PROGRAMMED CELL DEATH AND CARDIOVASCULAR DISEASE

EDITED BY: Zhi Qi, Rongxue Wu, Xiongwen Chen and Zhiqiang Lin

PUBLISHED IN: Frontiers in Cell and Developmental Biology

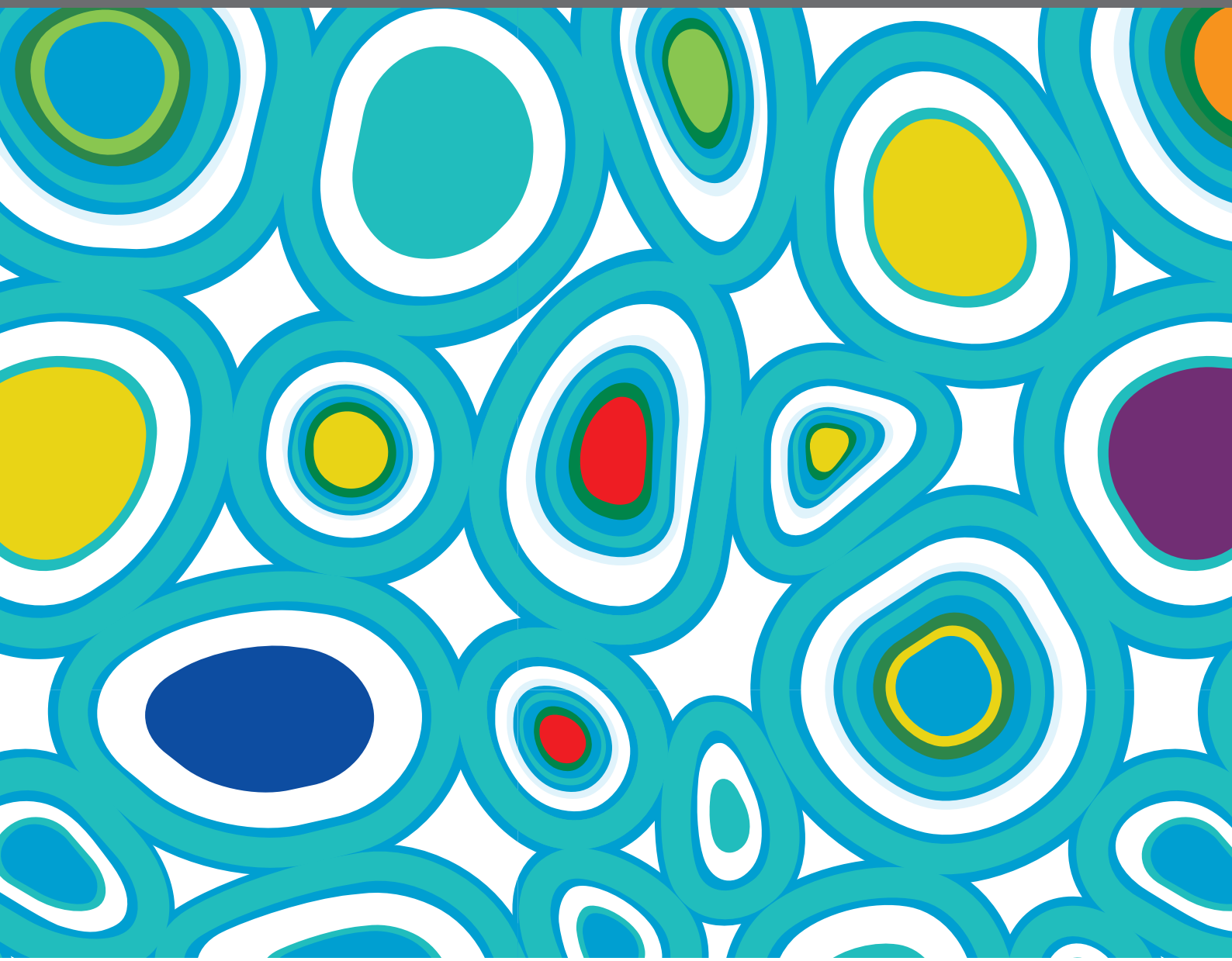

frontiers Research Topics

Frontiers eBook Copyright Statement

The copyright in the text of individual articles in this eBook is the property of their respective authors or their respective institutions or funders. The copyright in graphics and images within each article may be subject to copyright of other parties. In both cases this is subject to a license granted to Frontiers.

The compilation of articles constituting this eBook is the property of Frontiers.

Each article within this eBook, and the eBook itself, are published under the most recent version of the Creative Commons CC-BY licence. The version current at the date of publication of this eBook is CC-BY 4.0. If the CC-BY licence is updated, the licence granted by Frontiers is automatically updated to the new version.

When exercising any right under the CC-BY licence, Frontiers must be attributed as the original publisher of the article or eBook, as applicable.

Authors have the responsibility of ensuring that any graphics or other materials which are the property of others may be included in the CC-BY licence, but this should be checked before relying on the CC-BY licence to reproduce those materials. Any copyright notices relating to those materials must be complied with.

Copyright and source acknowledgement notices may not be removed and must be displayed in any copy, derivative work or partial copy which includes the elements in question.

All copyright, and all rights therein, are protected by national and international copyright laws. The above represents a summary only. For further information please read Frontiers' Conditions for Website Use and Copyright Statement, and the applicable CC-BY licence.

ISSN 1664-8714
ISBN 978-2-88976-919-3
DOI 10.3389/978-2-88976-919-3

About Frontiers

Frontiers is more than just an open-access publisher of scholarly articles: it is a pioneering approach to the world of academia, radically improving the way scholarly research is managed. The grand vision of Frontiers is a world where all people have an equal opportunity to seek, share and generate knowledge. Frontiers provides immediate and permanent online open access to all its publications, but this alone is not enough to realize our grand goals.

Frontiers Journal Series

The Frontiers Journal Series is a multi-tier and interdisciplinary set of open-access, online journals, promising a paradigm shift from the current review, selection and dissemination processes in academic publishing. All Frontiers journals are driven by researchers for researchers; therefore, they constitute a service to the scholarly community. At the same time, the Frontiers Journal Series operates on a revolutionary invention, the tiered publishing system, initially addressing specific communities of scholars, and gradually climbing up to broader public understanding, thus serving the interests of the lay society, too.

Dedication to Quality

Each Frontiers article is a landmark of the highest quality, thanks to genuinely collaborative interactions between authors and review editors, who include some of the world's best academicians. Research must be certified by peers before entering a stream of knowledge that may eventually reach the public - and shape society; therefore, Frontiers only applies the most rigorous and unbiased reviews.
Frontiers revolutionizes research publishing by freely delivering the most outstanding research, evaluated with no bias from both the academic and social point of view. By applying the most advanced information technologies, Frontiers is catapulting scholarly publishing into a new generation.

What are Frontiers Research Topics?

Frontiers Research Topics are very popular trademarks of the Frontiers Journals Series: they are collections of at least ten articles, all centered on a particular subject. With their unique mix of varied contributions from Original Research to Review Articles, Frontiers Research Topics unify the most influential researchers, the latest key findings and historical advances in a hot research area! Find out more on how to host your own Frontiers Research Topic or contribute to one as an author by contacting the Frontiers Editorial Office: frontiersin.org/about/contact

PROGRAMMED CELL DEATH AND CARDIOVASCULAR DISEASE

Topic Editors:
Zhi Qi, Nankai University, China
Rongxue Wu, The University of Chicago, United States
Xiongwen Chen, Temple University, United States
Zhiqiang Lin, Masonic Medical Research Institute (MMRI), United States

Citation: Qi, Z., Wu, R., Chen, X., Lin, Z., eds. (2022). Programmed Cell Death and Cardiovascular Disease. Lausanne: Frontiers Media SA.
doi: 10.3389/978-2-88976-919-3

Table of Contents

06 ***Targeting Ferroptosis to Treat Cardiovascular Diseases: A New Continent to Be Explored***
Fangze Huang, Ronghua Yang, Zezhou Xiao, Yu Xie, Xuefeng Lin, Peng Zhu, Pengyu Zhou, Jun Lu and Shaoyi Zheng

21 ***Normothermic* ex vivo *Heart Perfusion Combined With Melatonin Enhances Myocardial Protection in Rat Donation After Circulatory Death Hearts* via *Inhibiting NLRP3 Inflammasome-Mediated Pyroptosis***
Jun Lu, Liwei Xu, Zifeng Zeng, Chuqing Xue, Jiale Li, Xiong Chen, Pengyu Zhou, Shaoyan Lin, Yuhui Liao, Xianjin Du, Ronghua Yang and Shaoyi Zheng

34 ***IL-13 Alleviates Cardiomyocyte Apoptosis by Improving Fatty Acid Oxidation in Mitochondria***
Xiaoyu Guo, Ting Hong, Shen Zhang, Yazhong Wei, Haizhen Jin, Qing Miao, Kai Wang, Miao Zhou, Chong Wang and Bin He

44 ***IL-13 Derived Type 2 Innate Lymphocytes Ameliorates Cardiomyocyte Apoptosis Through STAT3 Signaling Pathway***
Ting Hong, Saiqi Li, Xiaoyu Guo, Yazhong Wei, Jingjing Zhang, Xiaohui Su, Miao Zhou, Haizhen Jin, Qing Miao, Lei Shen, Minfang Zhu and Bin He

55 ***Fundamental Mechanisms of the Cell Death Caused by Nitrosative Stress***
Fulin Wang, Qiuhuan Yuan, Fengying Chen, Jiaojiao Pang, Chang Pan, Feng Xu and Yuguo Chen

65 ***4-Hydroxy-2-Nonenal Promotes Cardiomyocyte Necroptosis* via *Stabilizing Receptor-Interacting Serine/Threonine-Protein Kinase 1***
Xiaoxuan Zhai, Wenjun Wang, Shukun Sun, Yu Han, Jiaxin Li, Shengchuan Cao, Ruochuan Li, Tonghui Xu, Qiuhuan Yuan, Jiali Wang, Shujian Wei and Yuguo Chen

78 ***Endogenous SO_2 Controls Cell Apoptosis: The State-of-the-Art***
Yingying Li, Yingjun Feng, Xiaoyun Ye, Hanlin Peng, Jiantong Du, Xiaoli Yao, Yaqian Huang, Hongfang Jin and Junbao Du

85 ***Iguratimod Alleviates Myocardial Ischemia/Reperfusion Injury Through Inhibiting Inflammatory Response Induced by Cardiac Fibroblast Pyroptosis via COX2/NLRP3 Signaling Pathway***
Mian Zhang, Yi-shan Lei, Xiao-wen Meng, Hua-yue Liu, Lin-gui Li, Jun Zhang, Jia-xin Zhang, Wen-hui Tao, Ke Peng, Jun Lin and Fu-hai Ji

101 ***Endothelial Dec1-PPARγ Axis Impairs Proliferation and Apoptosis Homeostasis Under Hypoxia in Pulmonary Arterial Hypertension***
Xiaoming Li, Chengcheng Liu, Wenwen Qi, Qiu Meng, Hui Zhao, Zhenxiao Teng, Runtong Xu, Xinhao Wu, Fangyuan Zhu, Yiming Qin, Miaoqing Zhao, Fenglei Xu and Ming Xia

116 ***Sacubitril Ameliorates Cardiac Fibrosis Through Inhibiting TRPM7 Channel***
Tian Jia, Xiaozhi Wang, Yiqun Tang, Wenying Yu, Chenhui Li, Shufang Cui, Juanjuan Zhu, Wei Meng, Chen Wang and Quanyi Wang

128 ***GSDMD Mediates LPS-Induced Septic Myocardial Dysfunction by Regulating ROS-dependent NLRP3 Inflammasome Activation***
Shanshan Dai, Bozhi Ye, Lingfeng Zhong, Yanghao Chen, Guangliang Hong, Guangju Zhao, Lan Su and Zhongqiu Lu

141 ***Programmed Cell Death: Complex Regulatory Networks in Cardiovascular Disease***
Liuhua Zhou, Jiateng Sun, Lingfeng Gu, Sibo Wang, Tongtong Yang, Tianwen Wei, Tiankai Shan, Hao Wang and Liansheng Wang

152 ***A Novel Insight Into the Fate of Cardiomyocytes in Ischemia-Reperfusion Injury: From Iron Metabolism to Ferroptosis***
Jing-yan Li, Shuang-qing Liu, Ren-qi Yao, Ying-ping Tian and Yong-ming Yao

166 ***YKL-40 Aggravates Early-Stage Atherosclerosis by Inhibiting Macrophage Apoptosis in an Aven-dependent Way***
Wei Huan, Liu Yandong, Wang Chao, Zou Sili, Bai Jun, Liao Mingfang, Chen Yu and Qu Lefeng

179 ***Ferroptosis Signaling and Regulators in Atherosclerosis***
Yuqin Wang, Yajie Zhao, Ting Ye, Liming Yang, Yanna Shen and Hong Li

192 ***The Function, Regulation and Mechanism of Programmed Cell Death of Macrophages in Atherosclerosis***
Chang Liu, Zecheng Jiang, Zhongjie Pan and Liang Yang

203 ***Autophagy, Pyroptosis, and Ferroptosis: New Regulatory Mechanisms for Atherosclerosis***
Lin Lin, Mu-Xin Zhang, Lei Zhang, Dan Zhang, Chao Li and Yun-lun Li

230 ***MicroRNA-223-3p Protect Against Radiation-Induced Cardiac Toxicity by Alleviating Myocardial Oxidative Stress and Programmed Cell Death* via *Targeting the AMPK Pathway***
Dao-ming Zhang, Jun-jian Deng, Yao-gui Wu, Tian Tang, Lin Xiong, Yong-fa Zheng and Xi-ming Xu

242 ***Sulphenylation of CypD at Cysteine 104: A Novel Mechanism by Which SO_2 Inhibits Cardiomyocyte Apoptosis***
Boyang Lv, Hanlin Peng, Bingquan Qiu, Lulu Zhang, Mei Ge, Dingfang Bu, Kun Li, Xiaoqi Yu, Jiantong Du, Liu Yang, Chaoshu Tang, Yaqian Huang, Junbao Du and Hongfang Jin

255 ***Ferroptosis: A Potential Target in Cardiovascular Disease***
Yanlong Leng, Xing Luo, Jiaying Yu, Haibo Jia and Bo Yu

270 ***Putative Prevention of XML Injection Against Myocardial Ischemia Is Mediated by PKC and PLA2 Proteins***
Ling Jin, Qianqian Yin, Yiqing Mao, Yuanxu Gao, Qing Han, Ruisi Mei, Lixiang Xue, Huanran Tan and Hui Li

282 ***Ferroptosis due to Cystathionine γ Lyase/Hydrogen Sulfide Downregulation Under High Hydrostatic Pressure Exacerbates VSMC Dysfunction***
Ruxi Jin, Ruixue Yang, Changting Cui, Haizeng Zhang, Jun Cai, Bin Geng and Zhenzhen Chen

293 ***$G\alpha_{12}$ and $G\alpha_{13}$: Versatility in Physiology and Pathology***
Paipai Guo, Yu Tai, Manman Wang, Hanfei Sun, Lingling Zhang, Wei Wei, Yang K. Xiang and Qingtong Wang

312 ***Atorvastatin Induces Mitochondria-Dependent Ferroptosis* via *the Modulation of Nrf2-xCT/GPx4 Axis***
Qi Zhang, Hang Qu, Yinghui Chen, Xueyang Luo, Chong Chen, Bing Xiao, Xiaowei Ding, Pengjun Zhao, Yanan Lu, Alex F. Chen and Yu Yu

330 ***Necroptosis and Viral Myocarditis: Tumor Necrosis Factor α as a Novel Biomarker for the Diagnosis of Viral Myocarditis***
Jin Zhou, Jing Xu, Peng Li, Shan Sun, Yimiti Kadier, Shiying Zhou and Aijuan Cheng

341 ***Higenamine Attenuates Doxorubicin-Induced Cardiac Remodeling and Myocyte Apoptosis by Suppressing AMPK Activation***
Cuiliu Jin, Yu Chai, Zhimin Hu, Wencong Tian, Wang Ling, Jing Li and Meiping Wu

frontiers in Cell and Developmental Biology

REVIEW
published: 30 August 2021
doi: 10.3389/fcell.2021.737971

Targeting Ferroptosis to Treat Cardiovascular Diseases: A New Continent to Be Explored

Fangze Huang[1†], Ronghua Yang[2†], Zezhou Xiao[1†], Yu Xie[1], Xuefeng Lin[1], Peng Zhu[1], Pengyu Zhou[1], Jun Lu[1*] and Shaoyi Zheng[1*]*

[1] Department of Cardiovascular Surgery, Nanfang Hospital, Southern Medical University, Guangzhou, China, [2] Department of Burn Surgery, The First People's Hospital of Foshan, Foshan, China

OPEN ACCESS

Edited by:
Zhi Qi,
Nankai University, China

Reviewed by:
Zhongkai Wu,
The First Affiliated Hospital of Sun Yat-sen University, China
Tian Hai,
The Second Affiliated Hospital of Harbin Medical University, China

***Correspondence:**
Pengyu Zhou
pyzhou@smu.edu.cn
Jun Lu
lujunwwwww@163.com
Shaoyi Zheng
zhsy@smu.edu.cn

† These authors have contributed equally to this work and share first authorship

Specialty section:
This article was submitted to Cell Death and Survival, a section of the journal Frontiers in Cell and Developmental Biology

Received: 08 July 2021
Accepted: 02 August 2021
Published: 30 August 2021

Citation:
Huang F, Yang R, Xiao Z, Xie Y, Lin X, Zhu P, Zhou P, Lu J and Zheng S (2021) Targeting Ferroptosis to Treat Cardiovascular Diseases: A New Continent to Be Explored. Front. Cell Dev. Biol. 9:737971. doi: 10.3389/fcell.2021.737971

Cardiovascular diseases, including cardiomyopathy, myocardial infarction, myocardial ischemia/reperfusion injury, heart failure, vascular injury, stroke, and arrhythmia, are correlated with cardiac and vascular cell death. Ferroptosis is a novel form of non-apoptotic regulated cell death which is characterized by an iron-driven accumulation of lethal lipid hydroperoxides. The initiation and execution of ferroptosis are under the control of several mechanisms, including iron metabolism, glutamine metabolism, and lipid peroxidation. Recently, emerging evidence has demonstrated that ferroptosis can play an essential role in the development of various cardiovascular diseases. Recent researches have shown the ferroptosis inhibitors, iron chelators, genetic manipulations, and antioxidants can alleviate myocardial injury by blocking ferroptosis pathway. In this review, we systematically described the mechanisms of ferroptosis and discussed the role of ferroptosis as a novel therapeutic strategy in the treatment of cardiovascular diseases.

Keywords: ferroptosis, cardiovascular disease, iron metabolism, cardiomyopathy, myocardial infarction, myocardial ischemia/reperfusion injury, heart failure, lipid peroxidation

INTRODUCTION

Cardiovascular diseases (CVDs) are the main cause of death and disability in developing and developed countries, including coronary artery disease, heart failure, aortic aneurysm and dissection, peripheral arterial disease, stroke, arrhythmia, and heart valve disorders (Graham et al., 2007; Arnett et al., 2019). In 2019, the prevalence of CVDs was up to 523 million, and the number of CVDs-related deaths reached 18.6 million (Roth et al., 2020). The pathogenesis of CVDs has been found correlated with the death of cardiac and vascular cells (Whelan et al., 2010; Moe and Marín-García, 2016; Del Re et al., 2019).

Fundamentally, cell death is divided into two different types: accidental cell death (ACD) and regulated cell death (RCD) (Tang et al., 2019). ACD can be triggered by unexpected attacks and injury resulting from any possible control molecular mechanisms (Galluzzi et al., 2015). On the contrary, RCD, also known as programmed cell death (PCD) in physiological conditions, involves precise signaling cascades that are executed by genetically defined effector molecules with unique immunological, functional, and biochemical consequences (Galluzzi et al., 2015). As a kind of adaptive response to restore cellular homeostasis, RCD can be modulated by inhibiting the transduction of lethal signals and improving the capacity of cells to adapt to stress (Taylor et al., 2008; Fuchs and Steller, 2011; Rubinsztein et al., 2012). Apoptosis is a classic form of RCD,

which can also be defined as programmed necrosis that functions as a homeostatic mechanism to maintain cell populations in tissues and a defense mechanism in immune reactions (Norbury and Hickson, 2001). Nowadays, more and more non-apoptotic forms of RCD have been shown to exert a significant influence on the occurrence and progress of diseases, such as necroptosis, pyroptosis, and autophagy-dependent cell death (Fearnhead et al., 2017; Tang et al., 2019).

Ferroptosis is an iron-dependent form of non-apoptotic RCD proposed by Dixon et al. (2012). It has been demonstrated that ferroptosis is essentially a process of overwhelming, iron-dependent accumulation of lethal lipid reactive oxygen species (ROS) (Dixon et al., 2012). Ferroptosis is morphologically and mechanistically distinguishable from other forms of RCD (**Table 1**).

Recently, several studies have indicated that ferroptosis contributes to the stress-induced deaths of cardiac and vascular cells (Gao et al., 2015; Fang et al., 2019; Wang and Tang, 2019). It has been pointed out that targeting ferroptosis can serve as a feasible approach for preventing cardiomyocyte death and managing cardiac pathologies (Ravingerová et al., 2020; Wu et al., 2021). In this review, we will describe the mechanism of ferroptosis and discuss the role of ferroptosis in the treatment of CVDs, thereby providing a novel therapeutic strategy for CVDs in the future.

OVERVIEW OF FERROPTOSIS

Dolma et al. (2003) found that erastin, a compound lethal to cells expressing RAS^{v12}, could selectively initiate a cell death procedure, which displayed no apoptotic features such as fragmented nuclei, DNA laddering, and activated caspase 3. Moreover, it was demonstrated by Yang and Stockwell (2008) that an inhibitor of glutathione peroxidase 4 (GPX4) named RAS-selective lethal 3 (RSL3), could induce rapid and non-apoptotic cell death in oncogenic RAS containing tumorigenic cells. This kind of non-apoptotic cell death could be prevented by genetic inhibition of cellular iron uptake or pharmacological iron chelation, which could not be completely reversed by the suppression of necrosis, apoptosis, autophagy, and necroptosis (Yagoda et al., 2007; Yang and Stockwell, 2008). Dixon et al. (2012) discovered that erastin triggered an iron-dependent accumulation of ROS and led to this novel non-apoptotic cell death, defined as *ferroptosis*. It was indicated that ferroptosis was induced by erastin through the inhibition of cystine uptake by the cystine/glutamate antiporter, which suppressed antioxidant defenses due to glutathione reduction (Dixon et al., 2012). This identified ferroptosis as a novel form of RCD and distinguished it from the other types of non-apoptotic cell death.

The occurrence of ferroptosis relies on enormous cellular iron and lipid hydroperoxide, which subsequently induce overwhelming lipid accumulation in cells and interfere with the homeostasis of redox reactions, thus promoting cell death (Xie et al., 2016; Dixon, 2017; Stockwell et al., 2017; Zhai et al., 2021). Ferroptosis can initiate the Fenton reaction and other peroxidation with excessive iron, which can convert the product of mitochondrial oxidative respiration, hydrogen peroxide, into hydroxyl-free radical under the catalysis of ferrous ion. This procedure leads to the accumulation of ROS that can destroy the integrity of cell membrane (Dixon et al., 2012; Qiu et al., 2020). The representative morphology of ferroptosis is shrunken mitochondria, which primarily exhibits increased membrane density, cristae degeneration, and breakdown (Xie et al., 2016). But few other significant morphological changes can be observed before the procedure of ferroptosis (Xie et al., 2016).

MECHANISM OF FERROPTOSIS

Ferroptosis is a complex process regulated by various mechanisms. Peroxidation of phospholipids (PLs) with polyunsaturated fatty acyl tails is considered as the primary driving factor for ferroptosis (Dixon et al., 2012). It has been demonstrated that the occurrence of ferroptosis requires three critical events: iron accumulation, glutathione (GSH) depletion, and lipid membrane oxidation (Bertrand, 2017). Based on those events and other related mechanisms, a large number of reagents have been discovered to induce or inhibit ferroptosis (**Table 2**). These mechanisms and regulators will be discussed below.

Iron Metabolism and Homeostasis

It has been proposed that the free radical generation by iron is a pivotal event during ferroptosis. A study in 2015 revealed that under amino acid starvation, ferroptosis occurred by incubating mouse embryonic fibroblasts in serum containing transferrin (Tf) (Gao et al., 2015). Moreover, the rate of cell death was reduced when Tf receptor expression was inhibited with RNA interference or when embryonic fibroblasts were incubated in the presence of iron-free Tf (Gao et al., 2015). These results demonstrate that iron metabolism is relevant to ferroptosis.

Concentrations and homeostasis of iron *in vivo* are regulated by various mechanisms, which control the metabolism, transfer, uptake, and export, as well as intracellular storage of iron (Ward and Kaplan, 2012; Drakesmith et al., 2015). Circulating iron exists in the form of ferric iron (Fe^{3+}) by the combination with Tf (Wang and Pantopoulos, 2011; Xie et al., 2016). The import of Fe^{3+} into cells is implemented through the membrane protein, Tf receptor 1 (TfR1) (Wang and Pantopoulos, 2011; Xie et al., 2016). After the import, Fe^{3+} is located in the endosome and then reduced to ferrous iron (Fe^{2+}) by the ferrireductase activity of STEAP3 (Hentze and Kühn, 1996; Wang and Pantopoulos, 2011; Xie et al., 2016). Subsequently, Fe^{2+} releases from the endosome into a labile iron pool (LIP) in the cytoplasm, mediated by divalent metal transporter 1 (DMT1) (Wang and Pantopoulos, 2011; Xie et al., 2016). The rest, excess iron is stored in ferritin (FT), an iron storage protein complex consisting of FTL and FTH1 subunits (Wang and Pantopoulos, 2011). The export of iron from cells is mediated by the membrane protein ferroportin (FPN), which can oxidize Fe^{2+} to Fe^{3+} (Xie et al., 2016). FPN is regulated by hepcidin, a 25-amino acid protein released mainly in the hepatocytes, which promotes the internalization and degradation of FPN when iron concentration is high (Ravingerová et al., 2020).

TABLE 1 | Characteristics of different types of regulated cell death.

Type	Morphological features	Biochemistry	Activation approach	Regulated genes
Ferroptosis	Smaller mitochondria with condensed mitochondrial membrane densities; reduction or vanishing of mitochondria crista, outer mitochondrial membrane rupture; normal nucleus	Iron-dependent lipid peroxidation, accumulation of iron and ROS	Iron overload, decreased cystine uptake, GSH depletion	Positive: VDAC2/3, RAS, NOX, TfR1, p53, CARS, ACSL4, NCOA4, GLS2s Negative: GPX4, NRF2, HSPB1/5, SLC7A11
Apoptosis	Plasma membrane blebbing without rupture; retraction of pseudopods; chromatin condensation and nuclear fragmentation; formation of apoptotic bodies	Caspase activation; Oligonucleosomal DNA fragment; phosphatidylserine exposure	Activated death receptor	Positive: initiator caspase (CASP2/8/9/10), effector caspase (CASP3/6/7), BCL2 family (BAX, BOK, BAK1, BBC3, BID, PMAIP1, and BCL2L11) and TP53, p53 Negative: Bcl-2 family
Necroptosis	Rupture of plasma membrane; cell swelling; moderate chromatin condensation; release of cell contents	Drop in ATP levels; RIPK1, RIPK3 and MLKL phosphorylation; ROS production; DAMPs release	TNF-α plus pan-Caspase inhibitor co-treatment; HSV-1 infection	Positive: RIPK1/3, MLKL
Autophagy	Accumulation of double-membraned autophagic vesicle	LC3-I to LC3-II conversion, p62 degradation	Nutritional deficiencies, oxidative stress	Positive: ATG5/7, Beclin 1, AMPK Negative: mTOR
Pyroptosis	Plasma membrane rupture, release of cell contents, unaffected mitochondrial integrity	Activation of caspase-1 and GSDMD, GSDMDN–induced pore formation, IL-1β release	Activation of inflammasomes	Positive: CASP1/11, GSDMD Negative: PKA, ESCRTIII, GPX4

Iron homeostasis is regulated by a post-transcriptional mechanism by the interaction of iron regulatory proteins (IRP) 1 and 2 with iron-responsive elements (IRE) on mRNA of respective genes, which modulate the synthesis of essential iron metabolism proteins that participate in iron uptake, storage, and release (Hentze and Kühn, 1996). Under conditions of low cellular iron concentration, IRP stabilizes the mRNA of TfR1 and DMT-1 to promote iron influx (Haddad et al., 2017; Paterek et al., 2019). Meanwhile, IRP prevents mRNA of FPN 1 and FT from translating to inhibit iron efflux and storage (Haddad et al., 2017; Paterek et al., 2019). This procedure results in a stable LIP, which is a crossroad of cellular iron metabolism. As a pool of chelatable and redox-active iron complexes, LIP is an intermediate or transitory pool between extracellular iron and cellular iron associated with proteins (Kakhlon and Cabantchik, 2002). When the concentration of the LIP increases to the homeostatic limits, severe oxidative damage occurs by initiating the Fenton reaction and other peroxidation, which will produce ROS and induce lipid peroxidation (Kakhlon and Cabantchik, 2002; Doll and Conrad, 2017; Qiu et al., 2020). The procedure of iron metabolism is presented in **Figure 1**.

Besides the iron homeostasis, it has been proposed that ferritinophagy, a process in which FT is selectively sequestered into autophagosomes and delivered to lysosomes for degradation, can trigger ferroptosis by promoting the accumulation of iron and ROS (Gao et al., 2015; Hou et al., 2016; Tang et al., 2018). Ferritinophagy can control iron availability and influence other proteins involving in ferroptosis to enhance the sensitivity of ferroptosis (Mancias et al., 2014; Sun et al., 2015; Hou et al., 2016; Tang et al., 2018). Therefore, iron metabolism and ferritinophagy can serve as the potential regulated targets for ferroptosis.

TABLE 2 | Common inducers and inhibitors of ferroptosis and their functioning mechanisms.

	Reagents	Mechanisms	References
Inducer	Erastin, Sulfasalazine	Inhibit system x_c^- and cause GSH depletion	Dixon et al., 2012
	Sorafenib		Dixon et al., 2014
	Glutamate		Zhang et al., 2019
	INF-γ	Downregulate expression of system x_c^-	Zitvogel and Kroemer, 2019
	RSL3, ML162	Inhibit GPX4 and lipid peroxidation	Yang et al., 2014
	FIN56	Deplete CoQ^{10} and degrade GPX4	Gaschler et al., 2018
	$FINO_2$	Deactivate GPX4 and oxidate iron	
	Statins	Inhibit mevalonate pathway to prevent CoQ^{10} synthesis	Viswanathan et al., 2017
Inhibitor	Ferrostatin-1	Block lipid peroxidation	Dixon et al., 2012
	Liproxstatins		Friedmann Angeli et al., 2014
	Glutathione		Schreiber et al., 2019
	CoQ^{10}		
	Vitamin E, α-Tocopherol	Suppress LOXs	Kagan et al., 2017
	Iron chelator	Deplete iron	Li N. et al., 2020
	Troglitazone, Rosiglitazone, Pioglitazone	Inhibit ACSL4	Doll et al., 2016

GSH, glutathione; GPX4, glutathione peroxidase 4; RSL3, RAS-selective lethal 3; LOX, lipoxygenase; ACSL4, acyl-CoA synthetase long-chain family member 4.

Abnormal Glutaminolysis

Amino acid metabolism is related to the regulation of ferroptosis (Angeli et al., 2017). Glutamine naturally exists at high concentrations in human tissues and plasma, and its degradation through glutaminolysis provides materials for the tricarboxylic acid cycle and essential biosynthetic processes such as lipid biosynthesis. This indicates that glutaminolysis is capable of

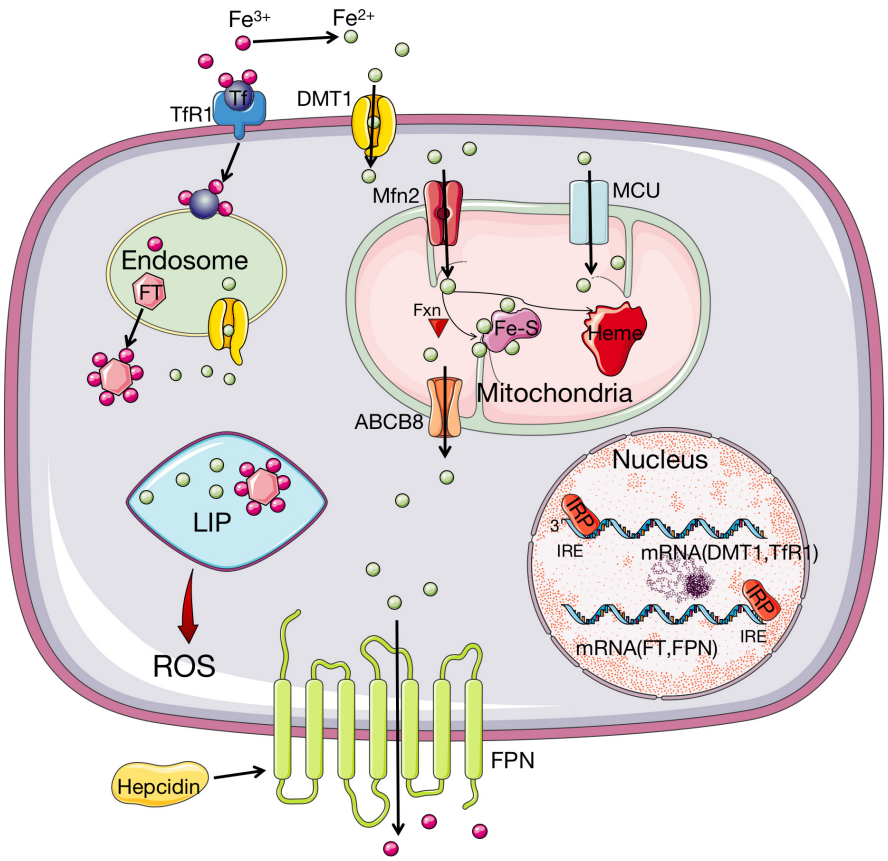

FIGURE 1 | Iron metabolism and homeostasis in organism. Fe^{3+} is imported into cells through Tf recognized by TfR1 while the uptake of Fe^{2+} is implemented through DMT1. Then Fe^{3+} is converted to Fe^{2+} in endosome, which is released from endosome by DMT1. In cell, iron is stored by binding FT, with a small amount staying at LIP. When the amount of iron in LIP increases to the homeostatic limits, ROS will be produced. The transport of iron to mitochondria is via MFRN and MCU. In mitochondria, iron can be synthesized to heme, or Fe–S under the participation of Fxn. The export of iron from mitochondria is through ABCB8 transporter and from cells is mediated through FPN. FPN can oxidize Fe^{2+} to Fe^{3+}, which is regulated by hepcidin. Iron homeostasis is controlled by IRP1/2, which can bind to IRE sites of mRNA of DMT-1, TfR1, FT, and FPN to regulate the influx and efflux of iron depending on the iron availability. When the intracellular iron level is low, IRPs bind to the 3′ UTR site of the mRNA of DMT1 and TfR1 to stabilize their transcript, whereas the 5′ UTR site mRNA of FT and FPN is also bound by IRPs to inhibit translation. Fe^{3+}, ferric; Tf, transferrin; TfR1, transferrin receptor 1; Fe^{2+}, ferrous; DMT1, divalent metal transporter 1; FT, ferritin; LIP, labile iron pool; ROS, reactive oxygen species; MRFN, mitoferrin; MCU, mitochondrial calcium uniporter; Fe–S: iron–sulfur cluster; Fxn, frataxin; FPN, ferroportin; ABCB8, adenosine triphosphate (ATP)-binding cassette subfamily B member 8; IRP1/2, iron regulatory protein 1/2; IRE, iron responsive elements.

reducing the accumulation of ROS and thus the occurrence of ferroptosis. It has been reported that ferroptosis can be initiated both by direct inhibition of GPX4, and an essential intracellular antioxidant, GSH, which are the crucial proteins in glutaminolysis (Wu et al., 2021).

When ferroptosis was first defined, it was induced by erastin which inhibited cystine uptake by the cystine/glutamate antiporter, leading to suppressed antioxidant defenses due to GSH reduction (Dixon et al., 2012). This is the classic pathway to initiate ferroptosis. It is indicated that erastin inhibits cystine uptake which is mediated by system x_c^-, a member of the heterodimeric amino acid transporter family (Dixon et al., 2012). Containing two subunits (SLC3A2 and SLC7A11), system x_c^- is the cystine/glutamate reverse transporter, which is expressed on cell membrane and capable of maintaining redox homeostasis (Bentea et al., 2020; Kim et al., 2020; Li et al., 2021). System x_c^- can transport glutamate into the extracellular space and meanwhile cystine into the cell on an equal ratio. After imported by system x_c^-, cystine is reduced and degraded to cysteine, which is utilized to synthesize antioxidant GSH (Bentea et al., 2020; Kim et al., 2020). Under the catalysis of GPX4, GSH converses to glutathione disulfide (GSSG) (Mirochnitchenko et al., 2000; Yang et al., 2014). In the meantime, free hydrogen peroxide is converted to water, or lipid hydroperoxides (L–OOH) are reduced to lipid hydroxy derivative (L–OH) by GPX4 (Mirochnitchenko et al., 2000; Yang et al., 2014). These procedures are essential for the maintenance of cellular redox homeostasis. When glutamine is absent or glutaminolysis is inhibited, cystine starvation and blockage of cystine import fail to induce the accumulation of ROS, lipid peroxidation, and ferroptosis (Gao et al., 2015; Stockwell et al., 2017). On the contrary, GSH depletion leads to the inactivation of GPX4 and thus produces excessive ROS (Yang et al., 2014). Hence, it is reasonable to hypothesize that system x_c^- and GPX4 serve as

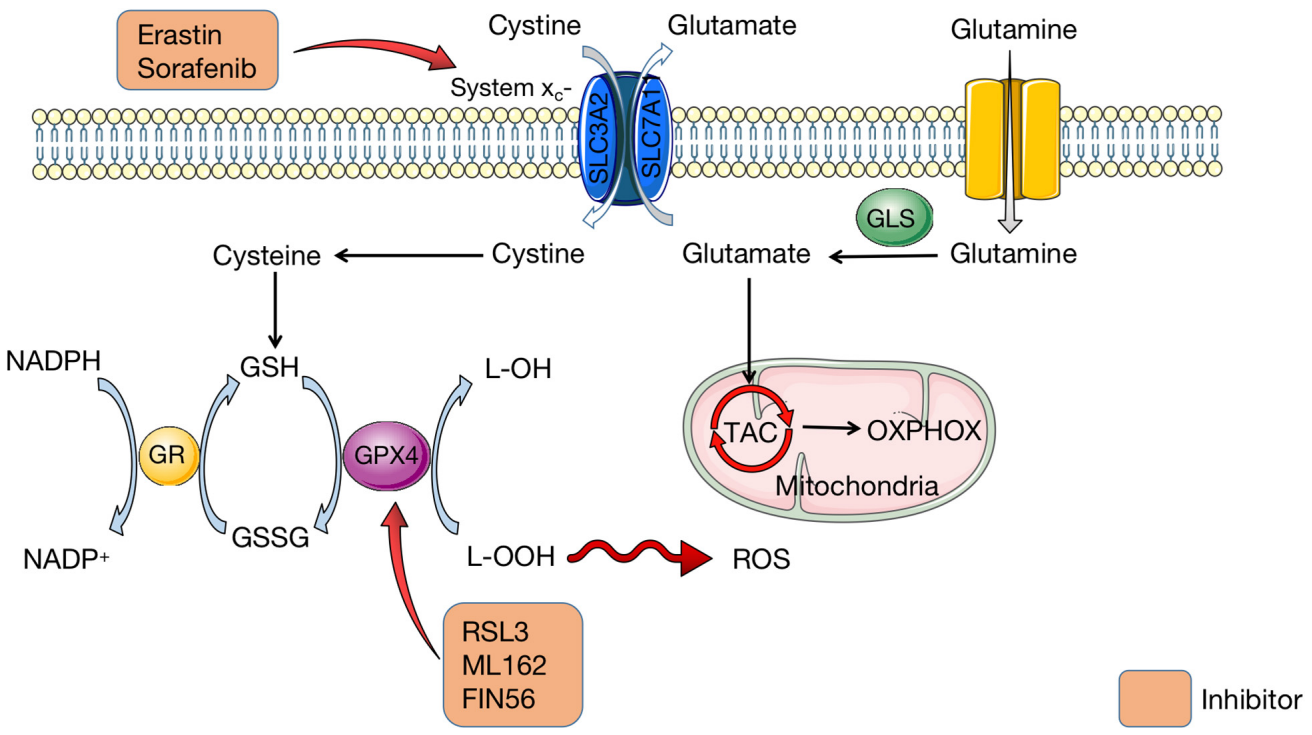

FIGURE 2 | Amio acid metabolism in ferroptosis. Containing two subunits (SLC3A2 and SLC7A11), system x_c^- is the cystine/glutamate reverse transporter on cell membrane, which transports cystine into cells and glutamate outside cells. Glutamate is transferred from glutamine, which is mediated by GLS. Then glutamate is imported into mitochondria for TAC to synthesize OXPHOX. In cells, cystine is degraded to cysteine for GSH synthesis. GSH is conversed to GSSG under the catalysis of GPX4, synchronized with conversion of L-OOH to L-OH. Meanwhile, NADPH is transferred to NADP+, which is catalyzed by GR. Erastin and sorafenib are inhibitors of system x_c^- to affect the amio acid metabolism. RSL3, ML162, and FIN56 can inhibit GPX4 and thus lead to excessive L-OOH in cells, which causes ROS accumulation. GLS, glutaminase; TAC, tricarboxylic acid cycle; OXPHOX, oxidative phosphorylation; GSH, glutathione; GSSG, glutathione disulfide; GPX4, glutathione peroxidase 4; NADPH, nicotinamide adenine dinucleotide phosphate; GR, glutathione reductase; RSL3, RAS-selective lethal 3; ROS, reactive oxygen species.

negative regulators of ferroptosis. **Figure 2** shows how amino acid metabolism is related to ROS production in organism.

Nevertheless, not all routes of glutaminolysis promote ferroptosis. The first step of glutaminolysis involves the conversion of glutamine into glutamate which is catalyzed by the glutaminases GLS1 and GLS2. Only GLS2 takes part in the initiation of ferroptosis, though GLS1 and GLS2 are structurally and enzymatically similar (Gao et al., 2015). The GLS2 gene is a transcriptional target of the tumor suppressor p53, and upregulation of GLS2 can promote p53-dependent ferroptosis (Jennis et al., 2016). Therefore, a precise target for inhibiting ferroptosis in amino acid metabolism still requires further researches.

Lipid Peroxidation

Lipid metabolism is intimately associated with cell death because it compromises membrane structural integrity, exerts downstream cytotoxic effects, and is involved in suicide signaling cascades (Reed, 2011; Yin et al., 2011; Ayala et al., 2014). As mentioned above, the inhibition of GPX4 causes lethal accumulation of lipid peroxides and thus leads to ferroptosis. This pathway has been demonstrated to mostly affect polyunsaturated fatty acid (PUFA), which contains bis-allylic hydrogen atoms that can be readily abstracted (Yang et al., 2016). Therefore, the abundance and localization of PUFA determine the degree of lipid peroxidation in cells, and the level of ferroptosis. PUFA must be esterified into membrane PLs and oxidated to become ferroptotic signals (Kagan et al., 2017). Also, accumulation of PL hydroperoxides has been detected in ferroptosis, including phosphatidylcholine, cardiolipin, and phosphatidylethanolamine (Yang et al., 2016). Hence, it has been proposed that PLs containing PUFA are the major substrates of ferroptotic lipid peroxidation and membrane damage is an essential event in ferroptosis (Friedmann Angeli et al., 2014; Yang et al., 2016; Kagan et al., 2017).

Recently, several lipidomic studies proposed that phosphatidylethanolamines (PEs) containing arachidonic acid (AA) or its elongation product, adrenic acid are pivotal PLs that undergo oxidation and actuate ferroptosis (Doll and Conrad, 2017; Kagan et al., 2017). As a result, coenzyme-A-derivatives that participate in the synthesis of these PUFAs and their insertion into PLs are required to produce ferroptotic signals. Two lipid metabolism-associated enzymes, lysophosphatidylcholine acyltransferase 3 (LPCAT3) and acyl-CoA synthetase long-chain family member 4 (ACSL4) are proved to participate in the

biosynthesis and restructuring of PUFA-PEs in cell membrane (Dixon et al., 2015). In fact, ACSL4 acylates AA and then LPCAT3 catalyzes the acylated AA into membrane PLs, which increases the oxidization of sensitive fatty acids such as PUFA in the membrane and eventually causes lipid peroxidation (Xie et al., 2016).

The formation of lipid hydroperoxides is demonstrated to be associated with enzymatic reactions and autoxidation catalyzed by lipoxygenase (LOX) (Yang et al., 2016). In ferroptosis, LOXs can promote the di-oxygenation of free and esterified PUFA to catalyze lipid peroxidation directly (Kuhn et al., 2015; Yang et al., 2016). The first step in LOXs catalysis is the abstraction of a labile hydrogen atom from a bis-allylic position on PUFA. Next, molecular oxygen adds to the intermediate carbon-centered radical to produce a peroxyl radical, which is then deoxidated by the enzyme to yield the hydroperoxide product (Kuhn et al., 2015). These products subsequently react with other PUFAs to pass on a chain reaction of lipid peroxidation, which yields PUFA peroxides and reactive aldehydes that cause cell damage (Yang et al., 2016; **Figure 3**).

Likewise, the progression of oxygen-driven free radical chain reaction, also named non-enzymatic lipid peroxidation, is believed to be involved in the occurrence of ferroptosis. Non-enzymatic lipid peroxidation includes the generation of early lipid radical L· based on the production of sufficiently reactive free radicals, the oxidation of L· in a chain reaction, and the termination of oxidation by antioxidants (Frank, 1950). Furthermore, lipid peroxidation spontaneously produces PLOO· and PLO·, which constantly recruit lipid molecules to free radical reactions and form a lipid peroxidation circle (Davies and Guo, 2014). It is believed that Fenton reaction can also provide the free radicals for lipid peroxidation metabolism, which can be a connecting point between iron metabolism and lipid peroxidation in ferroptosis (Zhai et al., 2021).

FERROPTOSIS AND CVDs

Iron Homeostasis in the Heart

The regulation of iron homeostasis in cardiac myocytes is similar to that of systemic iron homeostasis mentioned above. The import of iron is mediated by TfR1 and the export of iron from cells is implemented via FPN. Different from systemic cells, FPN in cardiomyocytes is regulated by both hepcidins produced by liver and locally in heart. Cardiac hepcidin has important autocrine effects and participates in autonomous regulation of iron in cardiomyocytes. Opposite to systemic hepcidin, loss of cardiac hepcidin upregulates FPN in cardiomyocytes to maintain cellular iron homeostasis (Lakhal-Littleton et al., 2016). It is indicated that iron level in cardiomyocytes is a balance between cellular iron efflux regulated by the cardiac hepcidin/FPN axis and systemic iron availability regulated by the systemic hepcidin/FPN axis (Lakhal-Littleton et al., 2016). In fact, cardiomyocytes are extra sensitive to iron overload with sufficient iron-importing mechanisms and only one export regulator. Nevertheless, either overload or deficiency of iron is harmful to homeostasis of cardiomyocytes. The import, utilization, storage, export, and regulation of iron in cardiomyocytes are presented in **Figure 4**. Interestingly, mitochondrial ferritin (mtFT) is an *H*-ferritin-like protein to store iron in mitochondria, which is mostly expressed in high oxygen-consuming and high metabolic cells. A recent study has demonstrated that mtFT can protect cardiomyocytes against the oxidative stress caused by cardiac injury via increasing the sensitivity of mitochondria (Li X. et al., 2017). The role of mtFT in iron homeostasis in cardiomyocytes still needs more researches to confirm.

Cardiomyocytes apoptosis can be induced by iron overload through mitochondrial dysfunction, in which increased mitochondrial oxidative stress triggers the release of cytochrome *c* and activates the caspase-dependent apoptotic pathway (Khamseekaew et al., 2017; Kumfu et al., 2018). This can result in iron-overload cardiomyopathy (IOC), which occurs in hemochromatosis and thalassemia major patients (Gulati et al., 2014). Moreover, the European Society of Cardiology currently recommended that the assessment of iron deficiency served as a comorbidity in chronic heart failure (CHF), due to the high prevalence of iron deficiency in patients with CHF (Klip et al., 2013).

The Role of Ferroptosis in CVDs

Ferroptosis and Cardiomyopathy

Several studies have indicated that ferroptosis is involved in many cardiomyopathies, including IOC, diabetic cardiomyopathy (DCM), doxorubicin (DOX)-induced cardiotoxicity, and so on.

As mentioned above, iron overload can destroy cardiac iron homeostasis, thereby leading to IOC through several mechanisms. IOC is regarded as a progressive electromechanical deterioration of the heart, which is the major reason for fatality in hemochromatosis patients (Nakamura et al., 2019). Also, several studies have demonstrated that high concentrations of intracellular iron induce ferroptosis in cardiomyocytes. Baba et al. (2018) verified that excessive iron induced cardiomyocytes ferroptosis as efficiently as erastin and RSL3 by directly incubating isolated mouse cardiomyocytes in ferric citrate. Furthermore, they found that cardiomyocytes treated with both Fe(III)-citrate and ferrostatin-1 (Fer-1), a specific ferroptosis inhibitor, were prevented from Fe(III)-citrate-induced cell death (Baba et al., 2018). This indicated that ferroptosis might play a significant role in the pathophysiological process of IOC, but the mechanism of how ferroptosis was associated with IOC remained unclear and needed further studies.

Diabetic cardiomyopathy, which is characterized by hypertrophy and fibrosis in the heart with the absence of clinical hypertension and coronary artery disease, is one of the most common complications of diabetes (Bugger and Abel, 2014; Parim et al., 2019). It can result in left ventricular remodeling event and subsequently develop into heart failure, which involves various mechanisms such as hyperglycemia, insulin resistance, increased fatty acid oxidation, oxidative stress, myocardial fibrosis and hypertrophy, endothelial dysfunction, myocyte cell death, autonomic neuropathy, arterial stiffness, autophagy, endoplasmic reticulum stress and so on

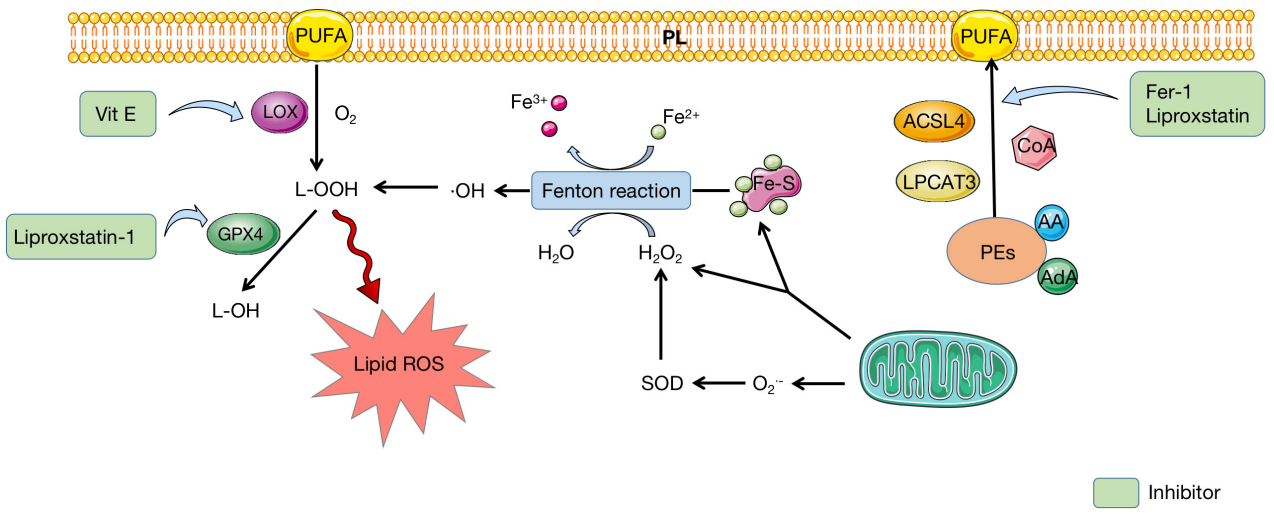

FIGURE 3 | Lipid metabolism in ferroptosis. PEs containing AA or AdA are fatty acid substrates, which are synthesized to PUFA under the catalysis of ACSL4, LPCAT3, and CoA. PUFA can insert to PL and be oxidated to produce L-OOH, which is catalyzed by LOX. Mitochondria provides Fe-S and H_2O_2 to participate in Fenton reaction, during which iron is oxidated and H_2O_2 is deoxidated. Reactive free radicals, ·OH, is produced and eventually conversed into L-OOH, which leads to accumulation of lipid ROS. GPX4 can mediate the transformation of L-OOH to L-OH, which can be inhibited by liproxstatin-1. Fer-1 and liproxstatin are inhibitors of PUFA synthesis, while Vit E can inhibit LOX to prevent PUFA oxidation. PEs, phosphatidylethanolamines; AA, arachidonic acid; AdA, adrenic acid; PUFA polyunsaturated fatty acid; PL, polyunsaturated fatty acid; LOX, lipoxygenase; Fe-S, iron–sulfur cluster; SOD, superoxide dismutase; ROS, reactive oxygen species; GPX4, glutathione peroxidase 4; Fer-1, ferrostatin-1; Vit E, vitamin E.

(Coats and Anker, 2000; Fiordaliso et al., 2001; Vinereanu et al., 2003; Brunner et al., 2006; Turan, 2010; Lakshmanan et al., 2013; Riehle et al., 2013; Brahmanaidu et al., 2017; Parim et al., 2019). Nowadays, it has been widely accepted that oxidative stress is the common pathogenesis of diabetic cardiomyopathy, which results from an imbalance between the production of ROS and the antioxidant capacity (Khullar et al., 2010; Huynh et al., 2014). Based on that, a recent research found that knockdown of nuclear factor-erythroid factor 2–related factor 2 (Nrf2), a main regulator of antioxidant defense, selectively suppressed glucolipotoxicity, while Fer-1 and iron chelator deferoxamine inhibited glucolipotoxicity in rat H9C2 cells cultured in high glucose (Zang et al., 2020). Moreover, the expression of ferroptosis markers, cyclooxygenase 2 (Cox2) and glutathione-specific γ-glutamylcyclotransferase 1 (Chac1), was upregulated, while the expressions of GPX4 and ferroptosis suppressor protein 1 (Fsp1) were downregulated in mice with streptozotocin-induced type 1 diabetes (T1D) (Zang et al., 2020). These results indicated that autophagy deficiency caused by diabetes initiated an Nrf2-operated ferroptosis in cardiomyocytes, thereby worsening the progression of diabetic cardiomyopathy. Hence, Nrf2 pathway-mediated ferroptosis should be focused on in the future, since it can be a novel target for treatment of DCM.

DOX is a class of anthracyclines that is commonly used to treat breast cancer, leukemia, and several types of malignancies (Young et al., 1981). Nevertheless, the clinical use of DOX is limited due to its cardiotoxicity, which can induce irreversible degenerative cardiomyopathy and congestive heart failure (Singal and Iliskovic, 1998). Fang et al. (2019) indicated that ferroptosis drove DOX-induced cardiomyopathy, owing to the results that DOX-treated cardiomyocytes in mice showed features of typical ferroptotic cell death and Fer-1 significantly decreased DOX-induced myocardial injury. Besides, by measuring mitochondrial lipid peroxidation to examine the effects of combining Fer-1 with zVAD-FMK (zVAD), an apoptosis inhibitor, in DOX-treated cardiomyocytes, Tadokoro et al. (2020) found that ferroptosis was the main form of RCD and triggered in mitochondria under DOX treatment. Luo et al. (2021) proved that DOX promoted ferroptosis in cardiomyocytes, whereas the administration of Astragaloside IV, an ingredient isolated from astragalus membranaceus, inhibited ferroptosis by activating Nrf2 signaling pathway and increased GPX4 expression (Luo et al., 2021). These studies demonstrated ferroptosis exerted a significant influence on DOX-induced cardiomyopathy and proved the therapeutic validity of inhibiting ferroptosis.

There is also a correlation between ferroptosis and sepsis-induced cardiomyopathy. Li N. et al. (2020) discovered that Fer-1 inhibited LPS-induced lipid peroxidation and injury of H9C2 myofibroblasts, which illustrated that ferroptosis served as a critical mechanism contributing to sepsis-induced cardiac injury. It is also proposed that targeting ferroptosis in cardiomyocytes may be a promising therapeutic strategy for preventing sepsis in the future.

Ferroptosis and Myocardial Infarction

Myocardial Infarction (MI) is a clinical term for heart attack, which is commonly caused by myocardial ischemia due to narrow or blocked coronary arteries. MI manifests as the death of cardiomyocytes and the replacement of damaged heart tissues by fibrotic scar tissue, which is unable to compensate for contraction function and thus causes heart failure (Hashimoto et al., 2018).

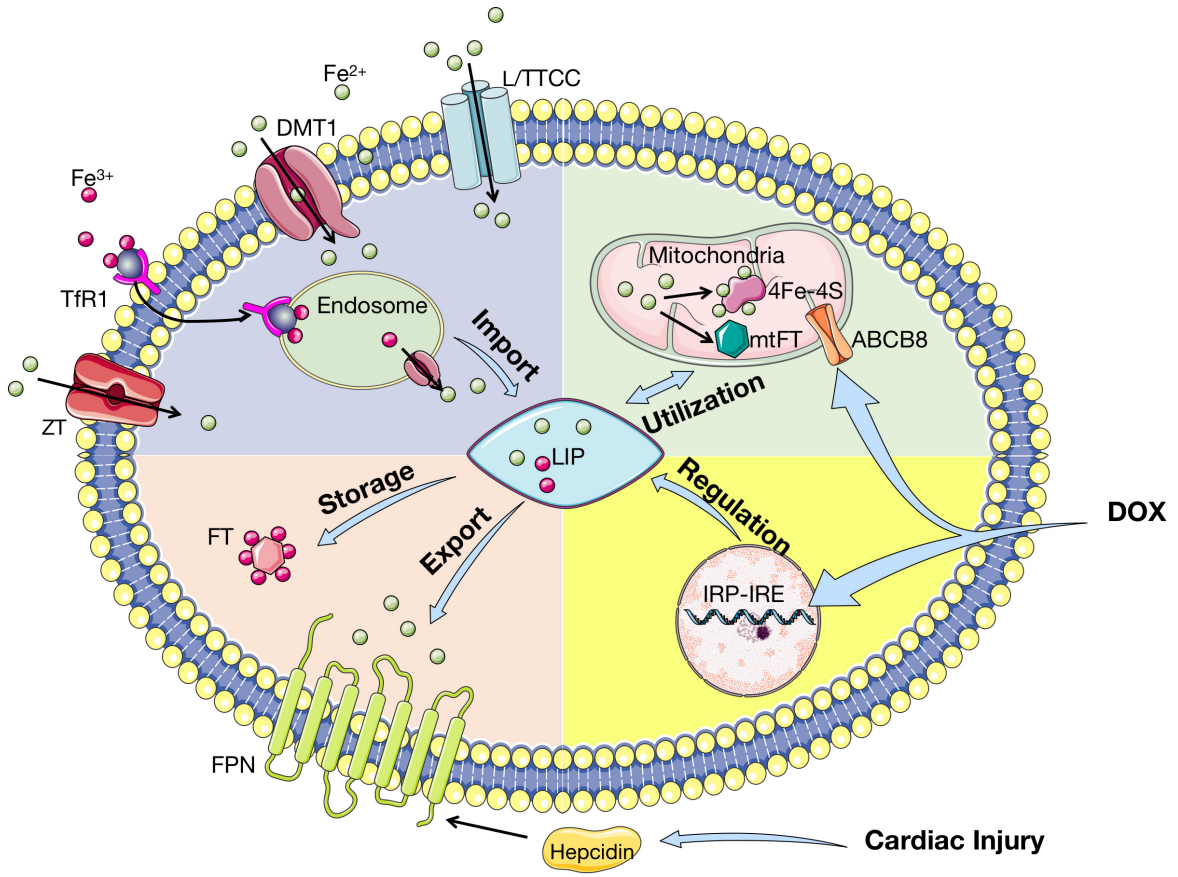

FIGURE 4 | Iron homeostasis in cardiomyocytes. Tf-bound iron is imported into cardiomyocytes via TfR1, whereas Non-Tf-bound iron enters via DMT1, L/TTCC, and ZT. After imported into cardiomyocytes, iron is located in endosome and deoxidated before stored in LIP. In cytoplasm, iron is stored by binding to FT and exported by FPN, which is regulated by hepcidin. Iron is transported into mitochondria for synthesis into 4Fe–4S and mtFT, which stores excessive iron during cardiac injury. ABCB8 is the iron exporter of mitochondria. Cardiac iron homeostasis is regulated by IRP-IRE with upregulation of TfR1 and downregulation of FT and FPN. Cardiac injury affects iron homeostasis by upregulating hepcidin, while DOX influences IRP-IRE and ABCB8. Tf, transferrin; TfR1: transferrin receptor 1; DMT1, divalent metal transporter 1; L/TTCC, L/T-type calcium channel; ZT, Zinc transporter; LIP, labile iron pool; FT, ferritin; FPN, ferroportin; Fe–S, iron–sulfur cluster; mtFT, mitochondrial ferritin; ABCB8, adenosine triphosphate (ATP)-binding cassette subfamily B member 8; IRP, iron regulatory protein; IRE, iron responsive elements; DOX, doxorubicin.

Currently, a variety of regulated cardiomyocyte deaths have been focused on and proved to play an important role in MI (Lee et al., 2003; Del Re et al., 2019). Bulluck et al. (2016) revealed that most of the ST-segment-elevation MI patients with IMH had residual myocardial iron at follow-up, which indicated that residual myocardial iron might be a potential therapeutic target to prevent adverse left ventricular remodeling in reperfused cardiac tissue of MI. By using quantitative proteomic analyses, Park et al. (2019) found that GPX4 and ROS pathway was downregulated significantly in early and middle stages of MI. This substantiates that ferroptosis contributes to cardiomyocyte death during MI under metabolic stress. Also, a recent research found that BTB and CNC homology 1 (BACH1), a regulator in heme and iron metabolism which could repress the transcription of erastin-induced protective genes, aggravates acute MI by promoting ferroptosis (Nishizawa et al., 2020). Tang et al. (2020) discovered autophagy in cardiomyocytes after MI could promote ferroptosis, which could be inhibited by microRNA-30d via binding to ATG5. Moreover, Song et al. (2021) examined the expression of DMT1 *in vivo* and *in vitro* acute MI models, and found that overexpression of DMT1 promoted cardiomyocyte ferroptosis. They also found that exosome of mesenchymal stem cells derived from human umbilical cord blood (HUCB-MSC) suppressed cardiomyocytes ferroptosis to mediate myocardial repair in acute MI by delivering miR-23a-3p (Song et al., 2021). Therefore, inhibition of ferroptosis might be a new insight for repairing cardiomyocyte injury in MI.

Ferroptosis and Myocardial Ischemia/Reperfusion Injury

Myocardial ischemia/reperfusion injury (IRI) is mostly caused by oxidative processes with ROS generation as the central pathogenesis. Although ROS from mitochondrion is considered as the primary cause of IRI in myocardium, several researches have purposed the significance of ferroptosis in induction of cardiomyocyte injury. By examining the level of myocardial iron in mouse models of IRI generated by 30-min left anterior descending coronary artery (LAD) ligation, Baba et al. (2018)

detected cardiomyocyte death with excessive iron accumulating around the myocardial scar, which proved to be ferroptosis by iron overload. Fang et al. (2019) treated mice with 30 min of myocardial ischemia followed by 24 h of reperfusion and discovered the occurrence of significantly increased cardiac non-heme iron. Also, they found that pretreatment of Fer-1 or iron chelator reduced ischemia/reperfusion-induced cardiac remodeling and fibrosis, with the decrease of cardiac *mt-Cytb* and *mt-Atp6* mRNA levels (Fang et al., 2019). Recently, Chen et al. (2021) discovered an increase in cellular iron levels but decreases in GPX4 activity as well as FTH1 and GSH levels in mice myocardial IRI model. Meanwhile, they found that the knockdown of embryonic lethal-abnormal vision like protein 1 (ELAVL1) could attenuate ischemia/reperfusion-induced ferroptosis by inhibiting autophagy, which was activated by Forkhead box C1 (FOXC1) in cardiomyocytes treated with hypoxia followed by reoxygenation (Chen et al., 2021). Fan et al. (2021) indicated that baicalin inhibited ACSL4-controlled ferroptosis to ameliorate myocardial IRI *in vitro*. Stamenkovic et al. (2021) put forward that increased oxidized phosphatidylcholines (OxPCs) generated in myocardial IRI provoked cardiomyocyte death through ferroptosis. Furthermore, several medications have been proposed to alleviate IRI by interfering with ferroptosis. Lv et al. (2021) proved that Etomidate suppressed ferroptosis in IRI model via upregulation of Nrf2 and heme oxygenase-1 (HO-1) protein expression. Cyanidin-3-glucoside, a kind of anthocyanin, is verified to attenuate myocardial IRI via ferroptosis inhibition by reducing oxidative stress and Fe^{2+} accumulation *in vivo* and *in vitro* (Shan et al., 2021). Ma et al. (2020) demonstrated that USP22 (ubiquitin-specific protease 22), a member of the deubiquitinase family, could inhibit ferroptosis in myocardial IRI via the SIRT1/p53/SLC7A11 association. On the contrary, USP7 is found to protect cardiomyocytes against ferroptosis caused by IRI via activation of the p53/TfR1 pathway (Tang et al., 2021b). Likewise, ferroptosis is demonstrated to be associated with diabetes myocardial IRI. Li et al. discovered that inhibiting ferroptosis reduced endoplasmic reticulum stress and mitigated myocardial damage (Li W. et al., 2020). These results suggested inhibiting ferroptosis could provide significant protection from myocardial IRI. Interestingly, a recent study found no significant changes in ACSL4, GPX4, iron, and malondialdehyde in cardiac ischemia region, whereas increased ACSL4, iron, and malondialdehyde as well as decreased GPX4 were observed in the reperfusion model (Tang et al., 2021a). Hence, it is believed that ferroptosis takes place in the phase of myocardial reperfusion instead of ischemia, which provides a fresh perspective for intervention of ferroptosis in IRI therapy.

Ischemia/reperfusion injury is one of the toughest challenges in heart transplantation, causing considerable sterile inflammation that leads to a high rate of primary graft dysfunction and even mortality in recipients (Kobashigawa et al., 2014). Li et al. (2019) found that Fer-1 reduced levels of hydroperoxy-arachidonoyl-phosphatidylethanolamine, a mediator of ferroptosis, which also repressed the ferroptosis of fibroblasts instead of endothelial cells in heart grafts submitted to IRI. They indicated that ferroptosis coordinated neutrophil recruitment to injured myocardium by promoting adhesion of neutrophils to coronary vascular endothelial cells through a TLR4/Trif/type I IFN signaling pathway (Li et al., 2019). Therefore, inhibition of ferroptosis in donor hearts before transplantation may reduce IRI and improve prognosis.

Ferroptosis and Heart Failure

Heart failure (HF), featured by cardiac hypertrophy and fibrosis, is a clinical syndrome, in which pumping function of heart is damaged and cardiac output fails to meet basic metabolic needs (Li et al., 2018; Miller et al., 2019). As loss of terminally differentiated cardiomyocytes is irreversible in HF, early prevention of cardiomyocyte death can maintain cardiac function and decelerate the progression of heart failure. A recent study observed ferroptotic cell death in the rat HF model induced by descending aortic banding (Liu et al., 2018). What's more, Puerarin, an antioxidant reagent, could reduce iron content and increase ROS elimination, suggesting that puerarin is a promising therapy for HF by inhibiting cardiomyocyte ferroptosis (Liu et al., 2018). By knockdown of TLR4 and NADPH oxidase 4 (NOX4) in HF rats, Chen et al. (2019) discovered a detainment of ferroptosis which was detected by expression of GPX4 and FTH1. Recently, Fang et al. (2020) found that a high-iron diet caused severe cardiac injury, hypertrophic cardiomyopathy, and eventually HF via inducing cardiomyocyte ferroptosis. Also, they revealed that cardiomyocytes deficient of FTH reduced expression of the SLC7A11 from system x_c^-, whereas overexpressing SLC7A11 selectively in cardiomyocytes increased GSH levels and prevented cardiac ferroptosis (Fang et al., 2020). Wang et al. (2020) indicated mixed lineage kinase 3 (MLK3), a member of MAP3K family, could regulate the JNK/p53 signaling pathway to initiate ferroptosis and cause myocardial fibrosis in the advanced stage of HF, which could be reversed by miR-351. Circular RNA (circRNA) is a new type of non-coding RNA, which is involved in the pathogenesis of cardiovascular diseases such as HF (Kolakofsky, 1976; Wang et al., 2017). Zheng et al. (2021) constructed a circRNA–miRNA–mRNA regulatory network based on competitive endogenous RNA and verified miR-224-5p, downstream target of circSnx12, could downregulate FTH1 expression in HF model. Altogether, these studies illustrate the significance of ferroptosis in cardiac hypertrophy and HF.

Ferroptosis and Vascular Injury

Vascular injury, a complicated type of CVDs including aortic dissection and abdominal aortic aneurysm, is caused by multifactorial damages such as genetic variant, diet, and environment. It is widely acknowledged that smoking is one of the main risk factors leading to aortic dissection and the rupture of abdominal aortic aneurysm (Lederle et al., 2003; Kakafika and Mikhailidis, 2007; Kihara et al., 2017). Sampilvanjil et al. (2020) found that cigarette smoke extract (CSE) initiated ferroptosis in vascular smooth muscle cells (VSMCs) rather than endothelial cells by depleting GSH rapidly and reducing the suppression of GPX4 overexpression, which resulted in medial VSMC loss in *ex vivo* aortas. These findings suggest that ferroptosis is the main cause of CSE-induced VSMC death and vascular injury.

TABLE 3 | Application of ferroptosis for treatment of cardiovascular diseases.

Reagents	Mechanisms	Protective effects	References
Knockdown of Nrf2	Reduce heme degradation	Prevent Hmox1-dependent ferroptosis in DIC.	Fang et al., 2019
Upregulation of GPX4	Decrease lipid ROS levels	Protect cardiomyocytes in MI.	Park et al., 2019
Overexpression of SLC7A11	Increase GSH levels	Mediate cardiac iron homeostasis and prevent hypertrophic cardiomyopathy.	Fang et al., 2020
Fer-1 DXZ	Prevent lipid peroxidation	Maintain the function of mitochondrial and prevent DIC.	Fang et al., 2019
Lip-1	Increase GPX4 protein levels and reduce ROS generation	Reduce myocardial infarct size and ischemia/reperfusion injury	Feng et al., 2019
Vitamin E	Suppress LOX	Inhibit PUFA oxidation and prevent ferroptosis.	Kagan et al., 2017

DIC, doxorubicin-induced cardiomyopathy; GPX4, glutathione peroxidase 4; ROS, reactive oxygen species; MI, myocardial infarction; GSH, glutathione; DXZ, dexrazoxane; Fer-1, ferrostatin-1; Lip-1, liproxstatin-1; LOX, lipoxygenase; PUFA, polyunsaturated fatty acid.

Further researches are expected to prove the role of ferroptosis in vascular diseases caused by other pathogenic factors such as atherosclerosis.

Ferroptosis and Stroke

Ischemic stroke refers to the restriction of blood supply to certain parts of the brain due to the occlusion of the internal carotid, middle cerebral, or vertebral/basilar arteries, which results in activation of ischemic cascade and ultimately cell death (Brouns and De Deyn, 2009; Au et al., 2017). Speer et al. (2013) hypothesized that ferroptosis might cause neuronal death induced by cerebral ischemia and that iron chelators prevented ferroptosis by inhibiting 2-oxoglutarate, oxygen-dependent dioxygenases, and the hypoxia-inducible factor (HIF) prolyl hydroxylases. Tuo et al. (2017) found that ferroptosis inhibition attenuated IRI in a middle cerebral artery occlusion model. More excitingly, they also found that tau-knockout mice were protected against hemispheric IRI, suggesting the tau–iron interaction as a pleiotropic modulator of ferroptosis and ischemic stroke outcome (Tuo et al., 2017). Recently, a research indicated that ACSL4 expression was downregulated in early ischemic stroke and its overexpression exacerbated ischemic cerebral injury, which proposed that ACSL4 expression might be a potential therapeutic target in ischemic stroke (Cui et al., 2021).

Intracerebral hemorrhage (ICH) occurs when a weakened vessel ruptures and bleeds, thereby leading to higher morbidity and mortality than ischemic stroke (Donnan et al., 2010). Hemoglobin/heme released from lysed erythrocytes after ICH is considered as a neurotoxin to induce lethal ROS after being metabolized into free iron and ultimately cause neuronal death (Ward et al., 2014; Xiong et al., 2014). A research showed that inhibition of iron-dependent hypoxia-inducible factor prolyl hydroxylase domain enzymes (HIF-PHDs) protected neurons from hemin-induced toxicity (Karuppagounder et al., 2016). Li Q. et al. (2017) found that Fer-1 prevented neuronal death and reduced iron deposition induced by hemoglobin in organotypic hippocampal slice cultures. Moreover, Zille et al. (2017) indicated that ICH *in vivo* and *in vitro* shared features of ferroptotic and necroptotic cell death, but not caspase-dependent apoptosis or autophagy. Collectively, all these studies suggest that ferroptosis contributes to neuronal death after ICH.

Ferroptosis and Arrhythmia

Cardiac arrhythmia can occur in terminal sudden unexpected death in epilepsy (SUDEP), due to a high rate of hypoxic stress induced by convulsions with excessive sympathetic overstimulation that triggers a neurocardiogenic injury (Nashef et al., 2012). Recently, arrhythmia in SUDEP is considered to be associated with iron overload in conditions of cardiac hypoxia. Akyuz et al. (2021) indicated ferroptosis might be a potential intrinsic mechanism that led to fatal cardiac arrhythmia, with hemosiderin observed in the cardiomyocytes in the SUDEP model. However, the deep mechanism of how ferroptosis is involved in arrhythmia remains unclear. Further investigations on this issue are expected to carry on in the future.

THE APPLICATION OF FERROPTOSIS IN TREATMENT OF CVDs

As mentioned above, ferroptosis plays a significant role in the occurrence and development of various CVDs. Therefore, targeting ferroptosis is proposed as a feasible approach for cardiac protection (**Table 3**).

Genetic manipulations in ferroptosis signaling pathway have been verified to successfully inhibit ferroptosis and decrease myocardial injury. The knockdown of Nrf2 to reduce heme degradation (Fang et al., 2019), upregulation of GPX4 (Park et al., 2019), and overexpression of SLC7A11 to increase GSH levels (Fang et al., 2020) are capable of inhibiting ferroptosis in cardiomyocytes.

Iron chelators are able to block redox reactions catalyzed by iron ions and to allow efficient transport and excretion without iron redistribution. Nowadays, 3 types of iron chelators including deferiprone, deferoxamine, and deferasirox are applied in clinical practice, mostly for the treatment of IOC (Pennell et al., 2013). Compared to the other two iron chelators, deferiprone targets hemorrhage-derived iron in IRI, which exerts a cardioprotective effect in acute MI by alleviating intramyocardial hemorrhage and cardiac hypertrophy (Behrouzi et al., 2020). Moreover, several retrospective studies revealed that deferiprone monotherapy showed better protection in heart than deferoxamine therapy or subcutaneous desferrioxamine therapy (Galanello et al., 2006; Pepe et al., 2011; Bilgin et al., 2020; Li et al., 2021).

The cardioprotective effects of antioxidants (e.g., Fer-1, liproxstatin-1, vitamin E) have been verified currently. Fer-1 is demonstrated to eliminate alkoxyl radicals produced by Fe^{2+} from lipid hydroperoxides in other excess iron-induced ferroptosis (Baba et al., 2018). Also, Fer-1 is beneficial to

cardiomyopathy in Fth-deficient mice (Fang et al., 2020). Likewise, liproxstatin-1 can decrease the levels of voltage-dependent anion channel 1 and rescue GPX4 levels to protect myocardium against IRI (Feng et al., 2019). Vitamin E and α-tocotrienol are capable of inhibiting ferroptosis by suppressing LOXs (Kagan et al., 2017).

PERSPECTIVE AND CONCLUSION

In this review, we summarized the main mechanisms of ferroptosis and discussed the role of ferroptosis in CVDs. As CVDs are a global health problem causing high rates of mortality, morbidity, and disability, understanding the pathology of cardiomyocyte damage is essential to develop a promising and novel therapeutic strategy for CVDs. With more and more focus on RCD in cardiomyocytes, ferroptosis, as an iron-dependent form of cell death, has received increasing attention.

Ferroptosis is mainly caused by the occurrence of lipid peroxidation of PUFA accumulation, which results from the accumulation of intracellular free Fe^{2+} and/or dysfunction of GSH peroxidation. Hence, the prominent features of ferroptosis are PUFA or PL peroxidation as well as accumulation of excessive iron. With overload of iron and lipid peroxidation, ROS accumulates and cell membrane is damaged, which eventually leads to cell death.

Iron overload is recently proved to be the significant cause of cardiomyocyte death, with cardiovascular imaging showing accumulation of iron in the damaged zone of heart. Also, verified by abundant studies with specific models *in vivo* and *in vitro*, ferroptosis has been demonstrated to play an important role in different types of CVDs, including cardiomyopathy, MI, IRI, HF, vascular injury, stroke, arrhythmia and so on. Inhibition of ferroptosis in CVDs can decrease cardiomyocyte death and improve cardiopathic conditions. Consequently, ferroptosis is a promising therapeutic target for CVDs.

However, the molecular mechanisms of ferroptotic cell death in cardiomyocytes remain unclear. Except for the destruction of iron metabolism, GSH depletion and lipid peroxidation, various pathways are also involved in the process of ferroptosis, such as high levels of extracellular glutamic acid, organelle-mediated pathways, Nrf2 pathway and so on (Zhai et al., 2021). Moreover, there are few researches on the relationship between ferroptosis and pathogenesis of arrhythmia. And further studies need to be performed to demonstrate the association between ferroptosis and vascular diseases. Though several inhibitors of ferroptosis, such as Fer-1 and GPX4, have been proposed to effectively repair cardiomyocyte injury, these novel methods are unsuitable for routine clinical therapy and their feasibility needs verification.

In conclusion, ferroptosis plays a significant role in the pathogenesis of various CVDs. With mechanisms and clinical feasibility under exploration, targeting ferroptosis to treat CVDs is a new continent to be explored.

AUTHOR CONTRIBUTIONS

FH, PYZ, JL, and SZ contributed to the conception and design of the study. FH, RY, and ZX searched the literature and wrote the manuscript. YX, XL, and PZ created the figure and table, and participated in drafting the manuscript. PYZ, JL, and SZ revised the manuscript. All the authors read and approved the final manuscript.

FUNDING

This research was supported by grants from the National Natural Science Foundation of China (81772136, 81972019, 21904145, 82170274, and 82100410), Guangdong Basic and Applied Basic Research Foundation (2021A1515011453), the Foundation of Foshan City (FS0AA-KJ218-1301-0034 and 2018AB003411), and Special fund of Foshan Summit plan (2019C002).

ACKNOWLEDGMENTS

We would like to express our gratitude to all the reviewers for the careful evaluation of the manuscript and appreciate the reviewers' insightful comments and suggestions which can help to improve our work. All figures were modified from Servier Medical Art (http://smart.servier.com/), licensed under a Creative Common Attribution 3.0 Generic License (https://creativecommons.org/licenses/by/3.0/).

REFERENCES

Akyuz, E., Doganyigit, Z., Eroglu, E., Moscovicz, F., Merelli, A., Lazarowski, A., et al. (2021). Myocardial iron overload in an experimental model of sudden unexpected death in epilepsy. *Front. Neurol.* 12:609236. doi: 10.3389/fneur.2021.609236

Angeli, J. P. F., Shah, R., Pratt, D. A., and Conrad, M. (2017). Ferroptosis inhibition: mechanisms and opportunities. *Trends Pharmacol. Sci.* 38, 489–498. doi: 10.1016/j.tips.2017.02.005

Arnett, D., Blumenthal, R., Albert, M., Buroker, A., Goldberger, Z., Hahn, E., et al. (2019). 2019 ACC/AHA guideline on the primary prevention of cardiovascular disease: executive summary: a report of the American college of cardiology/American heart association task force on clinical practice guidelines. *J. Am. Coll. Cardiol.* 74, 1376–1414.

Au, A., Griffiths, L. R., Irene, L., Kooi, C. W., and Wei, L. K. (2017). The impact of APOA5, APOB, APOC3 and ABCA1 gene polymorphisms on ischemic stroke: evidence from a meta-analysis. *Atherosclerosis* 265, 60–70. doi: 10.1016/j.atherosclerosis.2017.08.003

Ayala, A., Muñoz, M. F., and Argüelles, S. (2014). Lipid peroxidation: production, metabolism, and signaling mechanisms of malondialdehyde and 4-hydroxy-2-nonenal. *Oxid. Med. Cell. Longev.* 2014:360438. doi: 10.1155/2014/360438

Baba, Y., Higa, J. K., Shimada, B. K., Horiuchi, K. M., Suhara, T., Kobayashi, M., et al. (2018). Protective effects of the mechanistic target of rapamycin against excess iron and ferroptosis in cardiomyocytes. *Am. J. Physiol. Heart Circ. Physiol.* 314, H659–H668. doi: 10.1152/ajpheart.00452.2017

Behrouzi, B., Weyers, J. J., Qi, X., Barry, J., Rabadia, V., Manca, D., et al. (2020). Action of iron chelator on intramyocardial hemorrhage and cardiac remodeling following acute myocardial infarction. *Basic Res. Cardiol.* 115:24. doi: 10.1007/s00395-020-0782-6

Bentea, E., Villers, A., Moore, C., Funk, A. J., O'Donovan, S. M., Verbruggen, L., et al. (2020). Corticostriatal dysfunction and social interaction deficits in

mice lacking the cystine/glutamate antiporter. *Mol. Psychiatry* 10:1038. doi: 10.1038/s41380-020-0751-3

Bertrand, R. L. (2017). Iron accumulation, glutathione depletion, and lipid peroxidation must occur simultaneously during ferroptosis and are mutually amplifying events. *Med. Hypotheses* 101, 69–74. doi: 10.1016/j.mehy.2017.02.017

Bilgin, B. K., Yozgat, A. K., Isik, P., Çulha, V., Kacar, D., Kara, A., et al. (2020). The effect of deferasirox on endocrine complications in children with thalassemia. *Pediatr. Hematol. Oncol.* 37, 455–464. doi: 10.1080/08880018.2020.1734124

Brahmanaidu, P., Uddandrao, V. V. S., Sasikumar, V., Naik, R. R., Pothani, S., Begum, M. S., et al. (2017). Reversal of endothelial dysfunction in aorta of streptozotocin-nicotinamide-induced type-2 diabetic rats by S-Allylcysteine. *Mol. Cell. Biochem.* 432, 25–32. doi: 10.1007/s11010-017-2994-0

Brouns, R., and De Deyn, P. P. (2009). The complexity of neurobiological processes in acute ischemic stroke. *Clin. Neurol. Neurosurg.* 111, 483–495. doi: 10.1016/j.clineuro.2009.04.001

Brunner, F., Brás-Silva, C., Cerdeira, A. S., and Leite-Moreira, A. F. (2006). Cardiovascular endothelins: essential regulators of cardiovascular homeostasis. *Pharmacol. Ther.* 111, 508–531. doi: 10.1016/j.pharmthera.2005.11.001

Bugger, H., and Abel, E. D. (2014). Molecular mechanisms of diabetic cardiomyopathy. *Diabetologia* 57, 660–671. doi: 10.1007/s00125-014-3171-6

Bulluck, H., Rosmini, S., Abdel-Gadir, A., White, S. K., Bhuva, A. N., Treibel, T. A., et al. (2016). Residual myocardial iron following intramyocardial hemorrhage during the convalescent phase of reperfused ST-Segment-elevation myocardial infarction and adverse left ventricular remodeling. *Circ. Cardiovasc. Imaging* 9:e004940. doi: 10.1161/CIRCIMAGING.116.004940

Chen, H. Y., Xiao, Z. Z., Ling, X., Xu, R. N., Zhu, P., and Zheng, S. Y. (2021). ELAVL1 is transcriptionally activated by FOXC1 and promotes ferroptosis in myocardial ischemia/reperfusion injury by regulating autophagy. *Mol. Med.* 27:14. doi: 10.1186/s10020-021-00271-w

Chen, X., Xu, S., Zhao, C., and Liu, B. (2019). Role of TLR4/NADPH oxidase 4 pathway in promoting cell death through autophagy and ferroptosis during heart failure. *Biochem. Biophys. Res. Commun.* 516, 37–43. doi: 10.1016/j.bbrc.2019.06.015

Coats, A. J., and Anker, S. D. (2000). Insulin resistance in chronic heart failure. *J. Cardiovasc. Pharmacol.* 35(7 Suppl. 4), S9–S14. doi: 10.1097/00005344-200000004-00002

Cui, Y., Zhang, Y., Zhao, X., Shao, L., Liu, G., Sun, C., et al. (2021). ACSL4 exacerbates ischemic stroke by promoting ferroptosis-induced brain injury and neuroinflammation. *Brain Behav. Immun.* 93, 312–321. doi: 10.1016/j.bbi.2021.01.003

Davies, S. S., and Guo, L. (2014). Lipid peroxidation generates biologically active phospholipids including oxidatively N-modified phospholipids. *Chem. Phys. Lipids* 181, 1–33. doi: 10.1016/j.chemphyslip.2014.03.002

Del Re, D. P., Amgalan, D., Linkermann, A., Liu, Q., and Kitsis, R. N. (2019). Fundamental mechanisms of regulated cell death and implications for heart disease. *Physiol. Rev.* 99, 1765–1817. doi: 10.1152/physrev.00022.2018

Dixon, S. J. (2017). Ferroptosis: bug or feature? *Immunol. Rev.* 277, 150–157. doi: 10.1111/imr.12533

Dixon, S. J., Lemberg, K. M., Lamprecht, M. R., Skouta, R., Zaitsev, E. M., Gleason, C. E., et al. (2012). Ferroptosis: an iron-dependent form of nonapoptotic cell death. *Cell* 149, 1060–1072. doi: 10.1016/j.cell.2012.03.042

Dixon, S. J., Patel, D. N., Welsch, M., Skouta, R., Lee, E. D., Hayano, M., et al. (2014). Pharmacological inhibition of cystine-glutamate exchange induces endoplasmic reticulum stress and ferroptosis. *ELife* 3:e02523. doi: 10.7554/eLife.02523

Dixon, S. J., Winter, G. E., Musavi, L. S., Lee, E. D., Snijder, B., Rebsamen, M., et al. (2015). Human haploid cell genetics reveals roles for lipid metabolism genes in nonapoptotic cell death. *ACS Chem. Biol.* 10, 1604–1609. doi: 10.1021/acschembio.5b00245

Doll, S., and Conrad, M. (2017). Iron and ferroptosis: a still ill-defined liaison. *IUBMB Life* 69, 423–434. doi: 10.1002/iub.1616

Doll, S., Proneth, B., Tyurina, Y. Y., Panzilius, E., Kobayashi, S., Ingold, I., et al. (2016). ACSL4 dictates ferroptosis sensitivity by shaping cellular lipid composition. *Nat. Chem. Biol.* 13, 91–98. doi: 10.1038/nchembio.2239

Dolma, S., Lessnick, S. L., Hahn, W. C., and Stockwell, B. R. (2003). Identification of genotype-selective antitumor agents using synthetic lethal chemical screening in engineered human tumor cells. *Cancer Cell* 3, 285–296. doi: 10.1016/s1535-6108(03)00050-3

Donnan, G. A., Hankey, G. J., and Davis, S. M. (2010). Intracerebral haemorrhage: a need for more data and new research directions. *Lancet Neurol.* 9, 133–134. doi: 10.1016/S1474-4422(10)70001-6

Drakesmith, H., Nemeth, E., and Ganz, T. (2015). Ironing out ferroportin. *Cell Metab.* 22, 777–787. doi: 10.1016/j.cmet.2015.09.006

Fan, Z., Cai, L., Wang, S., Wang, J., and Chen, B. (2021). Baicalin prevents myocardial ischemia/reperfusion injury through inhibiting ACSL4 mediated ferroptosis. *Front. Pharmacol.* 12:628988. doi: 10.3389/fphar.2021.628988

Fang, X., Cai, Z., Wang, H., Han, D., Cheng, Q., Zhang, P., et al. (2020). Loss of cardiac ferritin H facilitates cardiomyopathy via Slc7a11-mediated ferroptosis. *Circ. Res.* 127, 486–501. doi: 10.1161/CIRCRESAHA.120.316509

Fang, X., Wang, H., Han, D., Xie, E., Yang, X., Wei, J., et al. (2019). Ferroptosis as a target for protection against cardiomyopathy. *Proc. Natl. Acad. Sci. U.S.A.* 116, 2672–2680. doi: 10.1073/pnas.1821022116

Fearnhead, H., Vandenabeele, P., and Vanden Berghe, T. (2017). How do we fit ferroptosis in the family of regulated cell death? *Cell Death Differ.* 24, 1991–1998. doi: 10.1038/cdd.2017.149

Feng, Y., Madungwe, N. B., Imam Aliagan, A. D., Tombo, N., and Bopassa, J. C. (2019). Liproxstatin-1 protects the mouse myocardium against ischemia/reperfusion injury by decreasing VDAC1 levels and restoring GPX4 levels. *Biochem. Biophys. Res. Commun.* 520, 606–611. doi: 10.1016/j.bbrc.2019.10.006

Fiordaliso, F., Leri, A., Cesselli, D., Limana, F., Safai, B., Nadal-Ginard, B., et al. (2001). Hyperglycemia activates p53 and p53-regulated genes leading to myocyte cell death. *Diabetes* 50, 2363–2375. doi: 10.2337/diabetes.50.10.2363

Frank, C. E. (1950). Hydrocarbon autoxidation. *Chem. Rev.* 46, 155–169. doi: 10.1021/cr60143a003

Friedmann Angeli, J. P., Schneider, M., Proneth, B., Tyurina, Y. Y., Tyurin, V. A., Hammond, V. J., et al. (2014). Inactivation of the ferroptosis regulator Gpx4 triggers acute renal failure in mice. *Nat. Cell Biol.* 16, 1180–1191. doi: 10.1038/ncb3064

Fuchs, Y., and Steller, H. (2011). Programmed cell death in animal development and disease. *Cell* 147, 742–758. doi: 10.1016/j.cell.2011.10.033

Galanello, R., Kattamis, A., Piga, A., Fischer, R., Leoni, G., Ladis, V., et al. (2006). A prospective randomized controlled trial on the safety and efficacy of alternating deferoxamine and deferiprone in the treatment of iron overload in patients with thalassemia. *Haematologica* 91, 1241–1243.

Galluzzi, L., Bravo-San Pedro, J. M., Vitale, I., Aaronson, S. A., Abrams, J. M., Adam, D., et al. (2015). Essential versus accessory aspects of cell death: recommendations of the NCCD 2015. *Cell Death Differ.* 22, 58–73. doi: 10.1038/cdd.2014.137

Gao, M., Monian, P., Quadri, N., Ramasamy, R., and Jiang, X. (2015). Glutaminolysis and transferrin regulate ferroptosis. *Mol. Cell* 59, 298–308. doi: 10.1016/j.molcel.2015.06.011

Gaschler, M. M., Andia, A. A., Liu, H., Csuka, J. M., Hurlocker, B., Vaiana, C. A., et al. (2018). FINO2 initiates ferroptosis through GPX4 inactivation and iron oxidation. *Nat. Chem. Biol.* 14, 507–515. doi: 10.1038/s41589-018-0031-6

Graham, I., Atar, D., Borch-Johnsen, K., Boysen, G., Burell, G., Cifkova, R., et al. (2007). European Society of Cardiology (ESC) Committee for Practice Guidelines (CPG). European guidelines on cardiovascular disease prevention in clinical practice: executive summary: fourth joint task force of the European society of cardiology and other societies on cardiovascular disease prevention in clinical practice (Constituted by representatives of nine societies and by invited experts). *Eur. Heart J.* 28, 2375–2414. doi: 10.1093/eurheartj/ehm316

Gulati, V., Harikrishnan, P., Palaniswamy, C., Aronow, W. S., Jain, D., and Frishman, W. H. (2014). Cardiac involvement in hemochromatosis. *Cardiol. Rev.* 22, 56–68. doi: 10.1097/CRD.0b013e3182a67805

Haddad, S., Wang, Y., Galy, B., Korf-Klingebiel, M., Hirsch, V., Baru, A. M., et al. (2017). Iron-regulatory proteins secure iron availability in cardiomyocytes to prevent heart failure. *Eur. Heart J.* 38, 362–372. doi: 10.1093/eurheartj/ehw333

Hashimoto, H., Olson, E. N., and Bassel-Duby, R. (2018). Therapeutic approaches for cardiac regeneration and repair. *Nat. Rev. Cardiol.* 15, 585–600. doi: 10.1038/s41569-018-0036-6

Hentze, M. W., and Kühn, L. C. (1996). Molecular control of vertebrate iron metabolism: mRNA-based regulatory circuits operated by iron, nitric oxide, and

oxidative stress. *Proc. Natl. Acad. Sci. U.S.A.* 93, 8175–8182. doi: 10.1073/pnas.93.16.8175

Hou, W., Xie, Y., Song, X., Sun, X., Lotze, M. T., Zeh, H. J. III, et al. (2016). Autophagy promotes ferroptosis by degradation of ferritin. *Autophagy* 12, 1425–1428. doi: 10.1080/15548627.2016.1187366

Huynh, K., Bernardo, B. C., McMullen, J. R., and Ritchie, R. H. (2014). Diabetic cardiomyopathy: mechanisms and new treatment strategies targeting antioxidant signaling pathways. *Pharmacol. Ther.* 142, 375–415. doi: 10.1016/j.pharmthera.2014.01.003

Jennis, M., Kung, C. P., Basu, S., Budina-Kolomets, A., Leu, J. I., Khaku, S., et al. (2016). An African-specific polymorphism in the TP53 gene impairs p53 tumor suppressor function in a mouse model. *Genes Dev.* 30, 918–930. doi: 10.1101/gad.275891.115

Kagan, V. E., Mao, G., Qu, F., Angeli, J. P., Doll, S., Croix, C. S., et al. (2017). Oxidized arachidonic and adrenic PEs navigate cells to ferroptosis. *Nat. Chem. Biol.* 13, 81–90. doi: 10.1038/nchembio.2238

Kakafika, A. I., and Mikhailidis, D. P. (2007). Smoking and aortic diseases. *Circ. J.* 71, 1173–1180. doi: 10.1253/circj.71.1173

Kakhlon, O., and Cabantchik, Z. I. (2002). The labile iron pool: characterization, measurement, and participation in cellular processes(1). *Free Radic. Biol. Med.* 33, 1037–1046. doi: 10.1016/s0891-5849(02)01006-7

Karuppagounder, S. S., Alim, I., Khim, S. J., Bourassa, M. W., Sleiman, S. F., John, R., et al. (2016). Therapeutic targeting of oxygen-sensing prolyl hydroxylases abrogates ATF4-dependent neuronal death and improves outcomes after brain hemorrhage in several rodent models. *Sci. Transl. Med.* 8:328ra29. doi: 10.1126/scitranslmed.aac6008

Khamseekaew, J., Kumfu, S., Wongjaikam, S., Kerdphoo, S., Jaiwongkam, T., Srichairatanakool, S., et al. (2017). Effects of iron overload, an iron chelator and a T-Type calcium channel blocker on cardiac mitochondrial biogenesis and mitochondrial dynamics in thalassemic mice. *Eur. J. Pharmacol.* 799, 118–127. doi: 10.1016/j.ejphar.2017.02.015

Khullar, M., Al-Shudiefat, A. A., Ludke, A., Binepal, G., and Singal, P. K. (2010). Oxidative stress: a key contributor to diabetic cardiomyopathy. *Can. J. Physiol. Pharmacol.* 88, 233–240. doi: 10.1139/Y10-016

Kihara, T., Yamagishi, K., Iso, H., Tamakoshi, A., and Jacc Study Group. (2017). Passive smoking and mortality from aortic dissection or aneurysm. *Atherosclerosis* 263, 145–150. doi: 10.1016/j.atherosclerosis.2017.06.022

Kim, D., Kim, W., Kim, S., Moon, D., and Lee, S. (2020). TGF-β1-mediated repression of SLC7A11 drives vulnerability to GPX4 inhibition in hepatocellular carcinoma cells. *Cell Death Dis.* 11:406.

Klip, I. T., Comin-Colet, J., Voors, A. A., Ponikowski, P., Enjuanes, C., Banasiak, W., et al. (2013). Iron deficiency in chronic heart failure: an international pooled analysis. *Am. Heart J.* 165, 575–582.e3. doi: 10.1016/j.ahj.2013.01.017

Kobashigawa, J., Zuckermann, A., Macdonald, P., Leprince, P., Esmailian, F., Luu, M., et al. (2014). Consensus Conference participants. Report from a consensus conference on primary graft dysfunction after cardiac transplantation. *J. Heart Lung Transplant.* 33, 327–340. doi: 10.1016/j.healun.2014.02.027

Kolakofsky, D. (1976). Isolation and characterization of Sendai virus DI-RNAs. *Cell* 8, 547–555. doi: 10.1016/0092-8674(76)90223-3

Kuhn, H., Banthiya, S., and van Leyen, K. (2015). Mammalian lipoxygenases and their biological relevance. *Biochim. Biophys. Acta* 1851, 308–330. doi: 10.1016/j.bbalip.2014.10.002

Kumfu, S., Khamseekaew, J., Palee, S., Srichairatanakool, S., Fucharoen, S., Chattipakorn, S. C., et al. (2018). A combination of an iron chelator with an antioxidant exerts greater efficacy on cardioprotection than monotherapy in iron-overload thalassemic mice. *Free Radic. Res.* 52, 70–79. doi: 10.1080/10715762.2017.1414208

Lakhal-Littleton, S., Wolna, M., Chung, Y. J., Christian, H. C., Heather, L. C., Brescia, M., et al. (2016). An essential cell-autonomous role for hepcidin in cardiac iron homeostasis. *Elife* 5:e19804. doi: 10.7554/eLife.19804

Lakshmanan, A. P., Harima, M., Suzuki, K., Soetikno, V., Nagata, M., Nakamura, T., et al. (2013). The hyperglycemia stimulated myocardial endoplasmic reticulum (ER) stress contributes to diabetic cardiomyopathy in the transgenic non-obese type 2 diabetic rats: a differential role of unfolded protein response (UPR) signaling proteins. *Int. J. Biochem. Cell Biol.* 45, 438–447. doi: 10.1016/j.biocel.2012.09.017

Lederle, F. A., Nelson, D. B., and Joseph, A. M. (2003). Smokers' relative risk for aortic aneurysm compared with other smoking-related diseases: a systematic review. *J. Vasc. Surg.* 38, 329–334. doi: 10.1016/s0741-5214(03)00136-8

Lee, P., Sata, M., Lefer, D. J., Factor, S. M., Walsh, K., and Kitsis, R. N. (2003). Fas pathway is a critical mediator of cardiac myocyte death and MI during ischemia-reperfusion in vivo. *Am. J. Physiol. Heart Circ. Physiol.* 284, H456–H463. doi: 10.1152/ajpheart.00777.2002

Li, N., Jiang, W., Wang, W., Xiong, R., Wu, X., and Geng, Q. (2021). Ferroptosis and its emerging roles in cardiovascular diseases. *Pharmacol. Res.* 166:105466. doi: 10.1016/j.phrs.2021.105466

Li, N., Wang, W., Zhou, H., Wu, Q., Duan, M., Liu, C., et al. (2020). Ferritinophagy-mediated ferroptosis is involved in sepsis-induced cardiac injury. *Free Radic. Biol. Med.* 160, 303–318. doi: 10.1016/j.freeradbiomed.2020.08.009

Li, N., Zhou, H., and Tang, Q. (2018). miR-133: a suppressor of cardiac remodeling? *Front. Pharmacol.* 9:903. doi: 10.3389/fphar.2018.00903

Li, Q., Han, X., Lan, X., Gao, Y., Wan, J., Durham, F., et al. (2017). Inhibition of neuronal ferroptosis protects hemorrhagic brain. *JCI Insight.* 2:e90777. doi: 10.1172/jci.insight.90777

Li, W., Feng, G., Gauthier, J. M., Lokshina, I., Higashikubo, R., Evans, S., et al. (2019). Ferroptotic cell death and TLR4/Trif signaling initiate neutrophil recruitment after heart transplantation. *J. Clin. Invest.* 129, 2293–2304. doi: 10.1172/JCI126428

Li, W., Li, W., Leng, Y., Xiong, Y., and Xia, Z. (2020). Ferroptosis is involved in diabetes myocardial ischemia/reperfusion injury through endoplasmic reticulum stress. *DNA Cell Biol.* 39, 210–225. doi: 10.1089/dna.2019.5097

Li, X., Wang, P., Wu, Q., Xie, L., Cui, Y., Li, H., et al. (2017). The construction and characterization of mitochondrial ferritin overexpressing mice. *Int. J. Mol. Sci.* 18:1518. doi: 10.3390/ijms18071518

Liu, B., Zhao, C., Li, H., Chen, X., Ding, Y., and Xu, S. (2018). Puerarin protects against heart failure induced by pressure overload through mitigation of ferroptosis. *Biochem. Biophys. Res. Commun.* 497, 233–240. doi: 10.1016/j.bbrc.2018.02.061

Luo, L. F., Guan, P., Qin, L. Y., Wang, J. X., Wang, N., and Ji, E. S. (2021). Astragaloside IV inhibits adriamycin-induced cardiac ferroptosis by enhancing Nrf2 signaling. *Mol. Cell. Biochem.* 476, 2603–2611. doi: 10.1007/s11010-021-04112-6

Lv, Z., Wang, F., Zhang, X., Zhang, X., Zhang, J., and Liu, R. (2021). Etomidate attenuates the ferroptosis in myocardial ischemia/reperfusion rat model via Nrf2 pathway. *Shock* doi: 10.1097/SHK.0000000000001751

Ma, S., Sun, L., Wu, W., Wu, J., Sun, Z., and Ren, J. (2020). USP22 protects against myocardial ischemia-reperfusion injury via the SIRT1-p53/SLC7A11-Dependent inhibition of ferroptosis-induced cardiomyocyte death. *Front. Physiol.* 11:551318. doi: 10.3389/fphys.2020.551318

Mancias, J. D., Wang, X., Gygi, S. P., Harper, J. W., and Kimmelman, A. C. (2014). Quantitative proteomics identifies NCOA4 as the cargo receptor mediating ferritinophagy. *Nature* 509, 105–109. doi: 10.1038/nature13148

Miller, P. E., van Diepen, S., and Ahmad, T. (2019). Acute decompensated heart failure complicated by respiratory failure. *Circ. Heart Fail.* 12:e006013. doi: 10.1161/CIRCHEARTFAILURE.119.006013

Mirochnitchenko, O., Prokopenko, O., Palnitkar, U., Kister, I., Powell, W. S., and Inouye, M. (2000). Endotoxemia in transgenic mice overexpressing human glutathione peroxidases. *Circ. Res.* 87, 289–295. doi: 10.1161/01.res.87.4.289

Moe, G. W., and Marín-García, J. (2016). Role of cell death in the progression of heart failure. *Heart Fail. Rev.* 21, 157–167. doi: 10.1007/s10741-016-9532-0

Nakamura, T., Naguro, I., and Ichijo, H. (2019). Iron homeostasis and iron-regulated ROS in cell death, senescence and human diseases. *Biochim. Biophys. Acta Gen. Subj.* 1863, 1398–1409. doi: 10.1016/j.bbagen.2019.06.010

Nashef, L., So, E. L., Ryvlin, P., and Tomson, T. (2012). Unifying the definitions of sudden unexpected death in epilepsy. *Epilepsia* 53, 227–233. doi: 10.1111/j.1528-1167.2011.03358.x

Nishizawa, H., Matsumoto, M., Shindo, T., Saigusa, D., Kato, H., Suzuki, K., et al. (2020). Ferroptosis is controlled by the coordinated transcriptional regulation of glutathione and labile iron metabolism by the transcription factor BACH1. *J. Biol. Chem.* 295, 69–82. doi: 10.1074/jbc.RA119.009548

Norbury, C. J., and Hickson, I. D. (2001). Cellular responses to DNA damage. *Annu. Rev. Pharmacol. Toxicol.* 41, 367–401.

Parim, B., Sathibabu Uddandrao, V. V., and Saravanan, G. (2019). Diabetic cardiomyopathy: molecular mechanisms, detrimental effects of conventional

treatment, and beneficial effects of natural therapy. *Heart Fail. Rev.* 24, 279–299. doi: 10.1007/s10741-018-9749-1

Park, T. J., Park, J. H., Lee, G. S., Lee, J. Y., Shin, J. H., Kim, M. W., et al. (2019). Quantitative proteomic analyses reveal that GPX4 downregulation during myocardial infarction contributes to ferroptosis in cardiomyocytes. *Cell Death Dis.* 10:835. doi: 10.1038/s41419-019-2061-8

Paterek, A., Mackiewicz, U., and Mączewski, M. (2019). Iron and the heart: a paradigm shift from systemic to cardiomyocyte abnormalities. *J. Cell. Physiol.* 234, 21613–21629. doi: 10.1002/jcp.28820

Pennell, D. J., Udelson, J. E., Arai, A. E., Bozkurt, B., Cohen, A. R., Galanello, R., et al. (2013). Cardiovascular function and treatment in β-thalassemia major: a consensus statement from the American Heart Association. *Circulation* 128, 281–308. doi: 10.1161/CIR.0b013e31829b2be6

Pepe, A., Meloni, A., Capra, M., Cianciulli, P., Prossomariti, L., Malaventura, C., et al. (2011). Deferasirox, deferiprone and desferrioxamine treatment in thalassemia major patients: cardiac iron and function comparison determined by quantitative magnetic resonance imaging. *Haematologica* 96, 41–47. doi: 10.3324/haematol.2009.019042

Qiu, Y., Cao, Y., Cao, W., Jia, Y., and Lu, N. (2020). The application of ferroptosis in diseases. *Pharmacol. Res.* 159:104919. doi: 10.1016/j.phrs.2020.104919

Ravingerová, T., Kindernay, L., Barteková, M., Ferko, M., Adameová, A., Zohdi, V., et al. (2020). The molecular mechanisms of iron metabolism and its role in cardiac dysfunction and cardioprotection. *Int. J. Mol. Sci.* 21:7889. doi: 10.3390/ijms21217889

Reed, T. T. (2011). Lipid peroxidation and neurodegenerative disease. *Free Radic. Biol. Med.* 51, 1302–1319. doi: 10.1016/j.freeradbiomed.2011.06.027

Riehle, C., Wende, A. R., Sena, S., Pires, K. M., Pereira, R. O., Zhu, Y., et al. (2013). Insulin receptor substrate signaling suppresses neonatal autophagy in the heart. *J. Clin. Invest.* 123, 5319–5333. doi: 10.1172/JCI71171

Roth, G. A., Mensah, G. A., Johnson, C. O., Addolorato, G., Ammirati, E., Baddour, L. M., et al. (2020). Global burden of cardiovascular diseases and risk factors, 1990-2019: update from the GBD 2019 study. *J. Am. Coll. Cardiol.* 76, 2982–3021. doi: 10.1016/j.jacc.2020.11.010

Rubinsztein, D. C., Codogno, P., and Levine, B. (2012). Autophagy modulation as a potential therapeutic target for diverse diseases. *Nat. Rev. Drug Discov.* 11, 709–730. doi: 10.1038/nrd3802

Sampilvanjil, A., Karasawa, T., Yamada, N., Komada, T., Higashi, T., Baatarjav, C., et al. (2020). Cigarette smoke extract induces ferroptosis in vascular smooth muscle cells. *Am. J. Physiol. Heart Circ. Physiol.* 318, H508–H518. doi: 10.1152/ajpheart.00559.2019

Schreiber, R., Buchholz, B., Kraus, A., Schley, G., Scholz, J., Ousingsawat, J., et al. (2019). Lipid peroxidation drives renal cyst growth in vitro through activation of TMEM16A. *J. Am. Soc. Nephrol. JASN* 30, 228–242. doi: 10.1681/ASN.2018010039

Shan, X., Lv, Z. Y., Yin, M. J., Chen, J., Wang, J., and Wu, Q. N. (2021). The protective effect of cyanidin-3-glucoside on myocardial ischemia-reperfusion injury through ferroptosis. *Oxid. Med. Cell. Longev.* 2021, 8880141. doi: 10.1155/2021/8880141

Singal, P. K., and Iliskovic, N. (1998). Doxorubicin-induced cardiomyopathy. *N. Engl. J. Med.* 339, 900–905. doi: 10.1056/NEJM199809243391307

Song, Y., Wang, B., Zhu, X., Hu, J., Sun, J., Xuan, J., et al. (2021). Human umbilical cord blood-derived MSCs exosome attenuate myocardial injury by inhibiting ferroptosis in acute myocardial infarction mice. *Cell Biol. Toxicol.* 37, 51–64. doi: 10.1007/s10565-020-09530-8

Speer, R. E., Karuppagounder, S. S., Basso, M., Sleiman, S. F., Kumar, A., Brand, D., et al. (2013). Hypoxia-inducible factor prolyl hydroxylases as targets for neuroprotection by "antioxidant" metal chelators: from ferroptosis to stroke. *Free Radic. Biol. Med.* 62, 26–36. doi: 10.1016/j.freeradbiomed.2013.01.026

Stamenkovic, A., O'Hara, K. A., Nelson, D. C., Maddaford, T. G., Edel, A. L., and Maddaford, G. (2021). Oxidized phosphatidylcholines trigger ferroptosis in cardiomyocytes during ischemia-reperfusion injury. *Am. J. Physiol. Heart Circ. Physiol.* 320, H1170–H1184. doi: 10.1152/ajpheart.00237.2020

Stockwell, B. R., Friedmann Angeli, J. P., Bayir, H., Bush, A. I., Conrad, M., Dixon, S. J., et al. (2017). Ferroptosis: a regulated cell death nexus linking metabolism. redox biology, and disease. *Cell* 171, 273–285. doi: 10.1016/j.cell.2017.09.021

Sun, X., Ou, Z., Xie, M., Kang, R., Fan, Y., Niu, X., et al. (2015). HSPB1 as a novel regulator of ferroptotic cancer cell death. *Oncogene* 34, 5617–5625. doi: 10.1038/onc.2015.32

Tadokoro, T., Ikeda, M., Ide, T., Deguchi, H., Ikeda, S., Okabe, K., et al. (2020). Mitochondria-dependent ferroptosis plays a pivotal role in doxorubicin cardiotoxicity. *JCI Insight.* 5:e132747. doi: 10.1172/jci.insight.132747

Tang, D., Kang, R., Berghe, T., Vandenabeele, P., and Kroemer, G. (2019). The molecular machinery of regulated cell death. *Cell Res.* 29, 347–364. doi: 10.1038/s41422-019-0164-5

Tang, L. J., Luo, X. J., Tu, H., Chen, H., Xiong, X. M., Li, N. S., et al. (2021a). Ferroptosis occurs in phase of reperfusion but not ischemia in rat heart following ischemia or ischemia/reperfusion. *Naunyn Schmiedebergs Arch. Pharmacol.* 394, 401–410. doi: 10.1007/s00210-020-01932-z

Tang, L. J., Zhou, Y. J., Xiong, X. M., Li, N. S., Zhang, J. J., Luo, X. J., et al. (2021b). Ubiquitin-specific protease 7 promotes ferroptosis via activation of the p53/TfR1 pathway in the rat hearts after ischemia/reperfusion. *Free Radic. Biol. Med.* 162, 339–352. doi: 10.1016/j.freeradbiomed.2020.10.307

Tang, M., Chen, Z., Wu, D., and Chen, L. (2018). Ferritinophagy/ferroptosis: iron-related newcomers in human diseases. *J. Cell. Physiol.* 233, 9179–9190. doi: 10.1002/jcp.26954

Tang, S., Wang, Y., Ma, T., Lu, S., Huang, K., Li, Q., et al. (2020). MiR-30d inhibits cardiomyocytes autophagy promoting ferroptosis after myocardial infarction. *Panminerva Med.* Advance online publication

Taylor, R. C., Cullen, S. P., and Martin, S. J. (2008). Apoptosis: controlled demolition at the cellular level. *Nat Rev. Mol. Cell Biol.* 9, 231–241. doi: 10.1038/nrm2312

Tuo, Q. Z., Lei, P., Jackman, K. A., Li, X. L., Xiong, H., Li, X. L., et al. (2017). Tau-mediated iron export prevents ferroptotic damage after ischemic stroke. *Mol. Psychiatry* 22, 1520–1530. doi: 10.1038/mp.2017.171

Turan, B. (2010). Role of antioxidants in redox regulation of diabetic cardiovascular complications. *Curr. Pharm. Biotechnol.* 11, 819–836. doi: 10.2174/138920110793262123

Vinereanu, D., Nicolaides, E., Boden, L., Payne, N., Jones, C. J., and Fraser, A. G. (2003). Conduit arterial stiffness is associated with impaired left ventricular subendocardial function. *Heart* 89, 449–450. doi: 10.1136/heart.89.4.449

Viswanathan, V. S., Ryan, M. J., Dhruv, H. D., Gill, S., Eichhoff, O. M., Seashore-Ludlow, B., et al. (2017). Dependency of a therapy-resistant state of cancer cells on a lipid peroxidase pathway. *Nature* 547, 453–457. doi: 10.1038/nature23007

Wang, J., and Pantopoulos, K. (2011). Regulation of cellular iron metabolism. *Biochem. J.* 434, 365–381. doi: 10.1042/BJ20101825

Wang, J., Deng, B., Liu, Q., Huang, Y., Chen, W., Li, J., et al. (2020). Pyroptosis and ferroptosis induced by mixed lineage kinase 3 (MLK3) signaling in cardiomyocytes are essential for myocardial fibrosis in response to pressure overload. *Cell Death Dis.* 11:574. doi: 10.1038/s41419-020-02777-3

Wang, K., Gan, T. Y., Li, N., Liu, C. Y., Zhou, L. Y., Gao, J. N., et al. (2017). Circular RNA mediates cardiomyocyte death via miRNA-dependent upregulation of MTP18 expression. *Cell Death Differ.* 24, 1111–1120. doi: 10.1038/cdd.2017.61

Wang, Y., and Tang, M. (2019). PM2.5 induces ferroptosis in human endothelial cells through iron overload and redox imbalance. *Environ. Pollut.* 254:112937. doi: 10.1016/j.envpol.2019.07.105

Ward, D. M., and Kaplan, J. (2012). Ferroportin-mediated iron transport: expression and regulation. *Biochim. Biophys. Acta* 1823, 1426–1433. doi: 10.1016/j.bbamcr.2012.03.004

Ward, R. J., Zucca, F. A., Duyn, J. H., Crichton, R. R., and Zecca, L. (2014). The role of iron in brain ageing and neurodegenerative disorders. *Lancet Neurol.* 13, 1045–1060. doi: 10.1016/S1474-4422(14)70117-6

Whelan, R. S., Kaplinskiy, V., and Kitsis, R. N. (2010). Cell death in the pathogenesis of heart disease: mechanisms and significance. *Annu. Rev. Physiol.* 72, 19–44. doi: 10.1146/annurev.physiol.010908.163111

Wu, X., Li, Y., Zhang, S., and Zhou, X. (2021). Ferroptosis as a novel therapeutic target for cardiovascular disease. *Theranostics* 11, 3052–3059. doi: 10.7150/thno.54113

Xie, Y., Hou, W., Song, X., Yu, Y., Huang, J., Sun, X., et al. (2016). Ferroptosis: process and function. *Cell Death Differ.* 23, 369–379. doi: 10.1038/cdd.2015.158

Xiong, X. Y., Wang, J., Qian, Z. M., and Yang, Q. W. (2014). Iron and intracerebral hemorrhage: from mechanism to translation. *Transl. Stroke Res.* 5, 429–441. doi: 10.1007/s12975-013-0317-7

Yagoda, N., von Rechenberg, M., Zaganjor, E., Bauer, A. J., Yang, W. S., Fridman, D. J., et al. (2007). RAS-RAF-MEK-dependent oxidative cell death involving voltage-dependent anion channels. *Nature* 447, 864–868. doi: 10.1038/nature05859

Yang, W. S., and Stockwell, B. R. (2008). Synthetic lethal screening identifies compounds activating iron-dependent, nonapoptotic cell death in oncogenic-RAS-harboring cancer cells. *Chem. Biol.* 15, 234–245. doi: 10.1016/j.chembiol.2008.02.010

Yang, W. S., Kim, K. J., Gaschler, M. M., Patel, M., Shchepinov, M. S., and Stockwell, B. R. (2016). Peroxidation of polyunsaturated fatty acids by lipoxygenases drives ferroptosis. *Proc. Natl. Acad. Sci. U.S.A.* 113, E4966–E4975. doi: 10.1073/pnas.1603244113

Yang, W. S., SriRamaratnam, R., Welsch, M. E., Shimada, K., Skouta, R., Viswanathan, V. S., et al. (2014). Regulation of ferroptotic cancer cell death by GPX4. *Cell* 156, 317–331. doi: 10.1016/j.cell.2013.12.010

Yin, H., Xu, L., and Porter, N. A. (2011). Free radical lipid peroxidation: mechanisms and analysis. *Chem. Rev.* 111, 5944–5972. doi: 10.1021/cr200084z

Young, R. C., Ozols, R. F., and Myers, C. E. (1981). The anthracycline antineoplastic drugs. *N. Engl. J. Med.* 305, 139–153. doi: 10.1056/NEJM198107163050305

Zang, H., Wu, W., Qi, L., Tan, W., Nagarkatti, P., Nagarkatti, M., et al. (2020). Autophagy inhibition enables Nrf2 to exaggerate the progression of diabetic cardiomyopathy in mice. *Diabetes* 69, 2720–2734. doi: 10.2337/db19-1176

Zhai, Z., Zou, P., Liu, F., Xia, Z., and Li, J. (2021). Ferroptosis is a potential novel diagnostic and therapeutic target for patients with cardiomyopathy. *Front. Cell Dev. Biol.* 9:649045. doi: 10.3389/fcell.2021.649045

Zhang, Y., Tan, H., Daniels, J. D., Zandkarimi, F., Liu, H., Brown, L. M., et al. (2019). Imidazole ketone erastin induces ferroptosis and slows tumor growth in a mouse lymphoma model. *Cell Chem. Biol.* 26, 623–633. doi: 10.1016/j.chembiol.2019.01.008

Zheng, H., Shi, L., Tong, C., Liu, Y., and Hou, M. (2021). circSnx12 is involved in ferroptosis during heart failure by targeting miR-224-5p. *Front. Cardiovasc. Med.* 8:656093. doi: 10.3389/fcvm.2021.656093

Zille, M., Karuppagounder, S. S., Chen, Y., Gough, P. J., Bertin, J., Finger, J., et al. (2017). Neuronal death after hemorrhagic stroke in vitro and in vivo shares features of ferroptosis and necroptosis. *Stroke* 48, 1033–1043. doi: 10.1161/STROKEAHA.116.015609

Zitvogel, L., and Kroemer, G. (2019). Interferon-γ induces cancer cell ferroptosis. *Cell Res.* 29, 692–693. doi: 10.1038/s41422-019-0186-z

Conflict of Interest: The authors declare that the research was conducted in the absence of any commercial or financial relationships that could be construed as a potential conflict of interest.

Publisher's Note: All claims expressed in this article are solely those of the authors and do not necessarily represent those of their affiliated organizations, or those of the publisher, the editors and the reviewers. Any product that may be evaluated in this article, or claim that may be made by its manufacturer, is not guaranteed or endorsed by the publisher.

Copyright © 2021 Huang, Yang, Xiao, Xie, Lin, Zhu, Zhou, Lu and Zheng. This is an open-access article distributed under the terms of the Creative Commons Attribution License (CC BY). The use, distribution or reproduction in other forums is permitted, provided the original author(s) and the copyright owner(s) are credited and that the original publication in this journal is cited, in accordance with accepted academic practice. No use, distribution or reproduction is permitted which does not comply with these terms.

frontiers in Cell and Developmental Biology

ORIGINAL RESEARCH
published: 31 August 2021
doi: 10.3389/fcell.2021.733183

Normothermic *ex vivo* Heart Perfusion Combined With Melatonin Enhances Myocardial Protection in Rat Donation After Circulatory Death Hearts *via* Inhibiting NLRP3 Inflammasome-Mediated Pyroptosis

Jun Lu[1†], Liwei Xu[1†], Zifeng Zeng[1†], Chuqing Xue[1†], Jiale Li[1], Xiong Chen[1], Pengyu Zhou[1], Shaoyan Lin[1], Yuhui Liao[2], Xianjin Du[3*], Ronghua Yang[4*] and Shaoyi Zheng[1*]*

[1] Department of Cardiovascular Surgery, Nanfang Hospital, Southern Medical University, Guangzhou, China, [2] Molecular Diagnosis and Treatment Center for Infectious Diseases, Dermatology Hospital, Southern Medical University, Guangzhou, China, [3] Department of Critical Care Medicine, Renmin Hospital of Wuhan University, Wuhan, China, [4] Department of Burn Surgery, The First People's Hospital of Foshan, Foshan, China

Objective: The adoption of hearts from donation after circulatory death (DCD) is a promising approach for the shortage of suitable organs in heart transplantation. However, DCD hearts suffer from serious ischemia/reperfusion injury (IRI). Recent studies demonstrate that nucleotide-binding oligomerization domain-like receptor family pyrin domain-containing 3 (NLRP3) inflammasome-mediated pyroptosis is a novel target to ameliorate myocardial IRI. Melatonin is shown to inhibit NLRP3 inflammasome-mediated pyroptosis. Therefore, this study is designed to verify the hypothesis that melatonin can protect the heart graft preserved with *ex vivo* heart perfusion (EVHP) against myocardial IRI *via* inhibiting NLRP3 inflammasome-mediated pyroptosis in a rat model of DCD.

Methods: Donor-heart rats were randomly divided into three groups: (1) Control group: non-DCD hearts were harvested from heart-beating rats and immediately preserved with allogenic blood-based perfusate at constant flow for 105 min in the normothermic EVHP system; (2) DCD-vehicle group; and (3) DCD-melatonin group: rats were subjected to the DCD procedure with 25 min of warm ischemia injury and preserved by the normothermic EVHP system for 105 min. Melatonin (200 μmol/L) or vehicle was perfused in the cardioplegia and throughout the whole EVHP period. Cardiac functional assessment was performed every 30 min during EVHP. The level of oxidative stress, inflammatory response, apoptosis, and NLRP3 inflammasome-mediated pyroptosis of heart grafts submitted to EVHP were evaluated.

Results: Twenty five-minute warm ischemia injury resulted in a significant decrease in the developed pressure (DP), dP/dt_{max}, and dP/dt_{min} of left ventricular of the DCD hearts, while the treatment with melatonin significantly increased the DP, dP/dt_{max} of

OPEN ACCESS

Edited by:
Zhi Qi,
Nankai University, China

Reviewed by:
Minxin Wei,
University of Hong Kong, China
Ping Hua,
Sun Yat-sen University, China

***Correspondence:**
Shaoyi Zheng
zhsy@smu.edu.cn
Ronghua Yang
21720091@qq.com
Xianjin Du
duxianjin@whu.edu.cn
Yuhui Liao
liaoyh8@mail.sysu.edu.cn

[†] These authors have contributed equally to this work and share first authorship

Specialty section:
This article was submitted to Cell Death and Survival, a section of the journal Frontiers in Cell and Developmental Biology

Received: 30 June 2021
Accepted: 11 August 2021
Published: 31 August 2021

Citation:
Lu J, Xu L, Zeng Z, Xue C, Li J, Chen X, Zhou P, Lin S, Liao Y, Du X, Yang R and Zheng S (2021) Normothermic ex vivo Heart Perfusion Combined With Melatonin Enhances Myocardial Protection in Rat Donation After Circulatory Death Hearts via Inhibiting NLRP3 Inflammasome-Mediated Pyroptosis. Front. Cell Dev. Biol. 9:733183. doi: 10.3389/fcell.2021.733183

the left ventricular of DCD hearts compared with DCD-vehicle group. Furthermore, warm ischemia injury led to a significant increase in the level of oxidative stress, inflammatory response, apoptosis, and NLRP3 inflammasome-mediated pyroptosis in the hearts preserved with EVHP. However, melatonin added in the cardioplegia and throughout the EVHP period significantly attenuated the level of oxidative stress, inflammatory response, apoptosis, and NLRP3 inflammasome-mediated pyroptosis compared with DCD-vehicle group.

Conclusion: EVHP combined with melatonin post-conditioning attenuates myocardial IRI in DCD hearts by inhibiting NLRP3 inflammasome-mediated pyroptosis, which might expand the donor pool by the adoption of transplantable DCD hearts.

Keywords: donation after circulatory death, normothermic *ex vivo* heart perfusion, melatonin, heart preservation, ischemia/reperfusion injury, pyroptosis

INTRODUCTION

Heart transplantation remains the gold standard for the treatment of patients with refractory heart failure (Burchill and Ross, 2012). Unfortunately, despite the ever-increasing population of heart failure patients, the development of heart transplantation has been limited by the shortage of suitable donor hearts (Christie et al., 2012). Recently, the adoption of hearts from donation after circulatory death (DCD) has been considered as a promising approach to expanding the donor pool (Smith et al., 2019). DCD heart transplantation has the potential to significantly increase transplant activity by 30% in the United States (Jawitz et al., 2020) and 48% in the United Kingdom (Messer et al., 2020), and will result in a substantial decrease in waiting list mortality. Furthermore, DCD heart transplantation provides comparable 30-day or 1-year postoperative survival in comparison with traditional donation after brain death (DBD) heart transplantation (Messer et al., 2017, 2020). Nevertheless, DCD hearts suffer from more serious ischemia/reperfusion injury (IRI) due to an obligatory warm ischemia time (from when the systolic blood pressure is lower than 50 mmHg after the withdrawal of life-sustaining therapy to reperfusion or cardioplegia) (Dhital et al., 2017; Niederberger et al., 2019).

Recent studies have demonstrated that nucleotide-binding oligomerization domain-like receptor pyrin domain-containing 3 (NLRP3) inflammasome-mediated pyroptosis can play an indispensable role in the myocardial IRI (Dai et al., 2020; Wei et al., 2020; Xu L.J. et al., 2020). Pyroptosis is a recently identified type of programmed cell death and is characterized as a NLRP3-caspase-1-dependent response during myocardial IRI (Wu et al., 2020). NLRP3, one of the best characterized intracellular pattern recognition receptors, can be activated by the generation of reactive oxygen species (ROS) shortly after reperfusion. NLRP3 can bind to apoptosis-associated specklike protein containing a caspase recruitment domain (ASC) and finally form an NLRP3 complex (Geldhoff et al., 2013; Cero et al., 2015; Martínez et al., 2015), which will lead to the activation of caspase-1 and the production of interleukin-1β (IL-1β) and IL-18, and the recruitment of pro-inflammatory response in the progression of myocardial IRI (Bracey et al., 2015). Moreover, active caspase-1 can result in the cleavage of gasdermin D (GSDMD), a member of the gasdermin family, thereby inducing pyroptosis (Wang et al., 2020). Therefore, the interference of NLRP3 inflammasome-mediated pyroptosis might be a promising target for alleviating myocardial IRI of DCD hearts.

Static cold storage has been regarded as a traditional and reliable heart preservation strategy, which is simple, cheap, and able to preserve standard-criteria donor hearts for 4–6 h with acceptable post-transplant outcomes (Lund et al., 2017). However, static cold storage may not be the optimal preservation method for DCD hearts since the energy-depleted DCD hearts can poorly tolerate additional cold ischemia (Iyer et al., 2015). Recently, normothermic *ex vivo* heart perfusion (EVHP) is introduced as a promising preservation strategy for DCD hearts. Normothermic EVHP can perfuse donated hearts with warm, oxygenated, and nutrient-enriched blood-based perfusate in a semi-physiologic state during the preservation period (Zhou et al., 2020). Therefore, compared with static cold storage, normothermic EVHP can alleviate myocardial IRI for DCD hearts, prolong preservation time, allow for a real-time assessment of contractile function for DCD hearts, and offer a unique platform to repair DCD hearts *via* directly delivering post-conditioning agents into machine perfusion circuit (Beuth et al., 2019; Xu J. et al., 2020).

Melatonin (N-acetyl-5-methoxytryptamine), which is mainly synthesized by the pineal gland in mammals, is regarded as an anti-oxidant (Manchester et al., 2015), anti-inflammatory (Agil et al., 2013), and anti-apoptotic (Li et al., 2014) molecule. Notably, the pharmacological actions of melatonin are closely related to the inhibition of NLRP3 inflammasome-mediated pyroptosis. One recent study conducted by Su et al. (2021) showed that melatonin alleviated lipopolysaccharide-induced myocardial injury by inhibiting NLRP3 inflammasome-mediated pyroptosis. The administration of melatonin prevented endothelial cell pyroptosis *via* MEG3/miR-223/NLRP3 axis in atherosclerosis (Zhang et al., 2018). What's more, melatonin can exert neuroprotective effects by inhibiting neuronal pyroptosis in the streptozotocin-induced diabetic mice (Che et al., 2020). However, it remains unclear whether normothermic EVHP combined with melatonin can ameliorate myocardial IRI for

DCD hearts *via* inhibiting NLRP3 inflammasome-mediated pyroptosis. Additionally, until now, no study investigated the cardioprotective effect of the normothermic EVHP combined with melatonin post-conditioning in the preservation of donor hearts.

Therefore, in the present study, we explored the cardioprotective potential of melatonin post-conditioning during our well-established normothermic EVHP protocol in a rat model of DCD. We hypothesized that the combination of normothermic EVHP and melatonin post-conditioning could be a novel and promising donor heart preservation strategy, which could ameliorate myocardial IRI and improve cardiac function of DCD hearts, thereby increasing the number of transplantable hearts in heart transplantation.

MATERIALS AND METHODS

Animals

Male Sprague-Dawley rats (Charles River Laboratories, Beijing, China) used in this study received care in compliance with the Guide for the Care and Use of Laboratory Animals (National Institutes of Health Publication No. 85-23, revised 1996). All animal experiments were reviewed and approved by the Ethical Committee of the Laboratory Animal Research Center of Southern Medical University Nanfang Hospital. The rats were housed in temperature-controlled (22 ± 2°C) rooms with a 12-h light-dark cycle, given food and sterilized water, and acclimatized for 1 week.

Experiment Design

Twenty four male Sprague-Dawley rats (200–300 g; 8 to 12-week-old) were introduced as donor-heart rats. Another 24 male Sprague-Dawley rats (300–400 g; 12 to 15-week-old) were regarded as blood donors for blood-based perfusate of the normothermic EVHP system. All donor hearts were harvested and preserved by the normothermic EVHP system. Functional assessment of hearts was performed during the EVHP period. Heart tissue was collected at the end of perfusion for the evaluation of the level of oxidative stress, apoptosis, inflammation, and NLRP3 inflammasome-mediated pyroptosis (**Figure 1**).

Donor-heart rats were randomly divided into three groups: (1) control group: eight non-DCD hearts were harvested from heart-beating rats and immediately preserved by the normothermic EVHP system for 105 min. During harvesting the donor heart, the heart was perfused with 20 ml cold Custodiol (Dr. Franz Köhler, Chemie GmbH, Bensheim, Germany) cardioplegic solution containing 116 μl ethanal. Before initiating normothermic EVHP, 87 μl ethanal was added into 15 ml blood-based perfusate; (2) DCD-vehicle group; and (3) DCD-melatonin group: 8 rats were subjected to the DCD procedure with 25 min of warm ischemia injury and preserved by the normothermic EVHP system for 105 min. During harvesting the donor heart, the heart was perfused with 20 ml cold Custodiol cardioplegic solution containing 116 μl ethanal or melatonin (34.44 μmol/ml, dissolved in ethanol). Before initiating normothermic EVHP, 87 μl ethanal or melatonin (34.44 μmol/ml, dissolved in ethanol) was added into 15 ml blood-based perfusate to make the concentration of melatonin in the perfusate of 200 μM.

Operative Procedure

Anesthesia

Sprague-Dawley rats were anesthetized with pentobarbital sodium (60 mg/kg, intraperitoneally). Pedal reflex was performed to determine adequate anesthetic depth before experiments. The rats were placed on a heating pad to maintain the body temperature.

Harvest of Blood From the Donor-Blood Rat

An 18 G, 2-inch I.V. catheter was cannulated into the abdominal artery. A 20 ml syringe containing 1,250 IU heparin was connected to the catheter to withdraw 9 ml blood. The blood-based perfusate consisted of 9 ml blood from the donor-blood rat, 6 ml modified Krebs–Henseleit solution (10 mM glucose, 117 mM NaCl, 4.5 mM KCl, 25 mM $NaHCO_3$, 1.2 mM NaH_2PO_4, 2 mM $CaCl_2$, 0.512 mM $MgCl_2$), mannitol (25 g/L), methylprednisolone sodium succinate (500 mg/L; Pfizer; Belgium; Switzerland), and insulin (160 IU/L; Novo Nordisk; Denmark) (see supplementary material). The blood-based perfusate was slowly added into the perfusion circuit to be oxygenated for 15 min (PaO_2 at 150–250 mmHg).

Procurement of Heart From the Donor-Heart Rat

The rat was intubated with a 16 G, 2-inch I.V. catheter after tracheotomy and mechanically ventilated. A 22 G, 1-inch I.V. catheter was cannulated into the right carotid artery for injection of heparin, real-time blood pressure monitoring, and delivery of Custodiol cardioplegic solution. The injection of heparin (2,000 IU/kg body weight) through the right carotid artery was performed to heparinize the donor-heart rat before the induction of circulatory death.

Rats in the DCD-vehicle and DCD-melatonin groups were subjected to the following DCD procedure. Briefly, the rat was extubated and the trachea was clamped by a mosquito forceps to induce circulatory death. Circulatory death could be declared when systolic pressure below 30 mmHg or asystole was observed (Kearns et al., 2017; Aceros et al., 2020). At the end of the 25-min warm ischemic time (WIT, equivalent to the hands-off period), we performed the sternotomy and clamped the aortic arch between the brachiocephalic trunk and left common carotid artery. After cutting the inferior vena cava and opening the left atrium, the DCD heart was immersed with ice and perfused with 20 ml cold Custodiol cardioplegic solution containing 116 μl ethanal (DCD-vehicle group) or melatonin (DCD-melatonin group) at a constant pressure *via* the right carotid artery. The aorta distal to the left subclavian artery and pulmonary artery were cut, respectively. Subsequently, the arrested heart was excised and cannulated with a homemade 14 G aortic catheter. The rats in the control group were treated similarly, but not submitted to 25-min WIT.

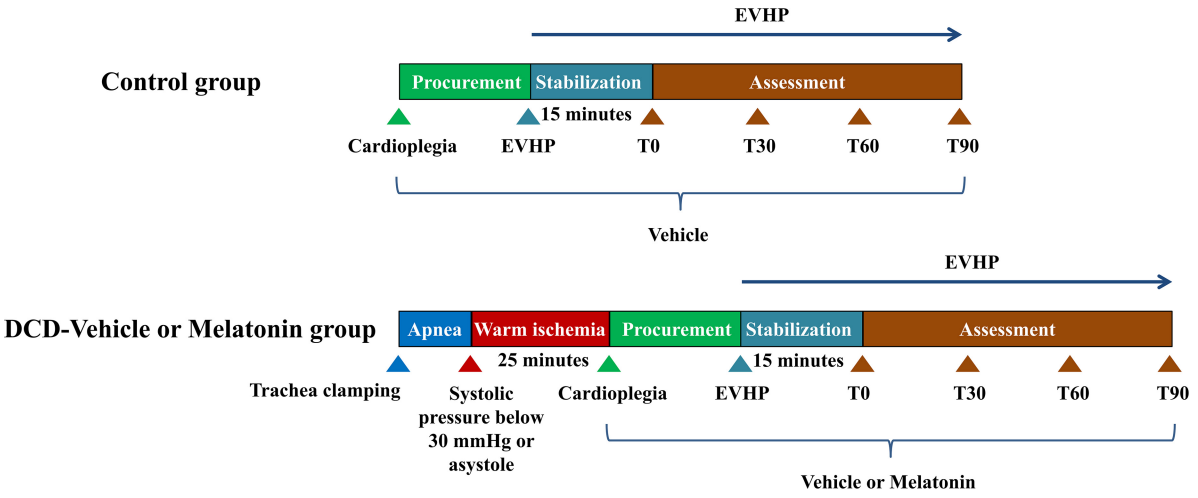

FIGURE 1 | Study protocol of *ex vivo* heart perfusion combined with melatonin in the DCD heart preservation. DCD, donation after circulatory death; EVHP, *ex vivo* heart perfusion.

The Operation of EVHP

The normothermic ESHP system (**Figure 2A**) consisted of a micro-peristaltic pump (BT101L; Lead Fluid; China; **Figure 2B**), an oxygenator (Micro-1 Rat Oxygenator; Dongguan Kewei; China; **Figure 2C**), 16# Tygon tubing, a reservoir, an infusion syringe pump (Perfusor-space; B. Braun; Germany; **Figure 2D**) for the administration of epinephrine, and a home-made water-bath box (**Figure 2E**) containing water, heater (**Figure 2F**), stirrer (**Figure 2G**), temperature-controlling switch (**Figure 2H**), and aortic cannula (**Figure 2I**). The oxygenator was gassed with a humidified gas mixture containing 95% O_2/5% CO_2.

The donor heart was connected to the EVHP system *via* the aortic cannula (**Figures 2J,K**). The reservoir was partially immersed in the water of the water-bath box and the isolated heart was placed below the horizontal plane of the water. The membrane oxygenator was wrapped by a thermal insulation bag and the temperature of water in the box was set at 41–42 °C to maintain the temperature of the inflow and isolated heart at 35–37°C (**Figure 2K**). The normothermic EVHP started with the perfusion flow rate of 2 ml/min, and slowly reached the target perfusion flow rate (1 ml/min/100 g body weight) within 10 min. The administration of epinephrine (4.8×10^{-5} mg/h/kg body weight) was performed *via* an infusion syringe pump throughout the perfusion after a 15-min stabilization period. During the normothermic EVHP, PaO_2 was maintained at 150–250 mmHg and the temperature of the isolated heart at 35–37°C. 20 μl 50% glucose solution and 40 μl 5% sodium bicarbonate solution were added into the perfusate every 15 min.

Cardiac Functional Assessment During EVHP

The latex balloon connected to a pressure sensor was inserted into the left ventricle through the left atrium at the end of the 15-min stabilization period. The intraventricular pressure measurement of the donor heart was performed by slowly filling the balloon with 0.15 ml saline at the beginning of the assessment phase (T0) and then every 30 min (T30, T60, and T90). The cardiac functional parameters of the donor heart during EVHP included developed pressure (DP, systolic blood pressure minus diastolic blood pressure), heart rate (HR), dP/dt_{max} (maximum rate of rise of left ventricular pressure), and dP/dt_{min} (maximum rate of pressure decline).

Sample Collection

At the end of 105-min EVHP, three ventricular slices (1- to 2-mm thick) were collected serially along the long axis. The first piece of myocardial tissue from the apex was applied for western blotting, the second one for histologic and immunohistochemical analysis, the third one for analyzing superoxide dismutase (SOD) activity, and the level of malonaldehyde (MDA).

Oxidative Stress

The SOD activity and the level of MDA in the heart tissue of donor heart were determined by colorimetric 5,5′-dithio-bis-(2-nitrobenzoic acid)-based method and thiobarbituric acid reactive substance assay, respectively (A001-3-2 and A003-1-2, Nanjing Jiancheng Bioengineering Institute, China). The analysis was performed using an automatic microplate reader (CLARIOstar, BMG LAGTECH, Germany). The expression of 4-hydroxynonenal (HNE), an indicator of oxidative stress, was determined by immunohistochemical analysis as described below.

Inflammatory Response

The expression of interleukin-6 (IL-6), tumor necrosis factor-α (TNF-α), and nuclear factor kappa-B p65 (NF-κB p65) were measured by immunohistochemistry as described below.

Immunohistochemistry

Myocardial tissue slices were fixed in paraformaldehyde solution (4%), embedded in paraffin, and cut into 4-μm-thick sections. The immunoreactivity to IL-6 (1:500, Abcam, ab9324, United States), TNF-α (1:200, Abcam, ab109322,

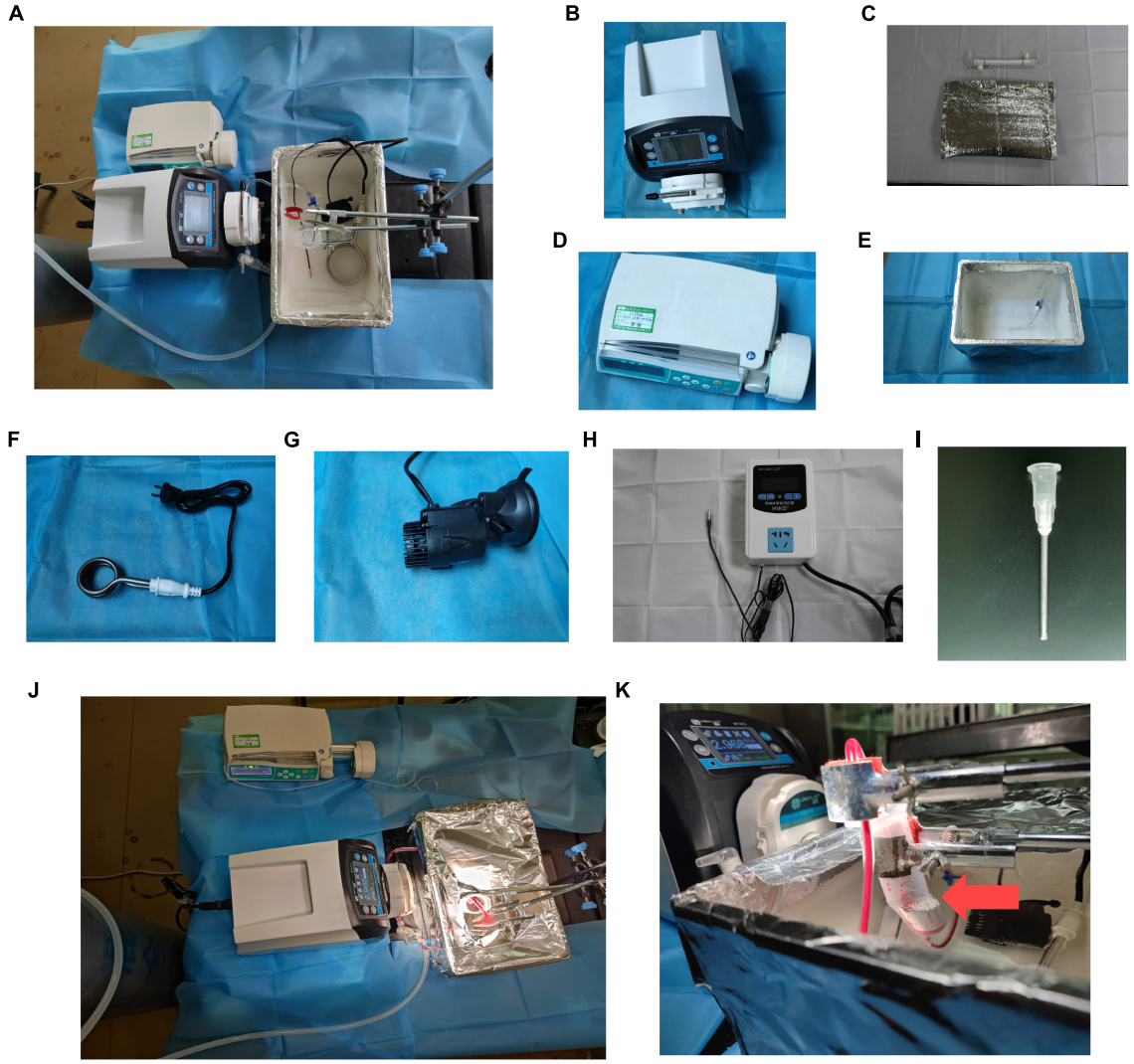

FIGURE 2 | *Ex vivo* heart perfusion system. **(A)** Schematic figure of the EVHP system; **(B)** micro-peristaltic pump; **(C)** oxygenator; **(D)** infusion syringe pump; **(E)** water-bath box; **(F)** heater; **(G)** stirrer; **(H)** temperature-controlling switch; **(I)** aortic catheter; **(J)** working EVHP system; and **(K)** beating heart (red arrow). EVHP, *ex vivo* heart perfusion.

United States), NF-κB p65 (1:500, Proteintech, 66535, China), HNE (1:1,000, Abcam, ab46545, United States) was assessed. The antigen–antibody reaction was visualized by diaminobenzidine reaction. The fields from each slice were randomly selected and recorded under a conventional light microscope in a blinded manner. Image analysis was performed using Image-Pro Plus software (Media Cybernetics, United States). The evaluation was performed in four random and non-overlapping fields of the heart tissue, and the average value was calculated for each animal. The expression of IL-6, TNF-α, NF-κB p65, and HNE was determined by counting integrated optical density (IOD).

Apoptosis

Terminal deoxynucleotidyl transferase dUTP nick end labeling (TUNEL) staining was performed to detect DNA-strand breaks of the donor hearts as previously described (Zhou et al., 2021). The number of TUNEL-positive cells was counted under a fluorescence microscope and the frequency of apoptosis in the donor heart was expressed as the ratio of 4′,6-diamidino-2-phenylindole (DAPI)-TUNEL double-labeled nuclei to the total number of nuclei stained with DAPI.

Western Blotting

Myocardial protein expression of donor heart was assessed by western blotting as previously described (Korkmaz-Icöz et al., 2020). The expression of cleaved caspase-3 (1:1,000 dilution, 9664, Cell Signaling Technology (Shanghai) Biological Reagents Company Limited, China), NLRP3 [1:1,000 dilution, 15101, Cell Signaling Technology (Shanghai) Biological Reagents Company Limited, China], ASC [1:1,000 dilution, 67824, Cell Signaling Technology (Shanghai)

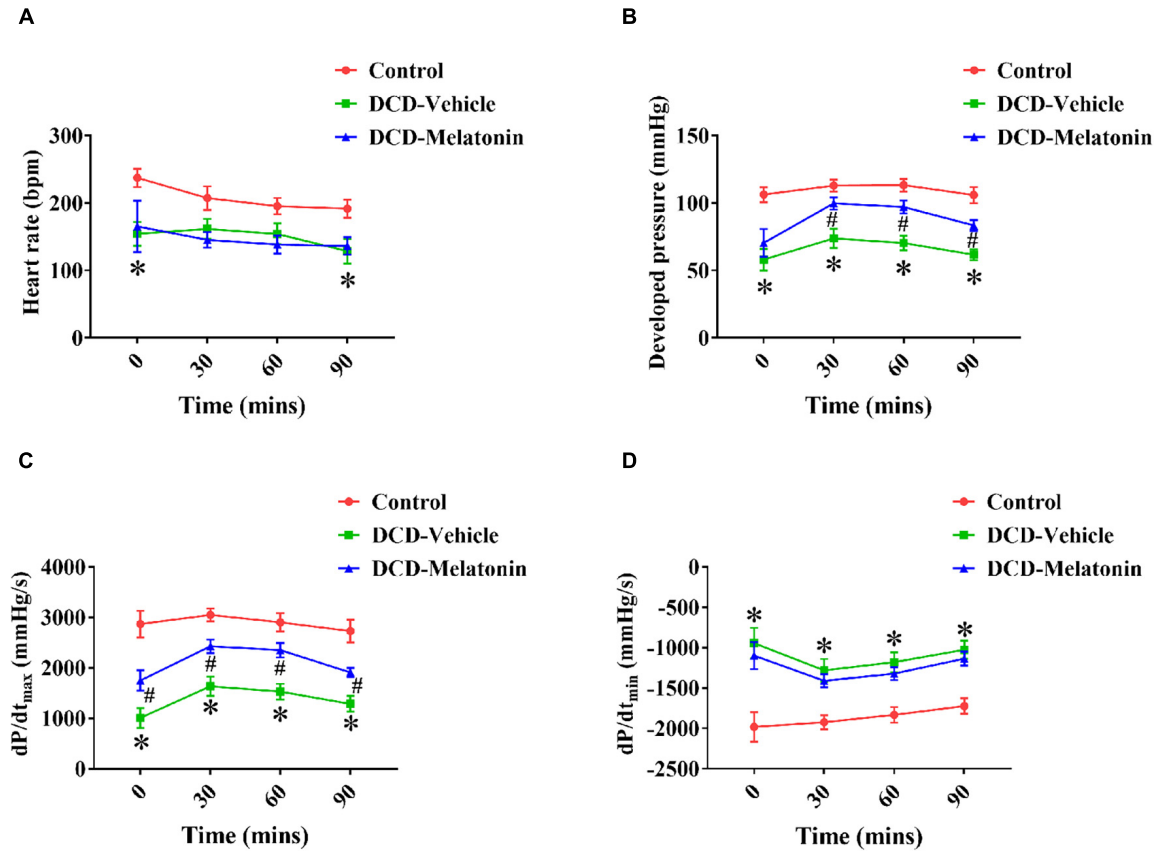

FIGURE 3 | Cardiac functional assessment of the DCD heart during EVHP. **(A)** Heart rate; **(B)** developed pressure; **(C)** dP/dt_{max}; and **(D)** dP/dt_{min}. Data represent mean ± standard error of the mean. $n = 8$ for each group. DCD, donation after circulatory death; EVHP, *ex vivo* heart perfusion; dP/dt_{max}, maximum rate of rise of left ventricular pressure; dP/dt_{min}, maximum rate of pressure decline. $^{*}p < 0.05$ vs. control; $^{\#}p < 0.05$ vs. DCD-vehicle.

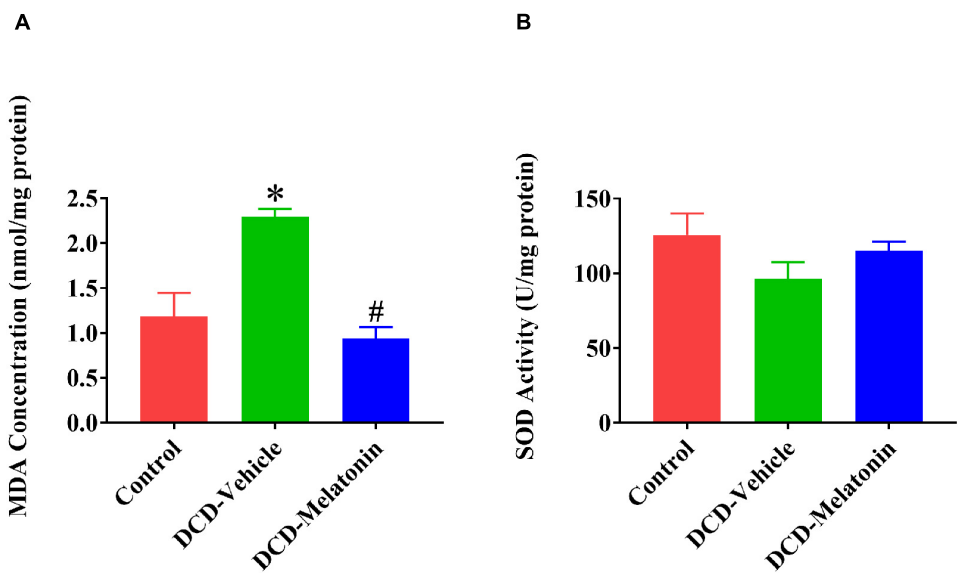

FIGURE 4 | Tissue content of MDA and SOD activity in the DCD heart preserved with EVHP. **(A)** Tissue content of MDA; and **(B)** SOD activity. Data represent mean ± standard error of the mean. $n = 5$ for each group. DCD, donation after circulatory death; EVHP, *ex vivo* heart perfusion; MDA, malonaldehyde; and SOD, superoxide dismutase. $^{*}p < 0.05$ vs. control; $^{\#}p < 0.05$ vs. DCD-vehicle.

Biological Reagents Company Limited, China], Caspase-1 (1:1,000 dilution, ab179515, Abcam, United States), IL-1β (1:1,000 dilution, ab9722, Abcam, United States), IL-18 (1:1,000 dilution, ab207323, Abcam, United States), and cleaved GSDMD [1:1,000 dilution, 10137, Cell Signaling Technology (Shanghai) Biological Reagents Company Limited, China] were evaluated.

Statistical Analysis

The results were expressed as mean ± standard error of the mean (SEM). GraphPad Prism 8.3 software (GraphPad Sofware, Inc., San Diego, CA, United States) was used to perform statistical analysis. Shapiro-Wilk test was performed to test the normality of data before statistical tests were applied. One-way ANOVA followed by Tukey's *post hoc*-test was performed for multiple comparisons between three experimental groups. If the data failed the normality test, the non-parametric Kruskal–Wallis test followed by Dunn's *post hoc*-test was used. Intraventricular pressure measurement recordings among control, DCD-vehicle, and DCD-melatonin groups were compared by two-way ANOVA according to different timepoints. A value of $p < 0.05$ was considered statistically significant.

RESULTS

Ex vivo Heart Perfusion Combined With Melatonin Post-conditioning Protects Against Cardiac Function Impairment Caused by Warm Ischemia Injury in the DCD Hearts

A WIT of 25 min results in a significant decrease in HR (T0 and T9, **Figure 3A**), DP (from T0 to T90, **Figure 3B**), dP/dt_{max} (from T0 to T90, **Figure 3C**), and dP/dt_{min} (from T0 to T90, **Figure 3D**) of DCD hearts preserved with EVHP in the DCD-vehicle group

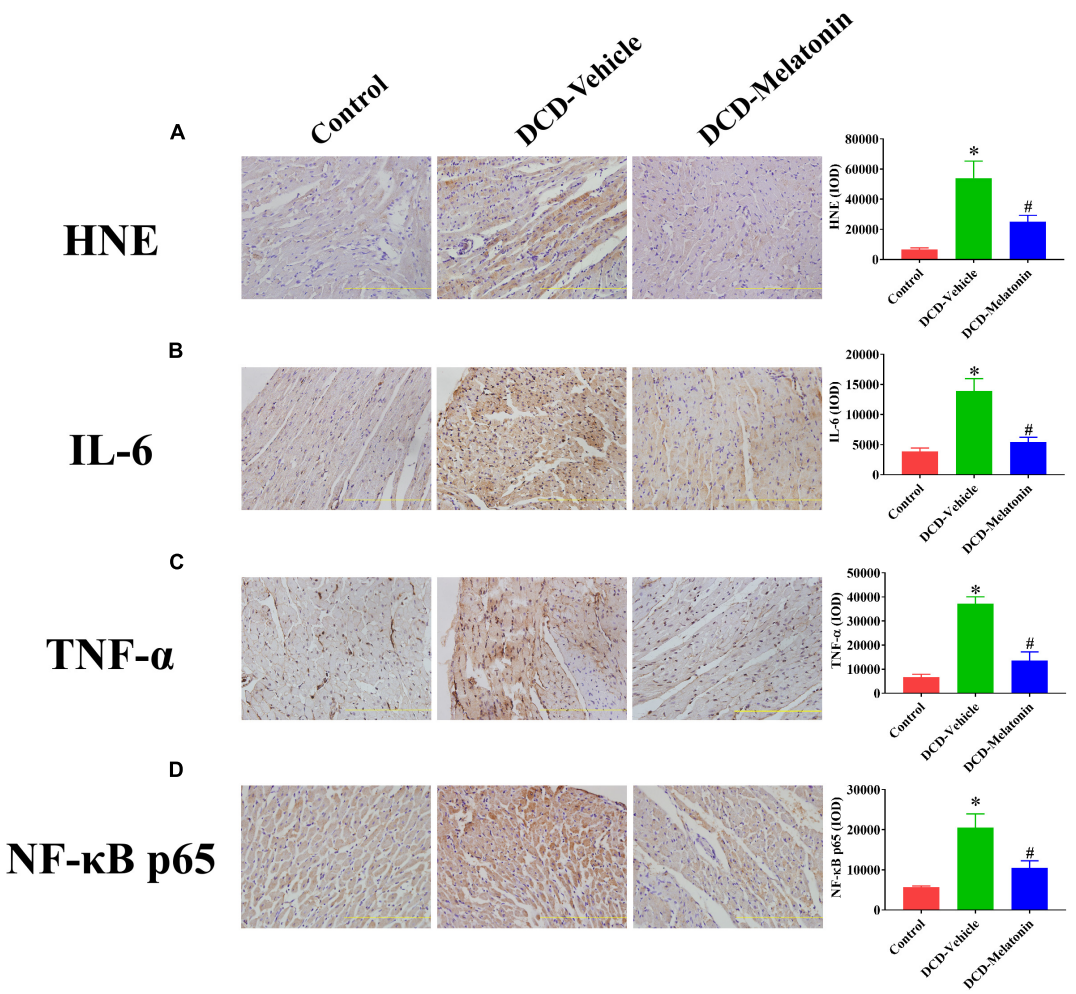

FIGURE 5 | The expression of HNE, IL-6, TNF-α, and NF-κB p65 in the DCD heart preserved with EVHP. Representative photomicrographs and quantitative analysis of immunohistochemistry for **(A)** HNE, **(B)** IL-6, **(C)** TNF-α, and **(D)** NF-κB p65 in the DCD heart. Data represent mean ± standard error of the mean. $n = 6$–8 for each group. DCD, donation after circulatory death; EVHP, *ex vivo* heart perfusion; HNE, 4-hydroxynonenal; IL-6, interleukin-6; IOD, integrated optical density; TNF-α, tumor necrosis factor-α; NF-κB, nuclear factor kappa-B. $^{*}p < 0.05$ vs. Control; $^{\#}p < 0.05$ vs. DCD-vehicle.

compared with the control group. Furthermore, melatonin post-conditioning leads to a significant increase in DP (from T30 to T90, **Figure 3B**) and dP/dt_{max} (from T0 to T90, **Figure 3C**) of DCD hearts preserved with EVHP in DCD-melatonin group compared with DCD-vehicle group.

Ex vivo Heart Perfusion Combined With Melatonin Post-conditioning Reduces Oxidative Stress in the DCD Hearts

Malonaldehyde is introduced as a reliable marker of oxidative stress since it is the end product of major reactions which can lead to significant oxidation of polyunsaturated fatty acids in cellular membranes (Reiter et al., 2009). A WIT of 25 min can significantly increase the level of MDA in the DCD hearts preserved with EVHP in the DCD-vehicle group compared with the control group. Treatment with melatonin at 200 μmol/L during cardioplegia and through the EVHP period can significantly reduce the level of MDA in the DCD hearts in the DCD-melatonin group compared with the DCD-vehicle group (**Figure 4A**). SOD is an enzyme that can catalyze the dismutation of the superoxide (O_2^-) radical into ordinary molecular oxygen (O_2), thereby exhibiting a great anti-oxidant effect (Hayyan et al., 2016). As shown in **Figure 4B**, the SOD activity of the heart graft in the control group and DCD-melatonin group is higher than that in the DCD-vehicle group without reaching a significant difference. The expression of HNE, an indicator of oxidative stress, among three groups was determined by immunohistochemical analysis. A WIT of 25 min leads to a significant increase in the expression of HNE in the DCD-vehicle group compared with the control group, whereas the treatment with melatonin can significantly down-regulate the expression of HNE in the DCD hearts preserved with EVHP (**Figure 5A**).

Collectively, 25-min warm ischemia injury increases the level of oxidative stress in the heart graft preserved with EVHP, while the addition with melatonin at 200 μmol/L during cardioplegia and EVHP period attenuates the level of oxidative stress in the DCD heart.

Ex vivo Heart Perfusion Combined With Melatonin Post-conditioning Attenuates Inflammation in the DCD Hearts

The expression of IL-6, TNF-α, and NF-κB in heart tissue was measured by immunohistochemistry to evaluate the inflammatory response in the myocardium. As shown in **Figure 5**, a WIT of 25 min can significantly up-regulate the levels of IL-6 (**Figure 5B**), TNF-α (**Figure 5C**), and NF-κB (**Figure 5D**) in the DCD heart submitted to EVHP, while the treatment of melatonin can lead to a significant decrease in the expression of IL-6, TNF-α, and NF-κB in the DCD heart.

Ex vivo Heart Perfusion Combined With Melatonin Post-conditioning Ameliorates Apoptosis in the DCD Hearts

After normothermic EVHP, a significantly increased number of TUNEL-positive nuclei in the heart graft can be observed in the DCD-vehicle group compared with the control group. Besides, treatment with melatonin significantly decreases DNA strand breaks and the expression of cleaved caspase-3 in the

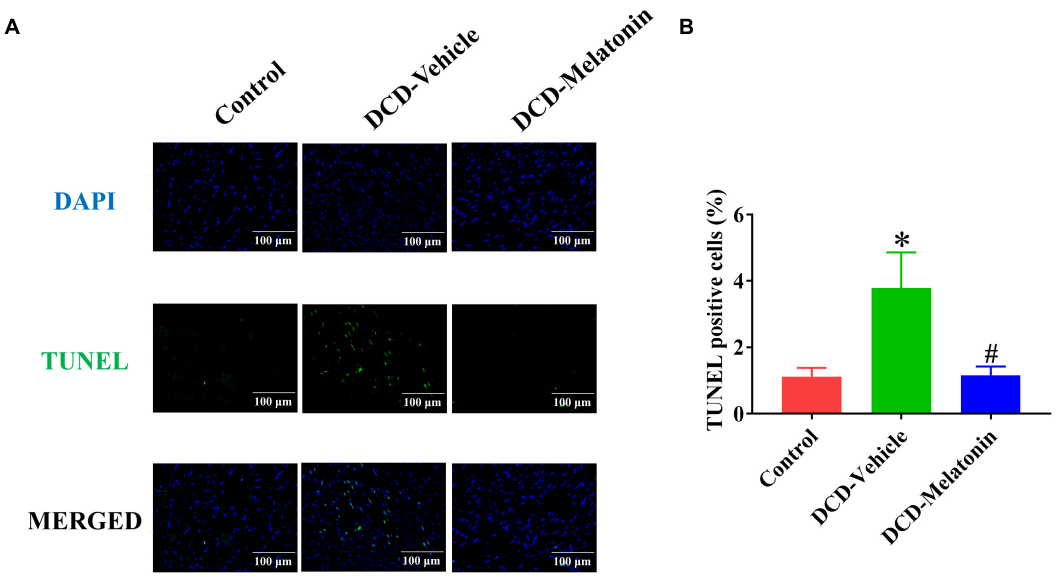

FIGURE 6 | Apoptosis evaluation of the DCD heart submitted to EVHP. **(A)** Representative photomicrographs of myocardial tissue stained with DAPI (blue), nuclei with fragmented DNA shown by TUNEL staining, and merged image (magnification of 40; scale length: 100 μm); and **(B)** quantification of TUNEL-positive cells (as a percentage). Data represent mean ± standard error of the mean. $n = 8$ for each group. DAPI, 4′,6-diamino-2-phenylindole (DAPI, blue); DCD, donation after circulatory death; EVHP, *ex vivo* heart perfusion; TUNEL, terminal deoxynucleotidyl transferase-mediated dUTP nick end-labeling. $^*p < 0.05$ vs. control; $^\#p < 0.05$ vs. DCD-vehicle.

myocardium of the DCD hearts preserved with EVHP compared with DCD-vehicle group (**Figures 6**, **7**).

Ex vivo Heart Perfusion Combined With Melatonin Post-conditioning Inhibits NLRP3 Inflammasome-Mediated Pyroptosis in the DCD Hearts

To investigate whether NLRP3 inflammasome-mediated pyroptosis is involved in myocardial IRI for the DCD heart, and the relationship between NLRP3 inflammasome-mediated pyroptosis and melatonin treatment in the DCD heart, the expression of NLRP3, ASC, cleaved caspase-1, IL-1β, IL-18, and cleaved GSDMD is evaluated by western blotting analysis.

As shown in **Figure 7**, the protein level of NLRP3, ASC, IL-1β, IL-18, and cleaved GSDMD in the heart submitted to EVHP is significantly higher in the DCD-vehicle group compared with the control group, while the treatment of melatonin can attenuate NLRP3 inflammasome-mediated pyroptosis (as evidenced by the significantly increased expression of NLRP3, ASC, cleaved caspase-1, IL-1β, IL-18, and cleaved GSDMD) in the DCD heart preserved with EVHP.

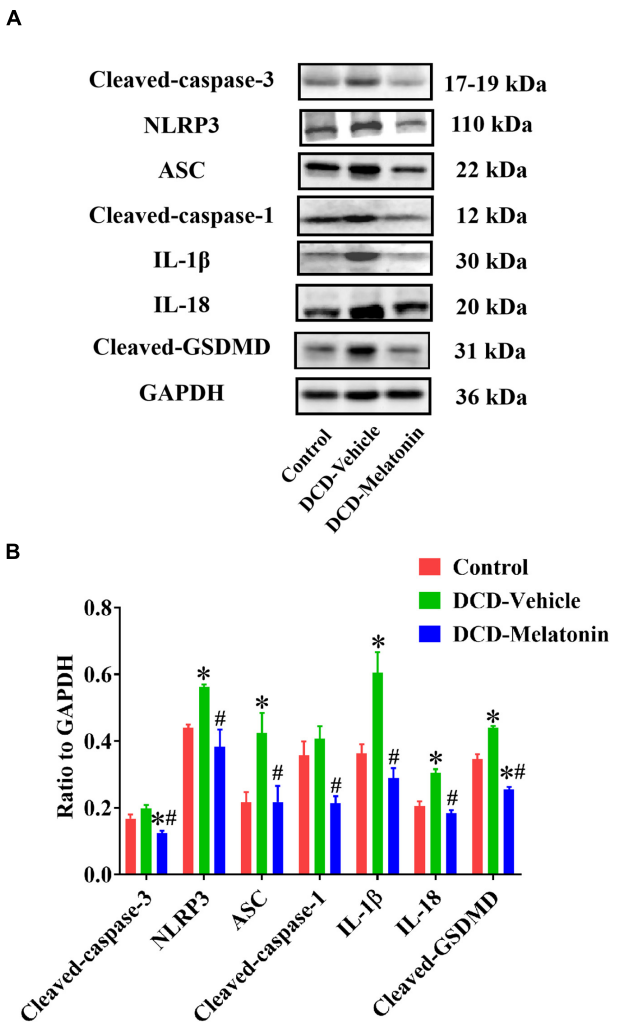

FIGURE 7 | Representative Western blotting and quantitative analysis of the effect of melatonin treatment on apoptosis and NLRP3 inflammasome-mediated pyroptosis in the hearts preserved with EVHP. **(A)** Representative protein band densities of cleaved caspase-3, NLRP3, ASC, cleaved caspase-1, IL-1β, IL-18, and cleaved GSDMD; and **(B)** quantitative analysis of protein expression in the DCD hearts. Data represent mean ± standard error of the mean. $n = 4$ for each group. DCD, donation after circulatory death; EVHP, *ex vivo* heart perfusion. $^{*}p < 0.05$ vs. Control; $^{\#}p < 0.05$ vs. DCD-vehicle.

DISCUSSION

Currently, heart transplantation with DCD hearts has received enormous attention over the past 15 years (Osaki et al., 2010; Manara et al., 2012) and is emerging as a promising strategy to expand the donor pool (Longnus et al., 2014). Nevertheless, the use of DCD hearts has been hampered by the severe IRI due to the inherent warm ischemia injury (Citerio et al., 2016; Stehlik et al., 2018; Smith et al., 2019). Normothermic EVHP is becoming a novel and ground-breaking strategy for DCD heart preservation in the clinical setting. Unlike static cold storage, the traditional organ preservation method, normothermic EVHP can preserve the donated heart in a perfused, semi-physiologic state (Van Raemdonck et al., 2013), thereby reducing myocardial IRI, allowing for a thorough evaluation for the viability of donor heart (Xu J. et al., 2020), and more excitingly, facilitating organ reconditioning during perfusion with pharmacological, gene, and stem cell therapy (Weissenbacher and Vrakas, 2019). Therefore, the combination of normothermic EVHP with some novel post-conditioning pharmacological agents could hopefully convert DCD hearts into transplantable donor hearts.

Previous studies proved the cardioprotective effect of melatonin, an important circadian molecule, which was either added into preservation solution in form of cold static storage (Rudd and Dobson, 2011) or administered for the donors (Lan et al., 2019) or recipients (Jung et al., 2004) in the heart transplantation. However, whether normothermic EVHP with the addition of melatonin can become a novel preservation strategy for the DCD heart remains unknown. The current study is the first time to demonstrate that melatonin has potent cardioprotective effects for the DCD heart when used throughout cardioplegia and EVHP period. Our results indicate that 25-min warm ischemia injury results in a significant decrease in cardiac functional parameters, and an increase in the level of oxidative stress, inflammatory response, apoptosis, and NLRP3 inflammasome-mediated pyroptosis of DCD hearts. However, the treatment with melatonin leads to a significant increase in cardiac functional parameters and attenuates myocardial IRI (as evidenced by the level of oxidative stress, inflammatory response, and apoptosis), and NLRP3 inflammasome-mediated pyroptosis of DCD hearts submitted to our well-established EVHP protocol (**Figure 8**).

Recently, an increasing number of studies have demonstrated that NLRP3 inflammasome-mediated pyroptosis is emerging as a novel target to attenuate myocardial IRI (Ding et al., 2020; Nie et al., 2021). Inhibiting microRNA-29a can alleviate

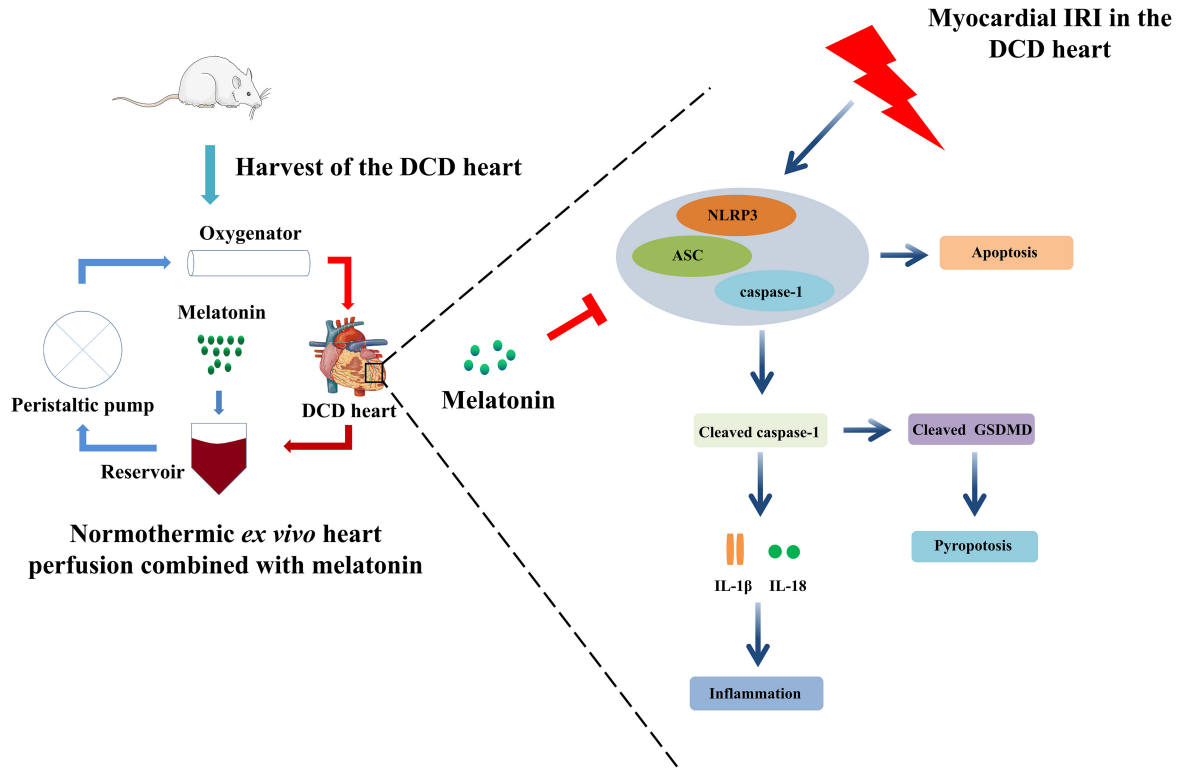

FIGURE 8 | *Ex vivo* heart perfusion combined with melatonin post-conditioning exerts a profound cardioprotective effect against myocardial IRI in the DCD heart, and this protection appears to be due to the inhibition of NLRP3 inflammasome-mediated pyroptosis. IRI, ischemia/reperfusion injury; DCD, donation after circulatory death.

myocardial IRI in mice by targeting SIRT1 and suppressing oxidative stress and the NLRP3-mediated pyroptosis pathway (Ding et al., 2020). Furthermore, hydrogen gas inhalation can attenuate myocardial IRI in rats by the inhibition of oxidative stress and NLRP3-mediated pyroptosis (Nie et al., 2021). Notably, Quader et al. (2020) reported that the DCD procedure resulted in the activation of the NLRP3 inflammasome, which contributed to myocardial damage and dysfunction, while NLRP3 inflammasome inhibition ameliorated myocardial warm ischemia injury and improved DCD heart function. In line with the above findings, our study shows 25-min warm ischemia in the DCD hearts impairs the cardiac function of hearts during 105-min EVHP and leads to a significant increase in the level of oxidative stress, inflammatory response, apoptosis, and NLRP3 inflammasome-mediated pyroptosis. Emerging studies have demonstrated that melatonin can effectively inhibit NLRP3 inflammasome-mediated pyroptosis. In agreement with these researches, the present study shows the mechanism of melatonin's cardioprotection against myocardial IRI in DCD hearts preserved with EVHP is partly due to the inhibition of NLRP3 inflammasome-mediated pyroptosis.

In our study, no difference was found in left ventricular relaxation, as evidenced by dP/dt_{min}, between DCD-melatonin and DCD-vehicle groups. Nevertheless, this may be due to the optimized protocol of DCD heart procurement and normothermic EVHP which can ensure cardioprotection from myocardial IRI. Besides, the current normothermic EVHP is limited to 105 min and a longer duration of reperfusion may be necessary to present better cardiac functional recovery in the melatonin-treated DCD hearts.

Apoptosis, another form of programmed cell death, can be characterized as cell shrinkage, nuclear fragmentation, and chromosomal DNA fragmentation. Furthermore, the inhibition of NLRP3 inflammasome can suppress the frequency of cell apoptosis (Wu et al., 2014; Li et al., 2015; Zhao et al., 2015). The current study reveals that the activation of NLRP3 inflammasome-mediated pyroptosis and increased apoptotic rate can contribute to myocardial IRI in the DCD heart, which can be inhibited by the treatment of melatonin. Therefore, we infer that normothermic EVHP combined with melatonin post-conditioning may attenuate myocardial apoptosis *via* inhibiting NLRP3 inflammasome-mediated pyroptosis.

There are several limitations to our present studies. Firstly, the duration of the current normothermic EVHP is limited to 105 min and should be prolonged in future studies to clearly present better cardiac functional recovery in the melatonin-treated DCD hearts. Secondly, a heart transplantation model should be introduced in the future to demonstrate the cardioprotective effect of normothermic EVHP combined with melatonin on the post-transplant donor heart.

Thirdly, the concentration of melatonin in the cardioplegic solution and perfusate may not be optimal although previous studies have demonstrated that melatonin, given either acutely or chronically at pharmacological doses, has virtually no toxicity (Jahnke et al., 1999; Seabra et al., 2000). Therefore, the dose-effect relationship of melatonin in the DCD hearts preserved with EVHP should be investigated in the future. In parallel, future research is necessary to confirm the cardioprotective effect of normothermic EVHP combined with melatonin in a porcine model to obtain more robust evidence for an efficient clinical translation. Finally, the precise mechanism for inhibition of the NLRP3 inflammasome-mediated pyroptosis by melatonin needs to be further studied.

CONCLUSION

Taken together, the present study reveals that normothermic EVHP combined with melatonin can attenuate myocardial IRI in the DCD hearts *via* inhibiting NLRP3 inflammasome-mediated pyroptosis. Therefore, the combination of normothermic EVHP and melatonin may facilitate the expansion of the DCD protocol for donor hearts by allowing the adoption of marginal organs, thereby improving the donor pool availability.

DATA AVAILABILITY STATEMENT

The original contributions presented in the study are included in the article/supplementary material, further inquiries can be directed to the corresponding authors.

ETHICS STATEMENT

The animal study was reviewed and approved by the Ethical Committee of the Animal Experimental Center of Southern Medical University Nanfang Hospital.

AUTHOR CONTRIBUTIONS

JuL, LX, ZZ, and CX performed the experiments, analyzed the data, and participated in the writing of the manuscript. JiL, XC, PZ, and SL conducted the experiments and collected the data. YL, XD, RY, and SZ designed the experiments and revised the manuscript. All authors read and approved the final manuscript.

FUNDING

This research was supported by grants from the National Natural Science Foundation of China (81772136, 81972019, 21904145, 82170274, and 82100410), the Guangdong Basic and Applied Basic Research Foundation (2021A1515011453), the Foundation of Foshan City (FS0AA-KJ218-1301-0034 and 2018AB003411), and Special Fund of Foshan Summit plan (2019C002).

ACKNOWLEDGMENTS

We would like to express our gratitude to all the reviewers for the careful evaluation of the manuscript and appreciate the reviewers' insightful comments and suggestions which can help to improve our work.

REFERENCES

Aceros, H., Der Sarkissian, S., Borie, M., Pinto Ribeiro, R. V., Maltais, S., Stevens, L. M., et al. (2020). Novel heat shock protein 90 inhibitor improves cardiac recovery in a rodent model of donation after circulatory death. *J. Thorac. Cardiovasc. Surg.* S0022-5223, 30707–30708. doi: 10.1016/j.jtcvs.2020.03.042

Agil, A., Reiter, R. J., Jiménez-Aranda, A., Ibán-Arias, R., Navarro-Alarcón, M., Marchal, J. A., et al. (2013). Melatonin ameliorates low-grade inflammation and oxidative stress in young Zucker diabetic fatty rats. *J. Pineal Res.* 54, 381–388. doi: 10.1111/jpi.12012

Beuth, J., Falter, F., Pinto Ribeiro, R. V., Badiwala, M., and Meineri, M. (2019). New strategies to expand and optimize heart donor pool: ex vivo heart perfusion and donation after circulatory death: a review of current research and future trends. *Anesth. Analg.* 128, 406–413. doi: 10.1213/ANE.0000000000003919

Bracey, N. A., Duff, H. J., and Muruve, D. A. (2015). Hierarchical regulation of wound healing by NOD-like receptors in cardiovascular disease. *Antioxid Redox Signal.* 22, 1176–1187. doi: 10.1089/ars.2014.6125

Burchill, L. J., and Ross, H. J. (2012). Heart transplantation in adults with end-stage congenital heart disease. *Future Cardiol.* 8, 329–342. doi: 10.2217/fca.12.11

Cero, F. T., Hillestad, V., Sjaastad, I., Yndestad, A., Aukrust, P., Ranheim, T., et al. (2015). Absence of the inflammasome adaptor ASC reduces hypoxia-induced pulmonary hypertension in mice. *Am. J. Physiol. Lung Cell Mol. Physiol.* 309, L378–L387. doi: 10.1152/ajplung.00342.2014

Che, H., Li, H., Li, Y., Wang, Y. Q., Yang, Z. Y., Wang, R. L., et al. (2020). Melatonin exerts neuroprotective effects by inhibiting neuronal pyroptosis and autophagy in STZ-induced diabetic mice. *Faseb J.* 34, 14042–14054. doi: 10.1096/fj.202001328R

Christie, J. D., Edwards, L. B., Kucheryavaya, A. Y., Benden, C., Dipchand, A. I., Dobbels, F., et al. (2012). The registry of the international society for heart and lung transplantation: 29th adult lung and heart-lung transplant report-2012. *J. Heart Lung. Transplant* 31, 1073–1086. doi: 10.1016/j.healun.2012.08.004

Citerio, G., Cypel, M., Dobb, G. J., Dominguez-Gil, B., Frontera, J. A., Greer, D. M., et al. (2016). Organ donation in adults: a critical care perspective. *Intensive Care Med.* 42, 305–315. doi: 10.1007/s00134-015-4191-5

Dai, Y., Wang, S., Chang, S., Ren, D., Shali, S., Li, C., et al. (2020). M2 macrophage-derived exosomes carry microRNA-148a to alleviate myocardial ischemia/reperfusion injury *via* inhibiting TXNIP and the TLR4/NF-κB/NLRP3 inflammasome signaling pathway. *J. Mol. Cell Cardiol.* 142, 65–79. doi: 10.1016/j.yjmcc.2020.02.007

Dhital, K. K., Chew, H. C., and Macdonald, P. S. (2017). Donation after circulatory death heart transplantation. *Curr. Opin. Organ. Transplant* 22, 189–197. doi: 10.1097/MOT.0000000000000419

Ding, S., Liu, D., Wang, L., Wang, G., and Zhu, Y. (2020). Inhibiting MicroRNA-29a protects myocardial ischemia-reperfusion injury by targeting SIRT1 and Suppressing Oxidative Stress and NLRP3-Mediated Pyroptosis Pathway. *J. Pharmacol. Exp. Ther.* 372, 128–135. doi: 10.1124/jpet.119.256982

Geldhoff, M., Mook-Kanamori, B. B., Brouwer, M. C., Troost, D., Leemans, J. C., Flavell, R. A., et al. (2013). Inflammasome activation mediates inflammation and outcome in humans and mice with pneumococcal meningitis. *BMC Infect. Dis.* 13:358. doi: 10.1186/1471-2334-13-358

Hayyan, M., Hashim, M. A., and AlNashef, I. M. (2016). Superoxide ion: generation and chemical implications. *Chem. Rev.* 116, 3029–3085. doi: 10.1021/acs.chemrev.5b00407

Iyer, A., Gao, L., Doyle, A., Rao, P., Cropper, J. R., Soto, C., et al. (2015). Normothermic ex vivo perfusion provides superior organ preservation and enables viability assessment of hearts from DCD donors. *Am. J. Transplant* 15, 371–380. doi: 10.1111/ajt.12994

Jahnke, G., Marr, M., Myers, C., Wilson, R., Travlos, G., and Price, C. (1999). Maternal and developmental toxicity evaluation of melatonin administered orally to pregnant Sprague-Dawley rats. *Toxicol. Sci.* 50, 271–279. doi: 10.1093/toxsci/50.2.271

Jawitz, O. K., Raman, V., DeVore, A. D., Mentz, R. J., Patel, C. B., Rogers, J., et al. (2020). Increasing the United States heart transplant donor pool with donation after circulatory death. *J. Thorac. Cardiovasc. Surg.* 159, e307–e309. doi: 10.1016/j.jtcvs.2019.09.080

Jung, F. J., Yang, L., Härter, L., Inci, I., Schneiter, D., Lardinois, D., et al. (2004). Melatonin in vivo prolongs cardiac allograft survival in rats. *J. Pineal Res.* 37, 36–41. doi: 10.1111/j.1600-079X.2004.00133.x

Kearns, M. J., Miller, S. D., Cheung, A., Bashir, J., Wong, S., Seidman, M. A., et al. (2017). A rodent model of cardiac donation after circulatory death and novel biomarkers of cardiac viability during ex vivo heart perfusion. *Transplantation* 101, e231–e239. doi: 10.1097/TP.0000000000001815

Korkmaz-Icöz, S., Li, K., Loganathan, S., Ding, Q., Ruppert, M., Radovits, T., et al. (2020). Brain-dead donor heart conservation with a preservation solution supplemented by a conditioned medium from mesenchymal stem cells improves graft contractility after transplantation. *Am. J. Transplant* 20, 2847–2856. doi: 10.1111/ajt.15843

Lan, H., Su, Y., Liu, Y., Deng, C., Wang, J., Chen, T., et al. (2019). Melatonin protects circulatory death heart from ischemia/reperfusion injury *via* the JAK2/STAT3 signalling pathway. *Life Sci.* 228, 35–46. doi: 10.1016/j.lfs.2019.04.057

Li, Y., Yang, J., Chen, M. H., Wang, Q., Qin, M. J., Zhang, T., et al. (2015). Ilexgenin A inhibits endoplasmic reticulum stress and ameliorates endothelial dysfunction *via* suppression of TXNIP/NLRP3 inflammasome activation in an AMPK dependent manner. *Pharmacol. Res.* 99, 101–115. doi: 10.1016/j.phrs.2015.05.012

Li, Y., Yang, Y., Feng, Y., Yan, J., Fan, C., Jiang, S., et al. (2014). A review of melatonin in hepatic ischemia/reperfusion injury and clinical liver disease. *Ann. Med.* 46, 503–511. doi: 10.3109/07853890.2014.934275

Longnus, S. L., Mathys, V., Dornbierer, M., Dick, F., Carrel, T. P., and Tevaearai, H. T. (2014). Heart transplantation with donation after circulatory determination of death. *Nat. Rev. Cardiol.* 11, 354–363. doi: 10.1038/nrcardio.2014.45

Lund, L. H., Khush, K. K., Cherikh, W. S., Goldfarb, S., Kucheryavaya, A. Y., Levvey, B. J., et al. (2017). The registry of the international society for heart and lung transplantation: thirty-fourth adult heart transplantation report-2017; focus theme: allograft ischemic time. *J. Heart Lung. Transplant* 36, 1037–1046. doi: 10.1016/j.healun.2017.07.019

Manara, A. R., Murphy, P. G., and O'Callaghan, G. (2012). Donation after circulatory death. *Br. J. Anaesth.* 108(Suppl. 1), i108–i121. doi: 10.1093/bja/aer357

Manchester, L. C., Coto-Montes, A., Boga, J. A., Andersen, L. P., Zhou, Z., Galano, A., et al. (2015). Melatonin: an ancient molecule that makes oxygen metabolically tolerable. *J. Pineal Res.* 59, 403–419. doi: 10.1111/jpi.12267

Martínez, G. J., Robertson, S., Barraclough, J., Xia, Q., Mallat, Z., Bursill, C., et al. (2015). Colchicine acutely suppresses local cardiac production of inflammatory cytokines in patients with an acute coronary syndrome. *J. Am. Heart Assoc.* 4:e002128. doi: 10.1161/jaha.115.002128

Messer, S., Cernic, S., Page, A., Berman, M., Kaul, P., Colah, S., et al. (2020). A 5-year single-center early experience of heart transplantation from donation after circulatory-determined death donors. *J. Heart Lung. Transplant* 39, 1463–1475. doi: 10.1016/j.healun.2020.10.001

Messer, S., Page, A., Axell, R., Berman, M., Hernández-Sánchez, J., Colah, S., et al. (2017). Outcome after heart transplantation from donation after circulatory-determined death donors. *J. Heart Lung. Transplant* 36, 1311–1318. doi: 10.1016/j.healun.2017.10.021

Nie, C., Ding, X., Rong, A., Zheng, M., Li, Z., Pan, S., et al. (2021). Hydrogen gas inhalation alleviates myocardial ischemia-reperfusion injury by the inhibition of oxidative stress and NLRP3-mediated pyroptosis in rats. *Life Sci.* 272:119248. doi: 10.1016/j.lfs.2021.119248

Niederberger, P., Farine, E., Raillard, M., Dornbierer, M., Freed, D. H., Large, S. R., et al. (2019). Heart transplantation with donation after circulatory death. *Circ. Heart Fail* 12:e005517. doi: 10.1161/CIRCHEARTFAILURE.118.005517

Osaki, S., Anderson, J. E., Johnson, M. R., Edwards, N. M., and Kohmoto, T. (2010). The potential of cardiac allografts from donors after cardiac death at the University of Wisconsin Organ Procurement Organization. *Eur. J. Cardiothorac. Surg.* 37, 74–79. doi: 10.1016/j.ejcts.2009.07.005

Quader, M., Mezzaroma, E., Kenning, K., and Toldo, S. (2020). Targeting the NLRP3 inflammasome to reduce warm ischemic injury in donation after circulatory death heart. *Clin. Transplant* 34:e14044. doi: 10.1111/ctr.14044

Reiter, R. J., Paredes, S. D., Manchester, L. C., and Tan, D. X. (2009). Reducing oxidative/nitrosative stress: a newly-discovered genre for melatonin. *Crit. Rev. Biochem. Mol. Biol.* 44, 175–200. doi: 10.1080/10409230903044914

Rudd, D. M., and Dobson, G. P. (2011). Eight hours of cold static storage with adenosine and lidocaine (Adenocaine) heart preservation solutions: toward therapeutic suspended animation. *J. Thorac. Cardiovasc. Surg.* 142, 1552–1561. doi: 10.1016/j.jtcvs.2011.05.023

Seabra, M. L., Bignotto, M., Pinto, L. R. Jr., and Tufik, S. (2000). Randomized, double-blind clinical trial, controlled with placebo, of the toxicology of chronic melatonin treatment. *J. Pineal Res.* 29, 193–200. doi: 10.1034/j.1600-0633.2002.290401.x

Smith, M., Dominguez-Gil, B., Greer, D. M., Manara, A. R., and Souter, M. J. (2019). Organ donation after circulatory death: current status and future potential. *Intensive Care Med.* 45, 310–321. doi: 10.1007/s00134-019-05533-0

Stehlik, J., Kobashigawa, J., Hunt, S. A., Reichenspurner, H., and Kirklin, J. K. (2018). Honoring 50 Years of clinical heart transplantation in circulation: in-depth state-of-the-art review. *Circulation* 137, 71–87. doi: 10.1161/CIRCULATIONAHA.117.029753

Su, Z. D., Wei, X. B., Fu, Y. B., Xu, J., Wang, Z. H., Wang, Y., et al. (2021). Melatonin alleviates lipopolysaccharide-induced myocardial injury by inhibiting inflammation and pyroptosis in cardiomyocytes. *Ann. Transl. Med.* 9:413. doi: 10.21037/atm-20-8196

Van Raemdonck, D., Neyrinck, A., Rega, F., Devos, T., and Pirenne, J. (2013). Machine perfusion in organ transplantation: a tool for ex-vivo graft conditioning with mesenchymal stem cells? *Curr. Opin. Organ. Transplant* 18, 24–33. doi: 10.1097/MOT.0b013e32835c494f

Wang, K., Sun, Q., Zhong, X., Zeng, M., Zeng, H., Shi, X., et al. (2020). Structural mechanism for GSDMD targeting by autoprocessed caspases in pyroptosis. *Cell* 180, 941.e20–955.e20. doi: 10.1016/j.cell.2020.02.002

Wei, X., Peng, H., Deng, M., Feng, Z., Peng, C., and Yang, D. (2020). MiR-703 protects against hypoxia/reoxygenation-induced cardiomyocyte injury *via* inhibiting the NLRP3/caspase-1-mediated pyroptosis. *J. Bioenerg. Biomembr.* 52, 155–164. doi: 10.1007/s10863-020-09832-w

Weissenbacher, A., and Vrakas, G. (2019). The future of organ perfusion and re-conditioning. *Transpl. Int.* 32, 586–597. doi: 10.1111/tri.13441

Wu, J., Xu, X., Li, Y., Kou, J., Huang, F., Liu, B., et al. (2014). Quercetin, luteolin and epigallocatechin gallate alleviate TXNIP and NLRP3-mediated inflammation and apoptosis with regulation of AMPK in endothelial cells. *Eur. J. Pharmacol.* 745, 59–68. doi: 10.1016/j.ejphar.2014.09.046

Wu, Y., Zhang, Y., Zhang, J., Zhai, T., Hu, J., Luo, H., et al. (2020). Cathelicidin aggravates myocardial ischemia/reperfusion injury *via* activating TLR4 signaling and P2X(7)R/NLRP3 inflammasome. *J. Mol. Cell Cardiol.* 139, 75–86. doi: 10.1016/j.yjmcc.2019.12.011

Xu, J., Buchwald, J. E., and Martins, P. N. (2020). Review of current machine perfusion therapeutics for organ Preservation. *Transplantation* 104, 1792–1803. doi: 10.1097/tp.0000000000003295

Xu, L. J., Chen, R. C., Ma, X. Y., Zhu, Y., Sun, G. B., and Sun, X. B. (2020). Scutellarin protects against myocardial ischemia-reperfusion injury by suppressing NLRP3 inflammasome activation. *Phytomedicine* 68:153169. doi: 10.1016/j.phymed.2020.153169

Zhang, Y., Liu, X., Bai, X., Lin, Y., Li, Z., Fu, J., et al. (2018). Melatonin prevents endothelial cell pyroptosis *via* regulation of long noncoding RNA MEG3/miR-223/NLRP3 axis. *J. Pineal Res.* 64:e12525. doi: 10.1111/jpi.12449

Zhao, Y., Li, Q., Zhao, W., Li, J., Sun, Y., Liu, K., et al. (2015). Astragaloside IV and cycloastragenol are equally effective in inhibition of endoplasmic reticulum stress-associated TXNIP/NLRP3 inflammasome activation in the endothelium. *J. Ethnopharmacol.* 169, 210–218. doi: 10.1016/j.jep.2015.04.030

Zhou, P., Liu, H., Liu, X., Ling, X., Xiao, Z., Zhu, P., et al. (2021). Donor heart preservation with hypoxic-conditioned medium-derived from bone marrow mesenchymal stem cells improves cardiac function in a heart transplantation model. *Stem Cell Res. Ther.* 12:56. doi: 10.1186/s13287-020-02114-7

Zhou, P., Liu, X., Xiao, Z., Xu, R., Lin, X., Zhu, P., et al. (2020). Machine perfusion of donor heart with normothermic blood versus hypothermic HTK in preserving coronary endothelium in a porcine model of DCD. *Ann. Palliat. Med.* 9, 1476–1487. doi: 10.21037/apm-20-131

Conflict of Interest: The authors declare that the research was conducted in the absence of any commercial or financial relationships that could be construed as a potential conflict of interest.

Publisher's Note: All claims expressed in this article are solely those of the authors and do not necessarily represent those of their affiliated organizations, or those of the publisher, the editors and the reviewers. Any product that may be evaluated in this article, or claim that may be made by its manufacturer, is not guaranteed or endorsed by the publisher.

Copyright © 2021 Lu, Xu, Zeng, Xue, Li, Chen, Zhou, Lin, Liao, Du, Yang and Zheng. This is an open-access article distributed under the terms of the Creative Commons Attribution License (CC BY). The use, distribution or reproduction in other forums is permitted, provided the original author(s) and the copyright owner(s) are credited and that the original publication in this journal is cited, in accordance with accepted academic practice. No use, distribution or reproduction is permitted which does not comply with these terms.

frontiers in Cell and Developmental Biology

ORIGINAL RESEARCH
published: 17 September 2021
doi: 10.3389/fcell.2021.736603

IL-13 Alleviates Cardiomyocyte Apoptosis by Improving Fatty Acid Oxidation in Mitochondria

Xiaoyu Guo[1†], Ting Hong[1†], Shen Zhang[1†], Yazhong Wei[1], Haizhen Jin[2], Qing Miao[1,3], Kai Wang[2], Miao Zhou[4], Chong Wang[5] and Bin He[1*]*

[1] Department of Critical Care Medicine, Shanghai Chest Hospital, Shanghai Jiao Tong University, Shanghai, China, [2] Central Laboratory of Shanghai Chest Hospital, Shanghai Jiao Tong University, Shanghai, China, [3] Department of Anesthesiology, Shanghai Chest Hospital, Shanghai Jiao Tong University, Shanghai, China, [4] Department of Anesthesiology and Intensive Care Medicine, Xinhua Hospital, School of Medicine, Shanghai Jiao Tong University, Shanghai, China, [5] Department of Cardiovascular Surgery, Shanghai Chest Hospital, Shanghai Jiao Tong University, Shanghai, China

OPEN ACCESS

Edited by:
Zhi Qi,
Nankai University, China

Reviewed by:
Ming Zhong,
Fudan University, China
Xiaolei Xu,
Mayo Clinic, United States

***Correspondence:**
Bin He
bin_he@sjtu.edu.cn
Chong Wang
wc001218@hotmail.com

[†] These authors have contributed equally to this work

Specialty section:
This article was submitted to Cell Death and Survival, a section of the journal Frontiers in Cell and Developmental Biology

Received: 05 July 2021
Accepted: 24 August 2021
Published: 17 September 2021

Citation:
Guo X, Hong T, Zhang S, Wei Y, Jin H, Miao Q, Wang K, Zhou M, Wang C and He B (2021) IL-13 Alleviates Cardiomyocyte Apoptosis by Improving Fatty Acid Oxidation in Mitochondria. Front. Cell Dev. Biol. 9:736603. doi: 10.3389/fcell.2021.736603

Sepsis-induced cardiac injury (*SIC*) is one of the most common complications in the intensive care unit (ICU) with high morbidity and mortality. Mitochondrial dysfunction is one of the main reasons for *SIC*, and Interleukin-13 (IL-13) is a master regulator of mitochondria biogenesis. The aim of the present study was to investigate the role of IL-13 in *SIC* and explore the underlying mechanism. It was found that reactive oxygen species (ROS) production and apoptosis were significantly increased in lipopolysaccharide (LPS)-stimulated primary cardiomyocytes, which was accompanied with obvious mitochondria dysfunction. The results of RNA-sequencing (RNA-seq), mitochondrial membrane potential, fatty acid uptake and oxidation rate suggested that treatment with IL-13 could restore the function and morphology of mitochondria, indicating that it played an important role in protecting septic cardiomyocytes. These findings demonstrated that IL-13 alleviated sepsis-induced cardiac inflammation and apoptosis by improving mitochondrial fatty acid uptake and oxidation, suggesting that IL-13 may prove to be a potential promising target for *SIC* treatment.

Keywords: sepsis, cardiomyocyte apoptosis, IL-13, mitochondria, fatty acid

INTRODUCTION

Sepsis-induced myocardial dysfunction is one of the main causes of death in the intensive care unit (ICU). Various theories and therapies have been proposed to treat septic patients with impaired cardiac function (Ichinose et al., 2007; Xu et al., 2012; Venet and Monneret, 2018). In recent years, mitochondrial dysfunction has been considered as a crucial cause of sepsis-induced cardiac injury (*SIC*) with augmented release of reactive oxygen species (ROS) and decreased mitochondrial oxidative phosphorylation (Drosatos et al., 2011, 2013; Schilling et al., 2011). Toxic ROS and insufficient energy metabolism finally lead to the impairment and apoptosis of cardiomyocytes (Sepúlveda et al., 2020).

Interleukin-13 (IL-13) is a protein secreted by many cell types and recognized as a type 2 immunity cytokine that plays an important role in a variety of diseases, including allergic inflammation, schistosomiasis, and tissue repair (Qian et al., 2021). Recently, IL-13 is reported to be increased after endurance exercise, probably due to type 2 innate lymphocytes (ILC2) expansion

in the muscle. IL-13 preserves the ability of fatty acid utilization and mitochondrial biogenesis in the muscle (Knudsen et al., 2020). Although IL-13 is known to have a protective effect in various diseases, whether IL-13 also has a cardioprotective effect in sepsis remains to be defined.

In this study, we investigated the potential role of IL-13 in protecting mitochondria and alleviating *SIC*. IL-13 decreased the apoptosis and increased the cardiac function in *SIC*. Furthermore, we evaluated the morphology of mitochondria and expression level of ROS in different conditions. Finally, we explored the possible mechanisms whereby IL-13 recovered the fatty acid utilization of mitochondria in the septic state. Our findings suggest that IL-13 may be a promising therapeutic target in *SIC*.

MATERIALS AND METHODS

Primary Cardiomyocyte Culture

Primary cardiomyocytes were isolated from neonatal rats aged 1–3 days (Wang et al., 2020). Briefly, the neonatal SD rat heart was digested into single cells in 0.1% trypsin (Gibco) diluted with Hank's balanced salt solution (HBSS, Cytiva) at 37°C. Then, low glucose Dulbecco's Modified Eagle's Medium (DMEM, Cytiva) containing fetal bovine serum (FBS) was added into the single cardiomyocyte suspension to neutralize the trypsin. In the end, the cardiomyocytes were cultured in low glucose DMEM containing 10% FBS at 37°C with 5% CO_2.

Model Establishment

The cellular model of *SIC* was established by lipopolysaccharide (LPS, Sigma-Aldrich, United States) incubation. Briefly, primary cardiomyocytes were cultured in low glucose DMEM containing 10 ug/ml LPS for 6 h. Morphology and pulse rhythm of cardiomyocytes were observed.

C57BL/6 mice (JSJ Co., Shanghai, China) were raised in the specific pathogen free (SPF)-grade environment, all biosecurity as well as institutional safety procedures were approved and supervised by the Ethics Committee of Shanghai Chest Hospital (Shanghai, China). C57BL/6 were intraperitoneally (i.p.) injected with LPS at a dosage of 10 mg/ml for 6 h.

Adenosine Triphosphate Measurement

Adenosine Triphosphate (ATP) production was measured by ATP measurement assay (Beyotime, China) according to the operating manual. Briefly, lysis solution was added into the cardiomyocytes and then centrifuged at 12000 × *g* at 4°C for 5 min. Then, the ATP standard solution was diluted to an appropriate concentration gradient with ATP test solution, and 100 ul ATP test solution was added into the microplate for 3 min in advance. Finally, 20 ul standard solution and sample solution were added into the prepared ATP test solution and detected by luminometry (Thermo Fisher Scientific, United States).

Reactive Oxygen Species Measurement

Generation of ROS was detected with ROS Assay Kit (Beyotime, China). In brief, DCFH-DA was diluted to a concentration of 10 uM. Cardiomyocytes were washed with PBS firstly and incubated with DCFH-DA at 37°C for 20 min. After that, cells were washed with PBS for 3 times and detected by fluorescent microscopy.

Mitochondrial Morphology

Mitochondria of primary cardiomyocytes were stained with MitoTracker^{TM} Deep Red (Invitrogen, United States). Briefly, 1 mM mitoTracker solution was diluted to the final work concentration of 50 nM with DMEM. Primary cardiomyocytes were washed with PBS and incubated with mitoTracker work solution for 30 min at 37°C. After staining, cells were washed with PBS for 3 times again and added fresh DMEM.

TUNEL Staining

TUNEL assays were performed with sections using One-step TUNEL Cell Apoptosis Detection Kit (Beyotime, China) principally according to the supplier's instruction. In addition, the nuclei in the slices were labeled with DAPI, and finally photographed with a fluorescence microscope.

Isolation of Mitochondria

Mitochondria from primary cardiomyocytes were extracted according to the instructions of QIAGEN (United States). Cells were collected and added with lysis buffer and incubated at 4°C for 10 min. After that, samples were centrifuged at 1000 × *g* at 4°C for 10 min. The precipitation was collected, incubated with disruption buffer, and then homogenized using a Dounce tissue grinder. The supernatant was collected in a new clear tube after 1000 × *g* centrifuge at 4°C for 10 min. Next, the samples were centrifuged again at 6000 × *g* for 10 min and added with 1 ml mitochondria, stored, and suspended until precipitation. Finally, the samples were centrifuged at 6000 × *g* for 20 min, resuspended and stored for future use.

Extraction and qPCR of Mitochondria DNA

The gene expression of mitochondria DNA (mtDNA) was determined by RT-qPCR with SYBR Green. Relative expression was quantified to Rplp0 as the internal standard control. All primer sequences are listed in **Supplementary Table 1**.

Western Blot Analysis

Protein lysates and Western blotting were performed using the classic methods. Briefly, each protein sample (30 ug) was resuspended in SDS-PAGE loading buffer, boiled at 95°C for 10 min and electrophoresed with appropriate gels. After that, the protein was electrotransferred to PVDF membrane (Millipore, United States) and blocked with 5% non-fat milk for 1 h at room temperature. Antibodies of Bcl2, Bax, Caspase3, α-tubulin, α-actin and Cox4 (Cell Signaling Technology, United States) and OXPHOS (Invitrogen, United States) were added to bind the membrane overnight at 4°C. Then, the membrane was washed with TBST for 3 times and incubated with HRP-conjugated secondary antibodies (Cell Signaling Technology, United States) for 1 h at room temperature. Finally, the PVDF

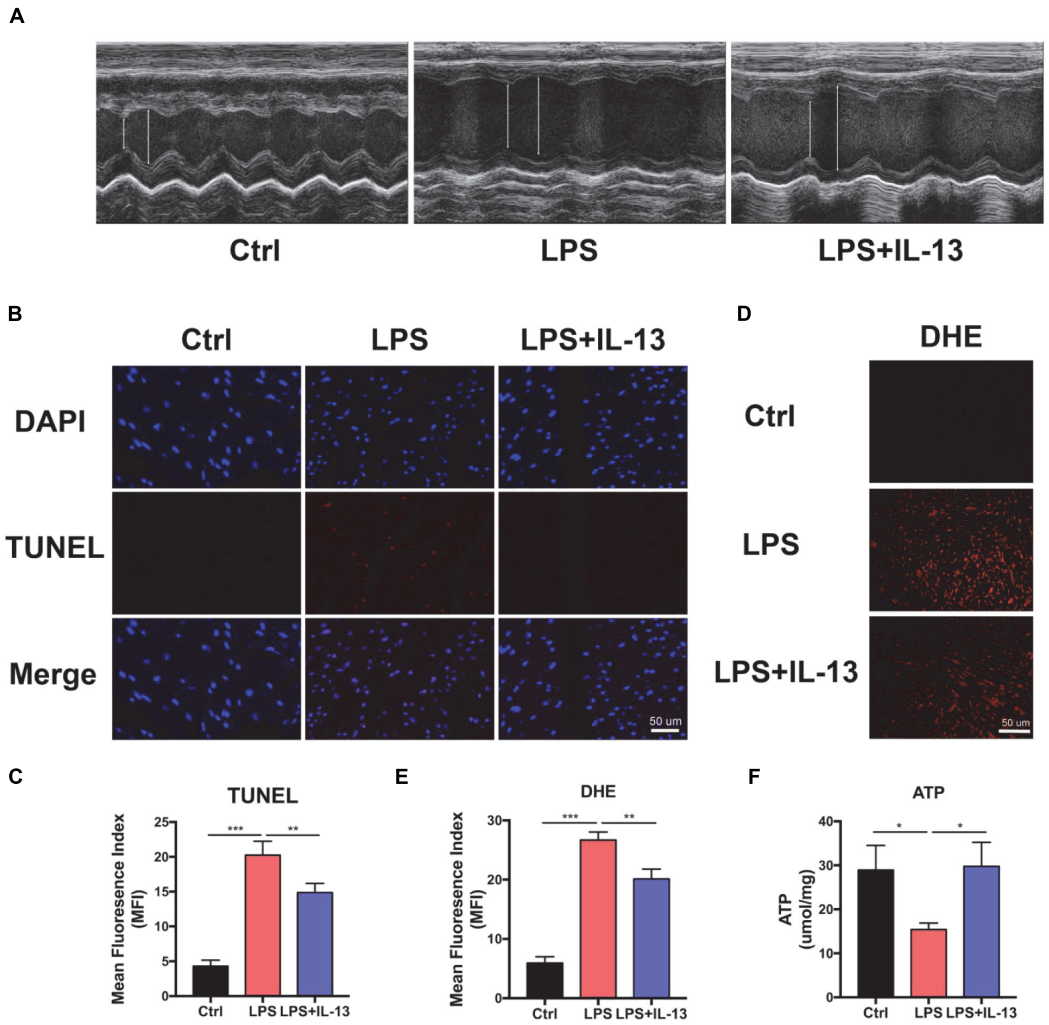

FIGURE 1 | Interleukin-13 (IL-13) alleviates cardiomyocyte apoptosis and reactive oxygen species (ROS) production *in vivo*. **(A)** Representative figures of echocardiography (ECG). **(B)** TUNEL staining was used to observe the level of apoptosis and **(C)** quantitative results were calculated with image J. **(D)** The level of ROS was observed with DHE probe and **(E)** calculated. **(F)** The level of Adenosine Triphosphate (ATP) production. Data are shown as the mean ± SEM (n = 3). $^{*}P < 0.05$; $^{**}P < 0.01$; $^{***}P < 0.001$.

membrane was washed with TBST for 3 times and developed with electrochemiluminescence solution (Millipore, United States).

Transmission Electron Microscope Investigation

The heart was isolated from the LPS-induced cardiac injury mice and cut into 1 mm^3 sections and incubated with fixative solution (Daixuan Biotechnology Co., Ltd., China) immediately, followed by incubation with 2.5% glutaraldehyde overnight. After that, the fixed samples were washed by ddH_2O and put into 30, 50 and 70% ethanol at 4°C for 10 min each in sequence. Then it was given to 80, 90 and 95% acetone for 10 min one by one, and to 100% acetone for 10 min × 2. Afterward, the specimen was immersed into epoxy resin and shaken at 30°C for 4 h. Finally, the prepared sample was sliced to ultrathin sections for transmission electron microscope (TEM) observation (Hitachi, Tokyo, Japan).

Mitochondrial Membrane Potential Detection

Mitochondrial membrane potential was detected with JC-10 Mitochondrial Membrane Potential Assay Kit (Yeasen, China). According to the instructions, JC-10 stock solution was diluted with ddH_2O at the ratio of 1:1000 to make JC-10 work solution. Primary cardiomyocytes were washed with PBS and incubated with 1 ml DMEM mixed with 1 ml JC-10 work solution at 37°C for 20 min. After that, cell samples were washed with PBS twice and added with fresh DMEM for confocal laser microscopic observation.

RNA Sequencing and Analysis

RNA was extracted from heart tissues that were grown under the appropriate conditions using the RNeasy mini kit (Qiagen, United States). After that, RNA-sequencing (RNA-seq) was

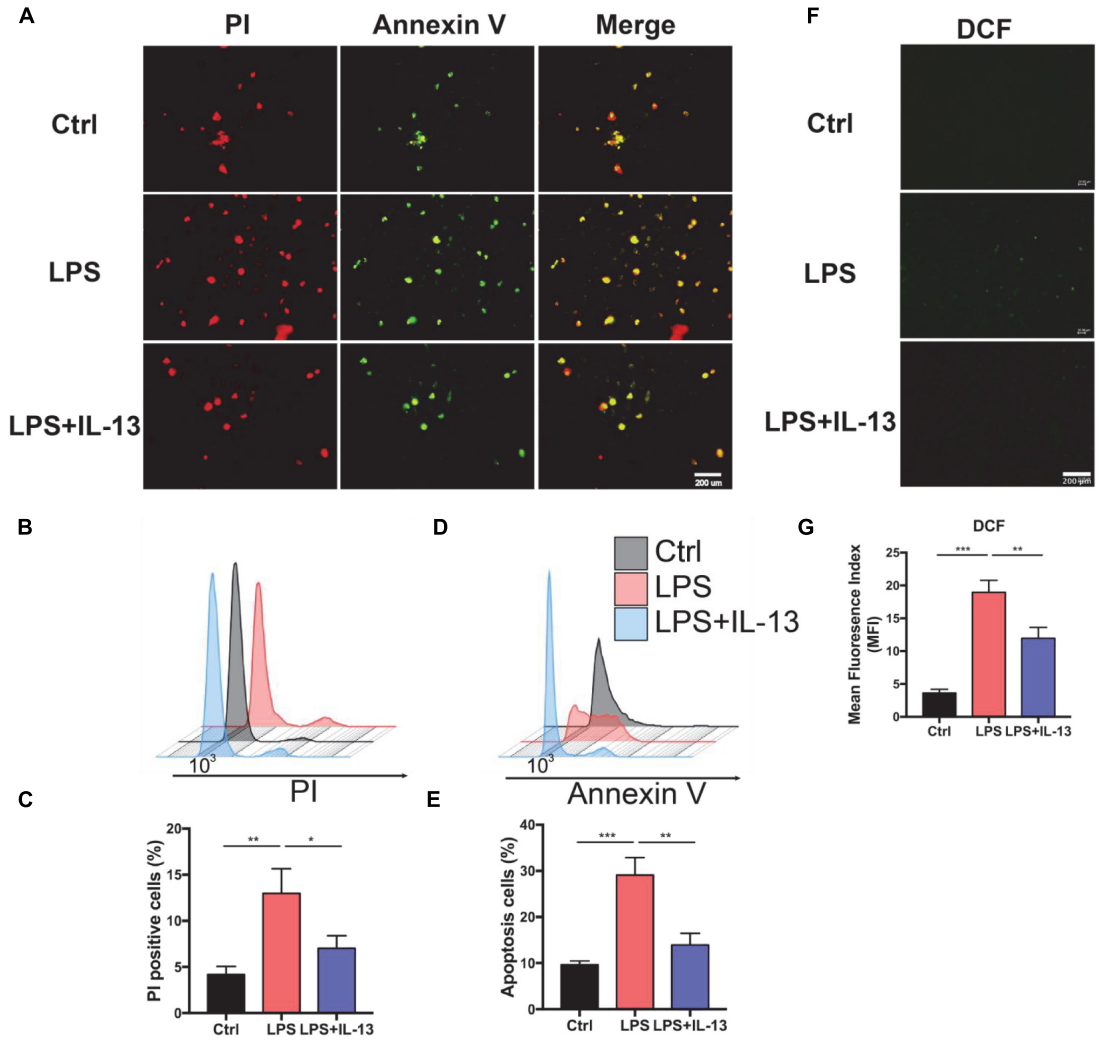

FIGURE 2 | Interleukin-13 alleviates cardiomyocyte apoptosis and ROS production *in vitro*. **(A)** PI and Annexin V dye was used to observe the level of apoptosis. **(B)** PI positive cells were counted by flow cytometry and **(C)** calculated. Annexin V positive cells **(D)** and the apoptosis ratio **(E)** were counted by flow cytometry and calculated. **(F)** DCFH-DA staining was applied to detect the level of ROS and **(G)** measured with image J. Data are shown as the mean ± SEM (n = 3). *P < 0.05; **P < 0.01; ***P < 0.001.

performed by GENEWIZ (Suzhou, China). Genes with a | fold-change (FC) | > 1 and P < 0.05 were defined as significant differential expressed genes for further analysis.

Fatty Acid Uptake Rate Detection

According to the instruction book, primary cardiomyocytes were seeded into black 96-well plate and incubated with LPS or IL-13. After that, 100 ul fatty acid dye solution (Sigma-Aldrich, United States) was added for 1 h incubation. Finally, fluorescence was detected with VARIOSKAN LUX (Thermo Fisher Scientific, United States) and reported as Fluorescence (RFU).

Fatty Acid Oxidation Rate Detection

Fatty acid oxidation rate assay (Genmed Scientifics Inc., United States) was applied to detect the rate of β-oxidation rate. According to the instruction manuscript, primary cardiomyocytes were seeded into 96-well plate. After stimulation, substrate of palmitoyl carnitine was added into the 96-well plates for β-oxidation. Finally, VARIOSKAN LUX was used to detect OD values at 420 nm. Fatty acid β-oxidation rate = [(ODsample-ODbackgroud) × system volume (ml)]/[sample protein content (mg) × 105 × reaction time(min)].

Statistical Analysis

Data are presented as the mean ± SEM at least three duplications of different samples. Student's t-test was applied for analysis between two groups and one-way analysis of variance (ANOVA) was used for comparisons between multiple groups. GraphPad Prism 7.0 (GraphPad Software Inc., United States) were used to analyze and illustrate the data. Differences with p-values < 0.05 were considered statistically significant.

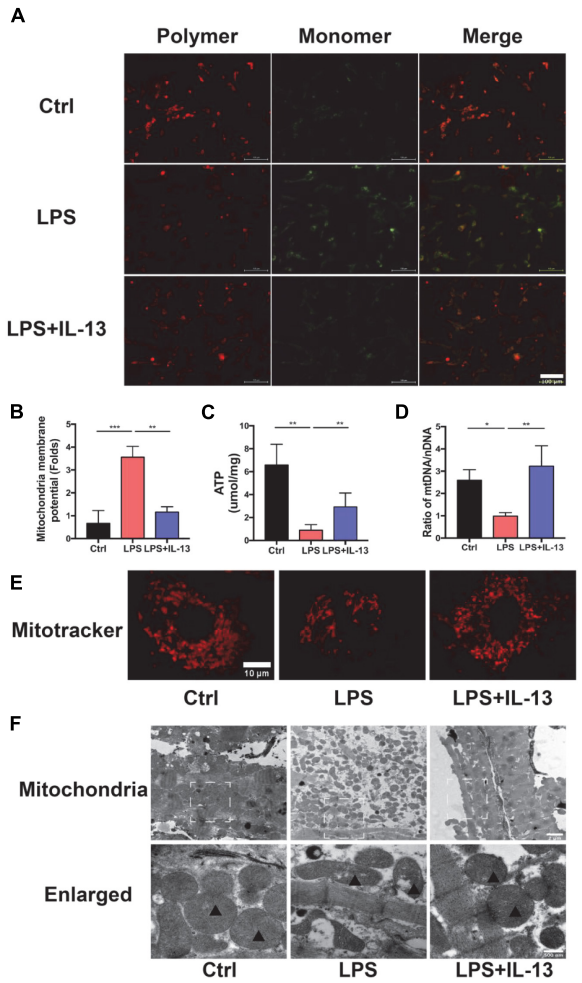

FIGURE 3 | Interleukin-13 recovers homeostasis and morphology of mitochondria. **(A)** Measurement of mitochondrial membrane potential using the JC-10 probe. **(B)** Calculation of the membrane potential change ratio with a monomer/polymer. **(C)** Level of ATP production. **(D)** mitochondria DNA (mtDNA)/nuclear DNA (nDNA) ratio. **(E)** Mitochondrial morphology shown by MitoTracker deep red staining. **(F)** Mitochondrial morphology shown by transmission electron microscope (TEM). Mitochondria was labeled with black triangle. Data are expressed as the mean ± SEM (n = 3). $^{*}P < 0.05$; $^{**}P < 0.01$; $^{***}P < 0.001$.

RESULTS

Interleukin-13 Alleviates LPS-Induced Cardiomyocyte Apoptosis and ROS Production *in vivo*

To understand the potential role of IL-13 in protection against *SIC*, LPS was injected i.p. to induce a cytokine storm. Echocardiography (ECG) was employed to determine the cardiac function in LPS-induced cardiac injury. As shown in **Figure 1A**, myocardial systolic function was decreased after LPS injection, and IL-13 mitigated cardiac injury and reversed to a certain extent. Eject fraction (EF) and fraction shorting (FS) were calculated in **Supplementary Figures 1A,B**. The heart was then harvested and TUNEL stained. As shown in **Figures 1B,C**, compared with the control group, LPS induced obvious cardiomyocyte apoptosis and IL-13 attenuated the apoptosis. In addition, DHE staining was employed to evaluate the ROS production in LPS-induced cardiac injury. As shown in **Figures 1D,E**, the change of ROS production was in accordance with the level of apoptosis, suggesting that ROS may be an important cause of cardiomyocyte apoptosis. Furthermore, H&E staining showed that LPS caused edema of the heart tissue as represented by enlarged tissue space (**Supplementary Figure 2**). We also observed the change of ATP in the heart of the septic mice, which is a crucial form of energy for the heart. Interestingly, LPS decreased the production of ATP and IL-13 treatment eliminated the disorder of energy metabolism (**Figure 1F**).

Interleukin-13 Alleviates LPS-Induced Cardiomyocyte Apoptosis and ROS Production *in vitro*

Next, we explored the therapeutic effect of IL-13 with primary cardiomyocytes. PBS, 10 ug/ml LPS and LPS + IL-13(50 ng/ml) was added to cardiomyocytes, respectively. After that, PI and Annexin V dyes were employed to mark the necrotic and apoptotic cells, respectively. As shown in **Figure 2A**, necrotic and apoptotic cells were increased conspicuously in LPS-stimulated group as compared with the control group, while IL-13 relieved the necrosis and apoptosis effectively. To obtain a quantification result of apoptosis, we used flow cytometry for more accurate investigation. As shown in **Figures 2B,C**, PI positive cells were decreased markedly in IL-13 treatment group as compared with LPS group (13.6% *vs.* 5.6%). Meanwhile, Annexin V positive cells, which represent the total apoptotic cells, were also decreased after IL-13 treatment (**Figures 2D,E**). In addition, we also detected the ROS production using the DCFH-DA assay kit. As shown in **Figures 2F–G**, the level of ROS in normal primary cardiomyocytes was very low but increased markedly after LPS induction. Together, we conclude that IL-13 could protect the cardiomyocytes and reduce the production of ROS.

Interleukin-13 Sustains the Homeostasis of Mitochondria

The above results suggest that IL-13 could alleviate the apoptosis of cardiomyocytes but the exact mechanism remains to be further understood. In consideration of the change in ATP production, IL-13 may play a protective role by maintaining the homeostasis of mitochondria. Next, we evaluated the mitochondria function by detecting the membrane potential by JC-10, which is a bicolourable membrane potential probe that reflects the function of mitochondria. JC-10 presents the polymer that displays red fluorescence in mitochondria of normal cardiomyocytes but resolves into a monomer with green fluorescence when damage occurs in mitochondria. As shown in **Figures 3A,B**, red fluorescence decreased, and green fluorescence increased after LPS stimulation. IL-13 recovered the membrane potential of mitochondria by regulating its homeostasis. After that, we detected the production of ATP in primary cardiomyocytes. As shown in **Figure 3C**, IL-13 increased ATP production as

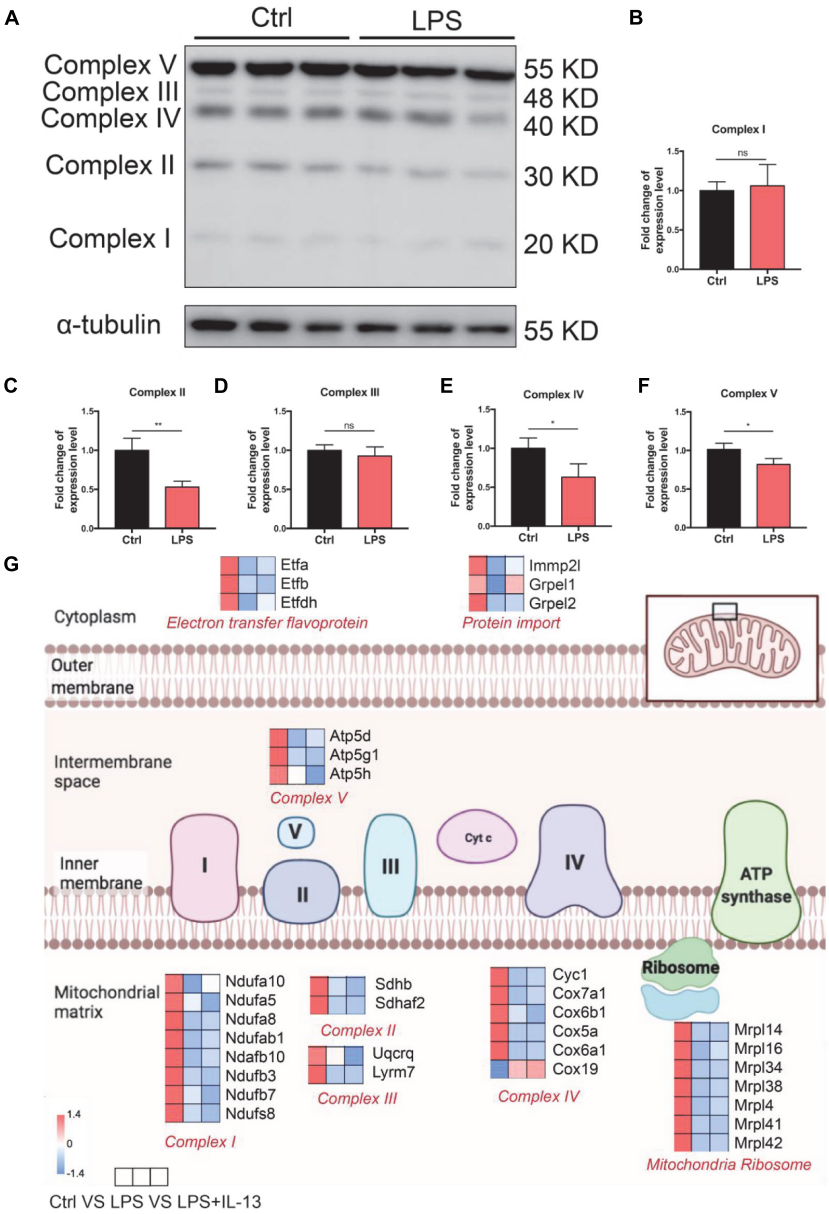

FIGURE 4 | Change of electronic delivery chain in lipopolysaccharide (LPS)-induced cardiomyocytes. **(A)** Western immunoblotting and **(B–F)** quantification of multiple OxPhos proteins from primary cardiomyocytes induced by LPS (n = 3). **(G)** Expression level of representative genes related to electronic delivery chain by RNA-sequencing (RNA-seq) in the mouse heart. Data are presented as a heatmap (n = 6). Data are shown as the mean ± SEM. $^{*}P < 0.05$; $^{**}P < 0.01$; $^{***}P < 0.001$.

expected. In addition, IL-13 treatment increased the biogenesis of mitochondria as determined by the ratio of mtDNA and nuclear DNA (nDNA; **Figure 3D**).

Interleukin-13 Sustains the Morphology of Mitochondria

In addition to the functional change of mitochondria, the morphology also restored to normal after IL-13 treatment. A deep red MitoTracker dye was applied to evaluate the change of mitochondria. As shown in **Figure 3E**, normal cardiomyocytes had more dense and dispersive mitochondria compared with those in LPS group. After LPS stimulation, the mean area of mitochondria became shorter (**Supplementary Figure 3A**), and the proportion of cardiomyocytes with fragmented mitochondria was increased (**Supplementary Figure 3B**). Next, we analyzed ultrastructural changes by TEM. As shown in **Figure 3F**, normal cardiomyocytes had more large mitochondria with regular arrangement as compared with LPS group. Supplementation of IL-13 restored the number, size and arrangement of mitochondria in inflammatory cardiomyocytes. In addition, LPS-stimulated mitochondria were characterized by the presence of fragmented cristae and swollen Vacuoles.

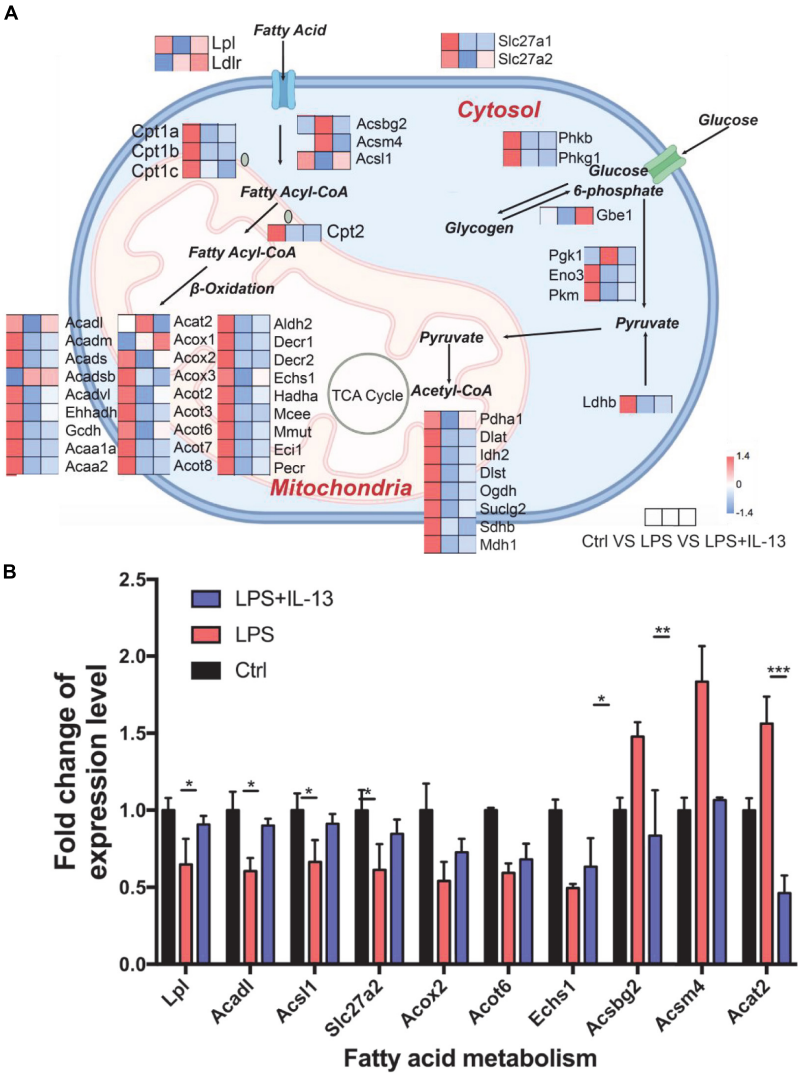

FIGURE 5 | Change of mitochondria biogenesis in LPS-induced cardiomyocytes. **(A)** Expression level of representative genes related to mitochondria biogenesis by RNA-seq in the mouse heart. Data are presented as a heatmap (n = 6). **(B)** The expression level of genes related to fatty acid metabolism was validated by RT-qPCR (n = 3). Data are shown as the mean ± SEM. *P < 0.05; **P < 0.01; ***P < 0.001.

LPS Leads to Damage of Electronic Delivery Chain

To investigate the cause of damaged ATP production, the expression level of OxPhos in control and LPS-induced cardiomyocytes was detected by Western Blot. It was found that the expression level of complex II, complex IV, and complex V was significantly decreased (**Figures 4A–F**). Furthermore, the hearts were harvested from the control and LPS-induced mice with or without IL-13 treatment for RNA-seq to explore the potential mechanisms. It was found that IL-13 treatment significantly up-regulated the expression of 62 genes and down-regulated the expression of 36 genes in the heart of LPS and IL-13 groups ($P < 0.05$ and $|\log_2 FC| > 1$) (**Supplementary Figure 4**). Interestingly, of the genes significantly related to electronic delivery chain, only Grprl1 underwent significant change (**Figure 4G**), knowing that Grprl1 is responsible to transport proteins from the membrane to mitochondria matrix in an ATP-dependent manner. This finding suggests that IL-13 could not restore the electronic delivery chain activity at transcriptional level, and there may be other potential pathways.

Interleukin-13 Reverts the LPS Induced Mitochondria Biogenesis Disorder

Knowing that IL-13 could not ameliorate LPS-induced mitochondria injury, we next analyzed the change of mitochondria biogenesis in LPS-induced cardiac injury. As shown in **Figure 5A**, totally 13 associated genes reverted after IL-13 treatment as compared with LPS group. Interestingly, among these genes, *Acadl*, *Acsl1*, *Acot6*, *Acat2*, *Acox2*, *Echs1*, *Acsm4*, *Acsbg2*, *Slc27a2*, and *Lpl* were responsible for fatty acid

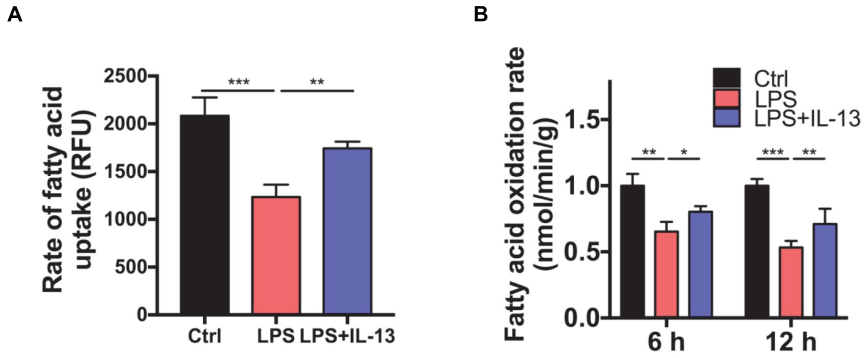

FIGURE 6 | Interleukin-13 ameliorates fatty acid uptake and oxidation in mitochondria. **(A)** Rate of fatty acid uptake in primary cardiomyocytes. **(B)** Rate of fatty acid oxidation in primary cardiomyocytes. Data are shown as the mean ± SEM (n = 3). *P < 0.05; **P < 0.01; ***P < 0.001.

uptake and β-oxidation, knowing that they are the main energy source for the heart. Only three genes (Gbe1, Pdha1, and Prkaa1) were related to carbohydrate metabolism. Based on the results of heatmap analysis, we validated the fatty acid metabolism gene expression level in primary cardiomyocytes by RT-qPCR, and found that Lpl, Acadl, Acsl1, Slc27a2, Acsbg2, Acsm4, and Acat2 underwent significant changes in LPS + IL-13 group compared with LPS, which is in consistent with the result of RNA-seq (**Figure 5B**). These results suggest that IL-13 may alleviate the LPS induced mitochondria biogenesis disorder by increasing the expression level of fatty acid uptake and β-oxidation.

Interleukin-13 Ameliorates Fatty Acid Uptake and Oxidation of Mitochondria

To determine whether IL-13 could ameliorate the fatty acid metabolism in LPS-stimulated primary cardiomyocytes, we detected the rate of fatty acid uptake and oxidation. As shown in **Figure 6A**, fatty acid uptake was impacted obviously by LPS compared with the control group, and IL-13 treatment improved the damaged uptake efficiency. In accordance with the results of uptake, IL-13 restored the activity of fatty acid oxidation at both 6 and 12 h after LPS stimulation (**Figure 6B**). These results suggest that IL-13 could effectively ameliorate sepsis-induced mitochondrial biogenesis dysfunction.

DISCUSSION

Sepsis-induced cardiac injury is one of the most common postoperative complications in the ICU, causing high morbidity and mortality. *SIC* is mainly characterized as systolic dysfunction in the serious inflammation environment. However, myocardial dysfunction in sepsis is a well-recognized but poorly understood condition without effective treatment.

Numerous mechanisms including calcium overload, ROS production, calcium overload, inactivation of ion channels and mitochondria dysfunction are involved in the development of *SIC*. Mitochondrial dysfunction is a hotspot of research on septic cardiomyopathy in recent years. Previous studies reported that LPS affected mitochondrial biosynthesis and eventually mediated the apoptosis of cardiomyocytes (Xin and Lu, 2020). Xu et al. (2018) demonstrated that several key regulators of mitochondria-associated apoptosis were abnormally expressed in the cecal ligation puncture (CLP) animal model, which may prove to be a promising potential target for the treatment of *SIC* with traditional Chinese medicine.

Sepsis-induced mitochondrial dysfunction is organ-specific and depends on the phase of the disease (Makrecka-Kuka et al., 2019). It is therefore significant to find a new regulator for mitochondrial dysfunction in the treatment of the disease. IL-13 is a key factor of type 2 immunity and plays an important role in fighting helminth infection, regulating asthma and tissue repair (Chu et al., 2021; Rodriguez-Rodriguez et al., 2021; Snodgrass et al., 2021). Previous research showed that IL-13 could maintain and increase the function and morphology of mitochondria in different diseases. For example, IL-13 could prevent and treat sepsis-induced brain dysfunction by enhancing the mitochondrial function and content in the brain microglia (Yan et al., 2020). In addition, latest research demonstrated that IL-13 mediated the mitochondrial metabolism from glycolysis switch into fatty acid oxidation, thus improving skeletal muscle endurance (Knudsen et al., 2020). These studies are consistent with the finding in our study that LPS induced obvious damage to mitochondrial function and morphology in terms of the decreased number, the smaller size, cell derangement and vacuolar formation in both *in vivo* and *in vitro SIC* models.

It is remarkable to note that β-oxidation of fatty acid, rather than glycolysis, is the primary energy supply for adult cardiomyocytes, which is different from other cells (Schulze et al., 2016; Cao et al., 2019). Recent studies reported that depressed cardiac function always accompanied with damaged mitochondrial fatty acid oxidation, and prevention of sepsis-induced fatty acid β-oxidation could improve heart function (Drosatos et al., 2011; Soraya et al., 2016). Our results also confirm that fatty acid oxidation plays a major role in the development of *SIC*. LPS mainly affects the transcription of genes involved in mitochondrial fatty acid uptake and β-oxidation, while IL-13 can restore the expression of these genes and rate of fatty acid uptake and oxidation to a certain extent, thereby

reducing the apoptosis of cardiomyocytes caused by sepsis induced mitochondrial injury.

Clinically, *SIC* is a heterogeneous disease with different damage degrees of cardiac function and mitochondria caused by different sources of infection (Ehrman et al., 2018; Hollenberg and Singer, 2021). In this study, we used 10 mg/mL LPS to induce relatively consistent and stable endotoxemia, but different concentration gradients were missing (Ndongson-Dongmo et al., 2019; Vico et al., 2019). Another limitation of the current study is that *SIC* is a dynamic disease over time. In this study, we mainly focused on the myocardial protection in the early stage of the disease and set 6 h after LPS injection as the time point of observation. Pathophysiological changes and possible mechanisms of *SIC* with different severities and at different time points will be further evaluated in our subsequent experiments.

In conclusion, mitochondrial dysfunction is an important cause of *SIC* as represented by production of large amounts of ROS and myocardial cell apoptosis. IL-13 could effectively improve the ability of fatty acid uptake and oxidation in mitochondria, thereby reducing mitochondrial dysfunction and ameliorating apoptosis of *SIC*. Our results demonstrated that IL-13, working as an important immunity regulator, may prove to be an important potential target for the treatment of *SIC*.

DATA AVAILABILITY STATEMENT

The original contributions presented in the study are included in the article/**Supplementary Material**, further inquiries can be directed to the corresponding authors.

ETHICS STATEMENT

The animal study was reviewed and approved by Ethics Committee of Shanghai Chest Hospital.

AUTHOR CONTRIBUTIONS

XG, TH, and SZ conducted the experiments. YW, HJ, and QM analyzed the data. KW and MZ wrote the manuscript. CW designed the manuscript. BH designed the methodology and supervised the study. All authors contributed to the article and approved the submitted version.

FUNDING

This work was financially supported through grants from the National Natural Science Foundation of China (No. 82072199 and No. 82172168); the Clinical Research Plan of Shanghai Hospital Development Center (No. SHDC2020CR3084B); Shanghai Collaborative Innovation Center for Translational Medicine Fund (No. TM202013); and the Translational Medicine Cross Research Fund of Shanghai Jiao Tong University (Nos. ZH2018ZDB01, YG2021QN124, and YG2021ZD27).

SUPPLEMENTARY MATERIAL

The Supplementary Material for this article can be found online at: https://www.frontiersin.org/articles/10.3389/fcell.2021.736603/full#supplementary-material

REFERENCES

Cao, T., Liccardo, D., LaCanna, R., Zhang, X., Lu, R., Finck, B., et al. (2019). Fatty acid oxidation promotes cardiomyocyte proliferation rate but does not change cardiomyocyte number in infant mice. *Front. Cell Dev. Biol.* 7:42. doi: 10.3389/fcell.2019.00042

Chu, C., Parkhurst, C., Zhang, W., Zhou, L., Yano, H., Arifuzzaman, M., et al. (2021). The ChAT-acetylcholine pathway promotes group 2 innate lymphoid cell responses and anti-helminth immunity. *Sci. Immunol.* 6:eabe3218. doi: 10.1126/sciimmunol.abe3218

Drosatos, K., Drosatos-Tampakaki, Z., Khan, R., Homma, S., Schulze, P., Zannis, V., et al. (2011). Inhibition of c-Jun-N-terminal kinase increases cardiac peroxisome proliferator-activated receptor alpha expression and fatty acid oxidation and prevents lipopolysaccharide-induced heart dysfunction. *J. Biol. Chem.* 286, 36331–36339. doi: 10.1074/jbc.M111.272146

Drosatos, K., Khan, R., Trent, C., Jiang, H., Son, N., Blaner, W., et al. (2013). Peroxisome proliferator-activated receptor-γ activation prevents sepsis-related cardiac dysfunction and mortality in mice. *Circ. Heart Fail.* 6, 550–562. doi: 10.1161/circheartfailure.112.000177

Ehrman, R., Sullivan, A., Favot, M., Sherwin, R., Reynolds, C., Abidov, A., et al. (2018). Pathophysiology, echocardiographic evaluation, biomarker findings, and prognostic implications of septic cardiomyopathy: a review of the literature. *Crit. Care* 22:112. doi: 10.1186/s13054-018-2043-8

Hollenberg, S., and Singer, M. (2021). Pathophysiology of sepsis-induced cardiomyopathy. *Nat. Rev. Cardiol.* 18, 424–434. doi: 10.1038/s41569-020-00492-2

Ichinose, F., Buys, E., Neilan, T., Furutani, E., Morgan, J., Jassal, D., et al. (2007). Cardiomyocyte-specific overexpression of nitric oxide synthase 3 prevents myocardial dysfunction in murine models of septic shock. *Circ. Res.* 100, 130–139. doi: 10.1161/01.RES.0000253888.09574.7a

Knudsen, N., Stanya, K., Hyde, A., Chalom, M., Alexander, R., Liou, Y., et al. (2020). Interleukin-13 drives metabolic conditioning of muscle to endurance exercise. *Science* 368:eaat3987. doi: 10.1126/science.aat3987

Makrecka-Kuka, M., Korzh, S., Vilks, K., Vilskersts, R., Cirule, H., Dambrova, M., et al. (2019). Mitochondrial function in the kidney and heart, but not the brain, is mainly altered in an experimental model of endotoxaemia. *Shock* 52, e153–e162. doi: 10.1097/shk.0000000000001315

Ndongson-Dongmo, B., Lang, G., Mece, O., Hechaichi, N., Lajqi, T., Hoyer, D., et al. (2019). Reduced ambient temperature exacerbates SIRS-induced cardiac autonomic dysregulation and myocardial dysfunction in mice. *Basic Res. Cardiol.* 114:26. doi: 10.1007/s00395-019-0734-1

Qian, N., Gao, Y., Wang, J., and Wang, Y. (2021). Emerging role of interleukin-13 in cardiovascular diseases: a ray of hope. *J. Cell. Mol. Med.* 25, 5351–5357. doi: 10.1111/jcmm.16566

Rodriguez-Rodriguez, N., Gogoi, M., and McKenzie, A. (2021). Group 2 innate lymphoid cells: team players in regulating asthma. *Annu. Rev. Immunol.* 39, 167–198. doi: 10.1146/annurev-immunol-110119-091711

Schilling, J., Lai, L., Sambandam, N., Dey, C., Leone, T., and Kelly, D. (2011). Toll-like receptor-mediated inflammatory signaling reprograms cardiac energy metabolism by repressing peroxisome proliferator-activated receptor γ coactivator-1 signaling. *Circ. Heart Fail.* 4, 474–482. doi: 10.1161/circheartfailure.110.959833

Schulze, P., Drosatos, K., and Goldberg, I. (2016). Lipid use and misuse by the heart. *Circ. Res.* 118, 1736–1751. doi: 10.1161/circresaha.116.306842

Sepúlveda, M., Burgos, J., Ciocci Pardo, A., González Arbelaez, L., Mosca, S., and Vila Petroff, M. (2020). CaMKII-dependent ryanodine receptor phosphorylation mediates sepsis-induced cardiomyocyte apoptosis. *J. Cell. Mol. Med.* 24, 9627–9637. doi: 10.1111/jcmm.15470

Snodgrass, R., Benatzy, Y., Schmid, T., Namgaladze, D., Mainka, M., Schebb, N., et al. (2021). Efferocytosis potentiates the expression of arachidonate 15-lipoxygenase (ALOX15) in alternatively activated human macrophages through LXR activation. *Cell Death Differ.* 28, 1301–1316. doi: 10.1038/s41418-020-00652-4

Soraya, H., Masoud, W., Gandhi, M., Garjani, A., and Clanachan, A. (2016). Myocardial mechanical dysfunction following endotoxemia: role of changes in energy substrate metabolism. *Basic Res. Cardiol.* 111:24. doi: 10.1007/s00395-016-0544-7

Venet, F., and Monneret, G. (2018). Advances in the understanding and treatment of sepsis-induced immunosuppression. *Nat. Rev. Nephrol.* 14, 121–137. doi: 10.1038/nrneph.2017.165

Vico, T., Marchini, T., Ginart, S., Lorenzetti, M., Adán Areán, J., Calabró, V., et al. (2019). Mitochondrial bioenergetics links inflammation and cardiac contractility in endotoxemia. *Basic Res. Cardiol.* 114:38. doi: 10.1007/s00395-019-0745-y

Wang, X., Li, X., Liu, S., Brickell, A., Zhang, J., Wu, Z., et al. (2020). PCSK9 regulates pyroptosis via mtDNA damage in chronic myocardial ischemia. *Basic Res. Cardiol.* 115:66. doi: 10.1007/s00395-020-00832-w

Xin, T., and Lu, C. (2020). SirT3 activates AMPK-related mitochondrial biogenesis and ameliorates sepsis-induced myocardial injury. *Aging* 12, 16224–16237. doi: 10.18632/aging.103644

Xu, C., Yi, C., Wang, H., Bruce, I., and Xia, Q. (2012). Mitochondrial nitric oxide synthase participates in septic shock myocardial depression by nitric oxide overproduction and mitochondrial permeability transition pore opening. *Shock* 37, 110–115. doi: 10.1097/SHK.0b013e3182391831

Xu, X., Liu, Q., He, S., Zhao, J., Wang, N., Han, X., et al. (2018). Qiang-Xin 1 formula prevents sepsis-induced apoptosis in murine cardiomyocytes by suppressing endoplasmic reticulum- and mitochondria-associated pathways. *Front. Pharmacol.* 9:818. doi: 10.3389/fphar.2018.00818

Yan, C., Ma, Z., Ma, H., Li, Q., Zhai, Q., Jiang, T., et al. (2020). Mitochondrial transplantation attenuates brain dysfunction in sepsis by driving microglial M2 polarization. *Mol. Neurobiol.* 57, 3875–3890. doi: 10.1007/s12035-020-01994-3

Conflict of Interest: The authors declare that the research was conducted in the absence of any commercial or financial relationships that could be construed as a potential conflict of interest.

Publisher's Note: All claims expressed in this article are solely those of the authors and do not necessarily represent those of their affiliated organizations, or those of the publisher, the editors and the reviewers. Any product that may be evaluated in this article, or claim that may be made by its manufacturer, is not guaranteed or endorsed by the publisher.

Copyright © 2021 Guo, Hong, Zhang, Wei, Jin, Miao, Wang, Zhou, Wang and He. This is an open-access article distributed under the terms of the Creative Commons Attribution License (CC BY). The use, distribution or reproduction in other forums is permitted, provided the original author(s) and the copyright owner(s) are credited and that the original publication in this journal is cited, in accordance with accepted academic practice. No use, distribution or reproduction is permitted which does not comply with these terms.

frontiers in Cell and Developmental Biology

ORIGINAL RESEARCH
published: 20 September 2021
doi: 10.3389/fcell.2021.742662

IL-13 Derived Type 2 Innate Lymphocytes Ameliorates Cardiomyocyte Apoptosis Through STAT3 Signaling Pathway

Ting Hong[1†], Saiqi Li[1†], Xiaoyu Guo[1†], Yazhong Wei[1], Jingjing Zhang[2], Xiaohui Su[2], Miao Zhou[3], Haizhen Jin[4], Qing Miao[5], Lei Shen[2], Minfang Zhu[1] and Bin He[1]**

[1] Department of Critical Care Medicine, Shanghai Chest Hospital, Shanghai Jiao Tong University, Shanghai, China, [2] Shanghai Institute of Immunology, Shanghai Jiao Tong University School of Medicine, Shanghai, China, [3] Department of Anesthesiology and Surgical Intensive Care Unit, Xinhua Hospital, Shanghai Jiaotong University School of Medicine, Shanghai, China, [4] Central Laboratory, Shanghai Chest Hospital, Shanghai Jiao Tong University, Shanghai, China, [5] Departments of Anesthesiology, Shanghai Chest Hospital, Shanghai Jiao Tong University, Shanghai, China

OPEN ACCESS

Edited by:
Zhi Qi,
Nankai University, China

Reviewed by:
Linlin Wang,
Zhejiang University, China
Hui Gong,
Fudan University, China

***Correspondence:**
Bin He
bin_he@sjtu.edu.cn
Minfang Zhu
zhuminfang97@sina.com

[†] These authors have contributed equally to this work and share first authorship

Specialty section:
This article was submitted to Cell Death and Survival, a section of the journal Frontiers in Cell and Developmental Biology

Received: 16 July 2021
Accepted: 30 August 2021
Published: 20 September 2021

Citation:
Hong T, Li S, Guo X, Wei Y, Zhang J, Su X, Zhou M, Jin H, Miao Q, Shen L, Zhu M and He B (2021) IL-13 Derived Type 2 Innate Lymphocytes Ameliorates Cardiomyocyte Apoptosis Through STAT3 Signaling Pathway. Front. Cell Dev. Biol. 9:742662. doi: 10.3389/fcell.2021.742662

The involvement of cardiomyopathy during sepsis means higher mortality and prolonged length of hospital stay. Many efforts have been made to alleviate the apoptosis of cardiomyocytes in sepsis. The huge potential of IL-13 in tissue repair has attracted increasing attention. In the present study, we used LPS-treated mice or primary cardiomyocytes as a sepsis model to explore the anti-apoptotic ability of IL-13. It was found that an increased level of exogenous IL-13 was beneficial to the recovery of heart function in sepsis, and this anti-apoptotic effect of IL-13 was probably through enhancing the phosphorylation of STAT3 Ser727. In addition, we identified that the heart protective effect of IL-13 was associated with type 2 innate lymphocytes (ILC2). All these findings may provide a potential promising treatment for sepsis-induced cardiomyopathy.

Keywords: sepsis, cardiomyocyte apoptosis, IL-13, ILC2, stat3

INTRODUCTION

Although sepsis-induced cardiac injury has been acknowledged as a leading cause of death in the intensive care unit (ICU), there is still limited knowledge about the underlying mechanism (Joseph et al., 2017; Ehrman et al., 2018). It is generally recognized that immoderate and excessive host immune responses play a central role in reducing the reactivity and exacerbating the apoptosis of cardiomyocytes (Kamisoglu et al., 2015; Akama et al., 2021). It is necessary to understand the variability of host immune responses, knowing that it may help decrease apoptosis of cardiomyocytes and develop new strategies for the treatment of sepsis-induced cardiac injury (Zechendorf et al., 2020).

IL-13 is a representative cytokine of type 2 immunity and participates in host protection through promoting tissue repair and controlling inflammation progress (Neill et al., 2010; Gause et al., 2013; Gieseck et al., 2018). IL-13 is a crucial regulator of cardiomyocyte fate by reversing transcription during heart generation, demonstrating the cardiac protection of IL-13 (O'Meara et al., 2015).

Although IL-13 shows great therapeutic potential in the treatment of cardiovascular diseases (Hofmann et al., 2014; Wodsedalek et al., 2019; Zlatanova et al., 2019), the role of IL-13 in protecting the septic cardiomyopathy remains to be further understood.

In this study, we investigated the expression level of IL-13 at different times after intraperitoneal (i.p.) injection of lipopolysaccharide (LPS), knowing that it could simulate endotoxemia during the sepsis state (Ehrman et al., 2018). Subsequently, we explored the protection mechanism of IL-13 in sepsis-induced cardiomyopathy through inhibiting the apoptosis of cardiomyocytes, and found that type 2 innate lymphocyte (ILC2) was the main source of IL-13. These results demonstrated that IL-13 played a significant cardioprotective role in sepsis-induced cardiac injury, which may provide a new remedy for clinical translation.

MATERIALS AND METHODS

Materials and Regents

Materials and reagents used in this study were lipopolysaccharide (LPS), DNase I and collagenase (Sigma, United States); 0.25% trypsin, 0.25% trypsin-EDTA and fetal bovine serum (FBS) (Gibco, United States); Dulbecco's Modified Eagle's Medium (DMEM) and D-Hank's balanced salt solution (D-Hank's) (Cytiva, United States); fluorescence-labeled antibodies (Biolegend, United States; details are listed in **Supplementary Table 1**); ermeabilization buffer, MitoTracker^{TM} Deep Red and DAPI (Invitrogen, United States); antibody of cleaved caspase 3, STAT3, phospho-STAT3 (Tyr705), phospho-STAT3 (Ser727), and β-actin (CST, United States); IL-13 and IL-13Rα1 antibodies (Santa Cruz Biotechnology, United States); primers (BioTNT, China); PVDF membrane (Millipore, United States); reactive oxygen species assay kit (DCFH-DA), red blood cell lysis buffer, cell mitochondria isolation kit and antibody of α-tubulin (Beyotime, China); GentleMACS C tubes (Miltenyi Biotech, United States); *Invivo* anti-CD90.2 (Bioxcell, Italy); FITC-Annexin V (BD, United States); RNA purification kit (EZBioscience, United States).

Cell Culture and Treatment

Primary cardiomyocytes were extracted from the rat hearts as previously described (Hong et al., 2020). In brief, the hearts were isolated from 2-day-old SD rats, washed with D-Hank's, cut into small pieces and incubated with 0.1% trypsin for 15 min to acquire single cardiomyocyte suspension. Then, low-glucose DMEM containing 10% FBS was added to the cardiomyocytes to terminate the digestion. This step is repeated five times until no lumps are visible. Finally, the primary cardiomyocytes were seeded into culture dishes at a density of 3–5 × 10^5 cells mL-1 in low-glucose DMEM containing 10% FBS for further use.

Experiment With the Sepsis-Induced Cardiac Injury Model

Sepsis-induced cardiac injury was established in animal and cell models.

Male C57BL/6 mice weighing 25–28 g (GemPharmatech Co., Jiangsu, China) were raised in a specific pathogen-free (SPF) environment in Shanghai Chest Hospital (Shanghai, China). All experimental procedures were approved and supervised by the Ethics Committee of the said hospital. 20 mg/kg LPS was injected i.p. to C57BL/6 LPS mice to establish LPS-induced cardiac injury.

In the cell model, primary cardiomyocytes were incubated with low-glucose DMEM containing 10% FBS and 10 μg/ml LPS to mimic endotoxin-induced cell damage.

RNA Extraction

RNA was extracted using the RNA purification kit. 40 mg heart tissue was put into a 1.5 ml centrifuge tube and added with 300 μl lysis buffer. Then, the tissue was homogenized in a rotor-stator homogenizer and centrifuged at 12,000 g for 2 min and mixed with an equal volume of ethanol. The mixture was added to the RNA column to bind RNA to the membrane, centrifuged at 4,000 g for 1 min, and after addition of 500 μl wash buffer into the spin column, centrifuged again at 12,000 g for 1 min. The spin column was transferred to a new RNase free tube, to which 20 μl elution buffer was added into the center of spin column at room temperature. Finally, the sample was centrifuged at 12,000 g for 1 min to remove the spin column.

Real-Time RT-PCR

Total RNA extracted from the mice heart was converted to cDNA for quantitative PCR (qPCR) using 4 × Reverse Transcription Master Mix Kits (EZBioscience, United States). The expression level of GAPDH was quantitated as an internal control according to the 2 × SYBR Green qPCR Master Mix (EZBioscience, United States) manufacturer's instructions. The primers used in the work were purchased from BioTNT, Shanghai.

Preparation of the Single-Cell Suspension and Flow Cytometry Analysis

The C57BL/6 mouse hearts were made into single-cell suspension via gentleMACS^{TM} Octo Dissociator for flow cytometry analysis. Briefly, the fresh mouse heart was washed with cold PBS to remove peripheral blood cells and cut into small pieces. The heart tissue was digested in D-Hank's containing 1 mg/ml collagenase II and 10 μg/ml DNase I under the program of 37_mmu Adult Heart Procedure. Then, red blood cells (RBCs) were lysed and washed with cold PBS twice.

After 200 mesh screen filtration, the cells were ready for staining. Firstly, cells were incubated with Live/Dead dye for 15 min at room temperature, surface stained using the standard protocol for 15 min at room temperature, fixed, permeabilized with permeabilization buffer at 4°C overnight, stained with corresponding antibodies for another 30 min, washed with PBS, resuspended in 100 μl PBS, and finally detected by BDFACSFortessa 4-Laser (BD, United States).

Protein Extraction and Western Blotting Assay

Protein extraction and Western blotting were performed as previously described (Virga et al., 2021). Briefly, the protein

sample (30 μg) was electrophoresed in SDS-PAGE and transferred to the PVDF membrane. The blots were incubated with the primary antibody at 4°C overnight, followed by incubation with the HRP-conjugated secondary antibody. The Western blot bands were detected by A6100 ECL imaging system (GE, United States) and quantitated with Image J software by measuring the intensity of each band compared with the internal control band.

Cell Apoptosis Assay

Apoptosis and morphology were detected simultaneously by fluorescence microscopy. Briefly, primary cardiomyocytes were incubated with FITC-labeled Annexin V diluted by the banding buffer at 37°C for 15 min. Then cells were washed with PBS and added with Mitotracker at 37°C for another 30 min. The stained cells were washed with PBS for 3 times and detected.

Deletion of Innate Lymphoid Cells

Innate lymphoid cells (ILCs) of C57BL/6 mice were deleted by i.p. injection of CD90.2 antibody at a dose of 12 mg/kg for 4 times at a 4-day interval. The deletion efficiency of ILC2 was determined by flow cytometry.

Data Analysis and Statistics

All experiments were repeated with three or more biological replicates. Data were analyzed by PRISM software (Graphpad, United States) and presented as the mean ± standard deviation (SD). One-way ANOVA was used to analyze differences between multiple groups and the two-tailed Student's *t*-test was used for comparison between two groups. P-value < 0.05 was considered statistically significant.

RESULTS

IL-13 Underwent Changes in a Time-Dependent Manner After Intraperitoneal Injection of Lipopolysaccharide in Mice

The protein expression of IL-13 in the mouse myocardium was continuously monitored by Western blot within 48 h after i.p. injection of LPS, showing a trend of rapid decline, transient rise and continuous low expression. At the same time, the two type receptors of IL-13, IL-13Rα1, and IL-13Rα2 increase steadily (**Figures 1A,B**). The mRNA of IL-13, and IL-13Rα1 showed similar changes in a time-dependent manner by qPCR (**Figure 1C** and **Supplementary Figure 1**). Although the transcription level of IL-13 increased continuously, the protein expression of IL-13 did not remain at a high level, indicating that IL-13 may be consumed heavily. Lactate dehydrogenase (LDH) and creatine kinase isoenzymes (CK-MB) as markers of myocardial injury were detected in the mouse plasma within 48 h after i.p. injection of LPS. It was found that the time-dependent change of LDH and CK-MB was related to the expression of IL-13 (**Figures 1D,E**). The critical turning point was observed at 12 h after LPS exposure, when the expression of IL-13 protein in the mouse myocardial tissue was reconfirmed to be significantly decreased as shown by immunofluorescence and histochemistry staining (**Figures 1F,G**). In addition, the level of IL-13 in the mouse plasma was also decreased significantly at this time point, suggesting that IL-13 may play an important role in septic cardiomyopathy.

IL-13 Alleviated Lipopolysaccharide-Induced Cardiac Dysfunction and Reduced Apoptosis in Mice

To explore the role of IL-13 in LPS-induced myocardial injury, mice injected i.p. with LPS were treated with recombinant IL-13 (rIL-13, 100 μg/kg). As shown in **Figures 2A,B**, rIL-13 effectively recovered the myocardial contractile function induced by LPS. Specifically, Cardiac output (CO), Ejection fraction (EF), and Fractional shortening (FS) all recovered in varying degrees. These results suggest that IL-13 could improve cardiac function. The production of reactive oxygen species (ROS), which is known to be closely related to myocardial injury, is shown in the images of dihydroethidium (DHE). As shown in **Figures 2D,F**, IL-13 significantly reduced the level of DHE oxidation induced by LPS. Furthermore, the degree of myocardial apoptosis was detected by TUNEL, and the result showed that IL-13 effectively reduced myocardial apoptosis (**Figures 2C,E**).

IL-13 Alleviated Lipopolysaccharide-Induced Cardiomyocyte Apoptosis

To identify the effect of IL-13 on cardiomyocytes, the primary cardiomyocytes were extracted as the experimental object *in vitro*. Firstly, the two receptors of IL-13 were detected by Western blot in the primary myocardium. The results showed that both receptors existed in the primary myocardium and increased upon LPS stimulation, with the increase of IL-13Rα1 more significant (**Figures 3A,B**). The production of reactive oxygen promoted DCFH transformation into DCF, and the mean fluorescence intensity of DCF was measured to represent the level of ROS in primary myocardiocytes. As shown in **Figures 3C,D**, cardiomyocytes ROS production induced by LPS was effectively inhibited by IL-13. Next, apoptosis was detected by flow cytometry. Compared with LPS treatment alone, the apoptosis of primary cardiomyocytes exposed to IL-13 (50 ng/ml) was significantly decreased, involving both early and late stages (**Figures 3E–G**). In the apoptosis process, phosphatidylserine (PS) was translocated from the inner to the outer leaflet of the plasma membrane, thus exposing PS to the external cellular environment. Annexin V labeled with a fluorophore was used to identify apoptotic cells by binding to PS exposed on the outer leaflet. As presented in **Figure 3H**, LPS accelerated PS exposure to the external environment of cells and weakened mitochondrial fluorescence. On the contrary, IL-13 effectively reversed this process.

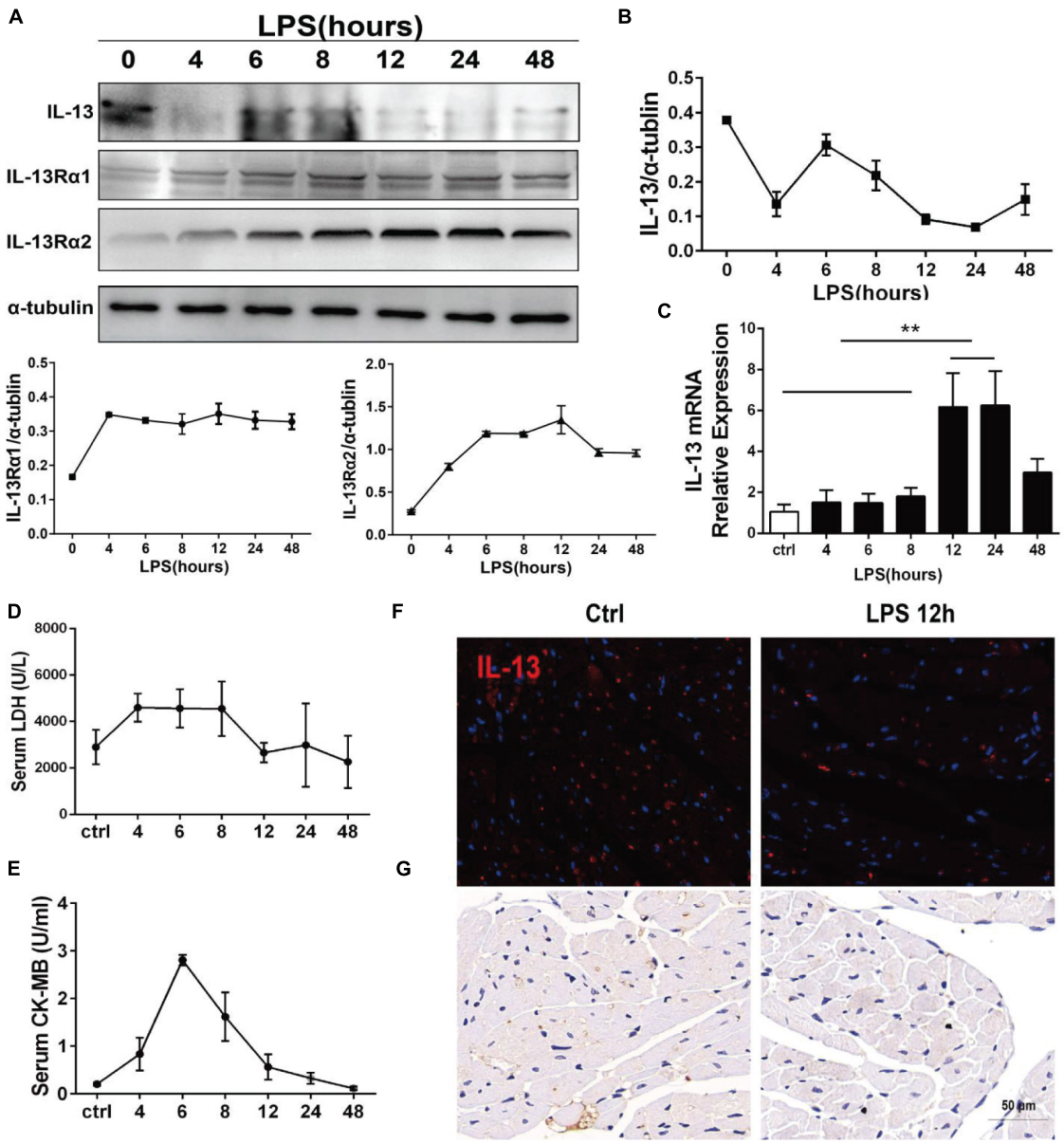

FIGURE 1 | IL-13 underwent changes in a time-dependent change after i.p. injection of LPS in mice. **(A)** Determination of IL-13, IL-13Rα1, and IL-13Rα2 relative expressions in the myocardial tissue by Western blot after i.p. injection of LPS in mice. **(B)** Quantification of **(A)**. **(C)** Detection of mRNA expression of IL-13 in the myocardial tissue by RT-qPCR. **(D)** Serum LDH change. **(E)** Serum CK-MB change. **(F,G)** Immunofluorescence and Immunohistochemical images of IL-13 in the mouse myocardium after 12-h exposure to LPS, Scale bar = 50 μm. All the experiments were repeated three times. Data were expressed as the mean ± SD ($n = 3$). $^{**}p < 0.01$.

The Transcription Level of STAT3 but Not STAT6 Was Altered in the Signaling Pathway Affected by IL-13

Heart tissues of LPS treated or untreated mice were collected for RNA sequence (RNA-seq). Gene Ontology (GO) analysis showed that a number of genes underwent changes in the three fields including the biological process, molecular function and cell composition with sepsis induced via i.p. injection of LPS (**Figure 4A**). The signaling pathways affected by LPS were further analyzed with Kyoto Encyclopedia of Genes and Genomes (KEGG) (**Figure 4B**). To determine the mechanism by which IL-13 reduced myocardial apoptosis caused by LPS, rIL-13 treatment of LPS-induced myocardial tissue in septic mice was included in RNA-seq. Stat6 is a typical transcription factor that mediates downstream transcription activated by IL-13 in immune cells. In other cell types, it is described that Stat3 is activated by Jak signaling downstream of IL-13Rα1. In the mouse myocardium, the Jak-STAT signaling pathway

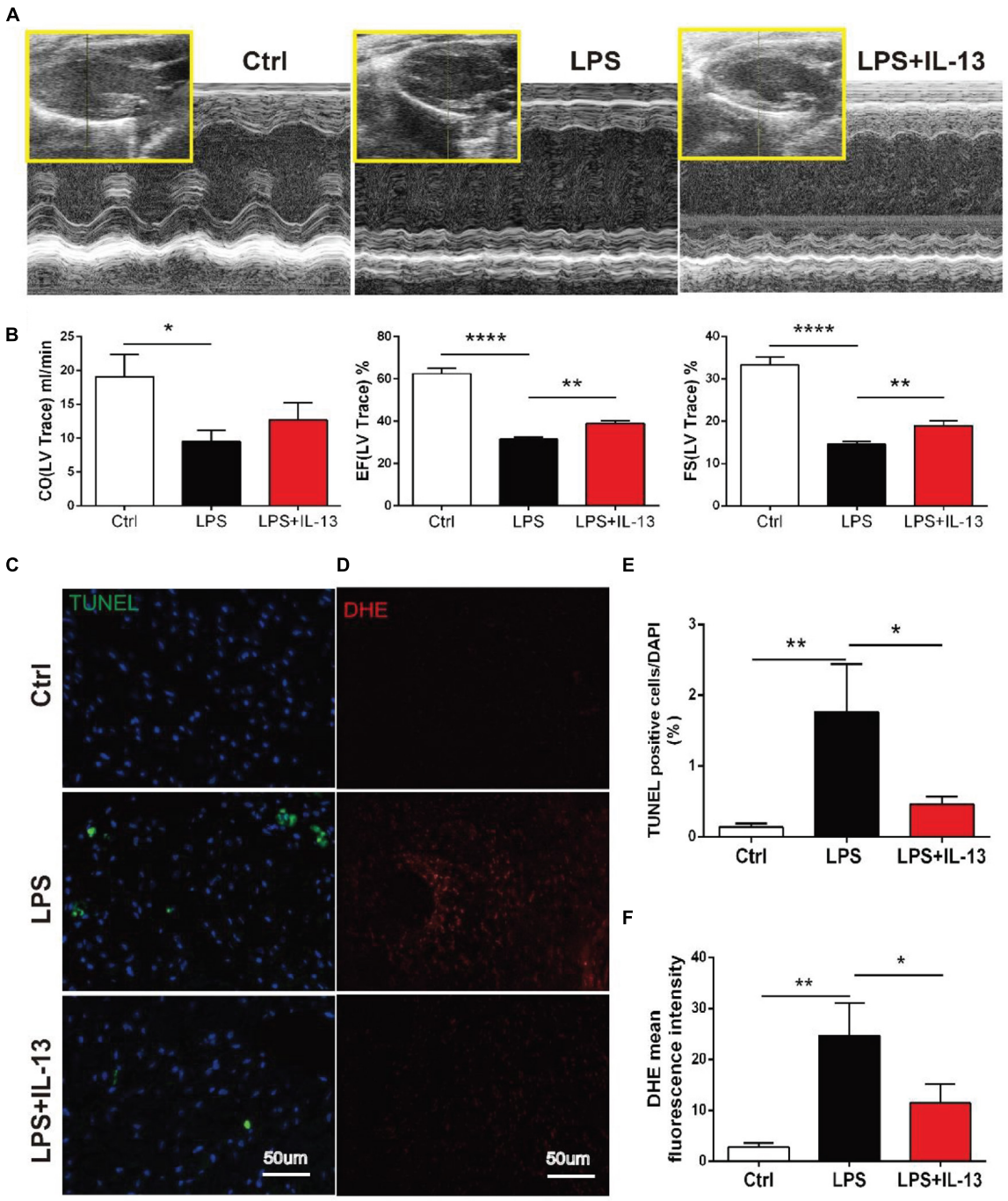

FIGURE 2 | IL-13 alleviated LPS-induced cardiac dysfunction and reduced apoptosis in mice. **(A)** Representative images of M-mode echocardiography. **(B)** Quantification of cardiac output (CO), ejection fraction (EF) and fractional shortening (FS) by echocardiography. **(C)** Representative TUNEL staining in the cardiac tissue, Scale bar = 50 μm. **(D)** Representative images of dihydroethidium (DHE) in the cardiac tissue, Scale bar = 50 μm. **(E)** Percentage of TUNEL-positive nuclei. **(F)** DHE oxidation values represent the mean fluorescent intensity (MFI). Data were expressed as the mean ± SD ($n = 6$). *$p < 0.05$, **$p < 0.01$, ****$p < 0.0001$.

was identified by RNA-seq as being significantly changed after LPS stimulation (**Figure 4B**). As shown in **Figure 4C**, the transcription of IL-13Rα1 and Stat3 was highly expressed under the action of LPS, while the transcription of Stat6 changed slightly, suggesting that IL-13 reduced apoptosis in the myocardial tissue through the transcription factor Stat3. IL-13Rα2 is a decoy receptor, and we did not explore its effect in this study.

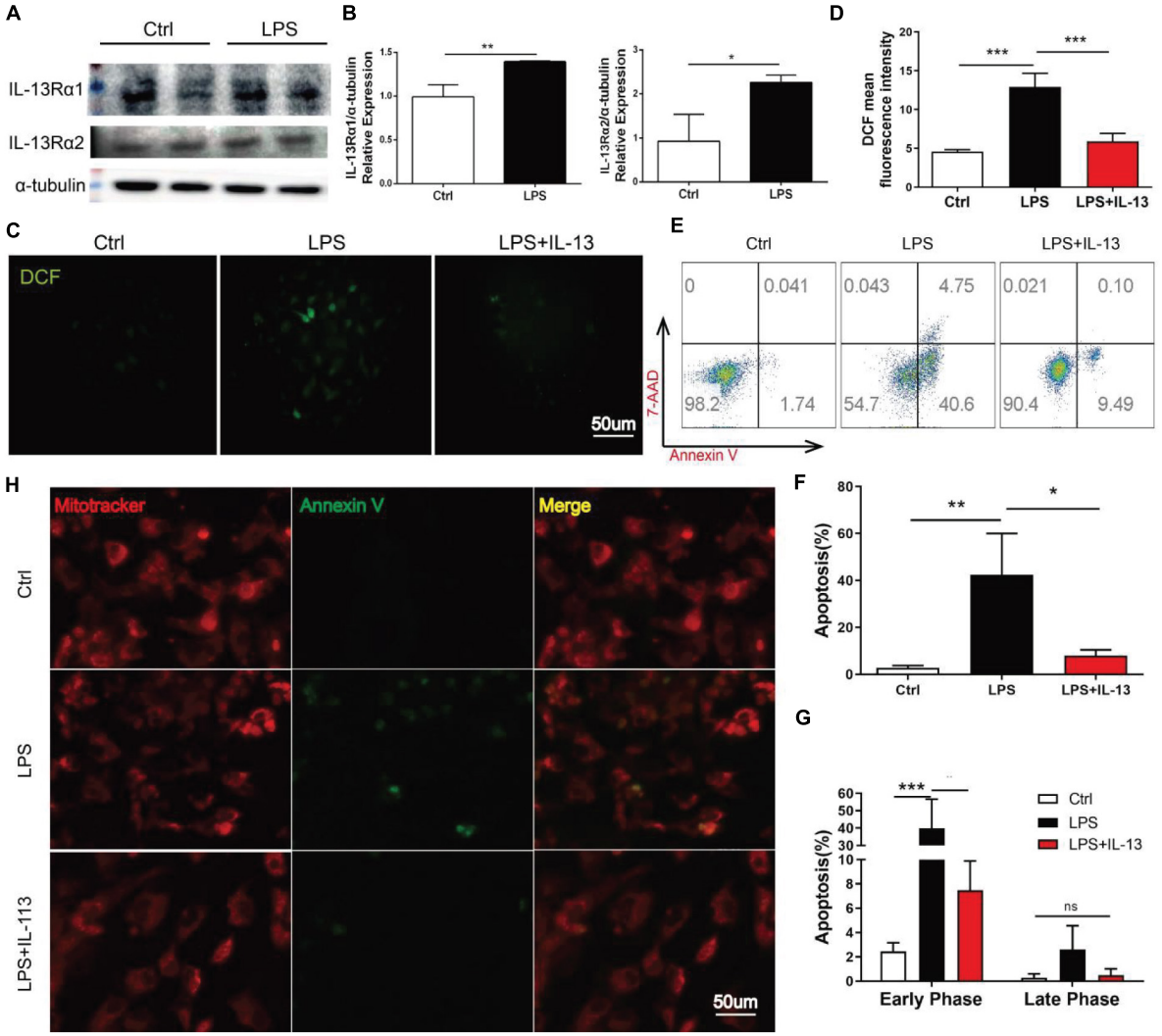

FIGURE 3 | IL-13 alleviated LPS-induced cardiomyocyte apoptosis. **(A)** Determination of IL-13Rα1 and IL-13Rα2 relative expressions in the primary cardiomyocytes by Western blot. **(B)** Quantification of **(A)**. **(C)** DCF fluorescent images, Scale bar = 50 μm. **(D)** DCF mean fluorescent intensity. **(E)** Flow cytometry analysis of apoptosis. **(F,G)** Quantification of apoptosis. **(H)** Cardiomyocytes stained with mitoitrcacker (red) and Annexin V(green), Scale bar = 50 μm. Data were expressed as the mean ± SD (n = 3). *$p < 0.05$, **$p < 0.01$, ***$p < 0.001$.

Effect of IL-13 on the Phosphorylation of STAT3 in Cardiomyocytes

Total protein, cytosol protein and mitochondrial protein were extracted from the primary cardiomyocytes and analyzed by Western blot. It was found that the LPS-induced increase of cleaved Caspase-3 was effectively inhibited by IL-13 (**Figures 5A,B**). Meanwhile, the expression of STAT3 Serine 727 (Ser727) and phosphorylation of STAT3 Tyrosine 705 (Tyr705) were both increased by IL-13. It is worth noting that the phosphorylation level of STAT3 Ser727 in the cytoplasm did not increase after LPS stimulation. In addition, the leakage of cytochrome C from mitochondria was increased after LPS stimulation, and IL-13 reduced this leakage (**Figures 5C,D**). Subsequently, mitochondrial protein expression was further confirmed by Western blot. Phosphorylation of STAT3 Tyr705 was not detected in the protein extracted from mitochondria. However, the phosphorylation of STAT3 Ser727 was increased by IL-13 in the mitochondrion (**Figures 5E,F**).

Change of ILC2 in the Myocardial Tissue After Lipopolysaccharide Treatment Was Correlated With the Change of IL-13

As ILC2 is one of the main sources of IL-13, we detected ILC2 change in the heart of mice treated with LPS by flow cytometry. The mouse heart tissue was first processed into single cells and incubated with fluorescence-labeled antibodies, and then ILC2 was further gated as Lineage-, $CD45^+$, $CD90.2^+$, and $ST2^+$ cell (**Supplementary Figure 3**). As shown in **Figures 6A,B**, the percentage of ILC2 exhibited a time-dependent change, and this trend was similar to that of IL-13. In addition, LPS

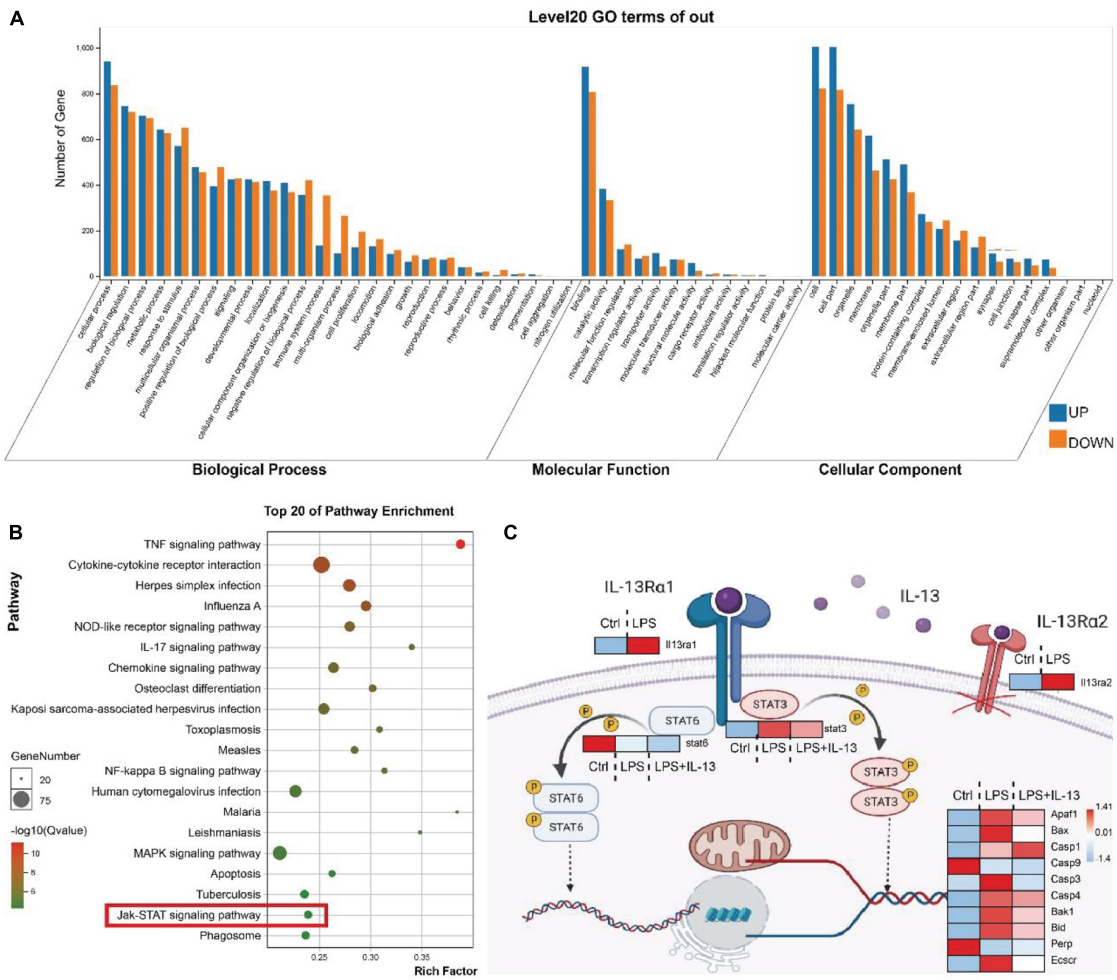

FIGURE 4 | The transcription level of STAT3 but not STAT6 was altered in the signaling pathway affected by IL-13. **(A)** GO analysis covered three domains including the biological process, molecular function and cellular component. The transcription of the heart tissue in mice receiving i.p. injection of LPS vs. control mice. **(B)** KEGG analysis revealed the most important signaling pathways involved in gene involvement. The transcription of the heart tissue of mice receiving i.p. injection of LPS vs. control mice. **(C)** Illustration of the downstream key genes in the heart tissue regulated by IL-13 as shown by RNA sequencing (RNA-seq). Data are presented as heatmap (log_2-fold change). Red indicates higher expression, and blue indicates lower expression (n = 6).

increased IL-13 positive ILC2 in the heart (**Figures 6C,D**). ILC2 is a CD3 negative T cell, and IL-13 in the heart appeared to be mainly derived from CD3 negative cells (**Figure 6E**). After treating the mice with CD90.2 antibody, ILC2 in the heart was almost completely eliminated (**Figure 6F**). At the same time, IL-13 of the myocardial tissue was almost cleared (**Figures 6G,H**). Interestingly, after ILC2 was cleared with CD90.2 antibody, not only IL-13 was reduced but the phosphorylation of STAT3 Ser727 was also inhibited. In contrast, the phosphorylation of STAT3 Tyr705 was enhanced by LPS (**Supplementary Figure 4**).

DISCUSSION

During sepsis, activation of type 1 immune response leads to the release of abundant cytokines, which is recognized as the common feature of sepsis, known as "cytokine storm" (Virga et al., 2021). Intriguingly, activation of anti-inflammatory type 2 immune response can antagonize proinflammatory type 1 immunity (Verhoef et al., 2019). A retrospective study observed that pre-existing type 2 immune activation could prevent the progression of sepsis (Krishack et al., 2017). Type 2 immunity is commonly observed in tissues repair and allergic inflammation as represented by the production of type 2 cytokines such as IL-4, IL-5, IL-9, and IL-13 (Flayer et al., 2021). Lai et al. showed that IL-9 derived from ILC2 mediated type 2 immune response and reduced inflammation following sepsis (Lai et al., 2018). In addition, IL-33, IL-13, and IL-5 have also been reported to prevent acute lung injury during sepsis (Linch et al., 2012; Nascimento et al., 2017; Califano et al., 2018). There is evidence that the protective effects of these type 2 cytokines are related to ILC2. The aim of the present study was to explore the effect of IL-13 on the heart during sepsis.

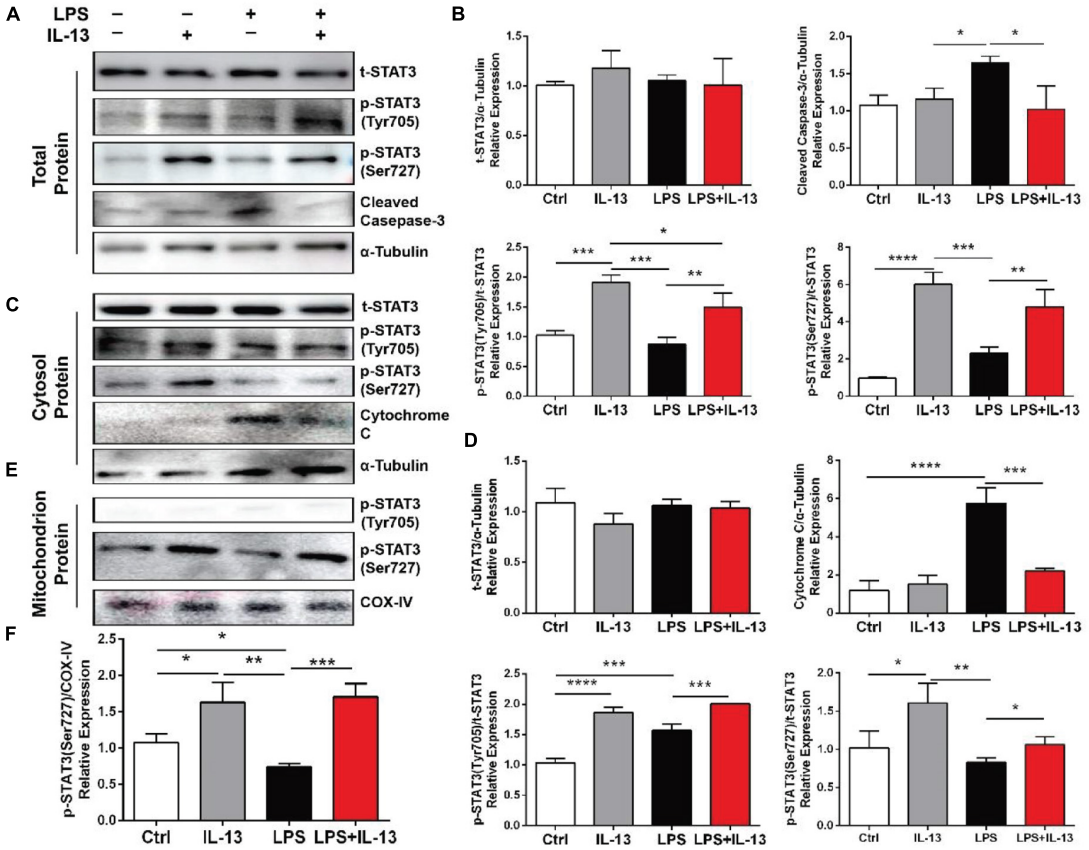

FIGURE 5 | Effect of IL-13 on the phosphorylation of STAT3 in cardiomyocytes. **(A)** Western blot images of total protein expression. **(B)** Quantification of **(A)**. **(C)** Western blot images of the cytosol protein expression. **(D)** Quantification of **(C)**. **(E)** Western blot images of the mitochondrial protein expression. **(F)** Quantification of **(C)**. Data are expressed as the mean ± SD (n = 3). *$p < 0.05$, **$p < 0.01$, ***$p < 0.001$, ****$p < 0.0001$.

IL-13 has been extensively studied as a classic type 2 cytokine for its effect on immune cells, and the direct effect of IL-13 on target tissue cells has also been explored more recently (Heredia et al., 2013; Wynn, 2015). Some studies reported that IL-13 level was increased after sepsis, while other studies argued that IL-13 was decreased after sepsis (Matsukawa et al., 2000; Akama et al., 2021). The possible reason for this discrepancy is that the specific time points of concern may be different between these studies. A more unified view is that IL-13 plays a protective role during sepsis. In the present study, we detected the expression level of IL-13 in the heart after sepsis over time and found that the expression of IL-13 was not simply a phenomenon of increase or decrease in the early stages of sepsis. Besides, unlike protein expression, the transcription level of IL-13 has always been increased. We found that the serum markers of myocardial injury were noted to return to the normal level 12 h after sepsis, when IL-13 transcription was further enhanced but protein expression was decreased. A possible explanation is that IL-13 is over-consumed. The results of this study showed that IL-13 protected cardiomyocytes against apoptosis during sepsis. IL-13 is known to polarize macrophages toward M2 phenotype, and this effect is beneficial to the survival of cardiomyocytes. To determine whether IL-13 had a direct effect on cardiomyocytes, primary cardiomyocytes were studied *in vitro*. The results showed that IL-13 directly inhibited cardiomyocyte apoptosis caused by LPS.

IL-13 is generally considered to function by activating STAT3 or STAT6 (Yu et al., 2018). However, our RNA-seq showed that Stat6 was not significantly changed in the myocardial tissue. STAT6 signaling has been described as transient in the field of heart research, whereas STAT3 activation is required for cardiomyocytes in response to injury (Fang et al., 2013). In this work, the treatment of rIL-13 did increase the phosphorylation of STAT3 and reduced the pro-apoptotic activity of cleaved-Caspase-3. However, the phosphorylation of STAT3 ser727 did not increase correspondingly in the cytosol. Cytochrome C plays a vital role in the mitochondrial electron transport chain in normal cells (Kalpage et al., 2019). It is reported that Cytochrome C in the cytosol resulted in a positive-feedback mechanism, causing more Cytochrome C release and activation of apoptosis (Li et al., 2000). Thus, the phenomenon that IL-13 suppressed cytochrome C in the cytosol attracted our attention. We hypothesized that the phosphorylated STAT3 Ser727 was transferred into the mitochondrion. The result of our experiment demonstrated that phosphorylated STAT3 Ser727 in mitochondria was increased by IL-13. At the same time, phosphorylated STAT3 Tyr705 was almost undetectable. Previous studies showed that the activation of STAT3 protected

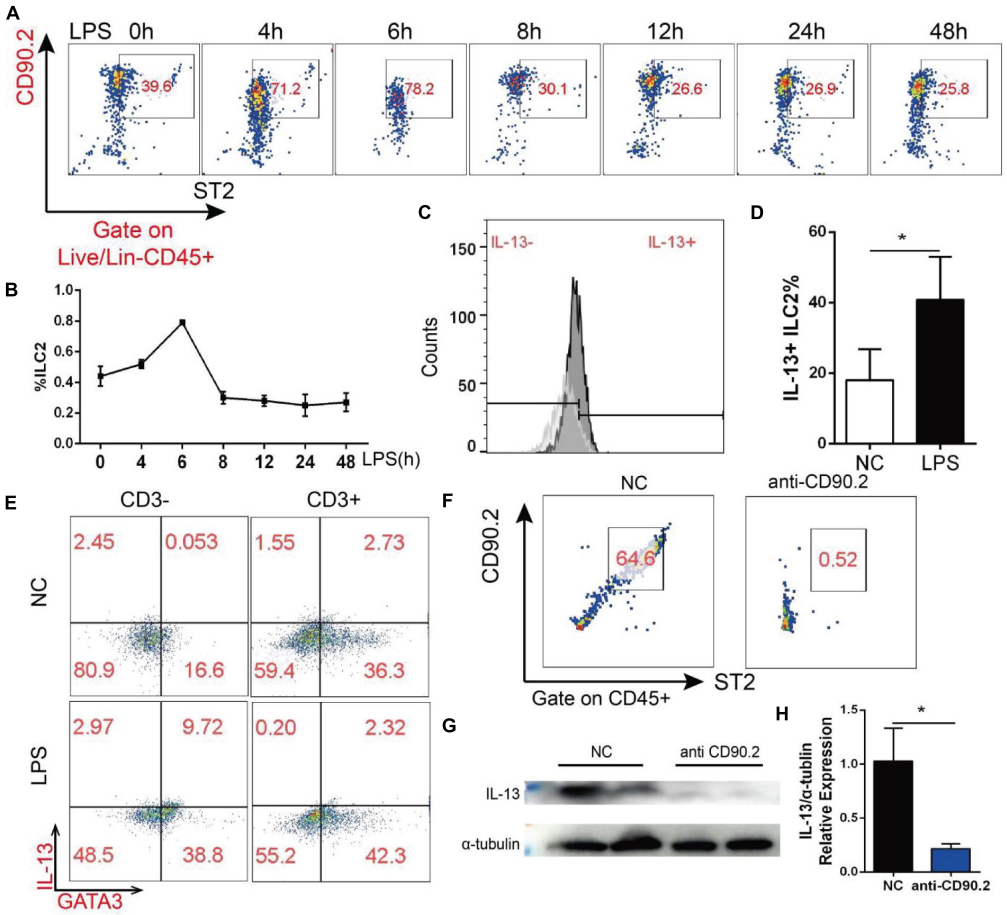

FIGURE 6 | ILC2 change in the myocardial tissue after LPS treatment was correlated with the change of IL-13. **(A)** Change of ILC2 in the myocardial tissue after LPS treatment. **(B)** Quantification of **(A)**. **(C)** Change of IL-13 positive ILC2 in the myocardial tissue of mice treated with LPS. **(D)** Quantification of **(B)**. **(E)** IL-13 secreted by CD3-negative or CD3-positive T cells; **(F)** CD90.2 antibody depletion efficiency of ILC2. **(G)** Expression of IL-13 in the myocardial tissue of mice after CD90.2 antibody treatment. **(H)** Quantification of **(G)**. Data were expressed as the mean ± SD ($n = 3$). $^*p < 0.05$.

cardiomyocytes against apoptosis (Wang et al., 2020). This study supports the protective effect of IL-13 on the myocardium to a certain extent based on the activation of STAT3.

As one of the main sources of IL-13, ILC2 is recognized in tissue repair and macrophage activation (Neill et al., 2010; Guo et al., 2012). However, few studies have focused on the source of IL-13 in the heart. Therefore, multi-label flow cytometry was applied to determine the source of IL-13 in the heart. According to the description of previous studies (Meyer et al., 2020), we applied CD90.2 antibody *in vivo* to eliminate ILC2 and found that IL-13 decreased drastically after eliminating ILC2. Based on these results, the main source of IL-13 in the heart is determined to be ILC2.

The *in vivo* application of CD90.2 antibody not only eliminates ILC2 and reduces IL-13 but directly reduces phosphorylated STAT3 Ser727. Combined with the results of the *in vitro* molecular experiments, it is supported that IL-13 activates the phosphorylation of STAT3 Ser727 to exert anti-apoptotic effects.

In summary, our investigations have demonstrated the importance of IL-13 in alleviating myocardial apoptosis caused by sepsis. IL-13 increases the phosphorylation of STAT3 Ser727 and transfers it into the mitochondria, and reduces the release of cytochrome C. In addition, IL-13 in the heart is derived from ILC2, and the absence of ILC2 will make this protective effect disappear. All these results suggest that IL-13 has therapeutic potential in cardiomyopathy caused by sepsis.

DATA AVAILABILITY STATEMENT

The original contributions presented in the study are included in the article/**Supplementary Material**, further inquiries can be directed to the corresponding author/s.

ETHICS STATEMENT

The animal study was reviewed and approved by Ethics Committee of Shanghai Chest Hospital.

AUTHOR CONTRIBUTIONS

TH, SL, and XG conducted the experiments. YW, JZ, and XS analyzed the data. MiaZ wrote the manuscript. HJ, QM, and LS designed the manuscript. MinZ and BH designed the methodology and supervised the study. All authors contributed to the article and approved the submitted version.

FUNDING

This work was financially supported through grants from the National Natural Science Foundation of China (Nos. 82072199 and 82172168), the Clinical Research Plan of Shanghai Hospital Development Center (No. SHDC2020CR3084B), the Shanghai Collaborative Innovation Center for Translational Medicine Fund (No. TM202013), and the Translational Medicine Cross Research Fund of Shanghai Jiao Tong University (Nos. ZH2018ZDB01, YG2021QN124, and YG2021ZD27).

SUPPLEMENTARY MATERIAL

The Supplementary Material for this article can be found online at: https://www.frontiersin.org/articles/10.3389/fcell.2021.742662/full#supplementary-material

REFERENCES

Akama, Y., Park, E. J., Satoh-Takayama, N., Gaowa, A., Ito, A., Kawamoto, E., et al. (2021). Sepsis induces deregulation of IL-13 production and PD-1 expression in lung group 2 innate lymphoid cells. *Shock* 55, 357–370. doi: 10.1097/shk.0000000000001647

Califano, D., Furuya, Y., Roberts, S., Avram, D., McKenzie, A. N. J., and Metzger, D. W. (2018). IFN-γ increases susceptibility to influenza a infection through suppression of group II innate lymphoid cells. *Mucosal Immunol.* 11, 209–219. doi: 10.1038/mi.2017.41

Ehrman, R. R., Sullivan, A. N., Favot, M. J., Sherwin, R. L., Reynolds, C. A., Abidov, A., et al. (2018). Pathophysiology, echocardiographic evaluation, biomarker findings, and prognostic implications of septic cardiomyopathy: a review of the literature. *Crit. Care* 22:112. doi: 10.1186/s13054-018-2043-8

Fang, Y., Gupta, V., Karra, R., Holdway, J. E., Kikuchi, K., and Poss, K. D. (2013). Translational profiling of cardiomyocytes identifies an early Jak1/Stat3 injury response required for zebrafish heart regeneration. *Proc. Natl. Acad. Sci. U.S.A.* 110, 13416–13421. doi: 10.1073/pnas.1309810110

Flayer, C. H., Perner, C., and Sokol, C. L. (2021). A decision tree model for neuroimmune guidance of allergic immunity. *Immunol. Cell Biol.* doi: 10.1111/imcb.12486 [Epub ahead of print].

Gause, W. C., Wynn, T. A., and Allen, J. E. (2013). Type 2 immunity and wound healing: evolutionary refinement of adaptive immunity by helminths. *Nat. Rev. Immunol.* 13, 607–614. doi: 10.1038/nri3476

Gieseck, R. L. III, Wilson, M. S., and Wynn, T. A. (2018). Type 2 immunity in tissue repair and fibrosis. *Nat. Rev. Immunol.* 18, 62–76. doi: 10.1038/nri.2017.90

Guo, L., Junttila, I. S., and Paul, W. E. (2012). Cytokine-induced cytokine production by conventional and innate lymphoid cells. *Trends Immunol.* 33, 598–606. doi: 10.1016/j.it.2012.07.006

Heredia, J. E., Mukundan, L., Chen, F. M., Mueller, A. A., Deo, R. C., Locksley, R. M., et al. (2013). Type 2 innate signals stimulate fibro/adipogenic progenitors to facilitate muscle regeneration. *Cell* 153, 376–388. doi: 10.1016/j.cell.2013.02.053

Hofmann, U., Knorr, S., Vogel, B., Weirather, J., Frey, A., Ertl, G., et al. (2014). Interleukin-13 deficiency aggravates healing and remodeling in male mice after experimental myocardial infarction. *Circ. Heart Fail.* 7, 822–830. doi: 10.1161/circheartfailure.113.001020

Hong, T., Wei, Y., Xue, X., Li, Y., Dong, H., Guo, X., et al. (2020). A novel anti-coagulative nanocomplex in delivering miRNA-1 inhibitor against microvascular obstruction of myocardial infarction. *Adv. Healthc. Mater.* 9:e1901783. doi: 10.1002/adhm.201901783

Joseph, L. C., Kokkinaki, D., Valenti, M. C., Kim, G. J., Barca, E., Tomar, D., et al. (2017). Inhibition of NADPH oxidase 2 (NOX2) prevents sepsis-induced cardiomyopathy by improving calcium handling and mitochondrial function. *JCI Insight* 2:e94248. doi: 10.1172/jci.insight.94248

Kalpage, H. A., Bazylianska, V., Recanati, M. A., Fite, A., Liu, J., Wan, J., et al. (2019). Tissue-specific regulation of cytochrome c by post-translational modifications: respiration, the mitochondrial membrane potential, ROS, and apoptosis. *FASEB J.* 33, 1540–1553. doi: 10.1096/fj.201801417R

Kamisoglu, K., Haimovich, B., Calvano, S. E., Coyle, S. M., Corbett, S. A., Langley, R. J., et al. (2015). Human metabolic response to systemic inflammation: assessment of the concordance between experimental endotoxemia and clinical cases of sepsis/SIRS. *Crit. Care* 19:71. doi: 10.1186/s13054-015-0783-2

Krishack, P. A., Wang, K., Rzhetsky, A., Solway, J., Sperling, A. I., and Verhoef, P. A. (2017). Preexisting type 2 immune activation protects against the development of sepsis. *Am. J. Respir. Cell Mol. Biol.* 57, 628–630. doi: 10.1165/rcmb.2017-0277LE

Lai, D., Tang, J., Chen, L., Fan, E., Scott, M., Li, Y., et al. (2018). Group 2 innate lymphoid cells protect lung endothelial cells from pyroptosis in sepsis. *Cell Death Dis.* 9:369. doi: 10.1038/s41419-018-0412-5

Li, K., Li, Y., Shelton, J. M., Richardson, J. A., Spencer, E., Chen, Z. J., et al. (2000). Cytochrome c deficiency causes embryonic lethality and attenuates stress-induced apoptosis. *Cell* 101, 389–399. doi: 10.1016/s0092-8674(00)80849-1

Linch, S. N., Danielson, E. T., Kelly, A. M., Tamakawa, R. A., Lee, J. J., and Gold, J. A. (2012). Interleukin 5 is protective during sepsis in an eosinophil-independent manner. *Am. J. Respir. Crit. Care Med.* 186, 246–254. doi: 10.1164/rccm.201201-0134OC

Matsukawa, A., Hogaboam, C. M., Lukacs, N. W., Lincoln, P. M., Evanoff, H. L., Strieter, R. M., et al. (2000). Expression and contribution of endogenous IL-13 in an experimental model of sepsis. *J. Immunol.* 164, 2738–2744. doi: 10.4049/jimmunol.164.5.2738

Meyer, A. R., Engevik, A. C., Madorsky, T., Belmont, E., Stier, M. T., Norlander, A. E., et al. (2020). Group 2 innate lymphoid cells coordinate damage response in the stomach. *Gastroenterology* 159, 2077–2091.e8. doi: 10.1053/j.gastro.2020.08.051

Nascimento, D. C., Melo, P. H., Piñeros, A. R., Ferreira, R. G., Colón, D. F., Donate, P. B., et al. (2017). IL-33 contributes to sepsis-induced long-term immunosuppression by expanding the regulatory T cell population. *Nat. Commun.* 8:14919. doi: 10.1038/ncomms14919

Neill, D. R., Wong, S. H., Bellosi, A., Flynn, R. J., Daly, M., Langford, T. K., et al. (2010). Nuocytes represent a new innate effector leukocyte that mediates type-2 immunity. *Nature* 464, 1367–1370. doi: 10.1038/nature08900

O'Meara, C. C., Wamstad, J. A., Gladstone, R. A., Fomovsky, G. M., Butty, V. L., Shrikumar, A., et al. (2015). Transcriptional reversion of cardiac myocyte fate during mammalian cardiac regeneration. *Circ. Res.* 116, 804–815. doi: 10.1161/circresaha.116.304269

Verhoef, P. A., Bhavani, S. V., Carey, K. A., and Churpek, M. M. (2019). Allergic immune diseases and the risk of mortality among patients hospitalized for acute infection. *Crit. Care Med.* 47, 1735–1742. doi: 10.1097/ccm.0000000000004020

Virga, F., Cappellesso, F., Stijlemans, B., Henze, A. T., Trotta, R., Van Audenaerde, J., et al. (2021). Macrophage miR-210 induction and metabolic reprogramming in response to pathogen interaction boost life-threatening inflammation. *Sci. Adv.* 7:eabf0466. doi: 10.1126/sciadv.abf0466

Wang, Q., Zhu, Q., Ye, Q., Wang, J., Dong, Q., Chen, Y., et al. (2020). STAT3 suppresses cardiomyocytes apoptosis in CVB3-induced myocarditis via survivin. *Front. Pharmacol.* 11:613883. doi: 10.3389/fphar.2020.613883

Wodsedalek, D. J., Paddock, S. J., Wan, T. C., Auchampach, J. A., Kenarsary, A., Tsaih, S. W., et al. (2019). IL-13 promotes in vivo neonatal cardiomyocyte cell cycle activity and heart regeneration. *Am. J. Physiol. Heart Circ. Physiol.* 316, H24–H34. doi: 10.1152/ajpheart.00521.2018

Wynn, T. A. (2015). Type 2 cytokines: mechanisms and therapeutic strategies. *Nat. Rev. Immunol.* 15, 271–282. doi: 10.1038/nri3831

Yu, Q. N., Guo, Y. B., Li, X., Li, C. L., Tan, W. P., Fan, X. L., et al. (2018). ILC2 frequency and activity are inhibited by glucocorticoid treatment via STAT pathway in patients with asthma. *Allergy* 73, 1860–1870. doi: 10.1111/all.13438

Zechendorf, E., O'Riordan, C. E., Stiehler, L., Wischmeyer, N., Chiazza, F., Collotta, D., et al. (2020). Ribonuclease 1 attenuates septic cardiomyopathy and cardiac apoptosis in a murine model of polymicrobial sepsis. *JCI Insight* 5:e131571. doi: 10.1172/jci.insight.131571

Zlatanova, I., Pinto, C., Bonnin, P., Mathieu, J. R. R., Bakker, W., Vilar, J., et al. (2019). Iron regulator hepcidin impairs macrophage-dependent cardiac repair after injury. *Circulation* 139, 1530–1547. doi: 10.1161/circulationaha.118.034545

Conflict of Interest: The authors declare that the research was conducted in the absence of any commercial or financial relationships that could be construed as a potential conflict of interest.

Publisher's Note: All claims expressed in this article are solely those of the authors and do not necessarily represent those of their affiliated organizations, or those of the publisher, the editors and the reviewers. Any product that may be evaluated in this article, or claim that may be made by its manufacturer, is not guaranteed or endorsed by the publisher.

Copyright © 2021 Hong, Li, Guo, Wei, Zhang, Su, Zhou, Jin, Miao, Shen, Zhu and He. This is an open-access article distributed under the terms of the Creative Commons Attribution License (CC BY). The use, distribution or reproduction in other forums is permitted, provided the original author(s) and the copyright owner(s) are credited and that the original publication in this journal is cited, in accordance with accepted academic practice. No use, distribution or reproduction is permitted which does not comply with these terms.

frontiers in Cell and Developmental Biology

REVIEW
published: 20 September 2021
doi: 10.3389/fcell.2021.742483

Fundamental Mechanisms of the Cell Death Caused by Nitrosative Stress

Fulin Wang[1,2,3,4,5†], Qiuhuan Yuan[1,2,3,4,5†], Fengying Chen[6], Jiaojiao Pang[1,2,3,4,5], Chang Pan[1,2,3,4,5], Feng Xu[1,2,3,4,5*] and Yuguo Chen[1,2,3,4,5*]*

[1] Department of Emergency Medicine, Qilu Hospital, Shandong University, Jinan, China, [2] Chest Pain Center, Qilu Hospital, Shandong University, Jinan, China, [3] Shandong Provincial Clinical Research Center for Emergency and Critical Care Medicine, Institute of Emergency and Critical Care Medicine of Shandong University, Qilu Hospital, Shandong University, Jinan, China, [4] Key Laboratory of Emergency and Critical Care Medicine of Shandong Province, Key Laboratory of Cardiopulmonary-Cerebral Resuscitation Research of Shandong Province, Shandong Provincial Engineering Laboratory for Emergency and Critical Care Medicine, Qilu Hospital, Shandong University, Jinan, China, [5] The Key Laboratory of Cardiovascular Remodeling and Function Research, Chinese Ministry of Education, Chinese Ministry of Health and Chinese Academy of Medical Sciences, The State and Shandong Province Joint Key Laboratory of Translational Cardiovascular Medicine, Qilu Hospital, Shandong University, Jinan, China, [6] Emergency Department, The Affiliated Hospital of Inner Mongolia Medical University, Hohhot, China

OPEN ACCESS

Edited by:
Zhi Qi,
Nankai University, China

Reviewed by:
Heng Ma,
Fourth Military Medical University, China
Jinwei Tian,
The Second Affiliated Hospital of Harbin Medical University, China

***Correspondence:**
Feng Xu
xufengsdu@126.com
Yuguo Chen
chen919085@sdu.edu.cn
Fengying Chen
fychen627@sohu.com

† These authors have contributed equally to this work

Specialty section:
This article was submitted to Cell Death and Survival, a section of the journal Frontiers in Cell and Developmental Biology

Received: *16 July 2021*
Accepted: *19 August 2021*
Published: *20 September 2021*

Citation:
Wang F, Yuan Q, Chen F, Pang J, Pan C, Xu F and Chen Y (2021) Fundamental Mechanisms of the Cell Death Caused by Nitrosative Stress. Front. Cell Dev. Biol. 9:742483. doi: 10.3389/fcell.2021.742483

Nitrosative stress, as an important oxygen metabolism disorder, has been shown to be closely associated with cardiovascular diseases, such as myocardial ischemia/reperfusion injury, aortic aneurysm, heart failure, hypertension, and atherosclerosis. Nitrosative stress refers to the joint biochemical reactions of nitric oxide (NO) and superoxide (O_2^-) when an oxygen metabolism disorder occurs in the body. The peroxynitrite anion ($ONOO^-$) produced during this process can nitrate several biomolecules, such as proteins, lipids, and DNA, to generate 3-nitrotyrosine (3-NT), which further induces cell death. Among these, protein tyrosine nitration and polyunsaturated fatty acid nitration are the most studied types to date. Accordingly, an in-depth study of the relationship between nitrosative stress and cell death has important practical significance for revealing the pathogenesis and strategies for prevention and treatment of various diseases, particularly cardiovascular diseases. Here, we review the latest research progress on the mechanisms of nitrosative stress-mediated cell death, primarily involving several regulated cell death processes, including apoptosis, autophagy, ferroptosis, pyroptosis, NETosis, and parthanatos, highlighting nitrosative stress as a unique mechanism in cardiovascular diseases.

Keywords: nitrosative stress, peroxynitrite, reactive nitrogen species, cell death, nitric oxide, cardiovascular diseases

INTRODUCTION

Cell death is a manifestation of the irreversible cessation and end of life, which occurs widely during development and pathological processes (Fricker et al., 2018; Green, 2019). Recent studies have shown that nitrosative stress plays an important role in the pathophysiological processes of cell death. Under physiological conditions, low-level nitrosative stress can be detected in almost all cells *in vivo*, including cardiomyocytes, endothelial cells, fibroblasts, mesenchymal stem cells, and vascular smooth muscle cells (Brunner and Wolkart, 2003; Borbely et al., 2005; Steinberg, 2013). However, little is known about nitrosative stress in pathological conditions and the degree to which nitrosative stress changes the structure and function of cells. Furthermore, the type of cell death

caused by stress is also less known. Additionally, what we still have to prove is that nitrosative stress and not other stresses related to oxygen metabolism disorders affects cell death. This review focuses on the biochemistry of nitrosative stress, as well as several new forms of cell death, and highlights its role in cell death, which provides important clues for studying the mechanism of cell death-related diseases (**Table 1**).

Nitrosative Stress

There are various oxygen metabolism disorders in human body, including hypoxia (West, 2017), oxidative stress (Sohal and Allen, 1990), nitrosative stress (Lim, 2019), endoplasmic reticulum stress (ERS) (Marciniak and Ron, 2006), mitochondria dysfunction (Rowlands, 2016), and carbonyl stress (Suzuki et al., 2001; Miyata and de Strihou, 2010), which are listed in **Table 2**. Nitrosative stress is closely associated with oxidative stress. Reactive oxygen species (ROS), such as the superoxide anion (O_2^-), singlet oxygen ($^1O_2$), hydroxyl radical (OH), hydrogen peroxide (H_2O_2), peroxynitrite anion ($ONOO^-$), and nitric oxide (NO), which are involved in oxidative stress, overlap with the formation and scavenging pathways of reactive nitrogen species (RNS) and regulate each other reciprocally (Espey et al., 2000; Maes et al., 2011). The $ONOO^-$ produced can nitrate several biomolecules, including proteins, lipids, and DNA, to generate 3-nitrotyrosine (3-NT). The most important characteristic of nitrosative stress is tyrosine nitration. Protein nitration modification is a post-translational modification of proteins caused by their interaction with RNS/ROS (Ischiropoulos, 2003; Velsor et al., 2003). In recent years, various studies have shown that the formation of 3-NT is a specific biomarker of nitrosative stress. It can be used to monitor the intracellular production and localization of $ONOO^-$ and the severity of cell death (Ahsan, 2013; Zhang and Wei, 2013).

A Brief History and the Biochemistry of Nitrosative Stress

Ohshima et al. (1990) reported the detection of 3-NT and 3-nitrophenylacetic acid in human urine and proposed that 3-NT could be used as a marker for endogenous protein nitration. In 1992, the Beckman group confirmed that $ONOO^-$ can promote the nitrification of proteins such as superoxide dismutase (SOD) and CuZnSOD *in vitro* and proposed that endogenous nitrifiers can cause protein nitrification in the body (Ischiropoulos et al., 1992). Thereafter, Beckman proposed the use of the antibody method to identify nitrifying proteins and confirmed their existence in human atherosclerotic lesions and acute respiratory distress syndrome lung tissues using the immunohistochemical method (Ye et al., 1996). Subsequently, increasing studies have focused on protein tyrosine nitration from biochemical and biomedical standpoints. As extensive studies have been carried out on protein nitration in nitrosative stress injury, we primarily reviewed the biological characteristics of protein nitration. Multiple pathways can lead to protein nitration, among which $ONOO^-$ and NO_2^-/H_2O_2/heme peroxidase are considered the most important pathways (Herold, 2004). The process by which NO and O_2^- produce $ONOO^-$ is irreversible and does not require enzyme catalysis. The protein nitration pathways induced by $ONOO^-$ can be broadly divided into three categories: direct redox reactions, reactions with carbon dioxide (CO_2), and homolysis after protonation (Alvarez and Radi, 2003; **Figure 1A**). Protein nitration *via* the NO_2^-/H_2O_2/heme peroxidase system also involves the formation of oxygen radicals (Bian et al., 2003; **Figure 1B**).

The Meaning of Nitrosative Stress

Nitrosative stress can promote protein tyrosine nitration, resulting in lipid peroxidation, DNA strand breaks, cell membrane damage, the inactivation of functional enzymes, and activation of cascade signal responses of cell death. Based on these basic biological functions, nitrosative stress affects diseases through various processes such as signal transduction in cells, mitochondrial energy metabolism, messenger ribonucleic acid transcription, protein post-translational modification, and ion channel function (Nobrega et al., 2019; Schiattarella et al., 2019; Paulus, 2020).

Cell Death

Cell death is defined by the phenomenon of the irreversible cessation of life, which is one of the leading causes of treatment failure and death in multiple diseases. The process of cell death comprises many steps, and the mechanism is complicated and has become the focus of life science and medical research (Chen et al., 2020). With the deepening of research, new progress has been made on the formation and mechanisms of cell death. To date, there are at least a dozen types of cell death, including apoptosis, necroptosis, pyroptosis, oncosis, ferroptosis, entotic cell death, NETotic cell death, parthanatos, phagocytosis, lysosome-dependent cell death, autophagy-dependent cell death, alkaliptosis, and oxeiptosis (Fricker et al., 2018; Tang et al., 2019; Bedoui et al., 2020).

MECHANISMS OF THE CELL DEATH CAUSED BY NITROSATIVE STRESS

Apoptosis

Nitrosative stress-mediated apoptosis is an important apoptotic pathway newly discovered following intrinsic and extrinsic apoptosis pathways associated with the pathogenesis of various diseases (Andreka et al., 2004). An increasing number of studies have shown that nitrosative stress-mediated apoptosis is involved in the pathogenesis of many diseases. To some extent, 3-NT can be used as a marker of apoptosis (Jumper et al., 2002; Zhang and Wei, 2013).

Mitoptosis

Studies have shown that nitrosative stress affects enzyme activity, including that of complex I (NADH dehydrogenase), complex III (cytochrome *c* reductase), complex IV (cytochrome *c* oxidase), and complex V (ATP synthase), in the mitochondrial respiratory chain and increases cytochrome *c* release from mitochondria into the cytoplasm, indicating mitochondrial dysfunction (Arnaiz et al., 1999; Mastrocola et al., 2005). Furthermore, severe nitrosative stress leads to excessive consumption of ATP, resulting

TABLE 1 | Cell death caused by nitrosative stress.

Type of cell death	When nitrosative stress increases	
	The upregulated mediators	**The downregulated mediators**
Apoptosis	Cytochrome *c*, Bax, caspases	Bcl-2
Autophagy	Autophagy-lysosome signaling (Beclin1, LC3, LAMP2, and cathepsin B)	Protein kinase B (PKB)–Akt pathway, and the Akt–mTOR pathway
Ferroptosis	Lethal lipid peroxidation	–
Pyroptosis	Nod-like receptor protein-3 (NLRP3) inflammasome	–
NETosis	Phosphoinositide 3-kinase (PI3K) and myeloperoxidase	Histones H2A and H2B
Parthanatos	Poly adenosine diphosphate-ribose polymerase-1 (PARP-1), and apoptosis-inducing factor (AIF)	–

TABLE 2 | Comparison of different types of abnormal oxygen metabolism.

Type of abnormal oxygen metabolism	Explanation	Mediators
Hypoxia	Any state of insufficient physiological oxygen or insufficient tissue oxygen demand	Hypoxia-inducible factor (HIF)
Oxidative stress	The imbalance between oxidation and antioxidation and a tendency for increased oxidation	Reactive oxygen species (ROS)
Nitrosative stress	The joint biochemical reaction of nitric oxide (NO) and the free radical superoxide (O_2^-)	Reactive nitrogen species (RNS)
Carbonyl stress	The joint biochemical reaction of oxidation and glycosylation, increasing the accumulation of reactive carbonyl compounds from unsaturated aldehyde ketone	Advanced glycation end product (AGEs)
Endoplasmic reticulum stress	In order to cope with the accumulation of misfolded and unfolded proteins in the endoplasmic reticulum lumen and the calcium ion imbalance, cells activate signal pathways such as unfolded protein response (UPR) and endoplasmic reticulum overload response	Inositol requiring (IRE) 1α, PKR-like ER kinase (PERK), and activating transcription factor (ATF) 6α
Mitochondrial dysfunction	Mitochondria are the primary source and direct target of ROS. Abnormal respiratory chain function and ATP synthesis disorders are the main characteristics of mitochondrial dysfunction.	Adenosine-triphosphate (ATP)

in an irreversible decline in mitochondrial membrane potential ($\Delta\Psi m$), which eventually leads to mitochondrial apoptosis. This indicates that nitrosative stress not only can directly cause mitochondrial damage but also can act synergistically with oxidative stress (Tao et al., 2014; Ma et al., 2018a). At present, mitochondrial permeability transition pore (mPTP) opening is considered a common pathway for endogenous apoptosis after cell injury. The generation of RNS and the opening of the mPTP are a vicious cycle of mutual promotion. Abnormal mPTP opening due to external or pathological brings about the production of large numbers of ROS, RNS, and malondialdehyde (MDA) in cells, which may lead to the conformational changes in structural proteins on the mPTP, mPTP opening, and an increase in mitochondrial permeability, which in turn leads to apoptosis (Salimi et al., 2019).

Endoplasmic Reticulum Stress

Nitrosative stress can synergistically induce cell apoptosis under oxidative and ERS. C/EBP-homologous protein (CHOP) and caspase-12 are key proteins involved in ERS-mediated apoptosis. Thus, nitrosative stress induces ERS-dependent apoptosis through ERS-mediated JNK activation, CHOP transcriptional activation, and caspase-12 activation (Zhao et al., 2013; Tao et al., 2014; Lv et al., 2020).

Caspases/Bcl-2 Family Proteins

Studies have shown that the activity of caspase-3 in nitrosative stress induced by H_2O_2 increases and positively correlates with the apoptosis ratio. As a direct substrate of caspase-3, Bcl-2 plays a vital role in apoptosis. Nitrosative stress causes a reduction in the expression levels of STAT3, which regulates the transcription of the Bcl-2 family of anti-apoptotic genes (Rosati et al., 2019). Additionally, nitrosative stress leads to the activation of inducible nitric oxide synthase (iNOS)/Bax/caspase-3-mediated apoptosis in the L132 cell line (Anand et al., 2014). Another study showed that α-ZAL, a natural phytoestrogen, reduces Bax expression and the expression and activity of caspase-9. These effects may be related to the inhibition of nitrosative stress (Liu et al., 2013).

Other Pathways in Apoptosis Signaling

Peroxisome proliferator-activated receptor gamma (PPARγ), a transcriptional regulator of energy balance, can regulate nitrosative stress and inflammation in endothelial cells. A recent

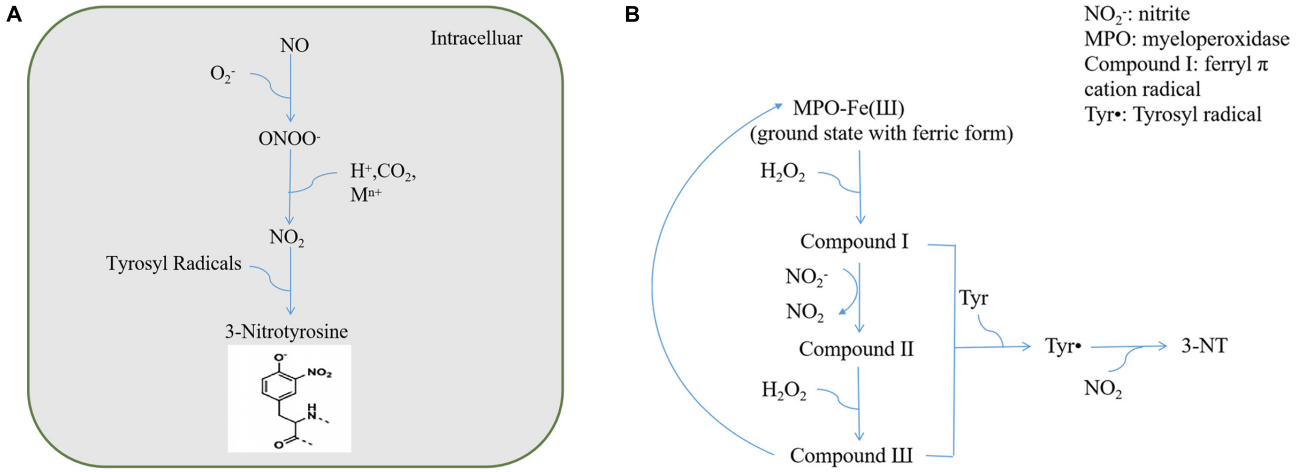

FIGURE 1 | (A) $ONOO^-$ reaction pathways. **(B)** NO_2^-/H_2O_2/heme peroxidase system.

study showed that salusin-β, a bioactive peptide composed of 20 amino acid residues, regulates PPARγ to attenuate nitrosative stress, thereby reducing apoptosis (Sun et al., 2017). Another protein kinase, NF-κB, stimulates IL-1β transferase protease and TNF-α gene expression and induces apoptosis. Nitrosative stress causes abnormal activation of the NF-κB signaling pathway, and its transcription activity increases, thereby triggering apoptosis signals, resulting in apoptosis (Cheng et al., 2014). Several studies found that 3-NT can bind to the C-terminus of α-tubulin through tubulin tyrosine ligase to produce tyrosine tubulin, which is insufficient to maintain microtubule stability, causing cell degeneration, eventually leading to apoptosis (Bisig et al., 2002; Peluffo et al., 2004; Blanchard-Fillion et al., 2006). Another study showed that 3-NT can be used as an indirect inhibitor of tubulin-specific carboxypeptidase, thereby blocking the production of glutamate microtubules and further causing apoptosis (Chang et al., 2002). In recent years, researchers utilize this mechanism to develop related antitumor drugs, which induce tumor cell apoptosis by mediating the nitration of tubulin in tumor cells (Xue et al., 2020).

Autophagy

Autophagy can be divided into macroautophagy, microautophagy, and chaperone-mediated autophagy (CMA) according to the mode of transportation of degraded substances to lysosomes (Filomeni et al., 2015; Doherty and Baehrecke, 2018). In macroautophagy, intracellular autophagy-associated proteins (Atg) form autophagosomes by wrapping damaged proteins or organelles in the cytoplasm, and autophagosomes fuse with lysosomes to form autolysosomes. Autophagy lysosomes degrade the encapsulated substances, and some small molecular substances can be reused by cells. Microautophagy is a method by which lysosomes actively and directly engulf cytoplasmic components, which has rarely been explored in mammals. In CMA, some molecular chaperones, such as hsp70, can help unfolded proteins translocate into lysosomes. In recent years, with advances in research, some autophagy forms with a specific selectivity for substrate degradation, including mitochondrial autophagy (mitophagy), peroxisome autophagy (pexophagy), aggregate autophagy (aggrephagy), endoplasmic reticulum autophagy (reticulophagy), and ribosomal autophagy (ribophagy), have emerged (Kiffin et al., 2006; Coliva et al., 2019). Various studies have shown that nitrosative stress is involved in the occurrence and development of autophagy and that it can induce autophagy through multiple signal transduction pathways.

Macroautophagy

ROS/RNS can induce autophagy by inhibiting the protein kinase B (PKB)-Akt pathway and the Akt-mTOR pathway (Ma et al., 2018b). RNS is related to the post-translational modification of target proteins in cells, including protein thiol oxidation or S-nitrosylation related to the autophagy pathway. The accumulation of ROS/RNS generates carbonyls, whose accumulation is positively correlated with the development of autophagy (Di Meo et al., 2016; Feng et al., 2017). The autophagy-related proteins Atg3, 7, and 10 use cysteine residues to catalyze ubiquitin transfer at their catalytic sites (Ornatowski et al., 2020). The sulfhydryl groups on cysteine residues are particularly vulnerable to the modification of ROS/RNS oxidation; therefore, these proteins may be sensitive to redox signals (Filomeni et al., 2015; Varga et al., 2015). Notch 1 signaling is a key regulator of autophagy and reduces nitrosative stress. For example, genistein (Gen), a natural biologically active flavonoid found in soy, attenuates burn-induced myocardial autophagy by activating cardiac Notch 1 signaling and reducing nitrosative stress (Fang et al., 2019). In addition, nitrosative stress potentiates autophagy-lysosome signaling, which involves Beclin1, LC3, LAMP2, and cathepsin B (Han et al., 2011).

Mitophagy

Nitrosative stress can decrease ΔΨm and cause mitochondrial dysfunction. When ΔΨm decreases, PTEN-induced putative kinase 1 (PINK1) accumulates in the outer membrane and

forms a large complex on the outer membrane surface to recruit Parkin to the damaged mitochondria, thereby causing mitochondrial autophagy (Redmann et al., 2016; Song et al., 2018). In a cerebral ischemia/reperfusion model, $ONOO^-$ induced the tyrosine nitration of dynamin-related protein 1 (Drp1) peptide and recruitment of Drp1 to damage mitochondria and subsequently induce PINK1/Parkin-mediated autophagy activation, thereby promoting brain ischemia/reperfusion injury (Feng et al., 2018a,b).

Pexophagy

Peroxisomes are critical metabolic organelles found in nearly all eukaryotic cells and are involved in ROS/RNS metabolism. Many peroxisomes cause severe nitrosative stress during metabolism (Jo et al., 2015; Sandalio and Romero-Puertas, 2015; Olmedilla and Sandalio, 2019). A recent study showed that certain miRNAs are associated with age-related degenerative changes. MiR-142 targets endothelial PAS domain protein 1 (Epas1), which is a known pexophagy regulatory protein. MiR-142 induces RNS/ROS accumulation by inducing pexophagy (Houri et al., 2020). The accumulation of ROS/RNS inhibits mTORC1 activity in the peroxisome, leading to the active translocation of the transcription factor EB (TFEB) into the nucleus, ultimately promoting autophagic flux and specifically inducing pexophagy through ubiquitin designation (Ganguli et al., 2019; Germain and Kim, 2020).

Ferroptosis

Ferroptosis was initially identified in small molecule erastin-induced cell death, which blocks cystine import, leading to glutathione depletion and inactivation of glutathione peroxidase 4 (GPX4) (Ursini et al., 1982; Yang et al., 2014). Ferroptosis is characterized by the accumulation of lethal lipid peroxidation, which is iron-dependent (Dixon et al., 2012; Stockwell et al., 2017; Lei et al., 2020). As the major component of lipid peroxidation, nitrosative stress was found to be related to the occurrence of ferroptosis (Uribe et al., 2018; Wu et al., 2020). Ferroptosis has been reported to be the prominent form of hepatocyte damage in Concanavalin A (ConA)-induced acute immune hepatitis, which is accompanied by RNS accumulation (Deng et al., 2020; Zeng et al., 2020). More importantly, the administration of an iNOS inhibitor or $ONOO^-$ scavenger diminishes RNS levels and reduces hepatocyte ferroptosis, suggesting that RNS, downstream of Caveolin-1 (Cav-1), is an important mediator that drives the hepatocellular ferroptosis induced by ConA. In addition, nitrosative stress is regulated by indoleamine 2,3-dioxygenase 1 (IDO1) during ferroptosis. IDO1 is an important cellular heme enzyme induced by pro-inflammatory mediators in response to inflammation and contributes to restraining the T and NK cells. Upregulation of IDO1 and nitrosative stress in ConA-induced hepatic damage are suppressed by ferroptosis abolishment. DO1 deficiency leads to ferroptosis inhibition by increasing the expression of solute carrier family 7 member 11 and RNS production, and the IDO1 inhibitor reduces iNOS and 3-NT expression during ferroptosis suppression (Zeng et al., 2020). Although few studies have paid close attention to the role of nitrosative stress in ferroptosis, the nature of ferroptosis caused by lethal lipid peroxidation suggests that nitrosative stress might significantly contribute to ferroptosis in various pathological conditions.

Pyroptosis

Nitrosative stress induces the activation of the nod-like receptor protein-3 inflammasome, which can cause pyroptosis through caspase-1- and caspase-11-mediated cytoplasmic protein gasdermin D (Mari and Colell, 2021). When acute and chronic inflammation occurs, the production rate of $ONOO^-$ exceeds the ability of the endogenous $ONOO^-$ defense system to scavenge it (Dedon and Tannenbaum, 2004; Galloway et al., 2014). Excessive $ONOO^-$ leads to an increase in inflammatory cytokine levels and induces tyrosine nitration, ultimately exacerbating the initial damage. A previous report suggested that TNF-α can activate various transcription factors, including NF-κB, activator protein 1, and interferon regulator factor 3, which induce the expression of target genes that encode various inflammatory factors (Pei et al., 2015). Furthermore, TNF-α induces nitrosative stress by upregulating the intercellular expression of adhesion molecule-1. Adiponectin (APN), an adipocyte-derived cytokine, attenuates TNF-α-induced inflammatory response through Cav-1-mediated ceramidase recruitment and activation in an AdipoR1-dependent manner (Wang et al., 2014). In addition, the upregulation of NF-E2-related factor-2, which is mainly secreted by macrophages, reduces nitrosative stress by blocking the NF-κB signal transduction (Li et al., 2019; Nadeem et al., 2020). The inflammatory response mediates the activation of phosphoinositide 3-kinase and the AKT (PI3K/AKT) and mitogen-activated protein kinase (MAPK) signaling pathways, which may also participate in the suppression of nitrosative stress (Ma et al., 2018b; Sarkozy et al., 2018).

NETosis

Some studies have shown that excessive intracellular RNS production in neutrophils is key to NETosis occurrence (Manda-Handzlik and Demkow, 2015; Lenin et al., 2018). Nitrosative stress mediates neutrophil activation, and activated neutrophils release neutrophil extracellular traps (NETs), a reticular structure that exerts a protective effect by surrounding and degrading pro-inflammatory cytokines (Boeltz et al., 2019). Recent research has shown that the formation of NETs induced by RNS depends on the activities of phosphoinositide 3-kinase and myeloperoxidase, as well as the selective degradation of histones H2A and H2B by neutrophil elastase (Chakraborty et al., 2011; Manda-Handzlik et al., 2020).

Parthanatos

A recent report showed that the overactivation of poly adenosine diphosphate-ribose polymerase-1 (PARP-1) leads to cell death. It is a new form of programmed cell death, termed "parthanatos," which differs from apoptosis and other forms of cell death (Lee et al., 2013, 2015; Tang et al., 2019). At present, research on parthanatos is in its infancy, and the molecular mechanism of its signaling pathway is still unclear. As a unique cell death pathway, parthanatos is characterized by the overactivation of PARP-1, accumulation of cytoplasmic

PAR polymers, mitochondrial depolarization, and apoptosis-inducing factor (AIF) nuclear translocation. When AIF enters the nucleus, it interacts with DNA through an as-of-yet unidentified PAAN, leading to large-scale DNA fragmentation and chromatin condensation (Fatokun et al., 2014). As DNA bases are sensitive to nitrosative stress, they are often modified by $ONOO^-$. One study showed that DNA nitration is upstream of PARP-1 activation. Spermidine is a naturally occurring polyamine that is widely involved in DNA replication, transcription, and translation. The use of exogenous spermidine effectively inhibits the activation of PARP-1 and DNA nitrosative stress (Kim, 2017). Under nitrosative stress, $ONOO^-$ not only induces DNA single-strand breaks but also activates PARP (Buelow et al., 2009), which consumes a large amount of NAD^+, resulting in energy depletion and necrotic cell death. One study showed that DNA nitration is upstream of PARP-1 activation (Barany et al., 2017; Horvath et al., 2018). The initial signaling of PARP-1 in mitochondria is mediated by the downstream activation of JNK-1, a stress-activated protein kinase (SAPK). When nitrosative stress occurs, JNK-1 is activated and participates in the regulation of parthanatos by regulating the intracellular ROS/RNS levels (Zheng et al., 2017).

NITROSATIVE STRESS AND CARDIOVASCULAR DISEASES

Cardiovascular diseases have become the most important causes of death worldwide. Therefore, clarifying its pathophysiological mechanisms is crucial for formulating prevention and treatment strategies. From a cardiovascular aspect, nitrosative stress is associated with the pathophysiological processes. Nitrosative stress can lead to key protein tyrosine nitration related to contractility, metabolism, and antioxidant defense mechanisms of the myocardium and skeletal muscle (Breitkreuz and Hamdani, 2015; Mozos and Luca, 2017). Furthermore, it induces myocardial hypertrophy, fibrosis, or cell death by activating inflammatory responses and stress signals (such as apoptosis and autophagy) (Frati et al., 2017). Myocardial ischemia/reperfusion injury and heart failure are the two main pathophysiological alterations associated with nitrosative stress. Recent studies demonstrated that melatonin receptor 2 (MT2) protects cardiomyocytes from nitrosative stress injury through the MT2/Notch1/Hes1/RORIα signaling pathway in a mouse myocardial ischemia/reperfusion model. Moreover, TNF-α-converting enzyme (TACE) protects against MRI *via* Notch1-mediated suppression of nitrosative stress. These results demonstrate that the upregulation of Notch1 may alleviate nitrosative stress-mediated myocardial ischemia/reperfusion injury (Pei et al., 2015; Yu et al., 2018; Zhang et al., 2020). In addition, $ONOO^-$ can interfere with the cellular calcium transport system, such as the oxidation of sulfhydryl groups of Na^+/Ca^{2+} exchangers, resulting in Na^+/Ca^{2+} exchanger protein dysfunction (Kitao et al., 2010). In heart failure, nitrosative stress causes sarcoplasmic reticulum Ca^{2+}-ATPase tyrosine nitration (Schoneich et al., 1999; Lokuta et al., 2005), further aggravating the dysfunction of left ventricular and vascular systolic functions (Kennedy et al., 2015; Schiattarella et al., 2019). Heart failure induces excessive production of iNOS by macrophages and cardiomyocytes, leading to the loss of myocardial contractility and decreased reactivity of β-adrenergic receptors (Kingery et al., 2017). Nitrosative stress adversely affects the regulation of muscle fiber energy. Myofibril creatine kinase plays an essential role in regulating cardiomyocyte contraction in patients with heart failure and is more susceptible to nitration modification. Creatine kinase activity can be inhibited by nitrosative stress, resulting in the decline of myocardial contractile function and promotion of the occurrence and development of heart failure (Mihm et al., 2001a,b).

CONCLUSION

Nitrosative stress falls under oxidative stress in the traditional category. However, in recent years, a growing body of knowledge has revealed that nitrosative stress, as an independent special biochemical phenomenon in the process of cell death, has unique pathophysiological characteristics that differ from those of oxidative stress in a general sense. This is because of the high responsiveness and short half-life of RNS. However, current research methods have not been able to accurately identify the RNS that induces nitrosative stress. In addition, there is a lack of practical methodologies for the positioning and quantification of nitrosative stress. Although a few antibodies can detect 3-NT, protein tyrosine nitration does not fully reflect the level of nitrosative stress. Therefore, future breakthroughs in biological methodology for detecting nitrosative stress will promote the development of research in this field and deepen our understanding of nitrosative stress biology. During nitrosative stress, the specific target protein tyrosine nitration in different diseases differs. Further studies on the relationship between specific protein tyrosine nitration and diseases will help reveal the pathogenesis of related diseases and identify new targets for drugs. The mechanisms underlying cell death due to nitrosative stress include target protein tyrosine nitration, mitochondrial dysfunction, and cell membrane destruction, which eventually lead to cell death. Revealing the mechanism of cell death induced by nitrosative stress is of great significance for the development of drugs targeting nitrosative stress. In recent years, significant progress has been made in determining the role of nitrosative stress injury in cell death; however, some key problems, such as the concentration threshold of $ONOO^-$ damage to various important cellular organs and the corresponding pathophysiological effects, have not been addressed. In summary, research on the mechanism of cell death induced by nitrosative stress helps us to further reveal the pathogenesis of cell injury, explore new sub-therapeutic targets, and provide new ways to prevent and treat diseases related to cell death. Cardiovascular disease is the first enemy of human health. Understanding nitrosative stress will help bridge the gap in the relationship between cell death and cardiovascular disease, thereby providing vital information for improving human health.

AUTHOR CONTRIBUTIONS

YC, FX, and FC designed the framework. FW and QY wrote the manuscript. JP and CP revised the manuscript. All authors read and approved the final version of the manuscript for publication.

FUNDING

This work was supported by the National Natural Science Foundation of China (81873950, 82072144, 81900435, 81772036, and 81873953), the State Key Program of the National Natural Science Foundation of China (82030059), the National Key R&D Program of China (2020YFC1512700, 2020YFC1512705, and 2020YFC1512703), National S&T Fundamental Resources Investigation Project (2018FY100600 and 2018FY100602), the Taishan Young Scholar Program of Shandong Province (tsqn20161065 and tsqn201812129), the Taishan Pandeng Scholar Program of Shandong Province (tspd20181220), and the Interdisciplinary Young Researcher Groups Program of Shandong University (2020QNQT004).

REFERENCES

Ahsan, H. (2013). 3-Nitrotyrosine: a biomarker of nitrogen free radical species modified proteins in systemic autoimmunogenic conditions. *Hum. Immunol.* 74, 1392–1399. doi: 10.1016/j.humimm.2013.06.009

Alvarez, B., and Radi, R. (2003). Peroxynitrite reactivity with amino acids and proteins. *Amino Acids* 25, 295–311. doi: 10.1007/s00726-003-0018-8

Anand, T., Pandareesh, M. D., Bhat, P. V., and Venkataramana, M. (2014). Anti-apoptotic mechanism of bacoside rich extract against reactive nitrogen species induced activation of iNOS/Bax/caspase 3 mediated apoptosis in L132 cell line. *Cytotechnology* 66, 823–838. doi: 10.1007/s10616-013-9634-7

Andreka, P., Tran, T., Webster, K. A., and Bishopric, N. H. (2004). Nitric oxide and promotion of cardiac myocyte apoptosis. *Mol. Cell. Biochem.* 263, 35–53. doi: 10.1023/b:mcbi.0000041847.63338.b8

Arnaiz, S. L., Coronel, M. F., and Boveris, A. (1999). Nitric oxide, superoxide, and hydrogen peroxide production in brain mitochondria after haloperidol treatment. *Nitric Oxide* 3, 235–243. doi: 10.1006/niox.1999.0229

Barany, T., Simon, A., Szabo, G., Benkő, R., Mezei, Z., Molnár, L., et al. (2017). Oxidative stress-related parthanatos of circulating mononuclear leukocytes in heart failure. *Oxid. Med. Cell. Longev.* 2017:1249614.

Bedoui, S., Herold, M. J., and Strasser, A. (2020). Emerging connectivity of programmed cell death pathways and its physiological implications. *Nat. Rev. Mol. Cell Biol.* 21, 678–695. doi: 10.1038/s41580-020-0270-8

Bian, K., Gao, Z., Weisbrodt, N., and Murad, F. (2003). The nature of heme/iron-induced protein tyrosine nitration. *Proc. Natl. Acad. Sci. U.S.A.* 100, 5712–5717. doi: 10.1073/pnas.0931291100

Bisig, C. G., Purro, S. A., Contin, M. A., Barra, H. S., and Arce, C. A. (2002). Incorporation of 3-nitrotyrosine into the C-terminus of alpha-tubulin is reversible and not detrimental to dividing cells. *Eur. J. Biochem.* 269, 5037–5045. doi: 10.1046/j.1432-1033.2002.03220.x

Blanchard-Fillion, B., Prou, D., Polydoro, M., Spielberg, D., Tsika, E., Wang, Z., et al. (2006). Metabolism of 3-nitrotyrosine induces apoptotic death in dopaminergic cells. *J. Neurosci.* 26, 6124–6130. doi: 10.1523/jneurosci.1038-06.2006

Boeltz, S., Amini, P., Anders, H. J., Andrade, F., Bilyy, R., Chatfield, S., et al. (2019). To NET or not to NET:current opinions and state of the science regarding the formation of neutrophil extracellular traps. *Cell Death Differ.* 26, 395–408.

Borbely, A., Toth, A., Edes, I., Virág, L., Papp, J. G., Varró, A., et al. (2005). Peroxynitrite-induced alpha-actinin nitration and contractile alterations in isolated human myocardial cells. *Cardiovasc. Res.* 67, 225–233.

Breitkreuz, M., and Hamdani, N. (2015). A change of heart: oxidative stress in governing muscle function? *Biophys. Rev.* 7, 321–341. doi: 10.1007/s12551-015-0175-5

Brunner, F., and Wolkart, G. (2003). Peroxynitrite-induced cardiac depression: role of myofilament desensitization and cGMP pathway. *Cardiovasc. Res.* 60, 355–364. doi: 10.1016/j.cardiores.2003.08.001

Buelow, B., Uzunparmak, B., Paddock, M., and Scharenberg, A. M. (2009). Structure/function analysis of PARP-1 in oxidative and nitrosative stress-induced monomeric ADPR formation. *PLoS One* 4:e6339. doi: 10.1371/journal.pone.0006339

Chakraborty, A., Chowdhury, S., and Bhattacharyya, M. (2011). Effect of metformin on oxidative stress, nitrosative stress and inflammatory biomarkers in type 2 diabetes patients. *Diabetes Res. Clin. Pract.* 93, 56–62. doi: 10.1016/j.diabres.2010.11.030

Chang, W., Webster, D. R., Salam, A. A., Gruber, D., Prasad, A., Eiserich, J. P., et al. (2002). Alteration of the C-terminal amino acid of tubulin specifically inhibits myogenic differentiation. *J. Biol. Chem.* 277, 30690–30698. doi: 10.1074/jbc.m204930200

Chen, Y., Hua, Y., Li, X., Arslan, I. M., Zhang, W., and Meng, G. (2020). Distinct types of cell death and the implication in diabetic cardiomyopathy. *Front. Pharmacol.* 11:42. doi: 10.3389/fphar.2020.00042

Cheng, C. Y., Lin, J. G., Tang, N. Y., Kao, S. T., and Hsieh, C. L. (2014). Electroacupuncture-like stimulation at the Baihui (GV20) and Dazhui (GV14) acupoints protects rats against subacute-phase cerebral ischemia-reperfusion injuries by reducing S100B-mediated neurotoxicity. *PLoS One* 9:e91426. doi: 10.1371/journal.pone.0091426

Coliva, G., Duarte, S., Perez-Sala, D., and Fedorova, M. (2019). Impact of inhibition of the autophagy-lysosomal pathway on biomolecules carbonylation and proteome regulation in rat cardiac cells. *Redox Biol.* 23:101123. doi: 10.1016/j.redox.2019.101123

Dedon, P. C., and Tannenbaum, S. R. (2004). Reactive nitrogen species in the chemical biology of inflammation. *Arch. Biochem. Biophys.* 423, 12–22. doi: 10.1016/j.abb.2003.12.017

Deng, G., Li, Y., Ma, S., Gao, Z., Zeng, T., Chen, L., et al. (2020). Caveolin-1 dictates ferroptosis in the execution of acute immune-mediated hepatic damage by attenuating nitrogen stress. *Free Radic. Biol. Med.* 148, 151–161.

Di Meo, S., Reed, T. T., Venditti, P., and Victor, V. M. (2016). Role of ROS and RNS sources in physiological and pathological conditions. *Oxid. Med. Cell. Longev.* 2016:1245049.

Dixon, S. J., Lemberg, K. M., Lamprecht, M. R., Skouta, R., Zaitsev, E. M., Gleason, C. E., et al. (2012). Ferroptosis: an iron-dependent form of nonapoptotic cell death. *Cell* 149, 1060–1072. doi: 10.1016/j.cell.2012.03.042

Doherty, J., and Baehrecke, E. H. (2018). Life, death and autophagy. *Nat. Cell Biol.* 20, 1110–1117.

Espey, M. G., Miranda, K. M., Feelisch, M., Fukuto, J., Grisham, M. B., Vitek, M. P., et al. (2000). Mechanisms of cell death governed by the balance between nitrosative and oxidative stress. *Ann. N. Y. Acad. Sci.* 899, 209–221.

Fang, Z., Wu, G., Zhang, D., Wang, K., Deng, X., Liu, M., et al. (2019). Genistein protects against burn-induced myocardial injury via Notch1 mediated suppression of oxidative/nitrative stress. *Shock* 54, 277–279

Fatokun, A. A., Dawson, V. L., and Dawson, T. M. (2014). Parthanatos: mitochondrial-linked mechanisms and therapeutic opportunities. *Br. J. Pharmacol.* 171, 2000–2016. doi: 10.1111/bph.12416

Feng, J., Chen, X., and Shen, J. (2017). Reactive nitrogen species as therapeutic targets for autophagy: implication for ischemic stroke. *Expert Opin. Ther. Targets* 21, 305–317. doi: 10.1080/14728222.2017.1281250

Feng, J., Chen, X., Guan, B., Li, C., Qiu, J., and Shen, J. (2018a). Inhibition of peroxynitrite-induced mitophagy activation attenuates cerebral ischemia-reperfusion injury. *Mol. Neurobiol.* 55, 6369–6386. doi: 10.1007/s12035-017-0859-x

Feng, J., Chen, X., Lu, S., Li, W., Yang, D., Su, W., et al. (2018b). Naringin attenuates cerebral ischemia-reperfusion injury through inhibiting peroxynitrite-mediated mitophagy activation. *Mol. Neurobiol.* 55, 9029–9042. doi: 10.1007/s12035-018-1027-7

Filomeni, G., De Zio, D., and Cecconi, F. (2015). Oxidative stress and autophagy: the clash between damage and metabolic needs. *Cell Death Differ.* 22, 377–388. doi: 10.1038/cdd.2014.150

Frati, G., Schirone, L., Chimenti, I., Yee, D., Biondi-Zoccai, G., Volpe, M., et al. (2017). An overview of the inflammatory signalling mechanisms in the myocardium underlying the development of diabetic cardiomyopathy. *Cardiovasc. Res.* 113, 378–388. doi: 10.1093/cvr/cvx011

Fricker, M., Tolkovsky, A. M., Borutaite, V., Coleman, M., and Brown, G. C. (2018). Neuronal cell death. *Physiol. Rev.* 98, 813–880.

Galloway, C. A., Lee, H., Brookes, P. S., and Yoon, Y. (2014). Decreasing mitochondrial fission alleviates hepatic steatosis in a murine model of nonalcoholic fatty liver disease. *Am. J. Physiol. Gastrointest. Liver Physiol.* 307, G632–G641.

Ganguli, G., Mukherjee, U., and Sonawane, A. (2019). Peroxisomes and oxidative stress: their implications in the modulation of cellular immunity during mycobacterial infection. *Front. Microbiol.* 10:1121. doi: 10.3389/fmicb.2019.01121

Germain, K., and Kim, P. K. (2020). Pexophagy: a model for selective autophagy. *Int. J. Mol. Sci.* 21:578. doi: 10.3390/ijms21020578

Green, D. R. (2019). The coming decade of cell death research: five riddles. *Cell* 177, 1094–1107. doi: 10.1016/j.cell.2019.04.024

Han, F., Chen, Y. X., Lu, Y. M., Huang, J. Y., Zhang, G. S., Tao, R. R., et al. (2011). Regulation of the ischemia-induced autophagy-lysosome processes by nitrosative stress in endothelial cells. *J. Pineal Res.* 51, 124–135. doi: 10.1111/j.1600-079x.2011.00869.x

Herold, S. (2004). Nitrotyrosine, dityrosine, and nitrotryptophan formation from metmyoglobin, hydrogen peroxide, and nitrite. *Free Radic. Biol. Med.* 36, 565–579. doi: 10.1016/j.freeradbiomed.2003.10.014

Horvath, E. M., Magenheim, R., Beres, N. J., Benkō, R., Pék, T., Tabák, ÁG., et al. (2018). Oxidative-nitrative stress and poly (ADP-ribose) polymerase activation 3 years after pregnancy. *Oxid. Med. Cell. Longev.* 2018:1743253.

Houri, K., Mori, T., Onodera, Y., Tsujimoto, T., Takehara, T., Nakao, S., et al. (2020). miR-142 induces accumulation of reactive oxygen species (ROS) by inhibiting pexophagy in aged bone marrow mesenchymal stem cells. *Sci. Rep.* 10:3735.

Ischiropoulos, H. (2003). Biological selectivity and functional aspects of protein tyrosine nitration. *Biochem. Biophys. Res. Commun.* 305, 776–783. doi: 10.1016/s0006-291x(03)00814-3

Ischiropoulos, H., Zhu, L., Chen, J., Tsai, M., Martin, J. C., Smith, C. D., et al. (1992). Peroxynitrite-mediated tyrosine nitration catalyzed by superoxide dismutase. *Arch. Biochem. Biophys.* 298, 431–437. doi: 10.1016/0003-9861(92)90431-u

Jo, D. S., Bae, D. J., Park, S. J., Seo, H. M., Kim, H. B., Oh, J. S., et al. (2015). Pexophagy is induced by increasing peroxisomal reactive oxygen species in 1'10-phenanthroline-treated cells. *Biochem. Biophys. Res. Commun.* 467, 354–360. doi: 10.1016/j.bbrc.2015.09.153

Jumper, J., Kalns, J., Batey, K., Lane, R., and Reed, J. (2002). The 3-nitrotyrosine marker of apoptosis shows time-dependent and tissue-specific variation in a porcine retinal laser injury model. *J. Investig. Ophthalmol. Vis. Sci.* 43:4528.

Kennedy, D. J., Shrestha, K., Sheehey, B., Li, X. S., Guggilam, A., Wu, Y., et al. (2015). Elevated plasma marinobufagenin, an endogenous cardiotonic steroid, is associated with right ventricular dysfunction and nitrative stress in heart failure. *Circ. Heart Fail.* 8, 1068–1076. doi: 10.1161/circheartfailure.114.001976

Kiffin, R., Bandyopadhyay, U., and Cuervo, A. M. (2006). Oxidative stress and autophagy. *Antioxid. Redox Signal.* 8, 152–162.

Kim, J. (2017). Spermidine is protective against kidney ischemia and reperfusion injury through inhibiting DNA nitration and PARP1 activation. *Anat. Cell Biol.* 50, 200–206. doi: 10.5115/acb.2017.50.3.200

Kingery, J. R., Hamid, T., Lewis, R. K., Ismahil, M. A., Bansal, S. S., Rokosh, G., et al. (2017). Leukocyte iNOS is required for inflammation and pathological remodeling in ischemic heart failure. *Basic Res. Cardiol.* 112:19. doi: 10.1016/b978-0-12-800039-7.00002-5

Kitao, T., Takuma, K., Kawasaki, T., Inoue, Y., Ikehara, A., Nashida, T., et al. (2010). The Na+/Ca2+ exchanger-mediated Ca2+ influx triggers nitric oxide-induced cytotoxicity in cultured astrocytes. *Neurochem. Int.* 57, 58–66. doi: 10.1016/j.neuint.2010.04.016

Lee, Y., Karuppagounder, S. S., Shin, J. H., Lee, Y. I., Ko, H. S., Swing, D., et al. (2015). Corrigendum: parthanatos mediates AIMP2-activated age-dependent dopaminergic neuronal loss. *Nat. Neurosci.* 18:1861. doi: 10.1038/nn1215-1861a

Lee, Y., Karuppagounder, S. S., Shin, J. H., Lee, Y. I., Ko, H. S., Swing, D., et al. (2013). Parthanatos mediates AIMP2-activated age-dependent dopaminergic neuronal loss. *Nat. Neurosci.* 16, 1392–1400. doi: 10.1038/nn.3500

Lei, J., Chen, Z., Song, S., Sheng, C., Song, S., and Zhu, J. (2020). Insight into the role of ferroptosis in non-neoplastic neurological diseases. *Front. Cell. Neurosci.* 14:231. doi: 10.3389/fncel.2020.00231

Lenin, R., Thomas, S. M., and Gangaraju, R. (2018). Endothelial activation and oxidative stress in neurovascular defects of the retina. *Curr. Pharm. Des.* 24, 4742–4754. doi: 10.2174/1381612825666190115122622

Li, Y., Deng, S. L., Lian, Z. X., and Yu, K. (2019). Roles of Toll-like receptors in nitroxidative stress in mammals. *Cells* 8:576. doi: 10.3390/cells8060576

Lim, G. B. (2019). New mouse model reveals nitrosative stress as a novel driver of HFpEF. *Nat. Rev. Cardiol.* 16:383. doi: 10.1038/s41569-019-0203-4

Liu, T., Hou, D. D., Zhao, Q., Liu, W., Zhen, P. P., Xu, J. P., et al. (2013). Phytoestrogen alpha-zearalanol attenuates homocysteine-induced apoptosis in human umbilical vein endothelial cells. *Biomed. Res. Int.* 2013:813450.

Lokuta, A. J., Maertz, N. A., Meethal, S. V., Potter, K. T., Kamp, T. J., Valdivia, H. H., et al. (2005). Increased nitration of sarcoplasmic reticulum Ca2+-ATPase in human heart failure. *Circulation* 111, 988–995. doi: 10.1161/01.cir.0000156461.81529.d7

Lv, S., Wu, N., Wang, Q., and Yang, L. H. (2020). Endogenous hydrogen sulfide alleviates methotrexate-induced cognitive impairment by attenuating endoplasmic reticulum stress-induced apoptosis via CHOP and caspase-12. *Fundam. Clin. Pharmacol.* 34, 559–570. doi: 10.1111/fcp.12543

Ma, L. L., Li, Y., Yin, P. P., Kong, F. J., Guo, J. J., Shi, H. T., et al. (2018a). Hypertrophied myocardium is vulnerable to ischemia/reperfusion injury and refractory to rapamycin-induced protection due to increased oxidative/nitrative stress. *Clin. Sci.* 132, 93–110. doi: 10.1042/cs20171471

Ma, L. L., Ma, X., Kong, F. J., Guo, J. J., Shi, H. T., Zhu, J. B., et al. (2018b). Mammalian target of rapamycin inhibition attenuates myocardial ischaemia-reperfusion injury in hypertrophic heart. *J. Cell. Mol. Med.* 22, 1708–1719. doi: 10.1111/jcmm.13451

Maes, M., Galecki, P., Chang, Y. S., and Berk, M. (2011). A review on the oxidative and nitrosative stress (O&NS) pathways in major depression and their possible contribution to the (neuro)degenerative processes in that illness. *Prog. Neuropsychopharmacol. Biol. Psychiatry* 35, 676–692.

Manda-Handzlik, A., and Demkow, U. (2015). Neutrophils: the role of oxidative and nitrosative stress in health and disease. *Adv. Exp. Med. Biol.* 857, 51–60. doi: 10.1007/5584_2015_117

Manda-Handzlik, A., Bystrzycka, W., Cieloch, A., Glodkowska-Mrowka, E., Jankowska-Steifer, E., Heropolitanska-Pliszka, E., et al. (2020). Nitric oxide and peroxynitrite trigger and enhance release of neutrophil extracellular traps. *Cell. Mol. Life Sci.* 77, 3059–3075. doi: 10.1007/s00018-019-03331-x

Marciniak, S. J., and Ron, D. (2006). Endoplasmic reticulum stress signaling in disease. *Physiol. Rev.* 86, 1133–1149. doi: 10.1152/physrev.00015.2006

Mari, M., and Colell, A. (2021). Mitochondrial oxidative and nitrosative stress as a therapeutic target in diseases. *Antioxidants* 10:314 doi: 10.3390/antiox10020314

Mastrocola, R., Restivo, F., Vercellinatto, I., Danni, O., Brignardello, E., Aragno, M., et al. (2005). Oxidative and nitrosative stress in brain mitochondria of diabetic rats. *J. Endocrinol.* 187, 37–44. doi: 10.1677/joe.1.06269

Mihm, M. J., Coyle, C. M., Schanbacher, B. L., Weinstein, D. M., and Bauer, J. A. (2001a). Peroxynitrite induced nitration and inactivation of myofibrillar creatine kinase in experimental heart failure. *Cardiovasc. Res.* 49, 798–807. doi: 10.1016/s0008-6363(00)00307-2

Mihm, M. J., Yu, F., Carnes, C. A., Reiser, P. J., McCarthy, P. M., Van Wagoner, D. R., et al. (2001b). Impaired myofibrillar energetics and oxidative injury during human atrial fibrillation. *Circulation* 104, 174–180. doi: 10.1161/01.cir.104.2.174

Miyata, T., and de Strihou, C. (2010). Diabetic nephropathy: a disorder of oxygen metabolism? *Nat. Rev. Nephrol.* 6, 83–95. doi: 10.1038/nrneph.2009.211

Mozos, I., and Luca, C. T. (2017). Crosstalk between oxidative and nitrosative stress and arterial stiffness. *Curr. Vasc. Pharmacol.* 15, 446–456.

Nadeem, A., Ahmad, S. F., Al-Ayadhi, L. Y., Attia, S. M., Al-Harbi, N. O., Alzahrani, K. S., et al. (2020). Differential regulation of Nrf2 is linked to elevated inflammation and nitrative stress in monocytes of children with autism. *Psychoneuroendocrinology* 113:104554. doi: 10.1016/j.psyneuen.2019.104554

Nobrega, N., Araujo, N. F., Reis, D., Facine, L. M., Miranda, C. A. S., Mota, G. C., et al. (2019). Hydrogen peroxide and nitric oxide induce anticontractile effect of perivascular adipose tissue via renin angiotensin system activation. *Nitric Oxide* 84, 50–59.

Ohshima, H., Friesen, M., Brouet, I., and Bartsch, H. (1990). Nitrotyrosine as a new marker for endogenous nitrosation and nitration of proteins. *Food Chem. Toxicol.* 28, 647–652. doi: 10.1016/0278-6915(90)90173-k

Olmedilla, A., and Sandalio, L. M. (2019). Selective autophagy of peroxisomes in plants: from housekeeping to development and stress responses. *Front. Plant Sci.* 10:1021. doi: 10.3389/fpls.2019.01021

Ornatowski, W., Lu, Q., Yegambaram, M., Garcia, A. E., Zemskov, E. A., Maltepe, E., et al. (2020). Complex interplay between autophagy and oxidative stress in the development of pulmonary disease. *Redox Biol.* 36:101679. doi: 10.1016/j.redox.2020.101679

Paulus, W. J. (2020). Unfolding discoveries in heart failure. *N. Engl. J. Med.* 382:679–682. doi: 10.1056/nejmcibr1913825

Pei, H., Song, X., Peng, C., Tan, Y., Li, Y., Li, X., et al. (2015). TNF-alpha inhibitor protects against myocardial ischemia/reperfusion injury via Notch1-mediated suppression of oxidative/nitrative stress. *Free Radic. Biol. Med.* 82, 114–121. doi: 10.1016/j.freeradbiomed.2015.02.002

Peluffo, H., Shacka, J. J., Ricart, K., Bisig, C. G., Martìnez-Palma, L., Pritsch, O., et al. (2004). Induction of motor neuron apoptosis by free 3-nitro-L-tyrosine. *J. Neurochem.* 89, 602–612. doi: 10.1046/j.1471-4159.2004.02363.x

Redmann, M., Darley-Usmar, V., and Zhang, J. (2016). The Role of autophagy, mitophagy and lysosomal functions in modulating bioenergetics and survival in the context of redox and proteotoxic damage: implications for neurodegenerative diseases. *Aging Dis.* 7, 150–162. doi: 10.14336/ad.2015.0820

Rosati, R., Shahab, M., Neumann, W. L., and Jamesdaniel, S. (2019). Inhibition of protein nitration prevents cisplatin-induced inactivation of STAT3 and promotes anti-apoptotic signaling in organ of Corti cells. *Exp. Cell Res.* 381, 105–111. doi: 10.1016/j.yexcr.2019.05.008

Rowlands, D. J. (2016). Mitochondria dysfunction: a novel therapeutic target in pathological lung remodeling or bystander? *Pharmacol. Ther.* 166, 96–105. doi: 10.1016/j.pharmthera.2016.06.019

Salimi, A., Neshat, M. R., Naserzadeh, P., and Pourahmad, J. (2019). Mitochondrial permeability transition pore sealing agents and antioxidants protect oxidative stress and mitochondrial dysfunction induced by naproxen, diclofenac and celecoxib. *Drug Res.* 69, 598–605. doi: 10.1055/a-0866-9356

Sandalio, L. M., and Romero-Puertas, M. C. (2015). Peroxisomes sense and respond to environmental cues by regulating ROS and RNS signalling networks. *Ann. Bot.* 116, 475–485. doi: 10.1093/aob/mcv074

Sarkozy, M., Kovacs, Z. Z. A., Kovacs, M. G., Gaspar, R., Szucs, G., and Dux, L. (2018). Mechanisms and modulation of oxidative/nitrative stress in type 4 cardio-renal syndrome and renal sarcopenia. *Front. Physiol.* 9:1648. doi: 10.3389/fphys.2018.01648

Schiattarella, G. G., Altamirano, F., Tong, D., French, K. M., Villalobos, E., Kim, S. Y., et al. (2019). Nitrosative stress drives heart failure with preserved ejection fraction. *Nature* 568, 351–356.

Schoneich, C., Viner, R. I., Ferrington, D. A., and Bigelow, D. J. (1999). Age-related chemical modification of the skeletal muscle sarcoplasmic reticulum Ca-ATPase of the rat. *Mech. Ageing Dev.* 107, 221–231. doi: 10.1016/s0047-6374(98)00158-4

Sohal, R. S., and Allen, R. G. (1990). Oxidative stress as a causal factor in differentiation and aging: a unifying hypothesis. *Exp. Gerontol.* 25, 499–522. doi: 10.1016/0531-5565(90)90017-v

Song, L., Huang, Y., Hou, X., Yang, Y., Kala, S., Qiu, Z., et al. (2018). PINK1/Parkin-mediated mitophagy promotes resistance to sonodynamic therapy. *Cell. Physiol. Biochem.* 49, 1825–1839. doi: 10.1159/000493629

Steinberg, S. F. (2013). Oxidative stress and sarcomeric proteins. *Circ. Res.* 112, 393–405. doi: 10.1161/circresaha.111.300496

Stockwell, B. R., Friedmann Angeli, J. P., Bayir, H., Bush, A. I., Conrad, M., Dixon, S. J., et al. (2017). Ferroptosis: a regulated cell death nexus linking metabolism, redox biology, and disease. *Cell* 171, 273–285. doi: 10.1016/j.cell.2017.09.021

Sun, H. J., Chen, D., Wang, P. Y., Wan, M. Y., Zhang, C. X., Zhang, Z. X., et al. (2017). Salusin-beta is involved in diabetes mellitus-induced endothelial dysfunction via degradation of peroxisome proliferator-activated receptor gamma. *Oxid. Med. Cell. Longev.* 2017:6905217.

Suzuki, D., Miyata, T., and Kurokawa, K. (2001). Carbonyl stress. *Contrib. Nephrol.* 134, 36–45.

Tang, D., Kang, R., Berghe, T. V., Vandenabeele, P., and Kroemer, G. (2019). The molecular machinery of regulated cell death. *Cell Res.* 29, 347–364. doi: 10.1038/s41422-019-0164-5

Tao, X., Wan, X., Xu, Y., Xu, L., Qi, Y., Yin, L., et al. (2014). Dioscin attenuates hepatic ischemia-reperfusion injury in rats through inhibition of oxidative-nitrative stress, inflammation and apoptosis. *Transplantation* 98, 604–611. doi: 10.1097/tp.0000000000000262

Uribe, P., Cabrillana, M. E., Fornes, M. W., Treulen, F., Boguen, R., Isachenko, V., et al. (2018). Nitrosative stress in human spermatozoa causes cell death characterized by induction of mitochondrial permeability transition-driven necrosis. *Asian J. Androl.* 20, 600–607. doi: 10.4103/aja.aja_29_18

Ursini, F., Maiorino, M., Valente, M., Ferri, L., and Gregolin, C. (1982). Purification from pig liver of a protein which protects liposomes and biomembranes from peroxidative degradation and exhibits glutathione peroxidase activity on phosphatidylcholine hydroperoxides. *Biochim. Biophys. Acta* 710, 197–211. doi: 10.1016/0005-2760(82)90150-3

Varga, Z. V., Giricz, Z., Liaudet, L., Hasko, G., Ferdinandy, P., and Pacher, P. (2015). Interplay of oxidative, nitrosative/nitrative stress, inflammation, cell death and autophagy in diabetic cardiomyopathy. *Biochim. Biophys. Acta* 1852, 232–242. doi: 10.1016/j.bbadis.2014.06.030

Velsor, L. W., Ballinger, C. A., Patel, J., and Postlethwait, E. M. (2003). Influence of epithelial lining fluid lipids on NO(2)-induced membrane oxidation and nitration. *Free Radic. Biol. Med.* 34, 720–733. doi: 10.1016/s0891-5849(02)01370-9

Wang, Y., Wang, X., Lau, W. B., Yuan, Y., Booth, D., Li, J. J., et al. (2014). Adiponectin inhibits tumor necrosis factor-alpha-induced vascular inflammatory response via caveolin-mediated ceramidase recruitment and activation. *Circ. Res.* 114, 792–805. doi: 10.1161/circresaha.114.302439

West, J. B. (2017). Physiological effects of chronic hypoxia. *N. Engl. J. Med.* 376, 1965–1971.

Wu, Y., Zhang, S., Gong, X., Tam, S., Xiao, D., Liu, S., et al. (2020). The epigenetic regulators and metabolic changes in ferroptosis-associated cancer progression. *Mol. Cancer* 19:39.

Xue, L., Zeng, Y., Fang, C., Cheng, W., and Li, Y. (2020). Effect of TTLL12 on tubulin tyrosine nitration as a novel target for screening anticancer drugs in vitro. *Oncol. Lett.* 20:340.

Yang, W. S., SriRamaratnam, R., Welsch, M. E., Shimada, K., Skouta, R., Viswanathan, V. S., et al. (2014). Regulation of ferroptotic cancer cell death by GPX4. *Cell* 156, 317–331. doi: 10.1016/j.cell.2013.12.010

Ye, Y. Z., Strong, M., Huang, Z. Q., and Beckman, J. S. (1996). Antibodies that recognize nitrotyrosine. *Methods Enzymol.* 269, 201–209. doi: 10.1016/s0076-6879(96)69022-3

Yu, L., Li, Z., Dong, X., Xue, X., Liu, Y., Xu, S., et al. (2018). Polydatin protects diabetic heart against ischemia-reperfusion injury via Notch1/Hes1-mediated activation of Pten/Akt signaling. *Oxid. Med. Cell. Longev.* 2018:2750695.

Zeng, T., Deng, G., Zhong, W., Gao, Z., Ma, S., Mo, C., et al. (2020). Indoleamine 2, 3-dioxygenase 1enhanceshepatocytes ferroptosis in acute immune hepatitis associated with excess nitrative stress. *Free Radic. Biol. Med.* 152, 668–679. doi: 10.1016/j.freeradbiomed.2020.01.009

Zhang, C., Yang, J. B., Quan, W., Feng, Y. D., Feng, J. Y., Cheng, L. S., et al. (2020). Activation of paraventricular melatonin receptor 2 mediates melatonin-conferred cardioprotection against myocardial ischemia/reperfusion injury. *J. Cardiovasc. Pharmacol.* 76, 197–206. doi: 10.1097/fjc.0000000000000851

Zhang, Y. L., and Wei, J. R. (2013). 3-nitrotyrosine, a biomarker for cardiomyocyte apoptosis induced by diabetic cardiomyopathy in a rat model. *Mol. Med. Rep.* 8, 989–994. doi: 10.3892/mmr.2013.1644

Zhao, S., Xiong, Z., Mao, X., Meng, D., Lei, Q., Li, Y., et al. (2013). Atmospheric pressure room temperature plasma jets facilitate oxidative and nitrative stress and lead to endoplasmic reticulum stress dependent apoptosis in HepG2 cells. *PLoS One* 8:e73665. doi: 10.1371/journal.pone.0073665

Zheng, L., Wang, C., Luo, T., Lu, B., Ma, H., Zhou, Z., et al. (2017). JNK activation contributes to oxidative stress-induced parthanatos in glioma cells via increase of intracellular ROS production. *Mol. Neurobiol.* 54, 3492–3505. doi: 10.1007/s12035-016-9926-y

Conflict of Interest: The authors declare that the research was conducted in the absence of any commercial or financial relationships that could be construed as a potential conflict of interest.

Publisher's Note: All claims expressed in this article are solely those of the authors and do not necessarily represent those of their affiliated organizations, or those of the publisher, the editors and the reviewers. Any product that may be evaluated in this article, or claim that may be made by its manufacturer, is not guaranteed or endorsed by the publisher.

Copyright © 2021 Wang, Yuan, Chen, Pang, Pan, Xu and Chen. This is an open-access article distributed under the terms of the Creative Commons Attribution License (CC BY). The use, distribution or reproduction in other forums is permitted, provided the original author(s) and the copyright owner(s) are credited and that the original publication in this journal is cited, in accordance with accepted academic practice. No use, distribution or reproduction is permitted which does not comply with these terms.

frontiers in Cell and Developmental Biology

ORIGINAL RESEARCH
published: 01 October 2021
doi: 10.3389/fcell.2021.721795

4-Hydroxy-2-Nonenal Promotes Cardiomyocyte Necroptosis *via* Stabilizing Receptor-Interacting Serine/Threonine-Protein Kinase 1

Xiaoxuan Zhai[1,2,3,4,5,6†], *Wenjun Wang*[1,2,3,4,5,6,7†], *Shukun Sun*[1,2,3,4,5,6], *Yu Han*[1,2,3,4,5,6], *Jiaxin Li*[1,2,3,4,5,6], *Shengchuan Cao*[1,2,3,4,5,6], *Ruochuan Li*[1,2,3,4,5,6], *Tonghui Xu*[1,2,3,4,5,6], *Qiuhuan Yuan*[1,2,3,4,5,6], *Jiali Wang*[1,2,3,4,5,6*], *Shujian Wei*[1,2,3,4,5,6*] and *Yuguo Chen*[1,2,3,4,5,6*]

[1] Department of Emergency and Chest Pain Center, Qilu Hospital, Cheeloo College of Medicine, Shandong University, Jinan, China, [2] Clinical Research Center for Emergency and Critical Care Medicine, Qilu Hospital, Institute of Emergency and Critical Care Medicine, Cheeloo College of Medicine, Shandong University, Jinan, China, [3] Key Laboratory of Emergency and Critical Care Medicine, Qilu Hospital, Cheeloo College of Medicine, Shandong University, Jinan, China, [4] Key Laboratory of Cardiopulmonary-Cerebral Resuscitation Research, Qilu Hospital, Cheeloo College of Medicine, Shandong University, Jinan, China, [5] The Key Laboratory of Cardiovascular Remodeling and Function Research, Chinese Ministry of Education, Chinese Ministry of Health and Chinese Academy of Medical Sciences, Qilu Hospital, Cheeloo College of Medicine, Shandong University, Jinan, China, [6] The State and Shandong Province Joint Key Laboratory of Translational Cardiovascular Medicine, Qilu Hospital, Cheeloo College of Medicine, Shandong University, Jinan, China, [7] Department of Critical Care Medicine, Shandong Provincial Hospital Affiliated to Shandong First Medical University, Jinan, China

OPEN ACCESS

Edited by:
Zhi Qi,
Nankai University, China

Reviewed by:
Qingbo Xu,
Zhejiang University, China
Jun Ren,
University of Washington, United States

***Correspondence:**
Jiali Wang
wangjiali_2000@126.com
Shujian Wei
weishujian@sdu.edu.cn
Yuguo Chen
chen919085@sdu.edu.cn

† These authors have contributed equally to this work and share first authorship

Specialty section:
This article was submitted to Cell Death and Survival, a section of the journal Frontiers in Cell and Developmental Biology

Received: *07 June 2021*
Accepted: *01 September 2021*
Published: *01 October 2021*

Citation:
Zhai X, Wang W, Sun S, Han Y, Li J, Cao S, Li R, Xu T, Yuan Q, Wang J, Wei S and Chen Y (2021) 4-Hydroxy-2-Nonenal Promotes Cardiomyocyte Necroptosis via Stabilizing Receptor-Interacting Serine/Threonine-Protein Kinase 1. Front. Cell Dev. Biol. 9:721795. doi: 10.3389/fcell.2021.721795

Background: Necroptosis is a vital regulator of myocardial ischemia/reperfusion (MI/R) injury. Meanwhile, 4-hydroxy-2-nonenal (4-HNE) is abundantly increased during MI/R injury. However, whether 4-HNE induces cardiomyocyte necroptosis during MI/R remains unknown.

Methods: To observe the relationship between 4-HNE and necroptosis during MI/R, C57BL/6 mice and aldehyde dehydrogenase 2-transgenic (ALDH2-Tg) mice were both exposed to left anterior descending artery ligation surgery to establish MI/R injury models. For further study, isolated mouse hearts and H9c2 cells were both treated with 4-HNE to elucidate the underlying mechanisms.

Results: Necroptosis and 4-HNE were both upregulated in I/R-injured hearts. Cardiomyocyte necroptosis was significantly decreased in I/R-injured hearts from ALDH2-Tg mice as compared with that of wild-type mice. *In vitro* studies showed that necroptosis was enhanced by 4-HNE perfusion in a time- and concentration-dependent manner. Knockdown of receptor-interacting serine/threonine-protein kinase 1 (RIP1) using small interfering RNA (siRNA) prevented 4-HNE-induced cardiomyocyte necroptosis, manifesting that RIP1 played a key role in the upregulation of cell necroptosis by 4-HNE. Further studies found that 4-HNE reduced the protein degradation of RIP1 by preventing K48-polyubiquitination of RIP1.

Conclusion: 4-HNE contributes to cardiomyocyte necroptosis by regulating ubiquitin-mediated proteasome degradation of RIP1.

Keywords: 4-hydroxynonenal (4-HNE), myocardial ischemia – reperfusion injury (MIRI), necroptosis, RIP1 (RIPK1), ubiquitination

INTRODUCTION

Reperfusion therapy is a medical treatment that restores the coronary artery blood perfusion and is regarded as the most effective intervention for the treatment of myocardial infarction (Yellon and Hausenloy, 2007). However, reperfusion can cause up to 50% at most of the total myocardial injury and results in malignant arrhythmia, myocardial stunning, and impaired heart function (Heusch and Gersh, 2017). Programmed cardiomyocyte death plays an initiating and central role in myocardial ischemia/reperfusion (MI/R) injury but may receive less clinical attention because of its insidious effects on cardiac structure and function (Zhu and Sun, 2018).

Necrosis used to be considered an "unprogrammed" cardiovascular cell death, while apoptosis and autophagy are denoted as "programmed cell death" and has gained a lot of attention. However, recent studies have shown that necroptosis is the most well-defined regulated necrosis that accounts for up to 30% of cell death during MI/R injury (Smith et al., 2007). It is characterized as loss of plasma membrane integrity and decreasing of cellular adenosine triphosphate (ATP) (Linkermann and Green, 2014; Zhang et al., 2018). Necroptosis is initiated by the activation of receptor-interacting serine/threonine-protein kinase 1 (RIP1) that binds to receptor-interacting serine/threonine-protein kinase 3 (RIP3) to form necrosome, followed by activation of downstream mixed lineage kinase domain-like pseudokinase (MLKL) and Ca^{2+}/calmodulin-dependent protein kinase II (CaMKII) (Cho et al., 2009; Chen et al., 2014). Thus, RIP1 plays a key role in transferring death signals and determines cell fate (Ofengeim and Yuan, 2013; Orozco et al., 2014).

4-Hydroxy-2-nonenal (4-HNE), one of the most toxic aldehydes, is the major secondary product of lipid peroxidation (Ayala et al., 2014). 4-HNE, at 0.3–5 μM under normal condition, plays physiological roles as a signaling molecule while 4-HNE is increased by 10–100 times under oxidative stress and plays cytotoxic roles by inhibiting gene expression or modifying proteins (Esterbauer et al., 1991; Ayala et al., 2014). During MI/R injury, 4-HNE is increased by 6-fold in reperfusion-injured hearts to 100 μM (Lucas and Szweda, 1999). Accumulation of 4-HNE increases the formation of 4-HNE adducts by binding to various proteins in the heart tissue and promotes cardiac dysfunction mainly through damaging mitochondria, impairing ATP production, and inducing cardiomyocyte death (Hwang et al., 2020; Santin et al., 2020). The role of 4-HNE in cardiomyocyte apoptosis was previously investigated, but the effects of 4-HNE on cardiomyocyte necroptosis remain unknown (Sun et al., 2014).

In this study, the effects of 4-HNE on necroptosis were investigated *in vivo* and *in vitro*. Using multiple approaches, we found that 4-HNE promoted necroptosis during MI/R by combination with RIP1 and then inhibiting the ubiquitination of RIP1.

MATERIALS AND METHODS

Reagents and Antibodies

Receptor-interacting serine/threonine-protein kinase 1 antibody (3493; 1:1,000), RIP3 antibody (15828; 1:1,000), phosphor-RIP1 antibody (p-RIP1; 1:1,000), Ser166 (31122; 1:1,000), CaMKII antibody (3362; 1:1,000), K48-ubiquitin antibody (8081; 1:1,000), and secondary antibodies (1:10,000) were bought from Cell Signaling Technology (Danvers, MA, United States). Phosphor-RIP3 antibody (p-RIP3) (ab195117; 1:1,000), 4-HNE antibody (ab46545; 1:1,000), phosphor-MLKL antibody (p-MLKL) (ab196436; 1:1,000), phosphor-CaMKII antibody (p-CaMKII) (ab32678; 1:1,000) were purchased from Abcam (Cambridge, MA, United States). β-Actin antibody (6008-1-Ig; 1:5,000) and MLKL antibody (66675; 1:1,000) were bought from Proteintech (Rosemont, IL, United States). Cycloheximide (CHX, 25 μg/ml) (5087390001) was bought from Sigma-Aldrich (Steinheim, Germany).

Animal Myocardial Ischemia/Reperfusion Injury Models

The present study was approved by the Animal Ethics Committee of Qilu Hospital of Shandong University. All procedures were in adherence with the National Institutes of Health guidelines. Aldehyde dehydrogenase 2-transgenic (ALDH2-Tg) mice were from Professor Jun Ren (University of Wyoming). Wild-type (WT) and ALDH2-Tg male mice (8–12 weeks) were used to perform MI/R injury surgery. After being anesthetized with isoflurane inhalation, the hearts were exposed by thoracotomy. The left anterior descending (LAD) artery was tied with 6-0 silk suture for 30 min and loosened for 4 or 24 h. Then, the hearts and blood of mice were harvested for the following experiments.

Langendorff Model

The Langendorff model was used to examine the direct effects of 4-HNE on the isolated mouse hearts. After being anesthetized and heparinized, the mouse hearts were harvested quickly and installed on the Langendorff apparatus. The isolated hearts were perfused with Krebs–Henseleit buffer (KH buffer) and stabilized at 37°C with 95% O_2 and 5% CO_2 for 20 min and then perfused the heart with KH buffer containing 60 μM 4-HNE or vehicles for 1 h. During that period, left ventricular developed pressure (LVDP) and left ventricular pressure rising rate (dp/dt) were recorded and compared with baseline to measure the left ventricular function.

Infarct Size Measurement and Echocardiography

To determine myocardial infarct size, the LAD artery was tied at previous place and then perfused with 1% Evans blue dye (EBD) through the aorta. After that, the hearts were frozen and cut into 2-mm slices. Then, the slices were incubated in 1% 2,3,5-triphenyl tetrazolium chloride (TTC) solution for 20 min at 37°C incubator. The red and white areas stood for the areas at risk, and the white area stood for the infarction area. After

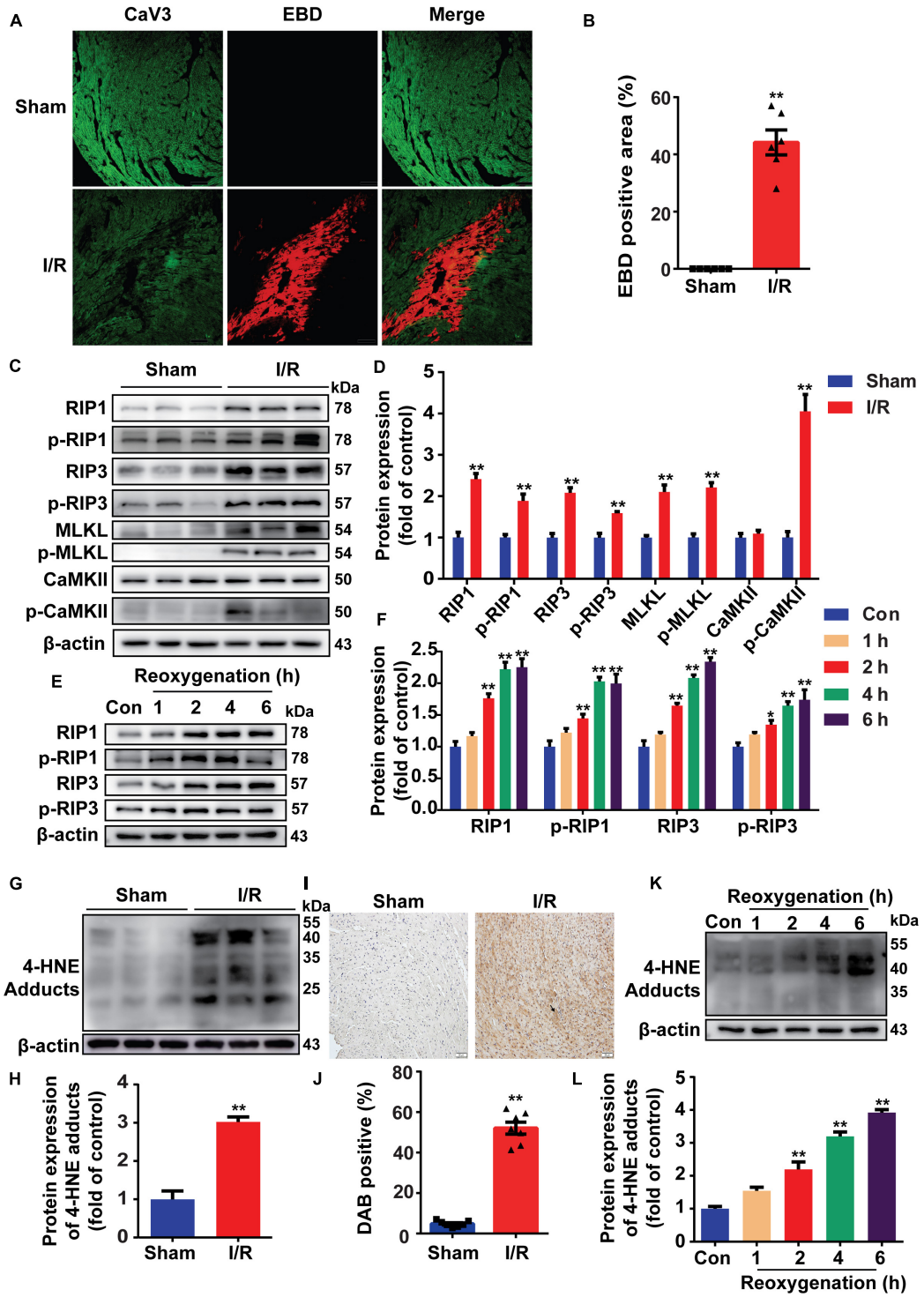

FIGURE 1 | Reperfusion injury induces cell necroptosis and increases 4-hydroxy-2-non-enal (4-HNE) production in mouse hearts and H9c2 cells. **(A,B)** Representative photomicrographs and analysis of necrotic area (red) and viable cardiomyocytes (green) in the sections of mouse hearts (n = 6). Scale bar = 100 μm. **(C,D)** Representative Western blots and relative expression of receptor-interacting serine/threonine-protein kinase 1 (RIP1), p-RIP1, RIP3, p-RIP3, mixed lineage kinase domain-like pseudokinase (MLKL), p-MLKL, Ca^{2+}/calmodulin-dependent protein kinase II (CaMKII), and p-CaMKII in mouse hearts (n = 6). **(E,F)** Representative immunoblots and relative expression of RIP1, p-RIP1, RIP3, and p-RIP3 in H9c2 cells under different reoxygenation times following hypoxia for 14 h (n = 5). **(G,H)** Protein expression and relative expression of 4-HNE adducts in mouse hearts (n = 6). **(I,J)** Representative immunohistochemical staining and analysis of mouse heart sections stained with anti-4-HNE antibodies (n = 7). Scale bar = 50 μm. **(K,L)** Protein expression of 4-HNE adducts in H9c2 cells under different reoxygenation times following hypoxia for 14 h (n = 5). *$p < 0.05$ vs. sham (control) group; **$p < 0.01$ vs. sham (control) group.

photographing with a camera, the images were analyzed by ImageJ software (NIH).

Cardiac function after MI/R injury including left ventricular fraction shortening (LVFS) and left ventricular ejection fraction (LVEF) was measured by the echocardiographic method (VEVO 2100, VisualSonics, Toronto, ON, Canada).

Cell Culture

H9c2 cells (ATCC) were cultured in Dulbecco's modified Eagle's medium (DMEM) (Gibco, Thermo Fisher Scientific, MA, United States) plus 10% fetal bovine serum and antibiotics. The cells were grown in the humified incubator with 20% O_2/5% CO_2 at 37°C. For hypoxia/reoxygenation (H/R) stimulation, the cells were maintained in the hypoxia chamber (2% O_2, 5% CO_2) with low glucose and serum-free DMEM overnight and then were moved to normoxic incubator with regular culture medium for different hours (1, 2, 4, or 6 h).

For 4-HNE stimulation, the cells were cultured in regular culture medium with vehicle or diverse concentration of 4-HNE (20, 40, 60, or 80 μM) and kept in incubator for various hours (1, 2, 4, or 6 h).

Necroptosis Assay

Myocardium necroptosis was measured by EBD-Caveolin 3 (CaV3) double staining. Mice were intraperitoneally given EBD (10 mg/ml) 14 h before the MI/R surgery. After surgerical operation, excised hearts were put into optimal cutting temperature (OCT) compound and were sliced into 5-μm cryosections. Finally, sections were incubated with CaV3 antibody and were imaged using a fluorescence microscope (Olympus, Tokyo, Japan).

Propidium iodide (PI)/Annexin V staining was used to distinguish the necroptotic cells. V-ZAD-FMK (Selleck Chemicals, TX, United States) was added to inhibit caspases accompanied with vehicle or 4-HNE, then the cells were harvested and washed twice. Cells were resuspended at the concentration of 1×10^6/ml and then were incubated with PI and Annexin V at 37°C for 20 min. The cells were detected using flow cytometry and were analyzed with CytExpert software (Beckman Coulter, IN, United States).

Receptor-Interacting Serine/Threonine-Protein Kinase 1 Knockdown

To silence the *RIP1* gene, the H9c2 cells were transfected with small interfering RNA (siRNA) using INTERFERin (Polyplus-transfection, NY, United States). The transfection effect was determined by Western blots. The sequence of siRNA1 was 5′-GCUACUGGGCAUCAUCAUA-3′; the sequence of siRNA2 was 5′-CCAGAAGACAGGCCAACAU-3′.

Western Blot Assay

Protein was extracted from myocardium tissue or H9c2 cells. Here, 20 μg protein was separated by sodium dodecyl sulfate–polyacrylamide gel electrophoresis (SDS-PAGE) and transferred to 0.25-μm polyvinylidene difluoride (PVDF) membrane (Merck Millipore, Billerica, MA, United States). The membranes were incubated with primary antibodies overnight at 4°C. After being washed, the membranes were incubated with corresponding horseradish peroxidase (HRP)-coupled secondary antibodies. Blots were visualized by chemiluminescence reagents and were analyzed with ImageJ software.

Co-immunoprecipitaion

The formation of necrosome and ubiquitination of RIP1 were assessed by immunoprecipitation method. H9c2 cells were lysed in NP-40 (Bosterbio, CA, United States). Then, protein was incubated with 2 μg RIP1 antibody or IgG overnight and then was added with 15 μl protein A/G agarose (Santa Cruz Biotechnology, TX, United States) for 2 h. After being washed, the beads were added 20 μl loading buffer and boiled. Supernatants were subjected to SDS-PAGE and analyzed.

Immunohistochemical Staining

The sections were incubated with anti-4-HNE antibody overnight at 4°C (Abcam, ab46545, Cambridge, MA, United States) followed by being washed and stained with secondary antibodies. After that, 3,3′-diaminobenzidine (DAB) was used as chromogenic substrate. And the slices were counterstained with hematoxylin.

Reverse Transcription Quantitative Polymerase Chain Reaction

To measure the mRNA levels of RIP1 in the myocardium tissues, RNA was extracted by EASYspin plus RNA extraction kit (Aidlab, Beijing, China) according to the instructions. Extracted RNA then was reverse transcribed to cDNA using Prime Script RT Master Mix (TaKaRa, Shiga, Japan). The amplifications and measurements were performed on ABI 7500 quantitative polymerase chain reaction instrument (Applied Biosystems; Thermo Fisher Scientific, MA, United States). The $2^{-\Delta\ \Delta\ CT}$ data of at least four independent experiments were recorded and analyzed.

Statistical Analysis

Data were expressed as the means ± SEM and were analyzed by two-sided unpaired Student's t-test. For multiple treatments, data were analyzed by one-way analysis of variance (ANOVA), followed by Tukey's multiple comparisons test. $p < 0.05$ was considered statistical significance. All data were analyzed using GraphPad Prism version 5.0.

RESULTS

Reperfusion Injury Induces Cell Necroptosis and Increases 4-Hydroxy-2-Nonenal Production in Mouse Hearts

Mice were subjected to 30 min ischemia followed by 4 h reperfusion to induce MI/R injury. EBD was used to indicate necrosis area, while viable cardiomyocytes were labeled by

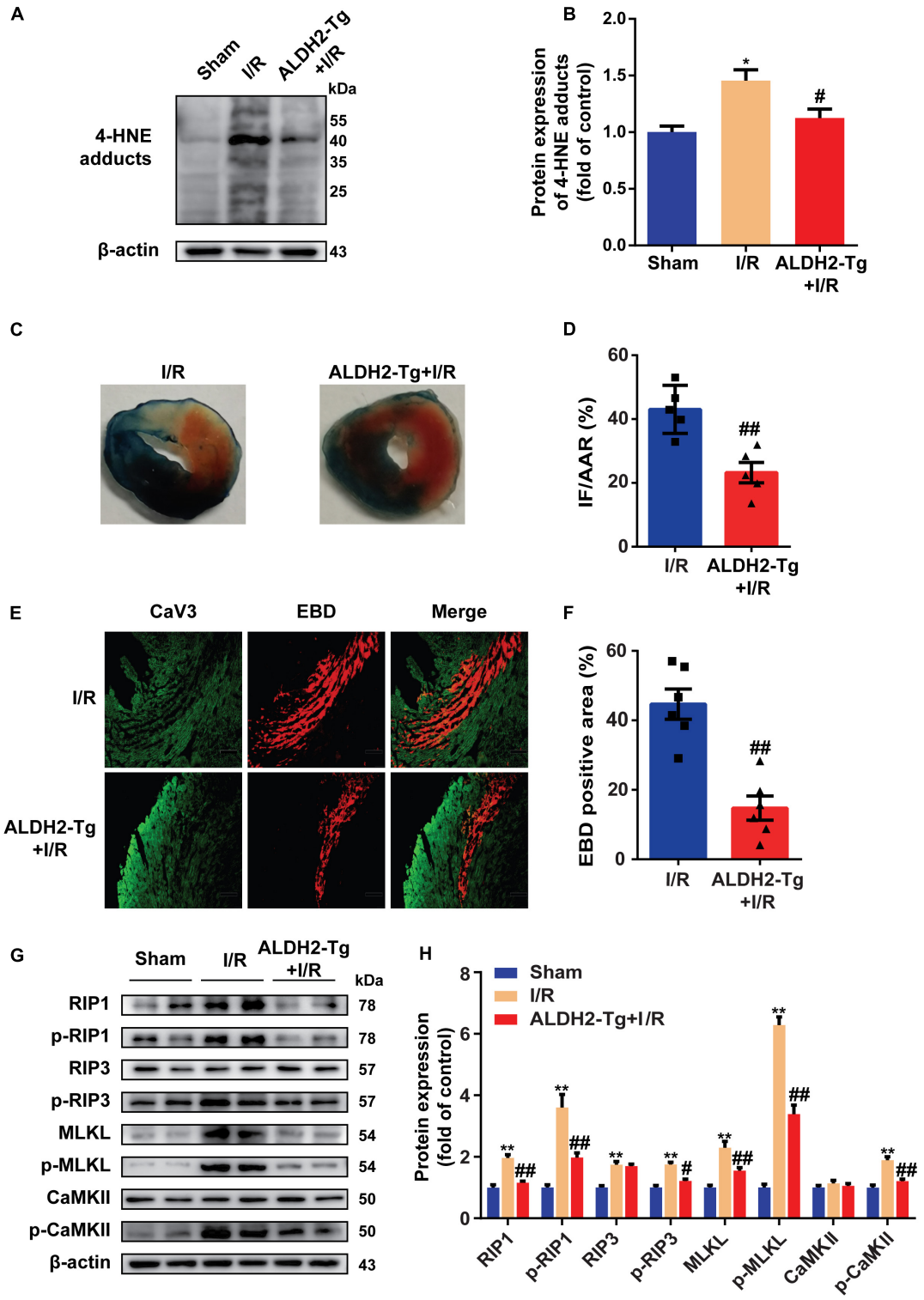

FIGURE 2 | Detoxifying 4-hydroxy-2-non-enal protects against myocardial ischemia/reperfusion (MI/R) injury by reducing necroptosis. **(A,B)** Representative Western blots and relative expression of 4-HNE adducts in mouse hearts (n = 5). **(C,D)** Representative sections and statistical analysis of mouse hearts stained with Evans blue dye (EBD)/2,3,5-triphenyl tetrazolium chloride (TTC). White area stands for infarction area (IF); white and red area stands for area at risk (AAR) (n = 5). **(E,F)** Representative sections and analysis of heart sections stained with EBD and CaV3 (n = 6). Scale bar = 100 μm. **(G,H)** Representative immunoblots and relative expression of receptor-interacting serine/threonine-protein kinase 1 (RIP1), p-RIP1, RIP3, p-RIP3, mixed lineage kinase domain-like pseudokinase (MLKL), p-MLKL, Ca^{2+}/CaMKII, and p-CaMKII in mouse hearts (n = 6). $^{*}p < 0.05$ vs. sham group, $^{**}p < 0.01$ vs. sham group; $^{\#}p < 0.05$ vs. I/R group, $^{\#\#}p < 0.01$ vs. I/R group.

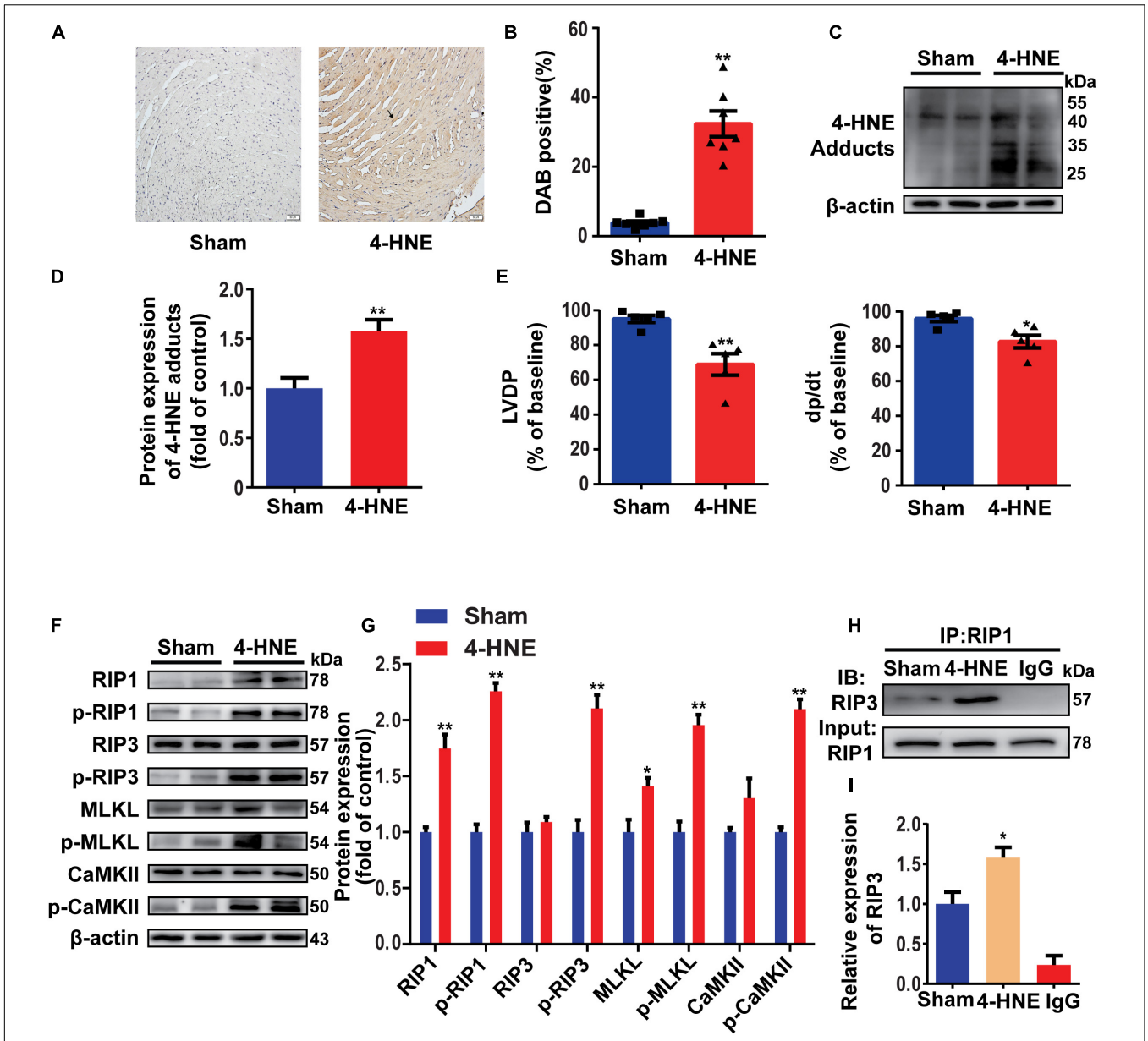

FIGURE 3 | 4-Hydroxy-2-non-enal induces myocardial necroptosis in Langendorff-perfused hearts. **(A,B)** Representative immunohistochemical staining and analysis of 4-HNE expression in mouse hearts (n = 7). Scale bar = 50 μm. **(C,D)** Representative Western blots and relative expression of 4-HNE adducts in mouse hearts (n = 6). **(E)** Cardiac function was evaluated by left ventricular developed pressure (LVDP) and left ventricular pressure rising rate (dp/dt) compared to the baseline (n = 5). **(F,G)** Representative Western blots and relative expression of receptor-interacting serine/threonine-protein kinase 1 (RIP1), p-RIP1, RIP3, p-RIP3, MLKL, p-MLKL, Ca^{2+}/CaMKII, p-CaMKII in mouse hearts (n = 6). **(H,I)** Co-immunoprecipitation using anti-RIP1 antibody indicating the combination between RIP1 and RIP3 (n = 3). *$p < 0.05$ vs. sham group, **$p < 0.01$ vs. sham group.

CaV3. As shown in **Figures 1A,B**, MI/R injury obviously induced myocardial necrosis. During cell necroptosis, activation of RIP1 and RIP3 is essential, and both CaMKII and MLKL are considered executors of cell necroptosis (Zhe-Wei et al., 2018). To determine whether cell necroptosis occurred during MI/R injury, these proteins were detected, and we found that RIP1, p-RIP1, RIP3, p-RIP3, MLKL, p-MLKL, and p-CaMKII were all upregulated in reperfusion-injured hearts (**Figures 1C,D**). To confirm the effect of reperfusion injury on cell necroptosis, H9c2 cells were exposed to H/R stimulation. In line with the results *in vivo*, RIP1, RIP3, and their phosphorylation were all upregulated in H/R-treated cells (**Figures 1E,F**).

Since lipid peroxidation is markedly increased during MI/R injury, we then detected the change of 4-HNE and found that more 4-HNE was immunoblotted or immunochemically stained in MI/R-injured hearts (**Figures 1G–J**). Identically, 4-HNE

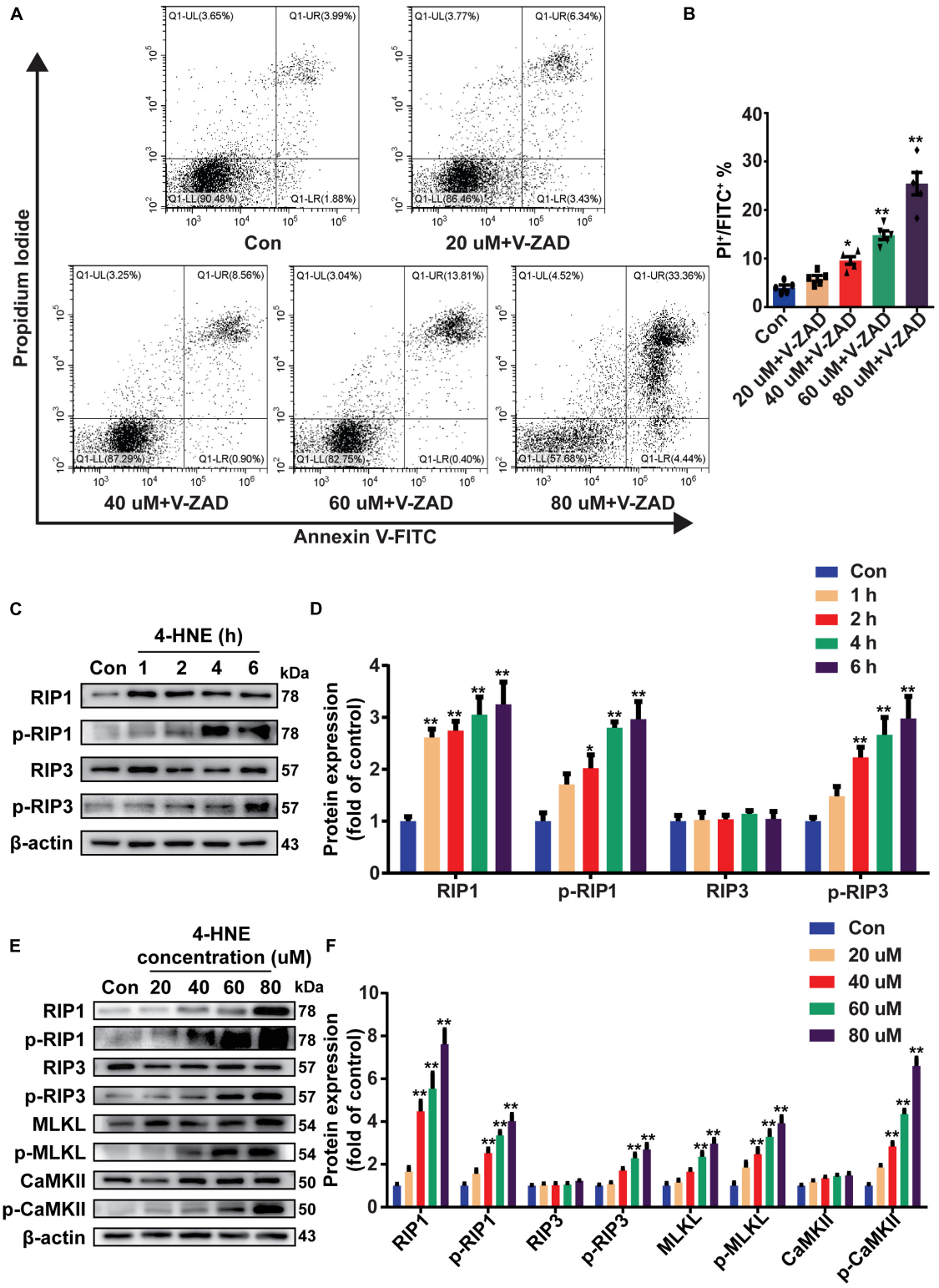

FIGURE 4 | 4-Hydroxy-2-non-enal induces cell necroptosis in H9c2 cells. **(A,B)** Necroptotic cells were determined using flow cytometry stained with Annexin V and propidium iodide (PI), and the cell necroptosis ratio was demonstrated as the percentage of Annexin V^+/PI^+ cells ($n = 5$). **(C,D)** Representative Western blots and relative expression of RIP1, p-RIP1, RIP3, and p-RIP3 under time gradients of 4-HNE treatment in H9c2 cells ($n = 5$). **(E,F)** Representative immunoblots and relative expression of RIP1, p-RIP1, RIP3, p-RIP3, MLKL, p-MLKL, Ca^{2+}/CaMKII, and p-CaMKII in H9c2 cells treated with different concentrations of 4-HNE ($n = 5$). $^*p < 0.05$ vs. control group, $^{**}p < 0.01$ vs. control group.

was also increased in H/R-treated H9c2 cells (**Figures 1K,L**). Moreover, we detected 4-HNE *in vivo* and *in vitro* by Western blots and found that 4-HNE was not changed in ischemia (hypoxia) group (**Supplementary Figures 1A,B**).

Detoxifying 4-Hydroxy-2-Nonenal Protects Against Myocardial Ischemia/Reperfusion Injury by Reducing Necroptosis

As ALDH2 is the main detoxifying enzyme of 4-HNE (Kimura et al., 2019), to elucidate the relationship between 4-HNE and necroptosis, ALDH2-Tg mice (**Supplementary Figures 2A,B**) and WT controls were exposed to MI/R injury. Less 4-HNE was detected in I/R-injured hearts from ALDH2-Tg group as compared with I/R group (**Figures 2A,B**). Cardiac function after I/R injury was improved by overexpression of ALDH2, as indicated by LVEF and LVFS (**Supplementary Figure 2C**). The myocardial infarct size was limited in ALDH2-Tg group compared to the I/R group (**Figures 2C,D**). Lactate dehydrogenase (LDH) was also decreased in ALDH2-Tg group (**Supplementary Figure 2D**). EBD-CaV3 staining showed that necrotic area was significantly reduced in ALDH2-Tg group (**Figures 2E,F**). Moreover, MI/R-induced upregulation of RIP1, p-RIP1, p-RIP3, MLKL, p-MLKL, and p-CaMKII was prevented by ALDH2 overexpression (**Figures 2G,H**). Because the formation of necrosome is critical to the happening of necroptosis (Chen et al., 2019), RIP1 was immunoprecipitated to detect the formation of necrosome and found that the binding of RIP1 to RIP3 was reduced in ALDH2-Tg group (**Supplementary Figures 2E,F**). These results demonstrated that 4-HNE might be a regulator of cell necroptosis in MI/R.

4-Hydroxy-2-Nonenal Induces Myocardial Necroptosis in Langendorff-Perfused Hearts

To explore the role of 4-HNE in cell necroptosis, the Langendorff-perfused mouse heart model was used. After being stabilized for 20 min, the hearts were perfused with 60 μM 4-HNE or vehicle for 1 h. 4-HNE adducts were significantly increased in 4-HNE-perfused hearts, as indicated by both Western blot and immunohistochemical staining (**Figures 3A–D**). The cardiac function was impaired by 4-HNE perfusion, as indicated by the decreased LVDP and dp/dt compared to baseline (**Figure 3E**). Importantly, the perfusion of 4-HNE increased RIP1, p-RIP1, p-RIP3, MLKL, p-MLKL, and p-CaMKII (**Figures 3F,G**). Furthermore, more RIP3 was co-immunoprecipitated with RIP1 in 4-HNE-perfused hearts (**Figures 3H,I**). These results provided support for the crucial role of 4-HNE in cardiomyocyte necroptosis.

4-Hydroxy-2-Non-enal Induces Cell Necroptosis in H9c2 Cells

To confirm the effect of 4-HNE on necroptosis, H9c2 cells were pretreated with Z-VAD-FMK (the pan-caspase inhibitor and was used to inhibit apoptosis) and then were stimulated with 4-HNE. Necroptotic cells were measured using flow cytometry and were defined as Annexin V^+/PI^+ cells. 4-HNE promoted cell necroptosis (**Figures 4A,B**). Moreover, RIP1, p-RIP1, and p-RIP3 were all upregulated by 4-HNE in a time-dependent manner (**Figures 4C,D**). Meanwhile, RIP1, p-RIP1, p-RIP3, MLKL, p-MLKL, and p-CaMKII were also upregulated by 4-HNE in a dose-dependent manner (**Figures 4E,F**).

Receptor-Interacting Serine/Threonine-Protein Kinase 1 Mediates the Effect of 4-Hydroxy-2-Nonenal on Cardiomyocyte Necroptosis

Receptor-interacting serine/threonine-protein kinase 1 is necessary for the regulation of RIP3 and the downstream pathways (Liu et al., 2019). To determine the critical role of RIP1 in the regulation of cardiomyocyte necroptosis by 4-HNE, the H9c2 cells were transfected with scramble or RIP1 siRNA (**Figures 5A,B**). The effect of 4-HNE (60 μM) on cell necroptosis was mitigated by knockdown of RIP1 (**Figures 5C,D**). Moreover, the 4-HNE-induced changes of p-RIP1, p-RIP3, MLKL, p-MLKL, and p-CaMKII were prevented by RIP1 deficiency (**Figures 5E,F**).

4-Hydroxy-2-Nonenal Reduces the Ubiquitin-Dependent Degradation of Receptor-Interacting Serine/Threonine-Protein Kinase 1

To investigate how 4-HNE upregulates the protein level of RIP1, the protein expression and degradation of RIP1 were both examined. The mRNA level of RIP1 was not changed by 4-HNE stimulation (**Figure 6A**). To assess the protein degradation of RIP1, CHX was used to inhibit the gene transcription, and we found that less protein was degraded in 4-HNE group (**Figures 6B,C**). These results suggested that 4-HNE upregulated RIP1 *via* preventing the protein degradation. K-48-linked polyubiquitination is a common type of ubiquitination that is associated with the degradation of RIP1 by proteasome (Samant et al., 2018). To verify whether 4-HNE regulated RIP1 degradation by decreasing the ubiquitination of RIP1, the K-48-linked polyubiquitination of RIP1 was detected, and we found that less K-48 ubiquitin was co-immunoprecipitated with RIP1 after 4-HNE stimulation (**Figures 6D,E**). Furthermore, the process of protein ubiquitination is divided into the combination of substrate protein with ubiquitin ligases and the transfer of ubiquitin to the substrate protein (Komander, 2009). To figure out which process was regulated by 4-HNE, cIAP1, and cIAP2, the important direct E3 ubiquitin ligases of RIP1 (Wang et al., 2008), were coimmunoprecipitated with RIP1, and we found the binding of cIAP1 and cIAP2 to RIP1 was not changed by 4-HNE stimulation (**Figures 6F,G**). To further underlie the mechanism of reduced ubiquitination of RIP1 by 4-HNE, the carbonylation of RIP1

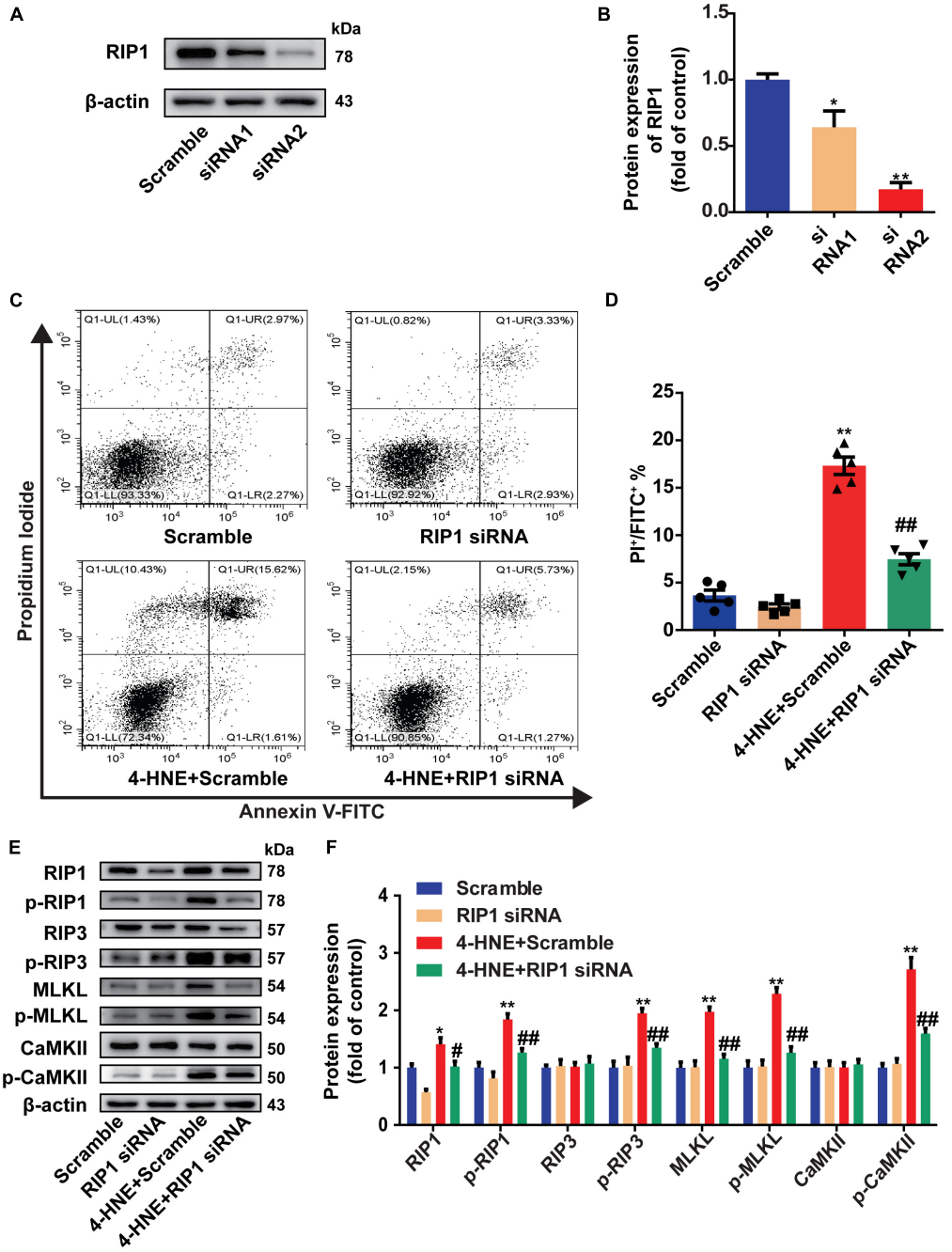

FIGURE 5 | Receptor-interacting serine/threonine-protein kinase 1 mediates the effect of 4-HNE on cardiomyocyte necroptosis. **(A,B)** Representative Western blots and relative expression of RIP1 in H9c2 cells treated with scrambled or RIP1-targeted siRNAs ($n = 3$). **(C,D)** Necroptotic cells were analyzed by Annexin V/PI staining using flow cytometry ($n = 5$). The necroptotic cells were indicated as Annexin V^+/PI^+ cells. **(E,F)** Representative immunoblots and relative expression of RIP1, p-RIP1, RIP3, p-RIP3, MLKL, p-MLKL, Ca^{2+}/CaMKII, and p-CaMKII in different groups treated with scramble or RIP1 siRNA with or without 4-HNE stimulation in H9c2 cells ($n = 5$). $^*p < 0.05$ vs. scramble group, $^{**}p < 0.01$ vs. scramble group; $^{\#}p < 0.05$ vs. 4-HNE + scramble group, $^{\#\#}p < 0.01$ vs. 4-HNE + scramble group.

was examined, and more 4-HNE was co-immunoprecipitated with RIP1 (**Figures 6H,I**). Taken together, we speculate that 4-HNE might prevent the K48 polyubiquitination-dependent protein degradation of RIP1 by enhancing the carbonylation of RIP1.

DISCUSSION

In this study, we found that 4-HNE played an important role in myocardial necroptosis during MI/R injury. 4-HNE induced cardiomyocyte necroptosis by increasing RIP1 and RIP3 and the

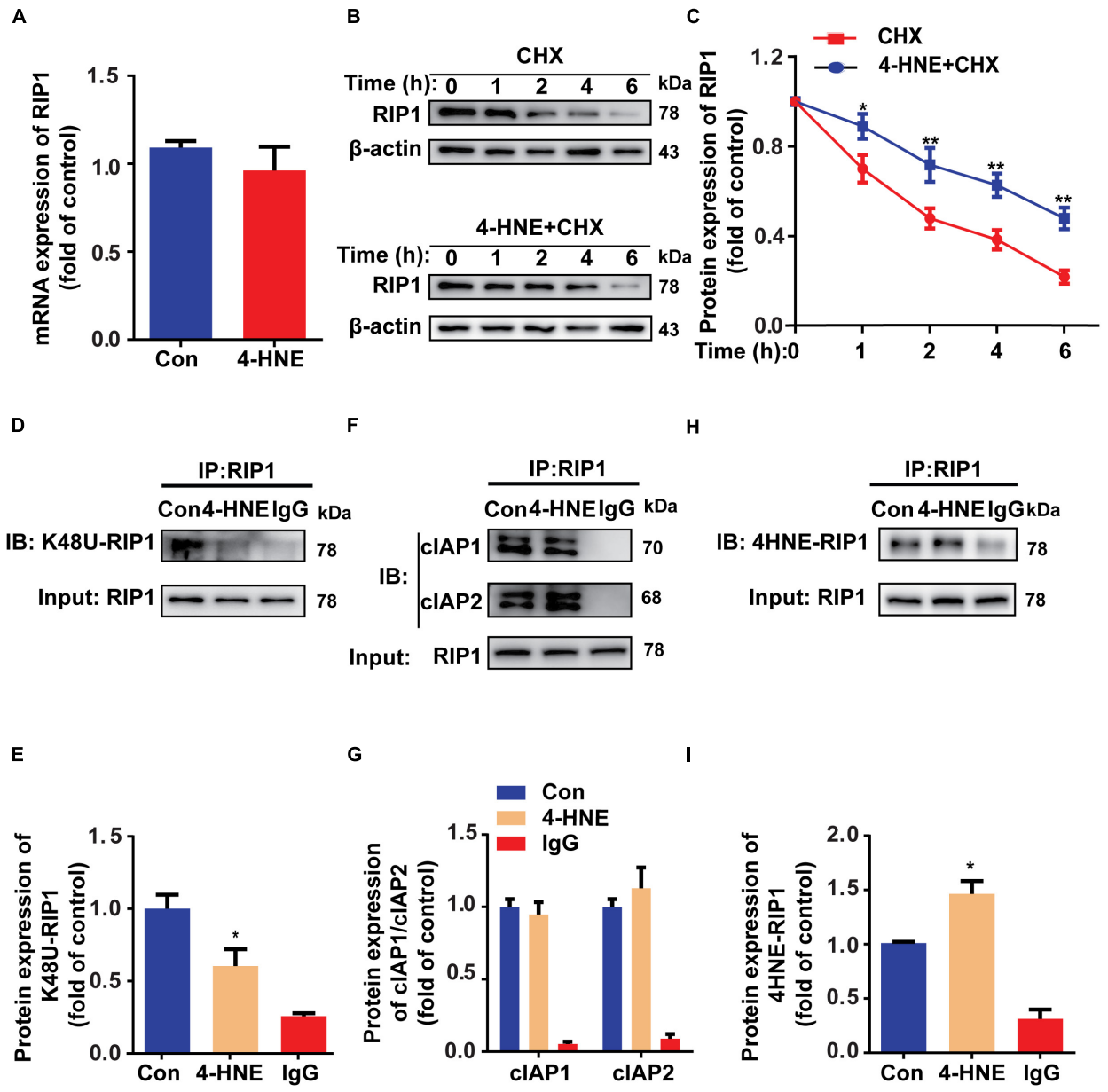

FIGURE 6 | 4-Hydroxy-2-non-enal reduces the ubiquitin-dependent degradation of RIP1. **(A)** RIP1 mRNA expression in H9c2 tested by quantitative real-time polymerase chain reaction ($n = 5$). **(B,C)** Protein expression of RIP1 in H9c2 cells treated with cycloheximide (CHX) and 4-HNE detected by Western blot ($n = 5$). **(D,E)** Co-immunoprecipitation using anti-RIP1 antibody showed the K48 ubiquitination of RIP1 ($n = 3$). **(F,G)** Co-immunoprecipitation using anti-RIP1 antibody to detect combination between RIP1 and cIAP1 or cIAP2 ($n = 3$). **(H,I)** Co-immunoprecipitation using anti-RIP1 antibody to detect the combination between RIP1 and 4-HNE ($n = 3$). $^{*}p < 0.05$ vs. control group, $^{**}p < 0.01$ vs. control group.

phosphorylation of the two proteins. Subsequently, the increase of MLKL and the phosphorylation of MLKL and CaMKII also evidenced that 4-HNE promoted cell necroptosis. Further studies found that 4-HNE favored the stabilization of RIP1 by suppressing K48 polyubiquitination of RIP1, leading to less protein degradation (**Figure 7**).

Myocardial ischemia reperfusion injury is characterized as the large burst of cardiomyocyte deaths (Whelan et al., 2010). Increasing evidence shows that necroptosis is the major type of programmed cell necrosis during MI/R. Preventing necroptosis was able to reduce myocardial infarct zone by nearly one third in animal MI/R models (Dmitriev et al., 2013; Zhang et al., 2014; Koudstaal et al., 2015).

4-Hydroxy-2-nonenal, an important product during oxidative stress, is abundantly produced during MI/R injury (Mali and Palaniyandi, 2014). 4-HNE regulates pathological

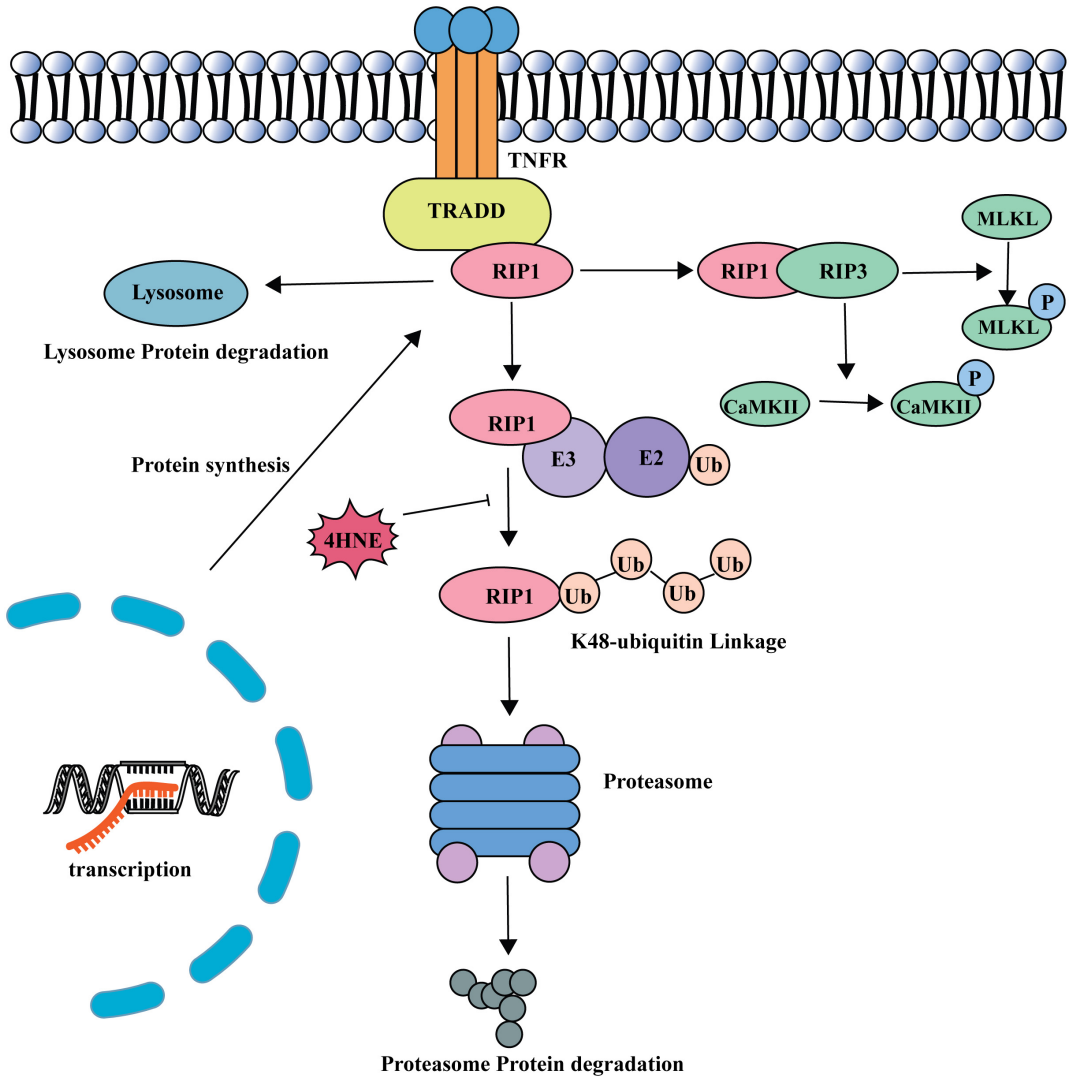

FIGURE 7 | A model of the role of 4-HNE in regulating cardiomyocyte necroptosis during MI/R.

processes through various ways. 4-HNE can bind to cysteine, histidine, and lysine amino residues by Michael reactions (Dubinina and Dadali, 2010). 4-HNE can also directly modify four DNA bases and then affect diverse biological processes (Zhong and Yin, 2015). Previous studies proved that 4-HNE regulated cell apoptosis or autophagy in different ways (Dodson et al., 2017; Yang et al., 2019). However, whether 4-HNE contributes to cell necroptosis was never reported. In the present study, we found that 4-HNE played an important role in cardiomyocyte necroptosis during MI/R injury or in the isolated perfused heart.

Necroptosis is usually initiated by the combination between pro-inflammatory factors and their corresponding receptors. The most well-studied pathway in cardiovascular diseases is tumor necrosis factor receptor 1 (TNFR1) signaling (Zhu and Sun, 2018). Once it is activated, RIP1, TNFR-associated death domain (TRADD), TNFR-associated factor (TRAF), and other factors are recruited to the intracellular part of TNFR1 to form necroptosis complex I. After the TNFR1 endocytosis, complex I shifts into complex II, which recruits and activates RIP3. MLKL and CaMKII are regarded as executors of necroptosis and activated by RIP3 (Galluzzi et al., 2017).

Receptor-interacting serine/threonine-protein kinase 1 has emerged as a vital upstream kinase that controls multiple cellular pathways involved in regulating cell death (Christofferson et al., 2014). RIP1 induces necroptosis by recruiting RIP3 and forming necrosome (Li et al., 2012). In this study, we found that increased RIP1 played a critical role in 4-HNE-induced cardiomyocyte necroptosis. RIP1 kinase is intricately regulated by ubiquitination, deubiquitination, and phosphorylation (Christofferson et al., 2014). Ubiquitination is a kind of post-translation modification during which ubiquitin protein is attached to substrate proteins. RIP1 can recruit E3 ligases such as cIAP1 and cIAP2, which mediate K11, K48,

K63, and linear polyubiquitination of RIP1 (Witt and Vucic, 2017). K48-linked ubiquitin modifications of RIP1 favor the combination with proteasomes and result in degradation of RIP1, while K63-linked ubiquitin modifications of RIP1 promote the activation of nuclear factor (NF)-κB (Lu et al., 2013; Ofengeim and Yuan, 2013). In this study, we found that 4-HNE reduced the K48 polyubiquitination of RIP1. Additionally, 4-HNE mainly affects the conjugation of ubiquitin molecules to the RIP1 instead of engagement of E3 ligases, as indicated by **Figures 6F,G**. As shown in **Supplementary Figure 3**, the structure of RIP1 is composed of lysine, cysteine, and histidine; thus, it is possible that 4-HNE modifies RIP1 directly (Ofengeim and Yuan, 2013). Thus, we speculate that the carbonylation of RIP1 might affect the ubiquitin binding sites and limit the binding of K48-linked ubiquitin.

In summary, we demonstrated that elevated 4-HNE directly combined with RIP1, which contributed to the decreasing of ubiquitin-mediated RIP1 degradation, thus resulting in activating the necroptosis pathway and promoting the myocardium necroptosis.

DATA AVAILABILITY STATEMENT

The raw data supporting the conclusion of this article will be made available by the authors, without undue reservation.

ETHICS STATEMENT

The animal study was reviewed and approved by Animal Ethics Committee of Qilu Hospital of Shandong University.

AUTHOR CONTRIBUTIONS

YC conceived the project. SW and JW planned and designed the experiments. XZ performed most of the experimental work and analyzed the data. WW performed some experimental work, interpreted the results, and drafted the manuscript. SS and JL participated in the performing of mouse I/R surgery. SC and RL participated in maintenance of H9c2 cell. TX and QY planned the Langendorff model and finished it. SW wrote the final version of the article. All authors contributed to the article and approved the submitted version.

FUNDING

This study was supported by the National Natural Science Foundation of China (82030059, 82072141, and 81873953), National S&T Fundamental Resources Investigation Project (2018FY100600 and 2018FY100602), Taishan Pandeng Scholar Program of Shandong Province (tspd20181220), Key R&D Program of Shandong Province (2019GSF108261, 2018GSF118003, and 2017GSF218040), Natural Science Foundation of Shandong Province (ZR2020MH030), Shandong Medical and Health Science Technology Development Plan Project (2018WS329), and Clinical Research Foundation of Shandong University (2020SDUCRCC014).

SUPPLEMENTARY MATERIAL

The Supplementary Material for this article can be found online at: https://www.frontiersin.org/articles/10.3389/fcell.2021.721795/full#supplementary-material

REFERENCES

Ayala, A., Munoz, M. F., and Arguelles, S. (2014). Lipid peroxidation: production, metabolism, and signaling mechanisms of malondialdehyde and 4-hydroxy-2-nonenal. *Oxid. Med. Cell Longev.* 2014:360438. doi: 10.1155/2014/360438

Chen, J., Kos, R., Garssen, J., and Redegeld, F. (2019). Molecular insights into the mechanism of necroptosis: the necrosome as a potential therapeutic target. *Cells* 8:1486. doi: 10.3390/cells8121486

Chen, X., Li, W., Ren, J., Huang, D., He, W. T., Song, Y., et al. (2014). Translocation of mixed lineage kinase domain-like protein to plasma membrane leads to necrotic cell death. *Cell Res.* 24, 105–121. doi: 10.1038/cr.2013.171

Cho, Y. S., Challa, S., Moquin, D., Genga, R., Ray, T. D., Guildford, M., et al. (2009). Phosphorylation-driven assembly of the RIP1-RIP3 complex regulates programmed necrosis and virus-induced inflammation. *Cell* 137, 1112–1123. doi: 10.1016/j.cell.2009.05.037

Christofferson, D. E., Li, Y., and Yuan, J. (2014). Control of life-or-death decisions by RIP1 kinase. *Annu. Rev. Physiol.* 76, 129–150. doi: 10.1146/annurev-physiol-021113-170259

Dmitriev, Y. V., Minasian, S. M., Demchenko, E. A., and Galagudza, M. M. (2013). Study of cardioprotective effects of necroptosis inhibitors on isolated rat heart subjected to global ischemia-reperfusion. *Bull. Exp. Biol. Med.* 155, 245–248.

Dodson, M., Wani, W. Y., Redmann, M., Benavides, G. A., Johnson, M. S., Ouyang, X., et al. (2017). Regulation of autophagy, mitochondrial dynamics, and cellular bioenergetics by 4-hydroxynonenal in primary neurons. *Autophagy* 13, 1828–1840. doi: 10.1080/15548627.2017.1356948

Dubinina, E. E., and Dadali, V. A. (2010). Role of 4-hydroxy- trans -2-nonenal in cell functions. *Biochemistry (Moscow)* 75, 1069–1087. doi: 10.1134/S0006297910090014

Esterbauer, H., Schaur, R. J., and Zollner, H. (1991). Chemistry and biochemistry of 4-hydroxynonenal, malonaldehyde and related aldehydes. *Free Radic. Biol. Med.* 11, 81–128. doi: 10.1016/0891-5849(91)90192-6

Galluzzi, L., Kepp, O., Chan, F. K.-M., and Kroemer, G. (2017). Necroptosis: mechanisms and relevance to disease. *Annu. Rev. Pathol.* 12, 103–130. doi: 10.1146/annurev-pathol-052016-100247

Heusch, G., and Gersh, B. J. (2017). The pathophysiology of acute myocardial infarction and strategies of protection beyond reperfusion: a continual challenge. *Eur. Heart J.* 38, 774–784. doi: 10.1093/eurheartj/ehw224

Hwang, H. V., Sandeep, N., Paige, S. L., Ranjbarvaziri, S., Hu, D. Q., Zhao, M., et al. (2020). 4HNE impairs myocardial bioenergetics in congenital heart disease-induced right ventricular failure. *Circulation* 142, 1667–1683. doi: 10.1161/CIRCULATIONAHA.120.045470

Kimura, M., Yokoyama, A., and Higuchi, S. (2019). Aldehyde dehydrogenase-2 as a therapeutic target. *Expert Opin. Ther. Targets* 23, 955–966. doi: 10.1080/14728222.2019.1690454

Komander, D. (2009). The emerging complexity of protein ubiquitination. *Biochem. Soc. Trans.* 37(Pt 5), 937–953. doi: 10.1042/BST0370937

Koudstaal, S., Oerlemans, M. I. F. J., Van der Spoel, T. I. G., Janssen, A. W. F., Hoefer, I. E., Doevendans, P. A., et al. (2015). Necrostatin-1 alleviates reperfusion injury following acute myocardial infarction in pigs. *Eur. J. Clin. Invest.* 45, 150–159. doi: 10.1111/eci.12391

Li, J., McQuade, T., Siemer, A. B., Napetschnig, J., Moriwaki, K., Hsiao, Y. S., et al. (2012). The RIP1/RIP3 necrosome forms a functional amyloid signaling

complex required for programmed necrosis. *Cell* 150, 339–350. doi: 10.1016/j.cell.2012.06.019

Linkermann, A., and Green, D. R. (2014). Necroptosis. *N. Engl. J. Med.* 370, 455–465. doi: 10.1056/NEJMra1310050

Liu, Y., Liu, T., Lei, T., Zhang, D., Du, S., Girani, L., et al. (2019). RIP1/RIP3-regulated necroptosis as a target for multifaceted disease therapy (review). *Int. J. Mol. Med.* 44, 771–786. doi: 10.3892/ijmm.2019.4244

Lu, T. T., Onizawa, M., Hammer, G. E., Turer, E. E., Yin, Q., Damko, E., et al. (2013). Dimerization and ubiquitin mediated recruitment of A20, a complex deubiquitinating enzyme. *Immunity* 38, 896–905. doi: 10.1016/j.immuni.2013.03.008

Lucas, D. T., and Szweda, L. I. (1999). Declines in mitochondrial respiration during cardiac reperfusion: age-dependent inactivation of alpha-ketoglutarate dehydrogenase. *Proc. Natl. Acad. Sci. U.S.A.* 96, 6689–6693.

Mali, V. R., and Palaniyandi, S. S. (2014). Regulation and therapeutic strategies of 4-hydroxy-2-nonenal metabolism in heart disease. *Free Radic. Res.* 48, 251–263. doi: 10.3109/10715762.2013.864761

Ofengeim, D., and Yuan, J. (2013). Regulation of RIP1 kinase signalling at the crossroads of inflammation and cell death. *Nat. Rev. Mol. Cell Biol.* 14, 727–736. doi: 10.1038/nrm3683

Orozco, S., Yatim, N., Werner, M. R., Tran, H., Gunja, S. Y., Tait, S. W., et al. (2014). RIPK1 both positively and negatively regulates RIPK3 oligomerization and necroptosis. *Cell Death Differ.* 21, 1511–1521. doi: 10.1038/cdd.2014.76

Samant, R. S., Livingston, C. M., Sontag, E. M., and Frydman, J. (2018). Distinct proteostasis circuits cooperate in nuclear and cytoplasmic protein quality control. *Nature* 563, 407–411. doi: 10.1038/s41586-018-0678-x

Santin, Y., Fazal, L., Sainte-Marie, Y., Sicard, P., Maggiorani, D., Tortosa, F., et al. (2020). Mitochondrial 4-HNE derived from MAO-A promotes mitoCa(2+) overload in chronic postischemic cardiac remodeling. *Cell Death Differ.* 27, 1907–1923. doi: 10.1038/s41418-019-0470-y

Smith, C. C., Davidson, S. M., Lim, S. Y., Simpkin, J. C., Hothersall, J. S., and Yellon, D. M. (2007). Necrostatin: a potentially novel cardioprotective agent? *Cardiovasc. Drugs Ther.* 21, 227–233. doi: 10.1007/s10557-007-6035-1

Sun, A., Zou, Y., Wang, P., Xu, D., Gong, H., Wang, S., et al. (2014). Mitochondrial aldehyde dehydrogenase 2 plays protective roles in heart failure after myocardial infarction via suppression of the cytosolic JNK/p53 pathway in mice. *J. Am. Heart Assoc.* 3:e000779. doi: 10.1161/JAHA.113.000779

Wang, L., Du, F., and Wang, X. (2008). TNF-alpha induces two distinct caspase-8 activation pathways. *Cell* 133, 693–703. doi: 10.1016/j.cell.2008.03.036

Whelan, R. S., Kaplinskiy, V., and Kitsis, R. N. (2010). Cell death in the pathogenesis of heart disease: mechanisms and significance. *Annu. Rev. Physiol.* 72, 19–44. doi: 10.1146/annurev.physiol.010908.163111

Witt, A., and Vucic, D. (2017). Diverse ubiquitin linkages regulate RIP kinases-mediated inflammatory and cell death signaling. *Cell Death Differ.* 24, 1160–1171. doi: 10.1038/cdd.2017.33

Yang, L.-l, Chen, H., Wang, J., Xia, T., Sun, H., Yuan, C.-h, et al. (2019). 4-HNE induces apoptosis of human retinal pigment epithelial cells by modifying HSP70. *Curr. Med. Sci.* 39, 442–448. doi: 10.1007/s11596-019-2057-8

Yellon, D. M., and Hausenloy, D. J. (2007). Myocardial reperfusion injury. *N. Engl. J. Med.* 357, 1121–1135. doi: 10.1056/NEJMra071667

Zhang, A., Mao, X., Li, L., Tong, Y., Huang, Y., Lan, Y., et al. (2014). Necrostatin-1 inhibits Hmgb1-IL-23/IL-17 pathway and attenuates cardiac ischemia reperfusion injury. *Transpl. Int.* 27, 1077–1085. doi: 10.1111/tri.12349

Zhang, Y., Chen, X., Gueydan, C., and Han, J. (2018). Plasma membrane changes during programmed cell deaths. *Cell Res.* 28, 9–21. doi: 10.1038/cr.2017.133

Zhe-Wei, S., Li-Sha, G., and Yue-Chun, L. (2018). The role of necroptosis in cardiovascular disease. *Front. Pharmacol.* 9:721. doi: 10.3389/fphar.2018.00721

Zhong, H., and Yin, H. (2015). Role of lipid peroxidation derived 4-hydroxynonenal (4-HNE) in cancer: focusing on mitochondria. *Redox Biol.* 4, 193–199. doi: 10.1016/j.redox.2014.12.011

Zhu, H., and Sun, A. (2018). Programmed necrosis in heart disease: molecular mechanisms and clinical implications. *J. Mol. Cell. Cardiol.* 116, 125–134. doi: 10.1016/j.yjmcc.2018.01.018

Conflict of Interest: The authors declare that the research was conducted in the absence of any commercial or financial relationships that could be construed as a potential conflict of interest.

Publisher's Note: All claims expressed in this article are solely those of the authors and do not necessarily represent those of their affiliated organizations, or those of the publisher, the editors and the reviewers. Any product that may be evaluated in this article, or claim that may be made by its manufacturer, is not guaranteed or endorsed by the publisher.

Copyright © 2021 Zhai, Wang, Sun, Han, Li, Cao, Li, Xu, Yuan, Wang, Wei and Chen. This is an open-access article distributed under the terms of the Creative Commons Attribution License (CC BY). The use, distribution or reproduction in other forums is permitted, provided the original author(s) and the copyright owner(s) are credited and that the original publication in this journal is cited, in accordance with accepted academic practice. No use, distribution or reproduction is permitted which does not comply with these terms.

frontiers in Cell and Developmental Biology

REVIEW
published: 07 October 2021
doi: 10.3389/fcell.2021.729728

Endogenous SO_2 Controls Cell Apoptosis: The State-of-the-Art

Yingying Li[1,2†], Yingjun Feng[2†], Xiaoyun Ye[1†], Hanlin Peng[1], Jiantong Du[3], Xiaoli Yao[2], Yaqian Huang[1], Hongfang Jin[1*] and Junbao Du[1,4*]*

[1] Department of Pediatrics, Peking University First Hospital, Beijing, China, [2] Department of Cardiovascular Medicine, Children's Hospital Affiliated to Zhengzhou University/Children's Hospital of Henan Province, Zhengzhou, China, [3] Department of Ophthalmology, Peking University First Hospital, Beijing, China, [4] Key Lab of Molecular Cardiology, Ministry of Education, Beijing, China

SO_2, previously known as the product of industrial waste, has recently been proven to be a novel gasotransmitter in the cardiovascular system. It is endogenously produced from the metabolism pathway of sulfur-containing amino acids in mammalians. Endogenous SO_2 acts as an important controller in the regulation of many biological processes including cardiovascular physiological and pathophysiological events. Recently, the studies on the regulatory effect of endogenous SO_2 on cell apoptosis and its pathophysiological significance have attracted great attention. Endogenous SO_2 can regulate the apoptosis of vascular smooth muscle cells, endothelial cells, cardiomyocytes, neuron, alveolar macrophages, polymorphonuclear neutrophils and retinal photoreceptor cells, which might be involved in the pathogenesis of hypertension, pulmonary hypertension, myocardial injury, brain injury, acute lung injury, and retinal disease. Therefore, in the present study, we described the current findings on how endogenous SO_2 is generated and metabolized, and we summarized its regulatory effects on cell apoptosis, underlying mechanisms, and pathophysiological relevance.

Keywords: sulfur dioxide, metabolism, apoptosis, mechanism, pathophysiology

OPEN ACCESS

Edited by:
Zhi Qi,
Nankai University, China

Reviewed by:
Linxi Chen,
University of South China, China
Liming Yang,
Harbin Medical University, China
Wei Yang,
The Fourth Hospital of Harbin Medical University, China

****Correspondence:***
Yaqian Huang
yaqianhuang@126.com
Hongfang Jin
jinhongfang51@126.com
Junbao Du
junbaodu1@126.com

† These authors have contributed equally to this work

Specialty section:
This article was submitted to Cell Death and Survival, a section of the journal Frontiers in Cell and Developmental Biology

Received: *23 June 2021*
Accepted: *13 September 2021*
Published: *07 October 2021*

Citation:
Li Y, Feng Y, Ye X, Peng H, Du J, Yao X, Huang Y, Jin H and Du J (2021) Endogenous SO_2 Controls Cell Apoptosis: The State-of-the-Art. Front. Cell Dev. Biol. 9:729728. doi: 10.3389/fcell.2021.729728

INTRODUCTION

Previously, SO_2 was recognized as a water-soluble, colorless, transparent exhaust gas and air pollutant with a sharp odor. High concentrations of SO_2 in the environment could cause various degrees of damage to humans, animals, plants, and even microorganisms. However, it was discovered that SO_2 can be endogenously produced in the mammalian metabolism of sulfur-containing amino acids (SAAs) (Stipanuk, 2004; Kimura, 2011). Many studies have shown that endogenous SO_2 has the unique characteristics of continuous production, rapid diffusion, low molecular weight, and extensive action (Du et al., 2008a; Huang et al., 2016). More interestingly, it was found to play an important role in regulating cardiovascular function and structure under physiologic and pathophysiologic conditions (Du et al., 2008a; Huang et al., 2016). Therefore, we proposed that SO_2 is a new cardiovascular gaseous signaling molecule. However, the molecular mechanisms underlying its biological action require further studies. It has been found recently that endogenous SO_2 regulates cell apoptosis, and therefore contributes to the pathogenesis of hypertension, pulmonary hypertension, myocardial injury, brain injury, retinal disease, and acute lung injury (Zhao et al., 2008, 2013, 2019; Wang et al., 2011; Ma et al., 2012; Jin et al., 2013; Han et al., 2014; Du et al., 2018; Liu et al., 2018; Niu et al., 2018; Yang et al., 2018; Zhou et al., 2020). In this article, we described the generation and metabolism of endogenous SO_2, and summarized

the latest findings of the regulation of endogenous SO_2 on cell apoptosis, its mechanisms, and pathophysiological significance.

GENERATION AND METABOLISM OF ENDOGENOUS SO_2

SO_2 can be produced endogenously through the biotransformation of SAAs in various mammal systems (**Figure 1**), such as the cardiovascular, respiratory, nervous, digestive, urinary, and immune systems. In the body, SAAs, such as methionine and cystine, are primarily metabolized to L-cysteine (L-Cys). L-Cys is a crucial precursor of endogenous SO_2 (Singer and Kearney, 1956; Stipanuk, 2004; Du et al., 2008a; Kimura, 2011; Huang et al., 2016). It can be oxidized to produce L-cysteinesulfinate, and this process involves a key enzyme cysteine dioxygenase. Subsequently, the metabolism of L-cysteinesulfinate involves two pathways. In one pathway, L-cysteinesulfinate is converted into β-sulfinylpyruvate via the catalysis of aspartate aminotransferase (AAT), which is followed by spontaneous decomposition of β-sulfinylpyruvate into SO_2 and pyruvic acid. In the other pathway, L-cysteinesulfinate is decarboxylated into hypotaurine and CO_2 via cysteinesulfinate decarboxylase. Hypotaurine is subsequently oxidized to taurine. There is a competition between these two pathways for the reaction tendency of L-cysteinesulfinate, which is ultimately determined by the activities of AAT and cysteinesulfinate decarboxylase (Singer and Kearney, 1956; Griffith, 1983). Studies have indicated that 3′-phosphoadenosine-5′-phosphosulfate in activated neutrophils functions as an endogenous sulfate donor (Stipanuk, 2004).

Besides, hydrogen sulfide (H_2S), another gaseous signaling molecule, metabolized from SAAs catalyzed by cystathionine γ-lyase or cystathionine β-synthase (Stipanuk, 2004; Kimura, 2011), can be transformed into SO_2 or sulfite through the following two pathways: (1) H_2S is oxidized directly to sulfite or SO_2 through reduced nicotinamide adenine dinucleotide phosphate (NADPH) oxidase (Mitsuhashi et al., 2005). (2) H_2S is firstly oxidized by sulfide oxidase into thiosulfate, and then the enzymes such as thiosulfate sulfurtransferase or glutathione-dependent thiosulfate reductase catalyze the transformation of thiosulfate to SO_2 (Shapiro, 1977).

In mammals, SO_2 can be hydrated to sulfite, and then converted into sulfate by sulfite oxidase, finally excreted in the urine in the kidney (Stipanuk, 2004; Huang et al., 2016). The half-life of SO_2 was supposed to be about 5–10 min, represented by the fact that serum SO_2 level decreased by 50% about 5–10 min after a bolus intravenous injection of SO_2 donor (Du et al., 2008b). It is known that AAT has two isozymes: cytosol AAT1 and mitochondrial AAT2. Huang et al. found that the overexpression of AAT1 or AAT2 increased but the knockdown of AAT1 or AAT2 inhibited the endogenous SO_2 production, suggesting that AAT1/2 is the main SO_2-generating enzyme (Liu et al., 2014).

SO_2 was detected in the headspace gas collected from a closed vial culturing porcine coronary arteries in 2003 by Balazy et al. (2003). Du et al. firstly found the SO_2/AAT pathway in the cardiovascular tissues of rats in 2008 (Du et al., 2008a). The SO_2 level in rat plasma was 15.54 ± 1.68 μmol/L while the SO_2 concentration in the aorta, pulmonary artery, mesenteric artery, tail artery, and renal artery were 3.27 ± 0.21, 2.67 ± 0.17, 2.50 ± 0.20, and 2.23 ± 0.19 μmol/g protein, respectively. To date, SO_2/AAT pathway has been found in almost all organs in mammals including vessels, heart, stomach, lung, liver, kidney, brain, retina, pancreas, and spleen, etc. (Luo et al., 2011; Du et al., 2018). It was found that the SO_2 level was the highest in the stomach, followed by the ventricle, and the activity of AAT and the expression of AAT1 mRNA are the highest in the left ventricle, whereas the expression of the AAT1 protein is the highest in the right ventricle. Furthermore, the expression of AAT2 mRNA is the highest in the liver, whereas the expression of the AAT2 protein is the highest in the renal medullary membrane (Luo et al., 2011).

MECHANISMS BY WHICH SO_2 REGULATES CELL APOPTOSIS AND THE SIGNIFICANCE

Apoptosis is the programmed cell death that occurs in multicellular organisms. Increasing evidence implies that endogenous SO_2 participates in regulating cell apoptosis (Zhao et al., 2008, 2013, 2019; Wang et al., 2011; Ma et al., 2012; Jin et al., 2013; Han et al., 2014; Du et al., 2018; Liu et al., 2018; Niu et al., 2018; Yang et al., 2018; Zhou et al., 2020, **Figure 2**). Three main pathways associated with the regulation of SO_2 on cell apoptosis have been revealed to date: (1) Extrinsic pathway (Wajant, 2002; Zhao et al., 2008): The combination of Fas ligand (FasL)/Fas causes the binding of the Fas-associated death domain proteins which activate caspase-8 precursor (caspase-10 in humans), initiate the cascade activation of caspase-3, caspase-6, and caspase-7 and then induce cell apoptosis. (2) Intrinsic pathway (Jin et al., 2013): The leakage of cytochrome c (Cytc) from impaired mitochondria to cytosol is the central event of the mitochondria-related intrinsic apoptosis pathway. Its preceding events include the deformation and swelling of mitochondria, the imbalance of apoptotic regulator B-cell lymphoma-2 (bcl-2)/bcl-2-associated X protein (bax), the destroy of mitochondrial membrane potential (MMP), and the opening of mitochondrial permeability transition pore (MPTP). The cytosol Cytc activates caspase-9 and caspase-3, finally induces cell apoptosis. (3) Endoplasmic reticulum stress (ERS)-related apoptosis (Wang et al., 2011): The overactivated ERS induces cell apoptosis via overexpressing C/EBP homologous protein (CHOP) and activating caspase-12.

Endogenous SO_2 Promotes Vascular Smooth Muscle Cell Apoptosis

As the main component cell of the vessel, the vascular smooth muscle cell (VSMC) apoptosis markedly affects vascular remodeling. Zhao et al. (2008) found that compared with the WKY rat, the plasma SO_2 level and the proportion of apoptotic VSMC in media were downregulated in the spontaneously hypertensive rat (SHR). Correspondingly, the blood pressure and

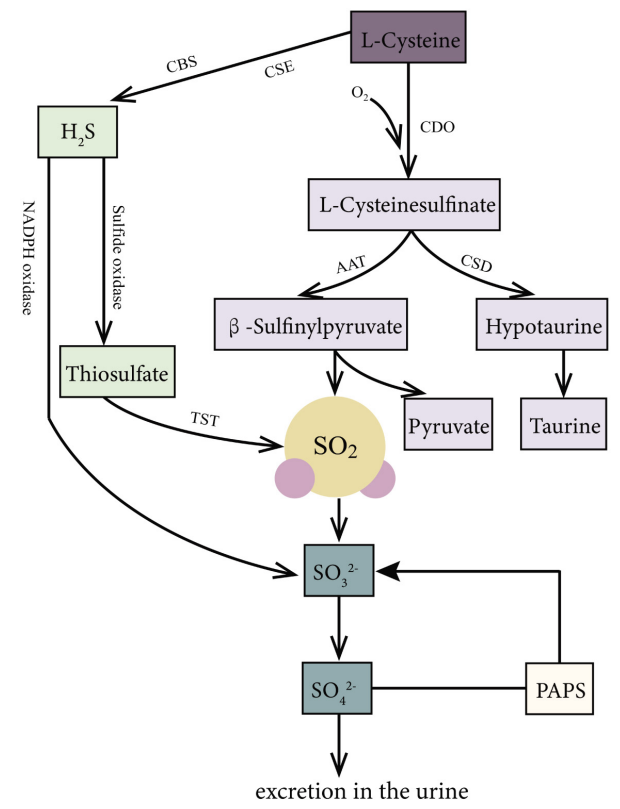

FIGURE 1 | Production and metabolism of endogenous SO_2 in mammals. L-Cys is metabolized through important enzymes including CDO, AAT, and CSD to generate endogenous SO_2, pyruvic acid, and hypotaurine. Moreover, H_2S, a product of the reaction catalyzed by CSE and CBS with L-Cys as substrate, can be metabolized to sulfite or SO_2 via the catalyzation of sulfide oxidase, TST, and NADPH oxidase. Thirdly, PAPS in activated neutrophils is also an origin of sulfite. In mammals, SO_2 can be hydrated to sulfite, then converted into sulfate by sulfite oxidase, and finally excreted in the urine in the kidney. AAT: aspartate aminotransferase; CBS, cystathionine β-synthase; CDO, cysteine dioxygenase; CSE, cystathionine γ-lyase; L-Cys, L-cysteine; NADPH, nicotinamide dinucleotide phosphate; PAPS, 3′-phosphoadenosine-5′-phosphosulfate; TST, thiosulfate sulfurtransferase.

the ratio of aorta media to lumen radius were increased by 53.6 and 28.1% in the SHR rat, respectively. Furthermore, SO_2 donor treatment recovered the decreased plasma SO_2 content, promoted the VSMC apoptosis, decreased blood pressure, and alleviated the thickening aorta media in the SHR rat. Mechanistically, the expression of antiapoptotic factor bcl-2 was increased but the expression of proapoptotic factor Fas and caspase-3 was decreased in the aorta media in the rats of the SHR + SO_2 group compared with those in the rats of the SHR group. These data suggested that SO_2 might alleviate the vascular remodeling by promoting VSMC apoptosis, which involved the regulation of bcl-2, Fas, and caspase-3.

However, SO_2 did not affect the apoptosis of VSMC with or without fetal bovine serum stimulation *in vitro* (Liu et al., 2014). The discrepant effects of SO_2 on VMSC apoptosis might be associated with the different experimental conditions such as *in vivo* and *in vitro*. For example, VSMCs are directly challenged by cyclic mechanical stretch and hydrostatic pressure and indirectly affected by endothelial cell (EC)-transduced shear stress under *in vivo* circumstances (Qiu et al., 2013; Chen et al., 2021). The abovementioned biomechanical stresses are reported to control the VSMC apoptosis, proliferation, and other behaviors and only are partly mimicked *in vivo*.

Endogenous SO_2 Inhibits Vascular Endothelial Cell Apoptosis

Vascular ECs constitute a huge divider separating the lumen and wall of the vessel, and therefore play a crucial role in maintaining the vascular function and microenvironment homeostasis. Especially, vascular EC apoptosis is a key process involved in the vascular physiological and pathophysiological regulation such as organ development, angiogenesis, vascular injury, and remodeling (Duan et al., 2021; Tisch and Ruiz de Al modóvar, 2021). During the development of hypoxic pulmonary artery structural remodeling, hypoxia-induced vascular EC apoptosis is a critical pathological change. Liu et al. explored the effect of SO_2 on the human pulmonary artery endothelial cell (HPAEC) apoptosis based on cobalt chloride ($CoCl_2$)-stimulated cell model (Liu et al., 2018). The endogenous SO_2 production and AAT1 expression were down-regulated but the percentage of terminal deoxynucleotidyl transferase-mediated nick end labeling (TUNEL)-positive nuclei was increased in HPAECs of the vehicle + $CoCl_2$ group as compared with those of the vehicle group. However, there was no difference in the endogenous SO_2/AAT1 pathway and apoptosis of HPAECs between the AAT1 overexpression and AAT1 overexpression + $CoCl_2$ groups, suggesting that the sufficient endogenous SO_2 was a powerful antagonist to chemical hypoxia-induced HPAEC apoptosis. Furthermore, AAT1 overexpression prevented the downregulation of antiapoptotic factor bcl-2, and the activation of caspase-3 in the $CoCl_2$-treated HPAECs. These data suggested that the endogenous SO_2 might inhibit the hypoxia-induced HPAEC apoptosis by increasing bcl-2 expression, and inactivating caspase-3.

Endogenous SO_2 Regulates Cardiomyocyte Apoptosis

Cardiomyocyte apoptosis is a keystone of cardiac pathological changes and is closely correlated with the development of heart failure, myocardial ischemia-reperfusion (I/R) injury and cardiomyopathy, etc. Endogenous SO_2 was found to protect against the myocardial I/R, isopropylarterenol (ISO)-induced cardiac injury, sepsis-induced cardiac dysfunction, myocardial infarction, and diabetic cardiomyopathy, suggesting that cardiomyocyte might be an important target cell of endogenous SO_2 (Liang et al., 2011; Wang et al., 2011, 2018; Chen et al., 2012; Jin et al., 2013; Zhao et al., 2013; Liu et al., 2017; Yang et al., 2018; Zhou et al., 2020).

SO_2 preconditioning significantly reduced the size of the myocardial infarction and decreased the percentage of TUNEL-positive cells in the rats of myocardial I/R (Wang et al., 2011). The mechanisms by which SO_2 preconditioning inhibited the cardiomyocyte apoptosis in the myocardial I/R

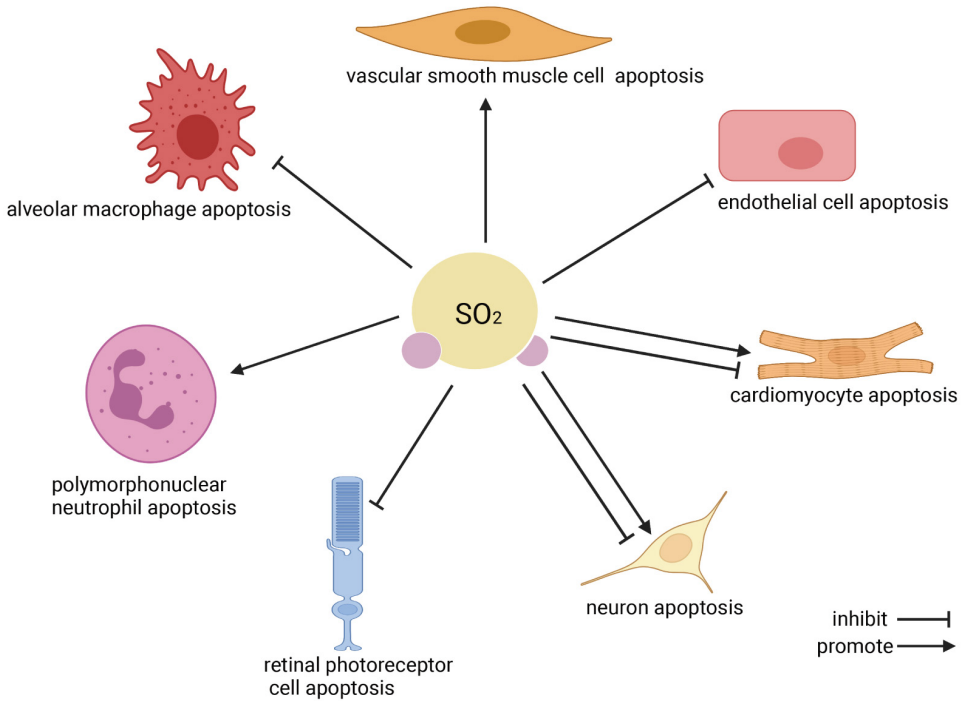

FIGURE 2 | The effect of endogenous SO_2 on cell apoptosis. According to the clockwise direction, the SO_2 target cells are shown beginning from vascular smooth muscle cells. In the cardiovascular system, endogenous SO_2 promotes vascular smooth muscle cell apoptosis, inhibits vascular endothelial cell apoptosis, and inhibits/promotes cardiomyocyte apoptosis. In the nervous system, endogenous SO_2 inhibits/promotes neuron apoptosis, and reduces the apoptosis of retinal photoreceptor cells. Regarding immune cells, SO_2 promotes polymorphonuclear neutrophil apoptosis but inhibits macrophage apoptosis.

might involve the following (Wang et al., 2011; Zhao et al., 2013): (1) SO_2 preconditioning induced a moderate ERS, and then inhibited vigorous ERS-initiated cardiomyocyte apoptosis in the development of myocardial I/R injury. The above process was supported by the fact that SO_2 induced early ERS markers glucose-regulated protein 78 (Grp78) expression and eukaryotic initiation factor 2α (eIF2α) phosphorylation, while myocardial I/R induced early and late ERS markers including Grp78 expression, eIF2α phosphorylation, CHOP expression and caspase-12 activation, which could be alleviated by SO_2 preconditioning. (2) SO_2 preconditioning inhibited the activation of caspase-9 and caspase-3 in the rats of the myocardial I/R group. Considering that caspase-9 activation subsequently follows the leakage of cytosol Cytc from injury mitochondria, the antiapoptotic effect of SO_2 preconditioning might involve mitochondrial protection. (3) The inhibitor of PI3K/Akt the pathway blocked the SO_2 preconditioning-inhibited caspase-3 activation, suggesting that the activation of the PI3K/Akt pathway might mediate the protective role of SO_2 preconditioning.

The effect of endogenous SO_2 on the ISO-induced cardiomyocyte apoptosis was examined targeting the mitochondrion (Liang et al., 2011; Jin et al., 2013). The SO_2 level in the myocardial tissue was decreased but the proportion of apoptotic cells was increased in the rats of the ISO group compared with those of the control group. SO_2 treatment restored the myocardial SO_2 level and inhibited cardiomyocyte apoptosis. Then, the study further focused on the mitochondria. Firstly, the stereological analysis of the mitochondria showed that SO_2 alleviated the cardiomyocytic mitochondria swelling and deformation, represented by the fact that SO_2 treatment decreased the mitochondrial mean surface area, mean volume and volume density, and increased the mitochondrial numerical density and surface-to-volume ratio in the myocardial tissue of ISO-treated rats. Secondly, SO_2 upregulated bcl-2 expression and downregulated bax expression, improved the impaired MMP, and reclosed the MPTP in rat myocardial tissues. Subsequently, SO_2 blocked the leakage of Cytc from the mitochondria and inhibited the activation of cytosol caspase-9 and caspase-3. These data suggested that endogenous SO_2 prevented ISO-induced cardiomyocytic apoptosis via maintaining the mitochondrial function and structure. Moreover, SO_2 decreased the protein and mRNA levels of ERS markers Grp78, CHOP, and caspase-12 in the myocardial tissues of ISO-treated rats, suggesting that the over-activated ERS might also be involved in the inhibitory effect of SO_2 on the ISO-induced cardiomyocytic apoptosis (Chen et al., 2012).

Similar to the ISO-induced myocardial injury, SO_2 treatment inhibited cardiomyocytic apoptosis in the myocardial tissue of rats with cecal ligation and puncture (CLP), accompanied by an increase in the bcl-2 expression, and a decrease in the bax/bcl-2 ratio and caspase-3 activation (Yang et al., 2018). Moreover, SO_2 decreased the level of inflammatory cytokines, inhibited TLR4 and NLRP3 expression, and reduced the inflammatory

caspase-1 expression in the myocardial tissue of CLP rats and the LPS-treated primary neonatal rat cardiac ventricular myocytes (Yang et al., 2018), suggesting that NLRP3/caspase-1-mediated cell pyroptosis might also participate in the protective role of SO_2 on the sepsis-induced cardiac dysfunction.

In some studies, SO_2 promoted cardiomyocytic apoptosis *in vitro* and *in vivo* (Li et al., 2019). The data showed that the SO_2 increased the proportion of apoptotic cells, activated caspase-9 and caspase-3, destroyed the MMP, reduced bcl-2 expression and the ratio of bcl-2/bax, and upregulated the expression of bax and p53, which could be blocked by antioxidant N-acetylcysteine. We speculated the following explanations for the different effects of SO_2 on cardiomyocyte apoptosis. (1) The experimental reagents were different. Li et al. used sodium bisulfite solution and SO_2 gas inhalation *in vitro* and *in vivo*, respectively, while a mixed solution of sodium sulfite and sodium bisulfite with a molar ratio of 3:1 was used in other studies. (2) The experimental conditions were different. Li et al. used untreated cardiomyocyte H9c2 cells and rats, while other studies were conducted on the different pathological cell and rat models.

Endogenous SO_2 Regulates Neuronal Apoptosis

The relationship between endogenous SO_2 and neuronal apoptosis in the neurological disease was investigated on the kainic acid (KA)-induced epilepsy, febrile seizure (FS), and transient global ischemia/reperfusion models (Han et al., 2014; Niu et al., 2018; Zare Mehrjerdi et al., 2018). The different effects of SO_2 on neuronal apoptosis depended on the neurological disorders and SO_2 donor concentrations.

In the KA-induced epileptic rats, plasma SO_2 level and AAT activity were upregulated compared with those in control rats (Niu et al., 2018). However, an AAT inhibitor HDX treatment retarded the occurrence of hippocampal neuronal apoptosis in the KA-treated rats, represented by the fact that a significant hippocampal neuronal apoptosis was detected in the rats 72 h after treatment with KA, while it was not observed in the rats treated with KA + HDX until 7 days after the intervention. The results suggested that the upregulated endogenous SO_2 might promote hippocampal neuronal apoptosis in the development of epilepsy-related brain injury. Furthermore, the KA-upregulated ERS markers Grp78 expression and phosphorylated PERK in the hippocampus could be inhibited by HDX, indicating that ERS might participate in the promotive effect of SO_2 on hippocampal neuronal apoptosis.

The endogenous SO_2/AAT pathway including SO_2 content and AAT1/2 expressions was upregulated in the hippocampus in rats of recurrent FS, accompanied by an increase in the neuronal apoptosis and mossy fiber sprouting (MFS) in the hippocampus (Han et al., 2014). Furthermore, HDX treatment aggravated the increased neuronal apoptosis and MFS in recurrent FS rats, while the supplement of a low concentration of SO_2 (1–10 μmol/kg) alleviated the above pathological change, suggesting that the upregulated endogenous SO_2 might be a defensive mechanism for antagonizing the neuronal apoptosis in the development of recurrent FS. However, the supplement of a high concentration of SO_2 donor (100 μmol/kg) worsened the neuronal apoptosis and MFS in recurrent FS rats, which reminded us to pay attention to the protective dose range of SO_2.

A global brain I/R injury increased CA1 neuronal apoptosis in the rats undergoing the occlusion of both common carotid arteries, accompanied by an increase in malondialdehyde level, and a decrease in glutathione level and activity of superoxide dismutase in the CA1 region (Zare Mehrjerdi et al., 2018). Furthermore, SO_2 donor treatment improved the learning and memory deficits in the rats with cerebral I/R injury, reduced CA1 neuronal apoptosis, decreased malondialdehyde level, and elevated GSH level and activity of superoxide dismutase in the CA1 region. These findings indicated that SO_2 donor prevented brain ischemic injury by decreasing neuronal apoptosis and the underlying mechanisms might involve the anti-oxidative effect of SO_2. However, the change of endogenous SO_2/AAT pathway in the brain ischemic rats was not detected, which merits further studies for exploring the role of endogenous SO_2 in the development of brain ischemic injury.

Endogenous SO_2 Inhibits Retinal Photoreceptor Cell Apoptosis

Oxidative stress can induce apoptosis of retinal photoreceptor cells, which is the main pathological change of blinding retinal diseases (Wenzel et al., 2005). Du et al. found that apoptosis was significantly induced in the 661w mouse photoreceptor cells exposed to H_2O_2 compared with those without H_2O_2 exposure, demonstrated by an increase in the percentage of TUNEL positive cells and the ratio of cleaved-caspase3/caspase3 (Du et al., 2018). Simultaneously, endogenous SO_2 production and AAT1 expression were decreased in the H_2O_2-treated 661w cells compared with control cells. HDX treatment mimicked the effects of H_2O_2 on 661w cells including an increase in the cell apoptosis and the downregulation of endogenous SO_2/AAT pathway, indicating that the apoptosis of 661W cells caused by oxidative stress might be mediated by the downregulation of the endogenous SO_2 pathway. However, the role of endogenous SO_2 in the development of retinal photoreceptor cell apoptosis and its mechanisms require further studies.

Endogenous SO_2 Promotes Polymorphonuclear Neutrophil Apoptosis

Lipopolysaccharide (LPS) was intratracheally instilled to induce acute lung injury (ALI) in adult male rats (Huang et al., 2009). The decrease in the apoptosis of polymorphonuclear neutrophils (PMNs) contribute to an increment of the number of PMN and a prolonged inflammatory reaction in the injured lung (Lee and Downey, 2001). LPS treatment reduced the SO_2 level in the lung tissue and peripheral blood, while the treatment of SO_2 donor alleviated the lung histopathological changes in the rats accompanied by a reduction of PMN number in the bronchoalveolar lavage fluid (Huang et al., 2009; Ma et al., 2012). Furthermore, SO_2 promoted the apoptosis of PMN in the bronchoalveolar lavage fluid and peripheral blood in the ALI

rats. Mechanistically, SO_2 treatment upregulated the expression of bax, downregulated the expression of bcl-2, and elevated the level of activated caspase-3 in the peripheral PMN in the ALI rats. Therefore, it is believed that SO_2 may antagonize ALI by promoting PMN apoptosis, in which the bax/bcl-2/caspase-3 pathway is involved.

Endogenous SO_2 Inhibits Alveolar Macrophage Apoptosis

Many studies focused on the role of alveolar macrophage (AM) in the pathogenesis of ALI (Cheng et al., 2021). It was found that AM apoptosis was significantly increased in the ALI rat model induced by limb I/R injury, resulting in the delayed clearance of inflammatory PMN and the prolongation of ALI (Zhao et al., 2016). Zhao et al. found that SO_2 donor prevented limb I/R-induced ALI in rats (Zhao et al., 2016). Furthermore, the primary AM was cultured with the plasma extracted from limb I/R to make the limb I/R-induced AM injury model (Zhao et al., 2019). Compared with the ALI group, the AM apoptosis was reduced in the AMs of the ALI + SO_2 group, with an increase in bcl-2 expression, an improvement of the impaired MMP, the reclosing of MPTP and the decrease in caspase-3 expression. These data suggested that the SO_2-inhibited AM apoptosis might be involved in the protective effect of SO_2 on ALI and mitochondrion was the possible target of SO_2.

CONCLUSION AND PERSPECTIVE

As a novel gaseous signaling molecule, endogenous SO_2 was reported to play a variety of biological effects by regulating cell apoptosis. In summary, endogenous SO_2 promoted VSMC apoptosis and inhibited vascular EC apoptosis to alleviate the vascular remodeling in hypertension and pulmonary hypertension. Endogenous SO_2 suppressed the apoptosis of cardiomyocytes, contributing to the cardioprotective effect of SO_2. In the nervous system, SO_2 increased KA-induced hippocampal neuronal apoptosis to aggravate the epileptic brain damage, while SO_2 reduced neuronal apoptosis to protect against the neuronal damage in the recurrent FS and global brain I/R injury. Moreover, the downregulation of endogenous SO_2 was accompanied by the increase in the 661w retinal photoreceptor cell apoptosis, suggesting that endogenous SO_2 might participate in the pathogenesis of blinding retinal disease. In the respiratory system, SO_2 facilitated PMN apoptosis and inhibited AM apoptosis to protect against ALI. The abovementioned apoptosis-related studies proved that the abnormal endogenous SO_2 was involved in the pathogenesis of many diseases such as cardiovascular disease, neurological disease, and respiratory disease, and then keeping endogenous SO_2 in the normal range might be a new and meaningful therapeutic strategy of related diseases in the future.

However, there remain some issues to be taken into account in future studies: (1) The endogenous SO_2 generation and its producing enzyme should be firstly detected in the animal and cell models to identify the role of endogenous SO_2 in the pathogenesis of diseases. (2) The concentration and type of SO_2 donors might affect the effect of SO_2, which should be paid attention to *in vitro* and *in vivo*. (3) Since mitochondria and their related apoptosis pathways were reported to be involved in almost all the anti- or pro-apoptotic effects of endogenous SO_2, the detailed target molecules, and mechanisms by which SO_2 affects mitochondria merit expectation in the future. (4) A recent study showed useful findings that plasma SO_2 as a practical biomarker could predict the occurrence of acute kidney injury in the patients staying in the surgical intensive care unit (Jiang et al., 2021). Therefore, as a biomarker, the level of SO_2 in clinical samples might have translational potential in the diagnosis, treatment decision, and prognosis prediction of the diseases. (5) In the future, the SO_2-released prodrug and AAT inhibitor in clinical application for apoptosis-related diseases are expected to further studies (Day et al., 2016; Wang and Wang, 2018; Huang et al., 2021).

AUTHOR CONTRIBUTIONS

All authors listed have made a substantial, direct and intellectual contribution to the work, and approved it for publication.

FUNDING

This research was funded by National Natural Science Foundation of China (81770422 to YH, 81770278 to JBD, and 81900872 to JTD), Beijing Natural Science Foundation (7191012 to HJ).

REFERENCES

Balazy, M., Abu-Yousef, I. A., Harpp, D. N., and Park, J. (2003). Identification of carbonyl sulfide and sulfur dioxide in porcine coronary artery by gas chromatography/mass spectrometry, possible relevance to EDHF. *Biochem. Biophys. Res. Commun.* 331, 728–734. doi: 10.1016/j.bbrc.2003.10.055

Chen, S., Du, J., Liang, Y., Ochs, T., Liu, D., Zhu, L., et al. (2012). Sulfur dioxide inhibits excessively activated endoplasmic reticulum stress in rats with myocardial injury. *Heart Vessels* 27, 505–516. doi: 10.1007/s00380-011-0192-7

Chen, Z., Zhang, H., Bai, Y., Cui, C., Li, S., Wang, W., et al. (2021). Single cell transcriptomic analysis identifies novel vascular smooth muscle subsets under high hydrostatic pressure. *Sci. China Life Sci.* doi: 10.1007/s11427-020-1852-x [Epub ahead of print].

Cheng, P., Li, S., and Chen, H. (2021). Macrophages in lung injury, repair, and fibrosis. *Cells* 10:436. doi: 10.3390/cells10020436

Day, J. J., Yang, Z., Chen, W., Pacheco, A., and Xian, M. (2016). Benzothiazole sulfinate: a water-soluble and slow-releasing sulfur dioxide donor. *ACS Chem. Biol.* 11, 1647–1651. doi: 10.1021/acschembio.6b00106

Du, J. T., Huang, Y. Q., Li, K., Yu, X. Q., Jin, H. F., and Yang, L. (2018). Retina-derived endogenous sulfur dioxide might be a novel anti-apoptotic factor. *Biochem. Biophys. Res. Commun.* 496, 955–960. doi: 10.1016/jbbrc.2018.01.103

Du, S. X., Jin, H. F., Bu, D. F., Zhao, X., Geng, B., Tang, C. S., et al. (2008a). Endogenously generated sulfur dioxide and its vasorelaxant effect in rats. *Acta Pharmacol. Sin.* 29, 923–930. doi: 10.1111/j.1745-7254.2008.00845.x

Du, S. X., Jin, H. F., Liang, Y. F., Zhao, X., Wei, H. L., Wang, L., et al. (2008b). Influence of sulfur dioxide and its derivatives on rats' blood pressure. *J. Appl. Clin. Pediatr.* 23, 22–24. doi: 10.3969/j.issn.1003-515X.2008.01.007

Duan, H., Zhang, Q., Liu, J., Li, R., Wang, D., Peng, W., et al. (2021). Suppression of apoptosis in vascular endothelial cell, the promising way for natural medicines to treat atherosclerosis. *Pharmacol. Res.* 168:105599. doi: 10.1016/j.phrs.2021.105599

Griffith, O. W. (1983). Cysteinesulfinate metabolism: altered partitioning between transamination and decarboxylation following administration of beta-methyleneaspartate. *J. Biol. Chem*. 258, 1591–1598.

Han, Y., Yi, W., Qin, J., Zhao, Y., Zhang, J., and Chang, X. (2014). Dose-dependent effect of sulfur dioxide on brain damage induced by recurrent febrile seizures in rats. *Neurosci. lett*. 563, 149–154. doi: 10.1016/j.neulet.2013.12.042

Huang, X. L., Zhou, J. L., Zhou, X. H., Xian, X. H., and Ding, C. H. (2009). Ameliorative effects of exogenous sulfur dioxide on lipopolysaccharide-induced acute lung injury in rats. *Acta Physiol. Sin*. 61, 499–503. doi: 10.3321/j.issn:0371-0874.2009.05.014

Huang, Y. Q., Tang, C. X., Du, J. B., and Jin, H. F. (2016). Endogenous sulfur dioxide: a new member of gasotransmitter family in the cardiovascular system. *Oxid. Med. Cell. Longev*. 2016:8961951. doi: 10.1155/2016/8961951

Huang, Y. Q., Zhang, H., Lv, B. Y., Tang, C. S., Du, J. B., and Jin, H. F. (2021). Endogenous sulfur dioxide is a new gasotransmitter with promising therapeutic potential in cardiovascular system. *Sci. Bull*. 66, 1604–1607. doi: 10.1016/j.scib.2021.04.00

Jiang, Y., Wang, J., Zheng, X., and Du, J. (2021). Plasma endogenous sulfur dioxide: a novel biomarker to predict acute kidney injury in critically Ill patients. *Int. J. Gen. Med.* 14, 2127–2136. doi: 10.2147/IJGM.S312058

Jin, H., Liu, A. D., Holmberg, L., Zhao, M., Chen, S., Yang, J., et al. (2013). The role of sulfur dioxide in the regulation of mitochondrion-related cardiomyocyte apoptosis in rats with isopropylarterenol-induced myocardial injury. *Int. J. Mol. Sci.* 14, 10465–10482. doi: 10.3390/ijms140510465

Kimura, H. (2011). Hydrogen sulfide: its production, release and functions. *Amino Acids* 41, 113–121. doi: 10.1007/s00726-010-0510-x

Lee, W. L., and Downey, G. P. (2001). Neutrophil activation and acute lung injury. *Curr. Opin. Crit Care*. 7, 1–7. doi: 10.1097/00075198-200102000-00001

Li, S., Xu, Z., Jin, X., Qin, G., and Nan, S. (2019). Sulfur dioxide induces apoptosis via reactive oxygen species generation in rat cardiomyocytes. *Environ. Sci. Pollut. Res*. 26, 8758–8767. doi: 10.1007/s11356-019-04319-7

Liang, Y., Liu, D., Ochs, T., Tang, C., Chen, S., Zhang, S., et al. (2011). Endogenous sulfur dioxide protects against isoproterenol-induced myocardial injury and increases myocardial antioxidant capacity in rats. *Lab. Invest.* 91, 12–23. doi: 10.1038/labinvest.2010.156

Liu, D., Huang, Y., Bu, D., Liu, A. D., Holmberg, L., Jia, Y., et al. (2014). Sulfur dioxide inhibits vascular smooth muscle cell proliferation via suppressing the ERK/MAP kinase pathway mediated by cAMP/PKA signaling. *Cell Death Dis.* 5:e1251. doi: 10.1038/cddis.2014.229

Liu, M., Liu, S., Tan, W., Tang, F., Long, J., Li, Z., et al. (2017). Gaseous signalling molecule SO_2 via Hippo-MST pathway to improve myocardial fibrosis of diabetic rats. *Mol. Med. Rep.* 16, 8953–8963. doi: 10.3892/mmr.2017.7714

Liu, X., Zhang, D., Li, K., Yu, X., Tang, C., Du, J., et al. (2018). Effect of endogenous sulfur dioxide on the apoptosis induced by cobalt chloride in the human pulmonary arterial endothelial cells. *Chin. J. Appl. Clin. Pediatr.* 33, 999–1003. doi: 10.3760/cma.j.issn.2095-428X.2018.13.009

Luo, L. L., Chen, S., Jin, H. F., Tang, C. S., and Du, J. B. (2011). Endogenous generation of sulfur dioxide in rat tissues. *Biochem. Biophys. Res. Commun*. 415, 61–67. doi: 10.1016/j.bbrc.2011.10.012

Ma, H. J., Huang, X. L., Liu, Y., and Fan, Y. M. (2012). Sulfur dioxide attenuates LPS-induced acute lung injury via enhancing polymorphonuclear neutrophil apoptosis. *Acta Pharmacol. Sin*. 33, 983–990. doi: 10.1038/aps.2012.70

Mitsuhashi, H., Yamashita, S., Ikeuchi, H., Kuroiwa, T., Kaneko, Y., Hiromura, K., et al. (2005). Oxidative stress-dependent conversion of hydrogen sulfide to sulfite by activated neutrophils. *Shock* 24, 529–534. doi: 10.1097/01.shk.0000183393.83272.de

Niu, M., Han, Y., Li, Q., and Zhang, J. (2018). Endogenous sulfur dioxide regulates hippocampal neuron apoptosis in developing epileptic rats and is associated with the PERK signaling pathway. *Neurosci. Lett.* 665, 22–28. doi: 10.1016/j.neulet.2017.11.036

Qiu, J., Zheng, Y., Hu, J., Liao, D., Gregersen, H., Deng, X., et al. (2013). Biomechanical regulation of vascular smooth muscle cell functions: from in vitro to in vivo understanding. *J. R. Soc. Interface* 11:20130852. doi: 10.1098/rsif.2013.0852

Shapiro, R. (1977). Genetic effects of bisulfite (sulfur dioxide). *Mutat. Res*. 39, 149–175. doi: 10.1016/0165-1110(77)90020-3

Singer, T. P., and Kearney, E. B. (1956). Intermediary metabolism of L-cysteinesulfinic acid in animal tissues. *Arch. Biochem. Biophys.* 61, 397–409. doi: 10.1016/0003-9861(56)90363-0

Stipanuk, M. H. (2004). Sulfur amino acid metabolism: pathways for production and removal of homocysteine and cysteine. *Annu. Rev. Nutr*. 24, 539–577. doi: 10.1146/annurev.nutr.24.012003.132418

Tisch, N., and Ruiz de Al modóvar, C. (2021). Contribution of cell death signaling to blood vessel formation. *Cell. Mol. Life Sci.* 78, 3247–3264. doi: 10.1007/s00018-020-03738-x

Wajant, H. (2002). The Fas signaling pathway: more than a paradigm. *Science* 296, 1635–1636. doi: 10.1126/science.1071553

Wang, W. Y., and Wang, B. H. (2018). SO_2 donors and prodrugs, and their possible applications: a review. *Front. Chem*. 6:559. doi: 10.3389/fchem.2018.00559

Wang, X. B., Cui, H., and Du, J. B. (2018). Sulfur dioxide ameliorates rat myocardial fibrosis by inhibiting endoplasmic reticulum stress. *Histol. Histopathol*. 33, 1089–1097. doi: 10.14670/HH-18-007

Wang, X. B., Huang, X. M., Ochs, T., Li, X. Y., Jin, H. F., Tang, C. S., et al. (2011). Effect of sulfur dioxide preconditioning on rat myocardial ischemia/reperfusion injury by inducing endoplasmic reticulum stress. *Basic Res. Cardiol.* 106, 865–878. doi: 10.1007/s00395-011-0176-x

Wenzel, A., Grimm, C., Samardzija, M., and Remé, C. E. (2005). Molecular mechanisms of light-induced photoreceptor apoptosis and neuroprotection for retinal degeneration. *Prog. Retin. Eye Res.* 24, 275–306. doi: 10.1016/j.preteyeres.2004.08.002

Yang, L., Zhang, H., and Chen, P. (2018). Sulfur dioxide attenuates sepsis-induced cardiac dysfunction via inhibition of NLRP3 inflammasome activation in rats. *Nitric Oxide*. 81, 11–20. doi: 10.1016/j.niox.2018.09.005

Zare Mehrjerdi, F., Shoshtari, A., Mohseni, F., Khastar, H., Norozi, P., Asadi, Y., et al. (2018). Sulfur dioxide reduces hippocampal cell death and improves learning and memory deficits in a rat model of transient global ischemia/reperfusion. *Iran. J. Basic Med. Sci.* 21, 998–1003. doi: 10.22038/IJBMS.2018.29404.7106

Zhao, M. M., Yang, J. Y., Wang, X. B., Tang, C. S., Du, J. B., and Jin, H. F. (2013). The PI3K/Akt pathway mediates the protection of SO_2 preconditioning against myocardial ischemia/reperfusion injury in rats. *Acta Pharmacol. Sin.* 34, 501–506. doi: 10.1038/aps.2012.204

Zhao, X., Jin, H. F., Tang, C. S., and Du, J. B. (2008). Effects of sulfur dioxide, on the proliferation and apoptosis of aorta smooth muscle cells in hypertension: experiments with rats. *Zhonghua Yi Xue Za Zhi* 88, 1279–1283. doi: 10.3321/j.issn:0376-2491.2008.18.011

Zhao, Y. R., Liu, Y., Wang, D., Lv, W. R., and Zhou, J. L. (2019). Effects of sulfur dioxide on alveolar macrophage apoptosis in acute lung injury induced by limb ischemia/reperfusion in rats. *J. Peking Univ*. 51, 239–244. doi: 10.19723/j.issn.1671-167X.2019.02.007

Zhao, Y. R., Wang, D., Liu, Y., Shan, L., and Zhou, J. L. (2016). The PI3K/Akt, p38MAPK, and JAK2/STAT3 signaling pathways mediate the protection of SO_2 against acute lung injury induced by limb ischemia/reperfusion in rats. *J. Physiol. Sci.* 66, 229–239. doi: 10.1007/s12576-015-0418-z

Zhou, D., Zhang, Y., Du, J., Jin, H., Tang, C., and Huang, Y. (2020). Sulfur dioxide: an endogenous protector against myocardial injury. *J. Cardiovasc. Pharmacol.* 76, 389–396. doi: 10.1097/FJC.0000000000000882

Conflict of Interest: The authors declare that the research was conducted in the absence of any commercial or financial relationships that could be construed as a potential conflict of interest.

Publisher's Note: All claims expressed in this article are solely those of the authors and do not necessarily represent those of their affiliated organizations, or those of the publisher, the editors and the reviewers. Any product that may be evaluated in this article, or claim that may be made by its manufacturer, is not guaranteed or endorsed by the publisher.

Copyright © 2021 Li, Feng, Ye, Peng, Du, Yao, Huang, Jin and Du. This is an open-access article distributed under the terms of the Creative Commons Attribution License (CC BY). The use, distribution or reproduction in other forums is permitted, provided the original author(s) and the copyright owner(s) are credited and that the original publication in this journal is cited, in accordance with accepted academic practice. No use, distribution or reproduction is permitted which does not comply with these terms.

frontiers in Cell and Developmental Biology

ORIGINAL RESEARCH
published: 25 October 2021
doi: 10.3389/fcell.2021.746317

Iguratimod Alleviates Myocardial Ischemia/Reperfusion Injury Through Inhibiting Inflammatory Response Induced by Cardiac Fibroblast Pyroptosis via COX2/NLRP3 Signaling Pathway

Mian Zhang[1,2†], Yi-shan Lei[1,2†], Xiao-wen Meng[1,2†], Hua-yue Liu[1,2†], Lin-gui Li[1,2], Jun Zhang[1,2], Jia-xin Zhang[1,2], Wen-hui Tao[1,2], Ke Peng[1,2], Jun Lin[3] and Fu-hai Ji[1,2]**

[1] Department of Anesthesiology, First Affiliated Hospital of Soochow University, Suzhou, China, [2] Institute of Anesthesiology, Soochow University, Suzhou, China, [3] Department of Orthopedics, First Affiliated Hospital of Soochow University, Suzhou, China

OPEN ACCESS

Edited by:
Zhi Qi,
Nankai University, China

Reviewed by:
Xu Junmei,
Central South University, China
Yonghao Yu,
Tianjin Medical University General Hospital, China

***Correspondence:**
Fu-hai Ji
jifuhai1968@163.com
Jun Lin
linjun@suda.edu.cn

[†] These authors have contributed equally to this work and share first authorship

Specialty section:
This article was submitted to Cell Death and Survival, a section of the journal Frontiers in Cell and Developmental Biology

Received: 23 July 2021
Accepted: 27 September 2021
Published: 25 October 2021

Citation:
Zhang M, Lei Y-s, Meng X-w, Liu H-y, Li L-g, Zhang J, Zhang J-x, Tao W-h, Peng K, Lin J and Ji F-h (2021) Iguratimod Alleviates Myocardial Ischemia/Reperfusion Injury Through Inhibiting Inflammatory Response Induced by Cardiac Fibroblast Pyroptosis via COX2/NLRP3 Signaling Pathway. Front. Cell Dev. Biol. 9:746317. doi: 10.3389/fcell.2021.746317

Background: NLRP3 inflammasome contributes a lot to sterile inflammatory response and pyroptosis in ischemia/reperfusion (I/R) injury. Cardiac fibroblasts (CFs) are regarded as semi-professional inflammatory cells and they exert an immunomodulatory role in heart. Iguratimod provides a protective role in several human diseases through exerting a powerful anti-inflammatory effect. However, it is still unclear whether iguratimod could alleviate myocardial I/R injury and whether inflammation triggered by NLRP3-related pyroptosis of CFs is involved in this process.

Methods: Transcriptomics analysis for GSE160516 dataset was conducted to explore the biological function of differentially expressed genes during myocardial I/R. *In vivo*, mice underwent ligation of left anterior descending coronary artery for 30 min followed by 24 h reperfusion. *In vitro*, primary CFs were subjected to hypoxia for 1 h followed by reoxygenation for 3 h (H/R). Iguratimod was used prior to I/R or H/R. Myocardial infarct area, serum level of cardiac troponin I (cTnI), pathology of myocardial tissue, cell viability, lactate dehydrogenase (LDH) release, and the expression levels of mRNA and protein for pyroptosis-related molecules were measured. Immunofluorescence was applied to determine the cellular localization of NLRP3 protein in cardiac tissue.

Results: During myocardial I/R, inflammatory response was found to be the most significantly enriched biological process, and nucleotide-binding oligomerization domain (NOD)-like receptor signaling was a crucial pathway in mediating cardiac inflammation. In our experiments, pretreatment with iguratimod significantly ameliorated I/R-induced myocardial injury and H/R-induced pyroptosis of CFs, as evidenced by reduced myocardial infarct area, serum cTnI level, and LDH release in supernatants, as well as improved pathology of cardiac tissue and cell viability. Immunofluorescence analysis

showed that NLRP3 was mainly localized in CFs. Moreover, iguratimod inhibited the expression of pro-inflammatory cytokines and pyroptosis-related molecules, including NLRP3, cleaved caspase-1, and GSDMD-N.

Conclusion: Our results suggested that inflammatory response mediated by NOD-like receptor signaling is of vital importance in myocardial I/R injury. Iguratimod protected cardiomyocytes through reducing the cascade of inflammation in heart by inhibiting cardiac fibroblast pyroptosis via the COX2/NLRP3 signaling pathway.

Keywords: iguratimod, pyroptosis, inflammatory response, myocardial ischemia/reperfusion injury, cardiac fibroblasts, COX2, NLRP3

INTRODUCTION

Cardiovascular disease is a major cause of death and disability worldwide, among which ischemic heart disease represents a leading threat to human health (Ferraro et al., 2020). Despite that restoring blood perfusion rapidly is considered to be a chief treatment to limit the extent of myocardial infarction after cardiovascular events (Fröhlich et al., 2013; Hausenloy and Yellon, 2015), however, studies have proven that reperfusion triggered further cardiomyocyte death up to 50% of the overall infarcted location, which is defined as "myocardial ischemia/reperfusion (I/R) injury" (Yellon and Hausenloy, 2007). The pathophysiological mechanism of I/R injury is a rather complex process (Davidson et al., 2019; Heusch, 2020), of which inflammatory response is indicated to be a crucial factor in secondary myocardial damage (Eltzschig and Eckle, 2011; Frangogiannis, 2014). It is worthy of paying attention that cardiac fibroblasts (CFs), the most abundant non-cardiomyocytes in heart tissue, can sense danger signals released during cardiac injury or stress and participate in inducing the recruitment of immune cells, thus activating inflammatory response (Smolgovsky et al., 2021).

The nucleotide-binding oligomerization domain (NOD)-like receptor (NLR) is a kind of pattern recognition receptors, and its family members mainly participate in inflammasome formation, among which NLR with a pyrin domain 3 (NLRP3) inflammasome is the most extensively studied. It has been well established that NLRP3 inflammasome, an important signaling sensor platform containing NLRP3, apoptosis-associated speck-like protein containing a CARD (ASC) and caspase-1, is essential for pyroptosis (Nagata and Tanaka, 2017; Bedoui et al., 2020). Pyroptosis, a newly discovered process of pro-inflammatory programmed cell death, is featured by pore formation in the plasma membrane and extracellular release of pro-inflammatory factors. Inflammatory caspases, including caspase-1, caspase-4, and caspase-5, cleave gasdermin family member gasdermin D (GSDMD) into C-terminal and N-terminal, with the latter translocating to the inner leaflet of plasma membrane and mediating cell pyroptosis (Shi et al., 2015; Nagata and Tanaka, 2017). Previous researches have indicated the critical role of pyroptosis in cardiovascular diseases and concluded that excessive pyroptosis may have a detrimental effect on cardiomyocytes (Zhou et al., 2018; An et al., 2019; Shi et al., 2021). Results from animal experiments demonstrated that inhibition of caspase-1 or knockdown of ASC and NLRP3 could prevent myocardium injury (Kawaguchi et al., 2011; Sandanger et al., 2013; Audia et al., 2018). In addition, it was reported that NLRP3 inflammasome induced by myocardial I/R was mainly expressed in non-cardiomyocytes, such as fibroblasts, endothelial cells, and infiltrated leukocytes within the myocardium (Kawaguchi et al., 2011; Sandanger et al., 2013; Liu et al., 2014). Therefore, interventions in NLRP3-mediated pyroptosis of CFs may reduce inflammatory counterparts and further exert myocardial protection.

Iguratimod, an emerging antirheumatic drug, has been characterized with selectively inhibitory role in the activity and induction of COX2 (Tanaka et al., 1992, 1995). Recently, investigators studied the therapeutic effect of iguratimod on multiple disease models (Jiang et al., 2018; Li et al., 2018, 2019), and the results suggested that iguratimod improved these diseases by exerting strong anti-inflammatory effect. Moreover, it was reported that iguratimod could inhibit NLRP3 inflammasome (Hou et al., 2019). Results from another study showed that COX2 positively regulated the expression of NLRP3 and IL-1β in macrophages (Hua et al., 2015). Nonetheless, to the best of our knowledge, the biological effect of iguratimod on COX2/NLRP3 signaling pathway in myocardial I/R model still remains elusive.

Transcriptomics studies gene transcription and function through analyzing all RNA from tissues or cells. Recently, transcriptomics has been widely applied in human disease-related researches and it can reveal underlying molecular mechanisms comprehensively (Singhania et al., 2018; Montaner et al., 2020). GSE160516 dataset stores expression data from mouse heart tissue treated with I/R, which can show the gene expression alteration associated with the development of cardiac injury. Therefore, we carried out bioinformatics analysis for GSE160516 dataset to identify differentially expressed genes (DEGs) and their biological function.

Collectively, the present study aimed to provide theoretical basis for a comprehensive understanding of myocardial I/R injury from a perspective of transcriptomics and to investigate the role and underlying mechanism of iguratimod on I/R-induced cardiomyocyte injury. We hypothesized that iguratimod pretreatment could reduce inflammatory response in cardiac tissue and protect the myocardium, and these effects were mediated by downregulation of CF pyroptosis via suppressing the COX2/NLRP3 signaling pathway.

MATERIALS AND METHODS

Microarray Data and Identification of Differentially Expressed Genes

The myocardial I/R microarray dataset was downloaded from the Gene Expression Omnibus (GEO) database[1]: GSE160516. There were four mouse heart tissues in the sham surgery group (sham), I/R for 6 h group (IR6h), I/R for 24 h group (IR24h), and I/R for 72 h group (IR72h), respectively. The gene expression data (GSE160516) were detected by the Affymetrix Clariom S Mouse Array platform (GPL23038). Boxplots and principal component analysis (PCA) were used to visualize the expression profiles of the four groups. GEO2R was utilized to identify DEGs in IR24h samples compared to sham samples, setting the thresholds of Benjamini-Hochberg (BH) method adjusted p-value <0.05 and $|\log_2 (\text{fold change})| \geq 1$ ($|\log_2 FC| \geq 1$) as the cutoff line. The visualization of the results was performed using the R software (version 4.0.4) and OmicShare tools[2], presented as volcano plot, bar charts, and heatmap.

Gene Ontology and Pathway Enrichment Analysis

Gene Ontology (GO) analysis is mainly applied to carry out the biological function enrichment of the proteins encoded by DEGs. The Metascape online database[3] was used to perform GO analysis, which contains three different terms for the molecular function, biological process, and cellular component categories (Zhou et al., 2019). Subsequently, the pathway enrichment analysis for the DEGs that were included in the most statistically significant GO term was conducted using the Kyoto Encyclopedia of Genes and Genomes (KEGG) pathways online tool[4]. The enrichment results of the GO term and KEGG pathway analysis were visualized by GraphPad Prism 8 software (GraphPad Software, San Diego, CA, United States). The process of analyzing data in GSE160516 dataset is shown in **Figure 1A**.

Experiment Design *in vivo* and *in vitro*

Experiment Design 1: Changes of COX2 and NLRP3 Expression in Heart Tissue of Myocardial Ischemia/Reperfusion Mice Model

In order to determine the changes of COX2 and NLRP3 mRNA expression in heart tissue at various reperfusion time points, mice were randomly allocated into the following five groups: sham group (Sham), reperfusion 3 h group [I/R(3h)], reperfusion 6 h group [I/R(6h)], reperfusion 24 h group [I/R(24h)], and reperfusion 48 h group [I/R(48h)]. All mice were sacrificed at an indicated time point after myocardial reperfusion and the heart tissue below ligated position was collected for real-time quantitative PCR (RT-qPCR) to access mRNA expression levels of COX2 and NLRP3 (**Figure 1B**). The experimental data were statistically analyzed, and thus, we chose 24 h as the optimal reperfusion time.

Experiment Design 2: Therapeutic Effect of Iguratimod on Ischemia/Reperfusion-Induced Cardiomyocyte Injury and the Potential Molecular Mechanisms

Adult male C57BL/6 mice were divided into the following three groups: Sham group, I/R group, and Iguratimod pretreatment (T-614) + I/R group. Mice in T-614 + I/R group received intraperitoneal injection of iguratimod (Cat no. HY-17009; MedChemExpress, Monmouth Junction, NJ, United States) at a dose of 5 mg/kg 1 h before myocardial ischemia. Mice in another two groups were administrated with equal volume solvent of 5% DMSO intraperitoneally (**Figure 1C**).

After myocardial reperfusion for 24 h, mice were sacrificed for following experiments. The myocardial infarct and ischemia area were assessed by Evans blue and 2,3,5-triphenyl tetrazolium chloride (TTC) double staining. The concentration of cardiac troponin I (cTnI) in serum was measured by enzyme-linked immunosorbent assay (ELISA). Hematoxylin and eosin (HE) staining was used to observe the pathological morphology of cardiac tissue. The expression of myeloperoxidase (MPO) in heart was detected by immunohistochemistry (IHC) staining. The mRNA levels of COX2, NLRP3, and some inflammatory factors including IL-1β, IL-6, IL-18, and TNF-α were measured by RT-qPCR. Western blotting was adopted to detect relative expression levels of COX2, NLRP3, caspase-1, ASC, cleaved caspase-1, GSDMD-N, and IL-1β. Additionally, the cellular localization of NLRP3 in cardiac tissue was determined by immunofluorescence (IF) staining.

Experiment Design 3: The Optimal Concentration of Iguratimod for *in vitro* Experiments in Primary Cardiac Fibroblasts

Cardiac fibroblasts were incubated with iguratimod of different concentrations (0, 0.1, 1, 5, 10 μM, respectively) for 24 h at normal culture condition, to find the optimal concentration with no cytotoxicity (**Figure 1D**). CFs were then pretreated with iguratimod (0, 0.1, 1, and 5 μM, respectively) for 6 h, followed by LPS (100 ng/ml) incubation for 18 h, and were then subjected to hypoxia for 1 h and reoxygenation for 3 h (H/R) (**Figure 1E**). Cell counting kit-8 (CCK-8) and lactate dehydrogenase (LDH) release were applied to select the optimal concentration of iguratimod *in vitro* H/R model.

Experiment Design 4: Effect of Iguratimod on H/R-Induced Pyroptosis of Cardiac Fibroblasts and Expression of Pro-inflammatory Factors

Murine primary CFs were divided into three groups: Con group, H/R group, and iguratimod pretreatment (T) + H/R group. Cells in the Con group were incubated with 100 ng/ml of LPS for 18 h followed by normal medium culture for 4 h. CFs in the H/R group were treated with LPS for 18 h before H/R. The T + H/R group was pretreated with iguratimod of 5 μM for 6 h, followed by the same procedure of the H/R group. At the end of reoxygenation, cells of all groups were harvested for accessing

[1] http://www.ncbi.nlm.nih.gov/geo
[2] https://www.omicshare.com/tools/
[3] http://metascape.org
[4] https://www.kegg.jp/kegg/

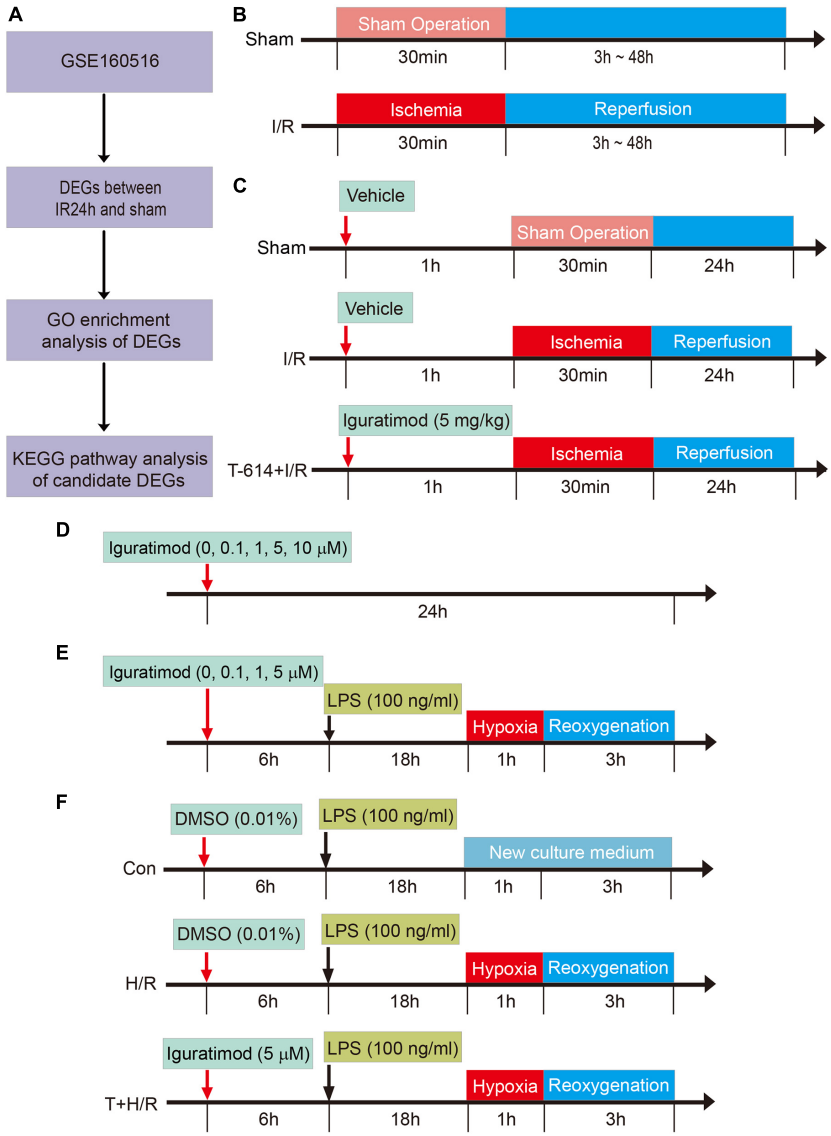

FIGURE 1 | Schematic diagram of the experimental design and major process in the present study. **(A)** Flow chart of processing data in GSE160516 dataset. **(B)** Experiment design 1 was performed to demonstrate the time course of changes in mRNA expression of COX2 and NLRP3 after myocardial reperfusion. **(C)** Experiment design 2 was conducted to investigate the therapeutic effect of Iguratimod pretreatment on myocardial injury induced by I/R and the underlying mechanism. **(D,E)** Experiment design 3 was carried out to explore the optimal concentration of iguratimod for mitigating H/R injury of primary cardiac fibroblasts. **(F)** Experiment design 4 assessed the implications of iguratimod on pyroptosis of cardiac fibroblasts in *vitro* H/R model. I/R, ischemia/reperfusion; H/R, hypoxia/reoxygenation.

the mRNA expressions of COX2, NLRP3, IL-1β, IL-6, IL-18, and TNF-α, and the protein levels of COX2, NLRP3, caspase-1, ASC, cleaved caspase-1, GSDMD-N, and IL-1β (**Figure 1F**).

Animals

Healthy adult male C57BL/6 mice (20–25 g weight) were purchased from Cavens Biogle (Suzhou) Model Animal Research Co., Ltd. (Animal license No. SCXK Jiang-su 2018-0002). All of the animals were housed in a specific room with controlled environmental condition (a normal 12 h light-dark cycle and constant temperature and humidity) and were fed with commercial food and water. The animal experimental procedures were carried out in line with the guide for the care and use of laboratory animals [National Institutes of Health (NIH), Bethesda, MD, United States] and also passed the review of the Institutional Animal Care and Use Committee of Soochow University (Suzhou, China).

Establishing Myocardial Ischemia/Reperfusion Model *in vivo*

Mice were anesthetized by intraperitoneal administration of 1% pentobarbital sodium at a dose of 50 mg/kg. They were ventilated

with a rodent respirator (Shenzhen Ruiwode Life Technology Co., Ltd., China) after tracheal intubation. The thorax was opened along the left fourth intercostal space to expose the heart. A 6-0 suture thread with needle was tied into a slipknot to ligate the left anterior descending coronary artery (LAD) at 3 mm under the extension line of the lower edge of the left auricle of the heart. The mark of successful ischemia was cyanosis in left ventricular myocardium wall or ST-segment elevation on the electrocardiograph. Following 30-min ischemia, the ligation was removed to allow reperfusion of the occluded coronary artery and then the incision was sutured carefully. All the mice were returned to their cages after recovering from anesthesia and were given free access to food and water.

Isolation and Culture of Primary Cardiac Fibroblasts

Murine primary CFs were isolated from hearts of neonatal C57BL/6 mice (aged 1–3 days) with a differential adhesion method as previously described (Wu et al., 2016). In brief, hearts from neonatal mice were harvested promptly and chopped into small pieces under aseptic condition. To gain suspension of CFs, cardiac tissue was digested with 0.25% trypsin (Cat no. C0201; Beyotime, China) at 37°C followed by dissociation in collagenase type 2 (0.5 mg/ml; Cat no. V900892; Sigma, St. Louis, MO, United States). The cell suspension was filtered through a 200-μm cell strainer and then centrifuged at 1000 × *g* for 5 min. DMEM/F12 medium (Cat no. C11330500BT, Gibco; Invitrogen, Carlsbad, CA, United States) containing 10% fetal bovine serum (FBS), and 1% penicillin/ streptomycin was added into the precipitation to resuspend the cells. After pre-culture for 70 min at 37°C, CFs were obtained by differential wall-adherence durations. Subsequently, the purity of primary CFs was confirmed by immunocytochemistry with an anti-vimentin monoclonal antibody (1:100, Cat no. 5741; CST, Danvers, MA, United States). CFs of passage 2, which were grown to 80% confluence in culture dishes, were used for *vitro* experiments.

Hypoxia/Reoxygenation Model *in vitro*

Primary CFs were treated with glucose-free DMEM (Cat no. PM150271; Procell, China) and pre-incubated in chamber filled with mixed gas (95% N_2 and 5% CO_2) at 37°C for 1 h. Subsequently, cells were cultured in complete medium with DMEM/F12 containing 10% FBS under normal atmosphere (95% air, 5% CO_2) at 37°C for 3 h.

Evans Blue and 2,3,5-Triphenyl Tetrazolium Chloride Double-Staining

At an indicated time point after reperfusion, mice were anesthetized and the LAD was ligated again *in situ*; 1% Evans blue solution (Cat no. E2129; Sigma) was injected into the inferior vena cava, after which hearts were resected, washed with cold saline, and frozen at −80°C for 15 min. Frozen hearts were then transversely sectioned into slices with 2-mm thickness and incubated in phosphate buffer solution (pH = 7.4) containing 1% TTC (Cat no. T8877; Sigma) at 37°C for 30 min. Subsequently, the slices were fixed in 4% paraformaldehyde fix solution (Cat no. BL539A; Biosharp, China). An Image J software (National Institutes of Health) was used to calculate the infarct area (INF) and area at risk (AAR). The infarcted size of the heart was regarded as the percentage of INF/AAR.

Enzyme-Linked Immunosorbent Assay

The serum level of cTnI was determined as a biomarker of myocardial damage. In the present study, murine blood sample was drawn from the inferior vena cava and collected in tubes for serum isolation. The concentration of cTnI was measured by an ELISA kit (Cat no. CTNI-1-HS; Life Diagnostics, West Chester, PA, United States) according to the manufacturer's instructions.

Hematoxylin and Eosin Staining

Hematoxylin and eosin staining was used to observe the histological structure of heart tissue. Briefly, paraformaldehyde-fixed and paraffin-embedded hearts were cut transversely into 5-μm-thick sections. After dewaxing with dimethylbenzene and dehydrating with graded ethanol series, the heart slices were stained with hematoxylin for 5 min and then alcohol- soluble eosin for 30 s. Finally, these sections were observed under a light microscope following sealing with neutral gum.

Immunohistochemistry Staining

For IHC, paraffin-embedded heart tissue sections were firstly deparaffinized and rehydrated. Subsequently, antigen was retrieved by heating samples in Tris-based buffer (pH = 9.0) to boil for 15 min. After three times of washing, the tissue slides were blocked with 5% BSA for 1 h and then incubated with primary antibody of myeloperoxidase (1:500, Cat no. ab208670; Abcam, Cambridge, MA, United States) at 4°C overnight in a humidified chamber. The following day, slices were incubated with appropriate HRP-conjugated secondary antibody (1:200, Cat no. ab6721; Abcam) for 1 h at 37°C. Positive staining could be visualized after using a DAB kit. At last, the representative images were further quantified for calculating the expression of MPO by using Image J software.

Western Blotting

After reperfusion for 24 h, cardiac tissues were harvested and homogenized in frozen RIPA lysis buffer (Cat no. P0013B; Beyotime) mixed with phenylmethylsulfonyl fluoride (Cat no. ST506; Beyotime). Then, the homogenate was centrifuged at 14,800 × *g* for 30 min, and the supernatant extracts were sucked out. The protein concentration was determined by BCA method. Equal amounts of total protein were loaded in each well and then separated by 10% sodium dodecyl sulfate–polyacrylamide gel electrophoresis. The protein was then transferred to a polyvinylidene difluoride (PVDF) membrane. Subsequently, the PVDF membrane was sealed with 5% non-fat milk in 1× Tris-buffered saline tween (TBST) buffer for 2 h followed by incubation with primary antibodies (**Table 1**) at 4°C overnight. After three times of washing, the PVDF membrane was incubated with corresponding horseradish peroxidase-labeled anti-rabbit or anti-mouse secondary antibodies (1:4000, Cat no. CW0102S, Cat no. CW0103S; CoWin Biosciences, China) at room temperature

TABLE 1 | Antibodies applied in Western blotting.

Antibodies	Cat. no. and company	Dilution ratio
COX2	ab14191, Abcam	1:1000
NLRP3	15101, CST	1:500
Caspase-1	CY10200, Abways	1:500
ASC	67824, CST	1:500
IL-1β	abs131179, absin	1:500
Cleaved caspase-1	89332, CST	1:500
GSDMD	ab219800, Abcam	1:500
β-Tubulin	abs137976, absin	1:20000

TABLE 2 | Primer sequences used in quantitative polymerase chain reaction in this study.

Primer name	Sequence (5′ → 3′)	
COX-2	Forward	ATTCCAAACCAGCAGACTCATA
	Reverse	CTTGAGTTTGAAGTGGTAACCG
NLRP3	Forward	CCAGACACTCATGTTGCCTGTTC
	Reverse	GAGGCTCCGGTTGGTGCTTA
IL-1β	Forward	CACTACAGGCTCCGAGATGAACAAC
	Reverse	TGTCGTTGCTTGGTTCTCCTTGTAC
IL-18	Forward	AGACCTGGAATCAGACAACTTT
	Reverse	TCAGTCATATCCTCGAACACAG
IL-6	Forward	ACAACCACGGCCTTCCCTACTT
	Reverse	CACGATTTCCCAGAGAACATGTG
TNF-α	Forward	AAGCCTGTAGCCCACGTCGTA
	Reverse	GGCACCACTAGTTGGTTGTCTTTG
β-Tubulin	Forward	GGGAGGTGATAAGCGATGAA
	Reverse	AGGGACATACTTGCCACCTG

for 2 h. The immunoblot bands were visualized by means of an electrochemiluminescence kit (Tanon, China) and the intensity of the bands was measured using the Image J software. The final semi-quantitative results were presented as the ratios of targeted molecular intensity relative to that of β-tubulin.

RNA Extraction and Real-Time Quantitative PCR

Total RNA of heart tissue was extracted using Trizol reagent (Cat no. 15596026; Thermo Fisher Scientific, Carlsbad, CA, United States) according to manufacturer's instructions. Quality and purity of RNA were identified by UV spectrophotometry (NanoDrop 2000; Thermo Fisher Scientific) at 260 and 280 nm, respectively; 1 μg of total RNA was used to synthesize cDNA. The qPCR reaction mixture contained 5 μl of SYBR qPCR SuperMix (Cat no. E096-01A; Novoprotein, China), 1 μl of forward and reverse primers, 1 μl of cDNA, and 2 μl of RNase-free water. The qPCR cycling was programmed for 40 cycles followed by the construction of a melting curve. Using a single predominant peak as quality control, qPCR was applied to estimate the transcript levels of selected genes: COX2, NLRP3, IL-1β, IL-18, TNF-α, and IL-6 with β-tubulin as normalization of mRNA expression. Data were analyzed by using the $2^{-\Delta\Delta Ct}$ method. Primer sequences of mice mRNA (**Table 2**) were synthesized by Shanghai Sangon Biotech Co., Ltd.

Immunofluorescence Staining

Hearts were resected and fixed in 4% paraformaldehyde for at least 1 day to prepare for immunofluorescence analysis. Thereafter, the specimens were soaked in gradient sucrose solutions in PBS to dehydrate and were processed into frozen sections. Representative sections from the ischemic region were permeabilized in 0.5% Triton X-100 for 15 min and sealed with 5% BSA for 1 h. Afterwards, the sections were incubated with the following primary antibodies at 4°C for 12 h: anti-COX2 (1:100, Cat no. ab15191; Abcam), anti-NLRP3 (1:100, Cat no. NBP2-12446; Novus, Littleton, CO, United States), anti-Vimentin (1:100, Cat no. 5741; CST) and anti-Smooth Muscle Actin (1:100, Cat no. sc-53142; Santa Cruz Biotechnology, Santa Cruz, CA, United States). Primary antibodies were detected by Alexa Fluor 488-conjugated goat anti-rabbit (1:500, Cat no. ab150077; Abcam), Alexa Fluor 568-conjugated goat anti-rabbit (1:500, Cat no. ab175471; Abcam), or Alexa Fluor 488-conjugated goat anti-mouse (1:500, Cat no. ab150113; Abcam) secondary antibodies, respectively, for 2 h at room temperature. Nuclei were identified with its marker of 4′,6-diamidino-2-phenylindole (DAPI) (Cat no. 62248; Thermo Fisher Scientific). Finally, the sections were observed with a fluorescence microscope.

Cell Counting Kit-8

Cell proliferation and cytotoxicity assay were measured using Cell Counting Kit-8 (CCK-8 kit) (Cat no. CK04; Dojindo, Japan). In brief, primary CFs were seeded in 96-well plates at a density of 10,000 cells/well and were pre-cultured for 24 h in a humid condition (5% CO_2, 37°C). After corresponding processing, the supernatant in each well was supplemented with 10 μl of CCK-8 solution and then the mixture was incubated at 37°C for 3 h. A microplate reader was used to detect the absorbance at 450 nm.

Lactate Dehydrogenase Release in Supernatant

Primary CFs were seeded in 96-well plates at a density of 15,000 cells/well and were pre-incubated for 24 h. To measure LDH release, 60 μl of supernatant in each well of the plate was transferred to a new plate. According to manufacturer's instructions, the homogeneous reaction solution containing 10 μl of lactic acid, 10 μl of diaphorase, and 10 μl of iodonitrotetrazolium (INT) was added into the supernatant and then this mixture was incubated at room temperature for 30 min in the dark. At last, the absorbance of each well was measured at 490 nm with a microplate reader.

Statistical Analysis

Data from the GSE160516 dataset were processed with the R software, online bioinformatic databases, and tools as mentioned before. The GraphPad Prism 8 software was applied to analyze experimental data. Continuous variables were presented as mean ± standard deviation (SD). Data between two groups with normal distribution were assessed using the two-sided unpaired Student *t*-test, and the differences among multiple

groups were evaluated using ordinary one-way or two-way analysis of variance (ANOVA) followed by Tukey's multiple comparisons test. In both cases, a *p*-value of less than 0.05 was considered statistically meaningful.

RESULTS

Inflammatory Response Mediated by Nucleotide-Binding Oligomerization Domain-Like Receptor Signaling Pathway Plays an Important Role in Myocardial Ischemia/Reperfusion Injury

The raw data in GSE160516 dataset were normalized and standardized (**Supplementary Figure 1**). The distribution of all samples was shown in the form of a two-dimensional scatter diagram with PCA (**Supplementary Figure 2**). The PCA plot also indicated that samples within each group were similar to each other and there were significant discriminations among four groups.

A total of 1860 DEGs (1240 upregulated genes and 620 downregulated genes) were identified in IR24h samples compared to sham samples (**Figures 2A,B**). The top 20 significant DEGs are listed in **Supplementary Table 1**. As shown in **Figure 2C**, the top 30 terms of GO enrichment analysis for DEGs were demonstrated as bar graphs, among which there were 26 items in the biological process group, three items in cellular component group, and one item in the molecular function group (more details shown in **Supplementary Table 2**). The result demonstrated that these DEGs were mainly enriched in leukocyte, cytokine, and cell migration-related processes. Among these GO terms, inflammatory response (GO:0006954) was the most significant enrichment process, with 176 DEGs included (gene list shown in **Supplementary Table 3**). The enriched top 20 KEGG pathways for these 176 DEGs were demonstrated in **Figure 2D** (details shown in **Supplementary Table 4**), among which there were 19 genes enriched in NOD-like receptor signaling pathway.

COX2 and Molecules Associated With Pyroptosis Were Both Upregulated After Myocardial Ischemia/Reperfusion

As shown in box plots (**Figures 3A,B**), the transcriptional expression of COX2 and NLRP3 in cardiac tissue changed dynamically with the reperfusion time, showing a trend of increasing first and then decreasing. To be specific, COX2 expression reached the peak at 6 h after myocardial reperfusion, and the expression peak of NLRP3 was at 24 h. The heatmap demonstrated that the expression levels of COX2, NLRP3, Caspase-1, IL-1β, IL-6, GSDMD, and IL-18 gene were all upregulated in IR24h samples (**Figure 3C**). Subsequently, we successfully established the mice model of myocardial I/R, which was identified by an elevation of ST segment on electrocardiograph (**Figure 3D**). qPCR results further confirmed similar expression trends of COX2 and NLRP3 in left ventricular myocardium after reperfusion (**Figures 3E,F**). Based on these findings, 24 h after myocardial reperfusion was selected as the optimal time point in subsequent *in vivo* experiments.

Iguratimod Ameliorated Myocardial Injury and Infiltration of Inflammatory Cells After Ischemia/Reperfusion

As shown in the Evans blue and TTC double stained heart sections, the AAR/LV ratio and IA/AAR ratio both increased significantly in I/R group and T-614 + I/R group compared with the Sham group. While there was no difference of AAR/LV ratio between the I/R group and T-614 + I/R group, the ratio of IA/AAR decreased significantly in the latter group, indicating that iguratimod pretreatment limited the infarct size after myocardial I/R (**Figures 4A,B**). The concentration of cTnI in serum was elevated after I/R and was reduced by iguratimod pretreatment (**Figure 4C**). HE staining showed that mice in the Sham group had clear and intact heart tissue structure, and the cardiomyocytes were arranged in order (**Figure 4D**). Nevertheless, the hearts from the I/R group were characterized with unclear tissue structure, swollen cardiomyocytes, disrupted myofibrils, and inflammatory cell infiltration. In the T-614 + I/R group, iguratimod ameliorated the above-mentioned morphological damage, with milder myofibril fracture and inflammatory cell infiltration. The result of IHC staining demonstrated that the MPO-positive stained area in the T-614 +I/R group was smaller than that in the I/R group, which indicated less neutrophil infiltration and mitigated inflammatory response (**Figures 4E,F**).

The Alleviated Myocardial Ischemia/Reperfusion Injury in Iguratimod Pre-treated Mice Was Associated With Inhibition of Pyroptosis and Inflammatory Response Mediated by COX2/NLRP3 Signaling Pathway

As shown in **Figures 5A–F**, cardiac tissue from I/R group exhibited obviously increased mRNA levels of COX2, NLRP3, IL-1β, IL-18, IL-6, and TNF-α in comparison to the Sham group. When mice were pre-treated with iguratimod before being subjected to myocardial ischemia, the mRNA levels of the above-mentioned molecules all reduced significantly. Moreover, results of the Western blotting analysis demonstrated that iguratimod pretreatment rendered a remarkable decline in the protein expression of COX2, NLRP3, caspase-1, cleaved caspase-1, GSDMD-N, and IL-1β, which were induced by I/R dramatically (**Figures 5G–M**). However, in the protein level of ASC, there was a lack of significant difference between the I/R group and T-614 + I/R group, though showing a trend of decrease after iguratimod pretreatment (**Figure 5N**). In addition, pictures of immunofluorescence staining showed lower expression of COX2 and NLRP3 in left the ventricular myocardium tissue within the T-614 + I/R group, when compared with the I/R group (**Figures 5O,P**). Taken together, these findings indicated that iguratimod attenuated pyroptosis

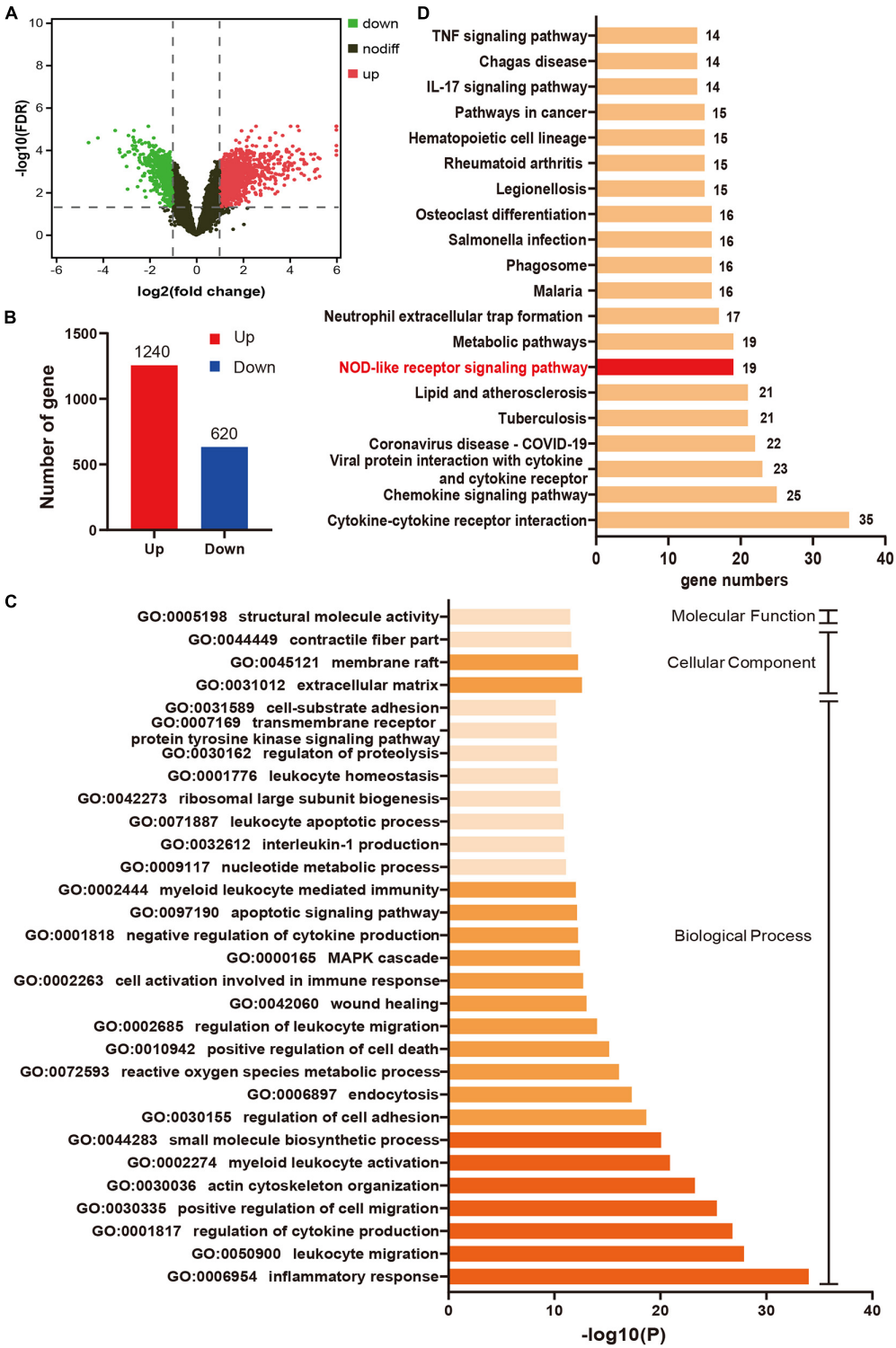

FIGURE 2 | Inflammatory response mediated by NOD-like receptor signaling pathway plays an important role in myocardial I/R injury. **(A)** Volcano plot for DEGs between IR24h samples and sham samples. Red dots and green dots respectively represent up-regulated and down-regulated genes in IR24h samples compared to sham samples (adjusted p-value < 0.05 and $|\log_2 FC| \geq 1$). Black dots indicate the genes without significant expression difference between the two groups (adjusted p-value ≥ 0.05 or $|\log_2 FC| < 1$). **(B)** The number of up-regulated and down-regulated genes in IR24h samples compared to sham samples. **(C)** Heatmap of GO analysis enriched terms colored by p-value. GO functional enrichment analysis classified the DEGs into three functional groups: molecular function group, biological process group, and cellular component group. **(D)** KEGG pathway analysis for the DEGs enriched in GO:0006954. NOD-like receptor signaling pathway is marked with red color. DEGs, differentially expressed genes; $\log_2 FC$, $\log_2$ (fold change); GO, Gene ontology; KEGG, Kyoto Encyclopedia of Genes and Genomes.

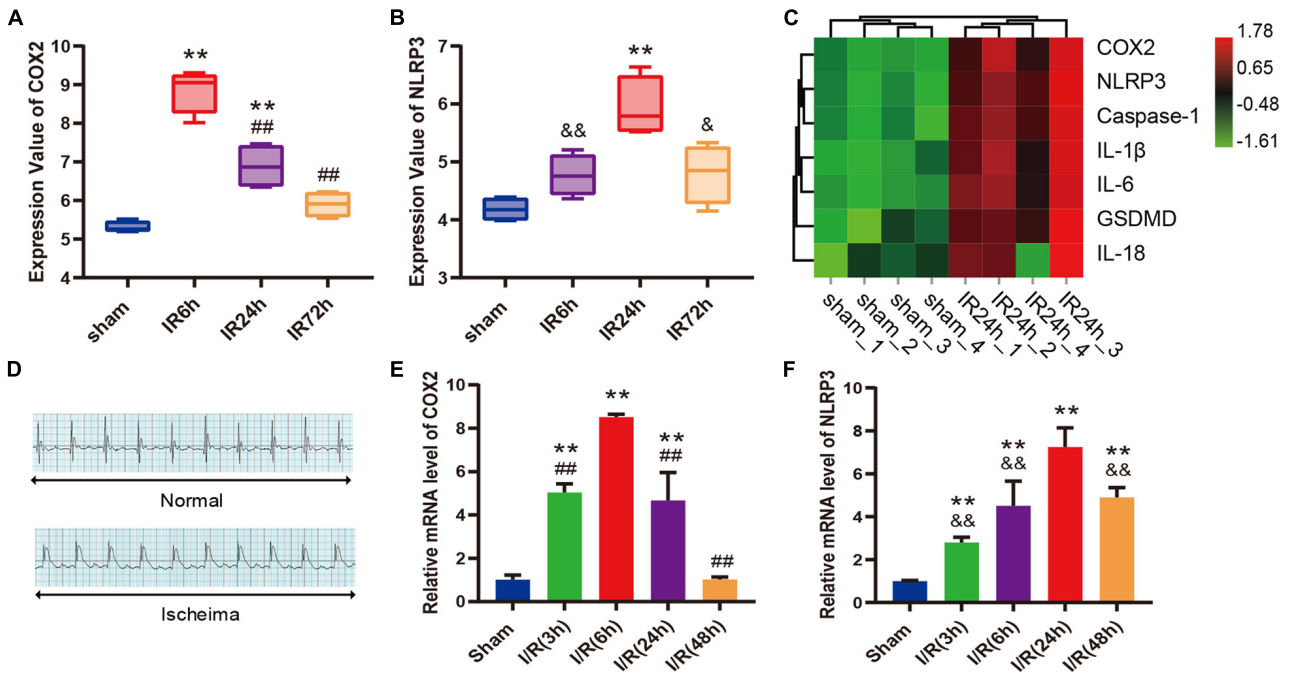

FIGURE 3 | COX2 and molecules associated with pyroptosis were both up-regulated after myocardial I/R. **(A,B)** Transcriptional expression values of COX2 and NLRP3 in sham samples and I/R samples of GSE160516 dataset. $n = 4$. **(C)** Expression heatmap of COX2, NLRP3, caspase-1, IL-1β, IL-6, GSDMD, and IL-18 in sham samples and IR24h samples. Each column represents a sample and each row represents expression profile of a specific gene. The color scale demonstrates the relative gene expression level in certain grid: green and red indicate the low and high expression values of the gene, respectively. **(D)** Representative electrocardiograph before and after ligation of LAD *in vivo* model of myocardial I/R. **(E,F)** Changes in mRNA expression levels of COX2 and NLRP3 after myocardial reperfusion. $n = 5$. Data are expressed as the mean ± SD; $^{**}p < 0.01$ versus sham group or Sham group; $^{\#\#}p < 0.01$ versus IR6h group or I/R(6h) group; $^{\&}p < 0.05$, $^{\&\&}p < 0.01$ versus IR24h group or I/R(24h) group. I/R, ischemia/reperfusion; LAD, left anterior descending coronary artery.

and inflammatory response triggered by I/R through the inhibition of COX2/NLRP3 pathway.

Iguratimod Attenuated Cell Injury of Primary Cardiac Fibroblasts Exposed to H/R Condition

The results of double immunofluorescence staining showed that there was more colocalization of NLRP3-positive cells with vimentin-positive cells in the left ventricular myocardium tissue after myocardial I/R (**Figure 6A**). Considering that vimentin was a special cytoskeleton protein of fibroblasts, we concluded that upregulated NLRP3 was expressed mainly in CFs instead of cardiomyocytes. Thereafter, primary CFs were isolated from mice aged 1–3 days to directly explore the effect of iguratimod on CFs exposed to H/R. The representative images of primary CFs, which were identified by immunofluorescence staining of vimentin, are presented in **Figure 6B**. The purity of primary CFs used in *in vitro* experiments was up to 93.3% (**Figure 6C**). As shown in **Supplementary Figures 3A,B**, iguratimod had no detrimental effect on CFs when its concentration ranged from 0 to 5 μM, as indicated by normal cell viability and low LDH release in the supernatants. Additionally, 100 ng/ml LPS did not cause injury to CFs (**Supplementary Figures 4A,B**). Therefore, LPS was used in simulated I/R experiments *in vitro* for priming of NLRP3 inflammasome. It can be seen from **Figures 6D,E** that H/R induced severe injury of CFs, as evidenced by decreased cell viability and elevated LDH release. Interestingly, compared with the H/R group, pretreatment with iguratimod increased cell viability only at a high concentration of 5 μM (**Figure 6D**), while it significantly decreased LDH release at concentration of both 1 and 5 μM (**Figure 6E**). Therefore, 5 μM of iguratimod was applied for the following experiments *in vitro*.

Iguratimod Ameliorated Pyroptosis and the Expression of Pro-inflammatory Cytokines of Cardiac Fibroblasts Subjected to H/R Through Inhibiting the COX2/NLRP3 Signaling Pathway

As shown in **Figures 7A–F**, H/R greatly elevated the mRNA levels of COX2, NLRP3, IL-1β, IL-18, IL-6, and TNF-α in primary CFs. However, the transcriptional levels of these genes were all downregulated by iguratimod of 5 μM. Similarly, the protein expression levels of COX2, NLRP3, caspase-1, ASC, cleaved caspase-1, GSDMD-N, and IL-1β were all significantly decreased in the T + H/R group in comparison with the H/R group (**Figures 7G–N**). Conclusively, the above results suggested that H/R greatly promoted pyroptosis of primary CFs, whereas pretreatment with Iguratimod remarkably mitigated pyroptosis and subsequent release of initial inflammatory mediators, as

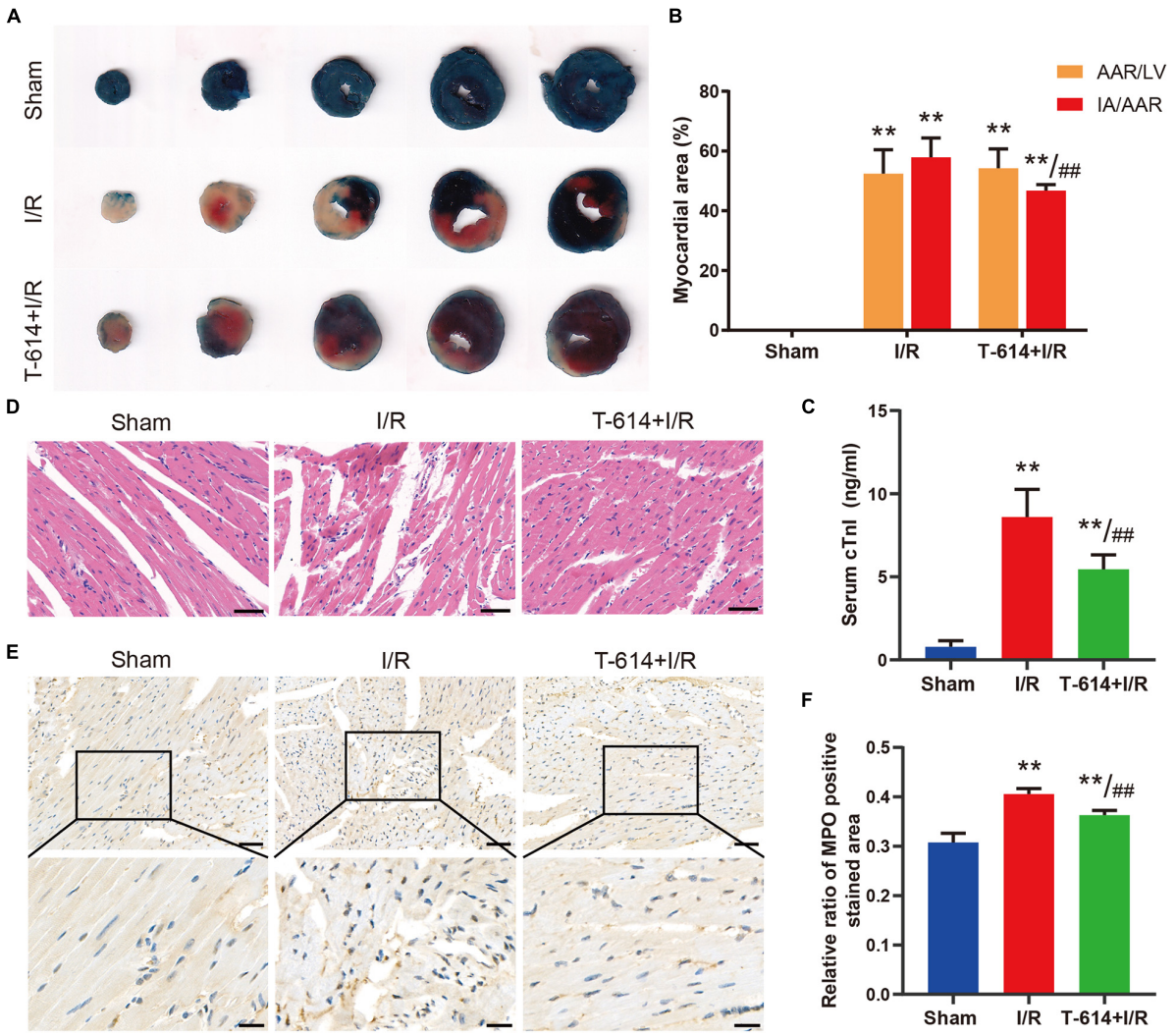

FIGURE 4 | Iguratimod ameliorated myocardial injury and infiltration of inflammatory cells after I/R. **(A)** Representative images of Evans blue and TTC double-stained heart sections. **(B)** Comparison of AAR/LV ratio and IA/AAR ratio among the three groups based on the results of **A**. $n = 5$. **(C)** The level of cTnI in serum determined by ELISA. $n = 5$. **(D)** Representative HE staining pictures of hearts from mice in three groups. Scale bar = 50 μm. **(E)** Representative immunohistochemistry staining images of MPO in cardiac tissue. Scale bar of the first row = 50 μm and scale bar of the second row = 20 μm. **(F)** Comparison of the MPO positive stained area among the three groups. $n = 4$. Data are expressed as mean ± SD; $^{**}p < 0.01$ versus Sham group; $^{\#\#}p < 0.01$ versus I/R group. I/R, ischemia/reperfusion; AAR, area at risk; LV, left ventricle; IA, infarct area; cTnI, cardiac troponin I; MPO, myeloperoxidase.

indicated by reduced expression of cell pyroptosis biomarker, GSDMD-N, and pro-inflammatory cytokines.

DISCUSSION

The present study found that DEGs mainly participated in inflammatory response during myocardial I/R, and NOD-like receptor signaling pathway played a crucial role in mediating inflammation of cardiac tissue. Pretreatment with iguratimod significantly ameliorated excessive cardiac inflammation and cardiomyocytes injury induced by I/R. Moreover, iguratimod decreased the expression of COX2, NLRP3 inflammasome, and pro-inflammatory factors in both *in vivo* and *in vitro* experiments, indicating that the cardioprotective effect of iguratimod was partly mediated through inhibiting CF pyroptosis-triggered inflammatory response via COX2/NLRP3 signaling pathway (**Figure 8**).

Myocardial I/R often causes irreversible changes in cardiac structure and function, as well as injury and death of cardiomyocytes, which involve in many complex pathological processes, including inflammatory response (Zuurbier et al., 2019), oxidative stress (Bugger and Pfeil, 2020), intracellular calcium overload (Wang et al., 2020), etc. Prior studies demonstrated that aseptic inflammation induced by myocardial ischemia was one of the important factors increasing myocardial infarct size (Mezzaroma et al., 2011; Frangogiannis, 2014). Consistently, the present study showed that DEGs during

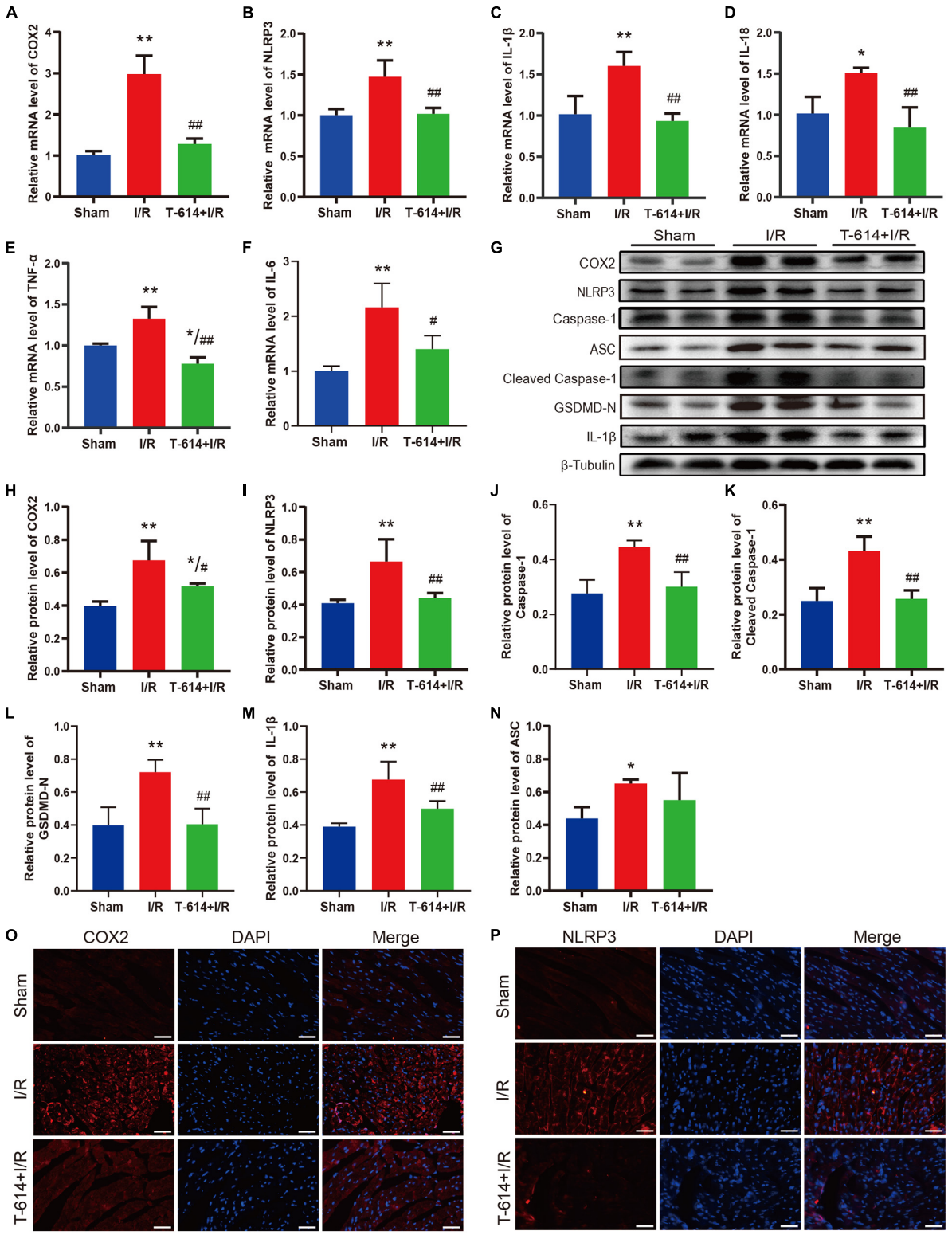

FIGURE 5 | Pyroptosis and inflammatory response mediated by COX2/NLRP3 signaling pathway were suppressed by iguratimod. **(A–F)** Relative mRNA expression levels of COX2, NLRP3, IL-1β, IL-18, IL-6, and TNF-α among Sham, I/R and T-614 + I/R group. $n = 4$. **(G)** Representative Western blotting luminogram of COX2, NLRP3, caspase-1, ASC, cleaved caspase-1, GSDMD-N, and IL-1β of the three groups. **(H–N)** Protein semiquantification standardized by β-Tubulin. $n = 5$. **(O,P)** Representative immunofluorescence staining pictures of COX2 and NLRP3 in left ventricular myocardium from hearts of different mice. Scale bar = 50 μm. Data are expressed as mean ± SD;$^{*}p < 0.05$, $^{**}p < 0.01$ versus Sham group; $^{\#}p < 0.05$, $^{\#\#}p < 0.01$ versus I/R group. I/R, ischemia/reperfusion.

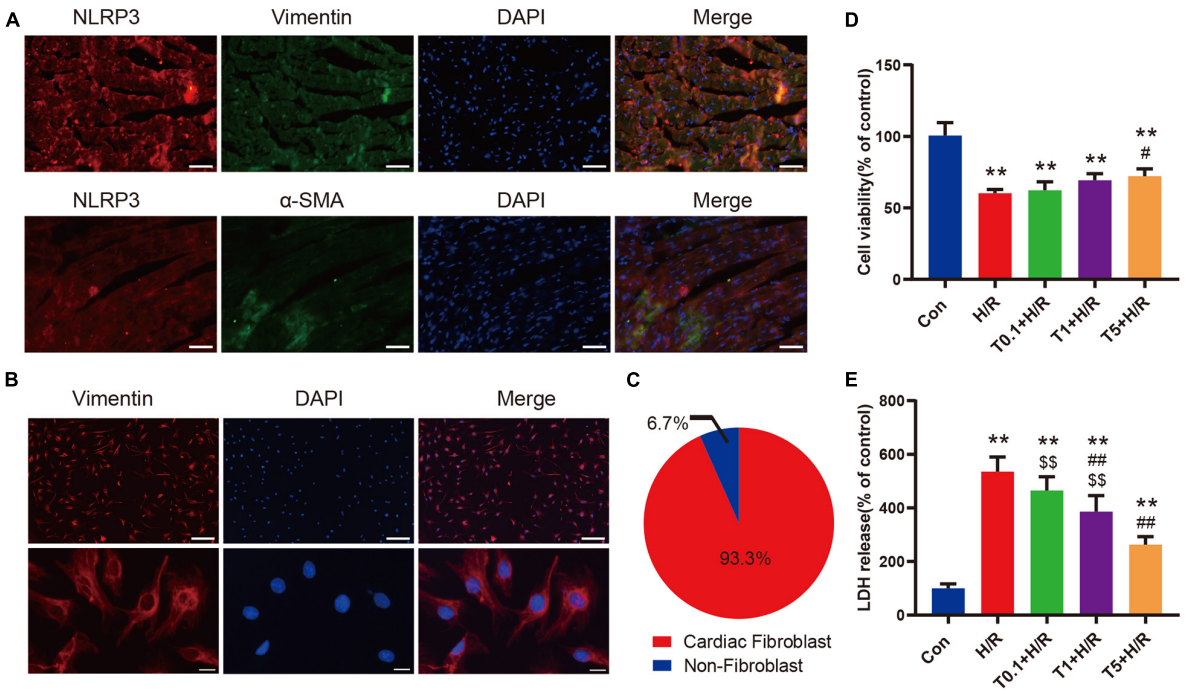

FIGURE 6 | Iguratimod attenuated cell injury of primary CFs exposed to H/R condition. **(A)** Double-immunofluorescence staining with antibodies against NLRP3 (red) and vimentin (green) or α-SMA (green) for left ventricular myocardium tissue. Scale bar = 50 μm. **(B)** Representative images of primary CFs isolated from hearts of neonatal mice. Scale bar of the first row = 50 μm and scale bar of the second row = 5 μm. **(C)** The purity of primary CFs in the present study. **(D)** Cell viability of primary CFs in Con, H/R and Iguratimod (0.1, 1, 5 μM, respectively) pretreatment + H/R group. $n = 5$. **(E)** Percentage of LDH release in cell culture supernatants among the five groups. $n = 6$. Data are expressed as mean ± SD; $^{**}p < 0.01$ versus Con group; $^{\#}p < 0.05$, $^{\#\#}p < 0.01$ versus H/R group; $^{\$\$}p < 0.01$ versus T5 + H/R group. CFs, cardiac fibroblasts; H/R, hypoxia/reoxygenation; α-SMA, α-smooth muscle actin; LDH: lactate dehydrogenase.

myocardial I/R were mainly involved in immune and inflammation-related biological processes, such as inflammatory response, leukocyte migration, regulation of cytokine production, positive regulation of cell migration, etc. I/R alters the balance between anti-inflammatory and pro-inflammatory cytokines, and the latter exacerbate inflammatory response and ischemic injury (Toldo et al., 2018). Specifically, subpopulations of blood-derived cells are delivered to the ischemic area with the help of pro-inflammatory molecules, and then they closely adhere to viable cardiomyocytes, release destructive enzymes into the environment, produce ROS and cause cytotoxic effect, thus extending I/R injury (Frangogiannis, 2014; Gunata and Parlakpinar, 2021).

Pyroptosis is one of the highly pro-inflammatory lytic forms of programmed cell death, which is featured by permeabilization of the plasma membrane, cell swelling, and release of pro-inflammatory factors (Shi et al., 2021). It is well accepted that cleaved caspase-1, the functional performer of activated NLRP3 inflammasome, cleaves GSDMD into C-terminal and N-terminal, and the latter mediates cell pyroptosis (Nagata and Tanaka, 2017; Bedoui et al., 2020). Moreover, cleaved caspase-1 also cuts inactive pro-IL-1β and pro-IL-18 to mature IL-1β and IL-18. Therefore, NLRP3 inflammasome, GSDMD, IL-1β, and IL-18 are all recognized as pyroptosis-related molecules (Zhang et al., 2020; Mo et al., 2021; Nie et al., 2021). These two interleukins, which are released to extracellular space through GSDMD-N pore in the cell membrane, are the upstream of the inflammation and can act as important signal amplifiers to induce the secretion of additional cytokines, chemokines, and adhesion molecules, thus triggering the inflammatory cascade and eventually causing cell damage (Venkatachalam et al., 2009; Eltzschig and Eckle, 2011; Kim et al., 2013). Similarly, we found that NLRP3-mediated pyroptosis signaling was differentially expressed and enriched in inflammatory response process during myocardial I/R through bioinformatics analysis.

In *in vivo* experiments, the up-regulation of pyroptosis-related molecules was observed in the left ventricular myocardium tissue, indicating that I/R triggered cell pyroptosis. Double immunofluorescence staining of cardiac tissue sections showed that I/R-induced NLRP3 had more co-localization with vimentin, the specific cytoskeleton of fibroblasts. This result was consistent with previous studies, which concluded that inflammasome-related genes trigged by myocardial I/R, including NLRP3, IL-1β, and IL-18, were expressed mainly in cardiac fibroblasts and microvascular endothelial cells, instead of cardiomyocytes (Kawaguchi et al., 2011; Sandanger et al., 2013). Activation of NLRP3 inflammasome in non-cardiomyocytes did not directly lead to the loss of contractile structure but caused cardiac dysfunction indirectly by amplifying the inflammatory response through IL-1β and IL-18 (Kawaguchi et al., 2011). According to a recent study, fibroblasts can sense the danger signals released during cardiac injury or stress and participate in inducing

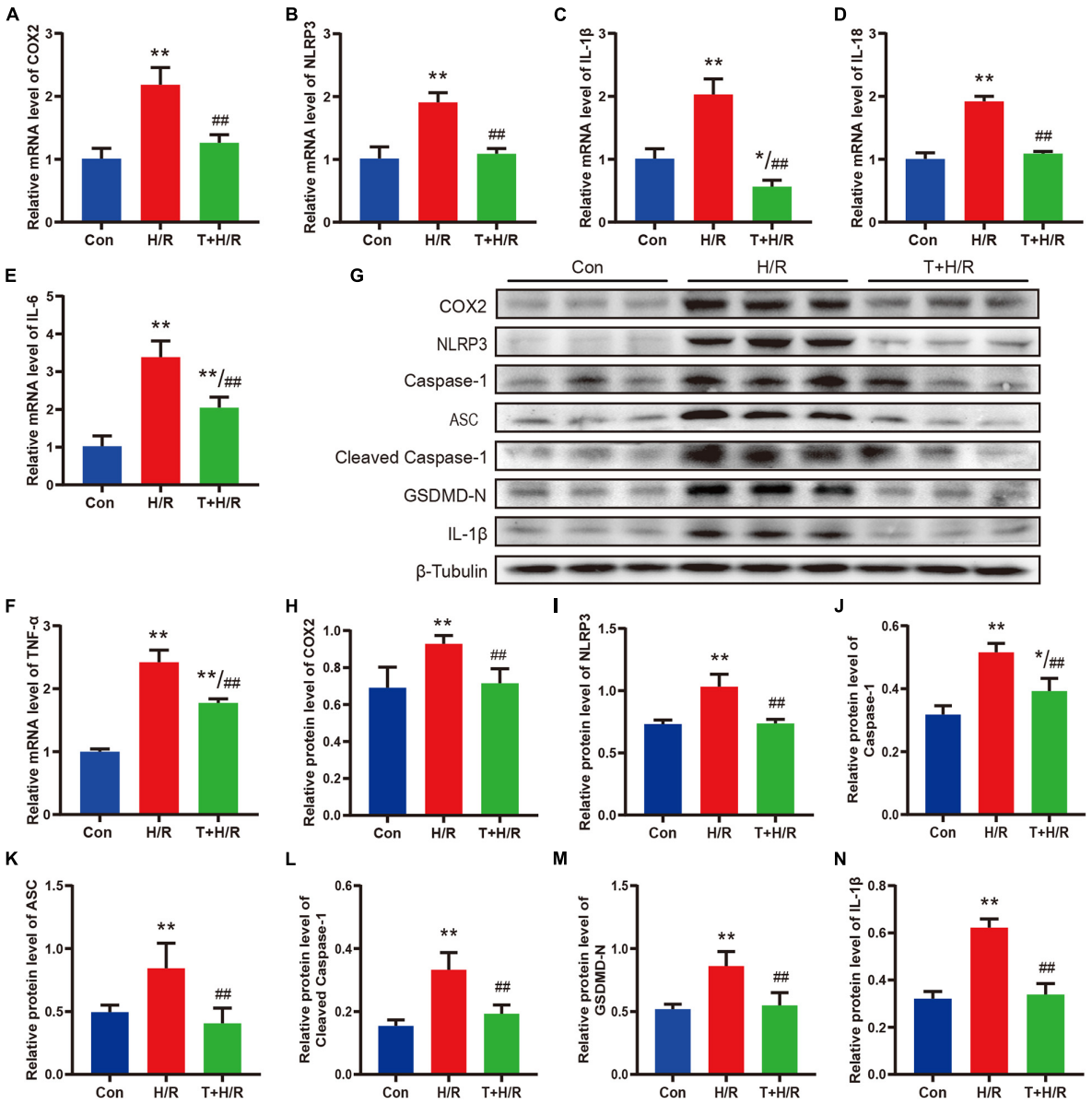

FIGURE 7 | Iguratimod ameliorated pyroptosis and the expression of pro-inflammatory cytokines of CFs subjected to H/R through inhibiting the COX2/NLRP3 signaling pathway. **(A–F)** Relative mRNA expression levels of COX2, NLRP3, IL-1β, IL-18, IL-6, and TNF-α among Con, H/R and T + H/R group. $n = 4$. **(G)** Representative Western blotting luminogram of COX2, NLRP3, caspase-1, ASC, cleaved caspase-1, GSDMD-N, and IL-1β of the three groups. **(H–N)** Protein semiquantification standardized by β-Tubulin. $n = 5$. Data are expressed as mean ± SD; $^{*}p < 0.05$, $^{**}p < 0.01$ versus Con group; $^{\#\#}p < 0.01$ versus H/R group. CFs, cardiac fibroblasts; H/R, hypoxia/reoxygenation.

the recruitment of immune cells to activate and maintain the inflammatory response (Smolgovsky et al., 2021). In view of the increasing focus on the immune role of CFs, we further investigated the effect of H/R on CFs in *in vitro* experiments, and the results demonstrated that H/R induced pyroptosis of primary CFs, confirmed by rupture of cell membrane (as assessed by LDH release) and enhanced expression of pyroptosis-related molecules. Taken together, NLRP3-mediated pyroptosis of CFs may cause injury to myocardium through triggering excessive inflammation.

Iguratimod, a novel drug commonly used in antirheumatic diseases, had been reported to possess therapeutic effect on colitis (Jiang et al., 2018), multiple sclerosis (Li et al., 2018), tumor, and neurodegenerative diseases in animal models (Li et al., 2019) due to its powerful anti-inflammatory ability. Likewise, our research was the first to explore the effect of iguratimod on myocardial I/R injury, and the results demonstrated that iguratimod reduced the myocardial infarct size, cTnI level in serum, and pathological changes of cardiac tissue, indicating its cardioprotective role. Moreover, iguratimod also suppressed

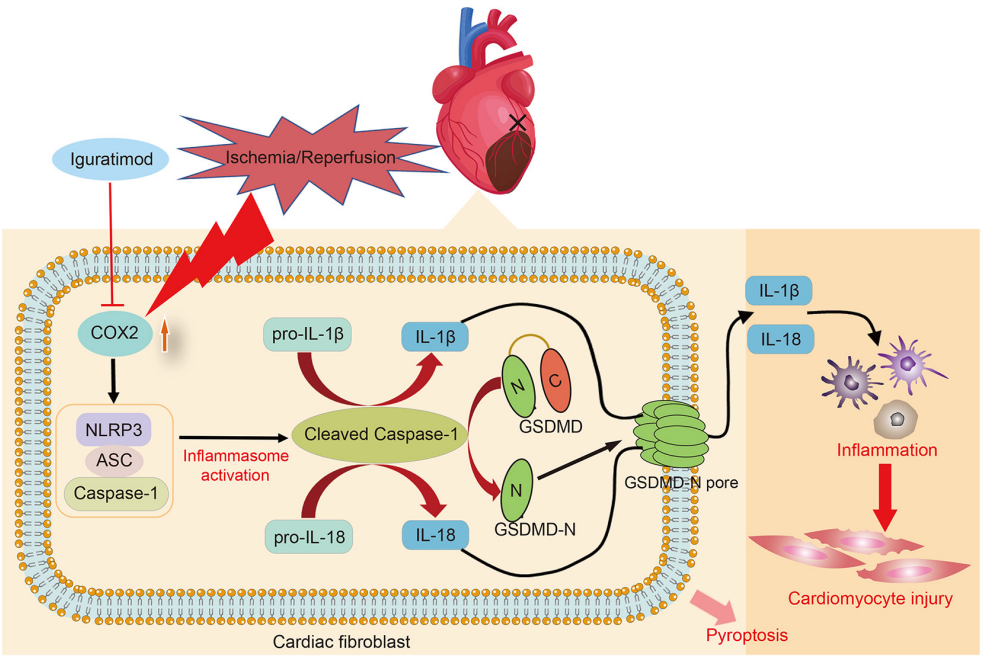

FIGURE 8 | Schematic diagram of this study: the primary mechanism of Iguratimod pretreatment ameliorating myocardial ischemia/reperfusion injury. Specifically, the expression of COX2 in cardiac fibroblasts was elevated after cardiac I/R, leading to the upregulation and activation of NLRP3 inflammasome. Activated caspase-1 cut GSDMD into GSDMD-N, which further executed pyroptosis. Additionally, pro-IL-1β and pro-IL-18 were also cleaved by activated caspase-1 and subsequently their mature forms were released into extracellular region and triggered amounts of inflammatory cells infiltration in the cardiac tissue, causing inflammatory reperfusion injury. Iguratimod reduced inflammatory cytokines secretion and cardiac inflammation response through inhibiting pyroptosis of cardiac fibroblasts via acting on COX2/NLRP3 signaling pathway, eventually improving myocardial I/R injury. I/R, ischemia/reperfusion.

the inflammatory response in heart, confirmed by decreased neutrophil infiltration and expression of inflammatory cytokines. Recently, investigators had revealed the inhibitory effect of iguratimod on NLRP3 inflammasome in mice model of acute pancreatitis (Hou et al., 2019). Similarly, in our study, the molecular expressions of NLRP3, caspase-1, cleaved caspase-1, GSDMD-N, and IL-1β were all decreased after iguratimod pretreatment in *in vivo* and *in vitro* experiments. Although the expression level of ASC protein in cardiac tissue was not dramatically reduced by iguratimod, it remarkably fell off in CFs exposed to H/R in *in vitro* experiments. This result suggested the specific effect of iguratimod on inflammasome in non-cardiomyocytes. Therefore, the cardioprotective role of iguratimod was closely associated with suppressing NLRP3 inflammasome-mediated pyroptosis of CFs.

It has been well-established that up-regulation of COX2 is clearly related to the pathogenesis of many inflammatory processes, and therapeutic treatment targeting COX2 is commonly recommended for inflammatory diseases (Bagi et al., 2006; Redondo et al., 2011; Díaz-Muñoz et al., 2012). Hua et al. (2015) reported for the first time that silencing COX2 gene or using COX2 inhibitors both reduced the expression and activation of NLRP3 inflammasome and downstream cytokines and ameliorated caspase-1-dependent cell apoptosis. Subsequently, results from other studies also supported the theory that COX2 was involved in the activation of NLRP3 inflammasome (Daniels et al., 2016; Lu et al., 2017; Hou et al., 2019). In this study, data from microarray dataset and *in vivo* experiment demonstrated that the transcriptional expression peak of COX2 gene was a little earlier than that of NLRP3 gene after myocardial I/R. Additionally, we found consistent changes in the expression of COX2 and NLRP3 with and without iguratimod pretreatment, indicating the potential regulatory role of COX2 for NLRP3 inflammasome in myocardial I/R. Evidence from previous literature has demonstrated that iguratimod is a highly selective inhibitor of COX2, with inhibition of its gene expression and enzyme activity (Tanaka et al., 1995). In pancreatitis model, the down-regulated expression of COX2 and NLRP3 was observed after preconditioning with iguratimod (Hou et al., 2019). Likewise, our experiments showed that I/R-induced COX2 expression was significantly decreased by iguratimod pretreatment, suggesting that the potential target of iguratimod in alleviating myocardial I/R injury could be COX2.

To sum up, the present study revealed the important role of inflammatory response in I/R-induced myocardial injury and the cardioprotective effect of iguratimod, which mitigated inflammation-mediated myocardium injury through inhibiting pyroptosis of cardiac fibroblasts via down-regulation of COX2/NLRP3 signaling pathway. These findings might provide important insights into the potential therapeutic role of iguratimod in myocardial I/R injury.

However, there were also limitations in the present study. Firstly, the secretion levels of inflammatory factors in cellular

culture supernatants, such as IL-1β and IL-18, were not detected with ELISA, which could directly illustrate the inflammatory microenvironment generated by pyroptosis of CFs and better demonstrate the initial immune role of CFs in the inflammatory cascade after I/R. Secondly, we did not transfect the CFs with overexpression plasmid of COX2. Therefore, there was insufficient evidence to further elucidate that iguratimod exerted an inhibitory role on NLRP3 through acting on COX2. Finally, although neonatal primary cells have been widely used in the study of cardiovascular disease, there may be difference between neonatal and adult primary cells. In the future, further researches are required to clarify other underlying mechanisms in the cardioprotective effect of iguratimod.

DATA AVAILABILITY STATEMENT

The dataset presented in this study can be found in Gene Expression Omnibus (GEO) database (http://www.ncbi.nlm.nih.gov/geo). The name of the repository and accession number is: GSE160516. The original contributions presented in the study are included in the article/**Supplementary Material**, further inquiries can be directed to the corresponding authors.

ETHICS STATEMENT

The animal study was reviewed and approved by the Institutional Animal Care and Use Committee of Soochow University (Suzhou, China).

AUTHOR CONTRIBUTIONS

MZ, X-WM, and F-HJ contributed to the conception and design of the study. MZ and L-GL processed GSE160516 dataset and drew the plots. MZ conducted the experiments and drafted the manuscript. Y-SL, JL, and F-HJ critically reviewed and offered significant modifications to the manuscript. J-XZ, JZ, KP, H-YL, and W-HT cooperatively helped collect the data and perform statistical analysis. All the authors approved the final version of the manuscript.

FUNDING

This work was supported by the National Natural Science Foundation of China (82072130 and 81873925 to F-HJ), Natural Science Foundation of Jiangsu Province (BK20191171 to F-HJ), Science and Technology Development Plan Clinical Trial Project (SLT201909 to F-HJ), Jiangsu Provincial Medical Innovation Team (CXTDA2017043 to F-HJ), 333 High-level Talent Training Project in Jiangsu Province (BRA2020089 to F-HJ), Six talent peaks project in Jiangsu Province (WSN-022 to F-HJ), and Youth Science and Sanitary Foundation of Suzhou (kjxw2018005 to Y-SL).

ACKNOWLEDGMENTS

We are grateful to Zhong-xue Su and Hui Wang for their skilled technical assistance in the establishment of experimental model. We thank Xiang Wei for helping us revise the experimental protocol and providing insightful advice.

SUPPLEMENTARY MATERIAL

The Supplementary Material for this article can be found online at: https://www.frontiersin.org/articles/10.3389/fcell.2021.746317/full#supplementary-material

REFERENCES

An, N., Gao, Y., Si, Z., Zhang, H., Wang, L., Tian, C., et al. (2019). Regulatory Mechanisms of the NLRP3 Inflammasome, a Novel Immune-Inflammatory Marker in Cardiovascular Diseases. *Front. Immunol.* 10:1592. doi: 10.3389/fimmu.2019.01592

Audia, J. P., Yang, X. M., Crockett, E. S., Housley, N., Haq, E. U., O'Donnell, K., et al. (2018). Caspase-1 inhibition by VX-765 administered at reperfusion in P2Y12 receptor antagonist-treated rats provides long-term reduction in myocardial infarct size and preservation of ventricular function. *Basic Res. Cardiol.* 113:32. doi: 10.1007/s00395-018-0692-z

Bagi, Z., Erdei, N., Papp, Z., Edes, I., and Koller, A. (2006). Up-regulation of vascular cyclooxygenase-2 in diabetes mellitus. *Pharmacol Rep.* 58(Suppl), 52–56.

Bedoui, S., Herold, M. J., and Strasser, A. (2020). Emerging connectivity of programmed cell death pathways and its physiological implications. *Nat. Rev. Mol. Cell Biol.* 21, 678–695. doi: 10.1038/s41580-020-0270-8

Bugger, H., and Pfeil, K. (2020). Mitochondrial ROS in myocardial ischemia reperfusion and remodeling. *Biochim. Biophys. Acta Mol. Basis Dis.* 1866:165768. doi: 10.1016/j.bbadis.2020.165768

Daniels, M. J., Rivers-Auty, J., Schilling, T., Spencer, N. G., Watremez, W., Fasolino, V., et al. (2016). Fenamate NSAIDs inhibit the NLRP3 inflammasome and protect against Alzheimer's disease in rodent models. *Nat. Commun.* 7:12504. doi: 10.1038/ncomms12504

Davidson, S. M., Ferdinandy, P., Andreadou, I., Bøtker, H. E., Heusch, G., Ibáñez, B., et al. (2019). Multitarget strategies to reduce myocardial ischemia/reperfusion injury: jacc review topic of the week. *J. Am. Coll. Cardiol.* 73, 89–99. doi: 10.1016/j.jacc.2018.09.086

Díaz-Muñoz, M. D., Osma-García, I. C., Fresno, M., and Iñiguez, M. A. (2012). Involvement of PGE2 and the cAMP signalling pathway in the up-regulation of COX-2 and mPGES-1 expression in LPS-activated macrophages. *Biochem. J.* 443, 451–461. doi: 10.1042/BJ20111052

Eltzschig, H. K., and Eckle, T. (2011). Ischemia and reperfusion–from mechanism to translation. *Nat. Med.* 17, 1391–1401. doi: 10.1038/nm.2507

Ferraro, R., Latina, J. M., Alfaddagh, A., Michos, E. D., Blaha, M. J., Jones, S. R., et al. (2020). Evaluation and management of patients with stable angina: beyond the ischemia paradigm: jacc state-of-the-art review. *J. Am. Coll. Cardiol.* 76, 2252–2266. doi: 10.1016/j.jacc.2020.08.078

Frangogiannis, N. G. (2014). The inflammatory response in myocardial injury, repair, and remodelling. *Nat. Rev. Cardiol.* 11, 255–265. doi: 10.1038/nrcardio.2014.28

Fröhlich, G. M., Meier, P., White, S. K., Yellon, D. M., and Hausenloy, D. J. (2013). Myocardial reperfusion injury: looking beyond primary PCI. *Eur. Heart J.* 34, 1714–1722. doi: 10.1093/eurheartj/eht090

Gunata, M., and Parlakpinar, H. (2021). A review of myocardial ischaemia/reperfusion injury: pathophysiology, experimental models, biomarkers, genetics and pharmacological treatment. *Cell Biochem. Funct.* 39, 190–217. doi: 10.1002/cbf.3587

Hausenloy, D. J., and Yellon, D. M. (2015). Targeting myocardial reperfusion injury–the search continues. *N. Engl. J. Med.* 373, 1073–1075. doi: 10.1056/NEJMe1509718

Heusch, G. (2020). Myocardial ischaemia-reperfusion injury and cardioprotection in perspective. *Nat. Rev. Cardiol.* 17, 773–789. doi: 10.1038/s41569-020-0403-y

Hou, C., Zhu, X., Shi, C., Peng, Y., Huang, D., Li, Q., et al. (2019). Iguratimod (T-614) attenuates severe acute pancreatitis by inhibiting the NLRP3 inflammasome and NF-κB pathway. *Biomed. Pharmacother.* 119:109455. doi: 10.1016/j.biopha.2019.109455

Hua, K. F., Chou, J. C., Ka, S. M., Tasi, Y. L., Chen, A., Wu, S. H., et al. (2015). Cyclooxygenase-2 regulates NLRP3 inflammasome-derived IL-1β production. *J. Cell. Physiol.* 230, 863–874. doi: 10.1002/jcp.24815

Jiang, X. P., Huang, X. L., Yang, Z. P., Wang, S. C., Xie, W., Miao, L., et al. (2018). Iguratimod ameliorates inflammatory responses by modulating the Th17/Treg paradigm in dextran sulphate sodium-induced murine colitis. *Mol. Immunol.* 93, 9–19. doi: 10.1016/j.molimm.2017.10.008

Kawaguchi, M., Takahashi, M., Hata, T., Kashima, Y., Usui, F., Morimoto, H., et al. (2011). Inflammasome activation of cardiac fibroblasts is essential for myocardial ischemia/reperfusion injury. *Circulation* 123, 594–604. doi: 10.1161/CIRCULATIONAHA.110.982777

Kim, H. J., Lee, D. W., Ravichandran, K., OKeys, D., Akcay, A., Nguyen, Q., et al. (2013). NLRP3 inflammasome knockout mice are protected against ischemic but not cisplatin-induced acute kidney injury. *J. Pharmacol. Exp. Ther.* 346, 465–472. doi: 10.1124/jpet.113.205732

Li, G., Yamasaki, R., Fang, M., Masaki, K., Ochi, H., Matsushita, T., et al. (2018). Novel disease-modifying anti-rheumatic drug iguratimod suppresses chronic experimental autoimmune encephalomyelitis by down-regulating activation of macrophages/microglia through an NF-κB pathway. *Sci. Rep.* 8:1933. doi: 10.1038/s41598-018-20390-5

Li, J., Bao, J., Zeng, J., Yan, A., Zhao, C., and Shu, Q. (2019). Iguratimod: a valuable remedy from the Asia Pacific region for ameliorating autoimmune diseases and protecting bone physiology. *Bone Res.* 7:27. doi: 10.1038/s41413-019-0067-6

Liu, Y., Lian, K., Zhang, L., Wang, R., Yi, F., Gao, C., et al. (2014). TXNIP mediates NLRP3 inflammasome activation in cardiac microvascular endothelial cells as a novel mechanism in myocardial ischemia/reperfusion injury. *Basic Res. Cardiol.* 109:415. doi: 10.1007/s00395-014-0415-z

Lu, G., Pan, Y., Kayoumu, A., Zhang, L., Yin, T., Tong, Z., et al. (2017). Indomethacin inhabits the NLRP3 inflammasome pathway and protects severe acute pancreatitis in mice. *Biochem. Biophys. Res. Commun.* 493, 827–832. doi: 10.1016/j.bbrc.2017.08.060

Mezzaroma, E., Toldo, S., Farkas, D., Seropian, I. M., Van Tassell, B. W., Salloum, F. N., et al. (2011). The inflammasome promotes adverse cardiac remodeling following acute myocardial infarction in the mouse. *Proc. Natl. Acad. Sci. U.S.A.* 108, 19725–19730. doi: 10.1073/pnas.1108586108

Mo, G., Liu, X., Zhong, Y., Mo, J., Li, Z., Li, D., et al. (2021). IP3R1 regulates Ca2+ transport and pyroptosis through the NLRP3/Caspase-1 pathway in myocardial ischemia/reperfusion injury. *Cell Death Discov.* 7, 31. doi: 10.1038/s41420-021-00404-4

Montaner, J., Ramiro, L., Simats, A., Tiedt, S., Makris, K., Jickling, G. C., et al. (2020). Multilevel omics for the discovery of biomarkers and therapeutic targets for stroke. *Nat. Rev. Neurol.* 16, 247–264. doi: 10.1038/s41582-020-0350-6

Nagata, S., and Tanaka, M. (2017). Programmed cell death and the immune system. *Nat. Rev. Immunol.* 17, 333–340. doi: 10.1038/nri.2016.153

Nie, C., Ding, X., Ar, Zheng, M., Li, Z., Pan, S., et al. (2021). Hydrogen gas inhalation alleviates myocardial ischemia-reperfusion injury by the inhibition of oxidative stress and NLRP3-mediated pyroptosis in rats. *Life Sci.* 272:119248. doi: 10.1016/j.lfs.2021.119248

Redondo, S., Ruiz, E., Gordillo-Moscoso, A., Navarro-Dorado, J., Ramajo, M., Rodríguez, E., et al. (2011). Overproduction of cyclo-oxygenase-2 (COX-2) is involved in the resistance to apoptosis in vascular smooth muscle cells from diabetic patients: a link between inflammation and apoptosis. *Diabetologia* 54, 190–199. doi: 10.1007/s00125-010-1947-x

Sandanger, Ø, Ranheim, T., Vinge, L. E., Bliksøen, M., Alfsnes, K., Finsen, A. V., et al. (2013). The NLRP3 inflammasome is up-regulated in cardiac fibroblasts and mediates myocardial ischaemia-reperfusion injury. *Cardiovasc. Res.* 99, 164–174. doi: 10.1093/cvr/cvt091

Shi, H., Gao, Y., Dong, Z., Yang, J., Gao, R., Li, X., et al. (2021). GSDMD-mediated cardiomyocyte pyroptosis promotes myocardial I/R injury. *Circ. Res.* 129, 383–396. doi: 10.1161/CIRCRESAHA.120.318629

Shi, J., Zhao, Y., Wang, K., Shi, X., Wang, Y., Huang, H., et al. (2015). Cleavage of GSDMD by inflammatory caspases determines pyroptotic cell death. *Nature* 526, 660–665. doi: 10.1038/nature15514

Singhania, A., Wilkinson, R. J., Rodrigue, M., Haldar, P., and O'Garra, A. (2018). The value of transcriptomics in advancing knowledge of the immune response and diagnosis in tuberculosis. *Nat. Immunol.* 19, 1159–1168. doi: 10.1038/s41590-018-0225-9

Smolgovsky, S., Ibeh, U., Tamayo, T. P., and Alcaide, P. (2021). Adding insult to injury - Inflammation at the heart of cardiac fibrosis. *Cell. Signal.* 77, 109828. doi: 10.1016/j.cellsig.2020.109828

Tanaka, K., Kawasaki, H., Kurata, K., Aikawa, Y., Tsukamoto, Y., and Inaba, T. (1995). T-614, a novel antirheumatic drug, inhibits both the activity and induction of cyclooxygenase-2 (COX-2) in cultured fibroblasts. *Jpn. J. Pharmacol.* 67, 305–314. doi: 10.1254/jjp.67.305

Tanaka, K., Shimotori, T., Makino, S., Aikawa, Y., Inaba, T., Yoshida, C., et al. (1992). Pharmacological studies of the new antiinflammatory agent 3-formylamino-7-methylsulfonylamino-6-phenoxy-4H-1-benzopyran-4-o ne. 1st communication: antiinflammatory, analgesic and other related properties. *Arzneimittelforschung* 42, 935–944.

Toldo, S., Mauro, A. G., Cutter, Z., and Abbate, A. (2018). Inflammasome, pyroptosis, and cytokines in myocardial ischemia-reperfusion injury. *Am. J. Physiol. Heart Circ. Physiol.* 315, H1553–H1568. doi: 10.1152/ajpheart.00158.2018

Venkatachalam, K., Prabhu, S. D., Reddy, V. S., Boylston, W. H., Valente, A. J., and Chandrasekar, B. (2009). Neutralization of interleukin-18 ameliorates ischemia/reperfusion-induced myocardial injury. *J. Biol. Chem.* 284, 7853–7865. doi: 10.1074/jbc.M808824200

Wang, R., Wang, M., He, S., Sun, G., and Sun, X. (2020). Targeting calcium homeostasis in myocardial ischemia/reperfusion injury: an overview of regulatory mechanisms and therapeutic reagents. *Front. Pharmacol.* 11:872. doi: 10.3389/fphar.2020.00872

Wu, D., Feng, J., Mo, X., and Liu, Y. (2016). An improved method for primary culture of neonatal mouse cardiomyocytes. *Chin. J. Comp. Med.* 26, 62–67.

Yellon, D. M., and Hausenloy, D. J. (2007). Myocardial reperfusion injury. *N. Engl. J. Med.* 357, 1121–1135. doi: 10.1056/NEJMra071667

Zhang, J., Huang, L., Shi, X., Yang, L., Hua, F., Ma, J., et al. (2020). Metformin protects against myocardial ischemia-reperfusion injury and cell pyroptosis via AMPK/NLRP3 inflammasome pathway. *Aging (Albany NY)* 12, 24270–24287. doi: 10.18632/aging.202143

Zhou, W., Chen, C., Chen, Z., Liu, L., Jiang, J., Wu, Z., et al. (2018). NLRP3: a Novel Mediator in Cardiovascular Disease. *J. Immunol. Res.* 2018:5702103. doi: 10.1155/2018/5702103

Zhou, Y., Zhou, B., Pache, L., Chang, M., Khodabakhshi, A. H., Tanaseichuk, O., et al. (2019). Metascape provides a biologist-oriented resource for the analysis of systems-level datasets. *Nat. Commun.* 10, 1523. doi: 10.1038/s41467-019-09234-6

Zuurbier, C. J., Abbate, A., Cabrera-Fuentes, H. A., Cohen, M. V., Collino, M., De Kleijn, D., et al. (2019). Innate immunity as a target for acute cardioprotection. *Cardiovasc. Res.* 115, 1131–1142. doi: 10.1093/cvr/cvy304

Conflict of Interest: The authors declare that the research was conducted in the absence of any commercial or financial relationships that could be construed as a potential conflict of interest.

Publisher's Note: All claims expressed in this article are solely those of the authors and do not necessarily represent those of their affiliated organizations, or those of the publisher, the editors and the reviewers. Any product that may be evaluated in this article, or claim that may be made by its manufacturer, is not guaranteed or endorsed by the publisher.

Copyright © 2021 Zhang, Lei, Meng, Liu, Li, Zhang, Zhang, Tao, Peng, Lin and Ji. This is an open-access article distributed under the terms of the Creative Commons Attribution License (CC BY). The use, distribution or reproduction in other forums is permitted, provided the original author(s) and the copyright owner(s) are credited and that the original publication in this journal is cited, in accordance with accepted academic practice. No use, distribution or reproduction is permitted which does not comply with these terms.

frontiers in Cell and Developmental Biology

ORIGINAL RESEARCH
published: 26 October 2021
doi: 10.3389/fcell.2021.757168

Endothelial Dec1-PPARγ Axis Impairs Proliferation and Apoptosis Homeostasis Under Hypoxia in Pulmonary Arterial Hypertension

Xiaoming Li[1,2], Chengcheng Liu[2,3], Wenwen Qi[4], Qiu Meng[1], Hui Zhao[1], Zhenxiao Teng[1], Runtong Xu[1], Xinhao Wu[1], Fangyuan Zhu[1], Yiming Qin[5], Miaoqing Zhao[6], Fenglei Xu[1]* and Ming Xia[1,2]**

[1] Department of Otolaryngology, Shandong Provincial Hospital Affiliated to Shandong First Medical University, Jinan, China, [2] Medical Science and Technology Innovation Center, Shandong First Medical University and Shandong Academy of Medical Sciences, Jinan, China, [3] Department of Central Laboratory, Shandong Provincial Hospital Affiliated to Shandong University, Jinan, China, [4] Department of Otolaryngology, Shandong Provincial Hospital, Cheeloo College of Medicine, Shandong University, Jinan, China, [5] College of Chemical Engineering and Materials Science, Shandong Normal University, Jinan, China, [6] Department of Pathology, Shandong Provincial Hospital Affiliated to Shandong First Medical University, Jinan, China

OPEN ACCESS

Edited by:
Zhiqiang Lin,
Masonic Medical Research Institute (MMRI), United States

Reviewed by:
Jichun Yang,
Peking University, China
Debia Wakhloo,
Stanford University, United States

***Correspondence:**
Miaoqing Zhao
zhaomqsd@163.com
Fenglei Xu
laifuju@126.com
Ming Xia
xiamingsdu@sohu.com

Specialty section:
This article was submitted to Cell Death and Survival, a section of the journal Frontiers in Cell and Developmental Biology

Received: 11 August 2021
Accepted: 27 September 2021
Published: 26 October 2021

Citation:
Li X, Liu C, Qi W, Meng Q, Zhao H, Teng Z, Xu R, Wu X, Zhu F, Qin Y, Zhao M, Xu F and Xia M (2021) Endothelial Dec1-PPARγ Axis Impairs Proliferation and Apoptosis Homeostasis Under Hypoxia in Pulmonary Arterial Hypertension. Front. Cell Dev. Biol. 9:757168. doi: 10.3389/fcell.2021.757168

Background: The hypoxia-induced pro-proliferative and anti-apoptotic characteristics of pulmonary arterial endothelial cells (PAECs) play critical roles in pulmonary vascular remodeling and contribute to hypoxic pulmonary arterial hypertension (PAH) pathogenesis. However, the mechanism underlying this hypoxic disease has not been fully elucidated.

Methods: Bioinformatics was adopted to screen out the key hypoxia-related genes in PAH. Gain- and loss-function assays were then performed to test the identified hypoxic pathways *in vitro*. Human PAECs were cultured under hypoxic (3% O_2) or normoxic (21% O_2) conditions. Hypoxia-induced changes in apoptosis and proliferation were determined by flow cytometry and Ki-67 immunofluorescence staining, respectively. Survival of the hypoxic cells was estimated by cell counting kit-8 assay. Expression alterations of the target hypoxia-related genes, cell cycle regulators, and apoptosis factors were investigated by Western blot.

Results: According to the Gene Expression Omnibus dataset (GSE84538), differentiated embryo chondrocyte expressed gene 1-peroxisome proliferative-activated receptor-γ (Dec1-PPARγ) axis was defined as a key hypoxia-related signaling in PAH. A negative correlation was observed between Dec1 and PPARγ expression in patients with hypoxic PAH. *In vitro* observations revealed an increased proliferation and a decreased apoptosis in PAECs under hypoxia. Furthermore, hypoxic PAECs exhibited remarkable upregulation of Dec1 and downregulation of PPARγ. Dec1 was confirmed to be crucial for the imbalance of proliferation and apoptosis in hypoxic PAECs. Furthermore, the pro-surviving effect of hypoxic Dec1 was mediated through PPARγ inhibition.

Conclusion: For the first time, Dec1-PPARγ axis was identified as a key determinant hypoxia-modifying signaling that is necessary for the imbalance between proliferation and apoptosis of PAECs. These novel endothelial signal transduction events may offer new diagnostic and therapeutic options for patients with hypoxic PAH.

Keywords: hypoxia, differentiated embryo-chondrocyte expressed gene 1 (Dec1), peroxisome proliferative activated receptor-γ (PPARγ), proliferation, apoptosis, pulmonary arterial hypertension

INTRODUCTION

As a complex, progressive, and lethal disease, pulmonary arterial hypertension (PAH) is characterized by the increased muscularity of pulmonary arteries (PAs), resistance to blood flow, irreversible right ventricular (RV) failure, and premature death (Humbert et al., 2018). Although its precise etiology is poorly understood, hypoxia has been identified as an important contributor to PAH (Stenmark et al., 2006). According to the Sixth World Symposium on Pulmonary Hypertension, PAH can be divided into five clinical groups. Hypoxic pulmonary hypertension (HPH) belongs to the third group and highly prevails in a wide range of hypoxia-associated diseases, such as chronic obstructive pulmonary diseases, obstructive sleep apnea (OSA), and high-altitude illness (Simonneau et al., 2014). The morbidity and mortality of PAH increase dramatically with OSA severity (Adir et al., 2021). This interaction can be explained by the hypoxia-induced endothelial dysfunction, which is critical in vascular remodeling and vasoconstriction (Sehgal and Mukhopadhyay, 2007; Houten, 2015).

Intermittent hypoxia, the physiological hallmark of OSA, increases oxidative stress in endothelial cells, which in turn results in endothelial dysfunction and remodeling (Bauters et al., 2016; Benjafield et al., 2019). The transcriptional factor peroxisome proliferative-activated receptor-γ (PPARγ) links these pathologies in vascular disease conditions and functions as a crucial mediator of the hypoxic response (Montaigne et al., 2021). As a ligand-activated nuclear hormone receptor, PPARγ can be stimulated in response to structurally diverse ligands and execute anti-inflammatory and antioxidant effects in many tissues to modulate cell differentiation, growth, inflammation, apoptosis, and angiogenesis (Polikandriotis et al., 2005). Insufficient PPARγ signaling is essential for PAH pathogenesis (Hansmann et al., 2008; Guignabert et al., 2009; Nisbet et al., 2010; Alastalo et al., 2011; Calvier et al., 2019), although the mechanisms have not been fully understood. PPARγ protein is highly expressed in the pulmonary vascular endothelium of normal individuals but is substantially decreased in the lungs and distal PAs of patients with PAH (Guignabert et al., 2009). PPARγ expression is also reduced in PASMCs and PAECs isolated from the PAs of HPH mice (Alastalo et al., 2011; Calvier et al., 2019). Mice with inducible deletion of PPARγ either in PAECs or PASMCs develop PAH (Hansmann et al., 2008). Pharmacological restoration of PPARγ with either pioglitazone or troglitazone shows therapeutic effects in preclinical animal models (Nisbet et al., 2010). The mechanism on how PPARγ is repressed under hypoxia in HPH must be explored.

In this study, the differentially expressed genes (DEGs) between PAH and normal control tissues were examined from the Gene Expression Omnibus (GEO) dataset (GSE84538), and the hypoxia-related DEGs for PAH were estimated. The differentiated embryo–chondrocyte-expressed gene 1 (Dec1), a hypoxia-induced transcriptional factor, was significantly upregulated in PAH. The protein–protein interaction (PPI) network was further established through the shared DEGs, and a Dec1-PPARγ interaction was found in PAH. Given that Dec1 is a hypoxia-regulated transcriptional factor and is involved in cell survival vs. death, the Dec1-PPARγ axis might be responsible for the proliferation promotion and apoptosis resistance of PAECs in hypoxic PAH.

MATERIALS AND METHODS

Ethics

All experiments were approved by the Ethics Committee of Shandong Provincial Hospital Affiliated to Shandong First Medical University. Written informed consent was obtained from all the participants.

Bioinformatic Analysis of Hypoxia-Related Differentially Expressed Genes in Patients With Pulmonary Arterial Hypertension

RNA-seq expression data of patients with PAH and the corresponding control subjects were extracted from the GEO database (GSE84538). These data were accessed by high throughput sequencing RNA from pulmonary arteries. The raw expression profiles were normalized in Deseq2 in the Affy installation package of R software, and the DEGs were screened out by the following selection criteria: $p < 0.05$ and $|\log_2$ fold change (FC)$| > 1$ (Rawal et al., 2021). Volcano plot and heatmaps were used to visualize the DEGs by using the R packages of ggplot2 (v3.3.0) and pheatmap, respectively (Wickham, 2009). The PPI networks were generated in Cytoscape (3.7.2) by the Search Tool for the Retrieval of Interacting Genes/Proteins database (StringDB[1]) protein query (Szklarczyk et al., 2019). Red and blue nodes represented the up and downregulated genes, respectively. GO functional enrichment analysis was performed by the R package "clusterProfiler," and the top 20 of the most significant entries were obtained with a threshold of a p-value set at 0.05 (Yu et al., 2012).

[1]https://string-db.org

Enzyme-Linked Immunosorbent Assay

Peripheral venous blood was collected from patients suffering from OSA with or without PAH, then centrifuged for 10 min at 3,000 rpm, and stored in frozen aliquots at −80°C. Human-specific commercial ELISA assays were applied to evaluate the serum concentrations of Dec1 (Shuangying Biological Technology Co., Ltd., Shanghai, China) and PPARγ (X-Y Biotechnology, Shanghai, China) in accordance with the instructions of the manufacturer. Absorbance was measured at 450 nm using a microtiter plate reader. Experiments were repeated three times.

Cell Culture

Human normal PAECs (hnPAECs) were purchased from Lonza (Basel, Switzerland) and cultured for three to six passages prior to use in the medium (EBM-2) provided by the manufacturers. PAH-PAECs were harvested from the explanted lung tissues of patients with PAH, and healthy-PAECs were obtained from the unused lungs of healthy donors. The isolated healthy- and PAH-PAECs were purified using CD31 antibody by the magnetic cell-sorting system (Miltenyi Biotec, Bergisch Gladbach, Germany) in accordance with the instructions of the manufacturer (Comhair et al., 2012). Cultured PAECs were placed in a standard normoxia incubator (21% O_2, 5% CO_2, 37°C) or a hypoxic incubator (3% O_2, 5% CO_2, 37°C). The hnPAECs were preconditioned with normoxia (pNor-PAECs) or hypoxia (pHyp-PAECs) for 1 week to observe the effect of hypoxia on the phenotype conversions of PAECs. In a separate experiment, the hnPAECs were treated with concentrations of various oxidative or inflammatory PAH stimuli (serum deprivation, H_2O_2 for 100 μM, TGF-β for 20 ng/ml, and IL-6 for 50 ng/ml) for 6, 12, and 24 h *in vitro*.

Construction and Transduction of Recombinant Lentiviral Vectors

Plasmids with Dec1 overexpression (Ov-Dec1), PPARγ overexpression (Ov- PPARγ), and empty control vectors (Ov-Ctrl) were generated as previously described (Li et al., 2016). Plasmids with the short-hairpin RNA of Dec1 (Sh-Dec1, sequence: 5′-GGACTCTTCCTTAATTGCGCC-3′) and nontargeting plasmids (Sh-Ctrl) were generated and recombined into the psi-LVRU6MP vectors in accordance with the instructions of the manufacturer (GeneCopoeia, Rockville, MD, United States). The plasmids were transfected by Lipofectamine 2000 following the instructions of the manufacturer (Thermo Fisher Scientific, San Jose, CA, United States).

Cell Counting Kit 8 Assessment and Flow Cytometry

Cell survival was measured by the CCK8 in accordance with the recommended instructions of the manufacturer (APExBIO, Houston, TX, United States), and cell apoptosis was detected by flow cytometry. After transfection or treatment with hypoxia for the indicated times, the PAECs were collected and double-stained with Annexin V-FITC and propidium iodide by using Annexin V-FITC Apoptosis Detection Kit I (Biosciences Pharmingen, CA, United States) following the instructions of the manufacturer. Apoptosis was measured and analyzed by a FACScan system (Becton Dickinson, Heidelberg, Germany). The cells with Annexin V-FITC positive and PI negative were considered as early apoptosis, and those with Annexin V-FITC positive and PI positive were considered as late apoptosis or necrosis. These experiments were repeated three times.

Ki-67 Immunofluorescence Staining

Ki-67 immunofluorescence staining was performed using the labeled streptavidin–biotin method to evaluate the proliferation of PAECs. After being washed three times with phosphate buffer saline (PBS), the PAECs were sequentially fixed in 4% paraformaldehyde at 4°C for 20 min, permeabilized with 0.2% Triton X-100 in PBS for 5 min, and blocked with 3% bovine serum albumin in PBS for 1 h at room temperature. The cells were then incubated with the Ki-67 primary antibodies (1:500 dilution, Abcam, Cambridge, MA, United States) at 4°C overnight, and then stained with goat anti-rabbit IgG antibody (1:500, Thermo Fisher Scientific, Alexa Fluor 488) at 37°C for 1 h. Finally, nuclei were stained with 4′,6-diamidino-2-phenylindole (DAPI; 1:500, Abcam). The Ki-67 immunostaining of PAECs were detected by a fluorescence microscope (Zeiss, Heidenheim, Germany). The percentage of Ki-67-positive cells was indicated as the proliferation rate of PAECs. Measurements were repeated three times.

Quantitative Real-Time Polymerase Chain Reaction

Total RNA of PAECs was extracted in accordance with the instructions of the Trizol reagent (Invitrogen), and reverse transcription was performed using reverse transcriptase (Thermo Fisher Scientific, Inc.) as reported previously (Zhao et al., 2017). The primers were designed and obtained from Sangon Biotech Co. (Shanghai, China) as follows: Dec1, forward primer 5′-GAAAGGATCGGCGCAATTAA-3′, reverse primer 5′-CATCATCCGAAAGCTGCATC-3′; and β-actin, forward primer 5′-TGGCACCACACCTTCTACAA-3′, reverse primer 5′-GCAGCTCGTAGCTCTTCTCC-3′. The relative level of mRNA was calculated by the $2^{-\Delta\Delta CT}$ method (Teng et al., 2012). Fold change of the relative mRNA expression was evaluated as the average fold change of the hypoxic PAECs compared with that of the normoxic PAECs. Measurements were repeated three times.

Western Blot

Proteins were extracted from human pulmonary artery tissues or PAECs and lysed in RIPA lysis buffer (RIPA, Beyotime, China) in accordance with the instructions of the manufacturer. Protein concentrations were evaluated using the BCA assay based on the albumin standard. The primary antibodies were used as follows: Dec1 and PPARγ (Abcam, United States, dilution: 1/1,000, for both), Cyclin B1 and Cyclin D1 (Sigma, United States,

dilution 1/1,000, for both), Bax (Cell Signaling Technology, United States, dilution: 1/1,000), Bcl-2 (Sigma, United States, dilution 1/1,000), cleaved caspase 3, and β-actin (Santa Cruz, United States, dilution 1/1,000, for both). Detailed information of Western blot was described previously (Li et al., 2020). β-actin was used as a loading control. Fold change of protein expression was evaluated as average fold change for the ratio of targeting genes/β-actin in treated samples compared with that in the controls. Measurements were repeated three times.

Statistical Analysis

All data were presented as mean ± SEM and independently repeated three times. SPSS 13.0 software (SPSS, Chicago, IL, United States) was applied for statistical analysis. GraphPad Prism 6 (GraphPad Software) was used to draw charts. Student's *t*-test was used for data comparison with the two groups. One-way or two-way ANOVA was performed for multiple comparisons. A value of $p < 0.05$ was considered to be statistically significant.

RESULTS

Identification and Validation of Differentiated Embryo-Chondrocyte-Expressed Gene 1-Peroxisome Proliferative-Activated Receptor-γ Axis by Bioinformatic Analysis in Patients With Pulmonary Arterial Hypertension

Gene expression data in eight lung tissue samples (four patients with PAH and four healthy control subjects) were extracted from the GEO (GSE84538) database. Deseq2 analysis identified 756 DEGs, including 446 upregulated (represented in red) and 310 downregulated genes (represented in blue) between the PAH and normal control samples (**Figure 1A**). With the use of STRING, the PPI network revealed 890 edges and 385 nodes in these DEGs (**Figure 1B**). These screened DEGs with all known hypoxia-related genes were overlapped to determine which DEGs have important functions in HPH. As shown in **Figure 1C**, five hypoxia-related genes showed differential expression in PAH. Among them, BHLHE40 (also named Dec1) and placental growth factor (PGF) were upregulated, whereas ENO1 (enolase 1), glycogen branching enzyme 1 (GBE1), and glycogen synthase 1 (GYS1) were downregulated. The volcano plot represented all the DEGs with statistical significance (upregulated and downregulated genes represented in red and blue, respectively) and indicated the prominently upregulated BHLHE40 in PAH (**Figure 1D**).

As the most robust hypoxia-related DEGs in PAH (**Figures 1B,C**), BHLHE40 was selected as a target gene for further study. The PPI network based on the DEGs showed a potential connection between BHLHE40 and PPARγ, a well-known mediator of PAH and a core DEG in the PPI network (as schematically highlighted by a black or green arrow, **Figure 1B**). This connection was also observed in the PPI network based on BHLHE40 and PPARγ (as schematically highlighted by a black or green arrow, **Figures 1E,F**). All these results indicated that the dysregulation of Dec1-PPARγ axis might play major roles in PAH development. However, the expression levels of Dec1 and PPARγ in HPH were still unclear. Therefore, the expression status of Dec1 and PPARγ in OSA patients with or without PAH ($n = 20$ for both groups) was further determined by ELISA. Compared with that in the healthy OSA group, Dec1 was significantly increased (445.8 ± 38.92 vs. 133.7 ± 12.71, $p < 0.001$, **Figure 1G**), and PPARγ was decreased (146.3 ± 13.22 vs. 261.3 ± 16.97, $p < 0.001$, **Figure 1H**) in OSA patients with PAH. A negative correlation was found between Dec1 and PPARγ ($r = -0.5830$, $p = 0.0070$, **Figure 1I**). The negative transcriptional regulating effect of Dec1 on PPARγ has been previously reported. The potential molecular biological role of the Dec1–PPARγ axis was further uncovered by GO enrichment analysis (**Figure 1J**). These data indicated a close relationship between the Dec1–PPARγ axis and the progression of OSA-associated PAH.

Pulmonary Arterial Hypertension Disrupts the Differentiated Embryo–Chondrocyte-Expressed Gene 1-Peroxisome Proliferative-Activated Receptor-γ Axis in Pulmonary Arterial Endothelial Cells

The expression of Dec1-PPARγ axis in human distal pulmonary arteries (PAs) was measured in individuals with or without PAH (control group, $n = 4$; PAH group, $n = 4$) for further understanding. Compared with the PAs in patients without PAH (used as control), Dec1 expression was significantly upregulated (>threefold increase, $p < 0.01$), and PPARγ expression was downregulated in the PAs of patients with PAH (**Figure 2A**, >fivefold decrease, $p < 0.001$). The protein levels of the Dec1–PPARγ axis were further examined in isolated PAECs from patients with or without PAH ($n = 4$ per group). A similar expression trend of the Dec1–PPARγ axis was found in the isolated PAECs. As shown in **Figure 2B**, the protein levels of Dec1 were significantly increased (>sixfold increase, <0.001), whereas those of PPARγ were decreased in PAH-PAECs compared with those in the control-PAECs (>fivefold decrease, $p < 0.001$). These results suggest that PAH exhibits disrupted expression of the Dec1-PPARγ axis.

The hnPAECs were cultured and treated with different PAH stimuli *in vitro* to further determine whether the disrupted expression of the Dec1-PPARγ axis is restricted to the presence of PAH. These stimuli promote PAH *via* oxidative stress and inflammation (Steiner et al., 2009; Wang et al., 2019; Reyes-Palomares et al., 2020). Consistent with the results for distal PAs and PAECs from patients with PAH, Dec1 was elevated, but PPARγ was declined in a time-dependent manner when the cells were treated with serum deprivation (**Figure 2C**), H_2O_2 (**Figure 2D**), TGF-β1 (**Figure 2E**), and IL-6 (**Figure 2F**). These findings indicate that the Dec1–PPARγ axis can also be disrupted

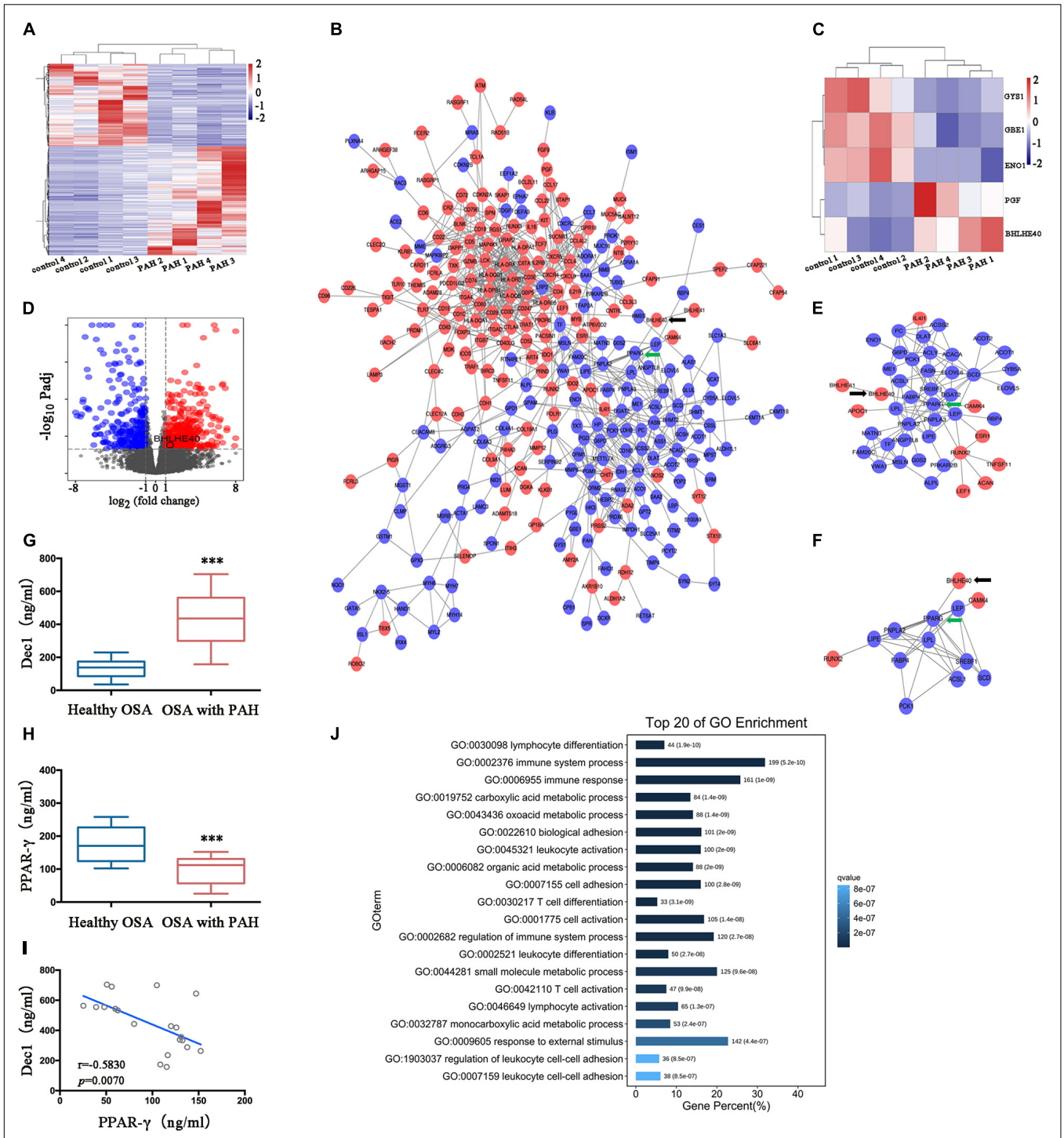

FIGURE 1 | The differentiated embryo-chondrocyte expressed gene 1-peroxisome proliferative activated receptor-γ (Dec1-PPARγ) axis is dysregulated in patients with PAH. **(A)** The heatmap of differentially expressed genes (DEGs) in patients with pulmonary arterial hypertension (PAH) from the GSE84538 database. **(B)** The protein-protein interactions (PPI) network of the DEGs. Black and green arrows indicate BHLHE40 (also named Dec1) and PPARγ, respectively. **(C)** The heatmap of the differentially expressed hypoxia-related genes in patients with PAH from the GSE84538 database. **(D)** The volcano plot showed the DEGs (upregulated in red and downregulated in blue) in patients with PAH from the GSE84538 database. **(E,F)** The PPI networks based on BHLHE40 (arrowed as black) and PPARγ (arrowed as green), respectively. **(G,H)** Plasma protein levels of Dec1 (G) and PPARγ **(H)** were determined by Enzyme-linked immunosorbent assay (ELISA) in obstructive sleep apnea (OSA) patients with or without PAH. One-way ANOVA tests were applied for statistical analysis. **(I)** Spearman's correlation analysis was performed to evaluate the correlations between Dec1 and PPARγ expressions in OSA patients combined with PAH. **(J)** The top 20 entries of the GO enrichment analysis of the gene set. ***$p < 0.001$.

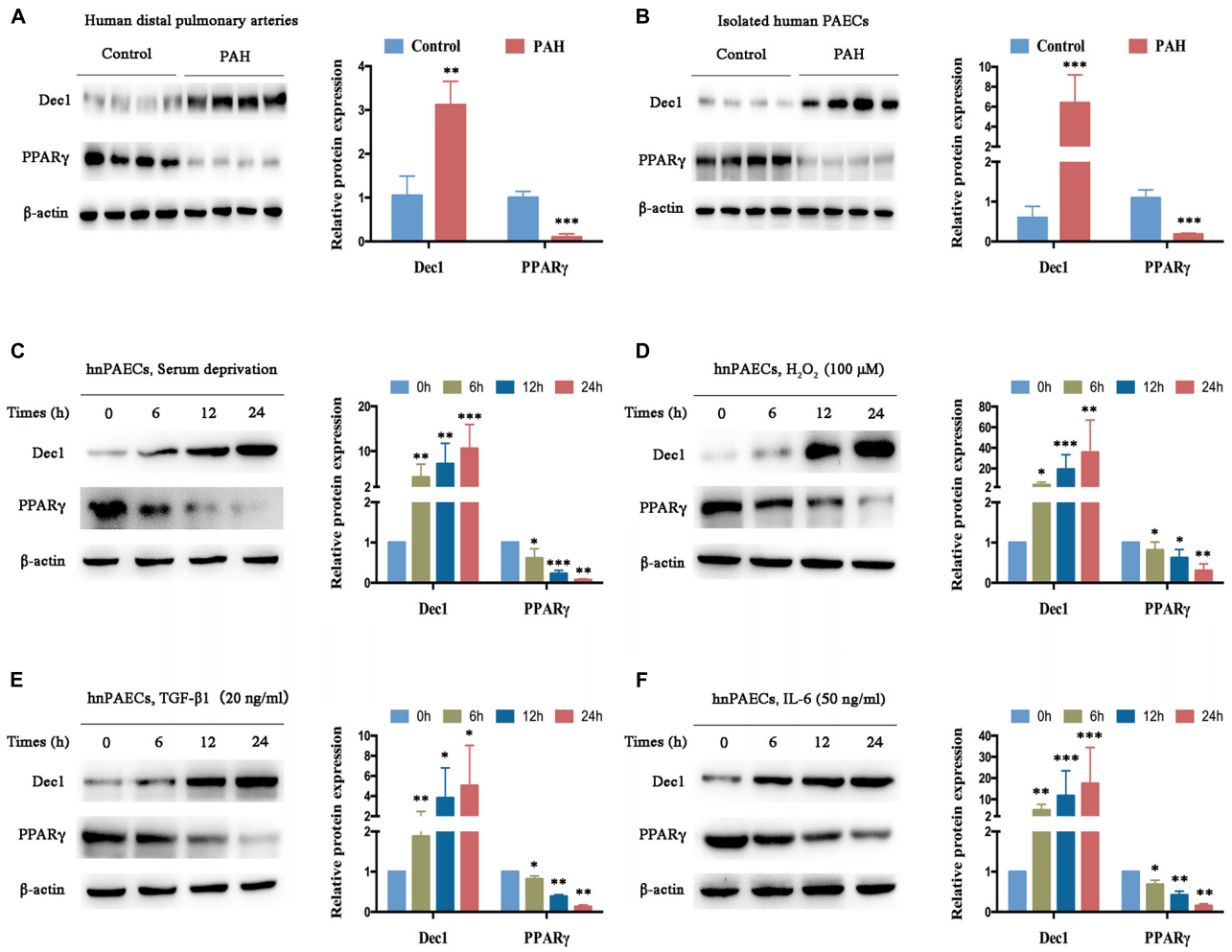

FIGURE 2 | Dec1 is upregulated and PPARγ is downregulated in PAH. **(A)** Expression levels of Dec1 and PPARγ were determined by western blot in pulmonary arteries from PAH (n = 4) and healthy control patients (n = 4). **(B)** Human pulmonary arterial endothelial cells (PAECs) were isolated from PAH and healthy control patients (n = 4 per group), and western blot was performed to determine expressions of the Dec1–PPARγ axis. **(C–F)** Human normal PAECs (hnPAECs) were treated with serum deprivation **(C)**, 100 μM H_2O_2 **(D)**, 20 ng/ml TGF-β1 **(E)**, and 50 ng/ml IL-6 **(F)** *in vitro*. Expression levels of Dec1 and PPARγ in PAECs were determined by western blot (left part) at the indicated times. One-way ANOVA test was applied for statistical analysis (right part). Data are represented as mean ± SEM. Experiments were repeated for three independent times. *$p < 0.05$; **$p < 0.01$; ***$p < 0.001$.

by the PAH stimuli *in vitro* and may play critical roles in PAH progression.

Differentiated Embryo–Chondrocyte-Expressed Gene 1 Modulates the Survival of Pulmonary Arterial Endothelial Cells Under Hypoxia

Differentiated embryo-chondrocyte expressed gene 1 is dysregulated by hypoxia-driven responses and plays important roles in cell death and survival (Park and Park, 2012; Sato et al., 2016; Jia et al., 2018; Nakashima et al., 2018; Le et al., 2019). Therefore, the hnPAECs were treated with hypoxia. The results showed that the mRNA and protein levels of Dec1 were gradually increased in the hnPAECs with the extent of hypoxia (**Figures 3A,B**). However, the protein levels of PPARγ showed the opposite trend (**Figure 3B**). These results suggested that the Dec1–PPARγ axis was also reprogrammed by hypoxia in PAECs.

The question of how PAECs can overcome hypoxia to survive has been extensively investigated. In this work, whether the dysregulated Dec1–PPARγ axis contributes to the cell survival under hypoxia in PAECs was further explored. Cell survival was determined by the CCK-8 assay. As shown in **Figure 3C**, over 75% of the isolated PAH-PAECs survived comparing with the healthy-PAECs (60%) under hypoxia. These results showed that the PAH–PAECs have a significant pro-surviving ability in hypoxia environment. The transfected PAH–PAECs with Dec1–shRNA were studied to further illustrate whether Dec1 is essential for the survival of PAH–PAECs under hypoxia. The results showed that the survival rate of these cells (PAH–PAECs + Sh-Dec1) declined 25% compared with that of the controlled cells (PAH–PAECs + Sh-Dec1, **Figure 3D**). Therefore,

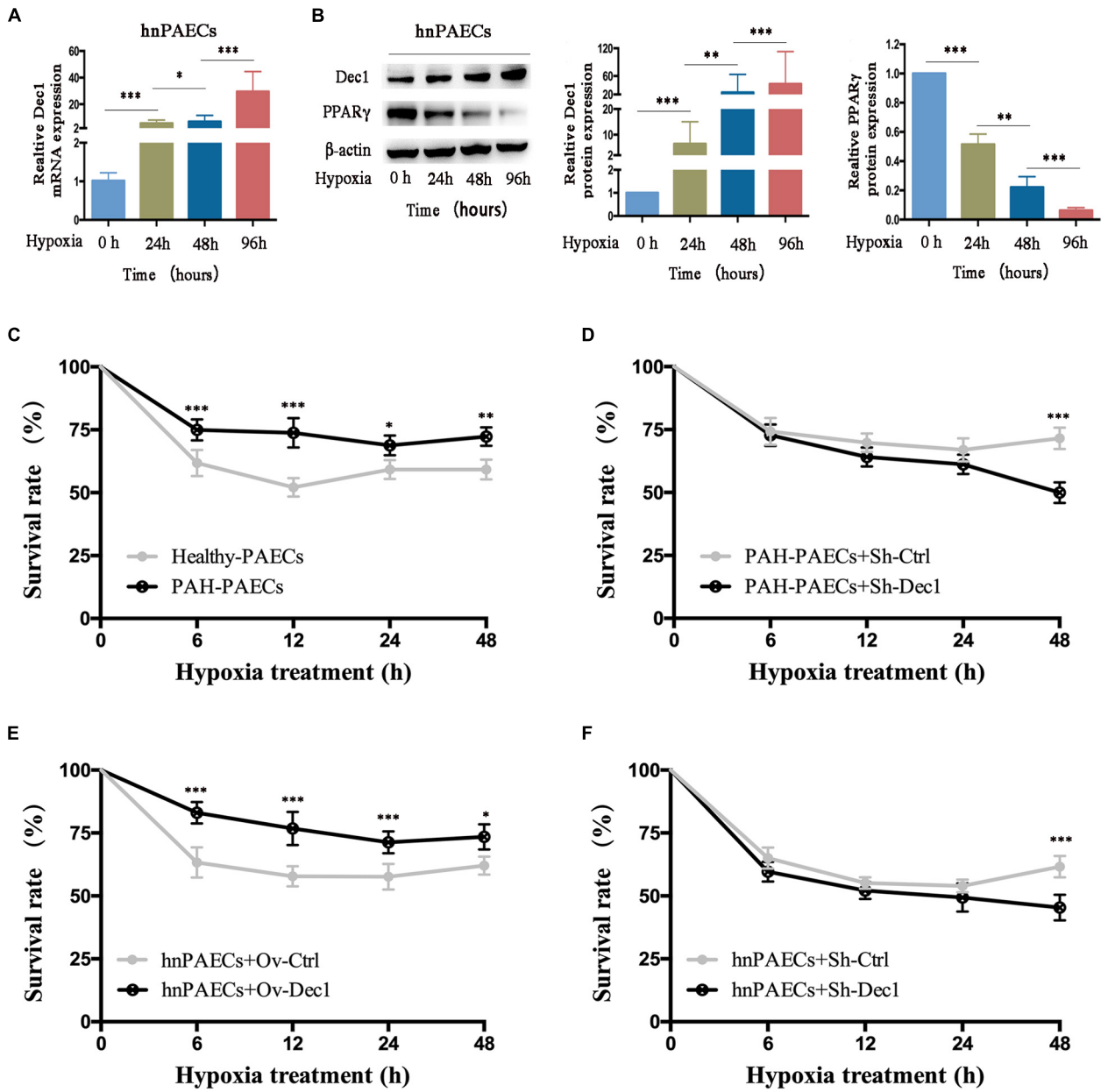

FIGURE 3 | Effect of Dec1 on PAECs survival under hypoxia. **(A,B)** Human normal PAECs (hnPAECs) were treated with 3% O_2 for 0, 24, 48, and 96 h and then performed real-time polymerase chain reaction (RT-PCR) or Western blot to determine the mRNA and protein levels of the target genes, respectively. **(A)** mRNA expression levels of Dec1. **(B)** Protein expression levels of Dec1 and PPARγ. One-way ANOVA test was applied for statistical analysis. **(C–F)** After 12 h of transient transfection, cells were treated with 3% O_2 for 6, 12, 24, and 48 h and monitored the cell viability vs. time by the cell counting kit 8 (CCK-8) assay. Cells were plotted cell viability at the indicated times. **(C)** Healthy- and PAH–PAECs with no transfections. **(D)** PAH–PAECs transfected with Dec1-shRNA (Sh-Dec1) or the scrambled RNA (Sh-Ctrl) plasmids. **(E)** hnPAECs transfected with Dec1 overexpression (Ov-Dec1) or the empty control (Ov-Ctrl) plasmids. **(F)** hnPAECs transfected with Dec1–shRNA (Sh-Dec1) or the scrambled RNA (Sh-Ctrl) plasmids. Two-way ANOVA test was applied for statistical analysis. Data are represented as mean ± SEM. Experiments were repeated for three independent times. $^{*}p < 0.05$; $^{**}p < 0.01$; $^{***}p < 0.001$.

Dec1 is responsible for the pro-surviving phenotype of PAH–PAECs under hypoxia. Dec1 was overexpressed or silenced in hnPAECs to further specify the role of Dec1 in this pro-surviving phenotype. The results showed the hnPAECs with Dec1 overexpression (hnPAECs + Ov-Dec1) under hypoxia showed an increase survival of up to 20% compared with the hnPAECs transfected with empty vectors (hnPAECs + Ov-Ctrl, **Figure 3E**). However, under half of the hnPAECs with deletion of Dec1 (hnPAECs + Sh-Dec1) survived compared with the controlled hnPAECs (65%, hnPAECs + Sh-Ctrl, **Figure 3F**) under hypoxia. All these data showed that Dec1 conferred to the ability of PAECs to survive under hypoxia.

Hypoxia Recapitulates the Pro-proliferative and Anti-apoptotic Phenotypes of Pulmonary Arterial Endothelial Cells

The imbalance between proliferation and apoptosis, which is considered as the PAH phenotype of PAECs, is a major hallmark of the surviving PAECs in PAH development. Therefore, the effects and mechanisms of hypoxia on proliferation and apoptosis of PAECs were investigated. Isolated healthy- or PAH–PAECs were treated with hypoxia (3% O_2) for 24 h, and their proliferation and apoptosis were determined by Ki-67 immunofluorescence staining and flow cytometry, respectively. Under hypoxia, the proliferation rate was higher in PAH-PAECs (46.45 ± 3.32) than in the healthy-PAECs (29.50 ± 3.57, $p < 0.05$, **Figure 4A**). Furthermore, the expression levels of proliferative factors, such as cyclin B1 and cyclin D1, were significantly upregulated in the PAH–PAECs compared with that in the healthy-PAECs (**Figure 4B**). By contrast, the apoptosis rate was lower in the PAH-PAECs than in the healthy-PAECs under hypoxia (7.22 ± 0.31 vs. 21.08 ± 0.80, $p < 0.001$, **Figure 4C**). The apoptotic indicators of Bax/Bcl-2 ratio and cleaved caspase-3 were significantly declined in the PAH-PAECs compared with that in the healthy-PAECs (**Figure 4D**). These data indicated a pro-proliferation and anti-apoptosis phenotypes of PAH-PAECs in hypoxic environments.

The hnPAECs were preconditioned under normoxia or hypoxia for 1 week to fully understand the influence of hypoxia in PAH progression. Compared with the normoxia-preconditioned PAECs (pNor-PAECs), the hypoxia-preconditioned PAECs (pHyp-PAECs) showed a significantly increased proliferation rate (38.05 ± 3.32 vs. 17.21 ± 3.57, $p < 0.05$, **Figure 4E**) but a decreased apoptosis rate (9.43 ± 0.68 vs. 20.01 ± 0.98, $p < 0.001$, **Figure 4G**) when cultured under hypoxia environment. In parallel with these data, the proliferative factors (Cyclin B1 and Cyclin D1) increased, but the apoptotic indicators (Bax/Bcl-2 ratio and cleaved caspase-3) decreased in the pHyp-PAECs compared with that of the pNor-PAECs (**Figures 4F,H**). Therefore, pHyp-PAECs had a PAH-like phenotype that exhibited a pro-proliferative and anti-apoptotic characteristic under hypoxia. These results were similar to those observed in PAH-PAECs and suggested that hypoxia environment promotes the pro-proliferative and anti-apoptotic phenotypes of PAECs.

Differentiated Embryo–Chondrocyte-Expressed Gene 1 Is Essential for the Hypoxia-Induced Pulmonary Arterial Hypertension Phenotypes of Pulmonary Arterial Endothelial Cells

Differentiated embryo-chondrocyte expressed gene 1 plays an important role in cell proliferation and apoptosis under various oxidative stress and inflammatory stimuli (Seino et al., 2015; Jia et al., 2018; Ming et al., 2018; Le et al., 2019). Therefore, the effects of Dec1 on proliferation and apoptosis of PAECs under hypoxia were examined. As shown in **Figure 5A**, the pHyp-PAECs were characterized by an increased proliferation rate compared with the pNor-PAECs (51.46 ± 1.89 vs. 12.44 ± 1.31, $p < 0.01$). The pHyp-PAECs with Dec1 knockdown (Sh-Dec1 + pHyp-PAECs) showed a lower proliferation rate than the corresponding control cells (Sh-Ctrl + pHyp-PAECs, 31.43 ± 3.36, $p < 0.05$) under hypoxia. Similarly, the expression levels of Cyclin B1 and Cyclin D1 were also upregulated by hypoxia but attenuated by Dec1 silencing (**Figures 5B,C**). In addition, a decrease in the apoptosis rate was also found in the pHyp-PAECs compared with that of the pNor-PAECs (12.54 ± 0.23 vs. 25.13 ± 1.65, $p < 0.05$). However, the apoptosis rate was reversed in pHyp-PAECs with Dec1 knockdown compared with that of corresponding control cells under hypoxia (12.54 ± 0.23 vs. 16.18 ± 0.34, $p < 0.001$, **Figure 5D**). In parallel, the decreased apoptotic indicators (Bax/Bcl-2 ratio and cleaved caspase-3) induced by the preconditioned hypoxia was also restored by Dec1 knockdown in PAECs (**Figures 5E,F**). Further comparison was conducted on the expression levels of the proliferative and apoptotic factors between Sh-Ctrl + pNor-PAECs and Sh-Dec1 + pHyp-PAECs groups. Cyclin D1, Bax/Bcl-2 ratio and cleaved caspase-3, but not Cyclin B1, showed significant expression (**Figures 5B,C,E,F**). These results indicated that knockout of Dec1 under hypoxia rescued the expression of Cyclin B1 normal to the greatest extent. Therefore, hypoxia induces the proliferation promotion and apoptosis resistance of PAECs, a PAH-like phenotype, which is regulated by Dec1.

Differentiated Embryo–Chondrocyte-Expressed Gene 1 Promotes the Pulmonary Arterial Hypertension Phenotype of Human Pulmonary Arterial Endothelial Cells *via* Inhibition of Peroxisome Proliferative-Activated Receptor-γ

Peroxisome proliferative activated receptor-γ, which was downregulated in experimental PAH models and clinical patients with PAH, has been widely proven as a protective factor for PAH (Crossno et al., 2007; Hansmann et al., 2007, 2008; Guignabert et al., 2009; Alastalo et al., 2011; Gong et al., 2011; Calvier et al., 2017, 2019). PPARγ expression in hnPAECs was detected by gain- and loss-function assays to understand whether hypoxia-induced downregulation of PPARγ, at least partially, is associated with Dec1. As shown in **Figure 6A**, PPARγ was significantly downregulated by hypoxia but partially restored by Dec1 deletion. Under normoxia, the protein level of PPARγ was also decreased in Dec1-overexpressing hnPAECs compared with that in the corresponding control PAECs (**Figure 6B**), suggesting that PPARγ suppression was a direct result of Dec1 upregulation. These results confirmed that PPARγ expression is negatively regulated by Dec1 under hypoxia.

The hnPAECs were co-transfected with Dec1 and PPARγ overexpressing vectors and treated under normoxia to further clarify whether Dec1 upregulation alone is responsible for the PAH phenotype of PAECs. PAECs transfected with empty vectors

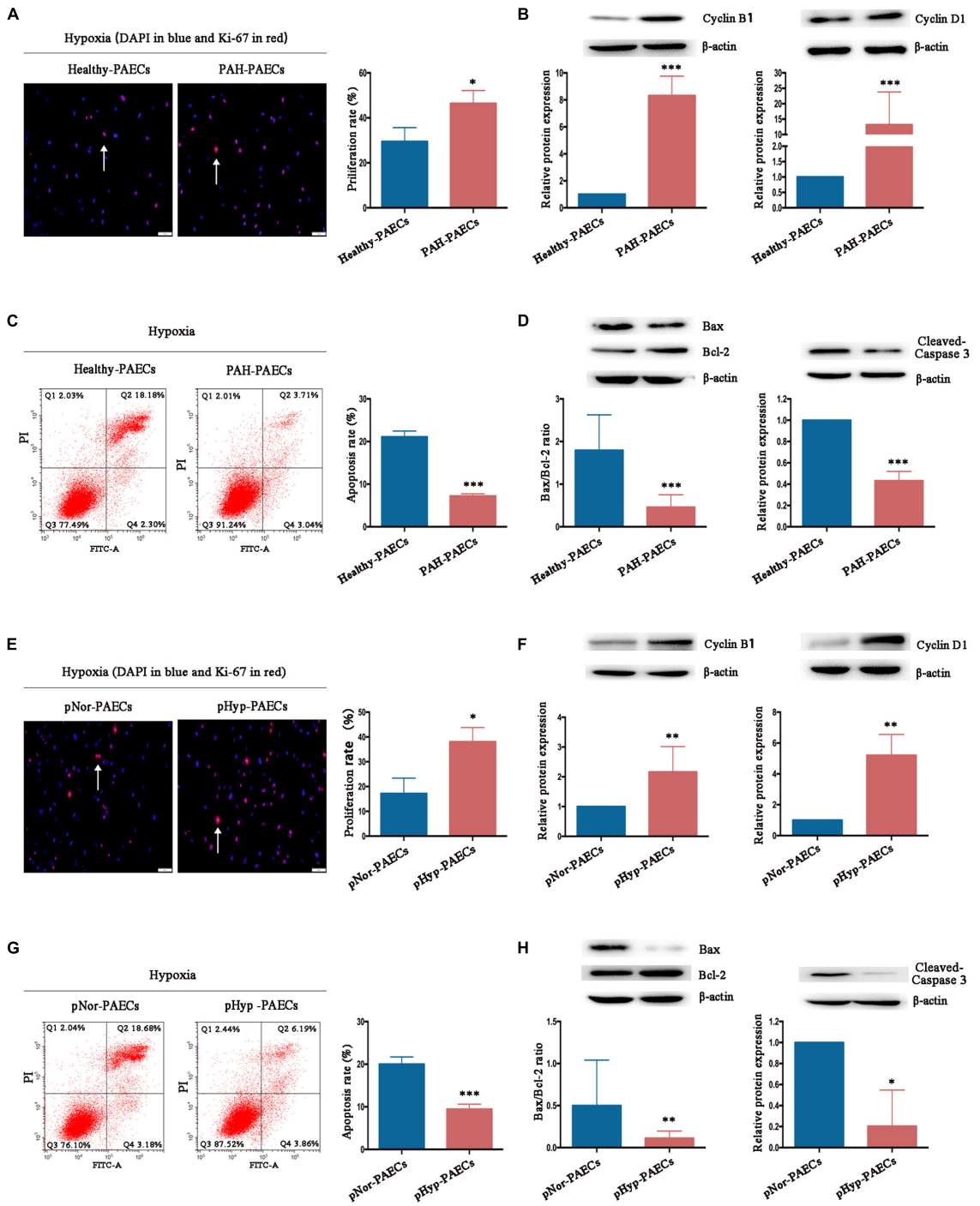

FIGURE 4 | Effect of hypoxia on phenotypes of PAECs. Isolated healthy- or PAH–PAECs were treated with hypoxia (3% O_2) for 24 h. Human normal PAECs (hnPAECs) were preconditioned with normoxia (21% O_2, pNor-PAECs) or hypoxia (3% O_2, pHyp-PAECs) for 1 week. Then these cells were assessed proliferation and apoptosis by immunofluorescence staining of Ki-67 and flow cytometry under hypoxia (3% O_2), respectively. In proliferation assay, Ki-67 positive cells (red) with nuclear DAPI counterstain (blue) indicated the proliferating cells. In apoptosis map, cells were divided into four subpopulations: necrotic cells (Q1: annexin V FITC–/PI+), late apoptotic cells (Q2: annexin V FITC+/PI+), live cells (Q3: annexin V FITC–/PI–), and early apoptotic cells (Q4: annexin V FITC+/PI–). The proliferative (Cyclin B1 and Cyclin D1) and apoptotic factors (Bax, Bcl-2, and cleaved-caspase 3) were detected by Western blot. **(A)** Immunofluorescence staining of Ki-67 (left part, scale bars = 50 μm) and the proliferation rate (right part). **(B)** Expressions of Cyclin B1 and Cyclin D1. **(C)** Flow cytometry (left part) and the apoptosis rate (right part). **(D)** Expressions of Bax, Bcl-2, and cleaved caspase 3. **(E)** Immunofluorescence staining of Ki-67 (left part, scale bars = 50 μm) and the proliferation rate (right part). **(F)** Expressions of Cyclin B1 and Cyclin D1. **(G)** Flow cytometry (left part) and the apoptosis rate (right part). **(H)** Expressions of Bax, Bcl-2, and cleaved caspase 3. One-way ANOVA test was applied for statistical analysis. Data are represented as mean ± SEM. Experiments were repeated for three independent times. $^{*}p < 0.05$; $^{**}p < 0.01$; $^{***}p < 0.001$.

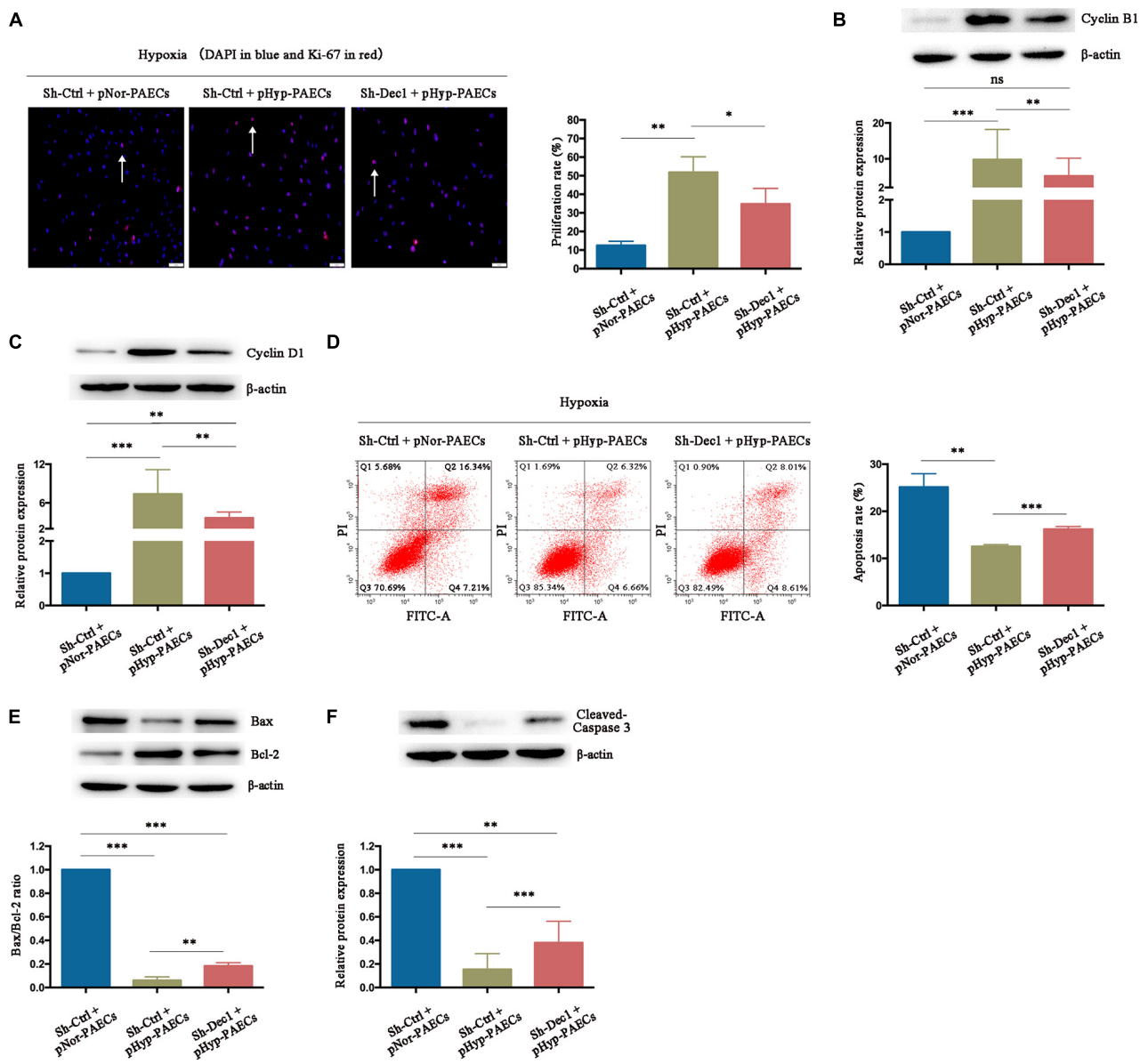

FIGURE 5 | Hypoxia promotes the PAH phenotypes of PAECs by induction of Dec1. Human normal PAECs (hnPAECs) were transfected with Dec1–shRNA (Sh-Dec1) or scrambled RNA (Sh-Ctrl) and then preconditioned with normoxia (21% O_2, pNor-PAECs) or hypoxia (3% O_2, pHyp-PAECs) for 1 week. Next, these cells were assessed proliferation and apoptosis by immunofluorescence staining of Ki-67 and flow cytometry under hypoxia (3% O_2), respectively. In proliferation assay, Ki-67-positive cells (red) with nuclear DAPI counterstain (blue) indicated the proliferating cells. In apoptosis map, cells were divided into four subpopulations: necrotic cells (Q1: annexin V FITC–/PI+), late apoptotic cells (Q2: annexin V FITC+/PI+), live cells (Q3: annexin V FITC–/PI–), and early apoptotic cells (Q4: annexin V FITC+/PI–). The proliferative (Cyclin B1 and Cyclin D1) and apoptotic factors (Bax, Bcl-2 and cleaved-caspase 3) were also detected by western blot.
(A) Immunofluorescence staining of Ki-67 (left part, scale bars = 50 μm) and the proliferation rate (right part). **(B,C)** The expressions of Cyclin B1 **(B)** and Cyclin D1 **(C)**. **(D)** Flow cytometry (left part) and the apoptosis rate (right part). **(E,F)** The expressions of Bax, Bcl-2 **(E)**, and cleaved caspase 3 **(F)**. One-way ANOVA test was applied for statistical analysis. Data are represented as mean ± SEM. Experiments were repeated for three independent times. $^{*}p < 0.05$; $^{**}p < 0.01$; $^{***}p < 0.001$.

was as control (Ov-Ctrl PAECs). Compared with that in Ov-Ctrl PAECs, Dec1 overexpression significantly increased the proliferation rate (59.26 ± 4.77 vs. 25.13 ± 2.17, $p < 0.01$, **Figure 6C**) and decreased the apoptosis rate of hnPAECs (8.040 ± 0.08 vs. 32.88 ± 0.30, $p < 0.001$, **Figure 6D**) under hypoxia. Furthermore, the proliferation rate of hnPAECs with Dec1 overexpression (Ov-Dec1 + Ov-Ctrl) was higher than that of the hnPAECs with co-overexpression of Dec1 and PPARγ (Ov-Dec1 Ov- PPARγ, 47.63 ± 4.16 vs. 19.51 ± 4.39, $p < 0.01$, **Figure 6C**). However, the apoptosis rate of hnPAECs with Dec1 overexpression (Ov-Dec1 + Ov-Ctrl) was significantly lower than that of the hnPAECs with co-overexpression of Dec1 and PPARγ (14.40 ± 0.51 vs. 20.67 ± 0.72, $p < 0.01$, **Figure 6D**). These results indicated that the increased proliferation rate and the

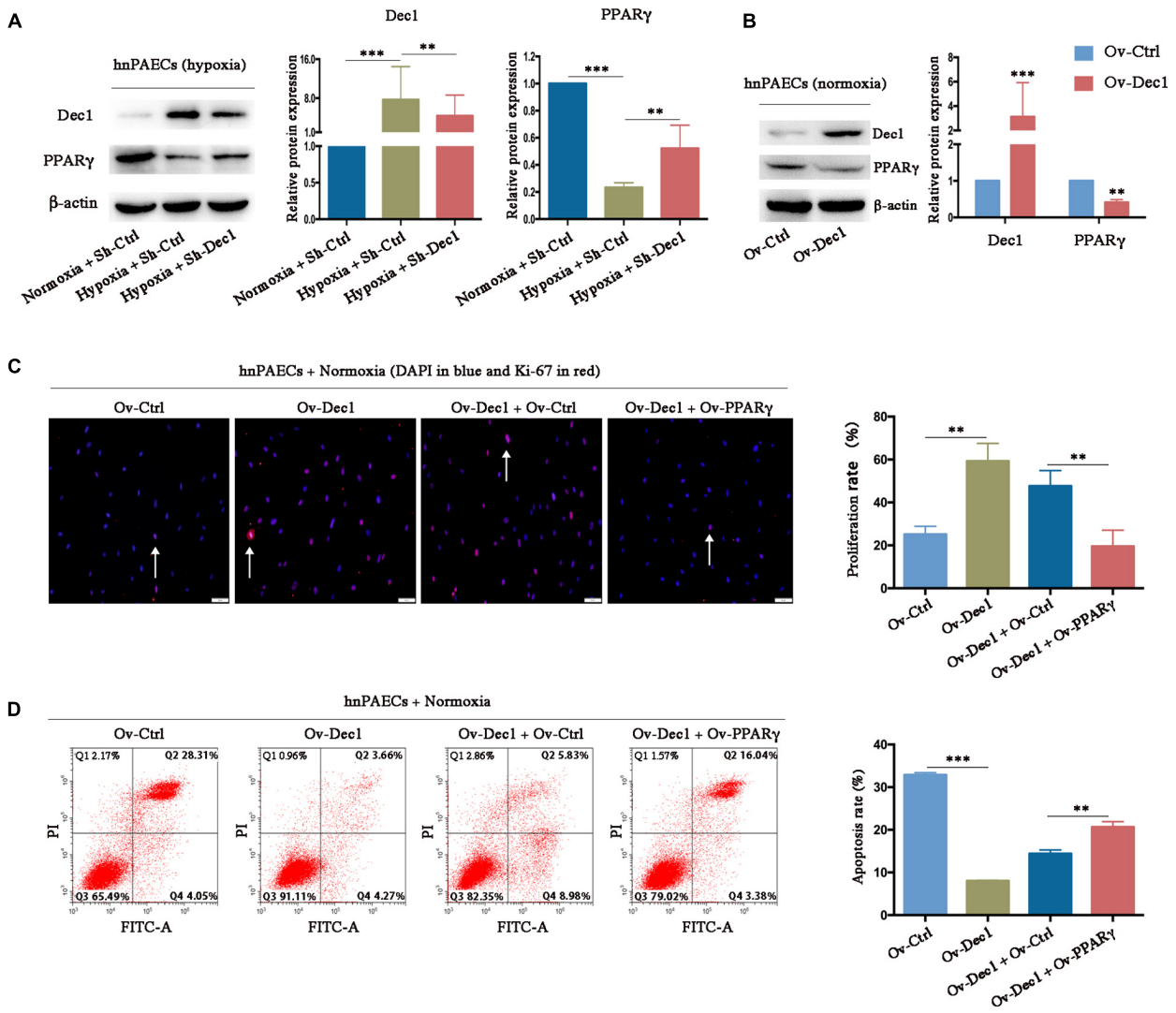

FIGURE 6 | Dec1 promotes the PAH phenotypes of PAECs by inhibition of PPARγ. **(A)** Human normal PAECs (hnPAECs) were transfected with Dec1 Sh-RNA (Sh-Dec1) or the scrambled control (Sh-Ctrl) plasmids and then treated with normoxia (21% O_2) or hypoxia (3% O_2) for 24 h. Protein levels of Dec1 and PPARγ were detected by Western blot in the indicated cells. **(B)** hnPAECs were transfected with Dec1 overexpression (Ov-Dec1) or the empty control (Ov-Ctrl) plasmids and treated with normoxia (21% O_2) for 24 h. Protein levels of Dec1 and PPARγ were detected by western blot in the indicated cells. **(C,D)** Human normal PAECs (hnPAECs) were transfected with Ov-Ctrl, Ov-Dec1, Ov-Dec1 + Ov-Ctrl, and Ov-Dec1 + Ov-PPARγ plasmids and treated with normoxia (21% O_2) for 24 h. Then these cells were assessed proliferation and apoptosis by immunofluorescence staining of Ki-67 (**C**, scale bars = 50 μm) and flow cytometry **(D)**, respectively. In proliferation assay, Ki-67-positive cells (red) with nuclear DAPI counterstain (blue) indicated the proliferating cells. In apoptosis map, cells were divided into four subpopulations: necrotic cells (Q1: annexin V FITC–/PI+), late apoptotic cells (Q2: annexin V FITC+/PI+), live cells (Q3: annexin V FITC–/PI–), and early apoptotic cells (Q4: annexin V FITC+/PI–). One-way ANOVA test was applied for statistical analysis. Data are represented as mean ± SEM. Experiments were repeated for three independent times. *$p < 0.05$; **$p < 0.01$; ***$p < 0.001$.

decreased apoptosis rate induced by Dec1 overexpression were at least partially attributed to PPARγ downregulation.

DISCUSSION

Hypoxia and hypoxia-related pathways contribute to the vascular remodeling of PAH, which is characterized by the phenotype conversions of endothelial proliferation and apoptosis. Under hypoxic environment, the hallmark of OSA, reprogram occurs for hypoxia-responsive genes causing the survival of hyper-proliferative and anti-apoptotic PAECs and the structural changes of PAs. Although the dysfunctions of PPARγ signaling are closely correlated with PAH progression (Hansmann et al., 2008; Alastalo et al., 2011; Gong et al., 2011; Calvier et al., 2017, 2019), the underlying mechanisms by which hypoxia-responsive genes dysregulate PPARγ to trigger the endothelial phenotypic conversions have remained elusive. In this study, bioinformatic analysis revealed that the Dec1-PPARγ axis was reprogrammed in PAH. Further evidence confirmed that Dec1 was the missing

link among the hypoxic environment, PPARγ dysfunctions, and endothelial phenotypic abnormalities.

Despite the underlying mechanisms are not entirely understood, OSA has been well-known as an important risk factor for PAH, which is closely relevant to the hypoxia-induced PA remodeling. The hypoxia-associated genes were screened in the public PAH database to fully explore the role of hypoxic signaling in HPH. The first hint provided by our bioinformatic studies showed a possible connection between the Dec1-PPARγ axis and PAH. In view of the dysregulation of the Dec1-PPARγ axis in PAH database (**Figures 1C,D**), we asked whether this hypoxic signaling was also reprogrammed in HPH. It is well established that hypoxic reprogramming induced by HIF-1α initiates intracellular signaling cascades leading to vascular remodeling, such as Notch, NF-κB, AKT, and PPARγ signaling, which play critical roles in PAH (Gong et al., 2011). As expected, we observed an increased Dec1 expression and decreased PPARγ expression in plasma of the OSA patients with PAH compared with OSA patients without PAH. This change was in a negative correlation (**Figure 1I**), suggesting that hypoxic Dec1 would be involved in downregulating of PPARγ. To the best of our knowledge, this is the first study demonstrating a role of the Dec1-PPARγ axis in the pulmonary vasculature of HPH.

A close relationship was found between hypoxia and the insufficient PPARγ signaling in the pathogenesis of PAH, although the mechanism is still unclear. This concept is supported by that genetic mutations or stimuli of PPARγ regulates development of PAH both *in vivo* and *in vitro* (Hansmann et al., 2008; Gong et al., 2011; Calvier et al., 2017, 2019). Several studies observed the spontaneous PAH developing in mice with conditional deletion of PPARγ in PASMCs and PAECs (Hansmann et al., 2008; Guignabert et al., 2009). Other experiments demonstrated that activation of PPARγ ligands by rosiglitazone attenuated pulmonary hypertension *via* suppressing oxidative, insulin resistance, and proliferative signals in mouse models treated with chronic hypoxia or apoE knockout mice fed a high-fat diet (Crossno et al., 2007; Hansmann et al., 2007; Nisbet et al., 2010). More recent investigations tried to provide the possible mechanism of how hypoxia downregulated the PPARγ expression (Gong et al., 2011; Yao et al., 2021). For example, Kaizheng et al. showed that hypoxia-induced downregulation of PPARγ expression is TGF-β-dependent through increasing Smad2/3/4 and HDAC1 binding at the transcriptional level (Gong et al., 2011). In the present study, we found that insufficient PPARγ signaling is dependent on the induction of Dec1 under hypoxia. These findings are very appealing as it provides an initial insight into the mechanism of which genes with oxygen availability exert a major effect in hypoxic endothelial dysfunctions.

The effects and mechanisms of Dec1 on regulation of PPARγ have been elaborated (**Figure 7**; Cho et al., 2009; Park and Park, 2012; Noshiro et al., 2018). First, Dec1 occupies the specific region of PPARγ promoter and negatively regulates PPARγ expression by interacting with CCAAT/Enhancer Binding Protein β (C/EBPβ) (Park and Park, 2012). Second, as a transcriptional regulator, Dec1 directly binds to the E-boxes or Sp1 sites of the target genes, therefore suppressing and promoting their transcriptions, respectively (Kato et al., 2014). Dec1 transcriptionally represses RXRα, which is a crucial heterodimer partner of PPARγ, via binding to the E-boxes of RXRα promoter (Cho et al., 2009; Noshiro et al., 2018). Third, peroxisome proliferator-activated receptor-γ coactivator-1α (PGC-1α) is also a key regulator of oxidative metabolism and mitochondrial function in PAH and hypoxia-induced repression of PGC-1α plays a critical role in PAH development (Ye et al., 2016). Dec1 could also directly target the E-box of the PGC-1α core promoter and transcriptionally represses PGC-1α (Hsiao et al., 2009; LaGory et al., 2015). Consistent with these studies, we found that PPARγ expression was not only significantly downregulated by induction of Dec1 but also obviously upregulated *via* silencing of Dec1 in PAECs (**Figures 6A,B**). Notably, we found that hypoxia-induced downregulation of PPARγ could be restored by inhibition of Dec1 (**Figure 6A**), which indicated that Dec1 was essential for the PPARγ deficiency under hypoxia.

Although Dec1 is well known as an oncogene in tumors (Nakamura et al., 2008; Feige et al., 2011; Sato et al., 2016; Jia et al., 2018), the present study also adds to a growing body of molecular evidence linking Dec1 to hypoxia-associated diseases (Nishiyama et al., 2012; Wu et al., 2017; Huang et al., 2018; Nakashima et al., 2018; Le et al., 2019). For example, Hue et al. previously reported that Dec1 expression was significantly upregulated in human cardiac hypertrophy and myocardial infarction, while Dec1 deficiency suppressed cardiac perivascular fibrosis and attenuated expressions of p21, TGF-β1, pSmad3, and TNF-α in transverse aortic constriction treated mouse models (Le et al., 2019). Although the potential mechanism remained to be specified, this study provided key findings regarding Dec1 in transverse aortic constriction induced by hypoxia, inflammation, and fibrosis in cardiovascular diseases. In addition, Ayumu et al. demonstrated that Dec1-deficient mice showed decreased blood pressure *in vivo*, and mechanistically, Dec1 suppressed activity of the Na^+/K^+-ATPase by transcriptional repression of Atp1b1 (Prabhakar et al., 2020). It is worth noting that this study also provided indirect evidence that Dec1 might have an important impact on regulating the contraction of pulmonary artery vascular smooth muscle and led to PAH. Owing to the critical roles of hypoxia in blood pressure, it is likely that besides PAH, hypoxic Dec1 may be involved in hypoxic hypertension. Along with these findings, we described Dec1 upregulation to be a key mediator regulating proliferation and apoptosis of PAECs *via* inhibition of PPARγ under hypoxia conditions. All these findings provided therapeutic interest that hypoxia enhanced Dec1 signaling, which in turn induced genetic reprogramming and promoted development of cardiovascular diseases.

The balance of pro-apoptotic and anti-apoptotic factors regulates cell death and survival. The anti-apoptotic effect of Dec1 has been observed under various environmental stimuli in cell lines and animal models, specifically in the field of tumor (Seino et al., 2015; Li et al., 2016; Sato et al., 2016; Jia et al., 2018). However, the role of Dec1 in endothelial apoptosis under hypoxia is poorly understood. For the first time, this work revealed the anti-apoptotic role of Dec1 in hypoxic PAECs by negatively regulating PPARγ expression. Hypoxia reduced number of apoptotic PAECs, which was restored by

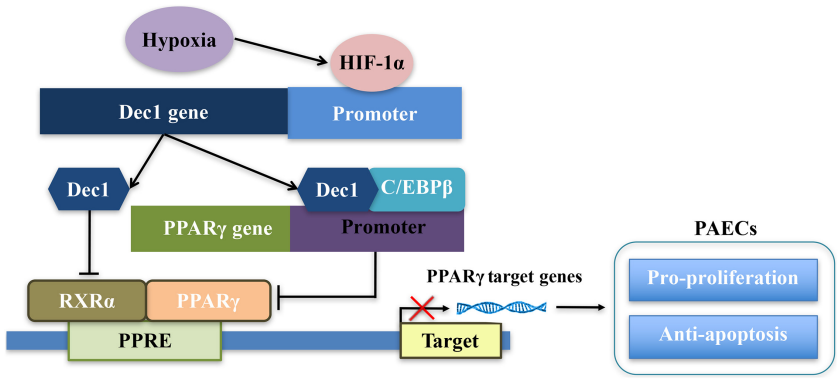

FIGURE 7 | Schema of the signaling pathways leading to disruption of Dec1-PPARγ axis in PAECs in response to hypoxia.

Dec1 knockdown (**Figure 5D**). Emerging evidence suggested that the Bax/Bcl-2 ratio and cleaved caspase 3 expression contribute to cell viability to apoptotic stimuli. Changes in the Bax/Bcl-2 ratio and cleaved caspase 3 expression were found in Dec1-overexpressed or silenced PAECs (**Figures 5E,F**), indicating the crucial role of Dec1 in the apoptotic sensitivity of endothelial cells under hypoxia. A recent study also revealed that Dec1 transcriptionally upregulates Survivin, a family member of the "anti-apoptotic factors," and facilitates the survival of gastric cancer cells under hypoxia (Jia et al., 2018). Xin et al. described Dec1 as a prosurvival factor because it upregulates clusterin, a cytoprotective protein that guards against genotoxic stresses to reduce DNA damage-induced apoptotic response (Ming et al., 2018). Therefore, Dec1 might be one of the key anti-apoptotic factors in hypoxic reprogramming during PAH development.

In addition to apoptosis resistance, the increased proliferation of vascular cells contributes to the progressive remodeling of pulmonary arteries and the formation of PAH (Kim et al., 2010). Recent evidence indicates that PPARγ dysfunction plays a crucial role in the excessive PASMC proliferation of hypoxic and other types of PAH (Ameshima et al., 2003; Kim et al., 2010; Xu et al., 2017), and further reveals the effect of PPARγ on anti-proliferation (Hansmann et al., 2008; Calvier et al., 2017, 2019). For instance, the TGF-β1-promoted VSMC proliferation is PPARγ dependent; on the one hand, PPARγ deletion activates TGF-β1 signaling, and on the other hand, TGF-β1 suppresses PPARγ by inducing miR-130a/301b (Calvier et al., 2017). However, the upstream mediators that downregulate PPARγ are yet to be defined. Hypoxia increases Dec1 (Wykoff et al., 2000) but decreases PPARγ (Kim et al., 2010), a transcriptional target of Dec1 (Park and Park, 2012). Therefore, Dec1-induced PPARγ repression might be important in HPH pathogenesis. As shown in **Figures 2**, **3**, PPARγ expression was significantly decreased by Dec1 overexpression in PAH-PAECs and hypoxia-treated PAECs but was enhanced by Dec1 knockdown (**Figures 6A,B**). These data clarified the hypothesis that hypoxic Dec1 facilitates PAH by inhibiting PPARγ.

Hypoxia is a well-known trigger of vascular remodeling, and PPARγ deficiency is a crucial contributor in PAH development. This study presents the missing link between hypoxia-responsive genes and insufficient PPARγ signaling in PAH pathogenesis. The findings further reveal a causative role of Dec1-PPARγ axis in the imbalance of endothelial proliferation and apoptosis under hypoxia. From the clinical point of view, the Dec1-PPARγ axis might be a novel therapeutic strategy for PAH, especially in HPH.

DATA AVAILABILITY STATEMENT

The original contributions presented in the study are included in the article/supplementary material, further inquiries can be directed to the corresponding author/s.

ETHICS STATEMENT

The studies involving human participants were reviewed and approved by Ethics Committee of Shandong Provincial Hospital Affiliated to Shandong First Medical University. The patients/participants provided their written informed consent to participate in this study. Written informed consent was obtained from the individual(s) for the publication of any potentially identifiable images or data included in this article.

AUTHOR CONTRIBUTIONS

XL, MX, and MZ designed the study. QM, HZ, ZT, RX, XW, FZ, and YQ were responsible for the experimental work. CL and WQ participated in the bioinformatic analysis. XL and MX were contributed to writing and/or revision of the manuscript. XL, MX, CL, MZ, and FX provided funding of this research. All authors approved the submitted version.

FUNDING

This work was supported by the National Natural Science Foundation of China (Nos. 81770979, 82071035, and 81900922) and Natural Science Foundation of Shandong Province (Nos. ZR2020QH155 and ZR2019BH019).

REFERENCES

Adir, Y., Humbert, M., and Chaouat, A. (2021). Sleep-related breathing disorders and pulmonary hypertension. *Eur. Respir. J.* 57:2002258. doi: 10.1183/13993003.02258-2020

Alastalo, T. P., Li, M., Perez Vde, J., Pham, D., Sawada, H., Wang, J. K., et al. (2011). Disruption of PPARγ/β-catenin-mediated regulation of apelin impairs BMP-induced mouse and human pulmonary arterial EC survival. *J. Clin. Invest.* 121, 3735–3746. doi: 10.1172/JCI43382

Ameshima, S., Golpon, H., Cool, C. D., Chan, D., Vandivier, R. W., Gardai, S. J., et al. (2003). Peroxisome proliferator-activated receptor gamma (PPARgamma) expression is decreased in pulmonary hypertension and affects endothelial cell growth. *Circ. Res.* 92, 1162–1169. doi: 10.1161/01.RES.0000073585.50092.14

Bauters, F., Rietzschel, E. R., Hertegonne, K., and Chirinos, J. A. (2016). The link between obstructive sleep apnea and cardiovascular disease. *Curr. Atheroscl. Rep.* 18:1. doi: 10.1007/s11883-015-0556-z

Benjafield, A., Ayas, N., Eastwood, P., Heinzer, R., Ip, M., Morrell, M., et al. (2019). Estimation of the global prevalence and burden of obstructive sleep apnoea: a literature-based analysis. *Lancet Respir. Med.* 7, 687–698. doi: 10.1016/S2213-2600(19)30198-5

Calvier, L., Boucher, P., Herz, J., and Hansmann, G. (2019). LRP1 deficiency in vascular SMC leads to pulmonary arterial hypertension that is reversed by PPARγ activation. *Circ. Res.* 124, 1778–1785. doi: 10.1161/CIRCRESAHA.119.315088

Calvier, L., Chouvarine, P., Legchenko, E., Hoffmann, N., Geldner, J., Borchert, P., et al. (2017). PPARγ links BMP2 and TGFβ1 pathways in vascular smooth muscle cells, regulating cell proliferation and glucose metabolism. *Cell Metab.* 25, 1118–1134.e7. doi: 10.1016/j.cmet.2017.03.011

Cho, Y., Noshiro, M., Choi, M., Morita, K., Kawamoto, T., Fujimoto, K., et al. (2009). The basic helix-loop-helix proteins differentiated embryo chondrocyte (DEC) 1 and DEC2 function as corepressors of retinoid X receptors. *Mol. Pharmacol.* 76, 1360–1369. doi: 10.1124/mol.109.057000

Comhair, S., Xu, W., Mavrakis, L., Aldred, M. A., Asosingh, K., and Erzurum, S. C. (2012). Human primary lung endothelial cells in culture. *Am. J. Respir. Cell Mol. Biol.* 46, 723–730. doi: 10.1165/rcmb.2011-0416TE

Crossno, J. T. Jr., Garat, C. V., Reusch, J. E., Morris, K. G., Dempsey, E. C., Mcmurtry, I. F., et al. (2007). Rosiglitazone attenuates hypoxia-induced pulmonary arterial remodeling. *Am. J. Physiol. Lung Cell Mol. Physiol.* 292, L885–L897. doi: 10.1152/ajplung.00258.2006

Feige, E., Yokoyama, S., Levy, C., Khaled, M., Igras, V., Lin, R., et al. (2011). Hypoxia-induced transcriptional repression of the melanoma-associated oncogene MITF. *Proc. Natl. Acad. Sci.U.S.A.* 108, E924–E933. doi: 10.1073/pnas.1106351108

Gong, K., Xing, D., Li, P., Aksut, B., Ambalavanan, N., Yang, Q., et al. (2011). Hypoxia induces downregulation of PPAR-γ in isolated pulmonary arterial smooth muscle cells and in rat lung via transforming growth factor-β signaling. *Am. J. Physiol. Lung Cell Mol. Physiol.* 301, L899–L907. doi: 10.1152/ajplung.00062.2011

Guignabert, C., Alvira, C. M., Alastalo, T. P., Sawada, H., Hansmann, G., Zhao, M., et al. (2009). Tie2-mediated loss of peroxisome proliferator-activated receptor-gamma in mice causes PDGF receptor-beta-dependent pulmonary arterial muscularization. *Am. J. Physiol. Lung Cell Mol. Physiol.* 297, L1082–L1090. doi: 10.1152/ajplung.00199.2009

Hansmann, G., de Jesus Perez, V. A., Alastalo, T. P., Alvira, C. M., Guignabert, C., Bekker, J. M., et al. (2008). An antiproliferative BMP-2/PPARγ/apoE axis in human and murine SMCs and its role in pulmonary hypertension. *J. Clin. Invest.* 118, 1846–1857. doi: 10.1172/JCI32503

Hansmann, G., Wagner, R. A., Schellong, S., Perez, V. A., Urashima, T., Wang, L., et al. (2007). Pulmonary arterial hypertension is linked to insulin resistance and reversed by peroxisome proliferator-activated receptor-gamma activation. *Circulation* 115, 1275–1284. doi: 10.1161/CIRCULATIONAHA.106.663120

Houten, B. V. (2015). Pulmonary arterial hypertension is associated with oxidative stress–induced genome instability. *Am. J. Respir. Crit. Care Med.* 192, 129–130. doi: 10.1164/rccm.201505-0904ED

Hsiao, S. P., Huang, K. M., Chang, H. Y., and Chen, S. L. (2009). P/CAF rescues the Bhlhe40-mediated repression of MyoD transactivation. *Biochem. J.* 422, 343–352. doi: 10.1042/BJ20090072

Huang, Y., Lai, X., Hu, L., Lei, C., Lan, X., Zhang, C., et al. (2018). Over-expression of DEC1 inhibits myogenic differentiation by modulating MyoG activity in bovine satellite cell. *J. Cell. Physiol.* 233, 9365–9374. doi: 10.1002/jcp.26471

Humbert, M., Guignabert, C., Bonnet, S., Dorfmüller, P., Klinger, J. R., Nicolls, M. R., et al. (2018). Pathology and pathobiology of pulmonary hypertension: state of the art and research perspectives. *Eur. Respir. J.* 53:1801887. doi: 10.1183/13993003.01887-2018

Jia, Y., Hu, R., Li, P., Zheng, Y., Wang, Y., and Ma, X. (2018). DEC1 is required for anti-apoptotic activity of gastric cancer cells under hypoxia by promoting Survivin expression. *Gastr. Cancer* 21, 632–642. doi: 10.1007/s10120-017-0780-z

Kato, Y., Kawamoto, T., Fujimoto, K., and Noshiro, M. (2014). DEC1/STRA13/SHARP2 and DEC2/SHARP1 coordinate physiological processes, including circadian rhythms in response to environmental stimuli. *Curr. Top. Dev. Biol.* 110, 339–372. doi: 10.1016/B978-0-12-405943-6.00010-5

Kim, E. K., Lee, J. H., Oh, Y. M., Lee, Y. S., and Lee, S. D. (2010). Rosiglitazone attenuates hypoxia-induced pulmonary arterial hypertension in rats. *Respirology* 15, 659–668. doi: 10.1111/j.1440-1843.2010.01756.x

LaGory, E. L., Wu, C., Taniguchi, C. M., Ding, C. C., Chi, J. T., Von Eyben, R., et al. (2015). Suppression of PGC-1alpha is critical for reprogramming oxidative metabolism in renal cell carcinoma. *Cell Rep.* 12, 116–127. doi: 10.1016/j.celrep.2015.06.006

Le, H. T., Sato, F., Kohsaka, A., Bhawal, U. K., Nakao, T., Muragaki, Y., et al. (2019). Dec1 deficiency suppresses cardiac perivascular fibrosis induced by transverse aortic constriction. *Int. J. Mol. Sci.* 20:4967. doi: 10.3390/ijms20194967

Li, X., Xu, F., Meng, Q., Gong, N., and Xia, M. (2020). Long noncoding RNA DLEU2 predicts a poor prognosis and enhances malignant properties in laryngeal squamous cell carcinoma through the miR-30c-5p/PIK3CD/Akt axis. *Cell Death Dis.* 11:472. doi: 10.1038/s41419-020-2581-2

Li, X. M., Lin, W., Wang, J., Zhang, W., Yin, A. A., Huang, Y., et al. (2016). Dec1 expression predicts prognosis and the response to temozolomide chemotherapy in patients with glioma. *Mol. Med. Rep.* 14, 5626–5636. doi: 10.3892/mmr.2016.5921

Ming, X., Bao, C., Hong, T., Yang, Y., Chen, X., Jung, Y. S., et al. (2018). Clusterin, a novel DEC1 target, modulates dna damage-mediated cell death. *Mol. Cancer Res.* 16, 1641–1651. doi: 10.1158/1541-7786.MCR-18-0070

Montaigne, D., Butruille, L., and Staels, B. (2021). PPAR control of metabolism and cardiovascular functions. *Nat. Rev. Cardiol.* doi: 10.1038/s41569-021-00569-6

Nakamura, H., Tanimoto, K., Hiyama, K., Yunokawa, M., Kawamoto, T., Kato, Y., et al. (2008). Human mismatch repair gene, MLH1, is transcriptionally repressed by the hypoxia-inducible transcription factors, DEC1 and DEC2. *Oncogene* 27, 4200–4209. doi: 10.1038/onc.2008.58

Nakashima, A., Kawamoto, T., Noshiro, M., Ueno, T., Doi, S., Honda, K., et al. (2018). Dec1 and CLOCK Regulate Na(+)/K(+)-ATPase β1 subunit expression and blood pressure. *Hypertension* 72, 746–754. doi: 10.1161/HYPERTENSIONAHA.118.11075

Nisbet, R. E., Bland, J. M., Kleinhenz, D. J., Mitchell, P. O., Walp, E. R., Sutliff, R. L., et al. (2010). Rosiglitazone attenuates chronic hypoxia-induced pulmonary hypertension in a mouse model. *Am. J. Respir. Cell Mol. Biol.* 42, 482–490. doi: 10.1165/rcmb.2008-0132OC

Nishiyama, Y., Goda, N., Kanai, M., Niwa, D., Osanai, K., Yamamoto, Y., et al. (2012). HIF-1α induction suppresses excessive lipid accumulation in alcoholic fatty liver in mice. *J. Hepatol.* 56, 441–447. doi: 10.1016/j.jhep.2011.07.024

Noshiro, M., Kawamoto, T., Nakashima, A., Ozaki, N., Ueno, T., Saeki, M., et al. (2018). Deficiency of the basic helix-loop-helix transcription factor DEC1 prevents obesity induced by a high-fat diet in mice. *Genes Cells* doi: 10.1111/gtc.12607

Park, Y. K., and Park, H. (2012). Differentiated embryo chondrocyte 1 (DEC1) represses PPARgamma2 gene through interacting with CCAAT/enhancer binding protein beta (C/EBPbeta). *Mol. Cells* 33, 575–581. doi: 10.1007/s10059-012-0002-9

Polikandriotis, J. A., Mazzella, L. J., Rupnow, H. L., and Hart, C. M. (2005). Peroxisome proliferator-activated receptor gamma ligands stimulate endothelial nitric oxide production through distinct peroxisome proliferator-activated receptor gamma-dependent mechanisms. *Arteriosc. Thromb. Vasc. Biol.* 25, 1810–1816. doi: 10.1161/01.ATV.0000177805.65864.d4

Prabhakar, N., Peng, Y., and Nanduri, J. (2020). Hypoxia-inducible factors and obstructive sleep apnea. *J. Clin. Invest.* 130, 5042–5051. doi: 10.1172/JCI137560

Rawal, H., Angadi, U., and Mondal, T. (2021). TEnGExA: an R package based tool for tissue enrichment and gene expression analysis. *Brief. Bioinform.* 22:bbaa221. doi: 10.1093/bib/bbaa221

Reyes-Palomares, A., Gu, M., Grubert, F., Berest, I., and Zaugg, J. B. (2020). Remodeling of active endothelial enhancers is associated with aberrant gene-regulatory networks in pulmonary arterial hypertension. *Nat. Commun.* 11:1673. doi: 10.1038/s41467-020-15463-x

Sato, F., Bhawal, U., Yoshimura, T., and Muragaki, Y. (2016). DEC1 and DEC2 crosstalk between circadian rhythm and tumor progression. *J. Cancer* 7, 153–159. doi: 10.7150/jca.13748

Sehgal, P., and Mukhopadhyay, S. (2007). Dysfunctional intracellular trafficking in the pathobiology of pulmonary arterial hypertension. *Am. J. Respir. Cell Mol. Biol.* 37, 31–37. doi: 10.1165/rcmb.2007-0066TR

Seino, H., Wu, Y., Morohashi, S., Kawamoto, T., Fujimoto, K., Kato, Y., et al. (2015). Basic helix-loop-helix transcription factor DEC1 regulates the cisplatin-induced apoptotic pathway of human esophageal cancer cells. *Biomed. Res.* 36, 89–96. doi: 10.2220/biomedres.36.89

Simonneau, G., Gatzoulis, M. A., Adatia, I., Celermajer, D., Denton, C., Ghofrani, A., et al. (2014). Updated clinical classification of pulmonary hypertension. *J. Am. Coll. Cardiol.* 62(25 Suppl), D34–D41. doi: 10.1016/j.jacc.2013.10.029

Steiner, M. K., Syrkina, O. L., Kolliputi, N., Mark, E. J., Hales, C. A., and Waxman, A. B. (2009). Interleukin-6 overexpression induces pulmonary hypertension. *Circ. Res.* 104, 236–244,228following244. doi: 10.1161/CIRCRESAHA.108.182014

Stenmark, K. R., Fagan, K. A., and Frid, M. G. (2006). Hypoxia-induced pulmonary vascular remodeling: cellular and molecular mechanisms. *Circ. Res.* 99, 675–691. doi: 10.1161/01.RES.0000243584.45145.3f

Szklarczyk, D., Gable, A. L., Lyon, D., Junge, A., Wyder, S., Huerta-Cepas, J., et al. (2019). STRING v11: protein-protein association networks with increased coverage, supporting functional discovery in genome-wide experimental datasets. *Nucleic Acids Res.* 47, D607–D613. doi: 10.1093/nar/gky1131

Teng, X., Zhang, Z., He, G., Yang, L., and Li, F. (2012). Validation of reference genes for quantitative expression analysis by real-time RT-PCR in four lepidopteran insects. *J. Insect Sci.* 12, 1–17. doi: 10.1673/031.012.6001

Wang, Y., Pandey, R. N., York, A. J., Mallela, J., Nichols, W. C., Hu, Y. C., et al. (2019). The EYA3 tyrosine phosphatase activity promotes pulmonary vascular remodeling in pulmonary arterial hypertension. *Nat. Commun.* 10:4143. doi: 10.1038/s41467-019-12226-1

Wickham, H. (2009). *Ggplot2: Elegant Graphics for Data Analysis*. Cham: Springer. doi: 10.1007/978-0-387-98141-3

Wu, L. H., Cheng, W., Yu, M., He, B. M., Sun, H., Chen, Q., et al. (2017). Nr3C1-Bhlhb2 axis dysregulation is involved in the development of attention deficit hyperactivity. *Mol. Neurobiol.* 54, 1196–1212. doi: 10.1007/s12035-015-9679-z

Wykoff, C. C., Pugh, C. W., Maxwell, P. H., Harris, A. L., and Ratcliffe, P. J. (2000). Identification of novel hypoxia dependent and independent target genes of the von Hippel-Lindau (VHL) tumour suppressor by mRNA differential expression profiling. *Oncogene* 19, 6297–6305. doi: 10.1038/sj.onc.1204012

Xu, Y., Gu, Q., Liu, N., Yan, Y., Yang, X., Hao, Y., et al. (2017). PPARgamma alleviates right ventricular failure secondary to pulmonary arterial hypertension in rats. *Int. Heart J.* 58, 948–956. doi: 10.1536/ihj.16-591

Yao, D., He, Q., Sun, J., Cai, L., Wei, J., Cai, G., et al. (2021). FGF21 attenuates hypoxia-induced dysfunction and inflammation in HPAECs via the microRNA-27b-mediated PPARγ pathway. *Int. J. Mol. Med.* 47:116. doi: 10.3892/ijmm.2021.4949

Ye, J. X., Wang, S. S., Ge, M., and Wang, D. J. (2016). Suppression of endothelial PGC-1alpha is associated with hypoxia-induced endothelial dysfunction and provides a new therapeutic target in pulmonary arterial hypertension. *Am. J. Physiol. Lung Cell Mol. Physiol.* 310, L1233–L1242. doi: 10.1152/ajplung.00356.2015

Yu, G., Wang, L. G., Han, Y., and He, Q. Y. (2012). clusterProfiler: an R package for comparing biological themes among gene clusters. *Omics* 16, 284–287. doi: 10.1089/omi.2011.0118

Zhao, M., Sun, D., Li, X., Xu, Y., Zhang, H., Qin, Y., et al. (2017). Overexpression of long noncoding RNA PEG10 promotes proliferation, invasion and metastasis of hypopharyngeal squamous cell carcinoma. *Oncol. Lett.* 14, 2919–2925. doi: 10.3892/ol.2017.6498

Conflict of Interest: The authors declare that the research was conducted in the absence of any commercial or financial relationships that could be construed as a potential conflict of interest.

Publisher's Note: All claims expressed in this article are solely those of the authors and do not necessarily represent those of their affiliated organizations, or those of the publisher, the editors and the reviewers. Any product that may be evaluated in this article, or claim that may be made by its manufacturer, is not guaranteed or endorsed by the publisher.

Copyright © 2021 Li, Liu, Qi, Meng, Zhao, Teng, Xu, Wu, Zhu, Qin, Zhao, Xu and Xia. This is an open-access article distributed under the terms of the Creative Commons Attribution License (CC BY). The use, distribution or reproduction in other forums is permitted, provided the original author(s) and the copyright owner(s) are credited and that the original publication in this journal is cited, in accordance with accepted academic practice. No use, distribution or reproduction is permitted which does not comply with these terms.

frontiers in Cell and Developmental Biology

ORIGINAL RESEARCH
published: 29 October 2021
doi: 10.3389/fcell.2021.760035

Sacubitril Ameliorates Cardiac Fibrosis Through Inhibiting TRPM7 Channel

Tian Jia[1†], Xiaozhi Wang[2†], Yiqun Tang[3], Wenying Yu[4], Chenhui Li[1], Shufang Cui[1], Juanjuan Zhu[1], Wei Meng[1], Chen Wang[1] and Quanyi Wang[1*]*

[1] State Key Laboratory of Natural Medicines, Department of Life Sciences and Technology, China Pharmaceutical University, Nanjing, China, [2] Department of Cardiology, The First Affiliated Hospital With Nanjing Medical University, Nanjing, China, [3] Department of Clinical Pharmacy, School of Basic Medicine and Clinical Pharmacy, China Pharmaceutical University, Nanjing, China, [4] State Key Laboratory of Natural Medicines, Department of Natural Medicinal Chemistry, China Pharmaceutical University, Nanjing, China

OPEN ACCESS

Edited by:
Zhi Qi,
Nankai University, China

Reviewed by:
Qinghua Cui,
Peking University, China
Yinchuan Xu,
Zhejiang University, China
Guang Li,
Southwest Medical University, China

***Correspondence:**
Chen Wang
cwang1971@cpu.edu.cn
Quanyi Wang
quanyiwang@cpu.edu.cn

[†] These authors have contributed equally to this work and share first authorship

Specialty section:
This article was submitted to Cell Death and Survival, a section of the journal Frontiers in Cell and Developmental Biology

Received: 17 August 2021
Accepted: 11 October 2021
Published: 29 October 2021

Citation:
Jia T, Wang XZ, Tang YQ, Yu WY, Li CH, Cui SF, Zhu JJ, Meng W, Wang C and Wang QY (2021) Sacubitril Ameliorates Cardiac Fibrosis Through Inhibiting TRPM7 Channel. Front. Cell Dev. Biol. 9:760035. doi: 10.3389/fcell.2021.760035

Heart failure caused by cardiac fibrosis has become a major challenge of public health worldwide. Cardiomyocyte programmed cell death (PCD) and activation of fibroblasts are crucial pathological features, both of which are associated with aberrant Ca^{2+} influx. Transient receptor potential cation channel subfamily M member 7 (TRPM7), the major Ca^{2+} permeable channel, plays a regulatory role in cardiac fibrosis. In this study, we sought to explore the mechanistic details for sacubitril, a component of sacubitril/valsartan, in treating cardiac fibrosis. We demonstrated that sacubitril/valsartan could effectively ameliorate cardiac dysfunction and reduce cardiac fibrosis induced by isoprotereno (ISO) *in vivo*. We further investigated the anti-fibrotic effect of sacubitril in fibroblasts. LBQ657, the metabolite of sacubitril, could significantly attenuate transforming growth factor-β 1 (TGF-β1) induced cardiac fibrosis by blocking TRPM7 channel, rather than suppressing its protein expression. In addition, LBQ657 reduced hypoxia-induced cardiomyocyte PCD *via* suppression of Ca^{2+} influx regulated by TRPM7. These findings suggested that sacubitril ameliorated cardiac fibrosis by acting on both fibroblasts and cardiomyocytes through inhibiting TRPM7 channel.

Keywords: sacubitril, cardiac fibrosis, PCD, TRPM7, Ca^{2+} influx

INTRODUCTION

Heart failure (HF), as a secondary disease of various cardiovascular diseases (CVDs), is the leading cause of death worldwide. Its prevalence is projected to continuously increase, with aging of the population (Virani et al., 2021). The American Heart Association (AHA) data predicts that from 2012 to 2030, the prevalence of HF will increase by 46%, and the total percentage will increase from 2.42% in 2012 to 2.97% in 2030 (Virani et al., 2020). Current therapeutic strategies for patients mainly focus on stimulating contractility and reducing vasoconstriction (Burke et al., 2019). Cardiomyocyte loss through programmed cell death (PCD), including apoptosis, necrosis and autophagy-dependent cell death, play important roles in the pathogenesis of heart failure (Del Re and Amgalan, 2019). The progression of HF is commonly accompanied by development of cardiac fibrosis (von Lueder et al., 2015). Pathological stimuli such as oxidative stress and inflammation mediate the differentiation of cardiac fibroblasts (CFs) into myofibroblasts, which synthesize and deposit excessive extracellular matrix protein (ECM), initiating cardiac fibrosis

(Tallquist, 2020; Wei et al., 2020). Fibrosis is a form of scarring that increases muscular tissue rigidity and decreases cardiac contractility. Currently, there is no effective treatment to block or reverse the development of fibrosis. The resulting abnormal cardiac conduction and stiffening of the ventricular walls severely damage the patients' cardiac function, which may further cause abnormalities in other tissues and organs, and eventually death (Schimmel et al., 2020).

LCZ696 (sacubitril/valsartan) is recommended for the management of HF patients according to current guidelines (Yandrapalli et al., 2018). LCZ696 is the first-in-class Angiotensin Receptor Neprilysin Inhibitor (ARNi); it is a 1:1 combination of the angiotensin receptor blocker (ARB) valsartan and the neprilysin inhibitor (NEPi) prodrug sacubitril (Gu et al., 2010). Many experimental and clinical studies have suggested that the dual action of LCZ696 represents a major therapeutic advance in the management of HF (McMurray et al., 2014; Ishii et al., 2017; Yandrapalli et al., 2018; Burke et al., 2019). A potential direct anti-fibrotic role for valsartan has been established (von Lueder et al., 2015). NEPi sustains biologically active natriuretic peptides (NPs), that has been demonstrated to have beneficial effects on heart failure (Song et al., 2015). LBQ657 is a metabolite of sacubitril. It has the effect of inhibiting neprilysin, which degrades the natriuretic peptides and many other vasoactive peptides (Hubers and Brown, 2016). Effects of stand-alone LBQ657 on cardiac fibrosis have not been examined.

Ca^{2+} is a critical second messenger for the activation of cell signaling pathways involved in myocardial fibrosis and subsequent heart failure (Falcón et al., 2019). Abnormal endoplasmic reticulum and mitochondria cause intracellular free Ca^{2+} imbalance, which can trigger heart failure and atrial fibrillation, leading to morbidity and mortality of cardiac diseases (Dridi et al., 2020; Meyer and Doroudgar, 2020). Understanding the molecular basis of Ca^{2+}-permeable channels is crucial for elucidating the mechanisms of abnormal cardiac function. Many studies have shown that transient receptor potential cation channel subfamily M (TRPM) channels participate in cardiac development and diseases (Wu et al., 2019; Simard and Magaud, 2020). TRPM member 7 (TRPM7) is a bifunctional protein with kinase structure and ion channel structure, which is responsible for Ca^{2+} influx (Yue et al., 2011; Duan et al., 2018). The important regulatory role of TRPM7 in cardiac hypertrophy, fibrosis and conduction disorders has been demonstrated sufficiently (Falcón et al., 2019). Our previous data confirmed that TRPM7 channel regulated hypoxia-induced myocardial fibrosis (Lu et al., 2017). Moreover, TRPM7 is broadly expressed and involved in many physiological and pathological processes such as cell proliferation and differentiation, cell death and transmembrane transport (Trapani and Wolf, 2020). Compelling evidences have demonstrated the pivotal roles of Ca^{2+} entry through TRPM7 in cardiac function and pathology (Du et al., 2010; Yu et al., 2014). Therefore, TRPM7 is becoming as a promising target to attenuate pathological cardiac fibrosis.

Herein reports direct evidence for anti-fibrotic function of sacubitril. We find sacubitril/valsartan has a better therapeutic effect on alleviating ISO-induced cardiac fibrosis and protecting against cardiac dysfunction *in vivo*, compared with valsartan alone. We further illustrate that LBQ657, the metabolite of sacubitril, ameliorates cardiac fibrosis through decreasing fibroblasts activation and reducing cardiomyocytes necrosis. The protective effect of LBQ657 against cardiac fibrosis is attributed to its impact on TRPM7-mediated Ca^{2+} entry by blocking TRPM7 channel. Taken together, the results of this study shed light on potential mechanism of sacubitril efficacy in heart fibrosis with reduced Ca^{2+} influx *via* acting on TRPM7 function.

MATERIALS AND METHODS

Animal Experiment and Histological Examination

All animal experiments were carried out in accordance with the Guidelines of Animals Experiments from Ethical Committee for Animal Research of China Pharmaceutical University. Adult male Sprague–Dawley (SD) rats (weight 220–250 g) were purchased from the Model Animal Research Center of Nanjing University. The rats were raised under pathogen-free conditions, under the 12 light-dark cycle, 25 ± 2°C condition and free to water and food. Isoprotereno (ISO) (Sigma-Aldrich, United States) was used for cardiac fibrosis modeling. The rats were randomized into control group, ISO group, ISO + valsartan group and ISO + sacubitril/valsartan group. Valsartan was purchased from Changzhou Siyao Pharm, China; and sacubitril/valsartan was purchased from Novatis Pharma, Schweiz AG. Rats in control group were subcutaneously injected with saline, while the other three groups were subcutaneously injected with ISO (7.5 mg/kg/day) for 14 days. From the 6th day to the 14th day, the rats in control group and ISO group were given saline by gavage (0.01 mL/g body weight), the rats in ISO + valsartan group were given valsartan by gavage (0.01 mL/g body weight, dissolved in 0.5% CMC-Na solution), and the rats in ISO + sacubitril/valsartan group were given sacubitril valsartan by gavage (0.01 mL/g body weight, dissolved in 0.5% CMC-Na solution). On the 15th day, rats were anesthetized with 2% isoflurane and kept on a 37°C heated platform. The chest hairs were removed using depilatory cream and acoustic coupling gel was applied to the thorax, then echocardiogram tests were performed using small animal ultrasound imaging system vevo3000 (VisualSonics, Canada). The cardiac function related indicators, including cardiac output, ejection fraction, fractional shortening, and stroke volume, were analyzed through the echocardiogram results. Then all rats were sacrificed and heart tissues were taken for follow-up analysis. The left ventricular apexes were resected and divided into two parts: one part was fixed in 10% formalin solution and then subjected to Masson trichrome staining to observe the histological changes, while the other part was frozen at −80°C for subsequent detection of mRNA and protein.

Cell Culture

Mouse embryonic fibroblast (MEF) and rat embryonic cardiomyocyte cell line H_9C_2 were cultured in DMEM (Gibco, United States) containing 10% FBS (Gibco, United States), 100 U/mL penicillin and 100 μg/mL streptomycin (Gibco,

United States). Cells were digested with 0.25% trypsin-EDTA (Gibco, United States) and subcultured for subsequent experiments when grew to 90% confluence.

Small Interfering RNA Transfection

Si-TRPM7 and si-NC were synthesized by GenePharm (Shanghai, China). MEF were seeded in 12-well cell culture plate (NEST, China) and transfected with small interfering RNAs (siRNAs) using Lipofectamine^{TM} 3000 Transfection Reagent (ThermoFisher, United States) in serum-free Opti-MEM medium (Gibco, United States). The cells were transfected for 8 h and then cultured in DMEM containing 10% FBS, 100 U/mL penicillin and 100 μg/mL streptomycin. The sequences of si-TRPM7 are as following:
si-TRPM7 sense 5′-GCGCUUUCCUUAUCCUCUUTT-3′;
si-TRPM7 antisense 5′-AAGAGGAUAAGGAAAGCGCTT-3′.

Quantitative Reverse Transcription-Polymerase Chain Reaction

Total RNA of cells or tissues was extracted with Trizol (Invitrogen, United States) according to the manufacturer's instructions, then reverse transcription was performed using a reverse transcription kit (Vazyme, China). The quantification of gene transcripts was performed by real-time PCR using SYBR Green PCR mix (Vazyme, China). All values were normalized to the level of *18S* mRNA. The primers used were listed below:
18S sense CGAACGTCTGCCCTATCAACT;
18S antisense CAGACTTGCCCTCCAATGGATCCTCGTT;
Rat-*Mmp9* sense CAGAGCGTTACTCGCTTGGA;
Rat-*Mmp9* antisense GGTTGTGGAAACTCACACGC;
Mouse-*Mmp9* sense GTCCAGACCAAGGGTACAGC;
Mouse-*Mmp9* antisense ATACAGCGGGTACATGAGCG;
Rat-α-*Sma* sense ACCATCGGGAATGAACGCTT;
Rat-α-*Sma* antisense CTGTCAGCAATGCCTGGGTA;
Mouse-α-*Sma* sense AGCCATCTTTCATTGGGATGG;
Mouse-α-*Sma* antisense CCCCTGACAGGACGTTGTTA;
Rat-*Trpm7* sense TGTTGCCGGATTGGTTACGA;
Rat-*Trpm7* antisense CTCGTGGAGGTACAGGAACG.

Western Blot

Cell protein was extracted by sonication and tissue protein was extracted by grinding. After centrifugation at 12,000 rpm for 15 min, the supernatant was collected for subsequent western blot analysis. Protein samples were boiled for 5 min, electrophoresed in SDS polyacrylamide gel, and then transferred onto PVDF membranes (Bio-Rad, United States). The blots were blocked with 5% skimmed milk in Tris-buffered saline solution-Tween 0.1% (TBST) (Sigma-Aldrich, United States) for 2 h at room temperature and probed with primary antibodies overnight at 4°C. The blots were washed four times with TBST for 8 min each time and incubated for 1 h at room temperature with the HRP-conjugated secondary antibodies (dilution 1:10,000; Sigma-Aldrich, United States), then developed with chemiluminescence (Vazyme, China). MMP9 antibody (10375-2-AP) was purchased from Proteintech, China, dilution 1:1,000; α-SMA (ab32575) and MLKL (ab243142) antibodies were purchased from Abcam, United States, dilution 1:1,000; TRPM7 antibody (BM5443) was purchased from Boster, China, dilution 1:200; LC3B (3868S), caspase3 (14220S) and cleaved caspase3 (9664S) were purchased from Cell Signaling Technology, United States, dilution 1:1,000; RIPK1 (AF7877), RIPK3 (AF7942) and phospho-MLKL (Ser358) (AF7420) antibodies were purchased from Affinity, China, dilution 1:1,000. The densitometry of protein bands was quantified using ImageJ software. All values were normalized to the level of β-actin.

Molecular Docking of TRPM7 Ligands

The crystal structure of TRPM7 (PDB ID: 5ZX5) (Duan et al., 2018) was retrieved from the RCSB Protein Data Bank. The protein structure was prepared for Glide docking calculations using the Protein Preparation Wizard utility. Water molecules were removed and the structure was treated and prepared by employing a protein preparation panel in the Schrödinger enterprise to magnify H-bond interactions. Structures of investigated compound (NEPi and Diprotic acid ARB) were built recruiting MAESTRO (Friesner et al., 2004) build panel and subsequently energy minimization by LigPrep module employing the OPLS2005 forcefield. Ionizable compounds were converted to their most probable charged forms at pH 7.0 ± 2.0 and explicit hydrogen atoms were added. The grid file for TRPM7 was generated by the Glide Grid Generation wizard in Schrödinger determining the co-crystallized ligands as the center point. Van der Waals scaling factor of the non-polar atoms was adjusted to 1.0 to enhance flexibility. The other parameters were fixed as defaults. The top conformations of investigated compounds were ranked by the corresponding values of docking score.

Isolation of Neonatal Rat Cardiac Fibroblasts

Hearts from the neonatal rats (1–3 days) were rapidly removed and washed in D-hanks solution and minced into 1 mm^3 pieces, then shake in 0.1% trypsin and 0.1% collagenase type II for several times to digest. The fully digested cell suspension was centrifuged and resuspended in Dulbecco's modified eagle's medium (DMEM) (Life Technologies, United States) containing 10% FBS, 100 U/mL penicillin and 100 μg/mL streptomycin, and incubated in a humidified atmosphere of 5% CO_2 at 37°C for 2 h. After removing non-adhered cells, the attached cells were cultured and inherited, the second or third generations were used in our experiments.

Whole Cell Patch Clamp

The third passage of neonatal rat cardiac fibroblasts was used in our experiments. TRPM7-like current was recorded by whole cell patch clamp at room temperature. The pipette solution contained (in mM) CsCl 145, NaCl 8, HEPES 10, EGTA 10, and CsOH was used to adjust to pH7.2. The bath solution contained (in mM) NaCl 145, KCl 5, HEPES 10, glucose10 and $CaCl_2$ 2, and NaOH was used to adjust to pH7.4. With a holding potential at 0 mV, TRPM7 current was recorded under the voltage stimulation from −100 mV to + 120 mV in 400 ms.

Hypoxia Treatment Procedure

H_9C_2 were divided into normoxic group, hypoxia group, hypoxia + BAPTA-AM group and hypoxia + LBQ657 group. BAPTA-AM and LBQ657 were purchased from MedChemExpress, China and Sigma-Aldrich, United States, respectively. Cells were seeded in 6-well cell culture plate (NEST, China) at a density of 5×10^5 per well. 8 h later, cells were treated with BAPTA-AM or LBQ657 for 8 h and then moved to a hypoxia environment by incubating into three-gas incubator (93% N_2, 5% CO_2 and 2% O_2) for 24 h to achieve, while the control groups were kept in normoxic incubator. All cell pellets were collected and total protein were extracted for western blot test.

Confocal Microscopy

H_9C_2 were loaded with the Ca^{2+} fluorescent dye, Fluo-4-AM (Invitrogen, United States) at 37°C for 1 h incubation, then washed by PBS solution and incubated at 37°C for 30 min. Cells were fixed by 4% paraformaldehyde and screened in 488 nm excitation light using Laser scanning confocal microscope LSM800 (Zeiss, Germany). The fluorescence ratio was analyzed using Image J software.

Statistical Analysis

Statistical analysis was performed using GraphPad Prism 6.0. The results were expressed as mean ± SD for experiments conducted at least in triplicates. Unpaired *t* test was used for comparison between two groups, and One-way ANOVA was used for three or more groups, and $P < 0.05$ was considered to be significantly different.

RESULTS

Sacubitril/Valsartan Effectively Protected Cardiac Function and Ameliorated Cardiac Fibrosis Induced by ISO in Rats

The rats were subcutaneous injected ISO to induce cardiac fibrosis and treated with normal saline, valsartan or sacubitril/valsartan, respectively (**Figure 1A**). Valsartan, a drug used for clinical treatment of heart failure, was used as positive control (Suematsu et al., 2016). The valsartan group and the sacubitril/valsartan group had lower heart weight to body weight ratio (**Figure 1B**). Echocardiogram showed that the cardiac output, ejection fraction, fractional shortening and stroke volume of ISO-induced rats were significantly increased after valsartan and sacubitril/valsartan treatment (**Figures 1C,D**). Especially, sacubitril/valsartan ameliorated stroke volume more efficiently than valsartan. Additionally, the valsartan group and the sacubitril/valsartan group had smaller area of fibrosis (**Figure 1E**) compared to non-treatment control group. These results indicate that sacubitril/valsartan effectively protected cardiac dysfunction in ISO-stimulated rats ($P < 0.01$ compared with control group).

Matrix metalloproteinase 9 (MMP9) is a biomarker associated with collagen degradation to cause heart failure (Zile et al., 2019). Alpha-smooth muscle actin (α-SMA) is an activation marker of fibrotic pathways in fibroblast differentiation (Jing et al., 2017). Accordingly, quantitative reverse transcription-polymerase chain reaction (qRT-PCR) was used to analyze the expression of these cardiac fibrosis related genes in the left ventricular apexes. We found that ISO induced a notable increase in *Mmp9* and α-*Sma* mRNA expression levels, while sacubitril/valsartan or valsartan treatment diminished the effect (**Figure 1F**). The protein expression levels of MMP9 and α-SMA detected by western blotting analysis showed a similar trend (**Figure 1G**). Moreover, sacubitril/valsartan significantly decreased α-*Sma* mRNA expression compared with valsartan. Taken together, the above results suggest that sacubitril/valsartan effectively ameliorated ISO induced cardiac fibrosis and improved cardiac function *in vivo*, superior to valsartan therapy alone. This indicates a potential anti-fibrotic function of sacubitril.

LBQ657 Significantly Extenuated TGF-β1 Induced Cardiac Fibroblast Activation *in vitro*

Transforming growth factor-β 1 (TGF-β1) is considered as a typical stimulus to mediate the differentiation of cardiac fibroblasts into myofibroblasts to acquire a fibrotic phenotype (Porter and Turner, 2009). To further examine the effect of sacubitril on cardiac fibrosis, we used TGF-β1 (10 ng/mL) to stimulate MEF for 24 h to induce a profibrotic phenotype. LBQ657, the metabolite of sacubitril, was used to treat MEF cells at a concentration of 50 μM prior to TGF-β1 stimulation. We found both the mRNA and protein expression of MMP9 and α-SMA was dramatically up-regulated by TGF-β1 stimulation, but this was prevented by LBQ657 pre-treatment ($P < 0.01$ comparison with the TGF-β1 group), indicating LBQ657 potently inhibited fibroblast activation *in vitro* (**Figures 2A,B**).

Because the previous reports suggested a close relationship between TRPM7 and cardiac fibrosis (Du et al., 2010; Wei et al., 2020), we further investigated the changes of TRPM7 expression in TGF-β1 induced cardiac fibrosis. We designed and selected a pair of TRPM7 siRNA with the best interference effect for follow-up experiments. The TRPM7 mRNA levels were reduced by 74% (**Figure 2C**). MEF were subjected to si-TRPM7 transfection and LBQ657 (50 μM) treatment, respectively, before TGF-β1 stimulation. The qRT-PCR and western blotting analysis indicated that si-TRPM7 suppressed the expression of TRPM7, but LBQ657 pre-treatment did not show discernible effects on TRPM7 protein expression in TGF-β1 treated MEF (**Figures 2E,F**). Meanwhile, both si-TRPM7 and LBQ657 reduced the expression of MMP9 and α-SMA induced by TGF-β1 (**Figures 2D,E**). These results suggest that LBQ657 attenuated TGF-β1-induced cardiac fibroblast activation without reducing the expression levels of TRPM7.

LBQ657 Protected Against Fibrosis by Blocking TRPM7 Channel

The inhibition of cardiac fibroblast activation by LBQ657 was not associated with reduced TRPM7 mRNA and protein levels, ruling out the possibility that LBQ657 functions by regulating TRPM7 channel current. Molecular docking was used

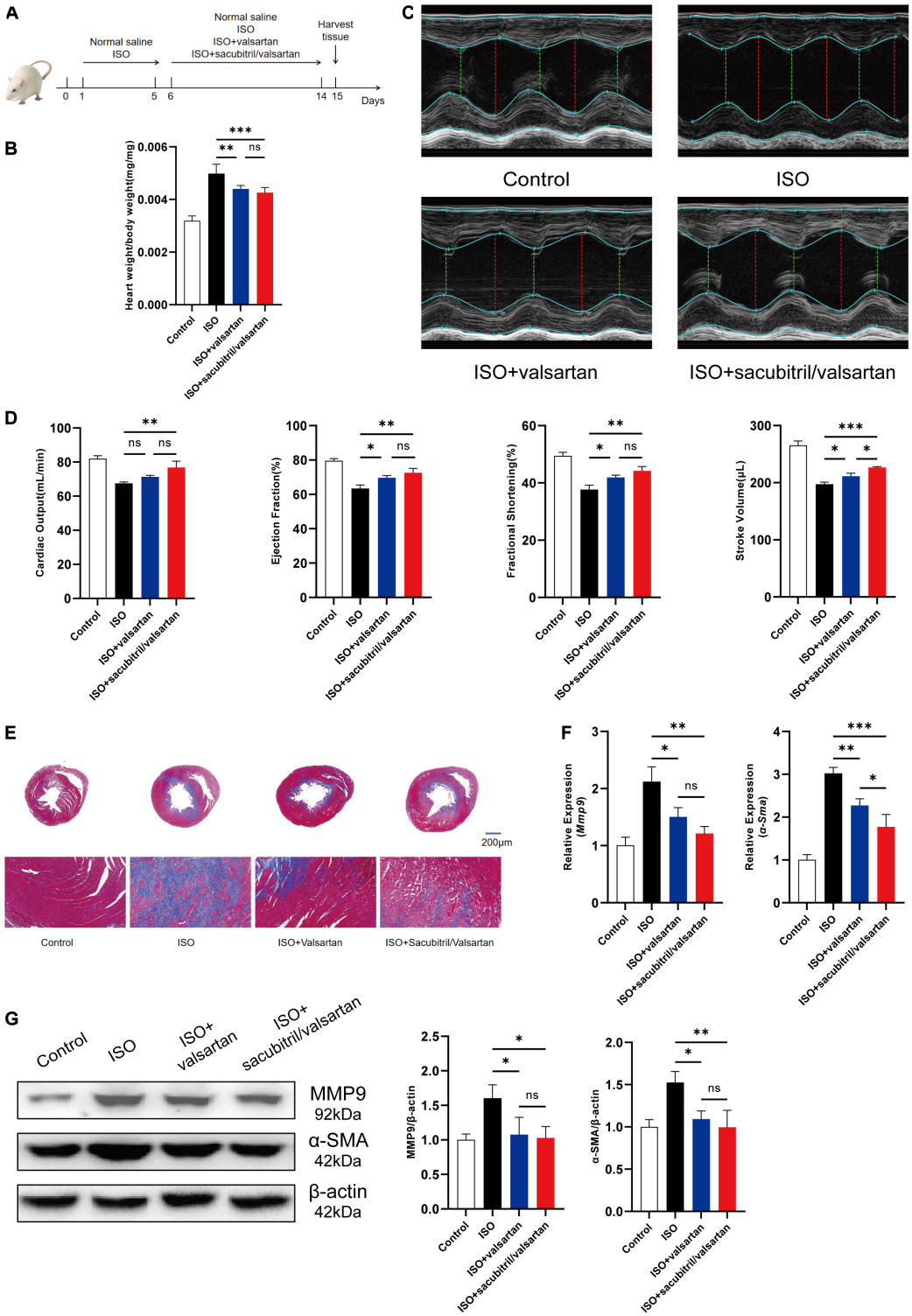

FIGURE 1 | Sacubitril/valsartan effectively protected cardiac function and ameliorated cardiac fibrosis induced by ISO in rats. **(A)** The flow chart of the cardiac fibrosis model and drug treatment in animal experiment. **(B)** Heart to body weight ratio of rats in the control group, the ISO group, the valsartan group and the sacubitril/valsartan group. **(C)** On the 15th day of the experiment, the heart function of rats was measured by echocardiography**. (D)** Cardiac output, ejection fraction, fractional shortening and stroke volume were analyzed and calculated according to the results of echocardiography. **(E)** Masson trichrome staining of heart tissue sections of rats. Scale bar = 200 μm. **(F)** mRNA expression levels of *Mmp9* and α-*Sma* in the left ventricular apexes of rats. **(G)** Protein levels of MMP9 and α-SMA in the left ventricular apexes of rats. The data presented are mean ± SD. $n = 5$/group. *18S* RNA was used as the internal reference gene and β-actin was used as the internal reference protein for normalization and statistical analysis. ***$P < 0.001$, **$P < 0.01$, and *$P < 0.05$.

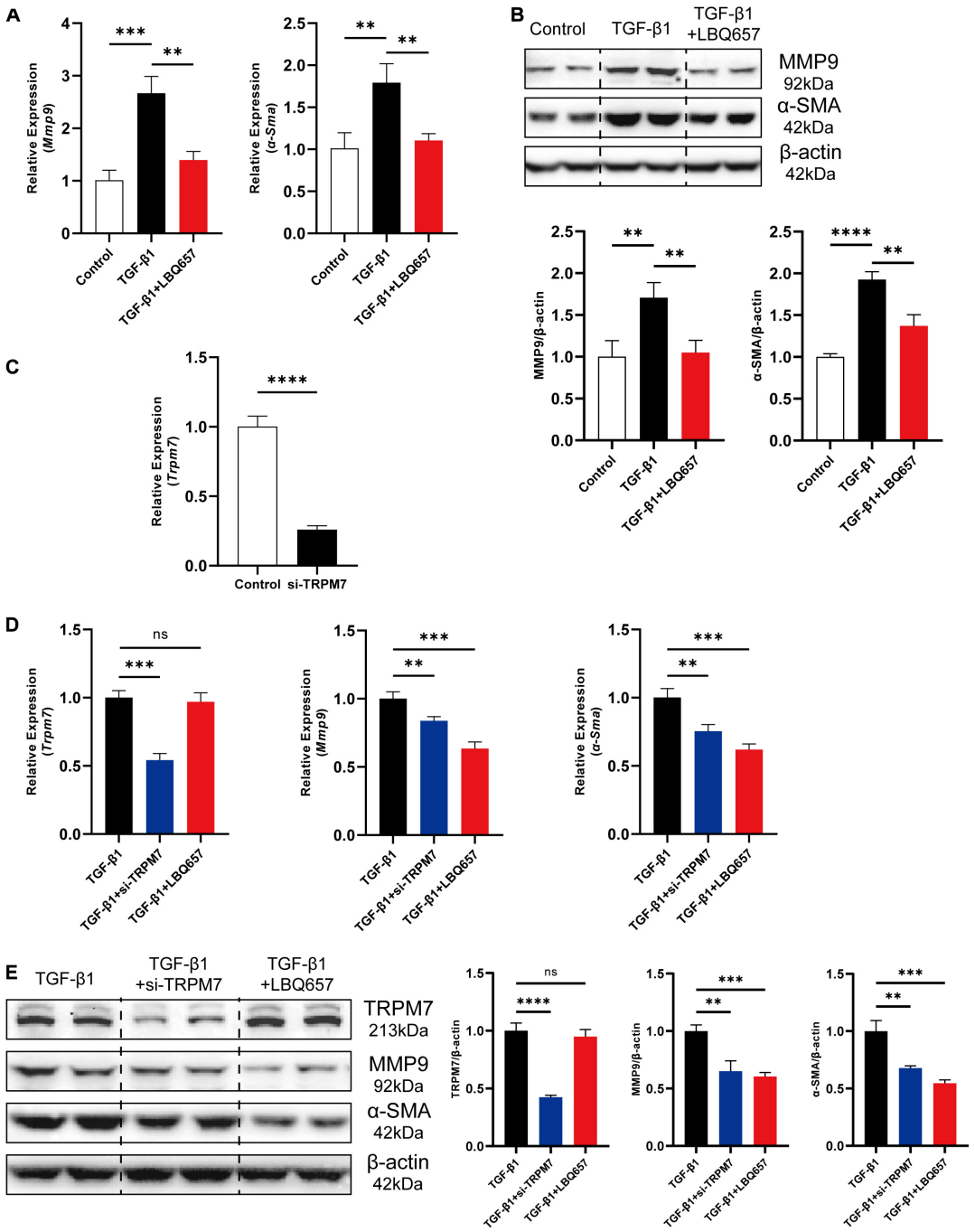

FIGURE 2 | LBQ657 significantly extenuated TGF-β1 induced cardiac fibroblast activation in MEF. **(A)** mRNA expression of *Mmp9* and α-*Sma* in control MEF, MEF treated with TGF-β1 and MEF treated with LBQ657 + TGF-β1. **(B)** Protein levels of MMP9 and α-SMA in the rats. **(C)** The efficiency of the siRNA used to reduce the mRNA expression of TRPM7 in MEF. **(D)** mRNA expression of *Trpm7*, *Mmp9* and α-*Sma* in MEF treated with TGF-β1, MEF transfected with si-TRPM7 and treated with TGF-β1, MEF treated with LBQ657 + TGF-β1. **(E)** Protein levels of TRPM7, MMP9 and α-SMA in the rats. The data presented are mean ± SD. Each group contained the results of three independent repeated trials. *18S* RNA was used as the internal reference gene and β-actin was used as the internal reference protein for normalization and statistical analysis. ****$P < 0.0001$, ***$P < 0.001$, and **$P < 0.01$.

to determine the interaction between TRPM7 (PDB ID: 5ZX5) and sacubitril/valsartan. Compound NEPi and Diprotic acid ARB of sacubitril/valsartan docked to the active site of TRPM7 with a free energy of −6.20 kcal/mol and −10.12 kcal/mol, respectively. This indicated that both sacubitril and valsartan docked to TRPM7 protein. The docking structure suggested that LBQ657, as the NEPi, occupied a similar position in TRPM7 compared with natural cholesterol hemisuccinateon ligand (**Figure 3A**).

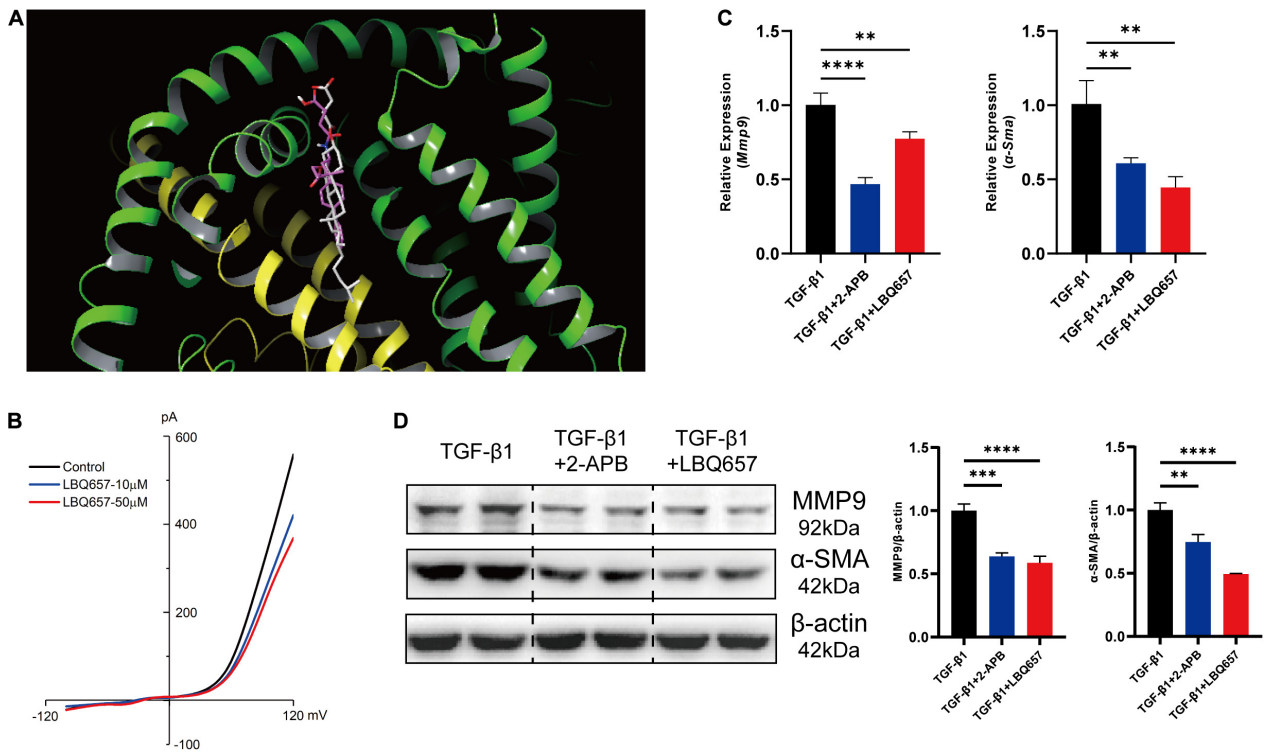

FIGURE 3 | LBQ657 protected against fibrosis by blocking TRPM7 channel. **(A)** The virtual binding mode of NEPi and natural cholesterol hemisuccinateon ligand (as control) on TRPM7. NEPi (red) and cholesterol hemisuccinate (gray) are shown as a stick model. **(B)** Current amplitude of TRPM7-like current recorded in neonatal rat cardiac fibroblasts in control cell (black), LBQ657-10 μM treated cell (blue) and LBQ657-50 μM treated cell (red). **(C)** mRNA expression of *Mmp9* and α-*Sma* in MEF treated with TGF-β1, MEF treated with 2-APB + TGF-β1, and MEF treated with LBQ657 + TGF-β1. **(D)** Protein levels of MMP9 and α-SMA in the rats. The data presented are mean ± SD. Each group contained the results of three independent repeated trials. *18S* RNA was used as the internal reference gene and β-actin was used as the internal reference protein for normalization and statistical analysis. ****$P < 0.0001$, ***$P < 0.001$, and **$P < 0.01$.

Aimed to validate the blocking of TRPM7 channel by LBQ657, TRPM7-like current was recorded by whole cell patch-clamp in neonatal rat cardiac fibroblasts. We observed that the current of TRPM7 channel was decreased by LBQ657 treatment in a clear dose-dependent manner (**Figure 3B**), strongly implying its direct influence on the channel function. And then we used 2-aminoethoxydiphenyl borate (2-APB), an inhibitor of TRPM7 channel, as a positive control to explore the anti-fibrotic effect of LBQ657 (Chokshi et al., 2012). As shown in **Figures 3C,D**, 2-APB (100 μM) indeed caused dramatic reduction of the MMP9 and α-SMA expression by ∼50%, so did LBQ657, in TGF-β1 stimulated MEF cells. We concluded from this set of experiments that the LBQ657 extenuated cardiac fibroblast activation through inhibiting the function of TRPM7 channel, rather than suppressing the expression of TRPM7.

LBQ657 Reduced Hypoxia-Induced Necrosis by Inhibiting TRPM7-Mediated Ca^{2+} Influx in Cardiomyocytes

The causal importance of hypoxia in cardiac fibrosis has been strongly supported by literature. Hypoxia occurs in myocardial infarction and causes large-scale loss of cardiomyocytes, which is the most common trigger of cardiac fibrosis. Cardiomyocyte death induces inflammatory responses, promoting the activation of fibroblasts into myofibroblasts, leading to cardiac fibrosis (Kong et al., 2014; Kumar and Choi, 2015). TRPM7 channel is mainly concentrated in myocardium during embryonic development and is indispensable for cardiac automaticity of cardiomyocytes (Sah et al., 2013). Therefore, we detected that TRPM7 was abundantly expressed in cardiomyocytes, approximately 1.5-fold greater than that in fibroblasts (**Figure 4A**). And then we measured the intracellular calcium concentration in H_9C_2 under hypoxia stimulation. The **Figure 4B** showed that Ca^{2+} influx was dramatically increased by hypoxia, but significantly deceased after LBQ657 treatment. These results demonstrated that LBQ657 inhibited Ca^{2+} entry though TRPM7 channel in cardiomyocytes.

While some studies had previously shown that activation of TRPM7 channels and produced Ca^{2+} overload significantly contributes to cell death (Wei et al., 2007; Cai et al., 2014), it was still to be determined whether LBQ657 attenuates cardiomyocyte PCD by TRPM7 mediated Ca^{2+} influx. We first studied the effect of LBQ657 on hypoxia-induced cardiomyocyte PCD. As shown in **Figure 4C**, there were no significant changes on the protein expression level of caspase3, cleaved caspase3, LC3B-I and LC3B-II in hypoxia-stimulated H_9C_2 pre-treated with LBQ657, suggesting that LBQ657 was incapable

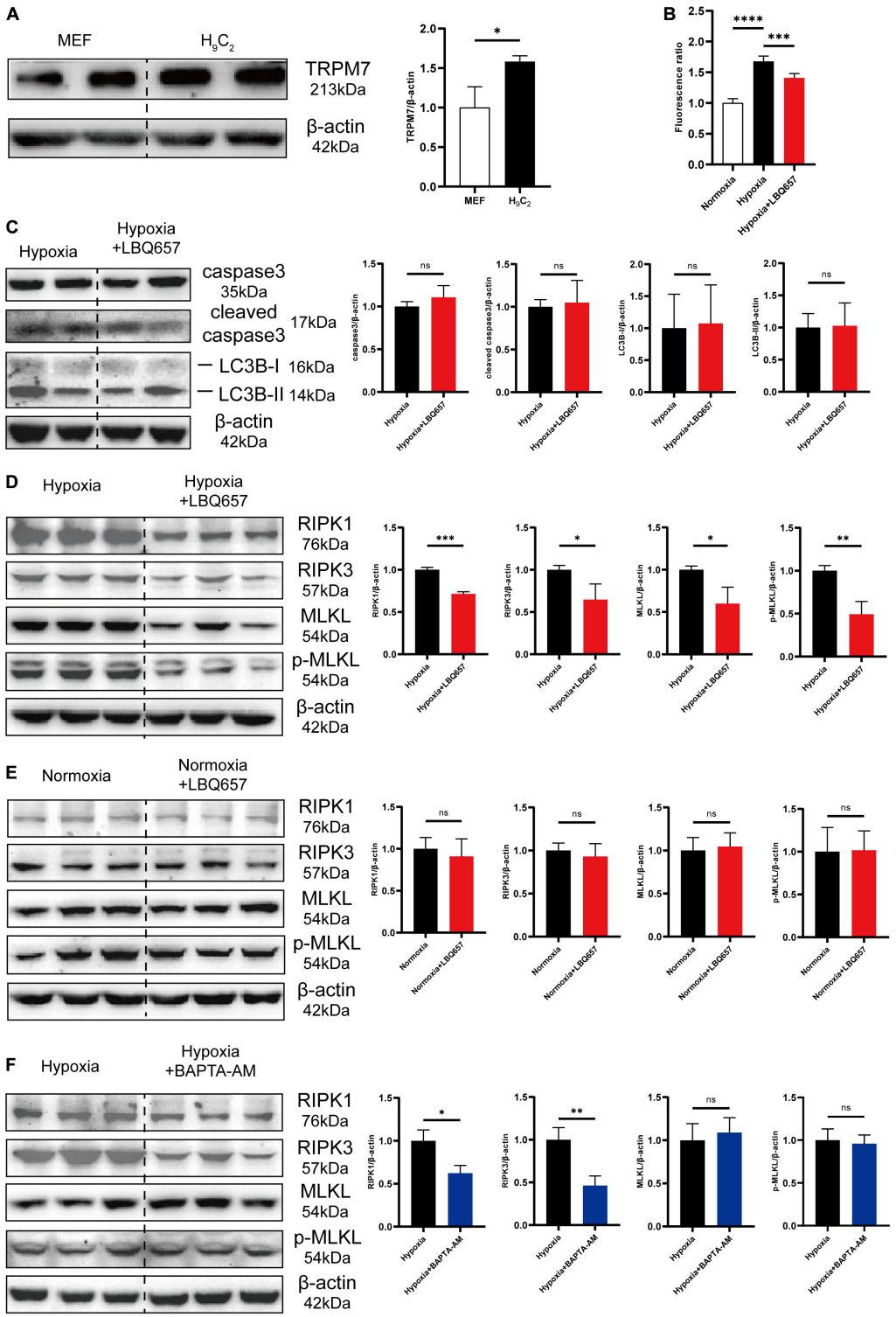

FIGURE 4 | LBQ657 reduced hypoxia-induced necrosis by inhibiting TRPM7-mediated Ca^{2+} influx in cardiomyocytes. **(A)** Comparison of TRPM7 protein levels in MEF and H_9C_2 cells. **(B)** Fluorescence intensity of Fluo-4-AM fluorescent dye in 488 nm excitation light of normoxic H_9C_2, hypoxic H_9C_2 and hypoxic H_9C_2 pre-treated with LBQ657. **(C)** Protein levels of caspase3, cleaved caspase3, LC3B-I and LC3B-II in hypoxic H_9C_2 and hypoxic H_9C_2 pre-treated with LBQ657. **(D)** Protein levels of RIPK1/RIPK3/MLKL/p-MLKL in hypoxic H_9C_2 and hypoxic H_9C_2 pre-treated with LBQ657. **(E)** Protein levels of RIPK1/RIPK3/MLKL/p-MLKL in normoxic H_9C_2 and normoxic H_9C_2 treated with LBQ657. **(F)** Protein levels of RIPK1/RIPK3/MLKL/p-MLKL in hypoxic H_9C_2 and hypoxic H_9C_2 pre-treated with BAPTA-AM. The data presented are mean ± SD. Each group contained the results of three independent repeated trials. β-actin was used as the internal reference protein for normalization and statistical analysis. ****$P < 0.0001$, ***$P < 0.001$, **$P < 0.01$, and *$P < 0.05$.

of regulating cardiomyocyte apoptosis or autophagy in hypoxic environment. The investigation of cell necrosis related proteins RIPK1/RIPK3/MLKL/p-MLKL expression in hypoxia-induced H_9C_2 under LBQ657 pre-treatment indicated the expression level of detected proteins declined to 70% or less compared with that in the hypoxia group (**Figure 4D**). We further found LBQ657 did not cause obvious changes in the expression level of RIPK1/RIPK3/MLKL/p-MLKL in normoxia cardiomyocytes (**Figure 4E**). Next, BAPTA-AM (5 μM) was used to chelate the intracellular calcium and caused down-regulated expression of RIPK1/RIPK3 in hypoxia-treated cardiomyocytes, but MLKL and p-MLKL protein expression were not notably altered (**Figure 4F**). These results suggested that the reduction of cardiomyocyte necrosis was closely associated with calcium influx. The cardiomyocyte necrosis was significantly reduced accompanied with decrease of TRPM7-mediated Ca^{2+} influx. Based on the above results, we conclude that LBQ657 could ameliorated cardiomyocyte necrosis induced by hypoxia *via* inhibiting TRPM7-mediated Ca^{2+} influx.

DISCUSSION

As one of the leading causes of deaths, HF places a tremendous burden to the healthcare systems of countries worldwide. LCZ696 (sacubitril/valsartan) represents a promising therapeutic drug in the treatment of CVD, particularly HF. LCZ696 can reduce cardiac fibrosis and hypertrophy to lower the risk of cardiovascular events in HF and attenuate cardiac remodeling and dysfunction after myocardial infarction (MI) (von Lueder et al., 2015; Ishii et al., 2017). In addition, LCZ696 reduces fibrosis and inflammation in chronic kidney disease (Jing et al., 2017), ameliorates cardiac function in diabetic mice (Suematsu et al., 2016), and improves clinical prognosis in patients with heart failure with reduced ejection fraction (HFrEF) (Cunningham et al., 2020). Since its development and commercialization, many studies have assessed its pathophysiological effects, as well as pharmacokinetics and pharmacodynamics (Ayalasomayajula et al., 2017; Hsiao et al., 2018; Zile et al., 2019). However, relatively few studies have deciphered the underlying mechanism involved in its anti-fibrotic effect. Our present study has shown that LBQ657 (active form of sacubitril) protected against cardiac fibrosis, probably due to the suppression of TRPM7 function in both cardiac fibroblasts and cardiomyocytes (**Figure 5**).

Published reports have shown that valsartan, the angiotensin receptor blocker component of LCZ696, inhibited the renin-angiotensin-aldosterone system to exert anti-fibrotic function (Lin et al., 2016). In addition, accumulating evidence also suggested that LCZ696 was more effective than valsartan alone in inhibiting fibrosis (Suematsu et al., 2016; Jing et al., 2017). However, the mechanism of anti-fibrosis by LBQ657, the neprilysin inhibitor component of LCZ696, is elusive. von Lueder et al. (2015) suggested that LBQ657 inhibited post-MI hypertrophy but not fibrosis. While Yandrapalli et al. (2017) revealed that augmenting the NPS inhibited the progression of HF. In this study, the anti-fibrotic effect of LBQ657 leads to the attenuation of ISO-dependent fibrosis, the inhibition of TGF-β1-induced fibroblast activation, and reduction of hypoxia-induced cardiomyocyte PCD. Based on above observations, we speculate that LBQ657 synergizes with valsartan in inhibiting cardiac fibrosis.

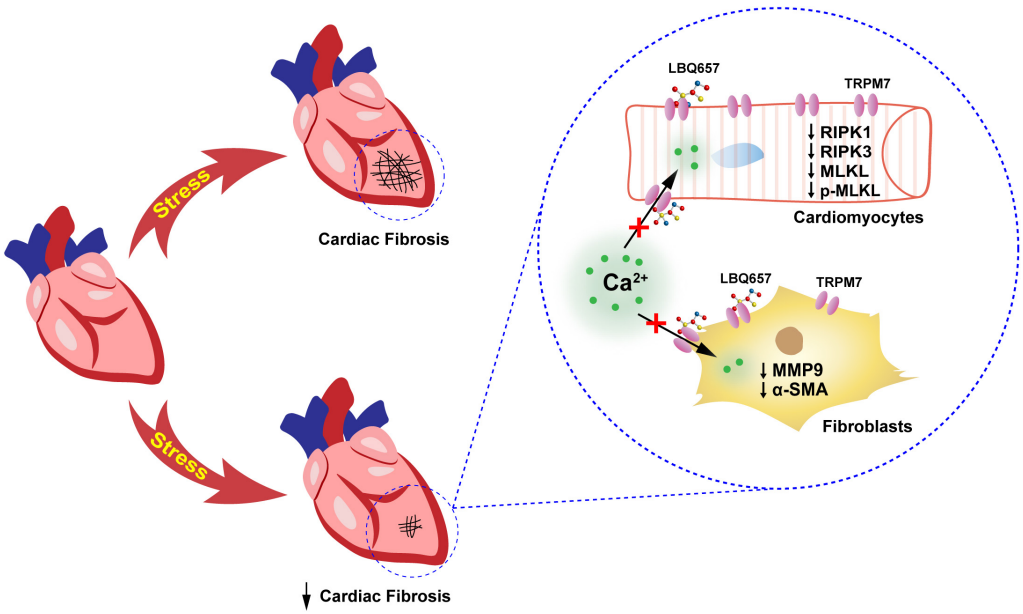

FIGURE 5 | Schematic showing that sacubitril ameliorates cardiac fibrosis through inhibiting TRPM7-mediated Ca^{2+} influx in cardiac fibroblasts and cardiomyocytes. This study demonstrated that sacubitril metabolite LBQ657 could relieve the fibrotic response of fibroblasts and reduce cardiomyocyte PCD by blocking TRPM7 channel, thereby ameliorating cardiac fibrosis.

The "chanzyme" TRPM7 contains both an ion channel and an α-kinase, which might be the molecular basis of the major divalent cation permeable channel in cardiac function and pathology (Falcón et al., 2019). In human atrial fibrillation, Ca^{2+} entry through TRPM7 channel plays a pivotal role in TGF-β1-elicited fibrogenesis in atrial fibroblasts (Du et al., 2010). While former attention was made to the altered expression of TRPM7 and the development of cardiac fibrosis (Xu et al., 2015), our current study indicated that LBQ657 administration improved cardiac function and attenuated the molecular markers (MMP9 and α-SMA) of fibrosis in fibroblasts by suppressing TRPM7 channel Ca^{2+} influx rather than by decreasing TRPM7 mRNA and protein levels. Ca^{2+} permeation may also account for the mechanism of TRPM7's action in cardiac dysfunction.

The term programmed cell death is applied broadly to refer to a number of cell death programs, including apoptosis, regulated necrosis, ferroptosis, pyroptosis, parthanatos, entotic cell death, lysosome-dependent cell death, autophagy-dependent cell death, and immunogenic cell death (Del Re and Amgalan, 2019; Bedoui et al., 2020; Khan et al., 2021). Autophagy is a process of cellular self-degradation for keeping the intracellular homeostasis (Bhardwaj et al., 2020). Although increased autophagy protects against various pathological factors in cardiomyocytes, the mistakenly degradation of essential cellular components by excessive autophagy exacerbates myocardial injury (Luo et al., 2021). Apoptosis is an intrinsic cell death program caused by diverse factors. There is a significant association between improved cardiac function and prevention of cardiomyocyte apoptosis in human HF (Li et al., 2021). The role for regulated forms of cardiomyocyte necrosis is critical in both myocardial infarction and heart failure. Cardiac Ca^{2+} overload has been proved to induce cardiomyocyte necrosis, heart failure, and premature death (Del Re and Amgalan, 2019). Previously, a systems biology approach has revealed that sacubitril attenuated cardiomyocyte cell death by inhibiting PTEN (Iborra-Egea et al., 2017). TRPM7-mediated Ca^{2+} influx was identified as a crucial mechanism of tumor necrosis factor (TNF)-induced necroptosis (Cai et al., 2014) and neuronal death during transient brain ischemia (Wei et al., 2007). Indeed, we show here that regulation of TRPM7-mediated Ca^{2+} influx by LBQ657 contributed to the reduction of hypoxia-induced cardiomyocyte necrosis, rather than apoptosis or autophagy. The protective effect of LBQ657 against cardiovascular fibrosis is demonstrated to be achieved at least partially through Ca^{2+}-sensitive PCD.

Taken together, our study sheds a new light in understanding the mechanisms by which sacubitril attenuates cardiac fibrosis, and has important guiding significance for clinical treatment. LBQ657, an active metabolite of sacubitril, inhibits cardiac fibrosis by acting on both cardiac fibroblasts and cardiomyocytes; and TRPM7 channel is the target of LBQ657 in these cells. As a major advance in the treatment of CVDs, sacubitril/valsartan should be evaluated as a direct anti-fibrotic therapy, better than valsartan. Importantly, our work identifies LBQ657 is a pharmacological compound that inhibits the TRPM7 channel function for the first time. This will open a door to develop LBQ657 as a new modulator to unravel TRPM7 channel vs. kinase function in cellular physiology and pathophysiology, and as a new therapy for various cardiovascular diseases.

DATA AVAILABILITY STATEMENT

The original contributions presented in the study are included in the article/supplementary material, further inquiries can be directed to the corresponding author/s.

ETHICS STATEMENT

The animal study was reviewed and approved by Ethical Committee for Animal Research of China Pharmaceutical University.

AUTHOR CONTRIBUTIONS

TJ, XW, CL, SC, JZ, and WM performed the molecular and animal experiments. YT performed the patch clamp. WY performed the compounds and protein docking analysis. QW and CW designed and supervised the whole project. All authors contributed to manuscript revision, read, and approved the submitted version.

FUNDING

This study was supported by the Open Project of State Key Laboratory of Natural Medicines (SKLNMZZCX201802), the National Natural Science Foundation of China (31730018), the "Double First-Class" Project of China Pharmaceutical University (CPU2018GF10), and the Jiangsu Innovative and Entrepreneurial Talents Program.

ACKNOWLEDGMENTS

We would like to thank Peng Li (The First Affiliated Hospital with Nanjing Medical University) for sharing the MEF and H_9C_2 cell lines.

REFERENCES

Ayalasomayajula, S., Langenickel, T., Pal, P., Boggarapu, S., and Sunkara, G. (2017). Clinical pharmacokinetics of Sacubitril/Valsartan (LCZ696): A novel angiotensin receptor-neprilysin inhibitor. *Clin. Pharmacokinet.* 56, 1461–1478. doi: 10.1007/s40262-017-0543-3

Bedoui, S., Herold, M. J., and Strasser, A. (2020). Emerging connectivity of programmed cell death pathways and its physiological implications. *Nat. Rev. Mol. Cell. Biol.* 21, 678–695. doi: 10.1038/s41580-020-0270-8

Bhardwaj, M., Leli, N. M., Koumenis, C., and Amaravadi, R. K. (2020). Regulation of autophagy by canonical and non-canonical ER stress responses. *Semin. Cancer Biol.* 66, 116–128. doi: 10.1016/j.semcancer.2019.11.007

Burke, R. M., Lighthouse, J. K., Mickelsen, D. M., and Small, E. M. (2019). Sacubitril/Valsartan decreases cardiac fibrosis in left ventricle pressure overload by restoring PKG signaling in cardiac fibroblasts. *Circ. Heart Fail.* 12:e005565. doi: 10.1161/circheartfailure.118.005565

Cai, Z., Jitkaew, S., Zhao, J., Chiang, H. C., Choksi, S., Liu, J., et al. (2014). Plasma membrane translocation of trimerized MLKL protein is required for TNF-induced necroptosis. *Nat. Cell. Biol.* 16, 55–65. doi: 10.1038/ncb2883

Chokshi, R., Fruasaha, P., and Kozak, J. A. (2012). 2-aminoethyl diphenyl borinate (2-APB) inhibits TRPM7 channels through an intracellular acidification mechanism. *Channels (Austin)* 6, 362–369. doi: 10.4161/chan.21628

Cunningham, J. W., Claggett, B. L., O'Meara, E., Prescott, M. F., Pfeffer, M. A., Shah, S. J., et al. (2020). Effect of Sacubitril/Valsartan on biomarkers of extracellular matrix regulation in patients with HFpEF. *J. Am. Coll. Cardiol.* 76, 503–514. doi: 10.1016/j.jacc.2020.05.072

Del Re, D. P., and Amgalan, D. (2019). Fundamental mechanisms of regulated cell death and implications for heart disease. *Physiol. Rev.* 99, 1765–1817. doi: 10.1152/physrev.00022.2018

Dridi, H., Kushnir, A., Zalk, R., Yuan, Q., Melville, Z., and Marks, A. R. (2020). Intracellular calcium leak in heart failure and atrial fibrillation: a unifying mechanism and therapeutic target. *Nat Rev Cardiol.* 17, 732–747. doi: 10.1038/s41569-020-0394-8

Du, J., Xie, J., Zhang, Z., Tsujikawa, H., Fusco, D., Silverman, D., et al. (2010). TRPM7-mediated Ca2+ signals confer fibrogenesis in human atrial fibrillation. *Circ. Res.* 106, 992–1003. doi: 10.1161/circresaha.109.206771

Duan, J., Li, Z., Li, J., Hulse, R. E., Santa-Cruz, A., and Valinsky, W. C. (2018). Structure of the mammalian TRPM7, a magnesium channel required during embryonic development. *Proc. Natl. Acad. Sci.* 115, E8201–E8210. doi: 10.1073/pnas.1810719115

Falcón, D., Galeano-Otero, I., Calderón-Sánchez, E., Del Toro, R., Martín-Bórnez, M., Rosado, J. A., et al. (2019). TRP Channels: current perspectives in the adverse cardiac remodeling. *Front. Physiol.* 10:159. doi: 10.3389/fphys.2019.00159

Friesner, R. A., Banks, J. L., Murphy, R. B., Halgren, T. A., Klicic, J. J., Mainz, D. T., et al. (2004). Glide: a new approach for rapid, accurate docking and scoring. 1. Method and assessment of docking accuracy. *J. Med. Chem.* 47, 1739–1749. doi: 10.1021/jm0306430

Gu, J., Noe, A., Chandra, P., Al-Fayoumi, S., Ligueros-Saylan, M., Sarangapani, R., et al. (2010). Pharmacokinetics and pharmacodynamics of LCZ696, a novel dual-acting angiotensin receptor-neprilysin inhibitor (ARNi). *J. Clin. Pharmacol.* 50, 401–414. doi: 10.1177/0091270009343932

Hsiao, H. L., Langenickel, T. H., Petruck, J., Kode, K., Ayalasomayajula, S., Schuehly, U., et al. (2018). Evaluation of pharmacokinetic and pharmacodynamic drug-drug interaction of Sacubitril/Valsartan (LCZ696) and sildenafil in patients with mild-to-moderate hypertension. *Clin. Pharmacol. Ther.* 103, 468–476. doi: 10.1002/cpt.759

Hubers, S. A., and Brown, N. J. (2016). Combined angiotensin receptor antagonism and neprilysin inhibition. *Circulation* 133, 1115–1124. doi: 10.1161/circulationaha.115.018622

Iborra-Egea, O., Gálvez-Montón, C., Roura, S., Perea-Gil, I., Prat-Vidal, C., Soler-Botija, C., et al. (2017). Mechanisms of action of sacubitril/valsartan on cardiac remodeling: a systems biology approach. *NPJ Syst. Biol. Appl.* 3:12. doi: 10.1038/s41540-017-0013-4

Ishii, M., Kaikita, K., Sato, K., Sueta, D., Fujisue, K., Arima, Y., et al. (2017). Cardioprotective effects of LCZ696 (Sacubitril/Valsartan) after experimental acute myocardial infarction. *JACC Basic Transl. Sci.* 2, 655–668. doi: 10.1016/j.jacbts.2017.08.001

Jing, W., Vaziri, N. D., Nunes, A., Suematsu, Y., Farzaneh, T., Khazaeli, M., et al. (2017). LCZ696 (Sacubitril/valsartan) ameliorates oxidative stress, inflammation, fibrosis and improves renal function beyond angiotensin receptor blockade in CKD. *Am. J. Transl. Res.* 9, 5473–5484.

Khan, I., Yousif, A., Chesnokov, M., Hong, L., and Chefetz, I. (2021). A decade of cell death studies: Breathing new life into necroptosis. *Pharmacol. Ther.* 220:107717. doi: 10.1016/j.pharmthera.2020.107717

Kong, P., Christia, P., and Frangogiannis, N. G. (2014). The pathogenesis of cardiac fibrosis. *Cell. Mol. Life Sci.* 71, 549–574. doi 10.1007/s00018-013-1349-6

Kumar, H., and Choi, D. K. (2015). Hypoxia inducible factor pathway and physiological adaptation: A cell survival pathway? *Mediators Inflamm.* 2015:584758. doi: 10.1155/2015/584758

Li, J., Salvador, A. M., Li, G., Valkov, N., Ziegler, O., Yeri, A., et al. (2021). Mir-30d regulates cardiac remodeling by intracellular and paracrine signaling. *Circ. Res.* 128, e1–e23. doi: 10.1161/circresaha.120.317244

Lin, L. M., Wu, Y., Wu, M. F., and Lin, J. X. (2016). Focus on the novel cardiovascular drug LZC696: from evidence to clinical consideration. *Cardiovasc. Drugs Ther.* 30, 623–633. doi: 10.1007/s10557-016-6699-5

Lu, J., Wang, Q. Y., Zhou, Y., Lu, X. C., Liu, Y. H., Wu, Y., et al. (2017). Astragaloside IV against cardiac fibrosis by inhibiting TRPM7 channel. *Phytomedicine* 30, 10–17. doi: 10.1016/j.phymed.2017.04.002

Luo, L. F., Qin, L. Y., Wang, J. X., Guan, P., Wang, N., and Ji, E. S. (2021). Astragaloside IV attenuates the myocardial injury caused by adriamycin by inhibiting autophagy. *Front. Pharmacol.* 12:669782. doi: 10.3389/fphar.2021.669782

McMurray, J. J., Packer, M., Desai, A. S., Gong, J., Lefkowitz, M. P., Rizkala, A. R., et al. (2014). Angiotensin-neprilysin inhibition versus enalapril in heart failure. *N. Engl. J. Med.* 371, 993–1004. doi: 10.1056/NEJMoa1409077

Meyer, B. A., and Doroudgar, S. (2020). ER stress-induced secretion of proteins and their extracellular functions in the heart. *Cells* 9:2066. doi: 10.3390/cells9092066

Porter, K. E., and Turner, N. A. (2009). Cardiac fibroblasts: at the heart of myocardial remodeling. *Pharmacol. Ther.* 123, 255–278. doi: 10.1016/j.pharmthera.2009.05.002

Sah, R., Mesirca, P., Van den Boogert, M., Rosen, J., Mably, J., Mangoni, M. E., et al. (2013). Ion channel-kinase TRPM7 is required for maintaining cardiac automaticity. *Proc. Natl. Acad. Sci. U S A* 110, E3037–E3046. doi: 10.1073/pnas.1311865110

Schimmel, K., Jung, M., Foinquinos, A., José, G. S., Beaumont, J., Bock, K., et al. (2020). Natural compound library screening identifies new molecules for the treatment of cardiac fibrosis and diastolic dysfunction. *Circulation* 141, 751–767. doi: 10.1161/circulationaha.119.042559

Simard, C., and Magaud, C. (2020). TRPM4 non-selective cation channel in human atrial fibroblast growth. *Pflugers Arch.* 472, 1719–1732. doi: 10.1007/s00424-020-02476-0

Song, W., Wang, H., and Wu, Q. (2015). Atrial natriuretic peptide in cardiovascular biology and disease (NPPA). *Gene* 569, 1–6. doi: 10.1016/j.gene.2015.06.029

Suematsu, Y., Miura, S., Goto, M., Matsuo, Y., Arimura, T., Kuwano, T., et al. (2016). LCZ696, an angiotensin receptor-neprilysin inhibitor, improves cardiac function with the attenuation of fibrosis in heart failure with reduced ejection fraction in streptozotocin-induced diabetic mice. *Eur. J. Heart Fail.* 18, 386–393. doi: 10.1002/ejhf.474

Tallquist, M. D. (2020). Cardiac fibroblast diversity. *Annu. Rev. Physiol.* 82, 63–78. doi: 10.1146/annurev-physiol-021119-034527

Trapani, V., and Wolf, F. I. (2020). The TRPM7 channel kinase: rekindling an old flame or not? *Cardiovasc. Res.* 116, 476–478. doi: 10.1093/cvr/cvz229

Virani, S. S., Alonso, A., Aparicio, H. J., Benjamin, E. J., Bittencourt, M. S., Callaway, C. W., et al. (2021). Heart disease and stroke statistics-2021 update: A report from the American Heart Association. *Circulation* 143, e254–e743. doi: 10.1161/cir.0000000000000950

Virani, S. S., Alonso, A., Benjamin, E. J., Bittencourt, M. S., Callaway, C. W., Carson, A. P., et al. (2020). Heart disease and stroke statistics-2020 update: A report from the American Heart Association. *Circulation* 141, e139–e596. doi: 10.1161/cir.0000000000000757

von Lueder, T. G., Wang, B. H., Kompa, A. R., Huang, L., Webb, R., Jordaan, P., et al. (2015). Angiotensin receptor neprilysin inhibitor LCZ696 attenuates cardiac remodeling and dysfunction after myocardial infarction by reducing cardiac fibrosis and hypertrophy. *Circ. Heart Fail.* 8, 71–78. doi: 10.1161/circheartfailure.114.001785

Wei, W. L., Sun, H. S., Olah, M. E., Sun, X., Czerwinska, E., Czerwinski, W., et al. (2007). TRPM7 channels in hippocampal neurons detect levels of extracellular divalent cations. *Proc. Natl. Acad. Sci. U S A* 104, 16323–16328. doi: 10.1073/pnas.0701149104

Wei, Y., Wu, Y., Feng, K., Zhao, Y., Tao, R., Xu, H., et al. (2020). Astragaloside IV inhibits cardiac fibrosis via miR-135a-TRPM7-TGF-β/Smads pathway. *J. Ethnopharmacol.* 249:112404. doi: 10.1016/j.jep.2019.112404

Wu, H. Y., Wu, J. L., and Ni, Z. L. (2019). Overexpression of microRNA-202-3p protects against myocardial ischemia-reperfusion injury through activation of TGF-β1/Smads signaling pathway by targeting TRPM6. *Cell Cycle* 18, 621–637. doi: 10.1080/15384101.2019.1580494

Xu, T., Wu, B. M., Yao, H. W., Meng, X. M., Huang, C., Ni, M. M., et al. (2015). Novel insights into TRPM7 function in fibrotic diseases: a potential therapeutic target. *J. Cell Physiol.* 230, 1163–1169. doi: 10.1002/jcp.24801

Yandrapalli, S., Aronow, W. S., Mondal, P., and Chabbott, D. R. (2017). The evolution of natriuretic peptide augmentation in management of heart failure and the role of sacubitril/valsartan. *Arch. Med. Sci.* 13, 1207–1216. doi: 10.5114/aoms.2017.68813

Yandrapalli, S., Khan, M. H., Rochlani, Y., and Aronow, W. S. (2018). Sacubitril/valsartan in cardiovascular disease: evidence to date and place in therapy. *Ther. Adv. Cardiovasc. Dis.* 12, 217–231. doi: 10.1177/1753944718784536

Yu, Y., Chen, S., Xiao, C., Jia, Y., Guo, J., Jiang, J., et al. (2014). TRPM7 is involved in angiotensin II induced cardiac fibrosis development by mediating calcium and magnesium influx. *Cell Calcium* 55, 252–260. doi: 10.1016/j.ceca.2014.02.019

Yue, L., Xie, J., and Nattel, S. (2011). Molecular determinants of cardiac fibroblast electrical function and therapeutic implications for atrial fibrillation. *Cardiovasc. Res.* 89, 744–753. doi: 10.1093/cvr/cvq329

Zile, M. R., O'Meara, E., Claggett, B., Prescott, M. F., Solomon, S. D., Swedberg, K., et al. (2019). Effects of Sacubitril/Valsartan on biomarkers of extracellular matrix regulation in patients with HFrEF. *J. Am. Coll. Cardiol.* 73, 795–806. doi: 10.1016/j.jacc.2018.11.042

Conflict of Interest: The authors declare that the research was conducted in the absence of any commercial or financial relationships that could be construed as a potential conflict of interest.

Publisher's Note: All claims expressed in this article are solely those of the authors and do not necessarily represent those of their affiliated organizations, or those of the publisher, the editors and the reviewers. Any product that may be evaluated in this article, or claim that may be made by its manufacturer, is not guaranteed or endorsed by the publisher.

Copyright © 2021 Jia, Wang, Tang, Yu, Li, Cui, Zhu, Meng, Wang and Wang. This is an open-access article distributed under the terms of the Creative Commons Attribution License (CC BY). The use, distribution or reproduction in other forums is permitted, provided the original author(s) and the copyright owner(s) are credited and that the original publication in this journal is cited, in accordance with accepted academic practice. No use, distribution or reproduction is permitted which does not comply with these terms.

frontiers in Cell and Developmental Biology

ORIGINAL RESEARCH
published: 08 November 2021
doi: 10.3389/fcell.2021.779432

GSDMD Mediates LPS-Induced Septic Myocardial Dysfunction by Regulating ROS-dependent NLRP3 Inflammasome Activation

Shanshan Dai[1†], Bozhi Ye[2†], Lingfeng Zhong[2], Yanghao Chen[2], Guangliang Hong[1], Guangju Zhao[1], Lan Su[2] and Zhongqiu Lu[1]**

[1]The Key Laboratory of Emergency and Disaster Medicine of Wenzhou, Department of Emergency, The First Affiliated Hospital of Wenzhou Medical University, Wenzhou, China, [2]The Key Laboratory of Cardiovascular Disease of Wenzhou, Department of Cardiology, The First Affiliated Hospital of Wenzhou Medical University, Wenzhou, China

OPEN ACCESS

Edited by:
Zhi Qi,
Nankai University, China

Reviewed by:
Wenwen Tang,
Yale University, United States
Jieli Li,
The Ohio State University,
United States

***Correspondence:**
Zhongqiu Lu
lzq_640815@163.com
Lan Su
2512057600@qq.com

[†]These authors have contributed equally to this work

Specialty section:
This article was submitted to Cell Death and Survival, a section of the journal Frontiers in Cell and Developmental Biology

Received: 18 September 2021
Accepted: 22 October 2021
Published: 08 November 2021

Citation:
Dai S, Ye B, Zhong L, Chen Y, Hong G, Zhao G, Su L and Lu Z (2021) GSDMD Mediates LPS-Induced Septic Myocardial Dysfunction by Regulating ROS-dependent NLRP3 Inflammasome Activation. Front. Cell Dev. Biol. 9:779432. doi: 10.3389/fcell.2021.779432

Myocardial dysfunction is a serious consequence of sepsis and contributes to high mortality. Currently, the molecular mechanism of myocardial dysfunction induced by sepsis remains unclear. In the present study, we investigated the role of gasdermin D (GSDMD) in cardiac dysfunction in septic mice and the underlying mechanism. C57BL/6 wild-type (WT) mice and age-matched *Gsdmd*-knockout (*Gsdmd*$^{-/-}$) mice were intraperitoneally injected with lipopolysaccharide (LPS) (10 mg/kg) to mimic sepsis. The results showed that GSDMD-NT, the functional fragment of GSDMD, was upregulated in the heart tissue of septic WT mice induced by LPS, which was accompanied by decreased cardiac function and myocardial injury, as shown by decreased ejection fraction (EF) and fractional shortening (FS) and increased cardiac troponin I (cTnI), creatine kinase isoenzymes MB (CK-MB), and lactate dehydrogenase (LDH). *Gsdmd*$^{-/-}$ mice exhibited protection against LPS-induced myocardial dysfunction and had a higher survival rate. *Gsdmd* deficiency attenuated LPS-induced myocardial injury and cell death. *Gsdmd* deficiency prevented LPS-induced the increase of interleukin-1β (IL-1β) and tumor necrosis factor-α (TNF-α) in serum, as well as IL-1β and TNF-α mRNA levels in myocardium. In addition, LPS-mediated inflammatory cell infiltration into the myocardium was ameliorated and activation of NF-κB signaling pathway and the NOD-like receptor protein 3 (NLPR3) inflammasome were suppressed in *Gsdmd*$^{-/-}$ mice. Further research showed that in the myocardium of LPS-induced septic mice, GSDMD-NT enrichment in mitochondria led to mitochondrial dysfunction and reactive oxygen species (ROS) overproduction, which further regulated the activation of the NLRP3 inflammasome. In summary, our data suggest that GSDMD plays a vital role in the pathophysiology of LPS-induced myocardial dysfunction and may be a crucial target for the prevention and treatment of sepsis-induced myocardial dysfunction.

Keywords: gasdermin D, sepsis, myocardial dysfunction, reactive oxygen species, NLRP3 inflammasome

Abbreviations: LPS, lipopolysaccharide; GSDMD, gasdermin D; GSDMD-NT, N-terminal fragment of GSDMD; GSDMD-FL, full-length GSDMD; NLRP3, NOD-like receptor protein 3; EF, ejection fraction; FS, fractional shortening; LVIDS, left ventricular end systolic inner diameter; LVIDD, left ventricular end diastolic inner diameter; LDH, lactate dehydrogenase; CK-MB, creatine kinase isoenzyme MB; MPO, myeloperoxidase; HE, hematoxylin and eosin staining; TNF-α, tumor necrosis factor α; IL-1β, interleukin-1β; MDA, malondialdehyde; SOD, superoxide dismutase; ROS, reactive oxygen species.

INTRODUCTION

Myocardial dysfunction is a serious complication of sepsis. It has been reported that 20–60% of patients with sepsis develop myocardial dysfunction (Charpentier et al., 2004; Vieillard-Baron et al., 2008). Patients exhibiting cardiac dysfunction have high mortality rates (Jeong et al., 2018). However, the molecular mechanisms of septic myocardial dysfunction remain unclear, and treatment for the disease is mainly supportive without any particularly effective therapies.

Currently, multiple mechanisms are thought to be participated in the pathogenesis of myocardial dysfunction in sepsis, including persistent inflammatory response, mitochondrial dysfunction, oxidative stress injury, autonomic nervous system dysregulation, and apoptosis (Cimolai et al., 2015; Essandoh et al., 2015; Neri et al., 2016). Among these mechanisms, excessive inflammation is an important one. During the inflammatory response, lots of inflammatory cytokines are produced. Tumor necrosis factor-α (TNF-α) and Interleukin-1β (IL-1β) are primary players in the hierarchy of proinflammatory mediator cascades (Loppnow et al., 1998). These inflammatory cytokines disturb energy metabolism, destroy β-adrenergic signaling, stimulate excess production of nitric oxide, and imbalance calcium homeostasis, leading to myocardial dysfunction (Zhong et al., 1997; Rudiger & Singer, 2007; Alves-Filho et al., 2008; de Montmollin et al., 2009; Smeding et al., 2012; Drosatos et al., 2015).

Pyroptosis is a type of death associated with inflammation, which can defense against microbial infection and induce excessive inflammatory response (Miao et al., 2010; Aachoui et al., 2013; Liang et al., 2016). Accumulating evidence has suggested that pyroptosis is involved in the pathophysiology of sepsis and cardiovascular diseases (Jia et al., 2019; Li et al., 2019). Gasdermin D (GSDMD) has been considered to be the critical mediator of pyroptosis (Kayagaki et al., 2015; Shi et al., 2015). In a stable state, GSDMD exists in an inactive form. When specific danger signals occur, GSDMD is cleaved into an N-terminal fragment (GSDMD-NT) and a C-terminal fragment (GSDMD-CT) (Agard et al., 2010). GSDMD-NT gradually transfers to the cell membrane and oligomerizes to form pores, destroying the integrity of the cell membrane and inducing cellular injury and inflammatory cytokine release (Ding et al., 2016). It has been reported that *Gsdmd*$^{-/-}$ mice are resistant to lethal doses of lipopolysaccharide (LPS) in animal models, and inflammatory and IL-Iβ secretion are inhibited in bone marrow-derived macrophages from *Gsdmd*$^{-/-}$ mice after LPS stimulation (Kayagaki et al., 2015). Chemical inhibition of GSDMD could reduce cellular injury and improve survival in septic mice (Rathkey et al., 2018). Evidence also demonstrates that GSDMD-mediated pyroptosis is involved in sepsis-associated acute kidney injury (AKI) and lung injury (Cheng et al., 2017; Ye Z. et al., 2019). However, the role of GSDMD in sepsis-induced cardiac dysfunction remains unknown. Therefore, in the present study, we investigated the effect of GSDMD in LPS-induced cardiac dysfunction and the underlying mechanisms, aiming to find a feasible target for the treatment of sepsis-induced myocardial dysfunction.

MATERIALS AND METHODS

Animals

All experimental procedures were approved by the Laboratory Animal Ethics Committee and Laboratory Animal Centre of Wenzhou Medical University (No. wydw 2019–0477). Male *Gsdmd*-knockout (*Gsdmd* $^{-/-}$) mice and age- and weight-matched C57BL/6 mice, 8 weeks old (22 ± 2 g), were obtained from GemPharmatech Co., Ltd. The animals were housed in the Animal Center of Wenzhou Medical University under temperature-controlled (25°C) and specific pathogen-free conditions. Mice had free access to water and food. A sepsis-induced myocardial dysfunction mouse model was established by intraperitoneal injection of LPS (10 mg/kg, from *Escherichia coli* O111:B4, Sigma-Aldrich). Mice in the control group received an equal volume of sterile saline. The 12 h time point for LPS treatment was chosen for the experiment based on the results that cardiac function and myocardial injury were most serious, accompanied by increased expression of GSDMD-NT in heart tissue induced by LPS at 12 h. Mice were randomly divided into four groups after adaptation to the environment: the wild-type (WT) control group, *Gsdmd*$^{-/-}$ control group, WT mice subjected to intraperitoneal LPS injection (WT-LPS group), and *Gsdmd*$^{-/-}$ mice subjected to intraperitoneal LPS injection (*Gsdmd*$^{-/-}$-LPS group). Each group included eight mice (n = 8). After 12 h, cardiac function was detected. Then mice were sacrificed, and serum and heart tissues were collected.

For survival analysis, *Gsdmd* $^{-/-}$ mice and WT mice (n = 10) were intraperitoneally injected with LPS to mimic septic myocardial dysfunction. After LPS administration, Mice were observed for 7 days and the survival rate was calculated based on the surviving mice number.

Echocardiography

The cardiac function of mice was measured by a preclinical ultrasound system (Vevo 3100, FUJIFILM Visual Sonics, Canada) after anesthetization with inhaled isoflurane. The left ventricular end systolic inner diameter (LVIDS) and left ventricular end diastolic inner diameter (LVIDD) were measured from the M-mode view. Then, ejection fraction (EF) and fractional shortening (FS) were calculated and analyzed.

Serum Biochemical Analysis

Serum samples from each group were carefully collected and stored at −80°C for subsequent analyses. The serum levels of cardiac troponin I (cTnI) (Xitang Biotechnology, Shanghai, China), creatine kinase isoenzyme MB (CK-MB) (Jiancheng Bioengineering Institute, Nanjing, China), and lactate dehydrogenase (LDH) (BC0685, Solarbio, Beijing, China) were tested by using commercial kits according to the manufacturer's instructions.

TABLE 1 | Primers for reverse transcription-quantitative polymerase chain reaction.

Target	Species	Primer	Sequence
IL-1β	mice	Forward	5′-TCGCAGCAGCACATCAACAAGAG-3′
	—	Reverse	5′-AGGTCCACGGGAAAGACACAGG-3′
TNF-α	mice	Forward	5′-ATGTCTCAGCCTCTTCTCATTC-3′
	—	Reverse	5′-GCTTGTCACTCGAATTTTGAGA-3′
β-actin	mice	Forward	5′-CTACCTCATGAAGATCCTGACC-3′
	—	Reverse	5′-CACAGCTTCTCTTTGATGTCAC-3′

Cell Culture and Treatments

H9c2 cardiomyocytes were purchased from the Shanghai Institute of Biochemistry and Cell Biology (Shanghai, China). Primary cardiomyocytes were isolated from the left ventricle of neonatal Sprague-Dawley (SD) rats as described previously (Ye B. et al., 2019). Cardiomyocytes were cultured in Dulbecco's modified Eagle's medium (DMEM, Thermo Fisher Scientific, United States) consisting of 10% fetal bovine serum (FBS, Thermo Fisher Scientific) and 1% penicillin-streptomycin (Thermo Fisher Scientific), and were maintained in a humidified environment with 5% CO_2 at 37°C. After achieving 80~90% confluence, cardiomyocytes were treated with LPS (10 μg/ml) for 6 h for priming (Zhang W. et al., 2017; Li et al., 2019), followed by nigericin (10 μM) for 1 h to establish the myocardial injury model. Cells in the control group were incubated with the same amounts of corresponding solvents.

In order to explore the role of GSDMD, *Gsdmd* gene silencing in cell was achieved by transfecting cells with small interfering RNA (siRNA) (5′- GTCAAGTCTAGG CCAGAAA -3′ for *Gsdmd*) using Lipofectamine 2000 (Invitrogen, Carlsbad, California). After 6 h, the medium was replaced with fresh DMEM containing 10% FBS, and the cells were incubated for 36 h. The effect of knockdown was verified by Western blotting. To confirm the role of the NOD-like receptor protein 3 (NLRP3) inflammasome, cells were treated with NLRP3 inhibitor (MCC950, Selleck Chemicals, Houston, TX) or caspase-1 inhibitor (Belnacasan, VX-765, Selleck Chemicals) or reactive oxygen species (ROS) scavenger, N-acetyl-L-cysteine (NAC) (Beyotime, Shanghai, China) for 1 h before LPS and nigericin treatment to mimic myocardial injury.

Cell Viability Assay

After various treatments, cell viability and death were detected by using the cell counting kit (CCK-8) (C0038, Beyotime, Shanghai, China) and LDH cytotoxicity assay kit (C0016, Beyotime, Shanghai, China) according to the specifications provided by the manufacturer.

Real-Time Quantitative Polymerase Chain Reaction

Total RNA was isolated from heart tissue using TRIzol reagent (Thermo Fisher Scientific) and reverse transcribed to cDNA by PrimeScript RT reagent kits (Thermo Fisher Scientific) according to the manufacturer's instructions. Quantitative PCR was run in an Applied Biosystems 7,300 system (United States) machine using SYBR Green reagent kits (TaKaRa, Tokyo, Japan). Relative mRNA expression of the target genes was normalized to β-actin, and data were analyzed based on the ΔΔCt method. The primers are presented in **Table 1**.

Western Blot Analysis

Proteins extracted from heart tissue and cardiomyocytes. Protein concentration was detected by the BCA Protein assay kit (PC0020, Solarbio, Beijing, China). Equal amounts of protein were added and separated by sodium dodecyl sulfate-polyacrylamide gel electrophoresis (SDS-PAGE) and transferred to a PVDF membrane. The membranes were then blocked with 5% fat-free milk solution at room temperature for 1 h. Then, the membranes were incubated with primary antibodies against GSDMD (1:1,000, ab219800, Abcam), NLRP3 (1:1,000, ab263899, Abcam), caspase-1 (1:200, sc-56036, Santa Cruz Biotechnology), NF-κB P65 (1:1,000, #8242, Cell Signaling Technology), phosphorylated P65 (p-P65) (1:1,000, #3033, Cell Signaling Technology) and GAPDH (1:1,000, #5174, Cell Signaling Technology) at 4°C overnight, followed by secondary antibody for 1 h at room temperature. After washing three times, enhanced chemiluminescence (ECL) reagent was added to the membrane. The signal was detected using an ECL system.

Histological Analysis

Heart tissue was immobilized in 4% paraformaldehyde at room temperature for 24 h. After embedded in paraffin, heart samples were cut into 5 μm sections. Subsequently, the slices were stained with hematoxylin and eosin (HE) (G1120, Solarbio, Beijing, China) according to the manufacturer's specifications. The slices prepared for immunohistochemistry were deparaffinized and rehydrated, incubated in citrate buffer (0.01 M, pH 6.0) in a pressure cooker for 10 min after water boiling, and then cooled to room temperature for antigen retrieval. Subsequently, the slices were incubated with 3% hydrogen peroxide for 10 min and blocked with 5% bovine serum albumin (BSA) (A8020, Solarbio, Beijing, China) for 30 min at room temperature. After that, sections were incubated with anti-CD68-antibody (1:50, ab955, Abcam) at 4°C overnight, followed by secondary antibody for 1 h at room temperature. Finally, the sections were treated with diaminobenzidine for histochemical visualization. Images were observed under a microscope (Olympus Corporation, Tokyo, Japan).

TdT-Mediated DUTP Nick End Labeling Assay

Cell death in heart sections was assessed by the TUNEL assay (Roche, Indianapolis, IN) according to the manufacturer's instructions. Positive staining was measured by a microscopy (Olympus Corporation, Tokyo, Japan).

Myeloperoxidase Activity Analysis

Heart tissues were homogenized and centrifuged, and the supernatant was collected. MPO activity was evaluated using a commercial kit (Jiancheng Bioengineering Institute, Nanjing, China) according to the instructions of the manufacturer.

Enzyme-Linked Immunosorbent Assay

The levels of IL-1β in serum and cell supernatants, as well as TNF-α in serum, were detected by using ELISA kits (Xitang Biotechnology, Shanghai, China) after various treatments, according to the instructions provided by the manufacturer.

Mitochondrial Membrane Potential Detection

MMP of cardiomyocytes was evaluated by the JC-1 fluorescence probe kit (C2006, Beyotime, Shanghai, China) according to the instructions of the manufacturer. Briefly, after the various treatments, cells were incubated with JC-1 (10 μg/ml) for 20 min at 37°C. Fluorescence was observed under a fluorescence microscope (Olympus Corporation, Tokyo, Japan). At high MMP, JC-1 accumulated in the mitochondrial matrix, forming polymers (J-aggregates), which yielded a red fluorescent light. At low MMP, JC-1 was unable to aggregate in the mitochondrial matrix, appearing as a monomer form. These monomers emitted a green fluorescent light. The change in fluorescence emission from red to green, indicating MMP depolarization.

Adenosine Triphosphate Determination

Cells were lysed and centrifuged at 12,000 g for 5 min after various treatments. And the supernatants were collected to detect ATP level using an ATP assay kit (S0026, Beyotime, Shanghai, China) according the instructions provided by the manufacturer.

Reactive Oxygen Species Activity Measurement

The intracellular level of ROS was measured by a dichloro-dihydro-luorescein diacetate (DCFH-DA) assay kit (S0033S, Beyotime, Shanghai, China). Cardiomyocytes were treated with DCFH-DA in the dark for 20 min at 37°C. After washing three times, images were examined using a fluorescence microscope (Olympus Corporation, Tokyo, Japan).

Malondialdehyde Concentration and Superoxide Dismutase Activity Detection

Heart tissues were homogenized and centrifuged, and the supernatant was collected. The corresponding kits (S0131S and S0103, Beyotime, Shanghai, China) were used to detect the concentration of MDA and activity of SOD, according to the instructions of the manufacturer.

Statistical Analysis

All experiments were randomized and blinded. Data were shown as the mean ± standard deviation (SD) from three independent experiments. SPSS 21.0 software was used to analyze the data. The comparisons among different groups were analyzed by one-way analysis of variance (ANOVA) followed by the LSD test. $p < 0.05$ was considered statistically significant.

RESULTS

Gasdermin D N-Terminal Was Upregulated in the Heart Tissue of Septic Mice Induced by Lipopolysaccharide

A sepsis-induced myocardial dysfunction mouse model was established by intraperitoneal injection of LPS. Transthoracic echocardiography and myocardial injury biomarkers cTnI, CK-MB and LDH were evaluated to assess cardiac dysfunction and myocardial injury. The results showed that cardiac function was significantly decreased by LPS, as shown by decreased EF and FS, especially at 12 h (**Figures 1A–C**). The concentrations of cTnI, CK-MB and LDH were significantly increased in the mice following LPS treatment compared with the control group (**Figures 1D–F**). In addition, HE staining showed that myocardial cells were swollen, myocardial fibers were irregularly arranged, and some myocardial fibers were broken and dissolved as LPS processing time was prolonged (**Figure 1G**). Meanwhile, the protein expression of GSDMD and its functional fragment GSDMD-NT in heart tissue were detected. The results exhibited that GSDMD-NT was markedly increased in the myocardium after treatment with LPS (**Figure 1H**). These findings indicate that GSDMD plays a role in septic myocardial dysfunction induced by LPS.

Gasdermin D Deficiency Improved the Survival Rate and Attenuated Myocardial Injury and Dysfunction in Lipopolysaccharide-Induced Septic Mice

To confirm our conjecture, *Gsdmd*$^{-/-}$ mice were used in subsequent experiments. *Gsdmd*$^{-/-}$ and WT mice, which were age-matched, were treated with or without LPS. The 7-days survival rate of mice treated with LPS was observed. The results displayed that the 7-days survival rate of WT mice after LPS injection was 50%, while no death occurred in *Gsdmd*$^{-/-}$ mice (**Figure 2A**). Compared with that of the WT group, the survival rate of *Gsdmd*$^{-/-}$ mice after intraperitoneal injection of LPS was significantly improved ($p < 0.05$). Further research showed that *Gsdmd* knockout ameliorated cardiac EF and FS decline induced by LPS (both $p < 0.001$, **Figures 2B–D**). The serum levels of cTnI, CK-MB, and LDH, biomarkers of myocardial injury, were detected. As shown in **Figures 2E–G**, LPS markedly increased the serum levels of cTnI, CK-MB, and LDH in WT mice (all $p < 0.001$), while these indicators were significantly decreased in *Gsdmd*$^{-/-}$ mice treated with LPS (all $p < 0.001$). There was no significant difference between the WT

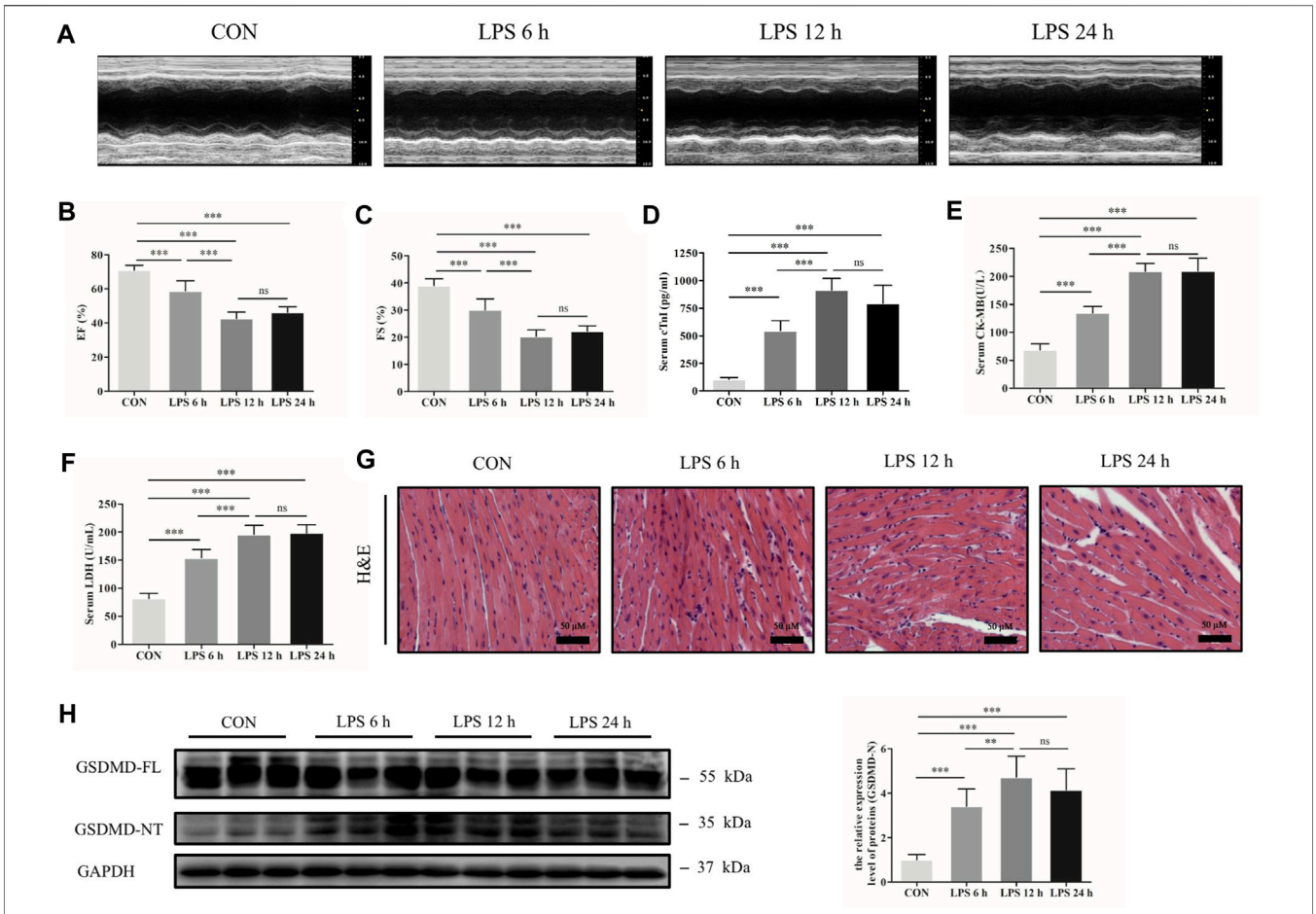

FIGURE 1 | GSDMD-NT was upregulated in the heart tissue of septic mice induced by LPS. **(A)** Representative echocardiography of mice from each group. **(B, C)** Myocardial function parameters, ejection fraction (EF) and fractional shortening (FS) of mice from each group were assessed by echocardiography (n = 6). **(D–F)** The levels of cardiac troponin I (cTnI), creatine kinase isoenzymes MB (CK-MB) and lactate dehydrogenase (LDH) in serum from each group (n = 6). **(G)** Representative HE images of heart tissue from each group (magnification × 400). **(H)** Expressions of GSDMD and GSDMD-NT protein in heart tissue were measured by Western blotting analysis. The results were normalized to the expression of GAPDH (n = 6). Data are expressed as the mean ± standard deviation (SD). $^{**}p < 0.01$, $^{***}p < 0.001$. ns: nonsignificance.

control group and the *Gsdmd*$^{-/-}$ control group (**Figures 2B–F**). In addition, HE staining and TUNEL staining of heart tissue were performed. The results showed that myocardial cells in the WT group following LPS treatment were disordered and swollen, myocardial muscle fibers were arranged irregularly, and cardiomyocyte death was increased, while these pathological changes were reversed in *Gsdmd*$^{-/-}$ mice (**Figures 3H,I**). All these results demonstrated that *Gsdmd*$^{-/-}$ mice were more resistant to LPS-induced myocardial injury than WT mice.

Gasdermin D Deficiency Attenuated Inflammatory Cytokine Secretion, Cardiac Inflammation, and Activation of the NF-κB Signaling Pathway Induced by Lipopolysaccharide

GSDMD has been considered to be the key mediator of pyroptosis and associated with inflammation. Therefore, in the follow-up experiment, levels of the serum inflammatory cytokines TNF-α and IL-1β were measured. As shown in **Figure 3**, compared with the control group, LPS dramatically increased the serum levels of TNF-α and IL-1β in WT mice (both $p < 0.001$). However, the LPS-induced increases in the levels of TNF-α and IL-1β were prevented in *Gsdmd*$^{-/-}$ mice (both $p < 0.001$). The mRNA expression levels of TNF-α and IL-1β in the myocardium were also measured. Consistent with the results of inflammation factors in the serum, *Gsdmd* knockout significantly attenuated LPS-increased mRNA levels of TNF-α and IL-1β in the myocardium (both $p < 0.001$, **Figures 3C,D**). In addition, mice intraperitoneally injected with LPS exhibited markedly increased numbers of CD-68-positive cells and MPO activity in the myocardium, which were attenuated in the *Gsdmd*$^{-/-}$-LPS group (**Figures 3E,F**). These data indicated that the GSDMD-mediated inflammatory response participated in the development of sepsis-induced myocardial dysfunction. The NF-κB signaling pathway has been reported to play an important role in

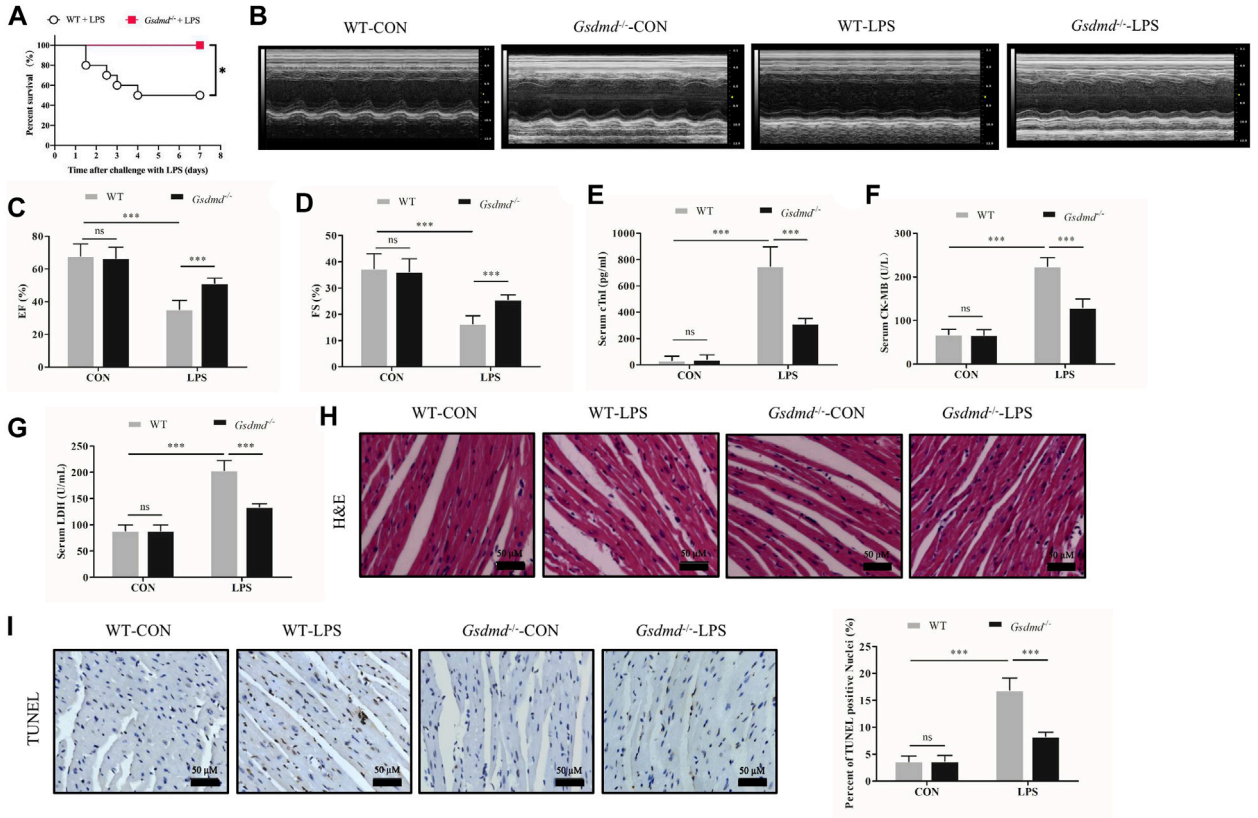

FIGURE 2 | *Gsdmd* deficiency improved the survival rate and attenuated myocardial injury and dysfunction in septic mice induced by LPS. **(A)** Survival rate of the WT-LPS group and *Gsdmd*$^{-/-}$-LPS group (n = 10). **(B)** Representative echocardiography of mice from each group. **(C, D)** Myocardial function parameters, EF and FS of mice from each group were measured by echocardiography (n = 8). **(E–G)** The levels of cTnI, CK-MB, and LDH in serum from each group (n = 8). **(H)** Representative HE images of heart tissue from each group (magnification × 400). **(I)** Representative TUNEL images of heart tissue from each group (magnification × 400) and quantitative data of positive cells from randomly selected five fields are shown on the right (n = 5). Data are expressed as the mean ± SD. *$p < 0.05$, ***$p < 0.001$.

coordinating inflammatory responses (Baker et al., 2011). Therefore, the effect of GSDMD on NF-κB activation was investigated. The results showed that compared to *Gsdmd*$^{-/-}$ mice, NF-κB was dramatically activated in WT mice treated with LPS, as evidenced by the increased phosphorylation of P65 (p-P65) (**Figures 3G,H**).

Gasdermin D Silencing Alleviated Myocardial Cell Injury Induced by Lipopolysaccharide

To explore the mechanism of GSDMD in cardiomyocytes, LPS combined with nigericin was used to induce myocardial injury in both primary cardiomyocytes and H9c2 cardiomyocytes *in vitro*. GSDMD protein expression and cell viability were analyzed. As shown in **Figures 4A–H**, the expression of GSDMD-NT protein was increased, cell viability was decreased, and LDH release and IL-1β content in the supernatant were increased in the model group of both primary cardiomyocytes and H9c2 cardiomyocytes compared to the respective control group. However, under the same stimulation, the cell viability was improved ($p < 0.01$), and LDH release ($p < 0.001$) and IL-1β content in supernatant ($p < 0.05$) were significantly decreased when GSDMD expression was interfered with (**Figures 4I–K**), indicating that cleaved GSDMD was involved in cell injury.

Gasdermin D Regulated NOD-Like Receptor Protein 3 Inflammasome Activation in Septic Myocardial Dysfunction Induced by Lipopolysaccharide

Gene sequencing analysis of myocardial tissue was further performed to screen the differentially expressed genes between the *Gsdmd*$^{-/-}$-LPS group and the WT-LPS group. The results showed that 19 genes were upregulated and 93 genes were downregulated in the *Gsdmd*$^{-/-}$-LPS group compared with the WT-LPS group (**Figure 5A**). Gene Ontology (GO) enrichment and Kyoto Encyclopedia of Genes and Genomes (KEGG) pathway analyses were performed, which indicated that the differentially expressed genes were significantly enriched in the NOD-like receptor (NLR) pathway (**Figure 5B**). Research has shown that NLRP3, a key protein in this pathway, plays a pivotal role in septic myocardial dysfunction (Baker et al.,

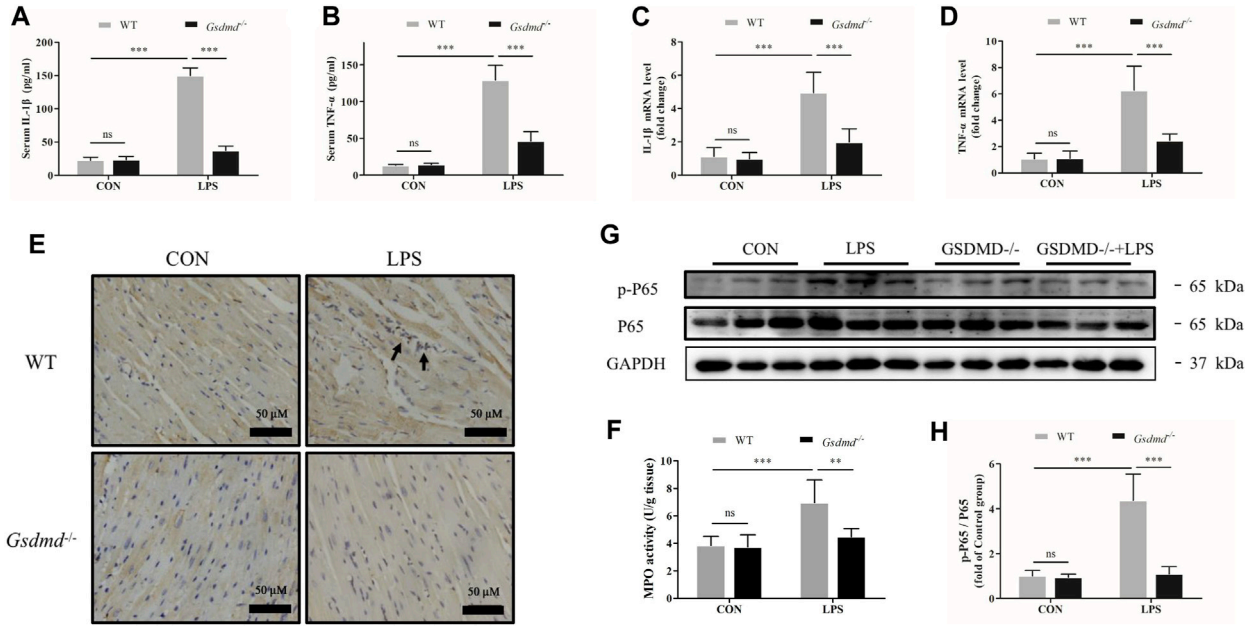

FIGURE 3 | *Gsdmd* deficiency attenuated inflammatory cytokine secretion, cardiac inflammation, and activation of the NF-κB signaling pathway induced by LPS. **(A,B)** The levels of Interleukin-1β (IL-1β) and Tumor necrosis factor-α (TNF-α) in serum from each group were detected by ELISA (n = 8). **(C,D)** The mRNA levels of IL-1β and TNF-α in heart tissue from each group were detected by PCR. The results were normalized to the expression of β-actin (n = 8). **(E)** Representative CD68 immunohistochemistry images of heart tissue from each group (magnification × 400). Arrow heads indicate positive staining. **(F)** MPO activity in heart tissue from each group (n = 5). **(G,H)** Expressions of NF-κB P65 and phosphorylated P65 protein in heart tissue were measured by Western blotting analysis. The results were normalized to the expression of P65 (n = 6). Data are expressed as the mean ± SD. $^{**}p < 0.01$, $^{***}p < 0.001$.

2011; Li et al., 2019; Yang et al., 2019). Our research showed that the NLRP3 inflammasome was activated in cardiomyocytes induced by LPS and nigericin (**Figure 5C**). Moreover, NLRP3 or caspase-1 inhibitors were applied to verify the effect of the NLRP3 inflammasome. As shown in **Figures 5D–F**, compared to the model group, the cell viability was improved (both $p < 0.01$), and the release of LDH and IL-1β in the supernatant were decreased in H9c2 cells pretreated with NLRP3 or caspase-1 inhibitors (all $p < 0.001$), suggesting that the NLRP3 inflammasome participated in myocardial injury induced by LPS.

NLRP3 inflammasome activation leads to GSDMD cleavage. However, it was interesting to note that the NLR pathway was downregulated in the *Gsdmd*$^{-/-}$-LPS group, indicating that GSDMD might be involved in the regulation of NLRP3 activation. Therefore, the effects of GSDMD on the NLRP3 inflammasome were examined. Compared to the control group, the expression of NLRP3 and cleaved caspase-1 proteins in myocardial tissue of WT mice treated with LPS was significantly increased (both $p < 0.001$, **Figure 5G**), while the expressions of the above proteins were decreased in *Gsdmd*$^{-/-}$ mice with the same treatment (both $p < 0.001$). Further study was conducted on H9c2 cardiomyocytes. The results showed that the protein expressions of NLRP3 and cleaved caspase-1, as well as the IL-1β concentration in the supernatant, were decreased in H9c2 cardiomyocytes transfected with si-*Gsdmd* after treatment with LPS and nigericin (**Figures 5H,I**), which was consistent with the results of animal experiments.

Gasdermin D N-Terminal Enrichment in Mitochondria Leads to Mitochondrial Dysfunction, Reactive Oxygen Species Generation, and NOD-Like Receptor Protein 3 Inflammasome Activation

It has been reported that ROS are involved in the activation of NLRP3 (Zhou et al., 2011), and mitochondria are the major source of cellular ROS. Studies have shown that GSDMD-NT aggregates not only on the cell membrane but also on the mitochondrial membrane, where it triggers mitochondrial injury (Platnich et al., 2018; Huang et al., 2020). Therefore, we hypothesized that GSDMD regulated NLRP3 inflammasome activation by acting on mitochondria. Mitochondrial protein was extracted, and mitochondrial function was examined in the follow-up experiment. The results showed that GSDMD-NT was enriched in mitochondria of both heart tissue and H9c2 cells (**Figures 6A,B**). The mitochondrial membrane potential and ATP level, as important indicators of mitochondrial function, were detected in H9c2 cells. The JC-1 assay results showed that LPS induced a significant change in fluorescence emission from red to green, which indicated MMP depolarization (**Figure 6C**). However, *Gsdmd* silencing reversed this shift and reduced the emission of green fluorescence. Moreover, GSDMD interference ameliorated the decline in ATP levels induced by LPS in H9c2 cells (**Figure 6D**). These results indicate that GSDMD-NT enrichment in mitochondria leads to mitochondrial dysfunction.

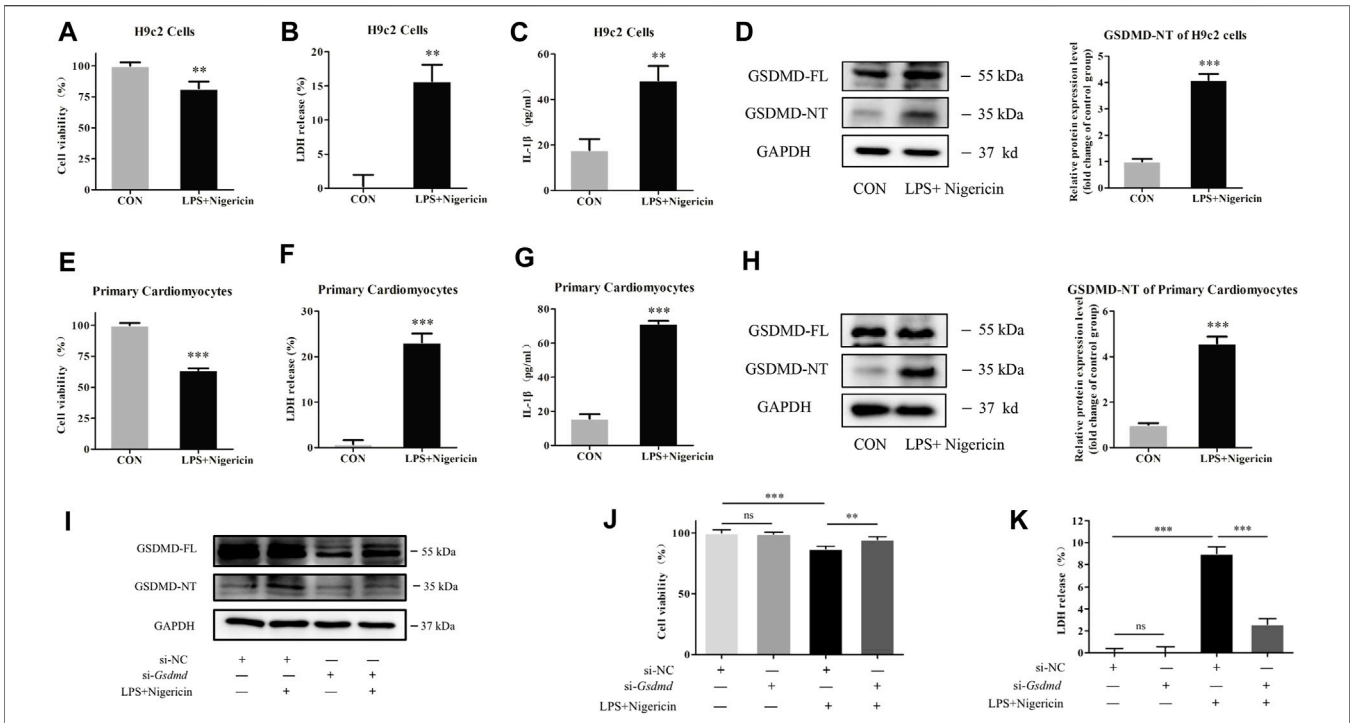

FIGURE 4 | GSDMD silencing alleviated myocardial cell injury induced by LPS. **(A and E)** CCK-8 assay was applied to measure cell viability of each group. **(B and F)** LDH release in supernatants of each group. **(C and G)** The level of IL-1β in supernatants of each group. **(D and H)** Expressions of GSDMD and GSDMD-NT protein in H9c2 cells and primary cardiomyocytes were measured by Western blotting analysis. The results were normalized to the expression of GAPDH. The data are expressed as the mean ± SD (n = 3). **(I)** After transfected with siRNA of *Gsdmd*, H9c2 cells were treated with LPS plus nigericin to establish the myocardial injury model. Expressions of GSDMD and GSDMD-NT protein in H9c2 cells were measured by Western blotting analysis (n = 3). **(J)** CCK-8 assay was applied to measure cell viability of each group. **(K)** LDH release in supernatants of each group. The data are expressed as the mean ± SD (n = 3). $^{**}p < 0.01$, $^{***}p < 0.001$.

GSDMD cleavage and insertion into the mitochondrial membrane likely drive ROS production. Next, ROS concentrations in H9c2 cells were evaluated. As shown in **Figure 6E**, LPS plus nigericin significantly increased the level of ROS in H9c2 cells. However, the ROS level was decreased when cells were transfected with siRNA targeting *Gsdmd*. Furthermore, the levels of MDA and SOD activity in the myocardium were detected to investigate oxidative stress injury induced by LPS. SOD is an antioxidant enzyme that is mainly responsible for the clearance of intracellular ROS. Its activity can reflect the ability of antioxidant enzymes to defend against free radical damage. MDA is a product of lipid oxidation and is related to the extent of oxidative damage (Haileselassie et al., 2017). The results showed that compared with the control group, LPS substantially increased MDA level and decreased SOD activity in myocardium of WT mice. While these changes were dramatically improved in the $Gsdmd^{-/-}$-LPS group (**Figures 6F,G**).

To investigate whether the increased ROS level is closely associated with the activation of the NLRP3 inflammasome and the corresponding induced cell injury, NAC, the ROS scavenger, was used in subsequent experiments to confirm the relationship between ROS and NLRP3 inflammasome. As shown in **Supplementary Figure S1A**, ROS production was increased by LPS and nigericin stimulation, while NAC treatment significantly decreased the production of ROS. Meanwhile, the cell death was remarkably reversed by NAC treatment in H9c2 cells induced by LPS and nigericin, indicated by increased cell viability and decreased LDH release ($p < 0.05$ and $p < 0.001$, **Supplementary Figure S1B,C**). Moreover, the expression of NLRP3 and cleaved caspase-1 proteins and IL-1β content in the supernatant were dramatically inhibited by NAC ($p < 0.001$, $p < 0.01$ and $p < 0.001$, **Supplementary Figures S1D,E**). These results showed that the activation of the NLRP3 inflammasome was closely linked with ROS generation.

DISCUSSION

The pathogenesis of sepsis-induced myocardial dysfunction has not been well clarified until now. It was reported that a persistent inflammatory response, elevated production of ROS, mitochondrial dysfunction, and autonomic nervous system dysregulation were involved. As a result, therapeutic approaches to reduce sepsis-induced myocardial dysfunction are limited. Treatment for this fatal condition is still based on antibiotics and supportive modalities (Howell & Davis, 2017). Therefore, it is essential to reveal the mechanisms of sepsis-induced myocardial dysfunction and explore new therapeutic targets and methods to reduce its damage. In this study, we found

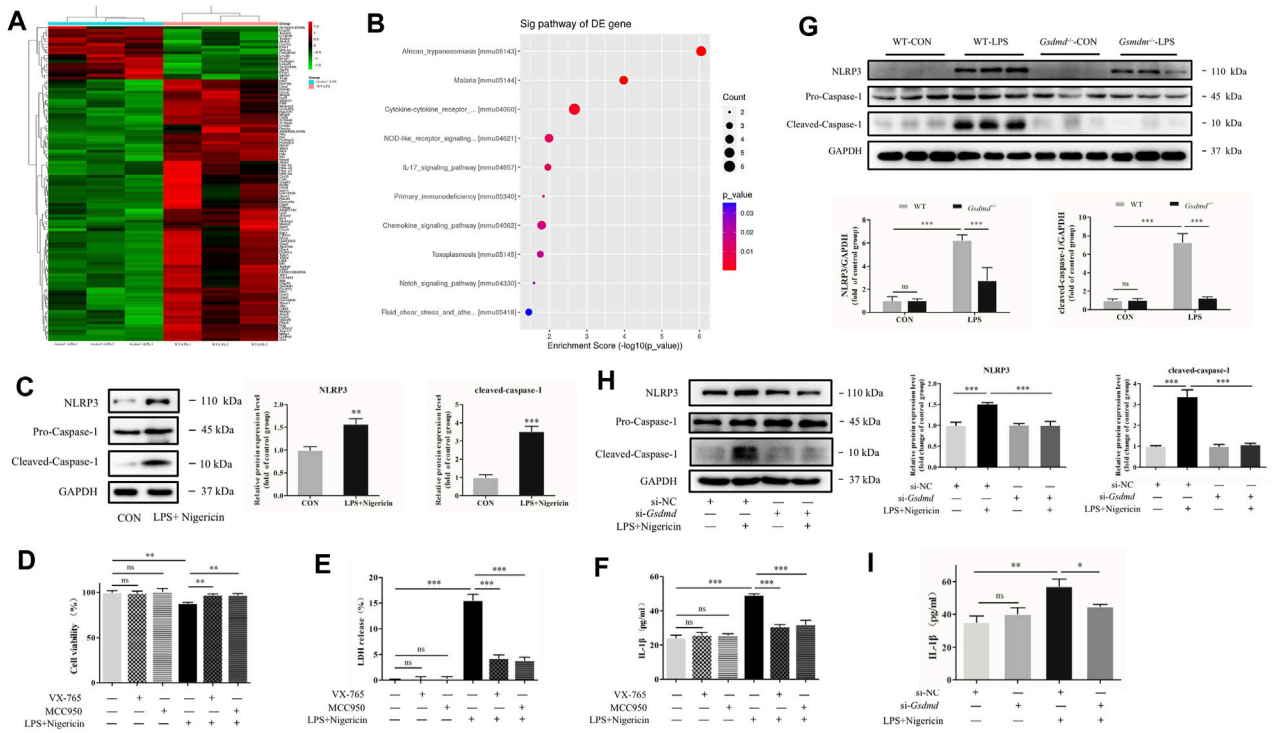

FIGURE 5 | GSDMD regulated NLRP3 inflammasome activation in septic myocardial dysfunction induced by LPS. **(A,B)** Heat map and Kyoto Encyclopedia of Genes and Genomes (KEGG) pathway analyses of the transcriptome of heart tissues from WT and *Gsdmd*$^{-/-}$ (n = 3) mice treated with LPS. **(C)** Expressions of NLRP3 and caspase-1 protein in H9c2 cells were measured by Western blotting analysis. The results were normalized to the expression of GAPDH. **(D)** H9c2 cells were pretreated with NLRP3 inhibitor or caspase-1 inhibitor for 1 h and subsequently stimulated with LPS plus nigericin. CCK-8 assay was applied to measure cell viability of each group (n = 4). **(E)** The LDH release in supernatants of each group (n = 3). **(F)** The level of IL-1β in supernatants of each group (n = 3). **(G)** Expressions of NLRP3 and caspase-1 protein in heart tissue were measured by Western blotting analysis. The results were normalized to the expression of GAPDH (n = 6). **(H)** After transfected with siRNA of *Gsdmd*, H9c2 cells were treated with LPS and nigericin to establish the myocardial injury model. Expressions of NLRP3, caspase-1, and P65 protein in H9c2 cells were measured by Western blotting analysis. The results were normalized to the expression of GAPDH (n = 3). **(I)** The level of IL-1β in supernatants of each group (n = 3). The data are expressed as the mean ± SD. *$p < 0.05$, **$p < 0.01$, ***$p < 0.001$.

that GSDMD-NT, the functional fragment of GSDMD, was upregulated in the heart tissue of septic WT mice induced by LPS, which was accompanied by decreased cardiac function and myocardial injury. GSDMD participated in cardiac inflammation, and resulted in LPS-induced myocardial injury and cell death, by enriching in mitochondria, leading to mitochondrial dysfunction and overproduction of ROS, further regulating the activation of the NLRP3 inflammasome. GSDMD plays an important role in the pathophysiology of LPS-induced myocardial dysfunction.

GSDMD, encoded by the *Gsdmd* gene of the gasdermin family, is widely expressed in different tissues and cells. After the action of relevant danger signals, canonical or noncanonical inflammasomes assemble, and activated inflammatory caspases cleave GSDMD to generate an N-terminal fragment (Liu et al., 2016; Yang J. et al., 2018). Then, GSDMD-NT transfers to the cell membrane and oligomerizes to form membrane pores, further destroying the cell membrane and mediating pyroptosis (Sborgi et al., 2016). In addition, study showed that overexpression of the N-terminal fragment could accelerate cell death, suggesting that GSDMD-NT is the functional component (Kayagaki et al., 2015). In this study, we found that the expression of GSDMD-NT in heart tissue was markedly increased after LPS treatment, accompanied by cardiac dysfunction and myocardial injury. However, *Gsdmd* deficiency attenuated myocardial injury and dysfunction in LPS-induced septic mice, and significantly improved survival outcomes. These results suggest that GSDMD is involved in the pathogenesis of sepsis-induced myocardial dysfunction. GSDMD might be used as a molecular target to protect the myocardium against LPS.

The molecular mechanisms by which GSDMD exerts its function in cardiac dysfunction induced by LPS were investigated subsequently. Inflammatory reaction is a prominent feature of sepsis. IL-1β and TNF-α have been proven to be important proinflammatory cytokines that drive the pathogenesis of cardiac inflammation and injury and magnify the effects of other cytokines, eventually resulting in cardiac dysfunction (Madorin et al., 2004; Kakihana et al., 2016). Moreover, inflammatory cytokines promote inflammatory cell extravasation into the cardiac interstitium. It was reported that there was an obvious negative relationship between the number of macrophages in the myocardium and cardiac function (Chen et al., 2016). Our results showed that *Gsdmd*$^{-/-}$ mice treated with LPS exhibited less severe inflammation than their WT littermates, as shown by reduced IL-1β and TNF-α levels in both the serum

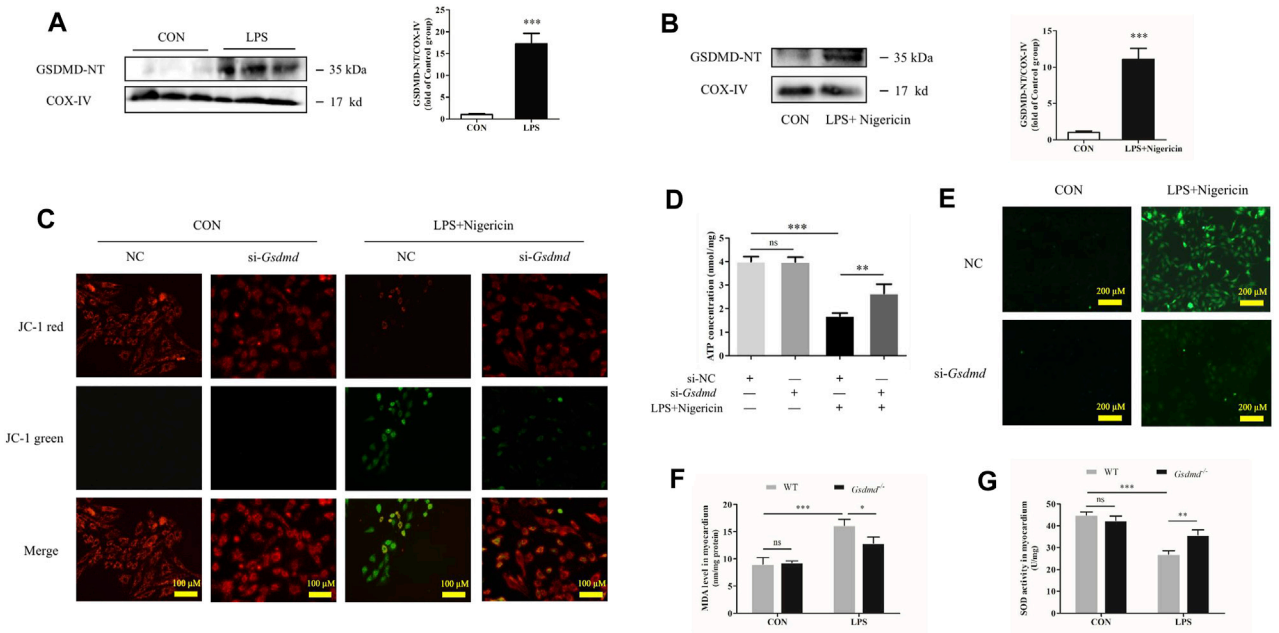

FIGURE 6 | GSDMD enrichment in mitochondria leads to mitochondrial dysfunction, ROS generation, and NLRP3 inflammasome activation. **(A)** Expressions of GSDMD-NT protein in mitochondria of heart tissue were measured by Western blotting analysis. The results were normalized to the expression of COX-IV (n = 6). **(B)** Expressions of GSDMD-NT protein in mitochondria of H9c2 cells were measured by Western blotting analysis. The results were normalized to the expression of COX-IV (n = 3). **(C)** Mitochondrial membrane potential was assessed by JC assays in each group. **(D)** ATP level in each group (n = 3). **(E)** ROS level in H9c2 cells. **(F)** MDA levels in heart tissue from each group. **(G)** SOD activity in heart tissue from each group. The data are expressed as the mean ± SD. $^{*}p < 0.05$, $^{**}p < 0.01$, $^{***}p < 0.001$.

and myocardium, as well as CD-68-positive cells and MPO activity in the myocardium. The NF-κB pathway has been reported to be a critical signaling pathway involved in the inflammatory response in sepsis, and cytokines, such as IL-1β and TNF-α, are associated with the activation of NF-κB (Sies et al., 2017). NF-κB is an important transcription factor that controls the expression of inflammatory cytokine genes (Zhang Q. et al., 2017). Therefore, key proteins in the NF-κB pathway were analyzed in this study. We found that the increased phosphorylation of p65 induced by LPS was markedly prevented by *Gsdmd* deficiency. These data suggested that the participation of GSDMD in sepsis-induced myocardial dysfunction might be partly relevant to the regulation of NF-κB activation and inflammatory response.

Moreover, gene sequencing analysis of myocardial tissue and further GO enrichment and KEGG pathway analyses were performed, which showed that the differentially expressed genes were significantly enriched in the NLR pathway. NLRP3, which belongs to the NLR family, plays a vital role in sepsis-induced myocardial dysfunction (Yang L. et al., 2018; Wang et al., 2018; Yang et al., 2019). Once activated, NLRP3 recruits apoptosis-associated speck-like protein containing a caspase recruitment domain (ASC) and caspase-1 to form NLRP3 inflammasomes. At the same time, caspase-1 is activated, which in turn promotes IL-1β and interleukin-18 (IL-18) maturation and secretion, leading to inflammatory responses (Lamkanfi & Dixit, 2014). Activated caspase-1 further cleaves GSDMD, resulting in inflammatory factor release and cellular injury (Liu et al., 2016; Sborgi et al., 2016). Our study found that the NLRP3 inflammasome was activated in myocardial injury induced by LPS. However, it is interesting to note that activation of the NLRP3 inflammasome induced by LPS is inhibited in *Gsdmd*$^{-/-}$ mice.

The NLRP3 inflammasome has been reported to be activated by potassium efflux and ROS (Zhou et al., 2011; Munoz-Planillo et al., 2013). Our study displayed the same finding that the activation of the NLRP3 inflammasome was closely linked with ROS generation. Evidence from previous studies reports that mitochondria are the main source of intracellular ROS in the myocardium during sepsis. Sepsis impairs cardiac mitochondria by damaging membrane integrity, which in turn increases ROS generation and oxidative stress (Zang et al., 2007). GSDMD-NT is a pore-forming protein with an affinity for cardiolipin-containing membranes (Liu et al., 2016). GSDMD-NT can not only bind to the plasmalemmal membrane, but also to the mitochondrial membrane (Ding et al., 2016), similar to other members of the gasdermin family, such as GSDMA and GSDME (Lin et al., 2015; Rogers et al., 2019). Cleaved GSDMD has been reported to be enriched in the mitochondrial membrane, leading to mitochondrial injury and mitochondrial ROS generation (Aglietti et al., 2016; Rogers et al., 2019). We speculate that GSDMD enrichment in the mitochondrial membrane triggers ROS generation and may be partially involved in the activation of NLRP3, as reported in a previous study (Platnich et al., 2018). Our study found that GSDMD-NT was enriched in mitochondria, which was accompanied by a decrease in MMP

and ATP in H9c2 cells. While interference with GSDMD expression improved MMP and ATP production. Normal MMP is required for mitochondrial oxidative phosphorylation and ATP production. The decreased MMP impairs mitochondrial oxidative phosphorylation, leading to abnormal electron transfer and increased ROS production (de Vasconcelos et al., 2019). Moreover, we also found that *Gsdmd* knockout reduced LPS-induced ROS production. The increase in MDA levels and decrease in SOD activity in LPS-WT mice were reversed in *Gsdmd*$^{-/-}$ mice treated with LPS, which supported the involvement of GSDMD in ROS production. These results suggest that the GSDMD-NT fragment aggregates in the mitochondrial membrane, leading to mitochondrial injury. Mitochondrial injury reduces mitochondrial membrane potential, resulting in increased ROS production and NLRP3 activation.

Mitochondria are energy production organelles that provide energy for heart contraction, and the heart is rich in mitochondria. It has been reported that the degree of mitochondrial dysfunction is tightly linked to sepsis-induced cardiac dysfunction and prognosis (Brealey et al., 2002; Suliman et al., 2004). Besides overproduction of ROS, mitochondrial dysfunction further mediates myocardial injury and dysfunction through impaired energy generation and metabolism. In addition, damaged mitochondria generate a significant amount of danger associated molecular patterns (DAMPs) during sepsis (Zhang et al., 2010), including mitochondrial ROS (mtROS), mitochondrial DNA (mtDNA) fragments and cytochrome C. These molecules participate in inciting inflammation or directly injure myocytes, resulting in myocardial dysfunction (Zang et al., 2012).

In conclusion, our study demonstrates that GSDMD not only mediates the release of inflammatory factors and the expansion of the inflammatory response but also causes mitochondrial injury, overproduction of ROS, and NLRP3 inflammasome activation. These factors interact with each other and ultimately lead to cardiac dysfunction. GSDMD plays an important role in septic myocardial dysfunction induced by LPS. Targeting GSDMD may serve as a therapeutic strategy for the prevention and treatment of septic myocardial dysfunction.

DATA AVAILABILITY STATEMENT

The original contributions presented in the study are included in the article/**Supplementary Material**, further inquiries can be directed to the corresponding authors.

ETHICS STATEMENT

All experimental procedures were approved by the Laboratory Animal Ethics Committee and Laboratory Animal Centre of Wenzhou Medical University.

AUTHOR CONTRIBUTIONS

ZL, LS, and SD contributed to design of the experiments. SD and BY conducted the entire study and wrote the manuscript. LZ and YC assisted in the experiments performed in animals. GH and GZ helped perform the analysis. All authors contributed to the article and approved the submitted version.

FUNDING

This work was supported by the National Natural Science Foundation of China (Grant No.81772112, 81871583 and 82003750), the Natural Science Foundation of Zhejiang Province (Grant No. LQ21H020009), the Key R and D Program Projects of Zhejiang Province (Grant No. 2021C03072), the Science and Technology Project of Wenzhou (Grant No. 20180105), and the Incubation Scientific Research Project of The First Affiliated Hospital of Wenzhou Medical University (Grant No. FHY2019018).

SUPPLEMENTARY MATERIAL

The Supplementary Material for this article can be found online at: https://www.frontiersin.org/articles/10.3389/fcell.2021.779432/full#supplementary-material

REFERENCES

Aachoui, Y., Leaf, I. A., Hagar, J. A., Fontana, M. F., Campos, C. G., Zak, D. E., et al. (2013). Caspase-11 Protects against Bacteria that Escape the Vacuole. *Science* 339, 975–978. doi:10.1126/science.1230751

Agard, N. J., Maltby, D., and Wells, J. A. (2010). Inflammatory Stimuli Regulate Caspase Substrate Profiles. *Mol. Cell Proteomics* 9, 880–893. doi:10.1074/mcp.M900528-MCP200

Aglietti, R. A., Estevez, A., Gupta, A., Ramirez, M. G., Liu, P. S., Kayagaki, N., et al. (2016). GsdmD P30 Elicited by Caspase-11 during Pyroptosis Forms Pores in Membranes. *Proc. Natl. Acad. Sci. USA* 113, 7858–7863. doi:10.1073/pnas.1607769113

Alves-Filho, J. C., de Freitas, A., Spiller, F., Souto, F. O., and Cunha, F. Q. (2008). The Role of Neutrophils in Severe Sepsis. *Shock* 30 (Suppl. 1), 3–9. doi:10.1097/SHK.0b013e3181818466

Baker, R. G., Hayden, M. S., and Ghosh, S. (2011). NF-κB, Inflammation, and Metabolic Disease. *Cel Metab.* 13, 11–22. doi:10.1016/j.cmet.2010.12.008

Brealey, D., Brand, M., Hargreaves, I., Heales, S., Land, J., Smolenski, R., et al. (2002). Association between Mitochondrial Dysfunction and Severity and Outcome of Septic Shock. *The Lancet* 360, 219–223. doi:10.1016/S0140-6736(02)09459-X

Charpentier, J., Luyt, C.-E., Fulla, Y., Vinsonneau, C., Cariou, A., Grabar, S., et al. (2004). Brain Natriuretic Peptide: A Marker of Myocardial Dysfunction and Prognosis during Severe Sepsis. *Crit. Care Med.* 32, 660–665. doi:10.1097/01.ccm.0000114827.93410.d8

Chen, J., Lai, J., Yang, L., Ruan, G., Chaugai, S., Ning, Q., et al. (2016). Trimetazidine Prevents Macrophage-Mediated Septic Myocardial Dysfunction via Activation of the Histone Deacetylase Sirtuin 1. *Br. J. Pharmacol.* 173, 545–561. doi:10.1111/bph.13386

Cheng, K. T., Xiong, S., Ye, Z., Hong, Z., Di, A., Tsang, K. M., et al. (2017). Caspase-11-mediated Endothelial Pyroptosis Underlies Endotoxemia-Induced Lung Injury. *J. Clin. Invest.* 127, 4124–4135. doi:10.1172/JCI94495

Cimolai, M., Alvarez, S., Bode, C., and Bugger, H. (2015). Mitochondrial Mechanisms in Septic Cardiomyopathy. *Ijms* 16, 17763–17778. doi:10.3390/ijms160817763

de Montmollin, E., Aboab, J., Mansart, A., and Annane, D. (2009). Bench-to-bedside Review: β-Adrenergic Modulation in Sepsis. *Crit. Care* 13, 230. doi:10.1186/cc8026

de Vasconcelos, N. M., Van Opdenbosch, N., Van Gorp, H., Parthoens, E., and Lamkanfi, M. (2019). Single-cell Analysis of Pyroptosis Dynamics Reveals Conserved GSDMD-Mediated Subcellular Events that Precede Plasma Membrane Rupture. *Cell Death Differ* 26, 146–161. doi:10.1038/s41418-018-0106-7

Ding, J., Wang, K., Liu, W., She, Y., Sun, Q., Shi, J., et al. (2016). Pore-forming Activity and Structural Autoinhibition of the Gasdermin Family. *Nature* 535, 111–116. doi:10.1038/nature18590

Drosatos, K., Lymperopoulos, A., Kennel, P. J., Pollak, N., Schulze, P. C., and Goldberg, I. J. (2015). Pathophysiology of Sepsis-Related Cardiac Dysfunction: Driven by Inflammation, Energy Mismanagement, or Both? *Curr. Heart Fail. Rep.* 12, 130–140. doi:10.1007/s11897-014-0247-z

Essandoh, K., Yang, L., Wang, X., Huang, W., Qin, D., Hao, J., et al. (2015). Blockade of Exosome Generation with GW4869 Dampens the Sepsis-Induced Inflammation and Cardiac Dysfunction. *Biochim. Biophys. Acta (Bba) - Mol. Basis Dis.* 1852, 2362–2371. doi:10.1016/j.bbadis.2015.08.010

Haileselassie, B., Su, E., Pozios, I., Niño, D. F., Liu, H., Lu, D.-Y., et al. (2017). Myocardial Oxidative Stress Correlates with Left Ventricular Dysfunction on Strain Echocardiography in a Rodent Model of Sepsis. *ICMx* 5, 21. doi:10.1186/s40635-017-0134-5

Howell, M. D., and Davis, A. M. (2017). Management of Sepsis and Septic Shock. *JAMA* 317, 847–848. doi:10.1001/jama.2017.0131

Huang, L. S., Hong, Z., Wu, W., Xiong, S., Zhong, M., Gao, X., et al. (2020). mtDNA Activates cGAS Signaling and Suppresses the YAP-Mediated Endothelial Cell Proliferation Program to Promote Inflammatory Injury. *Immunity* 52, 475–486. doi:10.1016/j.immuni.2020.02.002

Jeong, H. S., Lee, T. H., Bang, C. H., Kim, J.-H., and Hong, S. J. (2018). Risk Factors and Outcomes of Sepsis-Induced Myocardial Dysfunction and Stress-Induced Cardiomyopathy in Sepsis or Septic Shock. *Medicine (Baltimore)* 97, e0263. doi:10.1097/MD.0000000000010263

Jia, C., Chen, H., Zhang, J., Zhou, K., Zhuge, Y., Niu, C., et al. (2019). Role of Pyroptosis in Cardiovascular Diseases. *Int. Immunopharmacology* 67, 311–318. doi:10.1016/j.intimp.2018.12.028

Kakihana, Y., Ito, T., Nakahara, M., Yamaguchi, K., and Yasuda, T. (2016). Sepsis-induced Myocardial Dysfunction: Pathophysiology and Management. *J. Intensive Care* 4, 22. doi:10.1186/s40560-016-0148-1

Kayagaki, N., Stowe, I. B., Lee, B. L., O'Rourke, K., Anderson, K., Warming, S., et al. (2015). Caspase-11 Cleaves Gasdermin D for Non-canonical Inflammasome Signalling. *Nature* 526, 666–671. doi:10.1038/nature15541

Lamkanfi, M., and Dixit, V. M. (2014). Mechanisms and Functions of Inflammasomes. *Cell* 157, 1013–1022. doi:10.1016/j.cell.2014.04.007

Li, N., Zhou, H., Wu, H., Wu, Q., Duan, M., Deng, W., et al. (2019). STING-IRF3 Contributes to Lipopolysaccharide-Induced Cardiac Dysfunction, Inflammation, Apoptosis and Pyroptosis by Activating NLRP3. *Redox Biol.* 24, 101215. doi:10.1016/j.redox.2019.101215

Liang, Y.-D., Bai, W.-J., Li, C.-G., Xu, L.-H., Wei, H.-X., Pan, H., et al. (2016). Piperine Suppresses Pyroptosis and Interleukin-1β Release upon ATP Triggering and Bacterial Infection. *Front. Pharmacol.* 7, 390. doi:10.3389/fphar.2016.00390

Lin, P.-H., Lin, H.-Y., Kuo, C.-C., and Yang, L.-T. (2015). N-terminal Functional Domain of Gasdermin A3 Regulates Mitochondrial Homeostasis via Mitochondrial Targeting. *J. Biomed. Sci.* 22, 44. doi:10.1186/s12929-015-0152-0

Liu, X., Zhang, Z., Ruan, J., Pan, Y., Magupalli, V. G., Wu, H., et al. (2016). Inflammasome-activated Gasdermin D Causes Pyroptosis by Forming Membrane Pores. *Nature* 535, 153–158. doi:10.1038/nature18629

Loppnow, H., Werdan, K., Reuter, G., and Flad, H. D. (1998). The Interleukin-1 and Interleukin-1 Converting Enzyme Families in the Cardiovascular System. *Eur. Cytokine Netw.* 9, 675–680.

Madorin, W. S., Rui, T., Sugimoto, N., Handa, O., Cepinskas, G., and Kvietys, P. R. (2004). Cardiac Myocytes Activated by Septic Plasma Promote Neutrophil Transendothelial Migration. *Circ. Res.* 94, 944–951. doi:10.1161/01.res.0000124395.20249.ae

Miao, E. A., Leaf, I. A., Treuting, P. M., Mao, D. P., Dors, M., Sarkar, A., et al. (2010). Caspase-1-induced Pyroptosis Is an Innate Immune Effector Mechanism against Intracellular Bacteria. *Nat. Immunol.* 11, 1136–1142. doi:10.1038/ni.1960

Muñoz-Planillo, R., Kuffa, P., Martínez-Colón, G., Smith, B. L., Rajendiran, T. M., and Núñez, G. (2013). K+ Efflux Is the Common Trigger of NLRP3 Inflammasome Activation by Bacterial Toxins and Particulate Matter. *Immunity* 38, 1142–1153. doi:10.1016/j.immuni.2013.05.016

Neri, M., Riezzo, I., Pomara, C., Schiavone, S., and Turillazzi, E. (20162016). Oxidative-Nitrosative Stress and Myocardial Dysfunctions in Sepsis: Evidence from the Literature and Postmortem Observations. *Mediators Inflamm.* 2016, 1–12. doi:10.1155/2016/3423450

Platnich, J. M., Chung, H., Lau, A., Sandall, C. F., Bondzi-Simpson, A., Chen, H.-M., et al. (2018). Shiga Toxin/Lipopolysaccharide Activates Caspase-4 and Gasdermin D to Trigger Mitochondrial Reactive Oxygen Species Upstream of the NLRP3 Inflammasome. *Cel Rep.* 25, 1525–1536. doi:10.1016/j.celrep.2018.09.071

Rathkey, J. K., Zhao, J., Liu, Z., Chen, Y., Yang, J., Kondolf, H. C., et al. (2018). Chemical Disruption of the Pyroptotic Pore-Forming Protein Gasdermin D Inhibits Inflammatory Cell Death and Sepsis. *Sci. Immunol.* 3, eaat2738. doi:10.1126/sciimmunol.aat2738

Rogers, C., Erkes, D. A., Nardone, A., Aplin, A. E., Fernandes-Alnemri, T., and Alnemri, E. S. (2019). Gasdermin Pores Permeabilize Mitochondria to Augment Caspase-3 Activation during Apoptosis and Inflammasome Activation. *Nat. Commun.* 10, 1689. doi:10.1038/s41467-019-09397-2

Rudiger, A., and Singer, M. (2007). Mechanisms of Sepsis-Induced Cardiac Dysfunction. *Crit. Care Med.* 35, 1599–1608. doi:10.1097/01.CCM.0000266683.64081.02

Sborgi, L., Rühl, S., Mulvihill, E., Pipercevic, J., Heilig, R., Stahlberg, H., et al. (2016). GSDMD Membrane Pore Formation Constitutes the Mechanism of Pyroptotic Cell Death. *EMBO J.* 35, 1766–1778. doi:10.15252/embj.201694696

Shi, J., Zhao, Y., Wang, K., Shi, X., Wang, Y., Huang, H., et al. (2015). Cleavage of GSDMD by Inflammatory Caspases Determines Pyroptotic Cell Death. *Nature* 526, 660–665. doi:10.1038/nature15514

Sies, H., Berndt, C., and Jones, D. P. (2017). Oxidative Stress. *Annu. Rev. Biochem.* 86, 715–748. doi:10.1146/annurev-biochem-061516-045037

Smeding, L., Plötz, F. B., Groeneveld, A. B. J., and Kneyber, M. C. J. (2012). Structural Changes of the Heart during Severe Sepsis or Septic Shock. *Shock* 37, 449–456. doi:10.1097/SHK.0b013e31824c3238

Suliman, H., Weltywolf, K., Carraway, M., Tatro, L., and Piantadosi, C. (2004). Lipopolysaccharide Induces Oxidative Cardiac Mitochondrial Damage and Biogenesis. *Cardiovasc. Res.* 64, 279–288. doi:10.1016/j.cardiores.2004.07.005

Vieillard-Baron, A., Caille, V., Charron, C., Belliard, G., Page, B., and Jardin, F. (2008). Actual Incidence of Global Left Ventricular Hypokinesia in Adult Septic Shock. *Crit. Care Med.* 36, 1701–1706. doi:10.1097/CCM.0b013e318174db05

Wang, Z., Hu, W., Lu, C., Ma, Z., Jiang, S., Gu, C., et al. (2018). Targeting NLRP3 (Nucleotide-Binding Domain, Leucine-Rich-Containing Family, Pyrin Domain-Containing-3) Inflammasome in Cardiovascular Disorders. *Atvb* 38, 2765–2779. doi:10.1161/ATVBAHA.118.311916

Yang, C., Xia, W., Liu, X., Lin, J., and Wu, A. (2019). Role of TXNIP/NLRP3 in Sepsis-Induced Myocardial Dysfunction. *Int. J. Mol. Med.* 44, 417–426. doi:10.3892/ijmm.2019.4232

Yang, J., Liu, Z., Wang, C., Yang, R., Rathkey, J. K., Pinkard, O. W., et al. (2018a). Mechanism of Gasdermin D Recognition by Inflammatory Caspases and Their Inhibition by a Gasdermin D-Derived Peptide Inhibitor. *Proc. Natl. Acad. Sci. USA* 115, 6792–6797. doi:10.1073/pnas.1800562115

Yang, L., Zhang, H., and Chen, P. (2018b). Sulfur Dioxide Attenuates Sepsis-Induced Cardiac Dysfunction via Inhibition of NLRP3 Inflammasome Activation in Rats. *Nitric Oxide* 81, 11–20. doi:10.1016/j.niox.2018.09.005

Ye, B., Chen, X., Dai, S., Han, J., Liang, X., Lin, S., et al. (2019a). Emodin Alleviates Myocardial Ischemia/reperfusion Injury by Inhibiting Gasdermin D-Mediated Pyroptosis in Cardiomyocytes. *Dddt* 13, 975–990. doi:10.2147/DDDT.S195412

Ye, Z., Zhang, L., Li, R., Dong, W., Liu, S., Li, Z., et al. (2019b). Caspase-11 Mediates Pyroptosis of Tubular Epithelial Cells and Septic Acute Kidney Injury. *Kidney Blood Press. Res.* 44, 465–478. doi:10.1159/000499685

Zang, Q., Maass, D. L., Tsai, S. J., and Horton, J. W. (2007). Cardiac Mitochondrial Damage and Inflammation Responses in Sepsis. *Surg. Infections* 8, 41–54. doi:10.1089/sur.2006.033

Zang, Q. S., Sadek, H., Maass, D. L., Martinez, B., Ma, L., Kilgore, J. A., et al. (2012). Specific Inhibition of Mitochondrial Oxidative Stress Suppresses Inflammation and Improves

Cardiac Function in a Rat Pneumonia-Related Sepsis Model. *Am. J. Physiology-Heart Circulatory Physiol.* 302, H1847–H1859. doi:10.1152/ajpheart.00203.2011

Zhang, Q., Lenardo, M. J., and Baltimore, D. (2017a). 30 Years of NF-Kb: A Blossoming of Relevance to Human Pathobiology. *Cell* 168, 37–57. doi:10.1016/j.cell.2016.12.012

Zhang, Q., Raoof, M., Chen, Y., Sumi, Y., Sursal, T., Junger, W., et al. (2010). Circulating Mitochondrial DAMPs Cause Inflammatory Responses to Injury. *Nature* 464, 104–107. doi:10.1038/nature08780

Zhang, W., Tao, A., Lan, T., Cepinskas, G., Kao, R., Martin, C. M., et al. (2017b). Carbon Monoxide Releasing Molecule-3 Improves Myocardial Function in Mice with Sepsis by Inhibiting NLRP3 Inflammasome Activation in Cardiac Fibroblasts. *Basic Res. Cardiol.* 112, 16. doi:10.1007/s00395-017-0603-8

Zhong, J., Hwang, T.-C., Adams, H. R., and Rubin, L. J. (1997). Reduced L-type Calcium Current in Ventricular Myocytes from Endotoxemic guinea Pigs. *Am. J. Physiology-Heart Circulatory Physiol.* 273, H2312–H2324. doi:10.1152/ajpheart.1997.273.5.H2312

Zhou, R., Yazdi, A. S., Menu, P., and Tschopp, J. (2011). A Role for Mitochondria in NLRP3 Inflammasome Activation. *Nature* 469, 221–225. doi:10.1038/nature09663

Conflict of Interest: The authors declare that the research was conducted in the absence of any commercial or financial relationships that could be construed as a potential conflict of interest. The authors report no conflicts of interest in this work.

Publisher's Note: All claims expressed in this article are solely those of the authors and do not necessarily represent those of their affiliated organizations, or those of the publisher, the editors and the reviewers. Any product that may be evaluated in this article, or claim that may be made by its manufacturer, is not guaranteed or endorsed by the publisher.

Copyright © 2021 Dai, Ye, Zhong, Chen, Hong, Zhao, Su and Lu. This is an open-access article distributed under the terms of the Creative Commons Attribution License (CC BY). The use, distribution or reproduction in other forums is permitted, provided the original author(s) and the copyright owner(s) are credited and that the original publication in this journal is cited, in accordance with accepted academic practice. No use, distribution or reproduction is permitted which does not comply with these terms.

frontiers in Cell and Developmental Biology

REVIEW
published: 26 November 2021
doi: 10.3389/fcell.2021.794879

Programmed Cell Death: Complex Regulatory Networks in Cardiovascular Disease

*Liuhua Zhou†, Jiateng Sun†, Lingfeng Gu, Sibo Wang, Tongtong Yang, Tianwen Wei, Tiankai Shan, Hao Wang and Liansheng Wang**

Department of Cardiology, The First Affiliated Hospital of Nanjing Medical University, Nanjing, China

Abnormalities in programmed cell death (PCD) signaling cascades can be observed in the development and progression of various cardiovascular diseases, such as apoptosis, necrosis, pyroptosis, ferroptosis, and cell death associated with autophagy. Aberrant activation of PCD pathways is a common feature leading to excessive cardiac remodeling and heart failure, involved in the pathogenesis of various cardiovascular diseases. Conversely, timely activation of PCD remodels cardiac structure and function after injury in a spatially or temporally restricted manner and corrects cardiac development similarly. As many cardiovascular diseases exhibit abnormalities in PCD pathways, drugs that can inhibit or modulate PCD may be critical in future therapeutic strategies. In this review, we briefly describe the process of various types of PCD and their roles in the occurrence and development of cardiovascular diseases. We also discuss the interplay between different cell death signaling cascades and summarize pharmaceutical agents targeting key players in cell death signaling pathways that have progressed to clinical trials. Ultimately a better understanding of PCD involved in cardiovascular diseases may lead to new avenues for therapy.

Keywords: cardiovascular diseases, programmed cell death, apoptosis, necrosis, autophagy, pyroptosis, ferroptosis, drug therapy

OPEN ACCESS

Edited by:
Zhi Qi,
Nankai University, China

Reviewed by:
Yaozu Xiang,
Tongji University, China
Elena Grossini,
University of Eastern Piedmont, Italy

****Correspondence:***
Liansheng Wang
drlswang@njmu.edu.cn

†These authors have contributed equally to this work and share the first authorship

Specialty section:
This article was submitted to Cell Death and Survival, a section of the journal Frontiers in Cell and Developmental Biology

Received: *14 October 2021*
Accepted: *15 November 2021*
Published: *26 November 2021*

Citation:
Zhou L, Sun J, Gu L, Wang S, Yang T, Wei T, Shan T, Wang H and Wang L (2021) Programmed Cell Death: Complex Regulatory Networks in Cardiovascular Disease. Front. Cell Dev. Biol. 9:794879. doi: 10.3389/fcell.2021.794879

BACKGROUND

The development and homeostasis of multicellular organisms depend not only on the regulation of cell survival and renewal, but also on the processing of those cells that are no longer needed or pose a potential danger to the organism. This includes the removal of cells at risk of neoplastic transformation or those infected by pathogens (Kramer et al., 2012; Saunders et al., 2015; Zhu and Sun, 2018). Programmed cell death (PCD) is the primary approach organisms adapt to eliminate these abnormal cells, which stimulates membrane-bound and cytoplasmic proteins by developmental programs and stress-induced signaling, triggering cell death through complex cascade transcriptional and post-translational protein modifications (Shi et al., 2017). Several types of PCD have been discovered in the past 3 decades: autophagy, necrosis, ferroptosis, apoptosis, and pyroptosis (Bai et al., 2017). Each type of PCD has its unique characteristics. Apoptosis represents the coordinated disassembly of dead cells and typical "immune silencing" clearance, while pyroptosis and necrosis refer to the relatively "violent" type of cell death, characterized by the rupture of dead cells, from which effective inflammatory inducers are released (Kung et al., 2011). Autophagy is an evolutionarily conserved catabolic process that begins with forming autophagosomes, a double-membrane-bound structure surrounding

cytoplasmic macromolecules and organelles which are ultimately recycled (Nishida and Otsu, 2008; Oka et al., 2012). In addition, another novel iron-dependent PCD mode, ferroptosis, is mainly caused by the peroxidation of unsaturated fatty acids highly expressed on the cell membrane under the action of divalent iron or ester oxygenase inducing cell death (Dixon et al., 2012; Ma et al., 2017). At present, research on PCD is generally limited to a single type, and reports on synergistic or antagonistic effects between different types of PCD are rare.

At present, increasing studies suggest that PCD is a significant cause of cardiovascular diseases such as ischemia/reperfusion (I/R) injury, myocardial infarction (MI) and cardiomyopathy (Tower, 2015; Yang et al., 2016). Each PCD plays a vital role in maintaining cellular homeostasis. Apoptosis ensures the normal development and tissue homeostasis of mature organisms, as well as pyroptosis, ferroptosis, and necrosis protect the host from pathogens and other external threats (Kung et al., 2011; Dixon et al., 2012; Corbalan et al., 2016; Vande Walle and Lamkanfi, 2016). Unlike apoptosis and other PCD, autophagy may commit suicide by undergoing cell death and responding to excessive stress. This view is supported by the analysis of different PCD pathways (Sciarretta et al., 2012). Increasing evidence indicates that different PCD pathways in cardiovascular diseases are associated and interplayed at multiple levels. Still, no article had made a systematic study and report on this issue.

Moreover, many clinical trials have found that the application of appropriate drugs could target cell death signaling pathways in cardiovascular diseases. A clinical phase 2 trial of simvastatin found that targeting inhibition of apoptosis through miR-15a-5p could protect the myocardium in non-coronary surgery, and another trial of berberine found that it could regulate myocardial autophagy through AMPK/mTOR pathway to promote myocardial protection in postoperative patients (Qing et al., 2018; Zhou et al., 2018). However, all the existing studies focus on the targeted therapy through a single type of PCD signaling pathway in cardiovascular diseases. Hitherto, there are no relevant reviews systematically analyzing and collating the interplay of different drugs in cardiovascular diseases through crosstalk between different types of PCD signaling pathways.

Here, we discuss the role of PCD in cardiovascular disease, the interactions between different PCD signaling cascades, and describe the application of drugs targeting cell death signaling pathways in cardiovascular pathology. Moreover, we summarize the latest progress on the relevant studies that have progressed to clinical trials and put forward a novel understanding for the better transformation of PCD pathways in cardiovascular medicine.

DIFFERENT TYPES OF PCD AND MOLECULAR MECHANISMS IN CARDIOVASCULAR DISEASES

Apoptosis Pathways in Cardiovascular Diseases

Apoptosis is usually induced by intrinsic and extrinsic (also known as death receptor-mediated) triggers. The intrinsic pathway, also called the mitochondrial or Bcl-2-mediated pathway, is activated by Bh3 proteins (Bim, Puma, Bid, Bmf, Bad, Hrk, Bik, Noxa) to initiate apoptosis when facing intracellular stress caused by various physicochemical factors (Dong et al., 2019). Activated Bax and Bak then form oligomers that promote the activation of the caspase cascade by releasing downstream apoptotic factors such as cytochrome c and Smac/DIABLO from mitochondria, resulting in ultimate protein cleavage and cell death. Extrinsic pathway, also known as death receptor pathway, is the binding and activation of death receptors such as tumor necrosis factor receptor (TNFR) superfamily members, Fas/Fas ligand (FasL) system members and death receptor family members (DR3, DR4 and DR5) with corresponding ligands to form intracellular death-inducing signaling complexes, which activate caspase-8 and its effector (Wang et al., 2021a). However, in normal cells, the Bcl-2 protein family (Bcl-2, Bcl-xl, Mcl-1, Bcl-W, and A1/BFL1) protects cell survival by inhibiting Bax and Bak (**Figure 1**).

It has been found that myocardial apoptosis can simultaneously exert detrimental effects on cardiac function. For instance, Wu et al. found that bradykinin (BK) could reduce myocardial apoptosis by reducing caspase-3 expression in a human cardiac c-Kit + progenitor cell (hCPCs) myocardial infarction model, thereby improving ischemic heart disease (Wu et al., 2021a), Uberti F et al. showed that levosimendan could interfere with mitochondrial function by regulating mitoK (ATP) channels and NO, and could control the interaction between autophagy and apoptosis to protect H9c2 cells against oxidative damage (Uberti et al., 2011), Nie et al. reported that lncRNA AK006774 could reduce I/R-induced infarct size and myocardial apoptosis by regulating Bcl-2 expression through miR-448 in a mouse I/R model (Nie et al., 2021), Xu et al. found that GSK-3β upregulated CD47 expression in cardiac tissues after MI by activating NF-κb, and then regulated apoptosis leading to myocardial injury (Xu et al., 2021). Besides, AKT1/GSK3β, NF-κb, and other related signaling molecules can also regulate apoptosis in cardiovascular diseases (**Supplementary Table S1**) (Shen et al., 2020; Jiang et al., 2021a; Wang et al., 2021a; Jiang et al., 2021b; He et al., 2021; Lu et al., 2021; Sun et al., 2021; Xiong et al., 2021; Xu et al., 2021).

Necrosis Pathways in Cardiovascular Diseases

Necrosis is a type of PCD characterized by lytic necrosis and could drive inflammation, in which the RIPK1/RIPK3/MLKL axis may play an essential role (Chen et al., 2020; She et al., 2019). Receptor-interacting protein kinase1 (RIPK1) autophosphorylation is activated by RIPK3/MLKL sequence, induces membrane permeability and cell destruction to release cell damage-associated molecular pattern (cDAMP), and finally leads to the occurrence of cell necrosis (Zhu and Sun, 2018). Caspase-8 activation, on the other hand, could inhibit cell necrosis by cleaving RIPK1 and RIPK3 (**Figure 1**). In their study, M.I. Oerlemans et al. demonstrated that RIPK1, RIPK3, and mixed lineage kinase domain-like (MLKL) expression was up-regulated in the myocardium after reperfusion, and the

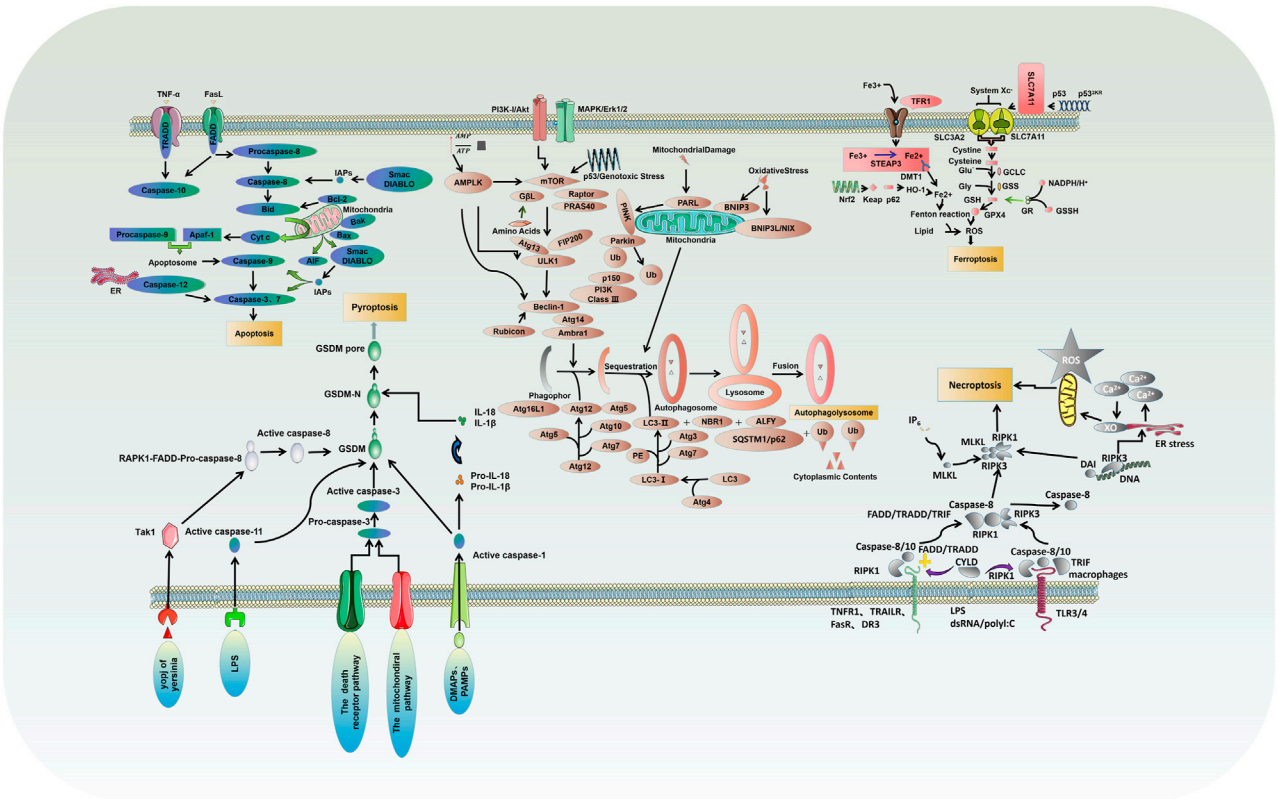

FIGURE 1 | Molecular mechanisms of different types of PCD: critical molecular pathways of autophagy, apoptosis, necrosis, pyroptosis and ferroptosis.

necrosis inhibitor Necrostatin-1 could reduce the phosphorylation levels of RIPK1 and RIPK3 and the recruitment of MLKL, thus inhibiting cell necrosis and reducing myocardial infarct size (Oerlemans et al., 2012). Currently, I/R models are preferred to elucidate the effect of different factors on cardiomyocyte necrosis through various pathways such as mechanistic target of rapamycin (mTOR), rate-oxygenation (ROX) and MLKL (**Supplementary Table S2**) (Yang et al., 2018a; Zhu et al., 2018; She et al., 2019; Chen et al., 2020; Jiang et al., 2021c; Han et al., 2021; Liu et al., 2021; Pullaiah et al., 2021; Zhang et al., 2021).

Ferroptosis Pathways in Cardiovascular Diseases

Ferroptosis, characterized by mitochondrial atrophy, increased membrane density, and reduced mitochondrial cristae, is a new form of PCD discovered recently, which proceeds with cell morphology and function different from the various modes of death described above (Dixon et al., 2012). Ferroptosis is usually executed by compressive lipid peroxidation and inhibited by iron chelators. In recent years, research has gradually unveiled its mystery, and many characteristic molecules are identified: acyl-CoA synthetase long-chain family 4 and lysophosphatidylcholine acyltransferase 3 (ACSL4 and LPCAT3) of membrane lipids susceptible to oxidation, xCT of the glutamate-cystine reverse transport system, glutathione peroxidase 4 (GPX4), and ferroptosis inhibitor protein 1, etc. (**Figure 1**) (Chen et al., 2019; Li et al., 2019).

Current studies have found that cardiovascular diseases caused by high iron levels are associated with ferroptosis (Wu et al., 2021b). Baba et al. have demonstrated that rapamycin could protect cardiomyocytes from excess iron-induced ferroptosis by reacting with mechanistic targets (Baba et al., 2018). Ferrostatin-1 (Fer-1) is an inhibitor of ferroptosis and can mediate the death of cardiomyocytes and neutrophil recruitment after heart transplantation through the toll-like receptor 4/interferon-β (TLR4/TRIF) signaling pathway (Li et al., 2019). Studies also indicate that other signaling molecules such as NADPH oxidase 4 (NOX4) and GPX4 regulate ferroptosis and thus affect heart disease (**Supplementary Table S3**). Ferroptosis is increasingly considered a potential cause of cardiovascular morbidity, and inhibition of ferroptosis represents a new strategy for these patients (Liu et al., 2018a; Bai et al., 2018; Chen et al., 2019; Fang et al., 2019; Feng et al., 2019; Fan et al., 2021).

Autophagy Pathways in Cardiovascular Diseases

Autophagy is a highly conserved catalytic process that leads to the autolysosomal degradation of primary cytoplasmic contents, removing abnormally aggregated proteins and excess

organelles. Generally, the activation of autophagy is triggered by undernutrition and oxidative stress (Dong et al., 2019). It is also associated with many other physiological and pathological processes, such as development, differentiation, neurodegenerative diseases, stress, infection, and cancer. Autophagy can be classified into three types: macroautophagy, microautophagy, and partner-mediated autophagy (Moujalled et al., 2021). mTOR is an important regulatory molecule that induces autophagy, and activating mTOR by phosphatidylinositol 3-kinase (PI3K) and mitogen-activated protein kinase (MARK) transduction can inhibit autophagy. In contrast, the negative regulation of mTOR by adenosine monophosphate-activated protein kinase (AMPK) and p53 signal transduction promotes autophagy (Dong et al., 2019; Shi et al., 2020). The formed mTOR complex is extensively linked to the downstream autophagy-related gene (ATG) family to construct the autophagosomes and ultimately complete the process of ubiquitin-like reactions. There is an extensive interaction between autophagy and apoptosis, which can be positively or negatively connected. Some studies have suggested the apoptosis-protective factor Bcl-2 could inhibit Beclin-1 dependent autophagy and function as its anti-autophagy regulatory molecule (**Figure 1**) (Oka et al., 2012; Grootaert et al., 2015; Dong et al., 2019).

In the normal physiological state of the heart, cardiomyocytes, vascular epithelial cells, and smooth muscle cells, autophagy plays an essential role in organelle function and cell renewal. Autophagy is also activated in response to cardiovascular stress, including I/R and heart failure. Sciarretta S et al. found that in ischemic stress, Rheb, as a GTP-binding protein, could inhibit autophagy by activating mTORC1, thereby aggravating post-ischemic infarct size (Sciarretta et al., 2012). During heart failure and aortic atherosclerosis, miR-212/132, laminar flow and Danqi pills regulated autophagy by modulating autophagy-related pathways and molecules, affecting cardiac function (**Supplementary Table S4**) (Oka et al., 2012; Shi et al., 2020; Grootaert et al., 2015; Ucar et al., 2012; Yuan et al., 2020; Wang et al., 2021b). As mentioned before, autophagy restricted to an appropriate extent protects against ischemic injury via maintaining cardiomyocyte homeostasis, degrading organelles, or misfolding proteins that produce adenosine triphosphate (ATP). However, it is also reported that overwhelming cardiac autophagy induction may also promote cell death and worsen cardiac function in the setting of severe ischemia. Some studies have found that knockdown of TLR4 or NOX4 in rats with heart failure significantly inhibited autophagy activation, thereby improving cardiac function. In addition, the PI3K/AKT/mTOR pathway is indicated to be involved in regulating the excessive autophagy process to protect cardiomyocytes (**Supplementary Table S5**) (Xuan and Jian, 2016; Xuan et al., 2017; Liu et al., 2018b; Chen et al., 2019; Zhang et al., 2020).

Pyroptosis Pathways in Cardiovascular Diseases

Pyroptosis is an inflammatory PCD process that rapidly initiates innate immune responses through pattern recognition receptors (PRRs), and different inflammatory bodies can sense different pathogen-associated molecular patterns and damage-associated molecular patterns (PAMPs and DAMPs) that induce pyroptosis (Zhu and Sun, 2018). Classical pyroptosis induction requires activating caspase-1, which cleaves and activates inflammatory cytokines (IL-1b, IL-18), caspase-1 cleaves and activates Gasdermin D (GSDMD), which is also key to the occurrence of pyroptosis (**Figure 1**) (Zhang et al., 2018a; Yue et al., 2019).

An increasing number of studies have shown that cardiovascular risk factors can activate nod-like receptor protein 3 (NLRP3) inflammasomes in cells. In addition, NLRP3 inflammasomes mediated pyroptosis was observed in various cardiovascular diseases. Studies suggested that NLRP3 inflammasomes and related pyrogenic signaling molecules played an essential role in the progression of cardiovascular diseases (**Supplementary Table S6**) (Liu et al., 2013; Jeyabal et al., 2016; Zhou et al., 2016; Huang et al., 2017; Nazir et al., 2017; Zhang et al., 2018a; Yang et al., 2018b; Li et al., 2018; Yue et al., 2019; Ding et al., 2020; Li et al., 2020). For example: in myocardial I/R model mice, Ding et al. found that Mi-29a expression was up-regulated and Sirtuin-1 (SIRT1) expression was down-regulated, which in turn regulated NLRP3 to attenuate myocardial I/R injury and enhanced cardiomyocytes survival (Ding et al., 2020).

Interconnections Between Different PCD Pathways

There is now increasing evidence that different PCD pathways in cardiovascular diseases are interconnected and affect each other on multiple levels. Studies have found that the PI3K/AKT pathway can regulate autophagy by targeting mTOR, and can also regulate apoptosis through the Bad pathway (Liu et al., 2018b; Wu et al., 2021a). mTOR kinase is an important regulatory molecule that induces PCD. Studies have found that the AMPK/mTOR pathway is not only involved in necrosis and pyroptosis, but can also regulate autophagy through Beclin-1 (Alers et al., 2012; Nazir et al., 2017; Han et al., 2021). Caspase-3 and caspase-7 act as executors and directly degrade structural and functional proteins, whereas caspase-8 and caspase-10 act as initiators and cause the caspase cascade after being activated by signaling stimuli (Kurokawa and Kornbluth, 2009). The caspase family is involved in the regulation of apoptosis and mediates necrosis and pyroptosis (Martin and Henry, 2013; Galluzzi et al., 2017; Yuan et al., 2018). Wu C et al. found that BK effectively improves cardiac function by reducing cardiomyocyte apoptosis, inflammatory infiltration, and myocardial fibrosis in the infarcted heart by reducing cleaved caspase-3 expression (Wu et al., 2021a). The study carried by Wang K et al. showed that miR-874 could regulate cardiomyocytes necrosis by affecting caspase-8 activity (Wang et al., 2013). Zheng X et al. found that BNIP3 mediated Doxorubicin-induced cardiomyocyte pyroptosis through activation of caspase-3 and cleavage of gasdermin D (GSDMD) (Zheng et al., 2020). In addition, it has been found that there is an interaction between TNF-α/TNFαR, PAMP/TLR, and DAMP/TLR that can activate NF-κB through the IKK pathway. Activation of NF-κb induces the expression of

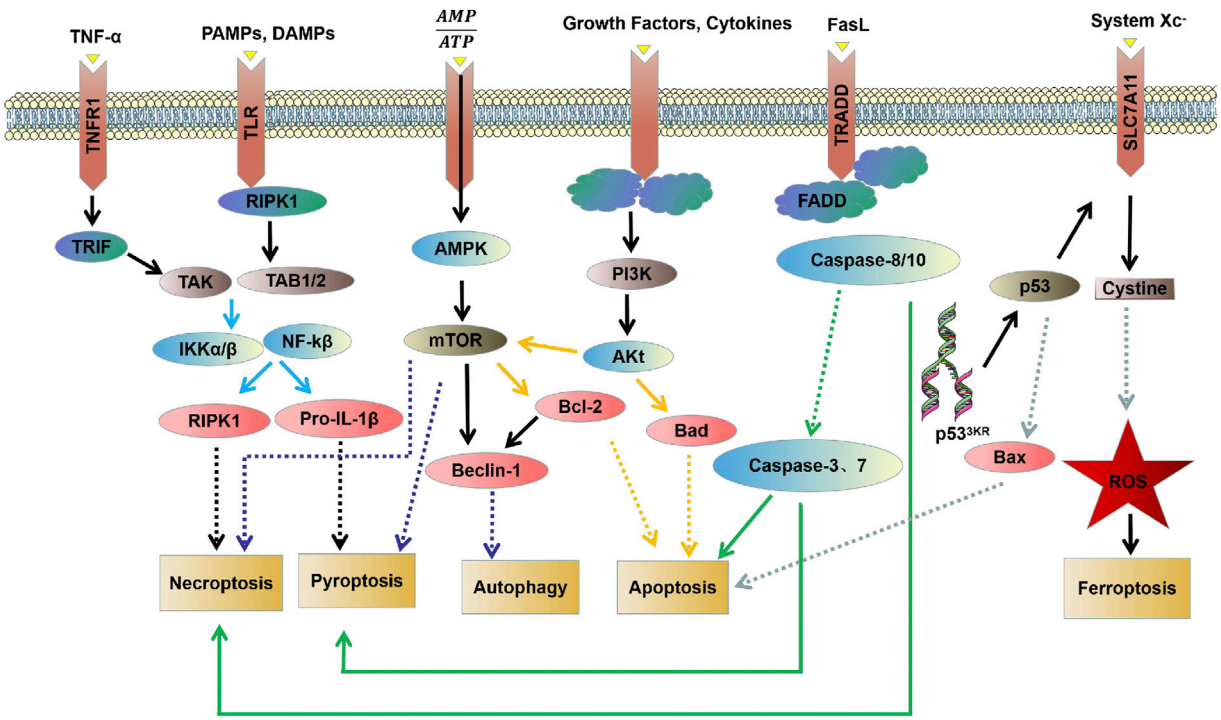

FIGURE 2 | The interrelationship between different PCD molecular mechanisms.

pro-survival genes, including RIPK1 and Pro-IL-1β (Wajant and Scheurich, 2011; Vande Walle and Lamkanfi, 2016). RIPK1 has been implicated in the regulation of necroptosis, whereas Pro-IL-1β mediated pyroptosis (Van Herreweghe et al., 2010; Yuan et al., 2018). An interaction between ferroptosis and apoptosis in cardiovascular diseases was also found in the present study (**Figure 2**).

DIFFERENT TYPES OF PCD AND CLINICAL DRUG THERAPY

Targeting Apoptosis in Clinical Practice

Currently, interventions targeting apoptosis may have a significant impact on the treatment of cardiovascular diseases. Bcl-2 family, p53 gene, IEG family, ICE gene family, and Fasl-Fas system play essential roles in initiating and developing apoptosis (Dispersyn and Borgers, 2001). Accumulating evidence from clinical trials suggested that modulation of the Bcl-2 family and the Fasl-Fas system as a novel intervention could improve myocardial function (Corbalan et al., 2016). Zhou et al. and Li et al. reported that statins could regulate the cardiomyocytes apoptosis in patients by regulating the expression of Bcl-2 and Bax, thereby protecting the cardiac function (Zhou et al., 2018; Li et al., 2016); Adamopoulos S et al. and Skudicky D et al. demonstrated that growth hormone (GH) and pentoxifylline could alleviate cardiac insults by modulating the apoptosis of cardiomyocytes and the level of soluble Fasl/Fas system (Adamopoulos et al., 2002; Skudicky et al., 2000). Other agents were also found to achieve the efficacy of myocardial protection in apoptosis-targeted ways (**Supplementary Table S7**) (Rössig et al., 2001; Zhang et al., 2005; Zhang et al., 2018b; Qing et al., 2018). Considering that apoptosis plays a vital role in cardiovascular pathologies, elucidating the underlying therapeutic mechanisms of these drugs in clinical trials provides us with a brand-new concept and idea for the occurrence and development of cardiovascular diseases.

Targeting Necrosis in Clinical Practice

Necrosis is a class of cell death initiated by death receptor ligands, mediated through death receptors, occurs in the inhibition of apoptotic pathways. The death receptor-receptor interaction protein-mitochondria-oxygen free radical pathway is proved to be an essential regulator of cardiac necrosis, and current clinical trials have found that drugs targeting this pathway can reduce cellular necrosis and improve cardiac function (Kim et al., 2011; Vandenabeele et al., 2010; Thévenod and Lee, 2013). Verma S et al. verified the effect of PZ-128 in a phase 2 clinical trial. The results indicated that it could reduce cyclic myocardial necrosis by targeting protease-activated receptor-1 (PAR1) on vascular cells on the inner surface of recipient cells, thereby further improving the outcome of patients with myocardial infarction (Wang, 2018); Silvain J et al. validated the combined efficacy of ticagrelor and clopidogrel on patients undergoing percutaneous coronary intervention (PCI) in a phase 3b clinical trial and found that apart from their anti-platelet aggregation and effect, it could also reduce perioperative myocardial necrosis by inhibiting NF-κb pathway and further improve the postoperative recovery of

patients with myocardial infarction (Silvain et al., 2020). Other studies found that some drugs could regulate cell necrosis by anti-aggregation, effect or reducing cell calcium overload, thereby improving myocardial necrosis in patients before and after surgery (**Supplementary Table S8**) (Alexander et al., 2008; Talarico et al., 2009; Lader et al., 2016; Nauck et al., 2018; Liu et al., 2019; Mohammad et al., 2020; Tcheng et al., 2020). At present, more and more attention has been focused on the clinical trials evaluating anti-necrosis therapies in cardiovascular diseases. The deepening of its targeted treatment in cardiovascular diseases will undoubtedly profoundly impact the clinical treatment of cardiovascular diseases.

Targeting Ferroptosis in Clinical Practice

Unlike classical apoptosis, there is no hallmark of apoptosis such as chromatin condensation during ferroptosis, but it is accompanied by mitochondrial shrinkage and accumulation of lipid oxides. Studies have revealed that overloaded iron would cause irreparable damage to multiple organs. The use of inhibitors of apoptosis in clinical trials does not also inhibit ferroptosis, while the use of iron chelators can inhibit the ferroptosis process of cells. Wongjaikam S et al. demonstrated that a combination of lamotrigine and desferrioxamine as chelation therapy could reduce the level of myocardial iron by restoring sarco/endoplasmic reticulum calcium ATPase (SERCA) levels (Wongjaikam et al., 2017). Farmaki K et al. also found that the combined chelation therapy of desferrioxamine and desferrioxone can prevent and reverse the cardiac complications caused by excessive iron in blood transfusion (Farmaki et al., 2010). Other clinical trials concerning iron chelators in cardiovascular diseases are shown in **Supplementary Table S9** (Penckofer and Schwertz, 2000; Al-Rousan et al., 2009; Farmaki et al., 2010; Lal et al., 2013; Jansová et al., 2014; Shakoor et al., 2014; Pennell et al., 2015; Ho et al., 2017; Eghbali et al., 2019). Although iron ion chelators are manifested as a promising drug target in clinical trials, their potential molecular signaling pathways and networks remain to be explored. Besides, the metabolism of iron at the systemic level is another challenge. Iron metabolism forms homeostasis between the body and target organs to regulate iron death in the clinical treatment of cardiovascular diseases.

Targeting Autophagy in Clinical Practice

Autophagy plays a broad role in developing cardiovascular pathology and can act as both a suppressor and a promoting factor of cardiovascular disease. Although some drugs and regimens can modulate autophagy, few clinical trials have assessed their role in the cardiovascular system. Among them, Qing et al. conducted a phase 2 clinical trial of berberine and found that it could reduce myocardial injury by regulating the AMPK/mTOR pathway; Hua et al. elucidated that simvastatin could reduce myocardial injury by regulating the expression of LC3-II/LC3-I, Beclin- 1, and AMPK phosphorylation, which in turn improved cardiac function (**Supplementary Table S10**) (Hua et al., 2017; Qing et al., 2018). Another significant limitation in this field is the lack of spatially specific delivery of exogenous autophagy modulators for cardiac or vascular repair, so there is still a long way to go for effective autophagy therapy. However, the insights gained from these works will inspire future clinical trials assessing autophagic responses to achieve therapeutic efficacies.

Targeting Pyroptosis in Clinical Practice

Pyroptosis is a new programmed inflammatory death mainly regulated by classical and non-classical pathways, the classical pathway of which is mediated by caspase-1 dependence, and the non-classical inflammasome pathway is mediated by caspase-4/5/11 (Li et al., 2020). Numerous studies have shown that pyroptosis is generally involved in the development and outcome of various cardiovascular diseases such as myocardial infarction, heart failure, and myocardial I/R (Zhu and Sun, 2018; Wang and Kanneganti, 2021). To date, few clinical trials have assessed its role in cardiovascular disease, mainly due to the lack of cell/organ-targeted delivery of exogenous pyroptosis modulators for cardiac or vascular repair. However, since pyroptosis is involved in the development of a variety of cardiovascular diseases, the subsequent in-depth study of cell/organ targeted delivery of apoptosis modulators will provide a new direction and effective target for the therapeutic research of related diseases.

SUMMARY AND DISCUSSION

While research into cardiovascular disease has focused on the molecular mechanisms of individual PCD types, it is now clear that different PCD pathways do not operate in isolation. Indeed, a more likely explanation basing on current knowledge about the various possibilities of triggering and reconnecting PCD signaling cascades suggests that autophagy, apoptosis, ferroptosis, pyroptosis, and necrosis constitute a pluralistic, coordinated cell death system in which one pathway can flexibly compensate for the other (Konstantinidis et al., 2012; Tower, 2015; Wang and Kanneganti, 2021). For example, it is demonstrated that in I/R injury models, both pyroptosis and necrosis could affect cardiovascular disease through AMPK/mTOR and other pathways (Oerlemans et al., 2013; Nazir et al., 2017). In this review, we describe the characteristics and molecular mechanisms of individual PCD types and discuss the interactions between different cell death signaling cascades to provide a better understanding of the relationship between PCD and cardiovascular diseases.

Up to now, while the increasingly important role of different PCD is unveiled, few clinical trial studies are conducted to treat cardiovascular diseases by pharmacological intervention to PCD (Mani, 2008). Therefore, we describe the critical role of drugs targeting cell death signaling pathways and their efficacy in various cardiovascular diseases by collecting currently available drugs studied in clinical trials. Multiple medications are targeted in cardiovascular disease by modulating different types of PCD in many clinical trials. For instance, statins can regulate myocardial apoptosis in patients by regulating the expression of Bcl-2 and Bax (Zhou et al., 2018). Simvastatin can regulate the autophagy of cardiomyocytes by regulating the expression of LC3-I/II,

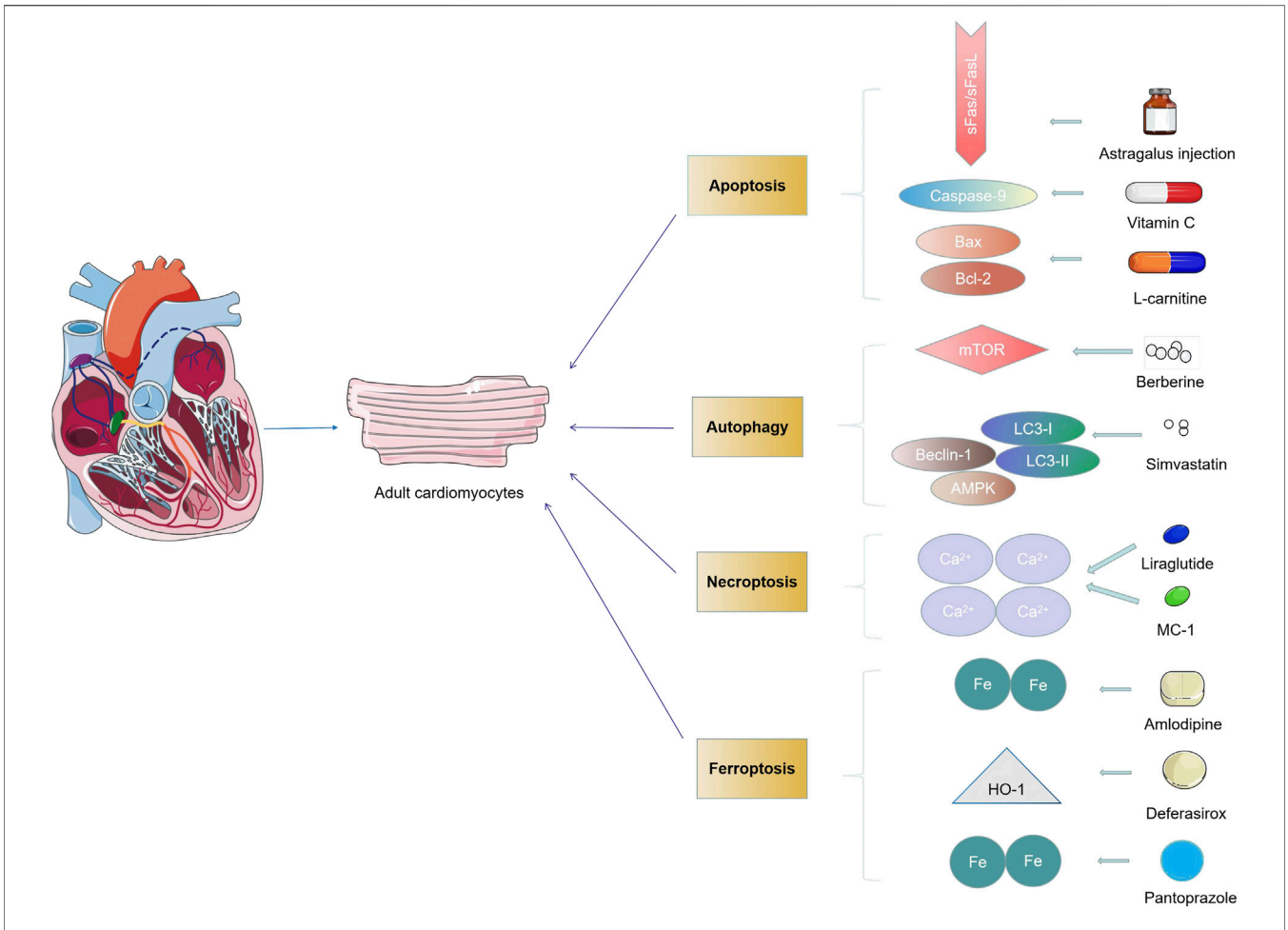

FIGURE 3 | Drugs target cardiomyocytes through different types of PCD.

Beclin-1, and other factors (Hua et al., 2017). Drugs such as liraglutide and pyridoxal 5′-phosphate (MC-1) can modulate the necrosis of cardiomyocytes by intervening calcium ions (Nauck et al., 2018; Alexander et al., 2008). Amlodipine and pantoprazole regulate ferroptosis in cardiomyocytes by affecting iron absorption (Shakoor et al., 2014; Eghbali et al., 2019) (**Figure 3**). Therefore, more work is needed to explore whether drugs can target therapy in various cardiac cells by handling multiple types of PCD. Most previous drug studies reported only a single PCD type, while recent studies found that drugs could act simultaneously by regulating multiple different types of PCD. For example, Qing et al., in phase 2 of clinical trials, found that berberine could reduce cardiomyocyte autophagy and apoptosis by regulating the AMPK/mTOR pathway, thereby reducing myocardial injury in PCI patients (Qing et al., 2018). In general, treatment for any type of PCD can reverse further damage to the heart to some extent (Moujalled et al., 2021). More research is needed to clarify whether PCD acts as an initiator or a critical node in the injury path when studying drugs acting through the PCD pathway.

Apart from cardiovascular disorders, PCD is also involved in other diseases, including respiratory and digestive tumors (Venderova and Park, 2012; Tai et al., 2018). However, current studies reported only PCD on a single type of cell, and the effects and differences between different types of cells are poorly informed. Therefore, in future work, we can start from various cell types and study the impact of drugs on cardiovascular diseases by intervening in various types of PCD in different cell types, which can not only reduce the adverse events of PCD-targeted therapy but also more accurately treat various types of cardiovascular diseases.

While the underlying biological mechanisms regarding the PCD remain uncovered, therapeutic manipulation of cell death pathways holds great promise. At present, among various types of diseases, the most studied is the intervention of drugs in various tumors: recent clinical trials reported that the combination of deferoxamine (DFO) and deferiprone (DFP) effectively improves hematologic malignancies (Wongjaikam et al., 2017). The combined therapy of drugs regulates ferroptosis in the clinical treatment of various diseases by affecting iron metabolism at the systemic level and allowing iron metabolism to form homeostasis between the body and target organs. Based on this, recently, Farmaki K et al. found that combination therapy with desferrioxamine drugs also improved prognosis in cardiovascular disease

and has been initiated in clinical trials (Farmaki et al., 2010). Moreover, combination therapy with DFO and DFP can improve cardiac function by inhibiting ferroptosis by reducing iron levels in the heart (Wongjaikam et al., 2017). Studies in future work can be carried out in different types of cardiovascular diseases based on drug-mediated signaling pathways.

Therefore, our review may pave the way for further novel research in the future. On the one hand, we hope to uncover complex signaling pathways between different PCD and clarify their functions in cardiovascular pathologies. On the other hand, acceleration in clinical transformation is warranted to enable PCD-targeted agents to be applied to detect, prevent, and treat cardiovascular diseases.

AUTHOR CONTRIBUTIONS

LW and JS designed the review; LZ and JS wrote the first draft of the manuscript; LZ and JS prepared the figures; All authors contributed to the editing of the review and approved the final version of the manuscript for submission.

FUNDING

This work was supported by grants from the National Natural Science Foundation of China (No. 81770361 and 82070367).

ACKNOWLEDGMENTS

We thank for the technical assistance support from Jiangsu Province Collaborative Innovation Center for Cardiovascular Disease Translational Medicine. Figures was modified from Servier Medical Art (http://smart.servier.com/), licensed under a Creative Common Attribution 3.0 Generic License (https://creativecommons.org/licenses/by/3.0/).

SUPPLEMENTARY MATERIAL

The Supplementary Material for this article can be found online at: https://www.frontiersin.org/articles/10.3389/fcell.2021.794879/full#supplementary-material

REFERENCES

Adamopoulos, S., Parissis, J. T., Georgiadis, M., Karatzas, D., Paraskevaidis, J., Kroupis, C., et al. (2002). Growth Hormone Administration Reduces Circulating Proinflammatory Cytokines and Soluble Fas/soluble Fas Ligand System in Patients with Chronic Heart Failure Secondary to Idiopathic Dilated Cardiomyopathy. *Am. Heart J.* 144 (2), 359–364. doi:10.1067/mhj.2002.124052

Al-Rousan, R. M., Paturi, S., Laurino, J. P., Kakarla, S. K., Gutta, A. K., Walker, E. M., et al. (2009). Deferasirox Removes Cardiac Iron and Attenuates Oxidative Stress in the Iron-Overloaded Gerbil. *Am. J. Hematol.* 84 (9), 565–570. doi:10.1002/ajh.21487

Alers, S., Löffler, A. S., Wesselborg, S., and Stork, B. (2012). Role of AMPK-mTOR-Ulk1/2 in the Regulation of Autophagy: Cross Talk, Shortcuts, and Feedbacks. *Mol. Cel Biol* 32 (1), 2–11. doi:10.1128/mcb.06159-11

Alexander, J. H., Alexander, J. H., Emery, R. W., Carrier, M., Ellis, S. J., Mehta, R. H., et al. (2008). Efficacy and Safety of Pyridoxal 5'-phosphate (MC-1) in High-Risk Patients Undergoing Coronary Artery Bypass Graft Surgery: the MEND-CABG II Randomized Clinical Trial. *Jama* 299 (15), 1777–1787. doi:10.1001/jama.299.15.joc80027

Baba, Y., Higa, J. K., Shimada, B. K., Horiuchi, K. M., Suhara, T., Kobayashi, M., et al. (2018). Protective Effects of the Mechanistic Target of Rapamycin against Excess Iron and Ferroptosis in Cardiomyocytes. *Am. J. Physiology-Heart Circulatory Physiol.* 314 (3), H659–h668. doi:10.1152/ajpheart.00452.2017

Bai, L., Mei, X., Wang, Y., Yuan, Y., Bi, Y., Li, G., et al. (2017). The Role of Netrin-1 in Improving Functional Recovery through Autophagy Stimulation Following Spinal Cord Injury in Rats. *Front. Cel. Neurosci.* 11, 350. doi:10.3389/fncel.2017.00350

Bai, Y.-T., Chang, R., Wang, H., Xiao, F.-J., Ge, R.-L., and Wang, L.-S. (2018). ENPP2 Protects Cardiomyocytes from Erastin-Induced Ferroptosis. *Biochem. Biophysical Res. Commun.* 499 (1), 44–51. doi:10.1016/j.bbrc.2018.03.113

Chen, H., Tang, L.-J., Tu, H., Zhou, Y.-J., Li, N.-S., Luo, X.-J., et al. (2020). Arctiin Protects Rat Heart against Ischemia/reperfusion Injury via a Mechanism Involving Reduction of Necroptosis. *Eur. J. Pharmacol.* 875, 173053. doi:10.1016/j.ejphar.2020.173053

Chen, X., Xu, S., Zhao, C., and Liu, B. (2019). Role of TLR4/NADPH Oxidase 4 Pathway in Promoting Cell Death through Autophagy and Ferroptosis during Heart Failure. *Biochem. Biophysical Res. Commun.* 516 (1), 37–43. doi:10.1016/j.bbrc.2019.06.015

Corbalan, J. J., Vatner, D. E., and Vatner, S. F. (2016). Myocardial Apoptosis in Heart Disease: Does the Emperor Have Clothes? *Basic Res. Cardiol.* 111 (3), 31. doi:10.1007/s00395-016-0549-2

Ding, S., Liu, D., Wang, L., Wang, G., and Zhu, Y. (2020). Inhibiting MicroRNA-29a Protects Myocardial Ischemia-Reperfusion Injury by Targeting SIRT1 and Suppressing Oxidative Stress and NLRP3-Mediated Pyroptosis Pathway. *J. Pharmacol. Exp. Ther.* 372 (1), 128–135. doi:10.1124/jpet.119.256982

Dispersyn, G. D., and Borgers, M. (2001). Apoptosis in the Heart: about Programmed Cell Death and Survival. *Physiology* 16, 41–47. doi:10.1152/physiologyonline.2001.16.1.41

Dixon, S. J., Lemberg, K. M., Lamprecht, M. R., Skouta, R., Zaitsev, E. M., Gleason, C. E., et al. (2012). Ferroptosis: an Iron-dependent Form of Nonapoptotic Cell Death. *Cell* 149 (5), 1060–1072. doi:10.1016/j.cell.2012.03.042

Dong, Y., Chen, H., Gao, J., Liu, Y., Li, J., and Wang, J. (2019). Molecular Machinery and Interplay of Apoptosis and Autophagy in Coronary Heart Disease. *J. Mol. Cell Cardiol.* 136, 27–41. doi:10.1016/j.yjmcc.2019.09.001

Eghbali, A., Khalilpour, A., Taherahmadi, H., and Bagheri, B. (2019). Pantoprazole Reduces Serum Ferritin in Patients with Thalassemia Major and Intermedia: A Randomized, Controlled Study. *Therapies* 74 (5), 507–512. doi:10.1016/j.therap.2018.11.013

Fan, K., Huang, W., Qi, H., Song, C., He, C., Liu, Y., et al. (2021). The Egr-1/miR-15a-5p/GPX4 axis Regulates Ferroptosis in Acute Myocardial Infarction. *Eur. J. Pharmacol.* 909, 174403. doi:10.1016/j.ejphar.2021.174403

Fang, X., Wang, H., Han, D., Xie, E., Yang, X., Wei, J., et al. (2019). Ferroptosis as a Target for protection against Cardiomyopathy. *Proc. Natl. Acad. Sci. USA* 116 (7), 2672–2680. doi:10.1073/pnas.1821022116

Farmaki, K., Tzoumari, I., Pappa, C., Chouliaras, G., and Berdoukas, V. (2010). Normalisation of Total Body Iron Load with Very Intensive Combined Chelation Reverses Cardiac and Endocrine Complications of Thalassaemia Major. *Br. J. Haematol.* 148 (3), 466–475. doi:10.1111/j.1365-2141.2009.07970.x

Feng, Y., Madungwe, N. B., Imam Aliagan, A. D., Tombo, N., and Bopassa, J. C. (2019). Liproxstatin-1 Protects the Mouse Myocardium against Ischemia/reperfusion Injury by Decreasing VDAC1 Levels and Restoring GPX4 Levels. *Biochem. Biophysical Res. Commun.* 520 (3), 606–611. doi:10.1016/j.bbrc.2019.10.006

Galluzzi, L., Kepp, O., Chan, F. K.-M., and Kroemer, G. (2017). Necroptosis: Mechanisms and Relevance to Disease. *Annu. Rev. Pathol. Mech. Dis.* 12, 103–130. doi:10.1146/annurev-pathol-052016-100247

Grootaert, M. O., da Costa Martins, P. A., Bitsch, N., Pintelon, I., De Meyer, G. R., Martinet, W., et al. (2015). Defective Autophagy in Vascular Smooth Muscle Cells Accelerates Senescence and Promotes Neointima Formation and Atherogenesis. *Autophagy* 11 (11), 2014–2032. doi:10.1080/15548627.2015.1096485

Han, Y. L., Chen, S., and Peng, X. (2021). Electroacupuncture Pretreatment at Neiguan (PC6) Attenuates Autophagy in Rats with Myocardial Ischemia Reperfusion through the Phosphatidylinositol 3-Kinase-Akt-Mammalian Target of Rapamycin Pathway. *J. Tradit Chin. Med.* 41 (3), 455–462. doi:10.19852/j.cnki.jtcm.2021.03.014

He, Z., Zeng, X., Zhou, D., Liu, P., Han, D., Xu, L., et al. (2021). LncRNA Chaer Prevents Cardiomyocyte Apoptosis from Acute Myocardial Infarction through AMPK Activation. *Front. Pharmacol.* 12, 649398. doi:10.3389/fphar.2021.649398

Ho, P. J., Tay, L., Teo, J., Marlton, P., Grigg, A., St Pierre, T., et al. (2017). Cardiac Iron Load and Function in Transfused Patients Treated with Deferasirox (The MILE Study). *Eur. J. Haematol.* 98 (2), 97–105. doi:10.1111/ejh.12793

Hua, P., Liu, J., Tao, J., Zou, R., Lin, X., Zhang, D., et al. (2017). Efficacy and Mechanism of Preoperative Simvastatin Therapy on Myocardial Protection after Extracorporeal Circulation. *Biomed. Res. Int.* 2017, 6082430. doi:10.1155/2017/6082430

Huang, W.-Q., Wei, P., Lin, R.-Q., and Huang, F. (2017). Protective Effects of Microrna-22 against Endothelial Cell Injury by Targeting NLRP3 through Suppression of the Inflammasome Signaling Pathway in a Rat Model of Coronary Heart Disease. *Cell Physiol Biochem* 43 (4), 1346–1358. doi:10.1159/000481846

Jansová, H., Macháček, M., Wang, Q., Hašková, P., Jirkovská, A., Potůčková, E., et al. (2014). Comparison of Various Iron Chelators and Prochelators as Protective Agents against Cardiomyocyte Oxidative Injury. *Free Radic. Biol. Med.* 74, 210–221. doi:10.1016/j.freeradbiomed.2014.06.019

Jeyabal, P., Thandavarayan, R. A., Joladarashi, D., Suresh Babu, S., Krishnamurthy, S., Bhimaraj, A., et al. (2016). MicroRNA-9 Inhibits Hyperglycemia-Induced Pyroptosis in Human Ventricular Cardiomyocytes by Targeting ELAVL1. *Biochem. Biophysical Res. Commun.* 471 (4), 423–429. doi:10.1016/j.bbrc.2016.02.065

Jiang, C., Zhao, Q., Wang, C., Peng, M., Hao, G., Liu, Z., et al. (2021). Downregulation of Long Noncoding RNA LINC00261 Attenuates Myocardial Infarction through the miR-522-3p/Trinucleotide Repeat-Containing Gene 6a (TNRC6A) Axis. *Cardiovasc. Ther.* 2021, 6628194. doi:10.1155/2021/6628194

Jiang, W., Song, J., Zhang, S., Ye, Y., Wang, J., and Zhang, Y. (2021). CTRP13 Protects H9c2 Cells against Hypoxia/Reoxygenation (H/R)-Induced Injury via Regulating the AMPK/Nrf2/ARE Signaling Pathway. *Cel Transpl.* 30, 9636897211033275. doi:10.1177/09636897211033275

Jiang, X., Wu, D., Jiang, Z., Ling, W., and Qian, G. (2021). Protective Effect of Nicorandil on Cardiac Microvascular Injury: Role of Mitochondrial Integrity. *Oxid Med. Cel Longev* 2021, 4665632. doi:10.1155/2021/4665632

Kim, J.-Y., Kim, Y.-J., Lee, S., and Park, J.-H. (2011). BNip3 Is a Mediator of TNF-Induced Necrotic Cell Death. *Apoptosis* 16 (2), 114–126. doi:10.1007/s10495-010-0550-4

Konstantinidis, K., Whelan, R. S., and Kitsis, R. N. (2012). Mechanisms of Cell Death in Heart Disease. *Atvb* 32 (7), 1552–1562. doi:10.1161/atvbaha.111.224915

Kramer, J. L. K., Lammertse, D. P., Schubert, M., Curt, A., and Steeves, J. D. (2012). Relationship between Motor Recovery and independence after Sensorimotor-Complete Cervical Spinal Cord Injury. *Neurorehabil. Neural Repair* 26 (9), 1064–1071. doi:10.1177/1545968312447306

Kung, G., Konstantinidis, K., and Kitsis, R. N. (2011). Programmed Necrosis, Not Apoptosis, in the Heart. *Circ. Res.* 108 (8), 1017–1036. doi:10.1161/circresaha.110.225730

Kurokawa, M., and Kornbluth, S. (2009). Caspases and Kinases in a Death Grip. *Cell* 138 (5), 838–854. doi:10.1016/j.cell.2009.08.021

Lader, A. S., Baguisi, A., Casale, R., Kates, S. A., and Beeuwkes, R. (2016). CMX-2043 Mechanisms of Action *In Vitro*. *J. Cardiovasc. Pharmacol.* 68 (3), 241–247. doi:10.1097/fjc.0000000000000408

Lal, A., Porter, J., Sweeters, N., Ng, V., Evans, P., Neumayr, L., et al. (2013). Combined Chelation Therapy with Deferasirox and Deferoxamine in Thalassemia. *Blood Cell Mol. Dis.* 50 (2), 99–104. doi:10.1016/j.bcmd.2012.10.006

Li, M., Xue, L., Sun, H., and Xu, S. (2016). Myocardial Protective Effects of L-Carnitine on Ischemia-Reperfusion Injury in Patients with Rheumatic Valvular Heart Disease Undergoing Cardiac Surgery. *J. Cardiothorac. Vasc. Anesth.* 30 (6), 1485–1493. doi:10.1053/j.jvca.2016.06.006

Li, P., Zhong, X., Li, J., Liu, H., Ma, X., He, R., et al. (2018). MicroRNA-30c-5p Inhibits NLRP3 Inflammasome-Mediated Endothelial Cell Pyroptosis through FOXO3 Down-Regulation in Atherosclerosis. *Biochem. Biophysical Res. Commun.* 503 (4), 2833–2840. doi:10.1016/j.bbrc.2018.08.049

Li, W., Feng, G., Gauthier, J. M., Lokshina, I., Higashikubo, R., Evans, S., et al. (2019). Ferroptotic Cell Death and TLR4/Trif Signaling Initiate Neutrophil Recruitment after Heart Transplantation. *J. Clin. Invest.* 129 (6), 2293–2304. doi:10.1172/jci126428

Li, Y., Niu, X., Xu, H., Li, Q., Meng, L., He, M., et al. (2020). VX-765 Attenuates Atherosclerosis in ApoE Deficient Mice by Modulating VSMCs Pyroptosis. *Exp. Cel Res.* 389 (1), 111847. doi:10.1016/j.yexcr.2020.111847

Liu, A., Gao, X., Zhang, Q., and Cui, L. (2013). Cathepsin B Inhibition Attenuates Cardiac Dysfunction and Remodeling Following Myocardial Infarction by Inhibiting the NLRP3 Pathway. *Mol. Med. Rep.* 8 (2), 361–366. doi:10.3892/mmr.2013.1507

Liu, B., Zhao, C., Li, H., Chen, X., Ding, Y., and Xu, S. (2018). Puerarin Protects against Heart Failure Induced by Pressure Overload through Mitigation of Ferroptosis. *Biochem. Biophysical Res. Commun.* 497 (1), 233–240. doi:10.1016/j.bbrc.2018.02.061

Liu, X., Deng, Y., Xu, Y., Jin, W., and Li, H. (2018). MicroRNA-223 Protects Neonatal Rat Cardiomyocytes and H9c2 Cells from Hypoxia-Induced Apoptosis and Excessive Autophagy via the Akt/mTOR Pathway by Targeting PARP-1. *J. Mol. Cell Cardiol.* 118, 133–146. doi:10.1016/j.yjmcc.2018.03.018

Liu, X., Wang, Y., Zhang, M., Liu, Y., Hu, L., and Gu, Y. (2019). Ticagrelor Reduces Ischemia-Reperfusion Injury through the NF-κb-dependent Pathway in Rats. *J. Cardiovasc. Pharmacol.* 74 (1), 13–19. doi:10.1097/fjc.0000000000000675

Liu, Y., Chen, J., Xia, P., Stratakis, C. A., and Cheng, Z. (2021). Loss of PKA Regulatory Subunit 1α Aggravates Cardiomyocyte Necrosis and Myocardial Ischemia/reperfusion Injury. *J. Biol. Chem.* 297 (1), 100850. doi:10.1016/j.jbc.2021.100850

Lu, C., Liu, L., Chen, S., Niu, J., Li, S., Xie, W., et al. (2021). Azathioprine Pretreatment Ameliorates Myocardial Ischaemia Reperfusion Injury in Diabetic Rats by Reducing Oxidative Stress, Apoptosis, and Inflammation. *Clin. Exp. Pharmacol. Physiol.* 48, 1621–1632. doi:10.1111/1440-1681.13569

Ma, S., Dielschneider, R. F., Henson, E. S., Xiao, W., Choquette, T. R., Blankstein, A. R., et al. (2017). Ferroptosis and Autophagy Induced Cell Death Occur Independently after Siramesine and Lapatinib Treatment in Breast Cancer Cells. *PLoS One* 12 (8), e0182921. doi:10.1371/journal.pone.0182921

Mani, K. (2008). Programmed Cell Death in Cardiac Myocytes: Strategies to Maximize post-ischemic Salvage. *Heart Fail. Rev.* 13 (2), 193–209. doi:10.1007/s10741-007-9073-7

Martin, S. J., and Henry, C. M. (2013). Distinguishing between Apoptosis, Necrosis, Necroptosis and Other Cell Death Modalities. *Methods* 61 (2), 87–89. doi:10.1016/j.ymeth.2013.06.001

Mohammad, H. M. F., Makary, S., Atef, H., El-Sherbiny, M., Atteia, H. H., Ibrahim, G. A., et al. (2020). Clopidogrel or Prasugrel Reduces Mortality and Lessens Cardiovascular Damage from Acute Myocardial Infarction in Hypercholesterolemic Male Rats. *Life Sci.* 247, 117429. doi:10.1016/j.lfs.2020.117429

Moujalled, D., Strasser, A., and Liddell, J. R. (2021). Molecular Mechanisms of Cell Death in Neurological Diseases. *Cell Death Differ* 28 (7), 2029–2044. doi:10.1038/s41418-021-00814-y

Nauck, M. A., Tornøe, K., Rasmussen, S., Treppendahl, M. B., and Marso, S. P. (2018). Cardiovascular Outcomes in Patients Who Experienced a Myocardial Infarction while Treated with Liraglutide versus Placebo in the LEADER Trial. *Diabetes Vasc. Dis. Res.* 15 (5), 465–468. doi:10.1177/1479164118783935

Nazir, S., Gadi, I., Al-Dabet, M. d. M., Elwakiel, A., Kohli, S., Ghosh, S., et al. (2017). Cytoprotective Activated Protein C Averts Nlrp3 Inflammasome-Induced

Ischemia-Reperfusion Injury via mTORC1 Inhibition. *Blood* 130 (24), 2664–2677. doi:10.1182/blood-2017-05-782102

Nie, S., Cui, X., Guo, J., Ma, X., Zhi, H., Li, S., et al. (2021). Long Non-coding RNA AK006774 Inhibits Cardiac Ischemia-Reperfusion Injury via Sponging miR-448. *Bioengineered* 12 (1), 4972–4982. doi:10.1080/21655979.2021.1954135

Nishida, K., and Otsu, K. (2008). Cell Death in Heart Failure. *Circ. J.* 72 Suppl A (Suppl. A), A17–A21. doi:10.1253/circj.cj-08-0669

Oerlemans, M. I. F. J., Koudstaal, S., Chamuleau, S. A., de Kleijn, D. P., Doevendans, P. A., and Sluijter, J. P. G. (2013). Targeting Cell Death in the Reperfused Heart: Pharmacological Approaches for Cardioprotection. *Int. J. Cardiol.* 165 (3), 410–422. doi:10.1016/j.ijcard.2012.03.055

Oerlemans, M. I. F. J., Liu, J., Arslan, F., Ouden, K., Middelaar, B. J., Doevendans, P. A., et al. (2012). Inhibition of RIP1-dependent Necrosis Prevents Adverse Cardiac Remodeling after Myocardial Ischemia-Reperfusion *In Vivo*. *Basic Res. Cardiol.* 107 (4), 270. doi:10.1007/s00395-012-0270-8

Oka, T., Hikoso, S., Yamaguchi, O., Taneike, M., Takeda, T., Tamai, T., et al. (2012). Mitochondrial DNA that Escapes from Autophagy Causes Inflammation and Heart Failure. *Nature* 485 (7397), 251–255. doi:10.1038/nature10992

Penckofer, S., and Schwertz, D. (2000). Improved Iron Status Parameters May Be a Benefit of Hormone Replacement Therapy. *J. Women's Health Gender-Based Med.* 9 (2), 141–151. doi:10.1089/152460900318632

Pennell, D. J., Porter, J. B., Piga, A., Lai, Y. R., El-Beshlawy, A., Elalfy, M., et al. (2015). Sustained Improvements in Myocardial T2* over 2 Years in Severely Iron-overloaded Patients with Beta Thalassemia Major Treated with Deferasirox or Deferoxamine. *Am. J. Hematol.* 90 (2), 91–96. doi:10.1002/ajh.23876

Pullaiah, C. P., Nelson, V. K., Rayapu, S., G v, N. K., and Kedam, T. (2021). Exploring Cardioprotective Potential of Esculetin against Isoproterenol Induced Myocardial Toxicity in Rats: *In Vivo* and *In Vitro* Evidence. *BMC Pharmacol. Toxicol.* 22 (1), 43. doi:10.1186/s40360-021-00510-0

Qing, Y., Dong, X., Hongli, L., and Yanhui, L. (2018). Berberine Promoted Myocardial protection of Postoperative Patients through Regulating Myocardial Autophagy. *Biomed. Pharmacother.* 105, 1050–1053. doi:10.1016/j.biopha.2018.06.088

Rössig, L., Hoffmann, J., Hugel, B., Mallat, Z., Haase, A., Freyssinet, J. M., et al. (2001). Vitamin C Inhibits Endothelial Cell Apoptosis in Congestive Heart Failure. *Circulation* 104 (18), 2182–2187. doi:10.1161/hc4301.098284

Saunders, L. L., Clarke, A., Tate, D. G., Forchheimer, M., and Krause, J. S. (2015). Lifetime Prevalence of Chronic Health Conditions Among Persons with Spinal Cord Injury. *Arch. Phys. Med. Rehabil.* 96 (4), 673–679. doi:10.1016/j.apmr.2014.11.019

Sciarretta, S., Zhai, P., Shao, D., Maejima, Y., Robbins, J., Volpe, M., et al. (2012). Rheb Is a Critical Regulator of Autophagy during Myocardial Ischemia. *Circulation* 125 (9), 1134–1146. doi:10.1161/circulationaha.111.078212

Shakoor, A., Zahoor, M., Sadaf, A., Alvi, N., Fadoo, Z., Rizvi, A., et al. (2014). Effect of L-type Calcium Channel Blocker (Amlodipine) on Myocardial Iron Deposition in Patients with Thalassaemia with Moderate-To-Severe Myocardial Iron Deposition: Protocol for a Randomised, Controlled Trial. *BMJ Open* 4 (12), e005360. doi:10.1136/bmjopen-2014-005360

She, L., Tu, H., Zhang, Y.-Z., Tang, L.-J., Li, N.-S., Ma, Q.-L., et al. (2019). Inhibition of Phosphoglycerate Mutase 5 Reduces Necroptosis in Rat Hearts Following Ischemia/Reperfusion through Suppression of Dynamin-Related Protein 1. *Cardiovasc. Drugs Ther.* 33 (1), 13–23. doi:10.1007/s10557-018-06848-8

Shen, Z., Shen, A., Chen, X., Wu, X., Chu, J., Cheng, Y., et al. (2020). Huoxin Pill Attenuates Myocardial Infarction-Induced Apoptosis and Fibrosis via Suppression of P53 and TGF-β1/Smad2/3 Pathways. *Biomed. Pharmacother.* 130, 110618. doi:10.1016/j.biopha.2020.110618

Shi, B., Huang, Y., Ni, J., Chen, J., Wei, J., Gao, H., et al. (2020). Qi Dan Li Xin Pill Improves Chronic Heart Failure by Regulating mTOR/p70S6k-Mediated Autophagy and Inhibiting Apoptosis. *Sci. Rep.* 10 (1), 6105. doi:10.1038/s41598-020-63090-9

Shi, Z., Zhou, H., Lu, L., Li, X., Fu, Z., Liu, J., et al. (2017). The Roles of microRNAs in Spinal Cord Injury. *Int. J. Neurosci.* 127 (12), 1104–1115. doi:10.1080/00207454.2017.1323208

Silvain, J., Lattuca, B., Beygui, F., Rangé, G., Motovska, Z., Dillinger, J. G., et al. (2020). Ticagrelor versus Clopidogrel in Elective Percutaneous Coronary Intervention (ALPHEUS): a Randomised, Open-Label, Phase 3b Trial. *Lancet* 396 (10264), 1737–1744. doi:10.1016/S0140-6736(20)32236-4

Skudicky, D., Sliwa, K., Bergemann, A., Candy, G., and Sareli, P. (2000). Reduction in Fas/APO-1 Plasma Concentrations Correlates With Improvement in Left Ventricular Function in Patients With Idiopathic Dilated Cardiomyopathy Treated with Pentoxifylline. *Heart* 84 (4), 438–441. doi:10.1136/heart.84.4.438

Sun, M., Zhang, W., Bi, Y., Xu, H., Abudureyimu, M., Peng, H., et al. (2021). NDP52 Protects against Myocardial Infarction-Provoked Cardiac Anomalies through Promoting Autophagosome-Lysosome Fusion via Recruiting TBK1 and RAB7. *Antioxid. Redox Signal.*. doi:10.1089/ars.2020.8253

Tai, Y.-T., Cho, K. C., and Anderson, K. C. (2018). Osteoclast Immunosuppressive Effects in Multiple Myeloma: Role of Programmed Cell Death Ligand 1. *Front. Immunol.* 9, 1822. doi:10.3389/fimmu.2018.01822

Talarico, G. P., Brancati, M., Burzotta, F., Porto, I., Trani, C., De Vita, M., et al. (2009). Glycoprotein IIB/IIIA Inhibitor to Reduce Postpercutaneous Coronary Intervention Myonecrosis and Improve Coronary Flow in Diabetics: the 'OPTIMIZE-IT' Pilot Randomized Study. *J. Cardiovasc. Med. (Hagerstown)* 10 (3), 245–251. doi:10.2459/jcm.0b013e32832180d9

Tcheng, J. E., Gibson, M., Krucoff, M. W., Patel, M. R., Ajit, M., Hiremath, J., et al. (2020). SUPPORT-1 (Subjects Undergoing PCI and Perioperative Reperfusion Treatment): A Prospective, Randomized Trial of CMX-2043 in Patients Undergoing Elective Percutaneous Coronary Intervention. *J. Cardiovasc. Pharmacol.* 76 (2), 189–196. doi:10.1097/fjc.0000000000000830

Thévenod, F., and Lee, W.-K. (2013). Cadmium and Cellular Signaling Cascades: Interactions between Cell Death and Survival Pathways. *Arch. Toxicol.* 87 (10), 1743–1786. doi:10.1007/s00204-013-1110-9

Tower, J. (2015). Programmed Cell Death in Aging. *Ageing Res. Rev.* 23 (Pt), 90–100. doi:10.1016/j.arr.2015.04.002

Uberti, F., Caimmi, P. P., Molinari, C., Mary, D., Vacca, G., and Grossini, E. (2011). Levosimendan Modulates Programmed Forms of Cell Death through KATP Channels and Nitric Oxide. *J. Cardiovasc. Pharmacol.* 57 (2), 246–258. doi:10.1097/fjc.0b013e318204bb55

Ucar, A., Gupta, S. K., Fiedler, J., Erikci, E., Kardasinski, M., Batkai, S., et al. (2012). The miRNA-212/132 Family Regulates Both Cardiac Hypertrophy and Cardiomyocyte Autophagy. *Nat. Commun.* 3, 1078. doi:10.1038/ncomms2090

Van Herreweghe, F., Festjens, N., Declercq, W., and Vandenabeele, P. (2010). Tumor Necrosis Factor-Mediated Cell Death: to Break or to Burst, That's the Question. *Cell. Mol. Life Sci.* 67 (10), 1567–1579. doi:10.1007/s00018-010-0283-0

Vande Walle, L., and Lamkanfi, M. (2016). Pyroptosis. *Curr. Biol.* 26 (13), R568–r572. doi:10.1016/j.cub.2016.02.019

Vandenabeele, P., Declercq, W., Van Herreweghe, F., and Vanden Berghe, T. (2010). The Role of the Kinases RIP1 and RIP3 in TNF-Induced Necrosis. *Sci. Signal.* 3 (115), re4. doi:10.1126/scisignal.3115re4

Venderova, K., and Park, D. S. (2012). Programmed Cell Death in Parkinson's Disease. *Cold Spring Harb Perspect. Med.* 2 (8). doi:10.1101/cshperspect.a009365

Wajant, H., and Scheurich, P. (2011). TNFR1-induced Activation of the Classical NF-Kb Pathway. *Febs j* 278 (6), 862–876. doi:10.1111/j.1742-4658.2011.08015.x

Wang, B., Xu, H., Kong, J., Liu, D., Qin, W. D., Bai, W., et al. (2021). Krüppel-like Factor 15 Reduces Ischemia-Induced Apoptosis Involving Regulation of P38/MAPK Signaling. *Hum. Gene Ther.* doi:10.1089/hum.2021.075

Wang, K., Liu, F., Zhou, L.-Y., Ding, S.-L., Long, B., Liu, C.-Y., et al. (2013). miR-874 Regulates Myocardial Necrosis by Targeting Caspase-8. *Cell Death Dis* 4, e709. doi:10.1038/cddis.2013.233

Wang, X., Jiang, Y., Zhang, Q., Tian, X., Sun, Q., Guo, D., et al. (2021). Autophagy as a Novel Insight into Mechanism of Danqi Pill against post-acute Myocardial Infarction Heart Failure. *J. Ethnopharmacology* 266, 113404. doi:10.1016/j.jep.2020.113404

Wang, Y., and Kanneganti, T.-D. (2021). From Pyroptosis, Apoptosis and Necroptosis to PANoptosis: A Mechanistic Compendium of Programmed Cell Death Pathways. *Comput. Struct. Biotechnol. J.* 19, 4641–4657. doi:10.1016/j.csbj.2021.07.038

Wang, Z., Wang, M., Hu, X., Li, Y., Ma, D., Li, S., et al. (2019). Liraglutide, a Glucagon-like Peptide-1 Receptor Agonist, Attenuates Development of Cardiac Allograft Vasculopathy in a Murine Heart Transplant Model. *Transplantation* 103 (3), 502–511. doi:10.1097/TP.0000000000002448

Wongjaikam, S., Kumfu, S., Khamseekaew, J., Chattipakorn, S. C., and Chattipakorn, N. (2017). Restoring the Impaired Cardiac Calcium Homeostasis and Cardiac Function in Iron Overload Rats by the Combined Deferiprone and N-Acetyl Cysteine. *Sci. Rep.* 7, 44460. doi:10.1038/srep44460

Wu, C., Zhou, X.-X., Li, J.-Z., Qiang, H.-F., Wang, Y., and Li, G. (2021). Pretreatment of Cardiac Progenitor Cells with Bradykinin Attenuates H2O2-Induced Cell Apoptosis and Improves Cardiac Function in Rats by Regulating Autophagy. *Stem Cel Res Ther* 12 (1), 437. doi:10.1186/s13287-021-02503-6

Wu, X., Li, Y., Zhang, S., and Zhou, X. (2021). Ferroptosis as a Novel Therapeutic Target for Cardiovascular Disease. *Theranostics* 11 (7), 3052–3059. doi:10.7150/thno.54113

Xiong, X., Liu, J., He, Q., Dai, R., Zhang, H., Cao, Z., et al. (2021). Long Non-coding RNA NORAD Aggravates Acute Myocardial Infarction by Promoting Fibrosis and Apoptosis via miR -577/ COBLL1 axis. *Environ. Toxicol.* 36 (11), 2256–2265. doi:10.1002/tox.23339

Xu, L.-N., Wang, S.-H., Su, X.-L., Komal, S., Fan, H.-K., Xia, L., et al. (2021). Targeting Glycogen Synthase Kinase 3 Beta Regulates CD47 Expression after Myocardial Infarction in Rats via the NF-Kb Signaling Pathway. *Front. Pharmacol.* 12, 662726. doi:10.3389/fphar.2021.662726

Xuan, F., and Jian, J. (2016). Epigallocatechin Gallate Exerts Protective Effects against Myocardial Ischemia/reperfusion Injury through the PI3K/Akt Pathway-Mediated Inhibition of Apoptosis and the Restoration of the Autophagic Flux. *Int. J. Mol. Med.* 38 (1), 328–336. doi:10.3892/ijmm.2016.2615

Xuan, F., Jian, J., Lin, X., Huang, J., Jiao, Y., Huang, W., et al. (2017). 17-Methoxyl-7-Hydroxy-Benzene-Furanchalcone Ameliorates Myocardial Ischemia/Reperfusion Injury in Rat by Inhibiting Apoptosis and Autophagy via the PI3K-Akt Signal Pathway. *Cardiovasc. Toxicol.* 17 (1), 79–87. doi:10.1007/s12012-016-9358-y

Yang, F., Qin, Y., Lv, J., Wang, Y., Che, H., Chen, X., et al. (2018). Silencing Long Non-coding RNA Kcnq1ot1 Alleviates Pyroptosis and Fibrosis in Diabetic Cardiomyopathy. *Cel Death Dis* 9 (10), 1000. doi:10.1038/s41419-018-1029-4

Yang, L., Zhang, Y., Zhu, M., Zhang, Q., Wang, X., Wang, Y., et al. (2016). Resveratrol Attenuates Myocardial Ischemia/reperfusion Injury through Up-Regulation of Vascular Endothelial Growth Factor B. *Free Radic. Biol. Med.* 101, 1–9. doi:10.1016/j.freeradbiomed.2016.09.016

Yang, Z., Li, C., Wang, Y., Yang, J., Yin, Y., Liu, M., et al. (2018). Melatonin Attenuates Chronic Pain Related Myocardial Ischemic Susceptibility through Inhibiting RIP3-MLKL/CaMKII Dependent Necroptosis. *J. Mol. Cell Cardiol.* 125, 185–194. doi:10.1016/j.yjmcc.2018.10.018

Yuan, P., Hu, Q., He, X., Long, Y., Song, X., Wu, F., et al. (2020). Laminar Flow Inhibits the Hippo/YAP Pathway via Autophagy and SIRT1-Mediated Deacetylation against Atherosclerosis. *Cel Death Dis* 11 (2), 141. doi:10.1038/s41419-020-2343-1

Yuan, Y.-Y., Xie, K.-X., Wang, S.-L., and Yuan, L.-W. (2018). Inflammatory Caspase-Related Pyroptosis: Mechanism, Regulation and Therapeutic Potential for Inflammatory Bowel Disease. *Gastroenterol. Rep. (Oxf)* 6 (3), 167–176. doi:10.1093/gastro/goy011

Yue, R.-C., Lu, S.-Z., Luo, Y., Wang, T., Liang, H., Zeng, J., et al. (2019). Calpain Silencing Alleviates Myocardial Ischemia-Reperfusion Injury through the NLRP3/ASC/Caspase-1 axis in Mice. *Life Sci.* 233, 116631. doi:10.1016/j.lfs.2019.116631

Zhang, B., Zhang, Y., Liu, B., Fang, L., Li, Y., Meng, S., et al. (2018). So-Osmolar Iodixanol Induces Less Increase in Circulating Endothelial Microparticles *In Vivo* and Less Endothelial Apoptosis *In Vitro* Compared with Low-Osmolar Iohexo. *Contrast Media Mol. Imaging. l*, 2018, 8303609. doi:10.1155/2018/8303609I

Zhang, H., Zhang, R.-H., Liao, X.-M., Yang, D., Wang, Y.-C., Zhao, Y.-L., et al. (2021). Discovery of β-Carboline Derivatives as a Highly Potent Cardioprotectant against Myocardial Ischemia-Reperfusion Injury. *J. Med. Chem.* 64 (13), 9166–9181. doi:10.1021/acs.jmedchem.1c00384

Zhang, J. G., Yang, N., He, H., Wei, G. H., Gao, D. S., Wang, X. L., et al. (2005). Effect of Astragalus Injection on Plasma Levels of Apoptosis-Related Factors in Aged Patients with Chronic Heart Failure. *Chin. J. Integr. Med.* 11 (3), 187–190. doi:10.1007/BF02836502

Zhang, X., Li, Y., Wang, Y., Zhuang, Y., Ren, X., Yang, K., et al. (2020). Dexmedetomidine Postconditioning Suppresses Myocardial Ischemia/reperfusion Injury by Activating the SIRT1/mTOR axis. *Biosci. Rep.* 40 (5). doi:10.1042/BSR20194030

Zhang, Y., Liu, X., Bai, X., Lin, Y., Li, Z., Fu, J., et al. (2018). Melatonin Prevents Endothelial Cell Pyroptosis via Regulation of Long Noncoding RNA MEG3/miR-223/NLRP3 axis. *J. Pineal Res.* 64 (2). doi:10.1111/jpi.12449

Zheng, X., Zhong, T., Ma, Y., Wan, X., Qin, A., Yao, B., et al. (2020). Bnip3 Mediates Doxorubicin-Induced Cardiomyocyte Pyroptosis via Caspase-3/GSDME. *Life Sci.* 242, 117186. doi:10.1016/j.lfs.2019.117186

Zhou, L., Liu, X., Wang, Z.-Q., Li, Y., Shi, M.-M., Xu, Z., et al. (2018). Simvastatin Treatment Protects Myocardium in Noncoronary Artery Cardiac Surgery by Inhibiting Apoptosis through miR-15a-5p Targeting. *J. Cardiovasc. Pharmacol.* 72 (4), 176–185. doi:10.1097/fjc.0000000000000611

Zhou, Z., Wang, Z., Guan, Q., Qiu, F., Li, Y., Liu, Z., et al. (2016). PEDF Inhibits the Activation of NLRP3 Inflammasome in Hypoxia Cardiomyocytes through PEDF Receptor/Phospholipase A2. *Int. J. Mol. Sci.* 17 (12). doi:10.3390/ijms17122064

Zhu, H., and Sun, A. (2018). Programmed Necrosis in Heart Disease: Molecular Mechanisms and Clinical Implications. *J. Mol. Cell Cardiol.* 116, 125–134. doi:10.1016/j.yjmcc.2018.01.018

Zhu, P., Hu, S., Jin, Q., Li, D., Tian, F., Toan, S., et al. (2018). Ripk3 Promotes ER Stress-Induced Necroptosis in Cardiac IR Injury: A Mechanism Involving Calcium overload/XO/ROS/mPTP Pathway. *Redox Biol.* 16, 157–168. doi:10.1016/j.redox.2018.02.019

Conflict of Interest: The authors declare that the research was conducted in the absence of any commercial or financial relationships that could be construed as a potential conflict of interest.

Publisher's Note: All claims expressed in this article are solely those of the authors and do not necessarily represent those of their affiliated organizations, or those of the publisher, the editors and the reviewers. Any product that may be evaluated in this article, or claim that may be made by its manufacturer, is not guaranteed or endorsed by the publisher.

Copyright © 2021 Zhou, Sun, Gu, Wang, Yang, Wei, Shan, Wang and Wang. This is an open-access article distributed under the terms of the Creative Commons Attribution License (CC BY). The use, distribution or reproduction in other forums is permitted, provided the original author(s) and the copyright owner(s) are credited and that the original publication in this journal is cited, in accordance with accepted academic practice. No use, distribution or reproduction is permitted which does not comply with these terms.

frontiers in Cell and Developmental Biology

REVIEW
published: 02 December 2021
doi: 10.3389/fcell.2021.799499

A Novel Insight Into the Fate of Cardiomyocytes in Ischemia-Reperfusion Injury: From Iron Metabolism to Ferroptosis

Jing-yan Li[1], Shuang-qing Liu[2], Ren-qi Yao[2], Ying-ping Tian[1] and Yong-ming Yao[1,2]**

[1]Department of Emergency, The Second Hospital of Hebei Medical University, Shijiazhuang, China, [2]Translational Medicine Research Center, Medical Innovation Research Division and Fourth Medical Center of the Chinese PLA General Hospital, Beijing, China

Ischemia-reperfusion injury (IRI), critically involved in the pathology of reperfusion therapy for myocardial infarction, is closely related to oxidative stress the inflammatory response, and disturbances in energy metabolism. Emerging evidence shows that metabolic imbalances of iron participate in the pathophysiological process of cardiomyocyte IRI [also termed as myocardial ischemia-reperfusion injury (MIRI)]. Iron is an essential mineral required for vital physiological functions, including cellular respiration, lipid and oxygen metabolism, and protein synthesis. Nevertheless, cardiomyocyte homeostasis and viability are inclined to be jeopardized by iron-induced toxicity under pathological conditions, which is defined as ferroptosis. Upon the occurrence of IRI, excessive iron is transported into cells that drive cardiomyocytes more vulnerable to ferroptosis by the accumulation of reactive oxygen species (ROS) through Fenton reaction and Haber–Weiss reaction. The increased ROS production in ferroptosis correspondingly leads cardiomyocytes to become more sensitive to oxidative stress under the exposure of excess iron. Therefore, ferroptosis might play an important role in the pathogenic progression of MIRI, and precisely targeting ferroptosis mechanisms may be a promising therapeutic option to revert myocardial remodeling. Notably, targeting inhibitors are expected to prevent MIRI deterioration by suppressing cardiomyocyte ferroptosis. Here, we review the pathophysiological alterations from iron homeostasis to ferroptosis together with potential pathways regarding ferroptosis secondary to cardiovascular IRI. We also provide a comprehensive analysis of ferroptosis inhibitors and initiators, as well as regulatory genes involved in the setting of MIRI.

Keywords: ischemia-reperfusion injury, cardiomyocyte, cell death, ferroptosis, iron metabolism

OPEN ACCESS

Edited by:
Zhi Qi,
Nankai University, China

Reviewed by:
Tianqing Peng,
Western University, Canada
Li Tao,
Third Military Medical University, China

****Correspondence:***
Ying-ping Tian
tianyingping999@163.com
Yong-ming Yao
c_ff@sina.com

Specialty section:
This article was submitted to Cell Death and Survival, a section of the journal Frontiers in Cell and Developmental Biology

Received: *21 October 2021*
Accepted: *15 November 2021*
Published: *02 December 2021*

Citation:
Li J-y, Liu S-q, Yao R-q, Tian Y-p and Yao Y-m (2021) A Novel Insight Into the Fate of Cardiomyocytes in Ischemia-Reperfusion Injury: From Iron Metabolism to Ferroptosis. Front. Cell Dev. Biol. 9:799499. doi: 10.3389/fcell.2021.799499

INTRODUCTION

To date, revascularization is commonly regarded as one of the efficacious treatments for ischemic cardiomyopathy in patients with critically acute myocardial infarction (Yang et al., 2018). However, reperfusion therapy is inevitably complicated with myocardial ischemia-reperfusion injury (MIRI), which is responsible for increased mortality and poor outcomes in myocardial infarction, thereby reducing the preponderance of reperfusion therapy to a large extent (Bell and Yellon, 2011). It has been demonstrated that ischemia-reperfusion injury (IRI) is especially involved in persistent

impairment of cardiac function, followed by myocardial remodeling. Therefore, timely recognition and prompt interference for MIRI are the currently clinical incidents that need to be urgently resolved to improve the survival and prognosis of myocardial infarction patients. Dysfunction in cardiomodulatory response compromised by IRI impairs cardiometabolisms, including oxidative stress, systemic inflammation, calcium metabolic disorders, mitochondrial damage, and iron overload, which ultimately results in a vicious cycle between progressive disturbance of cardiomyocyte metabolism and irreversible myocardial remodeling (Turer and Hill, 2010). Deep insights into the interplay between IRI and intracellular metabolism as well as cell death in cardiomyocytes are of great importance in extending the knowledge of the pathogenesis and development of MIRI.

As we know, iron is considered an essential mineral that serves as a prerequisite in pivotal biological processes, including oxygen transfer, enzymatic catalyzed reaction, aerobic respiration, lipid peroxidation, and intracellular metabolism (Hirst, 2013). Iron deficiency jeopardizes the contractility of cardiomyocytes by subduing mitochondrial function and decreasing energy generation, resulting in impairment of cardiac function (Hoes et al., 2018). Upon the physiological state, iron is capable of playing an important role in energy metabolism through multiple ways to enter cardiomyocytes, being utilized for storage or transported into the mitochondrion to take part in biosynthetic reaction (Valko et al., 2016). Under the challenge of continuous stress or decompensatory response however iron reversely drives a poisonous property resulting from the overproduction of reactive oxygen species (ROS), which collapses the balance between generation and depletion in free radicals *via* the Fenton reaction and Haber–Weiss reaction (Valko et al., 2016). Uncontrolled accumulation of iron concentration and redox efficacy of ferrous (Fe^{2+}) ions facilitate a perniciously metabolic network in cardiomyocytes, contributing to lipid peroxidation along with ROS overproduction, which exert a great threat to the function of basic cellular mechanisms (Gammella et al., 2016; He et al., 2019). Increased mitochondrial iron-related ROS generation is another regulatory contributor to both malfunction of intrinsic mitochondria and cardiac tissue injury. Mitochondrial iron is deemed as the major factor determining cardiomyocyte fate as evidenced by approximately one-third of cardiomyocyte iron reserves in the mitochondria. Moreover, it has been reported that the iron content in cardiomyocyte mitochondria is 50% higher than that of the other cells (Wofford et al., 2017). Increasing clinical studies have suggested that the level of cardiomyocyte iron is a prognostic factor of MIRI accounting for the deposition of iron in cardiac tissue in the occurrence of MIRI. Additionally, the impeded erythrocyte flow in the obstructive region might lead red blood cells to be lysed, resulting in the accumulation of iron from hemoglobin, which can eventually generate excessive ROS and trigger pathological events of MIRI. As is hypothesized that iron deposition might be recognized as an integral element of pathophysiology for triggering MIRI and increasing mortality risk, it is of great significance to clarify the underlying mechanisms of iron-mediated cell death to further provide potential targets for MIRI therapy.

As we all know, no matter what mechanisms are involved in the pathophysiology of MIRI, the final foreordination of the injured cardiomyocyte is the distinct forms of programmed cell death, which have been identified to play an essential role in MIRI, namely, apoptosis, necroptosis, pyroptosis, and ferroptosis. Over the past decades, regarded as the main types of cell death for cardiomyocytes, apoptosis is considered a form of programmed cell death, while necrosis is thought to be an accidental and uncontrolled type of cell death. In recent decades however, necrosis is precisely regulated by differently signaling pathways, including necroptosis, ferroptosis, pyroptosis, oxytosis, and parthanatos. Currently, noxious iron overload has been reported to induce non-apoptosis cell death, defined as ferroptosis, which presents with a deteriorative cross talk between lipid peroxidation, and a mass of ROS accumulation depended on excessive iron, together with the dominating causes of reduction in glutathione synthesis and deactivation of enzyme glutathione peroxidase 4 (GPX4) (Dixon et al., 2012). Indeed, multiple factors are involved in the pathogenesis of cardiac I/R injury implicated by ferroptosis, such as amino acid and lipid metabolism as well as iron mobilization and peroxidation through Fenton reaction (Fang et al., 2019). The regulatory effects of other factors, including activity of GPX4, ferroptosis-associated endoplasmic reticulum stress (ERS), and the mammalian target of rapamycin (mTOR)-mediated iron transport proteins, are also noteworthy but remain controversial (Baba et al., 2018; Li et al., 2020). From a molecular perspective, both ferroptosis-related initiators and inhibitors might be the potential targets for treatment of MIRI since ferroptosis accompanied by excess iron is confirmed to be the leading cause of cardiomyocyte death. Suppressing ferroptosis to prevent cardiac cell death and alleviate cardiac remodeling might become an efficacious therapeutic strategy for MIRI.

IRON HOMEOSTASIS AND ITS ROLE IN CARDIOMYOCYTES

The pathophysiological progression of cardiomyocyte injury reportedly results from a disorder of iron homeostasis attributed to the overproduction of ROS and formation of the mitochondrial permeability transition pore (mPTP), ultimately leading to the induction of cardiomyocyte death (Morciano et al., 2015; Pell et al., 2016). In fact, hyperactivation of hypoxia-inducible factor (HIF) upregulates the mitochondrial ferritin (FtMt) expression of transferrin receptor 1 (TfR1), followed by increased iron accumulation, which traps cardiomyocytes into a vicious cycle of exacerbated ROS-induced impairment (Tang et al., 2008). A unique cohort of FtMt, featured on ferroxidase activity and regulatory capacity of iron metabolism in mitochondria, acts as a prime contributor to myocardial vitality and ROS regulation in IRI (Wood, 2008; Wu et al., 2016). Since most of mitochondrial ROS arise from redox reaction in the initial stage of oxidative stress, it is reasonable to predicate that mitochondrial function serves as a bridge

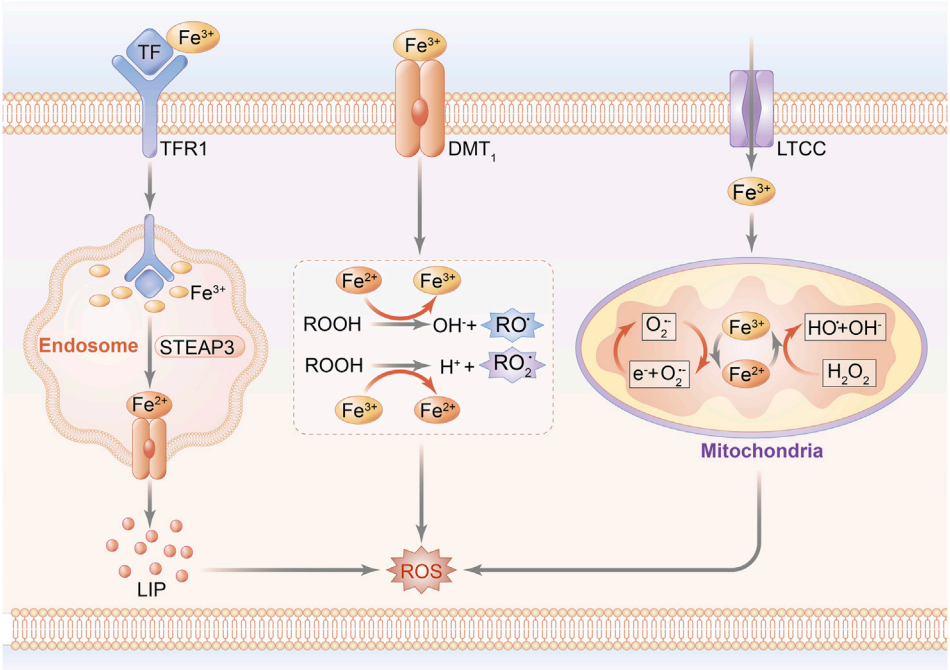

FIGURE 1 | Schematic diagram of iron homeostasis in cardiomyocytes. Peripheral iron is bound with Tf and imported into the intracellular area through the transport of TfR1, while non-Tf–combined iron is transported by DMT-1 and LTCC. The uptake of iron is internalized by endocytosis. A part of iron mediates lipid peroxidation by catalyzing ROOH into the formation of RO and RO_2 radicals. Other parts of Fe(II) and Fe(III) are transported into mitochondria to conduct peroxidative reaction through Fenton reaction, and eventually upregulate ROS generation.; Abbreviations: Tf, transferrin; TfR1: transferrin receptor 1; DMT-1, divalent metal transporter 1; LTCC, L-type voltage-dependent Ca^{2+} channels; ROOH, hydroperoxysides; RO, alkoxyl; RO_2, peroxyl; and STEAP3, STEAP family member 3.

connecting iron homeostasis to ROS production during the occurrence of MIRI, suggesting that reversal of mitochondrial iron–associated peroxidation reaction might be one of the beneficial interferences with MIRI. Notably, the schematic diagram of iron homeostasis in cardiomyocytes and mitochondria is shown in **Figure 1**.

Iron Transport in Cardiomyocytes

Cardiomyocyte intussuscepts iron mainly depending on ferritin (FT), either by means of combination with TfR1 and subsequently receptor-mediated endocytosis, or through the calcium channels and zinc transporters in the cardiac plasma membrane, which are mediated by divalent metal transporter 1 (DMT-1) protein (Hentze et al., 2010). In addition to being stored in FT cores in normal circumstances, ferrous ion can be mobilized and released to peripheral circulation *via* ferroportin (FPN), which is located on the basolateral membrane of enterocytes (Oudit et al., 2003). Upon entrance into the cardiomyocytes, iron is stored in the labile iron pool (LIP), where the level of iron is maintained stably on a normal range but abruptly increases under exposure to the pathological state, acting as an intermediator to promote heme and iron–sulfur cluster production in the mitochondrion through the biosynthetic pathway (Lane et al., 2015). Iron in LIP can be utilized for storage in FT, which serves as a ubiquitous intracellular buffer to prevent iron deficiency and iron overload, contributing to its efficacy in reserving as much as 5,000 atoms of iron in a soluble form and transporting iron to the requisite site (Watt, 2013). FT, composed of 24 subunits of both ferritin heavy chain (FTH) and ferritin light chain (FTL), is regarded as a key factor implicated with iron homeostasis for the reason that it combines and segregates iron in the case of redundant iron importing to protect against oxidative stress, whereas it releases and transports iron when suffering iron deficiency (Kawabata, 2019).

Notably, intracellular iron concentration and homeostasis are affected by several key regulators. Since the peroxidative peculiarity of iron prompts it to be a redox catalyst for the generation of noxious ROS, intracellular iron is exactly regulated by the ROS-dependent cell signaling pathway to maintain biological function. One of these catalytic responses is initiated in the Fenton reaction, for example, stimulating hydroxyl radical (HO) production, and another contributor concentrates on ferrous ion–mediating lipid peroxidation response, in turn inducing the accumulation of lipid radicals (Aisen et al., 2001). Moreover, transcriptional modification after the interconnection between iron regulatory proteins (IRPs) and iron responsive elements (IREs) is involved in the regulated mechanisms with regard to the cellular iron homeostatic process in iron intake, reservation, and release by modulating the synthetic function of iron metabolism–associated proteins (Haddad et al., 2017). Under the low content of cellular iron, bidirectional IRPs are responsible for either stabilizing the mRNA expression of TfR1 and DMT-1 to facilitate iron indrawal, or

conducting a suppressed impact on mRNA translation of FT in order to inhibit iron storage (Paterek et al., 2019). Additionally, the degradation of FPN has been proven to be independently related to hepcidin in cardiomyocytes, and it accounts for the inactivation of FPN, eventually resulting in reduced iron release. Actually, cardiac hepcidin is found to be a major cause for iron metabolism in cardiomyocytes, and it exhibits a distinction from systemic iron regulation due to its autologous secretive function that promotes cardiac hepcidin protein upregulation rather than downregulation onset of hypoxia (Lakhal-Littleton et al., 2016). Thus, the fact that only one FPN protein is available for iron exporting during iron accumulation might further confirm cardiomyocytes to be more sensitive to iron overload than other cell types.

The Role of Iron Metabolism in Myocardial Mitochondria

The mitochondrion, known as an essential organelle for systemic energy metabolism, confers an important impact on iron homeostasis and modulation of myocardial damage during IRI (Richardson et al., 2010; Lesnefsky et al., 2017; Vela, 2020). It has been documented that mitochondria provide available sites for heme synthesis and iron–sulfur cluster (ISC) generation, with formation of heme and ISC proteins to be integrated in the mitochondrial oxidative phosphorylation system, which supplies a physiological necessity of cardiac activity for continuous energy through catalyzing electron transport of oxidative iron (Paul et al., 2017). Thus, iron concentration in mitochondria is closely related to the fate of cardiomyocytes since the level of mitochondrial iron in cardiac myocytes is remarkably higher than other cells. As reported by Wofford et al., insufficient iron might impose restriction on energy export, whereas uncontrolled iron overload could lead to a disruption of the mitochondrion *via* redundant ROS generation (Kruszewski, 2003; Wofford et al., 2017). Along with ROS-associated toxicity in mitochondria, the productions of poisonous hydroxyl radicals, as a result of the reaction between ROS and mitochondria, contribute to depolarization in mitochondrial membrane potential (MMP) and openness in the mitochondrial penetrability pore, thereby leading to aberrant morphology of mitochondrial swelling as well as mitochondrial dysfunction (Sripetchwandee et al., 2014; Chan et al., 2018).

Despite explicit mechanisms concerning iron transportation through mitochondrial ectoblast remain to be ascertained, one of the most evident studies suggests that both the Tf-TfR complex and FT degradation in the lysosome are the major sources of importing iron from the cytoplasm to the mitochondrion, which is regulated by mitoferrin and mitochondrial calcium uniporter (Gordan et al., 2018). FtMt, another key regulator of mitochondrial iron homeostasis, especially expressing on cardiomyocytes and possessing a highly homologous sequence with FTH, conducts a pleiotropic effect on iron input by means of redistribution of iron from the cytosol to the mitochondrion (Santambrogio et al., 2007). On account of this regulatory mechanism, elevated expression of FtMt on cardiomyocytes is found to be a major cause for reduction of iron in mitochondrial LIP, subsequently resulting in decreased systemic ROS generation (Nie et al., 2005; Campanella et al., 2009). Further evidence has shown that the overexpression of FtMt significantly inhibits erastin-induced ferroptosis due to its impact on decreased ROS production (Wang et al., 2016). Of note, FtMt might be a potential target for maintaining iron homeostasis in cardiomyocytes.

MOLECULAR MECHANISMS OF IRON METABOLISM IN CARDIOMYOCYTE IRI

Iron metabolism imbalance, especially iron overload, has been demonstrated to be implicated in the pathology of cardiomyocyte IRI, resulting from the driving forces of excessive ROS and oxygen free radicals that attribute to antioxidant system disrupt onset of constant exposure to IRI (Zhou et al., 2015; Cadenas, 2018). Inherently, this pathological process further aggravates oxidative stress accompanied by myocardial membrane damage and cardiovascular endothelial dysfunction (Dongó et al., 2011). In the early stage of ischemia and reperfusion, intracellular iron is conductive to be released in the acid internal environment of cardiomyocytes, augmenting iron-mediated Fenton reaction, which converses hyporeactive hydrogen peroxide to hyperreactive hydroxyl radicals (Williams et al., 1991). In this case, the administration of iron inhibitors at the initial phase of reperfusion might diminish free radical generation and attenuate cardiomyocyte IRI (Drossos et al., 1995).

The Pathophysiology of Cardiomyocyte IRI

Increasing evidence indicates that multiple pathophysiological factors are involved in the development of MIRI, including oxidative stress, endothelial cell inflammation, calcium overload, and energy metabolism disorder. Cardiomyocyte IRI is commonly accompanied by redundant oxygen-free radicals and accumulated ROS after cardiovascular reperfusion, which finally evokes the peroxidation of proteins, lipids, and nucleic acids. These endogenous superoxide products can further accelerate membrane injury and organelle dysfunction (Matsushima et al., 2014). Along with hyperactivated inflammation compromised by conglutination and infiltration of neutrophils, cardiomyocyte IRI unexpectedly worsens as a result of robust feedback on increased metabolism of arachidonic acid, in turn leading to a massive production of inflammatory cytokines (Vinten-Johansen et al., 2007; Boag et al., 2017). During cardiomyocyte I/R injury, high levels of pro-inflammatory cytokines promote either the myocardial tissue to maintain a pro-inflammatory state or endothelial cells to induce autophagy, eventually exposing cardiomyocytes to a more vulnerable damage in structure and function (Russo et al., 2017; Schanze et al., 2019). Intracellular calcium, with the peculiar capacity of maintaining cardiomyocyte functions, appears to be more sensitive to reperfusion, and it is largely overloaded when cardiomyocytes suffer IRI (Verkhratsky and Parpura, 2014). Similar to excessive amounts of iron, calcium overload suppresses excitability and contractility of cardiomyocytes, attributed to the combination

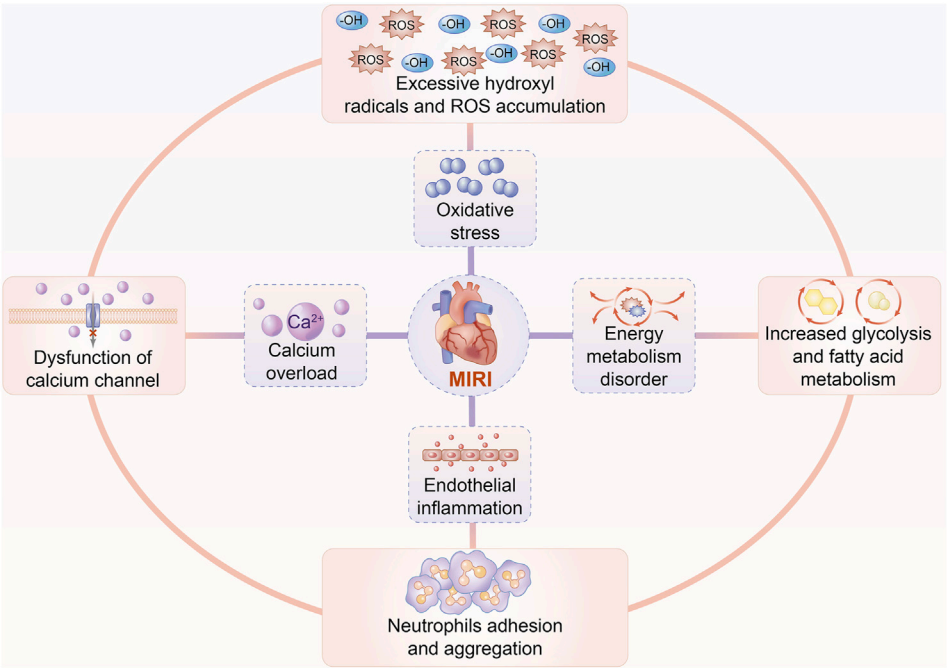

FIGURE 2 | Pathophysiology of cardiomyocyte IRI. Multiple factors are involved in the pathogenesis and progression of MIRI, including oxidative stress, endothelial cell inflammation, calcium overload, and energy metabolic disturbance. Excessive ROS and hydroxyl radicals are produced to trigger peroxidative stress. Chemotaxis, adhesion, and aggregation of neutrophils initiate inflammatory cytokine release, in turn inducing endothelial cell injury. Calcium overload suppresses excitability and contractility of cardiomyocytes due to the dysfunction of the L-type calcium channel as well as the ryanodine receptor. Increased glycolysis and fatty acid metabolism, as well as mitochondrial dysfunction, ultimately deteriorate the disorder of energy metabolism.

TABLE 1 | Mediators of iron metabolism in MIRI-associated diseases.

Molecule	Regulatory effects
HIF	Enhances TfR1 expression and exasperates iron overload and ROS production
FTH	Binds iron and suppresses cardiomyocyte capacity
MFRN	Regulates mitochondrial iron import
MCU	Regulates mitochondrial calcium uniporter
ABCB8	Augments mitochondrial iron output
IRP	Modulates iron intake, reservation, and release
IRE	Regulates the synthesis of iron metabolism–associated proteins
FPN	Mobilizes and releases ferrous ion to peripheral circulation
FtMt	Inputs iron and redistributes iron from the cytosol to mitochondria
DMT-1	Promotes iron indrawal and inputs iron

Abbreviations: HIF, hypoxia-inducible factor; FTH, ferritin heavy chain; MFRN, mitoferrin 2; MCU, mitochondrial calcium uniporter; ABCB8, ATP-binding cassette subfamily B member 8; IRP, iron regulatory proteins; IRE, iron-responsive elements; FPN, ferroportin; FtMt, mitochondrial ferritin; and DMT-1, divalent metal transporter 1.

between calcium and troponin, which finally debilitates the contraction of myocardial cells (Grueter et al., 2006). With regard to energy metabolism during cardiomyocyte IRI, ATP produced by glycolysis is considered to be the primary source of energy for the maintenance of cardiomyocyte vitality at the initial phase of reperfusion. Inevitably, this action causes cardiomyocytes to suffer a vicious cross talk between lactate accumulation and the acidic environment, resulting in fatty acid peroxidation together with an energy metabolism disorder (Tian et al., 2019). Taken together, cardiomyocyte IRI depends on the energy metabolism disorder initiated in the ischemia-hypoxia setting and enhances production of oxygen free radicals, which indirectly induce calcium along with inflammation, leading to mitochondrial damage (**Figure 2**).

The Mediators of Iron Metabolism in Cardiomyocyte IRI

It has been reported that multiple iron metabolism–associated factors are thought to be associated with the pathogenesis of cardiomyocyte IRI, including HIF and FTH signaling pathways and mitochondrial iron protein–regulated pathway (**Table 1**). The HIF, for instance, presents with visible hyperactivation, which, in turn, upregulates iron TfR1 expression and causes iron overload during cardiomyocyte IRI,

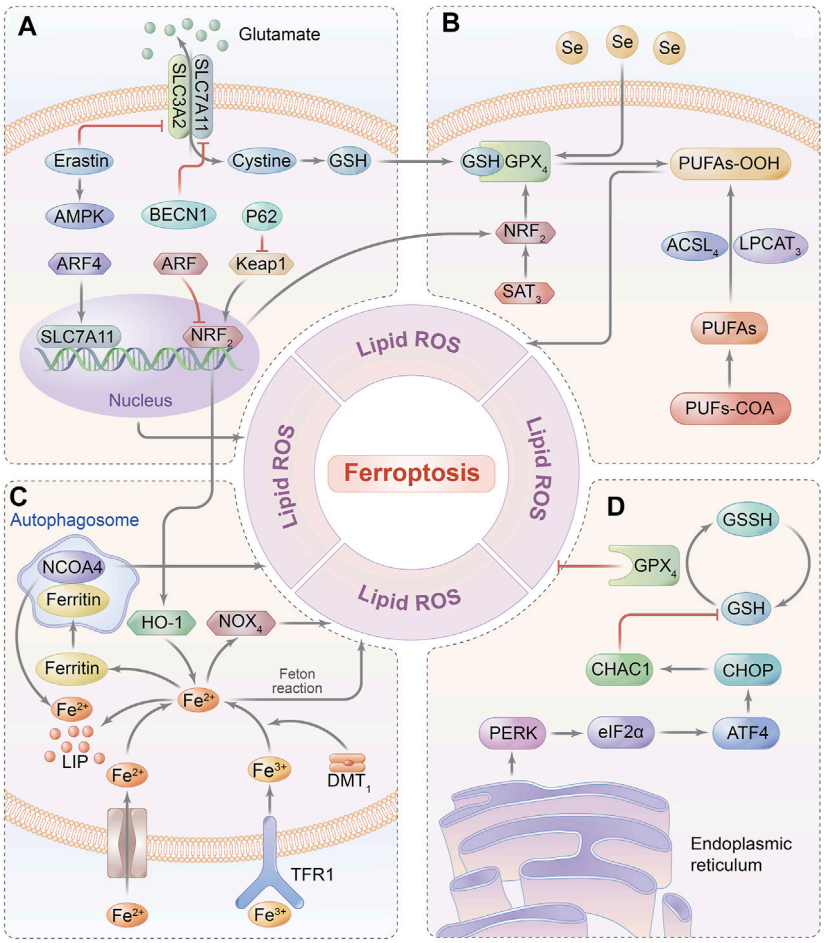

FIGURE 3 | Ferroptosis-related signaling pathway. **(A)** GSH relies on the molecular substrate called cysteine, which is transferred *via* a heterodimeric cell membrane antiporter, system Xc-that is composed of SLC7A11 and SLC3A2, regulating ferroptosis by exchanging glutamate and cystine at a 1:1 ratio. **(B)** Ferroptosis is triggered by the peroxidation of PUFAs and accumulation of ROS, which are catalyzed by ACSL4 and LPCAT3. GPX4 can hydrolyze lipid peroxides into innocuous alcohols. **(C)** Free iron bound with Tf is transported into intracellular area *via* TfR1 in endosomes. Fe (III) is reduced to redox-active iron (FeII) by ferrireductase of STEAP3, while Fe (II) is released from endosomes into LIP through DMT1. Under the oxidative stress, Fe^{2+} catalyzes the generation of hydroxyl radicals by Fenton reaction, which eventually initiates ferroptosis. Ferritin is utilized to iron storage and can be degraded by NCOA4-mediated ferritinophagy. **(D)** GSH synthesis is a requisite for GPX4 in mediating an antioxidant impact, thereby inhibiting the iron-dependent ROS production by catalyzing lipid hydroperoxides into lipid alcohols.; Abbreviations: GPX4, glutathione peroxidase 4; PUFAs, poly-unsaturated fatty acids; NCOA4, nuclear receptor coactivator 4; GSH, glutathione; SLC7A11: solute carrier family 7 member 11; SLC3A2, solute carrier family 3 member 2; ACSL4, acyl-coA synthetase long-chain family member 4; LPCAT3. lysophosphatidylcholine acyl-transferase 3; Tf, transferrin; TfR1, transferrin receptor 1; ATF4, activating transcription factor 4; and CHOP, C/EBP homologous protein.

eventually exasperating ROS-induced peroxidative injury (Zhang et al., 2019a). Further evidence has shown that the administration of cardiomyocytes with iron chelators after I/R injury is beneficial for the reversion on myocardiac malfunction (Paraskevaidis et al., 2005). Another mediator of FTH, as observed trending a down-expressed toward in the mouse model of MIRI, exerted a suppressed effect on the capacity of cardiomyocytes in binding free iron, leading to oxidative stress and even cell death (Omiya et al., 2009). Unique cohorts of mitochondrial iron proteins are demonstrated to complicate modulating cardiomyocyte IRI and play important roles in survival and prognosis of cardiomyocytes *via* controlling ROS generation. For instance, mitochondrial iron import is regulated by mitoferrin 2 (MFRN) and mitochondrial calcium uniporter (MCU), whereas its export is modulated *via* ABCB proteins (Ichikawa et al., 2012). The same verification goes for ATP-binding cassette subfamily B member 8 (ABCB8) that upregulated expression of ABCB8 through genetic modification is identified to effectively promote mitochondrial iron output and finally protect cardiomyocytes against IRI (Chang et al., 2016). Hence, mitochondrial iron regulators might become effective targets for improving outcomes in the setting of MIRI (Chang et al., 2016).

FERROPTOSIS IN CARDIOMYOCYTES AFTER IRI

Elevated concentration of the intracellular iron–induced poisonous ROS-dependent reaction is defined as ferroptosis,

which is a non-apoptotic programmed cell death and is characterized by overload iron-associated lipid peroxidation (Conrad et al., 2018). It can be initiated by either depletion of glutathione biosynthesis or inactivation of the antioxidant enzyme GPX4 that is deemed a consequence of iron-relevant ROS generation as well as polyunsaturated fatty acid (PUFA) peroxidation, contributing to the disruption of redox homeostasis (Dixon et al., 2012; Cao and Dixon, 2016). Currently, the major signaling pathways of ferroptosis are summarized in **Figure 3**. Moreover, recent studies have confirmed ferroptosis to be a substantial contributor to the pathogenesis of cardiomyocyte IRI, as evidenced by the protective effect on cardiomyocytes once the ferroptosis inhibitor is administered (e.g., liproxstatin-1, Lip-1) on a MIRI model, implicating that ferroptosis might provide a novel treatment targeted for diseases associated with cardiomyocyte IRI (Díez-López et al., 2018). Therefore, the effects of ferroptosis-related molecular pathways on MIRI are as follows.

Iron Metabolism Signaling Pathway

Iron overload resulted from either cytoplasm iron imbalance or mitochondrial iron disturbance exerts an impact on pathogenesis and progression of ferroptosis. One of the intracellular iron modulators nuclear receptor coactivator 4 (NCOA4), for example, can be regulated by ferritinophagy to further suppress transferrin exporting intracellular iron, while another key encoder named iron-responsive element-binding protein 2 (IREB2) mainly affects transferrin expression as well as iron transportation (Xie et al., 2016). Likewise, the cross talk of iron on the mitochondrial membrane is primarily regulated by the voltage-dependent anion channel (VDAC) located on the outer mitochondrial membrane (Tateda et al., 2012). VDAC 2/3 shows evident signs of opening under persistent exposure to mitochondrial iron accumulation, and this subsequently primes the response of ferroptosis *via* regulating the upstream protein of FtMt. Accordingly, the overexpression of FtMt can intercept mitochondrial iron to protect cells from ferroptosis (Maldonado et al., 2013).

Glutathione Metabolism Signaling Pathway

Intracellular reduced glutathione (GSH), considered the main antioxidant buffer, commonly displays the ability in protecting against lipid peroxidation in ferroptosis by donating an electron to GPX4, which can suppress the formation of iron-dependent ROS by transforming lipid hydroperoxides into lipid alcohols (Stockwell et al., 2017; Ingold et al., 2018). Originally, endogenous biosynthesis of GSH relies on the molecular substrate called cysteine, which is transferred *via* a heterodimeric cell membrane antiporter, system Xc- that is composed of a transmembrane protein transporter solute carrier family 7 member 11 (SLC7A11) and a single-pass transmembrane regulatory protein solute carrier family 3 member 2 (SLC3A2), regulating ferroptosis by exchanging glutamate and cystine at a 1: 1 ratio (Fujii et al., 2019). Importantly, the ferroptotic inhibitor of erastin can directly restrain system Xc- function resulting in GPX4 hypoactivation due to the depletion of GSH (Hayano et al., 2016). Consistent with this finding, the knockdown of GPX4 could exasperate lipid peroxidation–mediated ferroptosis, suggesting GPX4 to be the key negative regulator of ferroptosis (Gladyshev et al., 1999).

Lipid Peroxidation Signaling Pathway

Even though the systemic antioxidant effect dominates the enzyme-linked reactions, long-term exposure to oxidative stress can inevitably trigger the biosynthesis of PUFAs in decompensation by activating lipid metabolism–related enzymes, including acyl-coA synthetase long-chain family member 4 (ACSL4) and lysophosphatidylcholine acyl-transferase 3 (LPCAT3) (Anthonymuthu et al., 2018). PUFAs are catalyzed to generate subversive lipid peroxides that destruct cell morphology, such as mitochondrial membrane shrinkage and membrane imperfection, ultimately leading to ferroptosis (Ng et al., 2020). In accordance with these findings, exogenous unsaturated fatty acids might not only inhibit the susceptibility of cells to ferroptosis but also refrain the lipid bilayer of the cell membrane from peroxidative injury (Magtanong et al., 2019).

NOX4 Signaling Pathway

Previous studies have regarded NADPH oxidase 4 (NOX4) to be the major molecular medium of oxidative stress in cardiomyocytes that transfers electrons from NADPH to the oxygen atom, even producing superoxide (Kuroda et al., 2010). On account of its inductive ability in peroxidation, NOX4 deficiency inhibits the cardiomyocytotoxicity and mitochondrial injury induced by produced intracellular free radicals, implying that NOX4 is compromised in oxidative stress-mediated cell damage (Sun et al., 2017). As discovered by Chen et al., the knockdown of NOX4 dramatically reversed ventricular remodeling by means of improving iron overload in the heart failure model, which further inferred pharmaceutical inhibition or knockout of GPX4 to be effective in precaution of ferroptosis (Chen et al., 2019). Remarkably, apoptosis-inducing factor mitochondrion-associated 2 (AIFM2, also named FSP1) is another electronic carrier and lipid-soluble antioxidant independent of GPX4, which acts as a nicotinamide adenine dinucleotide phosphate (NADP)–dependent coenzyme Q (CoQ) oxidoreductase to suppress ferroptosis by directly modulating the CoQ antioxidant system (Marshall et al., 2005).

ATF4 Signaling Pathway

Activating transcription factor 4 (ATF4) has been documented to involve in the regulation of autophagy, oxidative stress, and inflammatory response, and partially expresses at a low level under the normal condition, whereas it is dramatically overexpresses upon stimulation with hypoxia or ERS (Pitale et al., 2017). A recent report revealed that activation of the ATF4-C/EBP homologous protein (CHOP) signaling pathway was closely related to ferroptosis-associated diseases such as cardiomyocyte IRI by modulating the ATF4-targeting gene of CHAC1 to induce GSH degradation (Chen et al., 2017a; Wang et al., 2019; Li et al., 2020). Based on the capacity of heat shock protein 5 (HSPA5) in mediating endoplasmic reticulum unfolding of the protein to negatively regulate GPX4, induction of HSPA5 expression can feedback on the

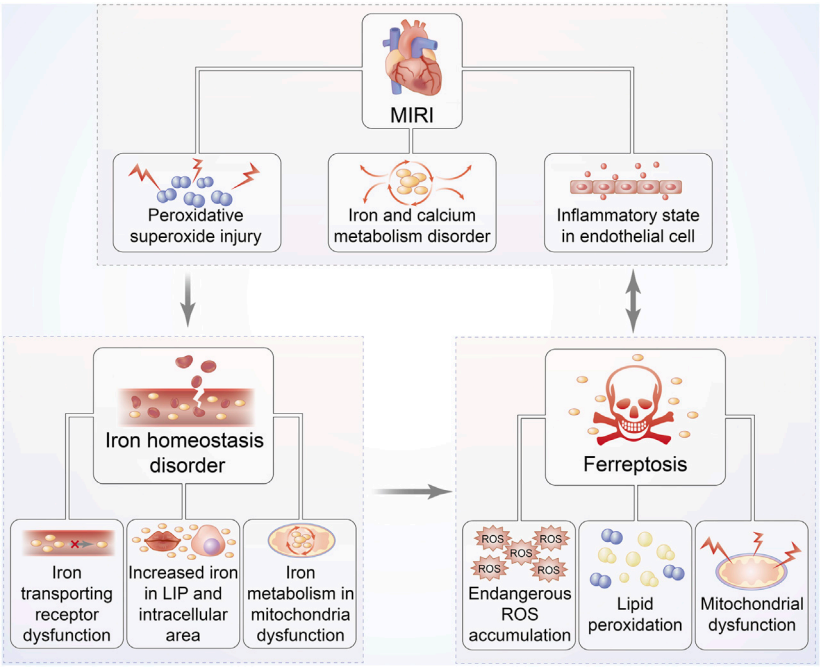

FIGURE 4 | Relationship between MIRI and iron homeostasis disorder as well as ferroptosis. The pathophysiological progression of MIRI is closely associated with iron homeostasis disorder, overproduction of ROS, and mitochondrial dysfunction, followed by increased iron accumulation. These responses can further trap cardiac cells into a vicious cycle of exacerbated ROS-induced impairment, eventually leading to ferroptosis. Hearts suffering I/R injury are exposed to persistent oxidative stress, especially iron-dependent lipid hydroperoxide generation, which might damage the contractility of cardiomyocytes.

upregulation of ATF4 activity to elevate the GPX4 level, eventually preventing cells from ferroptosis (Bai et al., 2020). Therefore, cascaded signals of ATF4-HSPA5-GPX4 implicated in oxidative response and the metabolic system might act as a negative feedback on ferroptosis *via* complex networks (Zhu et al., 2017).

NRF2 Signaling Pathway

A transcription factor in terms of nuclear factor erythroid 2–related factor 2 (NRF2) can mechanistically regulate ferroptosis by not only promoting iron storage to reduce iron accumulation, but also upregulating SLC7A11 activity to increase glutamate content (Fan et al., 2017; Kerins and Ooi, 2018; Mou et al., 2019). Meanwhile, NRF2 is modulated by upstream molecules, such as P62 and alternative reading frame (ARF). P62 likely suppresses the degradation of NRF2 to further enhance nuclear reservation, whereas ARF directly inhibits transcriptional function targeting to downregulate SLC7A11 expression; both of them effectively prevent ferroptosis (Sun et al., 2016; Chen et al., 2017b). Likely, ferroptosis-associated FT, together with heme oxygenase (HO-1), is affected by NRF2 as evidence showed that HO-1 knockdown deteriorated erastin-induced ferroptosis, but NRF activation might inversely upregulate HO-1 (Gai et al., 2020). Collectively, NRF2 is identified to be the main negative mediator in signaling cross-connection for protecting the cell against ferroptosis.

Since the viewpoint that abundant iron deposited on cardiac cells in the MIRI mouse model to induce ferroptosis was first recognized by Bata et al., it led us to further investigate the link between ferroptosis and cardiomyocyte IRI (Baba et al., 2018) **(Figure 4)**. Oxidative stress plays the predominant role in cardiomyocyte IRI that is manifested by chronic inflammation in vascular walls and lipid peroxidation deposition in the arterial wall (Berliner, 2002). Theoretically, membrane phospholipid compounds of PUFAs exhibit high susceptibility to esterification as evidenced by the signs on phospholipid oxidation products and subsequent damage *via* the production of ROS onset of MIRI (White et al., 2015). With continually increasing species of oxidized lipoacylcholine being discovered during cardiomyocyte IRI, the mechanisms underlying lipid peroxidation have been confirmed to be the connection between ferroptosis and MIRI (Yeang et al., 2019). Moreover, the exogenous supplement of these oxidized lipid products to cardiomyocytes can definitely trigger ferroptosis-associated cell death; thus, ferroptosis regulates cardiomyocyte IRI by affecting phospholipid metabolism (Ganguly et al., 2018).

The iron-related signaling pathway is recognized to be another prerequisite for ferroptosis-mediated cardiomyocyte IRI secondary to lipid oxidative stress, which might be attested by the protective effect of the iron chelator called deferoxamine in suppressing cardiac cells from ferroptosis by means of binding iron in an MIRI model (Kakhlon and Cabantchik, 2002; Gao et al., 2015). A previous study confirmed iron to be an indispensable substrate for NADPH oxidase that was capable of catalyzing to produce superoxides, finally initiating ferroptosis (Dixon and Stockwell, 2014). Consistently, ferroptosis-mediated

TABLE 2 | Ferroptosis initiators and inhibitors: targeting strategy for MIRI.

Reagent	Effects	Targets	Key mechanisms	References
Erastin	Induction	System Xc-	GSH depletion and GPX4 inactivation	Yagoda et al. (2007); Yang et al. (2014)
RSL3	Induction	GPX4	Binds GPX4 protein and increases ROS generation	Huang et al. (2021)
BSO	Induction	System Xc^-	Suppresses peripheral GSH biosynthesis	Harris et al. (2015)
Lanperisone	Induction	System Xc^-	Promotes ROS production	Shaw et al. (2011)
Sorafenib	Induction	System Xc^-	Interdicts GSH biosynthesis	Zhang et al. (2013); Louandre et al. (2015)
Sulfasalazine	Induction	System Xc^-	Downregulates SLC7A11 expression	Sehm et al. (2016)
DPI 7,10, 12	Induction	GPX4	Binds GPX4 and augments ROS production.	Sharma and Flora, (2021)
Ferrostatin-1	Inhibition	ROS	Prevents ROS generation	Yin et al. (2011)
Liproxstatin-1	Inhibition	ROS	Prevents lipid peroxidation	Zhang et al. (2019b)
Zileuton	Inhibition	5-Lipoxygenase	Inhibits PUFAs catalyzing into hyperoxide	Kagan et al. (2017)
Vitamin E	Inhibition	5-Lipoxygenase	Inhibits PUFAs catalyzing into hyperoxide	Liu et al. (2015)
Deferoxamine	Inhibition	Fe^{2+}	Chelates intracellular superfluous iron	Doll and Conrad, (2017)
XJB-5-131	Inhibition	ROS	Eliminates poisonous ROS	Doll and Conrad, (2017)
Mitoquinone	Inhibition	ROS	Eliminates mitochondrial ROS	Fuchs and Steller, (2011)

upregulation of NADPH oxidase and monocyte adhesion might account for cardiomyocyte IRI due to endothelial dysfunction following reperfused stress, hinting that the iron metabolism–associated pathway belongs to the leading cause for ferroptosis involved in MIRI (Sullivan, 2009; Kuo et al., 2014). The aforementioned notions were further validated by the subsequent fluorescence confocal analysis of cardiac muscle tissue from the MIRI mouse model, which manifested redundant iron accumulation and even non-apoptotic cell death of ferroptosis, showing an improved appearance after administration of ferrostatin-1 (Fer-1) (Stamenkovic et al., 2021). Moreover, rapamycin, discovered remarkably overexpressed in the early stage of MIRI, was identified to be the target for multiple iron transport proteins, which could modulate transferring receptor to upregulate ferroportin expression, suggesting that mTOR was implicated in the mechanistic process of ferroptosis-modulating MIRI (Bayeva et al., 2012; Guan and Wang, 2014). These documentations suggest that ferroptosis regulates MIRI *via* the iron metabolic signaling pathway, and the ferroptotic inhibitor of Fer-1 might be a potential approach to attenuate reperfusion damage.

Notably, some other ferroptotic-relevant molecules participate in the pathogenesis and progression of MIRI, including GPX4- and ERS-associated proteins. Lip-1, for instance, can prevent murine cardiomyocytes from IRI by inhibiting ferroptosis by enhancing GPX4 expression, and similarly another ferroptotic inhibitor of Fer-1 is found to alleviate MIRI of diabetes under constant hyperglycemia by weakening ERS (Li et al., 2019). These results suggest that GPX4, especially in GSH metabolism, as well as the ERS-mediated pathway may be driving factors for ferroptosis in regulating MIRI that need to be further clarified.

INITIATORS AND INHIBITORS OF FERROPTOSIS AS THE POTENTIAL TARGETS FOR MIRI

Initiators of Ferroptosis

Depending on whether directly targeting for GPX4 activity, all the ferroptotic initiators are classified into two categories (**Table 2**). One type of inducers shows efficacy in inhibiting GPX4 activity by GSH depletion including erastin, sulfasalazine, diphenyleneiodonium chloride 2 (DPI2), buthionine sulfoximine (BSO), and lanperisone, while another form of inducers mainly directly blocks GPX4 without GSH consumption, such as RSL3 and DPI family except for DPI2. Mechanistically, erastin triggers ferroptosis either by combining mitochondrial VDAC2/3 to disrupt the respiratory chain together with ROS accumulation or weakening Xc system activity to attenuate GSH concentration accompanied by GPX4 inactivation (Yagoda et al., 2007; Yang et al., 2014). RSL3, impervious to the upstream of GPX4 including GSH depletion and cysteine intussuscepts, is able to inactivate GPX4 by the binding protein site, in turn augmenting ROS generation to initiate ferroptosis (Huang et al., 2021). On account of the succedaneous antioxidant approach upregulated by blocking GSH synthesis, BSO, owning perciclular capacity in suppressing peripheral GSH biosynthesis and eventually inactivating GPX4 to induce ferroptosis, exhibits lower efficacy on occasioning ferroptosis-related chain reaction than RSL3 (Harris et al., 2015). Although lanperisone can effectively enhance ROS production mediated by the RAS/MEK/ERK signaling pathway to induce ferroptosis due to KRAS gene mutation in embryonic fibroblasts, it displays less competency than erastin in resisting against KRAS-driven tumor vitality (Shaw et al., 2011).

Similar to the reagent of erastin, sorafenib, a multikinase inhibitor utilized for hepatic cancer therapy, interdicts GSH biosynthesis, rather than Raf suppression, and induces ferroptosis in tumor cells manifested as attenuation in tumor angiogenesis and restriction in tumor proliferation (Zhang et al., 2013; Louandre et al., 2015). Sulfasalazine authorized by the drug institution for nonbacterial inflammatory treatment was also confirmed to be applied to induce ferroptosis in gliofibroma cells by downregulating SLC7A11 expression (Sehm et al., 2016). Except for DPI2 which initiates ferroptosis conformed to erastin-associated mechanism, other members of DPI directly induce ferroptosis targeting for GPX4, instead of GSH reduction (Sharma and Flora, 2021).

Inhibitors of Ferroptosis

Most varieties of ferroptotic inhibitors consist of antioxidants (e.g., Fer-1, Lip-1, and vitamin E), iron chelators (e.g., deferoxamine), and ROS scavengers (e.g., N-acetyl-L-cysteine, XJB-5-131, JP4-039, and mitoquinone), and they can potentially resist ferroptosis induced by RSL3 or erastin (Friedmann Angeli et al., 2014; Boonnoy et al., 2017; Zilka et al., 2017; Skouta et al., 2014; Krainz et al., 2016) (**Table 2**). Commonly, both Fer-1 and Lip-1, failing to suppress peroxidase activity, are able to capture free radicals to ameliorate ROS deposition, rather than inhibit ferroptosis as evidenced by the beneficial impact on the model of I/R injury (Yin et al., 2011; Zhang et al., 2019b). Based on the oxidant function of LOX in catalyzing unsaturated fatty acids into hyperoxides, the LOX inhibitor of zileuton and vitamin E antioxidant together with tocotrienol might protect cells from ferroptosis-induced oxidative stress (Liu et al., 2015; Kagan et al., 2017). Additionally, pretreatment of cells with deferoxamine, which chelates intracellular superfluous iron, may contribute to protecting cells against ferroptosis by disturbing the ROS-mediated Fenton reaction (Doll and Conrad, 2017). Currently, novel synthetic compounds defined as ROS scavengers, including XJB-5-131 and JP4-039, are reported to markedly suppress ferroptosis *via* eliminating poisonous ROS. In fact, the mitochondrion is considered the first line of defense in ROS clearance, and consequently, mitoquinone targets for mitochondrial ROS elimination (Fuchs and Steller, 2011).

CONCLUSION AND PERSPECTIVES

Cardiomyocyte IRI is commonly yet severely complicated by myocardial reperfusion intervention but is prone to be neglected in the clinical practice. The interplay between disorder of energy metabolism and massive accumulation of oxygen free radicals drives cardiomyocytes into a vicious circle in the setting of MIRI. Together with vascular endothelial inflammation, oxidative stress depending on iron homeostasis imbalance can damage cardiac function due to myocardial remodeling. Therefore, early interference of MIRI plays a critical role in the survival and prognosis of myocardial ischemia. Despite mechanisms with regard to ferroptosis in MIRI diseases being continually explored in experimental research studies and many progresses being achieved in clinical practice, certain limitations however remain to be overcome. First, precise downstream molecules of the signaling pathway in lipid peroxidation regulating ferroptotic myocardial remodeling appear unclear. Second, the potential mechanism of ferroptosis to activate the systematic inflammatory response in MIRI needs to be further explored. Third, more reasonable clinical trials are essential to be conducted in order to verify the outcomes in the established animal models of ferroptosis-related MIRI. In summary, ferroptosis appears to play an important role in pathogenic progression of MIRI; thus, targeting ferroptosis might provide a potential therapy for MIRI-associated diseases in the future.

AUTHOR CONTRIBUTIONS

J-YL conducted the literature review and drafted the manuscript, S-QL and R-QY helped with preparing the manuscript, which Y-MY and Y-PT conceptualized, supervised, and revised. All authors read and approved the final manuscript.

FUNDING

This study was supported by the grants from the National Natural Science Foundation of China (Nos. 81730057, 82130062, and 81873946), the National Tutorial System Training Program of Suzhou (2020-12), and the Provincial Key Project of Medical Science Research of Hebei (No. 20210013).

REFERENCES

Aisen, P., Enns, C., and Wessling-Resnick, M. (2001). Chemistry and Biology of Eukaryotic Iron Metabolism. *Int. J. Biochem. Cel Biol.* 33, 940–959. doi:10.1016/s1357-2725(01)00063-2

Anthonymuthu, T. S., Kenny, E. M., Shrivastava, I., Tyurina, Y. Y., Hier, Z. E., Ting, H.-C., et al. (2018). Empowerment of 15-Lipoxygenase Catalytic Competence in Selective Oxidation of Membrane ETE-PE to Ferroptotic Death Signals, HpETE-PE. *J. Am. Chem. Soc.* 140, 17835–17839. doi:10.1021/jacs.8b09913

Baba, Y., Higa, J. K., Shimada, B. K., Horiuchi, K. M., Suhara, T., Kobayashi, M., et al. (2018). Protective Effects of the Mechanistic Target of Rapamycin against Excess Iron and Ferroptosis in Cardiomyocytes. *Am. J. Physiol. Heart Circulatory Physiol.* 314, H659–H668. doi:10.1152/ajpheart.00452.2017

Bai, T., Liang, R., Zhu, R., Wang, W., Zhou, L., and Sun, Y. (2020). MicroRNA-214-3p Enhances Erastin-induced Ferroptosis by Targeting ATF4 in Hepatoma Cells. *J. Cel Physiol.* 235, 5637–5648. doi:10.1002/jcp.29496

Bayeva, M., Khechaduri, A., Puig, S., Chang, H.-C., Patial, S., Blackshear, P. J., et al. (2012). mTOR Regulates Cellular Iron Homeostasis through Tristetraprolin. *Cel Metab.* 16, 645–657. doi:10.1016/j.cmet.2012.10.001

Bell, R. M., and Yellon, D. M. (2011). There Is More to Life Than Revascularization: Therapeutic Targeting of Myocardial Ischemia/reperfusion Injury. *Cardiovasc. Ther.* 29, e67–e79. doi:10.1111/j.1755-5922.2010.00190.x

Berliner, J. (2002). Lipid Oxidation Products and Atherosclerosis. *Vasc. Pharmacol.* 38, 187–191. doi:10.1016/S1537-1891(02)00168-4

Boag, S. E., Andreano, E., and Spyridopoulos, I. (2017). Lymphocyte Communication in Myocardial Ischemia/reperfusion Injury. *Antioxid. Redox Signal.* 26, 660–675. doi:10.1089/ars.2016.6940

Boonnoy, P., Karttunen, M., and Wong-Ekkabut, J. (2017). Alpha-tocopherol Inhibits Pore Formation in Oxidized Bilayers. *Phys. Chem. Chem. Phys.* 19, 5699–5704. doi:10.1039/c6cp08051k

Cadenas, S. (2018). ROS and Redox Signaling in Myocardial Ischemia-Reperfusion Injury and Cardioprotection. *Free Radic. Biol. Med.* 117, 76–89. doi:10.1016/j.freeradbiomed.2018.01.024

Campanella, A., Rovelli, E., Santambrogio, P., Cozzi, A., Taroni, F., and Levi, S. (2009). Mitochondrial Ferritin Limits Oxidative Damage Regulating Mitochondrial Iron Availability: Hypothesis for a Protective Role in Friedreich Ataxia. *Hum. Mol. Genet.* 18, 1–11. doi:10.1093/hmg/ddn308

Cao, J. Y., and Dixon, S. J. (2016). Mechanisms of Ferroptosis. *Cell. Mol. Life Sci.* 73, 2195–2209. doi:10.1007/s00018-016-2194-1

Chan, S., Lian, Q., Chen, M.-P., Jiang, D., Ho, J. T. K., Cheung, Y.-F., et al. (2018). Deferiprone Inhibits Iron Overload-Induced Tissue Factor Bearing Endothelial Microparticle Generation by Inhibition Oxidative Stress Induced Mitochondrial Injury, and Apoptosis. *Toxicol. Appl. Pharmacol.* 338, 148–158. doi:10.1016/j.taap.2017.11.005

Chang, H. C., Wu, R., Shang, M., Sato, T., Chen, C., Shapiro, J. S., et al. (2016). Reduction in Mitochondrial Iron Alleviates Cardiac Damage during Injury. *EMBO Mol. Med.* 8, 247–267. doi:10.15252/emmm.201505748

Chen, M.-S., Wang, S.-F., Hsu, C.-Y., Yin, P.-H., Yeh, T.-S., Lee, H.-C., et al. (2017). CHAC1 Degradation of Glutathione Enhances Cystine-Starvation-Induced Necroptosis and Ferroptosis in Human Triple Negative Breast Cancer Cells via the GCN2-eIF2α-ATF4 Pathway. *Oncotarget* 8, 114588–114602. doi:10.18632/oncotarget.23055

Chen, D., Tavana, O., Chu, B., Erber, L., Chen, Y., Baer, R., et al. (2017). NRF2 Is a Major Target of ARF in P53-independent Tumor Suppression. *Mol. Cel* 68, 224–232. doi:10.1016/j.molcel.2017.09.009

Chen, X., Xu, S., Zhao, C., and Liu, B. (2019). Role of TLR4/NADPH Oxidase 4 Pathway in Promoting Cell Death through Autophagy and Ferroptosis during Heart Failure. *Biochem. Biophys. Res. Commun.* 516, 37–43. doi:10.1016/j.bbrc.2019.06.015

Conrad, M., Kagan, V. E., Bayir, H., Pagnussat, G. C., Head, B., Traber, M. G., et al. (2018). Regulation of Lipid Peroxidation and Ferroptosis in Diverse Species. *Genes Dev.* 32, 602–619. doi:10.1101/gad.314674.118

Díez-López, C., Comín-Colet, J., and González-Costello, J. (2018). Iron Overload Cardiomyopathy. *Curr. Opin. Cardiol.* 33, 334–340. doi:10.1097/HCO.0000000000000511

Dixon, S. J., and Stockwell, B. R. (2014). The Role of Iron and Reactive Oxygen Species in Cell Death. *Nat. Chem. Biol.* 10, 9–17. doi:10.1038/nchembio.1416

Dixon, S. J., Lemberg, K. M., Lamprecht, M. R., Skouta, R., Zaitsev, E. M., Gleason, C. E., et al. (2012). Ferroptosis: an Iron-dependent Form of Nonapoptotic Cell Death. *Cell* 149, 1060–1072. doi:10.1016/j.cell.2012.03.042

Doll, S., and Conrad, M. (2017). Iron and Ferroptosis: A Still Ill-defined Liaison. *IUBMB Life* 69, 423–434. doi:10.1002/iub.1616

Dongó, E., Hornyák, I., Benkő, Z., and Kiss, L. (2011). The Cardioprotective Potential of Hydrogen Sulfide in Myocardial Ischemia/reperfusion Injury (Review). *Acta Physiol. Hungarica* 98, 369–381. doi:10.1556/APhysiol.98.2011.4.1

Drossos, G., Lazou, A., Panagopoulos, P., and Westaby, S. (1995). Deferoxamine Cardioplegia Reduces Superoxide Radical Production in Human Myocardium. *Ann. Thorac. Surg.* 59, 169–172. doi:10.1016/0003-4975(94)00726-N

Fan, Z., Wirth, A.-K., Chen, D., Wruck, C. J., Rauh, M., Buchfelder, M., et al. (2017). Nrf2-Keap1 Pathway Promotes Cell Proliferation and Diminishes Ferroptosis. *Oncogenesis* 6, e371. doi:10.1038/oncsis.2017.65

Fang, X., Wang, H., Han, D., Xie, E., Yang, X., Wei, J., et al. (2019). Ferroptosis as a Target for protection against Cardiomyopathy. *Proc. Natl. Acad. Sci. USA* 116, 2672–2680. doi:10.1073/pnas.1821022116

Friedmann Angeli, J. P., Schneider, M., Proneth, B., Tyurina, Y. Y., Tyurin, V. A., Hammond, V. J., et al. (2014). Inactivation of the Ferroptosis Regulator Gpx4 Triggers Acute Renal Failure in Mice. *Nat. Cel Biol.* 16, 1180–1191. doi:10.1038/ncb3064

Fuchs, Y., and Steller, H. (2011). Programmed Cell Death in Animal Development and Disease. *Cell* 147, 742–758. doi:10.1016/j.cell.2011.10.033

Fujii, J., Homma, T., and Kobayashi, S. (2019). Ferroptosis Caused by Cysteine Insufficiency and Oxidative Insult. *Free Radic. Res.* 54, 969–980. doi:10.1080/10715762.2019.1666983

Gai, C., Yu, M., Li, Z., Wang, Y., Ding, D., Zheng, J., et al. (2020). Acetaminophen Sensitizing Erastin-induced Ferroptosis via Modulation of Nrf2/heme Oxygenase-1 Signaling Pathway in Non-small-cell Lung Cancer. *J. Cel Physiol.* 235, 3329–3339. doi:10.1002/jcp.29221

Gammella, E., Recalcati, S., and Cairo, G. (2016). Dual Role of ROS as Signal and Stress Agents: Iron Tips the Balance in Favor of Toxic Effects. *Oxid. Med. Cell Longev.* 2016, 1–9. doi:10.1155/2016/8629024

Ganguly, R., Hasanally, D., Stamenkovic, A., Maddaford, T. G., Chaudhary, R., Pierce, G. N., et al. (2018). Alpha Linolenic Acid Decreases Apoptosis and Oxidized Phospholipids in Cardiomyocytes during Ischemia/reperfusion. *Mol. Cel Biochem.* 437, 163–175. doi:10.1007/s11010-017-3104-z

Gao, M., Monian, P., Quadri, N., Ramasamy, R., and Jiang, X. (2015). Glutaminolysis and Transferrin Regulate Ferroptosis. *Mol. Cel* 59, 298–308. doi:10.1016/j.molcel.2015.06.011

Gladyshev, V. N., Stadtman, T. C., Hatfield, D. L., and Jeang, K.-T. (1999). Levels of Major Selenoproteins in T Cells Decrease during HIV Infection and Low Molecular Mass Selenium Compounds Increase. *Proc. Natl. Acad. Sci.* 96, 835–839. doi:10.1073/pnas.96.3.835

Gordan, R., Wongjaikam, S., Gwathmey, J. K., Chattipakorn, N., Chattipakorn, S. C., and Xie, L.-H. (2018). Involvement of Cytosolic and Mitochondrial Iron in Iron Overload Cardiomyopathy: an Update. *Heart Fail. Rev.* 23, 801–816. doi:10.1007/s10741-018-9700-5

Grueter, C. E., Colbran, R. J., and Anderson, M. E. (2006). CaMKII, an Emerging Molecular Driver for Calcium Homeostasis, Arrhythmias, and Cardiac Dysfunction. *J. Mol. Med.* 85, 5–14. doi:10.1007/s00109-006-0125-6

Guan, P., and Wang, N. (2014). Mammalian Target of Rapamycin Coordinates Iron Metabolism with Iron-Sulfur Cluster Assembly Enzyme and Tristetraprolin. *Nutrition* 30, 968–974. doi:10.1016/j.nut.2013.12.016

Haddad, S., Wang, Y., Galy, B., Korf-Klingebiel, M., Hirsch, V., Baru, A. M., et al. (2017). Iron-regulatory Proteins Secure Iron Availability in Cardiomyocytes to Prevent Heart Failure. *Eur. Heart J.* 38, ehw333–372. doi:10.1093/eurheartj/ehw333

Harris, I. S., Treloar, A. E., Inoue, S., Sasaki, M., Gorrini, C., Lee, K. C., et al. (2015). Glutathione and Thioredoxin Antioxidant Pathways Synergize to Drive Cancer Initiation and Progression. *Cancer Cell* 27, 211–222. doi:10.1016/j.ccell.2014.11.019

Hayano, M., Yang, W. S., Corn, C. K., Pagano, N. C., and Stockwell, B. R. (2016). Loss of Cysteinyl-tRNA Synthetase (CARS) Induces the Transsulfuration Pathway and Inhibits Ferroptosis Induced by Cystine Deprivation. *Cell Death Differ.* 23, 270–278. doi:10.1038/cdd.2015.93

He, H., Qiao, Y., Zhou, Q., Wang, Z., Chen, X., Liu, D., et al. (2019). Iron Overload Damages the Endothelial Mitochondria via the ROS/ADMA/DDAHII/eNOS/NO Pathway. *Oxid. Med. Cell Longev.* 2019, 1–19. doi:10.1155/2019/2340392

Hentze, M. W., Muckenthaler, M. U., Galy, B., and Camaschella, C. (2010). Two to Tango: Regulation of Mammalian Iron Metabolism. *Cell* 142, 24–38. doi:10.1016/j.cell.2010.06.028

Hirst, J. (2013). Mitochondrial Complex I. *Annu. Rev. Biochem.* 82, 551–575. doi:10.1146/annurev-biochem-070511-103700

Hoes, M. F., Grote Beverborg, N., Kijlstra, J. D., Kuipers, J., Swinkels, D. W., Giepmans, B. N. G., et al. (2018). Iron Deficiency Impairs Contractility of Human Cardiomyocytes through Decreased Mitochondrial Function. *Eur. J. Heart Fail.* 20, 910–919. doi:10.1002/ejhf.1154

Huang, F., YangXiao, R. Z. Z., Xiao, Z., Xie, Y., Lin, X., Zhu, P., et al. (2021). Targeting Ferroptosis to Treat Cardiovascular Diseases: a New Continent to Be Explored. *Front. Cel Dev. Biol.* 9, 737971. doi:10.3389/fcell.2021.737971

Ichikawa, Y., Bayeva, M., Ghanefar, M., Potini, V., Sun, L., Mutharasan, R. K., et al. (2012). Disruption of ATP-Binding Cassette B8 in Mice Leads to Cardiomyopathy through a Decrease in Mitochondrial Iron export. *Proc. Natl. Acad. Sci.* 109, 4152–4157. doi:10.1073/pnas.1119338109

Ingold, I., Berndt, C., Schmitt, S., Doll, S., Poschmann, G., Buday, K., et al. (2018). Selenium Utilization by GPX4 Is Required to Prevent Hydroperoxide-Induced Ferroptosis. *Cell* 172, 409–422. doi:10.1016/j.cell.2017.11.048

Kagan, V. E., Mao, G., Qu, F., Angeli, J. P. F., Doll, S., Croix, C. S., et al. (2017). Oxidized Arachidonic and Adrenic PEs Navigate Cells to Ferroptosis. *Nat. Chem. Biol.* 13, 81–90. doi:10.1038/nchembio.2238

Kakhlon, O., and Cabantchik, Z. I. (2002). The Labile Iron Pool: Characterization, Measurement, and Participation in Cellular Processes1 1This Article Is Part of a Series of Reviews on "Iron and Cellular Redox Status." the Full List of Papers May Be Found on the Homepage of the Journal. *Free Radic. Biol. Med.* 33, 1037–1046. doi:10.1016/S0891-5849(02)01006-7

Kawabata, H. (2019). Transferrin and Transferrin Receptors Update. *Free Radic. Biol. Med.* 133, 46–54. doi:10.1016/j.freeradbiomed.2018.06.037

Kerins, M. J., and Ooi, A. (2018). The Roles of NRF2 in Modulating Cellular Iron Homeostasis. *Antioxid. Redox Signal.* 29, 1756–1773. doi:10.1089/ars.2017.7176

Krainz, T., Gaschler, M. M., Lim, C., Sacher, J. R., Stockwell, B. R., and Wipf, P. (2016). A Mitochondrial-Targeted Nitroxide Is a Potent Inhibitor of Ferroptosis. *ACS Cent. Sci.* 2, 653–659. doi:10.1021/acscentsci.6b00199

Kruszewski, M. (2003). Labile Iron Pool: the Main Determinant of Cellular Response to Oxidative Stress. *Mutat. Res. Fund. Mol. Mech. Mutagen.* 531, 81–92. doi:10.1016/j.mrfmmm.2003.08.004

Kuo, K.-L., Hung, S.-C., Lee, T.-S., and Tarng, D.-C. (2014). Iron Sucrose Accelerates Early Atherogenesis by Increasing Superoxide Production and Upregulating Adhesion Molecules in CKD. *J. Am. Soc. Nephrol.* 25, 2596–2606. doi:10.1681/ASN.2013080838

Kuroda, J., Ago, T., Matsushima, S., Zhai, P., Schneider, M. D., and Sadoshima, J. (2010). NADPH Oxidase 4 (Nox4) Is a Major Source of Oxidative Stress in the

Failing Heart. *Proc. Natl. Acad. Sci.* 107, 15565–15570. doi:10.1073/pnas.1002178107

Lakhal-Littleton, S., Wolna, M., Chung, Y. J., Christian, H. C., Heather, L. C., Brescia, M., et al. (2016). An Essential Cell-Autonomous Role for Hepcidin in Cardiac Iron Homeostasis. *Elife* 5, e19804. doi:10.7554/eLife.19804

Lane, D., Bae, D.-H., Merlot, A., Sahni, S., and Richardson, D. (2015). Duodenal Cytochrome B (DCYTB) in Iron Metabolism: an Update on Function and Regulation. *Nutrients* 7, 2274–2296. doi:10.3390/nu7042274

Lesnefsky, E. J., Chen, Q., Tandler, B., and Hoppel, C. L. (2017). Mitochondrial Dysfunction and Myocardial Ischemia-Reperfusion: Implications for Novel Therapies. *Annu. Rev. Pharmacol. Toxicol.* 57, 535–565. doi:10.1146/annurev-pharmtox-010715-103335

Li, J., Zhao, Y., Zhou, N., Li, L., and Li, K. (2019). Dexmedetomidine Attenuates Myocardial Ischemia-Reperfusion Injury in Diabetes Mellitus by Inhibiting Endoplasmic Reticulum Stress. *J. Diabetes Res.* 2019, 1–12. doi:10.1155/2019/7869318

Li, W., Li, W., Leng, Y., Xiong, Y., and Xia, Z. (2020). Ferroptosis Is Involved in Diabetes Myocardial Ischemia/reperfusion Injury through Endoplasmic Reticulum Stress. *DNA Cel Biol.* 39, 210–225. doi:10.1089/dna.2019.5097

Liu, Y., Wang, W., Li, Y., Xiao, Y., Cheng, J., and Jia, J. (2015). The 5-lipoxygenase Inhibitor Zileuton Confers Neuroprotection against Glutamate Oxidative Damage by Inhibiting Ferroptosis. *Biol. Pharm. Bull.* 38, 1234–1239. doi:10.1248/bpb.b15-00048

Louandre, C., Marcq, I., Bouhlal, H., Lachaier, E., Godin, C., Saidak, Z., et al. (2015). The Retinoblastoma (Rb) Protein Regulates Ferroptosis Induced by Sorafenib in Human Hepatocellular Carcinoma Cells. *Cancer Lett.* 356, 971–977. doi:10.1016/j.canlet.2014.11.014

Magtanong, L., Ko, P.-J., To, M., Cao, J. Y., Forcina, G. C., Tarangelo, A., et al. (2019). Exogenous Monounsaturated Fatty Acids Promote a Ferroptosis-Resistant Cell State. *Cel Chem. Biol.* 26, 420–432. doi:10.1016/j.chembiol.2018.11.016

Maldonado, E. N., Sheldon, K. L., DeHart, D. N., Patnaik, J., Manevich, Y., Townsend, D. M., et al. (2013). Voltage-dependent Anion Channels Modulate Mitochondrial Metabolism in Cancer Cells. *J. Biol. Chem.* 288, 11920–11929. doi:10.1074/jbc.M112.433847

Marshall, K. R., Gong, M., Wodke, L., Lamb, J. H., Jones, D. J. L., Farmer, P. B., et al. (2005). The Human Apoptosis-Inducing Protein AMID Is an Oxidoreductase with a Modified Flavin Cofactor and DNA Binding Activity. *J. Biol. Chem.* 280, 30735–30740. doi:10.1074/jbc.M414018200

Matsushima, S., Tsutsui, H., and Sadoshima, J. (2014). Physiological and Pathological Functions of NADPH Oxidases during Myocardial Ischemia-Reperfusion. *Trends Cardiovasc. Med.* 24, 202–205. doi:10.1016/j.tcm.2014.03.003

Morciano, G., Giorgi, C., Bonora, M., Punzetti, S., Pavasini, R., Wieckowski, M. R., et al. (2015). Molecular Identity of the Mitochondrial Permeability Transition Pore and its Role in Ischemia-Reperfusion Injury. *J. Mol. Cell Cardiol.* 78, 142–153. doi:10.1016/j.yjmcc.2014.08.015

Mou, Y., Wang, J., Wu, J., He, D., Zhang, C., Duan, C., et al. (2019). Ferroptosis, a New Form of Cell Death: Opportunities and Challenges in Cancer. *J. Hematol. Oncol.* 12, 34. doi:10.1186/s13045-019-0720-y

Ng, S.-W., Norwitz, S. G., Taylor, H. S., and Norwitz, E. R. (2020). Endometriosis: the Role of Iron Overload and Ferroptosis. *Reprod. Sci.* 27, 1383–1390. doi:10.1007/s43032-020-00164-z

Nie, G., Sheftel, A. D., Kim, S. F., and Ponka, P. (2005). Overexpression of Mitochondrial Ferritin Causes Cytosolic Iron Depletion and Changes Cellular Iron Homeostasis. *Blood* 105, 2161–2167. doi:10.1182/blood-2004-07-2722

Omiya, S., Hikoso, S., Imanishi, Y., Saito, A., Yamaguchi, O., Takeda, T., et al. (2009). Downregulation of Ferritin Heavy Chain Increases Labile Iron Pool, Oxidative Stress and Cell Death in Cardiomyocytes. *J. Mol. Cell Cardiol.* 46, 59–66. doi:10.1016/j.yjmcc.2008.09.714

Oudit, G. Y., Sun, H., Trivieri, M. G., Koch, S. E., Dawood, F., Ackerley, C., et al. (2003). L-type Ca2+ Channels Provide a Major Pathway for Iron Entry into Cardiomyocytes in Iron-Overload Cardiomyopathy. *Nat. Med.* 9, 1187–1194. doi:10.1038/nm920

Paraskevaidis, I. A., Iliodromitis, E. K., Vlahakos, D., Tsiapras, D. P., Nikolaidis, A., Marathias, A., et al. (2005). Deferoxamine Infusion during Coronary Artery Bypass Grafting Ameliorates Lipid Peroxidation and Protects the Myocardium against Reperfusion Injury: Immediate and Long-Term Significance. *Eur. Heart J.* 26, 263–270. doi:10.1093/eurheartj/ehi028

Paterek, A., Mackiewicz, U., and Mączewski, M. (2019). Iron and the Heart: a Paradigm Shift from Systemic to Cardiomyocyte Abnormalities. *J. Cel. Physiol.* 234, 21613–21629. doi:10.1002/jcp.28820

Paul, B. T., Manz, D. H., Torti, F. M., and Torti, S. V. (2017). Mitochondria and Iron: Current Questions. *Expert Rev. Hematol.* 10, 65–79. doi:10.1080/17474086.2016.1268047

Pell, V. R., Chouchani, E. T., Frezza, C., Murphy, M. P., and Krieg, T. (2016). Succinate Metabolism: a New Therapeutic Target for Myocardial Reperfusion Injury. *Cardiovasc. Res.* 111, 134–141. doi:10.1093/cvr/cvw100

Pitale, P. M., Gorbatyuk, O., and Gorbatyuk, M. (2017). Neurodegeneration: Keeping ATF4 on a Tight Leash. *Front. Cel. Neurosci.* 11, 410. doi:10.3389/fncel.2017.00410

Richardson, D. R., Lane, D. J. R., Becker, E. M., Huang, M. L. H., Whitnall, M., Rahmanto, Y. S., et al. (2010). Mitochondrial Iron Trafficking and the Integration of Iron Metabolism between the Mitochondrion and Cytosol. *Proc. Natl. Acad. Sci.* 107, 10775–10782. doi:10.1073/pnas.0912925107

Russo, I., Penna, C., Musso, T., Popara, J., Alloatti, G., Cavalot, F., et al. (2017). Platelets, Diabetes and Myocardial Ischemia/reperfusion Injury. *Cardiovasc. Diabetol.* 16, 71. doi:10.1186/s12933-017-0550-6

Santambrogio, P., Biasiotto, G., Sanvito, F., Olivieri, S., Arosio, P., and Levi, S. (2007). Mitochondrial Ferritin Expression in Adult Mouse Tissues. *J. Histochem. Cytochem.* 55, 1129–1137. doi:10.1369/jhc.7A7273.2007

Schanze, N., Bode, C., and Duerschmied, D. (2019). Platelet Contributions to Myocardial Ischemia/reperfusion Injury. *Front. Immunol.* 10, 1260. doi:10.3389/fimmu.2019.01260

Sehm, T., Fan, Z., Ghoochani, A., Rauh, M., Engelhorn, T., Minakaki, G., et al. (2016). Sulfasalazine Impacts on Ferroptotic Cell Death and Alleviates the Tumor Microenvironment and Glioma-Induced Brain Edema. *Oncotarget* 7, 36021–36033. doi:10.18632/oncotarget.8651

Sharma, A., and Flora, S. J. S. (2021). Positive and Negative Regulation of Ferroptosis and its Role in Maintaining Metabolic and Redox Homeostasis. *Oxid. Med. Cell Longev.* 2021, 1–13. doi:10.1155/2021/9074206

Shaw, A. T., Winslow, M. M., Magendantz, M., Ouyang, C., Dowdle, J., Subramanian, A., et al. (2011). Selective Killing of K-Ras Mutant Cancer Cells by Small Molecule Inducers of Oxidative Stress. *Proc. Natl. Acad. Sci.* 108, 8773–8778. doi:10.1073/pnas.1105941108

Skouta, R., Dixon, S. J., Wang, J., Dunn, D. E., Orman, M., Shimada, K., et al. (2014). Ferrostatins Inhibit Oxidative Lipid Damage and Cell Death in Diverse Disease Models. *J. Am. Chem. Soc.* 136, 4551–4556. doi:10.1021/ja411006a

Sripetchwandee, J., Kenknight, S. B., Sanit, J., Chattipakorn, S., and Chattipakorn, N. (2014). Blockade of Mitochondrial Calcium Uniporter Prevents Cardiac Mitochondrial Dysfunction Caused by Iron Overload. *Acta Physiol.* 210, 330–341. doi:10.1111/apha.12162

Stamenkovic, A., O'Hara, K. A., Nelson, D. C., Maddaford, T. G., Edel, A. L., Maddaford, G., et al. (2021). Oxidized Phosphatidylcholines Trigger Ferroptosis in Cardiomyocytes during Ischemia-Reperfusion Injury. *Am. J. Physiol. Heart Circulatory Physiol.* 320, H1170–H1184. doi:10.1152/ajpheart.00237.2020

Stockwell, B. R., Friedmann Angeli, J. P., Bayir, H., Bush, A. I., Conrad, M., Dixon, S. J., et al. (2017). Ferroptosis: a Regulated Cell Death Nexus Linking Metabolism, Redox Biology, and Disease. *Cell* 171, 273–285. doi:10.1016/j.cell.2017.09.021

Sullivan, J. L. (2009). Iron in Arterial Plaque: A Modifiable Risk Factor for Atherosclerosis. *Biochim. Biophys. Acta Gen. Subjects* 1790, 718–723. doi:10.1016/j.bbagen.2008.06.005

Sun, X., Ou, Z., Chen, R., Niu, X., Chen, D., Kang, R., et al. (2016). Activation of the P62-Keap1-NRF2 Pathway Protects against Ferroptosis in Hepatocellular Carcinoma Cells. *Hepatology* 63, 173–184. doi:10.1002/hep.28251

Sun, X., Yang, Y., Shi, J., Wang, C., Yu, Z., and Zhang, H. (2017). NOX4- and Nrf2-Mediated Oxidative Stress Induced by Silver Nanoparticles in Vascular Endothelial Cells. *J. Appl. Toxicol.* 37, 1428–1437. doi:10.1002/jat.3511

Tang, W. H., Wu, S., Wong, T. M., Chung, S. K., and Chung, S. S. M. (2008). Polyol Pathway Mediates Iron-Induced Oxidative Injury in Ischemic-Reperfused Rat Heart. *Free Radic. Biol. Med.* 45, 602–610. doi:10.1016/j.freeradbiomed.2008.05.003

Tateda, C., Kusano, T., and Takahashi, Y. (2012). The Arabidopsis Voltage-dependent Anion Channel 2 Is Required for Plant Growth. *Plant Signal. Behav.* 7, 31–33. doi:10.4161/psb.7.1.18394

Tian, L., Cao, W., Yue, R., Yuan, Y., Guo, X., Qin, D., et al. (2019). Pretreatment with Tilianin Improves Mitochondrial Energy Metabolism and Oxidative Stress in Rats with Myocardial Ischemia/reperfusion Injury via AMPK/SIRT1/PGC-1 Alpha Signaling Pathway. *J. Pharmacol. Sci.* 139, 352–360. doi:10.1016/j.jphs.2019.02.008

Turer, A. T., and Hill, J. A. (2010). Pathogenesis of Myocardial Ischemia-Reperfusion Injury and Rationale for Therapy. *Am. J. Cardiol.* 106, 360–368. doi:10.1016/j.amjcard.2010.03.032

Valko, M., Jomova, K., Rhodes, C. J., Kuča, K., and Musílek, K. (2016). Redox- and Non-redox-metal-induced Formation of Free Radicals and Their Role in Human Disease. *Arch. Toxicol.* 90, 1–37. doi:10.1007/s00204-015-1579-5

Vela, D. (2020). Keeping Heart Homeostasis in Check through the Balance of Iron Metabolism. *Acta Physiol.* 228, e13324. doi:10.1111/apha.13324

Verkhratsky, A., and Parpura, V. (2014). Calcium Signalling and Calcium Channels: Evolution and General Principles. *Eur. J. Pharmacol.* 739, 1–3. doi:10.1016/j.ejphar.2013.11.013

Vinten-Johansen, J., Jiang, R., Reeves, J. G., Mykytenko, J., Deneve, J., and Jobe, L. J. (2007). Inflammation, Proinflammatory Mediators and Myocardial Ischemia-Reperfusion Injury. *Hematol. Oncol. Clin. North Am.* 21, 123–145. doi:10.1016/j.hoc.2006.11.010

Wang, Y.-Q., Chang, S.-Y., Wu, Q., Gou, Y.-J., Jia, L., Cui, Y.-M., et al. (2016). The Protective Role of Mitochondrial Ferritin on Erastin-Induced Ferroptosis. *Front. Aging Neurosci.* 8, 308. doi:10.3389/fnagi.2016.00308

Wang, N., Zeng, G.-Z., Yin, J.-L., and Bian, Z.-X. (2019). Artesunate Activates the ATF4-CHOP-CHAC1 Pathway and Affects Ferroptosis in Burkitt's Lymphoma. *Biochem. Biophys. Res. Commun.* 519, 533–539. doi:10.1016/j.bbrc.2019.09.023

Watt, R. K. (2013). A Unified Model for Ferritin Iron Loading by the Catalytic center: Implications for Controlling "Free Iron" during Oxidative Stress. *ChemBioChem* 14, 415–419. doi:10.1002/cbic.201200783

White, C. W., Hasanally, D., Mundt, P., Li, Y., Xiang, B., Klein, J., et al. (2015). A Whole Blood-Based Perfusate Provides superior Preservation of Myocardial Function during *Ex Vivo* Heart Perfusion. *J. Heart Lung Transplant.* 34, 113–121. doi:10.1016/j.healun.2014.09.021

Williams, R. E., Zweier, J. L., and Flaherty, J. T. (1991). Treatment with Deferoxamine during Ischemia Improves Functional and Metabolic Recovery and Reduces Reperfusion-Induced Oxygen Radical Generation in Rabbit Hearts. *Circulation* 83, 1006–1014. doi:10.1161/01.cir.83.3.1006

Wofford, J. D., Chakrabarti, M., and Lindahl, P. A. (2017). Mössbauer Spectra of Mouse Hearts Reveal Age-dependent Changes in Mitochondrial and Ferritin Iron Levels. *J. Biol. Chem.* 292, 5546–5554. doi:10.1074/jbc.M117.777201

Wood, J. C. (2008). Cardiac Iron across Different Transfusion-dependent Diseases. *Blood Rev.* 22 (Suppl. 2), S14–S21. doi:10.1016/S0268-960X(08)70004-3

Wu, W., Chang, S., Wu, Q., Xu, Z., Wang, P., Li, Y., et al. (2016). Mitochondrial Ferritin Protects the Murine Myocardium from Acute Exhaustive Exercise Injury. *Cell Death Dis* 7, e2475. doi:10.1038/cddis.2016.372

Xie, Y., Hou, W., Song, X., Yu, Y., Huang, J., Sun, X., et al. (2016). Ferroptosis: Process and Function. *Cel Death Differ.* 23, 369–379. doi:10.1038/cdd.2015.158

Yagoda, N., von Rechenberg, M., Zaganjor, E., Bauer, A. J., Yang, W. S., Fridman, D. J., et al. (2007). RAS-RAF-MEK-dependent Oxidative Cell Death Involving Voltage-dependent Anion Channels. *Nature* 447, 865–869. doi:10.1038/nature05859

Yang, W. S., SriRamaratnam, R., Welsch, M. E., Shimada, K., Skouta, R., Viswanathan, V. S., et al. (2014). Regulation of Ferroptotic Cancer Cell Death by GPX4. *Cell* 156, 317–331. doi:10.1016/j.cell.2013.12.010

Yang, F., Qin, Y., Lv, J., Wang, Y., Che, H., Chen, X., et al. (2018). Silencing Long Non-coding RNA Kcnq1ot1 Alleviates Pyroptosis and Fibrosis in Diabetic Cardiomyopathy. *Cel Death Dis.* 9, 1000. doi:10.1038/s41419-018-1029-4

Yeang, C., Hasanally, D., Que, X., Hung, M.-Y., Stamenkovic, A., Chan, D., et al. (2019). Reduction of Myocardial Ischaemia-Reperfusion Injury by Inactivating Oxidized Phospholipids. *Cardiovasc. Res.* 115, 179–189. doi:10.1093/cvr/cvy136

Yin, H., Xu, L., and Porter, N. A. (2011). Free Radical Lipid Peroxidation: Mechanisms and Analysis. *Chem. Rev.* 111, 5944–5972. doi:10.1021/cr200084z

Zhang, L., Gong, F., Zhang, F., Ma, J., Zhang, P. D., and Shen, J. (2013). Targeted Therapy for Human Hepatic Carcinoma Cells Using Folate-Functionalized Polymeric Micelles Loaded with Superparamagnetic Iron Oxide and Sorafenib *In Vitro*. *Int. J. Nanomedicine* 8, 1517–1524. doi:10.2147/IJN.S43263

Zhang, Y., Liu, D., Hu, H., Zhang, P., Xie, R., and Cui, W. (2019). HIF-1α/BNIP3 Signaling Pathway-Induced-Autophagy Plays Protective Role during Myocardial Ischemia-Reperfusion Injury. *Biomed. Pharmacother.* 120, 109464. doi:10.1016/j.biopha.2019.109464

Zhang, Y., Sun, C., Zhao, C., Hao, J., Zhang, Y., Fan, B., et al. (2019). Ferroptosis Inhibitor SRS 16-86 Attenuates Ferroptosis and Promotes Functional Recovery in Contusion Spinal Cord Injury. *Brain Res.* 1706, 48–57. doi:10.1016/j.brainres.2018.10.023

Zhou, T., Chuang, C.-C., and Zuo, L. (2015). Molecular Characterization of Reactive Oxygen Species in Myocardial Ischemia-Reperfusion Injury. *Biomed. Res. Int.* 2015, 1–9. doi:10.1155/2015/864946

Zhu, S., Zhang, Q., Sun, X., Zeh, H. J., Lotze, M. T., Kang, R., et al. (2017). HSPA5 Regulates Ferroptotic Cell Death in Cancer Cells. *Cancer Res.* 77, 2064–2077. doi:10.1158/0008-5472.CAN-16-1979

Zilka, O., Shah, R., Li, B., Friedmann Angeli, J. P., Griesser, M., Conrad, M., et al. (2017). On the Mechanism of Cytoprotection by Ferrostatin-1 and Liproxstatin-1 and the Role of Lipid Peroxidation in Ferroptotic Cell Death. *ACS Cent. Sci.* 3, 232–243. doi:10.1021/acscentsci.7b00028

Conflict of Interest: The authors declare that the research was conducted in the absence of any commercial or financial relationships that could be construed as a potential conflict of interest.

Publisher's Note: All claims expressed in this article are solely those of the authors and do not necessarily represent those of their affiliated organizations, or those of the publisher, the editors, and the reviewers. Any product that may be evaluated in this article, or claim that may be made by its manufacturer, is not guaranteed or endorsed by the publisher.

Copyright © 2021 Li, Liu, Yao, Tian and Yao. This is an open-access article distributed under the terms of the Creative Commons Attribution License (CC BY). The use, distribution or reproduction in other forums is permitted, provided the original author(s) and the copyright owner(s) are credited and that the original publication in this journal is cited, in accordance with accepted academic practice. No use, distribution or reproduction is permitted which does not comply with these terms.

GLOSSARY

ABCB8, ATP-binding cassette subfamily B member 8;
ACSL4, acyl-coA synthetase long-chain family member 4;
AIFM2, apoptosis-inducing factor mitochondrion-associated 2;
ATF4, activating transcription factor 4;
ARF, alternative reading frame;
BSO, buthionine sulfoximine
CHOP, C/EBP homologous protein;
CoQ, coenzyme Q;
DMT-1, divalent metal transporter 1;
DPI2, diphenyleneiodonium chloride 2;
ERS, endoplasmic reticulum stress;
Fer-1, ferrostatin-1;
FPN, ferroportin;
FtMt, mitochondrial ferritin;
FT, ferritin;
FTH, ferritin heavy chain;
FTL, ferritin light chain;
GSH, glutathione;
GPX4, glutathione peroxidase 4;
HO, hydroxyl radicals;
HO-1, heme oxygenase;
HIF, hypoxia-inducible factor;
HSPA5, heat shock protein five;
IRP, iron regulatory proteins;
IRE, iron-responsive elements;
IRI, ischemia-reperfusion injury;
ISCs, iron–sulfur clusters;
IREB2, element-binding protein 2;
LIP, labile iron pool;
Lip-1, liproxstatin-1;
LPCAT3, lysophosphatidylcholine acyl transferase 3;
MIRI, myocardial ischemia-reperfusion injury;
mTOR, mammalian target of rapamycin;
mPTP, mitochondrial permeability transition pore;
MCU, mitochondrial calcium uniporter;
MFRN, mitoferrin 2;
MMP, mitochondrial membrane potential;
NADP-, nicotinamide adenine dinucleotide phosphate;
NCOA4, nuclear receptor coactivator 4; I
NOX4, NADPH oxidase 4;
PUFAs, polyunsaturated fatty acids;
ROS, reactive oxygen species;
SLC7A11, solute carrier family seven member 11;
SLC3A2, solute carrier family three member 2;
TfR1, transferring receptor 1;
VDAC, voltage-dependent anion channel;

frontiers in Cell and Developmental Biology

ORIGINAL RESEARCH
published: 07 December 2021
doi: 10.3389/fcell.2021.752773

YKL-40 Aggravates Early-Stage Atherosclerosis by Inhibiting Macrophage Apoptosis in an Aven-dependent Way

Wei Huan[1†], Liu Yandong[1†], Wang Chao[1†], Zou Sili[1], Bai Jun[1], Liao Mingfang[1], Chen Yu[2] and Qu Lefeng[1]**

[1]Department of Vascular and Endovascular Surgery, Second Affiliated Hospital of Naval Medical University, Shanghai, China, [2]Yueyang Hospital of Integrated Traditional Chinese Medicine & Clinical Research Institute of Integrative Medicine, Shanghai University of Traditional Chinese Medicine, Shanghai, China

OPEN ACCESS

Edited by:
Zhi Qi,
Nankai University, China

Reviewed by:
Dawei Zhang,
University of Alberta, Canada
Andrew Newby,
University of Bristol, United Kingdom

***Correspondence:**
Qu Lefeng
qulefeng@smmu.edu.cn
Chen Yu
chenyu@shutcm.edu.cn

[†]These authors have contributed equally to this work and share first authorship

Specialty section:
This article was submitted to Cell Death and Survival, a section of the journal Frontiers in Cell and Developmental Biology

Received: 03 August 2021
Accepted: 22 November 2021
Published: 07 December 2021

Citation:
Huan W, Yandong L, Chao W, Sili Z, Jun B, Mingfang L, Yu C and Lefeng Q (2021) YKL-40 Aggravates Early-Stage Atherosclerosis by Inhibiting Macrophage Apoptosis in an Aven-dependent Way. Front. Cell Dev. Biol. 9:752773. doi: 10.3389/fcell.2021.752773

Objective: programmed cell removal in atherosclerotic plaques plays a crucial role in retarding lesion progression. Macrophage apoptosis has a critical role in PrCR, especially in early-stage lesions. YKL-40 has been shown to be elevated as lesions develop and is closely related to macrophages. This study aimed to determine the effect of YKL-40 on regulating macrophage apoptosis and early-stage atherosclerosis progression.

Research design and Methods: The correlations among the expression level of YKL-40, the area of early-stage plaque, and the macrophage apoptosis rate in plaques have been shown in human carotid atherosclerotic plaques through pathological and molecular biological detection. These results were successively confirmed *in vivo* (*Ldlr*$^{-/-}$ mice treated by YKL-40 recombinant protein/neutralizing antibody) and *in vitro* (macrophages that *Ykl40* up-/down-expressed) experiments. The downstream targets were predicted by iTRAQ analysis.

Results: In early-stage human carotid plaques and murine plaques, the YKL-40 expression level had a significant positive correlation with the area of the lesion and a significant negative correlation with the macrophage apoptosis rate. *In vivo*, the plaque area of aortic roots was significantly larger in the recomb-YKL-40 group than that in IgG group ($p = 0.0247$) and was significantly smaller in the anti-YKL-40 group than in the IgG group ($p = 0.0067$); the macrophage apoptosis rate of the plaque in aortic roots was significantly lower in the recomb-YKL-40 group than that in IgG group ($p = 0.0018$) and was higher in anti-YKL-40 group than that in VC group. *In vitro*, the activation level of caspase-9 was significantly lower in RAW264.7 with *Ykl40* overexpressed than that in controls ($p = 0.0054$), while the expression level of Aven was significantly higher than that in controls ($p = 0.0031$). The apoptosis rate of RAW264.7 treated by recomb-YKL40 was significantly higher in the *Aven* down-regulated group than that in the control group ($p < 0.001$). The apoptosis inhibitor Aven was confirmed as the target molecule of YKL-40. Mechanistically, YKL-40 could inhibit macrophage apoptosis by upregulating Aven to suppress the activation of caspase-9.

Conclusion: YKL-40 inhibits macrophage apoptosis by upregulating the apoptosis inhibitor Aven to suppress the activation of caspase-9, which may impede normal PrCR and promote substantial accumulation in early-stage plaques, thereby leading to the progression of atherosclerosis.

Keywords: atherosclerosis, macrophage, apoptosis, YKL-40, aven

INTRODUCTION

Cardio- and cerebrovascular diseases are the leading causes of mortality worldwide and account for well over 20% of all deaths, according to World Health Organization (WHO) estimates (Mathers and Loncar, 2006; Kim and Johnston, 2011). Statistics show that 9–35% of transient ischemic attacks (TIA) or strokes are associated with extracranial carotid atherosclerosis (Sacco et al., 1995; Wityk et al., 1996). Currently, treatments for carotid artery stenosis are most often performed at the late stage of carotid atherosclerosis, aiming to improve cerebral ischemia symptoms and prevent stroke or other serious ischemic complications. There are no definite effective means to inhibit plaque aggravation in the early stage to date.

Atherosclerosis is universally identified as a progressive inflammatory disease. In its initial stage, apolipoprotein B-containing lipoproteins accumulate in the arterial intima, triggering a chronic inflammatory response dominated by the recruitment of monocyte-derived macrophages (Tabas and Lichtman, 2017). Macrophages engulf lipids and form foam cells, a hallmark of the onset of early-stage atherosclerosis. Then apoptosis occurs and the cellular debris of macrophages is removed by efferocytosis. This programmed cell removal (PrCR) process can reduce the components of atherosclerotic plaque, which would effectively decrease plaque burden and inhibit lesion progression (Tabas, 2005; Vandivier et al., 2006; Gautier et al., 2009; Seimon and Tabas, 2009). Studies have shown that the inhibition of macrophage apoptosis significantly exacerbates the progression of early-stage atherosclerosis (Liu et al., 2005). Though the effect of macrophage apoptosis on atherosclerosis progression is reverse in advanced lesions, it is thought to be caused by impaired efferocytosis of phagocytes in the later-stage lesions (Tabas, 2005; Schrijvers et al., 2007). In our previous research, the impaired efferocytosis function of macrophages induced by the inflammatory factor YKL-40 contributed to enlarging the necrotic core and undermining the stability of later-stage atherosclerosis plaques.

YKL-40, also known as chitinase-3-like protein 1 (CHI3L1), is a 40 kD mammalian glycoprotein, belonging to the conserved mammalian chitinase family but without chitinase activity (Hakala et al., 1993; Rathcke and Vestergaard, 2006). YKL-40 has been identified as a novel biomarker of systemic inflammation and is expressed and secreted by macrophages, vascular smooth muscle cell (VSMC) and neutrophils under pathological conditions (Michelsen et al., 2010). Recent studies have shown that YKL-40 could play an important role in regulating apoptosis, pyroptosis, and activation of inflammasomes, etc. (Lee et al., 2009; Sohn et al., 2010; Chen et al., 2011; Areshkov et al., 2012). YKL-40 is lack of chitinase activity, while it still reserves certain biological function like possessing the carbohydrate-binding motif (CBM), which is considered the potential path that YKL-40 enhancing the AKT phosphorylation (Chen et al., 2011). Our previous research and other studies have found that serum levels of YKL-40 are markedly increased in patients with carotid atherosclerosis, especially in patients with ischemic symptoms (Kjaergaard et al., 2010; Michelsen et al., 2010; Wu et al., 2013). Moreover, a large population study confirmed that elevated plasma YKL-40 levels were positively correlated with an increased risk of ischemic stroke (Kjaergaard et al., 2010). We have known that YKL-40 could aggravate atherosclerosis progression. However, the effect of YKL-40 on the function of macrophages and the PrCR process in plaque and its mechanisms during early-stage atherosclerosis are still not known.

In this study, we focused on the effect of YKL-40 on regulating early-stage atherosclerotic plaque progression and explored its potential mechanisms.

MATERIALS AND METHODS

Human Study Population and Sample Preparation

Early-stage carotid plaques and corresponding blood samples were collected from 16 patients with carotid body tumors and five patients with carotid aneurysm undergoing surgical operations in the Department of Vascular and Endovascular Surgery, Changzheng Hospital, affiliated with the Naval Medical University (Shanghai, People's Republic of China) between July 2015 and September 2019. The inclusion criteria were patients with inchoate atherosclerosis in the carotid arteries. Exclusion criteria were patients with definite atherosclerotic carotid stenosis and renal/liver failure or other chronic disease that might result in metabolic abnormalities. As previously described, early-stage plaque samples were collected including foam cells and lipid particles accumulating in several pools in the thickening intima. Advanced lesions that had developed a massive, confluent, well-delineated accumulation of extracellular lipid (a lipid core) were excluded (Stary et al., 1994). For this study, all plaque samples were collected from patients intraoperatively, then flushed with phosphate buffered saline (PBS) and immediately stored in liquid nitrogen. All peripheral blood samples were collected before the procedure. Serum was acquired by centrifugation of the peripheral blood at 3,500 rpm for 10 min at room temperature and stored at −80°C before further processing. This research was conducted according to institutional and

ethical guidelines. Patients' informed consents were obtained. The study protocol was approved by the Independent Ethics Committee of the Changzheng Hospital affiliated with the Naval Medical University.

Calculating Relative Area and Grouping for Samples

H&E (hematoxylin-eosin) staining was performed on the cross-section of the plaques. The plaque area and total lesion area were calculated according to the staining outcomes, and the percentage of plaque area to total lesion area was counted as the relative area (%) of plaque (**Supplementary Figure S1**).

In order to compare the results between the groups on the basis of lesion size, all 21 samples were divided into a small group ($n = 10$) and a large group ($n = 11$) at the median value (51.32%) of plaque relative area. Baseline information on these patients in the two groups are compared in **Supplementary Table S1**.

Atherosclerosis Animal Model and *In Vivo* Administration Protocol

Ldlr$^{-/-}$ mice were bred based on C57BL/6 mice obtained from Jackson Laboratory. Male *Ldlr*$^{-/-}$ mice were weaned at 3 weeks old and fed a chow diet until 6 weeks old, then a high cholesterol diet (HCD) was maintained (0.4% fat +1.1% cholesterol +18.8% casein, Research Diets, America, D12104C) to construct the atherosclerosis model. The atherosclerotic plaque collected from the aorta of *Ldlr*$^{-/-}$ mice fed a HCD ≤12 weeks were regarded as early-stage lesions, according to the histological morphology and the criterion as previously described (Whitman, 2004).

At 12 weeks old (while HCD feeding has been lasted for 6 weeks), the administration was initiated. *Ldlr*$^{-/-}$ mice were randomly divided into three groups ($n = 5$), including the control group (IgG), YKL-40 recombinant protein group (recomb-YKL-40), and YKL-40 neutralizing antibody group (anti-YKL-40). At each week of age, IgG (1 mg/g), YKL-40 recombinant protein (500 ng/g) and YKL-40 neutralizing antibody (1 mg/g) was intraperitoneally injected for six successive weeks, while the high cholesterol diet was continued. Mice were euthanized after administration completed (while HCD feeding has been lasted for 12 weeks) and tissues were collected. Customized YKL-40 neutralizing antibody (Huiou Co., Ltd., Shanghai, China) was extracted from rabbit serum according to previously described (Mizoguchi, 2006) and the titer of the antiserum reached to 1: 72,900. The administration program was determined by the relatively large dose of agents (1 mg/g) and the protocols used in the previous studies (Kojima et al., 2016). After mice were euthanized, cold PBS was injected through the left ventricle to flush out blood or thrombus followed by an injection of 4% paraformaldehyde (10 ml per mouse) for internal fixation. The murine aorta tissue (from aortic root to iliac artery) was removed, the aortic root was immediately stored in liquid nitrogen, and the residual part was fixed in 4% formaldehyde at 4°C for further assay.

Histology and Immunofluorescent Staining

The human carotid plaques and murine aortic root were embedded in paraffin or optimal cutting temperature compound, followed by cutting into 5-μm-thick cryosections. H&E and Masson trichome staining was performed to examine plaque morphology. Human early-stage plaques were defined as previously described (Stary et al., 1994), according to the morphological assay. The murine aortic root cryosections and residual aorta tissue were stained with oil-red O for determination of lipids. Immunofluorescence staining was performed as previously described (Kojima et al., 2016). Briefly, after being blocked in 1% bovine serum albumin (BSA), sections were incubated with primary antibodies: human macrophages labeled with anti-CD68 Ab (Abcam ab201340 1:100); mouse macrophages labeled with anti-MOMA-2 Ab (Abcam ab33451 1:50); and human/mouse YKL-40 labeled with anti-YKL-40 Ab (Abcam ab180569 1:100). After being washed with PBS, the sections were incubated with fluorescein isothiocyanate (FITC)-conjugated secondary antibodies. Nuclei were stained with 4′, 6-diamidino-2-phenylindole (DAPI; 1:2000) for 5 min. After being rinsed three times in PBS, the sections were examined under a fluorescence microscope. The immunostaining was measured by ImageJ software.

Biochemical Assay

Mice were euthanized after being fasted overnight. Murine blood samples were centrifuged for collecting serum. Total cholesterol (TC), triglycerides (TG), low-density lipoprotein (LDL), and high-density lipoprotein (HDL) were measured by enzymatic colorimetric assays using colorimetric kits (Jiancheng, Nanjing, China) with an automatic biochemical analyzer.

Enzyme-Linked Immunosorbent Assay

Serum YKL-40 levels were measured with the related ELISA kits (R&D DC3L10) according to the manufacturer's instructions.

Measurement of Macrophage Apoptosis Rate Detection in Human and Murine Plaques

Human carotid plaque and murine aortic root sections were double stained for macrophages and apoptotic cells. Macrophages were labeled with anti-CD68 Ab (Abcam ab201340 1:100) or anti-MOMA-2 Ab (Abcam ab33451 1:50) antibody and apoptotic cells were stained with TUNEL kits (Progema G3250) according to the manufacturer's instructions. The proportion of TUNEL^{+} in CD68^{+} cells in each sample was calculated as the apoptosis rate of macrophages in the plaque. Nine randomized magnified fields were chosen to measure the apoptosis rate.

Cell Culture

Mouse bone marrow-derived macrophage (BMDM) were isolated from male C57BL/6 mice and differentiated in

Dulbecco's modified Eagle's medium (DMEM) supplemented with 10% fetal bovine serum, 1% penicillin/streptomycin (Invitrogen), and 10 ng/ml murine M-CSF (Peprotech). The murine macrophage cell line RAW264.7 (ATCC, SC-6003) was grown in DMEM growth media containing 10% fetal bovine serum (FBS) and 1% penicillin/streptomycin (Invitrogen). Cells were cultured in a 5% CO2 humidified atmosphere at 37°C.

In Vitro Apoptosis Rate Measurement

For the adherent cell assays, BMDM were embedded into Lab-Tek® chamber slides (Sigma). Apoptotic BMDM were induced via Ox-LDL (100 μg/ml for 24 h) combined with staurosporine (STS) (1 μM for 4 h). The apoptotic cells were stained with TUNEL kits (Progema G3250) according to the instructions. Nine randomized magnified fields were chosen to measure the apoptosis rate.

For the flow cytometry-based assays, apoptosis-induced BMDM were prepared into cell suspension. Apoptotic BMDM were detected with the FITC Annexin V Apoptosis Detection Kit with PI (BioLegend 640,914), according to the manufacturer's instructions. Apoptotic cells were quantified via flow cytometry using the FACS verse cell analyzer (Becton-Dickinson).

Plasmid Transfection

RAW264.7 were prepared in cell suspension then plated at 1–2 × 10^5 cells/well in a 24-well plate and cultured for 24 h. Commercially available plasmids for over-expressing or silencing *Ykl40*/*Aven* (Genechem Co.,Ltd., Shanghai, China) were used. Plasmids were transfected using Lipofectamine 3,000 (Invitrogen L3000001) according to the manufacturer's instructions. Cells were passaged or harvested for further experiments 48–72 h after transfection.

iTRAQ Labeling

iTRAQ-based proteomics analysis (Genechem Co.,Ltd., Shanghai, China) were performed to screen out the potential downstream target molecules of YKL-40. Three biological replicates were used for global proteome analysis. BMDM was treated with YKL-40 (500 ng/ml) or IgG as a control for 24 h to assay the potential pathways involved. We collected 20 mg protein from each sample and loaded into 12% SDS-PAGE for electrophoresis. The samples then underwent filter-aided sample preparation and were dissolved in 5X dissolution buffer. Then 100 μg peptide fragments from each sample were labeled with iTRAQ-8 plex reagents according to the protocol from AB SCIEX. The labeled peptides were separated by high-performance liquid chromatography (Agilent 1,260 Infinity II HPLC), followed by mass spectrometric analysis and identification. The raw data were processed with Mascot 2.5 software and Proteome Discoverer 2.1 to search the database. The experiment had been performed in our previous research, and the results were further explored in this study. The mass spectrometry proteomics data have been deposited to the ProteomeXchange Consortium with identifier PXD028305 via the PRIDE partner repository.

Western Blot Assay

Cells and homogenated human plaques were lysed in RIPA lysis buffer (ThermoFisher) for 60 min at 4°C. Protein samples were subjected to 10% Bis-Tris gels, electrophoresed, transferred to Immobilon-FL membranes (Millipore), and probed with the indicated primary antibody: caspase-3 (CST 9662S), cleaved caspase-3(Asp175) (CST 9661T), caspase-9 (CST 9508T), Aven (CST 2300S), Akt (CST 9272S), Phospho-Akt (Thr308) (CST 13038T), and β-Actin (CST 4970S), followed by incubation with horseradish peroxidase-conjugated secondary antibodies. Protein bands were visualized using an LAS 3000 Imager (Fujifilm) and were quantified using ImageJ software (ImageJ 1.51U, Fuji edition).

Ribonucleic Acid Extraction and Quantitative Real-Time Polymerase Chain Reaction

RNA was isolated from samples and cells using the RNeasy Kit (QIAGEN), and cDNA was synthesized from RNA (500 ng–1 μg per reaction) using Prime Script RT Master Mix (TaKaRa 2,621). Quantitative Real-time PCR (qRT-PCR) was performed using the LightCycler 480 Real-Time PCR System (Roche) and SYBR Green I Master (Roche 04,707,516,001). Primer sets used are listed in supplemental data (**Supplementary Table S1**).

Statistics Analysis

Independent experiments were replicated at least three times. All results are represented as mean ± SEM. Normality was determined using D'Agostino-Pearson and/or Shapiro-Wilk normality testing. *p*-values for normally distributed data were calculated using Student's *t*-test or one-way ANOVA analysis. *p*-values for non-normally distributed data were calculated using the Mann-Whitney U test. Percentages were analyzed with Chi-square testing or Fisher's exact test. Correlation coefficients (*r*) and related *p*-values were calculated using the Pearson product-moment correlation analysis. Statistical analysis was performed using Graphpad Prism 8.1. A *p*-value of <0.05 was deemed statistically significant.

RESULTS

Positive Correlation Was Determined Between Expression Level of YKL-40 and Carotid Early-Stage Plaque Area

The expression level of YKL-40 in the large group of human subjects was significantly higher than in the small group, according to immunohistochemical staining (p = 0.0034, **Figures 1A,B**). Significant positive correlation was confirmed between the *Ykl40* expression level in the plaque tissues and relative area of plaques (r = 0.6334, p = 0.0021, **Figure 1D**). Although the mean of *Ykl40* expression level was higher in the large group than in the small group, the difference was not significant (p > 0.05, **Figure 1C**), which may be due to the relatively low expression level of *Ykl40* in plaques. However,

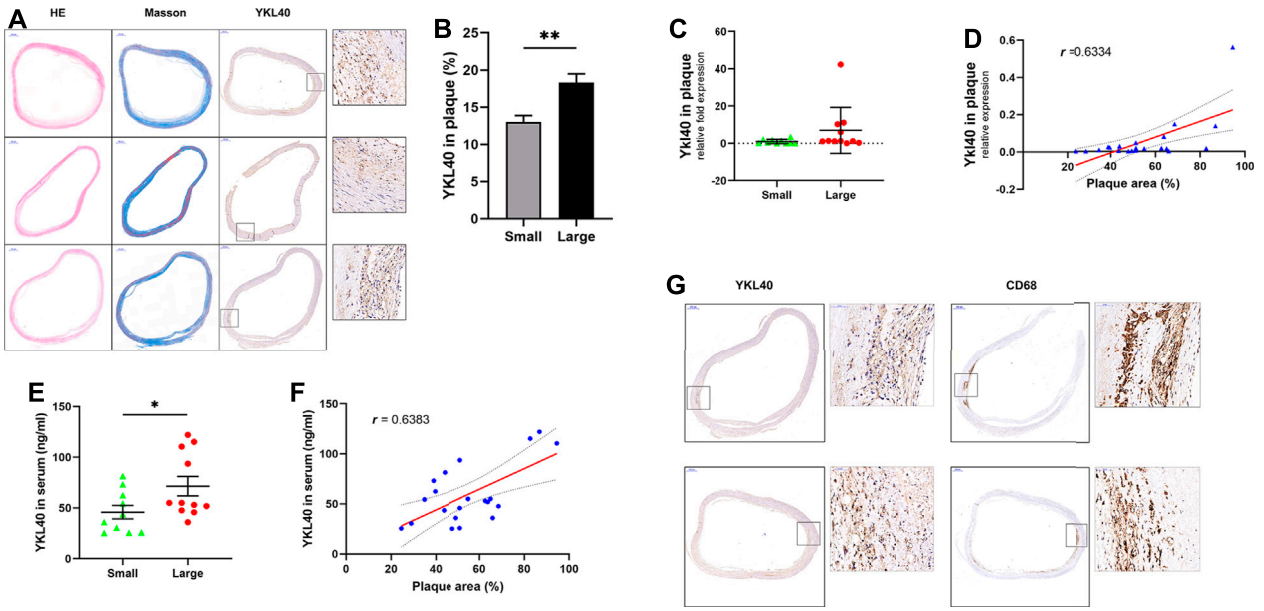

FIGURE 1 | (A) H&E, Masson staining and anti-YKL-40 Ab labeling were performed on carotid plauqe samples. **(B)** Relative expression level of YKL-40 in unit area of plaques were calculated based on immunohistochemistry. The YKL-40 expression level in the large group was significantly higher than in the small group ($p = 0.0034$). **(C,D)** The mRNA expression level of YKL-40 in plaque tissues were detected via qRT-PCR. Significant positive correlation existed between the Ykl40 expression level in the plaque tissues and plaque relative area ($r = 0.6334$, $p = 0.0021$), but the difference between two groups was not significant ($p > 0.05$). **(E,F)** YKL-40 expression level in serum samples were detected by ELISA assay. The YKL-40 expression level in serum was significantly higher in the large group than in the small group ($p = 0.0447$) and was significantly positively correlated with plaque relative area ($r = 0.6383$, $p = 0.0018$). **(G)** Colocalization between YKL-40 and macrophages in plaque tissues as indicated by immunohistochemical detection.

the expression level of YKL-40 in serum, which was detected by enzyme-linked immunosorbent assay (ELISA), was significantly higher in the large group than in the small group ($p = 0.0447$, **Figure 1E**) and was significantly positively correlated with plaque relative area ($r = 0.6383$, $p = 0.0018$, **Figure 1F**). These results indicated the positive correlation between the expression level of YKL-40 and the relative area of early-stage carotid plaque. Moreover, the location of YKL-40 had a significant correlation with CD68 in plaque tissues according to immunohistochemical staining (**Figure 1G**). The result suggests the potential association between YKL-40 and macrophages.

Negative Correlation Was Confirmed Between the Apoptosis Rate of Macrophages in Early-Stage Carotid Plaque Samples and the Lesion Area or the Serum Level of YKL-40

Immunofluorescent double-labelled staining for macrophages (CD68) and apoptotic cells (TUNEL) was performed on the above 21 human carotid plaque samples (**Figure 2A**). The macrophage apoptosis rate in the large group was significantly lower than that in the small group ($p = 0.0497$, **Figure 2B**). Moreover, a significant negative correlation was confirmed between the macrophage apoptosis rate in plaques and relative plaque area ($r = -0.5414$, $p = 0.0112$, **Figure 2C**). Meanwhile, a significant negative correlation was also confirmed between the macrophage apoptosis rate in plaques and expression level of YKL-40 in serum ($r = -4{,}373$, $p = 0.0475$, **Figure 2D**). These results indicated that the apoptosis of macrophages is strongly associated with YKL-40.

No Differences in Weight or Lipid Metabolism Among *Ldlr*$^{-/-}$ Mice of Three Groups

Weights of all *Ldlr*$^{-/-}$ mice in IgG group, YKL-40 recombinant protein group (recomb-YKL-40), and YKL-40 neutralizing antibody group (anti-YKL-40) were monitored and recorded weekly from the last day before intervention to the last day before harvest. Sera from all these mice were collected after euthanasia to test blood lipid levels including total cholesterol (TCHO), triglycerides (TG), high-density lipoprotein cholesterol (HDL-C), and low-density lipoprotein cholesterol (LDL-C). No statistical differences in weight or blood lipid levels of mice were found among the three groups, which indicated that the nutrition status and lipid metabolism of *Ldlr*$^{-/-}$mice were not affected by the intervention of the YKL-40 recombinant protein or YKL-40 neutralizing antibody ($p > 0.05$, **Figures 3A,B**).

Positive Correlation Was Confirmed Between the Plaque Area in Aortic Root and Expression Level of YKL-40 in *Ldlr*$^{-/-}$ Mice

In the process of establishing the atherosclerotic mice model by HCD feeding, we randomly selected mice at 8, 12, and

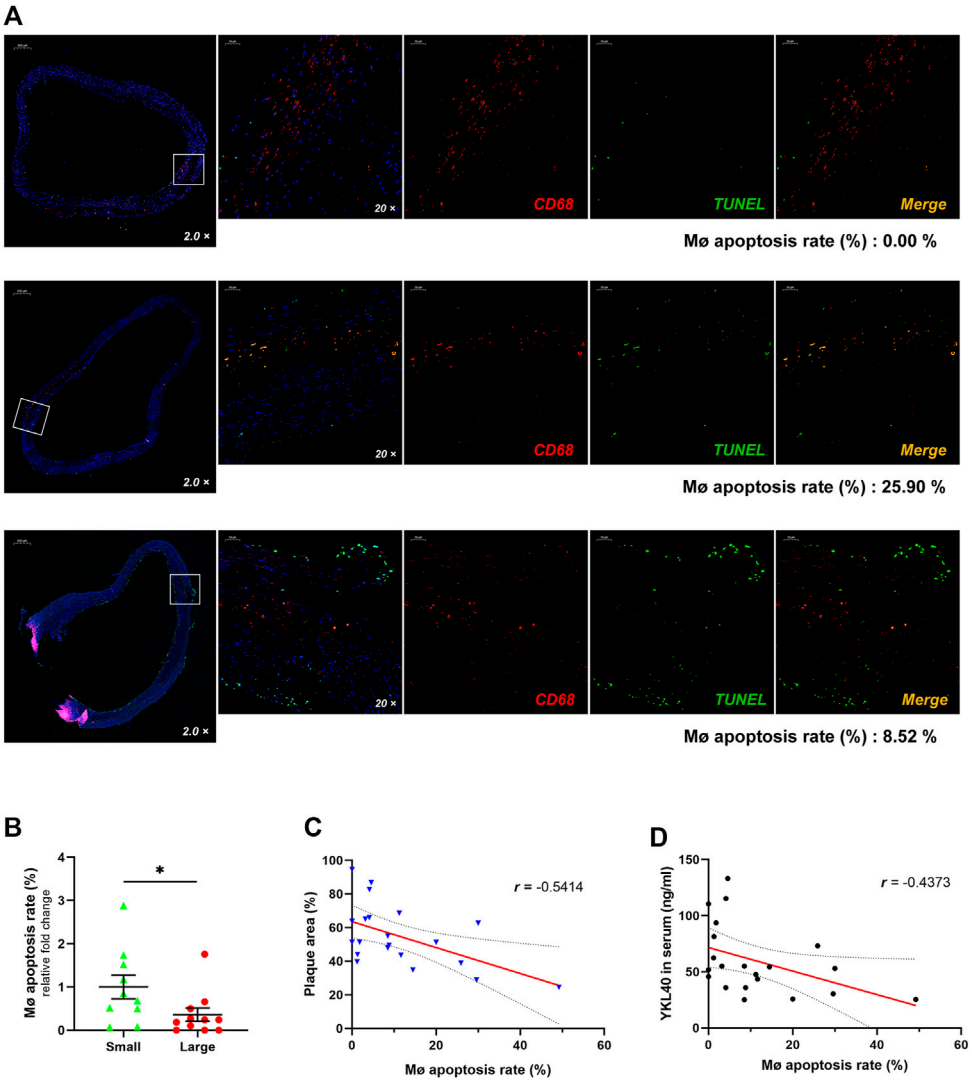

FIGURE 2 | (A) The immunofluorescent double-labelled staining for carotid plaque samples. CD68$^+$was presenting as red fluorescence while TUNEL$^+$ is shown as green and Merge as golden. The proportion of TUNEL$^+$ in CD68$^+$ cells was calculated as the apoptosis rate of macrophages, which is shown beneath each panel. **(B)** The macrophage apoptosis rate in the large group was significantly lower than that in the small group (p = 0.0497). **(C)** There was a significant negative correlation between the macrophage apoptosis rate and relative plaque area (r = –0.5414, p = 0.0112). **(D)** There was a significant negative correlation showed between the macrophage apoptosis rate and expression level of YKL-40 in serum (r = –0.4373, p = 0.0475).

16 weeks, respectively, to obtain the tissue samples, including aortic root and aortic arch. H&E and Masson staining were performed on the aortic root to measure the relative area of plaque. We detected the expression level of *Ykl40* in aortic arch tissues by qRT-PCR. Evidently, atherosclerotic plaques were formed on aortic roots at all three time periods, which confirmed the success of model construction (**Figure 3C**). Meanwhile, both the relative plaque area in the aortic root and *Ykl40* expression level in the aortic arch showed a consistently increasing trend as the HCD feeding time increased. The result confirmed the positive correlation between the progression of the plaque area and expression level of YKL-40 in *Ldlr*$^{-/-}$ mice (**Figures 3D,E**).

YKL-40 Resulted in Progression of Atherosclerotic Plaque in *Ldlr*$^{-/-}$ Mice

H&E, Masson, and oil-Red O staining were performed on aortic roots, and the plaque area as well as the lipid area were measured in the three mice groups (IgG, YKL-40 protein, YKL-40 neutralizing antibody) (**Figure 4A**). Oil-red O staining was performed on the whole aorta to measure the plaque relative area as well (**Figure 4D**). The plaque area in the aortic root was significantly larger in the recomb-YKL-40 group than that in IgG group (p = 0.0247) and was significantly smaller in the anti-YKL-40 group than in the IgG group (p = 0.0067, **Figure 4B**). The lipid area was significantly larger in the recomb-YKL-40 group than that in the IgG group (p = 0.0028) and in the anti-YKL-40 group

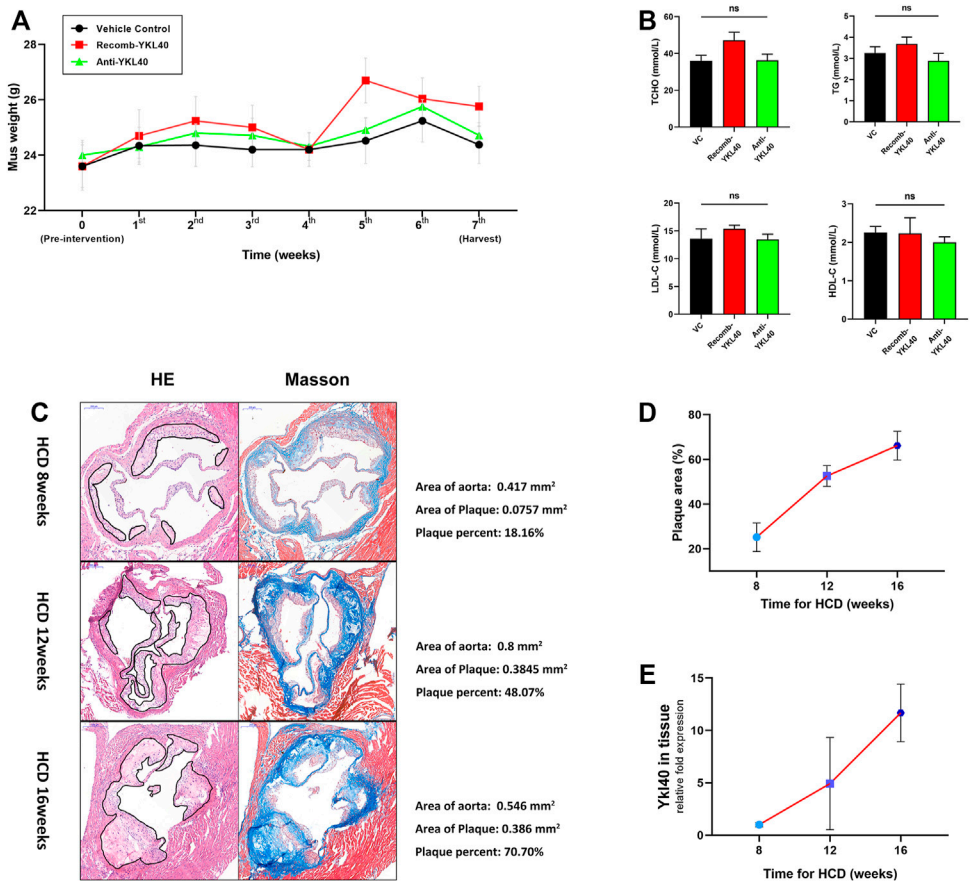

FIGURE 3 | (A) Weight curve of mice in different groups during intervention. No statistical differences were confirmed. **(B)** Blood lipid (TCHO, TG, LDL-c, HDL-c) levels of mice in different groups. No statistical differences were confirmed. **(C)** H&E and Masson staining on aortic valves of mice at 8, 12, and 16 weeks (the area of plaque is indicted by black lines). Calculations of the relative area are shown on the right side. **(D)** Increasing trend of aortic root plaque relative area as modeling time advanced. **(E)** Increasing trend of *Ykl-l40* expression level on the aortic arch as modeling time increased.

(p = 0.0001, **Figure 4C**). Similarly, the plaque area of the whole aorta was significantly larger in the recomb-YKL-40 group than that in the IgG group (p = 0.0126) and was significantly smaller in the anti-YKL-40 group than in the IgG group (p = 0.0464, **Figure 4E**). The results unequivocally confirmed that YKL-40 could result in progression of atherosclerotic plaque in *Ldlr*$^{-/-}$ mice, including lesion progression and lipid accumulation.

YKL-40 Inhibited Apoptosis of Macrophages in Atherosclerotic Plaque of *Ldlr*$^{-/-}$ Mice

Macrophages and apoptotic cells in aortic root plaques of *Ldlr*$^{-/-}$ mice were simultaneously assayed via immunofluorescent staining (for MOMA-2) and TUNEL, respectively (**Figure 4G**). The percentage of TUNEL^{+} in MOMA-2^{+} cells was calculated as the apoptosis rate of macrophages in each sample. The apoptosis rate of macrophages in aortic root plaques was significantly lower in the recomb-YKL-40 group than in the IgG group (p = 0.0018) and anti-YKL-40 group (p = 0.001). However, the rate was not significantly higher in the anti-YKL-40 group than in the VC group (p = 0.0513, **Figure 4F**). The results indicated that YKL-40 exerts an inhibitory effect on apoptosis of macrophages in atherosclerotic plaques in *Ldlr*$^{-/-}$ mice.

YKL-40 Inhibited Apoptosis of Macrophages *In Vitro*

BMDM apoptosis was induced by treatment with oxidized low-density lipoprotein (OX-LDL) 100 μg/ml for 24 h accompanied by staurosporine 4 μM for 4 h. After treatment with YKL-40 recombinant protein (500 ng/ml) for 24 h on apoptosis BMDM, TUNEL detection was performed on the cells *in situ* (**Figure 5A**). The staining result showed that the apoptosis rate of BMDM treated by YKL-40 recombinant protein was significantly lower than that in the apoptosis model (p = 0.0161). Flow cytometry (FCM) was performed while another cell group, the apoptosis BMDM synchronously treated by YKL-40 recombinant protein and YKL-40 neutralizing antibody (500 μg/ml) for 24 h, was added (**Figure 5B**). The FCM result showed that the

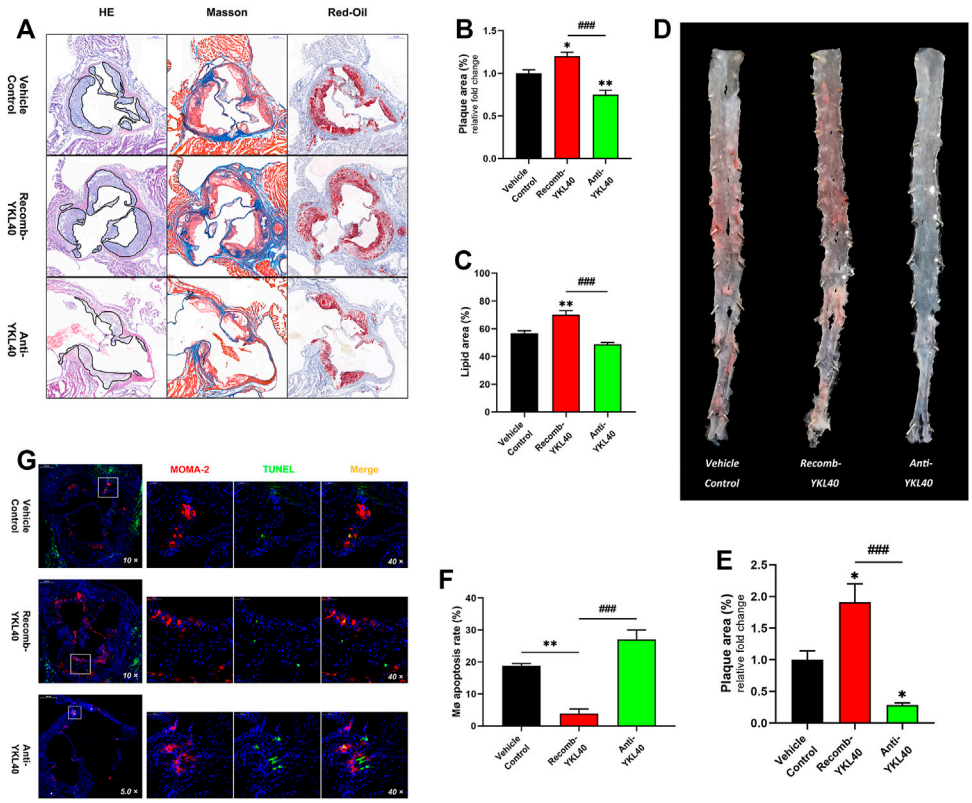

FIGURE 4 | (A–C) H&E, Masson, and oil-Red O staining of aortic roots (the area of plaque is outline in black). The plaque area of the aortic root was significantly larger in the recomb-YKL-40 group than that in IgG group ($p = 0.0247$) and in the anti-YKL-40 group ($p < 0.0001$), and which was significantly smaller in the anti-YKL-40 group than in the IgG group ($p = 0.0067$). The lipid area was significantly larger in the recomb-YKL-40 group than that in the IgG group ($p = 0.0028$) and in the anti-YKL-40 group ($p = 0.0001$). **(D,E)** Oil-Red O staining of the whole aortas. The plaque area of the whole aorta was significantly larger in the recomb-YKL-40 group than that in IgG group ($p = 0.0126$) and in the anti-YKL-40 group ($p = 0.0001$) and was significantly smaller in the anti-YKL-40 group than in the IgG group ($p = 0.0464$). **(F,G)** Immunofluorescence and TUNEL staining were performed on aortic root plaques (red indicates MOMA-2, green for TUNEL, and golden for MERGE). The macrophage apoptosis rate in aortic root plaques was significantly lower in the recomb-YKL-40 group than that in IgG group ($p = 0.0018$) and anti-YKL-40 group ($p = 0.001$) and was higher in the anti-YKL-40 group than that in the IgG group, but the difference was not statistically significant ($p = 0.0513$).

apoptosis rate of BMDM in the YKL-40 recombinant protein treated group was significantly lower than that in the apoptosis model group ($p = 0.0008$) and was significantly higher in the YKL-40 neutralizing antibody extra treated group than in the YKL-40 recombinant protein treated group ($p = 0.0042$). Moreover, the apoptosis rate of RAW264.7 was detected by FCM after overexpressing or silencing *Ykl40*. FCM results indicated the apoptosis rate of RAW264.7 was significantly lower in the *Ykl40* overexpressed group than that in apoptosis model group ($p = 0.0205$) and *Ykl40* knockdown group ($p = 0.0197$), but there was no significant difference between the *Ykl40* knockdown group and the model group ($p > 0.05$, **Figure 5C**). These results indicated that YKL-40 has an inhibitory effect on apoptosis of macrophages *in vitro*.

YKL-40 Inhibited Macrophage Apoptosis Via Suppressing Activation of Caspase-9

An iTRAQ-based proteomics analysis was performed on BMDM to screen out the potential downstream target molecules of YKL-40 in regulating macrophage apoptosis. Among all the apoptosis-regulating molecules, *Casp9* ($p = 0.0311$), *Casp8* ($p = 0.0399$), *Bak-1* ($p = 0.0014$), and *Dap* ($p = 0.0041$), all of which have the effect of promoting apoptosis, were significantly down-regulated in BMDM treated by YKL-40 recombinant protein, while the apoptosis inhibitor *Aven* was significantly up-regulated ($p = 0.0251$, **Figure 6A**). A *Volcano Plot* revealed that the most significant *fold change* (*FC*) on expression level among these molecules was *Casp9* (*FC* = 0.6411), which was followed by *Aven* (*FC* = 1.3006, **Figure 6B**), *Bak1* and *Dap*.

The expression level of activated caspase-9 in BMDM were detected by western blot. The value of cleaved caspase-9/β-actin were calculated as activation level of caspase-9, which was significantly lower in the BMDM group treated with the YKL-40 recombinant protein than in IgG group ($p = 0.0038$, $p = 0.0419$, **Figure 6C**).

These results were verified in aortic arch tissues of $Ldlr^{-/-}$ mice. The activation levels of caspase-3 and caspase-9 were significantly lower in the recomb-YKL-40 group than in the IgG group ($p = 0.0036$, $p = 0.0316$) and that in the anti-YKL-

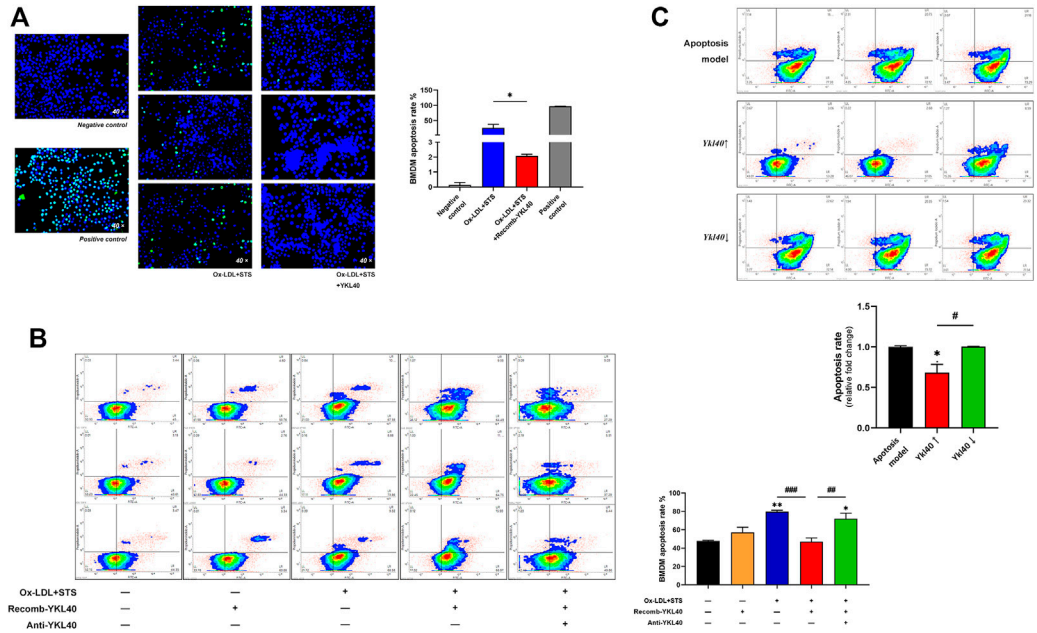

FIGURE 5 | (A) TUNEL detection performed on BMDM. The apoptosis rate of BMDM treated by YKL-40 recombinant protein was significantly lower than that in the apoptosis model that treated by Ox-LDL accompanied by staurosporine (p = 0.0161). **(B)** FCM indicated the apoptosis rate of BMDM was significantly lower in the recomb-YKL-40 group than that in apoptosis model group (p = 0.0008), as well as that in anti-YKL-40 group (p = 0.0042). **(C)** FCM indicated the apoptosis rate of RAW264.7 was significantly lower in the *Ykl40*↑ group than that in apoptosis model (p = 0.0205) and *Ykl40*↓ group (p = 0.0197).

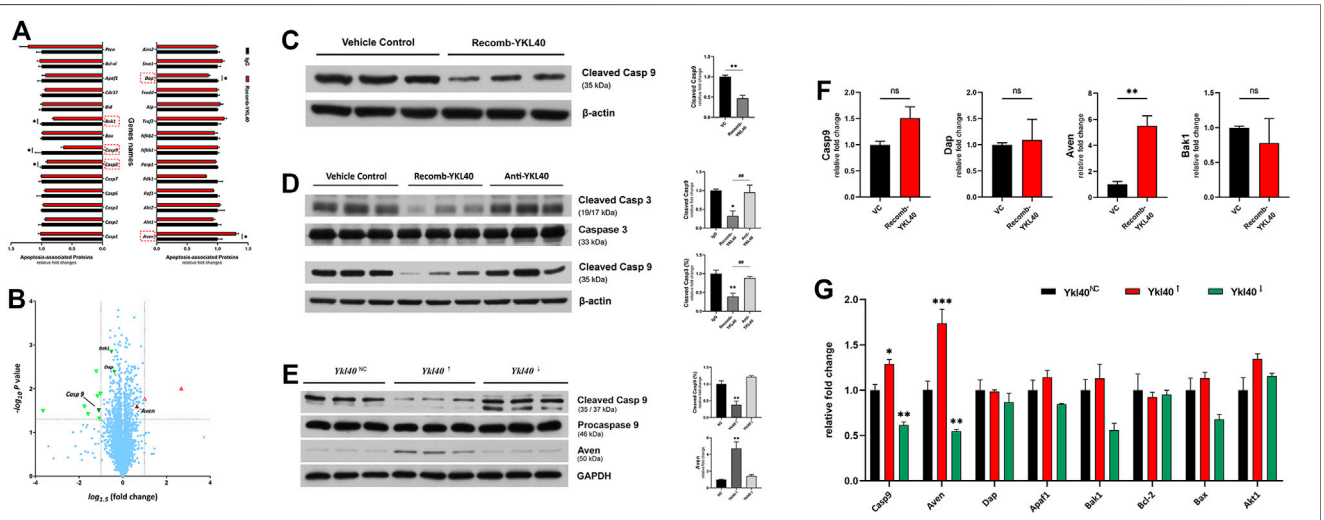

FIGURE 6 | (A,B) iTRAQ-based proteomics analysis. **(A)** Apoptosis promotors *Casp9*, *Casp8*, *Bak1,* and *Dap* were significantly down-regulated by YKL-40, while the apoptosis inhibitor *Aven* was significantly up-regulated. **(B)** ***Volcano Plot***. Molecules down-regulated by YKL-40 are presented in the upper left area (green down arrow) while those up-regulated are shown in the upper right area (red up arrow), and those involved in apoptosis regulation are marked with up/down solid arrows. The most significant *fold change* (*FC*) on the expression level of these molecules was caused by *Casp9* (*FC* = 0.6411), followed by *Aven* (*FC* = 1.3006). **(C,D)** Caspase-9 expression levels detected in BMDM and aorta tissues of $Ldlr^{-/-}$ mice. YKL-40 significantly down-regulated the activation level of caspase-9. **(E)** In RAW264.7, which was upregulated by *Ykl-40*, the activation level of caspase-9 was significantly lower than that in control group (p = 0.0054) while the expression level of Aven was significantly higher than in controls (p = 0.0031). There was no significant difference in caspase-9 activation and Aven expression level between the *Ykl40* downregulated group and normal controls (p > 0.05). **(F)** Genetic expression relative fold changes of *Casp9*, *Dap*, *Aven* and *Bak1.* No significant difference was indicated on *Casp9* in BMDM after being treated by YKL-40 recombinant protein, but *Aven* was significantly up-regulated. **(G)** *Casp9*, *Aven* expression levels were significantly upregulated in *Ykl40* upregulated RAW264.7 (p = 0.0154, p < 0.0001) and downregulated in the *Ykl40* downregulated group (p = 0.0039, p = 0.0037).

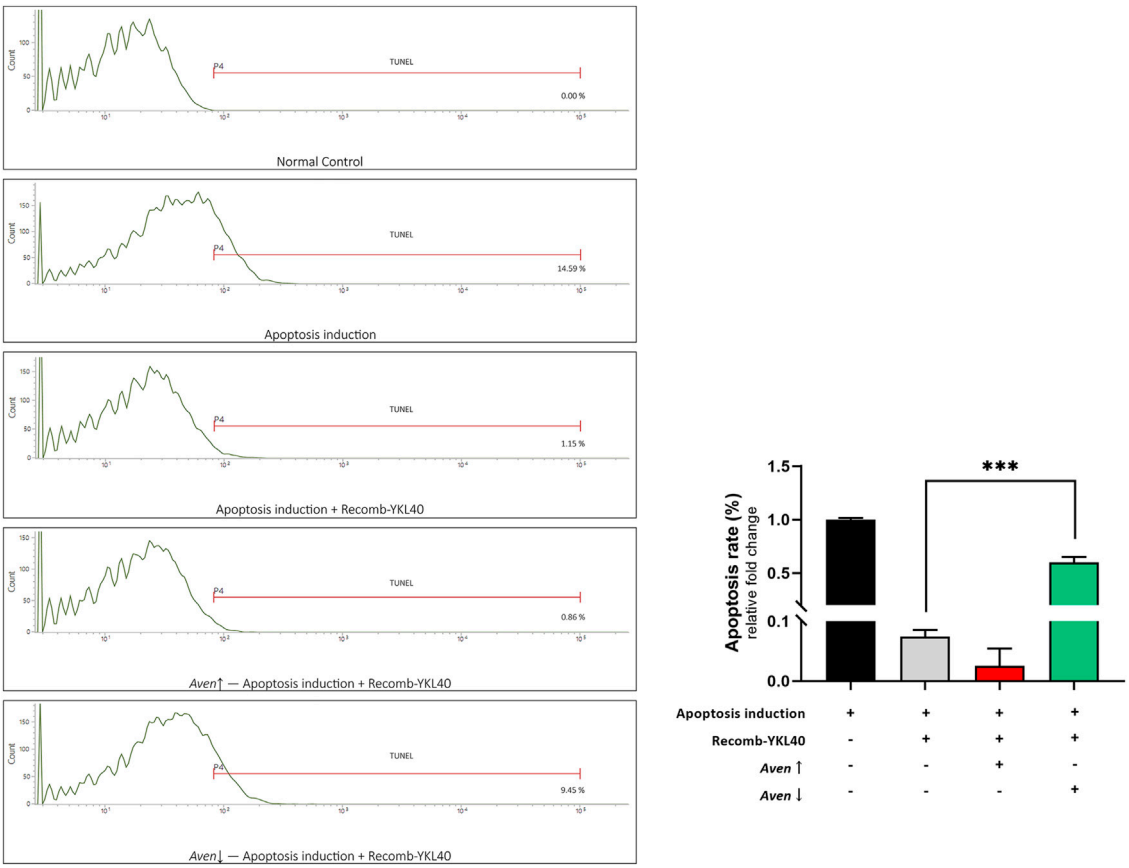

FIGURE 7 | FCM analysis of the apoptosis rate of RAW264.7 after TUNEL staining. Groups are presented as normal controls, the apoptosis model that treated by Ox-LDL accompanied by staurosporine, apoptosis induced combined with YKL-40 treatment, apoptosis induced combined with YKL-40 treatment and *Aven*↑, as well as apoptosis induced combined with YKL-40 treatment and *Aven*↓. The apoptosis rate of RAW264.7 in the recomb-YKL-40 treated group was certainly significantly lower than that in the apoptosis model group ($p < 0.001$); the apoptosis rate of RAW264.7 was significantly higher in *Aven*↓ group than that in Recomb-YKL40 group ($p < 0.001$).

40 group ($p = 0.0099$, $p = 0.0420$), but there was no significant difference between the anti-YKL-40 group and the IgG group ($p > 0.05$, **Figure 6D**).

However, there was no significant difference in the genetic expression level of *Casp9* between the recomb-YKL-40 group and IgG group in BMDM ($p > 0.05$). At the same time, the expression level of *Aven* was significantly higher in the recomb-YKL-40 group than in the IgG group ($p = 0.0048$, **Figure 6F**).

YKL-40 Inhibited Macrophage Apoptosis Via Suppressing Caspase-9 Activation by Up-Regulating *Aven*

In RAW264.7 with *Ykl40* overexpressed, the activation level of caspase-9 was significantly lower than that in the control group ($p = 0.0054$), while the expression level of Aven was significantly higher than in normal controls ($p = 0.0031$, **Figure 6E**). However, there was no significant difference on caspase-9 activation and *Aven* expression level between *Ykl40* downregulated group and normal control ($p > 0.05$). Interestingly, although the *Aven* expression level corresponded with protein expression, the expression level of *Casp9* was significantly upregulated in *Ykl40*-upregulated Raw264.7 and downregulated in the *Ykl40* downregulated group compared with normal controls ($p = 0.0154$, $p = 0.0039$), which was quite contrary to protein presentation (**Figure 6G**). The results indicated the suppression effect on caspase-9 activation of YKL40 was limited to the protein modification process, while Aven could be the potential target molecule.

Regulatory Role of Aven in YKL-40 Inhibition of Macrophage Apoptosis

We modified the expression of *Aven* in RAW264.7 to confirm the effect of Aven in YKL-40 inhibition of apoptosis. FCM analysis was performed to detect the apoptosis rate after TUNEL staining. Results showed that the apoptosis rate of RAW264.7 in the recomb-YKL-40 group was certainly significantly lower than that in the apoptosis model group ($p < 0.001$). When *Aven* expression was downregulated, the

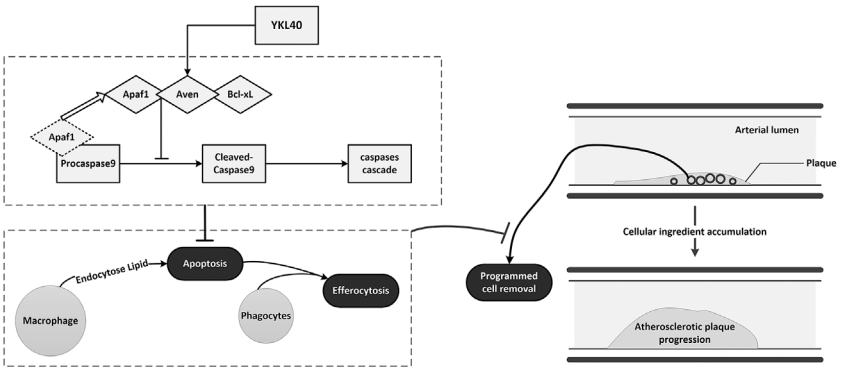

FIGURE 8 | Schematic diagram of the mechanism of YKL-40 aggravates early-stage atherosclerosis by inhibiting macrophage apoptosis in an Aven-dependent way.

apoptosis rate of RAW264.7 was significantly increased compared to that in the recomb-YKL-40 group ($p < 0.001$, **Figure 7**). The results suggested that the inhibitory effect of YKL-40 on macrophage apoptosis was mediated by its suppression of Aven.

DISCUSSION

In this study, the major findings are as follows: 1) the expression level of YKL-40 was positively correlated with the lesion size in early-stage carotid plaque; 2) the expression level of YKL-40 was negatively correlated with the macrophage apoptosis rate in early-stage carotid plaque; 3) YKL-40 treatment could suppress the apoptosis of murine macrophages and promote the progression of early-stage plaque in mice; 4) YKL-40 could inhibit the activation of the apoptosis promoter caspase-9 by upregulating the expression of apoptosis inhibitor Aven to suppress the apoptosis of macrophages.

Experimental results on the samples of early-stage carotid plaque patients indicated that the expression level of YKL-40 both in plaque tissues and in peripheral serum was positively correlated with the plaque area, suggesting that YKL-40 was significantly related to the progression of early-stage carotid plaques. Moreover, the correlation of location between YKL-40 and macrophages in plaques suggested its biological function in connection with macrophages. The results of experiments *in vivo* and *in vitro* confirmed that YKL-40 could not only promote the progression of atherosclerotic plaque but also suppress the apoptosis of macrophages in plaques.

Studies focused on advanced atherosclerotic lesions indicated that the elevated apoptosis rate of macrophages could enlarge the necrotic core (NC) and induce the instability of atherosclerotic plaques (Gautier et al., 2009). Many researchers are convinced that the enlarged NC has more to do with the impaired efferocytosis in later-stage atherosclerosis than macrophage apoptosis in plaques (Tabas, 2005; Schrijvers et al., 2007). However, in this study, we confirmed that in the early-stage plaque, impaired macrophage apoptosis induced by YKL-40 could certainly aggravate the atherosclerotic lesion.

Areshkov et al. thought that YKL-40 is a strong inductor of MAPK and PI3K signaling pathways, what would mediate the phosphorylation of ERK1/2 (Areshkov et al., 2012). Lee et al. have found that YKL-40 could inhibit apoptosis by inhibiting Fas (CD95) expression, activating the PKB/AKT and apoptosis inhibitor Faim3 (TOSO) (Lee et al., 2009). Unfortunately, like the most of other studies, they didn't refer to the specific mechanism of YKL-40 regulating the apoptosis pathways. However, based on the results of the experiments on molecular mechanisms in this study, we might propose a novel apoptosis-regulated pathway of YKL-40 depending on caspases cascade and apoptosis inhibitor Aven. We analyzed the differentially expressed apoptosis-related protein molecules in BMDM through iTRAQ analysis. The results showed that the apoptosis promoters caspase-9, caspase-8, BAK, and DAP were significantly down-regulated in BMDM treated by YKL-40 while the apoptosis inhibitor Aven was significantly up-regulated. Results of the protein expression level of caspase-9, an important initial promoter of the caspase cascade, was detected in BMDM and mice tissues, consistent with the iTRAQ analysis. However, the mRNA expression level of *Casp9* detected in BMDM treated by YKL-40 was contrary to protein detection. We repeatedly confirmed these phenomena on RAW264.7 whose *Ykl40* has been up/down-regulated. The results suggested that YKL40 may not directly regulate the expression of caspase-9 but may inhibit the activation from procaspase-9 to caspase-9. Meanwhile, there was no significant difference in the mRNA expression level of *BAK* and *DAP*, while *Aven* was significantly up-regulated in BMDM treated by YKL-40.

Most apoptosis processes are facilitated by the activation of the caspase family (Thornberry and Lazebnik, 1998). Some caspases are cleaved and activated by other caspases or regulated by bridging or regulatory factors, such as Bcl-2, a prototype of the anti-apoptotic protein family, which could suppress caspase-mediated cell death (Adams and Cory, 1998; Srinivasula et al., 1998; Yang et al., 1998). Studies have identified Aven as a new apoptosis inhibitor that can bind both Bcl-X_L, a member of Bcl-2 family, and caspase regulator Apaf-1, suppressing apoptosis induced by Apaf-1 plus caspase-9 (Chau et al., 2000). In this study, we confirmed by silencing or over-expressing *Ykl40* in RAW264.7 that Aven was significantly

regulated by YKL40 in both protein and mRNA expression levels. Moreover, flow cytometry on RAW264.7 confirmed that the suppressive effect of YKL-40 on macrophage apoptosis was significantly impaired when *Aven* was down-regulated.

Based on the above results, we suggest that YKL-40 can up-regulate the expression of Aven which could suppress the activation of caspase-9 by interfering with APAF-1 binding to it, then inhibit the activation of the caspase cascade and finally inhibit the apoptosis of macrophages. Moreover, in our previous study, we have found YKL-40 also exert an inhibiting effect on macrophage efferocytosis, a key part of PrCR. Which suggest YKL-40 might play an important role in impairing the entire process of PrCR in atherosclerotic lesion. However, it is ambiguous that YKL-40 promotes atherosclerosis mainly on account of its inhibiting effect on apoptosis or efferocytosis, and the specific mechanism of YKL-40 up-regulating Aven expression remains elusive. Which are worthy of further research and discussion. In addition, administration process that we performed in this study might provide more solid evidence on the global effect of YKL-40 affecting the plaque progression than the local effect *in Vivo*. However, it is our conjecture based on existing positive results that the YKL-40 might impair the PrCR to impact plaque macrophages and then aggravate atherosclerosis. Locally intervening experiments would be arranged to further confirm the local effect of YKL-40 in the future study.

In conclusion, YKL-40 might suppress the apoptosis of macrophages by inhibiting the activation of apoptosis promoter caspase-9 via up-regulating the expression of the apoptosis inhibitor Aven. Inhibited apoptosis of macrophages results in impaired PrCR in plaque. The accumulation of macrophages that should have been apoptotic and removed by efferocytosis could enlarge the plaques and aggravate early-stage atherosclerosis (**Figure 8**).

DATA AVAILABILITY STATEMENT

The datasets presented in this study can be found in online repositories. The names of the repository/repositories and accession number(s) can be found below: ProteomeXchange, PXD028305.

ETHICS STATEMENT

The studies involving human participants were reviewed and approved by Independent Ethics Committee of the Changzheng Hospital affiliated with the Naval Medical University. The patients/participants provided their written informed consent to participate in this study. The animal study was reviewed and approved by Independent Ethics Committee of the Changzheng Hospital affiliated with the Naval Medical University.

AUTHOR CONTRIBUTIONS

HW perforemed most experiments and completed the original manuscript; LY and WC made the important cooperations in this study; ZS, BJ and LM participated in collecting information of patients, pre-processing samples and assisting complete the experiments; QL and CY provided the crucial guidances and made final decision in this study.

FUNDING

This study was funded by the National Natural Science Foundation of China (81,870,347), the Specifically Invited Professor of Oriental Scholar of Shanghai Colleges and Universities Tracking Program (GZ2016008), the Program of Excellent Academic Leader of Shanghai (20XD1404900), Advanced Achievement Cultivation Program of the Naval Military Medical University (2018-CGPZ-B05), and the Advanced Achievement Cultivation Program of Changzheng Hospital (2020YCGPZ-205).

ACKNOWLEDGMENTS

We would like to thank Clinical Research Institute of Integrative Medicine, Yueyang Hospital, Shanghai University of Traditional Chinese Medicine, and all of the researchers for providing technical support and cooperation throughout the study.

SUPPLEMENTARY MATERIAL

The Supplementary Material for this article can be found online at: https://www.frontiersin.org/articles/10.3389/fcell.2021.752773/full#supplementary-material

REFERENCES

Adams, J. M., and Cory, S. (1998). The Bcl-2 Protein Family: Arbiters of Cell Survival. *Science* 281 (5381), 1322–1326. doi:10.1126/science.281.5381.1322

Areshkov, P. O., Avdieiev, S. S., Balynska, O. V., Leroith, D., and Kavsan, V. M. (2012). Two Closely Related Human Members of Chitinase-like Family, CHI3L1 and CHI3L2, Activate ERK1/2 in 293 and U373 Cells but Have the Different Influence on Cell Proliferation. *Int. J. Biol. Sci.* 8 (1), 39–48. doi:10.7150/ijbs.8.39

Chau, B. N., Cheng, E. H.-Y., Kerr, D. A., and Hardwick, J. M. (2000). Aven, a Novel Inhibitor of Caspase Activation, Binds Bcl-xL and Apaf-1. *Mol. Cel* 6 (1), 31–40. doi:10.1016/s1097-2765(05)00021-3

Chen, C.-C., Llado, V., Eurich, K., Tran, H. T., and Mizoguchi, E. (2011). Carbohydrate-binding Motif in Chitinase 3-like 1 (CHI3L1/YKL-40) Specifically Activates Akt Signaling Pathway in Colonic Epithelial Cells. *Clin. Immunol.* 140 (3), 268–275. doi:10.1016/j.clim.2011.04.007

Gautier, E. L., Huby, T., Witztum, J. L., Ouzilleau, B., Miller, E. R., Saint-Charles, F., et al. (2009). Macrophage Apoptosis Exerts Divergent Effects on Atherogenesis as a Function of Lesion Stage. *Circulation* 119 (13), 1795–1804. doi:10.1161/CIRCULATIONAHA.108.806158

Hakala, B. E., White, C., and Recklies, A. D. (1993). Human Cartilage Gp-39, a Major Secretory Product of Articular Chondrocytes and Synovial Cells, Is a Mammalian Member of a Chitinase Protein Family. *J. Biol. Chem.* 268 (34), 25803–25810. doi:10.1016/s0021-9258(19)74461-5

Kim, A. S., and Johnston, S. C. (2011). Global Variation in the Relative burden of Stroke and Ischemic Heart Disease. *Circulation* 124 (3), 314–323. doi:10.1161/CIRCULATIONAHA.111.018820

Kjaergaard, A. D., Bojesen, S. E., Johansen, J. S., and Nordestgaard, B. G. (2010). Elevated Plasma YKL-40 Levels and Ischemic Stroke in the General Population. *Ann. Neurol.* 68 (5), 672–680. doi:10.1002/ana.22220

Kojima, Y., Volkmer, J.-P., McKenna, K., Civelek, M., Lusis, A. J., Miller, C. L., et al. (2016). CD47-blocking Antibodies Restore Phagocytosis and Prevent Atherosclerosis. *Nature* 536 (7614), 86–90. doi:10.1038/nature18935

Lee, C. G., Hartl, D., Lee, G. R., Koller, B., Matsuura, H., Da Silva, C. A., et al. (2009). Role of Breast Regression Protein 39 (BRP-39)/chitinase 3-like-1 in Th2 and IL-13-induced Tissue Responses and Apoptosis. *J. Exp. Med.* 206 (5), 1149–1166. doi:10.1084/jem.20081271

Liu, J., Thewke, D. P., Su, Y. R., Linton, M. F., Fazio, S., and Sinensky, M. S. (2005). Reduced Macrophage Apoptosis Is Associated with Accelerated Atherosclerosis in Low-Density Lipoprotein Receptor-Null Mice. *Atvb* 25 (1), 174–179. doi:10.1161/01.ATV.0000148548.47755.22

Mathers, C. D., and Loncar, D. (2006). Projections of Global Mortality and burden of Disease from 2002 to 2030. *Plos Med.* 3 (11), e442. doi:10.1371/journal.pmed.0030442

Michelsen, A. E., Rathcke, C. N., Skjelland, M., Holm, S., Ranheim, T., Krohg-Sørensen, K., et al. (2010). Increased YKL-40 Expression in Patients with Carotid Atherosclerosis. *Atherosclerosis* 211 (2), 589–595. doi:10.1016/j.atherosclerosis.2010.02.035

Mizoguchi, E. (2006). Chitinase 3-like-1 Exacerbates Intestinal Inflammation by Enhancing Bacterial Adhesion and Invasion in Colonic Epithelial Cells. *Gastroenterology* 130 (2), 398–411. doi:10.1053/j.gastro.2005.12.007

Rathcke, C. N., and Vestergaard, H. (2006). YKL-40, a New Inflammatory Marker with Relation to Insulin Resistance and with a Role in Endothelial Dysfunction and Atherosclerosis. *Inflamm. Res.* 55 (6), 221–227. doi:10.1007/s00011-006-0076-y

Sacco, R. L., Kargman, D. E., Gu, Q., and Zamanillo, M. C. (1995). Race-Ethnicity and Determinants of Intracranial Atherosclerotic Cerebral Infarction. *Stroke* 26 (1), 14–20. doi:10.1161/01.str.26.1.14

Schrijvers, D., Demeyer, G., Herman, A., and Martinet, W. (2007). Phagocytosis in Atherosclerosis: Molecular Mechanisms and Implications for Plaque Progression and Stability. *Cardiovasc. Res.* 73 (3), 470–480. doi:10.1016/j.cardiores.2006.09.005

Seimon, T., and Tabas, I. (2009). Mechanisms and Consequences of Macrophage Apoptosis in Atherosclerosis. *J. Lipid Res.* 50 (Suppl. l), S382–S387. doi:10.1194/jlr.R800032-JLR200

Sohn, M. H., Kang, M.-J., Matsuura, H., Bhandari, V., Chen, N.-Y., Lee, C. G., et al. (2010). The Chitinase-like Proteins Breast Regression Protein-39 and YKL-40 Regulate Hyperoxia-Induced Acute Lung Injury. *Am. J. Respir. Crit. Care Med.* 182 (7), 918–928. doi:10.1164/rccm.200912-1793OC

Srinivasula, S. M., Ahmad, M., Fernandes-Alnemri, T., and Alnemri, E. S. (1998). Autoactivation of Procaspase-9 by Apaf-1-Mediated Oligomerization. *Mol. Cel.* 1 (7), 949–957. doi:10.1016/s1097-2765(00)80095-7

Stary, H. C., Chandler, A. B., Glagov, S., Guyton, J. R., Insull, W., Jr., Rosenfeld, M. E., et al. (1994). A Definition of Initial, Fatty Streak, and Intermediate Lesions of Atherosclerosis. A Report from the Committee on Vascular Lesions of the Council on Arteriosclerosis, American Heart Association. *Circulation* 89 (5), 2462–2478. doi:10.1161/01.cir.89.5.2462

Tabas, I. (2005). Consequences and Therapeutic Implications of Macrophage Apoptosis in Atherosclerosis. *Atvb* 25 (11), 2255–2264. doi:10.1161/01.ATV.0000184783.04864.9f

Tabas, I., and Lichtman, A. H. (2017). Monocyte-Macrophages and T Cells in Atherosclerosis. *Immunity* 47 (4), 621–634. doi:10.1016/j.immuni.2017.09.008

Thornberry, N. A., and Lazebnik, Y. (1998). Caspases: Enemies within. *Science* 281 (5381), 1312–1316. doi:10.1126/science.281.5381.1312

Vandivier, R. W., Henson, P. M., and Douglas, I. S. (2006). Burying the Dead. *Chest* 129 (6), 1673–1682. doi:10.1378/chest.129.6.1673

Whitman, S. C. (2004). A Practical Approach to Using Mice in Atherosclerosis Research. *Clin. Biochem. Rev.* 25 (1), 81–93.

Wityk, R. J., Lehman, D., Klag, M., Coresh, J., Ahn, H., and Litt, B. (1996). Race and Sex Differences in the Distribution of Cerebral Atherosclerosis. *Stroke* 27 (11), 1974–1980. doi:10.1161/01.str.27.11.1974

Wu, Y., Tao, Z., Song, C., Jia, Q., Bai, J., Zhi, K., et al. (2013). Overexpression of YKL-40 Predicts Plaque Instability in Carotid Atherosclerosis with CagA-Positive *Helicobacter pylori* Infection. *PLoS One* 8 (4), e59996. doi:10.1371/journal.pone.0059996

Yang, X., Chang, H. Y., and Baltimore, D. (1998). Autoproteolytic Activation of Pro-caspases by Oligomerization. *Mol. Cel* 1 (2), 319–325. doi:10.1016/s1097-2765(00)80032-5

Conflict of Interest: The authors declare that the research was conducted in the absence of any commercial or financial relationships that could be construed as a potential conflict of interest.

Publisher's Note: All claims expressed in this article are solely those of the authors and do not necessarily represent those of their affiliated organizations, or those of the publisher, the editors and the reviewers. Any product that may be evaluated in this article, or claim that may be made by its manufacturer, is not guaranteed or endorsed by the publisher.

Copyright © 2021 Huan, Yandong, Chao, Sili, Jun, Mingfang, Yu and Lefeng. This is an open-access article distributed under the terms of the Creative Commons Attribution License (CC BY). The use, distribution or reproduction in other forums is permitted, provided the original author(s) and the copyright owner(s) are credited and that the original publication in this journal is cited, in accordance with accepted academic practice. No use, distribution or reproduction is permitted which does not comply with these terms.

frontiers in Cell and Developmental Biology

REVIEW
published: 16 December 2021
doi: 10.3389/fcell.2021.809457

Ferroptosis Signaling and Regulators in Atherosclerosis

Yuqin Wang[1], Yajie Zhao[1], Ting Ye[1], Liming Yang[2], Yanna Shen[3]* and Hong Li[1]**

[1]Department of Pathophysiology, School of Basic Medical Sciences, Harbin Medical University, Harbin, China, [2]Department of Pathophysiology, Harbin Medical University-Daqing, Daqing, China, [3]School of Medical Laboratory, Tianjin Medical University, Tianjin, China

Atherosclerosis (AS) is a major cause of cardiovascular diseases such as coronary heart disease, heart failure and stroke. Abnormal lipid metabolism, oxidative stress and inflammation are the main features of AS. Ferroptosis is an iron-driven programmed cell death characterized by lipid peroxidation, which have been proved to participate in the development and progression of AS by different signal pathways. NRF2-Keap1 pathway decreases ferroptosis associated with AS by maintaining cellular iron homeostasis, increasing the production glutathione, GPX4 and NADPH. The p53 plays different roles in ferroptosis at different stages of AS in a transcription-dependent and transcription-independent manner. The Hippo pathway is involved in progression of AS, which has been proved the activation of ferroptosis. Other transcription factors, such as ATF3, ATF4, STAT3, also involved in the occurrence of ferroptosis and AS. Certain proteins or enzymes also have a regulatory role in AS and ferroptosis. In this paper, we review the mechanism of ferroptosis and its important role in AS in an attempt to find a new relationship between ferroptosis and AS and provide new ideas for the future treatment of AS.

Keywords: ferroptosis, atherosclerosis, Nrf2, p53, Hippo

OPEN ACCESS

Edited by:
Rongxue Wu,
University of Chicago, United States

Reviewed by:
Zhi Xin Shan,
Guangdong Provincial People's Hospital, China
Xiaoyan Dai,
Guangzhou Medical University, China

Correspondence:
Liming Yang
limingyanghmu@163.com
Yanna Shen
shenyanna@sina.com
Hong Li
drlihong1971@163.com

Specialty section:
This article was submitted to Cell Death and Survival, a section of the journal Frontiers in Cell and Developmental Biology

Received: *05 November 2021*
Accepted: *25 November 2021*
Published: *16 December 2021*

Citation:
Wang Y, Zhao Y, Ye T, Yang L, Shen Y and Li H (2021) Ferroptosis Signaling and Regulators in Atherosclerosis. Front. Cell Dev. Biol. 9:809457. doi: 10.3389/fcell.2021.809457

1. INTRODUCTION

The main lesion of AS is lipid deposition in the arterial wall, accompanied by proliferation of smooth muscle cells and fibrous matrix, which gradually forms atherosclerotic plaques (Zhu et al., 2018). AS is the pathological basis of cardiovascular disease, while rupture of unstable atherosclerotic plaques, platelet aggregation and thrombosis can lead to narrowing or occlusion of blood vessels, resulting in acute cardiovascular disease (Li and Chen, 2005; Kanter et al., 2012; Zhu et al., 2018). Inflammation plays an important role in all stages of the atherosclerotic process, especially involved in the formation of unstable plaques (Zhu et al., 2018).

Ferroptosis is a regulated cell death dependent on reactive oxygen species (ROS) production and iron overload (Wang et al., 2020a). The basic mechanism of ferroptosis is the interaction of intracellular free iron with hydrogen peroxide via the Fenton reaction, leading to the depletion of plasma membrane polyunsaturated fatty acids (PUFAs) (Stockwell et al., 2017). Ferroptosis is regulated by a variety of cellular metabolic pathways, including redox homeostasis, iron handling, mitochondrial activity and the metabolism of amino acids, lipids and sugars. Metabolic processes that affect cellular susceptibility to ferroptosis include the sulfhydryl-dependent redox system and the mevalonate pathway, while the Cysteine/GSH/GPX4 axis, the NAD(P)H/FSP1/CoQ10 system, and the GCH1/BH4/DHFR system inhibit ferroptosis (Zheng and Conrad, 2020). The transcription factors (such as p53, Nrf2, ATF3, ATF4, YAP1, HIF1a, EPAS1/HIF2A, BACH1, TFEB, Jun, HIC1 and HNF4a) play multiple roles in the regulation of ferroptosis through transcription-dependent or

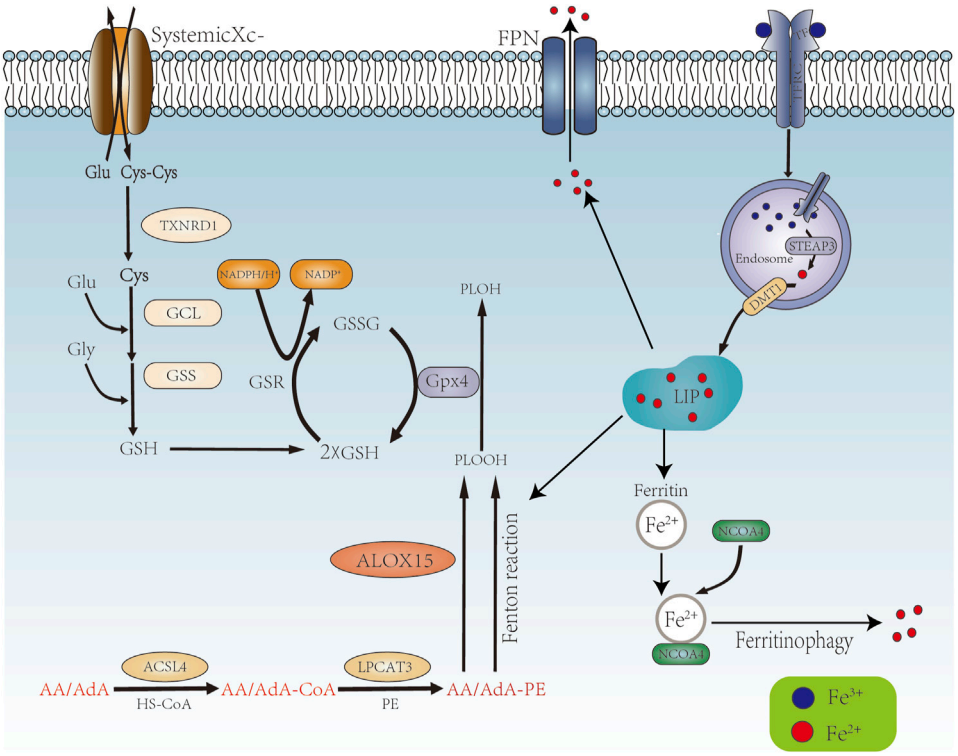

FIGURE 1 | Mechanism of ferroptosis occurrence. AA/AdA is activated by ACSL4 to become AA/AdA-CoA, then AA/AdA-CoA is esterified by LPCAT3 to AA/AdA-PE, AA/AdA-PE generates PLOOH through the Fenton reaction and the enzymatic reaction of ALOX15. Systemic Xc- promotes the synthesis of GSH, which together with GPX4 converts PLOOH to PLOH. Extracellular TF binds to Fe^{3+} and translocated into the cell via TFR1. The cell contains Fe3+, TF and TFR1 into the endosome by endocytosis. STEAP3 reduces Fe^{3+} to Fe^{2+}, which is transported to the cytoplasm via DMT1 to form LIP. Fe^{2+} in LIP promote ferroptosis by Fenton reaction. Ferritin reduces Fe^{2+} is decreased by storing of Ferritin and the excrete via FPN. Ferritin also binds to NCOA4 to release Fe^{2+} via ferritinphagy.

non-transcriptional mechanisms (Dai et al., 2020). In this review, we summarize the signaling pathways of ferroptosis associated with AS in order to provide new ideas for the prevention and treatment of AS.

2. FERROPTOSIS

2.1 Lipid Peroxidation and Ferroptosis

Lipid peroxidation, a process of oxidative degradation of lipids, plays a key role in driving ferroptosis. The phospholipid acyl chain remodeling pathway (Lands' cycle) is critical for achieving ferroptosis. Upon entry of extracellular free diffusible AA/AdA into the cell, acyl-CoA synthetase long chain family member 4 (ACSL4) can activate AA/Ada to generate AA/AdA- CoA, which can then be esterified to AA/AdA-PE by LPCAT3 (lysophosphatidylcholine acyltransferase 3) (Latunde-Dada, 2017). AA/AdA-PEs are the main target molecules for lipid peroxidation and are localized to the cytoplasmic face of the membrane during ferroptosis (Doll and Conrad, 2017). AA/AdA-PE undergoes iron-dependent lipid autoxidation/peroxidation via the Fenton reaction or enzymatic catalysis (e.g., Alox15) to produce phospholipid hydroperoxides (PLOOH) (Doll and Conrad, 2017), which ultimately leads to the formation of a large number of byproducts, including lipid peroxides (such as 4-hydroxynonenal and malondialdehyde) and breakdown products of oxidized and modified proteins, giving rise to the disruption of membrane integrity and ferroptosis (Jiang et al., 2021). As an amino acid reverse transporter protein distributed in the phospholipid bilayer consisting of two subunits, SLC7A11 and SLC3A2, system Xc^{-} exchanges cysteine and glutamate intracellularly and extracellularly in a 1:1 ratio. Cysteine is involved in the synthesis of GSH and the function of GPX4 (glutathione peroxidase 4) (Li et al., 2020) (**Figure 1**).

There are currently two explains about phenotypic features of ferroptosis observed *in vitro* experiments. One possibility is that the accumulation of PLOOH and breakdown products in the membrane during lipid peroxidation alters the properties of the membrane, leading to the formation of hydrophilic pores and altered permeability of water and other solutes through the cell membrane. Another possibility is that the formation of lipophilic and electrophilic substances during lipid peroxidation act as specific signaling molecules that mediate membrane

permeability by modifying downstream molecules (e.g., membrane proteins) (Doll and Conrad, 2017).

2.2 Iron Homeostasis and Ferroptosis

The regulation of iron homeostasis is particularly important for maintaining overall redox balance. On the one hand, iron is an essential element for physiological processes such as oxygen transport or energy production. On the other hand, overloaded iron acts as a catalyst for redox reactions, which can lead to oxidative stress-induced cytotoxicity (Galaris and Pantopoulos, 2008; Klóska et al., 2019). The bioavailability of intracellular iron is regulated by its import, storage and export (Klóska et al., 2019). Iron is present in two forms, Fe^{3+} and Fe^{2+}. Fe^{2+} can generate ROS via the Fenton reaction, leading to the accumulation of lipid peroxides, which is an important factor in the onset of ferroptosis. Extracellular Fe^{3+} can be bound to transferrin (TF) and transported into the cell via Trans-ferrin Receptor 1 (TFR1) on the cell membrane.

Fe^{3+}, TF and TFR1 are incorporated into endosomes by endocytosis, while the binding of TF and TFR1 and the binding of iron and TF are solubilized in an acidic environment. Fe^{3+} is reduced to Fe^{2+} in the endosome by STEAP3 (iron reductase), which then mediates the release of Fe^{2+} from the endosome into the cytoplasm via Divalent metal transporter 1 (DMT1/SLC11A2) to form LIP. Cytoplasmic Fe^{2+} can be reduced by ferritin and stored as Fe^{3+}, and Fe^{2+} can be transported out of the cell by ferroportin (FPN1/SLC40A1) (Anandhan et al., 2020). Ferritin is an important negative regulator of ferroptosis, consisting of the ferritin heavy chain (FTH1) and the ferritin light chain (FTL). FTH1 has ferrous oxidase activity and oxidizes Fe^{2+} to Fe^{3+}, which is then stored in ferritin (Finazzi and Arosio, 2014) (**Figure 1**).

Ferritinophagy, the autophagic degradation process of the iron storage protein ferritin, is essential for the regulation of cellular iron levels, and requires the co-regulation of NCOA4 (nuclear receptor coactivator 4) and autophagy. Knockout of NCOA4 inhibited erastin induced ferroptosis, while overexpression significantly enhanced intracellular iron levels promoting ferroptosis (Hou et al., 2016). NCOA4 binds to FTH1, autophagic vesicles and autolysosomes, which induce the releases of free iron (Mancias et al., 2014). Depletion or inhibition of NCOA4 or ATG proteins (e.g., ATG3, ATG5, ATG7 and ATG13) inhibits ferritin degradation, thereby reducing free iron levels and limiting ferroptosis (Hou et al., 2016; Gao et al., 2016; Liu et al., 2020) (**Figure 1**). Lipid peroxides can be produced by three pathways: iron-catalyzed lipid autoxidation, esterification and oxidation of polyunsaturated fatty acids (PUFAs), and the production of lipid ROS associated with the Fenton reaction, all of which require iron (Ying and Padanilam, 2016; Lei et al., 2019; Su et al., 2019; Li et al., 2020).

3. ATHEROSCLEROSIS

AS is characteristic by disorders of lipid metabolism, smooth muscle proliferation, endothelial dysfunction, apoptosis, necrosis, inflammation and the formation of foamy cells and lipid plaques (Wu et al., 2017). AS-associated inflammation is mediated by pro-inflammatory cytokines, inflammatory signaling pathways, bioactive lipids and adhesion molecules (Zhu et al., 2018). The main cells involved in AS are endothelial cells, smooth muscle cells and macrophages, etc. The damage and dysfunction of Endothelial cells is the initiating links in AS, and cholesterol-rich low-density lipoprotein (LDL)is deposited in the inner membrane of the vascular wall of endothelial cells, where it is oxidized to oxidized LDL during increased oxidative stress, which can be recognized by macrophages and other immune cells and destroy endothelial cells (Rafieian-Kopaei et al., 2014; Jinnouchi et al., 2020). The damaged endothelium is activated and expresses cytokines, chemokines and adhesion molecules that attract circulating monocytes to the atherosclerotic lesions and adhere to the vessel wal (Marchio et al., 2019). The main immune cells in atherosclerotic lesions are macrophages, which are divided into the pro-inflammatory macrophage phenotype M1 and the anti-inflammatory macrophage phenotype M2 (Tabas and Bornfeldt, 2016). Scavenger receptors (SR) on the macrophage take part in the lipids dynamic balance dependent on a number of enzymes, such as cholesterol acyltransferase-1 (ACAT1) and the cholesterol efflux transporters ABCA1 and ABCG1 (Linton et al., 2016). Reduced phagocytosis of lipids lead to the conversion of macrophages into foam cells, which induce the formation of plaques. Macrophage-derived foam cell-dominated atherosclerotic plaques are less stable and more likely to rupture.

4.SIGNALING PATHWAYS OF FERROPTOSIS ASSOCIATED WITH ATHEROSCLEROSIS

4.1 NRF2-Keap1 Pathway

Activated NRF2 improves the oxidative stress state of the body and promotes cell survival. Under non-stress conditions, NRF2 is ubiquitinated by the Keap1-CUL3 ubiquitin E3 ligase complex to mark it for degradation by the proteasome. However, redox interference leads to its functional inactivation by modifies of Keap1 when exposed to electrophilic substances or reactive oxygen species. Keap1-CUL3 ubiquitin E3 ligase activity is reduced, which promote the stabilization of NRF2. Stabilized and accumulated NRF2 translocate to the nucleus, forms a heterodimer with a small muscle tendon fibrosarcoma (Smaf), then initiates transcription of genes containing antioxidant response elements (ARE) and activates a range of cytoprotective genes. NRF2 has been shown to regulate the activity of ferroptosis and lipid peroxidation related proteins by three main pathways, iron/metal metabolism, intermediate metabolism and GSH synthesis/metabolism (Dodson et al., 2019) (**Figure 2**).

4.1.1 NRF2 Maintains Iron Homeostasis

Iron can also be released during heme degradation by HO-1 (heme oxygenase), a stress-inducible enzyme encoded by the Hmox1 gene. HO-1 metabolite performs an essential physiological function in the vascular system (Loboda et al.,

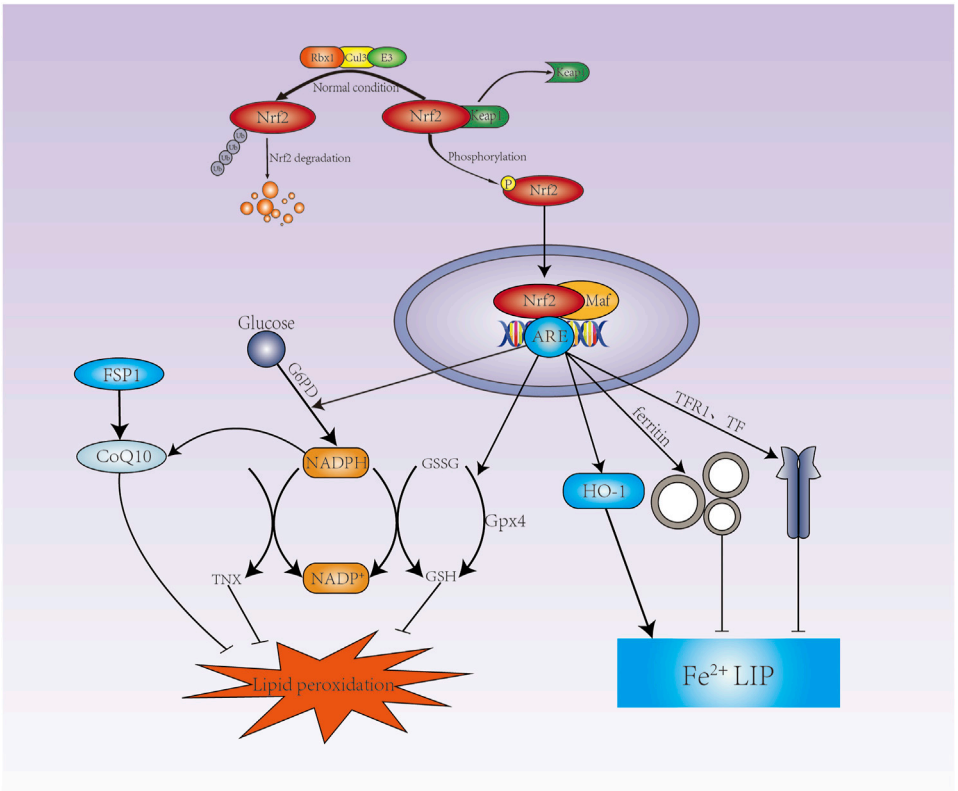

FIGURE 2 | NRF2 is involved in the regulation of ferroptosis. Under normal conditions, NRF2 is degraded by the Keap1-CUL3-RBX1 E3 ubiquitin ligase complex-targeted proteasome. Under oxidative stress conditions, NRF2 is no longer degraded, thus allowing nuclear translocation and binding to the ARE. NRF2 promotes G6PD expression to increases NADPH via the pentose phosphate pathway, GSH and TXN production is dependent on NADPH, which promotes CoQ10 production. NRF2 promotes the expression of SLC7A11, GCLC, GCLM, GSS to increase GSH synthesis, and NRF2 also promotes the expression of GPX4. GPX4 converts GSH to GSSG to reduce lipid hydrogen peroxide. NRF2 can promote the expression of ferritin and FPN to store Fe^{2+} and excrete Fe^{2+} respectively, and reduce Fe^{2+} in LIP; Nrf2 also promote the expression of HO-1.

2008). As a Metabolic product, biliverdin is rapidly reduced to bilirubin by biliverdin reductase, which is expressed in two forms: BVRa (predominant in adults and encoded by BLVRA) and BVRb (encoded by BLVRb and predominant in fetal life) (Baranano et al., 2002). Knockdown of BVR induced an increase in NRF2 transcription factor activity and HO-1 levels, accompanied by decrease of cellular heme content and increase of iron content (Klóska et al., 2019). The binding of NRF2 to the ABCB6 promoter region was first identified in airway epithelial cells of smokers with tissue specificity in the regulation of ABCB6 by NRF2 (Hübner et al., 2009; Campbell et al., 2013; Kerins and Ooi, 2018). Iron is transported from the cytoplasm to the mitochondria via mitoferrin 1 (MFRN1), where iron-containing porphyrins are synthesized to decrease iron ions. Up-regulation of ABCB6 promotes iron depletion by exporting iron-containing porphyrins, thereby inhibiting ferroptosis (Zhang et al., 2020). The lack of ABCB6 in bone marrow cells leads to increased oxidative stress and subsequent release of platelets. Subsequent thrombocytosis increases arterial deposition of the powerful myeloid cell-attracting chemokine CCL5 (RANTES), which ultimately promotes the development of atherosclerotic lesions (Murphy et al., 2014). In addition to ABCB6, ferrous iron chelatase (FECH) is located in the mitochondria and involved in the biosynthesis of hemoglobin. FECH inserts ferrous iron into protoporphyrin IX to produce hemoglobin cofactor (Khan and Quigley, 2011). NRF2 regulates heme synthesis via ABCB6, which is responsible for transporting porphyrins from the cytosol to the mitochondrial membrane gap (Kerins and Ooi, 2018).

NRF2 regulates intracellular iron homeostasis by regulating the expression of Tfr1, FTH1, FTL and FPN. It was found that p62 interacting with Keap1, promotes the translocation of NRF2 into the nucleus, up-regulate the expression of FTH, FPN and HO-1, which protects cells from ferroptosis (Zhao et al., 2021). TfR1 was found to be highly expressed in macrophage-derived foam cells and smooth muscle cells in human carotid plaque (Li et al., 2008). The expression of TfR1 was positively correlated with macrophage infiltration, ectopic lysosomal histone lyase L and ferritin expression (Li et al., 2008). Ox-LDL and pro-inflammatory cytokines promote macrophage iron retention and lipid accumulation, mainly due to NRF2-mediated increased expression of Hmox1 and FPN, a specific cellular

phenotype that may be associated with the development of atherosclerotic lesions and plaques instability (Marques et al., 2016).

4.1.2 NRF2 Increases the Expression of GSH and GPX4

NRF2 can regulate intracellular redox homeostasis through genes encoding GSH synthesis proteins, including SLC7A11, TXNRD1, GCLC, GCLM, and GSS (Song and Long, 2020). SLC7A11 is an essential subunit of system Xc- that regulates the reverse transport of glutamate and cystine. In contrast, NRF2 promotes the expression of SLC7A11 (Carpi-Santos and Calaza, 2018). Overexpression of NRF2 or knockdown of Keap1 increases SLC7A11 expression, whereas inhibition of expression of NRF2 or over-expression of Keap1 over-expression decreases SLC7A11 levels (Fan et al., 2017; Shin et al., 2017). It was found that inhibition of system Xc- induced GSH depletion increased the expression of TXNRD1, but not TXNRD2, compensated for the lack of GSH (Mandal et al., 2010). The synthesis of GSH is divided into two steps. The first step is catalyzed by GCL (glutamate-cysteine ligase), which consists of GCLC (GCL-catalytic subunit) and GCLM (GCL-modifier subunit), and cysteine combine with glutamate to produce γ-glutamylcysteine. The second step is catalyzed by GSS (Glutathione synthetase), which adds glycine to γ-glutamylcysteine to form γ-glutamylcysteine or GSH (Kalinina and Gavriliuk, 2020). GPX4 converts GSH to GSSG (oxidized glutathione) to reduce lipid hydrogen peroxide (Gaschler et al., 2018) (**Figure 2**).

Depletion of the antioxidant GSH or ox-LDL lead to the accumulation of intracellular lipid peroxide (Dixon et al., 2012; Kattoor et al., 2017; Ouyang et al., 2021). Over-expression of GPX4 in ApoE$^{-/-}$ mice attenuates the upregulation of endothelial cell adhesion molecule and monocyte-endothelial cell adhesion, thereby inhibiting the development of AS (Guo et al., 2008). Butyric acid treatment of VSMC not only up-regulates the expression of GPX4 but also enhances the catalytic activity of GPX4, which in turn inhibits VSMC proliferation and enhances arterial protective effect (Mathew et al., 2014). GPX4 also down-regulates lipoxygenase (LOX) and cyclooxygenase (COX) thereby reducing the level of pro-inflammatory factors (Chen et al., 2002). GPX4 reduces the release of pro-inflammatory mediators and inflammatory response associated with AS, which has been proved a chronic vascular inflammatory disease.

4.1.3 NRF2 Increases the Production of NADPH

The production of GSH (GSH) and thioredoxin (TRX) eliminates peroxides and thus inhibits ferroptosis (Chen et al., 2002), while NADPH deficiency will lead to a decrease of GSH and TRX, promoting the accumulation of lipid ROS (Yang et al., 2020a). The mammalian TRX system is an important reductase system (Arnér, 2020). AS a system that scavenges harmful lipid peroxides, FSP1 was found to be primarily localized in lipid droplets and plasma membranes.

Further studies have shown that FSP1 reduces coenzyme Q10 via NADPH to inhibit ferroptosis (Zhu et al., 2020). The NADPH/FSP1/CoQ10 system is therefore a negative regulator of ferroptosis. Glucose produces NADPH via the pentose phosphate pathway (PPP), which positively regulates ferroptosis via key enzyme G6PD (Zheng and Conrad, 2020). NRF2 can regulate the expression of G6PD (Dodson et al., 2019) (**Figure 2**).

The TRX system has been shown to play an important role in the regulation of metabolic processes, insulin signaling, regulation of blood pressure and inflammation (Poznyak et al., 2020a). It has been shown that Trx2 protects intravascular homeostasis by balancing mitochondrial ROS production in endothelial cells (Kirsch et al., 2016). Down-regulation of Trx1 inhibits the expression of VCAM-1 and ICAM-1 and blocks the initiation of AS (Chen et al., 2013). TRX also modulates macrophage inflammation and polarization (Tinkov et al., 2018). Hypercholesterolemia causes the accumulation of lipid peroxides in the aorta of ApoE$^{-/-}$ mice, and the antioxidant effect of coenzyme Q10 inhibits the development of AS (Witting et al., 2000; Bentzon et al., 2014). In addition to the pentose phosphate pathway (PPP), NADPH production also occur through NADH phosphorylation catalyzed by NAD kinase (NADK) and the NADP-dependent conversion of isocitrate to α-KG by isocitrate dehydrogenase (IDH) (Zheng and Conrad, 2020). NRF2 increases NADPH via G6PD, and NADPH acts as an antioxidant to cells by regulating GSH, TXN and CoQ10, which inhibits the development of AS.

4.2 p53

4.2.1 p53 Promotes the Development of Ferroptosis in AS

p53 can inhibit the synthesis of GSH by SLC7All in a transcription-dependent manner (Jiang et al., 2015). p53 increases the expression of GLS2 (glutaminase2) to catalyzes the hydrolysis of glutamine, which increases cellular susceptibility to ferroptosis by downregulating cellular antioxidant through massive hydrolysis of GSH and increasing ROS levels (Gao et al., 2015). PTGS2 is a key enzyme in the initiation step of prostaglandin synthesis and regulates the sensitivity of cells to ferroptosis by regulating the levels of key intracellular membrane phospholipids PE. When ferroptosis inducers such as GLS2 and erastin were applied to p53 wild-type cells, the cells exhibited upregulated PTGS2 gene expression and ferroptosis, but when p53-deficient cells were induced with GLS2 and erastin, PTGS2 gene expression levels were unchanged and ferroptosis did not occur. PTGS2 has been used as a marker of ferroptosis (Yang et al., 2014).

Deletion of SAT1, target gene of p53, decreases cell death induced by ROS. SATl increases the expression of ALOX15 (arachidonate-15-lipoxygenase), an iron-dependent PUFA oxidase that increases lipid peroxidation and thus promotes ferroptosis (Ou et al., 2016). p53 also promotes cellular ferroptosis by activating ALOX12 (arachidonate-12-lipoxygenase) (Chu et al., 2019). 12/15-LOX promotes increased trans-endothelial transport of ox-LDL and deposition of ox-LDL in the sub-endothelial space (Li et al., 2018). ALOX12 exhibits higher methylation levels in atherosclerotic plaques, particularly in endothelial cells,

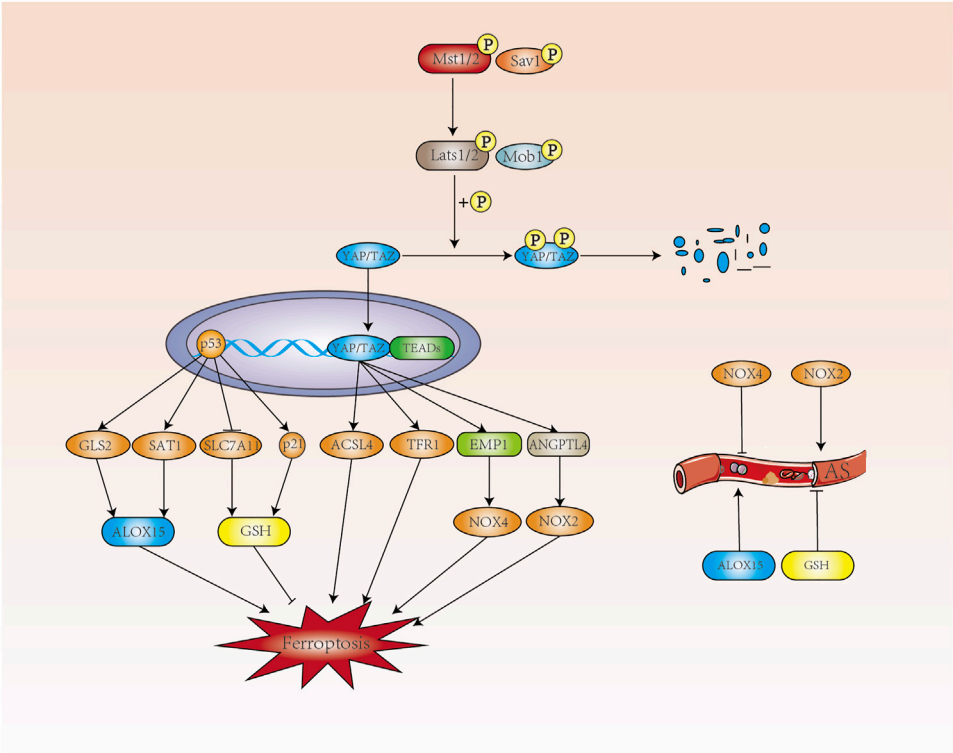

FIGURE 3 | The p53 and Hippo pathways regulate ferroptosis. p53 promotes the expression of ALOX15 in a transcription-dependent manner to promote ferroptosis, and ALOX15 can contribute to the development of AS. p53 regulates ferroptosis by inhibiting GSH through SLC7A11 and promoting GSH production through p21. In contrast, GSH can inhibit the development of AS. When the Hippo signaling pathway is opened, MST1/2 phosphorylates MOB1 and LATS1/2 and increases the interaction between them. Phosphorylated YAP/TAZ by LATS1/2 is degraded in the cytoplasm with the assistance of SAV1. When the Hippo signaling pathway is closed, the level of YAP phosphorylation decreases and translocates into the nucleus where it binds to the transcription factor TEAD to produce ACSL4, which promotes intracellular lipid peroxidation. TFR1, which increases intracellular Fe^{2+} concentration, and NOX4 and NOX2, induce intracellular ROS production and development of ferroptosis.

which is essential for p53-mediated ferroptosis following stress (Ouyang et al., 2021). The p53 gene also promotes ferroptosis through histone modification with non-dependent of p53 (Dai et al., 2020). p53 can form a nuclear p53-USP7 protein complex with de-ubiquitin specific peptidase 7 (USP7), further reduces the level of histone H2B monoubiquitylation (H2Bub1, a histone modification) mediated expression of SLC7A11, ultimately leading to ferroptosis (Wang et al., 2019a).

MDM2 and MDMX were found to be negative regulators of p53 by regulating FSP1 expression (Venkatesh et al., 2020) and suggests altering the lipid distribution of cells to promote the development of ferroptosis (Venkatesh et al., 2020). In addition, excess iron activates ROS production and induces lipid peroxidation in macrophage-derived foam cells, leading to instability of atherosclerotic plaques. Disturbed iron metabolism in macrophages is involved in the inflammatory response that exacerbates the severity of AS, and iron overload also closely related to the induction of macrophage polarization towards the inflammatory phenotype M1 via the ROS/acetyl-p53 pathway (Zhou et al., 2018; Handa et al., 2019; Ouyang et al., 2021).

4.2.2 p53 Inhibits the Onset of Ferroptosis in AS

p53 can also regulate cell cycle regulation to induce ferroptosis. p21 can inhibit ferroptosis by increasing intracellular GSH leading to increased synthesis of GPX4, while p53 directly regulates the activation of p21, although the exact mechanism is unclear (Tarangelo and Dixon, 2018; Tarangelo et al., 2018). Senescence and ROS production in human aortic endothelial cells are accompanied by significant increase in p53 and p21 (Iwabayashi et al., 2012). In addition, p21 also promote VSMC senescence (Moon et al., 2004; Kim and Moon, 2005; Wang et al., 2015). p53 inhibits ferroptosis by blocking dipeptidyl peptidase 4 (DPP4), a multifunctional serine protease involved in glucose control and a regulator of ferroptosis and lipid metabolism. DPP4 binds to nicotinamide adenine dinucleotide oxidase 1 (NOXl), leading to the production of ROS in cell membranes and plasma, resulting in a large accumulation of intracellular lipid peroxides and ferroptosis (Xie et al., 2017).

4.3 Hippo Pathway

The Hippo pathway consists of a series of protein kinase and transcription factors that is highly conserved from lower to higher animal. When the Hippo signaling pathway is shut down, the level of YAP phosphorylation is reduced and translocated into the nucleus, where it binds to the transcription factor TEAD, triggering the expression of a range of genes associated with cell proliferation. When the Hippo signaling pathway is turned on, MST1/2 phosphorylates and increases the interaction between MOB1 and LATS1/2 with the assistance of the co-factor SAV1 (Johnson and Halder, 2014). Hippo pathway plays an important role in cell growth, proliferation, metabolism and immunity, which has been a hot topic of research in the cardiovascular field (**Figure 3**).

The levels of AA (arachidonic acid) and AdA (adrenic acid) are closely related to the occurrence of ferroptosis. AA coenzyme A (AA-CoA) is produced by AA/AdA catalyzed by ACSL4 (acyl-coA synthetase long-chain family member 4) and eicosatetraenoic acid coenzyme A (AdA-CoA), both of which are key substrates for the onset of ferroptosis. Ferroptosis related with cell density in epithelial cells was mediated by E-calmodulin-mediated cell-cell contact, which activates Hippo signaling via the NF2 (also known as Merlin) tumor suppressor protein, thereby inhibiting the activity of the nuclear translocation and transcriptional co-regulator YAP, which can target including ACSL4 and TFR1 to promote ferroptosis (Wu et al., 2019a).

NADPH oxidase dysfunction plays an important role in the pathology of development of AS, including endothelial dysfunction, inflammation and vascular remodelling (Johnson and Halder, 2014). NADPH oxidase including NOX1, NOX2, NOX3 and NOX4, are the main sources of ROS during atherosclerotic formation (Poznyak et al., 2020b). In renal cell carcinoma, at low cell density, activated TAZ promotes the expression of epithelial membrane protein 1 (EMP1), followed by upregulation of NOX4 levels. NOX4 increases the level of intracellular lipid reactive oxygen species and induces ferroptosis (Yang et al., 2019). As a subtype of NADPH oxidase, NOX4 was shown to be AS-protective. Hydrogen peroxide released by NOX4 also inhibits the proliferation rate of vascular smooth muscle cells, prevents vascular remodeling and inflammation, and maintains the expression of eNOS under vascular stress (Schröder et al., 2012; Di Marco et al., 2016; Poznyak et al., 2020b).

In studying the role of TAZ in ferroptosis in ovarian cancer, angiopoietin like 4 was found to be a direct target gene regulated by TAZ, sensitizing ferroptosis through activation of NOX2 (Yang et al., 2020b). More importantly, ANGPTL4 maintains the integrity of the vascular endothelium by regulating vascular permeability, angiogenesis, inflammatory signaling, oxidative stress and lipid metabolism (Guo et al., 2014; Tsai et al., 2020). In addition, ANGPTL4 also regulates cellular energy homeostasis and reactive oxygen species and has been implicated in the pathogenesis of AS, including endothelial dysfunction, LDL oxidation and nitric oxide reduction (Zhu et al., 2012; Tsai et al., 2020). Hepatic ANGPTL4 deficiency significantly reduces triacylglycerol (TAG) and cholesterol levels, providing some protection against AS (Singh et al., 2021). When the Hippo pathway is closed, nuclear translocation of YAP induces endothelial cell proliferation and inflammation. YAP regulates the expression of ferroptosis-related target genes, including TFR1, ACSL4, EMP1 and ANGPTL4. Ferroptosis is promoted in terms of iron homeostasis, lipid metabolism and redox regulation, but whether ferroptosis is involved between Hippo and AS remains to be investigated.

5. OTHER TRANSCRIPTION FACTORS

5.1 ATF3 and ATF4

ATF3 was found to directly inhibit the expression of SLC7A11 in erastin-induced HT1080 cells, suggesting that ATF3 is a positive regulator of ferroptosis (Wang et al., 2020b). Endoplasmic reticulum stress promotes the upregulation of ATF3, which increases intracellular H_2O_2 levels through two pathways: ATF3 activates NOX4 transcription, overproduces of superoxide, inhibits SLC7A11 transcription, and deplets cysteine and GSH. H_2O_2 increases intracellular Fe^{2+} and restricts synthesis of GSH, leading to a continuous accumulation of toxic intracellular lipid peroxides (Lu et al., 2021).

Unlike ATF3, ATF4 plays a dual role in ferroptosis. Deletion of ATF4 increases ferroptosis in a variety of cancer cells (Chen et al., 2017; Zhu et al., 2017; Wang et al., 2019b). Inhibition of ATF4-HSPA5-GPX4 pathway-induced ferroptosis increases the anticancer activity of gemcitabine, which is related that ATF4 induces the binding of HSPA5 to GPX4, protecting against GPX4 protein degradation and subsequent lipid peroxidation (Zhu et al., 2017). Also, knockdown of SLC1A5 or CHAC1 or DDIT3 inhibited erastin or RSL3 induced ferroptosis (Dai et al., 2020). As the first cytoplasmic NADPH phosphatase, MESH1 leads to NADPH dephosphorylation, and the knockdown of MESH1 has been shown to increase NADPH and protect against ferroptosis (Ding et al., 2020). The knockdown of MESH1 induces different endoplasmic reticulum stress-related genes, particularly ATF3 gene. The knockdown of ATF4 sensitizes MESH1-deficient RCC4 cells to ferroptosis, suggesting a role in MESH1 knockdown-mediated protection against ferroptosis. The phenotypic similarity of stress tolerance caused by the removal of MESH1 and the accumulation of NADPH is achieved in part through the regulation of ferroptosis by ISR (Lin et al., 2021a).

In general, both ATF3 and ATF4 can regulate ferroptosis. ATF3 promotes ferroptosis by depleting intracellular GSH through inhibition of the system Xc-. Knockdown of ATF4 promotes ferroptosis, and protects against degradation of GPX4 through the ATF4-HSPA5-GPX4 pathway. In addition, endoplasmic reticulum stress promotes intracellular H_2O_2 levels by upregulating ATF3 and enhances intracellular Fe^{2+} by upregulating the expression of the transferritin receptor, leading to the accumulation of toxic lipid peroxides in cells. whether the high expression of ATF3 in AS is associated with ferroptosis needs to be further explored (Ouyang et al., 2021).

5.2 STAT3

Inhibition of STAT3 phosphorylation in endothelial cells down-regulates vascular endothelial growth factor (VEGF) expression, inhibits vascular endothelial cell proliferation and migration, and delays the formation of unstable plaques in AS (Dal Monte et al., 2011). STAT3 induces the proliferation and migration of vascular smooth muscle cells (Wang et al., 2016). STAT3 is involved in regulation of monocyte-to-macrophage differentiation, and inhibition of STAT3 activity decreases inflammation and monocyte-to-macrophage differentiation (Chen et al., 2019).

Protective effect of α6β4 integrin on erastin induced adherent epithelial cells and cancer cells is that α6β4-mediated activation of Src and STAT3 inhibits the expression of ACSL4 and suppresses lipid peroxidation (Brown et al., 2017). An earlier study showed that the onset of ferroptosis is not dependent on lysosomes, however, lysosomes play a potential role in promoting ferroptosis (Zhou et al., 2020). It has been shown that the transcriptional activity of NRF2 and STAT3 may jointly regulate ferroptosis-related gene expression, mainly because increased NRF2 can promote STAT3 phosphorylation, which amplifies downstream signaling and regulates SLC7A11 to inhibit ferroptosis (Liu and Wang, 2019; Qiang et al., 2020). The NF-κB/IL-6/STAT3 signaling pathway increases hepcidin expression and decreases serum iron and transferrin saturation (Yang et al., 2020a). Iron in macrophages is regulated by the hormone hepcidin, which reduces FPN-mediated iron export when iron is in sufficient supply. The expression of Hepcidin is associated with BMP signaling and its inhibition *in vivo* model has protective effect on AS, probably due to the fact that iron affects macrophage polarization and lipid metabolism levels (Wunderer et al., 2020).

Aberrant activation of STAT3 leads to endothelial cell dysfunction, macrophage polarization, inflammation and immunity, and thus may be an important regulator of the AS process (Chen et al., 2019). STAT3 regulates GSH synthesis by regulating SLC7A11 in ferroptosis and also inhibits ACSL4 expression, both of which can suppress the onset of ferroptosis. STAT3 also regulates intracellular iron homeostasis. How STAT3 regulates ferroptosis in AS needs to be further investigated.

6. OTHER REGULATORY MOLECULES

6.1 SCD1 and FADS2

LSH (lymphoid-specific helicase) is a DNA methylation modifier that inhibits the progression of ferroptosis by directly upregulating lipid metabolism genes, including SCD1 (searoyl CoA desaturase) and FADS2 (fatty acid desaturase 2) (Jiang et al., 2017). SCD1 was found to have a rate-limiting effect in catalyzing monounsaturated fatty acid synthesis, which promotes tumor growth, migration and resistance to ferroptosis (Wang et al., 2016). SCD1 converts saturated fatty acids into monounsaturated fatty acids (MUFAs) to inhibit ferroptosis (Magtanong et al., 2019; Wang et al., 2020c). Highly active mutations in PI3K-AKT-mTOR signaling protect cancer cells from oxidative stress and ferroptosis through SREBP1/SCD1-mediated adipogenesis (Gao et al., 2021). Inhibition of SCD1 through activation of AMPK/SREBP1 to promote ferroptosis (Yi et al., 2020). Research has shown that lead decreases SCD and FADS2 expression, leads to a significant increase in MDA and ROS content in macrophages and may lead to foam cell formation and inflammation (Zhao et al., 2020). *In vitro* and *in vivo* results show that laminar flow protects endothelial cells by increasing endothelial cell SCD1 mRNA expression through a PPARγ-specific mechanism (Sun et al., 2015). Up-regulation of SCD-1 leads to desaturation of saturated fatty acids, promotes esterification and storage of saturated fatty acids, which protects HAECs from lipotoxic damage (Qin et al., 2007). The absence of SCD1 attenuates adipocyte inflammation and its paracrine regulation in macrophages and endothelial cells. Reduced oleic acid levels are associated with inflammatory regulation of SCD1 deficiency (Peter et al., 2008). Hypoxia-inducible factor (HIF) plays a crucial role in regulating the hypoxic response of tumor by altering cellular energy metabolism, including altering the expression of genes related to glucose and lipid metabolism. SCD1 and HIF-2a in human renal tubular epithelial cell lines promote tumorigenesis by maintaining cell survival, triggering cell migration and enhancing proliferation of cancer cells (Liu et al., 2010; Liu et al., 2010). The over-expression of SCD1 promotes lipid droplet (LD)-lysosome fusion through activation of TFEB nuclear translocation and its activity, which promotes lysosome biosynthesis and inhibits the formation of VSMC foam cell. Regulation of SCD1/TFEB mediated lipophagy may provide new therapeutic avenues for the treatment of AS (Stoyanoff et al., 2016).

LSH induces ELAVL1 (ELAV-like) through inactivation the expression of p53 RNA-binding protein. ELAVL1 enhances the expression level of LINC00336 by interacting with LINC00336 (Long noncoding RNA), increases the expression of CBS (cystathionine-β-synthase) and inhibits ferroptosis in lung cancer (Pi et al., 2019). DCAF8 and WDR76 were recently reported to act as substrate connectors and molecular inhibitors of the CRL4 (Cullin-4 RING ubiquitin ligase) system for the control of LSH stability. WDR76 competitively inhibits DCAF8-targeted LSH protein hydrolysis for lipid hydroperoxide-induced ferroptosis (Wang et al., 2019c). LINC00618 decreases the expression of SLC7A11 by interacting with LSH, thereby inhibiting ferroptosis. Furthermore, over-expression of LINC00618 increases the levels of Bax and cleaved caspase-3, promoting apoptosis. Importantly, LINC00618 was found to accelerate ferroptosis via apoptosis, but the potential interaction between ferroptosis and apoptosis remains poorly understood (Huang et al., 2021).

6.2 HSPs

The heat shock response (HSR) is a highly conserved stress response to maintain dynamic protein homeostasis in almost all eukaryotic cells (Wang et al., 2021a). As molecular chaperone, heat shock proteins (HSPs) are classified mainly on the basis of their molecular size into seven large families: Hsp110, Hsp100, Hsp90, Hsp70, Hsp60, Hsp40 and small HSPs (approximately 15–30 kDa) (Wang et al., 2021a). HSPB1 (also known as HSP25 in mice and HSP27 in humans) is a small heat shock protein and also HSP27 is an estrogen receptor beta (ER-β)-related protein

(Miller et al., 2005; Barna et al., 2018). HSPB1 reduces cellular iron uptake by down-regulating TFR1 (Chiu et al., 2018). Protein kinase C-mediated phosphorylation of HSPB1 provides protection against ferroptosis by reducing iron-mediated production of lipid reactive oxygen species. Inhibition of the HSF1-HSPB1 pathway and HSPB1 phosphorylation increases erastin induced ferroptosis. This suggests that HSF1-HSPB1 is a negative regulator of ferroptosis (Chen et al., 2006).

HSP27 is a novel biomarker of AS that predicts adverse cardiovascular events (Sun et al., 2015). HSP27 prevents the formation of foam cell and plaques in female but not male mice (Inia and O'Brien, 2021). Intracellular HSPB1 stabilizes plaques by reducing vascular smooth muscle cell apoptosis (Rayner et al., 2009). Vascular wall infiltration of LDL may reduce VSMC adhesion and migration by inducing changes in HSP27/pHSP27 (Martin-Ventura et al., 2006). ROS were found to activate p38/MAPK phosphorylation, mediating the activation of HSF1, which in turn inhibits the development of ferroptosis (Garci´a-Arguinzonis et al., 2010). Another study showed that the lipid peroxidation metabolite 4-HNE could also mediate the activation of HSF1 through p38/MAPK phosphorylation, promoting the transcription of PROM2 (prominin2) and resisting the development of ferroptosis (Liu et al., 2021). Studies have shown that prominin2 promotes resistance to ferroptosis in mammary epithelial cells and breast cancer cells. Mechanistically, prominin2 promotes the formation of ferritin-containing multi-vesicular vesicles (MVBs) and exosomes transports iron out of cells (Brown et al., 2021). Oentin-1 inhibits VSMC migration by inactivating the NOX-ROS-p38-HSP27 pathway (Brown et al., 2019). PA (Palmitic acid) cause lipotoxic injury in cardiomyocytes, and over-expression of HSF1 restores the disturbance of iron homeostasis by mediating the expression of iron metabolism-related proteins such as TFRC, SLC40A1 and FTH1 (Lin et al., 2021b). Thus HSF1 appears to protect cardiomyocytes from PA induced ferroptosis by regulating the expression of iron-associated proteins and GPX4 (Wang et al., 2021b).

Heat shock protein A family (HSP70) member 5 (HSPA5, also known as BIP or GRP78) is a member of the HSP70 family and is mainly distributed in the endoplasmic reticulum (Zhang et al., 2010; Bailly and Waring, 2019). As mentioned above, ATF4 also induces the binding of HSPA5 to GPX4, thereby protecting GPX4 protein degradation and inhibiting ferroptosis. HSP70 facilitates over-expression of monocyte adhesion molecules and progression of AS (Xie et al., 2016). However, in parallel to the inhibition of HSP90 activity, a reduction in arterial wall inflammation and oxidative stress was also observed in association with increased HSP70 expression (Madrigal-Matute et al., 2010). HSP70 induces Treg to act as an anti-inflammatory agent (Wendling et al., 2000). When proteins carry a specific KFERQ-like motif to be degraded by CMA, GPX4 has a potential CMA-targeting motif that is recognized by HSPA8 and then transferred from the cytoplasm to the lysosomes via LAMP2A, ultimately causing protein degradation (Kaushik and Cuervo, 2018). HSP90-mediated LAMP2A protein stability promotes erastin induced ferroptosis by forming the HSPA8-LAMP2A-GPX4 protein complex to promote CMA-mediated GPX4 degradation (Wu et al., 2019b). LAMP2A and HSPA8-mediated CMA promote erastin induced GPX4 degradation via lysosomes, and HSP90 has been shown to increase the stability of LAMP2A protein, thereby linking autophagy and ferroptosis, known as chaperone-mediated autophagy (Liu et al., 2020).

Over-expression of HSP90 is associated with the characteristics of plaque instability. Inhibition of HSP90 reduces inflammatory responses and oxidative stress (Rodríguez-Iturbe and Johnson, 2018). HO-1 protein transcription is also regulated by HSF1 and NRF2 (Inouye et al., 2018; Rodríguez-Iturbe and Johnson, 2018). And HSF1 is also involved in nuclear translocation and stabilization of p53 (Zhang et al., 2021). Over-expression of HSP27 is protective against AS and is also a negative regulator of ferroptosis. Although HSP70 can inhibit ferroptosis via the ATF4-HSPA5-GPX4 pathway, the roles of HSP70 in AS are currently controversial (Bielecka-Dabrowa et al., 2009).

7. CONCLUSION

The pathogenesis of AS is complex and involves three major cell types including endothelial cells, smooth muscle cells and macrophages. The development of ferroptosis is associated with restricted GSH synthesis, disturbances in iron homeostasis, accumulation of lipid peroxides and fatty acid synthesis, which are also closely linked to the development of AS. In this review, we describe the role of ferroptosis signalling pathways and transcription factors and other regulatory molecules in the development of ferroptosis, with a focus on the linkage of these signalling pathways and transcription factors and other regulatory factors between ferroptosis and AS. The blood vessel is not just a simple anatomical organ, but one with complex functions. AS is the basis for many cardiovascular pathologies, including myocardial infarction and cerebral infarction, and ferroptosis also plays a very important role in many systemic cardiovascular diseases. Current research into ferroptosis in AS is still at a very early stage. What role does iron death play in the pathogenesis of atherosclerosis, and in the involvement of other organ lesions based on atherosclerosis. We hope that this review will provide new insights into the relationship between AS and ferroptosis.

AUTHOR CONTRIBUTIONS

YW and YZ contributed equally to collect the literature and write the review manuscript. YW, YZ, and TY revised the manuscript. YS gave the idea behind the manuscript compilation. HL and LY reviewed the article before final submission. All authors read and approved the manuscript prior to submission. YW and YZ contributed equally to this work.

FUNDING

This review was funded by the National Natural Science Foundation of China (91939104, 82070465, 82170469, 81772252, 32071263), Heilongjiang Province Science Foundation for Distinguished Young Scholars (JQ2021H001), General project of Heilongjiang Provincial Health Commission (2020-075),Construction Project of Scientific Research and Innovation Team of Harbin Medical University-Daqing (HD-CXTD-202001); Key Discipline Construction Project of Harbin Medical University-Daqing (HD-ZDXK-202001).

REFERENCES

Anandhan, A., Dodson, M., Schmidlin, C. J., Liu, P., and Zhang, D. D. (2020). Breakdown of an Ironclad Defense System: The Critical Role of NRF2 in Mediating Ferroptosis. *Cel Chem. Biol.* 27 (4), 436–447. doi:10.1016/j.chembiol.2020.03.011

Arnér, E. S. J. (2020). Effects of Mammalian Thioredoxin Reductase Inhibitors. *Handb Exp. Pharmacol.* 264, 289–309. doi:10.1007/164_2020_393

Bailly, C., and Waring, M. J. (2019). Pharmacological Effectors of GRP78 Chaperone in Cancers. *Biochem. Pharmacol.* 163, 269–278. doi:10.1016/j.bcp.2019.02.038

Baranano, D. E., Rao, M., Ferris, C. D., and Snyder, S. H. (2002). Biliverdin Reductase: a Major Physiologic Cytoprotectant. *Proc. Natl. Acad. Sci.* 99 (25), 16093–16098. doi:10.1073/pnas.252626999

Barna, J., Csermely, P., and Vellai, T. (2018). Roles of Heat Shock Factor 1 beyond the Heat Shock Response. *Cell. Mol. Life Sci.* 75 (16), 2897–2916. doi:10.1007/s00018-018-2836-6

Bentzon, J. F., Otsuka, F., Virmani, R., and Falk, E. (2014). Mechanisms of Plaque Formation and Rupture. *Circ. Res.* 114 (12), 1852–1866. doi:10.1161/CIRCRESAHA10.1161/circresaha.114.302721

Bielecka-Dabrowa, A., Barylski, M., Mikhailidis, D. P., Rysz, J., and Banach, M. (2009). HSP 70 and Atherosclerosis - Protector or Activator? *Expert Opin. Ther. Targets* 13 (3), 307–317. doi:10.1517/14728220902725149

Brown, C. W., Amante, J. J., Chhoy, P., Elaimy, A. L., Liu, H., Zhu, L. J., et al. (2019). Prominin2 Drives Ferroptosis Resistance by Stimulating Iron Export. *Dev. Cel.* 51 (5), 575–586. doi:10.1016/j.devcel.2019.10.007

Brown, C. W., Amante, J. J., Goel, H. L., and Mercurio, A. M. (2017). The α6β4 Integrin Promotes Resistance to Ferroptosis. *J. Cel Biol.* 216 (12), 4287–4297. doi:10.1083/jcb.201701136

Brown, C. W., Chhoy, P., Mukhopadhyay, D., Karner, E. R., and Mercurio, A. M. (2021). Targeting Prominin2 Transcription to Overcome Ferroptosis Resistance in Cancer. *EMBO Mol. Med.* 13 (8), e13792. doi:10.15252/emmm.202013792

Campbell, M. R., Karaca, M., Adamski, K. N., Chorley, B. N., Wang, X., and Bell, D. A. (2013). Novel Hematopoietic Target Genes in the NRF2-Mediated Transcriptional Pathway. *Oxidative Med. Cell Longevity* 2013, 1–12. doi:10.1155/2013/120305

Carpi-Santos, R., and Calaza, K. C. (2018). Alterations in System Xc– Expression in the Retina of Type 1 Diabetic Rats and the Role of Nrf2. *Mol. Neurobiol.* 55 (10), 7941–7948. doi:10.1007/s12035-018-0961-8

Chen, B., Wang, W., Shen, T., and Qi, R. (2013). Thioredoxin1 Downregulates Oxidized Low-Density Lipoprotein-Induced Adhesion Molecule Expression via Smad3 Protein. *PLoS One* 8 (9), e76226. doi:10.1371/journal.pone.0076226

Chen, C.-J., Huang, H.-S., and Chang, W.-C. (2002). Inhibition of Arachidonate Metabolism in Human Epidermoid Carcinoma A431 Cells Overexpressing Phospholipid Hydroperoxide Glutathione Peroxidase. *J. Biomed. Sci.* 9 (5), 453–459. doi:10.1007/BF02256540

Chen, D., Fan, Z., Rauh, M., Buchfelder, M., Eyupoglu, I. Y., and Savaskan, N. (2017). ATF4 Promotes Angiogenesis and Neuronal Cell Death and Confers Ferroptosis in a xCT-dependent Manner. *Oncogene* 36 (40), 5593–5608. doi:10.1038/onc.2017.146

Chen, H., Zheng, C., Zhang, Y., Chang, Y.-Z., Qian, Z.-M., and Shen, X. (2006). Heat Shock Protein 27 Downregulates the Transferrin Receptor 1-mediated Iron Uptake. *Int. J. Biochem. Cel Biol.* 38 (8), 1402–1416. doi:10.1016/j.biocel.2006.02.006

Chen, Q., Lv, J., Yang, W., Xu, B., Wang, Z., Yu, Z., et al. (2019). Targeted Inhibition of STAT3 as a Potential Treatment Strategy for Atherosclerosis. *Theranostics* 9 (22), 6424–6442. doi:10.7150/thno.35528

Chiu, M. H., Heydari, B., Batulan, Z., Maarouf, N., Subramanya, V., Schenck-Gustafsson, K., et al. (2018). Coronary Artery Disease in post-menopausal Women: Are There Appropriate Means of Assessment? *Clin. Sci. (Lond)* 132 (17), 1937–1952. doi:10.1042/CS20180067

Chu, B., Kon, N., Chen, D., Li, T., Liu, T., Jiang, L., et al. (2019). ALOX12 Is Required for P53-Mediated Tumour Suppression through a Distinct Ferroptosis Pathway. *Nat. Cel Biol* 21 (5), 579–591. doi:10.1038/s41556-019-0305-6

Dai, C., Chen, X., Li, J., Comish, P., Kang, R., and Tang, D. (2020). Transcription Factors in Ferroptotic Cell Death. *Cancer Gene Ther.* 27 (9), 645–656. doi:10.1038/s41417-020-0170-2

Dal Monte, M., Martini, D., Ristori, C., Azara, D., Armani, C., Balbarini, A., et al. (2011). Hypoxia Effects on Proangiogenic Factors in Human Umbilical Vein Endothelial Cells: Functional Role of the Peptide Somatostatin. *Naunyn-schmiedeberg's Arch. Pharmacol.* 383 (6), 593–612. doi:10.1007/s00210-011-0625-y

Di Marco, E., Gray, S. P., Kennedy, K., Szyndralewiez, C., Lyle, A. N., Lassègue, B., et al. (2016). NOX4-derived Reactive Oxygen Species Limit Fibrosis and Inhibit Proliferation of Vascular Smooth Muscle Cells in Diabetic Atherosclerosis. *Free Radic. Biol. Med.* 97, 556–567. doi:10.1016/j.freeradbiomed.2016.07.013

Ding, C.-K. C., Rose, J., Sun, T., Wu, J., Chen, P.-H., Lin, C.-C., et al. (2020). MESH1 Is a Cytosolic NADPH Phosphatase that Regulates Ferroptosis. *Nat. Metab.* 2 (3), 270–277. doi:10.1038/s42255-020-0181-1

Dixon, S. J., Lemberg, K. M., Lamprecht, M. R., Skouta, R., Zaitsev, E. M., Gleason, C. E., et al. (2012). Ferroptosis: an Iron-dependent Form of Nonapoptotic Cell Death. *Cell* 149 (5), 1060–1072. doi:10.1016/j.cell.2012.03.042

Dodson, M., Castro-Portuguez, R., and Zhang, D. D. (2019). NRF2 Plays a Critical Role in Mitigating Lipid Peroxidation and Ferroptosis. *Redox Biol.* 23, 101107. doi:10.1016/j.redox.2019.101107

Doll, S., and Conrad, M. (2017). Iron and Ferroptosis: A Still Ill-defined Liaison. *IUBMB Life* 69 (6), 423–434. doi:10.1002/iub.1616

Fan, Z., Wirth, A.-K., Chen, D., Wruck, C. J., Rauh, M., Buchfelder, M., et al. (2017). Nrf2-Keap1 Pathway Promotes Cell Proliferation and Diminishes Ferroptosis. *Oncogenesis* 6 (8), e371. doi:10.1038/oncsis.2017.65

Finazzi, D., and Arosio, P. (2014). Biology of Ferritin in Mammals: an Update on Iron Storage, Oxidative Damage and Neurodegeneration. *Arch. Toxicol.* 88 (10), 1787–1802. doi:10.1007/s00204-014-1329-0

Galaris, D., and Pantopoulos, K. (2008). Oxidative Stress and Iron Homeostasis: Mechanistic and Health Aspects. *Crit. Rev. Clin. Lab. Sci.* 45 (1), 1–23. doi:10.1080/10408360701713104

Gao, J., Zhang, Z., Liu, Y., Zhang, Z., Wang, M., Gong, A., et al. (2021). Stearoyl-CoA Desaturase 1 Potentiates Hypoxic Plus Nutrient-Deprived Pancreatic Cancer Cell Ferroptosis Resistance. *Oxidative Med. Cell Longevity* 2021, 1–14. doi:10.1155/2021/6629804

Gao, M., Monian, P., Pan, Q., Zhang, W., Xiang, J., and Jiang, X. (2016). Ferroptosis Is an Autophagic Cell Death Process. *Cell Res* 26 (9), 1021–1032. doi:10.1038/cr.2016.95

Gao, M., Monian, P., Quadri, N., Ramasamy, R., and Jiang, X. (2015). Glutaminolysis and Transferrin Regulate Ferroptosis. *Mol. Cel.* 59 (2), 298–308. doi:10.1016/j.molcel.2015.06.011

Garci´a-Arguinzonis, M., Padro´, T., Lugano, R., Llorente-Cortes, V., and Badimon, L. (2010). Low-density Lipoproteins Induce Heat Shock Protein 27 Dephosphorylation, Oligomerization, and Subcellular Relocalization in Human Vascular Smooth Muscle Cells. *Atvb* 30 (6), 1212–1219. doi:10.1161/ATVBAHA.109.198440

Gaschler, M. M., Andia, A. A., Liu, H., Csuka, J. M., Hurlocker, B., Vaiana, C. A., et al. (2018). FINO2 Initiates Ferroptosis through GPX4 Inactivation and Iron Oxidation. *Nat. Chem. Biol.* 14 (5), 507–515. doi:10.1038/s41589-018-0031-6

Guo, L., Li, S.-Y., Ji, F.-Y., Zhao, Y.-F., Zhong, Y., Lv, X.-J., et al. (2014). Role of Angptl4 in Vascular Permeability and Inflammation. *Inflamm. Res.* 63 (1), 13–22. doi:10.1007/s00011-013-0678-0

Guo, Z., Ran, Q., Roberts, L. J., 2nd, Zhou, L., Richardson, A., Sharan, C., et al. (2008). Suppression of Atherogenesis by Overexpression of Glutathione Peroxidase-4 in Apolipoprotein E-Deficient Mice. *Free Radic. Biol. Med.* 44 (3), 343–352. doi:10.1016/j.freeradbiomed.2007.09.009

Handa, P., Thomas, S., Morgan-Stevenson, V., Maliken, B. D., Gochanour, E., Boukhar, S., et al. (2019). Iron Alters Macrophage Polarization Status and Leads to Steatohepatitis and Fibrogenesis. *J. Leukoc. Biol.* 105 (5), 1015–1026. doi:10.1002/JLB.3A0318-108R

Hou, W., Xie, Y., Song, X., Sun, X., Lotze, M. T., Zeh, H. J., 3rd, et al. (2016). Autophagy Promotes Ferroptosis by Degradation of Ferritin. *Autophagy* 12 (8), 1425–1428. doi:10.1080/15548627.2016.1187366

Huang, D., Li, Q., Sun, X., Sun, X., Tang, Y., Qu, Y., et al. (2021). CRL4DCAF8 Dependent Opposing Stability Control over the Chromatin Remodeler LSH Orchestrates Epigenetic Dynamics in Ferroptosis. *Cell Death Differ* 28 (5), 1593–1609. doi:10.1038/s41418-020-00689-5

Hübner, R.-H., Schwartz, J. D., De, B. P., Ferris, B., Omberg, L., Mezey, J. G., et al. (2009). Coordinate Control of Expression of Nrf2-Modulated Genes in the Human Small Airway Epithelium Is Highly Responsive to Cigarette Smoking. *Mol. Med.* 15 (7-8), 203–219. doi:10.2119/molmed.2008.00130

Inia, J. A., and O'Brien, E. R. (2021). Role of Heat Shock Protein 27 in Modulating Atherosclerotic Inflammation. *J. Cardiovasc. Trans. Res.* 14 (1), 3–12. doi:10.1007/s12265-020-10000-z

Inouye, S., Hatori, Y., Kubo, T., Saito, S., Kitamura, H., and Akagi, R. (2018). NRF2 and HSF1 Coordinately Regulate Heme Oxygenase-1 Expression. *Biochem. Biophysical Res. Commun.* 506 (1), 7–11. doi:10.1016/j.bbrc.2018.10.030

Iwabayashi, M., Taniyama, Y., Sanada, F., Azuma, J., Iekushi, K., Okayama, K., et al. (2012). Inhibition of Lp(a)-Induced Functional Impairment of Endothelial Cells and Endothelial Progenitor Cells by Hepatocyte Growth Factor. *Biochem. Biophysical Res. Commun.* 423 (1), 79–84. doi:10.1016/j.bbrc.2012.05.086

Jiang, L., Kon, N., Li, T., Wang, S.-J., Su, T., Hibshoosh, H., et al. (2015). Ferroptosis as a P53-Mediated Activity during Tumour Suppression. *Nature* 520 (7545), 57–62. doi:10.1038/nature14344

Jiang, X., Stockwell, B. R., and Conrad, M. (2021). Ferroptosis: Mechanisms, Biology and Role in Disease. *Nat. Rev. Mol. Cel Biol.* 22 (4), 266–282. doi:10.1038/s41580-020-00324-8

Jiang, Y., Mao, C., Yang, R., Yan, B., Shi, Y., Liu, X., et al. (2017). EGLN1/c-Myc Induced Lymphoid-specific Helicase Inhibits Ferroptosis through Lipid Metabolic Gene Expression Changes. *Theranostics* 7 (13), 3293–3305. doi:10.7150/thno.19988

Jinnouchi, H., Guo, L., Sakamoto, A., Torii, S., Sato, Y., Cornelissen, A., et al. (2020). Diversity of Macrophage Phenotypes and Responses in Atherosclerosis. *Cel. Mol. Life Sci.* 77 (10), 1919–1932. doi:10.1007/s00018-019-03371-3

Johnson, R., and Halder, G. (2014). The Two Faces of Hippo: Targeting the Hippo Pathway for Regenerative Medicine and Cancer Treatment. *Nat. Rev. Drug Discov.* 13 (1), 63–79. doi:10.1038/nrd4161

Kalinina, E. V., and Gavriliuk, L. A. (2020). Glutathione Synthesis in Cancer Cells. *Biochem. Mosc.* 85 (8), 895–907. doi:10.1134/S0006297920080052

Kanter, J. E., Kramer, F., Barnhart, S., Averill, M. M., Vivekanandan-Giri, A., Vickery, T., et al. (2012). Diabetes Promotes an Inflammatory Macrophage Phenotype and Atherosclerosis through Acyl-CoA Synthetase 1. *Proc. Natl. Acad. Sci.* 109 (12), E715–E724. doi:10.1073/pnas.1111600109

Kattoor, A. J., Pothineni, N. V. K., Palagiri, D., and Mehta, J. L. (2017). Oxidative Stress in Atherosclerosis. *Curr. Atheroscler. Rep.* 19 (11), 42. doi:10.1007/s11883-017-0678-6

Kaushik, S., and Cuervo, A. M. (2018). The Coming of Age of Chaperone-Mediated Autophagy. *Nat. Rev. Mol. Cel Biol.* 19 (6), 365–381. doi:10.1038/s41580-018-0001-6

Kerins, M. J., and Ooi, A. (2018). The Roles of NRF2 in Modulating Cellular Iron Homeostasis. *Antioxid. Redox Signaling* 29 (17), 1756–1773. doi:10.1089/ars.2017.7176

Khan, A. A., and Quigley, J. G. (2011). Control of Intracellular Heme Levels: Heme Transporters and Heme Oxygenases. *Biochim. Biophys. Acta (Bba) - Mol. Cel Res.* 1813 (5), 668–682. doi:10.1016/j.bbamcr.2011.01.008

Kim, C.-H., and Moon, S.-K. (2005). Epigallocatechin-3-gallate Causes the p21/WAF1-Mediated G1-phase Arrest of Cell Cycle and Inhibits Matrix Metalloproteinase-9 Expression in TNF-α-Induced Vascular Smooth Muscle Cells. *Arch. Biochem. Biophys.* 435 (2), 264–272. doi:10.1016/j.abb.2004.12.022

Kirsch, J., Schneider, H., Pagel, J.-I., Rehberg, M., Singer, M., Hellfritsch, J., et al. (2016). Endothelial Dysfunction, and A Prothrombotic, Proinflammatory Phenotype Is Caused by Loss of Mitochondrial Thioredoxin Reductase in Endothelium. *Atvb* 36 (9), 1891–1899. doi:10.1161/ATVBAHA.116.307843

Klóska, D., Kopacz, A., Piechota-Polańczyk, A., Neumayer, C., Huk, I., Dulak, J., et al. (2019). Biliverdin Reductase Deficiency Triggers an Endothelial-To-Mesenchymal Transition in Human Endothelial Cells. *Arch. Biochem. Biophys.* 678, 108182. doi:10.1016/j.abb.2019.108182

Latunde-Dada, G. O. (2017). Ferroptosis: Role of Lipid Peroxidation, Iron and Ferritinophagy. *Biochim. Biophys. Acta (Bba) - Gen. Subjects* 1861 (8), 1893–1900. doi:10.1016/j.bbagen.2017.05.019

Lei, P., Bai, T., and Sun, Y. (2019). Mechanisms of Ferroptosis and Relations with Regulated Cell Death: A Review. *Front. Physiol.* 10, 139. doi:10.3389/fphys.2019.00139

Li, C., Chen, J. W., Liu, Z. H., Shen, Y., Ding, F. H., Gu, G., et al. (2018). CTRP5 Promotes Transcytosis and Oxidative Modification of Low-Density Lipoprotein and the Development of Atherosclerosis. *Atherosclerosis* 278, 197–209. doi:10.1016/j.atherosclerosis.2018.09.037

Li, J.-J., and Chen, J.-L. (2005). Inflammation May Be a Bridge Connecting Hypertension and Atherosclerosis. *Med. Hypotheses* 64 (5), 925–929. doi:10.1016/j.mehy.2004.10.016

Li, J., Cao, F., Yin, H.-l., Huang, Z.-j., Lin, Z.-t., Mao, N., et al. (2020). Ferroptosis: Past, Present and Future. *Cell Death Dis.* 11 (2), 88. doi:10.1038/s41419-020-2298-2

Li, W., Xu, L.-H., Forssell, C., Sullivan, J. L., and Yuan, X.-M. (2008). Overexpression of Transferrin Receptor and Ferritin Related to Clinical Symptoms and Destabilization of Human Carotid Plaques. *Exp. Biol. Med. (Maywood)* 233 (7), 818–826. doi:10.3181/0711-RM-320

Lin, C.-C., Ding, C.-K. C., Sun, T., Wu, J., Chen, K.-Y., Zhou, P., et al. (2021). The Regulation of Ferroptosis by MESH1 through the Activation of the Integrative Stress Response. *Cel Death Dis.* 12 (8), 727. doi:10.1038/s41419-021-04018-7

Lin, S., Li, X., Zhang, J., and Zhang, Y. (2021). Omentin-1: Protective Impact on Ischemic Stroke via Ameliorating Atherosclerosis. *Clinica Chim. Acta.* 517, 31–40. doi:10.1016/j.cca.2021.02.004

Linton, M. F., Babaev, V. R., Huang, J., Linton, E. F., Tao, H., and Yancey, P. G. (2016). Macrophage Apoptosis and Efferocytosis in the Pathogenesis of Atherosclerosis. *Circ. J.* 80 (11), 2259–2268. doi:10.1253/circj.CJ-16-0924

Liu, J., Kuang, F., Kroemer, G., Klionsky, D. J., Kang, R., and Tang, D. (2020). Autophagy-Dependent Ferroptosis: Machinery and Regulation. *Cel Chem. Biol.* 27 (4), 420–435. doi:10.1016/j.chembiol.2020.02.005

Liu, M., Fan, Y., Li, D., Han, B., Meng, Y., Chen, F., et al. (2021). Ferroptosis Inducer Erastin Sensitizes NSCLC Cells to Celastrol through Activation of the ROS-Mitochondrial Fission-Mitophagy axis. *Mol. Oncol.* 15 (8), 2084–2105. doi:10.1002/1878-0261.12936

Liu, Q., and Wang, K. (2019). The Induction of Ferroptosis by Impairing STAT3/Nrf2/GPx4 Signaling Enhances the Sensitivity of Osteosarcoma Cells to Cisplatin. *Cell Biol Int* 43 (11), 1245–1256. doi:10.1002/cbin.11121

Liu, X., Miyazaki, M., Flowers, M. T., Sampath, H., Zhao, M., Chu, K., et al. (2010). Loss of Stearoyl-CoA Desaturase-1 Attenuates Adipocyte Inflammation. *Atvb* 30 (1), 31–38. doi:10.1161/ATVBAHA.109.195636

Loboda, A., Jazwa, A., Grochot-Przeczek, A., Rutkowski, A. J., Cisowski, J., Agarwal, A., et al. (2008). Heme Oxygenase-1 and the Vascular Bed: from Molecular Mechanisms to Therapeutic Opportunities. *Antioxid. Redox Signaling* 10 (10), 1767–1812. doi:10.1089/ars.2008.2043

Lu, S., Wang, X.-z., He, C., Wang, L., Liang, S.-p., Wang, C.-c., et al. (2021). ATF3 Contributes to Brucine-Triggered Glioma Cell Ferroptosis via Promotion of Hydrogen Peroxide and Iron. *Acta Pharmacol. Sin* 42 (10), 1690–1702. doi:10.1038/s41401-021-00700-w

Madrigal-Matute, J., López-Franco, O., Blanco-Colio, L. M., Muñoz-García, B., Ramos-Mozo, P., Ortega, L., et al. (2010). Heat Shock Protein 90 Inhibitors Attenuate Inflammatory Responses in Atherosclerosis. *Cardiovasc. Res.* 86 (2), 330–337. doi:10.1093/cvr/cvq046

Magtanong, L., Ko, P.-J., To, M., Cao, J. Y., Forcina, G. C., Tarangelo, A., et al. (2019). Exogenous Monounsaturated Fatty Acids Promote a Ferroptosis-

Resistant Cell State. *Cel Chem. Biol.* 26 (3), 420–432. doi:10.1016/j.chembiol.2018.11.016

Mancias, J. D., Wang, X., Gygi, S. P., Harper, J. W., and Kimmelman, A. C. (2014). Quantitative Proteomics Identifies NCOA4 as the Cargo Receptor Mediating Ferritinophagy. *Nature* 509 (7498), 105–109. doi:10.1038/nature13148

Mandal, P. K., Seiler, A., Perisic, T., Kölle, P., Banjac Canak, A., Förster, H., et al. (2010). System Xc− and Thioredoxin Reductase 1 Cooperatively Rescue Glutathione Deficiency. *J. Biol. Chem.* 285 (29), 22244–22253. doi:10.1074/jbc.M110.121327

Marchio, P., Guerra-Ojeda, S., Vila, J. M., Aldasoro, M., Victor, V. M., and Mauricio, M. D. (2019). Targeting Early Atherosclerosis: A Focus on Oxidative Stress and Inflammation. *Oxidative Med. Cell Longevity* 2019, 1–32. doi:10.1155/2019/8563845

Marques, L., Negre-Salvayre, A., Costa, L., and Canonne-Hergaux, F. (2016). Iron Gene Expression Profile in Atherogenic Mox Macrophages. *Biochim. Biophys. Acta (Bba) - Mol. Basis Dis.* 1862 (6), 1137–1146. doi:10.1016/j.bbadis.2016.03.004

Martin-Ventura, J. L., Nicolas, V., Houard, X., Blanco-Colio, L. M., Leclercq, A., Egido, J., et al. (2006). Biological Significance of Decreased HSP27 in Human Atherosclerosis. *Atvb* 26 (6), 1337–1343. doi:10.1161/01.ATV.0000220108.97208.67

Mathew, O., Ranganna, K., and Milton, S. (2014). Involvement of the Antioxidant Effect and Anti-inflammatory Response in Butyrate-Inhibited Vascular Smooth Muscle Cell Proliferation. *Pharmaceuticals* 7 (11), 1008–1027. doi:10.3390/ph7111008

Miller, H., Poon, S., Hibbert, B., Rayner, K., Chen, Y.-X., and O'Brien, E. R. (2005). Modulation of Estrogen Signaling by the Novel Interaction of Heat Shock Protein 27, a Biomarker for Atherosclerosis, and Estrogen Receptor β. *Atvb* 25 (3), e10. doi:10.1161/01.ATV.0000156536.89752.8e

Moon, S.-K., Jung, S.-Y., Choi, Y.-H., Lee, Y.-C., Patterson, C., and Kim, C.-H. (2004). PDTC, Metal Chelating Compound, Induces G1 Phase Cell Cycle Arrest in Vascular Smooth Muscle Cells through Inducing p21Cip1 Expression: Involvement of P38 Mitogen Activated Protein Kinase. *J. Cel. Physiol.* 198 (2), 310–323. doi:10.1002/jcp.10728

Murphy, A. J., Sarrazy, V., Wang, N., Bijl, N., Abramowicz, S., Westerterp, M., et al. (2014). Deficiency of ATP-Binding Cassette Transporter B6 in Megakaryocyte Progenitors Accelerates Atherosclerosis in Mice. *Atvb* 34 (4), 751–758. doi:10.1161/ATVBAHA.113.302613

Ou, Y., Wang, S.-J., Li, D., Chu, B., and Gu, W. (2016). Activation of SAT1 Engages Polyamine Metabolism with P53-Mediated Ferroptotic Responses. *Proc. Natl. Acad. Sci. USA* 113 (44), E6806–E6812. doi:10.1073/pnas.1607152113

Ouyang, S., You, J., Zhi, C., Li, P., Lin, X., Tan, X., et al. (2021). Ferroptosis: the Potential Value Target in Atherosclerosis. *Cel Death Dis* 12 (8), 782. doi:10.1038/s41419-021-04054-3

Peter, A., Weigert, C., Staiger, H., Rittig, K., Cegan, A., Lutz, P., et al. (2008). Induction of Stearoyl-CoA Desaturase Protects Human Arterial Endothelial Cells against Lipotoxicity. *Am. J. Physiology-Endocrinology Metab.* 295 (2), E339–E349. doi:10.1152/ajpendo.00022.2008

Pi, H., Wang, Z., Liu, M., Deng, P., Yu, Z., Zhou, Z., et al. (2019). SCD1 Activation Impedes Foam Cell Formation by Inducing Lipophagy in oxLDL-treated Human Vascular Smooth Muscle Cells. *J. Cel Mol Med.* 23 (8), 5259–5269. doi:10.1111/jcmm.14401

Poznyak, A. V., Grechko, A. V., Orekhova, V. A., Chegodaev, Y. S., Wu, W.-K., and Orekhov, A. N. (2020). Oxidative Stress and Antioxidants in Atherosclerosis Development and Treatment. *Biology* 9 (3), 60. doi:10.3390/biology9030060

Poznyak, A. V., Grechko, A. V., Orekhova, V. A., Khotina, V., Ivanova, E. A., and Orekhov, A. N. (2020). NADPH Oxidases and Their Role in Atherosclerosis. *Biomedicines* 8 (7), 206. doi:10.3390/biomedicines8070206

Qiang, Z., Dong, H., Xia, Y., Chai, D., Hu, R., and Jiang, H. (2020). Nrf2 and STAT3 Alleviates Ferroptosis-Mediated IIR-ALI by Regulating SLC7A11. *Oxidative Med. Cell Longevity* 2020, 1–16. doi:10.1155/2020/5146982

Qin, X., Tian, J., Zhang, P., Fan, Y., Chen, L., Guan, Y., et al. (2007). Laminar Shear Stress Up-Regulates the Expression of Stearoyl-CoA Desaturase-1 in Vascular Endothelial Cells. *Cardiovasc. Res.* 74 (3), 506–514. doi:10.1016/j.cardiores.2007.02.014

Rafieian-Kopaei, M., Setorki, M., Doudi, M., Baradaran, A., and Nasri, H. (2014). Atherosclerosis: Process, Indicators, Risk Factors and New Hopes. *Int. J. Prev. Med.* 5 (8), 927–946.

Rayner, K., Sun, J., Chen, Y.-X., McNulty, M., Simard, T., Zhao, X., et al. (2009). Heat Shock Protein 27 Protects against Atherogenesis via an Estrogen-dependent Mechanism. *Atvb* 29 (11), 1751–1756. doi:10.1161/ATVBAHA.109.193656

Rodríguez-Iturbe, B., and Johnson, R. (2018). Heat Shock Proteins and Cardiovascular Disease. *Acta Physiol. Hung* 105 (1), 19–37. doi:10.1556/2060.105.2018.1.4

Schröder, K., Zhang, M., Benkhoff, S., Mieth, A., Pliquett, R., Kosowski, J., et al. (2012). Nox4 Is a Protective Reactive Oxygen Species Generating Vascular NADPH Oxidase. *Circ. Res.* 110 (9), 1217–1225. doi:10.1161/CIRCRESAHA.112.267054

Shin, C.-S., Mishra, P., Watrous, J. D., Carelli, V., D'Aurelio, M., Jain, M., et al. (2017). The Glutamate/cystine xCT Antiporter Antagonizes Glutamine Metabolism and Reduces Nutrient Flexibility. *Nat. Commun.* 8, 15074. doi:10.1038/ncomms15074

Singh, A. K., Chaube, B., Zhang, X., Sun, J., Citrin, K. M., Canfrán-Duque, A., et al. (2021). Hepatocyte-specific Suppression of ANGPTL4 Improves Obesity-Associated Diabetes and Mitigates Atherosclerosis in Mice. *J. Clin. Invest.* 131 (17), e140989. doi:10.1172/JCI140989

Song, X., and Long, D. (2020). Nrf2 and Ferroptosis: A New Research Direction for Neurodegenerative Diseases. *Front. Neurosci.* 14, 267. doi:10.3389/fnins.2020.00267

Stockwell, B. R., Friedmann Angeli, J. P., Bayir, H., Bush, A. I., Conrad, M., Dixon, S. J., et al. (2017). Ferroptosis: A Regulated Cell Death Nexus Linking Metabolism, Redox Biology, and Disease. *Cell* 171 (2), 273–285. doi:10.1016/j.cell.2017.09.021

Stoyanoff, T. R., Rodríguez, J. P., Todaro, J. S., Espada, J. D., Colavita, J. P. M., Brandan, N. C., et al. (2016). Tumor Biology of Non-metastatic Stages of clear Cell Renal Cell Carcinoma; Overexpression of Stearoyl Desaturase-1, EPO/EPO-R System and Hypoxia-Related Proteins. *Tumor Biol.* 37 (10), 13581–13593. doi:10.1007/s13277-016-5279-4

Su, L.-J., Zhang, J.-H., Gomez, H., Murugan, R., Hong, X., Xu, D., et al. (2019). Reactive Oxygen Species-Induced Lipid Peroxidation in Apoptosis, Autophagy, and Ferroptosis. *Oxidative Med. Cell Longevity* 2019, 1–13. doi:10.1155/2019/5080843

Sun, X., Ou, Z., Xie, M., Kang, R., Fan, Y., Niu, X., et al. (2015). HSPB1 as a Novel Regulator of Ferroptotic Cancer Cell Death. *Oncogene* 34 (45), 5617–5625. doi:10.1038/onc.2015.32

Tabas, I., and Bornfeldt, K. E. (2016). Macrophage Phenotype and Function in Different Stages of Atherosclerosis. *Circ. Res.* 118 (4), 653–667. doi:10.1161/CIRCRESAHA.115.306256

Tarangelo, A., and Dixon, S. (2018). The P53-P21 Pathway Inhibits Ferroptosis during Metabolic Stress. *Oncotarget* 9 (37), 24572–24573. doi:10.18632/oncotarget.25362

Tarangelo, A., Magtanong, L., Bieging-Rolett, K. T., Li, Y., Ye, J., Attardi, L. D., et al. (2018). p53 Suppresses Metabolic Stress-Induced Ferroptosis in Cancer Cells. *Cel Rep.* 22 (3), 569–575. doi:10.1016/j.celrep.2017.12.077

Tinkov, A. A., Bjørklund, G., Skalny, A. V., Holmgren, A., Skalnaya, M. G., Chirumbolo, S., et al. (2018). The Role of the Thioredoxin/thioredoxin Reductase System in the Metabolic Syndrome: towards a Possible Prognostic Marker? *Cel. Mol. Life Sci.* 75 (9), 1567–1586. doi:10.1007/s00018-018-2745-8

Tsai, M.-H., Kuo, C.-W., Lin, T.-K., Ho, C.-J., Wang, P.-W., Chuang, J.-H., et al. (2020). Ischemic Stroke Risk Associated with Mitochondrial Haplogroup F in the Asian Population. *Cells* 9 (8), 1885. doi:10.3390/cells9081885

Venkatesh, D., O'Brien, N. A., Zandkarimi, F., Tong, D. R., Stokes, M. E., Dunn, D. E., et al. (2020). MDM2 and MDMX Promote Ferroptosis by PPARα-Mediated Lipid Remodeling. *Genes Dev.* 34 (7-8), 526–543. doi:10.1101/gad.334219.119

Wang, C., Shi, M., Ji, J., Cai, Q., Zhao, Q., Jiang, J., et al. (2020). Stearoyl-CoA Desaturase 1 (SCD1) Facilitates the Growth and Anti-ferroptosis of Gastric Cancer Cells and Predicts Poor Prognosis of Gastric Cancer. *Aging* 12 (15), 15374–15391. doi:10.18632/aging.103598

Wang, H., Liu, C., Zhao, Y., and Gao, G. (2020). Mitochondria Regulation in Ferroptosis. *Eur. J. Cel Biol.* 99 (1), 151058. doi:10.1016/j.ejcb.2019.151058

Wang, J., Uryga, A. K., Reinhold, J., Figg, N., Baker, L., Finigan, A., et al. (2015). Vascular Smooth Muscle Cell Senescence Promotes Atherosclerosis and Features of Plaque Vulnerability. *Circulation* 132 (20), 1909–1919. doi:10.1161/CIRCULATIONAHA.115.016457

Wang, L., Liu, Y., Du, T., Yang, H., Lei, L., Guo, M., et al. (2020). ATF3 Promotes Erastin-Induced Ferroptosis by Suppressing System Xc-. *Cel Death Differ.* 27 (2), 662–675. doi:10.1038/s41418-019-0380-z

Wang, M., Mao, C., Ouyang, L., Liu, Y., Lai, W., Liu, N., et al. (2019). Long Noncoding RNA LINC00336 Inhibits Ferroptosis in Lung Cancer by Functioning as a Competing Endogenous RNA. *Cel Death Differ.* 26 (11), 2329–2343. doi:10.1038/s41418-019-0304-y

Wang, N., Ma, H., Li, J., Meng, C., Zou, J., Wang, H., et al. (2021). HSF1 Functions as a Key Defender against Palmitic Acid-Induced Ferroptosis in Cardiomyocytes. *J. Mol. Cell Cardiol.* 150, 65–76. doi:10.1016/j.yjmcc.2020.10.010

Wang, N., Zeng, G.-Z., Yin, J.-L., and Bian, Z.-X. (2019). Artesunate Activates the ATF4-CHOP-CHAC1 Pathway and Affects Ferroptosis in Burkitt's Lymphoma. *Biochem. Biophysical Res. Commun.* 519 (3), 533–539. doi:10.1016/j.bbrc.2019.09.023

Wang, X., Chen, L., Liu, J., Yan, T., Wu, G., Xia, Y., et al. (2016). *In Vivo* treatment of Rat Arterial Adventitia with Interleukin-1β Induces Intimal Proliferation via the JAK2/STAT3 Signaling Pathway. *Mol. Med. Rep.* 13 (4), 3451–3458. doi:10.3892/mmr.2016.4982

Wang, Y., Yang, L., Zhang, X., Cui, W., Liu, Y., Sun, Q. R., et al. (2019). Epigenetic Regulation of Ferroptosis by H2B Monoubiquitination and P53. *EMBO Rep.* 20 (7), e47563. doi:10.15252/embr.201847563

Wang, Z., Chen, X., Liu, N., Shi, Y., Liu, Y., Ouyang, L., et al. (2021). A Nuclear Long Non-coding RNA LINC00618 Accelerates Ferroptosis in a Manner Dependent upon Apoptosis. *Mol. Ther.* 29 (1), 263–274. doi:10.1016/j.ymthe.2020.09.024

Wendling, U., Paul, L., van der Zee, R., Prakken, B., Singh, M., and van Eden, W. (2000). A Conserved Mycobacterial Heat Shock Protein (Hsp) 70 Sequence Prevents Adjuvant Arthritis upon Nasal Administration and Induces IL-10-producing T Cells that Cross-React with the Mammalian Self-Hsp70 Homologue. *J. Immunol.* 164 (5), 2711–2717. doi:10.4049/jimmunol.164.5.2711

Witting, P. K., Pettersson, K., Letters, J., and Stocker, R. (2000). Anti-atherogenic Effect of Coenzyme Q10 in Apolipoprotein E Gene Knockout Mice. *Free Radic. Biol. Med.* 29 (3-4), 295–305. doi:10.1016/s0891-5849(00)00311-7

Wu, J., Minikes, A. M., Gao, M., Bian, H., Li, Y., Stockwell, B. R., et al. (2019). Intercellular Interaction Dictates Cancer Cell Ferroptosis via NF2-YAP Signalling. *Nature* 572 (7769), 402–406. doi:10.1038/s41586-019-1426-6

Wu, M.-Y., Li, C.-J., Hou, M.-F., and Chu, P.-Y. (2017). New Insights into the Role of Inflammation in the Pathogenesis of Atherosclerosis. *Ijms* 18 (10), 2034. doi:10.3390/ijms18102034

Wu, Z., Geng, Y., Lu, X., Shi, Y., Wu, G., Zhang, M., et al. (2019). Chaperone-mediated Autophagy Is Involved in the Execution of Ferroptosis. *Proc. Natl. Acad. Sci. USA* 116 (8), 2996–3005. doi:10.1073/pnas.1819728116

Wunderer, F., Traeger, L., Sigurslid, H. H., Meybohm, P., Bloch, D. B., and Malhotra, R. (2020). The Role of Hepcidin and Iron Homeostasis in Atherosclerosis. *Pharmacol. Res.* 153, 104664. doi:10.1016/j.phrs.2020.104664

Xie, F., Zhan, R., Yan, L.-C., Gong, J.-B., Zhao, Y., Ma, J., et al. (2016). Diet-induced Elevation of Circulating HSP70 May Trigger Cell Adhesion and Promote the Development of Atherosclerosis in Rats. *Cell Stress and Chaperones* 21 (5), 907–914. doi:10.1007/s12192-016-0716-2

Xie, Y., Zhu, S., Song, X., Sun, X., Fan, Y., Liu, J., et al. (2017). The Tumor Suppressor P53 Limits Ferroptosis by Blocking DPP4 Activity. *Cel Rep.* 20 (7), 1692–1704. doi:10.1016/j.celrep.2017.07.055

Yang, L., Wang, H., Yang, X., Wu, Q., An, P., Jin, X., et al. (2020). Auranofin Mitigates Systemic Iron Overload and Induces Ferroptosis via Distinct Mechanisms. *Sig Transduct Target. Ther.* 5 (1), 138. doi:10.1038/s41392-020-00253-0

Yang, W.-H., Ding, C.-K. C., Sun, T., Rupprecht, G., Lin, C.-C., Hsu, D., et al. (2019). The Hippo Pathway Effector TAZ Regulates Ferroptosis in Renal Cell Carcinoma. *Cel Rep.* 28 (10), 2501–2508. doi:10.1016/j.celrep.2019.07.107

Yang, W.-H., Huang, Z., Wu, J., Ding, C.-K. C., Murphy, S. K., and Chi, J.-T. (2020). A TAZ-ANGPTL4-NOX2 Axis Regulates Ferroptotic Cell Death and Chemoresistance in Epithelial Ovarian Cancer. *Mol. Cancer Res.* 18 (1), 79–90. doi:10.1158/1541-7786.MCR-19-0691

Yang, W. S., SriRamaratnam, R., Welsch, M. E., Shimada, K., Skouta, R., Viswanathan, V. S., et al. (2014). Regulation of Ferroptotic Cancer Cell Death by GPX4. *Cell* 156 (1-2), 317–331. doi:10.1016/j.cell.2013.12.010

Yi, J., Zhu, J., Wu, J., Thompson, C. B., and Jiang, X. (2020). Oncogenic Activation of PI3K-AKT-mTOR Signaling Suppresses Ferroptosis via SREBP-Mediated Lipogenesis. *Proc. Natl. Acad. Sci. USA* 117 (49), 31189–31197. doi:10.1073/pnas.2017152117

Ying, Y., and Padanilam, B. J. (2016). Regulation of Necrotic Cell Death: P53, PARP1 and Cyclophilin D-Overlapping Pathways of Regulated Necrosis? *Cel. Mol. Life Sci.* 73 (11-12), 2309–2324. doi:10.1007/s00018-016-2202-5

Zhang, B., Fan, Y., Cao, P., and Tan, K. (2021). Multifaceted Roles of HSF1 in Cell Death: A State-Of-The-Art Review. *Biochim. Biophys. Acta (Bba) - Rev. Cancer* 1876 (2), 188591. doi:10.1016/j.bbcan.2021.188591

Zhang, J., Zhang, X., Li, J., and Song, Z. (2020). Systematic Analysis of the ABC Transporter Family in Hepatocellular Carcinoma Reveals the Importance of ABCB6 in Regulating Ferroptosis. *Life Sci.* 257, 118131. doi:10.1016/j.lfs.2020.118131

Zhang, X., Min, X., Li, C., Benjamin, I. J., Qian, B., Zhang, X., et al. (2010). Involvement of Reductive Stress in the Cardiomyopathy in Transgenic Mice with Cardiac-specific Overexpression of Heat Shock Protein 27. *Hypertension* 55 (6), 1412–1417. doi:10.1161/HYPERTENSIONAHA.109.147066

Zhao, Y., Li, M., Yao, X., Fei, Y., Lin, Z., Li, Z., et al. (2020). HCAR1/MCT1 Regulates Tumor Ferroptosis through the Lactate-Mediated AMPK-SCD1 Activity and its Therapeutic Implications. *Cel Rep.* 33 (10), 108487. doi:10.1016/j.celrep.2020.108487

Zhao, Y., Lu, J., Mao, A., Zhang, R., and Guan, S. (2021). Autophagy Inhibition Plays a Protective Role in Ferroptosis Induced by Alcohol via the P62-Keap1-Nrf2 Pathway. *J. Agric. Food Chem.* 69 (33), 9671–9683. doi:10.1021/acs.jafc.1c03751

Zheng, J., and Conrad, M. (2020). The Metabolic Underpinnings of Ferroptosis. *Cel Metab.* 32 (6), 920–937. doi:10.1016/j.cmet.2020.10.011

Zhou, B., Liu, J., Kang, R., Klionsky, D. J., Kroemer, G., and Tang, D. (2020). Ferroptosis Is a Type of Autophagy-dependent Cell Death. *Semin. Cancer Biol.* 66, 89–100. doi:10.1016/j.semcancer.2019.03.002

Zhou, Y., Que, K.-T., Zhang, Z., Yi, Z. J., Zhao, P. X., You, Y., et al. (2018). Iron Overloaded Polarizes Macrophage to Proinflammation Phenotype through ROS/acetyl-p53 Pathway. *Cancer Med.* 7 (8), 4012–4022. doi:10.1002/cam4.1670

Zhu, J., Xiong, Y., Zhang, Y., Wen, J., Cai, N., Cheng, K., et al. (2020). The Molecular Mechanisms of Regulating Oxidative Stress-Induced Ferroptosis and Therapeutic Strategy in Tumors. *Oxidative Med. Cell Longevity* 2020, 1–14. doi:10.1155/2020/8810785

Zhu, P., Goh, Y. Y., Chin, H. F. A., Kersten, S., and Tan, N. S. (2012). Angiopoietin-like 4: a Decade of Research. *Biosci. Rep.* 32 (3), 211–219. doi:10.1042/BSR20110102

Zhu, S., Zhang, Q., Sun, X., Zeh, H. J., 3rd, Lotze, M. T., Kang, R., et al. (2017). HSPA5 Regulates Ferroptotic Cell Death in Cancer Cells. *Cancer Res.* 77 (8), 2064–2077. doi:10.1158/0008-5472.CAN-16-1979

Zhu, Y., Xian, X., Wang, Z., Bi, Y., Chen, Q., Han, X., et al. (2018). Research Progress on the Relationship between Atherosclerosis and Inflammation. *Biomolecules* 8 (3), 80. doi:10.3390/biom8030080

Conflict of Interest: The authors declare that the research was conducted in the absence of any commercial or financial relationships that could be construed as a potential conflict of interest.

Publisher's Note: All claims expressed in this article are solely those of the authors and do not necessarily represent those of their affiliated organizations, or those of the publisher, the editors and the reviewers. Any product that may be evaluated in this article, or claim that may be made by its manufacturer, is not guaranteed or endorsed by the publisher.

Copyright © 2021 Wang, Zhao, Ye, Yang, Shen and Li. This is an open-access article distributed under the terms of the Creative Commons Attribution License (CC BY). The use, distribution or reproduction in other forums is permitted, provided the original author(s) and the copyright owner(s) are credited and that the original publication in this journal is cited, in accordance with accepted academic practice. No use, distribution or reproduction is permitted which does not comply with these terms.

frontiers in Cell and Developmental Biology

REVIEW
published: 11 January 2022
doi: 10.3389/fcell.2021.809516

The Function, Regulation and Mechanism of Programmed Cell Death of Macrophages in Atherosclerosis

Chang Liu[1], Zecheng Jiang[1], Zhongjie Pan[2] and Liang Yang[1]**

[1]Department of Pharmacology, School of Medicine, Nankai University, Tianjin, China, [2]Tianjin Union Medical Center, Tianjin, China

Atherosclerosis is a chronic progressive inflammatory vascular disease, which is an important pathological basis for inducing a variety of cardio-cerebrovascular diseases. As a kind of inflammatory cells, macrophages are the most abundant immune cells in atherosclerotic plaques and participate in the whole process of atherosclerosis and are the most abundant immune cells in atherosclerotic plaques. Recent studies have shown that programmed cell death plays a critical role in the progression of many diseases. At present, it is generally believed that the programmed death of macrophages can affect the development and stability of atherosclerotic vulnerable plaques, and the intervention of macrophage death may become the target of atherosclerotic therapy. This article reviews the role of macrophage programmed cell death in the progression of atherosclerosis and the latest therapeutic strategies targeting macrophage death within plaques.

Keywords: atherosclerosis, macrophage, programmed cell death, apoptosis, autophagy, pyroptosis, ferroptosis, necroptosis

OPEN ACCESS

Edited by:
Xiongwen Chen,
Temple University, United States

Reviewed by:
Bin Geng,
Chinese Academy of Medical Sciences and Peking Union Medical College, China
Kui Cui,
Harvard University, United States

****Correspondence:***
Zhongjie Pan
jade09242003@aliyun.com
Liang Yang
yangliang@nankai.edu.cn

Specialty section:
This article was submitted to Cell Death and Survival, a section of the journal Frontiers in Cell and Developmental Biology

Received: *05 November 2021*
Accepted: *16 December 2021*
Published: *11 January 2022*

Citation:
Liu C, Jiang Z, Pan Z and Yang L (2022) The Function, Regulation and Mechanism of Programmed Cell Death of Macrophages in Atherosclerosis. Front. Cell Dev. Biol. 9:809516. doi: 10.3389/fcell.2021.809516

INTRODUCTION

Atherosclerosis is a chronic inflammatory vascular disease with complex pathogenesis, which is the pathological basis of a variety of cardiovascular and cerebrovascular diseases and has always been the focus of medical researchers. Atherosclerosis, especially ruptured or eroded plaque and subsequent acute cardio-cerebrovascular complications, remains the leading cause of mortality worldwide (Roth et al., 2017). The major immune cell in atherosclerotic lesions is the macrophage, the origin of which is circulating monocytes. Within plaques, macrophages participate in the progression of the atherosclerotic lesion via uptake of oxidized low-density lipoprotein (ox-LDL) and ensuing foam cell formation. Moreover, macrophages can create broad-spectrum cytokines and chemokines that cause atherosclerosis to influence plaque stability, and inflammatory responses of macrophages are also a driving force for atherosclerotic progression and plaque growth (Shashkin et al., 2005; Shimada, 2009).

Macrophage proliferation, aggregation, aging, and death have an impact on the occurrence and development of atherosclerosis. Therefore, these aspects can also be used as potential directions of anti-atherosclerotic therapy. Among them, macrophage programmed cell death plays a particularly important role in atherosclerosis. Within advanced atherosclerotic plaques, macrophages occupied nearly half of the dead cell population. The aggregation and death of macrophages may promote the formation and enlargement of lipid necrotic core and the instability of plaques (Lutgens et al., 1999). Previous studies have shown that macrophages in plaques may undergo several types of programmed death, including apoptosis, autophagy, pyroptosis, ferroptosis and necroptosis. Different

macrophage death patterns and occur stages will have a promotive or inhibitory effect on atherosclerosis. Based on the current knowledge of macrophages and atherosclerosis, diverse drugs can be designed to mitigate the progress of atherosclerosis and stabilize vulnerable plaques. Next, this review will concentrate on the research progress of various programmed death modes and targeted therapy of macrophages in atherosclerotic plaques.

Effect of Macrophage Apoptosis on Atherosclerosis

Apoptosis and Its Mechanism

Apoptosis is a form of programmed cell death, which is an active process of automatic termination of life determined by genes, with strict regulatory signal pathways (Fuchs and Steller, 2011). Apoptosis plays a key role in the normal ontogeny of multicellular organisms, the maintenance of self-stable balance and resistance to the interference of various external factors. Different from cell necrosis, apoptosis has the characteristic nuclear condensation in morphology, and the chromosomes are cut into 180bp-200 bp-sized fragments in nucleosomes. Then, the cells shrink and finally form apoptotic bodies. In the process of apoptosis, the phosphatidylserine (PtdSer) on the inside of the cell membrane is turned out to the surface of the membrane, but the structure of the cell membrane is still intact. Apoptotic bodies can be quickly swallowed by the surrounding professional or non-professional phagocytes, so it will not cause the surrounding inflammatory response (Jacobson et al., 1997).

Apoptosis mainly includes exogenous pathway and endogenous pathway. Exogenous pathway, also known as death receptor pathway, activates the caspase family of aspartate proteolytic enzymes and induces cell apoptosis mediated by transmembrane receptors. The endogenous pathway, also known as the mitochondrial pathway, stimulates the direct production of intracellular signals, causes changes in the structure of mitochondrial membrane, releases pro-apoptotic substances, and induces cell apoptosis (Peter, 2011).

Mechanism and Role of Macrophage Apoptosis in Different Stages of Atherosclerosis

In the area of atherosclerotic lesions, the macrophages with apoptosis account for the majority of the total apoptotic cells. The apoptosis of macrophages can ensue during all atherosclerotic stages and affect early lesion formation, plaque progression, and plaque stability. Previous studies have shown that there is a duality in the regulation of macrophage apoptosis on the development of atherosclerosis. Loss of JNK1, the pro-apoptotic effector, in hematopoietic cells protected macrophages from apoptosis and this accelerated early atherosclerosis in $Ldlr^{-/-}$ mice (Babaev et al., 2016). Myocardin-related transcription factor A (MRTF-A) was highly expressed in macrophages of human carotid atherosclerotic plaque. Experiments both *in vivo* and *in vitro* reveal that MRTF-A can elevate proliferation and attenuate apoptosis of macrophages and overexpression MRTF-A in monocytes aggravated atherosclerosis in ApoE knockout mice (An et al., 2019). Consistent with these findings, $Ldlr^{-/-}$ mice showed an increase in macrophage apoptosis and an inhibition of early atherosclerosis under the deletion of apoptosis inhibitor AIM (Spα/Api6) (Arai et al., 2005). These results support the concept that macrophage apoptosis is a negative regulator of atherosclerotic plaque development. It seems that increased macrophage apoptosis is related to diminished cellularity within the lesion area and decreased lesion progression in the early stage of atherosclerosis. However, other studies confirm that macrophage apoptosis positively regulates the development of atherosclerosis. Shan Shu et al. found that the expression of monocyte chemotactic protein-induced protein 1 (MCPIP1) can be promoted by Angiotensin II (Ang II) through an AMPK/p38 MAPK-dependent pathway. Increased MCPIP1 expression triggered endoplasmic reticulum (ER) stress to induce macrophage apoptosis and additionally participated in the formation of rupture-prone plaques (Shu et al., 2019). Overexpression of miR-10b in $ApoE^{-/-}$ mice mitigated plaque macrophage apoptosis, reduced late plaque size and increased plaque stability, but had no effect on early plaque formation (Wang et al., 2018). In addition, homocysteine (Hcy), via upregulation of endoplasmic reticulum oxidoreductase 1α (Ero1α) expression, activated ER stress-dependent macrophage apoptosis to expedite vulnerable plaque formation in advanced atherosclerosis (Zhang et al., 2021). It has been proposed that continuous apoptosis of macrophages in stable plaques contributes to the necrotic core expansion and fragility to rupture (Isner et al., 1995; Mallat et al., 1997). According to previous studies, the dual role of macrophage apoptosis in regulating atherosclerosis development depends on the stage of atherosclerotic plaque progression. Macrophage apoptosis decreases lesion cellularity and progression in early lesions but promotes plaque necrosis in more-advanced lesions. This may be due to the deficient efferocytotic removal of apoptotic cells and foam cells in advanced atherosclerotic plaques. In normal physiology, apoptotic cells in plaques can release "find me" signal molecules to effectively recruit phagocytes, and express "eat me" signals on the cell membrane to promote efferocytosis. For example, PtdSer of apoptotic cell membrane structure is a strong "eat me" signal. A variety of phagocytic receptors, such as brain-specific angiogenesis inhibitor one and TIM receptor family, can bind to it to facilitate efferocytosis (Elliott et al., 2017). In the context of this circumstance, the efficiency of apoptosis is very high, and both professional and non-professional phagocytes are able to remove apoptotic bodies rapidly. More importantly, the clearance of apoptotic cells can trigger a positive anti-inflammatory response in efferocytes (Fadok et al., 1998). Therefore, in early plaque, macrophage apoptosis can reduce inflammation and inhibit plaque progression through efficient efferocytosis (**Figure 1A**). However, in progressive plaques, despite the existence of a large number of "find me" and "eat me" signals, ox-LDL can block the effective phagocytic receptors on the surface of efferocytes, such as c-Mer tyrosine kinase (MerTK) receptors,

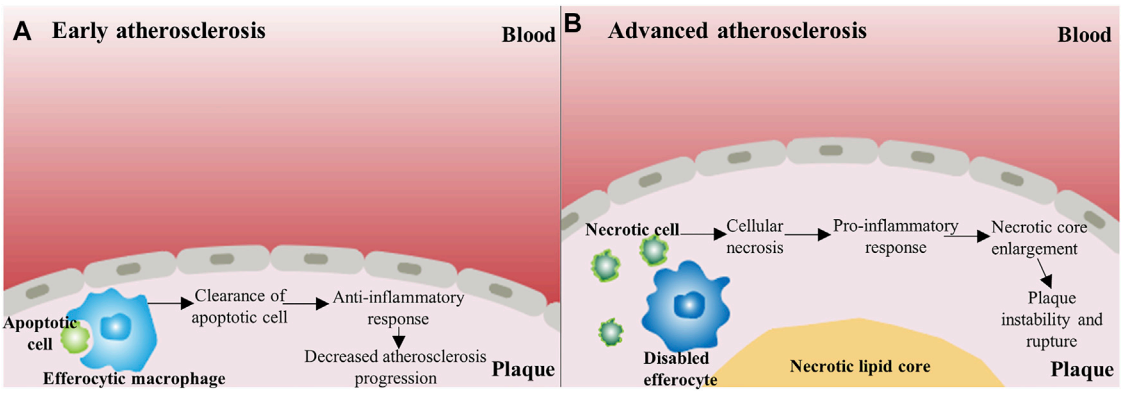

FIGURE 1 | The dual role of macrophage apoptosis in early and advanced atherosclerosis **(A)** In early atherosclerosis, efferocytosis is efficient, and apoptotic cells are rapidly cleared by efferocytes, which can trigger a positive anti-inflammatory response, then resulting in decreased atherosclerosis progression **(B)** In advanced atherosclerosis, disabled efferocytes cannot function properly. Subsequently, the accumulation of apoptotic cells results in secondary necrosis and an inflammatory response ensues. These phenomena may further increase the risk of plaque rupture.

and the efficient efferocytosis cannot play a full role. Gene knockout of MerTK receptors leads to plaque apoptotic cell accumulation and necrotic core expansion (Ait-Oufella et al., 2008). Especially in the inflammatory environment in plaques, the MerTK is cut to form soluble MerTK receptors, which significantly weakens the effective efferocytotic ability of efferocytes (Cai et al., 2017). Hence, in advanced plaques where efferocytosis is not efficient, the accumulation of apoptotic cells results in secondary necrosis and an inflammatory response ensues (Henson et al., 2001). These phenomena may further cause the release of cellular inflammatory contents, boost plaque instability and increase the risk of clinical events of acute atherosclerotic thrombosis (**Figure 1B**).

Pharmacological Intervention of Macrophage Apoptosis in the Treatment of Atherosclerosis

Macrophage apoptosis has a negative regulatory effect on the development of early atherosclerotic plaque, but positively regulates atherosclerotic lesion development in advanced atherosclerotic plaque. So, increasing macrophage apoptosis in early atherosclerotic plaque and reducing macrophage apoptosis in advanced atherosclerotic plaque may be an effective mechanism for the management and treatment of atherosclerosis. Existing drugs such as statins and drugs targeted by angiotensin converting enzyme inhibitors have been shown to regulate apoptosis in atherosclerotic plaques (Zhang et al., 2018). However, the side effects of these drugs are more serious, long-term use will cause muscle soreness, liver function damage and neurotoxicity and so on. In recent years, it has been found that sonodynamic therapy (SDT), as a new non-invasive targeted physiotherapy, has a good therapeutic effect on atherogenesis. Xin Sun et al. found that SDT can induce macrophage apoptosis, reduce the number and lipid content of macrophages, and stabilize atherosclerotic plaques. So it played an active role in delaying the progression of the disease (Sun et al., 2019). Moreover, Viorel Simion et al. showed that the macrophage-specific lncRNA MAARS regulated apoptosis via interacting with HuR which was a critical mediator of transcriptional stability and apoptosis. And MAARS deficiency in macrophages decreased apoptosis and increased their efferocytosis, consequently, reducing atherosclerotic lesion formation by 52% in $Ldlr^{-/-}$ mice. Therefore, either reducing MAARS expression or blocking MAARS–HuR interaction could presumably be effective strategies in limiting macrophage apoptosis in advanced plaques (Simion et al., 2020).

In addition, the treatment of atherosclerosis is mostly related to the enhancement of macrophage efferocytosis. A recent study has shown that synthetic simulated apoptotic cells such as PtdSer encapsulated nanoparticles can be used to enhance efferocytosis (Bagalkot et al., 2016). However, most of the studies on enhancing the role of macrophage efferocytosis to treat atherosclerosis only stay at the basic experimental level, so actively exploring whether these methods can be used in clinical anti-atherosclerosis by enhancing the effect of efferocytosis needs to be further discussed.

Effect of Macrophage Autophagy on Atherosclerosis

Autophagy and Its Occurrence Process

Autophagy is also a form of programmed cell death, also known as type II programmed cell death, which participates in the occurrence and development of many diseases. Autophagy refers to the process in which cells use lysosomes or vacuoles to degrade damaged organelles and macromolecular substances under the induction of nutritional deficiency, hypoxia and reactive oxygen species, which can provide raw materials for cell reconstruction, regeneration and repair. It is a compensatory and self-protecting catabolic cellular pathway and a defense and

protective mechanism to maintain cell homeostasis (Han et al., 2018). Based on the physiological function and delivery routine to the lysosomal lumen, autophagy is able to be divided into three different forms: macroautophagy, microautophagy and chaperone-mediated autophagy (Yang and Klionsky, 2010). The term autophagy commonly refers to macroautophagy, which is the most prevalent and extensively studied form of autophagy. Autophagy introduced later also refers to macroautophagy. The process of autophagy is that the degradation is wrapped by vesicles with bilayer structure to form autophagosomes, and the outer membrane of the latter then fuses with lysosomal membrane or tonoplast, releasing the encapsulated substance into lysosome or vacuole, and finally hydrolyzing it into small molecular compounds such as amino acids, carbohydrates, fatty acids and nucleotides under the action of a series of hydrolytic enzymes (Levine and Kroemer, 2008). Basal autophagy can remove excess or damaged substances in cells in time, and reuse degradation products, which helps to maintain the normal metabolic function and survival of cells.

The Protective Role of Macrophage Autophagy in Atherosclerosis

Autophagy is involved in the regulation of cell survival and death during atherosclerosis and runs through the whole process. In the process of plaque formation in mice, autophagic markers mainly colocalized with macrophages and dysfunctional autophagy is a characteristic of plaques (Razani et al., 2012). Studies have found that up-regulation of macrophage autophagy can slow down the progression of atherosclerosis and mitigate the vulnerability of atherosclerotic plaques. Shaohong Fang's findings indicated that arsenic trioxide (ATO) promoted reactive oxygen species (ROS) induction, which resulted in inhibition of the PI3K/AKT/mTOR pathway, ultimately promoting macrophage autophagy and reducing atherosclerotic lesions at early stages (Fang et al., 2021). The main reason for the foam formation of vascular wall macrophages is the imbalance of cholesterol in and out, and macrophage autophagy can mediate cholesterol efflux and reduce foam cell formation. Shuilong Leng et al. discovered that ursolic acid (UA) enhanced macrophage autophagy and facilitated macrophage cholesterol efflux. Both of these effects are anti-atherosclerotic, resulting in reduced atherogenesis in $Ldlr^{-/-}$ mice fed a Western diet (Leng et al., 2016). Mingxue Zhou et al. found that Shen-Yuan-Dan Capsule (SYDC) treatment can ameliorate the level of blood lipid, reduce the atherosclerotic index and plaque areas of aortic roots, and attenuate macrophage-derived foam cell formation in $ApoE^{-/-}$ mice by promoting macrophage autophagy via inhibiting the PI3K/Akt/mTORC1 signaling pathway (Zhou et al., 2019). Macrophage autophagy also plays an essential role in inflammatory response and oxidative stress. In ApoE-null mice, complete disruption of macrophage autophagy promotes hyperactivation of the macrophage inflammasome and excess interleukin-1β (IL-1β) production, thus increasing plaque instability (Razani et al., 2012). Basic autophagy can mitigate cell damage caused by oxidative stress by degrading intracellular oxidative damaged components and clearing dysfunctional mitochondria. It has been reported that macrophage ATG5 deficient $Ldlr^{-/-}$ mice showed increased oxidative stress in the context of atherosclerosis, which expedited the development of atherosclerotic plaque (Liao et al., 2012). In addition, when macrophages are being cleared, macrophage autophagy seems to facilitate efferocytosis. Xianghai Liao et al. showed that in the mouse model of advanced atherosclerosis, blocking autophagy rendered macrophages more susceptible to die, worsened the recognition and removal of dead cells via efferocytes, and accelerated plaque necrosis (Liao et al., 2012). In conclusion, a moderate increase of macrophage autophagy can reduce intracellular lipid accumulation, decrease foam cell formation, inhibit inflammatory and oxidative stress response, and promote efferocytosis in atherosclerotic plaques, thereby delaying the progression of atherogenesis (**Figure 2**).

Pharmacological Intervention of Macrophage Autophagy in the Treatment of Atherosclerosis

Accumulating evidence has indicated that macrophage autophagy plays a protective role in the occurrence and development of atherosclerosis. It can inhibit inflammatory reaction, attenuate oxidative stress and promote cholesterol efflux, which provides a new research direction for the treatment of atherosclerosis (Go et al., 2013). mTOR inhibitors are the most studied autophagy inducers. Many reports have confirmed that mTOR inhibitors or their derivatives have protective effects on atherogenesis. Inhibition of mTOR with pharmacological agents such as rapamycin appears to inhibit atherosclerosis in plenty of different animal models (Pakala et al., 2005; Mueller et al., 2008). Sirtuin1 (Sirt1), belonging to the conservative sirtuin family, exerts protective effects via regulating autophagy as an essential regulator during the progression of atherosclerosis. In Baoxin Liu's study, autophagy was upregulated by the Sirt1 activator resveratrol (RSV). When incubated with the appropriate dose of RSV, the efferocytosis of apoptotic RAW264.7 increased significantly, which alleviated inflammation in atherosclerotic plaques and avoided plaque rupture (Liu et al., 2014). Like Sirt1, Sirt6 also plays a crucial role in reducing plaque formation and promoting plaque stability via stimulating macrophage autophagy, and thereby revealing a novel target for therapeutic interventions (Wang et al., 2020). Additionally, Ismail Sergin et al. showed that therapeutical-related doses of trehalose can increase macrophage autophagy, TFEB (the master transcriptional regulator of autophagy–lysosomal biogenesis) and autophagy–lysosomal biogenesis both *in vitro* and *in vivo*, leading to reverse the dysfunction of macrophages in the plaque and mitigate atherosclerosis (Sergin et al., 2017). Therefore, inducing macrophage autophagy may be a potential therapeutic strategy for atherosclerosis.

Effect of Macrophage Pyroptosis on Atherosclerosis

Pyroptosis and Its Main Characteristics

Pyroptosis, also known as inflammatory necrosis, is a new way of programmed cell death, which depends on the caspase family.

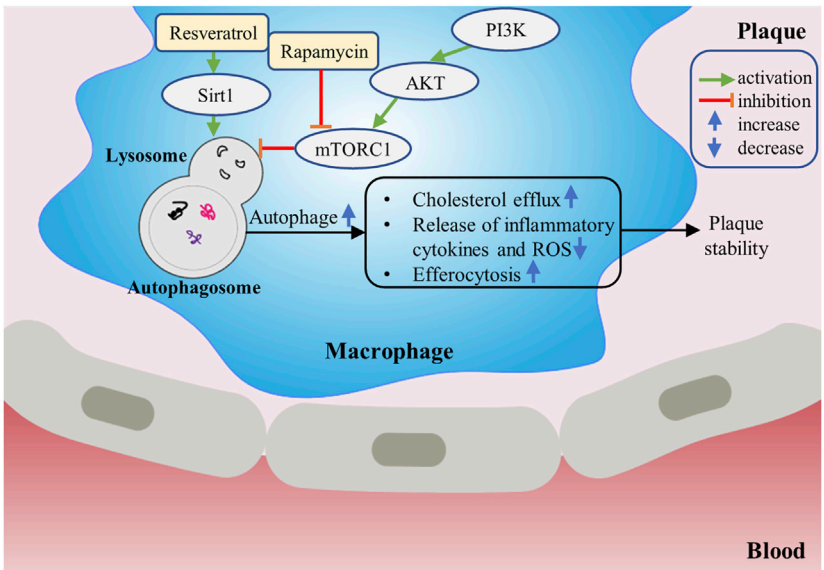

FIGURE 2 | The protective role of macrophage autophagy in atherosclerosis. Drugs such as rapamycin can increase autophagy of macrophages by inhibiting mTORC1. Up-regulation of macrophage autophagy can increase cholesterol efflux, promote efferocytosis, inhibit inflammatory response and suppress oxidative stress, thereby contributing to stabilizing the plaque.

Pyroptosis is accompanied by the maturation and release of inflammatory factors such as IL-1β and interleukin-18 (IL-18), and induces inflammatory cascade reaction. The pyroptosis signaling pathway can be divided into caspase-1-dependent classical pathways and caspase-4/5/11-dependent non-classical pathways. Pyroptosis is often induced by viral or bacterial infection and endogenous damage, which plays an essential role in antagonizing infection and endogenous danger signals. It is one of the innate immune defense mechanisms of hosts against intracellular pathogens infection (Miao et al., 2010).

Shao Feng's team and Vishva M Dixit's team discovered respectively in 2015 that caspase-1 and caspase-4/5/11 induced pyroptosis by cutting a protein called Gasdermin-D (GSDMD). After being cut by caspase-1 or caspase-4/5/11, GSDMD released its N-terminal domain which had the activity of binding to membrane lipids and drilling holes in the cell membrane, which led to changes in cell osmotic pressure and swelling until the final rupture of the cell membrane (Kayagaki et al., 2015; Shi et al., 2015). The pathway of pyroptosis is mainly regulated by inflammatory bodies. At present, the inflammatory bodies most closely related to atherosclerosis are mainly NLRP3 inflammatory bodies which are members of the NLR family. The NLR family's main biological function is to strengthen the ability of the immune system to detect microbial infection, produce proinflammatory cytokines, and regulate immune and inflammatory response. In the classical pathway of pyroptosis, related stimulation leads to the activation of NLRP3 which then recruits and activates caspase-1. The activated caspase-1 cleaves and activates inflammatory cytokines such as IL-1β and IL-18, and cleaves the N-terminal sequence of GSDMD which binds to the membrane to produce membrane pores, resulting in pyroptosis.

The Effectiveness of Macrophage Pyroptosis on Atherosclerosis

In recent years, a growing body of evidence suggests that macrophage pyroptosis plays a more significant role in the formation, rupture and immuno-inflammatory response of atherosclerotic vulnerable plaques than traditional ways of programmed cell death, such as apoptosis, autophagy and so on (Xu et al., 2018). Normal level of pyroptosis can cleave cells and release pathogens and inflammatory factors outside the cells, so as to recruit immune cells to remove pathogens and damaged cells, which is conducive to the maintenance of local homeostasis. However, in atherosclerosis, ox-LDL and cholesterol crystallization in the plaque will continuously activate NLRP3 inflammatory bodies and caspase-1, resulting in a continuous increase in the release of inflammatory factors, thus promoting the enhancement of inflammatory response in the atherosclerotic region and reducing the stability of the plaque (Hoseini et al., 2018) (**Figure 3**). It has been reported that NLRP3 inflammatory bodies are highly expressed in atherosclerotic areas, silencing ApoE$^{-/-}$ mice NLRP3 gene can inhibit the expression of inflammatory factors and atherosclerotic progression, reduce the content of lipids and matrix metalloproteinases in plaques, increase collagen fibers, promote plaque stability, and then reduce the risk of atherosclerotic plaque rupture (Zheng et al., 2014). In atherosclerotic plaques, in addition to overactivation of NLRP3, researchers also discovered that the site of plaque rupture demonstrated a highly immunoreactivity to caspase-1 in macrophages, while caspase-3 staining was weak, suggesting that macrophage pyroptosis may play a more vital role in atherosclerotic lesions than apoptosis (Kolodgie et al., 2000). Furthermore, IL-1β, IL-18 and other pro-inflammatory cytokines produced and released by macrophages in

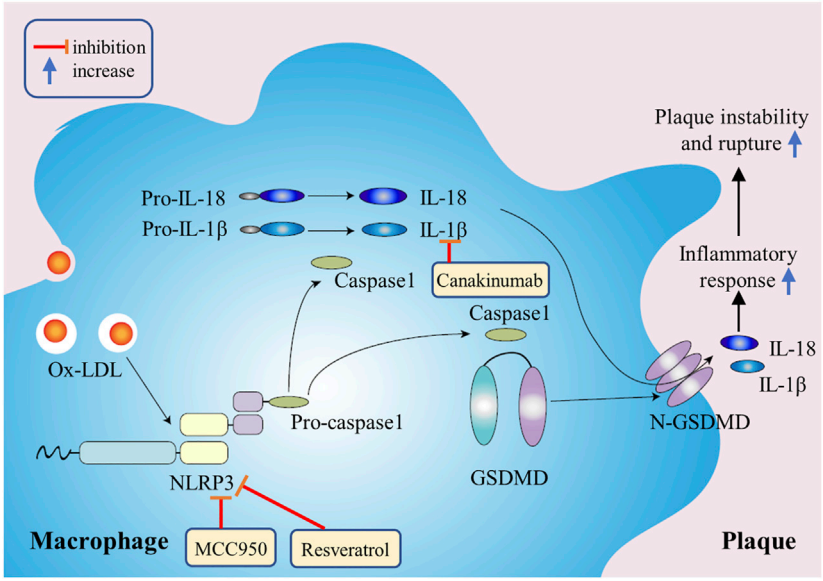

FIGURE 3 | The mechanism of macrophage pyroptosis in promoting atherosclerosis. Ox-LDL in plaques will continuously activate NLRP3 inflammatory bodies and caspase-1, resulting in a continuous increase in the release of inflammatory factors, thus promoting plaque instability and rupture.

atherosclerotic lesion are also closely associated with the development and stability of atherosclerotic plaques. IL-1β and IL-18 are predominantly derived from macrophages and are the main substrates of caspase-1. Hirokazu Kirii et al. reported that IL-1β deficiency reduced atherosclerotic lesions by about 33% in ApoE$^{-/-}$ mice (Kirii et al., 2003). In short, the release of inflammatory factors enhances the inflammatory environment and increases the aggregation of macrophages, thus promoting the development and instability of plaques.

Pharmacological Intervention of Macrophage Pyroptosis in the Treatment of Atherosclerosis

Many studies have confirmed that macrophage pyroptosis plays a crucial role in the formation, rupture and immune inflammation of atherosclerotic plaques. Regulation of macrophage pyroptosis is expected to become a new strategy to stabilize vulnerable plaques (Xu et al., 2018).

Activated NLRP3 inflammatory bodies and IL-1β signaling pathway may be essential to the atherosclerotic lesion progression. NLRP3 inflammatory body selective inhibitor MCC950 can reduce macrophage aggregation and inflammatory factor levels, significantly inhibit atherosclerotic plaque progression and increase plaque stability in ApoE$^{-/-}$ mice. MCC950 can also inhibit ox-LDL uptake, increase cholesterol efflux and inhibit the transformation of macrophages into foam cells (Chen et al., 2018). Canakinumab is a therapeutic monoclonal antibody targeting IL-1β with anti-inflammatory effects. The recurrence rate of cardiovascular events among atherosclerotic patients assigned to receive canakinumab was significantly lower than among those in the placebo group (Ridker et al., 2017). There were other researchers who used the effective ingredients of anti-inflammatory and detoxifying traditional Chinese medicine to carry out the research on the treatment of atherosclerosis. Misawa T et al. found that RSV was able to inhibit the assembly of NLRP3 and apoptosis-related spect-like protein containing a CARD (ASC) by inhibiting *a*-tubulin acetylation, and then inhibit the activation of NLRP3 inflammatory bodies and pyroptosis in mouse macrophages (Misawa et al., 2015). Berberine, an active component of coptis chinensis, can inhibit the activation of ROS-dependent NLRP3 inflammatory bodies and reduce the synthesis of pro-IL-1β by inhibiting NF-κB, so it can be used in the prevention and treatment of atherosclerosis (Ju et al., 2018).

Effect of Macrophage Ferroptosis on Atherosclerosis

Ferroptosis

Ferroptosis is a new type of iron-dependent programmed cell death, which occurs through the lethal accumulation of ROS when glutathione (GSH)-dependent lipid peroxidation repair system is compromised (Stockwell et al., 2017). Ferroptosis is closely related to a variety of human diseases, such as cancers, cardiovascular diseases and degenerative diseases. The essence of ferroptosis is the depletion of glutathione, the decrease of glutathione peroxidase (GPXs) activity (the decrease of GPX4 activity is the most important), and the impaired antioxidant capacity of cells dependent on GPX4. Lipid oxides cannot be metabolized by GPX4-catalyzed glutathione reductase reaction, and then Fe^{2+} oxidizes lipids to produce ROS, which eventually leads to cell oxidative death, that is, ferroptosis. There is a significant difference between ferroptosis and other forms of programmed cell death. In cell morphology, the changes of ferroptosis are mainly the increase of mitochondrial membrane density and mitochondrial contraction, but not accompanied by the decrease of nuclear volume, chromatin

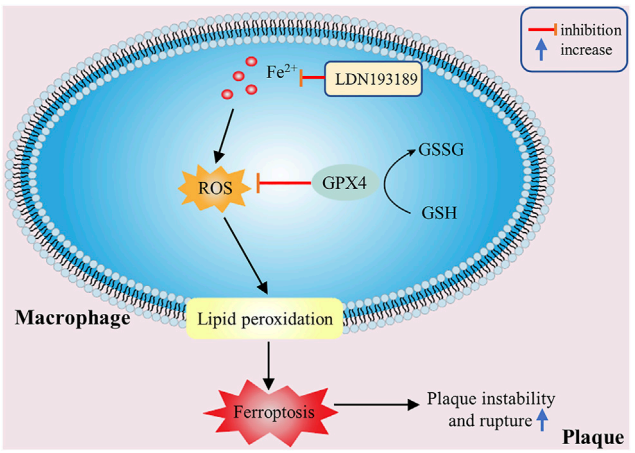

FIGURE 4 | The effectiveness of macrophage ferroptosis on atherosclerosis. Excessive ROS accumulation or iron overload in macrophages can promote lipid peroxidation and other pathological processes, then cause macrophage ferroptosis and increase plaque instability.

condensation and so on (Dixon et al., 2012). In the aspect of biochemical metabolism, ferroptosis is characterized by the increase of intracellular lipid peroxidation, the increase of ROS, the breaking of oxidation-antioxidation balance, the loss of cell integrity and cell death, which can be inhibited by antioxidants and iron chelating agents (Li et al., 2020).

The Effectiveness of Macrophage Ferroptosis on Atherosclerosis

Atherosclerosis is closely related to the changes of ROS and iron levels in the body. Excessive ROS accumulation or iron overload can promote cellular oxidative stress, lipid peroxidation and other pathological processes, and increase plaque instability (**Figure 4**). ROS accumulation in macrophages, lipid peroxidation, plaque hemorrhage and iron deposition are important characteristics of advanced atherosclerotic plaque, which indirectly indicates that ferroptosis may be involved in the development of atherosclerosis (Martinet et al., 2019). Besides, the increase of free iron can also accelerate inflammation and the formation of macrophage-derived foam cells (Hu et al., 2019). When Omar Saeed et al. used LDN 193189, a small molecular inhibitor of BMP signal transduction, to inhibit ferritin, thereby reducing macrophage intracellular iron levels, macrophages from LDN treated ApoE$^{-/-}$ mice demonstrated increased lipid efflux and reduced foam cell formation (Saeed et al., 2012). The loss of the activity of GPX4, the key enzyme of ferroptosis, will also lead to the accumulation of a large number of lipid peroxides and ROS, which further affect the progress of atherosclerosis (Feng and Stockwell, 2018). And overexpression of GPX4 can reduce lipid peroxidation and inhibit plaque development in ApoE$^{-/-}$ mice (Guo et al., 2008). These studies demonstrate that iron overload and lipid peroxidation play a significantly important role in the occurrence and development of atherosclerosis, and ferroptosis is closely related to atherogenesis. Therefore, removing excess iron and reducing ROS production may be new strategies for the treatment and prevention of atherosclerosis in the future.

Effect of Macrophage Necroptosis on Atherosclerosis

Necroptosis

Necroptosis, known as programmed cell necrosis, is also one of the important ways of programmed cell death, which was first proposed by Degterev et al., in 2005 (Degterev et al., 2005). Necroptosis has typical morphological features of necrosis, such as increase of cell size, swelling of organelles and rupture of cell plasma membrane. In terms of physiological and biochemical characteristics, necroptosis produces a large number of ROS and pro-inflammatory factors, and often forms necrosomes in the process of necrosis. However, compared with the usual necrosis, necroptosis is an ordered necrosis with the unique signal pathway and regulated by specific signal molecules (Kroemer et al., 2009). In necroptosis, receptor-interacting proteins (RIP) are a class of important signal molecules regulating cell death or survival, especially receptor-interacting protein kinase 1 (RIPK1) and receptor-interacting protein kinase 3 (RIPK3) play a key regulatory role in necroptosis signal pathway, and its expression level can indicate the degree of necroptosis (Silke et al., 2015). The classical pathway of necroptosis depends on the binding of tumor necrosis factor-α (TNF-α) to membrane receptors, which transduces signals to RIPK1 and RIPK3, so that they can phosphorylate each other to obtain kinase activity, and then phosphorylate downstream mixed lineage kinase domain-like protein (MLKL). The activated MLKLs oligomerize and form selective ion channels, which eventually lead to the rupture of cell membrane and cell necroptosis. In addition, when apoptosis is inhibited, necroptosis can be used as an alternative way to mediate cell death.

The Effectiveness of Macrophage Necroptosis on Atherosclerosis

The radiotracers labeling the necroptosis pathway were located in atherosclerotic plaques, which proved that necroptosis was involved in the pathological process of atherosclerosis (Leeper, 2016). Studies have shown that once programmed necrosis occurs, it will release a large number of inflammatory factors and chemokines, induce severe inflammatory reaction and promote the formation of atherosclerotic plaques (Galluzzi et al., 2017). Further study found that macrophage necroptosis can directly lead to the formation of atherosclerotic necrotic core and plaque instability (Kavurma et al., 2017) (**Figure 5**). Lingjun Meng et al. demonstrated that in RIPK3 knockout atherosclerotic mouse models, the levels of inflammatory factors such as IL-6 and IL-1β were significantly decreased, and the size of atherosclerotic plaque was reduced (Meng et al., 2016). Juan Lin et al. also found that in Ldlr$^{-/-}$ mice, the area of advanced atherosclerotic plaques in RIPK3

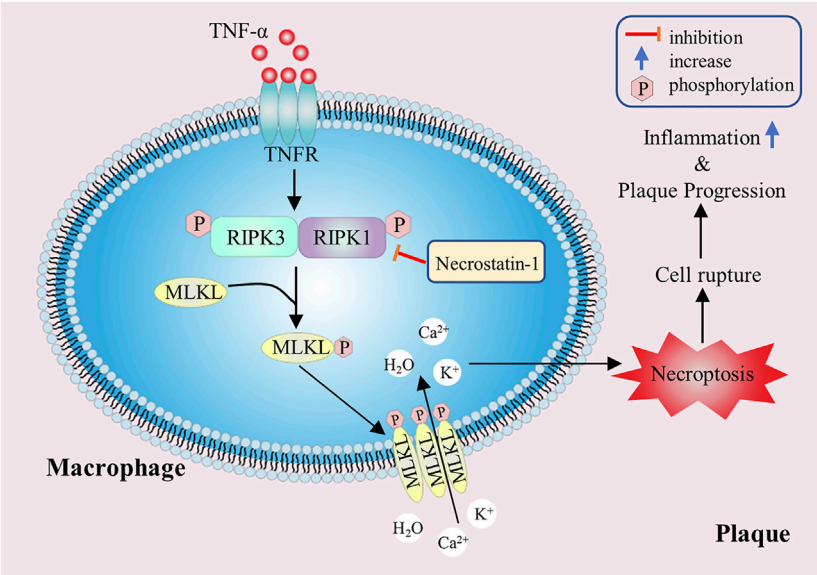

FIGURE 5 | The promoting effect of macrophage necroptosis on atherosclerosis. The RIPK1 and RIPK3 play a key regulatory role in necroptosis, and they can phosphorylate downstream MLKL. The activated MLKLs form selective ion channels, which eventually lead to cell membrane rupture, inflammatory factors release and plaque instability.

knockout mice was significantly reduced, and the number of programmed necrotic macrophages in the lesion was less than that in wild mice, but there was no significant difference in the number of apoptotic cells, suggesting that RIPK3-dependent necroptosis was closely related to the development of advanced atherosclerosis (Lin et al., 2013). Similar results were observed in RIPK1 knockout mice. According to Denuja Karunakaran's research results, knockout of RIPK1 in macrophages *in vitro* and *in vivo* can reduce inflammatory gene expression stimulated by TNF-α, inhibit nuclear factor κ-B (NF-κB) activity, markedly reduce atherosclerotic lesions, and have no effect on plasma cholesterol and body weight (Karunakaran et al., 2021). In ApoE$^{-/-}$ mice, necroptosis inhibitor necrostatin-1 (Nec-1) can inhibit the formation of RIPK1 and RIPK3 complex, then block the occurrence of macrophage necroptosis and mitigate the inflammatory response, thus inducing significant reduction in atherosclerotic lesions (Karunakaran et al., 2016). At present, Nec-1 has attracted wide attention as a new target for diagnosis, intervention and treatment of patients with atherosclerosis. Hence, inhibiting macrophage necroptosis in atherosclerotic lesions may have the effect of reducing intravascular load and stabilizing atherosclerotic plaques. Moreover, drugs or inhibitors targeting RIPK1 and RIPK3 can be designed to slow down atherosclerosis progression by mitigating macrophage necroptosis.

CONCLUSION

Macrophage programmed cell death is closely related to the formation and instability of atherosclerotic plaques, and it plays a vital role in the occurrence and development of atherosclerosis. This suggests that it can be a potential therapeutic target for vascular disease. Although the relationship between macrophage programmed cell death and atherosclerosis has been gradually recognized, many of the specific mechanisms are still not clear. In particular, the microenvironment in atherosclerotic plaques is complex, and a variety of inducing factors of macrophage death exist at the same time, so there are many ways of macrophage death in atherosclerotic plaques simultaneously. Moreover, the complicated relationship between diverse types of macrophage death requires us to target multiple types at the same time.

In addition, various death modes of macrophages have diverse effects on atherogenesis in different stages, so strategies should be adopted for different stages and modes of atherosclerosis. In the early stage of atherosclerosis, the efferocytosis of phagocytes is efficient, consequently, measures should be taken to enhance the specific apoptosis of macrophages, so as to reduce the production of macrophage-derived foam cells and inflammatory reaction, then mitigate disease development and stabilize plaques. In the late stage of efferocytosis dysfunction, macrophage apoptosis should be inhibited to prevent a large number of apoptotic cells from not being absorbed and cleared in time, from resulting in secondary cell necrosis and leading to inflammation and plaque rupture. Under controlled conditions, macrophage autophagy can promote plaque stability and delay disease development, so increasing macrophage autophagy can prevent the further development of plaques. But excessive autophagy which may cause apoptosis will exert harmful functions in atherosclerosis. Furthermore, the pyroptosis of macrophages that cause inflammation and ferroptosis that aggravate oxidative stress should be inhibited throughout the development of atherosclerosis. Macrophage necroptosis within plaques also

secretes large amounts of inflammatory cytokines and ROS, so it should be inhibited as well. In summary, although some progress has been made in the study of programmed macrophage death in atherosclerotic plaques, the specific mechanism, signal transduction pathway and significance in clinical treatment have not been clearly elucidated. Further research is needed to solve the existing obstacles.

AUTHOR CONTRIBUTIONS

CL wrote the manuscript. ZJ prepared the figures. ZP and LY designed the scope of the review and critically amended the manuscript. All authors listed have made a substantial and direct contribution to the work, and approved the submitted version.

FUNDING

This research was supported by the National Natural Science Foundation of China (Nos. 31971194, 81971887, 81772252), Tianjin Natural Science Foundation (Nos.16JCYBJC28100, 18JCQNJC13400), Science and Technology Fund of Tianjin Municipal Health Bureau (ZC20079), and Tianjin Union Medical Center Funding (2019XGPY01).

REFERENCES

Ait-Oufella, H., Pouresmail, V., Simon, T., Blanc-Brude, O., Kinugawa, K., Merval, R., et al. (2008). Defective Mer Receptor Tyrosine Kinase Signaling in Bone Marrow Cells Promotes Apoptotic Cell Accumulation and Accelerates Atherosclerosis. *Atvb* 28, 1429–1431. doi:10.1161/Atvbaha.108.169078

An, J., Naruse, T. K., Hinohara, K., Soejima, Y., Sawabe, M., Nakagawa, Y., et al. (2019). Mrtf-a Regulates Proliferation and Survival Properties of Pro-atherogenic Macrophages. *J. Mol. Cell Cardiol.* 133, 26–35. doi:10.1016/j.yjmcc.2019.05.015

Arai, S., Shelton, J. M., Chen, M., Bradley, M. N., Castrillo, A., Bookout, A. L., et al. (2005). A Role for the Apoptosis Inhibitory Factor AIM/Spα/Api6 in Atherosclerosis Development. *Cel Metab.* 1, 201–213. doi:10.1016/j.cmet.2005.02.002

Babaev, V. R., Yeung, M., Erbay, E., Ding, L., Zhang, Y., May, J. M., et al. (2016). Jnk1 Deficiency in Hematopoietic Cells Suppresses Macrophage Apoptosis and Increases Atherosclerosis in Low-Density Lipoprotein Receptor Null Mice. *Atvb* 36, 1122–1131. doi:10.1161/ATVBAHA.116.307580

Bagalkot, V., Deiuliis, J. A., Rajagopalan, S., and Maiseyeu, A. (2016). "Eat Me" Imaging and Therapy. *Adv. Drug Deliv. Rev.* 99, 2–11. doi:10.1016/j.addr.2016.01.009

Cai, B., Thorp, E. B., Doran, A. C., Sansbury, B. E., Daemen, M. J. A. P., Dorweiler, B., et al. (2017). Mertk Receptor Cleavage Promotes Plaque Necrosis and Defective Resolution in Atherosclerosis. *J. Clin. Invest.* 127, 564–568. doi:10.1172/Jci90520

Chen, L., Yao, Q., Xu, S., Wang, H., and Qu, P. (2018). Inhibition of the Nlrp3 Inflammasome Attenuates Foam Cell Formation of Thp-1 Macrophages by Suppressing Ox-Ldl Uptake and Promoting Cholesterol Efflux. *Biochem. Biophysical Res. Commun.* 495, 382–387. doi:10.1016/j.bbrc.2017.11.025

Degterev, A., Huang, Z., Boyce, M., Li, Y., Jagtap, P., Mizushima, N., et al. (2005). Chemical Inhibitor of Nonapoptotic Cell Death with Therapeutic Potential for Ischemic Brain Injury. *Nat. Chem. Biol.* 1, 112–119. doi:10.1038/nchembio711

Dixon, S. J., Lemberg, K. M., Lamprecht, M. R., Skouta, R., Zaitsev, E. M., Gleason, C. E., et al. (2012). Ferroptosis: An Iron-dependent Form of Nonapoptotic Cell Death. *Cell* 149, 1060–1072. doi:10.1016/j.cell.2012.03.042

Elliott, M. R., Koster, K. M., and Murphy, P. S. (2017). Efferocytosis Signaling in the Regulation of Macrophage Inflammatory Responses. *J.I.* 198, 1387–1394. doi:10.4049/jimmunol.1601520

Fadok, V. A., Bratton, D. L., Konowal, A., Freed, P. W., Westcott, J. Y., and Pm, H. (1998). Macrophages that Have Ingested Apoptotic Cells *In Vitro* Inhibit Proinflammatory Cytokine Production through Autocrine/Paracrine Mechanisms Involving Tgf-Beta, Pge2, and Paf. *J. Clin. Invest.* 101, 890–898. doi:10.1172/JCI1112

Fang, S., Wan, X., Zou, X., Sun, S., Hao, X., Liang, C., et al. (2021). Arsenic Trioxide Induces Macrophage Autophagy and Atheroprotection by Regulating Ros-dependent Tfeb Nuclear Translocation and Akt/Mtor Pathway. *Cell Death Dis* 12, 88. doi:10.1038/s41419-020-03357-1

Feng, H. Z., and Stockwell, B. R. (2018). Unsolved Mysteries: How Does Lipid Peroxidation Cause Ferroptosis? *Plos Biol.* 16, ARTN e2006203. doi:10.1371/journal.pbio.2006203

Fuchs, Y., and Steller, H. (2011). Programmed Cell Death in Animal Development and Disease. *Cell* 147, 742–758. doi:10.1016/j.cell.2011.10.033

Galluzzi, L., Kepp, O., Chan, F. K., and Kroemer, G. (2017). Necroptosis: Mechanisms and Relevance to Disease. *Annu. Rev. Pathol.* 12, 103–130. doi:10.1146/annurev-pathol-052016-100247

Go, A. S., Mozaffarian, D., Roger, V. L., Benjamin, E. J., Berry, J. D., Borden, W. B., et al. (2013). Executive Summary: Heart Disease and Stroke Statistics-2013 Update a Report from the American Heart Association. *Circulation* 127, 143–152. doi:10.1161/CIR.0b013e318282ab8f

Guo, Z., Ran, Q., Roberts, L. J., Zhou, L., Richardson, A., Sharan, C., et al. (2008). Suppression of Atherogenesis by Overexpression of Glutathione Peroxidase-4 in Apolipoprotein E-Deficient Mice. *Free Radic. Bio Med* 44, 343–352. doi:10.1016/j.freeradbiomed.2007.09.009

Han, X., Zhong, Z., Kou, J., Zheng, Y., Liu, Z., Jiang, Y., et al. (2018). Ros Generated by Upconversion Nanoparticle-Mediated Photodynamic Therapy Induces Autophagy via Pi3k/Akt/Mtor Signaling Pathway in M1 Peritoneal Macrophage (Retraction of Vol 48, Pg 1616, 2018). *Cell Physiol Biochem* 49, 2523. doi:10.1159/00049411910.1159/000492283

Henson, P. M., Bratton, D. L., and Fadok, V. A. (2001). Apoptotic Cell Removal. *Curr. Biol.* 11, R795–R805. doi:10.1016/s0960-9822(01)00474-2

Hoseini, Z., Sepahvand, F., Rashidi, B., Sahebkar, A., Masoudifar, A., and Mirzaei, H. (2018). Nlrp3 Inflammasome: Its Regulation and Involvement in Atherosclerosis. *J. Cel Physiol* 233, 2116–2132. doi:10.1002/jcp.25930

Hu, X. R., Cai, X. Y., Ma, R. S., Fu, W. W., Zhang, C. J., and Du, X. J. (2019). Iron-Load Exacerbates the Severity of Atherosclerosis via Inducing Inflammation and Enhancing the Glycolysis in Macrophages. *J. Cel Physiol* 234, 18792–18800. doi:10.1002/jcp.28518

Isner, J. M., Kearney, M., Bortman, S., and Passeri, J. (1995). Apoptosis in Human Atherosclerosis and Restenosis. *Circulation* 91, 2703–2711. doi:10.1161/01.cir.91.11.2703

Jacobson, M. D., Weil, M., and Raff, M. C. (1997). Programmed Cell Death in Animal Development. *Cell* 88, 347–354. doi:10.1016/s0092-8674(00)81873-5

Ju, J. Q., Li, J. E., Lin, Q., and Xu, H. (2018). Efficacy and Safety of Berberine for Dyslipidaemias: A Systematic Review and Meta-Analysis of Randomized Clinical Trials. *Phytomedicine* 50, 25–34. doi:10.1016/j.phymed.2018.09.212

Karunakaran, D., Geoffrion, M., Wei, L., Gan, W., Richards, L., Shangari, P., et al. (2016). Targeting Macrophage Necroptosis for Therapeutic and Diagnostic Interventions in Atherosclerosis. *Sci. Adv.* 2, e1600224. doi:10.1126/sciadv.1600224

Karunakaran, D., Nguyen, M. A., Geoffrion, M., Vreeken, D., Lister, Z., Cheng, H. S., et al. (2021). Ripk1 Expression Associates with Inflammation in Early Atherosclerosis in Humans and Can Be Therapeutically Silenced to Reduce Nf-Kappab Activation and Atherogenesis in Mice. *Circulation* 143, 163–177. doi:10.1161/CIRCULATIONAHA.118.038379

Kavurma, M. M., Rayner, K. J., and Karunakaran, D. (2017). The Walking Dead: Macrophage Inflammation and Death in Atherosclerosis. *Curr. Opin. Lipidol.* 28, 91–98. doi:10.1097/MOL.0000000000000394

Kayagaki, N., Stowe, I. B., Lee, B. L., O'Rourke, K., Anderson, K., Warming, S., et al. (2015). Caspase-11 Cleaves Gasdermin D for Non-canonical Inflammasome Signalling. *Nature* 526, 666–671. doi:10.1038/nature15541

Kirii, H., Niwa, T., Yamada, Y., Wada, H., Saito, K., Iwakura, Y., et al. (2003). Lack of Interleukin-1beta Decreases the Severity of Atherosclerosis in Apoe-Deficient Mice. *Arterioscler Thromb. Vasc. Biol.* 23, 656–660. doi:10.1161/01.ATV.0000064374.1523210.1161/01.atv.0000064374.15232.c3

Kolodgie, F. D., Narula, J., Burke, A. P., Haider, N., Farb, A., You, H. L., et al. (2000). Localization of Apoptotic Macrophages at the Site of Plaque Rupture in Sudden Coronary Death. *Am. J. Pathol.* 157, 1259–1268. doi:10.1016/S0002-9440(10)64641-X

Kroemer, G., Galluzzi, L., Vandenabeele, P., Abrams, J., Alnemri, E. S., Baehrecke, E. H., et al. (2009). Classification of Cell Death: Recommendations of the Nomenclature Committee on Cell Death 2009. *Cell Death Differ* 16, 3–11. doi:10.1038/cdd.2008.150

Leeper, N. J. (2016). The Role of Necroptosis in Atherosclerotic Disease. *JACC Basic Transl Sci.* 1, 548–550. doi:10.1016/j.jacbts.2016.08.002

Leng, S., Iwanowycz, S., Saaoud, F., Wang, J., Wang, Y., Sergin, I., et al. (2016). Ursolic Acid Enhances Macrophage Autophagy and Attenuates Atherogenesis. *J. Lipid Res.* 57, 1006–1016. doi:10.1194/jlr.M065888

Levine, B., and Kroemer, G. (2008). Autophagy in the Pathogenesis of Disease. *Cell* 132, 27–42. doi:10.1016/j.cell.2007.12.018

Li, J., Cao, F., Yin, H. L., Huang, Z. J., Lin, Z. T., Mao, N., et al. (2020). Ferroptosis: Past, Present and Future. *Cel Death Dis* 11. doi:10.1038/s41419-020-2298-2

Liao, X. H., Sluimer, J. C., Wang, Y., Subramanian, M., Brown, K., Pattison, J. S., et al. (2012). Macrophage Autophagy Plays a Protective Role in Advanced Atherosclerosis. *Cel Metab.* 15, 545–553. doi:10.1016/j.cmet.2012.01.022

Lin, J., Li, H., Yang, M., Ren, J., Huang, Z., Han, F., et al. (2013). A Role of Rip3-Mediated Macrophage Necrosis in Atherosclerosis Development. *Cell Rep* 3, 200–210. doi:10.1016/j.celrep.2012.12.012

Liu, B. X., Zhang, B. C., Guo, R., Li, S., and Xu, Y. W. (2014). Enhancement in Efferocytosis of Oxidized Low-Density Lipoprotein-Induced Apoptotic Raw264.7 Cells through Sirt1-Mediated Autophagy. *Int. J. Mol. Med.* 33, 523–533. doi:10.3892/ijmm.2013.1609

Lutgens, E., de Muinck, E. D., Kitslaar, P. J., Tordoir, J. H., Wellens, H. J., and Daemen, M. J. (1999). Biphasic Pattern of Cell Turnover Characterizes the Progression from Fatty Streaks to Ruptured Human Atherosclerotic Plaques. *Cardiovasc. Res.* 41, 473–479. doi:10.1016/s0008-6363(98)00311-3

Mallat, Z., Ohan, J., Leseche, G., and Tedgui, A. (1997). Colocalization of Cpp-32 with Apoptotic Cells in Human Atherosclerotic Plaques. *Circulation* 96, 424–428. doi:10.1161/01.cir.96.2.424

Martinet, W., Coornaert, I., Puylaert, P., and De Meyer, G. R. Y. (2019). Macrophage Death as a Pharmacological Target in Atherosclerosis. *Front. Pharmacol.* 10, ARTN 306. doi:10.3389/fphar.2019.00306

Meng, L., Jin, W., Wang, Y., Huang, H., Li, J., and Zhang, C. (2016). Rip3-Dependent Necrosis Induced Inflammation Exacerbates Atherosclerosis. *Biochem. Biophys. Res. Commun.* 473, 497–502. doi:10.1016/j.bbrc.2016.03.059

Miao, E. A., Leaf, I. A., Treuting, P. M., Mao, D. P., Dors, M., Sarkar, A., et al. (2010). Caspase-1-Induced Pyroptosis Is an Innate Immune Effector Mechanism against Intracellular Bacteria. *Nat. Immunol.* 11, 1136–U1194. doi:10.1038/ni.1960

Misawa, T., Saitoh, T., Kozaki, T., Park, S., Takahama, M., and Akira, S. (2015). Resveratrol Inhibits the Acetylated Alpha-Tubulin-Mediated Assembly of the Nlrp3-Inflammasome. *Int. Immunol.* 27, 425–434. doi:10.1093/intimm/dxv018

Mueller, M. A., Beutner, F., Teupser, D., Ceglarek, U., and Thiery, J. (2008). Prevention of Atherosclerosis by the Mtor Inhibitor Everolimus in Ldlr-/- Mice Despite Severe Hypercholesterolemia. *Atherosclerosis* 198, 39–48. doi:10.1016/j.atherosclerosis.2007.09.019

Pakala, R., Stabile, E., Dang, G. J., Clavijo, L., and Waksman, R. (2005). Rapamycin Attenuates Atherosclerotic Plaque Progression in Apolipoprotein E Knockout Mice - Inhibitory Effect on Monocyte Chemotaxis. *J. Cardiovasc. Pharm.* 46, 481–486. doi:10.1097/01.fjc.0000177985.14305.15

Peter, M. E. (2011). Programmed Cell Death: Apoptosis Meets Necrosis. *Nature* 471, 310–312. doi:10.1038/471310a

Razani, B., Feng, C., Coleman, T., Emanuel, R., Wen, H. T., Hwang, S., et al. (2012). Autophagy Links Inflammasomes to Atherosclerotic Progression. *Cel Metab.* 15, 534–544. doi:10.1016/j.cmet.2012.02.011

Ridker, P. M., Everett, B. M., Thuren, T., MacFadyen, J. G., Chang, W. H., Ballantyne, C., et al. (2017). Antiinflammatory Therapy with Canakinumab for Atherosclerotic Disease. *New Engl. J. Med.* 377, 1119–1131. doi:10.1056/NEJMoa1707914

Roth, G. A., Johnson, C., Abajobir, A., Abd-Allah, F., Abera, S. F., Abyu, G., et al. (2017). Global, Regional, and National Burden of Cardiovascular Diseases for 10 Causes, 1990 to 2015. *J. Am. Coll. Cardiol.* 70, 1–25. doi:10.1016/j.jacc.2017.04.052

Saeed, O., Otsuka, F., Polavarapu, R., Karmali, V., Weiss, D., Davis, T., et al. (2012). Pharmacological Suppression of Hepcidin Increases Macrophage Cholesterol Efflux and Reduces Foam Cell Formation and Atherosclerosis. *Arterioscl Throm Vas* 32, 299–U297. doi:10.1161/Atvbaha.111.240101

Sergin, I., Evans, T. D., Zhang, X. Y., Bhattacharya, S., Stokes, C. J., Song, E., et al. (2017). Exploiting Macrophage Autophagy-Lysosomal Biogenesis as a Therapy for Atherosclerosis. *Nat. Commun.* 8, ARTN 15750. doi:10.1038/ncomms15750

Shashkin, P., Dragulev, B., and Ley, K. (2005). Macrophage Differentiation to Foam Cells. *Curr. Pharm. Des.* 11, 3061–3072. doi:10.2174/1381612054865064

Shi, J. J., Zhao, Y., Wang, K., Shi, X. Y., Wang, Y., Huang, H. W., et al. (2015). Cleavage of Gsdmd by Inflammatory Caspases Determines Pyroptotic Cell Death. *Nature* 526, 660–665. doi:10.1038/nature15514

Shimada, K. (2009). Immune System and Atherosclerotic Disease - Heterogeneity of Leukocyte Subsets Participating in the Pathogenesis of Atherosclerosis. *Circ. J.* 73, 994–1001. doi:10.1253/circj.CJ-09-0277

Shu, S., Zhang, Y., Li, W., Wang, L., Wu, Y., Yuan, Z., et al. (2019). The Role of Monocyte Chemotactic Protein-Induced Protein 1 (Mcpip1) in Angiotensin Ii-Induced Macrophage Apoptosis and Vulnerable Plaque Formation. *Biochem. Biophys. Res. Commun.* 515, 378–385. doi:10.1016/j.bbrc.2019.05.145

Silke, J., Rickard, J. A., and Gerlic, M. (2015). Erratum: The Diverse Role of Rip Kinases in Necroptosis and Inflammation. *Nat. Immunol.* 16, 889. doi:10.1038/ni0815-889b

Simion, V., Zhou, H., Haemmig, S., Pierce, J. B., Mendes, S., Tesmenitsky, Y., et al. (2020). A Macrophage-specific Lncrna Regulates Apoptosis and Atherosclerosis by Tethering Hur in the Nucleus. *Nat. Commun.* 11, 6135. doi:10.1038/s41467-020-19664-2

Stockwell, B. R., Angeli, J. P. F., Bayir, H., Bush, A. I., Conrad, M., Dixon, S. J., et al. (2017). Ferroptosis: A Regulated Cell Death Nexus Linking Metabolism, Redox Biology, and Disease. *Cell* 171, 273–285. doi:10.1016/j.cell.2017.09.021

Sun, X., Guo, S., Yao, J., Wang, H., Peng, C., Li, B., et al. (2019). Rapid Inhibition of Atherosclerotic Plaque Progression by Sonodynamic Therapy. *Cardiovasc. Res.* 115, 190–203. doi:10.1093/cvr/cvy139

Wang, D., Wang, W., Lin, W., Yang, W., Zhang, P., Chen, M., et al. (2018). Apoptotic Cell Induction of Mir-10b in Macrophages Contributes to Advanced Atherosclerosis Progression in Apoe-/- Mice. *Cardiovasc. Res.* 114, 1794–1805. doi:10.1093/cvr/cvy132

Wang, T. T., Sun, C., Hu, L., Gao, E. H., Li, C. Y., Wang, H. C., et al. (2020). Sirt6 Stabilizes Atherosclerosis Plaques by Promoting Macrophage Autophagy and Reducing Contact with Endothelial Cells. *Biochem. Cel Biol* 98, 120–129. doi:10.1139/bcb-2019-0057

Xu, Y. J., Zheng, L., Hu, Y. W., and Wang, Q. (2018). Pyroptosis and its Relationship to Atherosclerosis. *Clin. Chim. Acta* 476, 28–37. doi:10.1016/j.cca.2017.11.005

Yang, Z., and Klionsky, D. J. (2010). Mammalian Autophagy: Core Molecular Machinery and Signaling Regulation. *Curr. Opin. Cel Biol* 22, 124–131. doi:10.1016/j.ceb.2009.11.014

Zhang, G. Q., Tao, Y. K., Bai, Y. P., Yan, S. T., and Zhao, S. P. (2018). Inhibitory Effects of Simvastatin on Oxidized Low-Density Lipoprotein-Induced Endoplasmic Reticulum Stress and Apoptosis in Vascular Endothelial Cells. *Chin. Med. J. (Engl)* 131, 950–955. doi:10.4103/0366-6999.229891

Zhang, N., Zhu, L., Wu, X., Yan, R., Yang, S., Jiang, X., et al. (2021). The Regulation of Ero1-Alpha in Homocysteine-Induced Macrophage Apoptosis and Vulnerable Plaque Formation in Atherosclerosis. *Atherosclerosis* 334, 39–47. doi:10.1016/j.atherosclerosis.2021.08.015

Zheng, F., Xing, S. S., Gong, Z. S., Mu, W., and Xing, Q. C. (20142014). Silence of Nlrp3 Suppresses Atherosclerosis and Stabilizes Plaques in Apolipoprotein E-Deficient Mice. *Mediat Inflamm.* Artn 507208. doi:10.1155/2014/507208

Zhou, M., Ren, P., Zhang, Y., Li, S., Li, M., Li, P., et al. (2019). Shen-Yuan-Dan Capsule Attenuates Atherosclerosis and Foam Cell Formation by Enhancing Autophagy and Inhibiting the Pi3k/Akt/Mtorc1 Signaling Pathway. *Front. Pharmacol.* 10, 603. doi:10.3389/fphar.2019.00603

Conflict of Interest: The authors declare that the research was conducted in the absence of any commercial or financial relationships that could be construed as a potential conflict of interest.

Publisher's Note: All claims expressed in this article are solely those of the authors and do not necessarily represent those of their affiliated organizations, or those of the publisher, the editors and the reviewers. Any product that may be evaluated in this article, or claim that may be made by its manufacturer, is not guaranteed or endorsed by the publisher.

Copyright © 2022 Liu, Jiang, Pan and Yang. This is an open-access article distributed under the terms of the Creative Commons Attribution License (CC BY). The use, distribution or reproduction in other forums is permitted, provided the original author(s) and the copyright owner(s) are credited and that the original publication in this journal is cited, in accordance with accepted academic practice. No use, distribution or reproduction is permitted which does not comply with these terms.

frontiers in Cell and Developmental Biology

REVIEW
published: 13 January 2022
doi: 10.3389/fcell.2021.809955

Autophagy, Pyroptosis, and Ferroptosis: New Regulatory Mechanisms for Atherosclerosis

Lin Lin[1], Mu-Xin Zhang[2], Lei Zhang[3], Dan Zhang[1], Chao Li[1]* and Yun-lun Li[1,4]**

[1]Chinese Medicine Innovation Research Institute, Shandong University of Traditional Chinese Medicine, Jinan, China, [2]The First Clinical Medical College, Shandong University of Traditional Chinese Medicine, Jinan, China, [3]College of Traditional Chinese Medicine, Shandong University of Traditional Chinese Medicine, Jinan, China, [4]Department of Cardiovascular, Affiliated Hospital of Shandong University of Traditional Chinese Medicine, Jinan, China

OPEN ACCESS

Edited by:
Zhi Qi,
Nankai University, China

Reviewed by:
Xianwei Wang,
Xinxiang Medical University, China
Aleksandr E. Vendrov,
University of Michigan, United States
W. Gray Jerome,
Vanderbilt University Medical Center, United States
Tatjana Radosavljević,
University of Belgrade, Serbia

***Correspondence:**
Yun-lun Li
yunlun.lee@hotmail.com
Dan Zhang
zhangdansdtcm@aliyun.com
Chao Li
lichao71795@hotmail.com

Specialty section:
This article was submitted to Cell Death and Survival, a section of the journal Frontiers in Cell and Developmental Biology

Received: 05 November 2021
Accepted: 27 December 2021
Published: 13 January 2022

Citation:
Lin L, Zhang M-X, Zhang L, Zhang D, Li C and Li Y-l (2022) Autophagy, Pyroptosis, and Ferroptosis: New Regulatory Mechanisms for Atherosclerosis. Front. Cell Dev. Biol. 9:809955. doi: 10.3389/fcell.2021.809955

Atherosclerosis is a chronic inflammatory disorder characterized by the gradual buildup of plaques within the vessel wall of middle-sized and large arteries. The occurrence and development of atherosclerosis and the rupture of plaques are related to the injury of vascular cells, including endothelial cells, smooth muscle cells, and macrophages. Autophagy is a subcellular process that plays an important role in the degradation of proteins and damaged organelles, and the autophagy disorder of vascular cells is closely related to atherosclerosis. Pyroptosis is a proinflammatory form of regulated cell death, while ferroptosis is a form of regulated nonapoptotic cell death involving overwhelming iron-dependent lipid peroxidation. Both of them exhibit distinct features from apoptosis, necrosis, and autophagy in morphology, biochemistry, and genetics. However, a growing body of evidence suggests that pyroptosis and ferroptosis interact with autophagy and participate in the development of cancers, degenerative brain diseases and cardiovascular diseases. This review updated the current understanding of autophagy, pyroptosis, and ferroptosis, finding potential links and their effects on atherogenesis and plaque stability, thus providing ways to develop new pharmacological strategies to address atherosclerosis and stabilize vulnerable, ruptured plaques.

Keywords: atherosclerosis, cell death, autophagy, pyroptosis, ferroptosis

1 INTRODUCTION

Atherosclerosis, caused by the accumulation of low-density lipoprotein (LDL) in the subendothelial matrix, is a progressive disease characterized by endothelial damage, inflammatory cell infiltration, cell proliferation, and fat deposition (Lusis, 2000). Proinflammatory and anti-inflammatory mechanisms, along with inadequate cellular inflammation resolution, are the initial factors that promote and accelerate the process of atherosclerotic plaque formation (Back et al., 2019). The composition and vulnerability of a plaque play a principally decisive role in plaque stability, thrombosis, and thrombus-mediated acute coronary events. The functional status, survival and death of vascular cells, including endothelial cells (ECs), vascular smooth muscle cells (VSMCs), and macrophages, can affect the formation and stability of plaques, thus affecting the progression of atherosclerosis.

The endothelial lining of lesion-prone areas of the arterial vasculature is highly susceptible to risk factors associated with atherosclerosis. Oxidized LDL (ox-LDL) is recognized by pattern-recognition receptors in ECs and induces endothelial dysfunction by triggering a cascade of oxidative stress and

TABLE 1 | The main features of autophagy, pyroptosis, and ferroptosis.

RCD	Autophagy	Pyroptosis	Ferroptosis
Morphological features	Formation of double-membraned autolysosomes	Cell swelling, pore formation, membrane rupture, massive leakage of cytoplasmic components	Cytoplasmic and organelles swelling, dysmorphic shrunken mitochondria with the reduced cristae and ruptured outer membrane, unchanged nucleus
Biochemical features	Increased lysosomal activity	Caspase-1/4/5/11 activation and proinflammatory cytokines release	Iron accumulation, lipid peroxidation
Immune features	Mostly anti-inflammatory	Proinflammatory	Proinflammatory
Key genes	ATG5, ATG7, ATG12, TFEB	NLPR3, caspase-1/4/5/11, IL-1β, IL-18	TFR1, GXP4, Nrf2, FSP1
Key regulatory pathways	PI3K–AKT–mTOR, MAPK–ERK1/2–mTOR pathway	NLRP3–Caspase-1–GSDMD pathway, Caspase-4/5/11–GSDMD pathway	System x_c^-–GSH–GPX4 pathway, Nrf2–Keap1 pathway
Released DAMP	HMGB-1	IL-1β, IL-18, ATP, HMGB-1	HMGB-1
Inducers	Rapamycin, C2-ceramide, lithium, sodium, valproate	Ivermectin, ZnO-NPs	Erastin, sulfasalazine, sorafenib, BSO, RSL3, ML162, ML210, $FINO_2$, FIN56, withaferin A
Inhibitors	3-MA, LY294002, Bafilomycin A1, hydroxychloroquine, PIK-III, compound 31, Vps34-In1	Necrosulfonami-de	Deferoxamine, dexrazoxane, ferritin, FPN1, vitamin E, ferrostatin-1, liproxstatin-1
References	Klionsky and Emr (2000), Ohsumi (2001), Thi and Reiner (2012), Xie et al. (2015)	Fink and Cookson (2006), Miao et al. (2011), Boucher et al. (2018), Hoseini et al. (2018)	Seiler et al. (2008), Dixon et al. (2015), Galluzzi et al. (2018), Bersuker et al. (2019), Bao et al. (2020), Riegman et al. (2020)

inflammatory responses (Marchio et al., 2019). Moreover, hyperlipidemia stimulates EC activation before monocyte recruitment (Yin et al., 2015) and activated ECs promote the infiltration of inflammatory cells into atherosclerotic lesions by increasing the release of adhesion molecules, resulting in plaque aggregation and eventually atherosclerosis (Libby et al., 2011). The subendothelial accumulation of foam cells is a major hallmark of early atherosclerotic lesions. It has been recently found that more than 50% of foam cells in plaques are contributed by VSMCs (Allahverdian et al., 2014; Wang Y. et al., 2019), which is the major constituent of the fibrous cap (Pan and Reilly, 2019). Therefore, the death of VSMCs and VSMCs-derived foam cells decreases lesion cellularity, weakens the fibrous cap of the plaque, and increases plaque instability (Clarke et al., 2010). Advanced plaques contain many macrophages with a proinflammatory phenotype, which secrete stromal degradation enzymes, growth factors, cytokines, and intracellular lipids into the extracellular space, leading to plaque instability, plaque rupture, and thrombotic events. Moreover, in advanced atherosclerotic plaques, up to 50% of dead cells are macrophages; the mechanisms of macrophage death involve the decay of lesion cellularity and the promotion of inflammation. Macrophage death is also a significant feature of advanced plaques in atherosclerosis and serves as a catalyst for the formation of necrotic core and plaque instability (Lutgens et al., 1999; Martinet et al., 2019). Atherosclerosis is still the leading cause of death worldwide because of the acute occlusion caused by the formation of a thrombus or blood clot. Hence, the different processes and mechanisms involved in plaque stabilization need to be further explored to find new therapies for atherosclerosis.

Regulated cell death (RCD) is a highly regulated cellular response that controls cell fate in multicellular organisms after they are subjected to various cellular pressures and/or external stimuli. The most common modulated form of cell death is called apoptosis (Kerr et al., 1972); other forms of RCD have been gradually discovered, such as autophagy (Ashford and Porter, 1962), pyroptosis (Fink and Cookson, 2005), and ferroptosis (Dixon et al., 2012). Different types of RCD display distinct features, meanwhile sharing many similar characteristics with considerable overlap and crosstalk (**Table 1**). The interactions between these cell death programs play a role in controlling the ultimate outcome during cell death (Lockshin and Zakeri, 2004). Under normal circumstances, various forms of RCD remove damaged or infected cells from the affected tissues so that the surrounding healthy cells can better perform their proper functions. Nevertheless, the loss of control over single or mixed types of RCD can lead to human diseases, such as cancer, neurodegeneration, autoimmune diseases, infectious diseases, and cardiovascular diseases. Multiple types of RCD have been identified in the pathological process of atherosclerosis, but the intricate overlapping effects and interactions have rarely been systematically summarized. Based on this, the present review provided a current overview of the known signal cascade and interaction of the common patterns of RCD, namely autophagy, pyroptosis, and ferroptosis, and the latest understanding of their functional role and significance in atherosclerosis.

2 THE ROLES OF AUTOPHAGY IN ATHEROSCLEROSIS

2.1 Overview of Autophagy

Autophagy is an evolutionarily conservative homeostatic mechanism consisting of three general subtypes: macroautophagy, microautophagy and chaperone-mediated autophagy (CMA) (Klionsky et al., 2016). Macroautophagy (hereafter referred to as autophagy) is a lysosome-dependent intracellular degradation system by which cytoplasmic organelles, macromolecules, proteins, and invading pathogens are degraded in the lysosome, with the ability to produce new building blocks and energy for cellular renovation and homeostasis (Mizushima and Komatsu, 2011; Parzych and Klionsky, 2014).

Morphologically, autophagy begins in the pre-autophagosomal structure in the cytoplasm and gradually develops into a phagophore, followed by an autophagosome, a double-membraned vacuole containing damaged organelles and denatured macromolecules. Subsequently, the outer membrane of autophagosome fuses with the lysosomal membrane to form autolysosome, and the inner membrane and encapsulated substances of autophagosome enter the lysosomal cavity and are degraded by activated lysosomal hydrolases (Klionsky and Emr, 2000).

Autophagy is a continuous and dynamic process that tightly regulated by autophagy-related genes (ATG) (Kang et al., 2011; Xie et al., 2015). Mammalian target of rapamycin (mTOR) is negatively involved in autophagy regulation. When the cell in the absence of growth factors and amino acids or is stimulated by rapamycin, unc-51 like autophagy-activating kinase 1 (ULK1) is separated from mTOR and undergoes rapid dephosphorylation; activated ULK1 promotes ATG13 phosphorylation and autophagy (Jung et al., 2009; Kim et al., 2011). The class III phosphatidylinositol 3-kinase (Class III PI3K) complex, which includes phosphatidylinositol 3-kinase, catalytic subunit type 3 (PIK3C3)/VPS34, Beclin-1, and ATG14, promotes the nucleation of phagophores by generating the phosphatidylinositol-3-phosphate and recruiting other factors involved in the process of autophagosome formation (Thi and Reiner, 2012; McKnight and Zhenyu, 2013; Bernard and Klionsky, 2014). Subsequently, the phagophore expands by membrane addition though two ubiquitin-like modification processes, among which ATG12-conjugation and microtubule-associated protein 1A/1B-light chain 3 (LC3)-modification play the most crucial roles (Ohsumi, 2001; Tanida et al., 2004). ATG12 is activated by ATG7, and then combines with ATG5 and ATG16L to form a ATG12-ATG5-ATG16L complex at phagophores. In the process of LC3-modification, proLC3 is first processed into LC3-I with the help of ATG4, activated by ATG7, transported to ATG3, and then processed into LC3-II, which is the membrane-bound form localized on preautophagosomes and autophagosomes. After the extension, the outer membrane of autophagosome fuses with lysosomes to form autolysosome and degrade encapsulated substances.

Autophagy plays a dual role, either preventing or promoting cell death, depending on the environment (Fitzwalter and Thorburn, 2015). On the one hand, autophagy-related stress tolerance protects cells against various kinds of cellular death stimuli. Free amino acids and fatty acids produced by the autophagy degradation of unused protein aggregates or damaged organelles can be used for protein synthesis and energy production to adapt to environmental stress (Kroemer et al., 2010). On the other hand, excessive or uncontrolled autophagy can result in the degradation of prosurvival proteins and promote cell death, termed "autophagy-dependent cell death" (Denton and Kumar, 2019). Autophagy regulates inflammatory responses and cell death pathways, thereby influencing the pathogenesis of diseases, including atherosclerosis.

2.2 Effects of Autophagy on Atherosclerosis

Autophagy is closely associated with atherosclerosis, which has been confirmed by the expression profile of ARGs (Chen Y. et al., 2021). Multiple autophagy triggers are present in atherosclerotic plaques, such as reactive oxygen species (ROS), LDL, inflammatory mediators, and tumor necrosis factor-α (TNF-α) (Shao et al., 2016; Zhu et al., 2019). Mild cellular stress, including oxidative stress, ox-LDL, and endoplasmic reticulum (ER) stress, stimulates mild adaptive autophagy of vascular cells (Menghini et al., 2014), which promotes cell survival by degrading damaged organelles and proteins, thereby protecting vascular tissues from oxidative stress or inflammation. It has been confirmed that autophagy can diminish the atherosclerotic plaque area and effectively preserve the stable plaque phenotype, including reduced lipid deposition and proinflammatory macrophages; increased anti-inflammatory macrophages, collagen content, and VSMCs; and lessened cell death within the plaques (Li et al., 2013). Nevertheless, similarly, dysfunction of autophagy has also been found to occur in the progression of atherosclerosis, regardless of the presence or absence of these autophagy stimulators in atherosclerotic plaques. The expression of autophagy markers ATG13 and LC3 in aortic intimal ECs with severe atherosclerosis was found to be significantly higher than the expression in those without atherosclerosis (Chen et al., 2017). Severe oxidative stress or inflammation stimulates excessive autophagy, leading to autophagy-dependent cell death, decreased collagen synthesis, thinning of the fibrous cap, plaque instability, lesions thrombosis, restenosis, and acute coronary events (Cai et al., 2018; Ge et al., 2021). Thus, the resistance to excessive autophagy in an early stage is critical in preventing arteriosclerosis, further leading to serious cardiovascular complications. Except excessive autophagy, the loss of autophagy is more prevalent and may be an important determinant of atherosclerosis. In addition, autophagy may also become insufficient, especially in advanced lesions with a large amount of oxidative stress. In this case, autophagy is functional, but is subsequently unable to cope with excess stress in the plaques, leading to cell apoptosis (Mollace et al., 2015). Therefore, the cytoprotective autophagic pathway may be transformed into a maladaptive pathway depending on the developmental stage of the plaques (**Figure 1**).

2.2.1 Autophagy Dysfunction Induces Endothelial Dysfunction and Inflammation

Endothelial dysfunction, leukocyte adhesion, and foam macrophage formation are the main pathogeneses of atherosclerosis. Endothelial dysfunction, in particular, is thought to be the first step in atherosclerosis (Gimbrone and Garcia-Cardena, 2016). The known mechanisms related to atherosclerosis and endothelial dysfunction include impaired eNOS ability to produce NO, increased oxidative stress, inflammation and impaired autophagy. EC autophagy deficiency improves the levels of vascular cell adhesion molecule-1 (VCAM-1), intercellular adhesion molecule-1 (ICAM-1), von Willebrand factor, and P-selectin, thus promoting the infiltration of macrophages and foam cells, as well as increasing the risk of arterial thrombosis (Wu Q. et al.,

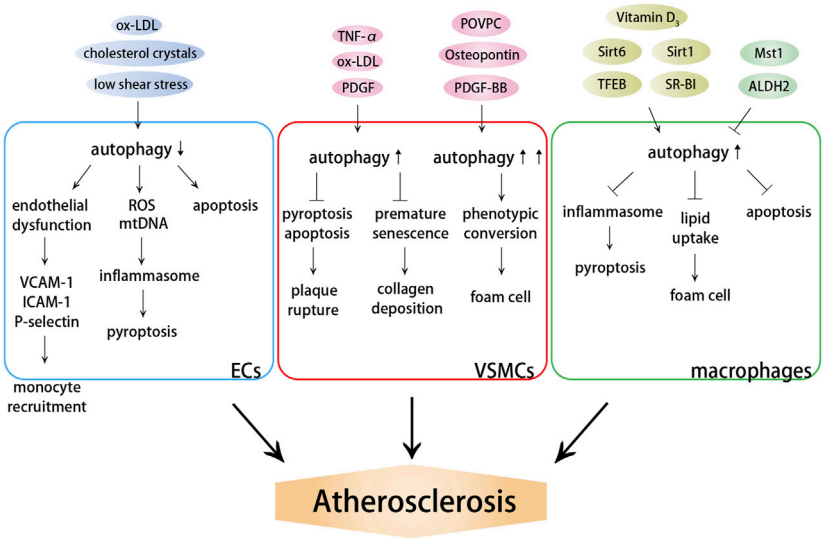

FIGURE 1 | Effects of autophagy on atherosclerosis. Autophagy dysfunction induces endothelial dysfunction and inflammation, promoting monocyte recruitment and cell death. Autophagy dysfunction aggravates plaque instability and promotes the formation of foam cells by influencing VSMC death and phenotypic conversion. Autophagy dysfunction induces lipid accumulation, macrophage foam cell formation and cell death.

2019; Perrotta et al., 2020). Furthermore, Vion et al. reported that specific deficiency in endothelial autophagy only stimulated the development of atherosclerotic lesions in atheroresistant areas, but not in atheroprone areas, in which the endothelial autophagic flux was already blocked (Vion et al., 2017). Thus, increasing basal autophagy and preventing the age-dependent decline in the autophagic flux are effective strategies for restoring endothelial health and inhibiting atherogenesis.

Current evidence supports the central role of EC inflammation in atherosclerosis. Oxidative stress is considered as a key signal in the progression of inflammation, and autophagy is a protective mechanism that protects plaque cells and ECs from certain stimulation on the arterial wall, especially oxidative damage (Cho and Choi, 2019). During oxidant stress, damaged mitochondrial DNA (mtDNA) that escaped autophagy resulted in a potent inflammatory response in atherosclerosis (Ding et al., 2013a). Increased autophagy significantly suppressed chronic vascular inflammation, restrained the formation of plaques, decreased plaque area, and attenuated atherogenesis (Pankratz et al., 2018; Meng Q. et al., 2021), whereas the inhibition or impairment of autophagy exacerbated the inflammation response (Guo F. X. et al., 2019). These studies implied that autophagy was a protective mechanism against endothelial inflammation and a potential target for treating atherosclerosis and related cardiovascular diseases.

Given the protective effect of autophagy on atherosclerotic resistance, the mechanisms of EC autophagy regulation in atherosclerosis have been gradually revealed. Arterial wall shear stress is considered to be one of the important factors in regulating EC autophagy. High shear stress triggers protective autophagy to limit atherosclerotic plaque formation by preventing endothelial apoptosis, senescence, and inflammation, whereas low shear stress, a potential proatherogenic factor, suppresses autophagy by activating the mTOR pathway (Vion et al., 2017; Yuan et al., 2020). The defect in endothelial autophagy may be the missing link between low shear stress and atherosclerosis. Moreover, caveolin-1 (CAV1) plays a critical role in atherogenesis by controlling NO production, vascular inflammation, and extracellular matrix remodeling (Pavlides et al., 2014; Ramirez et al., 2019). A recent study further found that CAV1 could interact with the ATG5–ATG12 complex and regulate the autophagosome formation by influencing the cellular localization of autophagosome components in lipid rafts. The increased autophagy activation and the autophagic flux of ECs caused by CAV1 deficiency mediated atheroprotection by attenuating EC activation in response to proatherogenic cytokines, inhibiting inflammation and macrophage recruitment (Zhang X. et al., 2020). Sun et al. reported that the deficiency of proprotein convertase subtilisin/kexin type 9 (PCSK9), which bound to the LDL reporter (LDLR) and thereby promoted its intracellular degradation, could affect atherogenesis by modulating the levels and properties of apolipoprotein B (ApoB)-containing lipoproteins dependent on increased autophagy signaling pathway and autophagic flux, rather on the effect of PCSK9 on cell surface LDLRs (Sun H. et al., 2018). This result revealed a critical mechanism by which PCSK9 inhibited atherosclerosis, in which autophagy was a major participant. Moreover, microRNAs (miRNAs), which have been identified as the critical regulators of gene expression in many organisms and biological processes, were studied extensively. MiR-214-3p regulates ox-LDL-initiated EC autophagy by directly targeting 3′-UTR of ATG5, which may play an appropriate role in the pathogenesis of atherosclerosis (Wang et al., 2018). Santovito et al. reported a noncanonical inhibition of caspase-3 by miR-126-5p, which was transported into the nucleus

and bound to caspase-3, preventing caspase dimerization and downregulating activity to limit apoptosis. The aforementioned antiapoptotic effect conferred endothelial protection by autophagy in atherosclerosis, and the nuclear import of miR-126-5p was blocked by the ablation of ATG5 (Santovito et al., 2020), reflecting the potential effect of ECs autophagy in cell death resistance and atheroprotection.

2.2.2 Autophagy Dysfunction Aggravates Plaque Instability by Influencing Vascular Smooth Muscle Cell Death and Phenotypic Conversion

Defective autophagy caused by VSMC-specific HuR knockout has recently been reported to trigger off plaque formation and plaque instability (Liu S. et al., 2021). Actually, the death of VSMCs and VSMC-derived foam cells is adverse to maintaining plaque stability, while autophagy promotes cell survival. Autophagy and mitophagy induced by oxidized lipids in the plaques protect VSMCs against apoptosis (Martinet et al., 2008; Swiader et al., 2016). In addition, several cytokines and growth factors, such as TNF-α and platelet-derived growth factor (PDGF), also promote autophagy to resist cell death (Jia et al., 2006; Salabei et al., 2013). Compared with healthy human VSMCs, VSMCs isolated from carotid plaque specimens showed increased autophagy (Yu et al., 2017). However, a fivefold decrease in LC3β expression was observed when comparing carotid plaques in symptomatic and asymptomatic patients, suggesting that decreased autophagy was associated with the clinical stage of atherosclerosis (Swaminathan et al., 2014). VSMC-specific ATG7 knockout in ApoE$^{-/-}$ mice significantly increased the susceptibility of VSMCs to apoptotic cell death, leading to plaque growth, medial disruption and aneurysm formation, which provided the evidence that autophagy deficiency of VSMCs aggravated atherosclerosis via inducing VSMC death (Osonoi et al., 2018). ATG7 deletion also accelerated the development of premature senescence, which was characterized by increased total collagen deposition, nuclear hypertrophy, and CDKN2A-RB-mediated G1 proliferative arrest (Grootaert et al., 2015). Furthermore, VSMC autophagy in ApoE$^{-/-}$ mice stimulated cholesterol efflux and inhibited lipid accumulation and necrotic core formation (Michiels et al., 2016), reflecting a regulatory effect of VSMC autophagy on lipid metabolism.

Phenotypic conversion promotes the migration and proliferation of VSMCs and the formation of VSMC-derived foam cells (Rong et al., 2003). Autophagy may play a critical role in the phenotypic conversion of VSMCs, as diverse stimuli promoting phenotypic conversions, such as ROS, oxidized lipids, and metabolic stress, are also associated with autophagy (Tai et al., 2016). Some autophagy-inducing stimuli, including PDGF-BB, POVPC, and osteopontin, promoted the loss of contractile phenotype and motivated VSMC proliferation and migration, whereas inhibiting autophagy could promote the maintenance of the contractile phenotype and prevent hyperproliferation (Chaulet et al., 2001; Li et al., 2012; Salabei and Hill, 2013). Furthermore, Wang et al. reported that nicotine-mediated autophagy in VSMCs triggered off phenotypic transition and accelerated atherosclerosis via the nAChRs/ROS/NF-κB signaling pathway (Wang Z. et al., 2019). Moreover, nicotine promoted the synthesis and secretion of cathepsin S that stimulated VSMC migration by activating autophagy (Ni et al., 2020). These results reflected that nicotine-modulated autophagy disorder in VSMCs induced and aggravated atherosclerosis, revealing the potential role of smoking in VSMCs and vascular diseases through the autophagic-lysosomal machinery. In brief, autophagy served as a safeguarding mechanism against VCMCs senescence and death; however, excessive activation of autophagy might aggravate atherosclerosis by triggering a synthetic phenotype of VSMCs.

2.2.3 Autophagy Dysfunction Induces Lipid Accumulation and Macrophage Foam Cell Formation

In macrophages, ox-LDL and one of its primary oxysterols, 7-ketonecholesterol, can directly or indirectly stimulate autophagy through ER stress, promoting the survival of macrophages by promoting the clearance of damaged proteins and organelles. Sergin et al. first described the functional status of the autophagy-lysosome system in murine and human atherosclerotic plaques through two key autophagy markers LC3 and SQSTM1/p62 (Sergin et al., 2017). They found that early atherosclerotic lesions had high levels of LC3 co-localized with SQSTM1, indicating the recruitment of autophagy as a stress response to burgeoning plaques. However, advanced lesions were characterized by reduced LC3 and dissociation from SQSTM1, suggesting an extensive dysfunction during the autophagic process (Sergin et al., 2017).

Autophagy of macrophages plays an important role in the pathogenesis of atherosclerosis by inhibiting oxidative stress, inflammation, and the formation of foam cells. For example, macrophage-specific overexpression of TFEB, a master transcriptional regulator of autophagy-lysosome biogenesis, induces a broad atheroprotection by reversing the autophagy dysfunction, including reduction of overall plaque burden and characteristics of plaque complexity, while the effect cannot be achieved in the absence of ATG5 or SQSTM1 (Sergin et al., 2017). Moreover, TFEB also modulates the inflammatory status and enhances the antioxidative capacity by increasing the transcription of genes encoding antioxidant factors (Lu et al., 2017). Arsenic trioxide promoted autophagy and autophagosome-lysosome fusion by triggering the nuclear translocation of TFEB, thus preventing atherosclerosis (Fang et al., 2021). MiR-761 regulates autophagy via the mTOR–ULK1 pathway and subsequently represses the production of inflammatory cytokines, as well as the formation of foam cells (Wang C. et al., 2020), reflecting the critical role of macrophage autophagy in inflammatory resistance and foam cell formation. The activation of autophagy in monocytes also prevents plaque vulnerability and subsequent plaque rupture (Cheng et al., 2015).

The formation of macrophage-derived foam cells is the initial stage of atherosclerosis. Autophagy activation of macrophages caused by sirtuin 6 (Sirt6) overexpression can restrain apoptosis, reduce macrophage foam cell formation, and stabilize atherosclerosis plaques (He et al., 2017; Wang T. et al., 2020). The upregulation of Sirt1 expression or enhanced interaction

between Sirt1 and FOXO1 also promotes autophagy and subsequently modulates macrophage polarization, thus attenuating foam cell formation (Luo et al., 2020; Hui et al., 2021). Vitamin D_3 can recover ox-LDL-impaired autophagy and attenuate the lipid accumulation in macrophages, and scavenger receptor class B type I (SR-BI) can also promote autophagy by regulating *Tfeb* expression and recruiting VPS34-Beclin-1 complex, which all inhibit the conversion of macrophages into foam cells (Kumar et al., 2021; Tao et al., 2021).

The differences in the polarization of macrophages lead to differences in the number and distribution of polarized macrophages in plaques. Classically activated (M1) and alternatively activated (M2) macrophages connect to produce atherosclerotic plaques, and M2 macrophages can suppress foam cell transformation (Moore et al., 2013). Sun et al. found that rapamycin stimulated M1 macrophages and inhibited early atherosclerosis by inducing autophagy, and FTY720 could transform foam cells into M2 macrophages through the autophagy pathway, alleviating advanced atherosclerosis (Sun R. Z. et al., 2018). Therefore, autophagy played a role in alleviating atherosclerosis by selectively removing macrophages or changing the polarization state within plaques.

The accumulation of lipid-rich macrophages is considered as a marker of plaque instability, and intact autophagic machinery is essential in limiting lipid uptake by macrophages. Macrophage-specific ATG7-deficient mice exhibited increased susceptibility to atherosclerosis by increasing macrophage LDL uptake and foam cell formation. Compared with $ApoE^{-/-}$ mice, the suppressed autophagic flux caused by mammalian Ste20-like kinase 1 (Mst1) overexpression increased plaque area, lipid core, and macrophage accumulation (Wang et al., 2016). Furthermore, acetaldehyde dehydrogenase 2 (ALDH2) has been reported to interact with adenosine monophosphate-activated protein kinase (AMPK) and then disturb lysosomal function and autophagy, thus repressing cholesterol hydrolysis in lysosomes and promoting lipid deposition and foam cell formation. LDLR can block the effect of ALDH2 through interaction with AMPK, whereas ALDH2 rs671 mutant attenuates this interaction and further promotes the release of ALDH2 to the nucleus where ALDH2 inhibits the transcription of a lysosomal proton pump protein ATP6V0E2 (Zhong et al., 2019). This result provides a possible molecular mechanism to explain why East Asians carrying the single nucleotide polymorphism ALDH2 rs671 have an increased risk of cardiovascular disease (Han et al., 2013). To sum up, the data revealed the function of macrophage autophagy in atherosclerosis and supported several practical methods of enhancing autophagy and degradative capacity of macrophages as a therapy for atherosclerotic vascular disease.

2.2.4 Effect of Lipophagy and Mitophagy in Atherosclerosis

In atherosclerosis, a majority of lipids stored in the foam cells in the form of lipid droplets consist mainly of free cholesterol and cholesterol esters. Therefore, promoting lipid droplet degradation and cholesterol efflux is an effective strategy to restrain foam cell formation and atherosclerosis process. Lipophagy prevents cellular lipid accumulation by autophagic degradation of lipid droplets via lysosomal acid lipases, thus playing a protective role in atherosclerosis (Ouimet et al., 2017). Sirt6 overexpression in foam cells accelerates cholesterol efflux via the autophagic pathway, which can be largely reversed by miR-33 (He et al., 2017). Ouimet et al. found that miR-33 restrained lipid droplet catabolism and cholesterol mobilization by repressing lipophagy. Importantly, the effect of miR-33 in regulating lipophagy lies the upstream of its effect on the ATP-binding cassette transporter A1-dependent cholesterol efflux, as miR-33 inhibitors cannot enhance the cholesterol efflux in autophagy-deficient macrophages, highlighting the importance of lipophagy in cellular lipid metabolism (Ouimet et al., 2017). Moreover, with aging and lipid accumulation, lipophagy activity decreases, leading to the excessive accumulation of lipid droplets, which further impairs lipophagy activity. Thus, improving the decreased activity of lipophagy may play a critical role in the blockage of foam cells formation and atherosclerosis development.

Aging within the aorta during normolipidemia results in mitochondrial dysfunction and an increase in the IL-6 level, accompanied by elevated mitophagy. Enhanced mitophagy pharmacologically during hyperlipidemia increased aortic mitochondrial function and inhibited atherosclerosis by removing damaged or dysfunctional mitochondria, implying that novel therapies to improve vascular mitochondrial bioenergy prior to hyperlipidemia may attenuate age-related atherosclerosis (Tyrrell et al., 2020). Furthermore, mitophagy in macrophages induced by melatonin scavenged mitochondrial ROS and subsequently repressed prolonged NLRP3 inflammasome activation, thus markedly attenuating atherosclerotic plaque area and vulnerability (Ma et al., 2018). These findings confirmed that mitophagy avails to atherosclerosis resistance. However, ox-LDL-stimulated nuclear receptor subfamily 4 group A member 1 (NR4A1) overexpression caused Parkin-mediated mitophagy through the post-transcriptional modification of Ca^{2+}/calmodulin-dependent protein kinase II, while excessive mitophagy significantly consumed mitochondrial mass, resulting in energy shortage and mitochondrial dysfunction and thus aggravating endothelial apoptosis and atherosclerosis (Li P. et al., 2018).

Taken together, the dysregulation of autophagy is present in atherosclerosis. Basic autophagy protects plaque cells from oxidative stress by degrading damaged intracellular substances, whereas overstimulated or deficient autophagic flux may lead to the death of vascular cells and plaque instability in a variety of ways, including promoting inflammation and lipid accumulation. Skyrocketing researches provide insight into the regulation of autophagic homeostasis as a critical way for therapeutic intervention for atherosclerosis. However, notably, in contrast to the proatherogenic role, a counter-regulatory response of autophagy disruption occurs in dendritic cells or T cells, which maintains immune homeostasis and limits atherogenesis (Amersfoort et al., 2018; Clement et al., 2019). Therefore, different types of cell-specific autophagy regulation have different effects on the development of atherosclerosis.

3 THE ROLES OF PYROPTOSIS IN ATHEROSCLEROSIS

3.1 Overview of Pyroptosis

Pyroptosis is a new caspase-dependent proinflammatory form of regulatory cell death, characterized by cell swelling, pore formation, and membrane rupture, resulting in the massive leakage of cytoplasmic components (Hoseini et al., 2018). Different from the immunologically silent cell death presented by apoptosis, pyroptosis is a response to pathogen-associated molecular patterns (PAMPs) derived from invading pathogens or damage-associated molecular patterns (DAMPs) induced by endogenous stress that leads to RCD and inflammatory response following the release of cytokines (Tavakoli Dargani et al., 2018). Caspases are cysteine proteases that initiate or execute cellular programs causing inflammation or cell death (Schroder and Tschopp, 2010). Pro-caspase-1 is stored in secretory lysosomes, where it awaits exocrine-induced stimulation; otherwise, these molecules may undergo lysosomal degradation (Andrei et al., 1999).

Caspase-dependent pyroptosis requires the activation of the typical inflammatory response (Xue et al., 2019). As proinflammatory caspases, the catalytic activity of caspase-1/4/5/11 is strictly regulated by signal-dependent autoactivation within multiprotein complexes called inflammasomes (Martinon et al., 2002). Inflammasomes are molecular platforms activated in response to cellular infection, toxic insults impinging on the cell, or intracellular stress releasing interleukin (IL)-1 family members, triggering the maturation of proinflammatory cytokines and inducing cell death in the form of pyroptosis (Schroder and Tschopp, 2010; Del Re et al., 2019). An important mechanism of inflammation is the induction of inflammasomes, which requires two signals: the priming signal occurs in response to receptor activation, including interferon (IFN) signaling and Toll-like receptors (TLR) ligands, and induces the transcriptional upregulation of inflammasome components via nuclear factor κB (NF-κB); then, the activating signal provided by an inflammasome activator in the form of a PAMP (e.g., Gram-positive and -negative bacteria, bacterial toxins, DNA and RNA viruses, and fungi) or DAMP (e.g., ATP, uric acid crystals, silica crystals, cholesterol crystals, saturated fatty acids, extracellular histones, lysophosphatidylcholine, mitochondrial ROS and DNA, and aluminum hydroxide) induces the assembly of the inflammasome mediated by kinase NEK7, apoptosis-associated speck-like protein (ASC), and caspase-1 (Bauernfeind et al., 2009; Mathur et al., 2018; Tang et al., 2019). Typical inflammasomes, such as NLRP1b, NLRP3, NAIP-NLRC4, AIM2, and Pyrin, have been found to activate caspase-1, ultimately inducing pyroptosis (Schroder and Tschopp, 2010).

Once activated in response to many stimuli, caspase-1 cleaves the N-terminal and C-terminal domains of the executive protein of pyroptosis, named gasdermin D (GSDMD). These peptides contain the N-terminal active domain of GSDMD, which oligomerizes on the cytoplasmic membrane, generating pores that act as the mediators of pyroptosis and as direct conduits for the transport of IL-1β and IL-18 (Shi J. et al., 2015; Boucher et al., 2018), ultimately causing pyroptosis and inflammatory response (Liu X. et al., 2016). Moreover, caspase-1 results in the cleavage of pro-IL-1β and pro-IL-18 and the release of active IL-1β and IL-18 (Miao et al., 2011), which recruit inflammatory cells and further amplify the inflammatory response. The plasma membrane pores allow the flow of ions, leading to the usual equilibrium of ion gradients between the intracellular and extracellular environments; the water then enters the cell, causing swelling and dissolution (Fink and Cookson, 2006). In the noncanonical caspase-4/5/11-dependent pathway of pyroptosis, the inflammatory agents, such as bacterial lipopolysaccharides (LPS), activate caspase-4/5/11, cleave GSDMD, and release GSDMD-p30 (Kayagaki et al., 2011; Kayagaki et al., 2015), which binds to the plasma membrane and the mitochondrial membrane to kill cells by forming the pyroptotic pores (Aglietti et al., 2016). Besides GSDMD, other members of the gasdermin family, such as GSDMA, GSDMB, GSDMC, GSDME/DFNA5, and GSDMA3, have similar functions in the cytotoxicity of cell membrane disruption (Ding et al., 2016). In the absence or blocking of canonical or noncanonical pyroptosis pathway (caspase1/4/5/11-GSDMD), pyroptosis can be engaged by mechanisms such as caspase-8-GSDMD (Orning et al., 2018) and caspase-3-GSDME (Wang et al., 2017), but their contribution to pyroptosis has not been determined *in vivo*.

Although originally discovered in bacterial immunity, pyroptosis has gradually become a recognized form of RCD in biological scenarios. Pyroptosis serves as an effective antimicrobial defense for the host during infection (Aachoui et al., 2013). However, the mutations in NOD-like receptor (NLR) proteins or the persistence of sterile inflammatory stimuli can lead to excessive pyroptosis, which is harmful to the host and can increase the levels of inflammatory mediators IL-1β, IL-18, and alarmin high mobility group box-1 (HMGB-1), leading to disease if left unchecked (Bergsbaken et al., 2009).

3.2 Effects of Pyroptotic Cell Death and Inflammation on Atherosclerosis

Inflammation is a primary response of innate immunity and is considered to be the initiator and driver of atherosclerosis. Pyroptosis, an inflammatory form of cell death, has been shown to be involved in atherosclerosis (An et al., 2019). Important functional molecules that result in pyroptosis, including NLRP3, AIM2, and caspase-1, are abundantly expressed and activated in atherosclerosis and are associated with the occurrence, accumulation, and destabilization of atherosclerotic plaques (Ozaki et al., 2015; Hoseini et al., 2018; Pan et al., 2018). The expression of NLRP1 and NLRC4 genes is upregulated in patients with atherosclerosis, and their receptors may result in the systemic alteration in inflammasome activation (Borborema et al., 2020). Caspase-11-GSDMD-mediated pyroptosis and the subsequent proinflammatory response in the pathogenesis of atherosclerosis have also been proved (Jiang M. et al., 2021). Considering that inflammasome and caspase-1 are important factors that induce pyroptosis, both the absence of inflammasome and caspase-1 deficiency

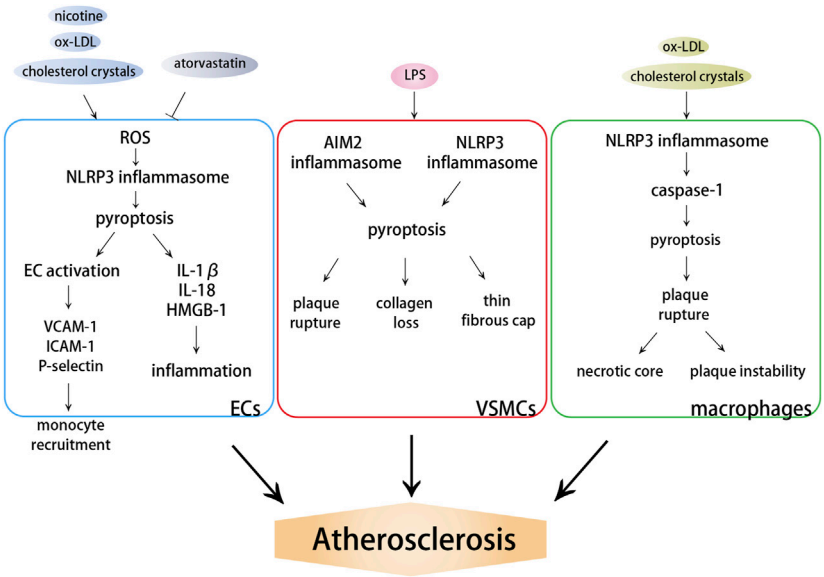

FIGURE 2 | Effects of pyroptosis on atherosclerosis. DAMPs induce the activation of NLRP3 or AIM2 inflammasome, which further activate caspase-dependent pyroptosis. ECs pyroptosis triggers monocyte recruitment into the intima in early atherogenesis. VSMC pyroptosis weakens fibrous caps and contributes to pathological instability in atherosclerosis. Macrophage pyroptosis promotes the formation of necrotic core and aggravates plaque instability in advanced atherosclerotic lesions.

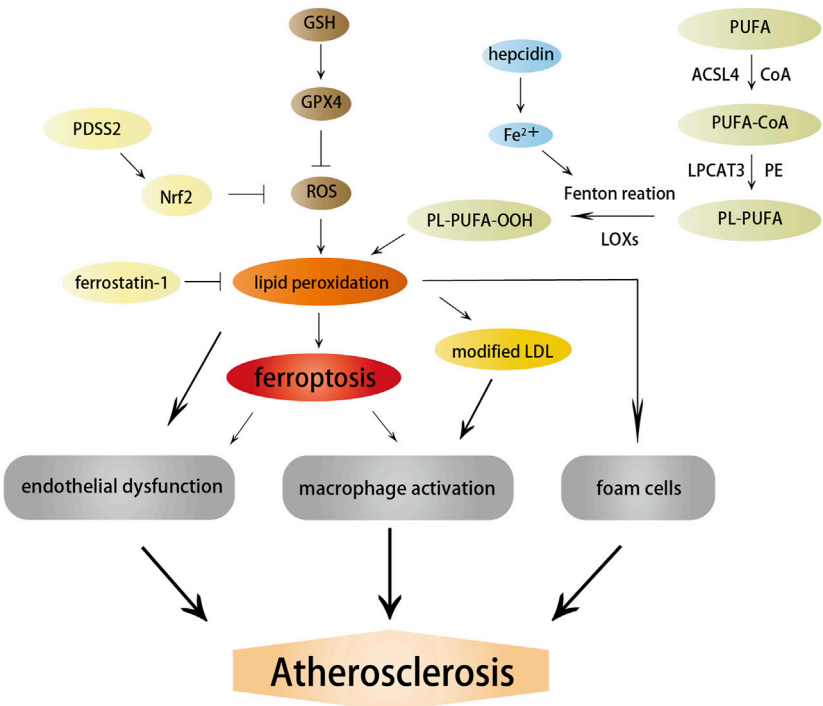

FIGURE 3 | Effects of ferroptosis on atherosclerosis. Ferroptosis and lipid peroxidation induce endothelial dysfunction, macrophage activation, and foam cell formation, contributing to the generation of atherosclerosis. ACSL4, LOXs, and hepcidin promote atherosclerosis by inducing lipid peroxidation and iron overload; in contrast, PDSS2 and ferrostatin-1 can inhibit ferroptosis and atherosclerosis by suppressing lipid peroxidation.

alleviate atherosclerosis (Zheng et al., 2014). Caspase-1 deficiency reduces endothelial cell activation and infiltration of monocytes into intima (Gage et al., 2012; Yin et al., 2015) and attenuates ox-LDL-induced VSMC pyroptosis and IL-1β processing (Li et al., 2020), which all suppress the development of atherosclerosis. The pyroptosis of ECs, VSMCs, and monocytes/macrophages is involved in the repair and injury of the intima, but plays different roles in the progression of atherosclerosis (**Figure 2**).

3.2.1 Endothelial Cells Pyroptosis Triggers Monocyte Recruitment Into the Intima in Early Atherogenesis

Caspase-1-dependent pyroptotic cell death of ECs and resulting increased inflammatory response are involved in atherosclerosis, especially in early atherosclerotic vascular injury. In the context of dyslipidemia and inflammation, the caspase-1–inflammasome pathway in ECs can sense the elevated lipids or DAMPs and other inflammatory mediators and activate ECs (Yin et al., 2015), which is the foremost step in the progress of atherosclerosis. The significantly increased levels of VCAM-1 and ICAM-1 caused by EC activation in ApoE$^{-/-}$ mice fed a high-fat diet were significantly reduced after caspase-1 knockout, indicating that hyperlipidemic stimulation triggered endothelial activation and upregulated adhesion molecule expression and cytokine secretion by activating caspase-1 and promoting EC pyroptosis (Yin et al., 2015). The upregulated expression of these adhesion molecules, which might be caused by pyroptosis, triggered monocyte adhesion. Based on this, EC pyroptosis promoted the recruitment of monocytes into the intima, exposure to hyperlipidemia, uptake of lipids, differentiation into macrophages, and lipid plaque formation, thus contributing to the formation and progression of atherosclerosis (Lopez-Pastrana et al., 2015; Yin et al., 2015). However, if caspase-1 activation and pyroptosis of ECs were attenuated, monocytes were not recruited into the intima and macrophages were removed from the atherosclerotic plaques (Potteaux et al., 2011; Lopez-Pastrana et al., 2015). In addition, the inhibition of caspase-1 in dyslipidemic and inflammatory environments prevented EC pyroptosis and improved EC survival and angiogenesis mediated by vascular endothelial growth factor receptor 2, thereby preserving vascular intima integrity (Lopez-Pastrana et al., 2015). This inhibited the migration and deposition of lipids, monocytes, and SMCs into the intima and further attenuated the progression of atherosclerosis. A recent study found that the protective effects against atherosclerosis of atorvastatin, as a commonly used lipid-lowering drug in clinical practice, did not depend on cholesterol-lowering capacity, but on the ability to restrain the pyroptosis of ECs through the lncRNA NEXN-AS1/NEXN pathway (Wu L. M. et al., 2020). These results proved that caspase-1-dependent pyroptosis induced by lipid metabolism disorder played a critical role in EC activation, inflammation, and early atherosclerosis.

Except for hyperlipidemia, ECs are affected by many other factors. Smoking has long been considered a risk factor for atherosclerosis. Recent studies revealed that the pyroptosis of ECs and macrophages might be a cellular mechanism for the pro-atherosclerotic properties of nicotine with the stimulation of ROS and activation of the NLRP3 inflammasome as the upstream mediators (Wu et al., 2018; Mao et al., 2021). Moreover, trimethylamine N-oxide (TMAO), an endothelial toxic factor, promoted EC pyroptosis through the increased ROS level induced by mitochondrial respiratory complex II subunit succinate dehydrogenase B (SDHB) oxidation, thereby promoting the development of atherosclerosis (Wu P. et al., 2020). The upregulation of SDHB expression and activity could also be induced by low shear stress-mediated TET2 deletion and reduced recruitment of histone deacetylase 2 (Chen J. et al., 2021). A low shear force also could to promote EC pyroptosis through the miR-181b-5p/STAT-3 axis, causing damage to the vascular wall and tissue remodeling and hence leading to the onset and development of atherosclerosis (Xu et al., 2021). In conclusion, ECs play a central role in mediating inflammation. Hyperlipidemia and other proatherogenic risk factors can promote the activation of the inflammasome and pyroptosis of ECs, increase the secretion of adhesion factors, and significantly promote monocyte recruitment and atherosclerosis progression.

3.2.2 Vascular Smooth Muscle Cell Pyroptosis Weakens Fibrous Caps and Contributes to Pathological Instability in Atherosclerosis

The death of VSMCs in atherosclerotic plaques can lead to significant thinning of fibrous caps, loss of collagen and extracellular matrix, and severe vascular inflammation, aggravating plaque instability. Except apoptosis, the pyroptosis of VSMCs is also tied up with the pathogenesis of atherosclerosis. The active pyroptotic indicators, including caspase-1 and IL-1β, overlapping with SMC marker α smooth muscle actin (α-SMA), were examined in human and mice atherosclerotic plaques, especially near the necrosis core, on the plaque surface, and in the intraplaque hemorrhage area, providing evidence that VSMC pyroptosis participated in atherosclerosis and contributed to plaque instability (Li et al., 2020). Pan et al. also reported the increased expression of GSDMD-N in ApoE$^{-/-}$ mice. AIM2 irritates GSDMD activity and pyroptosis through the ASC-caspase-1 pathway in VSMCs, thereby accelerating the atherosclerotic plaque progression (Pan et al., 2018). LPS derived from porphyromonas gingivalis (*Pg*-LPS) caused the pyroptosis of VSMCs and instability of atherosclerotic plaques, which played an important role in the occurrence and development of atherosclerosis (Liu G. et al., 2016). However, the blockage of circular RNA serine/threonine protein phosphatase PP1-gamma catalytic subunit (circPPP1CC) relieved the *Pg*-LPS-induced pyroptosis of VSMCs and atherosclerosis by inhibiting the HMGB-1/TLR9/AIM2 pathway (Liu J. et al., 2021). In advanced plaques, the proliferation of VSMCs promoted fibrous cap formation and contributed to plaque stability (Basatemur et al., 2019). To sum up, as a form of cell death of VSMCs in plaques, pyroptosis weakened the fibrous cap and promoted plaque rupture.

3.2.3 Macrophage Pyroptosis Promotes the Formation of Necrotic Core and Aggravates Plaque Instability in Advanced Atherosclerotic Lesions

Ox-LDL and cholesterol crystals could also trigger NLRP3 inflammasome activation and caspase-1 production in macrophages, leading to caspase-1-mediated pyroptosis (Duewell et al., 2010; Rajamaki et al., 2010). Rajamäki et al. reported that the silencing of NLRP3 receptors, one of the key components of the NLRP3 inflammasome, completely eliminated the cholesterol crystals-induced IL-1β secretion, thus confirming NLRP3 inflammasome as the cholesterol crystal-reactive element in macrophages (Rajamaki et al., 2010). The effect of cholesterol crystals and ox-LDL to activate the NLRP3 inflammasome depends on the destruction of lysosomes and the leakage of cathepsin, all of which promote the cleavage and activation of pro-caspase-1 and pyroptosis (Duewell et al., 2010; Karasawa and Takahashi, 2017; Grebe et al., 2018). Sequential pyroptosis occurs in response to ox-LDL or cholesterol crystals, in which one macrophage cannot digest the crystals and dies via pyroptosis. Then, another macrophage engulfs the same crystals and dies via pyroptosis repeatedly. This circulation reduces lesion cellularity, causes and exacerbates pronounced inflammation by releasing inflammatory mediators from pyroptotic cells, and promotes lesion instability (Chang et al., 2013).

Growing evidence shows that the pyroptosis of macrophages increases the risk of atherosclerotic plaque rupture, hence contributing to the formation of necrotic core and plaque instability in atherosclerotic lesions (Lu et al., 2021). Proinflammatory cytokines and mediators relying on caspase-1 in response to proatherogenic risk factors, such as ox-LDL and cholesterol crystals, trigger off pyroptosis of macrophage foam cells, resulting in the formation of lipid-rich pools, the necrotic core of plaques, in late stages of the lesion (Yan and Hansson, 2007). Additionally, the molecules including NLRP3, ASC, caspase-1, IL-1β, and IL-18 are more expressed in unstable plaques compared with stable plaques (Shi X. et al., 2015). Subsequently, Varghese et al. also demonstrated the close relationship between the upregulation of NLRP3 inflammasome-related components and plaque vulnerability, suggesting the possibility of NLRP3 inflammasome activation in promoting plaque instability (Paramel Varghese et al., 2016). Inhibiting NLRP3 expression and reducing macrophage pyroptosis could stabilize atherosclerotic plaques, which undoubtedly hinted at the potential value of blocking pyroptosis (Lin et al., 2021).

Vulnerable plaques are characterized by the accumulation of dead cells, in which up to 50% cells are macrophages. A large majority of dead cells in human atherosclerotic plaques had a typical cell lysis ultrastructure compared with apoptosis (Naghavi et al., 2003). The ruptured plaque showed strong immunoreactivity to caspase-1, but weak immunoreactivity to caspase-3, the executor caspase of apoptosis (Kolodgie et al., 2000). In plaque macrophages, the suppression of apoptosis by the targeted deletion of caspase-3 or p53, which all induced apoptosis, did not subside inflammation and atherosclerotic lesions (Merched et al., 2003). Conversely, macrophages showed the characteristics of cells undergoing pyroptosis accompanied by the increased caspase-1 activation in response to triglyceride treatment, suggesting that the cells in plaque died mainly via pyroptosis, not apoptosis (Son et al., 2013). Taken together, these data suggested that pyroptosis was involved in macrophage death in advanced atherosclerotic lesions and exacerbated inflammation through proinflammatory cytokines, ultimately leading to plaque rupture and acute coronary syndromes.

3.2.4 Recent Discovery of Inhibiting Pyroptosis and Improving Atherosclerosis

Based on the aforementioned understanding, the focus on novel targets and mechanisms has increased in recent years, so as to discover new approaches to intervene pyroptosis and atherosclerosis. For example, IFN regulatory factor-1, which has been found to be upregulated in macrophages of patients with acute coronary syndrome (Guo M. et al., 2019), facilitated macrophage pyroptosis and plaque rupture in atherosclerosis by restraining circ_0029589 through promoting its m6A modification (Guo et al., 2020). Brain-derived neurotrophic factor, which is found at lower levels in patients with coronary artery disease (CAD) than in those without CAD, inhibited ox-LDL-induced NLRP3 inflammasome formation and pyroptosis of ECs through KLF2/HK1-mediated regulation of glucose metabolism and mitochondrial homeostasis (Jin et al., 2021). Aldehyde dehydrogenase 2 has been reported to suppress ox-LDL-induced NLRP3 inflammasome priming and activation by attenuating oxidative stress (Xu et al., 2020). MicroRNA-302c-3p could directly target NLRP3 and ameliorate aortic inflammation and pyroptosis in ApoE$^{-/-}$ mice (Bai et al., 2021). Further studies are needed on the detailed mechanism of pyroptosis promoting atherosclerosis to find out better targets for atherosclerosis intervention.

4 THE ROLES OF FERROPTOSIS IN ATHEROSCLEROSIS

4.1 Overview of Ferroptosis

Ferroptosis is an iron-dependent form of RCD resulting from the overwhelming accumulation of lipid hydroperoxides and redox imbalance, characterized by a loss of plasma membrane integrity, cytoplasmic and organelles swelling, dysmorphic shrunken mitochondria with the loss of cristae, as well as condensed and ruptured outer membrane, but the morphology of the nucleus remains unchanged (Dixon et al., 2012; Dixon and Stockwell, 2014; Galluzzi et al., 2018). Ferroptosis occurs through iron-catalyzed lipid peroxidation initiated by nonenzymatic mechanisms such as Fenton reaction, and enzymatic mechanisms including lipoxygenases (LOXs) and EGLN prolyl hydroxylases (PHD), which are enzymes responsible for lipid peroxidation and oxygen homeostasis. The increased uptake of iron by transferrin receptor 1 (TFR1) and reduced iron export by ferroportin-1 (FPN1) trigger off iron overload, in which Fenton reaction-generated ferric iron (Fe^{3+}) increases ROS, activates LOXs or PHD, and results in ferroptosis

(Yang and Stockwell, 2008; Gao et al., 2015; Yang et al., 2016). Therefore, the lipid peroxidation and ferroptosis can be prevented by iron chelators such as deferoxamine and dexrazoxane (Dixon et al., 2012; Friedmann Angeli et al., 2014) or by knocking down TFR1 (Gao et al., 2015), whereas decreased expression of ferritin or FPN1 has been testified to be sensitized to ferroptosis (Bao et al., 2020; Chen et al., 2020). In addition to LOXs and PHD, the two other enzymes involved in phospholipid metabolism, especially in the oxidation of specific phosphatidylethanolamine-containing polyunsaturated fatty acids (PUFAs), acyl-CoA synthetase long-chain family member 4 (ACSL4) and lysophosphatidylcholine acyltransferase 3 (LPCAT3), also contribute to ferroptosis (Dixon et al., 2015; Doll et al., 2017; Muller et al., 2017; Xiao et al., 2019). In the presence of iron, PUFAs generate lipid hydroperoxides and then produce toxic lipid free radicals, which transfer protons near PUFAs and trigger a new round of lipid oxidation reactions (Yang et al., 2016). Some radical-trapping antioxidants, such as vitamin E, ferrostatin-1, and liproxstatin-1, exhibit oxidation resistance and ferroptosis resistance (Dixon et al., 2012; Hofmans et al., 2016); they directly trap chain-carrying peroxyl radicals rather than repressing LOXs (Zilka et al., 2017).

Except for increasing iron release into the labile iron pool (LIP) mentioned earlier, impeding the activation of glutathione peroxidase 4 (GPX4) is the classical channel that acts on the occurrence of ferroptosis. As the major protective mechanism of biomembranes against lipid peroxidation by catalyzing the conversion of lipid hydroperoxides into lipid alcohols, the function of GPX4 depends on its cofactor glutathione (GSH) and the plasma membrane cystine/glutamate antiporter system x_c^-, which imports cystine in exchange for intracellular glutamate and generates GSH (Seiler et al., 2008; Yang et al., 2014). GPX4 can be inactivated by the deprivation of GSH through the inhibition of the system x_c^-, as a result of the restrained function of overloaded extracellular glutamate, erastin, sulfasalazine, sorafenib, p53, and activating transcription factor 3 (ATF3) (Yang et al., 2014; Jiang et al., 2015; Hayano et al., 2016; Wang L. et al., 2020). Buthionine-(S, R)-sulfoximine (BSO) is also able to decrease GSH synthesis (Yang et al., 2014), furthermore, some compounds that directly bind and inactivate GPX4, such as RAS-selective-lethal compound 3 (RSL3), ML162, ML210, $FINO_2$, FIN56, and withaferin A, also have the ability to inhibit GPX4 and subsequently induce lipid peroxidation and ferroptosis (Weiwer et al., 2012; Friedmann Angeli et al., 2014; Yang et al., 2014; Shimada et al., 2016; Gaschler et al., 2018; Hassannia et al., 2018). In contrast, the Nrf2–Keap1 pathway has been confirmed to stimulate the system x_c^- and enhance resistance to ferroptosis through Nrf2 overexpression or Keap1 downregulation (Fan et al., 2017). Moreover, several other pathways that manage to regulate the peroxide state and prevent ferroptosis are gradually being discovered and studied. A newly discovered ferroptosis-resistance factor, FSP1, has also been shown to confer protection against ferroptosis as an oxidoreductase that catalyzes the regeneration of ubiquinone (also known as coenzyme Q10, CoQ10), which can trap lipid peroxyl radicals that mediate lipid peroxidation (Bersuker et al., 2019; Doll et al., 2019). GTP cyclohydrolase-1 (GCH1) and its metabolic derivatives tetrahydrobiopterin/dihydrobiopterin (BH4/BH2) have also recently been found to protect against ferroptosis because of the effect of BH4 that selectively deters the autoxidation of phospholipids and accelerates CoQ10 (Kraft et al., 2020). These redox pathways act on the progress of ferroptosis, but their roles and in-depth mechanisms in the pathophysiology of ferroptosis need to be further explored.

Ferroptosis induces the opening of plasma membrane pores, which may be caused by the lipid peroxidation-induced conformational changes in lipid domains and plasma membrane regions (Runas et al., 2016; Agmon et al., 2018). The formation of plasma membrane pores contributes to solute exchange with the external environment, resulting in cell swelling, and then ferroptotic cells undergo rupture and death (Riegman et al., 2020). Moreover, the intercellular propagation of the ferroptosis-inducing signal, including erastin and C' dot nanoparticles but not GPX4 inhibitor, occurs upstream of cell rupture and involves the spread of cell swelling effects through cell populations in an iron- and lipid peroxide-dependent manner (Dolma et al., 2003; Kim et al., 2016; Riegman et al., 2020). Because this wave-like propagation may cause widespread tissue damage (Katikaneni et al., 2020), ferroptosis has been demonstrated to be involved in multiple acute injury and degenerative diseases in various tissues including kidney, liver, heart, and brain (Abdalkader et al., 2018; Fang et al., 2019; Wang M. et al., 2020; Li et al., 2021), and also be a target in the treatment of cancers (Badgley et al., 2020).

4.2 Effects of Ferroptosis on Atherosclerosis

Ferroptosis is a nonapoptotic form of RCD driven by abnormal iron metabolism and lipid peroxidation, which are related to the pathogenesis of atherosclerosis (Vinchi et al., 2020) (**Figure 3**). Nontransferrin-bound serum iron-induced iron overload triggers off ROS production and stimulates monocyte recruitment, leading to vascular oxidative stress and plaque formation (Vinchi et al., 2020). Lipid peroxidation, intraplaque hemorrhages, and iron deposition, which are hallmarks of advanced plaques (Martinet et al., 2019), are also considered as indirect evidence for the onset of ferroptosis. Therefore, it is reasonable to believe that ferroptosis may participate in the occurrence and development of atherosclerosis. Indeed, a recent study confirmed this hypothesis and revealed that the inhibition of ferroptosis alleviated atherosclerosis by reducing lipid peroxidation and endothelial dysfunction in mouse aortic ECs (Bai T. et al., 2020).

Studies on the pathways and regulatory factors related to ferroptosis can also reflect the correlation between ferroptosis and atherosclerosis. GPX4 is responsible for transforming lipid hydroperoxides into nontoxic lipid alcohols, which can effectively abate the damage caused by oxidized lipids to vascular cells. A

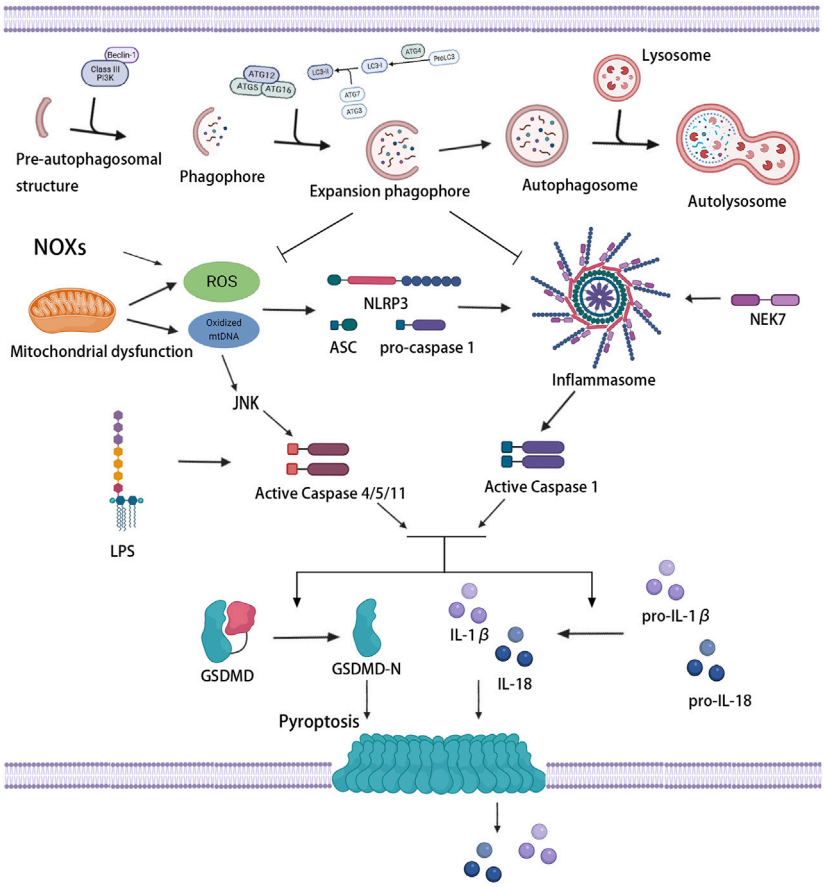

FIGURE 4 | Association between autophagy and pyroptosis. Mitochondrial dysfunction and NOXs induce the massive production of ROS and stimulate the activation of inflammasome and caspase-1. LPS and oxidized mtDNA induce caspase-4/5/11 activation. Activated caspase-1/4/5/11 cleaves GSDMD, induces pyroptotic cell death, and promotes the release of IL-1β and IL-18. Mild oxidative stress triggers off autophagy, which inhibits inflammasome signaling and ROS production, thus protecting against pyroptosis.

decreased GPX level has been demonstrated in atherosclerosis. Guo et al. found that the overexpression of GPX4 that could suppress ferroptosis reduced lipid peroxidation and alleviated atherosclerotic lesions in ApoE$^{-/-}$ mice (Guo et al., 2008). Moreover, the positive correlation between the severity of atherosclerosis and ACSL4 also implied that ferroptosis regulated the occurrence and progression of atherosclerosis (Zhou et al., 2021). Increased expression of ferroptosis-associated LOXs promoted atherosclerosis, while inhibiting 12/15-LOX significantly diminished ox-LDL subendothelial deposition and weakened the development of atherosclerosis (Li C. et al., 2018). Yang et al. recently found that prenyldiphosphate synthase subunit 2 (PDSS2), which was a key enzyme for the synthesis of CoQ10, could alleviate ferroptosis and atherosclerosis by activating antioxidant Nrf2 and suppressing ROS release and iron content (Yang et al., 2021). Radical-trapping antioxidant ferrostatin-1 has also been found to ameliorate iron overload, lipid peroxidation, and upregulation of ROS production induced by high glucose and high lipids, thereby effectively reducing ferroptosis and atherosclerosis (Meng Z. et al., 2021).

Ferritin-mediated iron homeostasis is instrumental in the cardiovascular system (Vinokur et al., 2016), and excessively increased ferritin levels can promote early atherosclerosis and its related complications (Sung et al., 2012). A clinical study found that circulating ferritin levels were independently associated with the changes in carotid intima-media thickness, suggesting that it could be used to monitor the risk of atherosclerosis (Prats-Puig et al., 2016). TFR1 promoted iron absorption and ferritin synthesis, and was found to accumulate significantly in the nuclear region of many foam cells, contributing to the development and rupture of atherosclerotic plaques (Li et al., 2008). Hepcidin, another hormone modulator of iron homeostasis, served as a catalyst for ferroptosis by increasing intracellular iron levels (Nemeth et al., 2004) and enhanced inflammatory atherosclerosis by inducing iron deposition (Habib et al., 2015). Therefore, the factors related to iron metabolism are important targets to the resistance of atherosclerosis, but whether they protect against atherosclerosis by affecting ferroptosis needs further exploration.

5 POSSIBLE ASSOCIATION BETWEEN AUTOPHAGY AND PYROPTOSIS IN ATHEROSCLEROSIS

As shown in **Figure 4**, the level of autophagy has a regulatory effect on pyroptosis. The effect has been verified and applied in treating tumors, infectious diseases, and cardiovascular and cerebrovascular diseases. In recent years, great strides have been made in the mutual regulation of autophagy and pyroptosis in atherosclerosis. Inducing an increase in autophagic activity in vulnerable atherosclerotic plaques restrains NLRP3 inflammasome activation and secretion of inflammatory cytokines, thus ameliorating inflammation and attenuating lipid deposition and pyroptosis (Peng et al., 2018; Cong et al., 2020). In contrast, repressing autophagy aggravates NLRP3 inflammasome activation and pyroptosis (Jiang et al., 2018). As previously mentioned, autophagy defects or autophagy deficiency are normally present in the progression of atherosclerosis. Autophagy deficiency has been shown to lead to atherosclerosis through multiple complementary mechanisms, including overactivation of the inflammasome, accumulation of cytotoxic protein aggregates, and impaired lipid degradation, which are all triggers of pyroptosis.

5.1 Autophagy, Pyroptosis and Oxidative Stress

Various signaling pathways of pyroptosis regulated by autophagy have always been a hot spot for research, especially oxidative stress signaling pathways. Oxidative stress occurs when the production of pro-oxidants or ROS exceeds the capacity of endogenous antioxidants. ROS, which are produced mainly by mitochondria and nicotinamide adenine dinucleotide phosphate (NADPH) oxidase (NOX), refer to the general term of oxygen-containing free radicals and peroxides that can easily form free radicals related to oxygen metabolism in the organism. Wang et al. found that NOX-mediated accumulation of ROS which stimulated by hypoxia promoted pyroptosis, meanwhile, autophagic activity was lessened in this process, suggesting that severe oxidative stress induced the upregulation of pyroptosis, as well as the inhibition of autophagy (Wang S. et al., 2019).

The increase in the levels of intracellular ROS give rise to pyroptosis through the execution of caspase (Li et al., 2015). The activation of caspase depends on the inflammasome, and oxidative stress is an initial signal that induces inflammasome activation and influences the priming phase of inflammasomes (Bauernfeind et al., 2011; Swanson et al., 2019). The massive accumulation of ROS can trigger off the activation of the NLRP3 inflammasome and then induce caspase-1-dependent pyroptosis (Qiu et al., 2017), which may be related to an ROS-sensitive NLRP3 ligand, thioredoxin-interacting protein (TXNIP/VDUP1) (Zhou et al., 2010). Ox-LDL, which is abundant in atherosclerotic lesions, has been certified to increase the activity of ROS and promote the activation of inflammasome and caspase-1, leading to pyroptosis (Ding et al., 2013b; Lin et al., 2013). Furthermore, increased mitochondria-derived ROS and oxidation of liberated mtDNA from damaged or dysfunctional mitochondria can also drive the assembly and activation of the NLRP3 inflammasome (Zhou et al., 2011; Zhong et al., 2018). Oxidized mtDNA was found to bind to NLRP3 directly, promoting inflammasome function and subsequent caspase-1 activation (Shimada et al., 2012). In contrast, the downregulation of NLRP3 inflammasome activation by ROS scavenger could effectively suppress caspase-1 cleavage, IL-1β production, and pyroptosis (Chen et al., 2016; Long et al., 2020). Antioxidants extracellular superoxide dismutase and catalase also showed the ability to prevent caspase-1 activation and pyroptosis (Xi et al., 2016). In addition, c-Jun N-terminal kinase (JNK) signaling played a role in the noncanonical caspase-4/5/11-dependent pathway of pyroptosis (Abe and Morrell, 2016). ROS activated JNK and transferred it into the nucleus, promoted the expression of caspase-11, and initiated pyroptosis (Lupfer et al., 2014). These results suggested that the activation of inflammasomes associated with oxidative stress induced the initiation of pyroptosis, and the extent of pyroptosis seemed to increase with the increase in inflammasome stimulation.

ROS mediates NLRP3 inflammasome activation, but also upregulates autophagy to inhibit the excessive activation of NLPR3 inflammasome (Jiang L. et al., 2021). For autophagy, ROS is one of the upstream modulator (Szumiel, 2011). Under acute or chronic oxidative stress, autophagy is increased or decreased, respectively (Mitter et al., 2014). Mild oxidative stress triggers some cellular survival and repair mechanisms, including autophagy pathways. Indeed, autophagy increases the bioavailability of NO and restrains oxidative stress and vascular inflammation (LaRocca et al., 2012). Autophagy can also selectively clear dysfunctional mitochondria which leads to massive production of ROS, thus inhibiting ROS accumulation and subsequent inflammasome activation (Li Q. et al., 2018; Lin et al., 2019). In addition, as a mitochondrial outer membrane protein that directly interacted with LC3, NIX was found to promote the degradation and removal of excess mitochondria and ROS by regulating autophagy, thus inhibiting ox-LDL-induced pyroptosis of macrophages in atherosclerosis (Peng et al., 2020). However, tumor necrosis factor receptor-associated factor 3 (TRAF3) has been reported to form a complex with TRAF2 and cIAP1 and mediate ubiquitin and degradation of ULK1, in which mitochondrial ROS production and pyroptosis were promoted (Shen et al., 2020). Therefore, ROS-activated autophagic machinery may represent a negative feedback mechanism that limits ROS-regulated caspase-1 activation through removing ROS-damaged organelles and proteins. Nevertheless, conversely, severe oxidative stress produces a large number of damaged proteins, which may lead to an overload of the autophagosome system, resulting in a reduced autophagic activity. Wang et al. reported that a decreased miR-103 level in oxidatively stressed ECs suppresses the interaction between autophagosomes and lysosomes, restraining the end-stage of autophagy, promoting the accumulation of inflammatory mediators, and thus increasing the occurrence of pyroptosis (Wang Y. et al., 2020).

Accordingly, considering that ROS can promote inflammasome activity but autophagy can suppress ROS

production, the suppression of autophagy on inflammasome activity and pyroptosis are related to oxidative stress. ROS blockade with subsequently suppressed inflammasome activity by autophagy is one of the important mechanisms to antagonize pyroptosis. An important feedback network exists between autophagy, NF-κB signaling pathway, and pyroptosis (Gao Y. et al., 2020). Wang et al. reported that enhanced autophagy prevented pyroptotic cell death by eliminating excess ROS and negatively mediating the nuclear translocation of NF-κB P65 and NLRP3 inflammasome activation (Wang X. et al., 2019). Li et al. found that adrenomedullin protected the steroidogenic functions of Leydig cells against pyroptosis by activating autophagy through the ROS-AMPK-mTOR axis (Li et al., 2019). Autophagy activation reversed the expression of pyroptosis-related proteins by downregulating the level of IL-13 and inhibiting the Janus kinase (JAK)-1/signal transducers and activators of transcription (STAT)-1 signaling pathway (Gao C. et al., 2020). Nrf2/ARE, one of the key pathways involved in oxidative stress, can regulate the expression of scavenger receptor-B in the macrophages of $ApoE^{-/-}$ $Nrf2^{+/+}$ mice, stimulate the rapid uptake of ox-LDL by macrophages, and promote the formation of atherosclerotic plaques (Bozaykut et al., 2014). A recent study further revealed that activation of the Nrf2/ARE pathway might be influenced by autophagy. The blockage of autophagy promoted the pyroptosis of ox-LDL-treated macrophages through the malignant activation between p62 and Nrf2/ARE pathway, which might provide a novel therapeutic target for atherosclerosis (Liu J. et al., 2021). Thereout, autophagy suppresses pyroptosis partly due to its regulation of oxidative stress, while devastating oxidative stress induces pyroptosis by inhibiting autophagy.

5.2 Autophagy, Pyroptosis and Inflammation

Atherosclerosis is a chronic inflammatory disease, and pyroptosis can release the cytoplasmic contents of dead host cells, thus providing an effective signal to initiate an inflammatory cascade, which exacerbates vascular inflammation and atherosclerosis (Man et al., 2017). Some proinflammatory cytokines are expressed in human atherosclerotic lesions, particularly in relation to infiltrating macrophages. Macrophages are considered as the primary sources of IL-1β and IL-18, which are two major substrates of caspase-1 and are mainly responsible for caspase-1-mediated pyroptosis in atherosclerosis, promoting plaque destruction and arterial thrombosis through the release of chemokines, matrix metalloproteinases, and proteases (Dinarello, 2011). Vromman et al. found that IL-1β inhibition promoted the tilt of monocytes toward a less inflammatory state during atherosclerosis and reduced the size of established atherosclerosis (Vromman et al., 2019). Moreover, IL-1β inhibition could recede the expression of VCAM-1 and monocyte chemotactic protein-1 (MCP-1), thus preventing the recruitment of monocytes or macrophages into the intima and significantly reducing atherosclerotic lesions (Kirii et al., 2003). The Canakinumab Anti-inflammatory Thrombosis Outcome Study trial involving 10,061 patients with previous myocardial infarction also revealed that anti-inflammatory therapy targeting the IL-1β innate immune pathway resulted in a significant reduction in the recurrence rate of cardiovascular events, independent of a decrease in lipid levels (Ridker et al., 2017). These results established a pivotal role for IL-1β in driving inflammation during atherogenesis and the evolution of advanced atheroma. Similarly, IL-18 has been found to promote the development of atherosclerosis by promoting lipoprotein oxidation, macrophage-derived foam cell formation, and immune cell activation (Bahrami et al., 2021). Even so, Gomez et al. demonstrated the atheroprotective effects of IL-1β in advanced atherosclerotic lesions. The results highlighted the importance of promoting inflammatory resolution, while the excessive repression of inflammation disrupted the formation and maintenance of SMC- and collagen-rich fibrous caps, leading to atherosclerotic plaque instability (Gomez et al., 2018). Thus, the excessive release of IL-1β and IL-18 attributed to pyroptosis is one of the factors that aggravate atherosclerosis, but meanwhile, the over-inhibition of inflammation also leads to plaque instability.

Pyroptosis and the release of these inflammatory factors requires the activation of inflammasome. Recent evidence has revealed a complex interplay between autophagy and inflammasome. Autophagy may be accompanied by the activation of inflammasomes. *Pseudomonas aeruginosa* can activate the NLRP3 inflammasome to trigger macrophage autophagy so as to escape intracellular killing (Deng et al., 2016). In addition, as mentioned earlier, mitochondria are involved in inflammasome activation; mitophagy is also stimulated in this process and regulates inflammasome activity by removing damaged mitochondria, thereby providing an important negative feedback mechanism (Green et al., 2011; Nakahira et al., 2011; Zhong et al., 2016). Autophagy moderates inflammation by eliminating active inflammasomes; however, lack of autophagy leads to the opposite effect and thus exacerbates inflammation. Resolvin D2, which is an innate suppressor of inflammation, has been found to promote the degradation of NLRP3 in an autophagy dependent manner; the suppression of autophagy could reverse the inhibition of NLRP3 inflammasome (Cao et al., 2021). LPS-dependent inflammasomes are activated in macrophages whose autophagy is blocked by the genetic ablation of the autophagy regulators ATG16L1 or ATG7, but not in wild-type macrophages, suggesting that autophagy generally suppresses inflammasome activation induced by LPS (Saitoh et al., 2008). The NLRP3 inflammasome can also be activated by oxidative or apoptosis-induced mtDNA, which is released during autophagy repression (Sollberger et al., 2015). Impaired CMA has also been proven to increase NLRP3 inflammasome activation and secretion of IL-1β, promoting vascular inflammation and atherosclerosis (Qiao et al., 2021). Therefore, autophagy can negatively regulate pyroptosis by restraining the activation of the inflammasome and caspase-1/GSDMD pathway (Wang X. et al., 2020). A clinical trial found that excessive inflammation and the pyroptosis of vascular ECs triggered off atherosclerosis in postmenopausal women, which could be ameliorated with estrogen treatment by alleviating EC pyroptosis through estrogen receptor α-mediated activation of autophagy (Meng Q. et al., 2021). For the mechanism underlying

autophagy-dependent inflammation inhibition, it has been suggested that autophagy typically restrains inflammasome signaling and IL-1β production by directing ubiquitinated inflammasome complexes and pro-IL-1β to lysosomes for degradation (Katsnelson et al., 2016; Kimura et al., 2017). In other words, the inflammasome itself may serve as a target for autophagic degradation, thereby facilitating the resolution of the inflammatory responses.

In spite of an activation effect on autophagy, the NLRP3 inflammasome has also been found to suppress protective autophagy through the E2/ERβ/AMPK/mTOR pathway or through caspase-1-mediated cleavage of the TLR adaptor (Lai et al., 2018; Wei et al., 2019). Moreover, the triggering of pyroptosis releases a large number of proinflammatory factors, further aggravating the inflammatory response, which in turn aggravates the autophagy defect; the two synergistically exacerbate atherosclerosis. For example, a high level of myeloid cells trigger receptors 1 (TREM-1) and a low level of Sirt6 are associated with increased risk for all-cause mortality and major adverse cardiovascular events. Also, TREM-1 negatively regulates the expression of Sirt6. TREM-1-mediated pyroptosis may underlie the proatherogenic effects of ox-LDL, which may be limited by Sirt6-induced EC autophagy (Zi et al., 2019). In conclusion, autophagy activation could inhibit pyroptosis and excessive inflammation, thereby improving atherosclerosis and reducing the incidence of adverse cardiovascular events, which associated with decreased inflammasome activity.

5.3 Autophagy, Pyroptosis and Lipid Accumulation

Dyslipidemia, which involves pathologically elevated concentrations of cholesterol and other lipids, is a major risk factor for atherosclerotic diseases (Kopin and Lowenstein, 2017). The inflammasome may be a potential target of atherosclerosis induced by abnormal lipid metabolism. The NLRP3 inflammasome is positively correlated with the severity and prognosis of atherosclerosis in patients with acute coronary syndrome (Afrasyab et al., 2016). When the $LDLR^{-/-}$ mice were transplanted with NLRP3-deficient, ASC-deficient, or IL-1α/β-deficient bone marrow and fed a high cholesterol diet, they had significantly reduced early atherosclerosis and inflammasome-dependent IL-18 levels (Duewell et al., 2010), suggesting that the deficiency of the NLRP3 inflammasome significantly protected proatherogenic mice from disease. Given that pyroptosis is an inflammasome-dependent form of cell death, possible lipotoxic mediators including ox-LDL, cholesterol crystals, saturated fatty acids, and palmitic acid were found to induce pyroptosis in ECs (Hu et al., 2018), which involve mitochondrial injury, oxidative stress, activation of JNK and release of DAMPs. LDL entered the arterial wall and was transformed into ox-LDL due to changes in endothelial permeability and extracellular matrix composition located under the endothelium (Tabas et al., 2007). Ox-LDL might induce EC pyroptosis and promote the development of atherosclerosis by regulating the miR-125a-5p/ten-eleven translocation 2 (TET2) pathway, resulting in mitochondrial dysfunction, increased ROS generation, and NF-κB nuclear transposition that triggered the activation of the NLRP3 inflammasome and inflammatory response (Zhaolin et al., 2019). The effect of ox-LDL on the NLRP3 inflammasome also depended on the upregulated expression of mixed lineage kinase domain-like protein (Wu Q. et al., 2020). Cholesterol crystals, a key pathological marker of atherosclerotic plaque vulnerability, which were observed in human atherosclerotic lesions as they progressed from fatty streaks to more advanced lesions (Katz et al., 1976), could induce ROS production, NLRP3 inflammasome activation, and ultimately pyroptosis of ECs (Yang et al., 2020). The major lipid component of the plasma membrane, lysophosphatidylcholine, was also proved to elicit the activation of the inflammasome and pyroptosis though potassium efflux and lysosomal damage in both ECs and monocytes; this process was involved in the maintenance of inflammation in tissues adjacent to blood vessels and the pathological process of atherosclerosis (Correa et al., 2019). These results suggested that dyslipidemia was an important factor to induce pyroptosis, and inflammasome activation might be an important link between lipid metabolism and inflammation in atherosclerotic lesions. Therefore, regulation of lipid metabolism and inhibition of lipid overaccumulation are important ways to inhibit inflammasome activation and pyroptosis in atherosclerosis.

Besides pyroptosis, lipid accumulation may also lead to defects in autophagy. In advanced human carotid atherosclerosis, accompanied by lipid accumulation, the levels of autophagic proteins ATG5 and LC3β were decreased, while the levels of dysfunctional autophagy markers SQSTM1/p62 and ubiquitin were increased (Li et al., 2016). Defects in autophagic machinery might occur during the formation and maturation of autophagosomes or during the fusion of autophagosomes with lysosomes or lysosomal-mediated degradation. It was widely considered that an autophagy defect in atherosclerosis was attributable to defects in the lysosomal-dependent pathway. Abundant cholesterol crystals in atherosclerotic plaques jeopardized the lysosomal membrane, consequently impeding the autophagy process (Duewell et al., 2010). These findings suggested that lysosomal-mediated cytoplasmic degradation might be restrained in advanced atherosclerosis, rather than the initiation of autophagy itself. Therefore, autophagy may still be actuated in response to the autophagy activator in the plaques, such as ROS and oxidative lipids, but the process becomes dysfunctional in the second stage of lysosomal-dependent degradation.

Endothelial autophagy represents an important mechanism to regulate excess, exogenous lipids and limit lipid accumulation in the vascular wall. Oxidized and natural LDL promotes the formation of autophagosomes, while excess natural or modified LDL appears to be engulfed in the autophagic structure, which is intercepted by endothelial-specific ATG7 knockdown, showing an increase in lipid deposition (Torisu et al., 2016). Recently, Kim et al. found that endothelial lipid accumulation in atherosclerosis is caused by autophagy-related lysosomal dysfunction (Kim et al., 2021). Moreover, autophagy deficiency disturbs the degradation of CAV1, which interacts with caveolae associated protein 1 (CAVIN1) and LC3B, and is

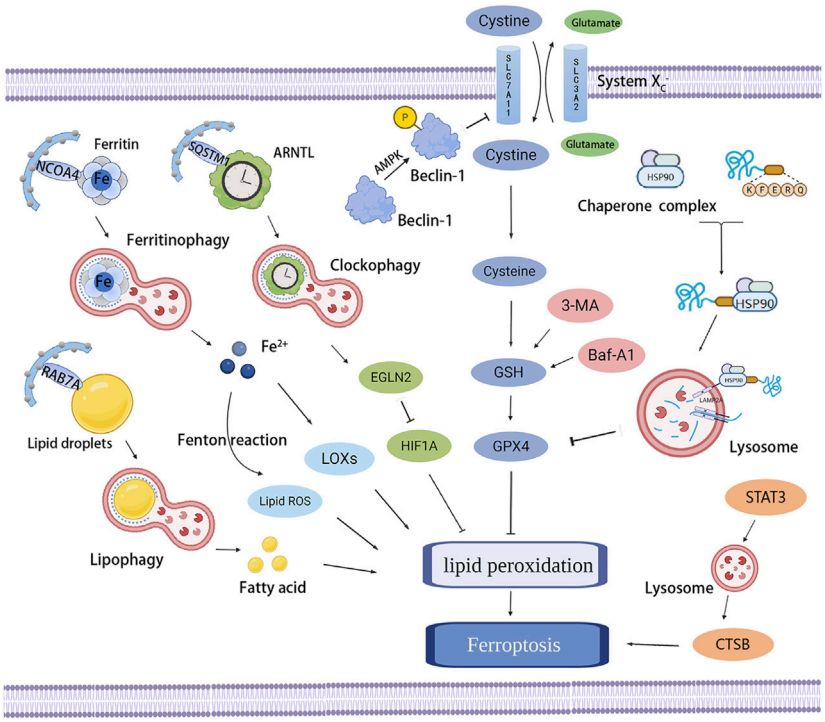

FIGURE 5 | Association between autophagy and ferroptosis. Several types of selective autophagy, including ferritinophagy, lipophagy, clockophagy, and CMA, promote lipid peroxidation and ferroptosis by promoting the degradation of ferritin, lipid droplets, ARNTL, and GPX4, respectively. Beclin-1 is phosphorylated by AMPK and then facilitates ferroptosis by binding and blocking the activity of system x_c^-. Autophagy inhibitors (e.g., 3-MA, Baf-A1) can prevent GSH depletion-dependent ferroptosis. STAT3-mediated CTSB expression and lysosomal cell death promote ferroptosis.

used to form more caveolae in the cell membrane, contributing to LDL transcytosis across ECs (Bai X. et al., 2020). Therefore, the absence of autophagy of ECs is responsible for the prolonged retention of oxidized and natural LDL and increased atherosclerotic burden. Some researchers reported that ox-LDL in atherosclerosis induced EC autophagy, accompanied by apoptosis and increased monolayer permeability; however, when ox-LDL-mediated autophagy was partly inhibited, apoptosis and monolayer permeability were further increased (Wei et al., 2013; Wang Y. et al., 2019).

A recent study demonstrated that activation of the P2RY12 receptor reduced cholesterol efflux and promoted the formation of VSMC-derived foam cells by blocking autophagy in advanced atherosclerosis, suggesting that autophagy is essential in maintaining lipophagic flux and cholesterol homeostasis in VSMCs (Pi et al., 2021). Similarly, as mentioned earlier, intact autophagic machinery is also essential in limiting lipid uptake by macrophages. C1q/tumor necrosis factor-related protein 13 can diminish ox-LDL uptake, retention, and foam cell formation, meanwhile reducing inflammatory responses and lesion areas, which is attributed to the enhanced autophagy in macrophages and accelerated autophagy-lysosome-dependent degradation of CD36 (Wang C. et al., 2019). Gustafsson and colleagues also found that perilipin-2, whose Pro251 variant had a negative correlation with intima-media thickness at baseline and over 30 months of follow-up, initiated a feed-forward cycle in which liver-X-receptor and autophagy activate each other, thus influencing the susceptibility to atherosclerosis through the increased activation of autophagy and stimulation of cholesterol efflux (Saliba-Gustafsson et al., 2019). Based on this, we have reason to believe that enhancing autophagy can inhibit pyroptosis by regulating lipid accumulation in vascular cells, although there is no clear literature confirming this viewpoint.

6 POSSIBLE ASSOCIATION BETWEEN AUTOPHAGY AND FERROPTOSIS IN ATHEROSCLEROSIS

6.1 Regulation of Autophagy on Ferroptosis

It has shown that the knockout or knockdown of ATG5 and ATG7 prevents erastin-induced ferroptosis by diminishing intracellular iron levels and lipid peroxidation (Hou et al., 2016), suggesting that autophagy may play a critical role in the progress of ferroptosis. As shown in **Figure 5**, Song et al. found that the autophagy regulator Beclin-1 was phosphorylated by AMPK and translocated to the plasma membrane, which ultimately facilitated ferroptosis through binding and blocking the activity of system x_c^- (Song et al., 2018). Autophagy also decreases intracellular GSH levels, and thus, autophagy inhibitors such as 3-MA and Baf-A1 can prevent GSH depletion-dependent

ferroptosis (Desideri et al., 2012; Sun Y. et al., 2018). Since lysosomes recycle endogenous iron sources like ferritin and mitochondria, it participates in ferroptosis by influencing cellular iron equilibria and ROS generation (Torii et al., 2016). STAT3 positively regulated ferroptosis by mediating cathepsin B (CTSB) expression. Erastin increased lysosomal membrane permeability and subsequent lysosomal cell death, which could be inhibited by the pharmacological blockade of cathepsin activity. The repression of lysosomal activity and the release of acidic hydrolases into the cytoplasm could restrain ferroptosis (Torii et al., 2016; Gao et al., 2018).

Apart from nonselective autophagy, the excessive activation of selective autophagy that recognizes specific targets and recruits corresponding receptors for subsequent lysosomal degradation mediates ferroptosis. Excess iron can prompt the overproduction of mitochondrial ROS and actuate ferroptosis. Ferritin is the main iron storage protein, which inhibits oxidative stress caused by Fe^{2+}-mediated Fenton reaction and maintains iron homeostasis. Excessive degradation of ferritin can significantly increase intracellular unstable iron levels and enhance sensitivity to ferroptosis (Dufrusine et al., 2019). Ferritin-targeted autophagy, known as ferritinophagy, induces ferroptosis by promoting the release of iron stored in ferritin to the LIP and also lipid peroxidation (Tang et al., 2018). An increasing number of studies reported that activating ferritinophagy promoted ferroptosis by degrading ferritin and inducing TFR1 expression (Du et al., 2019; Sui et al., 2019; Sui et al., 2021), while ferritinophagy deficiency led to cell survival during ferroptosis (Masaldan et al., 2018; Zhang Z. et al., 2020). Ferritinophagy is mediated by nuclear receptor coactivator 4 (NCOA4), which is a cargo receptor for the degradation of ferritin. NCOA4 increases the amount of intracellular iron by binding to FTH1 in autophagosomes and sending the autophagosomes to lysosomes to degrade ferritin (Mancias et al., 2014). Therefore, silencing NCOA4 prevents ferroptosis by abrogating the accumulation of iron and ROS, while the overexpression of NCOA4 increases ferritin degradation and promotes ferroptosis (Gao et al., 2016; Qin et al., 2021). Furthermore, Park et al. confirmed that ferritinophagy was indeed actuated by erastin-induced ROS, providing evidence that the activation of ferritinophagy induced by the ferroptosis inducer was necessary for the initiation of ferroptosis (Park and Chung, 2019).

In addition to ferritinophagy, Yang et al. first revealed that clockophagy, which was a novel mode of selective autophagy, could degrade the core circadian clock protein aryl hydrocarbon receptor nuclear translocator-like protein 1 (ARNTL) depending on the cargo receptor sequestosme 1 (SQSTM1), and favored lipid peroxidation and ferroptosis resulting from type II ferroptosis activators such as RSL3 and FIN56 (Yang et al., 2019). ARNTL could directly repress transcriptional factor egl-9 family hypoxia inducible factor 2 (EGLN2) expression and subsequently increase the level of prosurvival factor hypoxia-inducible factor 1 subunit α (HIF1A), while HIF1A suppressed ferroptosis by regulating lipid metabolism and facilitating the storage of lipids in droplets (Bai et al., 2019). Thus, the clockophagy-mediated degradation of ARNTL induced ferroptosis through the activation of lipid peroxidation. In addition, lipid droplets or increased lipid storage protected against ferroptosis (Kamili et al., 2015). Lipophagy was found to promote ferroptosis by degrading lipid droplets into free fatty acids that then trigger off mitochondrial oxidation, which could be suppressed by the knockout of ATG5 (Bai et al., 2019). In lipophagy, as the key mediator of transporting multivesicular bodies and lysosomes to the lipid droplet surface, RAB7A (a member of the RAS oncogene family) promoted lipid peroxidation and ferroptosis (Schroeder et al., 2015; Bai et al., 2019). Moreover, CMA is a selective autophagy that uses molecular chaperone such as heat shock proteins (HSPs) to stimulate the direct translocation of certain cytoplasmic proteins across the lysosomal membrane by recognizing specific amino acid sequences. It has been shown that autophagy of HSP70 stabilizes lysosomes and inhibits ferroptosis by promoting the transformation of lysosomal redox-active iron into a non-redox-active form (Kurz and Brunk, 2009). HSP member 5 (HSPA5) protected against GPX4 degradation and lipid peroxidation by bounding GPX4 (Zhu et al., 2017). However, Wu et al. found that ferroptosis activators facilitated the degradation of GPX4 protein by increasing the levels of lysosome-associated membrane protein 2a (LAMP2A) and inducing CMA, besides, the inhibition of CMA stabilizes GPX4 and reduces ferroptotic cell death through HSP90 inhibitor (Wu Z. et al., 2019), supporting that HSPs-mediated CMA plays a critical role in ferroptosis. In a nutshell, these findings overturned the previous conclusion that ferroptosis was non-autophagic cell death and confirmed that ferroptosis was an autophagy-mediated form of cell death. The initiation of ferroptosis required autophagy, and ferroptosis was an autophagic process.

6.2 Effect of Ferroptosis on Inflammation

Like pyroptosis, ferroptosis can also promote sterile inflammation and the development of inflammatory diseases by releasing DAMPs (Gong et al., 2020), in which GSH and GPX4 play an important role. As the most abundant antioxidant, GSH can buffer increasing ROS and protect cell from inflammation-associated damage (Mak et al., 2017). Moreover, GPX4 inhibited inflammatory response by suppressing arachidonic acid oxidation and NF-κB pathway activation, meanwhile reducing ROS production (Li C. et al., 2018). In contrast, the disruption of GPX4 could upregulate the expression of 12-lipoxygenase and cyclooxygenase 1, thereby triggering an inflammatory response (Chen et al., 2003). Kang et al. have found that the deficiency of GPX4 in myeloid cells increased the production of caspase-1/11-mediated GSDMD and promoted pyroptosis, which also could promote inflammatory response by releasing plenty of inflammatory factors (Kang et al., 2018).

Ferroptosis-associated peroxidation of LDL induces endothelial dysfunction and macrophages activation; besides, lipid peroxidation increases ROS, decreases NO, and promotes the formation of foam cells, all of these contributing to atherosclerosis (Yu et al., 2021). A recent study found that activation of Sirt1 inhibited excess iron-induced ferroptosis of foam cells through autophagy, providing a novel therapeutic

target for atherosclerosis (Su et al., 2021). However, as mentioned earlier, autophagy induces ferroptosis through a variety of pathways, but the role of these regulatory mechanisms of autophagy in ferroptosis of vascular cells in atherosclerosis remains unclear. Furthermore, although we have manifested a correlation between atherosclerosis and ferroptosis, of course, which mainly involved the ferroptosis-related factors including iron overload and redox pathways, whether ferroptosis is active or passive, in other words, whether it is an automatic response to a stimulus that disrupts metabolic homeostasis or it is a stimulus that directly disrupts the homeostasis is still controversial. Therefore, further studies are needed to explore the exact relationship between ferroptosis and pathophysiological conditions of atherosclerosis, and also the interaction between autophagy and ferroptosis in atherosclerosis.

7 CONCLUSIONS AND FUTURE PERSPECTIVES

Oxidative stress plays a key role in the pathogenesis of numerous types of vascular diseases including atherosclerosis. Once exceeding the capacity of the cellular reductase mechanisms, an overwhelming concentration of ROS triggers off direct or indirect functional damage to different molecules, such as proteins, lipids, and nucleic acids, eventually leading to cell death, which unfortunately leads to, rather than ameliorating, atherosclerosis and plaque instability. ROS-induced inflammasome activation and lipid peroxidation are important features of atherosclerosis, therefore, pyroptosis and ferroptosis as nexus linking oxidative stress, inflammation and lipid metabolism are inevitable to play important roles in the pathogenesis of atherosclerosis. Autophagy is a promising pathway for maintaining plaque cell survival and function. Increasing evidence has shown the crosstalk between autophagy, pyroptosis, and ferroptosis, but whether these different modes of RCD can be integrated into a complete regulatory network remains to be explored.

In atherosclerosis, excessive oxidative stress, inflammation, and lipid peroxidation lead to autophagy dysfunction, pyroptosis, and ferroptosis. The regulation of autophagy, pyroptosis, and ferroptosis is thought to be the potential therapeutic option of atherosclerosis. However, the current studies still have significant limitations. Firstly, atherosclerosis is a complex pathological process involving multiple cells, and the results of a single cell type or a single cell process can hardly explain the actual disease. It is a pity that although we have found clues from separate studies, the specific mechanism of mutual regulation of multiple RCDs and the mutual influence of multiple vascular cells on atherosclerosis has not been implemented. Second, although some studies have used animal models, a large number of experiments *in vivo* are still urgently needed, especially clinical experiments.

In summary, the abnormal states of autophagy, pyroptosis, and ferroptosis in vascular cells including ECs, VSMCs and macrophages associated with oxidative stress, inflammation, and lipid peroxidation are important pathogenesis of atherosclerosis. However, their regulatory mechanisms of atherosclerosis need to be further explored, especially the interaction between multiple RCDs. Therefore, further researches on RCD will develop a broader field for exploring the pathogenesis of atherosclerosis and provide a better clinical treatment for atherosclerosis.

AUTHOR CONTRIBUTIONS

LL, M-XZ, and LZ took the lead in writing the manuscript. DZ, CL, and Y-LL discussed the contents and edited the manuscript.

FUNDING

This work received support by the National Natural Science Foundation of China (81974566, 82004276), Jinan independent innovation team—blood circulation and blood vessel reconstruction innovation team (2020GXRC017), Natural Science Foundation of the Shandong Province (ZR2020KH034), China Postdoctoral Science Foundation (2020M672125, 2021T140429) and Shandong Province Postdoctoral Innovation Project (202003027), Medical and Health Science and Technology Development Project of Shandong Province (2019WS553).

ACKNOWLEDGMENTS

This work is supported by Shandong Provincial Engineering Laboratory of TCM Precision Therapy for Cardiovascular Diseases.

REFERENCES

Aachoui, Y., Sagulenko, V., Miao, E. A., and Stacey, K. J. (2013). Inflammasome-mediated Pyroptotic and Apoptotic Cell Death, and Defense against Infection. *Curr. Opin. Microbiol.* 16 (3), 319–326. doi:10.1016/j.mib.2013.04.004

Abdalkader, M., Lampinen, R., Kanninen, K. M., Malm, T. M., and Liddell, J. R. (2018). Targeting Nrf2 to Suppress Ferroptosis and Mitochondrial Dysfunction in Neurodegeneration. *Front. Neurosci.* 12, 466. doi:10.3389/fnins.2018.00466

Abe, J., and Morrell, C. (2016). Pyroptosis as a Regulated Form of Necrosis: PI+/Annexin V-/High Caspase 1/Low Caspase 9 Activity in Cells = Pyroptosis. *Circ. Res.* 118 (10), 1457–1460. doi:10.1161/CIRCRESAHA.116.308699

Afrasyab, A., Qu, P., Zhao, Y., Peng, K., Wang, H., Lou, D., et al. (2016). Correlation of NLRP3 with Severity and Prognosis of Coronary Atherosclerosis in Acute Coronary Syndrome Patients. *Heart Vessels* 31 (8), 1218–1229. doi:10.1007/s00380-015-0723-8

Aglietti, R. A., Estevez, A., Gupta, A., Ramirez, M. G., Liu, P. S., Kayagaki, N., et al. (2016). GsdmD P30 Elicited by Caspase-11 during Pyroptosis Forms Pores in Membranes. *Proc. Natl. Acad. Sci. U S A.* 113 (28), 7858–7863. doi:10.1073/pnas.1607769113

Agmon, E., Solon, J., Bassereau, P., and Stockwell, B. R. (2018). Modeling the Effects of Lipid Peroxidation during Ferroptosis on Membrane Properties. *Sci. Rep.* 8 (1), 5155. doi:10.1038/s41598-018-23408-0

Allahverdian, S., Chehroudi, A. C., McManus, B. M., Abraham, T., and Francis, G. A. (2014). Contribution of Intimal Smooth Muscle Cells to Cholesterol

Accumulation and Macrophage-like Cells in Human Atherosclerosis. *Circulation* 129 (15), 1551–1559. doi:10.1161/CIRCULATIONAHA.113.005015

Amersfoort, J., Douna, H., Schaftenaar, F. H., Foks, A. C., Kroner, M. J., van Santbrink, P. J., et al. (2018). Defective Autophagy in T Cells Impairs the Development of Diet-Induced Hepatic Steatosis and Atherosclerosis. *Front. Immunol.* 9, 2937. doi:10.3389/fimmu.2018.02937

An, N., Gao, Y., Si, Z., Zhang, H., Wang, L., Tian, C., et al. (2019). Regulatory Mechanisms of the NLRP3 Inflammasome, a Novel Immune-Inflammatory Marker in Cardiovascular Diseases. *Front. Immunol.* 10, 1592. doi:10.3389/fimmu.2019.01592

Andrei, C., Dazzi, C., Lotti, L., Torrisi, M. R., Chimini, G., and Rubartelli, A. (1999). The Secretory Route of the Leaderless Protein Interleukin 1beta Involves Exocytosis of Endolysosome-Related Vesicles. *Mol. Biol. Cel* 10 (5), 1463–1475. doi:10.1091/mbc.10.5.1463

Ashford, T. P., and Porter, K. R. (1962). Cytoplasmic Components in Hepatic Cell Lysosomes. *J. Cel Biol* 12, 198–202. doi:10.1083/jcb.12.1.198

Back, M., Yurdagul, A., Jr., Tabas, I., Oorni, K., and Kovanen, P. T. (2019). Inflammation and its Resolution in Atherosclerosis: Mediators and Therapeutic Opportunities. *Nat. Rev. Cardiol.* 16 (7), 389–406. doi:10.1038/s41569-019-0169-2

Badgley, M. A., Kremer, D. M., Maurer, H. C., DelGiorno, K. E., Lee, H. J., Purohit, V., et al. (2020). Cysteine Depletion Induces Pancreatic Tumor Ferroptosis in Mice. *Science* 368 (6486), 85–89. doi:10.1126/science.aaw9872

Bahrami, A., Sathyapalan, T., and Sahebkar, A. (2021). The Role of Interleukin-18 in the Development and Progression of Atherosclerosis. *Curr. Med. Chem.* 28 (9), 1757–1774. doi:10.2174/0929867327666200427095830

Bai, B., Yang, Y., Ji, S., Wang, S., Peng, X., Tian, C., et al. (2021). MicroRNA-302c-3p Inhibits Endothelial Cell Pyroptosis via Directly Targeting NOD-, LRR- and Pyrin Domain-Containing Protein 3 in Atherosclerosis. *J. Cel Mol Med* 25 (9), 4373–4386. doi:10.1111/jcmm.16500

Bai, T., Li, M., Liu, Y., Qiao, Z., and Wang, Z. (2020). Inhibition of Ferroptosis Alleviates Atherosclerosis through Attenuating Lipid Peroxidation and Endothelial Dysfunction in Mouse Aortic Endothelial Cell. *Free Radic. Biol. Med.* 160, 92–102. doi:10.1016/j.freeradbiomed.2020.07.026

Bai, X., Yang, X., Jia, X., Rong, Y., Chen, L., Zeng, T., et al. (2020). CAV1-CAVIN1-LC3B-mediated Autophagy Regulates High Glucose-Stimulated LDL Transcytosis. *Autophagy* 16 (6), 1111–1129. doi:10.1080/15548627.2019.1659613

Bai, Y., Meng, L., Han, L., Jia, Y., Zhao, Y., Gao, H., et al. (2019). Lipid Storage and Lipophagy Regulates Ferroptosis. *Biochem. Biophys. Res. Commun.* 508 (4), 997–1003. doi:10.1016/j.bbrc.2018.12.039

Bao, W. D., Zhou, X. T., Zhou, L. T., Wang, F., Yin, X., Lu, Y., et al. (2020). Targeting miR-124/Ferroportin Signaling Ameliorated Neuronal Cell Death through Inhibiting Apoptosis and Ferroptosis in Aged Intracerebral Hemorrhage Murine Model. *Aging Cell* 19 (11), e13235. doi:10.1111/acel.13235

Basatemur, G. L., Jorgensen, H. F., Clarke, M. C. H., Bennett, M. R., and Mallat, Z. (2019). Vascular Smooth Muscle Cells in Atherosclerosis. *Nat. Rev. Cardiol.* 16 (12), 727–744. doi:10.1038/s41569-019-0227-9

Bauernfeind, F., Bartok, E., Rieger, A., Franchi, L., Nunez, G., and Hornung, V. (2011). Cutting Edge: Reactive Oxygen Species Inhibitors Block Priming, but Not Activation, of the NLRP3 Inflammasome. *J. Immunol.* 187 (2), 613–617. doi:10.4049/jimmunol.1100613

Bauernfeind, F. G., Horvath, G., Stutz, A., Alnemri, E. S., MacDonald, K., Speert, D., et al. (2009). Cutting Edge: NF-kappaB Activating Pattern Recognition and Cytokine Receptors License NLRP3 Inflammasome Activation by Regulating NLRP3 Expression. *J. Immunol.* 183 (2), 787–791. doi:10.4049/jimmunol.0901363

Bergsbaken, T., Fink, S. L., and Cookson, B. T. (2009). Pyroptosis: Host Cell Death and Inflammation. *Nat. Rev. Microbiol.* 7 (2), 99–109. doi:10.1038/nrmicro2070

Bernard, A., and Klionsky, D. J. (2014). Defining the Membrane Precursor Supporting the Nucleation of the Phagophore. *Autophagy* 10 (1), 1–2. doi:10.4161/auto.27242

Bersuker, K., Hendricks, J. M., Li, Z., Magtanong, L., Ford, B., Tang, P. H., et al. (2019). The CoQ Oxidoreductase FSP1 Acts Parallel to GPX4 to Inhibit Ferroptosis. *Nature* 575 (7784), 688–692. doi:10.1038/s41586-019-1705-2

Borborema, M. E. A., Crovella, S., Oliveira, D., and de Azevedo Silva, J. (2020). Inflammasome Activation by NLRP1 and NLRC4 in Patients with Coronary Stenosis. *Immunobiology* 225 (3), 151940. doi:10.1016/j.imbio.2020.151940

Boucher, D., Monteleone, M., Coll, R. C., Chen, K. W., Ross, C. M., Teo, J. L., et al. (2018). Caspase-1 Self-Cleavage Is an Intrinsic Mechanism to Terminate Inflammasome Activity. *J. Exp. Med.* 215 (3), 827–840. doi:10.1084/jem.20172222

Bozaykut, P., Karademir, B., Yazgan, B., Sozen, E., Siow, R. C., Mann, G. E., et al. (2014). Effects of Vitamin E on Peroxisome Proliferator-Activated Receptor Gamma and Nuclear Factor-Erythroid 2-related Factor 2 in Hypercholesterolemia-Induced Atherosclerosis. *Free Radic. Biol. Med.* 70, 174–181. doi:10.1016/j.freeradbiomed.2014.02.017

Cai, X., She, M., Xu, M., Chen, H., Li, J., Chen, X., et al. (2018). GLP-1 Treatment Protects Endothelial Cells from Oxidative Stress-Induced Autophagy and Endothelial Dysfunction. *Int. J. Biol. Sci.* 14 (12), 1696–1708. doi:10.7150/ijbs.27774

Cao, L., Wang, Y., Wang, Y., Lv, F., Liu, L., and Li, Z. (2021). Resolvin D2 Suppresses NLRP3 Inflammasome by Promoting Autophagy in Macrophages. *Exp. Ther. Med.* 22 (5), 1222. doi:10.3892/etm.2021.10656

Chang, W., Lin, J., Dong, J., and Li, D. (2013). Pyroptosis: an Inflammatory Cell Death Implicates in Atherosclerosis. *Med. Hypotheses* 81 (3), 484–486. doi:10.1016/j.mehy.2013.06.016

Chaulet, H., Desgranges, C., Renault, M. A., Dupuch, F., Ezan, G., Peiretti, F., et al. (2001). Extracellular Nucleotides Induce Arterial Smooth Muscle Cell Migration via Osteopontin. *Circ. Res.* 89 (9), 772–778. doi:10.1161/hh2101.098617

Chen, C. J., Huang, H. S., and Chang, W. C. (2003). Depletion of Phospholipid Hydroperoxide Glutathione Peroxidase Up-Regulates Arachidonate Metabolism by 12S-Lipoxygenase and Cyclooxygenase 1 in Human Epidermoid Carcinoma A431 Cells. *FASEB J.* 17 (12), 1694–1696. doi:10.1096/fj.02-0847fje

Chen, H., Lu, Y., Cao, Z., Ma, Q., Pi, H., Fang, Y., et al. (2016). Cadmium Induces NLRP3 Inflammasome-dependent Pyroptosis in Vascular Endothelial Cells. *Toxicol. Lett.* 246, 7–16. doi:10.1016/j.toxlet.2016.01.014

Chen, P. H., Wu, J., Ding, C. C., Lin, C. C., Pan, S., Bossa, N., et al. (2020). Kinome Screen of Ferroptosis Reveals a Novel Role of ATM in Regulating Iron Metabolism. *Cell Death Differ* 27 (3), 1008–1022. doi:10.1038/s41418-019-0393-7

Chen, P. S., Wang, K. C., Chao, T. H., Chung, H. C., Tseng, S. Y., Luo, C. Y., et al. (2017). Recombinant Thrombomodulin Exerts Anti-autophagic Action in Endothelial Cells and Provides Anti-atherosclerosis Effect in Apolipoprotein E Deficient Mice. *Sci. Rep.* 7 (1), 3284. doi:10.1038/s41598-017-03443-z

Chen, J., Zhang, J., Wu, J., Zhang, S., Liang, Y., Zhou, B., et al. (2021). Low Shear Stress Induced Vascular Endothelial Cell Pyroptosis by TET2/SDHB/ROS Pathway. *Free Radic. Biol. Med.* 162, 582–591. doi:10.1016/j.freeradbiomed.2020.11.017

Chen, Y., Zeng, A., He, S., He, S., Li, C., Mei, W., et al. (2021). Autophagy-Related Genes in Atherosclerosis. *J. Healthc. Eng.* 2021, 6402206. doi:10.1155/2021/6402206

Cheng, J., Qiao, L., Xu, X., Zhai, C., Zhao, K., Ji, X., et al. (2015). Lower AMP-Activated Protein Kinase Level Is Associated with the Vulnerability of Coronary Atherosclerotic Plaques by Attenuating the Expression of Monocyte Autophagy. *Coron. Artery Dis.* 26 (4), 322–327. doi:10.1097/MCA.0000000000000243

Cho, K., and Choi, S. H. (2019). ASK1 Mediates Apoptosis and Autophagy during oxLDL-CD36 Signaling in Senescent Endothelial Cells. *Oxid Med. Cel Longev* 2019, 2840437. doi:10.1155/2019/2840437

Clarke, M. C., Talib, S., Figg, N. L., and Bennett, M. R. (2010). Vascular Smooth Muscle Cell Apoptosis Induces Interleukin-1-Directed Inflammation: Effects of Hyperlipidemia-Mediated Inhibition of Phagocytosis. *Circ. Res.* 106 (2), 363–372. doi:10.1161/CIRCRESAHA.109.208389

Clement, M., Raffort, J., Lareyre, F., Tsiantoulas, D., Newland, S., Lu, Y., et al. (2019). Impaired Autophagy in CD11b(+) Dendritic Cells Expands CD4(+) Regulatory T Cells and Limits Atherosclerosis in Mice. *Circ. Res.* 125 (11), 1019–1034. doi:10.1161/CIRCRESAHA.119.315248

Cong, L., Gao, Z., Zheng, Y., Ye, T., Wang, Z., Wang, P., et al. (2020). Electrical Stimulation Inhibits Val-boroPro-Induced Pyroptosis in THP-1 Macrophages

via Sirtuin3 Activation to Promote Autophagy and Inhibit ROS Generation. *Aging (Albany NY)* 12 (7), 6415–6435. doi:10.18632/aging.103038

Correa, R., Silva, L. F. F., Ribeiro, D. J. S., Almeida, R. D. N., Santos, I. O., Correa, L. H., et al. (2019). Lysophosphatidylcholine Induces NLRP3 Inflammasome-Mediated Foam Cell Formation and Pyroptosis in Human Monocytes and Endothelial Cells. *Front. Immunol.* 10, 2927. doi:10.3389/fimmu.2019.02927

Del Re, D. P., Amgalan, D., Linkermann, A., Liu, Q., and Kitsis, R. N. (2019). Fundamental Mechanisms of Regulated Cell Death and Implications for Heart Disease. *Physiol. Rev.* 99 (4), 1765–1817. doi:10.1152/physrev.00022.2018

Deng, Q., Wang, Y., Zhang, Y., Li, M., Li, D., Huang, X., et al. (2016). *Pseudomonas aeruginosa* Triggers Macrophage Autophagy to Escape Intracellular Killing by Activation of the NLRP3 Inflammasome. *Infect. Immun.* 84 (1), 56–66. doi:10.1128/IAI.00945-15

Denton, D., and Kumar, S. (2019). Autophagy-dependent Cell Death. *Cel Death Differ* 26 (4), 605–616. doi:10.1038/s41418-018-0252-y

Desideri, E., Filomeni, G., and Ciriolo, M. R. (2012). Glutathione Participates in the Modulation of Starvation-Induced Autophagy in Carcinoma Cells. *Autophagy* 8 (12), 1769–1781. doi:10.4161/auto.22037

Dinarello, C. A. (2011). A Clinical Perspective of IL-1beta as the Gatekeeper of Inflammation. *Eur. J. Immunol.* 41 (5), 1203–1217. doi:10.1002/eji.201141550

Ding, J., Wang, K., Liu, W., She, Y., Sun, Q., Shi, J., et al. (2016). Pore-forming Activity and Structural Autoinhibition of the Gasdermin Family. *Nature* 535 (7610), 111–116. doi:10.1038/nature18590

Ding, Z., Liu, S., Wang, X., Khaidakov, M., Dai, Y., and Mehta, J. L. (2013a). Oxidant Stress in Mitochondrial DNA Damage, Autophagy and Inflammation in Atherosclerosis. *Sci. Rep.* 3, 1077. doi:10.1038/srep01077

Ding, Z., Wang, X., Schnackenberg, L., Khaidakov, M., Liu, S., Singla, S., et al. (2013b). Regulation of Autophagy and Apoptosis in Response to Ox-LDL in Vascular Smooth Muscle Cells, and the Modulatory Effects of the microRNA Hsa-Let-7 G. *Int. J. Cardiol.* 168 (2), 1378–1385. doi:10.1016/j.ijcard.2012.12.045

Dixon, S. J., Lemberg, K. M., Lamprecht, M. R., Skouta, R., Zaitsev, E. M., Gleason, C. E., et al. (2012). Ferroptosis: an Iron-dependent Form of Nonapoptotic Cell Death. *Cell* 149 (5), 1060–1072. doi:10.1016/j.cell.2012.03.042

Dixon, S. J., and Stockwell, B. R. (2014). The Role of Iron and Reactive Oxygen Species in Cell Death. *Nat. Chem. Biol.* 10 (1), 9–17. doi:10.1038/nchembio.1416

Dixon, S. J., Winter, G. E., Musavi, L. S., Lee, E. D., Snijder, B., Rebsamen, M., et al. (2015). Human Haploid Cell Genetics Reveals Roles for Lipid Metabolism Genes in Nonapoptotic Cell Death. *ACS Chem. Biol.* 10 (7), 1604–1609. doi:10.1021/acschembio.5b00245

Doll, S., Freitas, F. P., Shah, R., Aldrovandi, M., da Silva, M. C., Ingold, I., et al. (2019). FSP1 Is a Glutathione-independent Ferroptosis Suppressor. *Nature* 575 (7784), 693–698. doi:10.1038/s41586-019-1707-0

Doll, S., Proneth, B., Tyurina, Y. Y., Panzilius, E., Kobayashi, S., Ingold, I., et al. (2017). ACSL4 Dictates Ferroptosis Sensitivity by Shaping Cellular Lipid Composition. *Nat. Chem. Biol.* 13 (1), 91–98. doi:10.1038/nchembio.2239

Dolma, S., Lessnick, S. L., Hahn, W. C., and Stockwell, B. R. (2003). Identification of Genotype-Selective Antitumor Agents Using Synthetic Lethal Chemical Screening in Engineered Human Tumor Cells. *Cancer Cell* 3 (3), 285–296. doi:10.1016/s1535-6108(03)00050-3

Du, J., Wang, T., Li, Y., Zhou, Y., Wang, X., Yu, X., et al. (2019). DHA Inhibits Proliferation and Induces Ferroptosis of Leukemia Cells through Autophagy Dependent Degradation of Ferritin. *Free Radic. Biol. Med.* 131, 356–369. doi:10.1016/j.freeradbiomed.2018.12.011

Duewell, P., Kono, H., Rayner, K. J., Sirois, C. M., Vladimer, G., Bauernfeind, F. G., et al. (2010). NLRP3 Inflammasomes Are Required for Atherogenesis and Activated by Cholesterol Crystals. *Nature* 464 (7293), 1357–1361. doi:10.1038/nature08938

Dufrusine, B., Di Francesco, A., Oddi, S., Scipioni, L., Angelucci, C. B., D'Addario, C., et al. (2019). Iron-Dependent Trafficking of 5-Lipoxygenase and Impact on Human Macrophage Activation. *Front. Immunol.* 10, 1347. doi:10.3389/fimmu.2019.01347

Fan, Z., Wirth, A. K., Chen, D., Wruck, C. J., Rauh, M., Buchfelder, M., et al. (2017). Nrf2-Keap1 Pathway Promotes Cell Proliferation and Diminishes Ferroptosis. *Oncogenesis* 6 (8), e371. doi:10.1038/oncsis.2017.65

Fang, S., Wan, X., Zou, X., Sun, S., Hao, X., Liang, C., et al. (2021). Arsenic Trioxide Induces Macrophage Autophagy and Atheroprotection by Regulating ROS-dependent TFEB Nuclear Translocation and AKT/mTOR Pathway. *Cell Death Dis* 12 (1), 88. doi:10.1038/s41419-020-03357-1

Fang, X., Wang, H., Han, D., Xie, E., Yang, X., Wei, J., et al. (2019). Ferroptosis as a Target for protection against Cardiomyopathy. *Proc. Natl. Acad. Sci. U S A.* 116 (7), 2672–2680. doi:10.1073/pnas.1821022116

Fink, S. L., and Cookson, B. T. (2005). Apoptosis, Pyroptosis, and Necrosis: Mechanistic Description of Dead and Dying Eukaryotic Cells. *Infect. Immun.* 73 (4), 1907–1916. doi:10.1128/IAI.73.4.1907-1916.2005

Fink, S. L., and Cookson, B. T. (2006). Caspase-1-dependent Pore Formation during Pyroptosis Leads to Osmotic Lysis of Infected Host Macrophages. *Cell Microbiol* 8 (11), 1812–1825. doi:10.1111/j.1462-5822.2006.00751.x

Fitzwalter, B. E., and Thorburn, A. (2015). Recent Insights into Cell Death and Autophagy. *FEBS J.* 282 (22), 4279–4288. doi:10.1111/febs.13515

Friedmann Angeli, J. P., Schneider, M., Proneth, B., Tyurina, Y. Y., Tyurin, V. A., Hammond, V. J., et al. (2014). Inactivation of the Ferroptosis Regulator Gpx4 Triggers Acute Renal Failure in Mice. *Nat. Cel Biol* 16 (12), 1180–1191. doi:10.1038/ncb3064

Gage, J., Hasu, M., Thabet, M., and Whitman, S. C. (2012). Caspase-1 Deficiency Decreases Atherosclerosis in Apolipoprotein E-Null Mice. *Can. J. Cardiol.* 28 (2), 222–229. doi:10.1016/j.cjca.2011.10.013

Galluzzi, L., Vitale, I., Aaronson, S. A., Abrams, J. M., Adam, D., Agostinis, P., et al. (2018). Molecular Mechanisms of Cell Death: Recommendations of the Nomenclature Committee on Cell Death 2018. *Cel Death Differ* 25 (3), 486–541. doi:10.1038/s41418-017-0012-4

Gao, H., Bai, Y., Jia, Y., Zhao, Y., Kang, R., Tang, D., et al. (2018). Ferroptosis Is a Lysosomal Cell Death Process. *Biochem. Biophys. Res. Commun.* 503 (3), 1550–1556. doi:10.1016/j.bbrc.2018.07.078

Gao, M., Monian, P., Pan, Q., Zhang, W., Xiang, J., and Jiang, X. (2016). Ferroptosis Is an Autophagic Cell Death Process. *Cell Res* 26 (9), 1021–1032. doi:10.1038/cr.2016.95

Gao, M., Monian, P., Quadri, N., Ramasamy, R., and Jiang, X. (2015). Glutaminolysis and Transferrin Regulate Ferroptosis. *Mol. Cel* 59 (2), 298–308. doi:10.1016/j.molcel.2015.06.011

Gao, C., Yan, Y., Chen, G., Wang, T., Luo, C., Zhang, M., et al. (2020). Autophagy Activation Represses Pyroptosis through the IL-13 and JAK1/STAT1 Pathways in a Mouse Model of Moderate Traumatic Brain Injury. *ACS Chem. Neurosci.* 11 (24), 4231–4239. doi:10.1021/acschemneuro.0c00517

Gao, Y., You, X., Liu, Y., Gao, F., Zhang, Y., Yang, J., et al. (2020). Induction of Autophagy Protects Human Dental Pulp Cells from Lipopolysaccharide-Induced Pyroptotic Cell Death. *Exp. Ther. Med.* 19 (3), 2202–2210. doi:10.3892/etm.2020.8475

Gaschler, M. M., Andia, A. A., Liu, H., Csuka, J. M., Hurlocker, B., Vaiana, C. A., et al. (2018). FINO2 Initiates Ferroptosis through GPX4 Inactivation and Iron Oxidation. *Nat. Chem. Biol.* 14 (5), 507–515. doi:10.1038/s41589-018-0031-6

Ge, P., Gao, M., Du, J., Yu, J., and Zhang, L. (2021). Downregulation of microRNA-512-3p Enhances the Viability and Suppresses the Apoptosis of Vascular Endothelial Cells, Alleviates Autophagy and Endoplasmic Reticulum Stress as Well as Represses Atherosclerotic Lesions in Atherosclerosis by Adjusting Spliced/unspliced Ratio of X-Box Binding Protein 1 (XBP-1S/XBP-1U). *Bioengineered* 12 (2), 12469–12481. doi:10.1080/21655979.2021.2006862

Gimbrone, M. A., Jr., and Garcia-Cardena, G. (2016). Endothelial Cell Dysfunction and the Pathobiology of Atherosclerosis. *Circ. Res.* 118 (4), 620–636. doi:10.1161/CIRCRESAHA.115.306301

Gomez, D., Baylis, R. A., Durgin, B. G., Newman, A. A. C., Alencar, G. F., Mahan, S., et al. (2018). Interleukin-1beta Has Atheroprotective Effects in Advanced Atherosclerotic Lesions of Mice. *Nat. Med.* 24 (9), 1418–1429. doi:10.1038/s41591-018-0124-5

Gong, T., Liu, L., Jiang, W., and Zhou, R. (2020). DAMP-sensing Receptors in Sterile Inflammation and Inflammatory Diseases. *Nat. Rev. Immunol.* 20 (2), 95–112. doi:10.1038/s41577-019-0215-7

Grebe, A., Hoss, F., and Latz, E. (2018). NLRP3 Inflammasome and the IL-1 Pathway in Atherosclerosis. *Circ. Res.* 122 (12), 1722–1740. doi:10.1161/CIRCRESAHA.118.311362

Green, D. R., Galluzzi, L., and Kroemer, G. (2011). Mitochondria and the Autophagy-Inflammation-Cell Death axis in Organismal Aging. *Science* 333 (6046), 1109–1112. doi:10.1126/science.1201940

Grootaert, M. O., da Costa Martins, P. A., Bitsch, N., Pintelon, I., De Meyer, G. R., Martinet, W., et al. (2015). Defective Autophagy in Vascular Smooth Muscle

Cells Accelerates Senescence and Promotes Neointima Formation and Atherogenesis. *Autophagy* 11 (11), 2014–2032. doi:10.1080/15548627.2015.1096485

Guo, M., Yan, R., Ji, Q., Yao, H., Sun, M., Duan, L., et al. (2020). IFN Regulatory Factor-1 Induced Macrophage Pyroptosis by Modulating m6A Modification of Circ_0029589 in Patients with Acute Coronary Syndrome. *Int. Immunopharmacol* 86, 106800. doi:10.1016/j.intimp.2020.106800

Guo, F. X., Wu, Q., Li, P., Zheng, L., Ye, S., Dai, X. Y., et al. (2019). The Role of the LncRNA-Fa2h-2-MLKL Pathway in Atherosclerosis by Regulation of Autophagy Flux and Inflammation through mTOR-dependent Signaling. *Cel Death Differ* 26 (9), 1670–1687. doi:10.1038/s41418-018-0235-z

Guo, M., Yan, R., Yao, H., Duan, L., Sun, M., Xue, Z., et al. (2019). IFN Regulatory Factor 1 Mediates Macrophage Pyroptosis Induced by Oxidized Low-Density Lipoprotein in Patients with Acute Coronary Syndrome. *Mediators Inflamm.* 2019, 2917128. doi:10.1155/2019/2917128

Guo, Z., Ran, Q., Roberts, L. J., 2nd, Zhou, L., Richardson, A., Sharan, C., et al. (2008). Suppression of Atherogenesis by Overexpression of Glutathione Peroxidase-4 in Apolipoprotein E-Deficient Mice. *Free Radic. Biol. Med.* 44 (3), 343–352. doi:10.1016/j.freeradbiomed.2007.09.009

Habib, A., Polavarapu, R., Karmali, V., Guo, L., Van Dam, R., Cheng, Q., et al. (2015). Hepcidin-ferroportin axis Controls Toll-like Receptor 4 Dependent Macrophage Inflammatory Responses in Human Atherosclerotic Plaques. *Atherosclerosis* 241 (2), 692–700. doi:10.1016/j.atherosclerosis.2015.06.025

Han, H., Wang, H., Yin, Z., Jiang, H., Fang, M., and Han, J. (2013). Association of Genetic Polymorphisms in ADH and ALDH2 with Risk of Coronary Artery Disease and Myocardial Infarction: a Meta-Analysis. *Gene* 526 (2), 134–141. doi:10.1016/j.gene.2013.05.002

Hassannia, B., Wiernicki, B., Ingold, I., Qu, F., Van Herck, S., Tyurina, Y. Y., et al. (2018). Nano-targeted Induction of Dual Ferroptotic Mechanisms Eradicates High-Risk Neuroblastoma. *J. Clin. Invest.* 128 (8), 3341–3355. doi:10.1172/JCI99032

Hayano, M., Yang, W. S., Corn, C. K., Pagano, N. C., and Stockwell, B. R. (2016). Loss of Cysteinyl-tRNA Synthetase (CARS) Induces the Transsulfuration Pathway and Inhibits Ferroptosis Induced by Cystine Deprivation. *Cel Death Differ* 23 (2), 270–278. doi:10.1038/cdd.2015.93

He, J., Zhang, G., Pang, Q., Yu, C., Xiong, J., Zhu, J., et al. (2017). SIRT6 Reduces Macrophage Foam Cell Formation by Inducing Autophagy and Cholesterol Efflux under Ox-LDL Condition. *FEBS J.* 284 (9), 1324–1337. doi:10.1111/febs.14055

Hofmans, S., Vanden Berghe, T., Devisscher, L., Hassannia, B., Lyssens, S., Joossens, J., et al. (2016). Novel Ferroptosis Inhibitors with Improved Potency and ADME Properties. *J. Med. Chem.* 59 (5), 2041–2053. doi:10.1021/acs.jmedchem.5b01641

Hoseini, Z., Sepahvand, F., Rashidi, B., Sahebkar, A., Masoudifar, A., and Mirzaei, H. (2018). NLRP3 Inflammasome: Its Regulation and Involvement in Atherosclerosis. *J. Cel Physiol* 233 (3), 2116–2132. doi:10.1002/jcp.25930

Hou, W., Xie, Y., Song, X., Sun, X., Lotze, M. T., Zeh, H. J., 3rd, et al. (2016). Autophagy Promotes Ferroptosis by Degradation of Ferritin. *Autophagy* 12 (8), 1425–1428. doi:10.1080/15548627.2016.1187366

Hu, Q., Zhang, T., Yi, L., Zhou, X., and Mi, M. (2018). Dihydromyricetin Inhibits NLRP3 Inflammasome-dependent Pyroptosis by Activating the Nrf2 Signaling Pathway in Vascular Endothelial Cells. *Biofactors* 44 (2), 123–136. doi:10.1002/biof.1395

Hui, B., Hou, X., Liu, R., Liu, X. H., and Hu, Z. (2021). Gypenoside Inhibits Ox-LDL Uptake and Foam Cell Formation through Enhancing Sirt1-FOXO1 Mediated Autophagy Flux Restoration. *Life Sci.* 264, 118721. doi:10.1016/j.lfs.2020.118721

Jia, G., Cheng, G., Gangahar, D. M., and Agrawal, D. K. (2006). Insulin-like Growth Factor-1 and TNF-Alpha Regulate Autophagy through C-Jun N-Terminal Kinase and Akt Pathways in Human Atherosclerotic Vascular Smooth Cells. *Immunol. Cel Biol* 84 (5), 448–454. doi:10.1111/j.1440-1711.2006.01454.x

Jiang, C., Jiang, L., Li, Q., Liu, X., Zhang, T., Dong, L., et al. (2018). Acrolein Induces NLRP3 Inflammasome-Mediated Pyroptosis and Suppresses Migration via ROS-dependent Autophagy in Vascular Endothelial Cells. *Toxicology* 410, 26–40. doi:10.1016/j.tox.2018.09.002

Jiang, L., Kon, N., Li, T., Wang, S. J., Su, T., Hibshoosh, H., et al. (2015). Ferroptosis as a P53-Mediated Activity during Tumour Suppression. *Nature* 520 (7545), 57–62. doi:10.1038/nature14344

Jiang, L., Luo, S., Qiu, T., Li, Q., Jiang, C., Sun, X., et al. (2021). Bidirectional Role of Reactive Oxygen Species during Inflammasome Activation in Acrolein-Induced Human EAhy926 Cells Pyroptosis. *Toxicol. Mech. Methods* 31 (9), 680–689. doi:10.1080/15376516.2021.1953204

Jiang, M., Sun, X., Liu, S., Tang, Y., Shi, Y., Bai, Y., et al. (2021). Caspase-11-Gasdermin D-Mediated Pyroptosis Is Involved in the Pathogenesis of Atherosclerosis. *Front. Pharmacol.* 12, 657486. doi:10.3389/fphar.2021.657486

Jin, H., Zhu, Y., Wang, X. D., Luo, E. F., Li, Y. P., Wang, B. L., et al. (2021). BDNF Corrects NLRP3 Inflammasome-Induced Pyroptosis and Glucose Metabolism Reprogramming through KLF2/HK1 Pathway in Vascular Endothelial Cells. *Cell Signal* 78, 109843. doi:10.1016/j.cellsig.2020.109843

Jung, C. H., Jun, C. B., Ro, S. H., Kim, Y. M., Otto, N. M., Cao, J., et al. (2009). ULK-Atg13-FIP200 Complexes Mediate mTOR Signaling to the Autophagy Machinery. *Mol. Biol. Cel* 20 (7), 1992–2003. doi:10.1091/mbc.E08-12-1249

Kamili, A., Roslan, N., Frost, S., Cantrill, L. C., Wang, D., Della-Franca, A., et al. (2015). TPD52 Expression Increases Neutral Lipid Storage within Cultured Cells. *J. Cel Sci* 128 (17), 3223–3238. doi:10.1242/jcs.167692

Kang, R., Zeh, H. J., Lotze, M. T., and Tang, D. (2011). The Beclin 1 Network Regulates Autophagy and Apoptosis. *Cel Death Differ* 18 (4), 571–580. doi:10.1038/cdd.2010.191

Kang, R., Zeng, L., Zhu, S., Xie, Y., Liu, J., Wen, Q., et al. (2018). Lipid Peroxidation Drives Gasdermin D-Mediated Pyroptosis in Lethal Polymicrobial Sepsis. *Cell Host Microbe* 24 (1), 97–108. e104. doi:10.1016/j.chom.2018.05.009

Karasawa, T., and Takahashi, M. (2017). Role of NLRP3 Inflammasomes in Atherosclerosis. *J. Atheroscler. Thromb.* 24 (5), 443–451. doi:10.5551/jat.RV17001

Katikaneni, A., Jelcic, M., Gerlach, G. F., Ma, Y., Overholtzer, M., and Niethammer, P. (2020). Lipid Peroxidation Regulates Long-Range Wound Detection through 5-lipoxygenase in Zebrafish. *Nat. Cel Biol* 22 (9), 1049–1055. doi:10.1038/s41556-020-0564-2

Katsnelson, M. A., Lozada-Soto, K. M., Russo, H. M., Miller, B. A., and Dubyak, G. R. (2016). NLRP3 Inflammasome Signaling Is Activated by Low-Level Lysosome Disruption but Inhibited by Extensive Lysosome Disruption: Roles for K+ Efflux and Ca2+ Influx. *Am. J. Physiol. Cel Physiol* 311 (1), C83–C100. doi:10.1152/ajpcell.00298.2015

Katz, S. S., Shipley, G. G., and Small, D. M. (1976). Physical Chemistry of the Lipids of Human Atherosclerotic Lesions. Demonstration of a Lesion Intermediate between Fatty Streaks and Advanced Plaques. *J. Clin. Invest.* 58 (1), 200–211. doi:10.1172/JCI108450

Kayagaki, N., Stowe, I. B., Lee, B. L., O'Rourke, K., Anderson, K., Warming, S., et al. (2015). Caspase-11 Cleaves Gasdermin D for Non-canonical Inflammasome Signalling. *Nature* 526 (7575), 666–671. doi:10.1038/nature15541

Kayagaki, N., Warming, S., Lamkanfi, M., Vande Walle, L., Louie, S., Dong, J., et al. (2011). Non-canonical Inflammasome Activation Targets Caspase-11. *Nature* 479 (7371), 117–121. doi:10.1038/nature10558

Kerr, J. F., Wyllie, A. H., and Currie, A. R. (1972). Apoptosis: a Basic Biological Phenomenon with Wide-Ranging Implications in Tissue Kinetics. *Br. J. Cancer* 26 (4), 239–257. doi:10.1038/bjc.1972.33

Kim, J., Kundu, M., Viollet, B., and Guan, K. L. (2011). AMPK and mTOR Regulate Autophagy through Direct Phosphorylation of Ulk1. *Nat. Cel Biol* 13 (2), 132–141. doi:10.1038/ncb2152

Kim, S. E., Zhang, L., Ma, K., Riegman, M., Chen, F., Ingold, I., et al. (2016). Ultrasmall Nanoparticles Induce Ferroptosis in Nutrient-Deprived Cancer Cells and Suppress Tumour Growth. *Nat. Nanotechnol* 11 (11), 977–985. doi:10.1038/nnano.2016.164

Kim, S., Lee, W., and Cho, K. (2021). P62 Links the Autophagy Pathway and the Ubiquitin-Proteasome System in Endothelial Cells during Atherosclerosis. *Int. J. Mol. Sci.* 22 (15), 7791. doi:10.3390/ijms22157791

Kimura, T., Jia, J., Kumar, S., Choi, S. W., Gu, Y., Mudd, M., et al. (2017). Dedicated SNAREs and Specialized TRIM Cargo Receptors Mediate Secretory Autophagy. *EMBO J.* 36 (1), 42–60. doi:10.15252/embj.201695081

Kirii, H., Niwa, T., Yamada, Y., Wada, H., Saito, K., Iwakura, Y., et al. (2003). Lack of Interleukin-1beta Decreases the Severity of Atherosclerosis in ApoE-Deficient Mice. *Arterioscler Thromb. Vasc. Biol.* 23 (4), 656–660. doi:10.1161/01.ATV.0000064374.15232.C3

Klionsky, D. J., Abdelmohsen, K., Abe, A., Abedin, M. J., Abeliovich, H., Acevedo Arozena, A., et al. (2016). Guidelines for the Use and Interpretation of Assays

for Monitoring Autophagy (3rd Edition). *Autophagy* 12 (1), 1–222. doi:10.1080/15548627.2015.1100356

Klionsky, D. J., and Emr, S. D. (2000). Autophagy as a Regulated Pathway of Cellular Degradation. *Science* 290 (5497), 1717–1721. doi:10.1126/science.290.5497.1717

Kolodgie, F. D., Narula, J., Burke, A. P., Haider, N., Farb, A., Hui-Liang, Y., et al. (2000). Localization of Apoptotic Macrophages at the Site of Plaque Rupture in Sudden Coronary Death. *Am. J. Pathol.* 157 (4), 1259–1268. doi:10.1016/S0002-9440(10)64641-X

Kopin, L., and Lowenstein, C. (2017). Dyslipidemia. *Ann. Intern. Med.* 167 (11), ITC81–ITC96. doi:10.7326/AITC201712050

Kraft, V. A. N., Bezjian, C. T., Pfeiffer, S., Ringelstetter, L., Muller, C., Zandkarimi, F., et al. (2020). GTP Cyclohydrolase 1/Tetrahydrobiopterin Counteract Ferroptosis through Lipid Remodeling. *ACS Cent. Sci.* 6 (1), 41–53. doi:10.1021/acscentsci.9b01063

Kroemer, G., Marino, G., and Levine, B. (2010). Autophagy and the Integrated Stress Response. *Mol. Cel* 40 (2), 280–293. doi:10.1016/j.molcel.2010.09.023

Kumar, S., Nanduri, R., Bhagyaraj, E., Kalra, R., Ahuja, N., Chacko, A. P., et al. (2021). Vitamin D3-VDR-PTPN6 axis Mediated Autophagy Contributes to the Inhibition of Macrophage Foam Cell Formation. *Autophagy* 17 (9), 2273–2289. doi:10.1080/15548627.2020.1822088

Kurz, T., and Brunk, U. T. (2009). Autophagy of HSP70 and Chelation of Lysosomal Iron in a Non-redox-active Form. *Autophagy* 5 (1), 93–95. doi:10.4161/auto.5.1.7248

Lai, M., Yao, H., Shah, S. Z. A., Wu, W., Wang, D., Zhao, Y., et al. (2018). The NLRP3-Caspase 1 Inflammasome Negatively Regulates Autophagy via TLR4-TRIF in Prion Peptide-Infected Microglia. *Front. Aging Neurosci.* 10, 116. doi:10.3389/fnagi.2018.00116

LaRocca, T. J., Henson, G. D., Thorburn, A., Sindler, A. L., Pierce, G. L., and Seals, D. R. (2012). Translational Evidence that Impaired Autophagy Contributes to Arterial Ageing. *J. Physiol.* 590 (14), 3305–3316. doi:10.1113/jphysiol.2012.229690

Li, C., Chen, J. W., Liu, Z. H., Shen, Y., Ding, F. H., Gu, G., et al. (2018). CTRP5 Promotes Transcytosis and Oxidative Modification of Low-Density Lipoprotein and the Development of Atherosclerosis. *Atherosclerosis* 278, 197–209. doi:10.1016/j.atherosclerosis.2018.09.037

Li, C., Deng, X., Xie, X., Liu, Y., Friedmann Angeli, J. P., and Lai, L. (2018). Activation of Glutathione Peroxidase 4 as a Novel Anti-inflammatory Strategy. *Front. Pharmacol.* 9, 1120. doi:10.3389/fphar.2018.01120

Li, P., Bai, Y., Zhao, X., Tian, T., Tang, L., Ru, J., et al. (2018). NR4A1 Contributes to High-Fat Associated Endothelial Dysfunction by Promoting CaMKII-Parkin-Mitophagy Pathways. *Cell Stress Chaperones* 23 (4), 749–761. doi:10.1007/s12192-018-0886-1

Li, Q., Gao, S., Kang, Z., Zhang, M., Zhao, X., Zhai, Y., et al. (2018). Rapamycin Enhances Mitophagy and Attenuates Apoptosis after Spinal Ischemia-Reperfusion Injury. *Front. Neurosci.* 12, 865. doi:10.3389/fnins.2018.00865

Li, H., Huang, S., Wang, S., Zhao, J., Su, L., Zhao, B., et al. (2013). Targeting Annexin A7 by a Small Molecule Suppressed the Activity of Phosphatidylcholine-specific Phospholipase C in Vascular Endothelial Cells and Inhibited Atherosclerosis in Apolipoprotein E(-)/(-)mice. *Cel Death Dis* 4, e806. doi:10.1038/cddis.2013.317

Li, H., Li, J., Li, Y., Singh, P., Cao, L., Xu, L. J., et al. (2012). Sonic Hedgehog Promotes Autophagy of Vascular Smooth Muscle Cells. *Am. J. Physiol. Heart Circ. Physiol.* 303 (11), H1319–H1331. doi:10.1152/ajpheart.00160.2012

Li, L., Tan, J., Miao, Y., Lei, P., and Zhang, Q. (2015). ROS and Autophagy: Interactions and Molecular Regulatory Mechanisms. *Cell Mol Neurobiol* 35 (5), 615–621. doi:10.1007/s10571-015-0166-x

Li, M. Y., Zhu, X. L., Zhao, B. X., Shi, L., Wang, W., Hu, W., et al. (2019). Adrenomedullin Alleviates the Pyroptosis of Leydig Cells by Promoting Autophagy via the ROS-AMPK-mTOR axis. *Cel Death Dis* 10 (7), 489. doi:10.1038/s41419-019-1728-5

Li, S., Zheng, L., Zhang, J., Liu, X., and Wu, Z. (2021). Inhibition of Ferroptosis by Up-Regulating Nrf2 Delayed the Progression of Diabetic Nephropathy. *Free Radic. Biol. Med.* 162, 435–449. doi:10.1016/j.freeradbiomed.2020.10.323

Li, W., Sultana, N., Siraj, N., Ward, L. J., Pawlik, M., Levy, E., et al. (2016). Autophagy Dysfunction and Regulatory Cystatin C in Macrophage Death of Atherosclerosis. *J. Cel Mol Med* 20 (9), 1664–1672. doi:10.1111/jcmm.12859

Li, W., Xu, L. H., Forssell, C., Sullivan, J. L., and Yuan, X. M. (2008). Overexpression of Transferrin Receptor and Ferritin Related to Clinical Symptoms and Destabilization of Human Carotid Plaques. *Exp. Biol. Med. (Maywood)* 233 (7), 818–826. doi:10.3181/0711-RM-320

Li, Y., Niu, X., Xu, H., Li, Q., Meng, L., He, M., et al. (2020). VX-765 Attenuates Atherosclerosis in ApoE Deficient Mice by Modulating VSMCs Pyroptosis. *Exp. Cel Res* 389 (1), 111847. doi:10.1016/j.yexcr.2020.111847

Libby, P., Ridker, P. M., and Hansson, G. K. (2011). Progress and Challenges in Translating the Biology of Atherosclerosis. *Nature* 473 (7347), 317–325. doi:10.1038/nature10146

Lin, J., Shou, X., Mao, X., Dong, J., Mohabeer, N., Kushwaha, K. K., et al. (2013). Oxidized Low Density Lipoprotein Induced Caspase-1 Mediated Pyroptotic Cell Death in Macrophages: Implication in Lesion Instability. *PLoS One* 8 (4), e62148. doi:10.1371/journal.pone.0062148

Lin, Q., Li, S., Jiang, N., Shao, X., Zhang, M., Jin, H., et al. (2019). PINK1-parkin Pathway of Mitophagy Protects against Contrast-Induced Acute Kidney Injury via Decreasing Mitochondrial ROS and NLRP3 Inflammasome Activation. *Redox Biol.* 26, 101254. doi:10.1016/j.redox.2019.101254

Lin, Y., Liu, M., Chen, E., Jiang, W., Shi, W., and Wang, Z. (2021). Bone Marrow-Derived Mesenchymal Stem Cells Microvesicles Stabilize Atherosclerotic Plaques by Inhibiting NLRP3-Mediated Macrophage Pyroptosis. *Cell Biol Int* 45 (4), 820–830. doi:10.1002/cbin.11526

Liu, G., Deng, J., Zhang, Q., Song, W., Chen, S., Lou, X., et al. (2016). Porphyromonas Gingivalis Lipopolysaccharide Stimulation of Vascular Smooth Muscle Cells Activates Proliferation and Calcification. *J. Periodontol.* 87 (7), 828–836. doi:10.1902/jop.2016.150602

Liu, X., Zhang, Z., Ruan, J., Pan, Y., Magupalli, V. G., Wu, H., et al. (2016). Inflammasome-activated Gasdermin D Causes Pyroptosis by Forming Membrane Pores. *Nature* 535 (7610), 153–158. doi:10.1038/nature18629

Liu, J., Wang, C., Li, J., Yu, Y., Liu, Y., Liu, H., et al. (2021). Autophagy Blockage Promotes the Pyroptosis of Ox-LDL-Treated Macrophages by Modulating the p62/Nrf2/ARE axis. *J. Physiol. Biochem.* 77 (3), 419–429. doi:10.1007/s13105-021-00811-2

Liu, J., Wang, Y., Liao, Y., Zhou, Y., and Zhu, J. (2021). Circular RNA PPP1CC Promotes Porphyromonas Gingivalis-Lipopolysaccharide-Induced Pyroptosis of Vascular Smooth Muscle Cells by Activating the HMGB1/TLR9/AIM2 Pathway. *J. Int. Med. Res.* 49 (3), 300060521996564. doi:10.1177/0300060521996564

Liu, S., Jiang, X., Cui, X., Wang, J., Liu, S., Li, H., et al. (2021). Smooth Muscle-specific HuR Knockout Induces Defective Autophagy and Atherosclerosis. *Cel Death Dis* 12 (4), 385. doi:10.1038/s41419-021-03671-2

Lockshin, R. A., and Zakeri, Z. (2004). Apoptosis, Autophagy, and More. *Int. J. Biochem. Cel Biol* 36 (12), 2405–2419. doi:10.1016/j.biocel.2004.04.011

Long, Y., Liu, X., Tan, X. Z., Jiang, C. X., Chen, S. W., Liang, G. N., et al. (2020). ROS-induced NLRP3 Inflammasome Priming and Activation Mediate PCB 118- Induced Pyroptosis in Endothelial Cells. *Ecotoxicol Environ. Saf.* 189, 109937. doi:10.1016/j.ecoenv.2019.109937

Lopez-Pastrana, J., Ferrer, L. M., Li, Y. F., Xiong, X., Xi, H., Cueto, R., et al. (2015). Inhibition of Caspase-1 Activation in Endothelial Cells Improves Angiogenesis: A Novel Therapeutic Potential for Ischemia. *J. Biol. Chem.* 290 (28), 17485–17494. doi:10.1074/jbc.M115.641191

Lu, H., Fan, Y., Qiao, C., Liang, W., Hu, W., Zhu, T., et al. (2017). TFEB Inhibits Endothelial Cell Inflammation and Reduces Atherosclerosis. *Sci. Signal.* 10 (464), eaah4214. doi:10.1126/scisignal.aah4214

Lu, L. Q., Tian, J., Luo, X. J., and Peng, J. (2021). Targeting the Pathways of Regulated Necrosis: a Potential Strategy for Alleviation of Cardio-Cerebrovascular Injury. *Cell Mol Life Sci* 78 (1), 63–78. doi:10.1007/s00018-020-03587-8

Luo, Y., Lu, S., Gao, Y., Yang, K., Wu, D., Xu, X., et al. (2020). Araloside C Attenuates Atherosclerosis by Modulating Macrophage Polarization via Sirt1-Mediated Autophagy. *Aging (Albany NY)* 12 (2), 1704–1724. doi:10.18632/aging.102708

Lupfer, C. R., Anand, P. K., Liu, Z., Stokes, K. L., Vogel, P., Lamkanfi, M., et al. (2014). Reactive Oxygen Species Regulate Caspase-11 Expression and Activation of the Non-canonical NLRP3 Inflammasome during Enteric Pathogen Infection. *Plos Pathog.* 10 (9), e1004410. doi:10.1371/journal.ppat.1004410

Lusis, A. J. (2000). Atherosclerosis. *Nature* 407 (6801), 233–241. doi:10.1038/35025203

Lutgens, E., de Muinck, E. D., Kitslaar, P. J., Tordoir, J. H., Wellens, H. J., and Daemen, M. J. (1999). Biphasic Pattern of Cell Turnover Characterizes the Progression from Fatty Streaks to Ruptured Human Atherosclerotic Plaques. *Cardiovasc. Res.* 41 (2), 473–479. doi:10.1016/s0008-6363(98)00311-3

Ma, S., Chen, J., Feng, J., Zhang, R., Fan, M., Han, D., et al. (2018). Melatonin Ameliorates the Progression of Atherosclerosis via Mitophagy Activation and NLRP3 Inflammasome Inhibition. *Oxid Med. Cel Longev* 2018, 9286458. doi:10.1155/2018/9286458

Mak, T. W., Grusdat, M., Duncan, G. S., Dostert, C., Nonnenmacher, Y., Cox, M., et al. (2017). Glutathione Primes T Cell Metabolism for Inflammation. *Immunity* 46 (4), 675–689. doi:10.1016/j.immuni.2017.03.019

Man, S. M., Karki, R., and Kanneganti, T. D. (2017). Molecular Mechanisms and Functions of Pyroptosis, Inflammatory Caspases and Inflammasomes in Infectious Diseases. *Immunol. Rev.* 277 (1), 61–75. doi:10.1111/imr.12534

Mancias, J. D., Wang, X., Gygi, S. P., Harper, J. W., and Kimmelman, A. C. (2014). Quantitative Proteomics Identifies NCOA4 as the Cargo Receptor Mediating Ferritinophagy. *Nature* 509 (7498), 105–109. doi:10.1038/nature13148

Mao, C., Li, D., Zhou, E., Zhang, J., Wang, C., and Xue, C. (2021). Nicotine Exacerbates Atherosclerosis through a Macrophage-Mediated Endothelial Injury Pathway. *Aging (Albany NY)* 13 (5), 7627–7643. doi:10.18632/aging.202660

Marchio, P., Guerra-Ojeda, S., Vila, J. M., Aldasoro, M., Victor, V. M., and Mauricio, M. D. (2019). Targeting Early Atherosclerosis: A Focus on Oxidative Stress and Inflammation. *Oxid Med. Cel Longev* 2019, 8563845. doi:10.1155/2019/8563845

Martinet, W., Coornaert, I., Puylaert, P., and De Meyer, G. R. Y. (2019). Macrophage Death as a Pharmacological Target in Atherosclerosis. *Front. Pharmacol.* 10, 306. doi:10.3389/fphar.2019.00306

Martinet, W., Schrijvers, D. M., Timmermans, J. P., and Bult, H. (2008). Interactions between Cell Death Induced by Statins and 7-ketocholesterol in Rabbit Aorta Smooth Muscle Cells. *Br. J. Pharmacol.* 154 (6), 1236–1246. doi:10.1038/bjp.2008.181

Martinon, F., Burns, K., and Tschopp, J. (2002). The Inflammasome: a Molecular Platform Triggering Activation of Inflammatory Caspases and Processing of proIL-Beta. *Mol. Cel* 10 (2), 417–426. doi:10.1016/s1097-2765(02)00599-3

Masaldan, S., Clatworthy, S. A. S., Gamell, C., Meggyesy, P. M., Rigopoulos, A. T., Haupt, S., et al. (2018). Iron Accumulation in Senescent Cells Is Coupled with Impaired Ferritinophagy and Inhibition of Ferroptosis. *Redox Biol.* 14, 100–115. doi:10.1016/j.redox.2017.08.015

Mathur, A., Hayward, J. A., and Man, S. M. (2018). Molecular Mechanisms of Inflammasome Signaling. *J. Leukoc. Biol.* 103 (2), 233–257. doi:10.1189/jlb.3MR0617-250R

McKnight, N. C., and Zhenyu, Y. (2013). Beclin 1, an Essential Component and Master Regulator of PI3K-III in Health and Disease. *Curr. Pathobiol Rep.* 1 (4), 231–238. doi:10.1007/s40139-013-0028-5

Meng, Q., Li, Y., Ji, T., Chao, Y., Li, J., Fu, Y., et al. (2021). Estrogen Prevent Atherosclerosis by Attenuating Endothelial Cell Pyroptosis via Activation of Estrogen Receptor Alpha-Mediated Autophagy. *J. Adv. Res.* 28, 149–164. doi:10.1016/j.jare.2020.08.010

Meng, Q., Pu, L., Lu, Q., Wang, B., Li, S., Liu, B., et al. (2021). Morin Hydrate Inhibits Atherosclerosis and LPS-Induced Endothelial Cells Inflammatory Responses by Modulating the NFkappaB Signaling-Mediated Autophagy. *Int. Immunopharmacol* 100, 108096. doi:10.1016/j.intimp.2021.108096

Meng, Z., Liang, H., Zhao, J., Gao, J., Liu, C., Ma, X., et al. (2021). HMOX1 Upregulation Promotes Ferroptosis in Diabetic Atherosclerosis. *Life Sci.* 284, 119935. doi:10.1016/j.lfs.2021.119935

Menghini, R., Casagrande, V., Marino, A., Marchetti, V., Cardellini, M., Stoehr, R., et al. (2014). MiR-216a: a Link between Endothelial Dysfunction and Autophagy. *Cel Death Dis* 5, e1029. doi:10.1038/cddis.2013.556

Merched, A. J., Williams, E., and Chan, L. (2003). Macrophage-specific P53 Expression Plays a Crucial Role in Atherosclerosis Development and Plaque Remodeling. *Arterioscler Thromb. Vasc. Biol.* 23 (9), 1608–1614. doi:10.1161/01.ATV.0000084825.88022.53

Miao, E. A., Rajan, J. V., and Aderem, A. (2011). Caspase-1-induced Pyroptotic Cell Death. *Immunol. Rev.* 243 (1), 206–214. doi:10.1111/j.1600-065X.2011.01044.x

Michiels, C. F., Kurdi, A., Timmermans, J. P., De Meyer, G. R. Y., and Martinet, W. (2016). Spermidine Reduces Lipid Accumulation and Necrotic Core Formation in Atherosclerotic Plaques via Induction of Autophagy. *Atherosclerosis* 251, 319–327. doi:10.1016/j.atherosclerosis.2016.07.899

Mitter, S. K., Song, C., Qi, X., Mao, H., Rao, H., Akin, D., et al. (2014). Dysregulated Autophagy in the RPE Is Associated with Increased Susceptibility to Oxidative Stress and AMD. *Autophagy* 10 (11), 1989–2005. doi:10.4161/auto.36184

Mizushima, N., and Komatsu, M. (2011). Autophagy: Renovation of Cells and Tissues. *Cell* 147 (4), 728–741. doi:10.1016/j.cell.2011.10.026

Mollace, V., Gliozzi, M., Musolino, V., Carresi, C., Muscoli, S., Mollace, R., et al. (2015). Oxidized LDL Attenuates Protective Autophagy and Induces Apoptotic Cell Death of Endothelial Cells: Role of Oxidative Stress and LOX-1 Receptor Expression. *Int. J. Cardiol.* 184, 152–158. doi:10.1016/j.ijcard.2015.02.007

Moore, K. J., Sheedy, F. J., and Fisher, E. A. (2013). Macrophages in Atherosclerosis: a Dynamic Balance. *Nat. Rev. Immunol.* 13 (10), 709–721. doi:10.1038/nri3520

Muller, T., Dewitz, C., Schmitz, J., Schroder, A. S., Brasen, J. H., Stockwell, B. R., et al. (2017). Necroptosis and Ferroptosis Are Alternative Cell Death Pathways that Operate in Acute Kidney Failure. *Cel Mol Life Sci* 74 (19), 3631–3645. doi:10.1007/s00018-017-2547-4

Naghavi, M., Libby, P., Falk, E., Casscells, S. W., Litovsky, S., Rumberger, J., et al. (2003). From Vulnerable Plaque to Vulnerable Patient: a Call for New Definitions and Risk Assessment Strategies: Part II. *Circulation* 108 (15), 1772–1778. doi:10.1161/01.CIR.0000087481.55887.C9

Nakahira, K., Haspel, J. A., Rathinam, V. A., Lee, S. J., Dolinay, T., Lam, H. C., et al. (2011). Autophagy Proteins Regulate Innate Immune Responses by Inhibiting the Release of Mitochondrial DNA Mediated by the NALP3 Inflammasome. *Nat. Immunol.* 12 (3), 222–230. doi:10.1038/ni.1980

Nemeth, E., Tuttle, M. S., Powelson, J., Vaughn, M. B., Donovan, A., Ward, D. M., et al. (2004). Hepcidin Regulates Cellular Iron Efflux by Binding to Ferroportin and Inducing its Internalization. *Science* 306 (5704), 2090–2093. doi:10.1126/science.1104742

Ni, H., Xu, S., Chen, H., and Dai, Q. (2020). Nicotine Modulates CTSS (Cathepsin S) Synthesis and Secretion through Regulating the Autophagy-Lysosomal Machinery in Atherosclerosis. *Arterioscler Thromb. Vasc. Biol.* 40 (9), 2054–2069. doi:10.1161/ATVBAHA.120.314053

Ohsumi, Y. (2001). Molecular Dissection of Autophagy: Two Ubiquitin-like Systems. *Nat. Rev. Mol. Cel Biol* 2 (3), 211–216. doi:10.1038/35056522

Orning, P., Weng, D., Starheim, K., Ratner, D., Best, Z., Lee, B., et al. (2018). Pathogen Blockade of TAK1 Triggers Caspase-8-dependent Cleavage of Gasdermin D and Cell Death. *Science* 362 (6418), 1064–1069. doi:10.1126/science.aau2818

Osonoi, Y., Mita, T., Azuma, K., Nakajima, K., Masuyama, A., Goto, H., et al. (2018). Defective Autophagy in Vascular Smooth Muscle Cells Enhances Cell Death and Atherosclerosis. *Autophagy* 14 (11), 1991–2006. doi:10.1080/15548627.2018.1501132

Ouimet, M., Ediriweera, H., Afonso, M. S., Ramkhelawon, B., Singaravelu, R., Liao, X., et al. (2017). microRNA-33 Regulates Macrophage Autophagy in Atherosclerosis. *Arterioscler Thromb. Vasc. Biol.* 37 (6), 1058–1067. doi:10.1161/ATVBAHA.116.308916

Ozaki, E., Campbell, M., and Doyle, S. L. (2015). Targeting the NLRP3 Inflammasome in Chronic Inflammatory Diseases: Current Perspectives. *J. Inflamm. Res.* 8, 15–27. doi:10.2147/JIR.S51250

Pan, H., and Reilly, M. P. (2019). A Protective Smooth Muscle Cell Transition in Atherosclerosis. *Nat. Med.* 25 (8), 1194–1195. doi:10.1038/s41591-019-0541-0

Pan, J., Han, L., Guo, J., Wang, X., Liu, D., Tian, J., et al. (2018). AIM2 Accelerates the Atherosclerotic Plaque Progressions in ApoE-/- Mice. *Biochem. Biophys. Res. Commun.* 498 (3), 487–494. doi:10.1016/j.bbrc.2018.03.005

Pankratz, F., Hohnloser, C., Bemtgen, X., Jaenich, C., Kreuzaler, S., Hoefer, I., et al. (2018). MicroRNA-100 Suppresses Chronic Vascular Inflammation by Stimulation of Endothelial Autophagy. *Circ. Res.* 122 (3), 417–432. doi:10.1161/CIRCRESAHA.117.311428

Paramel Varghese, G., Folkersen, L., Strawbridge, R. J., Halvorsen, B., Yndestad, A., Ranheim, T., et al. (2016). NLRP3 Inflammasome Expression and Activation in Human Atherosclerosis. *J. Am. Heart Assoc.* 5 (5), e003031. doi:10.1161/JAHA.115.003031

Park, E., and Chung, S. W. (2019). ROS-mediated Autophagy Increases Intracellular Iron Levels and Ferroptosis by Ferritin and Transferrin

Receptor Regulation. *Cel Death Dis* 10 (11), 822. doi:10.1038/s41419-019-2064-5

Parzych, K. R., and Klionsky, D. J. (2014). An Overview of Autophagy: Morphology, Mechanism, and Regulation. *Antioxid. Redox Signal.* 20 (3), 460–473. doi:10.1089/ars.2013.5371

Pavlides, S., Gutierrez-Pajares, J. L., Iturrieta, J., Lisanti, M. P., and Frank, P. G. (2014). Endothelial Caveolin-1 Plays a Major Role in the Development of Atherosclerosis. *Cell Tissue Res* 356 (1), 147–157. doi:10.1007/s00441-013-1767-7

Peng, S., Xu, L. W., Che, X. Y., Xiao, Q. Q., Pu, J., Shao, Q., et al. (2018). Atorvastatin Inhibits Inflammatory Response, Attenuates Lipid Deposition, and Improves the Stability of Vulnerable Atherosclerotic Plaques by Modulating Autophagy. *Front. Pharmacol.* 9, 438. doi:10.3389/fphar.2018.00438

Peng, X., Chen, H., Li, Y., Huang, D., Huang, B., and Sun, D. (2020). Effects of NIX-Mediated Mitophagy on Ox-LDL-Induced Macrophage Pyroptosis in Atherosclerosis. *Cel Biol Int* 44 (7), 1481–1490. doi:10.1002/cbin.11343

Perrotta, P., Van der Veken, B., Van Der Veken, P., Pintelon, I., Roosens, L., Adriaenssens, E., et al. (2020). Partial Inhibition of Glycolysis Reduces Atherogenesis Independent of Intraplaque Neovascularization in Mice. *Arterioscler Thromb. Vasc. Biol.* 40 (5), 1168–1181. doi:10.1161/ATVBAHA.119.313692

Pi, S., Mao, L., Chen, J., Shi, H., Liu, Y., Guo, X., et al. (2021). The P2RY12 Receptor Promotes VSMC-Derived Foam Cell Formation by Inhibiting Autophagy in Advanced Atherosclerosis. *Autophagy* 17 (4), 980–1000. doi:10.1080/15548627.2020.1741202

Potteaux, S., Gautier, E. L., Hutchison, S. B., van Rooijen, N., Rader, D. J., Thomas, M. J., et al. (2011). Suppressed Monocyte Recruitment Drives Macrophage Removal from Atherosclerotic Plaques of Apoe-/- Mice during Disease Regression. *J. Clin. Invest.* 121 (5), 2025–2036. doi:10.1172/JCI43802

Prats-Puig, A., Moreno, M., Carreras-Badosa, G., Bassols, J., Ricart, W., Lopez-Bermejo, A., et al. (2016). Serum Ferritin Relates to Carotid Intima-Media Thickness in Offspring of Fathers with Higher Serum Ferritin Levels. *Arterioscler Thromb. Vasc. Biol.* 36 (1), 174–180. doi:10.1161/ATVBAHA.115.306396

Qiao, L., Ma, J., Zhang, Z., Sui, W., Zhai, C., Xu, D., et al. (2021). Deficient Chaperone-Mediated Autophagy Promotes Inflammation and Atherosclerosis. *Circ. Res.* 129 (12), 1141–1157. doi:10.1161/CIRCRESAHA.121.318908

Qin, X., Zhang, J., Wang, B., Xu, G., Yang, X., Zou, Z., et al. (2021). Ferritinophagy Is Involved in the Zinc Oxide Nanoparticles-Induced Ferroptosis of Vascular Endothelial Cells. *Autophagy* 17 (12), 4266–4285. doi:10.1080/15548627.2021.1911016

Qiu, Z., Lei, S., Zhao, B., Wu, Y., Su, W., Liu, M., et al. (2017). NLRP3 Inflammasome Activation-Mediated Pyroptosis Aggravates Myocardial Ischemia/Reperfusion Injury in Diabetic Rats. *Oxid Med. Cel Longev* 2017, 9743280. doi:10.1155/2017/9743280

Rajamaki, K., Lappalainen, J., Oorni, K., Valimaki, E., Matikainen, S., Kovanen, P. T., et al. (2010). Cholesterol Crystals Activate the NLRP3 Inflammasome in Human Macrophages: a Novel Link between Cholesterol Metabolism and Inflammation. *PLoS One* 5 (7), e11765. doi:10.1371/journal.pone.0011765

Ramirez, C. M., Zhang, X., Bandyopadhyay, C., Rotllan, N., Sugiyama, M. G., Aryal, B., et al. (2019). Caveolin-1 Regulates Atherogenesis by Attenuating Low-Density Lipoprotein Transcytosis and Vascular Inflammation Independently of Endothelial Nitric Oxide Synthase Activation. *Circulation* 140 (3), 225–239. doi:10.1161/CIRCULATIONAHA.118.038571

Ridker, P. M., Everett, B. M., Thuren, T., MacFadyen, J. G., Chang, W. H., Ballantyne, C., et al. (2017). Antiinflammatory Therapy with Canakinumab for Atherosclerotic Disease. *N. Engl. J. Med.* 377 (12), 1119–1131. doi:10.1056/NEJMoa1707914

Riegman, M., Sagie, L., Galed, C., Levin, T., Steinberg, N., Dixon, S. J., et al. (2020). Ferroptosis Occurs through an Osmotic Mechanism and Propagates Independently of Cell Rupture. *Nat. Cel Biol* 22 (9), 1042–1048. doi:10.1038/s41556-020-0565-1

Rong, J. X., Shapiro, M., Trogan, E., and Fisher, E. A. (2003). Transdifferentiation of Mouse Aortic Smooth Muscle Cells to a Macrophage-like State after Cholesterol Loading. *Proc. Natl. Acad. Sci. U S A.* 100 (23), 13531–13536. doi:10.1073/pnas.1735526100

Runas, K. A., Acharya, S. J., Schmidt, J. J., and Malmstadt, N. (2016). Addition of Cleaved Tail Fragments during Lipid Oxidation Stabilizes Membrane Permeability Behavior. *Langmuir* 32 (3), 779–786. doi:10.1021/acs.langmuir.5b02980

Saitoh, T., Fujita, N., Jang, M. H., Uematsu, S., Yang, B. G., Satoh, T., et al. (2008). Loss of the Autophagy Protein Atg16L1 Enhances Endotoxin-Induced IL-1beta Production. *Nature* 456 (7219), 264–268. doi:10.1038/nature07383

Salabei, J. K., Cummins, T. D., Singh, M., Jones, S. P., Bhatnagar, A., and Hill, B. G. (2013). PDGF-mediated Autophagy Regulates Vascular Smooth Muscle Cell Phenotype and Resistance to Oxidative Stress. *Biochem. J.* 451 (3), 375–388. doi:10.1042/BJ20121344

Salabei, J. K., and Hill, B. G. (2013). Implications of Autophagy for Vascular Smooth Muscle Cell Function and Plasticity. *Free Radic. Biol. Med.* 65, 693–703. doi:10.1016/j.freeradbiomed.2013.08.003

Saliba-Gustafsson, P., Pedrelli, M., Gertow, K., Werngren, O., Janas, V., Pourteymour, S., et al. (2019). Subclinical Atherosclerosis and its Progression Are Modulated by PLIN2 through a Feed-Forward Loop between LXR and Autophagy. *J. Intern. Med.* 286 (6), 660–675. doi:10.1111/joim.12951

Santovito, D., Egea, V., Bidzhekov, K., Natarelli, L., Mourao, A., Blanchet, X., et al. (2020). Noncanonical Inhibition of Caspase-3 by a Nuclear microRNA Confers Endothelial protection by Autophagy in Atherosclerosis. *Sci. Transl Med.* 12 (546), eaaz2294. doi:10.1126/scitranslmed.aaz2294

Schroder, K., and Tschopp, J. (2010). The Inflammasomes. *Cell* 140 (6), 821–832. doi:10.1016/j.cell.2010.01.040

Schroeder, B., Schulze, R. J., Weller, S. G., Sletten, A. C., Casey, C. A., and McNiven, M. A. (2015). The Small GTPase Rab7 as a central Regulator of Hepatocellular Lipophagy. *Hepatology* 61 (6), 1896–1907. doi:10.1002/hep.27667

Seiler, A., Schneider, M., Forster, H., Roth, S., Wirth, E. K., Culmsee, C., et al. (2008). Glutathione Peroxidase 4 Senses and Translates Oxidative Stress into 12/15-lipoxygenase Dependent- and AIF-Mediated Cell Death. *Cell Metab* 8 (3), 237–248. doi:10.1016/j.cmet.2008.07.005

Sergin, I., Evans, T. D., Zhang, X., Bhattacharya, S., Stokes, C. J., Song, E., et al. (2017). Exploiting Macrophage Autophagy-Lysosomal Biogenesis as a Therapy for Atherosclerosis. *Nat. Commun.* 8, 15750. doi:10.1038/ncomms15750

Shao, B. Z., Han, B. Z., Zeng, Y. X., Su, D. F., and Liu, C. (2016). The Roles of Macrophage Autophagy in Atherosclerosis. *Acta Pharmacol. Sin* 37 (2), 150–156. doi:10.1038/aps.2015.87

Shen, Y., Liu, W. W., Zhang, X., Shi, J. G., Jiang, S., Zheng, L., et al. (2020). TRAF3 Promotes ROS Production and Pyroptosis by Targeting ULK1 Ubiquitination in Macrophages. *FASEB J.* 34 (5), 7144–7159. doi:10.1096/fj.201903073R

Shi, J., Zhao, Y., Wang, K., Shi, X., Wang, Y., Huang, H., et al. (2015). Cleavage of GSDMD by Inflammatory Caspases Determines Pyroptotic Cell Death. *Nature* 526 (7575), 660–665. doi:10.1038/nature15514

Shi, X., Xie, W. L., Kong, W. W., Chen, D., and Qu, P. (2015). Expression of the NLRP3 Inflammasome in Carotid Atherosclerosis. *J. Stroke Cerebrovasc. Dis.* 24 (11), 2455–2466. doi:10.1016/j.jstrokecerebrovasdis.2015.03.024

Shimada, K., Crother, T. R., Karlin, J., Dagvadorj, J., Chiba, N., Chen, S., et al. (2012). Oxidized Mitochondrial DNA Activates the NLRP3 Inflammasome during Apoptosis. *Immunity* 36 (3), 401–414. doi:10.1016/j.immuni.2012.01.009

Shimada, K., Skouta, R., Kaplan, A., Yang, W. S., Hayano, M., Dixon, S. J., et al. (2016). Global Survey of Cell Death Mechanisms Reveals Metabolic Regulation of Ferroptosis. *Nat. Chem. Biol.* 12 (7), 497–503. doi:10.1038/nchembio.2079

Sollberger, G., Strittmatter, G. E., Grossi, S., Garstkiewicz, M., Auf Dem Keller, U., French, L. E., et al. (2015). Caspase-1 Activity Is Required for UVB-Induced Apoptosis of Human Keratinocytes. *J. Invest. Dermatol.* 135 (5), 1395–1404. doi:10.1038/jid.2014.551

Son, S. J., Rhee, K. J., Lim, J., Kim, T. U., Kim, T. J., and Kim, Y. S. (2013). Triglyceride-induced Macrophage Cell Death Is Triggered by Caspase-1. *Biol. Pharm. Bull.* 36 (1), 108–113. doi:10.1248/bpb.b12-00571

Song, X., Zhu, S., Chen, P., Hou, W., Wen, Q., Liu, J., et al. (2018). AMPK-mediated BECN1 Phosphorylation Promotes Ferroptosis by Directly Blocking System Xc(-) Activity. *Curr. Biol.* 28 (15), 2388–2399 e2385. doi:10.1016/j.cub.2018.05.094

Su, G., Yang, W., Wang, S., Geng, C., and Guan, X. (2021). SIRT1-autophagy axis Inhibits Excess Iron-Induced Ferroptosis of Foam Cells and Subsequently

Increases IL-1Beta and IL-18. *Biochem. Biophys. Res. Commun.* 561, 33–39. doi:10.1016/j.bbrc.2021.05.011

Sui, M., Xu, D., Zhao, W., Lu, H., Chen, R., Duan, Y., et al. (2021). CIRBP Promotes Ferroptosis by Interacting with ELAVL1 and Activating Ferritinophagy during Renal Ischaemia-Reperfusion Injury. *J. Cel Mol Med* 25 (13), 6203–6216. doi:10.1111/jcmm.16567

Sui, S., Zhang, J., Xu, S., Wang, Q., Wang, P., and Pang, D. (2019). Ferritinophagy Is Required for the Induction of Ferroptosis by the Bromodomain Protein BRD4 Inhibitor (+)-JQ1 in Cancer Cells. *Cel Death Dis* 10 (5), 331. doi:10.1038/s41419-019-1564-7

Sun, H., Krauss, R. M., Chang, J. T., and Teng, B. B. (2018). PCSK9 Deficiency Reduces Atherosclerosis, Apolipoprotein B Secretion, and Endothelial Dysfunction. *J. Lipid Res.* 59 (2), 207–223. doi:10.1194/jlr.M078360

Sun, R. Z., Fan, Y., Liang, X., Gong, T. T., Wang, Q., Liu, H., et al. (2018). Rapamycin and FTY720 Alleviate Atherosclerosis by Cross Talk of Macrophage Polarization and Autophagy. *Biomed. Res. Int.* 2018, 1010248. doi:10.1155/2018/1010248

Sun, Y., Zheng, Y., Wang, C., and Liu, Y. (2018). Glutathione Depletion Induces Ferroptosis, Autophagy, and Premature Cell Senescence in Retinal Pigment Epithelial Cells. *Cel Death Dis* 9 (7), 753. doi:10.1038/s41419-018-0794-4

Sung, K. C., Kang, S. M., Cho, E. J., Park, J. B., Wild, S. H., and Byrne, C. D. (2012). Ferritin Is Independently Associated with the Presence of Coronary Artery Calcium in 12,033 Men. *Arterioscler Thromb. Vasc. Biol.* 32 (10), 2525–2530. doi:10.1161/ATVBAHA.112.253088

Swaminathan, B., Goikuria, H., Vega, R., Rodriguez-Antiguedad, A., Lopez Medina, A., Freijo Mdel, M., et al. (2014). Autophagic Marker MAP1LC3B Expression Levels Are Associated with Carotid Atherosclerosis Symptomatology. *PLoS One* 9 (12), e115176. doi:10.1371/journal.pone.0115176

Swanson, K. V., Deng, M., and Ting, J. P. (2019). The NLRP3 Inflammasome: Molecular Activation and Regulation to Therapeutics. *Nat. Rev. Immunol.* 19 (8), 477–489. doi:10.1038/s41577-019-0165-0

Swiader, A., Nahapetyan, H., Faccini, J., D'Angelo, R., Mucher, E., Elbaz, M., et al. (2016). Mitophagy Acts as a Safeguard Mechanism against Human Vascular Smooth Muscle Cell Apoptosis Induced by Atherogenic Lipids. *Oncotarget* 7 (20), 28821–28835. doi:10.18632/oncotarget.8936

Szumiel, I. (2011). Autophagy, Reactive Oxygen Species and the Fate of Mammalian Cells. *Free Radic. Res.* 45 (3), 253–265. doi:10.3109/10715762.2010.525233

Tabas, I., Williams, K. J., and Boren, J. (2007). Subendothelial Lipoprotein Retention as the Initiating Process in Atherosclerosis: Update and Therapeutic Implications. *Circulation* 116 (16), 1832–1844. doi:10.1161/CIRCULATIONAHA.106.676890

Tai, S., Hu, X. Q., Peng, D. Q., Zhou, S. H., and Zheng, X. L. (2016). The Roles of Autophagy in Vascular Smooth Muscle Cells. *Int. J. Cardiol.* 211, 1–6. doi:10.1016/j.ijcard.2016.02.128

Tang, D., Kang, R., Berghe, T. V., Vandenabeele, P., and Kroemer, G. (2019). The Molecular Machinery of Regulated Cell Death. *Cel Res* 29 (5), 347–364. doi:10.1038/s41422-019-0164-5

Tang, M., Chen, Z., Wu, D., and Chen, L. (2018). Ferritinophagy/ferroptosis: Iron-Related Newcomers in Human Diseases. *J. Cel Physiol* 233 (12), 9179–9190. doi:10.1002/jcp.26954

Tanida, I., Ueno, T., and Kominami, E. (2004). LC3 Conjugation System in Mammalian Autophagy. *Int. J. Biochem. Cel Biol* 36 (12), 2503–2518. doi:10.1016/j.biocel.2004.05.009

Tao, H., Yancey, P. G., Blakemore, J. L., Zhang, Y., Ding, L., Jerome, W. G., et al. (2021). Macrophage SR-BI Modulates Autophagy via VPS34 Complex and PPARalpha Transcription of Tfeb in Atherosclerosis. *J. Clin. Invest.* 131 (7), e94229. doi:10.1172/JCI94229

Tavakoli Dargani, Z., Singla, R., Johnson, T., Kukreja, R., and Singla, D. K. (2018). Exosomes Derived from Embryonic Stem Cells Inhibit Doxorubicin and Inflammation-Induced Pyroptosis in Muscle Cells. *Can. J. Physiol. Pharmacol.* 96 (3), 304–307. doi:10.1139/cjpp-2017-0340

Thi, E. P., and Reiner, N. E. (2012). Phosphatidylinositol 3-kinases and Their Roles in Phagosome Maturation. *J. Leukoc. Biol.* 92 (3), 553–566. doi:10.1189/jlb.0212053

Torii, S., Shintoku, R., Kubota, C., Yaegashi, M., Torii, R., Sasaki, M., et al. (2016). An Essential Role for Functional Lysosomes in Ferroptosis of Cancer Cells. *Biochem. J.* 473 (6), 769–777. doi:10.1042/BJ20150658

Torisu, K., Singh, K. K., Torisu, T., Lovren, F., Liu, J., Pan, Y., et al. (2016). Intact Endothelial Autophagy Is Required to Maintain Vascular Lipid Homeostasis. *Aging Cell* 15 (1), 187–191. doi:10.1111/acel.12423

Tyrrell, D. J., Blin, M. G., Song, J., Wood, S. C., Zhang, M., Beard, D. A., et al. (2020). Age-Associated Mitochondrial Dysfunction Accelerates Atherogenesis. *Circ. Res.* 126 (3), 298–314. doi:10.1161/CIRCRESAHA.119.315644

Vinchi, F., Porto, G., Simmelbauer, A., Altamura, S., Passos, S. T., Garbowski, M., et al. (2020). Atherosclerosis Is Aggravated by Iron Overload and Ameliorated by Dietary and Pharmacological Iron Restriction. *Eur. Heart J.* 41 (28), 2681–2695. doi:10.1093/eurheartj/ehz112

Vinokur, V., Weksler-Zangen, S., Berenshtein, E., Eliashar, R., and Chevion, M. (2016). The Loss of Myocardial Benefit Following Ischemic Preconditioning Is Associated with Dysregulation of Iron Homeostasis in Diet-Induced Diabetes. *PLoS One* 11 (7), e0159908. doi:10.1371/journal.pone.0159908

Vion, A. C., Kheloufi, M., Hammoutene, A., Poisson, J., Lasselin, J., Devue, C., et al. (2017). Autophagy Is Required for Endothelial Cell Alignment and Atheroprotection under Physiological Blood Flow. *Proc. Natl. Acad. Sci. U S A.* 114 (41), E8675–E8684. doi:10.1073/pnas.1702223114

Vromman, A., Ruvkun, V., Shvartz, E., Wojtkiewicz, G., Santos Masson, G., Tesmenitsky, Y., et al. (2019). Stage-dependent Differential Effects of Interleukin-1 Isoforms on Experimental Atherosclerosis. *Eur. Heart J.* 40 (30), 2482–2491. doi:10.1093/eurheartj/ehz008

Wang, J., Wang, W. N., Xu, S. B., Wu, H., Dai, B., Jian, D. D., et al. (2018). MicroRNA-214-3p: A Link between Autophagy and Endothelial Cell Dysfunction in Atherosclerosis. *Acta Physiol. (Oxf)* 222 (3), e12973. doi:10.1111/apha.12973

Wang, C., Xu, W., Liang, M., Huang, D., and Huang, K. (2019). CTRP13 Inhibits Atherosclerosis via Autophagy-lysosome-dependent Degradation of CD36. *FASEB J.* 33 (2), 2290–2300. doi:10.1096/fj.201801267RR

Wang, S., Ji, L. Y., Li, L., and Li, J. M. (2019). Oxidative Stress, Autophagy and Pyroptosis in the Neovascularization of Oxygeninduced Retinopathy in Mice. *Mol. Med. Rep.* 19 (2), 927–934. doi:10.3892/mmr.2018.9759

Wang, X., Jiang, L., Shi, L., Yao, K., Sun, X., Yang, G., et al. (2019). Zearalenone Induces NLRP3-dependent Pyroptosis via Activation of NF-kappaB Modulated by Autophagy in INS-1 Cells. *Toxicology* 428, 152304. doi:10.1016/j.tox.2019.152304

Wang, Y., Che, J., Zhao, H., Tang, J., and Shi, G. (2019). Paeoniflorin Attenuates Oxidized Low-Density Lipoprotein-Induced Apoptosis and Adhesion Molecule Expression by Autophagy Enhancement in Human Umbilical Vein Endothelial Cells. *J. Cel Biochem* 120 (6), 9291–9299. doi:10.1002/jcb.28204

Wang, Y., Dubland, J. A., Allahverdian, S., Asonye, E., Sahin, B., Jaw, J. E., et al. (2019). Smooth Muscle Cells Contribute the Majority of Foam Cells in ApoE (Apolipoprotein E)-Deficient Mouse Atherosclerosis. *Arterioscler Thromb. Vasc. Biol.* 39 (5), 876–887. doi:10.1161/ATVBAHA.119.312434

Wang, Z., Liu, B., Zhu, J., Wang, D., and Wang, Y. (2019). Nicotine-mediated Autophagy of Vascular Smooth Muscle Cell Accelerates Atherosclerosis via nAChRs/ROS/NF-kappaB Signaling Pathway. *Atherosclerosis* 284, 1–10. doi:10.1016/j.atherosclerosis.2019.02.008

Wang, C., Yang, W., Liang, X., Song, W., Lin, J., Sun, Y., et al. (2020). MicroRNA-761 Modulates Foam Cell Formation and Inflammation through Autophagy in the Progression of Atherosclerosis. *Mol. Cel Biochem* 474 (1-2), 135–146. doi:10.1007/s11010-020-03839-y

Wang, L., Liu, Y., Du, T., Yang, H., Lei, L., Guo, M., et al. (2020). ATF3 Promotes Erastin-Induced Ferroptosis by Suppressing System X_c^-. *Cel Death Differ* 27 (2), 662–675. doi:10.1038/s41418-019-0380-z

Wang, M., Liu, C. Y., Wang, T., Yu, H. M., Ouyang, S. H., Wu, Y. P., et al. (2020). (+)-Clausenamide Protects against Drug-Induced Liver Injury by Inhibiting Hepatocyte Ferroptosis. *Cel Death Dis* 11 (9), 781. doi:10.1038/s41419-020-02961-5

Wang, T., Sun, C., Hu, L., Gao, E., Li, C., Wang, H., et al. (2020). Sirt6 Stabilizes Atherosclerosis Plaques by Promoting Macrophage Autophagy and Reducing Contact with Endothelial Cells. *Biochem. Cel Biol* 98 (2), 120–129. doi:10.1139/bcb-2019-0057

Wang, X., Li, H., Li, W., Xie, J., Wang, F., Peng, X., et al. (2020). The Role of Caspase-1/gsdmd-Mediated Pyroptosis in Taxol-Induced Cell Death and a Taxol-Resistant Phenotype in Nasopharyngeal Carcinoma Regulated by Autophagy. *Cell Biol Toxicol* 36 (5), 437–457. doi:10.1007/s10565-020-09514-8

Wang, Y., Song, X., Li, Z., Liu, N., Yan, Y., Li, T., et al. (2020). MicroRNA-103 Protects Coronary Artery Endothelial Cells against H2O2-Induced Oxidative Stress via BNIP3-Mediated End-Stage Autophagy and Antipyroptosis Pathways. *Oxid Med. Cel Longev* 2020, 8351342. doi:10.1155/2020/8351342

Wang, T., Zhang, L., Hu, J., Duan, Y., Zhang, M., Lin, J., et al. (2016). Mst1 Participates in the Atherosclerosis Progression through Macrophage Autophagy Inhibition and Macrophage Apoptosis Enhancement. *J. Mol. Cel Cardiol* 98, 108–116. doi:10.1016/j.yjmcc.2016.08.002

Wang, Y., Gao, W., Shi, X., Ding, J., Liu, W., He, H., et al. (2017). Chemotherapy Drugs Induce Pyroptosis through Caspase-3 Cleavage of a Gasdermin. *Nature* 547 (7661), 99–103. doi:10.1038/nature22393

Wei, D. H., Jia, X. Y., Liu, Y. H., Guo, F. X., Tang, Z. H., Li, X. H., et al. (2013). Cathepsin L Stimulates Autophagy and Inhibits Apoptosis of Ox-LDL-Induced Endothelial Cells: Potential Role in Atherosclerosis. *Int. J. Mol. Med.* 31 (2), 400–406. doi:10.3892/ijmm.2012.1201

Wei, Q., Zhu, R., Zhu, J., Zhao, R., and Li, M. (2019). E2-Induced Activation of the NLRP3 Inflammasome Triggers Pyroptosis and Inhibits Autophagy in HCC Cells. *Oncol. Res.* 27 (7), 827–834. doi:10.3727/096504018X15462920753012

Weiwer, M., Bittker, J. A., Lewis, T. A., Shimada, K., Yang, W. S., MacPherson, L., et al. (2012). Development of Small-Molecule Probes that Selectively Kill Cells Induced to Express Mutant RAS. *Bioorg. Med. Chem. Lett.* 22 (4), 1822–1826. doi:10.1016/j.bmcl.2011.09.047

Wu, X., Zhang, H., Qi, W., Zhang, Y., Li, J., Li, Z., et al. (2018). Nicotine Promotes Atherosclerosis via ROS-NLRP3-Mediated Endothelial Cell Pyroptosis. *Cel Death Dis* 9 (2), 171. doi:10.1038/s41419-017-0257-3

Wu, Q., Hu, Y., Jiang, M., Wang, F., and Gong, G. (2019). Effect of Autophagy Regulated by Sirt1/FoxO1 Pathway on the Release of Factors Promoting Thrombosis from Vascular Endothelial Cells. *Int. J. Mol. Sci.* 20 (17), 4132. doi:10.3390/ijms20174132

Wu, Z., Geng, Y., Lu, X., Shi, Y., Wu, G., Zhang, M., et al. (2019). Chaperone-mediated Autophagy Is Involved in the Execution of Ferroptosis. *Proc. Natl. Acad. Sci. U S A.* 116 (8), 2996–3005. doi:10.1073/pnas.1819728116

Wu, L. M., Wu, S. G., Chen, F., Wu, Q., Wu, C. M., Kang, C. M., et al. (2020). Atorvastatin Inhibits Pyroptosis through the lncRNA NEXN-AS1/NEXN Pathway in Human Vascular Endothelial Cells. *Atherosclerosis* 293, 26–34. doi:10.1016/j.atherosclerosis.2019.11.033

Wu, P., Chen, J., Chen, J., Tao, J., Wu, S., Xu, G., et al. (2020). Trimethylamine N-Oxide Promotes apoE(-/-) Mice Atherosclerosis by Inducing Vascular Endothelial Cell Pyroptosis via the SDHB/ROS Pathway. *J. Cel Physiol* 235 (10), 6582–6591. doi:10.1002/jcp.29518

Wu, Q., He, X., Wu, L. M., Zhang, R. Y., Li, L. M., Wu, C. M., et al. (2020). MLKL Aggravates Ox-LDL-Induced Cell Pyroptosis via Activation of NLRP3 Inflammasome in Human Umbilical Vein Endothelial Cells. *Inflammation* 43 (6), 2222–2231. doi:10.1007/s10753-020-01289-8

Xi, H., Zhang, Y., Xu, Y., Yang, W. Y., Jiang, X., Sha, X., et al. (2016). Caspase-1 Inflammasome Activation Mediates Homocysteine-Induced Pyrop-Apoptosis in Endothelial Cells. *Circ. Res.* 118 (10), 1525–1539. doi:10.1161/CIRCRESAHA.116.308501

Xiao, F. J., Zhang, D., Wu, Y., Jia, Q. H., Zhang, L., Li, Y. X., et al. (2019). miRNA-17-92 Protects Endothelial Cells from Erastin-Induced Ferroptosis through Targeting the A20-ACSL4 axis. *Biochem. Biophys. Res. Commun.* 515 (3), 448–454. doi:10.1016/j.bbrc.2019.05.147

Xie, Y., Kang, R., Sun, X., Zhong, M., Huang, J., Klionsky, D. J., et al. (2015). Posttranslational Modification of Autophagy-Related Proteins in Macroautophagy. *Autophagy* 11 (1), 28–45. doi:10.4161/15548627.2014.984267

Xu, X., Yang, Y., Wang, G., Yin, Y., Han, S., Zheng, D., et al. (2021). Low Shear Stress Regulates Vascular Endothelial Cell Pyroptosis through miR-181b-5p/STAT-3 axis. *J. Cel Physiol* 236 (1), 318–327. doi:10.1002/jcp.29844

Xu, Y., Yuan, Q., Cao, S., Cui, S., Xue, L., Song, X., et al. (2020). Aldehyde Dehydrogenase 2 Inhibited Oxidized LDL-Induced NLRP3 Inflammasome Priming and Activation via Attenuating Oxidative Stress. *Biochem. Biophys. Res. Commun.* 529 (4), 998–1004. doi:10.1016/j.bbrc.2020.06.075

Xue, Y., Enosi Tuipulotu, D., Tan, W. H., Kay, C., and Man, S. M. (2019). Emerging Activators and Regulators of Inflammasomes and Pyroptosis. *Trends Immunol.* 40 (11), 1035–1052. doi:10.1016/j.it.2019.09.005

Yan, Z. Q., and Hansson, G. K. (2007). Innate Immunity, Macrophage Activation, and Atherosclerosis. *Immunol. Rev.* 219, 187–203. doi:10.1111/j.1600-065X.2007.00554.x

Yang, K., Song, H., and Yin, D. (2021). PDSS2 Inhibits the Ferroptosis of Vascular Endothelial Cells in Atherosclerosis by Activating Nrf2. *J. Cardiovasc. Pharmacol.* 77 (6), 767–776. doi:10.1097/FJC.0000000000001030

Yang, M., Chen, P., Liu, J., Zhu, S., Kroemer, G., Klionsky, D. J., et al. (2019). Clockophagy Is a Novel Selective Autophagy Process Favoring Ferroptosis. *Sci. Adv.* 5 (7), eaaw2238. doi:10.1126/sciadv.aaw2238

Yang, M., Lv, H., Liu, Q., Zhang, L., Zhang, R., Huang, X., et al. (2020). Colchicine Alleviates Cholesterol Crystal-Induced Endothelial Cell Pyroptosis through Activating AMPK/SIRT1 Pathway. *Oxid Med. Cel Longev* 2020, 9173530. doi:10.1155/2020/9173530

Yang, W. S., Kim, K. J., Gaschler, M. M., Patel, M., Shchepinov, M. S., and Stockwell, B. R. (2016). Peroxidation of Polyunsaturated Fatty Acids by Lipoxygenases Drives Ferroptosis. *Proc. Natl. Acad. Sci. U S A.* 113 (34), E4966–E4975. doi:10.1073/pnas.1603244113

Yang, W. S., SriRamaratnam, R., Welsch, M. E., Shimada, K., Skouta, R., Viswanathan, V. S., et al. (2014). Regulation of Ferroptotic Cancer Cell Death by GPX4. *Cell* 156 (1-2), 317–331. doi:10.1016/j.cell.2013.12.010

Yang, W. S., and Stockwell, B. R. (2008). Synthetic Lethal Screening Identifies Compounds Activating Iron-dependent, Nonapoptotic Cell Death in Oncogenic-RAS-Harboring Cancer Cells. *Chem. Biol.* 15 (3), 234–245. doi:10.1016/j.chembiol.2008.02.010

Yin, Y., Li, X., Sha, X., Xi, H., Li, Y. F., Shao, Y., et al. (2015). Early Hyperlipidemia Promotes Endothelial Activation via a Caspase-1-Sirtuin 1 Pathway. *Arterioscler Thromb. Vasc. Biol.* 35 (4), 804–816. doi:10.1161/ATVBAHA.115.305282

Yu, E. P. K., Reinhold, J., Yu, H., Starks, L., Uryga, A. K., Foote, K., et al. (2017). Mitochondrial Respiration Is Reduced in Atherosclerosis, Promoting Necrotic Core Formation and Reducing Relative Fibrous Cap Thickness. *Arterioscler Thromb. Vasc. Biol.* 37 (12), 2322–2332. doi:10.1161/ATVBAHA.117.310042

Yu, Y., Yan, Y., Niu, F., Wang, Y., Chen, X., Su, G., et al. (2021). Ferroptosis: a Cell Death Connecting Oxidative Stress, Inflammation and Cardiovascular Diseases. *Cell Death Discov* 7 (1), 193. doi:10.1038/s41420-021-00579-w

Yuan, P., Hu, Q., He, X., Long, Y., Song, X., Wu, F., et al. (2020). Laminar Flow Inhibits the Hippo/YAP Pathway via Autophagy and SIRT1-Mediated Deacetylation against Atherosclerosis. *Cel Death Dis* 11 (2), 141. doi:10.1038/s41419-020-2343-1

Zhang, X., Ramirez, C. M., Aryal, B., Madrigal-Matute, J., Liu, X., Diaz, A., et al. (2020). Cav-1 (Caveolin-1) Deficiency Increases Autophagy in the Endothelium and Attenuates Vascular Inflammation and Atherosclerosis. *Arterioscler Thromb. Vasc. Biol.* 40 (6), 1510–1522. doi:10.1161/ATVBAHA.120.314291

Zhang, Z., Guo, M., Li, Y., Shen, M., Kong, D., Shao, J., et al. (2020). RNA-binding Protein ZFP36/TTP Protects against Ferroptosis by Regulating Autophagy Signaling Pathway in Hepatic Stellate Cells. *Autophagy* 16 (8), 1482–1505. doi:10.1080/15548627.2019.1687985

Zhaolin, Z., Jiaojiao, C., Peng, W., Yami, L., Tingting, Z., Jun, T., et al. (2019). OxLDL Induces Vascular Endothelial Cell Pyroptosis through miR-125a-5p/TET2 Pathway. *J. Cel Physiol* 234 (5), 7475–7491. doi:10.1002/jcp.27509

Zheng, F., Xing, S., Gong, Z., Mu, W., and Xing, Q. (2014). Silence of NLRP3 Suppresses Atherosclerosis and Stabilizes Plaques in Apolipoprotein E-Deficient Mice. *Mediators Inflamm.* 2014, 507208. doi:10.1155/2014/507208

Zhong, S., Li, L., Zhang, Y. L., Zhang, L., Lu, J., Guo, S., et al. (2019). Acetaldehyde Dehydrogenase 2 Interactions with LDLR and AMPK Regulate Foam Cell Formation. *J. Clin. Invest.* 129 (1), 252–267. doi:10.1172/JCI122064

Zhong, Z., Liang, S., Sanchez-Lopez, E., He, F., Shalapour, S., Lin, X. J., et al. (2018). New Mitochondrial DNA Synthesis Enables NLRP3 Inflammasome Activation. *Nature* 560 (7717), 198–203. doi:10.1038/s41586-018-0372-z

Zhong, Z., Umemura, A., Sanchez-Lopez, E., Liang, S., Shalapour, S., Wong, J., et al. (2016). NF-kappaB Restricts Inflammasome Activation via Elimination of Damaged Mitochondria. *Cell* 164 (5), 896–910. doi:10.1016/j.cell.2015.12.057

Zhou, R., Tardivel, A., Thorens, B., Choi, I., and Tschopp, J. (2010). Thioredoxin-interacting Protein Links Oxidative Stress to Inflammasome Activation. *Nat. Immunol.* 11 (2), 136–140. doi:10.1038/ni.1831

Zhou, R., Yazdi, A. S., Menu, P., and Tschopp, J. (2011). A Role for Mitochondria in NLRP3 Inflammasome Activation. *Nature* 469 (7329), 221–225. doi:10.1038/nature09663

Zhou, Y., Zhou, H., Hua, L., Hou, C., Jia, Q., Chen, J., et al. (2021). Verification of Ferroptosis and Pyroptosis and Identification of PTGS2 as the Hub Gene in

Human Coronary Artery Atherosclerosis. *Free Radic. Biol. Med.* 171, 55–68. doi:10.1016/j.freeradbiomed.2021.05.009

Zhu, L., Wu, G., Yang, X., Jia, X., Li, J., Bai, X., et al. (2019). Low Density Lipoprotein Mimics Insulin Action on Autophagy and Glucose Uptake in Endothelial Cells. *Sci. Rep.* 9 (1), 3020. doi:10.1038/s41598-019-39559-7

Zhu, S., Zhang, Q., Sun, X., Zeh, H. J., 3rd, Lotze, M. T., Kang, R., et al. (2017). HSPA5 Regulates Ferroptotic Cell Death in Cancer Cells. *Cancer Res.* 77 (8), 2064–2077. doi:10.1158/0008-5472.CAN-16-1979

Zi, Y., Yi-An, Y., Bing, J., Yan, L., Jing, T., Chun-Yu, G., et al. (2019). Sirt6-induced Autophagy Restricted TREM-1-Mediated Pyroptosis in Ox-LDL-Treated Endothelial Cells: Relevance to Prognostication of Patients with Acute Myocardial Infarction. *Cel Death Discov* 5, 88. doi:10.1038/s41420-019-0168-4

Zilka, O., Shah, R., Li, B., Friedmann Angeli, J. P., Griesser, M., Conrad, M., et al. (2017). On the Mechanism of Cytoprotection by Ferrostatin-1 and Liproxstatin-1 and the Role of Lipid Peroxidation in Ferroptotic Cell Death. *ACS Cent. Sci.* 3 (3), 232–243. doi:10.1021/acscentsci.7b00028

Conflict of Interest: The authors declare that the research was conducted in the absence of any commercial or financial relationships that could be construed as a potential conflict of interest.

Publisher's Note: All claims expressed in this article are solely those of the authors and do not necessarily represent those of their affiliated organizations, or those of the publisher, the editors and the reviewers. Any product that may be evaluated in this article, or claim that may be made by its manufacturer, is not guaranteed or endorsed by the publisher.

Copyright © 2022 Lin, Zhang, Zhang, Zhang, Li and Li. This is an open-access article distributed under the terms of the Creative Commons Attribution License (CC BY). The use, distribution or reproduction in other forums is permitted, provided the original author(s) and the copyright owner(s) are credited and that the original publication in this journal is cited, in accordance with accepted academic practice. No use, distribution or reproduction is permitted which does not comply with these terms.

frontiers in Cell and Developmental Biology

ORIGINAL RESEARCH
published: 17 January 2022
doi: 10.3389/fcell.2021.801661

MicroRNA-223-3p Protect Against Radiation-Induced Cardiac Toxicity by Alleviating Myocardial Oxidative Stress and Programmed Cell Death *via* Targeting the AMPK Pathway

Dao-ming Zhang[1†], Jun-jian Deng[1†], Yao-gui Wu[1], Tian Tang[1], Lin Xiong[2], Yong-fa Zheng[1] and Xi-ming Xu[1*]*

[1]Cancer Center, Renmin Hospital of Wuhan University, Wuhan, China, [2]Department of Pathology, Renmin Hospital of Wuhan University, Wuhan, China

OPEN ACCESS

Edited by:
Zhi Qi,
Nankai University, China

Reviewed by:
Ming Liu,
Sichuan University, China
Liang Liu,
Fudan University, China

***Correspondence:**
Yong-fa Zheng
Zyf0322@126.com
Xi-ming Xu
doctorxu120@aliyun.com

[†]These authors have contributed equally to this work

Specialty section:
This article was submitted to Cell Death and Survival, a section of the journal Frontiers in Cell and Developmental Biology

Received: 25 October 2021
Accepted: 29 November 2021
Published: 17 January 2022

Citation:
Zhang D-m, Deng J-j, Wu Y-g, Tang T, Xiong L, Zheng Y-f and Xu X-m (2022) MicroRNA-223-3p Protect Against Radiation-Induced Cardiac Toxicity by Alleviating Myocardial Oxidative Stress and Programmed Cell Death via Targeting the AMPK Pathway. Front. Cell Dev. Biol. 9:801661. doi: 10.3389/fcell.2021.801661

Objectives: Radiotherapy improves the survival rate of cancer patients, yet it also involves some inevitable complications. Radiation-induced heart disease (RIHD) is one of the most serious complications, especially the radiotherapy of thoracic tumors, which is characterized by cardiac oxidative stress disorder and programmed cell death. At present, there is no effective treatment strategy for RIHD; in addition, it cannot be reversed when it progresses. This study aims to explore the role and potential mechanism of microRNA-223-3p (miR-223-3p) in RIHD.

Methods: Mice were injected with miR-223-3p mimic, inhibitor, or their respective controls in the tail vein and received a single dose of 20 Gy whole-heart irradiation (WHI) for 16 weeks after 3 days to construct a RIHD mouse model. To inhibit adenosine monophosphate activated protein kinase (AMPK) or phosphodiesterase 4D (PDE4D), compound C (CompC) and AAV9-shPDE4D were used.

Results: WHI treatment significantly inhibited the expression of miR-223-3p in the hearts; furthermore, the levels of miR-223-3p decreased in a radiation time-dependent manner. miR-223-3p mimic significantly relieved, while miR-223-3p inhibitor aggravated apoptosis, oxidative damage, and cardiac dysfunction in RIHD mice. In addition, we found that miR-223-3p mimic improves WHI-induced myocardial injury by activating AMPK and that the inhibition of AMPK by CompC completely blocks these protective effects of miR-223-3p mimic. Further studies found that miR-223-3p lowers the protein levels of PDE4D and inhibiting PDE4D by AAV9-shPDE4D blocks the WHI-induced myocardial injury mediated by miR-223-3p inhibitor.

Conclusion: miR-223-3p ameliorates WHI-induced RIHD through anti-oxidant and anti-programmed cell death mechanisms *via* activating AMPK by PDE4D regulation. miR-223-3p mimic exhibits potential value in the treatment of RIHD.

Keywords: RIHD, MiR-223-3p, apoptosis, oxidative stress, AMPK

INTRODUCTION

With the increasing cancer incidence, radiotherapy (RT) has become an important treatment approach. On the one hand, RT improves the survival rate of cancer patients, but on the other, it also involves some inevitable complications of RT (Wang et al., 2019). Radiation-induced heart disease (RIHD) is one of the most serious complications, which is characterized by oxidative stress and cell loss (Ping et al., 2020). Mediastinal radiation therapy stimulates the atherosclerosis process, resulting in early onset coronary artery disease. Valvular disease caused by RT usually affects the left valve, with aortic regurgitation being the most common. In rare cases, it can lead to aortic stenosis that requires surgical intervention. Pericardial involvement includes acute and chronic pericardial disease and pericardial effusion (Raghunathan et al., 2017). A number of large clinical studies have confirmed that radiation therapy increases the risk of heart disease-related deaths (Laugaard Lorenzen et al., 2020). There is no clear treatment program to avoid or effectively eradicate the onset and subsequent development of RIHD. It is currently believed that RIHD is the result of the interaction of multiple mechanisms through multiple perturbed pathways; however, oxidative stress is considered to be the main one of them (Ping et al., 2020).

MicroRNAs (miRNAs) have gradually become the hot spot of RIHD research (Sarkozy et al., 2019). It has been considered that miRNAs regulate the signaling pathways and thus play a key role in the development of RIHD (Hawkins et al., 2019). miRNA is a type of single-stranded non-coding RNA with a length of approximately 19–25 nucleotides, which acts as a negative regulator of gene expression by binding to the 3′-untranslated region (UTR) of the target mRNA (Gomes et al., 2020). Emerging studies have shown that miRNAs participate in the regulation of the development of RIHD by influencing inflammation and oxidative damage (O'Connell et al., 2012; Bodega et al., 2019). A number of studies have shown that miR-223-3p is expressed in macrophages, platelets, hepatocytes, and cardiomyocytes and other cells (Zhang MW. et al., 2020). By targeting a variety of genes to regulate its cell activity, it is involved in the pathological progress of a variety of cardiovascular diseases (Zhang MW. et al., 2020). Chen et al. demonstrated that miR-223-3p inhibits the activation of inflammasomes by regulating the polarization of dendritic cells and then reduces the injury of autoimmune myocarditis (Chen et al., 2020). A recent study from Wu and colleagues showed that the expression level of serum miR-223-3p is closely related to the prognostic efficacy of patients with coronary heart disease (Wu et al., 2021). In addition, Han et al. demonstrated that miR-223-3p can inhibit atherosclerotic vascular calcification by regulating IL-6/STAT3 signal-mediated vascular smooth muscle cell (VSMC) transdifferentiation (Han et al., 2021). The results from Qin et al. showed that miR-223-3p can inhibit cardiac necrosis induced by myocardial ischemia-reperfusion. Adenosine monophosphate activated protein kinase (AMPK) is a key signal molecule that regulates energy metabolism, cell fate, and oxidative stress signal transduction in cardiomyocytes (Sun et al., 2006). Recent studies have shown that activating AMPK alleviated oxidative stress and apoptosis (Ichihara et al., 2006). Furthermore, miR-223-3p exhibited an indispensable role in regulating apoptosis and redox homeostasis in a variety of diseases (Matsuzaki and Ochiya, 2018; Tang et al., 2018; Zhang and Cheng, 2021). In this study, we aim to explore the role and potential mechanism of miR-223-3p in the progression of RIHD.

MATERIALS AND METHODS

Material

Enzyme-linked immunosorbent assay (ELISA) assay including lactate dehydrogenase (LDH), creatine kinase MB isoenzyme (CK-MB), were purchased from MyBioSource (CA, United States). PKA (protein kinase A) colorimetric activity kit. Dihydrodichlorofluorescein diacetate (DCF-DA) and caspase-3 assay kit were obtained from ThermoFisher Scientific (CA, United States). Total antioxidant capacity (TAOC) assay kits, total superoxide dismutase (SOD) activity assay kits, malondialdehyde (MDA) assay kits, 3-nitrotyrosine (3-NT) assay kits, and 8-hydroxy 2 deoxy guanosine (8-OHdG) assay kits were purchased from Abcam (Cambridge, United Kingdom). ELISA^{PLUS} kit was purchased from Roche Applied Science (Mannheim, Germany). Caspase 3/7 activity using a kit from Promega (WI, United States). Total collagen assay kit and soluble collagen assay kit were purchased from Abcam (Cambridge, United Kingdom). Phosphorylated (P–) AMPK, total (T–) AMPK, antibodies, and β-actin were purchased from Cell Signaling Technology (MA, United States). p53, cAMP, PKA, NRF2, HO-1, α-SMA, fibronectin, and phosphodiesterase 4D (PDE4D) were purchased from Abcam (Cambridge, United Kingdom). Compound C was obtained from Selleck Chemicals (Texas, United States). An AAV9 system harboring shPDE5D, shRNA, miR-223-3p mimic, miR-223-3p mimic inhibitor, or negative control was generated by HanBio Technology (Shanghai, China).

Animals

C57BL/6 mice (6–8 weeks) were purchased from Chinese Academy of Medical Sciences and Peking Union Medical College. Mice received a single dose of 20 Gy whole-heart irradiation (WHI) or sham therapy under anesthesia using an X-RAD 160–225 radiator (CT, United States) with a 2 mm AI filter (Lee et al., 2012). To overexpress miR-223-3p, mice received 1×10^{11} viral genome of AAV9-miR-223-3p mimic (mimic) or AAV9-scramble (con) by tail vein injection according to a previous study. To investigate miR-223-3p deficiency in WHI model, mice received 1×10^{11} viral genome of AAV9-miR-223-3p inhibitor (inhibitor) or AAV9-negative control (NC) by tail vein injection. After the 4th week injection, mice were subjected to WHI. For AMPK inhibition, compound C (20 mg/kg) was intraperitoneally injected every 2 days at 1 week before WHI stimulation (Zhang X. et al., 2020). For PDE4D inhibition, mice received 1×10^{11} viral genome of AAV9-shPDE4D (shPDE4D) or AAV9-shRNA (shRNA) by tail vein injection at 4 weeks before WHI therapy (Ma et al., 2021). After 15 weeks WHI, the cardiac echocardiographic and hemodynamic

measurements were performed, and then all mice were sacrificed with euthanasia by an overdose of sodium pentobarbital. The animal experiments were performed according to the Guide for the Care and Use of Laboratory Animals published by the US National Institutes of Health. The protocol was approved by the institutional animal care and use committee of Renmin Hospital of Wuhan University.

Echocardiography and Hemodynamic

Serial transthoracic echocardiography was performed according to previously described method (Fan D. et al., 2017; Liu et al., 2019). For pressure–volume loops, a pressure probe catheter (TX, United States) was inserted into the left carotid artery and then retrogradely advanced into the left ventricle to record the hemodynamic parameters.

ELISA Assay

The DNA damage biomarkers, apoptosis biomarkers, and oxidation/antioxidation biomarker level in serum or cardiac from each group were detected by utilizing ELISA kits according to the manufacturer's protocol.

Collagen Assay

Total collagen content was determined by measuring hydroxyproline levels in the left ventricles as previously described. In order to evaluate the content of soluble collagen, mouse heart tissues of each group were placed in pepsin solution, and the supernatant was precipitated with trichloroacetic acid. The precipitate was hydrolyzed with HCL, and the hydroxyproline level was detected by the commercial kit. The total collagen content minus the amount of soluble collagen equals the insoluble collagen content.

Cardiac Injury Biomarkers Measurement

To detect plasma LDH and CK-MB levels, blood samples were collected from mice. CK-MB and LDH were detected to reflect the cardaic injury according to standard procedures.

Real-Time PCR

We used TRIzol reagent to isolate total mRNA. We used the SmartSpec Plus Spectrophotometer (Bio-Rad) to detect mRNA purity with OD260/OD280 ratios. A total of 2 μg of mRNA was reverse transcribed into cDNA with cDNA Synthesis Kit (Roche Diagnostics). Gene expression analysis was carried out using the Fast SYBR Green master mix (Applied Biosystems) and the QuantStudio 12k Flex real-time PCR (RT-PCR) system (Switzerland). Results were normalized to β-actin mRNA as an internal control. miRNA level was determined using Bulge-Loop miRNA qRT-PCR Starter Kit (Guangzhou, China). U6 was used as the internal control of miRNA.

Western Blotting

Western blotting was performed according to previously described method (Guo et al., 2020). Protein samples were prepared from heart tissues. Whole-cell lysates or tissue lysates were prepared in radioimmunoprecipitation assay (RIPA) buffer supplemented with 1 mmol/L phenylmethanesulfonyl fluoride (PMSF) and 1% protease inhibitor cocktail before use. For Western blotting analysis, the lysates were clarified, denatured, separated on 10% polyacrylamide gels by sodium dodecyl sulfate polyacrylamide gel electrophoresis (SDS-PAGE) and transferred to polyvinylidene difluoride (PVDF) membranes. Detection of the target proteins on membranes was performed using standard techniques. The abundance 1 of the proteins was determined by densitometry. Raw data of band intensity were normalized to a control protein such as β-actin.

Data and Statistical Analysis

All experiments were randomized and blinded. Data are presented as means ± standard deviation. Statistical analysis was performed with GraphPad Prism version 8.0.1 and the SPSS 18.0 software package (IL, United States). Multiple comparisons were carried out using Tukey's test following significant one-way or two-way ANOVA. Unpaired *t*-test was to compare significance between the two groups. p-values <0.05 were considered to be statistically significant.

RESULTS

miR-223-3p Mimic Reduces Myocardial Damage and Dysfunction in RIHD Mice

As shown in **Figure 1A**, WHI treatment significantly reduced the expression of miR-223-3p in mice hearts in a radiation-time dependent manner. At the 15th week after WHI stimulation, the level of miR-223-3p reached the lowest. To clarify the role of miR-223-3p, mice were injected with adenovirus harboring miR-223-3p mimic, the efficiency of which is shown in **Figure 1B**. After 15 weeks of WHI therapy, the levels of heart failure biomarkers *ANP* and *BNP* were increased, while miR-223-3p mimic alleviated this alternation (**Figure 1C**). The serum CK-MB and LDH, indicators associated with cardiac injury, were reduced with miR-223-3p mimic treatment (**Figure 1D**). Then, we examined the cardiac function and found that miR-223-3p mimic ameliorated WHI-induced cardiac dysfunction by improving the left fractional shortening (FS), left ventricular ejection fraction (EF), maximal rate of the left ventricular pressure fall or increase (±dP/dt), and cardiac output (CO) (**Figures 1E, F**). In addition, the end-diastolic pressure in the left ventricle (LVEDP) of WHI mice was restored with miR-223-3p mimic treatment (**Figure 1G**). These data indicate that miR-223-3p mimic alleviates cardiac injury and dysfunction in mice with WHI stimulation.

miR-223-3p Mimic Inhibits Oxidative Stress Damage and Programmed Cell Death

Due to the critical role of oxidative stress and programmed cell death in the progression of RIHD, we assessed the effect of miR-223-3p mimic on redox reaction and cell loss in the hearts of RIHD mice. As shown in **Figures 2A, B**, WHI increased the accumulation of reactive oxygen species (ROS) and superoxide but decreased in miR-223-3p mimic-treated mice. The increase of peroxides needs to be swept by antioxidants, such as SOD and

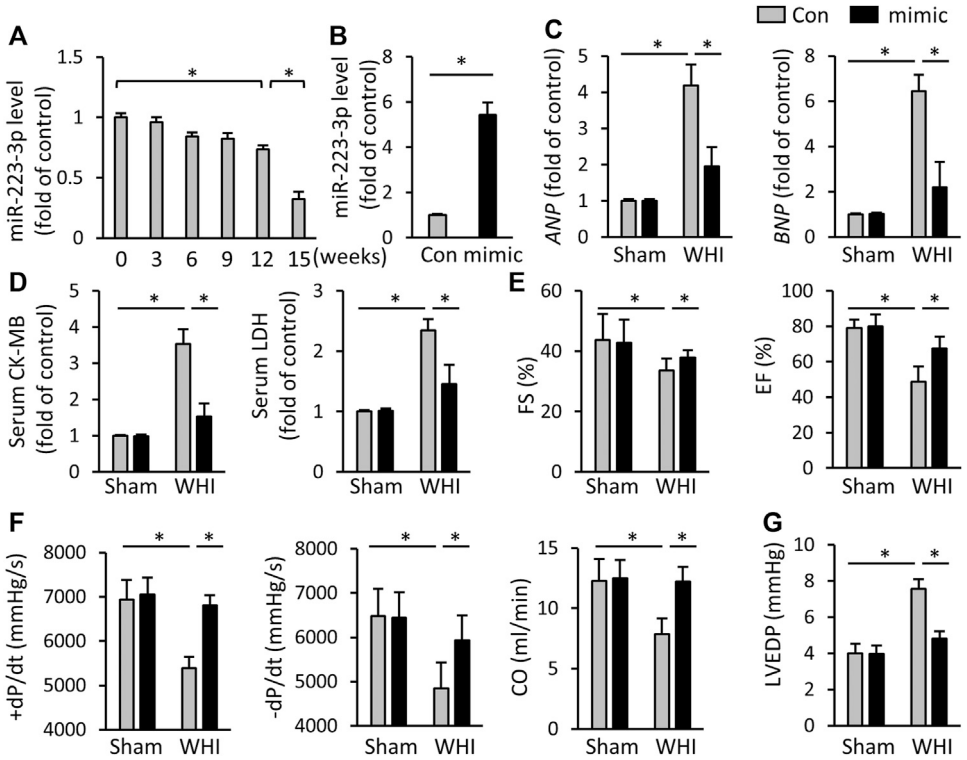

FIGURE 1 | miR-223-3p mimic attenuates cardiac injury and dysfunction. **(A)** Relative level of miR-223-3p in cardiac with 20 Gy WHI were detected at the indicated times (n = 6). **(B)** Relative level of miR-223-3p in mice hearts with or without miR-223-3p mimic treatment (n = 5). **(C)** Relative mRNA levels of *ANP* and *BNP* in the hearts (n = 6). **(D)** Serum biomarkers related to cardiac injury with or without miR-30d-5p mimic treatment upon WHI stimulation, including CK-MB and LDH (n = 6). **(E–G)** Echocardiographic and hemodynamic parameters were detected at 16 weeks after WHI or sham therapy (n = 6). CO, cardiac output; All data are presented as means ± SD. *p < 0.05 vs. the matched group.

glutathione (GSH). We tested the TAOC and the levels of SOD and GSH and found that miR-223-3p mimic also reduced WHI-related SOD and GSH consumption and increased the TAOC (**Figure 2B**). In addition, increased production of 4-HNE and MDA were found in WHI mice, indicating increased oxidative stress, which were also alleviated with miR-223-3p mimic treatment (**Figure 2C**). Radiation, both acute and chronic exposure, induces oxidative stress, causing oxidative damage and DNA damage. Cellular DNA damage includes single strand breaks and double strand breaks in cellular DNA and also 8-OHdG in cellular DNA. Therefore, by detecting DNA biomarkers in myocardial tissue, we detected that DNA biomarkers, such as 8-OHdG, p53, and DNA fragments, were elevated in the myocardial tissue of WHI mice and reduced by miR-223-3p (**Figure 2D**). RT-PCR results showed that the hearts of WHI mice exhibited higher programmed cell death compared with WHI mice treated with miR-223-3p mimic, as reflected by levels of *Bax* and *Bcl-2* and the ratio of Bax/Bcl-2 (**Figure 2E**). Consistent with the RT-PCR results, the levels of Caspase-3 and Caspase3/7, as programmed cell death executive molecules, were decreased in miR-223-3p mimic-treated mice, detected by ELISA (**Figure 2F**). It has been reported that NRF2 acts as a redox-sensitive transcription factor, which inhibits oxidative damage in RIHD (Fan Z. et al., 2017; Cao et al., 2021). As shown in **Figures 2G, H**, WHI significantly reduced the protein levels of NRF2 and its downstream HO-1 in mice hearts, which was rescued by miR-223-3p mimic treatment. Therefore, we conclude that miR-223-3p mimic inhibits oxidative stress damage and programmed cell death in radiated hearts.

miR-223-3p Mimic Reduces Myocardial Fibrosis in RIHD Mice

Radiation-induced myocardial fibrosis is a chronic stage of RIHD, which is the main cause of cardiac stiffness and cardiac dysfunction (Ma et al., 2019; Sarkozy et al., 2019). Next, we assessed the role of miR-223-3p mimic on the transcription of key molecules related to myocardial fibrosis, such as *TGF-β*, *Ctgf*, *col-1*, *col-3*, and *α-SMA*. As shown in **Figure 3A**, after the mice received 15 weeks WHI, the mRNA elevation of the pro-fibrosis markers induced by WHI was alleviated by miR-223-3p mimic administration. MMP2 and MMP9 are both main components of the extracellular matrix, which are elevated in WHI mice (**Figure 3B**). Interestingly, MMP2 (WHI+Con vs. WHI+mimic, 3.63 vs. 3.40) and MMP9 (WHI+Con vs. WHI+mimic, 2.89 vs. 2.74) in WHI mice were unaffected by miR-223-3p mimic. ELISA data also showed that the total insoluble (mainly cross-linked) collagen content in the left

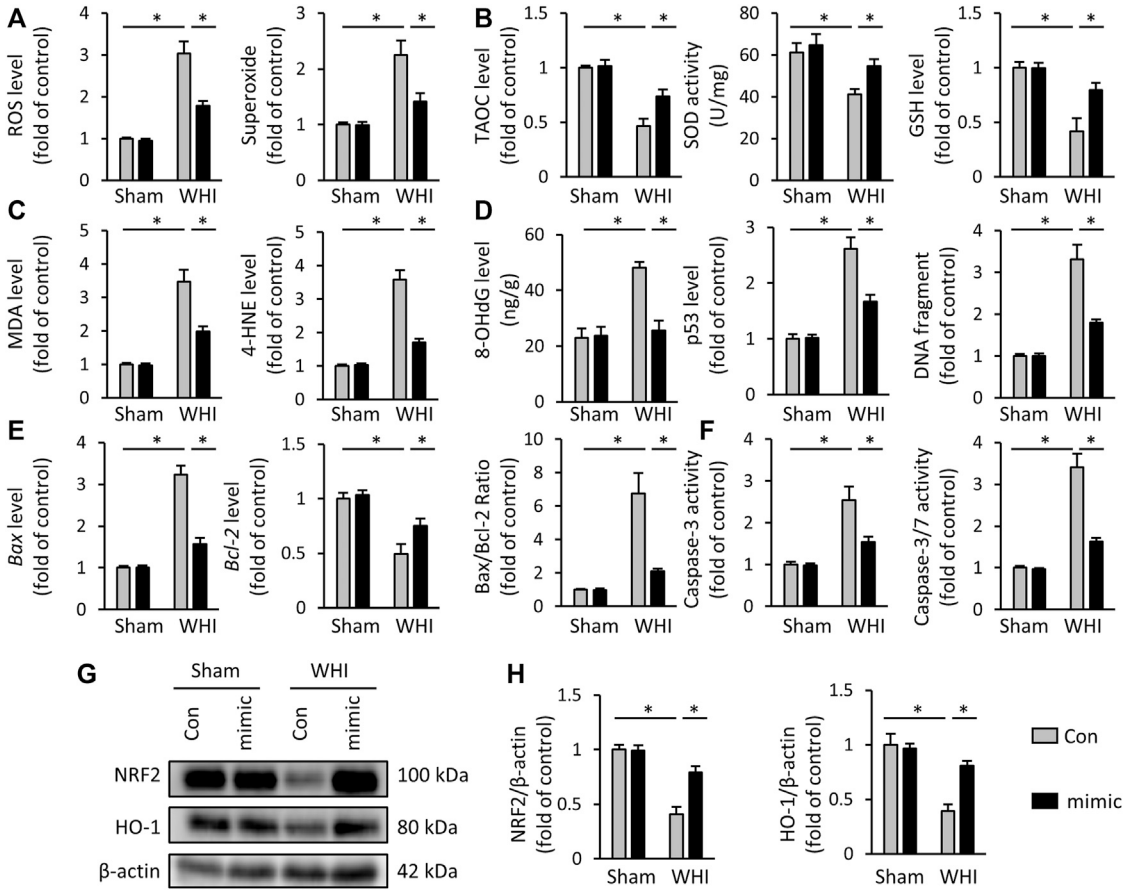

FIGURE 2 | miR-223-3p mimic inhibits oxidative stress and programmed cell death in WHI mice. **(A)** ROS and superoxide level in the hearts with or without miR-223-3p mimic (n = 6). **(B)** TAOC and total SOD activity and GSH level detected by ELISA assay (n = 6). **(C)** Oxidative products levels in mice hearts (n = 6). **(D)** Quantitative results of 8-OHdG, p53, and DNA fragment in each group (n = 6). **(E)** Relative mRNA levels of *Bax* and *Bcl-2* and the ratio of Bax/Bcl-2 in the hearts (n = 6). **(F)** Quantitative results of caspase-3 and caspase-3/7 activity in each group (n = 6). **(G, H)** Relative protein expression of NRF2 and HO-1 in each group (n = 6). All data are presented as means ± SD. *$p < 0.05$ vs. the matched group.

ventricle of mice was decreased in miR-223-3p mimic treatment mice with WHI stimulation, without alteration of the soluble forms (**Figure 3C**). Western blot detection revealed that the elevation of α-SMA and fibronectin expression induced by WHI were alleviated by miR-223-3p mimic injection (**Figures 3D, E**). These data indicated that miR-223-3p mimic reduced myocardial fibrosis in RIHD mice.

miR-223-3p Inhibitor Aggravates Oxidative Stress and Programmed Cell Death in RIHD Mice

We also used miR-223-3p inhibitor to determine whether inhibiting miR-223-3p would aggravate oxidative stress and programmed cell death in RIHD mice. As shown in **Figures 4A–C**, the miR-223-3p inhibitor significantly increases the accumulation of ROS and peroxide in the hearts after WHI therapy, with lower levels of the TAOC, SOD, and GSH, Correspondingly, the productions of MDA and 4-HNE were enhanced with miR-223-3p inhibitor injection. Correspondingly, miR-223-3p inhibitor administration increased the DNA damage, as determined by the levels of 8-OHdG, p53, and DNA fragments (**Figure 4D**). As expected, we found that miR-223-3p inhibitor significantly increased the level of pro-apoptotic marker Bax mRNA and reduced the anti-apoptotic Bcl-2 mRNA expression under WHI stimulation (**Figure 4E**). Accordingly, miR-223-3p inhibitor further promoted the increase of Caspase-3 and Caspase-3/7 levels in WHI mice. These data provide evidence that miR-223-3p inhibitor aggravate oxidative stress and programmed cell death induced by WHI therapy.

miR-223-3p Inhibitor Aggravates Myocardial Damage and Dysfunction in RIHD Mice

Because of miR-223-3p aggravating oxidative stress and programmed cell death in RIHD mice, we also investigated the effect of miR-223-3p inhibitor on cardiac injury and dysfunction induced by WHI. As shown in **Figure 5A**, compared with WHI mice, miR-223-3p inhibitor further increased the levels of *ANP*

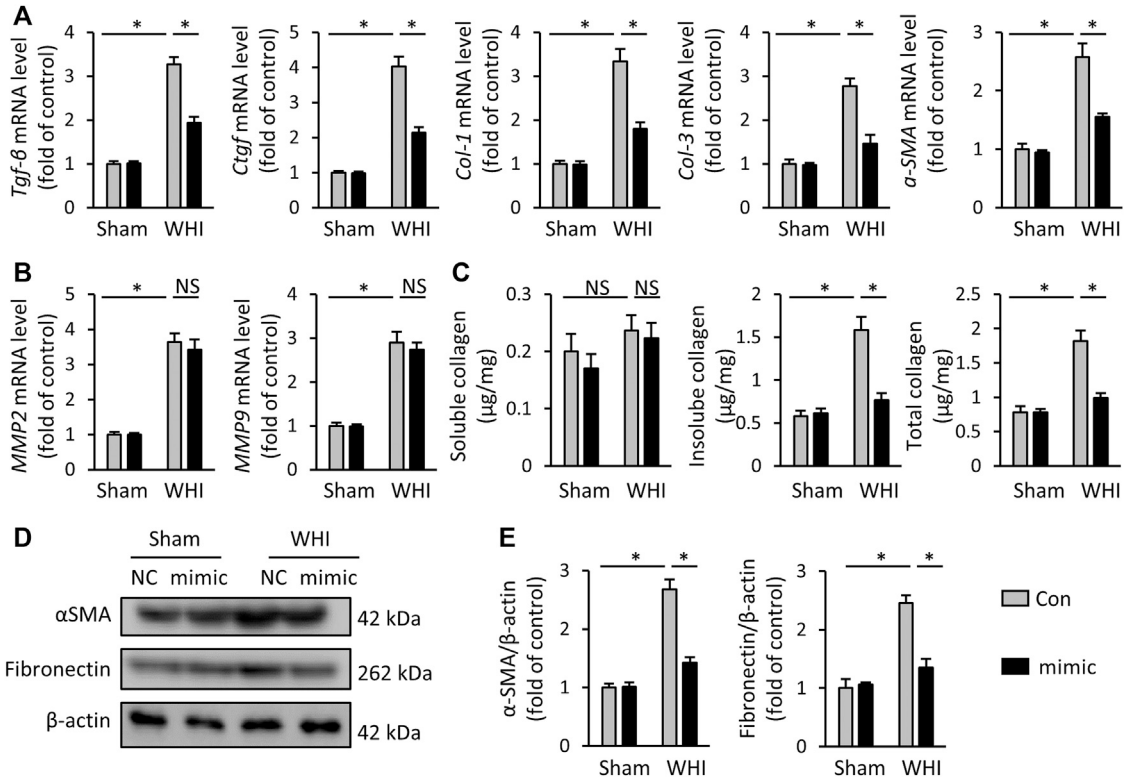

FIGURE 3 | miR-223-3p mimic reduces myocardial fibrosis in RIHD mice. **(A)** Relative mRNA levels of *Tgf-β*, *Ctgf*, *Col-1*, *Col-3*, and *α-SMA* in the hearts (n = 6). **(B)** Relative mRNA levels of *MMP2* and *MMP9* in each group (n = 6). **(C)** Total, soluble, and insoluble collagen content were assessed in each group (n = 6). **(D, E)** Relative protein expression of α-SMA and fibronectin in each group (n = 6). All data are presented as means ± SD. *p < 0.05 vs. the matched group.

and *BNP* (**Figure 5A**). As expected, miR-223-3p inhibitor also promotes cardiac injury, as reflected by serum levels of CK-MB and LDH, as well as LDH levels in cardiac tissue (**Figure 5B**). The greater deterioration of EF and FS in the mice with pretreatment of miR-223-3p inhibitor compared with WHI+NC group was detected by echocardiographic examination (**Figure 5C**). Correspondingly, the hemodynamic analysis showed that CO, ±dP/dt, and LVEDP further worsened after miR-223-3p inhibitor injection (**Figures 5D, E**). Furthermore, mice pretreated with miR-223-3p inhibitor promoted the transcription of the pro-fibrotic gene (*TGF-β* and *CTGF*) with WHI stimulation and accordingly increased the deposition of total collagen and insoluble collagen in the left ventricle (**Figures 5F, G**). Besides, the levels of MMP2 and MMP9 were not significantly different between the WHI+NC group and WHI+inhibitor group, further indicating that miR-223-3p unaffected the MMP2 and MMP9 (data not shown). Therefore, we concluded that miR-223-3p inhibitor aggravates cardiac injury and dysfunction induced by WHI.

miR-223-3p Mimic Improves WHI-Induced RIHD by Activating AMPK

To further explore the mechanism of miR-223-3p in RIHD, we collected heart tissues from each group of mice. Western blot data showed that miR-223-3p mimic prevented the decrease of AMPK phosphorylation induced by WHI, while miR-223-3p inhibitor further aggravated the reduction of AMPK phosphorylation (**Figures 6A, B**). Next, the AMPK inhibitor CompC was used to block AMPK activity *in vivo* to verify whether the effect of miR-223-3p was dependent on AMPK activation. We found that miR-223-3p mimic-mediated cardiac protection was significantly eliminated by CompC administration, as shown by unchanged *ANP*, *BMP*, and serum CK-MB levels (**Figures 6C, D**). Consistent with unaltered cardiac injury markers, the protective effect of miR-223-3p mimic on RIHD was also blocked by AMPK inhibitors, as reflected by FS, EF, and LVEDP (**Figures 6E, F**). In addition, CompC also blocked the effect of miR-223-3p mimic on oxidative stress, as determined by ROS, superoxide, MDA, 4-HNE, and TAOC (**Figure 6G**). Correspondingly, miR-223-3p mimic failed to ameliorate myocardial fibrosis, DNA damage, and programmed cell death in WHI mice with CompC administration (**Figures 6H–J**). Hence, we consider that miR-223-3p exerted a cardioprotective role in WHI mice by activating AMPK.

miR-223-3p Regulates PDE4D/AMPK Signaling

Finally, we investigated the possible mechanism of AMPK activation regulation by miR-223-3p. In predicting the miR-

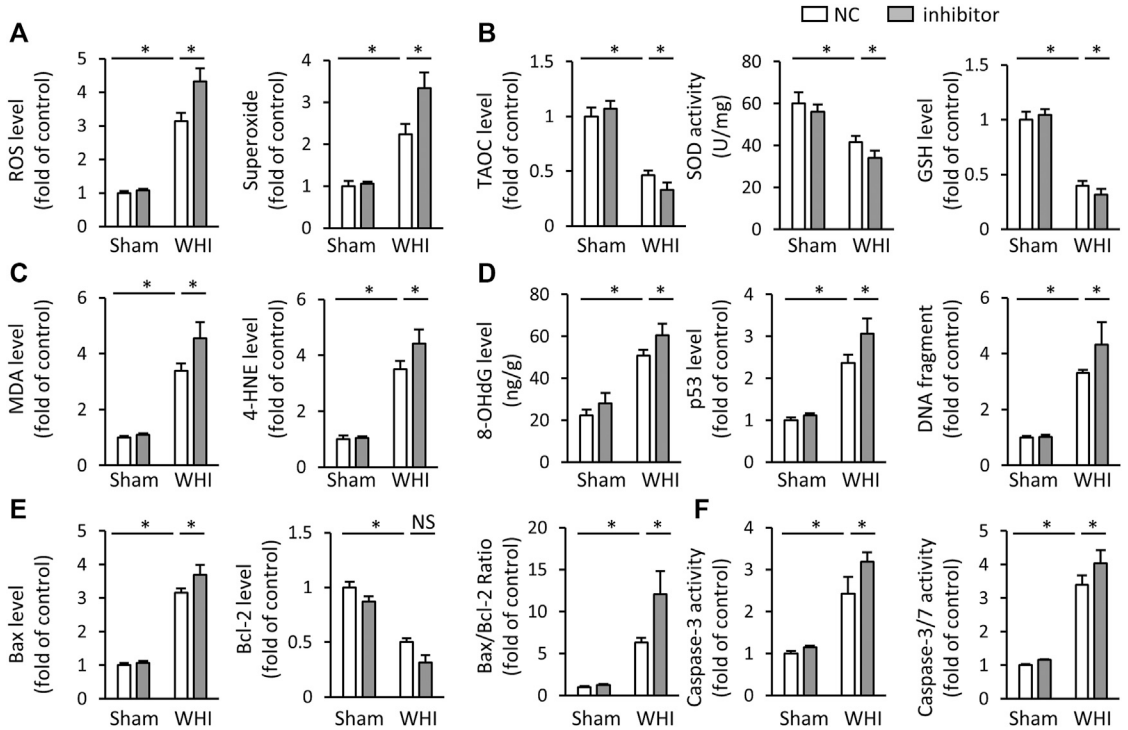

FIGURE 4 | miR-223-3p inhibitor aggravates oxidative stress and programmed cell death in RIHD mice. **(A)** ROS and superoxide level in the hearts with or without miR-223-3p inhibitor (n = 6). **(B)** The relative levels of TAOC and total SOD activity and GSH (n = 6). **(C)** Oxidative products levels in mice with or without miR-223-3p inhibitor (n = 6). **(D)** Quantitative results of 8-OHdG, p53, and DNA fragment in each group (n = 6). **(E)** Relative mRNA levels of *Bax* and *Bcl-2* and the ratio of Bax/Bcl-2 in the hearts (n = 6). **(F)** Quantitative results of caspase-3 and caspase-3/7 activity in each group (n = 6). All data are presented as means ± SD. *$p < 0.05$ vs. the matched group.

223-3p regulatory target site by TargetScan Mouse 7.1, we revealed that the supposed banding site of miR-223-3p is in the 3′-UTR of PDE4D (**Figure 7A**). PDE4D is a specific phosphodiesterase (PDE) isoenzyme that regulates the hydrolysis of cAMP and the downstream PKA pathway (Yun et al., 2019). Therefore, the reduction of PDE4D downstream cAMP and PKA activity were found in the mice with miR-223-3p inhibitor treatment, while it is increased by miR-223-3p mimic (**Figures 7B, C**). In addition, miR-223-3p significantly inhibits the expression of PDE4D in WHI mice (**Figures 7D, E**). In order to verify whether miR-223-3p is involved in the regulation of AMPK activation *via* PDE4D, mice were injected with AAV9-shPDE4D into the tail vein to silence the expression of PDE4D in the mice hearts. As shown in **Figure 7F**, shPDE4D significantly inhibited the protein expression of PDE4D in myocardial tissue and rescued the inhibition of AMPK phosphorylation mediated by miR-223-3p inhibitor. Moreover, PDE4D deficiency restored the deterioration of cardiac dysfunction mediated by miR-223-3p inhibitor (**Figure 7G**), as suggested by EF and FS. miR-223-3p inhibitor-associated increased level of serum CK-MB was also blunted by shPDE4D injection (**Figure 7H**). Consistent with the cardiac function, AAV9-shPDE4D reduced the effects of miR-223-3p inhibitor in WHI mice, as suggested by the levels of total collagen, superoxide, ROS, and caspase-3 activity (**Figures 7I–K**). Collectively, we demonstrated that miR-223-3p suppressed the expression of PDE4D by directly binding to the 3′-UTR of PDE4D and subsequently activated AMPK to regulate the progression of RIHD.

DISCUSSION

With the increasing cancer incidence, RT has become an important treatment approach. Long-term radiation therapy, especially chest cancer radiation therapy, leads to RIHD. In this study, we aimed to explore the role and mechanism of miR-223-3p in RIHD. The main findings are as follows: 1) the expression of miR-223-3p in the hearts of WHI mice with a radiation time-dependent manner; 2) miR-223-3p exerted cardioprotective effects on WHI induced heart injury *via* reducing cardiac oxidative damage and programmed cell death; 3) miR-223-3p mimic ameliorates WHI-induced radiocardiotoxicity *via* AMPK activation; and 4) PDE4D is involved in AMPK activation by miR-223-3p. In conclusion, our results demonstrated for the first time that miR-223-3p showed potential value in RIHD treatment.

As we know, the heart is an organ with high oxygen consumption, and cardiomyocytes contain a large number of mitochondria. The ROS are mainly produced by the mitochondria in the heart (Pohjoismaki and Goffart, 2017).

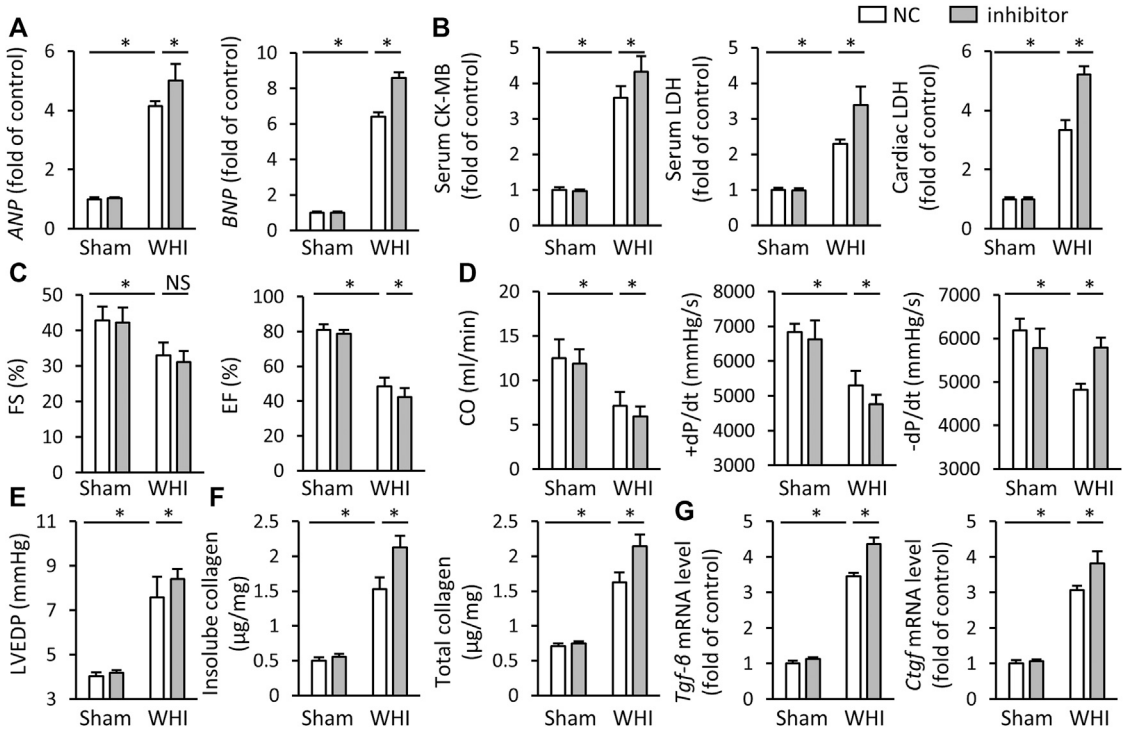

FIGURE 5 | miR-223-3p inhibitor aggravates myocardial damage and dysfunction in RIHD mice. **(A)** Relative mRNA levels of *ANP* and *BNP* in the hearts (n = 6). **(B)** Serum and cardiac biomarkers related to cardiac injury with or without miR-30d-5p mimic treatment upon WHI stimulation, including CK-MB and LDH (n = 6). **(C–E)** Echocardiographic and hemodynamic parameters (n = 6). **(F)** Total and insoluble collagen content were assessed in each group (n = 6). **(G)** Relative mRNA levels of *Tgf-β* and *Ctgf* in the hearts (n = 6). All data are presented as means ± SD. *p < 0.05 vs. the matched group.

Therefore, it is important to explore the mechanism of ROS regulation in the progression of heart disease. When ROS are produced in large quantities, excess free radicals are neutralized by increasing the production of intracellular antioxidants (including GSH, SOD, etc.). However, along with the antioxidants consumed, the fracture of the balance between the oxidation and the antioxidant system leads to ROS accumulation, which causes cardiac injury (Boengler et al., 2017). Studies have shown that oxidative stress also plays an important role in RIHD (Cuomo et al., 2016). Myocardial tissue contains a large amount of water, and the onset of water decomposition during radiation exposure subsequently produces a large amount of ROS (Vorotnikova et al., 2010). When the production of oxygen-free radicals exceeds the antioxidant capacity of cardiomyocytes, DNA damage occurs. According to previous reports, there are many forms of DNA damage, which can significantly change the structure of DNA and ultimately lead to cell cycle arrest, cell death, mutation, and other effects (Marnett et al., 2003; Yamamori et al., 2012). The DNA damage repair (DDR) pathway is mediated by a variety of functional proteins and is an important mechanism for repairing DNA damage and ensuring the integrity of the genome (Martinet et al., 2002). The p53 gene is one of the main effectors of the DDR signaling pathway (Bhattacharya and Asaithamby, 2016). Analogously, the Bax family also alters with radiation stimulation, leading to increased apoptosis (Sridharan et al., 2014). In addition to DNA damage, ROS can also cause lipid and protein peroxidation and activate a variety of signaling pathways (Dent et al., 2003). Consistent with the results of previous studies, we found that the markers of myocardial injury in WHI mice were significantly increased, accompanied by cardiac dysfunction and hemodynamic alternation. However, cardiac injury and dysfunction was improved in WHI mice with miR-223-3p mimic pretreatment. In addition, we found that WHI increased the production of ROS, superoxide, MDA, and 4-HNE and reduced the antioxidant-related biomarkers, including TAOC, SOD, and GSH. However, miR-223-3p mimic alleviated the alternations of oxidative stress induced by WHI. NRF2 is an antioxidant transcription factor that regulates the expression of a variety of antioxidant enzymes (Tonelli et al., 2018) and is particularly important for maintaining the balance of the oxidation/antioxidant system in WHI mice. In this study, we observed that miR-223-3p mimic significantly upregulated the protein levels of NRF2 and its downstream HO-1 in WHI mice, which also partly accounts for the fact that miR-223-3p mimic alleviated oxidative stress level induced by WHI stimulation.

Apoptosis is a main form of myocardial programmed cell death that is regulated by the Bcl-2 family and caspase family of proteins (Brentnall et al., 2013; Shi et al., 2017). Numerous studies have shown that animal models with cardiac disease involve apoptosis (Baba et al., 2018; Bruni et al., 2018). Programmed cell

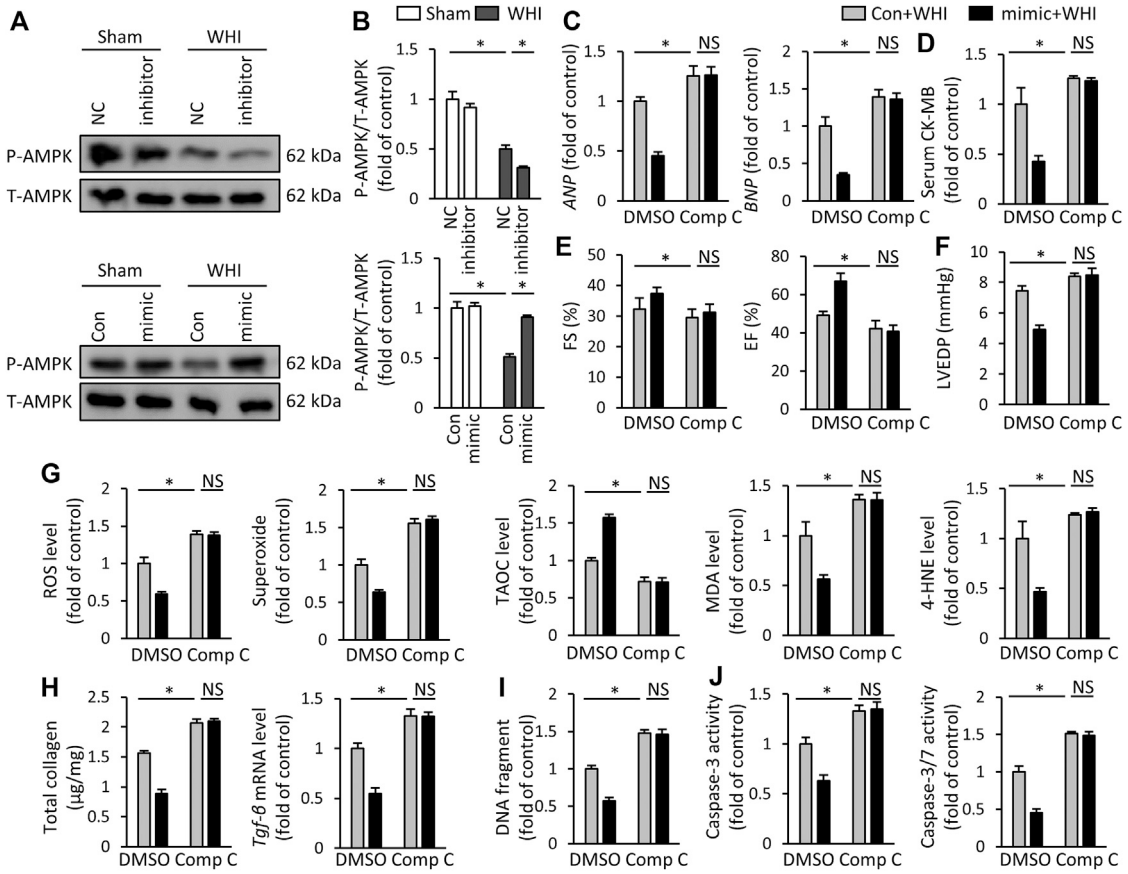

FIGURE 6 | miR-223-3p mimic improves WHI-induced RIHD by activating AMPK **(A, B)** Protein expression of total AMPK and phosphorylation AMPK (n = 6). **(C)** Relative mRNA levels of *ANP* and *BNP* (n = 6). **(D)** Serum CK-MB level (n = 6). **(E, F)** The alteration in FS, EF, and LVEDP in mice with or without compound C administration (n = 6). **(G)** ROS content and oxidative products in mice (n = 6). **(H)** Determination of the total collagen content and relative mRNA level of TGF-β (n = 6). **(I)** Quantitative results of DNA fragments (n = 6). **(J)** Quantitative results of caspase-3 activity and caspase-3/7 activity (n = 6). All data are presented as means ± SD. *p < 0.05 vs. the matched group.

death is a tightly regulated signaling process required for myocardial homeostasis. Intrinsic apoptosis, mediated by the mitochondrial outer membrane permeabilizatione, is mitochondrial-centered cell death. The initiation and execution of these processes are regulated by the Bcl-2 and caspase protein family (Danial and Korsmeyer, 2004; Galluzzi et al., 2012). The activation of Bcl-2 family member Bax results in the release of mitochondrial outer membrane permeabilization and cytochrome c from the interstitial space into the cytoplasm (Eskes et al., 2000; Wei et al., 2000; Wei et al., 2001). Subsequently, cytochrome c binds Apaf-1 to form apoptotic bodies and activate caspase-9. Once activated, caspase-9 directly cleaves and activates caspase-3 and caspase-7 (Li et al., 1997; Srinivasula et al., 1998). Hence, the level of caspase-3 and caspase-7 together with mRNA levels of Bcl-2 and Bax reflect the degree of programmed cell death. Our data suggested that miR-223-3p mimic ameliorated WHI-induced programmed cell death. The reduction of programmed cell death implied more viable cardiomyocytes involved in the pumping force of the heart. Replacement fibrosis replaces dead cardiomyocytes with extracellular matrix tissue and fibroblasts, preserving tissue integrity at the expense of muscle bundle continuity (Talman and Ruskoaho, 2016). The reduction of myocardial fibrosis improves the elevation of myocardial compliance, which partly accounts for the effects of miR-223-3p mimic in improving cardiac function. Consist with the result of cell death. The DNA damage and myocardial fibrosis were aggravated in mice with miR-223-3p inhibitor but alleviated with miR-223-3p mimic treatment. Overall, our data indicated that miR-223-3p prevents WHI-induced cardiac injury and dysfunction through anti-oxidant and anti-programmed cell death mechanisms.

Many studies have shown that AMPK, as the core protein of heart energy metabolism, plays a critical role in the regulation of oxidative stress (Lai et al., 2016). AMPK activating promotes Nrf2 nuclear transfer, and then Nrf2 enters the nucleus and combines with the HO-1 promoter to promote the transcription of antioxidants (Lv et al., 2017). Meanwhile, activated AMPK is also essential for the introduction of cytosolic fatty acids into mitochondria. Phosphorylation of AMPK inactivates acetyl-CoA carboxylase (ACC), resulting in a decrease in the concentration of malonyl-CoA (Qi and Young, 2015). Consistently, we found miR-223-3p mimic alleviated WHI-induced cardiac injury by activating AMPK and further verified that inhibition of AMPK by the CompC administration completely offset the anti-apoptotic

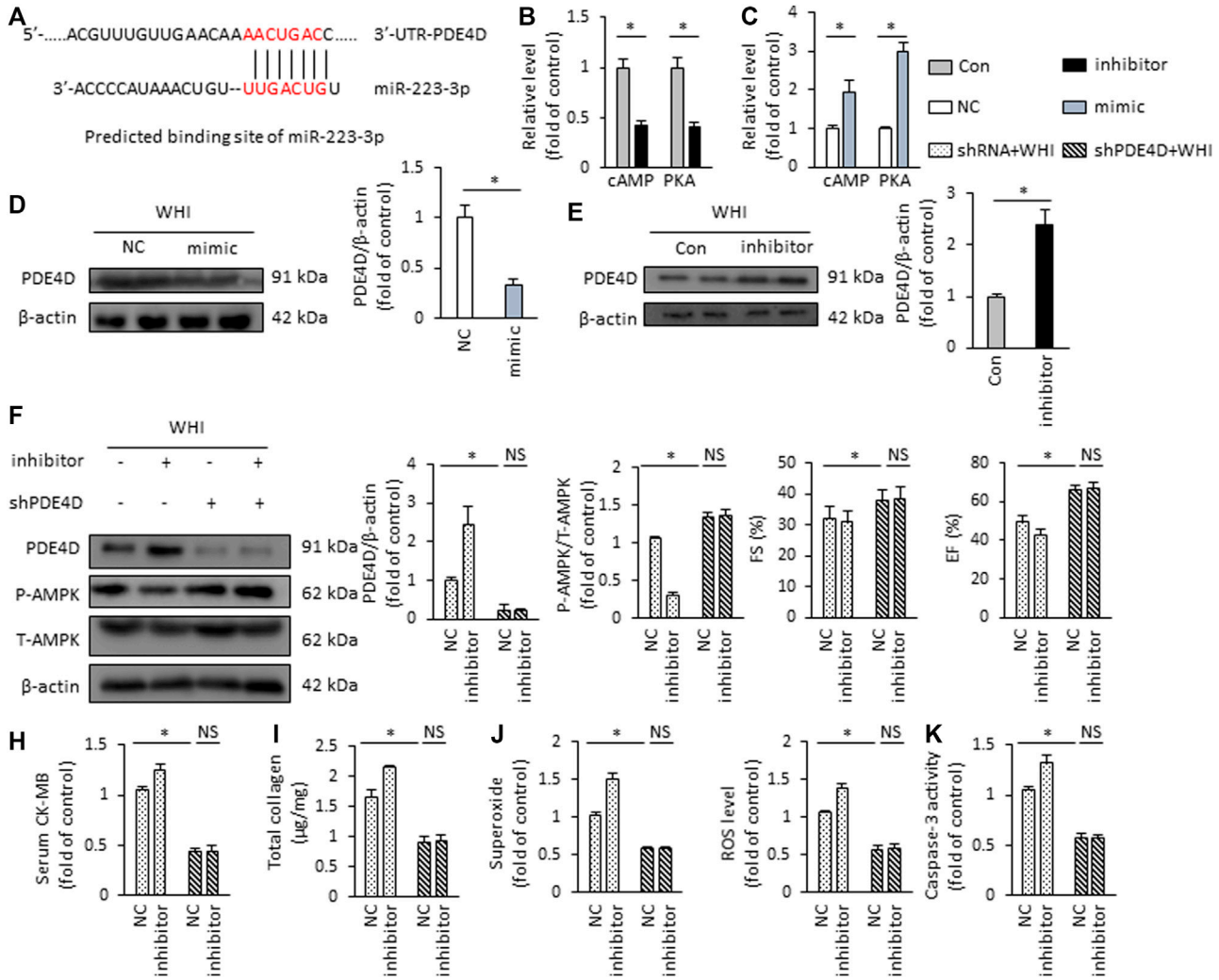

FIGURE 7 | miR-223-3p regulates PDE4D/AMPK signaling **(A)** Putative binding site of miR-223-3p by TargetScan Mouse 7.1. **(B, C)** Relative cAMP level and PKA activity in the hearts (n = 6). **(D, E)** Protein expression of PDE4D detected by Western blot (n = 6). **(F)** The protein expression alteration of PDE4D and AMPK in the hearts (n = 6). **(G)** The alteration in FS and EF in mice (n = 6). **(H)** Serum CK-MB level detected by ELISA kit (n = 6). **(I)** Total collagen content in the mice hearts (n = 6). **(J)** ROS content in the hearts (n = 6). **(K)** Quantitative results of caspase-3 activity (n = 6). All data are presented as means ± SD. *p < 0.05 vs. the matched group.

and antioxidant effects of miR-223-3p mimic in WHI mice. According to TargetScan Mouse 7.1 software, we determined the putative binding site of miR-223-3p in PDE4D 3′-UTR. Western blot results verified that miR-223-3p inhibits the expression of PDE4D. PDE4D, as a hydrolase of cAMP, inhibits the activity of downstream PKA by reducing the concentration of cAMP. PKA is a key kinase activated by AMPK (Chen et al., 2019). Furthermore, PDE4D inhibition by AAV9-shPDE4D injection reversed the inhibitory effect of miR-223-3p inhibitor on AMPK phosphorylation. Consequently, the pro-inflammatory and pro-oxidant effects of miR-223-3p inhibitor in WHI mice were also alleviated with AAV9-shPDE4D injection.

However, there are still some limitations in the current research. First, why is miR-223-3p downregulated in WHI mice hearts? Secondly, it is uncertain whether miR-223-3p inhibits WHI-induced programmed cell death depending on the production of ROS. Third, whether there are other signal pathways involved in the regulation of miR-223-3p on RIHD is not known. Finally, does miR-223-3p inhibit the effect of RT on tumors? All these issues need to be explored in future research.

In conclusion, we found for the first time that miR-223-3p inhibits programmed cell death and oxidative stress at least in part by regulating AMPK activation to protect against RIHD. This study provides potential ideas for RIHD treatment.

DATA AVAILABILITY STATEMENT

The original contributions presented in the study are included in the article/Supplementary Material; further inquiries can be directed to the corresponding authors.

ETHICS STATEMENT

The animal study was reviewed and approved by the Committee of Renmin Hospital of Wuhan University.

AUTHOR CONTRIBUTIONS

X-MX designed the experiments. D-MZ, J-JD, LX, Y-GW, and X-MX performed the experiments and analyzed the data. Y-FZ supervised the project and provided materials and technical support. D-MZ, TT, Y-FZ, and X-MX drafted the manuscript. All authors contributed to the completion of the manuscript.

FUNDING

This work was supported by funding from the National Natural Science Foundation of China (No. 31971166).

REFERENCES

Baba, Y., Higa, J. K., Shimada, B. K., Horiuchi, K. M., Suhara, T., Kobayashi, M., et al. (2018). Protective Effects of the Mechanistic Target of Rapamycin Against Excess Iron and Ferroptosis in Cardiomyocytes. *Am. J. Physiology-Heart Circulatory Physiol.* 314, H659–H668. doi:10.1152/ajpheart.00452.2017

Bhattacharya, S., and Asaithamby, A. (2016). Ionizing Radiation and Heart Risks. *Semin. Cel Develop. Biol.* 58, 14–25. doi:10.1016/j.semcdb.2016.01.045

Bodega, G., Alique, M., Puebla, L., Carracedo, J., and Ramírez, R. M. (2019). Microvesicles: ROS Scavengers and ROS Producers. *J. Extracellular Vesicles* 8, 1626654. doi:10.1080/20013078.2019.1626654

Boengler, K., Kosiol, M., Mayr, M., Schulz, R., and Rohrbach, S. (2017). Mitochondria and Ageing: Role in Heart, Skeletal Muscle and Adipose Tissue. *J. Cachexia, Sarcopenia Muscle* 8, 349–369. doi:10.1002/jcsm.12178

Brentnall, M., Rodriguez-Menocal, L., De Guevara, R. L., Cepero, E., and Boise, L. H. (2013). Caspase-9, Caspase-3 and Caspase-7 Have Distinct Roles During Intrinsic Apoptosis. *BMC Cel Biol* 14, 32. doi:10.1186/1471-2121-14-32

Bruni, A., Bornstein, S., Linkermann, A., and Shapiro, A. M. J. (2018). Regulated Cell Death Seen Through the Lens of Islet Transplantation. *Cel Transpl.* 27, 890–901. doi:10.1177/0963689718766323

Cao, L., Xu, C., Yi, P., Li, H., Lin, Y., Cai, G., et al. (2021). Asparaginyl Endopeptidase (AEP) Regulates Myocardial Apoptosis in Response to Radiation Exposure via Alterations in NRF2 Activation. *Am. J. Cancer Res.* 11, 1206–1225. doi:10.3389/fonc.2021.603932

Chen, L., Hou, X., Zhang, M., Zheng, Y., Zheng, X., Yang, Q., et al. (2020). MicroRNA-223-3p Modulates Dendritic Cell Function and Ameliorates Experimental Autoimmune Myocarditis by Targeting the NLRP3 Inflammasome. *Mol. Immunol.* 117, 73–83. doi:10.1016/j.molimm.2019.10.027

Chen, M.-Y., Hsu, W.-C., Hsu, S.-C., Yang, Y.-S., Chuang, T.-H., Lin, W.-J., et al. (2019). PP4 Deficiency Leads to DNA Replication Stress that Impairs Immunoglobulin Class Switch Efficiency. *Cell Death Differ* 26, 1221–1234. doi:10.1038/s41418-018-0199-z

Cuomo, J. R., Sharma, G. K., Conger, P. D., and Weintraub, N. L. (2016). Novel Concepts in Radiation-Induced Cardiovascular Disease. *World J. Cardiol.* 8, 504–519. doi:10.4330/wjc.v8.i9.504

Danial, N. N., and Korsmeyer, S. J. (2004). Cell Death. *Cell* 116, 205–219. doi:10.1016/s0092-8674(04)00046-7

Dent, P., Yacoub, A., Fisher, P. B., Hagan, M. P., and Grant, S. (2003). MAPK Pathways in Radiation Responses. *Oncogene* 22, 5885–5896. doi:10.1038/sj.onc.1206701

Eskes, R., Desagher, S., Antonsson, B., and Martinou, J.-C. (2000). Bid Induces the Oligomerization and Insertion of Bax into the Outer Mitochondrial Membrane. *Mol. Cel Biol* 20, 929–935. doi:10.1128/mcb.20.3.929-935.2000

Fan, D., Yang, Z., Yuan, Y., Wu, Q.-Q., Xu, M., Jin, Y.-G., et al. (2017a). Sesamin Prevents Apoptosis and Inflammation After Experimental Myocardial Infarction by JNK and NF-Kb Pathways. *Food Funct.* 8, 2875–2885. doi:10.1039/c7fo00204a

Fan, Z., Han, Y., Ye, Y., Liu, C., and Cai, H. (2017b). l -Carnitine Preserves Cardiac Function by Activating P38 MAPK/Nrf2 Signalling in Hearts Exposed to Irradiation. *Eur. J. Pharmacol.* 804, 7–12. doi:10.1016/j.ejphar.2017.04.003

Galluzzi, L., Vitale, I., Abrams, J. M., Alnemri, E. S., Baehrecke, E. H., Blagosklonny, M. V., et al. (2012). Molecular Definitions of Cell Death Subroutines: Recommendations of the Nomenclature Committee on Cell Death 2012. *Cel Death Differ* 19, 107–120. doi:10.1038/cdd.2011.96

Gomes, C. P. D. C., Schroen, B., Kuster, G. M., Robinson, E. L., Ford, K., Squire, I. B., et al. (2020). Regulatory RNAs in Heart Failure. *Circulation* 141, 313–328. doi:10.1161/circulationaha.119.042474

Guo, Z., Tang, N., Liu, F. Y., Yang, Z., Ma, S. Q., An, P., et al. (2020). TLR9 Deficiency Alleviates Doxorubicin-Induced Cardiotoxicity via the Regulation of Autophagy. *J. Cel Mol Med* 24, 10913–10923. doi:10.1111/jcmm.15719

Han, Y., Zhang, J., Huang, S., Cheng, N., Zhang, C., Li, Y., et al. (2021). MicroRNA-223-3p Inhibits Vascular Calcification and the Osteogenic Switch of Vascular Smooth Muscle Cells. *J. Biol. Chem.* 296, 100483. doi:10.1016/j.jbc.2021.100483

Hawkins, P. G., Sun, Y., Dess, R. T., Jackson, W. C., Sun, G., Bi, N., et al. (2019). Circulating microRNAs as Biomarkers of Radiation-Induced Cardiac Toxicity in Non-Small-Cell Lung Cancer. *J. Cancer Res. Clin. Oncol.* 145, 1635–1643. doi:10.1007/s00432-019-02903-5

Ichihara, S., Noda, A., Nagata, K., Obata, K., Xu, J., Ichihara, G., et al. (2006). Pravastatin Increases Survival and Suppresses an Increase in Myocardial Matrix Metalloproteinase Activity in a Rat Model of Heart Failure. *Cardiovasc. Res.* 69, 726–735. doi:10.1016/j.cardiores.2005.08.001

Lai, Y.-C., Tabima, D. M., Dube, J. J., Hughan, K. S., Vanderpool, R. R., Goncharov, D. A., et al. (2016). SIRT3-AMP-Activated Protein Kinase Activation by Nitrite and Metformin Improves Hyperglycemia and Normalizes Pulmonary Hypertension Associated with Heart Failure with Preserved Ejection Fraction. *Circulation* 133, 717–731. doi:10.1161/circulationaha.115.018935

Laugaard Lorenzen, E., Christian Rehammar, J., Jensen, M.-B., Ewertz, M., and Brink, C. (2020). Radiation-induced Risk of Ischemic Heart Disease Following Breast Cancer Radiotherapy in Denmark, 1977-2005. *Radiother. Oncol.* 152, 103–110. doi:10.1016/j.radonc.2020.08.007

Lee, C. L., Moding, E. J., Cuneo, K. C., Li, Y., Sullivan, J. M., Mao, L., et al. (2012). p53 Functions in Endothelial Cells to Prevent Radiation-Induced Myocardial Injury in Mice. *Sci. Signal.* 5, ra52. doi:10.1126/scisignal.2002918

Li, P., Nijhawan, D., Budihardjo, I., Srinivasula, S. M., Ahmad, M., Alnemri, E. S., et al. (1997). Cytochrome C and dATP-Dependent Formation of Apaf-1/Caspase-9 Complex Initiates an Apoptotic Protease Cascade. *Cell* 91, 479–489. doi:10.1016/s0092-8674(00)80434-1

Liu, F.-Y., Fan, D., Yang, Z., Tang, N., Guo, Z., Ma, S.-Q., et al. (2019). TLR9 Is Essential for HMGB1-Mediated Post-Myocardial Infarction Tissue Repair Through Affecting Apoptosis, Cardiac Healing, and Angiogenesis. *Cell Death Dis* 10, 480. doi:10.1038/s41419-019-1718-7

Lv, H., Liu, Q., Wen, Z., Feng, H., Deng, X., and Ci, X. (2017). Xanthohumol Ameliorates Lipopolysaccharide (LPS)-Induced Acute Lung Injury via Induction of AMPK/GSK3β-Nrf2 Signal Axis. *Redox Biol.* 12, 311–324. doi:10.1016/j.redox.2017.03.001

Ma, C. X., Zhao, X. K., and Li, Y. D. (2019). New Therapeutic Insights into Radiation-Induced Myocardial Fibrosis. *Ther. Adv. Chronic Dis.* 10, 2040622319868383. doi:10.1177/2040622319868383

Ma, S. Q., Guo, Z., Liu, F. Y., Hasan, S. G., Yang, D., Tang, N., et al. (2021). 6-Gingerol Protects Against Cardiac Remodeling by Inhibiting the P38 Mitogen-Activated Protein Kinase Pathway. *Acta Pharmacol. Sin* 42 (10), 1575–1586. doi:10.1038/s41401-020-00587-z

Marnett, L. J., Riggins, J. N., and West, J. D. (2003). Endogenous Generation of Reactive Oxidants and Electrophiles and Their Reactions with DNA and Protein. *J. Clin. Invest.* 111, 583–593. doi:10.1172/jci200318022

Martinet, W., Knaapen, M. W. M., De Meyer, G. R. Y., Herman, A. G., and Kockx, M. M. (2002). Elevated Levels of Oxidative DNA Damage and DNA Repair

Enzymes in Human Atherosclerotic Plaques. *Circulation* 106, 927–932. doi:10.1161/01.cir.0000026393.47805.21

Matsuzaki, J., and Ochiya, T. (2018). Extracellular microRNAs and Oxidative Stress in Liver Injury: A Systematic Mini Review. *J. Clin. Biochem. Nutr.* 63, 6–11. doi:10.3164/jcbn.17-123

O'Connell, R. M., Rao, D. S., and Baltimore, D. (2012). microRNA Regulation of Inflammatory Responses. *Annu. Rev. Immunol.* 30, 295–312. doi:10.1146/annurev-immunol-020711-075013

Ping, Z., Peng, Y., Lang, H., Xinyong, C., Zhiyi, Z., Xiaocheng, W., et al. (2020). Oxidative Stress in Radiation-Induced Cardiotoxicity. *Oxid Med. Cel Longev* 2020, 3579143. doi:10.1155/2020/3579143

Pohjoismäki, J. L., and Goffart, S. (2017). The Role of Mitochondria in Cardiac Development and Protection. *Free Radic. Biol. Med.* 106, 345–354. doi:10.1016/j.freeradbiomed.2017.02.032

Qi, D., and Young, L. H. (2015). AMPK: Energy Sensor and Survival Mechanism in the Ischemic Heart. *Trends Endocrinol. Metab.* 26, 422–429. doi:10.1016/j.tem.2015.05.010

Raghunathan, D., Khilji, M. I., Hassan, S. A., and Yusuf, S. W. (2017). Radiation-Induced Cardiovascular Disease. *Curr. Atheroscler. Rep.* 19, 22. doi:10.1007/s11883-017-0658-x

Sárközy, M., Gáspár, R., Zvara, Á., Kiscsatári, L., Varga, Z., Kővári, B., et al. (2019). Selective Heart Irradiation Induces Cardiac Overexpression of the Pro-Hypertrophic miR-212. *Front. Oncol.* 9, 598. doi:10.3389/fonc.2019.00598

Shi, J., Gao, W., and Shao, F. (2017). Pyroptosis: Gasdermin-Mediated Programmed Necrotic Cell Death. *Trends Biochem. Sci.* 42, 245–254. doi:10.1016/j.tibs.2016.10.004

Sridharan, V., Aykin-Burns, N., Tripathi, P., Krager, K. J., Sharma, S. K., Moros, E. G., et al. (2014). Radiation-Induced Alterations in Mitochondria of the Rat Heart. *Radiat. Res.* 181, 324–334. doi:10.1667/rr13452.1

Srinivasula, S. M., Ahmad, M., Fernandes-Alnemri, T., and Alnemri, E. S. (1998). Autoactivation of Procaspase-9 by Apaf-1-Mediated Oligomerization. *Mol. Cel* 1, 949–957. doi:10.1016/s1097-2765(00)80095-7

Sun, W., Lee, T.-S., Zhu, M., Gu, C., Wang, Y., Zhu, Y., et al. (2006). Statins Activate AMP-Activated Protein Kinase In Vitro and In Vivo. *Circulation* 114, 2655–2662. doi:10.1161/circulationaha.106.630194

Talman, V., and Ruskoaho, H. (2016). Cardiac Fibrosis in Myocardial Infarction-From Repair and Remodeling to Regeneration. *Cell Tissue Res* 365, 563–581. doi:10.1007/s00441-016-2431-9

Tang, Q., Li, M.-Y., Su, Y.-F., Fu, J., Zou, Z.-Y., Wang, Y., et al. (2018). Absence of miR-223-3p Ameliorates Hypoxia-Induced Injury Through Repressing Cardiomyocyte Apoptosis and Oxidative Stress by Targeting KLF15. *Eur. J. Pharmacol.* 841, 67–74. doi:10.1016/j.ejphar.2018.10.014

Tonelli, C., Chio, I. I. C., and Tuveson, D. A. (2018). Transcriptional Regulation by Nrf2. *Antioxid. Redox Signaling* 29, 1727–1745. doi:10.1089/ars.2017.7342

Vorotnikova, E., Rosenthal, R. A., Tries, M., Doctrow, S. R., and Braunhut, S. J. (2010). Novel Synthetic SOD/Catalase Mimetics Can Mitigate Capillary Endothelial Cell Apoptosis Caused by Ionizing Radiation. *Radiat. Res.* 173, 748–759. doi:10.1667/rr1948.1

Wang, H., Wei, J., Zheng, Q., Meng, L., Xin, Y., Yin, X., et al. (2019). Radiation-Induced Heart Disease: A Review of Classification, Mechanism and Prevention. *Int. J. Biol. Sci.* 15, 2128–2138. doi:10.7150/ijbs.35460

Wei, M. C., Lindsten, T., Mootha, V. K., Weiler, S., Gross, A., Ashiya, M., et al. (2000). tBID, A Membrane-Targeted Death Ligand, Oligomerizes BAK to Release Cytochrome C. *Genes Dev.* 14, 2060–2071. doi:10.1101/gad.14.16.2060

Wei, M. C., Zong, W.-X., Cheng, E. H.-Y., Lindsten, T., Panoutsakopoulou, V., Ross, A. J., et al. (2001). Proapoptotic BAX and BAK: A Requisite Gateway to Mitochondrial Dysfunction and Death. *Science* 292, 727–730. doi:10.1126/science.1059108

Wu, Y., Fan, Y., Huang, N., Zhang, S., Zhang, H., Liu, X., et al. (2021). Effect of Nicorandil Combined with Trimetazidine on miR-223-3p and NRF2 Expression in Patients with Coronary Heart Disease. *Am. J. Transl Res.* 13, 4804–4811. https://pubmed.ncbi.nlm.nih.gov/34150061/.

Yamamori, T., Yasui, H., Yamazumi, M., Wada, Y., Nakamura, Y., Nakamura, H., et al. (2012). Ionizing Radiation Induces Mitochondrial Reactive Oxygen Species Production Accompanied by Upregulation of Mitochondrial Electron Transport Chain Function and Mitochondrial Content Under Control of the Cell Cycle Checkpoint. *Free Radic. Biol. Med.* 53, 260–270. doi:10.1016/j.freeradbiomed.2012.04.033

Yun, S., Hu, R., Schwaemmle, M. E., Scherer, A. N., Zhuang, Z., Koleske, A. J., et al. (2019). Integrin α5β1 Regulates PP2A Complex Assembly Through PDE4D in Atherosclerosis. *J. Clin. Invest.* 129, 4863–4874. doi:10.1172/jci127692

Zhang, M., and Cheng, K. (2021). Long Non-Coding RNA KCNQ1OT1 Promotes Hydrogen Peroxide-Induced Lens Epithelial Cell Apoptosis and Oxidative Stress by Regulating miR-223-3p/BCL2L2 Axis. *Exp. Eye Res.* 206, 108543. doi:10.1016/j.exer.2021.108543

Zhang, M. W., Shen, Y. J., Shi, J., and Yu, J. G. (2020a). MiR-223-3p in Cardiovascular Diseases: A Biomarker and Potential Therapeutic Target. *Front. Cardiovasc. Med.* 7, 610561. doi:10.3389/fcvm.2020.610561

Zhang, X., Hu, C., Kong, C.-Y., Song, P., Wu, H.-M., Xu, S.-C., et al. (2020b). FNDC5 Alleviates Oxidative Stress and Cardiomyocyte Apoptosis in Doxorubicin-Induced Cardiotoxicity via Activating AKT. *Cel Death Differ* 27, 540–555. doi:10.1038/s41418-019-0372-z

Conflict of Interest: The authors declare that the research was conducted in the absence of any commercial or financial relationships that could be construed as a potential conflict of interest.

Publisher's Note: All claims expressed in this article are solely those of the authors and do not necessarily represent those of their affiliated organizations, or those of the publisher, the editors and the reviewers. Any product that may be evaluated in this article, or claim that may be made by its manufacturer, is not guaranteed or endorsed by the publisher.

Copyright © 2022 Zhang, Deng, Wu, Tang, Xiong, Zheng and Xu. This is an open-access article distributed under the terms of the Creative Commons Attribution License (CC BY). The use, distribution or reproduction in other forums is permitted, provided the original author(s) and the copyright owner(s) are credited and that the original publication in this journal is cited, in accordance with accepted academic practice. No use, distribution or reproduction is permitted which does not comply with these terms.

frontiers in Cell and Developmental Biology

ORIGINAL RESEARCH
published: 18 January 2022
doi: 10.3389/fcell.2021.784799

Sulphenylation of CypD at Cysteine 104: A Novel Mechanism by Which SO_2 Inhibits Cardiomyocyte Apoptosis

Boyang Lv[1], Hanlin Peng[1], Bingquan Qiu[1], Lulu Zhang[1], Mei Ge[1], Dingfang Bu[1], Kun Li[2], Xiaoqi Yu[2], Jiantong Du[3], Liu Yang[3], Chaoshu Tang[4,5], Yaqian Huang[1], Junbao Du[1,4]* and Hongfang Jin[1]**

[1]Department of Pediatrics, Peking University First Hospital, Beijing, China, [2]Key Laboratory of Green Chemistry and Technology, Ministry of Education, College of Chemistry, Sichuan University, Chengdu, China, [3]Department of Ophthalmology, Peking University First Hospital, Beijing, China, [4]Key Laboratory of Molecular Cardiology, Ministry of Education, Beijing, China, [5]Department of Physiology and Pathophysiology, Peking University Health Science Centre, Beijing, China

OPEN ACCESS

Edited by:
Zhi Qi,
Nankai University, China

Reviewed by:
Jie Tian,
Children's Hospital of Chongqing Medical University, China
Zhi-Ren Zhang,
Harbin Medical University, China

***Correspondence:**
Yaqian Huang
yaqianhuang@126.com
Junbao Du
junbaodu1@126.com
Hongfang Jin
jinhongfang51@126.com

Specialty section:
This article was submitted to Cell Death and Survival, a section of the journal Frontiers in Cell and Developmental Biology

Received: 28 September 2021
Accepted: 13 December 2021
Published: 18 January 2022

Citation:
Lv B, Peng H, Qiu B, Zhang L, Ge M, Bu D, Li K, Yu X, Du J, Yang L, Tang C, Huang Y, Du J and Jin H (2022) Sulphenylation of CypD at Cysteine 104: A Novel Mechanism by Which SO_2 Inhibits Cardiomyocyte Apoptosis. Front. Cell Dev. Biol. 9:784799. doi: 10.3389/fcell.2021.784799

Objectives: The study was designed to explore the role of endogenous gaseous signaling molecule sulfur dioxide (SO_2) in the control of cardiomyocyte apoptosis and its molecular mechanisms.

Methods: Neonatal mouse cardiac myocytes (NMCMs) and H9c2 cells were used in the cell experiments. The endogenous SO_2 pathway including SO_2 level and the expression of SO_2-generating enzyme aspartate aminotransferase 1/2 (AAT1/2) were detected in NMCMs. The apoptosis of cardiomyocytes was examined by a TUNEL assay. The cleavage and the activity of apoptotic proteins caspase9 and caspase3 were measured. The content of ATP, the opening of mitochondrial permeability transition pore (mPTP), and the cytochrome c (cytc) leakage were detected by immunofluorescence. The sulphenylation of cyclophilin-D (CypD) was detected by biotin switch analysis. The four CypD mutant plasmids in which cysteine sites were mutated to serine were constructed to identify the SO_2-affected site *in vitro*.

Results: ISO down-regulated the endogenous SO_2/AAT pathway of cardiomyocytes in association with a significant increase in cardiomyocyte apoptosis, demonstrated by the increases in apoptosis, cleaved-caspase3/caspase3 ratio, and caspase3 activity. Furthermore, ISO significantly reduced ATP production in H9c2 cells, but the supplement of SO_2 significantly restored the content of ATP. ISO stimulated mPTP opening, resulting in an increase in the release of cytc, which further increased the ratio of cleaved caspase9/caspase9 and enhanced the protein activity of caspase9. While, the supplementation of SO_2 reversed the above effects. Mechanistically, SO_2 did not affect CypD protein expression, but sulphenylated CypD and inhibited mPTP opening, resulting in an inhibition of cardiomyocyte apoptosis. The C104S mutation in CypD abolished SO_2-induced sulphenylation of CypD, and thereby blocked the inhibitory effect of SO_2 on the mPTP opening and cardiomyocyte apoptosis.

Conclusion: Endogenous SO_2 sulphenylated CypD at Cys104 to inhibit mPTP opening, and thus protected against cardiomyocyte apoptosis.

Keywords: sulfur dioxide, cardiomyocyte, apoptosis, sulphenylation, CypD

1 INTRODUCTION

Myocardial injury is an important pathophysiological process in a variety of cardiovascular diseases (Jin et al., 2013), including hypertension, heart failure, and coronary heart disease (Leong et al., 2017). Cardiomyocyte apoptosis plays a crucial part in cardiovascular diseases (Singh et al., 2011). Therefore, clarifying the mechanisms underlying cardiomyocyte apoptosis in cardiovascular diseases has always been the focus of the research (Abbate and Narula, 2012). However, the exact mechanisms for cardiomyocyte apoptosis have not yet been fully clarified.

Sulfur dioxide (SO_2) had been regarded as a waste gas in air pollution. Recent literature has shown that cardiovascular tissues can produce SO_2 endogenously (Du et al., 2008a). Increasing evidences have confirmed that the endogenous SO_2 exerts crucial cardiovascular pathophysiologic functions (Zhou et al., 2020). Our previous animal study showed that the down-regulated endogenous SO_2/AAT pathway might be involved in the mechanisms underlying isoproterenol (ISO)-induced myocardial damage, and the protective role of SO_2 might be related to the enhancement of myocardial antioxidant capacity in rats (Liang et al., 2011). In addition, Jin et al. (2013) found that myocardial injury is related to the inhibition of the bcl2/cytc/caspase9/caspase3 pathway mediated by SO_2. However, the molecular mechanisms by which endogenous SO_2 protected cardiomyocyte injury and apoptosis are completely not clear.

Mitochondrial permeability transition refers to the process that the inner membrane of mitochondria allows solutes up to 1.5 kDa to pass freely (Kwong and Molkentin, 2015). Prolonged opening of mitochondrial permeability transition pore (mPTP) can lead to mitochondrial energy dysfunction, swelling, rupture, apoptosis, and necrotic cell death (Zhou et al., 2019). Cyclophilin-D (CypD) locates in the mitochondrial matrix and is a peptidyl-prolyl isomerase. CypD translocates from mitochondrial matrix to mitochondrial inner membrane and binds to adenine nucleotide translocator (ANT) to initiate the formation of mPTP complex. Therefore, CypD acts as an important regulator of switching the mPTP opening (Sun et al., 2019). It has been reported that a variety of post-translational modifications occur in CypD (Elrod and Molkentin, 2013), such as S-nitrosylation (Nguyen et al., 2011), acetylation (Amanakis et al., 2021), and phosphorylation (Hurst et al., 2020). As a small gaseous signaling molecule, SO_2 regulates downstream proteins and exerts biological effects through post-translational sulphenylation. As a reversible form of post-translational modification, sulphenylation can oxidize cysteine mercaptan to sulphenic acid (Cys-SOH) and regulate protein function (Song et al., 2020). According to the amino acid sequence analysis of the CypD, the human CypD protein contains four cysteines. However, it is not clear whether endogenous SO_2 can inhibit the opening of mPTP to reduce cardiomyocyte apoptosis through the sulphenylation of CypD.

Therefore, in this study, the role of the endogenous SO_2 in the development of ISO-induced cardiomyocyte apoptosis was investigated. Moreover, we explored its mechanism from a new point of view that SO_2 likely inhibits the opening of mPTP by chemically modifying CypD, thus alleviating cardiomyocyte apoptosis.

2 MATERIALS AND METHODS

2.1 Reagent

Sodium hydrogen sulfite and sodium sulfite ($NaHSO_3/Na_2SO_3$, freshly mixed at 1:3 M ratio, pH 7.4) were used as SO_2 donors and purchased from Sigma (Zhang et al., 2021). Isoprenaline hydrochloride was purchased from Sigma (I5627). A chemically selective fluorescent probe SS-1 was provided by Professor Kun Li and Xiaoqi Yu. DAz-2 was used as a protein sulphenylation probe (13382, Cayman, Michigan, USA) to capture and enrich the sulphenylated protein. The primary antibodies in the present study included CypD (abcam, USA), AAT1 (Sigma, USA), AAT2 (Sigma, USA), β-actin (Zsbio, China), caspase9 (CST, USA), caspase3 (Beyotime, China), cleaved caspase3 (Beyotime, China), cytc (santa, USA), His (Zsbio, China), and β-tubulin (Zsbio, China). Human CypD wild type (WT), and C104S, C82S, C157S, and C203S mutant plasmids were constructed by Sangon Biotech. The information of three kinds of ATP plasmids used in this study are as follows: EcAT3.10 (Conley et al., 2017) was deposited at Addgene by Mathew Tantama (Addgene plasmid #107215); pm-iATPSnFR1.1 (Lobas et al., 2019) (Addgene plasmid #102549) and cyto-iATPSnFR1.0 (Lobas et al., 2019) (Addgene plasmid #102550) were deposited at Addgene by Baljit Khakh.

2.2 Cell Culture and Treatment

Culture of NMCMs: The kit for isolation of primary mouse cardiomyocytes was purchased from Thermo Fisher (Waltham, USA). In brief, the ventricular tissue parts from 1–2 days old C57BL/6J mouse neonates were subjected to modified enzymatic digestion. The enriched cardiomyocytes were cultured in DMEM with 1% penicillin-streptomycin solution (PS) and 10% fetal bovine serum (FBS). A cardiomyocyte growth supplement was added to inhibit the growth of the remaining fibroblasts.

NMCMs were divided randomly into control, ISO, ISO + SO_2, and SO_2 groups. For the control group, the cells were treated with the equivalent amount of saline for 48 h. For the ISO group, they were treated with 10 μmol/L ISO for 48 h. For the ISO + SO_2 group, the cells were given 100 μmol/L SO_2 donor for 30 min and 10 μmol/L ISO for 48 h (Ding et al., 2005). For the SO_2 group, cells were treated with 100 μmol/L SO_2 donor for 0.5 h and the equivalent amount of saline for 48 h.

H9c2 cell culture: H9c2 rat embryonic cardiomyocytes were purchased from the National Infrastructure of Cell Line Resource (China) and they were cultured in DMEM medium containing 10% FBS, 1% PS, and 1% glutathione in 5% CO_2 at 37°C. After a 6 h of synchronous treatment in serum-free medium, the cell treatment and grouping were similar to those in NMCMs, except that in H9c2 cells the ISO treatment was 200 μmol/L for 24 h (Deng et al., 2017).

2.3 *In situ* Fluorescent Imaging of SO_2

SS-1 is a chemically selective fluorescent probe for *in situ* visualization of SO_2, developed and presented by Kun Li from Sichuan University, Sichuan, China (Yang et al., 2017). As mentioned in the previous study, SO_2 in NMCMs was tested with an SS-1 probe (Huang et al., 2021a). The cells were incubated with a 10 μM probe for 30 min at 37°C and then they were washed with PBS for removing the unlabeled probe. Subsequently, the cells were fixed with 4% paraformaldehyde solution. Finally, DAPI was added to stain nuclei. The green fluorescence detected by Olympus confocal laser scanning microscope (CK40, Olympus, Japan) is considered to be a positive signal.

2.4 AAT Activity Detected by Colorimetric Assay

AAT assay kit (Njjcbio, Nanjing, China) was used as described previously (Zhang et al., 2021). Firstly, cells were collected and lysed on ice with pre-cooled PBS for 30 min. The substrate solution and tested samples were added into the 96-well plate, and reacted at 37°C for 30 min. Then, 2,4-dinitrophenylhydrazine was added to each well, and the plate was placed at 37°C for 20 min. Finally, sodium hydroxide solution (200 μl, 0.4 mol/L) was added and gently mixed into each well. The plate was incubated at room temperature for 15 min. Finally, the optical density was measured at the absorption wavelength of 510 nm.

2.5 *In situ* Detection of Apoptosis in NMCMs and H9c2 Cells by TdT-Mediated dUTP Nick End Labeling Assay

In situ cell death detection kit (Roche, Mannheim, Germany) was used as described previously (Du et al., 2018). Firstly, after gently rinsed with PBS, the cells were fixed in 4% paraformaldehyde for 1 h. Subsequently, they were permeabilized in 0.3% triton-X100 solution for 2 min. They were incubated with the TUNEL reaction mixture for 60 min at 37°C, preventing from light after washing with PBS. Finally, the nuclei were stained by a DAPI dye. The fluorescence images were captured with the help of a confocal laser scanning microscope (CK40, Olympus, Japan). The cell apoptosis was measured by using the percentage of TUNEL positive cells to the total DAPI positive cells (Du et al., 2018).

2.6 ATP Fluorescence Intensity of Cytoplasm and Cell Surface Monitored by Immunofluorescence Method in H9c2 Cells

H9c2 cells were seeded and grown to 50% confluency, and then pmiATPSnFR1.1 and cyto-iATPSnFR1.0 were respectively transfected into H9c2 cells, which were replaced with a complete culture medium after a 6 h-transfection. The cells were imaged under a confocal laser scanning microscope (TCS SP8, Leica, Wetzlar, Germany) by the excitation at 473 nm and the emission at 525 nm.

2.7 ATP Fluorescence Intensity of Extracellular Matrix Monitored by Immunofluorescence Method in H9c2 Cells

The plasmid ecAT3.10 was transfected into 50% confluent H9c2 cells with a lipofectamine 3000 transfection reagent (Invitrogen, Carlsbad, CA, United States). After a 6 h-transfection, the freshly completed culture medium was replaced. The activity of the ecATeam sensor was measured by examining the fluorescence intensities in CFP, CFP-YFPFRET, and YFP channels as described in the previous study. The settings of the bandpass filter were identical to those previously reported (Conley et al., 2017). The ratio of CFP-YFPFRET to YFP is expressed as the activity of the ecATeam biosensor. The conformational change of the probe induced by ATP binding to the ecATeam probe increases the Förster resonance energy transfer (FRET) between the CFP donor and the YFP receptor (Imamura et al., 2009). Therefore, the higher the ratio of CFP-YFPFRET to CFP, the more extracellular ATP binding, which indirectly reflects the extracellular ATP content.

2.8 Detection of Enzymatic Activities of Caspase3 and Caspase9 in H9c2 Cells

The enzymatic activities of caspase3 and caspase9 in H9c2 cells were detected with the commercial caspase3 and caspase9 activity kit, respectively (Applygen, Beijing, China) (Wang X. et al., 2019). Briefly, with the lysis buffer, the cells were lysed for 30 min at 4°C, and then centrifuged at 12,000 g for 5 min to harvest the supernatant. The concentration of protein was measured by the Bradford method. Then, 50 μg of cell lysate mixed with a reaction reagent was added to each well in a 96-well plate in order and then incubated for a period of 2 h at 37°C away from light. The activity of caspase3 or caspase9 was calculated from the absorbance value at 405 nm.

2.9 Detection of the mPTP Opening in NMCMs and H9c2 Cells

The mPTP opening was detected using the mPTP detection kit (Genmed, Shanghai, China) according to the instruction of the manufacture. The detection principle is that the fluorescence of calcein-AM is quenched when it leaks from mitochondria via the opening mPTP. Therefore, the strong green fluorescence represents the closed mPTP while the faint green fluorescence represents the opening mPTP. After completing the cell experiment, the cells were rinsed and incubated with the staining working solution for 20 min at 37°C in the dark. The remaining staining solution was removed by twice rinse with the cleaning solution. After the fixation with 4% paraformaldehyde, the fluorescence was observed by using a laser confocal microscopy (CK40, Olympus, Japan) with 488 nm excitation (Ex) and 505 nm emission (Em) settings (Song et al., 2018).

2.10 Detection of the Leakage of Mitochondrial Cytc in NMCMs

To determine the cytc subcellular localization, NMCMs were firstly incubated with the pre-warmed medium which contained 200 nmol/L MitoTracker (Life Technologies, USA) for 1 h. After the fixation with 4% paraformaldehyde, the cells were permeabilized in 0.1% Triton-X100 solution for 30 min, and then the cells were incubated with the cytc primary antibody at 4°C overnight. After the triplicate rinses with PBS buffer, an Alexa 594-conjugated secondary antibody (Life Technologies, USA) was added and then incubated for 90 min at 37°C in a dark container. Finally, images were captured with laser confocal microscopy (SP8-STED, Leica, Germany) (Wang X. et al., 2019).

2.11 CypD Sulphenylation Detection by Biotin Switch Analysis

Sulphenylation of CypD in the H9c2 cells and purified CypD protein was detected by the BSA method as previously reported (Huang et al., 2021a). The H9c2 cells were lysed in a non-denaturing lysis buffer (Applygen, Beijing, China) containing 5 mM DAz-2 for 20 min. The supernatant was collected by centrifuging at 16,000 g for 4 min at 4°C and gently shaken for 2.5 h at 37°C to label the DAZ-2. The DAz-2-labelled samples reacted with 250 μM p-biotin in a water bath for 2 h at 37°C. Then, the hyperlinked Neutral Affinity Protein™ was added at a volume ratio of 1–10 (Thermo Fisher Science) and incubated in a shaker for 4 h to capture the sulfenylated protein at 4°C. The sulphenylated proteins were mixed with a non-denaturing sample buffer and boiled for 10 min. Then, the supernatant was collected by centrifuging at 5,000 g for 10 min and it was subjected to western blot for the sulphenylation of CypD.

The human purified CypD protein (Abnova) was randomly divided into 3 groups: control, SO_2, and SO_2+DTT groups. The amount of purified protein used in each group was 0.1 μg. The protein was incubated for 2 h at 37°C. After the termination of the incubation experiment, the purified protein was divided into two portions to detect the sulphenylation of CypD and total CypD, respectively. The CypD sulphenylation was detected according to the abovementioned protocol in the cell experiment.

2.12 *In situ* Detection of CypD Sulphenylation in H9c2 Cells

A sulphenylated protein cell-based detection kit (Cayman, USA) with a DAz-2-based fluorescence probe was used to visualize the sulphenylated proteins in cells (Song et al., 2020). The cells were treated with 100 μM SO_2 for 1 h or SO_2 plus 200 μM DTT for 15 min. The sulphenylation of CypD in H9c2 cells was observed by the co-localization of the fluorescent signals indicating CypD and sulphenylated proteins. Nuclei were stained with DAPI dye. The sulphenylated protein, CypD protein, and nuclei exhibited green, red, and blue fluorescence, respectively, with confocal laser-scanning microscope (Leica, Germany).

2.13 CypD Plasmid Transfection

The pcDNA3.1 vector for human CypD-WT, CypD-C82S, CypD-C104S, CypD-C157S, and CypD-C203S mutant plasmids was constructed by Sangon Biotech (Shanghai, China). When H9c2 cells grew to approximately 50–60% confluence, the cells were treated with jetPEI TM reagent (Polyplus-transfection, France) before treatment.

2.14 Western Blotting Analysis

The protein expression of AAT1, AAT2, cleaved caspase3, caspase3, cleaved caspase9, caspase9, CypD, and His in NMCMs and H9c2 cells was detected by a standard western blotting analysis as described in the previous study (Huang, et al., 2021a). Briefly, the cells were lysed using protein lysis buffer for 20 min at 4°C. The total protein was harvested and quantitated by the BCA method. The proteins were subjected to electrophoresis and they were subsequently transferred to nitrocellulose membranes. The protein bands were treated with primary antibodies at 4°C overnight, respectively. Then, at room temperature, they were incubated with the corresponding horseradish peroxidase-coupled secondary antibody for 1 h. Finally, the protein bands were incubated by using the enhanced chemiluminescent western blotting substrate kit (GE, Pittsburgh, PA, United States) in a FluorChem M MultiFluor System (Protein Simple, San Francisco, CA, United States).

2.15 Gene Ontology Cellular Component Analysis

A dataset containing a total of 658 SO_2-mediated sulfenylated vascular smooth muscle cell (VSMC) proteins was from Huang's research (Huang et al., 2021a). The gene ontology cellular component analysis of the 658 SO_2-mediated sulfenylated VSMC proteins was performed by g: Profiler (https://biit.cs.ut.ee/gprofiler) (version e104_eg51_p15_3922dba). The parameters were set as follows: organism (Rattus norvegicus); statistical domain scope (only annotated genes); significance threshold (g:SCS threshold); and p values <0.05 indicated statistical significance.

2.16 Statistical Analysis

The statistical analysis was conducted using SPSS 17.0 (IBM, USA) and Graphpad Prism 8.0 (GraphPad Software Inc., San Diego, CA, United States). The data are expressed as mean ± standard error. A comparison among multiple groups was performed by ANOVA followed by LSD post-doc analysis if the data were normally distributed, while followed by Dunnett T3 post-doc analysis if the data were not normally distributed. A statistical significance is set by $p < 0.05$.

3 RESULTS

3.1 Endogenous SO_2 Controls ISO-Induced Apoptosis of Cardiomyocytes

ISO-stimulated NMCMs showed a marked decrease in SO_2 content as compared with the control group as evidenced by a significant

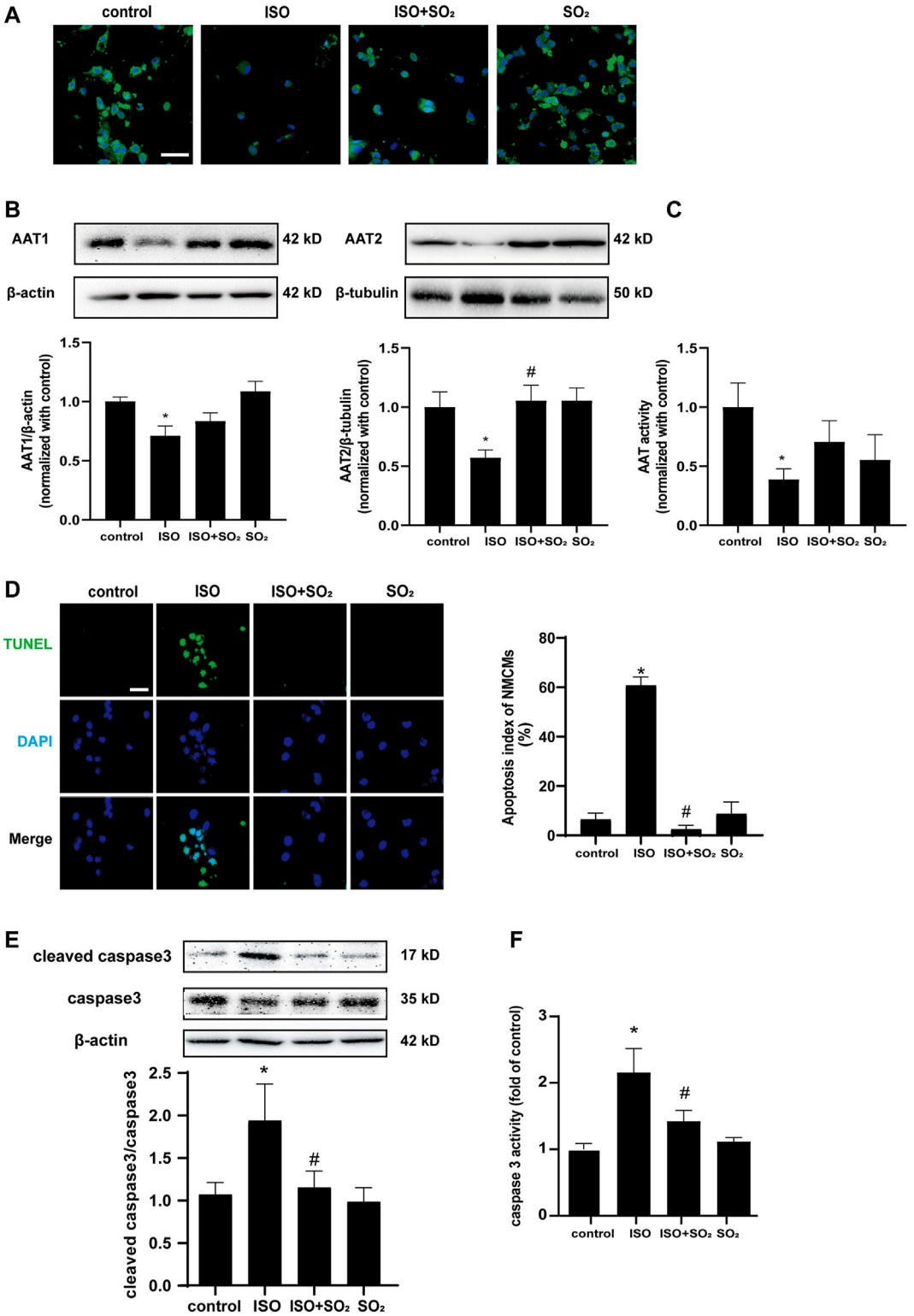

FIGURE 1 | Endogenous SO_2 controls ISO-induced apoptosis of cardiomyocytes. **(A)** SO_2 production in NMCMs was tested with *in situ* fluorescent SO_2 probe (green color, magnification, ×600; scale bar: 40 μm). **(B)** AAT1 and AAT2 expressions in NMCMs were measured by western blot. **(C)** AAT activity in NMCMs was detected by colorimetric assay. **(D)** The apoptosis of NMCMs was tested by TdT-mediated dUTP nick end labeling (TUNEL) assays (magnification, ×600; scale bar: 40 μm). **(E)** The caspase3 cleavage in H9c2 cells was measured by using western blot method. **(F)** A quantitative caspase3 activity analysis was done by the colorimetric kit. Data are expressed as mean ± SEM. $*p < 0.05$ versus control group; $^{\#}p < 0.05$ versus ISO group.

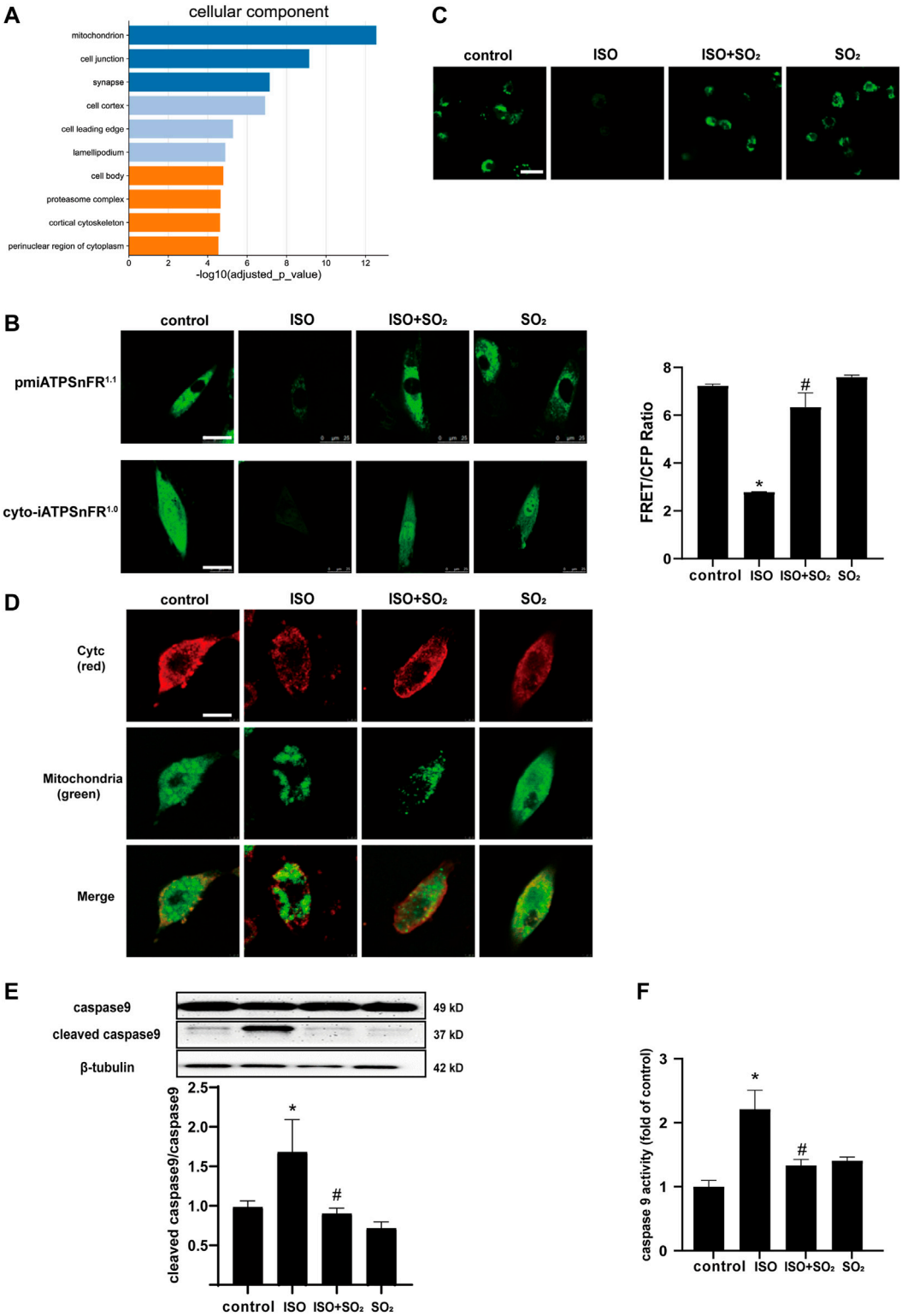

FIGURE 2 | SO_2 blocked ISO-induced mPTP opening and subsequent cardiomyocyte apoptosis. **(A)** GO-enriched cellular component (CC) reanalysis of the SO_2-affected redox proteomic dataset. **(B)** The fluorescence intensity of cell surface and cytoplasmic ATP were investigated by the transfection of H9c2 cells with pmiATPSnFR$^{1.1}$ and cyto-iATPSnFR$^{1.0}$, respectively (magnification, ×600; scale bar: 25 μm). The ATP fluorescence intensity of extracellular matrix monitored by immunofluorescence method in H9c2 cells. **(C)** The mPTP opening in H9c2 cells was tested with calcein-AM. The green fluorescence quenching indicated the opening of mPTP (magnification, ×600; scale bar: 20 μm). **(D)** The cytochrome c (cytc) leakage from the mitochondria was tested by using immunofluorescence microscopy, with red fluorescence representing cytc and green fluorescence representing mitochondria (magnification, ×600; scale bar: 50 μm). **(E)** Caspase9 cleavage measured by western blotting. **(F)** A quantitative caspase9 activity analysis was done by using a commercial colorimetric kit. Data are expressed as mean ± SEM. $*p < 0.05$ versus control group; $^{\#}p < 0.05$ versus ISO group.

decrease in SO_2-specific green fluorescence, and an obvious decrease in AAT1 and AAT2 protein expression, and AAT activity in the ISO-stimulated NMCMs (**Figures 1A–C**), accompanied by a significant increase in cell apoptosis, as evidenced by an increase in apoptotic cells, the cleaved-caspase3/caspase3 ratio, and caspase3 activity demonstrated by colorimetric assay (**Figures 1D–F**). The supplementation of SO_2 donors in ISO-stimulated NMCMs restored SO_2 content while significantly reduced the apoptotic cells, lowered the cleaved-caspase3/caspase3 ratio, and inhibited caspase3 activity (**Figure 1**). Therefore, the abovementioned data suggested that ISO stimulation downregulated the endogenous SO_2/AAT pathway and promoted cardiomyocyte apoptosis; whereas adequate endogenous SO_2 inhibited the apoptosis of cardiomyocytes.

3.2 SO_2 Blocked ISO-Induced mPTP Opening and Subsequent Cardiomyocyte Apoptosis

We performed a GO-enriched cellular component (CC) reanalysis of the SO_2-affected redox proteomic dataset and showed that differential proteins regulated by SO_2 were significantly enriched in mitochondria ($p = 2.829 \times 10^{-13}$) (**Figure 2A**). Furthermore, we compared the ATP fluorescence intensity in the cytoplasm, membrane, and extracellular matrix of H9c2 cells and found that ATP production was significantly reduced in H9c2 cells in the ISO group in comparison with the control group, and the supplementation with SO_2 significantly restored the ATP content (**Figures 2B,C**), suggesting that mitochondria might be an important target for the cytoprotective effect of SO_2 on cardiomyocytes.

The mPTP opening is an important event in the development of cardiomyocyte apoptosis under a variety of cardiac pathological conditions (Ahmad et al., 2019). Therefore, the present study analyzed the mitochondrial mPTP opening and downstream events. The results showed that ISO-stimulated NMCMs showed an increased mitochondrial mPTP opening, an increased cytc leakage from mitochondria, and an enhanced cleaved caspase9/caspase9 ratio and caspase9 activity in comparison with the control group; while SO_2 inhibited ISO-induced mPTP opening, suppressed the cytc release and reduced the ratio of cleaved caspase9/caspase9, thereby inhibiting apoptosis (**Figures 2D–F**). The results suggested that SO_2 significantly blocked ISO-opened mPTP, which might be involved in the mechanisms by which SO_2 inhibited cardiomyocyte apoptosis.

3.3 SO_2 Sulphenylated CypD and Thereby Blocked the mPTP Opening and Cardiomyocyte Apoptosis

CypD, a peptidyl-prolylcis-trans isomerase (PPI) present in the mitochondrial matrix, is an important redox-regulation-dependent mPTP regulator (Lam et al., 2015). Therefore, we tested if CypD was a candidate target of SO_2 to explore the possible mechanism by which SO_2 blocked mitochondrial mPTP opening.

Firstly, there were no significant effects of SO_2 on the protein level of CypD either in NMCMs or in H9c2 cells as shown in **Figures 3A,B** ($p > 0.05$). However, the sulphenylation of CypD in human purified CypD protein in the SO_2 group was markedly higher than that of the control group, which was blocked by a sulfhydryl reducing agent DTT treatment (p all<0.05) (**Figure 3C**).

Furthermore, the quantitative analysis and *in situ* visualization of CypD sulphenylation in the H9c2 cells were performed. The results revealed that in comparison with the control, the sulphenylation of CypD was increased in H9c2 cells of the SO_2 group, which was also successfully blocked by DTT (p all<0.05) (**Figure 3D**). The multi-color confocal images showed that the co-localization of the fluorescent signals indicating CypD and sulphenylated proteins was strong in H9c2 cells of the SO_2 group but weak in that of the control group and SO_2+DTT group (**Figure 3E**). Correspondingly, the mPTP opening and cell apoptosis were inhibited in the cells of the ISO + SO_2 group in comparison with the ISO group, while DTT treatment reversed the above protective effect of SO_2 (**Figures 3F,H**).

The above facts indicate that SO_2 can directly sulphenylate CypD protein, which might be associated with SO_2-inhibited mPTP opening and cell apoptosis.

3.4 The CypD Cys104 Might Be a Novel Target for SO_2 to Inhibit mPTP Opening and Cardiomyocyte Apoptosis

The human purified CypD protein has four cysteine sites: Cys82, Cys104, Cys157, and Cys203 (Linard et al., 2009). Homology analysis of CypD protein sequences among diverse species including human, goat, rat, mouse, pig, rabbit, chick and zebrafish showed that these four cysteine sites are all highly conserved among these different species (**Figure 4A**). Therefore, we mutated the four cysteine sites Cys82, Cys104, Cys157, and Cys203 to serine in the CypD protein, respectively, to clarify the precise site on which SO_2 affected CypD and then inhibited the cardiomyocyte apoptosis. The sulphenylation site screening results showed that the sulphenylation of CypD-His could be induced by SO_2 treatment in the H9c2 cells transfected with CypD-WT, C82S, C157S, and C203S plasmids, except in the cells transfected with CypD C104S plasmid (**Figure 4B**). The results suggested that the Cys104 in the CypD protein might be the sulphenylation site of SO_2.

Furthermore, the mPTP opening and the apoptosis of H9c2 cells was examined to identify if the CypD Cys104 might be the target of SO_2 affecting the cardiomyocyte apoptosis. The results showed that in the H9c2 cells transfected with CypD-WT plasmid, the mPTP opening in the ISO-stimulated cells was increased and the percentage of apoptotic cells was decreased by the SO_2 treatment, while DTT could reverse the effect of SO_2. In contrast, in the H9c2 cells transfected with CypD-C104S plasmid, SO_2 treatment failed to affect the ISO-stimulated mPTP opening and the apoptosis (**Figures 4C,D**). The result further confirmed that SO_2 sulphenylated CypD cysteine at Cys104, thereby inhibiting cardiomyocyte apoptosis.

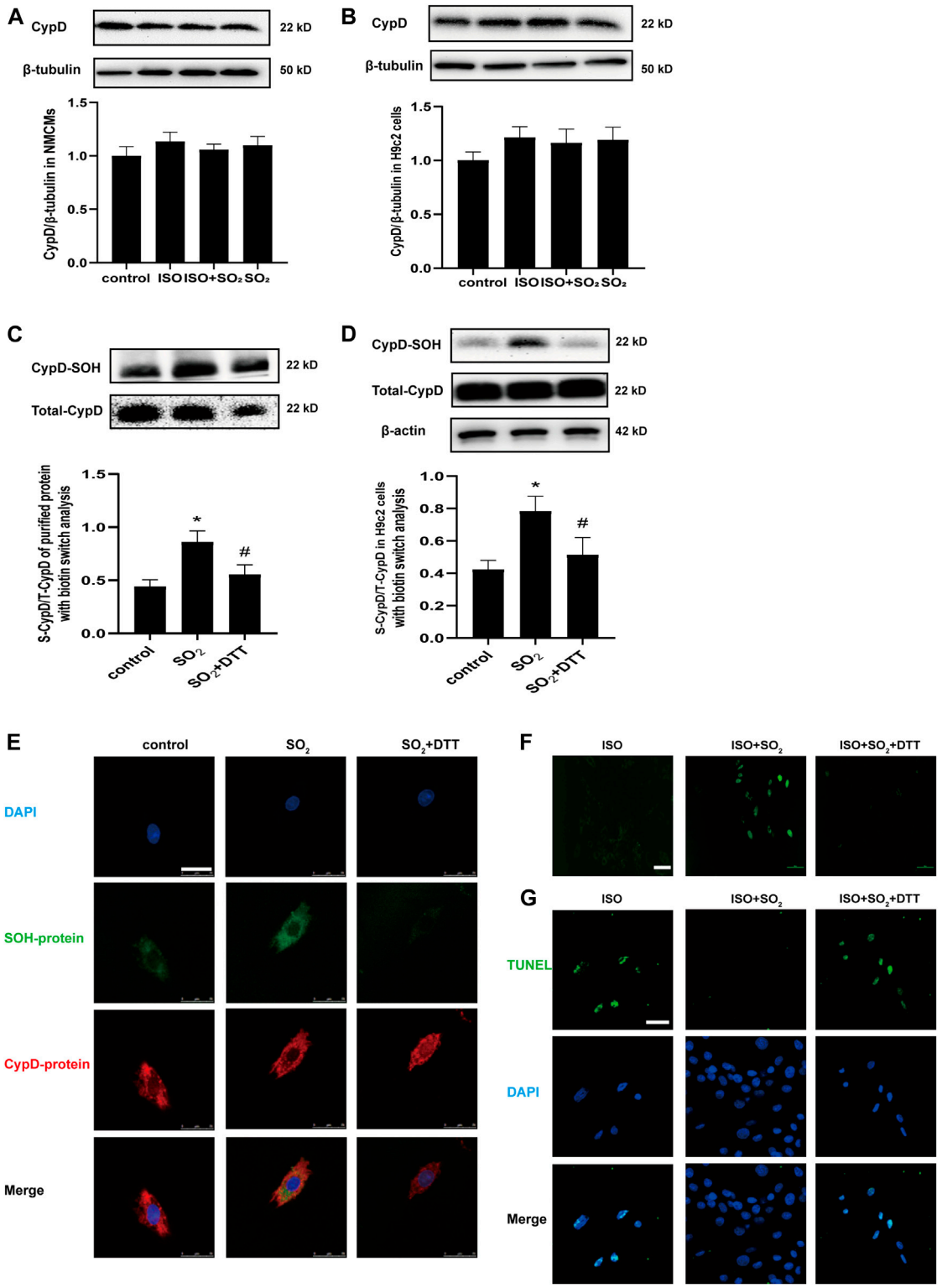

FIGURE 3 | SO_2 sulphenylated CypD and thereby blocked mitochondrial mPTP opening and apoptosis. CypD expressions in NMCMs and H9c2 cells were measured by western blot in **(A)** and **(B)**, respectively. **(C)** Sulphenylation of CypD in the purified protein with biotin switch analysis. **(D)** Sulphenylation of CypD in H9c2 cells with biotin switch analysis. **(E)** The co-localization of sulphenylated protein and CypD in H9c2 cells as detected with a DAz-2-based fluorescent probe and CypD antibody under a confocal laser-scanning microscope (magnification, ×600; scale bar: 25 μm). **(F)** The mPTP opening in H9c2 cells was detected with calcein-AM (magnification, ×400; scale bar: 40 μm). **(G)** The apoptosis of H9c2 cells was tested by using the TdT-mediated dUTP nick end labeling (TUNEL) method (magnification, ×600; scale bar: 25 μm).

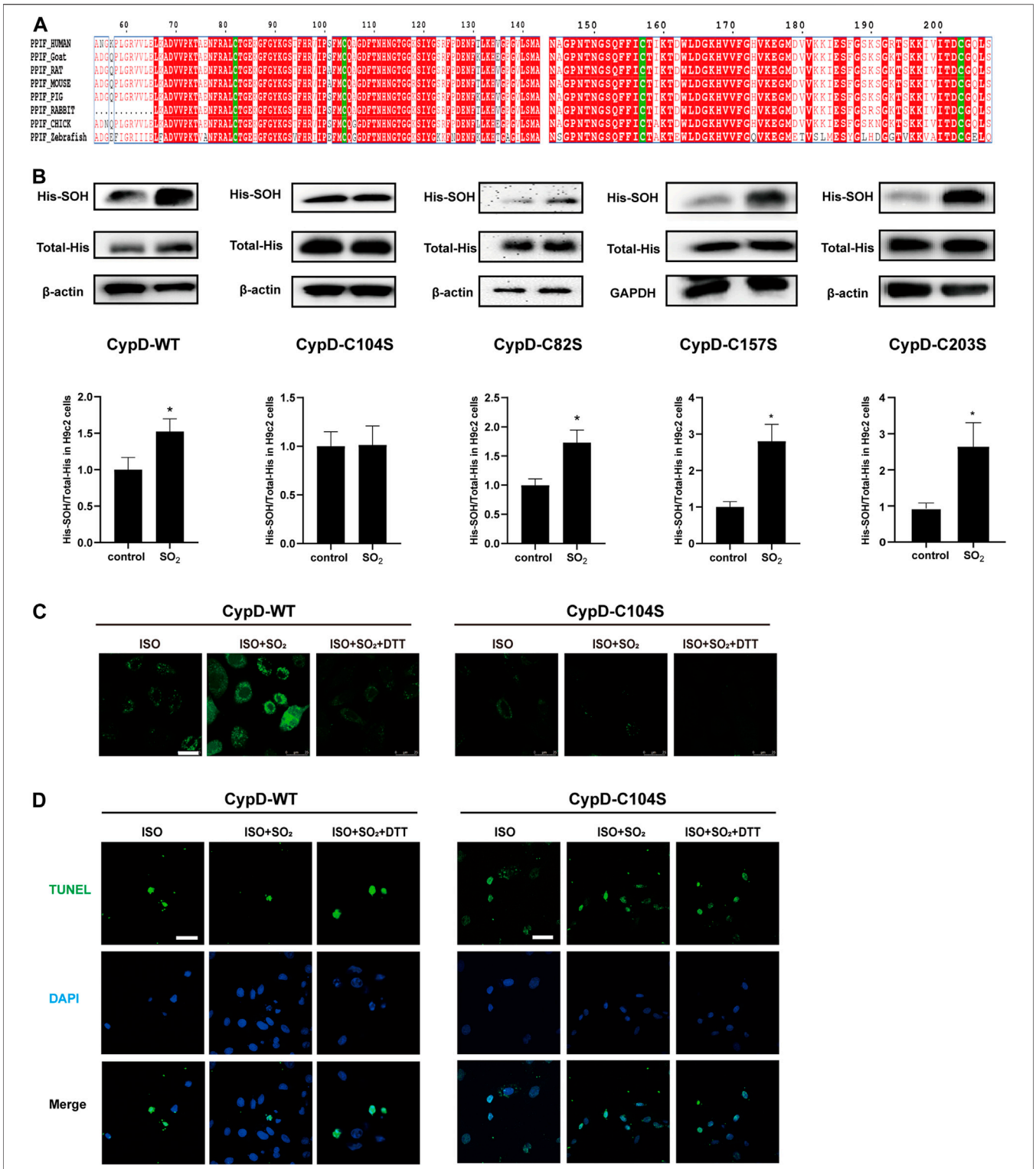

FIGURE 4 | The CypD Cys104 might be a novel target for SO_2 to inhibit cardiomyocyte apoptosis. **(A)** Analysis of sequence homology of CypD proteins from different species. The sequences were archived from the UniProt database. **(B)** Sulphenylation of CypD in H9c2 cells transfected with WT or C104S, C82S, C157S, C203S-mutated CypD plasmids was measured by biotin switch analysis. **(C)** The mPTP opening in H9c2 cells transfected with WT or C104S-mutated CypD plasmid measured by the mPTP detection kit (magnification, ×600; scale bar: 25 μm). **(D)** The apoptosis in H9c2 cells transfected with WT or C104S-mutated CypD plasmid measured by using the TdT-mediated dUTP nick end labeling (TUNEL) method (magnification, ×600; scale bar: 40 μm).

4 DISCUSSION

In the present study, we revealed, for the first time, a novel mechanism by which the endogenous SO_2/AAT pathway controlled ISO-induced cardiomyocyte apoptosis, and the SO_2-induced CypD sulphenylation inhibited the opening of mPTP, the downstream cytc leakage, and the activation of caspase9, thereby attenuating cardiomyocyte apoptosis. The sulphenylation of CypD cys104 is a key target for SO_2 to inhibit apoptosis in cardiomyocytes.

Previously, SO_2 was considered to be a toxic gas and environmental pollutant. In recent years, it is shown that the SO_2 can be endogenously synthesized via an enzymatic reaction catalyzed by AAT in cardiovascular tissues (Huang et al., 2016). The half-life time of SO_2 was about 5–10 min, demonstrated by the fact that serum SO_2 level was decreased by 50% about 5–10 min after the intravenous injection of SO_2 donor (Du et al., 2008b). It has features of low molecular weight, continuous production, and fast diffusion and has extensive biological action independent of the membrane receptors (Huang et al., 2016). Endogenous SO_2 exerts important cardiovascular effects. For example, the reduction of endogenous SO_2 promotes the proliferation and migration of cardiac fibroblasts (Zhang et al., 2018). SO_2 inhibits the VSMC proliferation by activating Cl^-/HCO_3^- exchangers and acidifying cells (Wang Y. et al., 2019). Endogenous SO_2 alleviates angiotensin II-induced myocardial hypertrophy and cardiomyocyte autophagy (Chen et al., 2016). It was reported that the downregulated endogenous SO_2/AAT pathway might be involved in the possible mechanisms underlying the myocardial injury. Liang *et al* found that the *in vivo* protective effect of SO_2 on the myocardial injury was related to the increased myocardial antioxidant capacity (Liang et al., 2011). Jin et al. (2013) found that SO_2 attenuated myocardial injury, in association with the inhibition of myocardial apoptosis. However, the mechanisms by which SO_2 protects cardiomyocytes against apoptosis have not yet been elucidated.

In this study, we showed that ISO treatment resulted in a downregulation of the endogenous SO_2/AAT2 pathway in NMCMs, as evidenced by a significantly downregulated AAT2 expression and SO_2 content in the ISO-stimulated cardiomyocytes. Simultaneously, cell apoptosis was evident. While the supplementation of SO_2 donors in ISO-stimulated NMCMs restored SO_2 content accompanied with a decreased cell apoptosis, cleaved-caspase3/caspase3 ratio, and caspase3 activity. These results demonstrate that endogenous SO_2 significantly inhibits ISO-induced apoptosis in cardiomyocytes.

Up to now, the possible molecular mechanisms by which endogenous SO_2 controls ISO-induced myocardial apoptosis have been unclear. A previous study suggested that SO_2 could significantly affect signaling pathways associated with cellular energy metabolism in the VSMCs (Huang et al., 2021a). A cellular component reanalysis of gene ontology enrichment on the previously reported SO_2-affected protein dataset was conducted in the present study. The data showed that mitochondrion is one of the important subcellular components in which SO_2-affected proteins were highly enriched. Furthermore, considering that the mitochondrion acts as a cell energy mill, the change of ATP level affected by the ISO and/or SO_2 treatment was investigated. As single-wavelength and genetically encoded fluorescent sensors, pmiATPSnFR1.1 and cyto-iATPSnFR1.0 were used for imaging cell surface and cytosolic ATP, respectively. The structure of pmiATPSnFR1.1 and cyto-iATPSnFR1.0 contains epsilon subunit F0F1-ATP synthase which binds to ATP. The conformation of these sensors changes and the fluorescence changes from dim to bright when bound to ATP (Lobas et al., 2019). Additionally, extracellular matrix ATP binding to ecAT3.10 induces a conformational change that increases FRET between the CFP donor and YFP acceptor (Conley et al., 2017). Therefore, the higher the ratio of CFP-YFPFRET to CFP, the more extracellular ATP binding, which indirectly reflects the extracellular ATP content. The results showed that ISO significantly reduced cytoplasmic ATP, cell surface ATP, and extracellular matrix ATP, while the supplementation with SO_2 significantly reversed the reduced ATP fluorescence intensity in the H9c2 cells of the ISO group. Taken together, the abovementioned results suggested that SO_2 might target the mitochondria to exert anti-apoptosis effects in cardiomyocytes.

The function of mitochondria is finely regulated by intrinsic factors, such as mPTP (Penna et al., 2013). Therefore, we, for the first time, examined the effect of SO_2 on the opening of mPTP and its downstream events (cytc release, caspase9 activation, and apoptosis). The results showed that under ISO stimulation, the opening of mPTP was increased, the downstream leakage of cytc increased, the ratio of cleaved caspase9/caspase9 increased, and caspase9 activity was enhanced. While, SO_2 supplementation reversed the above effects of ISO on the opening of mPTP and the downstream apoptosis, suggesting that SO_2 might turn off mitochondrial mPTP and then inhibit cardiomyocyte apoptosis.

However, the possible mechanism by which SO_2 blocks the mitochondrial mPTP opening has not yet been known. CypD is known to be the only protein identified to regulate the mPTP opening (Alam et al., 2015). CypD is a prolyl isomerase encoded by the Ppif gene and located within the mitochondrial matrix. Baines et al. (2005) found that the gene deletion of the Ppif in mice protected against ischemia/reperfusion-induced cell death, whereas the mice with CypD overexpression exhibited mitochondrial swelling and spontaneous cell death. Therefore, we firstly examined whether SO_2 affected CypD protein expression in this study. The results revealed that SO_2 did not impact the expression of CypD protein in the H9c2 cells with or without ISO stimulation. As discovered in the previous studies, the post-translational modifications might impact CypD activity (Nguyen et al., 2011; Sanchez et al., 2011; Hurst et al., 2020; Amanakis et al., 2021). For example, S-glutathionylation of CypD at the Cys203 prevented the binding between CypD and ANT, and therefore blocked mPTP (Nguyen et al., 2011; Sanchez et al., 2011). While, due to its oxidative capacity, SO_2 was found to control the protein function by a sulfhydryl-dependent oxidative modification on the specific cysteinyl residue. Yao et al. found that SO_2 promoted the disulfide-dependent dimerization of soluble guanylate cyclase to induce the vasodilate effect (Yao et al., 2016). More importantly, SO_2 was reported to regulate the

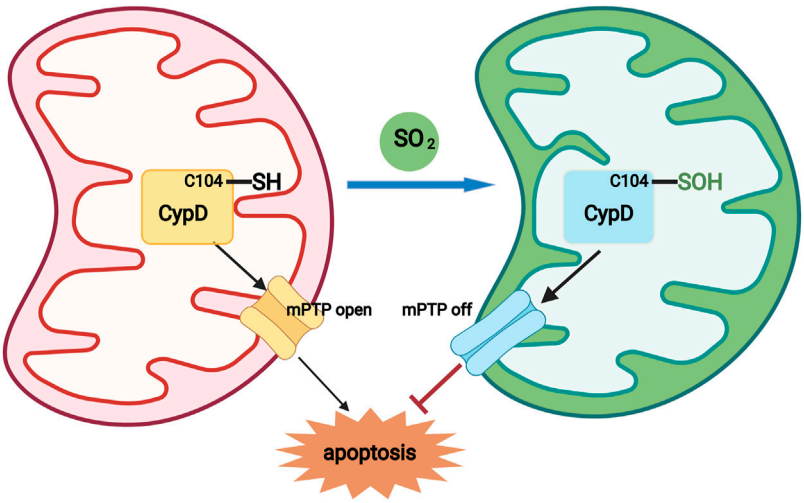

FIGURE 5 | A diagram showing that a novel redox mechanism by which SO_2 inhibits cardiomyocyte apoptosis. SO_2 sulphenylated mitochondrial CypD at Cys 104, which acted as a switch-off to close the mPTP opening, thereby inhibiting mitochondria-dependent cardiomyocyte apoptosis.

vascular function and structure by the sulphenylation, an important post-translational modification regulating protein function, on the target proteins such as AAT, Smad3 and NF-κB p65 (Chen et al., 2017; Song et al., 2020; Huang et al., 2021a). Sulphenylation refers to the oxidation of cysteine thiol groups (Cys-SH) to cysteine sulfenic acid (Cys-SOH) (Chen et al., 2017). Therefore, we explored whether CypD was able to be sulphenylated by SO_2. Interestingly, the present cellular experiments and CypD purified protein assays demonstrated that SO_2 could sulphenylate CypD protein to inhibit mPTP opening and cardiomyocyte apoptosis.

To further reveal the target site by which SO_2 sulphenylated CypD and thereby inhibited cardiomyocyte apoptosis, we firstly performed the homology analysis of CypD protein sequences among diverse species and found that Cys82, Cys104, Cys157, and Cys203 are highly conserved. And then, the mutated CypD plasmids containing the site-directed mutant of C82S, C104S, C157S, and C203S were constructed and transfected into H9c2 cells, respectively. The screening results showed that the SO_2 could sulfenylate the CypD in the H9c2 cells transfected with the mutant Cys82, Cys157, and Cys203, but, interestingly, SO_2 failed to do so in the H9c2 cells transfected with the mutant CypD C104S. In accordance with the sulphenylation screening results, SO_2 failed to prevent ISO-stimulated cell apoptosis in the H9c2 cells transfected with the mutant CypD C104S. These results further confirm that SO_2 exerts an inhibitory effect on cardiomyocyte apoptosis by the sulphenylation of CypD at the Cys104.

As well known, the interaction among the different post-translational modifications on the same protein provided a fine mechanism for adjusting the protein function. For example, the persulfidation of p66Shc at Cys59 inhibited the phosphorylation at Ser36, and then blocked p66Shc activation to prevent H_2O_2-induced cellular senescence (Xie et al., 2014). In the oleic acid-induced A549 cell inflammatory experiment, endogenous SO_2 sulphenylated NF-κB p65 in association with a decrease in the phosphorylation, nuclear translocation and DNA binding activity of NF-κB p65, suggesting that there might be interaction between the sulphenylation and phosphorylation of protein. While, it was reported that the phosphorylation of the Ser191 site of CypD leads to its binding to oligomycin sensitivity-conferring protein, which sensitizes mPTP opening (Hurst et al., 2020). Hence, the impact of the sulphenylation of CypD on the other post-translational modifications at other sites might also contribute to the sophisticated tuning of CypD and mPTP opening.

The mPTP opening and the loss of mitochondrial membrane potential (MMP) are two key elements involved in the cell apoptosis (Kroemer and Reed, 2000). Moreover, the opening of mPTP is closely related with the decrease in the MMP (Bossy-Wetzel et al., 1998; Hüser and Blatter, 1999; Joiner et al., 2012). Briefly, as a highly conductive and non-selective channel, the opening of mPTP increases the permeability of the inner mitochondrial membrane to ions and small solutes, and destroys the MMP and the proton gradient, resulting in the insufficient ATP production and cell apoptosis (Galluzzi et al., 2009; Kalani et al., 2018). Zhao et al. found that SO_2 restored the destroyed MMP in the alveolar macrophages treated with the serum from rats of acute lung injury and prevented the cell apoptosis (Zhao et al., 2019). However, the effect of SO_2-sulphenylated CypD on the MMP in the cardiomyocyte apoptosis is still unclear and merits further study.

5 CONCLUSION

Taken together, our data highlight the important protective role of SO_2-dependent site-specific CypD S-sulphenylation in inhibiting

mPTP opening and reducing apoptosis in cardiomyocytes (**Figure 5**). Along with the in-depth studies on the biological effect of endogenous SO_2 and its mechanisms, the discovery of SO_2-related prodrugs has become a hot topic for their potential therapeutic application (Day et al., 2016; Wang and Wang, 2018; Huang et al., 2021b). A variety of SO_2 prodrugs based on the different releasing mechanisms, such as thiol-activated SO_2 prodrug, thermally activated SO_2 prodrug, hydrolysis-based SO_2 prodrug, click reaction-based SO_2 prodrug, and esterase-sensitive SO_2 prodrug, developed to meet the different research requirement or clinical application in the future. Therefore, our results would not only deepen the understanding of the mechanisms by which endogenous SO_2 inhibits myocardial apoptosis, but also provide new research ideas and potential therapeutic targets for myocardial protection in the future.

DATA AVAILABILITY STATEMENT

All data supporting the findings of this study are available within this article or from the corresponding authors on request.

AUTHOR CONTRIBUTIONS

BL, HP, BQ, LZ, MG, DB, KL, XY, JTD, and LY conducted experiments, analyzed data, and interpreted the results. BL, HP, YH, JBD, and HJ wrote the manuscript. CT, YH, JBD, and HJ designed the research, interpreted the results, and edited the manuscript.

FUNDING

This work was supported by National Natural Science Foundation of China (81970872, 81970424, 81770422, 82070445, 81921001), and Beijing Natural Science Foundation (7191012).

ACKNOWLEDGMENTS

We thank for the scientists Mathew Tantama and Baljit Khakh that deposited the plasmids ecAT3.10, pm-iATPSnFR1.1, and cyto-iATPSnFR1.0 at Addgene.

REFERENCES

Abbate, A., and Narula, J. (2012). Role of Apoptosis in Adverse Ventricular Remodeling. *Heart Fail. Clin.* 8 (1), 79–86. doi:10.1016/j.hfc.2011.08.010

Ahmad, F., Singh, A. P., Tomar, D., Rahmani, M., Zhang, Q., Woodgett, J. R., et al. (2019). Cardiomyocyte-GSK-3α Promotes mPTP Opening and Heart Failure in Mice with Chronic Pressure Overload. *J. Mol. Cell. Cardiol.* 130, 65–75. doi:10.1016/j.yjmcc.2019.03.020

Alam, M. R., Baetz, D., and Ovize, M. (2015). Cyclophilin D and Myocardial Ischemia-Reperfusion Injury: a Fresh Perspective. *J. Mol. Cell. Cardiol.* 78, 80–89. doi:10.1016/j.yjmcc.2014.09.026

Amanakis, G., Sun, J., Fergusson, M. M., McGinty, S., Liu, C., Molkentin, J. D., et al. (2021). Cysteine 202 of Cyclophilin D Is a Site of Multiple post-translational Modifications and Plays a Role in Cardioprotection. *Cardiovasc. Res.* 117 (1), 212–223. doi:10.1093/cvr/cvaa053

Baines, C. P., Kaiser, R. A., Purcell, N. H., Blair, N. S., Osinska, H., and Hambleton, M. A. (2005). Loss of cyclophilin D reveals a critical role for mitochondrial permeability transition in cell death. *Nature* 434 (7033), 658–662. doi:10.1038/nature03434

Bossy-Wetzel, E., Newmeyer, D. D., and Green, D. R. (1998). Mitochondrial Cytochrome C Release in Apoptosis Occurs Upstream of DEVD-specific Caspase Activation and Independently of Mitochondrial Transmembrane Depolarization. *EMBO. J.* 17 (1), 37–49. doi:10.1093/emboj/17.1.37

Chen, Q., Zhang, L., Chen, S., Huang, Y., Li, K., Yu, X., et al. (2016). Downregulated Endogenous Sulfur Dioxide/Aspartate Aminotransferase Pathway Is Involved in Angiotensin II-Stimulated Cardiomyocyte Autophagy and Myocardial Hypertrophy in Mice. *Int. J. Cardiol.* 225, 392–401. doi:10.1016/j.ijcard.2016.09.111

Chen, S., Huang, Y., Liu, Z., Yu, W., Zhang, H., Li, K., et al. (2017). Sulphur Dioxide Suppresses Inflammatory Response by Sulphenylating NF-κB p65 at Cys38 in a Rat Model of Acute Lung Injury. *Clin. Sci. (Lond)* 131 (21), 2655–2670. doi:10.1042/CS20170274

Conley, J. M., Radhakrishnan, S., Valentino, S. A., and Tantama, M. (2017). Imaging Extracellular ATP with a Genetically-Encoded, Ratiometric Fluorescent Sensor. *PLoS. One.* 12 (11), e0187481. doi:10.1371/journal.pone.0187481

Day, J. J., Yang, Z., Chen, W., Pacheco, A., and Xian, M. (2016). Benzothiazole Sulfinate: a Water-Soluble and Slow-Releasing Sulfur Dioxide Donor. *ACS Chem. Biol.* 11 (6), 1647–1651. doi:10.1021/acschembio.6b00106

Deng, S., Zhao, Q., Zhen, L., Zhang, C., Liu, C., Wang, G., et al. (2017). Neonatal Heart-Enriched miR-708 Promotes Proliferation and Stress Resistance of Cardiomyocytes in Rodents. *Theranostics.* 7 (7), 1953–1965. doi:10.7150/thno.16478

Ding, B., Abe, J.-i., Wei, H., Huang, Q., Walsh, R. A., Molina, C. A., et al. (2005). Functional Role of Phosphodiesterase 3 in Cardiomyocyte Apoptosis. *Circulation.* 111 (19), 2469–2476. doi:10.1161/01.CIR.0000165128.39715.87

Du, J., Huang, Y., Li, K., Yu, X., Jin, H., and Yang, L. (2018). Retina-derived Endogenous Sulfur Dioxide Might Be a Novel Anti-apoptotic Factor. *Biochem. Biophys. Res. Commun.* 496, 955–960. doi:10.1016/j.bbrc.2018.01.103

Du, S., Jin, H.-f., Bu, D.-f., Zhao, X., Geng, B., Tang, C.-s., et al. (2008a). Endogenously Generated Sulfur Dioxide and its Vasorelaxant Effect in Rats. *Acta. Pharmacol. Sin.* 29 (8), 923–930. doi:10.1111/j.1745-7254.2008.00845.x

Du, S., Jin, H., Liang, Y., Zhao, X., Wei, H., Wang, L., et al. (2008b). Influence of Sulfur Dioxide and its Derivatives on Rats' Blood Pressure. *J. Appl. Clin. Pediatr.* 23 (1), 22–24. doi:10.3969/j.issn.1003-515X.2008.01.007

Elrod, J. W., and Molkentin, J. D. (2013). Physiologic Functions of Cyclophilin D and the Mitochondrial Permeability Transition Pore. *Circ. J.* 77 (5), 1111–1122. doi:10.1253/circj.cj-13-0321

Galluzzi, L., Blomgren, K., and Kroemer, G. (2009). Mitochondrial Membrane Permeabilization in Neuronal Injury. *Nat. Rev. Neurosci.* 10 (7), 481–494. doi:10.1038/nrn2665

Huang, Y., Tang, C., Du, J., and Jin, H. (2016). Endogenous Sulfur Dioxide: a New Member of Gasotransmitter Family in the Cardiovascular System. *Oxid. Med. Cell. Longev.* 2016, 1–9. doi:10.1155/2016/8961951

Huang, Y., Li, Z., Zhang, L., Tang, H., Zhang, H., Wang, C., et al. (2021a). Endogenous SO_2-dependent Smad3 Redox Modification Controls Vascular Remodeling. *Redox. Biol.* 41, 101898. doi:10.1016/j.redox.2021.101898

Huang, Y., Zhang, H., Lv, B., Tang, C., Du, J., and Jin, H. (2021b). Sulfur Dioxide: Endogenous Generation, Biological Effects, Detection, and Therapeutic Potential. *Antioxid. Redox. Signal.* doi:10.1089/ars.2021.0213

Hurst, S., Gonnot, F., Dia, M., Crola Da Silva, C., Gomez, L., and Sheu, S.-S. (2020). Phosphorylation of Cyclophilin D at Serine 191 Regulates Mitochondrial Permeability Transition Pore Opening and Cell Death after Ischemia-Reperfusion. *Cell. Death. Dis.* 11 (8), 661. doi:10.1038/s41419-020-02864-5

Hüser, J., and Blatter, L. A. (1999). Fluctuations in Mitochondrial Membrane Potential Caused by Repetitive Gating of the Permeability Transition Pore. *Biochem. J.* 343, 311–317. doi:10.1042/bj3430311

Imamura, H., Huynh Nhat, K. P., Togawa, H., Saito, K., Iino, R., Kato-Yamada, Y., et al. (2009). Visualization of ATP Levels inside Single Living Cells with

Fluorescence Resonance Energy Transfer-Based Genetically Encoded Indicators. *Proc. Natl. Acad. Sci. U. S. A.* 106, 15651–15656. doi:10.1073/pnas.0904764106

Jin, H., Liu, A., Holmberg, L., Zhao, M., Chen, S., Yang, J., et al. (2013). The Role of Sulfur Dioxide in the Regulation of Mitochondrion-Related Cardiomyocyte Apoptosis in Rats with Isopropylarterenol-Induced Myocardial Injury. *Int. J. Mol. Sci.* 14 (5), 10465–10482. doi:10.3390/ijms140510465

Joiner, M.-l. A., Koval, O. M., Li, J., He, B. J., Allamargot, C., Gao, Z., et al. (2012). CaMKII Determines Mitochondrial Stress Responses in Heart. *Nature.* 491 (7423), 269–273. doi:10.1038/nature11444

Kalani, K., Yan, S. F., and Yan, S. S. (2018). Mitochondrial Permeability Transition Pore: a Potential Drug Target for Neurodegeneration. *Drug. Discov. Today.* 23 (12), 1983–1989. doi:10.1016/j.drudis.2018.08.001

Kroemer, G., and Reed, J. C. (2000). Mitochondrial Control of Cell Death. *Nat. Med.* 6 (5), 513–519. doi:10.1038/74994

Kwong, J. Q., and Molkentin, J. D. (2015). Physiological and Pathological Roles of the Mitochondrial Permeability Transition Pore in the Heart. *Cell. Metab.* 21 (2), 206–214. doi:10.1016/j.cmet.2014.12.001

Lam, C. K., Zhao, W., Liu, G. S., Cai, W. F., Gardner, G., Adly, G., et al. (2015). HAX-1 Regulates Cyclophilin-D Levels and Mitochondria Permeability Transition Pore in the Heart. *Proc. Natl. Acad. Sci. U. S. A.* 112 (47), E6466–E6475. doi:10.1073/pnas.1508760112

Leong, D. P., Joseph, P. G., McKee, M., Anand, S. S., Teo, K. K., Schwalm, J. D., et al. (2017). Reducing the Global Burden of Cardiovascular Disease, Part 2: Prevention and Treatment of Cardiovascular Disease. *Circ. Res.* 121 (6), 695–710. doi:10.1161/CIRCRESAHA.117.311849

Liang, Y., Liu, D., Ochs, T., Tang, C., Chen, S., Zhang, S., et al. (2011). Endogenous Sulfur Dioxide Protects against Isoproterenol-Induced Myocardial Injury and Increases Myocardial Antioxidant Capacity in Rats. *Lab. Invest.* 91 (1), 12–23. doi:10.1038/labinvest.2010.156

Linard, D., Kandlbinder, A., Degand, H., Morsomme, P., Dietz, K.-J., and Knoops, B. (2009). Redox Characterization of Human Cyclophilin D: Identification of a New Mammalian Mitochondrial Redox Sensor? *Arch. Biochem. Biophys.* 491 (1-2), 39–45. doi:10.1016/j.abb.2009.09.002

Lobas, M. A., Tao, R., Nagai, J., Kronschläger, M. T., Borden, P. M., Marvin, J. S., et al. (2019). A Genetically Encoded Single-Wavelength Sensor for Imaging Cytosolic and Cell Surface ATP. *Nat. Commun.* 10 (1), 711. doi:10.1038/s41467-019-08441-5

Nguyen, T. T., Stevens, M. V., Kohr, M., Steenbergen, C., Sack, M. N., and Murphy, E. (2011). Cysteine 203 of Cyclophilin D Is Critical for Cyclophilin D Activation of the Mitochondrial Permeability Transition Pore. *J. Biol. Chem.* 286 (46), 40184–40192. doi:10.1074/jbc.M111.243469

Penna, C., Perrelli, M.-G., and Pagliaro, P. (2013). Mitochondrial Pathways, Permeability Transition Pore, and Redox Signaling in Cardioprotection: Therapeutic Implications. *Antioxid. Redox. Signal.* 18 (5), 556–599. doi:10.1089/ars.2011.4459

Sánchez, G., Fernández, C., Montecinos, L., Domenech, R. J., and Donoso, P. (2011). Preconditioning Tachycardia Decreases the Activity of the Mitochondrial Permeability Transition Pore in the Dog Heart. *Biochem. Biophysical. Res. Commun.* 410 (4), 916–921. doi:10.1016/j.bbrc.2011.06.095

Singh, K. P., Jaffe, A. S., and Liang, B. T. (2011). The Clinical Impact of Circulating Caspase3 P17 Level: a Potential New Biomarker for Myocardial Injury and Cardiovascular Disease. *Future. Cardiol.* 7 (4), 443–445. doi:10.2217/fca.11.29

Song, Y., Li, S., Geng, W., Luo, R., Liu, W., Tu, J., et al. (2018). Sirtuin 3-dependent Mitochondrial Redox Homeostasis Protects against AGEs-Induced Intervertebral Disc Degeneration. *Redox. Biol.* 19, 339–353. doi:10.1016/j.redox.2018.09.006

Song, Y., Peng, H., Bu, D., Ding, X., Yang, F., Zhu, Z., et al. (2020). Negative Auto-Regulation of Sulfur Dioxide Generation in Vascular Endothelial Cells: AAT1 S-Sulfenylation. *Biochem. Biophysical. Res. Commun.* 525, 231–237. doi:10.1016/j.bbrc.2020.02.040

Sun, T., Ding, W., Xu, T., Ao, X., Yu, T., Li, M., et al. (2019). Parkin Regulates Programmed Necrosis and Myocardial Ischemia/reperfusion Injury by Targeting Cyclophilin-D. *Antioxid. Redox. Signal.* 31 (16), 1177–1193. doi:10.1089/ars.2019.7734

Wang, W., and Wang, B. (2018). SO_2 Donors and Prodrugs, and Their Possible Applications: A Review. *Front. Chem.* 6, 559. doi:10.3389/fchem.2018.00559

Wang, X., Wang, Y., Zhang, L., Zhang, D., Bai, L., Kong, W., et al. (2019). L-cystathionine Protects against Homocysteine-Induced Mitochondria-dependent Apoptosis of Vascular Endothelial Cells. *Oxid. Med. Cell. Long.* 2019, 1–13. doi:10.1155/2019/1253289

Wang, Y., Wang, X., Chen, S., Tian, X., Zhang, L., Huang, Y., et al. (2019). Sulfur Dioxide Activates Cl^-/HCO_3^- Exchanger via Sulphenylating AE2 to Reduce Intracellular pH in Vascular Smooth Muscle Cells. *Front. Pharmacol.* 10, 313. doi:10.3389/fphar.2019.00313

Xie, Z. Z., Shi, M. M., Xie, L., Wu, Z. Y., Li, G., Hua, F., et al. (2014). Sulfhydration of p66Shc at Cysteine59 Mediates the Antioxidant Effect of Hydrogen Sulfide. *Antioxid. Redox. Signal.* 21 (18), 2531–2542. doi:10.1089/ars.2013.5604

Yang, J., Li, K., Hou, J. T., Lu, C. Y., Li, L. L., Yu, K. K., et al. (2017). A Novel Coumarin-Based Water-Soluble Fluorescent Probe for Endogenously Generated SO_2 in Living Cells. *Sci. China. Chem.* 60 (6), 793–798. doi:10.1007/s11426-016-0411-7

Yao, Q., Huang, Y., Liu, A. D., Zhu, M., Liu, J., Yan, H., et al. (2016). The Vasodilatory Effect of Sulfur Dioxide via sGC/cGMP/PKG Pathway in Association with Sulfhydryl-dependent Dimerization. *Am. J. Physiol. Regul. Integr. Comp. Physiol.* 310 (11), R1073–R1080. doi:10.1152/ajpregu.00101.2015

Zhang, L. L., Du, J. B., Tang, C. S., Jin, H. F., and Huang, Y. Q. (2018). Inhibitory Effects of Sulfur Dioxide on Rat Myocardial Fibroblast Proliferation and Migration. *Chin. Med. J. (Engl).* 131 (14), 1715–1723. doi:10.4103/0366-6999.235875

Zhang, L., Jin, H., Song, Y., Chen, S. Y., Wang, Y., Sun, Y., et al. (2021). Endogenous Sulfur Dioxide Is a Novel Inhibitor of Hypoxia-Induced Mast Cell Degranulation. *J. Adv. Res.* 29, 55–65. doi:10.1016/j.jare.2020.08.017

Zhao, Y. R., Liu, Y., Wang, D., Lv, W. R., and Zhou, J. L. (2019). Effects of Sulfur Dioxide on Alveolar Macrophage Apoptosis in Acute Lung Injury Induced by Limb Ischemia/reperfusion in Rats. *Beijing. Da. Xue. Xue. Bao. Yi. Xue. Ban.* 51 (2), 239–244. doi:10.19723/j.issn.1671-167X.2019.02.007

Zhou, B., Kreuzer, J., Kumsta, C., Wu, L., Kamer, K. J., Cedillo, L., et al. (2019). Mitochondrial Permeability Uncouples Elevated Autophagy and Lifespan Extension. *Cell.* 177 (2), 299–314. doi:10.1016/j.cell.2019.02.013

Zhou, D., Zhang, Y., Du, J., Jin, H., Tang, C., and Huang, Y. (2020). Sulfur Dioxide: an Endogenous Protector against Myocardial Injury. *J. Cardiovasc. Pharmacol.* 76 (4), 389–396. doi:10.1097/FJC.0000000000000882

Conflict of Interest: The authors declare that the research was conducted in the absence of any commercial or financial relationships that could be construed as a potential conflict of interest.

Publisher's Note: All claims expressed in this article are solely those of the authors and do not necessarily represent those of their affiliated organizations, or those of the publisher, the editors and the reviewers. Any product that may be evaluated in this article, or claim that may be made by its manufacturer, is not guaranteed or endorsed by the publisher.

Copyright © 2022 Lv, Peng, Qiu, Zhang, Ge, Bu, Li, Yu, Du, Yang, Tang, Huang, Du and Jin. This is an open-access article distributed under the terms of the Creative Commons Attribution License (CC BY). The use, distribution or reproduction in other forums is permitted, provided the original author(s) and the copyright owner(s) are credited and that the original publication in this journal is cited, in accordance with accepted academic practice. No use, distribution or reproduction is permitted which does not comply with these terms.

frontiers in Cell and Developmental Biology

REVIEW
published: 20 January 2022
doi: 10.3389/fcell.2021.813668

Ferroptosis: A Potential Target in Cardiovascular Disease

Yanlong Leng[1,2†], Xing Luo[1,2†], Jiaying Yu[2,3], Haibo Jia[1,2] and Bo Yu[1,2]*

[1]Department of Cardiology, The Second Affiliated Hospital of Harbin Medical University, Harbin, China, [2]Key Laboratory of Myocardial Ischemia, Harbin Medical University, Harbin, China, [3]Department of Obstetrics and Gynecology, The Second Affiliated Hospital of Harbin Medical University, Harbin, China

Ferroptosis is a new form of regulatory cell death characterized by iron-dependent and intracellular lipid peroxidation. Ferroptosis can be divided into two stages. The first stage is iron overload in the cell, which generates a large amount of reactive oxygen species through the Fenton reaction, and the second stage results from an imbalance of the intracellular antioxidant system. Excessive phospholipid hydroperoxides cannot be removed by reduction reactions, as this could destroy the cell membrane structure and interfere with mitochondrial function, eventually leading to ferroptosis of the cell. Cardiovascular diseases have gradually become the leading cause of death in modern society. The relationship between ferroptosis and the occurrence and progression of cardiovascular disease has become a research hotspot in recent years. In this review, we summarize the mechanism of ferroptosis and its specific role in cardiovascular disease.

Keywords: ferroptosis, cardiovascular disease, iron homeostasis, antioxidant metabolism, lipid metabolism, ischemia reperfusion, heart failure, coronary atherosclerotic heart disease

OPEN ACCESS

Edited by:
Chunying Li,
Fourth Military Medical University, China

Reviewed by:
Takashi Matsui,
University of Hawaii, United States
Weinan Guo,
Fourth Military Medical University, China
Xin Wei,
Second Hospital of Anhui Medical University, China

****Correspondence:***
Haibo Jia
jhb101180@163.com

†These authors have contributed equally to this work and share first authorship

Specialty section:
This article was submitted to Cell Death and Survival, a section of the journal Frontiers in Cell and Developmental Biology

Received: *12 November 2021*
Accepted: *31 December 2021*
Published: *20 January 2022*

Citation:
Leng Y, Luo X, Yu J, Jia H and Yu B (2022) Ferroptosis: A Potential Target in Cardiovascular Disease. Front. Cell Dev. Biol. 9:813668. doi: 10.3389/fcell.2021.813668

INTRODUCTION

Cell death is an important cornerstone for maintaining the balance of development and homeostasis of the body. There are two main types of cell death: regulatory cell death (RCD) and non-regulatory cell death (Lockshin and Zakeri, 2001). Nonregulatory cell death refers mainly to the severe damage of cells under the stimulation of various pathogenic factors, leading to passive cell death. However, according to the different signaling pathways involved in the process, regulatory cell death can be divided into apoptosis, necroptosis, pyroptosis, autophagy, and ferroptosis (Del Re et al., 2019). Among them, ferroptosis is a new type of regulatory cell death discovered only recently. In fact, in 2003, Dolma et al. (Dolma et al., 2003) identified a new type of compound that caused tumor cell death and named it erastin. However, due to limitations in research on regulatory cell death at that time, the authors failed to identify the special regulatory cell death mode induced by erastin. Until 2012, when Dixon et al. defined erastin-induced cell death as iron-dependent regulatory cell death induced by lipid peroxidation and named it ferroptosis (Dixon et al., 2012). The morphological characteristics of ferroptosis cells are as follows: mitochondrial shrinkage, decreased mitochondrial cristae, and decreased membrane density, which are different from the characteristic apoptotic body formation of apoptotic cells.

Cardiovascular disease is one of the most threatening diseases to human health today. Cardiovascular diseases mainly include coronary atherosclerotic heart disease, myocardial ischemia/reperfusion injury (IRI), and heart failure (HF). Severe coronary artery stenosis can lead to IRI after recanalization, HF after myocardial injury, and even ischemic cardiomyopathy (Ezekowitz et al., 2009). Therefore, a clear understanding of the pathophysiological basis behind the onset of cardiovascular diseases is of great significance for the prevention, early diagnosis, and precise treatment of cardiovascular diseases. At present, a variety of regulatory cell deaths are thought to

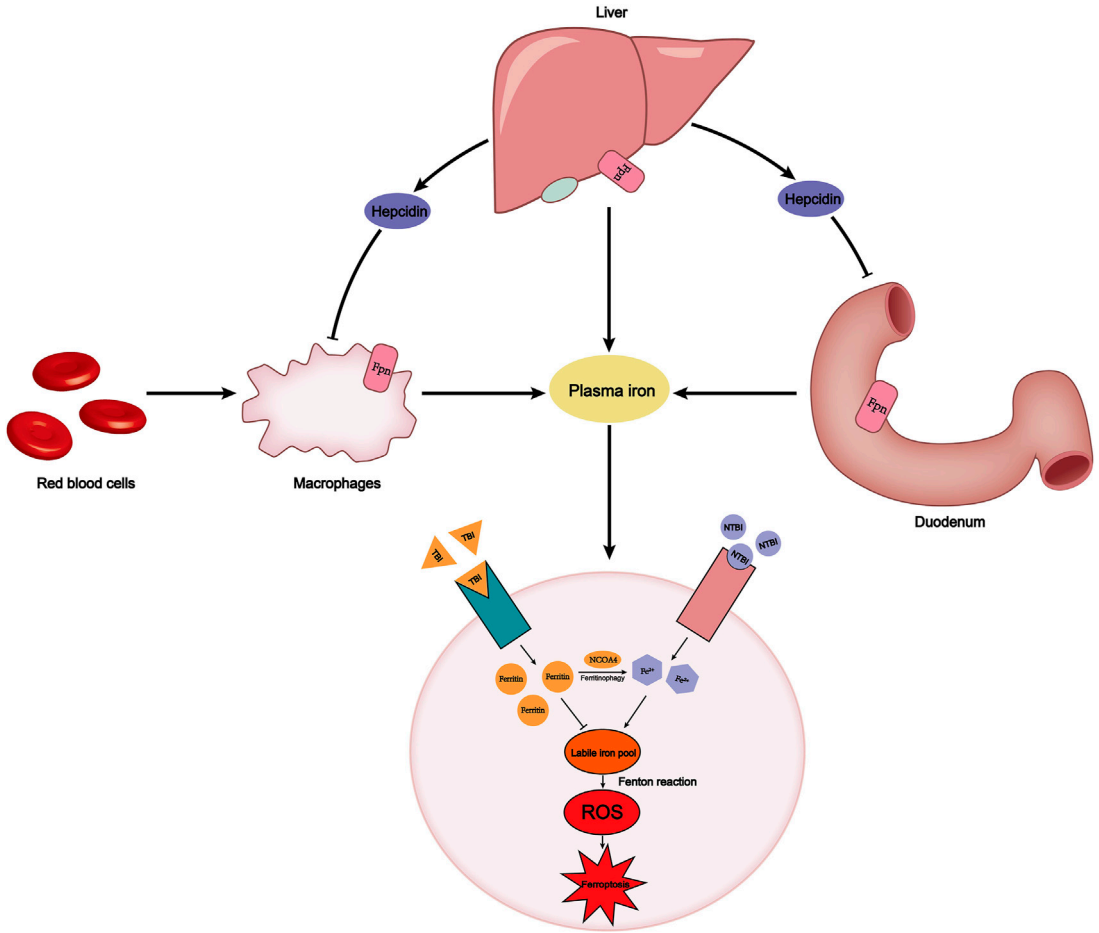

FIGURE 1 | Plasma iron concentration is always maintained within a certain range. This relies on the precise dynamic balance of iron metabolism. FPN on the surface of macrophages, the duodenum, and liver transports iron into the plasma. The endogenous source of iron is mainly hemoglobin iron that is swallowed by macrophages, while the exogenous source is iron in food absorbed by the duodenum. Hepcidin secreted by the liver can degrade FPN to reduce iron export. Plasma iron is divided into TBI and NTBI according to whether it binds to transferrin. TBI binds to the TfR1 on the cell membrane surface and stores iron in the form of ferritin, avoiding the occurrence of Fenton reaction. However, labile iron pool, derived from NCOA4-mediated ferritinophagy or NTBI absorbed by SLC39A14, will cause an increase in intracellular ROS and ferroptosis. FPN, ferroportin; TBI, transferrin-bound iron; NTBI, non-transferrin-bound iron; TfR1, transferrin receptor.

regulate the death of related cells in cardiovascular disease (Choi et al., 2019; Dong et al., 2019; Zhaolin et al., 2019). Ferroptosis, as an emerging mode of regulatory cell death, has become a new focus of research in the field of cardiovascular disease. Understanding the mechanism by which ferroptosis occurs or is inhibited in cardiovascular disease is a prerequisite to reducing morbidity and mortality in the future. In this review, we enumerate the latest developments in different aspects of the mechanism of ferroptosis and then will specifically review the unique pathological characteristics of ferroptosis in different cardiovascular diseases, which will be a reference for the prevention and treatment strategies.

REGULATION OF IRON HOMEOSTASIS

Iron is an essential trace element for the human body; it participates in the formation of a variety of proteins, including hemoglobin, myoglobin, and ferritin, and various redox reactions in cells. It is not only involved in the above-mentioned biological processes but is also the most important initiation and promotion factor for ferroptosis. Under physiological conditions, the complex and precise mechanism of iron homeostasis regulation ensures that iron concentration in the cell remains stable and prevents intracellular iron overload from triggering the Fenton reaction, which in turn leads to ferroptosis (Ganz, 2013). The regulation of iron homeostasis mainly includes mechanisms involving import, export, storage, and utilization of iron.

Iron Export

Ferroportin (Fpn), also known as SLC40A1, is the only protein known to export nonheme iron to the outside of the cell. Fpn is widely distributed on the surface of duodenal epithelial cells, macrophages, and hepatocytes. The main source of iron in the human body is hemoglobin iron recovered by macrophages phagocytosing senescent red blood cells. The macrophages

TABLE 1 | The regulatory mechanism of ferroptosis.

Target	Regulation mechanism	Effect	References
Iron export	Hepcidin-Fpn pathway	Hepcidin promotes FPN internalization and degradation, causing iron accumulation in cells, which promotes ferroptosis	Bao et al. (2021)
	MiR-124/Fpn pathway	High serum levels of miR-124 inhibit FPN expression and promote ferroptosis	Bao et al. (2020)
Iron import	Serum transferrin level, NTBI and SLC39A14	When serum transferrin levels decrease, NTBI levels increase. NTBI accelerates cellular iron accumulation and ferroptosis. But at this time, SLC39A14, which is not the main transport protein under normal circumstances, can antagonize the effect of NTBI.	Yu et al. (2020)
	SREBF2 and transferrin	SREBF2 induces ferritin at the transcriptional level and inhibits ferroptosis	Hong et al. (2021)
	USP7/P53/TfR1 pathway	USP7 promotes P53 ubiquitination and increases TfR1 transcription. And TfR1 is one of the markers of ferroptosis	Tang et al. (2021b)
Iron storage and utilization	Ferritinophagy	NCOA4 facilitates degradation of ferritin in a selective cargo-mediated autophagy manner, which is an important source of iron for labile iron pool	Ito et al. (2021)
Other iron metabolism	HSF1/HSPB1/TfR1 pathway	HSF1 indirectly regulates cellular iron homeostasis and reduces the expression of TfR1 through HSPB1	Sun et al. (2015)
GPX4	Selenium metabolism	Selenium not only participates in the synthesis of GPX4 but also promotes the transcription of GPX4 through TFAP2C and SP1	Alim et al. (2019)
	mTORC1/4EBP/GPX4 pathway	MTORC1 and 4EBP act as a bridge between cystine, cysteine and GPX4, and can accelerate the synthesis of GPX4	Zhang et al. (2021)
System Xc^-	ATF3 and ATF4 transcriptional regulation	ATF3 binds to the SLC7A11 promoter to inhibit transcription, while ATF4 does the opposite	Wang L et al. (2020), Chen et al. (2017)
	KEAP1/NRF2/SLC7A11	After separation of NRF2 from KEAP1, NRF2 enters the nucleus and binds with the ARE of the SLC7A11 promoter to up-regulate the expression of SLC7A11	Habib et al. (2015)
	BECN1 post-translational modification	BECN1 directly binds to SLC7A11 to inhibit its activity	Song et al. (2018)
	Amino acid metabolism	AMPK/SREBP1/BCAT2 pathway reduces intracellular glutamate concentration and inhibits system Xc^-. Increasing the concentration of extracellular glutamate produce the same result	Gao et al. (2015); Wang et al. (2021)
	Immunotherapy and chemotherapy	IFNγ secreted by $CD8^+$ cells inhibits SLC7A11 and SLC3A2. Radiotherapy can also interfere with the function of SLC7A11	Lang et al., (2019), Wang W et al. (2019)
FSP1-CoQ10-NADPH	MDM2 and MDMX	The MDM2-MDMX heterodimer can up-regulate the antioxidant system activity of FSP1-CoQ10	Venkatesh et al. (2020)
Lipid metabolism	ACSLs	ACSL4 promotes phosphatidylethanolamine containing AA and AdA to participate in phospholipid synthesis and increase the proportion of phospholipids that are prone to be oxidized. And ACSL1 adjusts the lipid composition by assembling αESA into DAG and TAG.	Doll et al. (2017) , Beatty et al. (2021)
	Lipoxygenase	ALOX12 catalyzes the oxidation of arachidonic acid. 15LOX and PEBP1 combine to form a complex and then oxidize PUFA to form 15-HpETE-PE, which is an important signaling molecule of ferroptosis	Chu et al., (2019), Anthonymuthu et al. (2021), Wenzel et al. (2017)
	MDM2 and MDMX	MDM2 and MDMX form a complex to inhibit the transcription factor PPARα, and up-regulate the sensitivity to ferroptosis	Venkatesh et al. (2020)

FPN, ferroportin; NTBI, non-transferrin-bound iron; USP7, ubiquitin-specific protease 7; TfR1, transferrin receptor 1; HSF1, heat shock factor 1; HSPB1, heat shock protein beta-1; GPX4, glutathione peroxidase 4; mTORC1, mechanistic target of rapamycin complex 1; ATF3, activating transcription factor 3; ATF4, activating transcription factor 4; KEAP1, Kelch-like ech-associated protein 1; NRF2, NF E2 Related Factor 2; ARE, antioxidant response element; AMPK, AMP-activated protein kinase; SREBP1, sterol response element binding protein 1; BCAT2, branched-chain amino acid aminotransferase 2; IFNγ, interferon γ; FSP1, Ferrop-Suppressor-Protein 1; ACSLs, acyl-CoA synthetase long-chain family; ACSL4, long-chain acyl-CoA synthetase 4; AA, arachidonic acid; AdA, adrenal acid; ACSL1, long-chain acyl-CoA synthetase 1; DAG, diacylglycerols; TAG, triacylglycerols; ALOX12, arachidonate 12-lipoxygenase; 15LOX, 15-lipoxygenase; PEBP1, phospholipid-ethanolamine binding protein-1; PUFA, polyunsaturated fatty acid; 15-HpETE-PE, 15-hydroperoxy-eicosatetraenoyl phosphatidylethanolamine.

then transport the iron into plasma through Fpn. Simultaneously, the duodenum absorbs iron ions from food into the human body through Fpn (**Figure 1**) (Ganz, 2013). The lack of Fpn on the membrane surface of other tissues leads to intracellular iron enrichment (Donovan et al., 2005). Bao et al. found that Fpn was down-regulated, leading to accumulation of lipid peroxide and neuronal cell ferroptosis in a mouse model of Alzheimer's disease (**Table 1**) (Bao et al., 2021). Hepcidin, a hepatic-secreted peptide hormone, binds to Fpn and promotes internalization and degradation of Fpn, resulting in the decreased export of non-heme iron (Nemeth et al., 2004). In addition to the Hepcidin-Fpn signaling pathway, the miR-124/Fpn signaling pathway has also been confirmed to affect the occurrence of ferroptosis. High levels of miR-124 in serum inhibit the expression of Fpn, leading to iron accumulation and ferroptosis in cells (Bao et al., 2020).

Iron Import

Under physiological conditions, ferric iron exported from cells binds to transferrin, which is a protein secreted primarily by the liver and transports iron to the bone marrow and other tissues. Conversely, if transferrin in plasma decreases, iron binds to albumin and anions to form non-transferrin-bound iron

(NTBI), which can be absorbed by tissue cells, causing iron overload (Ganz, 2013). Yu et al. reported that when transferrin levels in serum decreased, the vulnerability of liver fibrosis in both humans and mice increased significantly, which was due to the accumulation of NTBI in liver cells and leads to ferroptosis of liver cells. In this case, SLC39A14, which is not the main transporter under physiological conditions, can act as a transporter for NTBI to induce ferroptosis (Yu et al., 2020). However, research has found that SREBF2, the principal regulator of cholesterol synthesis, can directly induce transferrin expression at the transcription level, reduce intracellular iron pools, and suppress ferroptosis induced by iron accumulation (Hong et al., 2021). Transferrin receptor 1 (TfR1) can transfer transferrin into cells through receptor-mediated endocytosis, and release iron carried by transferrin into the iron pool. TfR1 has been identified as a specific target antigen related to ferroptosis (Feng et al., 2020). The research by Tang et al. (2021a) demonstrated that Ubiquitin-specific protease 7 (USP7) promotes ubiquitination of P53, leading to increased transcription of TfR1 and ferroptosis (Tang et al., 2021a).

Iron Storage and Utilization

Ferritin is an intracellular protein that oxidizes ferrous iron to ferric iron to avoid the occurrence of Fenton reaction, composed of light subunits (Ftl) and heavy subunits (Fth1). Ferritin is an inhibitor of ferroptosis, knockdown of Fth1 expression significantly increases the occurrence of ferroptosis (Rui et al., 2021). Ferritin is a form of iron storage in cells, and ferroptosis requires ferritin degradation to release stored iron. Quantitative proteomics found that NCOA4 can deliver ferritin to lysosomes and degrade ferritin in a selective cargo-mediated autophagy manner. Therefore, this process is called ferritinophagy (Mancias et al., 2014). Iron-independent ROS in the cell induces ferritinophagy and will increase intracellular iron levels (Park and Chung, 2019). The ferrous ions produced by ferritinophagy and the NTBI participate in the formation of labile iron pool in the cell, which is the chief culprit for the generation of ROS through the Fenton reaction (Ito et al., 2021). Therefore, iron storage and iron utilization are involved in the occurrence of ferroptosis.

Other Iron Metabolism

Novel regulators of iron homeostasis have been described. Sun et al. found that phosphorylated heat shock protein beta-1(HSPB1) acted as a negative regulator of ferroptosis by reducing iron uptake by cells and the production of lipids. Transphosphorylation of HSPB1 increases ferritin expression and reduces TfR1 expression. HSPB1 is expressed in a heat shock factor 1(HSF1) dependent manner. Protein kinase C (PKC) regulates the phosphorylation of HSPB1 and indirectly regulates ferroptosis (Sun et al., 2015). The HSF1-HSPB1 pathway and PKC are novel regulators of iron homeostasis.

ANTIOXIDANT METABOLISM

Glutathione Peroxidase 4

Not only does abnormal iron homeostasis regulation play an important role in ferroptosis but ferroptosis also requires the dysregulation of the intracellular antioxidant system. Yang et al. found that in ferroptosis cells, reduced glutathione (GSH), one of the most important endogenous antioxidants, was depleted, leading to the inactivation of glutathione peroxidase 4 (GPX4) (Yang et al., 2014). GSH-dependent GPX4 transforms toxic lipid peroxides in cells into non-toxic fatty alcohols, and prevents membrane phospholipids from reacting with ROS to produce lipid peroxides that directly lead to ferroptosis (**Figure 2**) (Magtanong et al., 2016). GSH is an essential substrate for GPX4 and exerts antiferroptosis activity. It is synthesized from cysteine and glutamic acid through a two-step enzymatic reaction and is oxidized to oxidized glutathione (GSSG) after reacting with lipid peroxides. Therefore, the antioxidant system comprising the GPX4 core is considered one of the most powerful regulators for protecting cells from ferroptosis. The appearance of a variety of diseases has been closely associated with the knockout of GPX4, such as neuronal degeneration (Hambright et al., 2017) and acute renal failure (Friedmann Angeli et al., 2014). Conversely, inhibiting GPX4 in drug-tolerant persisted cancer cells increases their vulnerability to ferroptosis. This discovery suggests a new treatment strategy for tumors (Hangauer et al., 2017; Viswanathan et al., 2017).

Selenoproteins are unique and rare proteins among a large protein family with unique physiological functions. Selenocysteine, which is not one of the 20 proteinogenic amino acids, is involved in the synthesis of GPX4. Selenocysteine ensures the need for unexpected antioxidant capacity (Ingold et al., 2018). Moreover, selenium is not only related to the synthesis of GPX4 but also promotes GPX4 transcription by coordinating and activating the transcription factors TFAP2C and SP1, allowing cells to respond to ferroptosis stimulation in an adaptive manner (Alim et al., 2019). In addition to the regulation of the transcription level, cystine and cysteine, as raw materials that simultaneously participate in the synthesis of GSH and GPX4, can activate the mechanistic target of rapamycin complex 1 (mTORC1) to inhibit the downstream 4EBP axis and promote GPX4 synthesis instead of indirectly regulating GSH levels (Zhang et al., 2021). In fact, mTORC1 acts as a bridge to link cystine and cysteine availability with the regulation of GPX4 and ferroptosis. Gaschler et al. recently discovered a new type of ferroptosis inducer FINO2 that inhibits GPX4. This is different from the class II ferroptosis inducer represented by RSL3. FINO2 can inhibit GPX4 while directly oxidizing polyunsaturated fatty acids (PUFAs), and provides a new perspective for the intervention of ferroptosis by adjusting GPX4 levels (Gaschler et al., 2018).

System Xc^-

System Xc^- is an amino acid reverse transporter located on the surface of the cell membrane, which can transport cystine outside the cell and glutamate inside the cell in a 1:1 ratio across the membrane. Therefore, System Xc^- activity is closely related to intracellular GSH content and GPX4 function. Ferroptosis is induced if system Xc^- activity is inhibited by erastin treatment (Dixon et al., 2012; Dixon et al., 2014). System Xc^- is a dimer composed of two subunits, SLC7A11 and SLC3A2, of which SLC7A11 makes a critical difference in limiting the rate of amino

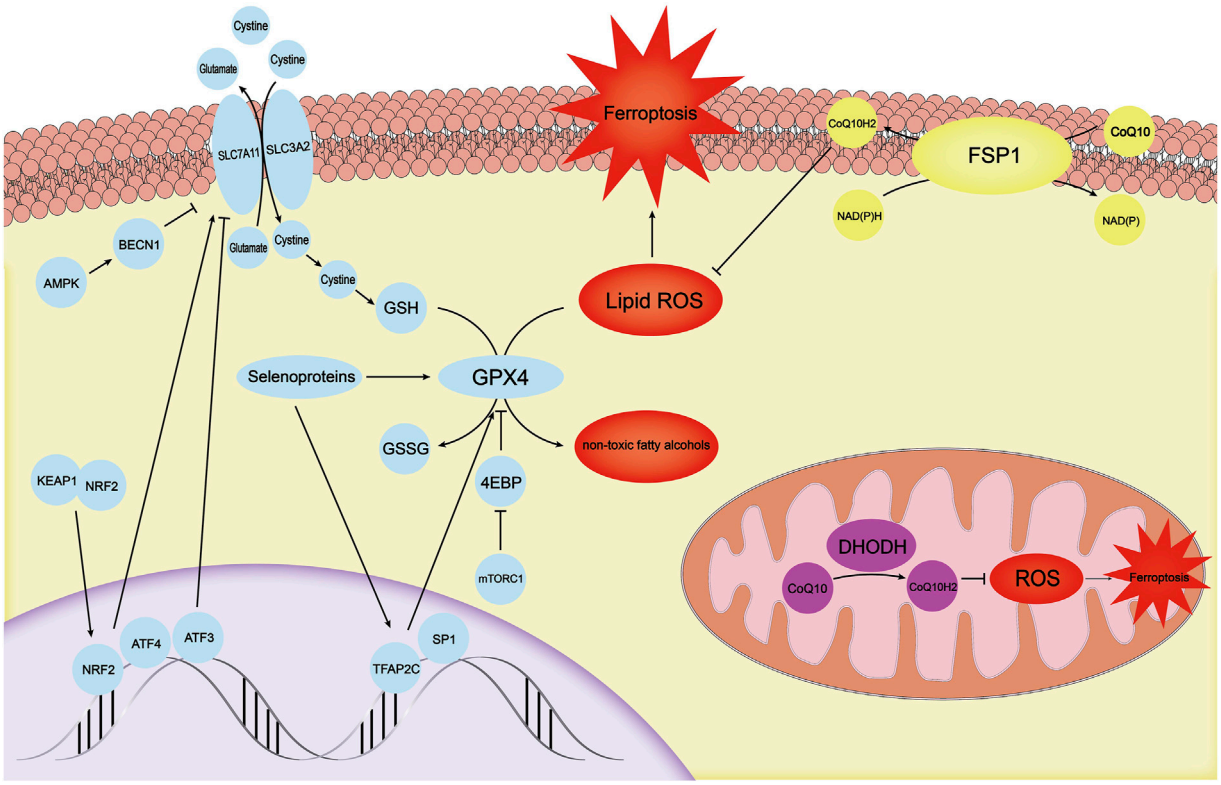

FIGURE 2 | There are three independent antioxidant systems in cells. The antioxidant system with GPX4 as the core is the first antioxidant system discovered. It is regulated by mechanisms such as TFAP2C, SP1, mTOR-4EBP, and selenoproteins. SLC7A11, which provides a substrate for GPX4, is regulated by ATF3, ATF4, KEAP1-NRF2, and AMPK-BECN1. The FSP1-CoQ10-NADPH system, another antioxidant system in the cell membrane, can inhibit ferroptosis through CoQ10H2. DHODH primarily inhibits ROS in mitochondria by synthesizing CoQ10H2 to avoid the ferroptosis process in mitochondria. GPX4, glutathione peroxidase 4; mTOR, mechanistic target of the rapamycin complex 1; ATF3, activating transcription factor 3; ATF4, activating transcription factor 4; KEAP1, kelch-like ech-associated protein 1; NRF2, NF E2 Related Factor 2; AMPK, AMP-activated protein kinase; FSP1, Ferrop-Suppressor-Protein 1; NADPH, nicotinamide adenine dinucleotide phosphate; DHODH, dihydroorotate dehydrogenase; ROS, reactive oxygen species.

acid transport (Lewerenz et al., 2013). Multiple regulatory mechanisms at transcription, post-translational modification (PTMS), and protein levels determine the ability of System Xc^- to uptake cystine.

Activating transcription factors are a family of transcription factors that includes activating transcription factor 3 (ATF3) and activating transcription factor 4 (ATF4), which have been confirmed to be related to the function of the system Xc^- (Wang J et al., 2020; Chen et al., 2017). In the presence of the intracellular redox imbalance, the mRNA level of ATF3 increased. Activated ATF3 binds tightly to the SLC7A11 promoter, inhibits the expression of SLC7A11, and promotes the occurrence of ferroptosis in oxidatively stressed cells (Wang L et al., 2020). Interestingly, the effects of ATF4 is completely opposite. Increased expression of ATF4 up-regulates system Xc^- expression and increases cell resistance to ferroptosis (Chen et al., 2017). There are other transcription factors, such as the redox-sensitive transcription factor NF E2 Related Factor 2 (NRF2) and P53, which regulate the function of system Xc^- (Habib et al., 2015). In the basal state, Kelch-like ech-associated protein 1 (KEAP1) ubiquitinates NRF2, and when cells are under oxidative stress, NRF2 separates from KEAP1. Subsequently, NRF2 enters the nucleus and binds to the antioxidant response element (ARE) of the proximal promoter of its target gene SLC7A11 to up-regulate the expression of SLC7A11 (Habib et al., 2015). As the most famous tumor suppressor gene, P53 has unique and diverse functions in the regulation of ferroptosis. Under stimulation of low or moderate levels of ROS, P53 can prevent the accumulation of lethal ROS, but when high levels of ROS are produced, P53 causes ferroptosis in cells by inhibiting SLC7A11 transcription (Jiang et al., 2015). Multiple transcription factors can be considered indirect regulatory targets of ferroptosis.

Unlike regulation at the transcriptional level, BECN1 can regulate the activity of system Xc^- through post-translational modification. BECN1 binds directly to SLC7A11 to form the BECN1-SLC7A11 complex, rather than interfering with the transcription of SLC7A11. Prior to this, BECN1 requires phosphorylation at Ser90/93/96 *via* AMP-activated protein kinase (AMPK) (Song et al., 2018).

Amino acid metabolism is the main mechanism regulating protein levels, and both cysteine and glutamate within and outside the cell have an impact on system Xc^-. High extracellular glutamate concentrations inhibit the activity of

system Xc^-, whereas elevated intracellular glutamate concentrations have the opposite effect. If cells are treated with erastin or sorafenib, the intracellular labile iron level will increase and subsequently induce ferritinophagy (Park and Chung, 2019). Wang et al. showed that ferritinophagy activated downstream AMPK and inhibited nuclear translocation of the sterol response element binding protein 1 (SREBP1), resulting in reduced transcription of the branched-chain amino acid aminotransferase 2 (BCAT2). BCAT2 is involved in the *de novo* synthesis of intracellular glutamate, and inhibition of BCAT2 reduces intracellular glutamate, which induces ferroptosis in cells (Wang et al., 2021). Similarly, inhibition of extracellular glutamine breakdown, which creates extracellular conditions of high glutamate, inhibits ferroptosis (Gao et al., 2015).

Recently, unique mechanisms by which immunotherapy and chemotherapy affect the system Xc^- have been reported. It was found that immune-activated $CD8^+T$ cells secreted interferon γ (IFNγ) that downregulated the expression of SLC7A11 and SLC3A2 expression (Lang et al., 2019; Wang W et al., 2019). SLC7A11 has also been shown to be a key target for the simultaneous action of immunotherapy and radiation therapy to induce ferroptosis (Lang et al., 2019). These novel studies provide a new research perspective to explore the mechanism of regulation of the system Xc^-, and future studies may focus on the effect of the intervention of physiological factors.

Other Parallel Antioxidant Mechanisms

Do cells have only one barrier against ferroptosis? Whether there is a parallel but completely independent antioxidant system with GPX4 and system Xc^- has become the key question regarding its antioxidant mechanism. Two research groups, Doll et al. (2019) and Bersuker et al. (2019) described independent mechanisms for cell resistance to ferroptosis almost simultaneously. The researchers determined that in some tumor cell lines, cells were able to resist ferroptosis even when the antiferroptosis system with the core of GPX4 was absent. Through gene sequencing of a large number of cells, the authors identified a previously unrecognized new mitochondrial-associated 2 apoptosis inducing factor (AIFM2), and renamed it "Ferrop-Suppressor-Protein 1" (FSP1). FSP1 must be recruited to the lipid membrane after myristoylation to perform its reductase function (Bersuker et al., 2019). The lipid membrane is rich in ubiquinone (CoQ10), and its reduced form, ubiquinol, can act as a lipophilic radical that traps antioxidant harvesting lipid peroxyl radicals (Doll et al., 2019). To reduce CoQ10, FSP1 must be supported by the coenzyme nicotinamide dinucleotide phosphate (NADPH), so FSP1-CoQ10-NADPH constitutes an independent antiferroptotic system.

In fact, cells contain other parallel antioxidant mechanisms. According to a recent study by Mao et al., there is a unique ferroptosis resistance system in mitochondria, which is dominated by dihydroorotate dehydrogenase (DHODH) (Mao et al., 2021). DHODH in GPX4-deficient cells leads to significant mitochondrial lipid peroxidation. Similarly, to the activity of the FSP1-CoQ10-NADPH axis, DHODH promotes the regeneration of CoQ10, which traps lipid peroxides in the mitochondrial membrane. Intervention with other parallel antioxidant mechanisms is a promising target to inhibit ferroptosis.

LIPID METABOLISM

The Fenton reaction triggered by abnormal iron metabolism leads to an increase in ROS, and an antioxidant system represented by GPX4 can eliminate ROS toxicity to cells, but the link between the two is lipid metabolism within the cell. Phospholipids are a component of cell membranes. ROS generated by the Fenton reaction tends to react with phospholipids (PL) to form hydroperoxy-phospholipids (PLOOH), which are the main elimination target of GPX4 (Magtanong et al., 2016). Phospholipids are lipids containing phosphoric acid, including a hydrophobic part composed of fatty acids and a hydrophilic part containing phosphoric acid. Phospholipids composed of polyunsaturated fatty acids are the main substrate for ROS oxidation (Kagan et al., 2017). Polyunsaturated fatty acids refer to straight chain fatty acids containing two or more double bonds, divided mainly into the omega-6 and omega-3 series (Wiktorowska-Owczarek et al., 2015). In the process of lipid synthesis, the first reaction using fatty acids is to catalyze the conversion of fatty acids into fatty acyl-CoA. The acyl-CoA synthetase long-chain family (ACSLs) is the first enzyme to catalyze the synthesis of phospholipids by acyl-CoA. Among them, long-chain acyl-CoA synthetase 4 (ACSL4) was identified as the key executor of ferroptosis (Yuan et al., 2016).

The preferred substrate for oxidation is phosphatidylethanolamine containing arachidonic acid (AA) and adrenal acid (AdA), and ACSL4 has a strong selectivity for AA-CoA and AdA-CoA (Doll et al., 2017; Dierge et al., 2021). ACSL4 promotes more peroxidable fatty acids to participate in the phospholipid synthesis process, and changes the composition ratio of fatty acids in lipids (Doll et al., 2017). Long-chain acyl-CoA synthetase 1 (ACSL1) adjusts the lipid composition by assembling αESA into diacylglycerols (DAG) and triacylglycerols (TAG). ACSL4 and ACSL1 adjust the content of non-conjugated fatty acids and conjugated fatty acids in lipids to adjust the vulnerability to ferroptosis. Unlike ACSL, lipoxygenase consists of a series of enzymes that catalyze the oxidation of PUFA double bonds to form lipid peroxides. Arachidonate 12-lipoxygenase (ALOX12) mainly catalyzes the oxidation of arachidonic acid, which is closely related to P53-mediated ferroptosis (Chu et al., 2019). P53 can indirectly activate ALOX12 by inhibiting SLC7A11 transcription, causing ferroptosis. It should be noted that although the transcription of SLC7A11 is reduced, it does not have a significant effect on GPX4 and GSH, indicating that this is an independent ferroptosis mechanism of GPX4 and ACSL4 (Chu et al., 2019), which involves 15-lipoxygenase (15LOX) and phospholipid-ethanolamine binding protein-1 (PEBP1) to combine and form a complex. The 15LOX/PEBP1 complex oxidizes various PUFAs to form 15-hydroperoxy-eicosatetraenoyl phosphatidylethanolamine (15-HpETE-PE), an important signaling molecule of ferroptosis (Wenzel et al., 2017; Anthonymuthu et al., 2021).

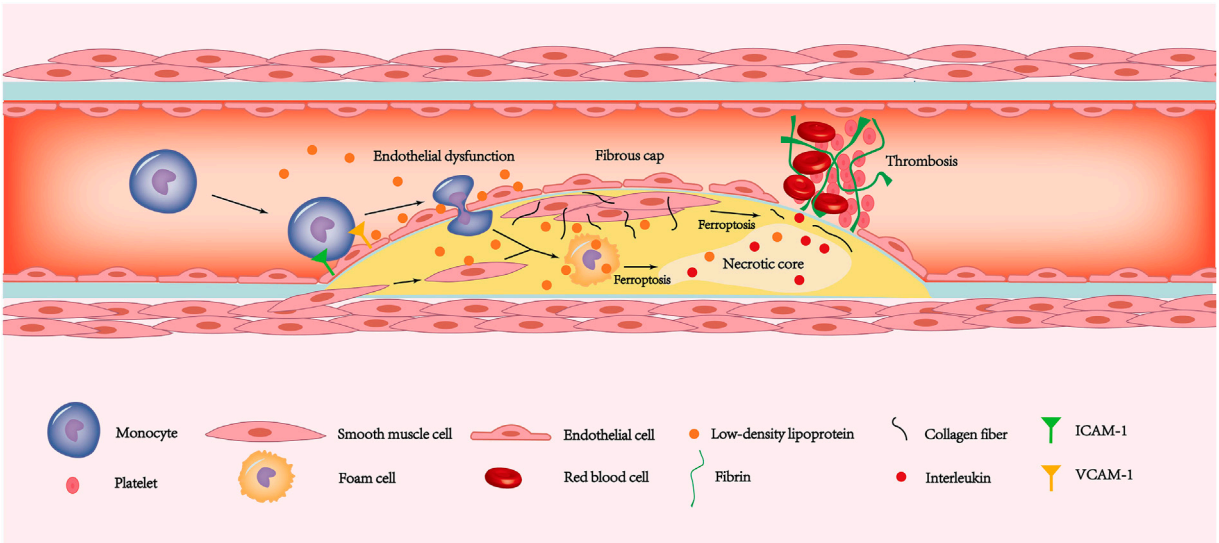

FIGURE 3 | The ferroptosis of endothelial cells, smooth muscle cells and macrophages is involved in the pathogenesis of coronary atherosclerotic heart disease. The increased expression of ICAM-1 and VCAM-1 allows monocytes to adhere to the endothelial surface. Due to ferroptosis leading to endothelial dysfunction, monocytes have the opportunity to deform and enter the inner membrane. The monocytes under the inner membrane gradually transform into macrophages. Then some macrophages and smooth muscle cells phagocytose LDL and then form foam cells. In addition, some smooth muscle cells migrate to the plaque surface and secrete a large amount of extracellular matrix such as collagen fibers, forming thick fibrous caps. As the disease progresses, ferroptosis in smooth muscle cells leads to gradual thinning of the fibrous cap. Similarly, foam cells ferroptosis promotes the release of interleukins in the necrotic core. Exfoliation of the endothelium caused by ferroptosis exposes fibrinogen to the tissue. The combination of thin fibrous caps, endothelial stripping, and large amounts of interleukin released from the necrotic core leads to a rapidly forming thrombosis that blocks the coronary artery and causes ACS. LDL, low-density lipoprotein; ACS, acute coronary syndrome.

MDM2 and MDMX are negative regulatory proteins of the P53 gene. However, their role in ferroptosis has nothing to do with P53, but with lipid metabolism (Venkatesh et al., 2020). During ferroptosis, the MDM2-MDMX heterodimer formed by MDM2 and MDMX inhibits the activity of the transcription factor PPARα in a post-translational manner. The PPAR transcription factor family is a large-scale regulator of lipid components, and reduced PPARα activity increases susceptibility to ferroptosis. At the same time, the MDM2-MDMX heterodimer can up-regulate the antioxidant system activity of FSP1-CoQ10 (Venkatesh et al., 2020). In conclusion, the lipid composition of the cell membrane is both the substrate and site of ferroptosis execution, and the regulation of the lipid composition of the cell membrane is an independent mechanism able to regulate ferroptosis.

FERROPTOSIS AND CORONARY ATHEROSCLEROTIC HEART DISEASE

Coronary artery disease refers to a series of diseases with angina pectoris as the main symptom caused by the inability of the coronary blood supply to meet the metabolic needs of the myocardium. Coronary artery disease is a general term for a series of diseases that include coronary atherosclerotic heart disease, coronary artery spasm, and myocardial bridge—of which coronary atherosclerotic heart disease accounts for the vast majority. Coronary atherosclerotic heart disease is a disease characterized by hyperplasia of atherosclerotic plaques. In the early stage of atherosclerosis, endothelial cell ability to resist blood cell attachment is reduced under stimulation of high levels of low-density lipoprotein (LDL) (Verhoye and Langlois, 2009; Trpkovic et al., 2015), hypertension (Quyyumi and Patel, 2010) and inflammation (Weissberg and Bennett, 1999). The expression of adhesion molecules on the surface of endothelial cells is dramatically increased, and the permeability of endothelial cells and the subendothelial extracellular matrix are simultaneously altered (**Figure 3**). This process is called endothelial dysfunction. Circulating monocytes adhere to the surface of the artery intima under the impact of endothelial cell adhesion molecules and gradually penetrate the arterial intima (Libby et al., 2011). Monocytes entering the intima differentiate into mononuclear macrophages under stimulation of inflammatory factors. Under stimulation of inflammation, the smooth muscle cells of the arterial media are recruited into the intima and merge with smooth muscle cells that settle in the inner membrane (Libby et al., 2011).

Endothelial dysfunction also causes the lipid composition of the blood to gradually accumulate under the inner membrane. To remove deposited lipids, especially LDL, monocytes, macrophages, and smooth muscle cells will phagocytose lipids to form foam cells. As lipids and foam cells accumulate and lipid deposition under the inner membrane, a fatty streak gradually forms in the intima, which are the early lesions of atherosclerosis (Maguire et al., 2019; Wang D et al., 2019). However, the phagocytic ability of foam cells is limited and the deposited lipid cannot be engulfed completely. Therefore, a large number of cell components are wrapped by the lipid pool

formed by extracellular lipids, and these components together become the basis for the formation of the lipid core. Long-term hypoxia and inflammation in the lipid core cause foam cells to die in a variety of ways, including necrosis and apoptosis. This process releases components such as cell debris, which constitute the main component of the necrotic core (Tabas, 2010). Smooth muscle cells secrete a large amount of extracellular matrix, including collagen fibers and elastin, covering the surface of the necrotic core, which is called the fibrous cap. The necrotic core and fibrous cap together constitute the pathological basis of coronary atherosclerotic heart disease and coronary atherosclerotic plaque formation.

As plaque size increases, coronary lumen stenosis reduces blood supply to cardiomyocytes and presents as angina pectoris. A potentially more lethal process may occur if the plaque thrombus suddenly occludes the coronary arteries and blood flow is drastically reduced. The produces a lack of collateral circulation compensation and can cause acute coronary syndromes (ACS), including unstable angina (UA) and acute myocardial infarction (AMI) (Crea and Libby, 2017). According to current opinions, the causes of acute thrombosis on the plaque surface are divided mainly into two types: plaque rupture (Davies and Thomas, 1984) and plaque erosion (Dai et al., 2018). Plaque rupture is the main cause of ACS. About two-thirds of ACSs are caused by plaque rupture (Arbustini et al., 1999). Plaques that are prone to rupture are called vulnerable plaques. Pathological features of vulnerable plaques include thin fibrous caps, large necrotic cores, and few smooth muscle cells (Finn et al., 2010). Macrophages cause vulnerable plaque rupture and thrombosis through a variety of regulatory cell death methods, including apoptosis (Hutter et al., 2004) and necroptosis (Karunakaran et al., 2016). Unlike macrophages, smooth muscle cells secrete an extracellular matrix to protect vulnerable plaques. The reduction in smooth muscle cells caused by multiple cell death pathways can significantly increase plaque vulnerability (Bennett et al., 2016).

Another vital pathogen that causes the occurrence of ACS is plaque erosion, which is responsible for up to about a third of ACS incidence. Compared to plaque rupture, plaque erosion has smaller necrotic cores, a higher number of smooth muscle cells, and thicker fibrous caps (Crea and Libby, 2017). In fact, the current explanation for the mechanism of plaque erosion is the two-hit hypothesis. De-endothelization of the plaque surface is the initial step of plaque erosion, which is the first hit. Endothelial cell dysfunction or death leads to the activation of platelets in the blood and the release of neutrophil extracellular traps (NETs) by neutrophils (Döring et al., 2017). The above factors are called the second hit, which induces thrombosis on the surface of the plaque. Through the study of the atherosclerosis process, it is easy to see that the death of various cells plays a key role in the occurrence and development of atherosclerosis. Current studies have confirmed that RCD methods such as apoptosis (Hutter et al., 2004), necroptosis (Karunakaran et al., 2016), and pyrolysis (Zhou et al., 2021) all occur in the plaque evolution process. Thus, do macrophages, smooth muscle cells and endothelial cells undergo ferroptosis during plaque progression?

As early as 30 years ago, Sullivan proposed the iron hypothesis, which pointed out that iron accumulation in atherosclerosis increases the risk of cardiovascular disease (Sullivan, 1981). The iron hypothesis is still controversial because the mechanism of iron accumulation leading to coronary atherosclerotic heart disease is not yet fully understood. The iron hypothesis has been widely questioned because hereditary hemochromatosis, a disease characterized by iron deposition throughout the body, not only reduces the risk of coronary atherosclerotic heart disease but also reduces the incidence (Mascitelli and Goldstein, 2014). Recent studies have shown that HFE gene mutations in patients with hemochromatosis regulate the expression of LDL receptors in liver cells and Kupffer cells. Under iron stimulation, HFE-deficient Kupffer cells phagocytose LDL-C in large amounts and reduce blood lipid levels (Demetz et al., 2020). Therefore, the reduced risk of coronary atherosclerosis in patients with hemochromatosis patients is actually related to the secondary low plasma level of LDL-C, which once again perfects and verifies the correctness of the iron hypothesis. Since the iron hypothesis was proposed, it has been widely recognized after continuous improvement, but the specific mechanism of iron deposition leading to atherosclerosis has not yet been fully elucidated.

The discovery of ferroptosis may explain the biological effects of iron accumulation. A recent study found that the SIRT1 autophagy axis in foam cells can inhibit ferroptosis induced by excessive iron (Su et al., 2021). By adding the exogenous iron agent ferric ammonium citrate to THP-1 cells, Su et al. confirmed that excessive iron induced ferroptosis in foam cells. Excess iron inhibits the SIRT1-autophagy axis of foam cells and reduces GPX4, both of which together induce foam cell ferroptosis (Su et al., 2021). Ferroptosis foam cells will release large amounts of inflammatory mediators such as IL-1β and IL-18. IL-1β and IL-18 belong to the IL-1 family of cytokines, and both are processed by caspase-1 for their activation (Pfeiler et al., 2019). Furthermore, early studies have confirmed that IL-1β and IL-18 can not only promote the progression of atherosclerosis (Mallat et al., 2001; Kirii et al., 2003) but also cause late plaque instability (Mallat et al., 2001) and induce myocardial infarction (Seta et al., 2000). Therefore, macrophage ferroptosis and foam cells derived from macrophage ferroptosis are present throughout the process, from early plaque formation to late plaque instability.

Regulating macrophage ferroptosis and foam cells derived from macrophages has become a novel target for the treatment of coronary atherosclerotic heart disease. Iron is a necessary condition for macrophage ferroptosis, and the most important pathway for macrophage iron regulation is the hepcidin-FPN axis (Wunderer et al., 2020). Hepcidin degrades FPN on the surface of macrophages, the only iron export protein, thus increasing the iron content of macrophages (Donovan et al., 2005). If hepcidin expression is suppressed, macrophages can excrete excess iron and cholesterol, which reduces foam cell formation and the progression of atherosclerosis (Saeed et al., 2012). When the iron content is increased or under inflammatory conditions, bone morphogenetic protein (BMP) stimulates the expression of hepcidin. Similarly, inhibition of BMP can also significantly delay atherosclerosis and vascular calcification (Derwall et al., 2012). Although current studies have confirmed the two facts that macrophage ferroptosis promotes

the progression of atherosclerosis and hepcidin interferes with the process of atherosclerosis by regulating iron content, the link between macrophage ferroptosis and hepcidin has not been confirmed. Whether hepcidin can affect the development of atherosclerosis by regulating macrophage ferroptosis has become a current research hotspot.

Smooth muscle cells are the cellular components of the fatty streak and the most important source of extracellular matrix secretion in plaques. Unlike macrophages, smooth muscle cell death interferes mainly with plaque vulnerability by affecting the components of the fibrous cap on the surface of the plaque (Bennett et al., 2016). Smooth muscle cells secrete collagen fibers, the main component of the fibrous cap. As smooth muscle cells die through various pathways, the thickness of the fibrous cap becomes thinner due to reduced secretion and degradation of collagen fibers (Allahverdian et al., 2018). Thin cap fibrous atheroma is usually responsible for acute cardiovascular events. Therefore, when smooth muscle cells die in the form of ferroptosis caused by various triggers, such as smoking and diabetes, it is likely to promote plaque rupture and lead to ACS. Sampilvanjil et al. extracted the components of the gas phase of cigarettes, which are the main components of cigarettes that induce cardiovascular disease, mainly including acrolein and methyl vinyl ketone (Sampilvanjil et al., 2020). Smooth muscle cells treated with components of the gas phase of cigarettes showed obvious ferroptosis characteristics, such as increased expression of PTGS2, increased active oxygen content of lipids, and depletion of GSH. Smooth muscle cells overexpressing GPX4 cannot escape ferroptosis induced by gas phase extracts. However, iron chelators and N-Acetyl-L-cysteine (an antioxidant that can replace GSH) can prevent ferroptosis of smooth muscle cells, demonstrating that cigarettes can induce ferroptosis by depleting GSH within smooth muscle cells (Sampilvanjil et al., 2020). Moreover, ferroptosis can also promote vascular calcification to cause coronary atherosclerotic heart disease (Durham et al., 2018).

Coronary artery calcification is an independent risk factor for coronary atherosclerotic heart disease and is closely related to plaque rupture (Nicoll and Henein, 2014). Smoking, diabetes, metabolic syndrome, chronic kidney disease, and oxidative stress are closely related to smooth muscle cell-induced vascular calcification (Durham et al., 2018). Oxidative stress has been identified as an initiating factor for smooth muscle cell-mediated phenotypic transformation and calcium salt secretion (Byon et al., 2008). Ma et al. used palmitic acid to stimulate smooth muscle cells to construct an *in vitro* model of oxidative stress, and found that smooth muscle cells produce ferroptosis and promote calcification deposition (Ma et al., 2021). In terms of mechanism, the extracellular matrix protein periostin (POSTN) negatively regulates the expression of SLC7A11 by inhibiting the expression of the smooth muscle cell P53 gene. After pretreatment with metformin, the ferroptosis of smooth muscle cells was significantly reduced, and the calcification deposition disappeared. In conclusion, metformin activates the antioxidant system of smooth muscle cells to resist ferroptosis and secondary calcification through the Nrf2 signaling pathway, which finally confirmed the close connection between ferroptosis and vascular calcification. Preventing coronary heart disease by intervening in smooth muscle cell ferroptosis will become another promising independent therapeutic target.

It was reported that endothelial cell ferroptosis contributes to the activation of adhesion factor and thrombus formation. The mechanism that triggers endothelial dysfunction is mainly related to endothelial cell oxidative stress, and ferroptosis also plays a role in oxidized low-density lipoprotein (oxLDL)-induced endothelial cell dysfunction (Bai et al., 2020). When endothelial cell dysfunction occurs, adhesion molecules on the surface of endothelial cells are overexpressed, including the intercellular adhesion molecule-1 (ICAM-1) and the vascular cell adhesion molecule-1 (VCAM-1) (Habas and Shang, 2018). The ferroptosis inhibitor Fer-1 reversed ICAM-1 and VCAM-1 expression secondary to the reduction in ferroptosis of endothelial cells and restored vascular endothelial cell function. GPX4, as an important protein of cellular antioxidant system, plays an important protective role in ferroptosis. Surprisingly, the endothelial cell-specific knockout of GPX4 did not damage vascular homeostasis in mice with a normal diet (Wortmann et al., 2013). Similarly, *in vitro* treatment of vitamin E deficient medium resulted in GPX4 knockout endothelial cell ferroptosis. Under these conditions, when mice were fed a diet deficient in antioxidant vitamin E, thrombotic events occurred in almost all mice. This may indicate that we can avoid ferroptosis and endothelial cell dysfunction by regular intake of antioxidants such as vitamin E. Besides, when the human body inhales PM2.5, the molecular mechanisms of ferroptosis in endothelial cells as the first line of defense include GSH depletion combined with iron metabolism disorder (Wang and Tang, 2019). Zinc oxide nanoparticles (ZnONPs), widely used in cosmetics, rubber, and pigments, promote NCOA4-mediated ferritinophagy in endothelial cells (Qin et al., 2021). Ferroptosis of endothelial cells mediated by ferritinophagy causes endothelial dysfunction and intense vascular inflammation. In summary, endothelial cells ferroptosis plays an important role in promoting atherosclerosis, and inhibition of ferroptosis by improving antioxidant metabolism may be a new target for protecting atherosclerosis.

FERROPTOSIS AND MYOCARDIAL ISCHEMIA REPERFUSION INJURY

Coronary artery subtotal occlusion or complete thrombosis-induced occlusion is likely to cause the onset of AMI. When AMI occurs, the blood supply to myocardial cells is interrupted and the cells are in a state of severe hypoxia. Unfortunately, the rapid improvement in blood supply in the ischemic myocardium can aggravate the degree of myocardial injury. Ischemia-reperfusion is one of the main mechanisms of myocardial injury (IRI) caused by AMI, and can be responsible for up to 50% of the infracted myocardial area (Lillo-Moya et al., 2021). The previous theory believed that IRI was related to xanthine oxidase and NADPH oxidase levels, and to mitochondrial activity, but new research shows that ferroptosis also plays an important role. (Tang et al., 2021b). found that only during the reperfusion period, the expression of ferroptosis markers MDA

and ACSL4 was significantly increased, accompanied by a down-regulation of GPX4 expression in the Sprague-Dawley rats (SD) model of IRI (Tang et al., 2021a). SD rats injected with the ferroptosis inhibitor DFO before IRI have up-regulated GPX4 expression during reperfusion, accompanied by a decrease in myocardial infarction area and a decrease in creatine kinase (CK) levels. After ischemia-reperfusion, the up-regulation of USP7 expression promotes the progression of ferroptosis through the USP7/P53/TfR1 pathway (Tang et al., 2021b). TfR1 takes transferrin in the blood into cardiomyocytes and provides the initiating factor iron for cardiomyocyte ferroptosis. These studies confirmed that ferroptosis was involved in myocardial IRI. More importantly, ferroptosis of myocardial cells occurs primarily during reperfusion (Tang et al., 2021a).

Diabetes is one of the most important risk factors for AMI. The incidence of myocardial ischemia in patients with diabetes is significantly higher than in the normal population (Ndumele et al., 2016). If diabetic patients experience myocardial IRI, ferroptosis and stress of the endoplasmic reticulum can promote each other and aggravate myocardial IRI within a state of high glucose and hypoxia (Li et al., 2020). In the study, compared to the control group, the degree of myocardial damage in the diabetes group increased dramatically, accompanied by ferroptosis and endoplasmic reticulum stress. Application of the ferroptosis inhibitor Fer-1 or the endoplasmic reticulum stress inhibitor salubrinal or tunicamycin can significantly reduce ferroptosis and endoplasmic reticulum stress, demonstrating that ferroptosis and endoplasmic reticulum stress mutually induce and promote diabetic myocardial IRI.

Existing studies have confirmed the important role of ferroptosis in myocardial ischemia-reperfusion. Therefore, suppressing ferroptosis during ischemia-reperfusion may become a new therapeutic strategy to protect the myocardium. Before reperfusion, Feng et al. administered Lip-1 to mice, a potent specific inhibitor of ferroptosis, which reduced the level of VDAC1 and increased the activity of GPX4 (Feng et al., 2019). Lip-1 also has the ability to maintain mitochondrial function and reduce the area of myocardial infarction. A variety of VDACs are embedded on the surface of the outer mitochondrial membrane (OMM), including VDAC1, VDAC2, and VDAC3. Among them, the oligomerization of VDAC1 induced the occurrence of apoptosis. A mechanism by which erastin induces ferroptosis is that of binding directly to VDAC2 on the surface of the OMM, which changes the permeability of mitochondria (Keinan et al., 2013). Lip-1 induces the opposite effect of erastin and cannot act on VDAC2. Lip-1 shuts down VDAC1 on the surface of OMM and weakens the ability of the VDAC1/GRP75/IP3R1 complex to transport Ca^{2+} to mitochondria, which inhibits cardiomyocyte apoptosis. Moreover, Lip-1 can strongly eliminate ROS and significantly reduces the ferroptosis of myocardial cells (Keinan et al., 2013). Therefore, Lip-1 may be a drug with great potential to protect cardiomyocytes from IRI.

FERROPTOSIS AND HEART FAILURE

Subsequent to insufficient blood supply and myocardial IRI caused by coronary atherosclerotic heart disease, a considerable number of patients exhibit a reduction in the number of myocardial cells and present severely damaged cardiac contractile function (Yancy et al., 2013). HF is a highly heterogeneous disease and is the common final result of various cardiovascular diseases, including coronary heart disease, cardiomyopathy, IRI, valvular disease, and hypertension, which develop to the advanced stage (Lakhal-Littleton et al., 2015). In addition to the fact that ferroptosis plays a driving role in various diseases causing HF there are also unique factors that induce ferroptosis to accelerate the progression of HF. In the development of HF, the imbalance of cardiac iron homeostasis can accelerate ferroptosis-mediated HF. Various iron metabolism abnormalities ultimately affect the content of labile iron pool in cells. If the FPN expressed by cardiomyocytes is specifically knocked out, the mice will show a significant increase in left ventricular diameter with a decrease in the ejection fraction (Fang et al., 2020). The non-specific knockout of the Hamp gene, which encodes hepcidin, in mice has been reported to lead to increased iron accumulation in the mouse heart, but did not significantly lead to the onset of cardiovascular disease (Zheng et al., 2021). This is because after hepcidin knockout, although the overall iron content in the heart increased significantly, iron was deposited mainly in noncardiomyocytes, which is the key difference between the two models. Similarly, knocking out Fth in the mouse heart specifically causes intracellular iron metabolism disorders, which can also lead to severe myocardial hypertrophy and myocardial damage (Chen et al., 2019). In addition, the study by Ito et al. found that the mice that specifically knocked out NCOA4 had significantly stronger cardiac function than the wild group after performing transverse aortic constriction (Ito et al., 2021). Their study confirmed that knocking out NCOA4 reduces the occurrence of ferritinophagy, which provides a beneficial help for inhibiting labile iron pool. Other studies confirmed that overexpression of SLC7A11 or exposure to of Fer-1 treatment in mice abolished pathological changes in the myocardium, which showed that myocardial iron metabolism disorder caused heart failure through ferroptosis of myocardial cells (Stevenson et al., 2019).

The noncoding RNA circSnx12 can up-regulate the downstream target miR224-5p, and can combine with the 3′UTR region of FTH1 to down-regulate its expression (Zheng et al., 2021). In addition to iron metabolism disorders, there are other mechanisms involved in the process of HF. The receptor 4 (TLR4)-NADPH oxidase 4 (NOX4) pathway is up-regulated in cardiomyocytes of mouse models of HF (Chen et al., 2019). TLR4 is the key to activating inflammation, and activation of inflammation promotes the appearance of cardiomyocyte autophagy and the up-regulation of NOX4. NOX4 is the downstream executor of cardiomyocyte ferroptosis. Another study found that NOX4 in heart samples from patients with advanced HF of ischemic cardiomyopathy promoted myocardial inflammation and myocardial fibrosis, which can be mutually verified with the above study (Stevenson et al., 2019). Myocardial fibrosis is the pathological basis for the heart remodeling process in HF. Mixed lineage kinase 3 (MLK3), a member of the MAP3K family, causes myocardial fibrosis by promoting ferroptosis in the late stage of congestive HF (J. Wang et al., 2020). It is worth

mentioning that the plant antioxidant puerarin is an effective inhibitor of ferroptosis during heart failure. Puerarin can inhibit NOX4 activity and, at the same time, up-regulate the expression of GPX4 and FTH1, and thus, it can delay cardiomyocyte damage and deterioration of heart function (Liu et al., 2018). In the future, including ferroptosis as a therapeutic target may represent an effective breakthrough in the treatment of heart failure.

FERROPTOSIS AND CLINICAL APPLICATION

With the development of basic research related to ferroptosis, combining ferroptosis with clinical applications has gradually become the next important research direction. The clinical application of ferroptosis-related targets is currently in its infancy. The current clinical research results may enlighten us several potential intervention targets in clinical applications. Since it is difficult to collect ferroptosis indicators in clinical practice, most studies focus on iron metabolity-related indicators, such as serum iron, serum ferritin, transferrin and soluble transferrin receptors. These targets with translational medicine potential could be key to controlling the progression of cardiovascular disease in the future.

Since Sullivan's hypothesis, people have focused on the relationship between serum iron and atherosclerotic diseases (Sullivan, 1981). The incidence of acute myocardial infarction was significantly higher in patients with elevated serum ferritin than in patients with reduced serum ferritin (Moradi et al., 2015). However, lower ferritin levels did not improve all-cause mortality from cardiovascular disease (Zacharski et al., 2007). There are many factors influencing the level of serum ferritin. Under pathological conditions such as inflammation and tumors, the level of serum ferritin will increase significantly. Therefore, we need more accurate predictors to link ferroptosis with coronary atherosclerotic heart disease. The soluble transferrin receptor (sTfR) is derived from the cell membrane surface receptor through hydrolysis, and it exists as a complex with transferrin in the blood. Although the concentration of soluble ferritin receptors is not directly related to the risk of coronary atherosclerotic heart disease, the concentration of sTfR increases with the number of affected coronary arteries (Braun et al., 2004). Hepcidin concentration also has limited predictive value for the risk of future myocardial infarction or cardiovascular death (Zeller et al., 2018). However, intrinsic Iron release, defined as low levels of hepcidin (<24 ng/ml) and high levels of sTfR (≥2 mg/L), has been associated with a significant reduction in cardiovascular mortality in patients with coronary atherosclerotic heart disease (Ruhe et al., 2018).

Elevated levels of ferritin and hepcidin were highly associated with a higher risk of new-onset heart failure in women but not in men (Klip et al., 2017). Alternatively, disorders in iron intake and absorption in patients with heart failure often result in iron deficiency (ID). Iron not only causes ferroptosis in the body, but also assists in oxygen transport and mitochondrial function. Hence, iron supplementation has become a widely accepted treatment for heart failure patients with ID. Intravenous administration of ferric carboxymaltose for 1 year significantly improves the results of 6-min walking trials in both anemic and non-anemic patients (Ponikowski et al., 2015). In patients with heart failure with ID, serum iron metabolism-related proteins could not correctly predict cardiac ferroptosis levels and heart failure mortality. All in all, it is difficult to use ferroptosis indicators as accurate predictors or therapeutic targets in clinical practice so far.

DISCUSSION

In recent years, research on the occurrence of ferroptosis and disease has gradually improved. More and more mechanisms related to the regulation of ferroptosis have been discovered, such as the FSP1-CoQ10-NADPH axis and DHODH antioxidant system. But there are still many unsolved mysteries. To date, the major research directions have focused on ferroptosis and tumors. By studying the regulatory pathways that promote tumor cell ferroptosis, we can provide new directions to prolong the survival of tumor patients. In addition, degenerative diseases of the nervous system, liver disease, and kidney disease are also hotspots in ferroptosis research. Due to the high incidence and mortality of cardiovascular diseases, these have gradually become the number one killer of human health. However, our understanding of the pathogenesis and treatment of cardiovascular disease is limited. After the discovery of apoptosis, researchers have confirmed its important role in cardiovascular disease. With the improved understanding of regulatory cell death, other modalities of regulatory cell death, such as necroptosis and pyrolysis, are believed to occur in cardiovascular diseases. Research on ferroptosis and cardiovascular disease is still in its infancy, and most existing studies have confirmed the existence of ferroptosis in cardiovascular disease. As we gradually deepen our understanding of the role of ferroptosis, this mechanism will become a potential breakthrough point in the treatment of cardiovascular disease.

Research on the mechanism of ferroptosis is a prerequisite for clinical treatment and application. The iron hypothesis has been a controversial issue for many years since it was put forward. The recent discovery that iron metabolism disorder is the first step in ferroptosis may be a strategy to quell the controversial issue of iron hypothesis. According to previous theories, the antioxidant system with GPX4 at the core is the only anti-ferroptosis mechanism. The FSP1-CoQ10-NADPH axis and the DHODH antioxidant system suggest that ferroptosis may be regulated by a variety of independent antioxidant mechanisms. The chemical structure of phospholipids is also a target for regulating ferroptosis. The structure of the phospholipid bilayer membrane of different ratios of fatty acid composition gives cells different degrees of vulnerability to ferroptosis. The discovery that conjugated and nonconjugated fatty acids have different ferroptosis characteristics has provided a novel insight for a strategies for intervention, that is, in the future, it is possible to alter the proportion of fatty acids by optimizing dietary intake by the population as a strategy to achieve the goals of prevention and treatment.

In terms of basic research, ferroptosis has been investigated in terms of coronary atherosclerotic heart disease progression to IRI and even HF. Existing research is limited to *in vitro* cell-based experiments and animal studies, and there is almost no verification of the pathological development process mentioned above in human samples. Further verification of the role of ferroptosis in human specimens will be the goal of the next stage of research. Arrhythmia-related diseases have so far been the blind spot in ferroptosis studies. In the future, exploring whether ferroptosis is related to arrhythmia may be part of the research prospects.

In clinical application, iron metabolism indicators can only predict the risk of AMI or initial heart failure in a limited manner. Since iron metabolism-related indicators are interfered by many other factors in the human body, more independent predictors of ferroptosis need to be discovered in the future.

In summary, current research has preliminarily shown that ferroptosis is closely related to a variety of cardiovascular diseases. Regulating ferroptosis will be one of the most promising emerging targets to improve the prognosis and the survival rate of cardiovascular diseases.

AUTHOR CONTRIBUTIONS

YL, XL, and JY: Conceptualization and writing, HJ and BY: Review and editing.

FUNDING

This research is supported by the National Natural Science Foundation of China (No. 82061130223 and No. 82072031), HMU Marshal Initiative Funding (HMUMIF-21016) and Fund of Key Laboratory of Myocardial Ischemia, Ministry of Education (KF202020/LX).

ACKNOWLEDGMENTS

We sincerely thank Charlesworth for assistance in language editing and manuscript writing.

REFERENCES

Alim, I., Caulfield, J. T., Chen, Y., Swarup, V., Geschwind, D. H., Ivanova, E., et al. (2019). Selenium Drives a Transcriptional Adaptive Program to Block Ferroptosis and Treat Stroke. *Cell* 177, 1262–1279. e25. doi:10.1016/j.cell.2019.03.032

Allahverdian, S., Chaabane, C., Boukais, K., Francis, G. A., and Bochaton-Piallat, M.-L. (2018). Smooth Muscle Cell Fate and Plasticity in Atherosclerosis. *Cardiovasc. Res.* 114, 540–550. doi:10.1093/cvr/cvy022

Anthonymuthu, T. S., Tyurina, Y. Y., Sun, W.-Y., Mikulska-Ruminska, K., Shrivastava, I. H., Tyurin, V. A., et al. (2021). Resolving the Paradox of Ferroptotic Cell Death: Ferrostatin-1 Binds to 15lox/Pebp1 Complex, Suppresses Generation of Peroxidized Ete-Pe, and Protects against Ferroptosis. *Redox Biol.* 38, 101744. doi:10.1016/j.redox.2020.101744

Arbustini, E., Dal Bello, B., Morbini, P., Burke, A. P., Bocciarelli, M., Specchia, G., et al. (1999). Plaque Erosion Is a Major Substrate for Coronary Thrombosis in Acute Myocardial Infarction. *Heart* 82, 269–272. doi:10.1136/hrt.82.3.269

Bai, T., Li, M., Liu, Y., Qiao, Z., and Wang, Z. (2020). Inhibition of Ferroptosis Alleviates Atherosclerosis through Attenuating Lipid Peroxidation and Endothelial Dysfunction in Mouse Aortic Endothelial Cell. *Free Radic. Biol. Med.* 160, 92–102. doi:10.1016/j.freeradbiomed.2020.07.026

Bao, W.-D., Pang, P., Zhou, X.-T., Hu, F., Xiong, W., Chen, K., et al. (2021). Loss of Ferroportin Induces Memory Impairment by Promoting Ferroptosis in Alzheimer's Disease. *Cell Death Differ* 28, 1548–1562. doi:10.1038/s41418-020-00685-9

Bao, W. D., Zhou, X. T., Zhou, L. T., Wang, F., Yin, X., Lu, Y., et al. (2020). Targeting miR-124/Ferroportin Signaling Ameliorated Neuronal Cell Death through Inhibiting Apoptosis and Ferroptosis in Aged Intracerebral Hemorrhage Murine Model. *Aging cell* 19, e13235. doi:10.1111/acel.13235

Bennett, M. R., Sinha, S., and Owens, G. K. (2016). Vascular Smooth Muscle Cells in Atherosclerosis. *Circ. Res.* 118, 692–702. doi:10.1161/circresaha.115.306361

Bersuker, K., Hendricks, J. M., Li, Z., Magtanong, L., Ford, B., Tang, P. H., et al. (2019). The Coq Oxidoreductase Fsp1 Acts Parallel to Gpx4 to Inhibit Ferroptosis. *Nature* 575, 688–692. doi:10.1038/s41586-019-1705-2

Braun, S., Ndrepepa, G., Beckerath, N. v., Vogt, W., Schömig, A., and Kastrati, A. (2004). Value of Serum Ferritin and Soluble Transferrin Receptor for Prediction of Coronary Artery Disease and its Clinical Presentations. *Atherosclerosis* 174, 105–110. doi:10.1016/j.atherosclerosis.2004.01.011

Byon, C. H., Javed, A., Dai, Q., Kappes, J. C., Clemens, T. L., Darley-Usmar, V. M., et al. (2008). Oxidative Stress Induces Vascular Calcification through Modulation of the Osteogenic Transcription Factor Runx2 by Akt Signaling. *J. Biol. Chem.* 283, 15319–15327. doi:10.1074/jbc.M800021200

Chen, D., Fan, Z., Rauh, M., Buchfelder, M., Eyupoglu, I. Y., and Savaskan, N. (2017). Atf4 Promotes Angiogenesis and Neuronal Cell Death and Confers Ferroptosis in a Xct-dependent Manner. *Oncogene* 36, 5593–5608. doi:10.1038/onc.2017.146

Chen, X., Xu, S., Zhao, C., and Liu, B. (2019). Role of Tlr4/Nadph Oxidase 4 Pathway in Promoting Cell Death through Autophagy and Ferroptosis during Heart Failure. *Biochem. biophysical Res. Commun.* 516, 37–43. doi:10.1016/j.bbrc.2019.06.015

Choi, M. E., Price, D. R., Ryter, S. W., and Choi, A. M. K. (2019). Necroptosis: A Crucial Pathogenic Mediator of Human Disease. *JCI insight* 4. doi:10.1172/jci.insight.128834

Chu, B., Kon, N., Chen, D., Li, T., Liu, T., Jiang, L., et al. (2019). Alox12 Is Required for P53-Mediated Tumour Suppression through a Distinct Ferroptosis Pathway. *Nat. Cel Biol* 21, 579–591. doi:10.1038/s41556-019-0305-6

Crea, F., and Libby, P. (2017). Acute Coronary Syndromes. *Circulation* 136, 1155–1166. doi:10.1161/circulationaha.117.029870

Dai, J., Xing, L., Jia, H., Zhu, Y., Zhang, S., Hu, S., et al. (2018). *In Vivo* Predictors of Plaque Erosion in Patients with St-Segment Elevation Myocardial Infarction: A Clinical, Angiographical, and Intravascular Optical Coherence Tomography Study. *Eur. Heart J.* 39, 2077–2085. doi:10.1093/eurheartj/ehy101

Davies, M. J., and Thomas, A. (1984). Thrombosis and Acute Coronary-Artery Lesions in Sudden Cardiac Ischemic Death. *N. Engl. J. Med.* 310, 1137–1140. doi:10.1056/nejm198405033101801

Del Re, D. P., Amgalan, D., Linkermann, A., Liu, Q., and Kitsis, R. N. (2019). Fundamental Mechanisms of Regulated Cell Death and Implications for Heart Disease. *Physiol. Rev.* 99, 1765–1817. doi:10.1152/physrev.00022.2018

Demetz, E., Tymoszuk, P., Hilbe, R., Volani, C., Haschka, D., Heim, C., et al. (2020). The Haemochromatosis Gene Hfe and Kupffer Cells Control Ldl Cholesterol Homeostasis and Impact on Atherosclerosis Development. *Eur. Heart J.* 41, 3949–3959. doi:10.1093/eurheartj/ehaa140

Derwall, M., Malhotra, R., Lai, C. S., Beppu, Y., Aikawa, E., Seehra, J. S., et al. (2012). Inhibition of Bone Morphogenetic Protein Signaling Reduces Vascular Calcification and Atherosclerosis. *Arterioscler Thromb. Vasc. Biol.* 32, 613–622. doi:10.1161/atvbaha.111.242594

Dierge, E., Debock, E., Guilbaud, C., Corbet, C., Mignolet, E., Mignard, L., et al. (2021). Peroxidation of N-3 and N-6 Polyunsaturated Fatty Acids in the Acidic Tumor Environment Leads to Ferroptosis-Mediated Anticancer Effects. *Cel Metab.* 33, 1701–1715. doi:10.1016/j.cmet.2021.05.016

Dixon, S. J., Lemberg, K. M., Lamprecht, M. R., Skouta, R., Zaitsev, E. M., Gleason, C. E., et al. (2012). Ferroptosis: An Iron-dependent Form of Nonapoptotic Cell Death. *Cell* 149, 1060–1072. doi:10.1016/j.cell.2012.03.042

Dixon, S. J., Patel, D. N., Welsch, M., Skouta, R., Lee, E. D., Hayano, M., et al. (2014). Pharmacological Inhibition of Cystine-Glutamate Exchange Induces Endoplasmic Reticulum Stress and Ferroptosis. *eLife* 3, e02523. doi:10.7554/eLife.02523

Doll, S., Freitas, F. P., Shah, R., Aldrovandi, M., da Silva, M. C., Ingold, I., et al. (2019). Fsp1 Is a Glutathione-independent Ferroptosis Suppressor. *Nature* 575, 693–698. doi:10.1038/s41586-019-1707-0

Doll, S., Proneth, B., Tyurina, Y. Y., Panzilius, E., Kobayashi, S., Ingold, I., et al. (2017). Acsl4 Dictates Ferroptosis Sensitivity by Shaping Cellular Lipid Composition. *Nat. Chem. Biol.* 13, 91–98. doi:10.1038/nchembio.2239

Dolma, S., Lessnick, S. L., Hahn, W. C., and Stockwell, B. R. (2003). Identification of Genotype-Selective Antitumor Agents Using Synthetic Lethal Chemical Screening in Engineered Human Tumor Cells. *Cancer cell* 3, 285–296. doi:10.1016/s1535-6108(03)00050-3

Dong, Y., Chen, H., Gao, J., Liu, Y., Li, J., and Wang, J. (2019). Molecular Machinery and Interplay of Apoptosis and Autophagy in Coronary Heart Disease. *J. Mol. Cell. Cardiol.* 136, 27–41. doi:10.1016/j.yjmcc.2019.09.001

Donovan, A., Lima, C. A., Pinkus, J. L., Pinkus, G. S., Zon, L. I., Robine, S., et al. (2005). The Iron Exporter Ferroportin/Slc40a1 Is Essential for Iron Homeostasis. *Cel Metab.* 1, 191–200. doi:10.1016/j.cmet.2005.01.003

Döring, Y., Soehnlein, O., and Weber, C. (2017). Neutrophil Extracellular Traps in Atherosclerosis and Atherothrombosis. *Circ. Res.* 120, 736–743. doi:10.1161/circresaha.116.309692

Durham, A. L., Speer, M. Y., Scatena, M., Giachelli, C. M., and Shanahan, C. M. (2018). Role of Smooth Muscle Cells in Vascular Calcification: Implications in Atherosclerosis and Arterial Stiffness. *Cardiovasc. Res.* 114, 590–600. doi:10.1093/cvr/cvy010

Ezekowitz, J. A., Kaul, P., Bakal, J. A., Armstrong, P. W., Welsh, R. C., and McAlister, F. A. (2009). Declining In-Hospital Mortality and Increasing Heart Failure Incidence in Elderly Patients with First Myocardial Infarction. *J. Am. Coll. Cardiol.* 53, 13–20. doi:10.1016/j.jacc.2008.08.067

Fang, X., Cai, Z., Wang, H., Han, D., Cheng, Q., Zhang, P., et al. (2020). Loss of Cardiac Ferritin H Facilitates Cardiomyopathy via Slc7a11-Mediated Ferroptosis. *Circ. Res.* 127, 486–501. doi:10.1161/circresaha.120.316509

Feng, H., Schorpp, K., Jin, J., Yozwiak, C. E., Hoffstrom, B. G., Decker, A. M., et al. (2020). Transferrin Receptor Is a Specific Ferroptosis Marker. *Cel Rep.* 30, 3411–3423. e7. doi:10.1016/j.celrep.2020.02.049

Feng, Y., Madungwe, N. B., Imam Aliagan, A. D., Tombo, N., and Bopassa, J. C. (2019). Liproxstatin-1 Protects the Mouse Myocardium against Ischemia/Reperfusion Injury by Decreasing Vdac1 Levels and Restoring Gpx4 Levels. *Biochem. biophysical Res. Commun.* 520, 606–611. doi:10.1016/j.bbrc.2019.10.006

Finn, A. V., Nakano, M., Narula, J., Kolodgie, F. D., and Virmani, R. (2010). Concept of Vulnerable/Unstable Plaque. *Atvb* 30, 1282–1292. doi:10.1161/atvbaha.108.179739

Friedmann Angeli, J. P., Schneider, M., Proneth, B., Tyurina, Y. Y., Tyurin, V. A., Hammond, V. J., et al. (2014). Inactivation of the Ferroptosis Regulator Gpx4 Triggers Acute Renal Failure in Mice. *Nat. Cel Biol* 16, 1180–1191. doi:10.1038/ncb3064

Ganz, T. (2013). Systemic Iron Homeostasis. *Physiol. Rev.* 93, 1721–1741. doi:10.1152/physrev.00008.2013

Gao, M., Monian, P., Quadri, N., Ramasamy, R., and Jiang, X. (2015). Glutaminolysis and Transferrin Regulate Ferroptosis. *Mol. Cel.* 59, 298–308. doi:10.1016/j.molcel.2015.06.011

Gaschler, M. M., Andia, A. A., Liu, H., Csuka, J. M., Hurlocker, B., Vaiana, C. A., et al. (2018). FINO2 Initiates Ferroptosis through GPX4 Inactivation and Iron Oxidation. *Nat. Chem. Biol.* 14, 507–515. doi:10.1038/s41589-018-0031-6

Habas, K., and Shang, L. (2018). Alterations in Intercellular Adhesion Molecule 1 (Icam-1) and Vascular Cell Adhesion Molecule 1 (Vcam-1) in Human Endothelial Cells. *Tissue and Cell* 54, 139–143. doi:10.1016/j.tice.2018.09.002

Habib, E., Linher-Melville, K., Lin, H.-X., and Singh, G. (2015). Expression of xCT and Activity of System Xc− Are Regulated by NRF2 in Human Breast Cancer Cells in Response to Oxidative Stress. *Redox Biol.* 5, 33–42. doi:10.1016/j.redox.2015.03.003

Hambright, W. S., Fonseca, R. S., Chen, L., Na, R., and Ran, Q. (2017). Ablation of Ferroptosis Regulator Glutathione Peroxidase 4 in Forebrain Neurons Promotes Cognitive Impairment and Neurodegeneration. *Redox Biol.* 12, 8–17. doi:10.1016/j.redox.2017.01.021

Hangauer, M. J., Viswanathan, V. S., Ryan, M. J., Bole, D., Eaton, J. K., Matov, A., et al. (2017). Drug-Tolerant Persister Cancer Cells Are Vulnerable to Gpx4 Inhibition. *Nature* 551, 247–250. doi:10.1038/nature24297

Hong, X., Roh, W., Sullivan, R. J., Wong, K. H. K., Wittner, B. S., Guo, H., et al. (2021). The Lipogenic Regulator Srebp2 Induces Transferrin in Circulating Melanoma Cells and Suppresses Ferroptosis. *Cancer Discov.* 11, 678–695. doi:10.1158/2159-8290.Cd-19-1500

Hutter, R., Valdiviezo, C., Sauter, B. V., Savontaus, M., Chereshnev, I., Carrick, F. E., et al. (2004). Caspase-3 and Tissue Factor Expression in Lipid-Rich Plaque Macrophages. *Circulation* 109, 2001–2008. doi:10.1161/01.Cir.0000125526.91945

Ingold, I., Berndt, C., Schmitt, S., Doll, S., Poschmann, G., Buday, K., et al. (2018). Selenium Utilization by Gpx4 Is Required to Prevent Hydroperoxide-Induced Ferroptosis. *Cell* 172, 409–422. e21. doi:10.1016/j.cell.2017.11.048

Ito, J., Omiya, S., Rusu, M.-C., Ueda, H., Murakawa, T., Tanada, Y., et al. (2021). Iron Derived from Autophagy-Mediated Ferritin Degradation Induces Cardiomyocyte Death and Heart Failure in Mice. *eLife* 10. doi:10.7554/eLife.62174

Jiang, L., Kon, N., Li, T., Wang, S.-J., Su, T., Hibshoosh, H., et al. (2015). Ferroptosis as a P53-Mediated Activity during Tumour Suppression. *Nature* 520, 57–62. doi:10.1038/nature14344

Kagan, V. E., Mao, G., Qu, F., Angeli, J. P. F., Doll, S., Croix, C. S., et al. (2017). Oxidized Arachidonic and Adrenic Pes Navigate Cells to Ferroptosis. *Nat. Chem. Biol.* 13, 81–90. doi:10.1038/nchembio.2238

Karunakaran, D., Geoffrion, M., Wei, L., Gan, W., Richards, L., Shangari, P., et al. (2016). Targeting Macrophage Necroptosis for Therapeutic and Diagnostic Interventions in Atherosclerosis. *Sci. Adv.* 2, e1600224. doi:10.1126/sciadv.1600224

Keinan, N., Pahima, H., Ben-Hail, D., and Shoshan-Barmatz, V. (2013). The Role of Calcium in Vdac1 Oligomerization and Mitochondria-Mediated Apoptosis. *Biochim. Biophys. Acta (Bba) - Mol. Cel Res.* 1833, 1745–1754. doi:10.1016/j.bbamcr.2013.03.017

Kirii, H., Niwa, T., Yamada, Y., Wada, H., Saito, K., Iwakura, Y., et al. (2003). Lack of Interleukin-1β Decreases the Severity of Atherosclerosis in ApoE-Deficient Mice. *Atvb* 23, 656–660. doi:10.1161/01.Atv.0000064374.15232.C3

Klip, I. T., Voors, A. A., Swinkels, D. W., Bakker, S. J. L., Kootstra-Ros, J. E., Lam, C. S., et al. (2017). Serum Ferritin and Risk for New-Onset Heart Failure and Cardiovascular Events in the Community. *Eur. J. Heart Fail.* 19, 348–356. doi:10.1002/ejhf.622

Lakhal-Littleton, S., Wolna, M., Carr, C. A., Miller, J. J. J., Christian, H. C., Ball, V., et al. (2015). Cardiac Ferroportin Regulates Cellular Iron Homeostasis and Is Important for Cardiac Function. *Proc. Natl. Acad. Sci. USA* 112, 3164–3169. doi:10.1073/pnas.1422373112

Lang, X., Green, M. D., Wang, W., Yu, J., Choi, J. E., Jiang, L., et al. (2019). Radiotherapy and Immunotherapy Promote Tumoral Lipid Oxidation and Ferroptosis via Synergistic Repression of Slc7a11. *Cancer Discov.* 9, 1673–1685. doi:10.1158/2159-8290.Cd-19-0338

Lewerenz, J., Hewett, S. J., Huang, Y., Lambros, M., Gout, P. W., Kalivas, P. W., et al. (2013). The Cystine/Glutamate Antiporter System Xc− in Health and Disease: From Molecular Mechanisms to Novel Therapeutic Opportunities. *Antioxid. Redox Signaling* 18, 522–555. doi:10.1089/ars.2011.4391

Li, W., Li, W., Leng, Y., Xiong, Y., and Xia, Z. (2020). Ferroptosis Is Involved in Diabetes Myocardial Ischemia/Reperfusion Injury through Endoplasmic Reticulum Stress. *DNA Cel. Biol.* 39, 210–225. doi:10.1089/dna.2019.5097

Libby, P., Ridker, P. M., and Hansson, G. K. (2011). Progress and Challenges in Translating the Biology of Atherosclerosis. *Nature* 473, 317–325. doi:10.1038/nature10146

Lillo-Moya, J., Rojas-Solé, C., Muñoz-Salamanca, D., Panieri, E., Saso, L., and Rodrigo, R. (2021). Targeting Ferroptosis against Ischemia/Reperfusion Cardiac Injury. *Antioxidants* 10, 667. doi:10.3390/antiox10050667

Liu, B., Zhao, C., Li, H., Chen, X., Ding, Y., and Xu, S. (2018). Puerarin Protects against Heart Failure Induced by Pressure Overload through Mitigation of Ferroptosis. *Biochem. biophysical Res. Commun.* 497, 233–240. doi:10.1016/j.bbrc.2018.02.061

Lockshin, R. A., and Zakeri, Z. (2001). Programmed Cell Death and Apoptosis: Origins of the Theory. *Nat. Rev. Mol. Cel Biol* 2, 545–550. doi:10.1038/35080097

Ma, W.-Q., Sun, X.-J., Zhu, Y., and Liu, N.-F. (2021). Metformin Attenuates Hyperlipidaemia-Associated Vascular Calcification through Anti-ferroptotic Effects. *Free Radic. Biol. Med.* 165, 229–242. doi:10.1016/j.freeradbiomed.2021.01.033

Magtanong, L., Ko, P. J., and Dixon, S. J. (2016). Emerging Roles for Lipids in Non-apoptotic Cell Death. *Cel Death Differ* 23, 1099–1109. doi:10.1038/cdd.2016.25

Maguire, E. M., Pearce, S. W. A., and Xiao, Q. (2019). Foam Cell Formation: A New Target for Fighting Atherosclerosis and Cardiovascular Disease. *Vasc. Pharmacol.* 112, 54–71. doi:10.1016/j.vph.2018.08.002

Mallat, Z., Corbaz, A., Scoazec, A., Graber, P., Alouani, S., Esposito, B., et al. (2001). Interleukin-18/Interleukin-18 Binding Protein Signaling Modulates Atherosclerotic Lesion Development and Stability. *Circ. Res.* 89, E41–E45. doi:10.1161/hh1901.098735

Mancias, J. D., Wang, X., Gygi, S. P., Harper, J. W., and Kimmelman, A. C. (2014). Quantitative Proteomics Identifies Ncoa4 as the Cargo Receptor Mediating Ferritinophagy. *Nature* 509, 105–109. doi:10.1038/nature13148

Mao, C., Liu, X., Zhang, Y., Lei, G., Yan, Y., Lee, H., et al. (2021). Dhodh-Mediated Ferroptosis Defence Is a Targetable Vulnerability in Cancer. *Nature* 593, 586–590. doi:10.1038/s41586-021-03539-7

Mascitelli, L., and Goldstein, M. R. (2014). Hereditary Hemochromatosis, Iron, Hepcidin, and Coronary Heart Disease. *Med. hypotheses* 82, 402–403. doi:10.1016/j.mehy.2013.12.013

Moradi, M., Fariba, F., and Mohasseli, A. S. (2015). Relation between the Serum Ferritin Level and the Risk for Acute Myocardial Infarction. *J. Res. Health Sci.* 15, 147–151.

Ndumele, C. E., Matsushita, K., Lazo, M., Bello, N., Blumenthal, R. S., Gerstenblith, G., et al. (2016). Obesity and Subtypes of Incident Cardiovascular Disease. *Jaha* 5. doi:10.1161/jaha.116.003921

Nemeth, E., Tuttle, M. S., Powelson, J., Vaughn, M. B., Donovan, A., Ward, D. M., et al. (2004). Hepcidin Regulates Cellular Iron Efflux by Binding to Ferroportin and Inducing its Internalization. *Science* 306, 2090–2093. doi:10.1126/science.1104742

Nicoll, R., and Henein, M. Y. (2014). The Predictive Value of Arterial and Valvular Calcification for Mortality and Cardiovascular Events. *IJC Heart & VesselsHeart & vessels.* 3, 1–5. doi:10.1016/j.ijchv.2014.02.001

Park, E., and Chung, S. W. (2019). Ros-Mediated Autophagy Increases Intracellular Iron Levels and Ferroptosis by Ferritin and Transferrin Receptor Regulation. *Cell Death Dis* 10, 822. doi:10.1038/s41419-019-2064-5

Pfeiler, S., Winkels, H., Kelm, M., and Gerdes, N. (2019). Il-1 Family Cytokines in Cardiovascular Disease. *Cytokine* 122, 154215. doi:10.1016/j.cyto.2017.11.009

Ponikowski, P., van Veldhuisen, D. J., Comin-Colet, J., Ertl, G., Komajda, M., Mareev, V., et al. (2015). Beneficial Effects of Long-Term Intravenous Iron Therapy with Ferric Carboxymaltose in Patients with Symptomatic Heart Failure and Iron Deficiency. *Eur. Heart J.* 36, 657–668. doi:10.1093/eurheartj/ehu385

Qin, X., Zhang, J., Wang, B., Xu, G., Yang, X., Zou, Z., et al. (2021). Ferritinophagy Is Involved in the Zinc Oxide Nanoparticles-Induced Ferroptosis of Vascular Endothelial Cells. *Autophagy* 17, 4266–4285. doi:10.1080/15548627.2021.1911016

Quyyumi, A. A., and Patel, R. S. (20101979). 55. Dallas, Tex, 1092–1094. doi:10.1161/hypertensionaha.109.148957Endothelial Dysfunction and Hypertension*Hypertension*

Ruhe, J., Waldeyer, C., Ojeda, F., Altay, A., Schnabel, R., Schäfer, S., et al. (2018). Intrinsic Iron Release Is Associated with Lower Mortality in Patients with Stable Coronary Artery Disease-First Report on the Prospective Relevance of Intrinsic Iron Release. *Biomolecules* 8, 72. doi:10.3390/biom8030072

Rui, T., Wang, H., Li, Q., Cheng, Y., Gao, Y., Fang, X., et al. (2021). Deletion of Ferritin H in Neurons Counteracts the Protective Effect of Melatonin against Traumatic Brain Injury-induced Ferroptosis. *J. Pineal Res.* 70, e12704. doi:10.1111/jpi.12704

Saeed, O., Otsuka, F., Polavarapu, R., Karmali, V., Weiss, D., Davis, T., et al. (2012). Pharmacological Suppression of Hepcidin Increases Macrophage Cholesterol Efflux and Reduces Foam Cell Formation and Atherosclerosis. *Arterioscler Thromb. Vasc. Biol.* 32, 299–307. doi:10.1161/atvbaha.111.240101

Sampilvanjil, A., Karasawa, T., Yamada, N., Komada, T., Higashi, T., Baatarjav, C., et al. (2020). Cigarette Smoke Extract Induces Ferroptosis in Vascular Smooth Muscle Cells. *Am. J. Physiology-Heart Circulatory PhysiologyHeart circulatory Physiol.* 318, H508–H518. doi:10.1152/ajpheart.00559.2019

Seta, Y., Kanda, T., Tanaka, T., Arai, M., Sekiguchi, K., Yokoyama, T., et al. (2000). Interleukin 18 in Acute Myocardial Infarction. *Heart (British Cardiac Society)* 84, 668–669. doi:10.1136/heart.84.6.668

Song, X., Zhu, S., Chen, P., Hou, W., Wen, Q., Liu, J., et al. (2018). AMPK-mediated BECN1 Phosphorylation Promotes Ferroptosis by Directly Blocking System Xc- Activity. *Curr. Biol.* 28, 2388–2399. e5. doi:10.1016/j.cub.2018.05.094

Stevenson, M. D., Canugovi, C., Vendrov, A. E., Hayami, T., Bowles, D. E., Krause, K.-H., et al. (2019). Nadph Oxidase 4 Regulates Inflammation in Ischemic Heart Failure: Role of Soluble Epoxide Hydrolase. *Antioxid. Redox Signaling* 31, 39–58. doi:10.1089/ars.2018.7548

Su, G., Yang, W., Wang, S., Geng, C., and Guan, X. (2021). SIRT1-autophagy axis Inhibits Excess Iron-Induced Ferroptosis of Foam Cells and Subsequently Increases IL-1B and IL-18. *Biochem. biophysical Res. Commun.* 561, 33–39. doi:10.1016/j.bbrc.2021.05.011

Sullivan, J. (1981). Iron and the Sex Difference in Heart Disease Risk. *The Lancet* 317, 1293–1294. doi:10.1016/s0140-6736(81)92463-6

Sun, X., Ou, Z., Xie, M., Kang, R., Fan, Y., Niu, X., et al. (2015). Hspb1 as a Novel Regulator of Ferroptotic Cancer Cell Death. *Oncogene* 34, 5617–5625. doi:10.1038/onc.2015.32

Tabas, I. (2010). Macrophage Death and Defective Inflammation Resolution in Atherosclerosis. *Nat. Rev. Immunol.* 10, 36–46. doi:10.1038/nri2675

Tang, L.-J., Luo, X.-J., Tu, H., Chen, H., Xiong, X.-M., Li, N.-S., et al. (2021a). Ferroptosis Occurs in Phase of Reperfusion but Not Ischemia in Rat Heart Following Ischemia or Ischemia/Reperfusion. *Naunyn-schmiedeberg's Arch. Pharmacol.* 394, 401–410. doi:10.1007/s00210-020-01932-z

Tang, L.-J., Zhou, Y.-J., Xiong, X.-M., Li, N.-S., Zhang, J.-J., Luo, X.-J., et al. (2021b). Ubiquitin-Specific Protease 7 Promotes Ferroptosis via Activation of the P53/Tfr1 Pathway in the Rat Hearts after Ischemia/Reperfusion. *Free Radic. Biol. Med.* 162, 339–352. doi:10.1016/j.freeradbiomed.2020.10.307

Trpkovic, A., Resanovic, I., Stanimirovic, J., Radak, D., Mousa, S. A., Cenic-Milosevic, D., et al. (2015). Oxidized Low-Density Lipoprotein as a Biomarker of Cardiovascular Diseases. *Crit. Rev. Clin. Lab. Sci.* 52, 70–85. doi:10.3109/10408363.2014.992063

Venkatesh, D., O'Brien, N. A., Zandkarimi, F., Tong, D. R., Stokes, M. E., Dunn, D. E., et al. (2020). MDM2 and MDMX Promote Ferroptosis by PPARα-Mediated Lipid Remodeling. *Genes Dev.* 34, 526–543. doi:10.1101/gad.334219.119

Verhoye, E., and Langlois, M. R. (2009). Circulating Oxidized Low-Density Lipoprotein: A Biomarker of Atherosclerosis and Cardiovascular Risk? *Clin. Chem. Lab. Med.* 47, 128–137. doi:10.1515/cclm.2009.037

Viswanathan, V. S., Ryan, M. J., Dhruv, H. D., Gill, S., Eichhoff, O. M., Seashore-Ludlow, B., et al. (2017). Dependency of a Therapy-Resistant State of Cancer Cells on a Lipid Peroxidase Pathway. *Nature* 547, 453–457. doi:10.1038/nature23007

Wang, D., Yang, Y., Lei, Y., Tzvetkov, N. T., Liu, X., Yeung, A. W. K., et al. (2019). Targeting Foam Cell Formation in Atherosclerosis: Therapeutic Potential of Natural Products. *Pharmacol. Rev.* 71, 596–670. doi:10.1124/pr.118.017178

Wang, J., Deng, B., Liu, Q., Huang, Y., Chen, W., Li, J., et al. (2020). Pyroptosis and Ferroptosis Induced by Mixed Lineage Kinase 3 (Mlk3) Signaling in Cardiomyocytes Are Essential for Myocardial Fibrosis in Response to Pressure Overload. *Cel Death Dis* 11, 574. doi:10.1038/s41419-020-02777-3

Wang, K., Zhang, Z., Tsai, H.-i., Liu, Y., Gao, J., Wang, M., et al. (2021). Branched-Chain Amino Acid Aminotransferase 2 Regulates Ferroptotic Cell Death in Cancer Cells. *Cel Death Differ* 28, 1222–1236. doi:10.1038/s41418-020-00644-4

Wang, L., Liu, Y., Du, T., Yang, H., Lei, L., Guo, M., et al. (2020). ATF3 Promotes Erastin-Induced Ferroptosis by Suppressing System Xc-. *Cel Death Differ* 27, 662–675. doi:10.1038/s41418-019-0380-z

Wang, W., Green, M., Choi, J. E., Gijón, M., Kennedy, P. D., Johnson, J. K., et al. (2019). CD8+ T Cells Regulate Tumour Ferroptosis during Cancer Immunotherapy. *Nature* 569, 270–274. doi:10.1038/s41586-019-1170-y

Wang, Y., and Tang, M. (2019). Pm2.5 Induces Ferroptosis in Human Endothelial Cells through Iron Overload and Redox Imbalance. *Environ. Pollut.* 254, 112937. doi:10.1016/j.envpol.2019.07.105

Weissberg, P. L., and Bennett, M. R. (1999). Atherosclerosis - an Inflammatory Disease. *N. Engl. J. Med.* 340, 1928–1929. doi:10.1056/nejm199906173402418

Wenzel, S. E., Tyurina, Y. Y., Zhao, J., St. Croix, C. M., Dar, H. H., Mao, G., et al. (2017). Pebp1 Wardens Ferroptosis by Enabling Lipoxygenase Generation of Lipid Death Signals. *Cell* 171, 628–641. e26. doi:10.1016/j.cell.2017.09.044

Wiktorowska-Owczarek, A., Berezińska, M., and Nowak, J. (2015). Pufas: Structures, Metabolism and Functions. *Adv. Clin. Exp. Med.* 24, 931–941. doi:10.17219/acem/31243

Wortmann, M., Schneider, M., Pircher, J., Hellfritsch, J., Aichler, M., Vegi, N., et al. (2013). Combined Deficiency in Glutathione Peroxidase 4 and Vitamin E Causes Multiorgan Thrombus Formation and Early Death in Mice. *Circ. Res.* 113, 408–417. doi:10.1161/circresaha.113.279984

Wunderer, F., Traeger, L., Sigurslid, H. H., Meybohm, P., Bloch, D. B., and Malhotra, R. (2020). The Role of Hepcidin and Iron Homeostasis in Atherosclerosis. *Pharmacol. Res.* 153, 104664. doi:10.1016/j.phrs.2020.104664

Yancy, C. W., Jessup, M., Bozkurt, B., Butler, J., Casey, D. E., Drazner, M. H., et al. (2013). 2013 ACCF/AHA Guideline for the Management of Heart Failure. *J. Am. Coll. Cardiol.* 62, e147–e239. doi:10.1016/j.jacc.2013.05.019

Yang, W. S., SriRamaratnam, R., Welsch, M. E., Shimada, K., Skouta, R., Viswanathan, V. S., et al. (2014). Regulation of Ferroptotic Cancer Cell Death by Gpx4. *Cell* 156, 317–331. doi:10.1016/j.cell.2013.12.010

Yu, Y., Jiang, L., Wang, H., Shen, Z., Cheng, Q., Zhang, P., et al. (2020). Hepatic Transferrin Plays a Role in Systemic Iron Homeostasis and Liver Ferroptosis. *Blood* 136, 726–739. doi:10.1182/blood.2019002907

Yuan, H., Li, X., Zhang, X., Kang, R., and Tang, D. (2016). Identification of Acsl4 as a Biomarker and Contributor of Ferroptosis. *Biochem. biophysical Res. Commun.* 478, 1338–1343. doi:10.1016/j.bbrc.2016.08.124

Zacharski, L. R., Chow, B. K., Howes, P. S., Shamayeva, G., Baron, J. A., Dalman, R. L., et al. (2007). Reduction of Iron Stores and Cardiovascular Outcomes in Patients with Peripheral Arterial Disease. *JAMA* 297, 603–610. doi:10.1001/jama.297.6.603

Zeller, T., Altay, A., Waldeyer, C., Appelbaum, S., Ojeda, F., Ruhe, J., et al. (2018). Prognostic Value of Iron-Homeostasis Regulating Peptide Hepcidin in Coronary Heart Disease-Evidence from the Large Atherogene Study. *Biomolecules* 8, 43. doi:10.3390/biom8030043

Zhang, Y., Swanda, R. V., Nie, L., Liu, X., Wang, C., Lee, H., et al. (2021). Mtorc1 Couples Cyst(E)Ine Availability with Gpx4 Protein Synthesis and Ferroptosis Regulation. *Nat. Commun.* 12, 1589. doi:10.1038/s41467-021-21841-w

Zhaolin, Z., Guohua, L., Shiyuan, W., and Zuo, W. (2019). Role of Pyroptosis in Cardiovascular Disease. *Cell Prolif* 52, e12563. doi:10.1111/cpr.12563

Zheng, H., Shi, L., Tong, C., Liu, Y., and Hou, M. (2021). Circsnx12 Is Involved in Ferroptosis during Heart Failure by Targeting Mir-224-5p. *Front. Cardiovasc. Med.* 8, 656093. doi:10.3389/fcvm.2021.656093

Zhou, Y., Zhou, H., Hua, L., Hou, C., Jia, Q., Chen, J., et al. (2021). Verification of Ferroptosis and Pyroptosis and Identification of Ptgs2 as the Hub Gene in Human Coronary Artery Atherosclerosis. *Free Radic. Biol. Med.* 171, 55–68. doi:10.1016/j.freeradbiomed.2021.05.009

Conflict of Interest: The authors declare that the research was conducted in the absence of any commercial or financial relationships that could be construed as a potential conflict of interest.

Publisher's Note: All claims expressed in this article are solely those of the authors and do not necessarily represent those of their affiliated organizations, or those of the publisher, the editors and the reviewers. Any product that may be evaluated in this article, or claim that may be made by its manufacturer, is not guaranteed or endorsed by the publisher.

Copyright © 2022 Leng, Luo, Yu, Jia and Yu. This is an open-access article distributed under the terms of the Creative Commons Attribution License (CC BY). The use, distribution or reproduction in other forums is permitted, provided the original author(s) and the copyright owner(s) are credited and that the original publication in this journal is cited, in accordance with accepted academic practice. No use, distribution or reproduction is permitted which does not comply with these terms.

frontiers in Cell and Developmental Biology

ORIGINAL RESEARCH
published: 24 January 2022
doi: 10.3389/fcell.2022.827691

Putative Prevention of XML Injection Against Myocardial Ischemia Is Mediated by PKC and PLA2 Proteins

Ling Jin[1], Qianqian Yin[1], Yiqing Mao[2], Yuanxu Gao[3], Qing Han[2], Ruisi Mei[2], Lixiang Xue[1], Huanran Tan[2] and Hui Li[2]**

[1]Center of Basic Medical Research, Institute of Medical Innovation and Research, Peking University Third Hospital, Beijing, China, [2]Department of Pharmacology, Peking University, Health Science Center, Beijing, China, [3]State Key Laboratory of Lunar and Planetary Sciences, Macau University of Science and Technology, Macau, China

Background: Xinmailong (XML) injection is a CFDA-approved traditional Chinese medicine with clinical value for heart failure treatment. The present investigation was aimed to evaluate the potential protective roles of this injection on myocardial ischemia and the underlying molecular mechanism.

Methods: In our study, we selected two models of myocardial ischemia rats. Rats were randomly divided into six groups, with saline or XML administrated 4 days before ischemia model establishment. ECG of different time intervals and biochemical parameters of end point were measured. The potential mechanisms of the protective role of XML were explored using system pharmacology and molecular biology approaches.

Results: Myocardial ischemia rats demonstrated abnormal ECG and serum levels of cTnT. Pretreatment with XML significantly attenuated these damages, especially the medium doses. GO and KEGG analysis revealed that the 90 putative target genes were associated with pathways of fatty acid absorption/metabolism, inflammation, RAAS, and vascular smooth muscle. Further network pharmacology method identified five main chemical ingredients and potential targets of XML injection for myocardial ischemia. Mechanically, the beneficial effect of XML injection was mediated by the reactive oxygen species (ROS) inhibition and inflammation attenuation via regulating the expression levels of targets of PKC and PLA2.

Conclusion: These findings indicate that XML exerts protective effects against myocardial injury, with attenuated ROS production, apoptosis, and inflammation. Therefore, we speculate that XML may be an alternative supplementary therapeutic agent for myocardial ischemia prevention.

Keywords: xinmailong injection, myocardial ischemia, network pharmacology, Protein kinase C, PLA 2

OPEN ACCESS

Edited by:
Zhi Qi,
Nankai University, China

Reviewed by:
Liming Yang,
Harbin Medical University, China
Yangyang Zhang,
Shanghai Jiaotong University, China

****Correspondence:***
Huanran Tan
tanlab@bjmu.edu.cn
Hui Li
lihui@bjmu.edu.cn

Specialty section:
This article was submitted to Cell Death and Survival, a section of the journal Frontiers in Cell and Developmental Biology

Received: *02 December 2021*
Accepted: *03 January 2022*
Published: *24 January 2022*

Citation:
Jin L, Yin Q, Mao Y, Gao Y, Han Q, Mei R, Xue L, Tan H and Li H (2022) Putative Prevention of XML Injection Against Myocardial Ischemia Is Mediated by PKC and PLA2 Proteins. Front. Cell Dev. Biol. 10:827691. doi: 10.3389/fcell.2022.827691

INTRODUCTION

The cockroach has a long history of the treatment of disease in traditional Chinese medicine. It is bitter in taste and cold in nature, with the component activities associated with heart function enhancement, increased urine amount, and improved microcirculation (Luo et al., 2014). Xinmailong (XML) injection is a bioactive composite extracted from the cockroach that has

been approved by the China State Food and Drug Administration (CFDA) in 2006 (2016). XML has been shown to have outstanding curative effects against cardiovascular injury in chronic heart failure owing to its activities of dilating the coronary arteries, antagonizing activation of neuroendocrine systems, increasing blood supply to cardiac muscle, improving cardiac function, and antagonizing ventricular restructuring (Ma et al., 2013; Liu et al., 2014). XML is currently adopted as an optional treatment for chronic congestive heart failure patients in the clinic (Ma et al., 2013; Liu et al., 2014). In addition, XML injection was reported to mitigate epirubicin (EPI)-induced cardiotoxicity *in vivo* (Li et al., 2016).

Myocardial ischemia is a pathological state of the heart that leads to the decrease of oxygen supply to the heart and abnormalities in myocardial energy metabolism, both of which result in further damage to the heart (Heusch, 2016). This disease results in a reduction of the blood flow to the myocardium. A prolonged duration of ischemia can induce myocardial infarction (MI), which is a common cause of heart failure (HF) (Gheorghiade and Bonow, 1998; Tanai and Frantz, 2015). Thus, early intervention in myocardial ischemia should restore blood flow and improve the clinical outcomes for patients with cardiovascular diseases (CVDs) such as HF and MI.

In the present study, we aim to explore whether XML injection is an effective pharmacological intervention for the early treatment of myocardial ischemia. Since Chinese herbal medicines contain multiple active compounds, and each compound can target different genes and proteins, we hoped to identify the key herbal ingredients and therapeutic targets involved in its disease prevention properties.

MATERIALS AND METHODS

Chemicals

XML injection was provided by Tengchong Pharmaceutical Company Limited by shares Yunnan (Yunnan, China). This drug is manufactured in accordance with applicable Good Manufacturing Practice (GMP) and CFDA standards. HPLC analysis was performed to identify its chemical characteristics. Isoproterenol was obtained from Harvest Pharmaceutical Co., Ltd. (Shanghai, China). Propranolol was purchased from Sigma-Aldrich Co. (St. Louis, MO, United States).

Animals

Adult male Sprague–Dawley (SD) rats, weighing 160–180 g, were purchased from the Animal Center of the Peking University Health Science Center (Beijing, China). Animals were housed in light-controlled and air-conditioned rooms for 7 days for adaptation before experiments. Standard laboratory chow and water were provided ad libitum. Animal experiments were performed in accordance with the "Guidelines for Animal Experiment" and approved by the Animal Care Committee of the Peking University Health Science Center.

SD rats were randomly selected into groups that received normal saline or three different concentrations of XML injection or propranolol (10 mg/kg) every day for a total of 4 days. 30 min after the final administration, two types of *in vivo* myocardial ischemia models were induced. The rats were either subcutaneously injected with isoproterenol (5 mg/kg) or their left anterior descending coronary artery was ligated, while control rats were not (Wu et al., 2011). Heart myocardial ischemia was assessed using the noninvasive cardiac imaging technology of echocardiography (ECG) and by measuring the serum levels of cardiac troponin T (cTnT) biomarker.

TABLE 1 | Primers used for quantitative real-time RT-PCR.

Gene	Primer
PRKCA	F: 5′-CCCAGAAGCAAGCACAAGTT-3′
	R:5′-GACATTGATCACGCACTGCT-3′
PRKCE	F: 5′-ACGGTGGAGACCTCATGTTC-3′
	R: 5′-TTGCAGTGACCTTCTGCATC-3′
MAPK3	F: 5′-GGCCCGAAACTACCTACAGT-3′
	R: 5′-TCCAGCTCCATGTCAAAGGT-3′
PLA2GA4A	F: 5′-TTAACCTGCCGTATCCCTTG-3′
	R: 5′-CTTCAATCCTTCCCGATCAA-3′
CYBA	F: 5′-CATGTGGGCCAACGAACAG-3′
	R: 5′-CACTGTGTGAAACGTCCAGCAGTA-3′
CYBB	F: 5′-TGATCCTGCTGCCAGTGTGTC-3′
	R: 5′-GTGAGGTTCCTGTCCAGTTGTCTTC-3′
GAPDH	F: 5′-ACAAAGTGGACATTGTTGCC-3′
	R: 5′-AAACATGGTGGTGAAGACGC-3′

Electrocardiographic Recordings

Surface electrocardiographic (ECG) recordings were obtained from rats that were anesthetized with sodium pentobarbital. For the ECG analysis, the onsets and offsets of the P, Q, R, S, and T waves were determined by measuring the earliest (onset) and the latest (offset) times from lead II.

Network Pharmacology-Based Analysis

Published literature and the BATMAN-TCM databases were used to identify XML ingredients. Active ingredients were identified using SwissADME, while candidate targets for each ingredient were predicted using the SwissTargetPrediction database. Disease-associated target prediction was performed using DisGeNET, Therapeutic Target Database (TTD), and OMIM databases. The relevant protein–protein interaction networks were extracted from the Human Protein Reference and STRING databases. The Kyoto Encyclopedia of Genes and Genomes (KEGG) pathway database and Gene Ontology (GO) map were used to analyze the disease-related targets and pathways. Finally, an ingredient-target-pathway network was constructed using Cytoscape software (version 3.8.2) to provide a systematic overview of potential target genes and mechanisms for XML action.

Reverse Transcription and Real-Time PCR

Heart tissue was homogenized and lysed with Trizol reagent (Invitrogen, United States) according to the manufacturer's

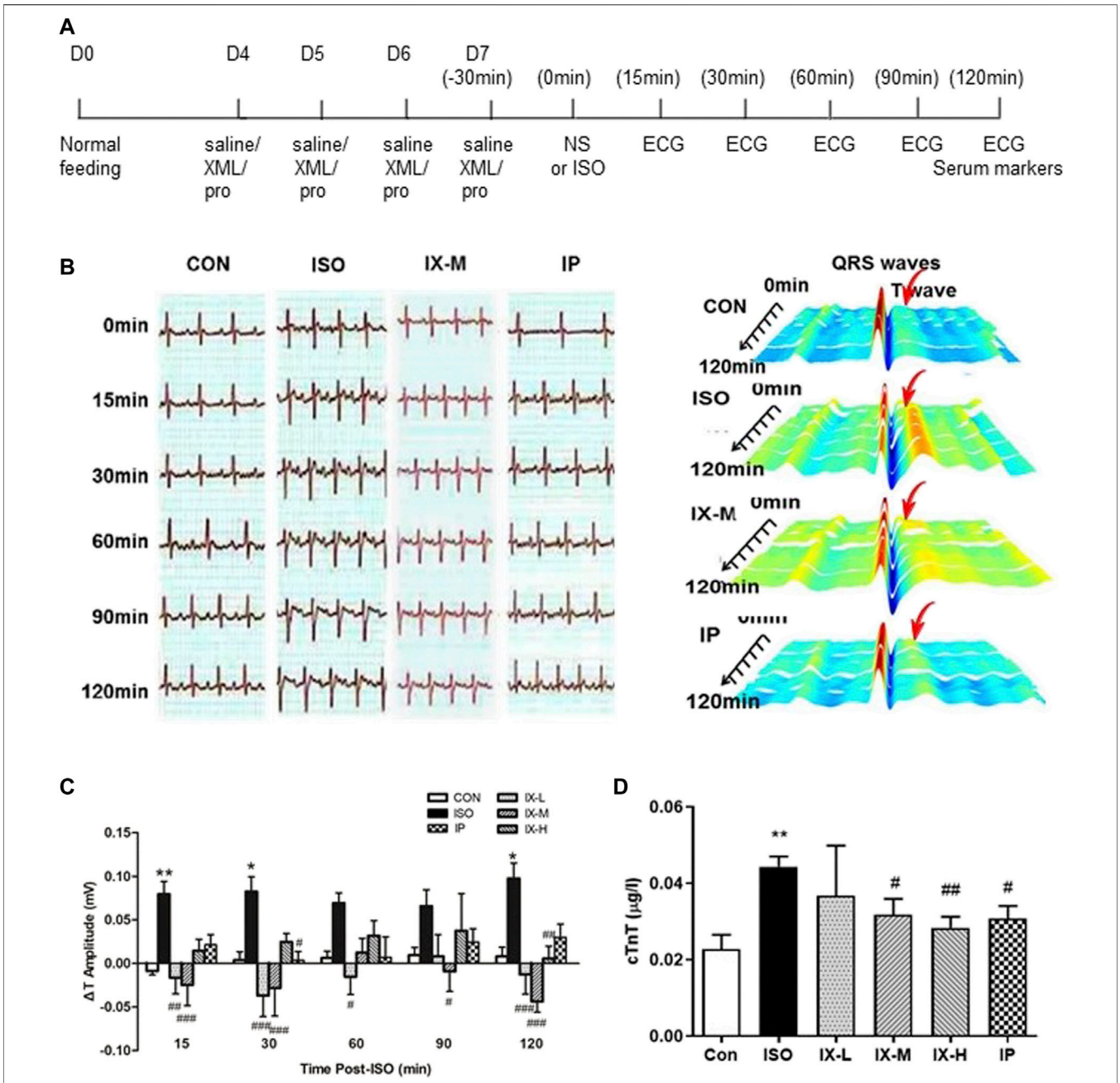

FIGURE 1 | Protective effect of XML on isoproterenol-induced myocardial ischemia in a rat model. **(A)** Timeline of drug administration. CON rats ($n = 5$) were treated with normal saline, while test groups received an XML injection (low dose—L ($n = 5$), medium dose—M ($n = 6$), high dose—H ($n = 5$)), or propranolol (10 mg/kg) ($n = 5$) for a total of 4 days 30 min after the final administration, rats were subcutaneously injected with isoproterenol (5 mg/kg) to induce the myocardial ischemia model. Heart contractile function was assessed using the noninvasive cardiac imaging technology of echocardiography (ECG) and by measuring the levels of the cardiac troponin T (cTnT) biomarker. **(B)** Electrocardiogram recordings of SD rats. **(C)** T interval of rats in each group. **(D)** cTnT levels for each group. Asterisk (*) refers to statistical significance in comparisons with the CON group ($^{*}p < 0.05$, $^{**}p < 0.01$), while # refers to comparisons with the ISO group ($^{\#}p < 0.05$, $^{\#\#}p < 0.01$, $^{\#\#\#}p < 0.005$).

instructions. Extracted RNA samples were transcribed into cDNA using the RevertAid RT Reverse Transcription Kit (Thermo, United States). Amplifications were performed with the ROCHE LightCycler 480 Real-Time PCR with the primers listed in **Table 1**, with the conditions of initial denaturation at 95°C for 2 min followed by 40 cycles of 95°C for 15 s and 60°C for 1 min. Gene transcript abundance levels were normalized to those for GAPDH.

Measurement of Serum Cardiac Troponin T (cTnT) Levels

Blood was collected from the orbital venous of rats 2 hours after isoproterenol administration or coronary artery ligation. Serum was collected by centrifugation, and the cTnT content was quantified using a double-antibody sandwich ELISA.

Western Blot Analysis

Heart tissue was homogenized and tissue protein was quantified using the Bradford method. Sixty micrograms of protein was loaded onto an SDS-PAGE gel, separated, and transferred onto a PVDF membrane (Millipore, United States). Antibodies for Bcl-2 (CST, United States), Bax (CST, United States), and GPADH (CST, United States) were diluted 1:1000 and incubated with the membrane overnight at 4°C. The next day, the membrane was washed and incubated with secondary antibodies and then visualized using a luminescence ChemiDoc XRS (Bio-Rad, United States).

Statistical Analysis

Results are shown as mean ± standard error. Differences between the control and experimental groups were evaluated by one-way ANOVA. $p < 0.05$ were considered to be statistically significant.

RESULTS

XML Pretreatment Improves Response to Myocardial Ischemia

To explore whether XML injection could be an effective pharmacological intervention for myocardial ischemia, two different types of animal models were established. The first is the isoproterenol-induced myocardial ischemia rat model (Viswanadha et al., 2021), and the second is the acute myocardial infarction rat model induced by the ligation of the left anterior descending coronary artery (Li et al., 2021).

Isoproterenol-induced myocardial ischemia is a classical model used to screen for the cardioprotective effects of pharmacological interventions (Allawadhi et al., 2018). In our study, six groups of SD rats were generated: CON (saline pretreatment for 4 days followed by normal saline injection, n = 5), ISO (saline pretreatment for 4 days followed by isoproterenol injection, n = 5), IX-L (31.25 mg/kg XML pretreatment for 4 days followed by isoproterenol injection, n = 5), IX-M (62.5 mg/kg XML pretreatment for 4 days followed by isoproterenol injection, n = 6), IX-H (125 mg/kg XML pretreatment for 4 days followed by isoproterenol injection, n = 5), and IP (propranolol pretreatment for 4 days followed by isoproterenol injection, n = 5) (**Figure 1A**). Electrocardiograph (ECG) is the most common test used in the clinic to assess suspected or known cases of myocardial ischemia (Fabiszak et al., 2021). Changes in the ST segment and T-wave should be observed if myocardial ischemia has occurred (Thygesen et al., 2018). Our study showed significant alterations in the ECG patterns in ISO-induced rats compared to normal CON rats (**Figure 1B**). ECG recordings showed significantly longer T intervals in the ISO rats (**Figure 1C**). Low and medium doses of XML injection to ISO rats significantly reduced the changes in T intervals, while the medium and high doses of XML reduced the prolonged time for heart rate (**Figure 1C**, **Supplementary Figure S1**). Serum cTnT levels have been considered to be a specific marker for myocardial damage, with increases in levels supporting the involvement of myocardial dysfunction (Cullen et al., 2017). cTnT levels were significantly increased in the treatment groups compared with the CON group, with pretreatment with medium and high doses of XML injection reducing the increases in cTnT levels (**Figure 1D**). These findings suggest that XML pretreatment attenuated cardiac injury induced by isoproterenol exposure, especially for the medium dose.

For the second myocardial ischemia model, the left coronary artery was ligated, which should lead to a variable degree of left ventricular myocardial ischemia (Okninska et al., 2021). As above, in this study, our SD rats were also assigned into six groups: Sham (saline pretreatment for 4 days following sham, n = 5), MI (saline pretreatment for 4 days followed by coronary artery ligation, n = 4), MX-L (15.625 mg/kg XML pretreatment for 4 days followed by coronary artery ligation, n = 5), MX-M (31.25 mg/kg XML pretreatment for 4 days followed by coronary artery ligation, n = 6), MX-H (62.5 mg/kg XML pretreatment for 4 days followed by coronary artery ligation, n = 5), and MP (propranolol pretreatment for 4 days followed by coronary artery ligation, n = 6) (**Figure 2A**). After ligation of the coronary artery, heart function was assessed by ECG and measurement of serum cTnT levels. Ml rats showed significantly longer T intervals and higher cTnT levels (**Figures 2B–D**), which is consistent with previous findings that coronary occlusion causes an immediate cessation of aerobic metabolism in the ischemic myocardium and durations of coronary occlusion exceeding 60–90 min is considered to be irreversible (Ilic et al., 2021). XML pretreatment significantly altered the upregulation of ΔT amplitude and cTnT level, especially for the MX-M group. For this model, a decreased heart rate was observed in each group with the prolonged time; however, XML injection had no effect on it (suppl. **Figure 2**). The above data indicate that XML administration for 4 days has protective activity against myocardial ischemia induced by coronary artery ligation.

Network Pharmacology Analysis of XML

To elucidate the molecular mechanisms of the beneficial effects of XML injection on myocardial ischemia, we first used the network pharmacology method. Published literature and the BATMAN-TCM database were used to identify XML ingredients, and the active components were screened using the SwissADME database. A total of 17 ingredients with high levels of GI absorption and drug-likeness were identified in XML injection (**Table 2**). From these ingredients, a total of 198 targets, with duplicates removed, were predicted by the Swiss Target Prediction database (**Figure 3A**). Potential targets for myocardial ischemia were screened using the GeneCards, OMIM, and DisGeNET databases. In total, 1658 gene targets were identified after duplicates were removed (**Figure 3A**). A Venn diagram was created to visualize the overlap in genes related to active XML ingredients and

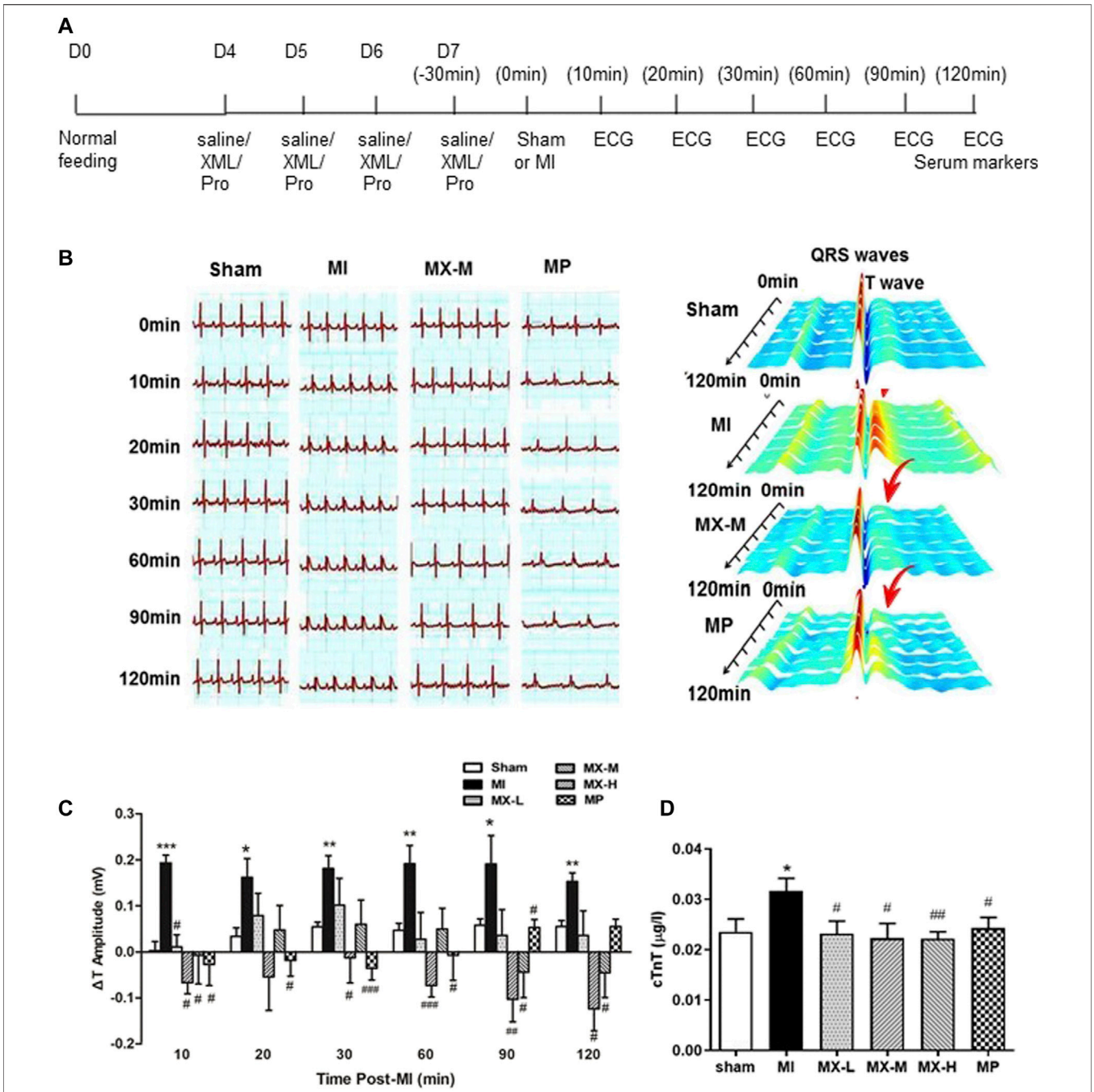

FIGURE 2 | Protective effect of XML on myocardial ischemia induced by ligation of the left anterior descending coronary artery in the rat. **(A)** Timeline of drug administration. Rats received a pretreatment with normal saline (n = 4) or XML injection (low dose—L (n = 5), medium dose—M (n = 6), high dose—H (n = 5)), or propranolol (10 mg/kg) (n = 6) for a total of 4 days. The left anterior descending coronary artery of rats was ligated 30 min after the final administration to induce the myocardial ischemia model. Heart contractile function was assessed by the noninvasive cardiac imaging technology of echocardiography (ECG) and measurement of serum cardiac troponin T (cTnT) biomarker levels. **(B)** Electrocardiogram recordings of SD rats. **(C)** T interval of the rats in each group. **(D)** cTnT levels for each group. Asterisk (*) refers to statistical significance in comparisons with the CON group (*p < 0.05, **p < 0.01, ***p < 0.005), while # refers to comparisons with the MI group ($^{\#}p$ < 0.05, $^{\#\#}p$ < 0.01, $^{\#\#\#}p$ < 0.005).

TABLE 2 | Basic information on the active compounds in XML injection.

No	Chemical composition	Molecular formula	PK GI absorption	Drug likeness Number
XML1	4-(2-amino-1-hydroxyethyl)-2-benzenediol	C8H11NO3	High	4
XML2	3-hydroxy-4-(N,N,N-trimethyl)-butyric acid	C7H15O3N	High	3
XML3	2,3-butanediol	C4H10O2	High	3
XML4	Pentanoic acid	C5H10O2	High	3
XML5	2-[(2-aminoethyl) amino]-ethanol	C4H12N2O	High	3
XML6	2-piperidine ketone	C5H9NO	High	3
XML7	Dihydro-5-(1-hydroxyethyl)-2(3H)-furanone	C6H10O3	High	3
XML8	catechol	C6H6O2	High	3
XML9	5-oxo-2-pyrrolidinecarboxylic ethyl ester	C7H10NO3	High	3
XML10	1-isopropylcyclobutyl methylamine	C8H16N	High	3
XML11	2-methyl-3-vinyl cyclopentene carboxylic acid	C7H8O2	High	3
XML12	3-pyrrolidin-2-yl-propionic acid	C7H13NO2	High	3
XML13	2,5,5-trimethyl-1,3-cyclohexanedione	C9H14O2	High	3
XML14	Hexadecanoic acid	C16H32O2	High	3
XML15	Hexadecanoic acid, methyl ester	C17H34O2	High	2
XML16	Tridecanoic acid, 12-methyl-, methyl ester	C15H30O2	High	3
XML17	11-Hexadecanoic acid, methyl ester	C17H32O2	High	3

myocardial ischemia (**Figure 3A**), which identified 90 intersecting genes.

The 90 intersected genes were analyzed using STRING software, with a coefficient of 0.4 indicating correlation (**Figure 3B**). A PPI network should facilitate our understanding of the regulatory roles of targets. The importance of the functional module in the PPI network is described by the MCODE score (**Supplementary Figure S3**), and we named the two largest as MCODE1 (containing 64 nodes) and MCODE2 (containing 43 nodes) (**Figure 3C**). The biological processes of these top 2 MCODEs include "adenylate cyclase–modulating G protein–coupled receptor signaling pathway," "regulation of catecholamine secretion," "blood circulation," and "fatty acid transport," all of which were strongly associated with the pathological mechanisms of myocardial ischemia (**Table 3**).

To further examine the functions of the 90 overlapping target genes, GO and KEGG enrichment analyses were carried out. As shown in **Figure 3D**, pathways related to fatty acid absorption/metabolism, inflammation, RAAS, and vascular smooth muscle were identified, including the terms "PPAR signaling," "arachidonic acid metabolism," "renin-angiotensin system," "regulation of lipolysis in adipocytes," "aldosterone-regulated sodium reabsorption," and "VEGF signaling pathway". The GO map contains the top molecular functions of "oxidoreductase activity" and "protein kinase C activity," and the top biological processes of "circulatory system process," "lipid localization and transport," and "inflammation response" (suppl. **Figure 4**).

Network pharmacology can analyze the relationship between drugs, targets, metabolic pathways, and diseases by constructing a network model (Hopkins, 2008). Based on the target and pathway analyses, an entire ingredient-target-pathway network was constructed (**Figure 4**). In this network, we identified the top five chemical ingredients in XML injection, which were "11-hexadecenoic acid, methyl ester," "hexadecanoic acid," "tridecanoic acid, 12-methyl-, methyl ester," "hexadecanoic acid, methyl ester," and "pentanoic acid" (**Table 4**). In addition, we screened for the top ten genes based on their degree values as potential core targets (**Table 5**) and speculate that these genes might contribute to the molecular mechanisms by which XML injection attenuates myocardial damage.

Putative Involvement of Protein Kinase C (PKC) and PLA2 (Phospholipase A2 Group IVA) in the Prevention of Myocardial Ischemia by XML Injection

Clinically, myocardial ischemia is caused by the blockage of the coronary artery and is defined as an interrupted supply of blood to the left ventricle (Kompa and Summers, 2000). The surgical ligation of the left coronary artery animal model is more similar to human myocardial ischemia (Seong et al., 2021); thus, we evaluated gene changes in this rat model.

Based on the results of network pharmacology analysis (**Figure 4**; **Table 5**), first, the top four genes (PRKCA/MAPK3/PRKCG/PLA2G4A) and PRKCE (an isoform of the large PKC family) were picked up for validation in the animal model of surgery-induced myocardial ischemia.

In our study, the expression level of heart PRKCA was enhanced, while PRKCE was reduced upon myocardial ischemia, and their levels returned to normal following the pretreatment of XML injection (**Figure 5A**). Approximately, 11 isozymes have been identified in the Protein kinase C (PKC) family (Perveen et al., 2021). PKCα is encoded by the PRKCA gene and is the predominant PKC isoform expressed in the heart (Aslam, 2020). Activated or increased PKCα expression is associated with hypertrophy, dilated cardiomyopathy, ischemic injury, and mitogen stimulation (Steinberg, 2012). Another novel PKC isozyme, PKCε, is encoded by the PRKCE gene and is involved in ischemia tolerance following ischemic preconditioning and ischemia injury (Chen et al., 2021). NADPH oxidase is a main downstream protein complex of Protein kinase C activation,

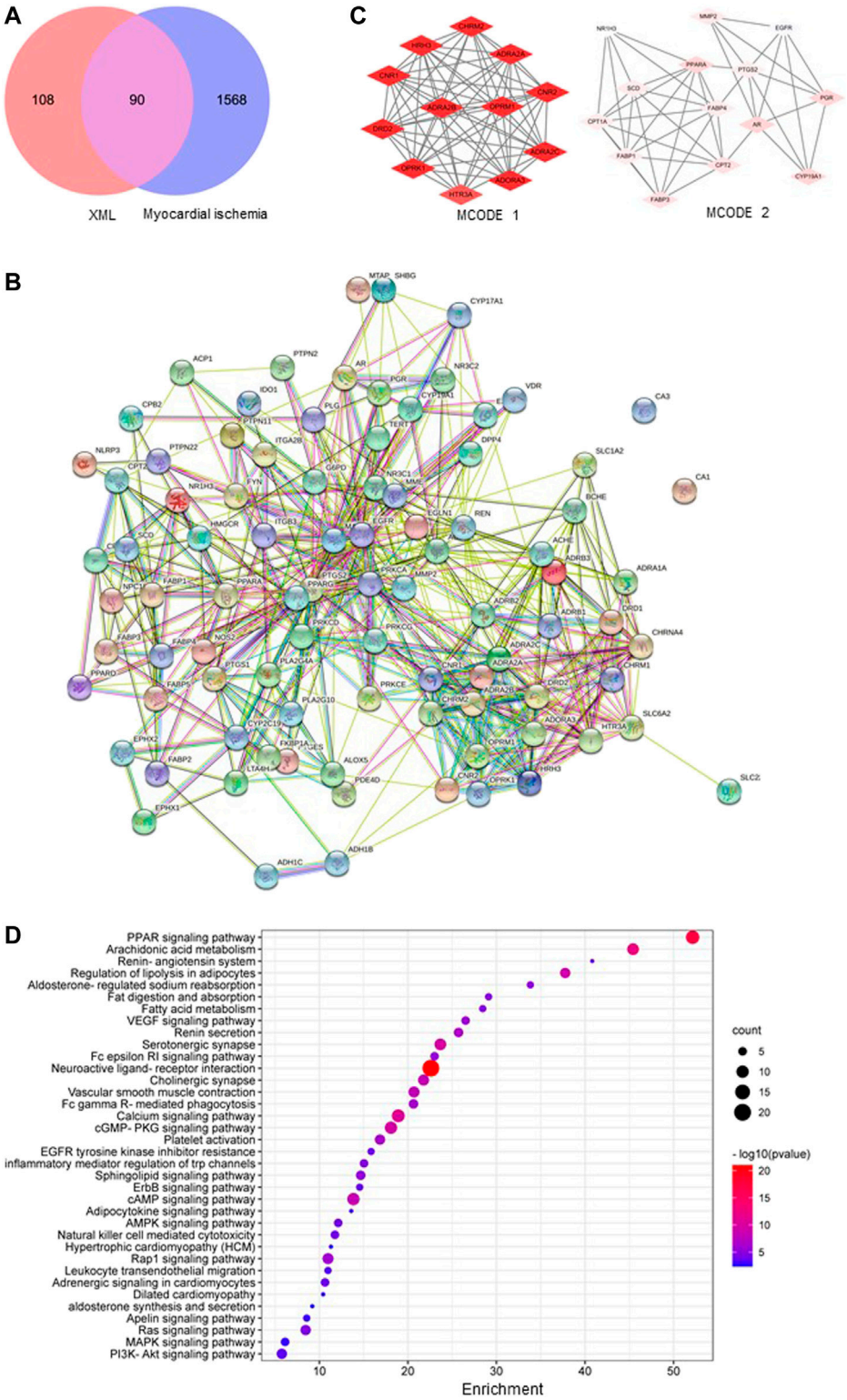

FIGURE 3 | Overlap of genes associated with XML treatment and myocardial ischemia and their functions. **(A)** An intersection generated between genes related to XML-active targets and myocardial ischemia. **(B)** Protein–protein interaction network of the overlapped genes for XML and myocardial ischemia. **(C)** The top 2 MCODEs from the PPI network. **(D)** Most enriched KEGG pathways for XML and myocardial ischemia overlapped genes.

TABLE 3 | Main biological processes of the top 2 MCODE gene functions.

GO	Description	Log10(p)
GO: 0007188	Adenylate cyclase–modulating G protein-coupled receptor signaling pathway	−14.2
GO:1903531	Negative regulation of secretion by cell	−14.2
GO:0050433	Regulation of catecholamine secretion	−13.3
GO:0008015	Blood circulation	−12.4
GO:0015908	Fatty acid transport	−11.9

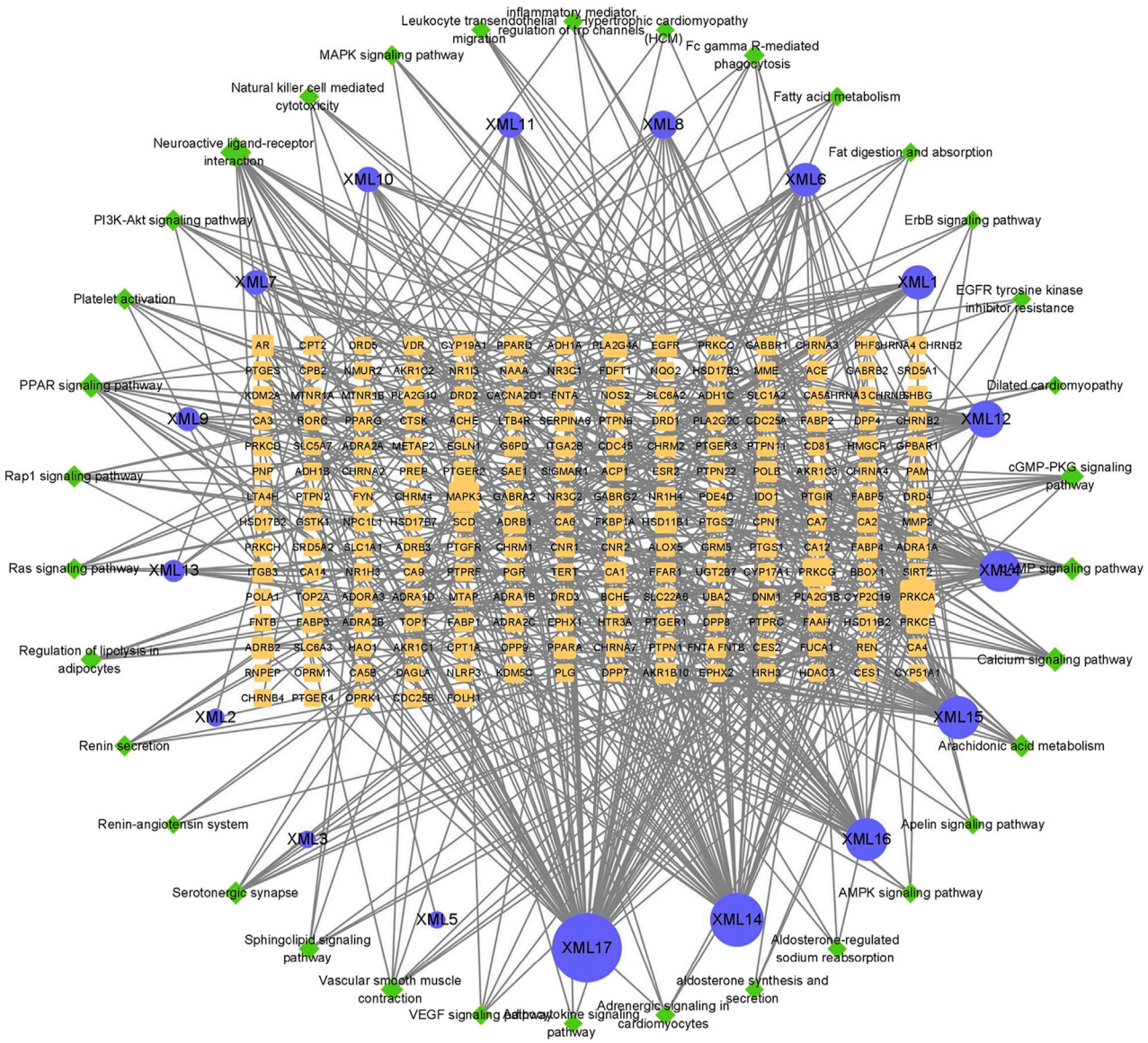

FIGURE 4 | XML ingredient-target-pathway network. Blue circles represent active components, yellow rectangles represent target genes, and green diamonds represent pathways. The size of a node represents its degree. The larger the area, the more important the node.

and the two mitochondrial function-related indicators of CYBA and CYBB encode the membrane-spanning subunits of this complex (Deng et al., 2012). In the present study, XML pretreatment was shown to mitigate the upregulation of myocardial ischemia induced by CYBA/CYBB levels (**Figure 5D**).

TABLE 4 | Putative main compounds in XML injection associated with prevention of myocardial ischemia.

Molid	Chemical name	Degree	Betweenness Centrality	Closeness Centrality
XML17	11-Hexadecanoic acid, methyl ester	74	0.43112	0.44345
XML14	Hexadecanoic acid	51	0.16506	0.35953
XML16	Tridecanoic acid, 12-methyl-, methyl ester	36	0.04302	0.33514
XML15	Hexadecanoic acid, methyl ester	36	0.04302	0.33514
XML4	Pentanoic acid	35	0.06230	0.32203

TABLE 5 | Putative targets of XML injection in the prevention of myocardial ischemia.

Target	Degree	Betweenness Centrality	Closeness Centrality
PRKCA	25	0.08158	0.35235
MAPK3	19	0.04513	0.34163
PRKCG	17	0.01314	0.29025
PLA2G4A	10	0.01579	0.29581
ADRB1	9	0.01387	0.29440
EGFR	8	0.02173	0.27784
PRKCE	8	0.00354	0.26361
HSD11B1	8	0.06382	0.38775
PPARA	8	0.02203	0.35336
ADRB2	8	0.00997	0.29231

PLA2 (encoded by the Pla2g4a gene) can hydrolyze phospholipids into arachidonic acid and mediate inflammation (Marsche, 2015). Similarly, XML pretreatment was revealed to significantly lower the ischemia-induced upregulation of PLA2G4A abundance (**Figure 5C**).

Generally, during ischemia, in addition to the excessive production of ROS and inflammation, programmed cardiomyocyte death (through apoptosis) is also activated (Hotchkiss et al., 2009; Malek and Nematbakhsh, 2015). To clarify how XML injection regulates myocardial cell apoptosis, protein levels for B-cell lymphoma 2 (Bcl2) and Bcl-2–associated X protein (Bax) were measured. Our study revealed that the abundance of Bax and Bcl2 were significantly changed in the MI model and restored in XML pretreated cardiomyopathy (**Figure 5E**). These results indicate a role for XML in the independent anti-apoptosis mechanism.

Taken together, our study indicates that XML pretreatment augments the abundance of PKCε and suppresses the levels of PKCα, both of which then decrease NADPH oxidase and inhibit apoptosis activity. Meanwhile, reduction of PLA2 levels induced by XML injection results in decreased inflammation (**Figure 5F**). Thus, the actions of XML injection likely are responsible, at least in part, for the antioxidative, anti-inflammatory, and anti-apoptotic activities via the PKC and PLA pathways. These results closely coincide with our findings from the GO and KEGG analyses and indicate the potential functions of XML injection as an alternative supplementary therapeutic agent for the prevention of myocardial ischemia.

DISCUSSION AND CONCLUSION

Myocardial ischemia is defined as reduced blood flow to the heart that inhibits heart muscle from receiving enough oxygen (Heusch, 2019). It is a leading cause of morbidity and mortality for CVDs, though certain risk factors such as arteriosclerosis and treatments via surgical intervention can be controlled. According to the 2018 universal definition of myocardial ischemia, it is a disease with clinical events that includes myocardial cell death (seen as ischemic symptoms, ischemic electrocardiographic changes, and coronary artery intervention), and myocardial injury (which results in elevations of cardiac troponin levels) (Thygesen et al., 2018).

Early intervention to the blocked vessel is critical for restoring blood flow to the heart muscle and improving clinical outcomes. Suitable preventative medicines for the treatment of myocardial ischemia are still at an early stage of development. XML injection is an optional treatment for chronic congestive heart failure patients in the clinic. Our results, in the present study, show that XML pretreatment for 4 days can protect rats from myocardial ischemia-induced myocardial injury (**Figure 1C**, **Figure 1E**, **Figure 2C**, **Figure 2D**, **Supplementary Figure S1A**), indicating its potential for prevention of injury.

The causes of myocardial ischemia are various and include atherosclerosis, blood clots, and coronary artery spasms (Heusch, 2019). Atherosclerosis may result in myocardial ischemia *via* two different identities, acute coronary syndrome (ACS, type 1 MI) and prolonged myocardial oxygen supply–demand imbalance (type 2 MI) (Smit et al., 2020). ACS occurs because of an unstable plaque rupture or endothelial ulceration and is influenced by factors such as inflammation (Casscells et al., 2003) and hyperlipidemia (Lai et al., 2021). Our study showed that among the top ten KEGG pathways associated with XML injection treatment, five were associated with inflammation and hyperlipidemia, including "PPAR signaling pathway," "arachidonic acid metabolism," "regulation of lipolysis in adipocytes," and "fat digestion and absorption" (**Figure 3D**). It is also reported that atherosclerotic arteries lead to a dysfunctional endothelium in combination with increased α adrenergic receptors (Naghavi et al., 2003), which is consistent with our findings that the pathways "VEGF signaling pathway" and "vascular smooth muscle contraction" were identified in the KEGG analysis **Figure 3D**). In addition to ACS and type 2 MI, a further cause for myocardial ischemia is coronary artery spasm. The most important causative factor for this pathophysiology is an increased intracellular calcium concentration in combination with elevated calcium sensitivity (Yasue et al., 2008), which is consistent with our identification of changes in the "calcium signaling pathway" with XML injection treatment (**Figure 3D**).

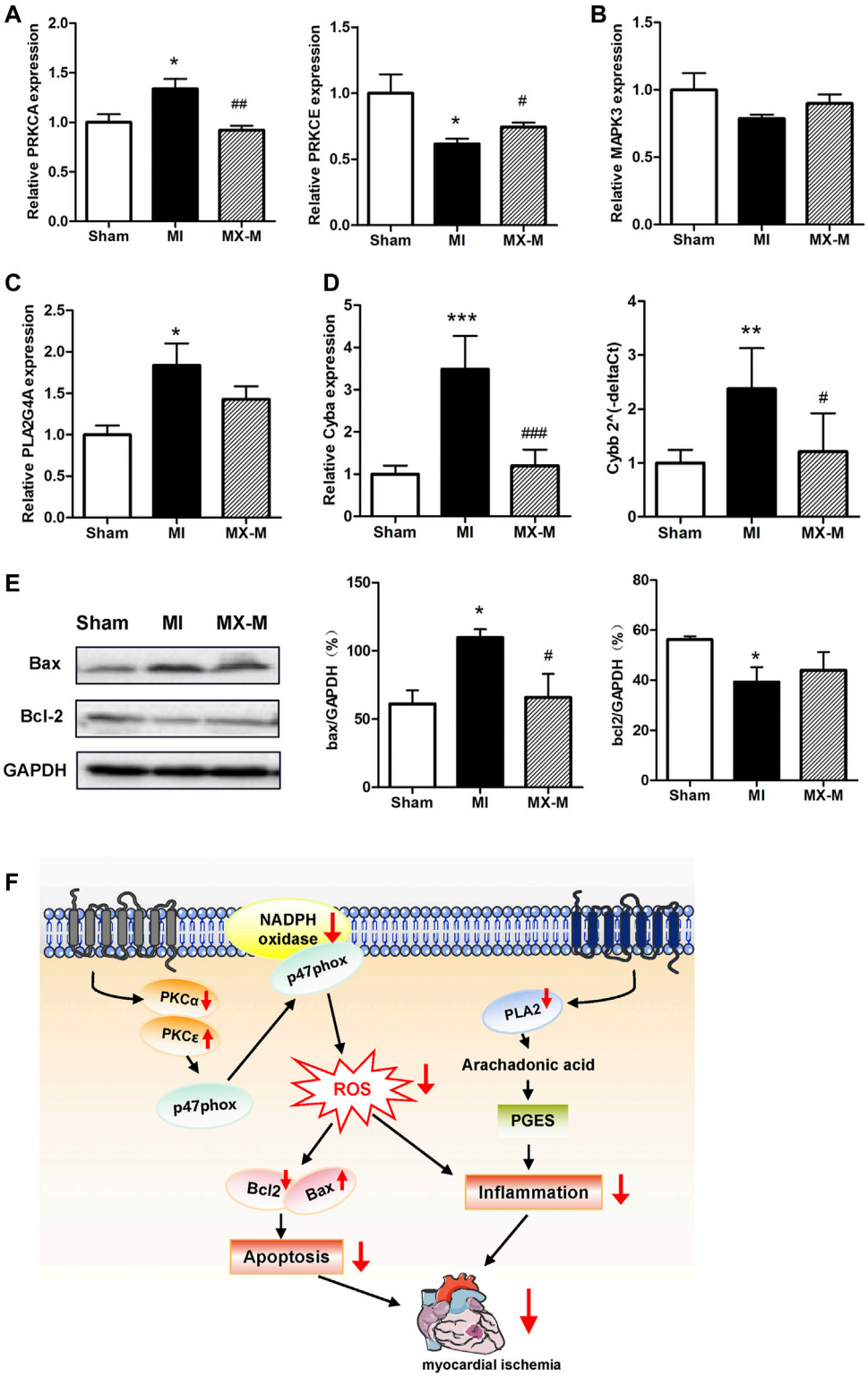

FIGURE 5 | Mechanisms of the protective effects of XML injection on myocardial ischemia. **(A)** Relative PRKCA and PRKCE transcript levels in the Sham ($n = 5$), MI ($n = 4$), and MX-M ($n = 6$) groups. **(B,C)** Relative MAPK3 **(B)** and PLA2G4A **(C)** transcript levels in the Sham ($n = 5$), MI ($n = 4$), and MX-M ($n = 6$) groups. **(D)** CYBA and CYBB gene transcript abundance in the Sham ($n = 5$), MI ($n = 4$), and MX-M ($n = 6$) groups. **(E)** Abundance of Bax and Bcl-2 proteins in the Sham, MI, and MX-M groups ($n = 3$). **(F)** Schematic model for the molecular mechanisms associated with the protective effect of XML injection against myocardial ischemia. Asterisk (*) refers to statistical significance in comparisons with the CON group ($^{*}p < 0.05$, $^{**}p < 0.01$, $^{***}p < 0.005$), while # refers to comparisons with the EPI group ($^{\#}p < 0.05$, $^{\#\#}p < 0.01$, $^{\#\#\#}p < 0.005$).

The human body is a complex regulatory network; therefore, the therapeutic effects of compounds likely affect more than just their direct targets. Traditional Chinese medicine is a comprehensive medical health-care system and has been applied for centuries to prevent or heal diseases by restoring balance. Herbal medicines contain multiple active compounds, with each compound potentially targeting multiple genes or proteins (Hopkins, 2008; Schenone et al., 2013). XML injection has been reported to contain compounds that include polyhydric alcohols, organic acids, alkaloids, and other micro-constituents; however, the active ingredients have not yet been reported. Our study identified five main components associated with myocardial ischemia prevention (**Table 4**). XML injection, like other traditional Chinese medicine, contains many components and has multi-target effects. Among the five main components, hexadecanoic acid methyl esters are vasoactive and can dilate blood vessels (Lin et al., 2014). In addition, these components can protect against myocardial ischemia by regulating the metabolism of fatty acids and activating numerous signaling pathways (Cheng et al., 2021). In addition, the ingredient-target-pathway network shown in **Figure 4** revealed multiple targets and pathways for XML injection and its attenuation of myocardial ischemia disease and indicated multiple pharmacological activities. This suggests that therapeutic medications that interact with multiple targets might be more effective for complex or chronic diseases such as myocardial ischemia.

Based on the integrated-network-pathway and molecular experiment analysis, we identified PKC and PLA2 as potential targets of XML injection for the improved response to myocardial ischemia (**Figure 4**, **Figure 5A**, **Figure 5C**, **Table 4**). Protein kinase C (PKC) is a group of multifunctional proteins that phosphorylate target proteins that have biological functions involved in redox signaling, oxidative stress, cell apoptosis, and mitochondrial dysfunction (Bright and Mochly-Rosen, 2005). PLA2 (encoded by the Pla2g4a gene) promotes chronic inflammation by inducing the production of free fatty acids and lysophosphatides (Wang et al., 2021). Both pathways are associated with myocardial ischemia (Marsche, 2015). It is suggested that the overproduction of reactive oxygen species, intracellular calcium overload, and inflammatory cell infiltration are the most important features of myocardial ischemia injury, all of which could be alleviated by XML injection pretreatment. Of course, in addition to the mechanisms of antioxidant, anti-apoptotic, and immune modulation, more accurate mechanisms of XML injection could be identified by high-throughput methods of RNA sequencing, metabolome, and proteome. We will extend this work in near future.

In conclusion, this study revealed the preventative effects of XML injection, a CFDA-approved injection adopted as an optional treatment for chronic congestive heart failure patients in the clinic, for ischemic heart diseases. Pretreatment with XML significantly alleviates the cardiac-linked pathologies, attenuates the release of cTnT, and prevents cardiovascular effects mediated by antioxidant, anti-apoptotic, and immune modulation. Further network pharmacology method analysis identified the five main chemical ingredients, and their potential targets, for XML injection for myocardial ischemia. Our results indicate that XML injection could be used as an alternative supplementary therapeutic agent for the treatment and prevention of myocardial ischemia.

DATA AVAILABILITY STATEMENT

The original contributions presented in the study are included in the article/**Supplementary Material**, and further inquiries can be directed to the corresponding authors.

ETHICS STATEMENT

The animal study was reviewed and approved by the Peking University Health Science Center.

AUTHOR CONTRIBUTIONS

LJ, LX, HL, and HT designed the experiment, analyzed the data, and wrote and modified the manuscript. YM, QH, and RM assisted with the animal experiments. YG and QY assisted with carrying out the network pharmacology analysis.

FUNDING

This study was supported by grants from the National Natural Science Foundation of China (NSFC, Grant Nos. 81874321, 81700374, 81673459, and 81102484) and interdisciplinary Medicine Seed Fund of Peking University (BMU2020MX021).

ACKNOWLEDGMENTS

XML Injection was provided by Tengchong Pharmaceutical Company Limited by shares Yunnan (Yunnan, China).

SUPPLEMENTARY MATERIAL

The Supplementary Material for this article can be found online at: https://www.frontiersin.org/articles/10.3389/fcell.2022.827691/full#supplementary-material

REFERENCES

Allawadhi, P., Khurana, A., Sayed, N., Kumari, P., and Godugu, C. (2018). Isoproterenol-induced Cardiac Ischemia and Fibrosis: Plant-Based Approaches for Intervention. *Phytotherapy Res.* 32, 1908–1932. doi:10.1002/ptr.6152

Aslam, N. (2020). Increase in PKCα Activity during Heart Failure Despite the Stimulation of PKCα Braking Mechanism. *Int. J. Mol. Sci.* 21, 2561. doi:10.3390/ijms21072561

Bright, R., and Mochly-Rosen, D. (2005). The Role of Protein Kinase C in Cerebral Ischemic and Reperfusion Injury. *Stroke* 36, 2781–2790. doi:10.1161/01.str.0000189996.71237.f7

Casscells, W., Naghavi, M., and Willerson, J. T. (2003). Vulnerable Atherosclerotic Plaque. *Circulation* 107, 2072–2075. doi:10.1161/01.cir.0000069329.70061.68

Chen, L., Shi, D., and Guo, M. (2021). The Roles of PKC-δ and PKC-ε in Myocardial Ischemia/reperfusion Injury. *Pharmacol. Res.* 170, 105716. doi:10.1016/j.phrs.2021.105716

Cheng, T.-Y., Li, J.-X., Chen, J.-Y., Chen, P.-Y., Ma, L.-R., Zhang, G.-L., et al. (2021). Gut Microbiota: a Potential Target for Traditional Chinese Medicine Intervention in Coronary Heart Disease. *Chin. Med.* 16, 108. doi:10.1186/s13020-021-00516-0

Cullen, L. A., Mills, N. L., Mahler, S., and Body, R. (2017). Early Rule-Out and Rule-In Strategies for Myocardial Infarction. *Clin. Chem.* 63, 129–139. doi:10.1373/clinchem.2016.254730

Deng, B., Xie, S., Wang, J., Xia, Z., and Nie, R. (2012). Inhibition of Protein Kinase C β2 Prevents Tumor Necrosis Factor-α-Induced Apoptosis and Oxidative Stress in Endothelial Cells: The Role of NADPH Oxidase Subunits. *J. Vasc. Res.* 49, 144–159. doi:10.1159/000332337

Fabiszak, T., Kasprzak, M., Koziński, M., and Kubica, J. (2021). Assessment of Selected Baseline and Post-PCI Electrocardiographic Parameters as Predictors of Left Ventricular Systolic Dysfunction after a First ST-Segment Elevation Myocardial Infarction. *J. Clin. Med.* 10, 5445. doi:10.3390/jcm10225445

Gheorghiade, M., and Bonow, R. O. (1998). Chronic Heart Failure in the United States. *Circulation* 97, 282–289. doi:10.1161/01.cir.97.3.282

Heusch, G. (2016). Myocardial Ischemia. *Circ. Res.* 119, 194–196. doi:10.1161/circresaha.116.308925

Heusch, G. (2019). Myocardial Ischemia: Lack of Coronary Blood Flow, Myocardial Oxygen Supply-Demand Imbalance, or what? *Am. J. Physiology-Heart Circulatory Physiol.* 316, H1439–H1446. doi:10.1152/ajpheart.00139.2019

Hopkins, A. L. (2008). Network Pharmacology: the Next Paradigm in Drug Discovery. *Nat. Chem. Biol.* 4, 682–690. doi:10.1038/nchembio.118

Hotchkiss, R. S., Strasser, A., Mcdunn, J. E., and Swanson, P. E. (2009). Cell Death. *N. Engl. J. Med.* 361, 1570–1583. doi:10.1056/nejmra0901217

Ilic, A., Todorovic, D., Mutavdzin, S., Boricic, N., Bozic Nedeljkovic, B., Stankovic, S., et al. (2021). Translocator Protein Modulation by 4'-Chlorodiazepam and NO Synthase Inhibition Affect Cardiac Oxidative Stress, Cardiometabolic and Inflammatory Markers in Isoprenaline-Induced Rat Myocardial Infarction. *Int. J. Mol. Sci.* 22, 2867. doi:10.3390/ijms22062867

Kompa, A. R., and Summers, R. J. (2000). Lidocaine and Surgical Modification Reduces Mortality in a Rat Model of Cardiac Failure Induced by Coronary Artery Ligation. *J. Pharmacol. Toxicol. Methods* 43, 199–203. doi:10.1016/s1056-8719(00)00103-9

Lai, J., Han, Y., Huang, C., Li, B., Ni, J., Dong, M., et al. (2021). Non-invasive Skin Cholesterol Testing: a Potential Proxy for LDL-C and apoB Serum Measurements. *Lipids Health Dis.* 20, 137. doi:10.1186/s12944-021-01571-0

Li, H., Mao, Y., Zhang, Q., Han, Q., Man, Z., Zhang, J., et al. (2016). Xinmailong Mitigated Epirubicin-Induced Cardiotoxicity via Inhibiting Autophagy. *J. Ethnopharmacology* 192, 459–470. doi:10.1016/j.jep.2016.08.031

Li, Q., Xu, M., Li, Z., Li, T., Wang, Y., Chen, Q., et al. (2021). Maslinic Acid Attenuates Ischemia/Reperfusion Injury-Induced Myocardial Inflammation and Apoptosis by Regulating HMGB1-TLR4 Axis. *Front. Cardiovasc. Med.* 8, 768947. doi:10.3389/fcvm.2021.768947

Lin, H. W., Saul, I., Gresia, V. L., Neumann, J. T., Dave, K. R., and Perez-Pinzon, M. A. (2014). Fatty Acid Methyl Esters and Solutol HS 15 Confer Neuroprotection after Focal and Global Cerebral Ischemia. *Transl. Stroke Res.* 5, 109–117. doi:10.1007/s12975-013-0276-z

Liu, H. Y., Zhu, M. J., Mao, J. Y., and Lin, Q. (2016). [Consensus on Standardized Using Xinmailong Injection for Treating Chronic Heart Failure]. *Zhongguo Zhong Xi Yi Jie He Za Zhi* 36, 280–284.

Liu, Y., Wang, Z., Xiao, W., and Li, Y. (2014). Use of Gated Myocardial Perfusion Imaging to Assess Clinical Value of Xinmailong Injection in Chronic Congestive Heart Failure. *J. Traditional Chin. Med.* 34, 555–559. doi:10.1016/s0254-6272(15)30062-5

Luo, S.-L., Huang, X.-J., Wang, Y., Jiang, R.-W., Wang, L., Bai, L.-L., et al. (2014). Isocoumarins from American Cockroach (*Periplaneta americana*) and Their Cytotoxic Activities. *Fitoterapia* 95, 115–120. doi:10.1016/j.fitote.2014.03.004

Ma, Q., Luo, Y., Guo, P., Gao, G., Yang, M., Sablok, G., et al. (2013). Clinical Effects of Xinmailong Therapy in Patients with Chronic Heart Failure. *Int. J. Med. Sci.* 10, 624–633. doi:10.7150/ijms.5779

Malek, M., and Nematbakhsh, M. (2015). Renal Ischemia/reperfusion Injury; from Pathophysiology to Treatment. *J. Ren. Inj Prev* 4, 20–27. doi:10.12861/jrip.2015.06

Marsche, G. (2015). Lp-PLA2, Plaque Inflammation and Lesion Development Vary Fundamentally between Different Vascular Sites. *J. Am. Heart Assoc.* 4. doi:10.1161/JAHA.115.001800

Naghavi, M., Libby, P., Falk, E., Casscells, S. W., Litovsky, S., Rumberger, J., et al. (2003). From Vulnerable Plaque to Vulnerable Patient. *Circulation* 108, 1772–1778. doi:10.1161/01.cir.0000087481.55887.c9

Okninska, M., Paterek, A., Bierla, J., Czarnowska, E., Maczewski, M., and Mackiewicz, U. (2021). Effect of Age and Sex on the Incidence of Ventricular Arrhythmia in a Rat Model of Acute Ischemia. *Biomed. Pharmacother.* 142, 111983.

Perveen, K., Quach, A., Stark, M. J., Prescott, S. L., Barry, S. C., Hii, C. S., et al. (2021). Characterization of the Transient Deficiency of PKC Isozyme Levels in Immature Cord Blood T Cells and its Connection to Anti-allergic Cytokine Profiles of the Matured Cells. *Int. J. Mol. Sci.* 22. doi:10.3390/ijms222312650

Schenone, M., Dančík, V., Wagner, B. K., and Clemons, P. A. (2013). Target Identification and Mechanism of Action in Chemical Biology and Drug Discovery. *Nat. Chem. Biol.* 9, 232–240. doi:10.1038/nchembio.1199

Seong, E., Lee, J. H., Lim, S., Park, E. H., Kim, E., Kim, C. W., et al. (2021). Activation of Aryl Hydrocarbon Receptor by ITE Improves Cardiac Function in Mice after Myocardial Infarction. *J. Am. Heart Assoc.* 10, e020502. doi:10.1161/JAHA.120.020502

Smit, M., Coetzee, A. R., and Lochner, A. (2020). The Pathophysiology of Myocardial Ischemia and Perioperative Myocardial Infarction. *J. Cardiothorac. Vasc. Anesth.* 34, 2501–2512. doi:10.1053/j.jvca.2019.10.005

Steinberg, S. F. (2012). Cardiac Actions of Protein Kinase C Isoforms. *Physiology* 27, 130–139. doi:10.1152/physiol.00009.2012

Tanai, E., and Frantz, S. (2015). Pathophysiology of Heart Failure. *Compr. Physiol.* 6, 187–214. doi:10.1002/cphy.c140055

Thygesen, K., Alpert, J. S., Jaffe, A. S., Chaitman, B. R., Bax, J. J., Morrow, D. A., et al. (2018). Fourth Universal Definition of Myocardial Infarction (2018). *J. Am. Coll. Cardiol.* 13, e618-e651 .

Viswanadha, V. P., Dhivya, V., Somasundaram, B., Beeraka, N. M., Huang, C.-Y., Mikhaleva, L. M., et al. (2021). The Role of Mitochondria in Piperine Mediated Cardioprotection in Isoproterenol Induced Myocardial Ischemia. *Cpd* 27, 2975–2989. doi:10.2174/1381612826666200909125750

Wang, R., Wang, X., Zhang, E., Li, F., Zhang, P., and Shi, J. (2021). Correlation of Plasma Galectin-3 and Plasma Lipoprotein-Associated Phospholipase A2 with the Severity and Prognosis of Coronary Artery Disease. *Am. J. Transl Res.* 13, 8997–9004.

Wu, Y., Yin, X., Wijaya, C., Huang, M. H., and Mcconnell, B. K. (2011). Acute Myocardial Infarction in Rats. *J. Vis. Exp.* doi:10.3791/2464

Yasue, H., Nakagawa, H., Itoh, T., Harada, E., and Mizuno, Y. (2008). Coronary Artery Spasm-Clinical Features, Diagnosis, Pathogenesis, and Treatment. *J. Cardiol.* 51, 2–17. doi:10.1016/j.jjcc.2008.01.001

Conflict of Interest: The authors declare that the research was conducted in the absence of any commercial or financial relationships that could be construed as a potential conflict of interest.

Publisher's Note: All claims expressed in this article are solely those of the authors and do not necessarily represent those of their affiliated organizations, or those of the publisher, the editors, and the reviewers. Any product that maybe evaluated in this article, or claim that may be made by its manufacturer, is not guaranteed or endorsed by the publisher.

Copyright © 2022 Jin, Yin, Mao, Gao, Han, Mei, Xue, Tan and Li. This is an open-access article distributed under the terms of the Creative Commons Attribution License (CC BY). The use, distribution or reproduction in other forums is permitted, provided the original author(s) and the copyright owner(s) are credited and that the original publication in this journal is cited, in accordance with accepted academic practice. No use, distribution or reproduction is permitted which does not comply with these terms.

frontiers in Cell and Developmental Biology

ORIGINAL RESEARCH
published: 03 February 2022
doi: 10.3389/fcell.2022.829316

Ferroptosis due to Cystathionine γ Lyase/Hydrogen Sulfide Downregulation Under High Hydrostatic Pressure Exacerbates VSMC Dysfunction

Ruxi Jin, Ruixue Yang, Changting Cui, Haizeng Zhang, Jun Cai, Bin Geng and Zhenzhen Chen**

State Key Laboratory of Cardiovascular Disease, National Center for Cardiovascular Diseases, Hypertension Center, Fuwai Hospital, Chinese Academy of Medical Sciences and Peking Union Medical College, Beijing, China

OPEN ACCESS

Edited by:
Zhi Qi,
Nankai University, China

Reviewed by:
Yongsheng Chang,
Tianjin Medical University, China
Jinwei Tian,
The Second Affiliated Hospital of Harbin Medical University, China

***Correspondence:**
Bin Geng
bingeng@hsc.pku.edu.cn
Zhenzhen Chen
chenzhenzhen@bjmu.edu.cn

Specialty section:
This article was submitted to Cell Death and Survival, a section of the journal Frontiers in Cell and Developmental Biology

Received: *05 December 2021*
Accepted: *10 January 2022*
Published: *03 February 2022*

Citation:
Jin R, Yang R, Cui C, Zhang H, Cai J, Geng B and Chen Z (2022) Ferroptosis due to Cystathionine γ Lyase/Hydrogen Sulfide Downregulation Under High Hydrostatic Pressure Exacerbates VSMC Dysfunction. Front. Cell Dev. Biol. 10:829316. doi: 10.3389/fcell.2022.829316

Hydrostatic pressure, stretch, and shear are major biomechanical forces of vessels and play critical roles in genesis and development of hypertension. Our previous work demonstrated that high hydrostatic pressure (HHP) promoted vascular smooth muscle cells (VSMCs) two novel subsets: inflammatory and endothelial function inhibitory VSMCs and then exacerbated VSMC dysfunction. However, the underlying mechanism remains unknown. Here, we first identified that aortic GPX4 (a core regulator of ferroptosis) significantly downregulated association with VSMC novel phenotype elevation in SHR rats and hypertension patients. In primary VSMCs, HHP (200 mmHg) increased iron accumulation, ROS production, and lipid peroxidation compared with normal pressure (100 mmHg). Consistently, the ferroptosis-related gene (*COX-2*, *TFRC*, *ACSL4*, and *NOX-1*) expression was also upregulated. The ferroptosis inhibitor ferrostatin-1 (Fer-1) administration blocked HHP-induced VSMC inflammatory (CXCL2 expression) and endothelial function inhibitory (AKR1C2 expression) phenotyping switch association with elevation in the GPX4 expression, reduction in the reactive oxygen species (ROS), and lipid peroxidation production. In contrast, the ferroptosis inducer RLS3 increased HHP-induced CXCL2 and AKR1C2 expressions. These data indicate HHP-triggering ferroptosis contributes to VSMC inflammatory and endothelial function inhibitory phenotyping switch. In mechanism, HHP reduced the VSMC GSH content and cystathionine gamma-lyase (CSE)/hydrogen sulfide (H_2S)—an essential system for GSH generation. Supplementation of the H_2S donor-NaHS increased the VSMC GSH level, alleviated iron deposit, ROS and lipid peroxidation production. NaHS administration rescues both HHP- and RLS3-induced ferroptosis. Collectively, HHP downregulated VSMC CSE/H_2S triggering GSH level reduction, resulting in ferroptosis, which contributed to the genesis of VSMC inflammation and endothelial function inhibitory phenotypes.

Keywords: hydrostatic pressure, ferroptosis, hydrogen sulfide, VSMCs, hypertension

INTRODUCTION

Biomechanical forces within the vasculature contain wall shear stress, circumferential wall tensile stress, and hydrostatic pressure (Takayama et al., 2013), and these biomechanics contribute to pathogenesis and development of hypertension and its complications (Hayashi and Naiki, 2009). Shear stress disorder impaired endothelial function and involved in vascular remodeling, atherosclerosis, plaque progression, and vascular malformations (Zhou et al., 2014). The mechanical cyclic stretch force also contributes to vascular smooth muscle cell functions (e.g., apoptosis, proliferation, and migration), which is crucial in vascular remodeling during hypertension (Cheng et al., 2012; Qi et al., 2018), whereas little attention is paid to hydrostatic pressure regulation. A recent study has shown that high hydrostatic pressure (HHP)–driving VSMCs differentiated into inflammatory subset (elevating CXCL2, CXCL3, and CCL2) and endothelial function inhibitory subset (upregulating AKR1C2, AKR1C3, and PEDF) by single-cell sequencing and exacerbated the VSMC dysfunction (Chen Z. et al., 2021). However, the underlying mechanism remains unknown.

Ferroptosis is a novel type of programmed cell death, characteristic as iron overload, reactive oxygen species (ROS) accumulation, iron-dependent lipid peroxidation, and mitochondrial shrinkage (Wu et al., 2021). Ferroptosis is triggered by the cystine/glutamate antiporter system (Xc^- system) dysfunction, glutathione (GSH) depletion, and glutathione-dependent antioxidant enzyme glutathione peroxidase 4 (GPX4) inactivation (Yang and Stockwell, 2016). GSH is an important antioxidant, synthesized from cysteine and oxidizes to oxidized glutathione (GSSG) dependent on GPX4 (Badgley et al., 2020). Meanwhile, GPX4 also reduced cytotoxic lipid peroxide (L-OOH) into nontoxic alcohol L-OH in the presence of the cofactor GSH (Stockwell et al., 2017). Thus, GPX4/GSH is an essential regulatory system in ferroptosis. Recently, many studies highlighted that ferroptosis is a crucial pathophysiological process in chronic diseases such as cancer, diabetes, and nervous system disease (Qiu et al., 2020). Over iron deposits induced ferroptosis causing cardiomyopathy (Gujja et al., 2010) or development of vulnerable plaques (Vinchi et al., 2020). Recombinant human GPX4 (Liu et al., 2021) and ferroptosis inhibitor Fer-1 (Li et al., 2020) treatment attenuated myocardial injuries. These works indicate that ferroptosis contributes to the pathogenesis of cardiovascular diseases.

Cystathionine-γ-lyase (CSE) endogenously produces hydrogen sulfide (H_2S) exerting a cardiovascular protective role and as the key enzyme for L-cysteine (precursor of GSH) (Kimura, 2021). H_2S plays an antioxidative role by facilitating the GSH content and removing ROS (Tabassum and Jeong, 2019), also inhibiting GPX4 activity and maintaining the Xc^- system stability to mitigate ferroptosis (Chen S. et al., 2021; Wang et al., 2021b). In the present study, we seek to clarify whether VSMC ferroptosis involve into the HHP-induced VSMC phenotyping switch. In mechanism, we investigate the CSE/H_2S-dependent GSH level in ferroptosis in the HHP condition.

MATERIALS AND METHODS

Human Samples

Human internal mammary arteries were obtained from patients undergoing off-pump coronary artery bypass graft. The internal mammary artery (about 5 mm) was acquired from the patient's surgical donor artery; then, the paraffin slices were prepared for immunofluorescent staining. This study was approved by Fuwai Hospital Ethics Committee and performed in accordance with ethical standards.

Animal and Materials

Adult male Wistar–Kyoto (WKY) and spontaneously hypertensive rats (SHR) aged 12–16 weeks were housed in controlled temperature at a 12:12-h light–dark cycle with free access to water and standard diet. All animal protocols complied with all relevant ethical regulations and were approved by the Institutional Animal Care and Use Committee, the Experimental Animal Center, Fuwai Hospital, and the National Center for Cardiovascular Diseases, China. The primary antibodies used in this study are as follows: anti-GPX4 (ab125066, Abcam); anti-CXCL2 (PA5-47015, Invitrogen); anti-AKR1C2 (ab166900, Abcam); anti-CSE (ab151769); ferrostatin-1 (S7243, Selleck); RLS3 (S8155, Selleck); and NaHS (161527, Sigma).

H_2S Production Measurement

H_2S production was measured by the modified methylene blue method, as mentioned previously (Niu et al., 2021). In detail, the inner ring of the Erlenmeyer flask was added with zinc acetate and a filter paper to absorb H_2S. The outer ring was added with an incubation buffer (potassium phosphate buffer, L-cysteine and pyridoxal 5′-phosphate). The cell lysate in the potassium phosphate buffer was added into the outer ring of the conical flasks. The reaction was performed in 37°C shaking water bath by incubation. After sufficient reaction, trichloroacetic acid was added into the outer ring and incubated for another 1 h to terminate the reaction. Followed by adding N, N-dimethyl-*p*-phenylenediamine sulfate and 10% ammonium ferric sulfate, absorbance at 670 nm was measured by spectrophotometry.

Cell Culture and Treatment

Primary human aorta vascular smooth muscle cells (HASMCs) were purchased from ScienCell Research Laboratories, Inc. HAMSCs were cultured in a smooth muscle cell medium (1,101, ScienCell Research Laboratories.) containing 2% FBS, 100 U/mL penicillin–streptomycin, and 1% smooth muscle cell growth factor at 37°C in a 5% CO_2 atmosphere. HASMCs in passages three to six were used in this study. We used a specific hydrostatic pressure device for hydrostatic pressure treatment, as described previously (Chen Z. et al., 2021). HASMCs (~70% confluence) were set in a hydrostatic pressure device at 100 mmHg or 200 mmHg for culturing for 24 h. For inhibition or activation of ferroptosis, HASMCs were treated with Fer-1 (10 μM, 24 h) or RLS3 (0.1 μM, 6 h) under hydrostatic pressure. For increasing exogenous H_2S, HASMCs were treated with NaHS (100 μM, 24 h) under hydrostatic pressure.

Primary Mouse Vascular Smooth Muscle Cell Isolation

Aortic smooth muscle cells were isolated from wild-type male 6–8-week and CSE-knockout mice. Mice were sacrificed by decapitation, followed by separating the aorta *via* removing the fatty tissue and vascular adventitia. Then, the mouse aorta was cut into pieces and allowed for digestion for 8 h in the DMEM containing collagenase type 1. The obtained VSMCs were centrifuged at 300 xg for 5 min, and the pellet was resuspended in the DMEM supplemented with 10% FBS, 2 mM L-glutamine, and 100 U/mL penicillin/streptomycin. The medium was replaced every 2 days. All experimental procedures were conducted in an incubator at a temperature of 37°C, in an atmosphere of 95% air and 5% CO_2. Primary SMCs with the passage number three to eight were used in the study.

Iron and GSH Detection

We used two different methods to detect the iron content. After treatment, the intracellular ferrous iron level was assessed with an iron colorimetric assay kit (ab83366, Abcam) according to the manufacturer's instruction protocol. For FeRhoNox-1 staining, 5 μM of the FeRhoNox-1 staining working solution (MX4558 and MKBIO) was added and incubated in a 37°C, 5% CO_2 incubator for 60 min after treatment for 24 h in a hydrostatic pressure chamber. After washing three times with PBS, cells were imaged with a confocal microscope. The cellular level of glutathione was determined using the Glutathione Assay Kit (S0035, Beyotime) according to the manufacturer's instruction protocol.

Reactive Oxygen Species (ROS) Measurement

ROS was measured by using a fluorometric intracellular ROS kit (MAK143, sigma). HASMCs were incubated with 10 μM DCFH-DA for 1 h. After washing with PBS three times, fluorescence signals were observed by using a fluorescence microscope.

Mitochondrial Superoxide Measurement

We use the MitoSOX™ Red mitochondrial superoxide indicator (M36008, Invitrogen) to detect ROS in the mitochondria. After treatment, HASMCs were stained with 5 μM MitoSOX Red for 10 min, followed by washing with PBS. The images were observed by using a confocal microscope.

Lipid Peroxidation Detection

HASMCs were labeled with a lipid peroxidation sensor BODIPY™ 581/591 C11 (D3861, Invitrogen) at 2 μM in a living cell imaging solution for 1 h at 37°C. The images were observed by using a confocal microscope. The fluorescence signals correspond to the oxidized (orange) form of BODIPY 581/591 C11. Oxidation of BODIPY-C11 was calculated by the orange fluorescence intensity.

Immunofluorescence Staining

For aorta immunofluorescent staining, paraffin sections were incubated with 3% hydrogen peroxide to block the endogenous peroxidase activity. Antigen retrieval was performed for 20 min at 97°C in a citrate buffer, and sections were cooled to room temperature. For HAMSC immunofluorescent staining, cells were fixed with 4% paraformaldehyde for 15 min at room temperature. After washed with PBS three times, cells were permeabilized with 0.5% Triton X-100 for 15 min at room temperature. Subsequently, above tissue sections or cells were blocked with 1% BSA for 1 h and incubated with the primary antibody at 4°C overnight, followed by incubating with a fluorescent-labeled secondary antibody for 1 h at room temperature according to the manufacturer's instructions. After washing three times with PBS, the nuclei were stained with Hoechst for 8 min. The images of tissues or cells were collected using a fluorescence microscope or by confocal microscopy.

Western Blot

Cells were lysed in RIPA buffer containing protease- and phosphatase-inhibitor cocktails, followed by sonication and centrifugation. Total protein of cells was quantified by BCA assay. For the assay, 40 μg protein samples were separated by SDS-PAGE and transferred to polyvinylidene fluoride membranes. Then, the PVDF membranes were blocked by 5% defatted milk for 1 h and probed with the primary antibody at 4°C overnight. After washing and incubating with the horseradish peroxidase–conjugated secondary antibody for 1 h at room temperature, the membranes were visualized using the chemiluminescence kit.

RNA Extraction and qRT-PCR

Total RNA from HASMCs was extracted using TRIzol reagent (Invitrogen) according to the manufacturer's instructions. cDNA was reverse transcribed from 1 μg total RNA by using the cDNA synthesis kit (K1622, Thermo scientific). The real-time PCR was performed in a final volume of 20 μl, which contained 10 μl of the 2×SYBR Mix (Yeasen, China), 1 μl of forward and reverse primers, respectively, 4 μl of template cDNA, and 5 μl of RNase-free H_2O. A sample without cDNA was subjected to an identical protocol as a negative control. The PCR amplification was accomplished with initial denaturation at 95°C for 10 min, followed by 40 cycles at 95°C for 15 s and 1 min at 60°C for primer annealing and extension. The relative expression of target genes was normalized to that of GAPDH and analyzed by the $2^{-\Delta\Delta CT}$ method. The primer sequences used for qRT-PCR are provided in **Supplementary Table S1**.

Statistical Analysis

All data are presented as the mean ± SD. The statistical significance of differences between groups was analyzed by the *t*-test or by one-way analysis of variance (ANOVA) when more than two groups were compared. p values <0.05 were considered as statistically significant.

RESULTS

Elevation of Ferroptosis in Aortic Media of SHR and Hypertensive Patients Associated With VSMC Novel Phenotypes

High hydrostatic pressure drives VSMC differentiation into two novel phenotypes: the inflammatory phenotype (marker genes

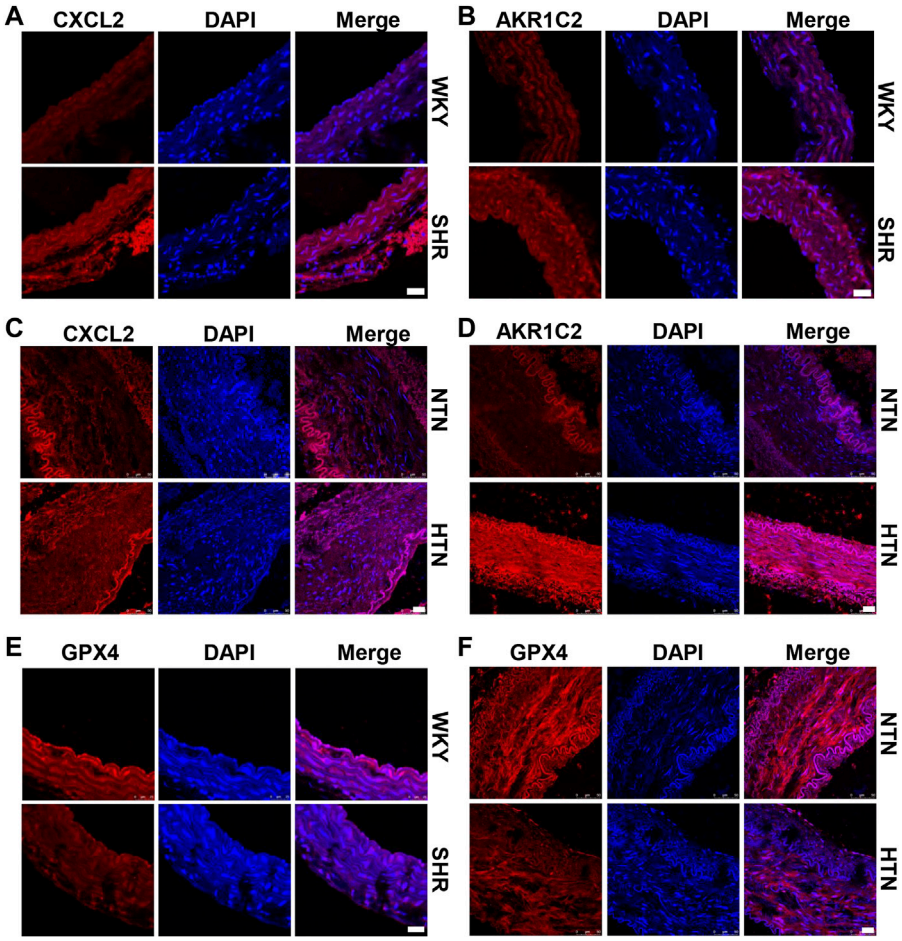

FIGURE 1 | GPX4 expression positively correlated with the VSMC-specific phenotype in SHR and hypertensive patients. Immunofluorescent staining of CXCL2 **(A)** and *AKR1C2* **(B)** in the arterial media of SHR. Immunofluorescence of CXCL2 **(C)** and *AKR1C2* **(D)** on paraffin-embedded human normotension (NTN) and hypertension (HTN) internal mammary arteries. The GPX4 expression was detected by immunofluorescent staining in SHR **(E)** and human hypertensive patients **(F)**. Nuclei were counterstained with Hoechst. Scale bar = 25 μM.

are CXCL2/CXCL3/CCL2) and endothelial function inhibitory phenotype (marker genes are AKR1C2/AKR1C3/PEDF), and promote VSMC dysfunction (Chen Z. et al., 2021). Compared with WKY rats, SHR exhibits CXCL2 and AKR1C2 increase in the media of aorta (**Figures 1A,B** and **Supplementary Figure S1A**). Similarly, CXCL2 and AKR1C2 expressions were significantly enhanced in the human internal mammary artery of hypertensive patients in comparison with normotensive patients (**Figures 1C,D** and **Supplementary Figure S1B**). To investigate ferroptosis involved in HHP-induced VSMC novel phenotypes, we measured the GPX4 (a key enzyme of ferroptosis) protein level. Here, we showed that aortic media GPX4 dramatically downregulated in the SHR and hypertensive patients compared with the related control (**Figures 1E,F** and **Supplementary Figure S1A–B**). These results indicated that ferroptosis associated with the VSMC phenotype switch in the hypertensive animal model and hypertensive patients.

High Hydrostatic Pressure Induces Ferroptosis

To seek whether HHP induces VSMC ferroptosis, we constructed a specific cell culture chamber and set 200 mmHg as HHP and 100 mmHg as normal (simulates hydrostatic pressure of the aortic wall in normotensive and hypertensive individuals). For evaluation ferroptosis, HHP (200 mmHg)-treatment increased the VSMC total ROS production (**Figure 2A** and **Supplementary Figure S2A**), mitochondria-derived ROS releasing by MitoSOX Red staining (**Figure 2B** and **Supplementary Figure S2B**), lipid peroxidation production by BODIPY 588/591 C11 (**Figure 2C** and **Supplementary Figure S2C**), iron accumulation by FeRhoNox-1 staining (**Figure 2D**), and iron content by the iron assay kit (**Figure 2E**) in comparison to normal pressure. In line with the ROS enhancing and lipid peroxidation, the GPX4 protein (**Figure 2F**) and mRNA level (**Figure 2G**) also lowered under the HHP condition. Indeed, the ferroptosis-related gene (*COX-2*, *TFRC*, *ACSL4*, and *NOX-1*) mRNA expression was

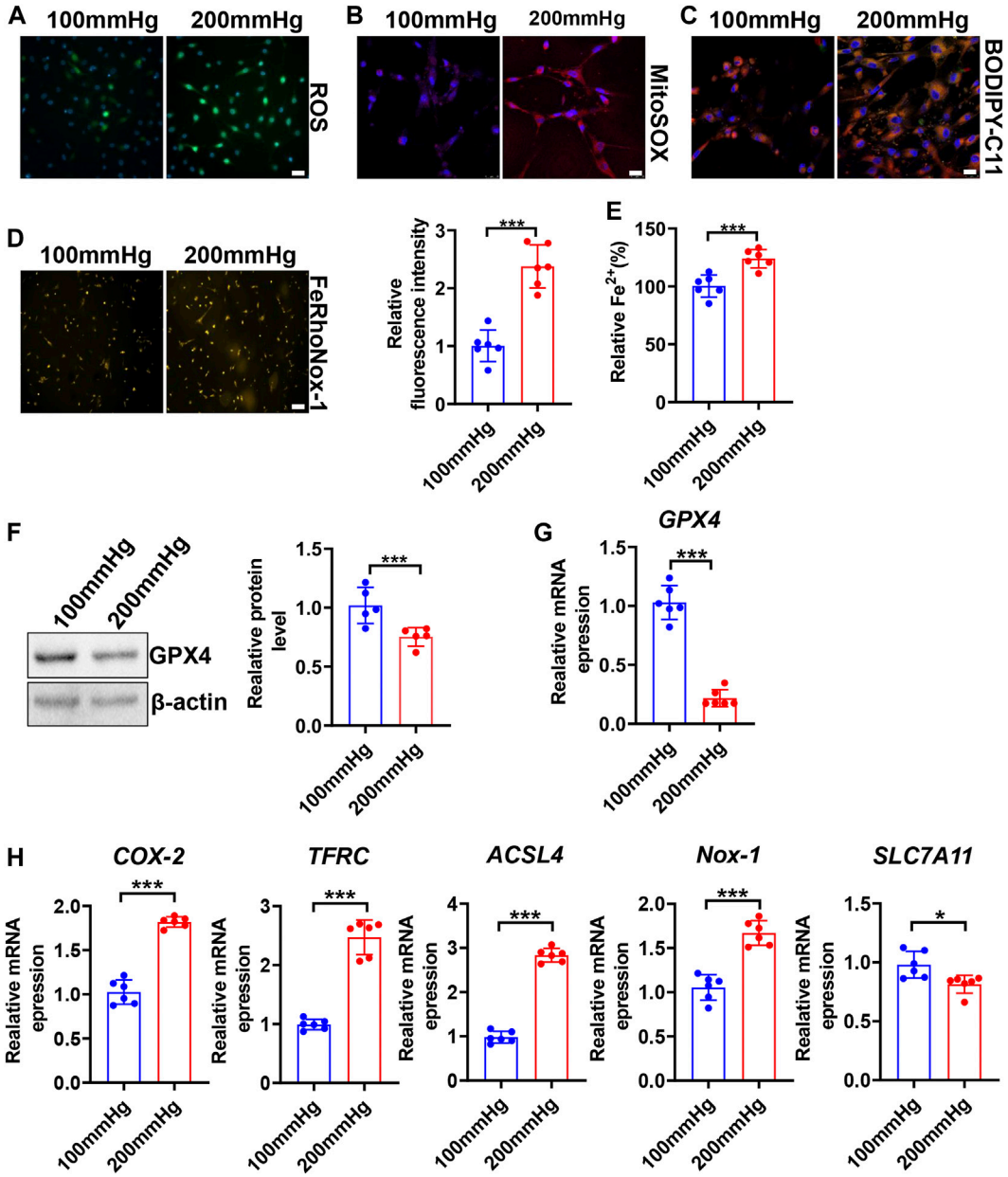

FIGURE 2 | High hydrostatic pressure promoted ferroptosis. HASMCs were treated with hydrostatic pressure for 24 h. Immunofluorescent staining of total ROS, scale bar = 50 μM **(A)**. MitoSOX Red staining of HASMCs for mitochondrial ROS, scale bar = 25 μM **(B)**. BODIPY-C11 staining measured the lipid peroxidation; orange indicated oxidized C11, scale bar = 25 μM **(C)**. Iron level was detected by FeRhoNox-1 staining **(D)** and iron assay kit **(E)**, scale bar = 100 μM. Western blot assay measured the GPX4 protein level; the left panel is the representative image, and the right panel is the statistical graph **(F)**. The mRNA levels of GPX4 **(G)**, COX-2, TFRC, ACSL4, NOX-1, and SLC7A11 were measured by real-time PCR **(H)** under HHP conditions. Nuclei were counterstained with Hoechst. $^{*}p < 0.05$, $^{***}p < 0.001$.

upregulated, and SLC7A11 mRNA was downregulated while exposed to HHP (**Figure 2H**). Overall, these results indicate high hydrostatic pressure promotes VSMC ferroptosis.

Ferroptosis Contributes to the HHP-Induced Specific VSMC Phenotype Switch

To investigate the effect of ferroptosis on HHP-induced specific VSMC subsets, we treated HASMCs with the ferroptosis suppressor Fer-1. Fer-1 supplementation upregulated the VSMC GPX4 expression under normal or high hydrostatic pressure conditions (**Figure 3A**). In line with GPX4 upregulation, Fer-1 administration also blocked HHP-stimulated ROS production (**Figure 3B**), mitochondrial ROS production (**Figure 3C**), and lipid oxidation (**Figure 3D**), similar to other ferroptosis inducers (Dixon et al., 2012). These results confirmed Fer-1 blocked HHP-associated ferroptosis. In association with ferroptosis inhibition, Fer-1

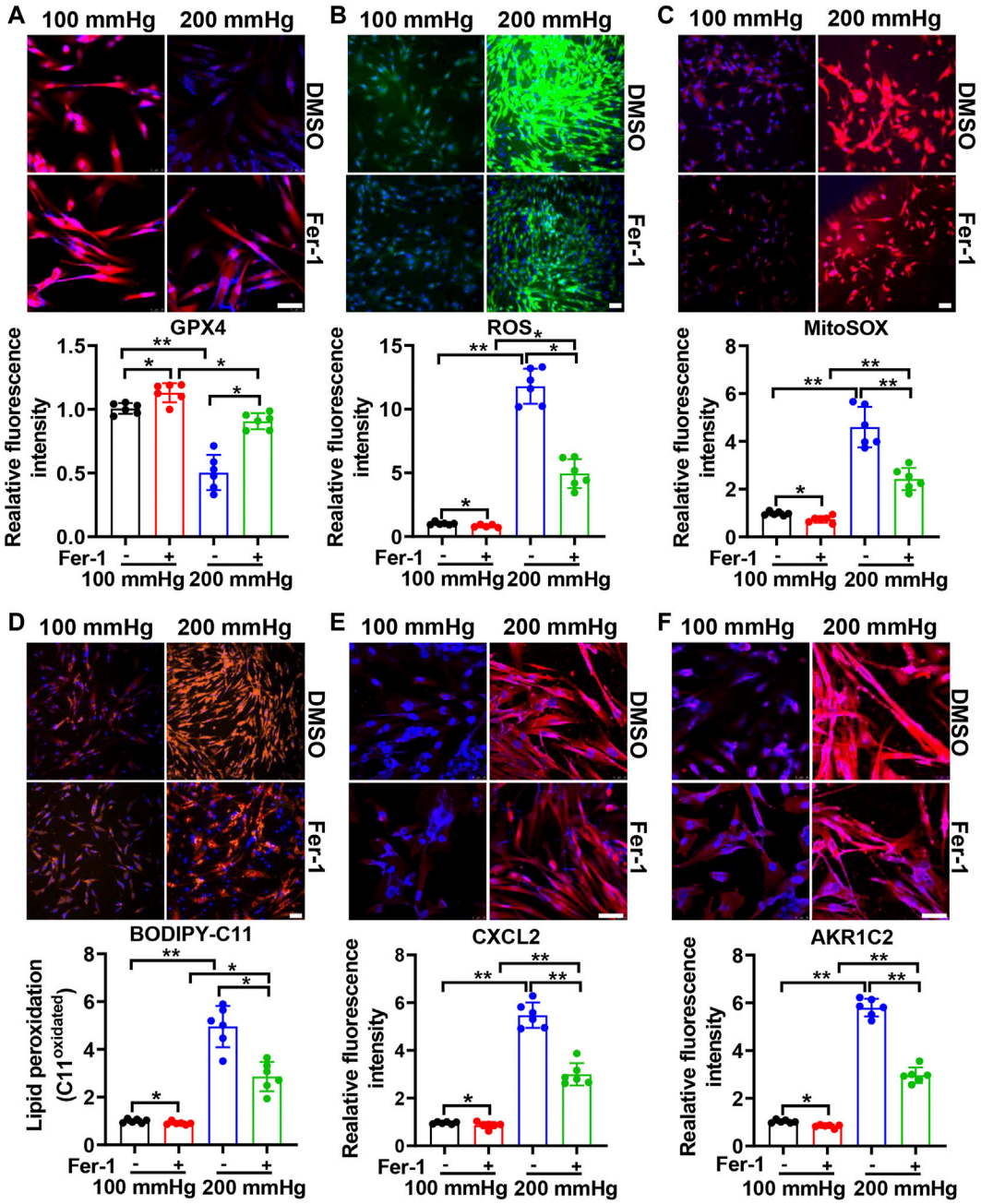

FIGURE 3 | Ferroptosis inhibitor Fer-1 mitigates the HHP-induced VSMC phenotype switch. HASMCs in a 100 mmHg or 200 mmHg incubator were treated with or without 10 μM Fer-1 for 24 h. The GPX4 protein level was evaluated by immunofluorescent staining; the upper panel is the representative image, and the lower panel is the statistical graph **(A)**. ROS production was determined by the ROS staining kit; the upper panel is the representative image, and the lower panel is the statistical graph **(B)**. Mitochondrial ROS was visualized by use of the fluorescent probe MitoSOX Red **(C)**. BODIPY 581/591 C11 lipid oxidation in HASMCs was measured by immunofluorescent staining; the statistical graph is the oxidized (orange signal) BODIPY 581/591 C11 fluorescence intensity **(D)**. Confocal images of the CXCL2 expression **(E)** and AKR1C2 expression **(F)** in HASMCs. Nuclei were counterstained with Hoechst. All scale bar = 50 μM $^{*}p < 0.05$, $^{**}p < 0.01$, $^{***}p < 0.001$.

also blocked HHP-induced VSMC CXCL2 (**Figure 3E**) and AKR1C2 (**Figure 3F**) elevation.

Since HHP-induced ferroptosis is in part of the GPX4/GSH pathway, we used a ferroptosis inducer RLS3 (GPX4 inactivation) to confirm its role in the VSMC novel phenotype switch. Under 200 mmHg hydrostatic pressure condition, RLS3 ulteriorly reduced the GPX4 expression (**Figure 4A**). Consistently, RLS3 exacerbated ferroptosis by increasing ROS production (**Figure 4B**), mitochondrial ROS production(**Figure 4C**), and lipid oxidation (**Figure 4D**). Correspondingly, RLS3 further increases the HHP-induced VSMC CXCL2 (**Figure 4E**) and AKR1C2 expression (**Figure 4F**). Taken together, these data

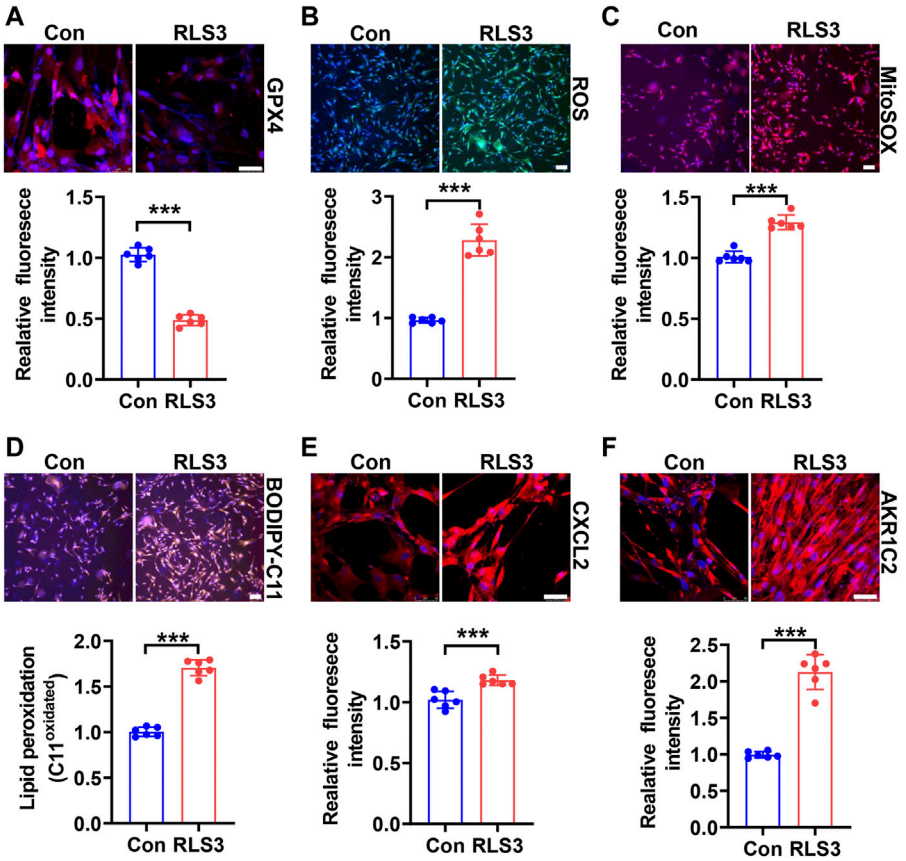

FIGURE 4 | Ferroptosis inducer RLS3 aggravates VSMC dysfunction in response to HHP. HASMCs were treated with RLS3 0.1 μM for 6 h in the presence of 200 mmHg. Immunofluorescent staining of GPX4 (red) in HASMCs **(A)**. Intracellular ROS were measured by ROS staining; the upper panel is the representative image, and the lower panel is the statistical graph **(B)**. HASMCs were labeled with the MitoSOX Red probe to detect mitochondrial ROS **(C)**. Confocal images of the BODIPY 588/591 C11 staining; lipid oxidation was measured by the relative intensity of oxidized (orange fluorescence signal) BODIPY 581/591 C11 **(D)**. CXCL2 **(E)**, and AKR1C2 **(F)** protein levels were detected by immunofluorescent staining. All scale bar = 50 μM ***$p < 0.001$.

indicated that ferroptosis contributed to the pathophysiological process of HHP-induced VSMC-specific phenotypes.

CSE/H_2S Alleviate HHP-Induced VSMC Ferroptosis

CSE/H_2S plays a crucial role in GSH synthesis due to controlling the GSH precursor-L-cysteine generation, and CSE/H_2S plays an essential protection in VSMC function (Kimura, 2021). To investigate whether CSE/H_2S involved in the modulation of HHP-induced ferroptosis, we first measured the CSE/H_2S changes exposed to HHP (200 mmHg). As **Figure 5A** showed, HHP treatment for 48 h dramatically reduced the HASMC H_2S production (about 27%). The CSE protein (**Figure 5B**) and mRNA expression (**Figure 5C**) were also downregulated under HHP. The association with CSE/H_2S downregulation and the intracellular GSH level reduced about 28% (**Figure 5D**).

In contrast, supplementation H_2S donor-NaHS under HHP culture, upregulated the GSH level and GPX4 expression (**Figures 5E,F** and **Supplementary Figure S3A**) but lowered the HASMC iron concentration (**Figure 5G** and **Supplementary Figure S3B**), ROS production (**Figure 5H** and **Supplementary Figure S3C**), mitochondrial ROS production (**Figure 5I** and **Supplementary Figure S3D**), and lipid peroxidative production (**Figure 5J** and **Supplementary Figure S3E**). Next, we isolated primary CSE-knockout mouse VSMCs to confirm its role in HHP-induced ferroptosis. Under HHP conditions, CSE deficiency further decreased the GPX4 expression (**Figure 5K** and **Supplementary Figure S3F**), enhanced iron accumulation (**Figure 5L** and **Supplementary Figure S3G**), cellular and mitochondrial ROS (**Figure 5M–N** and **Supplementary Figure S3H–I**), and lipid peroxidative production (**Figure 5O** and **Supplementary Figure S3J**). Our present data highlight HHP decreases CSE/H_2S causing GSH level reduction attribution to pathogenesis of VSMC ferroptosis.

To confirm the effect of CSE/H_2S on ferroptosis, we first used RLS3 to induce ferroptosis. In line with the above findings, NaHS administration also rescued the RLS3-induced GPX4 expression (**Figure 6A** and **Supplementary Figure S4A**), iron accumulation (**Figure 6B** and **Supplementary Figure S4B**), ROS production (**Figure 6C** and **Supplementary Figure S4C**), mitochondrial ROS production (**Figure 6D** and **Supplementary Figure S4D**), and

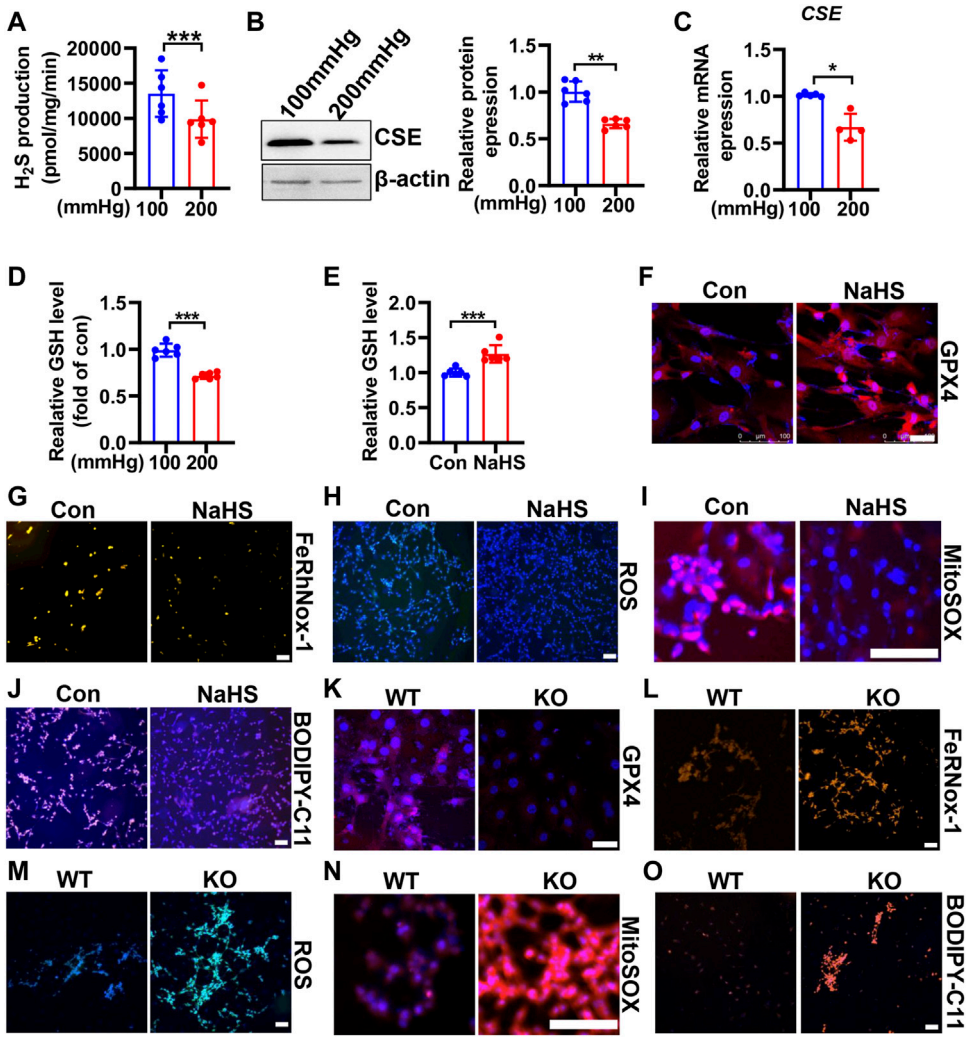

FIGURE 5 | CSE/H_2S attenuates HHP-induced ferroptosis in VSMCs. H_2S production was measured by the modified methylene blue method under 100 or 200 mmHg **(A)**. Western blot assay analysis of the CSE expression under hydrostatic pressure; the left panel is the representative image, and the right panel is the statistical graph **(B)**. CSE mRNA level under hydrostatic pressure **(C)**. GSH assay kit measured the GSH level in response to hydrostatic pressure **(D)**. After NaHS administration (0.1mM, 24 h) in the presence of 200 mmHg, the GSH content was measured **(E)**. Representative image of GPX4 staining after NaHS treatment under HHP conditions **(F)**. Effect of NaHS on Fe^{2+} **(G)**, ROS **(H)**, mitochondrial ROS **(I)**, and lipid oxidation **(J)** under 200 mmHg by immunofluorescent staining. In isolated primary mouse VSMCs, the effect of deletion of CSE on the GPX4 expression **(K)**, iron level **(L)**, ROS production **(M)**, mitochondrial ROS production **(N)**, and lipid peroxidation **(O)** under HHP conditions by immunofluorescent staining. All scale bar = 50 μM $^*p < 0.05$, $^{**}p < 0.01$, $^{***}p < 0.001$.

lipid oxidation (**Figure 6E** and **Supplementary Figure S4E**). In summary, our result indicated that CSE/H_2S contributes to the regulation of ferroptosis under HHP conditions.

DISCUSSION

Mechanical forces play an important role in vasculature and circulation, such as rapid regulation of vascular wall elasticity, administration of vascular remodeling, and the modulation of VSMC and endothelial function (Qiu et al., 2014). Our previous study identifies a novel cellular taxonomy of VSMCs under hydrostatic pressure by single-cell RNA sequencing. HHP derived VSMCs into inflammatory and endothelial-function inhibitory VSMCs, resulting in VSMC dysfunction (cytokine secretion and angiogenesis inhibition) (Chen Z. et al., 2021). However, the underlying mechanism is unclear. In the current study, we first demonstrated that HHP induced VSMC ferroptosis evidence as iron accumulation, ROS generation, and lipid peroxidation. Furthermore, inhibiting ferroptosis by Fer-1 alleviated, promoting ferroptosis by RLS3 increased inflammatory and endothelial function inhibitory VSMC phenotypes. For the mechanism, we demonstrated that HHP downregulated CSE/H_2S and then lowered GSH generation, resulting in ferroptosis. Our findings highlight that ferroptosis is a novel pathophysiological regulatory mechanism for VSMC function and as a new druggable target for therapeutic hypertension concomitant vascular diseases.

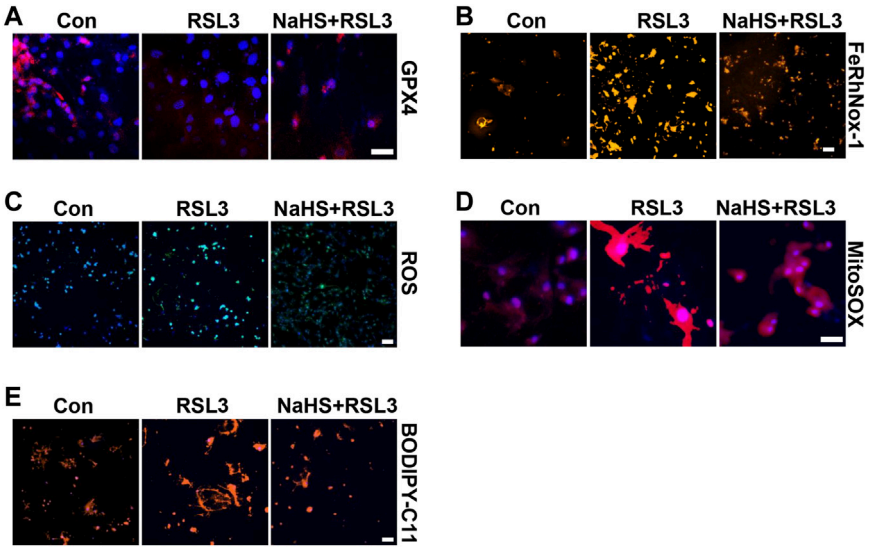

FIGURE 6 | CSE/H_2S rescue RLS3-induced ferroptosis under HHP conditions. Under 200 mmHg conditions, HASMCs were pretreated with NaHS 24 h and followed by RLS3 treatment for another 6 h. Immunofluorescent staining of GPX4 **(A)**. HASMCs were incubated with the FeRhNOX-1 probe for measuring iron **(B)**. HASMCs were labeled with the ROS probe to detect cellular ROS **(C)**, MitoSOX Red to detect mitochondrial ROS **(D)**, and BODIPY-C11 to detect lipid peroxidation **(E)** by immunofluorescent staining. All scale bar = 50 μM.

Hypertension is tightly associated with oxidation stress (McMaster et al., 2015; Touyz et al., 2018). An imbalance between the oxidant and antioxidant system leads to ROS production exaggeration in the arterial media from hypertension patients with hypertension and experimental animal models of hypertension (Touyz and Schiffrin, 2001). Overproduced ROS promoted VSMC proliferation, induced VSMC migration, and switched to the differentiated phenotype (Badran et al., 2020). Dedifferentiated VSMCs synthesize and secrete a repertoire of growth factors and inflammatory cytokines which is a key initiating factor for vascular remodeling. ROS promotes MMP2, MMP9, and collagen expressions and disturbs the extracellular matrix (Rajagopalan et al., 1996; Branchetti et al., 2013). Additionally, oxidation stress induces calcification, stiffness, and aging leading to VSMC dysfunction (Takaishi et al., 2021). ROS overproduction, a center of oxidation stress, is a main characteristic of ferroptosis. Our study first identified GPX4, a key enzyme of ferroptosis, which was dramatically downregulated in arterial media of SHR. *In vitro,* VSMCs exhibited intracellular and mitochondrial ROS overproduction, lipid peroxidation, and iron accumulation under high hydrostatic stress. Ferroptosis upregulation under high hydrostatic stress is a novel pathophysiological process in VSMC dysfunction.

Compelling evidence has indicated that ferroptosis is an essential regulator of inflammation. GPX4 deficiency blocked T-cell survival and B-cell development (Matsushita et al., 2015; Muri et al., 2019). The ferroptosis inducer erastin promoted human peripheral blood mononuclear cells differentiating into B cells and natural killer cells (Tang et al., 2021). Ferroptotic death cells recruited macrophages by secreting CCL2 and CCL7 (Wang et al., 2021a). Ferroptosis inhibitors exhibited the anti-inflammation effect by suppressing TNF-α, IL-6, and IL-1β releasing (Tsurusaki et al., 2019). Consistent with the previous study, Fer-1 treatment attenuated, while RLS3 treatment augmented the HHP-stimulated CXCL2 (one marker gene of inflammatory VSMCs) protein level. In addition, high hydrostatic pressure also induced *AKR1C2* (one marker gene of endothelial function inhibitory VSMCs) which was lowered by Fer-1 but enhanced by RLS3. Studies indicated ferroptosis led to endothelial dysfunction which is a critical pathogenetic factor of hypertension. Iron accumulation resulted in endothelial damage (Vinchi et al., 2020). Fer-1 administration attenuated ox-LDL-induced inflammation and endotheliocyte death, while erastin induced ROS production and ferroptotic death of HUVECs (Xiao et al., 2019; Bai et al., 2020). Combined with our results, ferroptosis may be a potential therapeutic target to hypertension *via* modulating endothelial function.

One important characteristic of ferroptosis is GSH depletion. GSH, an intracellular antioxidant, is the synthesis from the homocysteine/methionine cycle (Rodrigues and Percival, 2019). GSH precursor L-cysteine is also a main source of hydrogen sulfide. Growing evidence demonstrated that H_2S enhances GSH production to attenuate oxidative stress. In a neurocyte, mitochondrial H_2S production increases the GSH level and promotes its redistribution to the mitochondria to protect the neurocyte from oxidative stress (Kimura et al., 2010). In a myotube, H_2S promotes GSH synthesis to improve impaired glucose homeostasis (Parsanathan and Jain, 2018). H_2S donor NaHS administration enhances GSH production to decrease oxidative stress and delay cell senescence (Yang et al., 2013). Consistently, our study showed that exogenous (NaHS administration) H_2S production significantly rescued GSH reduction in response to HHP. Thus, H_2S downregulation–mediated GSH reduction may be a novel mechanism of ferroptosis under HHP.

Recently, studies showed the protective role of H_2S is associated with ferroptosis inhibition. Wang and Chen et al. identified H_2S restrains ferroptosis *via* inhibiting ALOX12 acetylation and regulating the xCT (the functional submit of the Xc^- system) stability (Chen S. et al., 2021; Wang et al., 2021c). H_2S donor GYY4137 treatment alleviates ferroptosis to attenuate acute lung injury (Li et al., 2021). Inhibition of H_2S production *via* the CBS inhibitor CH004 supplement aggravates ferroptosis in hepatocellular carcinoma (Wang et al., 2018). These studies suggested H_2S could restrain ferroptosis to exert a protective effect. However, experimental evidence in the cardiovascular system is still missing. Our present study illustrated that H_2S donor NaHS administration significantly increased the GPX4 expression, downregulated ROS production, and lipid peroxidation, thus reversing high hydrostatic-induced ferroptosis. In addition, NaHS rescued RLS3-induced ferroptosis. Overall, H_2S inhibits ferroptosis to attenuate HHP-induced VSMC dysfunction.

Taken together, the present study highlights the essential regulator role of ferroptosis in the HHP-triggered VSMC novel phenotype switch. The novel pathophysiological process also accounts for HHP, a direct biomechanical force, triggers VSMC ferroptosis, then drives vascular inflammation and limitation vascular relaxation, and contributes to vascular remodeling and aging even if calcified, thus exacerbating concomitant vascular damages and diseases (such as atherosclerosis). More interestingly, our study also indicates a new pathway about the ROS-GSH-iron-ferroptosis signal cascade in CSE/H_2S cardiovascular protection.

DATA AVAILABILITY STATEMENT

The original contributions presented in the study are included in the article/**Supplementary Material**; further inquiries can be directed to the corresponding authors.

ETHICS STATEMENT

The studies involving human participants were reviewed and approved by the Institutional Animal Care and Use Committee, the Experimental Animal Center, Fuwai Hospital, National Center for Cardiovascular Diseases, China. The ethics committee waived the requirement of written informed consent for participation. The animal study was reviewed and approved by the Institutional Animal Care and Use Committee, the Experimental Animal Center, Fuwai Hospital, National Center for Cardiovascular Diseases, China.

AUTHOR CONTRIBUTIONS

ZC and BG conceived the project and designed the experiments. RJ conducted most of the experiments and data analyses. RY conducted a part of experiments. CC and HZ provided the technical assistance. The manuscript was written by ZC and revised and edited by BG and JC.

FUNDING

The study was supported by the CAMS Innovation Fund for Medical Sciences (CIFMS, 2021-I2M-1-007), the National Natural Science Foundation of China (81800367, 81870318, 81825002), the National Key R&D Program of China (2018YFC1312703), and the Beijing Outstanding Young Scientist Program (BJJWZYJH01201910023029).

SUPPLEMENTARY MATERIAL

The Supplementary Material for this article can be found online at: https://www.frontiersin.org/articles/10.3389/fcell.2022.829316/full#supplementary-material

REFERENCES

Badgley, M. A., Kremer, D. M., Maurer, H. C., DelGiorno, K. E., Lee, H.-J., Purohit, V., et al. (2020). Cysteine Depletion Induces Pancreatic Tumor Ferroptosis in Mice. *Science* 368 (6486), 85–89. doi:10.1126/science.aaw9872

Badran, A., Nasser, S. A., Mesmar, J., El-Yazbi, A. F., Bitto, A., Fardoun, M. M., et al. (2020). Reactive Oxygen Species: Modulators of Phenotypic Switch of Vascular Smooth Muscle Cells. *Int. J. Mol. Sci.* 21 (22), 8764. doi:10.3390/ijms21228764

Bai, T., Li, M., Liu, Y., Qiao, Z., and Wang, Z. (2020). Inhibition of Ferroptosis Alleviates Atherosclerosis through Attenuating Lipid Peroxidation and Endothelial Dysfunction in Mouse Aortic Endothelial Cell. *Free Radic. Biol. Med.* 160, 92–102. doi:10.1016/j.freeradbiomed.2020.07.026

Branchetti, E., Poggio, P., Sainger, R., Shang, E., Grau, J. B., Jackson, B. M., et al. (2013). Oxidative Stress Modulates Vascular Smooth Muscle Cell Phenotype via CTGF in Thoracic Aortic Aneurysm. *Cardiovasc. Res.* 100 (2), 316–324. doi:10.1093/cvr/cvt205

Chen, S., Bu, D., Zhu, J., Yue, T., Guo, S., Wang, X., et al. (2021). Endogenous Hydrogen Sulfide Regulates xCT Stability through Persulfidation of OTUB1 at Cysteine 91 in colon Cancer Cells. *Neoplasia* 23 (5), 461–472. doi:10.1016/j.neo.2021.03.009

Chen, Z., Zhang, H., Bai, Y., Cui, C., Li, S., Wang, W., et al. (2021). Single Cell Transcriptomic Analysis Identifies Novel Vascular Smooth Muscle Subsets under High Hydrostatic Pressure. *Sci. China Life Sci.* 64 (10), 1677–1690. doi:10.1007/s11427-020-1852-x

Cheng, W.-P., Wang, B.-W., Chen, S.-C., Chang, H., and Shyu, K.-G. (2012). Mechanical Stretch Induces the Apoptosis Regulator PUMA in Vascular Smooth Muscle Cells. *Cardiovasc. Res.* 93 (1), 181–189. doi:10.1093/cvr/cvr280

Dixon, S. J., Lemberg, K. M., Lamprecht, M. R., Skouta, R., Zaitsev, E. M., Gleason, C. E., et al. (2012). Ferroptosis: an Iron-dependent Form of Nonapoptotic Cell Death. *Cell* 149 (5), 1060–1072. doi:10.1016/j.cell.2012.03.042

Gujja, P., Rosing, D. R., Tripodi, D. J., and Shizukuda, Y. (2010). Iron Overload Cardiomyopathy. *J. Am. Coll. Cardiol.* 56 (13), 1001–1012. doi:10.1016/j.jacc.2010.03.083

Hayashi, K., and Naiki, T. (2009). Adaptation and Remodeling of Vascular wall; Biomechanical Response to Hypertension. *J. Mech. Behav. Biomed. Mater.* 2 (1), 3–19. doi:10.1016/j.jmbbm.2008.05.002

Kimura, H. (2021). Hydrogen Sulfide (H2S) and Polysulfide (H2Sn) Signaling: The First 25 Years. *Biomolecules* 11 (6), 896. doi:10.3390/biom11060896

Kimura, Y., Goto, Y.-I., and Kimura, H. (2010). Hydrogen Sulfide Increases Glutathione Production and Suppresses Oxidative Stress in Mitochondria. *Antioxid. Redox Signaling* 12 (1), 1–13. doi:10.1089/ars.2008.2282

Li, J., Li, M., Li, L., Ma, J., Yao, C., and Yao, S. (2022). Hydrogen Sulfide Attenuates Ferroptosis and Stimulates Autophagy by Blocking mTOR Signaling in Sepsis-

Induced Acute Lung Injury. *Mol. Immunol.* 141, 318–327. doi:10.1016/j.molimm.2021.12.003

Li, N., Wang, W., Zhou, H., Wu, Q., Duan, M., Liu, C., et al. (2020). Ferritinophagy-mediated Ferroptosis Is Involved in Sepsis-Induced Cardiac Injury. *Free Radic. Biol. Med.* 160, 303–318. doi:10.1016/j.freeradbiomed.2020.08.009

Liu, C., Li, B., Yan, Q., Niu, S., Zhao, Y., Xiong, C., et al. (2021). Protective Effects and Mechanisms of Recombinant Human Glutathione Peroxidase 4 on Isoproterenol-Induced Myocardial Ischemia Injury. *Oxidative Med. Cell Longevity* 2021, 1–17. doi:10.1155/2021/6632813

Matsushita, M., Freigang, S., Schneider, C., Conrad, M., Bornkamm, G. W., and Kopf, M. (2015). T Cell Lipid Peroxidation Induces Ferroptosis and Prevents Immunity to Infection. *J. Exp. Med.* 212 (4), 555–568. doi:10.1084/jem.20140857

McMaster, W. G., Kirabo, A., Madhur, M. S., and Harrison, D. G. (2015). Inflammation, Immunity, and Hypertensive End-Organ Damage. *Circ. Res.* 116 (6), 1022–1033. doi:10.1161/CIRCRESAHA.116.303697

Muri, J., Thut, H., Bornkamm, G. W., and Kopf, M. (2019). B1 and Marginal Zone B Cells but Not Follicular B2 Cells Require Gpx4 to Prevent Lipid Peroxidation and Ferroptosis. *Cel Rep.* 29 (9), 2731–2744.e4. doi:10.1016/j.celrep.2019.10.070

Niu, Y., Du, C., Cui, C., Zhang, H., Deng, Y., Cai, J., et al. (2021). Norswertianolin Promotes Cystathionine γ-Lyase Activity and Attenuates Renal Ischemia/Reperfusion Injury and Hypertension. *Front. Pharmacol.* 12, 677212. doi:10.3389/fphar.2021.677212

Parsanathan, R., and Jain, S. K. (2018). Hydrogen Sulfide Increases Glutathione Biosynthesis, and Glucose Uptake and Utilisation in C2C12 Mouse Myotubes. *Free Radic. Res.* 52 (2), 288–303. doi:10.1080/10715762.2018.1431626

Qi, Y.-X., Han, Y., and Jiang, Z.-L. (2018). Mechanobiology and Vascular Remodeling: From Membrane to Nucleus. *Adv. Exp. Med. Biol.* 1097, 69–82. doi:10.1007/978-3-319-96445-4_4

Qiu, J., Zheng, Y., Hu, J., Liao, D., Gregersen, H., Deng, X., et al. (2014). Biomechanical Regulation of Vascular Smooth Muscle Cell Functions: from *In Vitro* to *In Vivo* Understanding. *J. R. Soc. Interf.* 11 (90), 20130852. doi:10.1098/rsif.2013.0852

Qiu, Y., Cao, Y., Cao, W., Jia, Y., and Lu, N. (2020). The Application of Ferroptosis in Diseases. *Pharmacol. Res.* 159, 104919. doi:10.1016/j.phrs.2020.104919

Rajagopalan, S., Meng, X. P., Ramasamy, S., Harrison, D. G., and Galis, Z. S. (1996). Reactive Oxygen Species Produced by Macrophage-Derived Foam Cells Regulate the Activity of Vascular Matrix Metalloproteinases *In Vitro*. Implications for Atherosclerotic Plaque Stability. *J. Clin. Invest.* 98 (11), 2572–2579. doi:10.1172/JCI119076

Rodrigues, C., and Percival, S. (2019). Immunomodulatory Effects of Glutathione, Garlic Derivatives, and Hydrogen Sulfide. *Nutrients* 11 (2), 295. doi:10.3390/nu11020295

Stockwell, B. R., Friedmann Angeli, J. P., Bayir, H., Bush, A. I., Conrad, M., Dixon, S. J., et al. (2017). Ferroptosis: A Regulated Cell Death Nexus Linking Metabolism, Redox Biology, and Disease. *Cell* 171 (2), 273–285. doi:10.1016/j.cell.2017.09.021

Tabassum, R., and Jeong, N. Y. (2019). Potential for Therapeutic Use of Hydrogen Sulfide in Oxidative Stress-Induced Neurodegenerative Diseases. *Int. J. Med. Sci.* 16 (10), 1386–1396. doi:10.7150/ijms.36516

Takaishi, K., Kinoshita, H., Kawashima, S., and Kawahito, S. (2021). Human Vascular Smooth Muscle Function and Oxidative Stress Induced by NADPH Oxidase with the Clinical Implications. *Cells* 10 (8), 1947. doi:10.3390/cells10081947

Takayama, K., Ogawa, M., Mochizuki, M., and Takeuchi, M. (2013). Cytomegalovirus Retinitis in a Patient with Proliferative Diabetes Retinopathy. *Ocul. Immunol. Inflamm.* 21 (3), 225–226. doi:10.3109/09273948.2012.762983

Tang, D., Chen, X., Kang, R., and Kroemer, G. (2021). Ferroptosis: Molecular Mechanisms and Health Implications. *Cell Res* 31 (2), 107–125. doi:10.1038/s41422-020-00441-1

Touyz, R. M., Alves-Lopes, R., Rios, F. J., Camargo, L. L., Anagnostopoulou, A., Arner, A., et al. (2018). Vascular Smooth Muscle Contraction in Hypertension. *Cardiovasc. Res.* 114 (4), 529–539. doi:10.1093/cvr/cvy023

Touyz, R. M., and Schiffrin, E. L. (2001). Increased Generation of Superoxide by Angiotensin II in Smooth Muscle Cells from Resistance Arteries of Hypertensive Patients: Role of Phospholipase D-dependent NAD(P)H Oxidase-Sensitive Pathways. *J. Hypertens.* 19 (7), 1245–1254. doi:10.1097/00004872-200107000-00009

Tsurusaki, S., Tsuchiya, Y., Koumura, T., Nakasone, M., Sakamoto, T., Matsuoka, M., et al. (2019). Hepatic Ferroptosis Plays an Important Role as the Trigger for Initiating Inflammation in Nonalcoholic Steatohepatitis. *Cell Death Dis* 10 (6), 449. doi:10.1038/s41419-019-1678-y

Vinchi, F., Porto, G., Simmelbauer, A., Altamura, S., Passos, S. T., Garbowski, M., et al. (2020). Atherosclerosis Is Aggravated by Iron Overload and Ameliorated by Dietary and Pharmacological Iron Restriction. *Eur. Heart J.* 41 (28), 2681–2695. doi:10.1093/eurheartj/ehz112

Wang, L., Cai, H., Hu, Y., Liu, F., Huang, S., Zhou, Y., et al. (2018). A Pharmacological Probe Identifies Cystathionine β-synthase as a New Negative Regulator for Ferroptosis. *Cel Death Dis* 9 (10), 1005. doi:10.1038/s41419-018-1063-2

Wang, Y., Quan, F., Cao, Q., Lin, Y., Yue, C., Bi, R., et al. (2021a). Quercetin Alleviates Acute Kidney Injury by Inhibiting Ferroptosis. *J. Adv. Res.* 28, 231–243. doi:10.1016/j.jare.2020.07.007

Wang, Y., Wang, S., Xin, Y., Zhang, J., Wang, S., Yang, Z., et al. (2021b). Hydrogen Sulfide Alleviates the Anxiety-like and Depressive-like Behaviors of Type 1 Diabetic Mice via Inhibiting Inflammation and Ferroptosis. *Life Sci.* 278, 119551. doi:10.1016/j.lfs.2021.119551

Wang, Y., Yu, R., Wu, L., and Yang, G. (2021c). Hydrogen Sulfide Guards Myoblasts from Ferroptosis by Inhibiting ALOX12 Acetylation. *Cell Signal.* 78, 109870. doi:10.1016/j.cellsig.2020.109870

Wu, X., Li, Y., Zhang, S., and Zhou, X. (2021). Ferroptosis as a Novel Therapeutic Target for Cardiovascular Disease. *Theranostics* 11 (7), 3052–3059. doi:10.7150/thno.54113

Xiao, F.-J., Zhang, D., Wu, Y., Jia, Q.-H., Zhang, L., Li, Y.-X., et al. (2019). miRNA-17-92 Protects Endothelial Cells from Erastin-Induced Ferroptosis through Targeting the A20-ACSL4 axis. *Biochem. Biophysical Res. Commun.* 515 (3), 448–454. doi:10.1016/j.bbrc.2019.05.147

Yang, G., Zhao, K., Ju, Y., Mani, S., Cao, Q., Puukila, S., et al. (2013). Hydrogen Sulfide Protects against Cellular Senescence via S-Sulfhydration of Keap1 and Activation of Nrf2. *Antioxid. Redox Signaling* 18 (15), 1906–1919. doi:10.1089/ars.2012.4645

Yang, W. S., and Stockwell, B. R. (2016). Ferroptosis: Death by Lipid Peroxidation. *Trends Cel Biol.* 26 (3), 165–176. doi:10.1016/j.tcb.2015.10.014

Zhou, J., Li, Y.-S., and Chien, S. (2014). Shear Stress-Initiated Signaling and its Regulation of Endothelial Function. *Arterioscler Thromb. Vasc. Biol.* 34 (10), 2191–2198. doi:10.1161/ATVBAHA.114.303422

Conflict of Interest: The authors declare that the research was conducted in the absence of any commercial or financial relationships that could be construed as a potential conflict of interest.

Publisher's Note: All claims expressed in this article are solely those of the authors and do not necessarily represent those of their affiliated organizations, or those of the publisher, the editors, and the reviewers. Any product that may be evaluated in this article, or claim that may be made by its manufacturer, is not guaranteed or endorsed by the publisher.

Copyright © 2022 Jin, Yang, Cui, Zhang, Cai, Geng and Chen. This is an open-access article distributed under the terms of the Creative Commons Attribution License (CC BY). The use, distribution or reproduction in other forums is permitted, provided the original author(s) and the copyright owner(s) are credited and that the original publication in this journal is cited, in accordance with accepted academic practice. No use, distribution or reproduction is permitted which does not comply with these terms.

frontiers in Cell and Developmental Biology

REVIEW
published: 14 February 2022
doi: 10.3389/fcell.2022.809425

$G\alpha_{12}$ and $G\alpha_{13}$: Versatility in Physiology and Pathology

Paipai Guo[1], Yu Tai[1], Manman Wang[1], Hanfei Sun[1], Lingling Zhang[1], Wei Wei[1], Yang K. Xiang[2,3] and Qingtong Wang[1]**

[1]Key Laboratory of Anti-inflammatory and Immune Medicine, Ministry of Education, Collaborative Innovation Center of Anti-inflammatory and Immune Medicine, Institute of Clinical Pharmacology, Anhui Medical University, Hefei, China, [2]Department of Pharmacology, University of California, Davis, Davis, CA, United States, [3]VA Northern California Health Care System, Mather, CA, United States

G protein-coupled receptors (GPCRs), as the largest family of receptors in the human body, are involved in the pathological mechanisms of many diseases. Heterotrimeric G proteins represent the main molecular switch and receive cell surface signals from activated GPCRs. Growing evidence suggests that $G\alpha_{12}$ subfamily ($G\alpha_{12/13}$)-mediated signaling plays a crucial role in cellular function and various pathological processes. The current research on the physiological and pathological function of $G\alpha_{12/13}$ is constantly expanding, Changes in the expression levels of $G\alpha_{12/13}$ have been found in a wide range of human diseases. However, the mechanistic research on $G\alpha_{12/13}$ is scattered. This review briefly describes the structural sequences of the $G\alpha_{12/13}$ isoforms and introduces the coupling of GPCRs and non-GPCRs to $G\alpha_{12/13}$. The effects of $G\alpha_{12/13}$ on RhoA and other signaling pathways and their roles in cell proliferation, migration, and immune cell function, are discussed. Finally, we focus on the pathological impacts of $G\alpha_{12/13}$ in cancer, inflammation, metabolic diseases, fibrotic diseases, and circulatory disorders are brought to focus.

Keywords: G protein-coupled receptor, $G\alpha_{12}$, $G\alpha_{13}$, cell pathophysiology, diseases

OPEN ACCESS

Edited by:
Zhiqiang Lin,
Masonic Medical Research Institute (MMRI), United States

Reviewed by:
Amanda Mackenzie,
BioAscent, United Kingdom
Henry Alexander Dunn,
Western University, Canada

****Correspondence:***
Yang K. Xiang
ykxiang@ucdavis.edu
Qingtong Wang
hfwqt727@163.com

Specialty section:
This article was submitted to Cell Death and Survival, a section of the journal Frontiers in Cell and Developmental Biology

Received: *05 November 2021*
Accepted: *17 January 2022*
Published: *14 February 2022*

Citation:
Guo P, Tai Y, Wang M, Sun H, Zhang L, Wei W, Xiang YK and Wang Q (2022) $G\alpha_{12}$ and $G\alpha_{13}$: Versatility in Physiology and Pathology. Front. Cell Dev. Biol. 10:809425. doi: 10.3389/fcell.2022.809425

INTRODUCTION

G protein-coupled receptors (GPCRs) family are a superfamily of membrane receptors responsible for signal transduction in cells. GPCRs are extensively studied drug targets because they participate in a broad range of human physiological and pathological processes. There are currently 481 drugs (about 34% of all drugs approved by the FDA) acting on 107 unique GPCRs to treat different diseases, including neurological disorders, metabolic and cardiovascular diseases, cancer, and inflammation (Hauser et al., 2017; Wang et al., 2020). Heterotrimeric G proteins are sensors for GPCR active conformations and trigger intracellular signal transduction (Maziarz et al., 2020). Heterotrimeric G proteins are composed of Gα, Gβ, and Gγ subunits, which are mainly located on the inner leaflet of the plasma membrane (Bondar and Lazar, 2021). Gα proteins are divided into four categories based on sequence homology and downstream effectors: $G\alpha_s$ (s stands for stimulation), $G\alpha_{i/o}$ (i stands for inhibition), $G\alpha_{q/11}$, and $G\alpha_{12/13}$ (Hilger et al., 2018; Yang et al., 2020). The function of $G\alpha_s$, $G\alpha_{i/o}$, and $G\alpha_q$ have been well documented. Meanwhile, the progress in understanding the function of the $G\alpha_{12/13}$ family, which was discovered in the early 1990s, has been relatively slow (Kim et al., 2018a). Nevertheless, with the development of new research tools (for example, constitutively active mutants, fusion proteins, and gene knockout, etc.), progress has been made in further to understanding the function of $G\alpha_{12/13}$ in recent years (Worzfeld et al., 2008).

$G\alpha_{12/13}$ subunits are expressed in most cell types and are able to induce diversified cellular signaling and responses that are important players in health and disease. $G\alpha_{12}$ and $G\alpha_{13}$ share 67% of their amino acid sequence and have many downstream signaling targets in commm (Montgomery et al., 2014; Stecky et al., 2020). Some of the pathways that are triggered by both $G\alpha_{12}$ and $G\alpha_{13}$ include phospholipase C (PLC)-ε and phospholipase D, mitogen-activated protein kinase (MAPK), and Na/H-exchange which promote cytoskeletal alterations, carcinogenic responses, and apoptosis (Litosch, 2012; Dusaban et al., 2013; Xie et al., 2016). Moreover, $G\alpha_{12/13}$ interacts with specific guanine nucleotide exchange factors (GEFs) (e.g., p115RhoGEF, leukemia-related RhoGEF, and PDZ-RhoGEF) to activate downstream effectors, including ras homolog family member A (RhoA), PLC, adenylate cyclase, and a variety of ion channels (Mikelis et al., 2013). These effectors, in turn, regulate the concentration of secondary messengers in the cells, such as diglycerides, cyclic adenosine monophosphate (cAMP), sodium ions, and calcium ions. Together, the activated RhoA and sencodary messengers eventually lead to physiological responses (Jiang et al., 2008; Kalwa et al., 2015; Wang et al., 2019). Furthermore, $G\alpha_{12/13}$ subunits also regulate the activity of a variety of transcription factors, such as signal transducer and activator of transcription 3, serum response factor (SRF), activator protein 1 (AP-1), and activated T cell nuclear factor (NFAT) (Kumar et al., 2006; Lee et al., 2009; Song et al., 2018; Yagi et al., 2019). Abnormally elevated upstream stimuli promote the incidence and development of diseases by increasing the corresponding receptor coupling to $G\alpha_{12}$ and/or $G\alpha_{13}$ (Yang et al., 2020; Rasheed et al., 2021). In this review, the structure of $G\alpha_{12}$ and $G\alpha_{13}$ is reviewed along with their roles in GPCR signal pathways, cell function, and disease pathogenesis.

The Amino Acid Structure of $G\alpha_{12}$ and $G\alpha_{13}$

The $G\alpha_{12/13}$ subfamily consists of two α subunits encoded by *GNA12* and *GNA13*. The $G\alpha_{12/13}$ subunits were originally discovered based on the amino acid sequence similarity with other Gα subunits and their insensitivity to pertussis toxin (Arang and Gutkind, 2020). The structure of $G\alpha_{12/13}$ subunit consists of an amino-terminal α-helical domain and a Ras-like GTPase domain. There is a link between these two domains involved in binding to GDP and GTP (Syrovatkina et al., 2016; Smrcka and Fisher, 2019). In response to activation of GPCR, the conformation of GDP-bound inactive $G\alpha_{12/13}$ is transformed into the active form with GTP binding, triggering the dissociation of $G\alpha_{12/13}$ from Gβγ and activation of downstream effectors (Arthofer et al., 2016). After dissociation, free Gβγ subunits transmit signals through regulating canonical effectors, including adenylate cyclase, PLC, and various ion channels (Senarath et al., 2018). Gβγ subunits also regulate a series of non-canonical effectors, such as the nuclear import of the extracellular regulated protein kinases (ERK) 1/2, oxidative phosphorylation, and mRNA processing (Khan et al., 2016). The large number of Gβγ subunits in mammal cells define much of the diversity that occurs within GPCR signaling with resepect to spatial and temporal bias and are extensively involved in the pathogenesis of diseases (Masuho et al., 2021). Gβγ signaling has been previously well summarized.

Although Gβγ-mediated effects of GPCR signaling are diverse, the assorted isoforms of Gα also have a wide variety of influences. These varied functions are highly related to their structures. Under present consideration, $G\alpha_{12}$ has four isoforms, of which isoform 1 is the longest isoform containing 381 amino acids (**Figure 1**). Compared with isoform 1, the encoded isoform 2 (305 amino acids) and isoform 3 (322 amino acids) are shorter and have different N-termini. Both $G\alpha_{12}$ isoform 2 and 3 have distinct 5′ untranslated region and 5′ coding region for different N-termini. The isoform 4 of $G\alpha_{12}$ lacks in-frame exons in the 3′ coding region relative to the isoform 1; the encoded isoform 4 (364 amino acids) is also shorter than isoform 1. $G\alpha_{13}$ has two isoforms, of which isoform 1 is the longer isoform containing 377 amino acids. The isoform 2 of $G\alpha_{13}$ uses an alternative 5′ exons resulting in a downstream start codon AUG. Thus, the encoded isoform 2 of $G\alpha_{13}$ has a shorter N-terminus than the isoform 1. The isoform sequences of $G\alpha_{12}$ or $G\alpha_{13}$ show similar structural domains, including an adenylyl cyclase binding site, a β-γ complex binding site, a switch I region (one of two surface loops that undergo conformational changes upon GTP binding), a switch II region, and a putative receptor binding site, respectively, (Lambright et al., 1996; Sunahara et al., 1997; Tesmer et al., 1997). Additional difference in the amino acid sequence of each isoform may provide tissue specific expression and cellular localization to fulfill the broad functional roles of the $G\alpha_{12}$ or $G\alpha_{13}$.

While literature clearly show that $G\alpha_{12/13}$ has different functions from other Gα subtypes, the functional difference between the isoforms of $G\alpha_{12}$ and $G\alpha_{13}$ has not been reported. Future studies on the structure-functional relationship between these isoforms will help understanding their roles in cells and diseases.

Regulation Network of $G\alpha_{12/13}$

$G\alpha_{12/13}$ has been shown to couple to more than 30 GPCRs. Activated by various upstream stimuli, $G\alpha_{12/13}$ can transmit to divergent downstream signaling pathways and regulates cell function in pathophysiological processes (Ackerman et al., 2015; Yung et al., 2017; Yanagida et al., 2018; Spoerri et al., 2020). $G\alpha_{12}$ and $G\alpha_{13}$ are broadly expressed, yet gene deficiency in mice shows that they are not interchangeable (Yang et al., 2020). Some GPCRs preferentially couple to either $G\alpha_{12}$ or $G\alpha_{13}$ (Ayoub and Pin, 2013; Yung et al., 2017; Mackenzie et al., 2019). Moreover, non-GPCRs are also shown to couple to $G\alpha_{12}$ and $G\alpha_{13}$ (Shen et al., 2013; Shen et al., 2015; Piccinin et al., 2019) (**Table 1**).

GPCRs Triggered $G\alpha_{12/13}$ Signaling

Lysophosphatidic Acid Receptors

Lysophosphatidic acid (LPA) is a biologically active phospholipid, which mediates various biological functions through six homologous LPA receptors (LAPRs) (Plastira et al., 2020). Activated LPARs promote $G\alpha_{12}$, but not $G\alpha_{13}$, association with v-raf murine sarcoma viral oncogene homolog A which than activates ERK. The activated ERK promotes ring

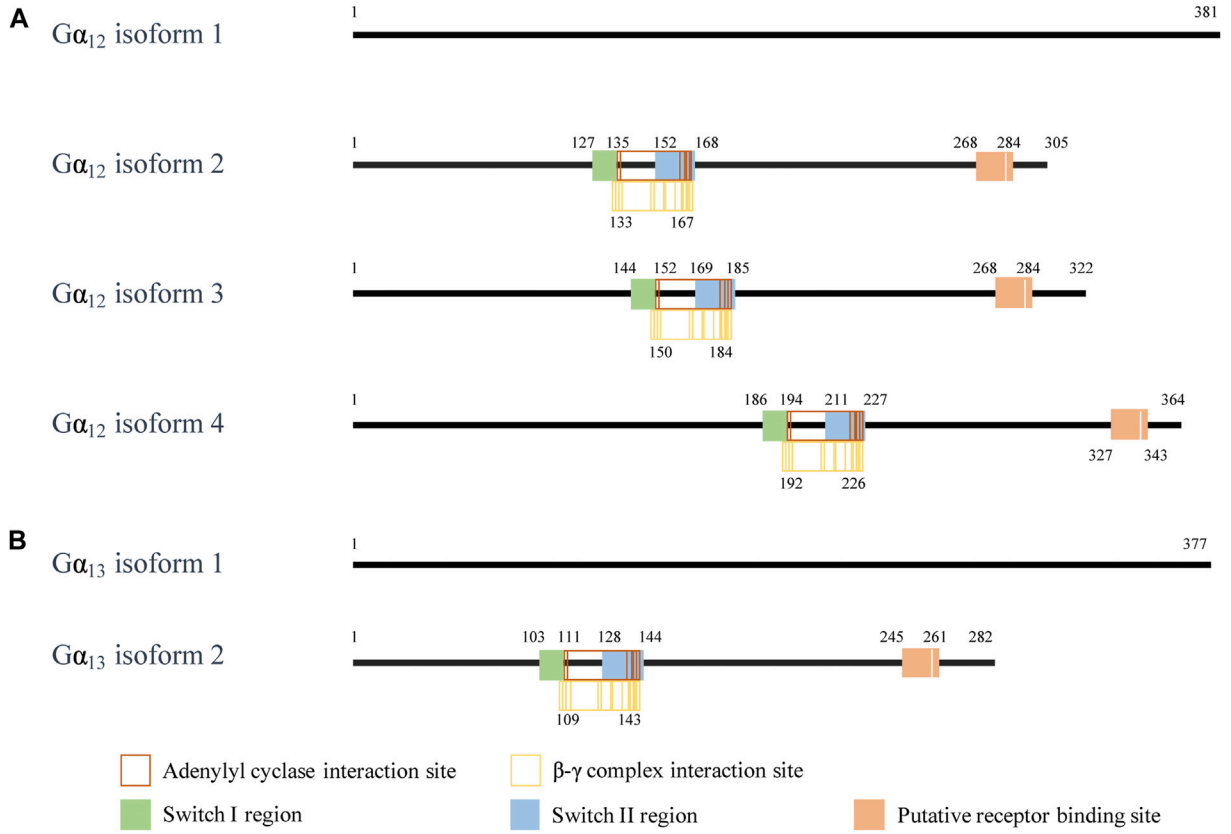

FIGURE 1 | The interaction site of the $G\alpha_{12/13}$ isoform. **(A)** The interaction sites on the amino acid fragment of $G\alpha_{12}$ isoforms. **(B)** The interaction sites on the amino acid fragment of $G\alpha_{13}$ isoforms. The information on the interaction sites of $G\alpha_{12}$ and $G\alpha_{13}$ is from NCBI. In NCBI reference sequence database, the human *GNA12* isoforms are NP_031379.2, NP_001269369.1, NP_001269370.1, and NP_001280021.1. (https://www.ncbi.nlm.nih.gov/gene/2768). The human *GNA13* isoforms are NP_006563.2 and NP_001269354.1. (https://www.ncbi.nlm.nih.gov/gene/10672).

finger and FYVE like domain-containing E3 ubiquitin protein ligase transcription and fibroblast migration (Gan et al., 2013). LPAR-$G\alpha_{12/13}$ signaling also plays an important role in embryonic blood vessel development (Tanaka et al., 2006). Additionally, LPAR1/2 couple with $G\alpha_{i/o}$, $G\alpha_{q/11}$, as well as $G\alpha_{12/13}$ to activate a variety of downstream pathways, such as protein kinase B (PKB, commonly known as AKT), RhoA, MAPK, and phosphatidylinositol 3-kinase (PI3K), and regulates cell proliferation, migration, and cytoskeleton rearrangement (Kihara et al., 2014). Previous studies have identified that LPAR4/6 can effectively couple to $G\alpha_{12/13}$ to stimulate Rho GTPase, which subsequently activates Rho-associated protein kinase (ROCK) I/II, leading to changes in the tension of the actin cytoskeleton (Noguchi et al., 2003; Yanagida et al., 2009). The LPAR4/6-activated $G\alpha_{12/13}$-Rho-ROCK signal also promotes nuclear translocation of Yes-associated protein/transcriptional coactivator with PDZ-binding motif (YAP/TAZ) (Yasuda et al., 2019). YAP/TAZ promotes the proliferation of cancer cells (such as liver, bladder, and lung cancers) and accelerates the progress of cancer (Yagi et al., 2016; Maziarz et al., 2020). Activation of LPAR5 also induces axon retraction and stress fiber formation through an LPA-LPAR5-$G\alpha_{12/13}$ pathway (Lee et al., 2006). As of today, there is no evidence supporting a coupling between LPAR3 and $G\alpha_{12/13}$.

Frizzleds

Frizzled (FZD) receptors are unconventional GPCRs, which can be activated by the *Wingless/Int-1* lipoglycoprotein (WNT) family (Janda et al., 2017). FZD4 interacts with $G\alpha_{12/13}$ and does not interact with other subunits of the G protein family. The complex formed by FZD4 and $G\alpha_{12/13}$ is dissociated under WNT stimulation. The FZD4-$G\alpha_{12/13}$ signaling mediates cytoskeletal rearrangement and Rho signaling through p115RhoGEF, affecting angiogenesis in embryonic and tumor development (Arthofer et al., 2016). WNT5a/b and WNT3a bind to the receptor tyrosine kinase-like orphan receptor 1/2-FZD complex, activating Rho GTPases through $G\alpha_{12/13}$. The activated Rho inhibits the activity of large tumor suppressor 1/2 (LATS1/2), leading to YAP/TAZ dephosphorylation and nuclear translocation and promoting bone formation and cell migration (Park et al., 2015). Interestingly, a similar mechanism has been found in brain endothelial cells. The FZD10-$G\alpha_{13}$ complex dissociates under WNT5a/7a stimulation, and $G\alpha_{13}$ transmits a signal to YAP/TAZ through Rho family members (Hot et al., 2017). In osteoblasts, WNT family member 16 binds to

TABLE 1 | List of biologically significant $G\alpha_{12/13}$-associated receptors and their physiological functions.

Receptors	G proteins	Functions	References
		GPCRs	
LPA receptor	$G\alpha_{12}$	Migration of fibroblasts	Gan et al. (2013)
LPA receptor	$G\alpha_{12/13}$	Embryonic blood vessel development	Tanaka et al. (2006)
LPAR1	$G\alpha_{12}$	Proliferation of astrocytes	Loskutov et al. (2018)
LPAR1/LPAR2	$G\alpha_{12/13}$	Cell proliferation, migration, and cytoskeleton changes	Kihara et al. (2014)
LPAR4/LPAR6	$G\alpha_{12/13}$	Changes in the tension of the actin cytoskeleton	(Noguchi et al. (2003), Yanagida et al. (2009)
LPAR4/LPAR6	$G\alpha_{12/13}$	Angiogenesis	Yasuda et al. (2019)
LPAR5	$G\alpha_{12/13}$	Axon retraction and stress fiber formation	Lee et al. (2006)
FZD	$G\alpha_{12/13}$	Bone formation and cell migration	Park et al. (2015)
FZD	$G\alpha_{12/13}$	Bone homeostasis	Hendrickx et al. (2020)
FZD4	$G\alpha_{12/13}$	Angiogenesis	Arthofer et al. (2016)
FZD10	$G\alpha_{13}$	Angiogenesis	Hot et al. (2017)
PAR1/PAR2	$G\alpha_{13}$	Fibroblast adhesion maturation, spreading, and migration	Spoerri et al. (2020)
PAR1	$G\alpha_{12/13}$	Stress fiber formation	Regué et al. (2013)
PAR2	$G\alpha_{13}$	Smooth muscle contraction	Sriwai et al. (2013)
S1PR1/S1PR3/S1PR5	$G\alpha_{12}$	Inflammation	Ki et al. (2007)
S1PR2	$G\alpha_{12/13}$	Vascular smooth muscle cell migration and neointimal hyperplasia	Kim et al. (2011)
S1PR2	$G\alpha_{12/13}$	Myofibroblast contraction	Sobel et al. (2015)
S1PR2	$G\alpha_{13}$	Cardiomyocyte migration	Ye and Lin, (2013)
S1PR2/S1PR3	$G\alpha_{12/13}$	Stress fiber formation	Olivera et al. (2003)
S1PR2/S1PR3	$G\alpha_{12/13}$	Cardiac progenitor cell proliferation	Castaldi et al. (2016)
S1PR3	$G\alpha_{12/13}$	Inflammation	Dusaban et al. (2017)
S1PR3	$G\alpha_{13}$	Cardioprotection	Yung et al. (2017)
M1R	$G\alpha_{13}$	Impaired growth	Sabbir et al. (2018)
M3R	$G\alpha_{12}$	Human airway smooth muscle cells contraction	Yoo et al. (2017)
CXCR4	$G\alpha_{13}$	Tumor cell migration and adhesion	Scarlett et al. (2018)
CXCR4	$G\alpha_{13}$	Breast cancer metastasis	Yagi et al. (2011)
Calcium-sensing receptor	$G\alpha_{12/13}$	Gene expression, cytoskeleton, and cell shape	Leach et al. (2012), Leach et al. (2013)
AT_1R	$G\alpha_{12/13}$	Vasoconstriction	Lymperopoulos et al. (2021)
Thromboxane A2 receptor	$G\alpha_{12/13}$	Neointima formation and restenosis	Feng et al. (2016)
Ghrelin receptor	$G\alpha_{12}$	Food intake	Mende et al. (2018)
Dopamine D3 receptor	$G\alpha_{12}$	Inhibit inflammation	Wang et al. (2015)
5-HT_4R	$G\alpha_{13}$	Hippocampal synaptic function	Müller et al. (2021)
5-HT_4R	$G\alpha_{13}$	Angiogenesis	Profirovic et al. (2013)
UII receptor	$G\alpha_{13}$	Tumor invasion	Lecointre et al. (2015)
Complement C5a receptor	$G\alpha_{12/13}$	Macrophage tail retraction	Raghavan et al. (2018)
GPR56	$G\alpha_{12/13}$	Myelination	Ackerman et al. (2015)
Purinergic receptor 6	$G\alpha_{13}$	Cell migration	Girard et al. (2020)
Gastrin type 2 cholecystokinin receptor	$G\alpha_{13}$	Cell migration	Masià-Balagué et al. (2015)
GPR40	$G\alpha_{12/13}$	Release of insulin vesicles	Rives et al. (2018)
GPR56	$G\alpha_{12/13}$	Muscle protein synthesis and myotube hypertrophy	White et al. (2014)
GPR91	$G\alpha_{12}$	Mitochondrial fission and cell migration	Ko et al. (2017)
ET-1 type A receptor	$G\alpha_{12/13}$	Formation of myofibroblasts	Nishida et al. (2007)
		Non-GPCRs	
Integrin β_1	$G\alpha_{13}$	Cell migration	Shen et al. (2013), Shen et al. (2015)
Integrin $\alpha_{IIb}\beta_3$	$G\alpha_{13}$	Cell retraction and migration	Gong et al. (2010)
Integrin $\alpha_{IIb}\beta_3$	$G\alpha_{13}$	Promote thrombosis	Pang et al. (2018)
PPARγ	$G\alpha_{13}$	Inhibit thrombosis	Unsworth et al. (2017)
Smoothened	$G\alpha_{12}$	Tumor growth and anti-apoptosis	Qu et al. (2013)

FZD receptors to activate canonical WNT signaling and non-canonical $G\alpha_{12/13}$ signaling and regulate bone homeostasis (Hendrickx et al., 2020).

Protease-Activated Receptors

Protease-activated receptors (PARs) consist of four subtypes (PAR1-4). PARs play an important role in blood vessel development, cell proliferation, tumorigenesis, and thrombosis (Chandrabalan and Ramachandran, 2021). In fibroblasts, PAR1/2 send signals to integrin $\alpha_5\beta_1$ through Gβγ and PI3K to induce fibronectin binding and initiate cell adhesion. PAR1/2 also send signals through $G\alpha_{13}$, $G\alpha_i$, ROCK, and Src to enhance integrin $\alpha_5\beta_1$-mediated adhesion (Spoerri et al., 2020). The PAR1-mediated $G\alpha_{12/13}$ activation stimulates RhoGEF and simultaneously activates the RhoA-ROCK pathway and myosin light chain (Flaumenhaft and De Ceunynck, 2017). Stimulation of PAR1 also initiates the assembly of F-actin through the $G\alpha_{12/13}$-RhoA pathway, which induces YAP dephosphorylation and nuclear translocation, thereby promoting cell migration and invasion (Regué et al., 2013). PAR2 couples with $G\alpha_q$, $G\alpha_i$, and $G\alpha_{13}$ to stimulate RhoA-ROCK activity independently of the cyclic adenosine

monophosphate-protein kinase A pathway to induce smooth muscle contraction (Sriwai et al., 2013). An earlier study found that in endothelial cells, PAR3 directly interacts with PAR1 to change the binding conformation of PAR1/$G\alpha_{13}$, induce the activation of downstream signaling pathways, and promote endothelial barrier dysfunction (McLaughlin et al., 2007). Presently, there is no clear evidence showing a direct interaction between PAR3/4 and $G\alpha_{12/13}$.

Sphingosine 1-Phosphate Receptors

Sphingosine 1-phosphate (S1P) is a natural biologically active lipid molecule that binds to five different S1P receptors (S1PR1-5). Activated S1PRs couple with $G\alpha_{12/13}$ to induce downstream signals (Zhang et al., 2020). An earlier study shows that S1PR2/S1PR3 couple to $G\alpha_{12/13}$ and send an "inside-out" signal to mediate the formation of stress fibers (Olivera et al., 2003). After binding to S1P, S1PR1/3/5 couple with $G\alpha_{12}$ and activate the c-Jun N-terminal kinase (JNK)-nuclear factor-kappa B (NF-κB) pathway to promote the expression of cyclooxygenase-2 and accelerate local inflammation (Ki et al., 2007). S1PR3 activates the $G\alpha_{12/13}$-RhoA pathway and promotes the expression of inflammatory gene in astrocytes (Dusaban et al., 2017). S1PR3 activates $G\alpha_{13}$-RhoA in cardiomyocytes and mediates cardio-protection during ischemia/reperfusion (I/R) (Yung et al., 2017). In vascular smooth muscle cells, S1PR2 couples to $G\alpha_{12/13}$ to activate AP-1-dependent induction of cysteine-rich protein 61 and promote the migration of vascular smooth muscle cells and neointimal hyperplasia (Kim et al., 2011). S1PR2 also induces the contraction of myofibroblasts through the $G\alpha_{12/13}$-Rho-ROCK pathway (Sobel et al., 2015). Moreover, $G\alpha_{12}$, activated by S1PR2, is recruited to E-cadherin to form a complex after mechanical stress. $G\alpha_{12}$ then recruits and activates p114RhoGEF, driving RhoA signaling and increasing the tensile strength of multicellular connections (Acharya et al., 2018).

Muscarinic Acetylcholine Receptors

Muscarinic acetylcholine receptors have five different subtypes (M1R-M5R) (Ruan et al., 2021). The increase of acetylcholine signal in neurons leads to the overexpression of M1R, promoting the polymerization of $G\alpha_{13}$ and Gβγ (Sabbir et al., 2018). $G\alpha_{13}$ disrupts the stability of tubulin polymer through the RhoA-ROCK signal, reducing mitochondrial transport and impairing growth in neurites (Sabbir et al., 2018). Early study has shown that M3R promotes the activity of phospholipase D through $G\alpha_{12}$ in HEK-293 cells (Rümenapp et al., 2001). It has also been found that $G\alpha_{12}$ binds to M3R in human airway smooth muscle cells. The M3R-$G\alpha_{12}$ signaling is important in promoting the contraction of human airway smooth muscle cells by inducing PI3K-mediated ROCK activation in a RhoA-dependent manner (Yoo et al., 2017).

Chemokine Receptors

The binding of chemokine C-X-C motif chemokine 12 (CXCL12) to C-X-C chemokine receptor 4 (CXCR4) activates RhoA through $G\alpha_{13}$, which leads to ROCK phosphorylation of myosin light chain and promotes cell migration and adhesion (Scarlett et al., 2018). In metastatic breast cancer cells, CXCR4 activates small Rho GTPases through $G\alpha_{13}$ to initiate cell motility and trans-endothelial migration (Yagi et al., 2011).

Non-GPCRs Triggered $G\alpha_{12/13}$ Signaling

Integrin "outside-in" signaling requires $G\alpha_{13}$ and monomeric small G proteins (i.e., Rho) to mediate cell retraction, migration, and spreading (Shen et al., 2012). $G\alpha_{13}$ directly binds to the ExE motif in the cytoplasmic domain of the integrin β_3 subunits, which is important in transducing the "outside-in" integrin signaling (Shen et al., 2013). $G\alpha_{13}$ also binds to the cytoplasmic domain of the integrin β_1 subunit in platelets, which mediates the Src-dependent transient inhibition of RhoA, activates the Rac1 and PI3K pathways, and promotes cell migration (Shen et al., 2013; Shen et al., 2015). Interfering with the expression of $G\alpha_{13}$ reduces $\alpha_{IIb}\beta_3$-dependent activation of c-Src, inhibits cell migration, and accelerates cell contraction, thereby spreading platelets on fibrinogen (Gong et al., 2010). Integrin $\alpha_{IIb}\beta_3$ also serves as a mechanical sensor that transmits "outside-in" signals through $G\alpha_{13}$-Src-Rac1-dependent pathways in platelets and facilitates coagulation *in vitro* and intravascularly *in vivo* (Pang et al., 2018). Therefore, the $G\alpha_{13}$-integrin interaction is important in thrombosis.

Additionally, peroxisome proliferator-activated receptor-γ (PPARγ), a member of the nuclear hormone superfamily, regulates lipid and glucose metabolism and homeostasis in many metabolic pathways (Piccinin et al., 2019). Treatment of platelets with PPARγ agonists leads to decreased binding between $G\alpha_{13}$ and integrin β_3, which prevents c-Src-dependent integrin β_3 phosphorylation and talin dissociation and weakens the downstream signal transduction of integrin $\alpha_{IIb}\beta_3$, thereby regulating platelet activation and reducing thrombosis (Unsworth et al., 2017). Moreover, in diffuse large B-cell lymphoma (DLBCL), smoothened recruits $G\alpha_i$ and $G\alpha_{12}$ and activates the protein kinase C (PKC)-caspase recruitment domain and membrane-associated guanylate kinase-like domain protein 1-dependent signaling cascade, which promotes activation of NF-κB, tumor growth, and anti-apoptosis (Qu et al., 2013).

$G\alpha_{12/13}$ and Biased Signaling

Traditionally, each GPCR is thought to initiate the "canonical" signal transduction through a single homologous G protein class (Seyedabadi et al., 2019). With the advances in the study of the ligand-receptor-effector relationship, it has been found that specific ligands induce a GPCR to selectively bind to a particular G protein subunit, transducing biased intracellular signaling toward one of many downstream pathways. This phenomenon is called "biased signaling"; and functionally selective ligands are called "biased ligands" (Tan et al., 2018).

Up to now, only a few GPCRs have shown biased signaling, but it is still the early days of understanding the biased signaling mechanisms. The characteristics of biased ligands, which have strong or weak activity in different pathways, may provide significant clinical advantages for developing new drugs. However, attention should be paid to testing conditions, ligand verification, and patient and disease selection to achieve successful biased ligand therapy (Seyedabadi et al., 2019). So far a few of the receptor types seen to produce biased signaling

involving Gα subunit switch include calcium-sensing receptors, angiotensin receptors, PARs, prostaglandin receptors, and ghrelin receptor.

The biased signaling can occur due to different underlying principles. The well-documented biased signaling is triggered by biased ligands. For instance, calcium-sensing receptor induces the activation of four G protein subfamilies ($G\alpha_{q/11}$, $G\alpha_{i/o}$, $G\alpha_{12/13}$, and $G\alpha_s$) (Abid et al., 2021). The ligands NPS-2143/NPS-R568 binds to a calcium-sensing receptor to specifically mediate the activation of $G\alpha_{12/13}$-RhoA signal, which in turn activates various other signal checkpoints that regulate gene expression, cytoskeleton, and cell shape (Leach et al., 2012; Leach et al., 2013). Similarly, the prostaglandin F2α receptor, a $G\alpha_q$-coupled GPCR, is activated by prostaglandin F2α (Pathe-neuschäfer-rube et al., 2005). PDC113.824 acts on the prostaglandin F2α receptor, which biasedly increases $G\alpha_q$-PKC-ERK1/2 signaling while inhibiting $G\alpha_{12}$-Rho-ROCK signaling, blocking cell contraction and skeletal reorganization, and inhibiting uterine contraction (Goupil et al., 2010). PAR2 is activated mainly by trypsin-like serine proteases and regulates various signaling pathways in coupling with $G\alpha_{i/o}$, $G\alpha_{q/11}$, and $G\alpha_{12/13}$ (Kim et al., 2018b). Among PAR2 antagonists, I-287 inhibits $G\alpha_q$, but biasedly activates $G\alpha_{12/13}$ without affecting $G\alpha_{i/o}$ signaling and β-arrestin recruitment, thereby attenuating the PAR2-mediated inflammatory response (Avet et al., 2020). Likewise, the ghrelin receptor in the arcuate nucleus of the hypothalamus, activated by Ghrelin, induces an intracellular signaling cascade through $G\alpha_q$, $G\alpha_{i/o}$, $G\alpha_{12/13}$, and β-arrestin (Hedegaard and Holst, 2020). The biased ligand YIL781 selectively activates $G\alpha_{q/11}$ and $G\alpha_{12}$ through the ghrelin receptor without intrinsic activity for β-arrestin recruitment, leading to an increased food intake and a reduced gastric emptying (Mende et al., 2018). However, other factors, including ionic strength, lipid environments, and downstream signaling partners, can also contribute to biased signaling observed in native cells and tissues. For instance, receptors can couple in a cell type-specific manner. The binding of angiotensin II (Ang II) to the Ang II type 1 receptor (AT_1R) causes AT_1R interaction with $G\alpha_{q/11}$, $G\alpha_{12/13}$, and $G\alpha_i$, depending on cell type (Forrester et al., 2018). When Ang II stimulates vascular smooth muscle cells, AT_1R binds to $G\alpha_{12/13}$ instead of $G\alpha_{q/11}$ to activate RhoA-ROCK and promote vasoconstriction (Lymperopoulos et al., 2021). Cleaving a receptor is another method that often leads to a change in downstream signaling. For PAR1, the endogenous ligand thrombin promotes PAR1 binding to heterotrimeric G proteins of the $G\alpha_{q/11}$, $G\alpha_{12/13}$, $G\alpha_i$, and $G\alpha_s$ families. The activation of matrix metalloproteinase-1 in platelets cleaves the N-terminal extracellular domain of PAR1, activating the $G\alpha_{12/13}$-Rho-MAPK signal instead of $G\alpha_{q/11}$, and promotes cell shape changes and platelet thrombosis (Trivedi et al., 2009).

$G\alpha_{12/13}$Signaling and Cell Function

As discussed above, the well-characterized downstream effector of active $G\alpha_{12/13}$ is the Rho GTPases through stimulating RhoGEF, which regulates the actin cytoskeleton and participates in various cellular functions, including cell proliferation, migration, contractility, and gene expression (Bodmann et al., 2017) (**Figure 2**).

Cell Growth and Apoptosis

$G\alpha_{12/13}$ was initially identified as an oncogene with the potential for tumor transformation of fibroblasts (Chan et al., 1993; Xu et al., 1993). Subsequent studies have shown that $G\alpha_{12/13}$ can promote mitogenic response and cell growth by transducing a RhoA-dependent signal, which increases YAP/TAZ-dependent gene expression (Goldsmith and Dhanasekaran, 2007; Syrovatkina and Huang, 2019).

Subsequent publications have revealed that $G\alpha_{12/13}$ coupling with several different receptor types promotes proliferation. S1P activates S1PR2/3 to trigger $G\alpha_{12/13}$-RhoA signaling, leading to the proliferation of mouse cardiac progenitor cells and regulating gene transcription in hearts (Castaldi et al., 2016). Stimulation of the thromboxane A2 receptor also promotes the activity of Rho GTPase through $G\alpha_{12/13}$. The activated Rho GTPase regulates actin cytoskeleton, increases nuclear translocation of YAP/TAZ, and promotes proliferation and migration of T/G HA-vascular smooth muscle cells (Feng et al., 2016). After the loss of primary cilia on human astrocytes, LPA promotes association between LPAR1 and $G\alpha_{12}$/$G\alpha_q$, augmenting mitogenic signaling and cell proliferation (Loskutov et al., 2018). Furthermore, the acetylcholine signaling via M1R activates $G\alpha_{13}$ protein to disrupt tubulin polymerization in axons and inhibit mitochondrial transport, thereby limiting the growth of neurites (Sabbir et al., 2018). G protein-coupled receptor 56 (GPR56) interacts with $G\alpha_{12/13}$ to mediate RhoA signaling and regulates zebrafish oligodendrocytes' development and subsequent myelination (Ackerman et al., 2015).

$G\alpha_{12/13}$ is also very important in the proliferation of tumor cells. The activation of $G\alpha_{12/13}$ promotes cell growth and tumor development of hepatocellular, small cell lung carcinoma, and ovarian cancer cells, but not in breast and prostate cancer cells (Grzelinski et al., 2010; Rasheed et al., 2013; Yagi et al., 2016; Syrovatkina and Huang, 2019). The synthetic ligand, Clozapine N-oxide, stimulates GPCR-$G\alpha_{12/13}$ signaling and promotes the proliferation of ovarian cancer cells by activating YAP1 (Yagi et al., 2016). Bombesin secreted by small cell lung carcinoma cells activates the gastrin-releasing peptide receptor (GRPR)-$G\alpha_{12/13}$-Rho-NF-κB signaling cascade. Subsequently, the activated NF-κB increases the production of Sonic Hedgehog, which activates the Gli transcription factor and promotes cell proliferation, survival, blood vessel generation, and local invasion (Castellone et al., 2015).

Meanwhile, the combination of muscle-restricted coiled-coil protein and caveolin-1 promotes $G\alpha_{13}$-mediated p115RhoGEF activation, leading to subsequent activation of the Rho-ROCK signal and enhancing the proliferation and migration of human pulmonary artery smooth muscle cells (Nakanishi et al., 2016). Moreover, $G\alpha_{13}$ dynamically regulates the RhoA signaling through the combination of RhoGEF GTPase and integrin β_1, promoting integrin β_1-mediated proliferation of CHO cell lines (Shen et al., 2015). In addition to autophagy-mediated

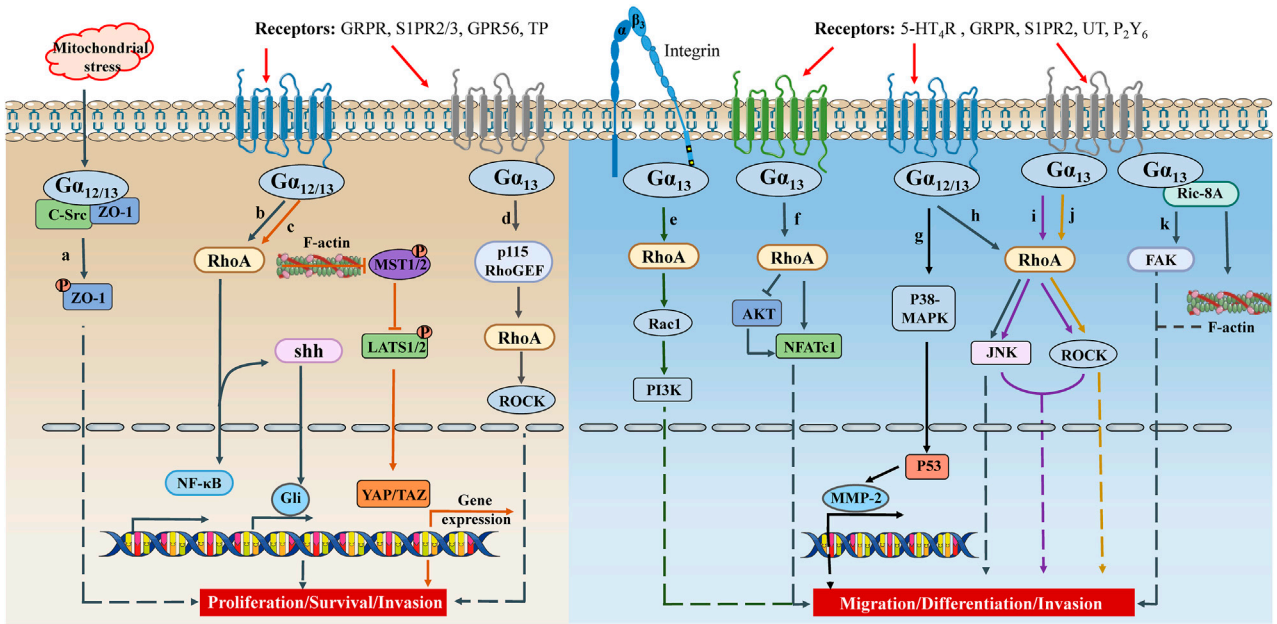

FIGURE 2 | The crosstalk between $G\alpha_{12/13}$ signaling and cell proliferation/migration. Under different physiological/pathological environments, GPCRs on the cell membrane receive different signals, couple $G\alpha_{12}$ or $G\alpha_{13}$, activate signal cascades, and promote synthesis of transcription factors or secretion of inflammatory factors. These signals ultimately lead to different cell activities, such as cell proliferation, survival, differentiation, migration, invasion, etc. TP, thromboxane A2 receptor; UT, urotensin II receptor; P_2Y_6, purinergic receptor 6; shh, sonic hedgehog; MST1/2, mammalian sterile 20-like kinases 1/2.

mitochondrial damage and oxidative stress, lysosomal dysfunction in cystopathy stimulates $G\alpha_{12}$/Src-mediated phosphorylation of zona occludin-1. The activated zona occludin-1-related signaling cascade promotes the proliferation of epithelial cells and disrupts the cell lining along the proximal tubules of mouse kidneys (Festa et al., 2018).

Studies have also found that $G\alpha_{12}$ and $G\alpha_{13}$ regulate apoptosis. In Madin-Darby canine kidney cells, the activation of endogenous $G\alpha_{12}$ and thrombin stimulation increase the activity of JNK1, inhibit the activity of NF-κB, and promote cell apoptosis (Yanamadala et al., 2007). In melanoma cells, US28, a GPCR encoded by human cytomegalovirus, is coupled with $G\alpha_{13}$ to induce cell apoptosis; silencing $G\alpha_{13}$ inhibits cell apoptosis driven by US28 (Joshi et al., 2015). Notably, this event has been only observed in human melanoma cell lines but not in murine cells. The emerging discovery of ligand-GPCR-$G\alpha_{12/13}$ signals will offer insight into the regulation of apoptosis on cancer cells.

Cell Migration

The ability of cell migration is essential for cell growth, proliferation, the inputs and outputs of nutrients and signal intermediates, and normal cell physiology. Cell movement also enhances tumor cell invasion and metastasis (Svitkina, 2018). The process of cell migration is usually accompanied by changes in the actin cytoskeleton. $G\alpha_{12/13}$ activates RhoA through their respective RhoGEF effectors and promotes the dynamic changes of cell shape controlled by actin cytoskeleton reorganization (Castillo-Kauil et al., 2020).

$G\alpha_{12/13}$ plays pivotal roles in cell migration that occurs during development. For instance, the 5-hydroxytryptamine type 4 receptor (5-HT_4R) triggers $G\alpha_{13}$-mediated RhoA signal transduction, promoting the reorganization of filamentous actin and the morphology of mouse astrocytes, and enhancing hippocampal synaptic function (Müller et al., 2021). The 5-HT_4R also mediates human endothelia cell migration and angiogenesis through the $G\alpha_{13}$-RhoA-ROCK pathway *in vitro* (Profirovic et al., 2013). In zebrafish development, the S1PR2-$G\alpha_{13}$-RhoGEF signal is necessary for the convergent movement of the endoderm by promoting myocardial migration at all stages of heart development (Ye et al., 2015). Disrupting the S1PR2-$G\alpha_{13}$-RhoGEF pathway jeopardizes the endoderm's convergence and the myocardium's migration during the segmentation process (Ye and Lin, 2013). With the high concentrations of urotensin II stimulation, urotensin II receptors recruit $G\alpha_{13}$ to activate the Rho-ROCK pathway and promote actin polymerization, which contributes to glioma cells invasion and new blood vessel formation (Lecointre et al., 2015). $G\alpha_{12}$ participates in cell differentiation through the nuclear factor of activated T-cell c1 (NFATc1) and regulates cell migration and resorption through RhoA in the process of osteoclast formation in mice (Song et al., 2018). Resistance to inhibitors of cholinesterase 8A (Ric-8A) is a guanine nucleotide exchange factor of Gα subunits and an important partner of $G\alpha_i$, $G\alpha_q$, and $G\alpha_{13}$ proteins (Papasergi-Scott et al., 2018). In *Xenopus* cranial neural crest cells, the Ric-8A-$G\alpha_{13}$-focal adhesion kinase (FAK) signal regulates focal adhesion dynamics and neurite formation to control cell migration (Toro-Tapia et al., 2018). The activated Ric-8A catalyzes the nucleotide exchange on $G\alpha_{13}$, induces the

reorganization of the actin cytoskeleton, and promotes the migration of mouse embryonic fibroblasts (Wang et al., 2011).

Cell migration that is mediated by $G\alpha_{12/13}$ is also important in metastasis. For example, the activated purinergic receptor 6 increases the number of filopodia and adhesions of human lung cancer cells (A549) and colorectal cancer cells (Caco-2) through both $G\alpha_q$-Ca^{2+}-PKCα and $G\alpha_{13}$-ROCK signals, regulating cell migration (Girard et al., 2020). The GRPR-$G\alpha_{13}$-RhoA-ROCK signaling is necessary for GRP to stimulate the migration of human colon cancer cells. This signaling also promotes the expression of COX-2, which contributes to cell migration (Patel et al., 2014). Similarly, $G\alpha_{12/13}$ signal facilitates the invasion of human cervical cancer cells through a RhoA-ROCK-JNK signal axis (Yuan et al., 2016). $G\alpha_{12/13}$ increases the gene expression of metalloproteinase-2 through p53, which is necessary for inducing the invasion and migration phenotypic changes of untransformed human breast epithelial cells (Kim et al., 2010). $G\alpha_{12}$, which is overexpressed in many hepatocellular carcinoma patients, relieves the regulation of p53-responsive miRNA and promotes the metastasis and invasion of tumor cells (Yang et al., 2015). The $G\alpha_{12}$-mediated pathway promotes metastasis and invasion of human nasopharyngeal carcinoma cells by regulating the reorganization of the actin cytoskeleton (Liu et al., 2009).

Increased $G\alpha_{12/13}$ mediated cell migration also greatly contributes to primary solid tumor growth. Take as example that $G\alpha_{13}$, which is up-regulated in breast cancer, inhibits the transcription of kallikreins through the RhoA-ROCK pathway and promotes the invasion and metastasis of breast cancer cells (Teo et al., 2016). The expression of *GNA13* in breast cancer cells is primarily regulated by MicroRNA (miR)-31, and the absence of miR-31 increases the expression of *GNA13* and the invasion of cancer cells (Rasheed et al., 2015). Similarly, $G\alpha_{13}$ is overexpressed in pancreatic ductal adenocarcinoma and enhances the invasion of human pancreatic cancer cells in three-dimensional collagen by destroying cell adhesion; however, this process does not go through ROCK signal transduction (Chow et al., 2016). $G\alpha_{13}$ is also involved in cell fusion (Carloni et al., 2013). Disintegrins and metalloproteinases stimulate $G\alpha_{13}$ to activate RhoA. The up-regulated RhoA activity causes dephosphorylation of ezrin/radixin/moesin proteins and destruction of plasma membrane-cortical actin interaction, promoting fusion of human metastatic colon cancer cells and cell acquisition of drug resistance (Carloni et al., 2013).

These observations highlight the importance of $G\alpha_{12/13}$-RhoA signaling in cell proliferation or migration. The expression of $G\alpha_{12/13}$ and the downstream signaling are often elevated in cancer cells. However, in some disease states (especially cancer), the upstream ligand and receptor of $G\alpha_{12/13}$ remain unknown.

Immune Cell Function

Due to the lack of specific inhibitors of $G\alpha_{12/13}$, the research of $G\alpha_{12/13}$ in immune cells was stagnant for many years. However, with various transgenic models, the studies on the role of $G\alpha_{12/13}$ in immune cells are accelerating.

T Cells

After naive T cells are activated, $CD4^+$ T cells differentiate into different effector subsets: T helper (Th) 1, Th2, Th17, and T follicular helper (Tfh) cells, which perform their specific auxiliary functions (Dong, 2021). During T cell activation, $G\alpha_{12/13}$ regulates actin polymerization and contributes to cell adhesion and migration (Wang et al., 2013). A recent study has found that $G\alpha_{13}$-RhoA-ROCK2 signaling plays a key regulatory role in the differentiation and function of early Tfh cells. The $G\alpha_{13}$-deficient Tfh cells impair the function of adhering B cells to form conjugates and stimulating B cells to produce immunoglobulins (Kuen et al., 2021). Morover, receptors coupled to $G\alpha_{12/13}$ have been demonstrated to be essential for T cell adhesion, differentiation, and retention in lymph nodes (Moriyama et al., 2014; Mathew et al., 2019). For example, S1PR2 promotes the maturation of Tfh cells by directing co-localization with B cells in the germinal center; and the deficiency of S1PR2 in Tfh cells inhibits the retention in lymph nodes (Moriyama et al., 2014). In response to the stimulation of CXCL12, the $G\alpha_{13}$-Rho signal in human T cells mediates the endosomal trafficking of CXCR4 (Kumar et al., 2011). CXCL12 also promotes the migration of Jurkat T cells through the CXCR4-$G\alpha_{13}$-Rho signal axis (Tan et al., 2006). Meanwhile, $G\alpha_{12/13}$ negatively regulates the activation state of integrin leukocyte-function-antigen-1 to modulate $CD4^+$T cells trafficking and proliferation and susceptibility to immune diseases (Herroeder et al., 2009). In response to the activation of T cell receptor signals, the interleukin-2 inducible T cell kinase directly interacts with $G\alpha_{13}$ to mediate the activation of SRF transcriptional activity (Huang et al., 2013). Conversely, $G\alpha_{12}$ is a key mediator of T cell receptor-mediated interleukin-2 production and controls the differentiation of Th2 and Th17 cells (Won et al., 2010). Additionally, $G\alpha_{13}$, but not $G\alpha_{12}$, mediated signal transduction is necessary for early thymocyte proliferation and survival (McNeil Coffield et al., 2004).

B Cells

Mature B lymphocytes express LPAR2/5, LPA negatively regulates B cell receptor signaling through the LPAR5–$G\alpha_{12/13}$–Arhgef1 pathway, inhibiting the release of calcium stored in the cell and the antibody response (Hu et al., 2014). $G\alpha_{12/13}$ also regulates the maturation, migration, and polarization of marginal zone B cells. In mice with depletion of $G\alpha_{12/13}$ in B cells, the number of zone B cells and zone B cell precursors are significantly reduced, but the formation of pseudopods is increased (Rieken et al., 2006).

Knockout of $G\alpha_{13}$ also results in the loss of restriction of B cells in the germinal center, thus spreading to lymph nodes and blood (Muppidi et al., 2014). Meanwhile, $G\alpha_{13}$ plays a direct role in the growth inhibition of B cells, affecting their survival and differentiation. It has been noted that the impaired phosphorylation of AKT at the Ser473 site is related to $G\alpha_{13}$ activity and may affect the growth and survival of B cells (Green et al., 2011; O'Hayre et al., 2016). The mechanism by which the $G\alpha_{12/13}$-RhoA axis inhibits the growth of B cells needs to be further explored.

Macrophages

In macrophages, complement C5a couples to $G\alpha_{12/13}$ to activate Rho GTPases and tail retraction in migrating cells. Macrophages without $G\alpha_{12/13}$ show complete chemotaxis but increased migration speed and a moderately impaired tail contraction (van den Bos et al., 2020). Thrombin, a major platelet activator, selectively induces the expression of CD36, a plasma membrane fatty acid transporter, and foam cell formation of RAW264.7 cells through PAR1-$G\alpha_{12}$ signaling and facilitates atherosclerosis (Raghavan et al., 2018). Thrombin also induces the migration of monocytes or macrophages through the PAR1-$G\alpha_{12}$ pathway (Gadepalli et al., 2013). The loss of Ric-8A in lymphocytes and bone marrow-derived macrophages leads to a decrease in the expression of $G\alpha_{i2/3}$, $G\alpha_q$, and $G\alpha_{13}$, but not $G\alpha_{12}$, leading to anemia and leukocytosis (Boularan et al., 2015).

The above studies suggest that dysregulation of $G\alpha_{12}$ or $G\alpha_{13}$ in immune cells may lead to pathophysiological consequences, such as cancer and autoimmunity. So far, the research of $G\alpha_{12/13}$ in immune cells is relatively scarce. More research is needed to bring new therapeutic targets for cancers and autoimmune diseases.

$G\alpha_{12/13}$ Signaling and Diseases

$G\alpha_{12/13}$ plays an important role in multiple stages of disease development in different tissues and organs. An increasing number of cancers have shown overexpressed $G\alpha_{12/13}$, which is correlated to abnormal cell proliferation, metastasis, and invasion (Montgomery et al., 2014). The high abundance or constitutive activation of $G\alpha_{12}$ and $G\alpha_{13}$ are effective stimulators of oncogenic transformation. $G\alpha_{12/13}$ also interacts with cell surface GPCRs and participates in the inflammation regulation (Dusaban et al., 2013; Hou et al., 2021). Meanwhile, $G\alpha_{12/13}$ levels in metabolic organs, including liver and muscle, are altered in metabolic diseases (Koo et al., 2017; Kim et al., 2019). However, the mechanism by which $G\alpha_{12/13}$ regulates the progression of these diseases has not been fully elucidated.

$G\alpha_{12/13}$ and Cancer

$G\alpha_{12/13}$ are called the *gep* proto-oncogenes and are usually overexpressed in cancers (Yagi et al., 2016). Besides the functional roles in cancer cell migration and invasion, $G\alpha_{12/13}$ and Rho GTPases exert pro- or anti-cancer effects in a cancer type and background-dependent manner.

The results of Gene Expression Omnibus and The Cancer Genome Atlas database analysis have shown that *GNA12* can be used as a biomarker for the personalized treatment of head and neck squamous cell carcinoma (HNSCC) patients and one of the prognostic genes for patients with HNSCC (Liu et al., 2021). *GNA13* is also a biomarker for the prognosis and metastasis of solid tumors, including HNSCC, ovarian cancer, lung cancer, and gastric cancer (Cerami et al., 2012; Gao et al., 2013; Cancer Genome Atlas, 2015). *GNA13* mutations are present at a high frequency in gastric cancer, nasopharyngeal cancer, prostate cancer, breast cancer, lymphoma, and bladder cancer (Muppidi et al., 2014; Wu et al., 2019; Arang and Gutkind, 2020).

The increased expression and activity of $G\alpha_{12/13}$ contribute to the pathogenesis of different cancers. The copy number of *GNA12* is significantly increased in ovarian cancer, which enhances the function of $G\alpha_{12}$ to promote cancer growth and metastasis (Wu et al., 2019). In two prostate cancer cell lines (C4-2B and PC3), both $G\alpha_{12}$ and $G\alpha_{13}$ are abundantly expressed (El-Haibi et al., 2013). The highly expressed *GNA13* also acts through Rho GTPase to drive the NF-κB transcription program and induce the expression of CXCL5 (Lim et al., 2019). A study on HNSCC has demonstrated that *GNA13* promotes the aggressive phenotype and drug resistance of tumor-initiating cells through the MAPK/AP-1 and NF-κB pathways (Rasheed et al., 2018). In bladder cancer, the Arg-200 (residue required to hydrolyze GTP) mutation of $G\alpha_{13}$ strongly activates YAP/TAZ-dependent TEAD and myocardin-related transcription factor-A/B-dependent SRF transcriptional activities through the RhoGEF-Rho GTPase cascade (Maziarz et al., 2020). Additionally, the low expression of MiR-30b-5p in renal cell carcinoma up-regulates the activity of $G\alpha_{13}$, which promotes cell proliferation, metastasis, and epithelial cell-mesenchymal transition (Liu et al., 2017). The reduction of regulators of G protein signaling protein (RGS) 12 promotes the $G\alpha_{12/13}$-RhoA-YAP pathway and Ezrin expression, which leads to the growth and progression of osteosarcoma and lung metastasis (Li et al., 2021). Moreover, $G\alpha_{13}$-mediated down-regulation of LATS1 promotes phenotypic changes of epithelial cell-mesenchymal transition in ovarian cancer cells (Yagi et al., 2019). These findings identify the $G\alpha_{13}$-Hippo signaling as a potential target for cancer therapeutic interventions.

A few GPCR ligands have been identified upstream of $G\alpha_{12/13}$ in cancers. LPA promotes the combination of $G\alpha_{12}$ and EFA6 through LPAR2 and activates the ADP-ribosylation factors 6 mesenchymal pathway, thereby promoting the invasion, metastasis, and drug resistance of renal cancer cells (Hashimoto et al., 2016). High concentrations of LPA are also accumulated in the ascites of patients with ovarian cancer (Yu et al., 2016). The heterodimerization of LPAR1 and CD97 amplifies the LPA-mediated $G\alpha_{12/13}$-Rho signal transduction and promotes the invasion of prostate cancer cells (Ward et al., 2011). Gastrin induces the activation of paxillin and FAK through the cholecystokinin B receptor-$G\alpha_{12/13}$-RhoA-ROCK signaling pathway, thereby promoting the redirection of the Golgi apparatus and the directional migration of pancreatic cancer cells (Mu et al., 2018). Gastrin also promotes the activation of $G\alpha_{13}$ through the gastrin type 2 cholecystokinin receptor in colon cancer cells. The recruitment of p190RhoGEF by $G\alpha_{13}$ enhances the phosphorylation of FAK and paxillin, leading to RhoA activation and promoting the migration of cancer cells (Masià-Balagué et al., 2015). In addition, the down-regulated GPR65 in a variety of hematological malignancies promotes $G\alpha_{13}$/Rho signal transduction, which leads to the decrease of c-myc oncogene expression and promotes growth, migration, and metastasis of blood cancer cells (Justus et al., 2017). $G\alpha_{13}$ binds to CXCR5 in response to CXCL13 treatment and promotes prostate cancer cell

movements; however, silencing $G\alpha_{13}$ does not affect CXCL13-dependent cell invasion (El-Haibi et al., 2013).

Interestingly, the $G\alpha_{13}$-Rho GTPase signaling has also been shown to alleviate hematological malignancies (Justus et al., 2017). In malignant tumors of the hematopoietic and lymphatic system, *GNA13* and RhoA mutations are present in B-cell lymphomas, mainly in DLBCL and Burkitt's lymphoma (Justus et al., 2017). The mutation of *GNA13* in germinal center B cells is resistant to programmed cell death (Healy et al., 2016). These B cells are differentiated, facilitating genetic instability through continuous somatic hypermutation (Muppidi et al., 2014). Over time, the accumulation of driver mutations in persistent germinal center B cells may cause lymphoma. Loss of $G\alpha_{13}$ facilitates germinal center B cells to spread to the lymph node and blood, leading to the pathogenesis of DLBCL (Healy et al., 2016). Moreover, in the absence of $G\alpha_{13}$ signaling, S1P acts through S1PR3 to promote mouse germinal center B cells migration into the circulation (Muppidi et al., 2015). S1PR2 signals through $G\alpha_{13}$ to induce tumor cell apoptosis and exert its tumor suppressor function (Flori et al., 2016). However, in DLBCL, the forkhead box protein 1 directly inhibits S1PR2 and promotes tumor cell survival (Flori et al., 2016). The restoration and activation of the $G\alpha_{13}$-Rho pathway help reduce tumor growth and progression, supporting that the $G\alpha_{13}$-RhoA axis has a tumor suppressor effect (Justus et al., 2017). Meanwhile, analyzing the genome of tumor tissues from patients with classical Hodgkin lymphoma has revealed that *GNA13* is one of the genes repeatedly mutated (Tiacci et al., 2018). *GNA13* variants are mostly heterozygous, including nonsense, frameshift, and missense mutations, like the mutation patterns in DLBCL and Burkitt's lymphoma (Muppidi et al., 2014; Justus et al., 2017).

Despite the emerging evidence supporting the critical roles of $G\alpha_{12/13}$ in cancers, many questions remain about how the ligands and receptors trigger $G\alpha_{12}$ or $G\alpha_{13}$ signaling in a cancer type-specific manner. A comprehensive understanding of these mechanisms may provide a promising prospect for targeting specific $G\alpha_{12/13}$ signaling processes in cancer therapies.

$G\alpha_{12/13}$ and Inflammation

$G\alpha_{12/13}$ has been implicated in both induction and suppression of inflammation. In the context of inflammation, thrombin, LPA, and S1P transmit signals through $G\alpha_{12/13}$-coupled receptors to amplify inflammatory responses (Gavard and Gutkind, 2008; Dusaban et al., 2017; Lee et al., 2019).

Early studies have found a direct connection between $G\alpha_{12/13}$ signaling and arachidonic acid in cells (Dermott et al., 1999; Mariggiò et al., 2006). NIH-3T3 cells transformed with $G\alpha_{12}$QL show increased secretion of arachidonic acid and transcriptional activation of cyclooxygenase-2 (Dermott et al., 1999). Thrombin stimulates CHO cells to activate the $G\alpha_{13}$-RhoA-ERK1/2 signaling through PAR1, leading to the phosphorylation of cytosolic phospholipase A2 and the increase of arachidonic acid (Mariggiò et al., 2006). The activation of LPAR and S1PR also promotes the expression of inflammatory genes (such as cyclooxygenase-2) and the proliferation of astrocytes through $G\alpha_{12/13}$-RhoA-PLCε-protein kinase D (PKD)-NF-κB signaling, which contributes to neuroinflammation (Dusaban et al., 2013).

Recent work has shown that S1P promotes the NLRP3 inflammasome-mediated inflammatory response and the secretion of pro-inflammatory cytokines such as interleukin-1β and interleukin-18 through the S1PR2-$G\alpha_{12/13}$-MAPK pathway (Hou et al., 2021). Meanwhile, a variety of pro-inflammatory ligands promote the interaction of $G\alpha_{13}$ to VE-cadherin, inducing Src activation and VE-cadherin phosphorylation, leading to the internalization of VE-cadherin, the loss of endothelial barrier function, and vascular inflammation (Gong et al., 2014). The deficiency of $G\alpha_{13}$ in leukocytes and platelets inhibits thrombosis and inflammation and significantly optimizes the survival rate of septic mice (Cheng et al., 2021).

$G\alpha_{12}$ and $G\alpha_{13}$ have opposite effects on osteoclasts. The silencing of $G\alpha_{13}$ enhances the AKT-GSK3β-NFATc1 signal cascade by inhibiting RhoA, strongly promoting the formation and size of osteoclasts (Wu et al., 2017). This observation depicts that $G\alpha_{13}$ is the main endogenous negative switch for osteoclast production. $G\alpha_{13}$ also protects against various bone loss disease models from inflammation (Wu et al., 2017; Nakano et al., 2019). In comparison, a study has shown $G\alpha_{12}$ is involved in the pathophysiology of bone diseases such as osteoporosis or rheumatoid arthritis (Song et al., 2018). Interestingly, the volume of trabecular bone increases in $G\alpha_{12}$ knockout mice, whereas the number of osteoclasts decreases, contrary to the phenotype of $G\alpha_{13}$ deletion (Song et al., 2018). The underlying mechanisms of these opposite phenotypes are unclear, possibly because that $G\alpha_{12}^{-/-}$ mice are whole body knocked out, whereas $G\alpha_{13}^{-/-}$ mice undergo an osteoclast lineage-specific conditional knockout.

$G\alpha_{12/13}$ and Metabolic Diseases

$G\alpha_{12}$ is extensively expressed in metabolic organs, for instance, the liver (Strathmann and Simon, 1991; Kim et al., 2018a). Fasting of normal mice for 24–48 h significantly enhances the expression of $G\alpha_{12}$ in the liver (Kim et al., 2018a). *GNA12*-knockout mice are prone to hepatic steatosis and obesity after being fed a high-fat diet due to reduced energy consumption (Kim et al., 2018a). A study using cDNA microarray analysis with the liver of *GNA12*-knockout mice has found that $G\alpha_{12}$ regulates mitochondrial respiration through the Sirtuin 1/PPARα network (Kim et al., 2018a). Sirtuin 1, a class III histone deacetylases activated by NAD^+, is an important regulator involved in the fatty acid oxidation transcription network (Kalliora et al., 2019). $G\alpha_{12}$ induces ubiquitin-specific peptidase 22 through HIF-1α to promote the stability of Sirtuin 1, controlling lipid metabolism and mitochondrial respiration (Kim et al., 2018a). Interestingly, $G\alpha_{12}$ also exists in the endoplasmic reticulum and participates in the endoplasmic reticulum export (Subramanian et al., 2019). With the coat protein II subunit Sec24 binds to the cargo, it acts as a GEF to activate $G\alpha_{12}$ at the export site of the endoplasmic reticulum, promoting cargo export and inhibiting protein synthesis (Subramanian et al., 2019).

The role of $G\alpha_{13}$ in energy metabolism has opposite effects in skeletal muscle (prodiabetic) and liver (antidiabetic) (Koo et al., 2017; Kim et al., 2019). $G\alpha_{13}$ is more highly expressed in skeletal muscle than other metabolic organs (Koo et al., 2017). The

knockout $G\alpha_{13}$ in skeletal muscles contributes to systemic energy homeostasis, increasing glucose metabolism and insulin sensitivity and inhibiting diet-induced obesity and hepatic steatosis (Koo et al., 2017). The level of $G\alpha_{13}$ in skeletal muscle is reduced by exercise but is increased under conditions of metabolic diseases. Loss of $G\alpha_{13}$ in skeletal muscle inhibits the RhoA-ROCK2 pathway and activates NFATc1, which induces the conversion of skeletal muscle fibers into oxidized form and enhances energy metabolism (Koo et al., 2017). On the contrary, the lack of $G\alpha_{13}$ in the liver of mice leads to the overproduction of inter-α-trypsin inhibitor heavy chain 1, which exacerbates systemic insulin resistance (Kim et al., 2019).

GPR40 is a clinically proven molecular target for the treatment of diabetes. A GPR40 allosteric full agonist promotes glucose-stimulated insulin secretion in pancreatic β cells through GPR40-mediated $G\alpha_{12}$ signaling (Rives et al., 2018). In response to mechanical overload, GPR56 elevates the expression of the mammalian target of rapamycin and insulin-like growth factor 1 through $G\alpha_{12/13}$ and promotes muscle protein synthesis and myotube hypertrophy (White et al., 2014). Succinate activates the $G\alpha_{12}$-PKC-p38-dynamin-related protein 1 signaling through GPR91 to increase mitochondrial fission, enhances ATP production and membrane potential of mitochondria, and promote the migration of human mesenchymal stem cells (Ko et al., 2017). LPA is a key product of fatty acid metabolism. LPAR4 is selectively coupled with $G\alpha_{12/13}$ in adipocytes to limit the remodeling and healthy expansion of white adipose tissue in high-fat diet mice (Yanagida et al., 2018). The above studies have shown that the GPCR-$G\alpha_{12/13}$ axis can be an attractive target for treating metabolic diseases.

$G\alpha_{12/13}$ and Fibrotic Diseases

$G\alpha_{12/13}$ has a pro-fibrotic effect mainly mediated by the RhoA-ROCK activation (Haak et al., 2020). Early studies have demonstrated that $G\alpha_{12/13}$ play a key role in regulating the phenotype of cardiac fibroblasts (Fujii et al., 2005; Nishida et al., 2007). The stimulation of Ang II induces the production of reactive oxygen species (ROS) through the AT_1R-$G\alpha_{12/13}$-Rac pathway. The ROS-mediated JNK activation promotes the activity of AP-1 and NFAT, leading to the proliferation of cardiac fibroblasts (Fujii et al., 2005). Recently, it has been found that targeted inhibition of the $G\alpha_{12/13}$-RhoA-ROCK pathway successfully alleviates Ang II-induced cardiac dysfunction and the fibrotic response of cardiac fibroblasts (He et al., 2017). Endothelin-1 activates the Endothelin-1 type A receptor-$G\alpha_{12/13}$ axis in cardiac fibroblasts and promotes the formation of myofibroblasts through Rac-dependent ROS production and JNK activation (Nishida et al., 2007). The osteoglycin in the heart binds to LPAR3 and mediates the $G\alpha_{12/13}$-Rho-ROCK signal to attenuate the transactivation of epidermal growth factor receptors, thus inhibiting the proliferation and migration of cardiac myofibroblasts and negatively regulating cardiac fibrotic remodeling (Zuo et al., 2018).

Among numerous G protein members, $G\alpha_{12}$ is expressed abundantly in hepatic stellate cells of the fibrotic liver, whereas $G\alpha_{13}$ is not (Kim et al., 2018c). The imbalance of miR-16 in hepatic stellate cells leads to the overexpression of $G\alpha_{12}$, which promotes autophagy through the transcription of JNK-dependent autophagy-related genes 12-5 and accelerates the progression of liver fibrosis (Kim et al., 2018c). Meanwhile, deficiency of $G\alpha_{12}$ significantly blocks bleomycin-induced pulmonary fibrosis in mice. LPA stimulates the phosphorylation and activation of PKC-δ through $G\alpha_{12}$ and the mammalian target of rapamycin complex 2, which is important for fibroblast migration and the development of pulmonary fibrosis (Gan et al., 2012).

In short, the role of $G\alpha_{12}$ or $G\alpha_{13}$ in fibrotic diseases is unclear. Using various omics (e.g., genomics, proteomics) to detect the expression of $G\alpha_{12/13}$ in specific tissues/cells of fibrotic diseases, exploring its upstream receptors and downstream signals may lead to a better understanding of the pathological mechanisms of the fibrotic diseases.

$G\alpha_{12/13}$ and Circulatory and Renal Disorders

$G\alpha_{13}$ is involved in heart remodeling induced by pressure overload and plays a central role in the transition to heart failure (Takefuji et al., 2012). The Ang II-AT_1R-$G\alpha_{13}$-RhoA-myocardin-related transcription factor signal cascade regulates the expression of hypertrophy and fibrosis genes in cardiomyocytes (Takefuji et al., 2012). In response to low concentrations of thrombin, disabled-2, a linker protein, regulates $G\alpha_{12/13}$-mediated RhoA-ROCK activation and enhances ADP release, which increases the activity of AKT and mammalian target of rapamycin and promotes platelet aggregation and thrombosis (Tsai et al., 2014). Thrombin also stimulates platelets to promote the interaction of $G\alpha_{13}$ and receptor-interacting protein kinase 3. Receptor-interacting protein kinase 3 participates in the integrin-$G\alpha_{13}$ signal to promote platelet activation and thrombosis (Zhang et al., 2017). The newly developed high-load ExE peptide nanoparticles, based on the $G\alpha_{13}$ binding ExE motif on the cytoplasmic domain of integrin β_3, inhibit thrombosis and protect mice from cardiac I/R injury (Pang et al., 2020). This study supports that the integrin-$G\alpha_{13}$-RhoA-YAP pathway can be targeted for anti-atherosclerosis therapy (Wang et al., 2016). Inhibiting proteins that specifically interact with $G\alpha_{13}$ is a promising approach for the treatment of diseases such as macular degeneration, atherosclerosis, and tumor angiogenesis (Wang et al., 2017). In the process of angiogenesis, RGS5 converts $G\alpha_{q/11}$-mediated calcium-dependent contraction to $G\alpha_{12/13}$-mediated RhoA activation, leading to the formation of stress fibers in the vascular smooth muscle cells of the artery and the process of vascular remodeling (Arnold et al., 2014). $G\alpha_{12/13}$ are also essential for blood vessel formation. $G\alpha_{13}$ interacts with Abl1 to form a complex, which regulates actin cytoskeleton reorganization, remodeling, and endothelial cell migration and promotes blood vessel formation (Wang et al., 2017).

$G\alpha_{12}$ also plays a key role in inducing renal I/R injury through various mechanisms, such as destruction of tight cell connections, oxidative stress, inflammation, and cell apoptosis. $G\alpha_{12}$ knockout mice are almost completely protected from I/R injury (Yu et al., 2012). In addition, kidney injury molecule-1 prevents tissue damage by blocking the binding of GTP to $G\alpha_{12}$ in renal I/R

(Ismail et al., 2015). $G\alpha_{12}$ is also necessary for the development of a mouse renal cyst model induced by polycystin-1 mutation. The lack of polycystin-1 promotes the activation of $G\alpha_{12}$, leading to alteration in the form of N-cadherin, destroying cell-matrix/cell adhesion, inhibiting FAK, but promoting the formation of stress fibers (Wu et al., 2016). The activation of $G\alpha_{12}$ in mouse podocytes also leads to the imbalance of collagen expression in glomeruli, age-dependent proteinuria, and focal glomerular sclerosis (Boucher et al., 2012). However, a study has found that the activation of the dopamine D3 receptor increases coupling to $G\alpha_{12}$, leading to the reduction in ROS production and inflammation, ultimately preventing renal I/R injury (Wang et al., 2015).

The coupling of different GPCRs to $G\alpha_{12/13}$ and the impacts on the pathophysiology have not been fully elucidated. The identification of the reciprocal binding domains of $G\alpha_{12/13}$ to related cellular proteins will facilitate the development of more specific inhibitors to selectively disrupt the interaction. A comprehensive understanding of the complex regulatory mechanisms of $G\alpha_{12/13}$ signaling may lead to novel therapeutics targeting specific functions of $G\alpha_{12}$ or $G\alpha_{13}$ in a disease-specific manner.

CONCLUSION

The mechanisms of signal transduction through $G\alpha_{12/13}$ are still one of the most enchanting problems in biology. Many crucial questions remain to be addressed: what determines the specificity of the receptor-$G\alpha_{12/13}$ interaction (Montgomery et al., 2014; Lymperopoulos et al., 2021)? What determines the specific selectivity of the receptor to $G\alpha_{12}$ or $G\alpha_{13}$ (Corbisier et al., 2015; Mackenzie et al., 2019)? Do receptor and $G\alpha_{12/13}$ form a pre-coupling complex (Ayoub et al., 2012; Zhang et al., 2017)? The importance of $G\alpha_{12/13}$ in mediating the complexity of signals, affecting the diversity of cell functions, and participating in the pathogenesis of diseases are continuously being explored. $G\alpha_{12/13}$ are pathologically relevant to cancer, bone diseases, liver steatosis, and pulmonary fibrosis. $G\alpha_{12/13}$ are considered an attractive biomarker and target for diagnosing and treating related diseases. However, it is unwise to directly stimulate or inhibit the activity of $G\alpha_{12/13}$ due to the complexity of its regulatory network, the diversity of functions, and the high likelihood of off-target effects. In comparison, stimulating/inhibiting the upstream receptor/downstream pathways of $G\alpha_{12}$ or $G\alpha_{13}$ in specific organs/cells may offer a chance of successful therapy. A better understanding of the ligand-receptor-$G\alpha_{12/13}$-downstream signaling networks may guide new drug development in the future.

AUTHOR CONTRIBUTIONS

PG wrote the manuscript; YT and MW drew the figures; HS made the table; LZ and WW gave comments; QW and YX gave instructions and revised the manuscript.

FUNDING

This work was financially supported by the National Natural Science Foundation of China (81973314, 81202541, and 81973332), the Anhui Provincial Natural Science Foundation for Distinguished Young Scholars (1808085J28), Collaborative Innovation Project of Key Scientific Research Platform in Anhui Universities (GXXT-2020-066), Program for Upgrading Scientific Research Level of Anhui Medical University (2019xkjT008), Academic Funding for Top-notch Talents in University Disciplines (Majors) of Anhui Province (gxbjZD2021047), National Institute of Health R01HL147263, and Veteran Affair 1I01BX005100 and IK6BX005753.

ACKNOWLEDGMENTS

We appreciate Huijuan Cheng, Tiantian Su, Chunru Jiang, and Zhenduo Zhu for the literature search.

REFERENCES

Abid, H. A., Inoue, A., and Gorvin, C. M. (2021). Heterogeneity of G Protein Activation by the Calcium-Sensing Receptor. *J. Mol. Endocrinol.* 67, 41–53. doi:10.1530/jme-21-0058

Acharya, B. R., Nestor-Bergmann, A., Liang, X., Gupta, S., Duszyc, K., Gauquelin, E., et al. (2018). A Mechanosensitive RhoA Pathway that Protects Epithelia against Acute Tensile Stress. *Developmental Cell* 47, 439–452. doi:10.1016/j.devcel.2018.09.016

Ackerman, S. D., Garcia, C., Piao, X., Gutmann, D. H., and Monk, K. R. (2015). The Adhesion GPCR Gpr56 Regulates Oligodendrocyte Development via Interactions with Gα12/13 and RhoA. *Nat. Commun.* 6, 6122. doi:10.1038/ncomms7122

Arang, N., and Gutkind, J. S. (2020). G Protein-Coupled Receptors and Heterotrimeric G Proteins as Cancer Drivers. *FEBS Lett.* 594, 4201–4232. doi:10.1002/1873-3468.14017

Arnold, C., Feldner, A., Pfisterer, L., Hödebeck, M., Troidl, K., Genové, G., et al. (2014). RGS 5 Promotes Arterial Growth during Arteriogenesis. *EMBO Mol. Med.* 6, 1075–1089. doi:10.15252/emmm.201403864

Arthofer, E., Hot, B., Petersen, J., Strakova, K., Jäger, S., Grundmann, M., et al. (2016). WNT Stimulation Dissociates a Frizzled 4 Inactive-State Complex with Gα12/13. *Mol. Pharmacol.* 90, 447–459. doi:10.1124/mol.116.104919

Avet, C., Sturino, C., Grastilleur, S., Gouill, C. L., Semache, M., Gross, F., et al. (2020). The PAR2 Inhibitor I-287 Selectively Targets Gαq and Gα12/13 Signaling and Has Anti-inflammatory Effects. *Commun. Biol.* 3, 719. doi:10.1038/s42003-020-01453-8

Ayoub, M. A., Al-Senaidy, A., and Pin, J.-P. (2012). Receptor-G Protein Interaction Studied by Bioluminescence Resonance Energy Transfer: Lessons from Protease-Activated Receptor 1. *Front. Endocrin.* 3, 82. doi:10.3389/fendo.2012.00082

Ayoub, M. A., and Pin, J.-P. (2013). Interaction of Protease-Activated Receptor 2 with G Proteins and β-Arrestin 1 Studied by Bioluminescence Resonance Energy Transfer. *Front. Endocrinol.* 4, 196. doi:10.3389/fendo.2013.00196

Bodmann, E. L., Krett, A. L., and Bünemann, M. (2017). Potentiation of Receptor Responses Induced by Prolonged Binding of Gα 13 and Leukemia-associated RhoGEF. *FASEB j.* 31, 3663–3676. doi:10.1096/fj.201700026r

Bondar, A., and Lazar, J. (2021). Optical Sensors of Heterotrimeric G Protein Signaling. *FEBS J.* 288, 2570–2584. doi:10.1111/febs.15655

Boucher, I., Yu, W., Beaudry, S., Negoro, H., Tran, M., Pollak, M. R., et al. (2012). Gα12 Activation in Podocytes Leads to Cumulative Changes in Glomerular Collagen Expression, Proteinuria and Glomerulosclerosis. *Lab. Invest.* 92, 662–675. doi:10.1038/labinvest.2011.198

Boularan, C., Hwang, I.-Y., Kamenyeva, O., Park, C., Harrison, K., Huang, Z., et al. (2015). B Lymphocyte-specific Loss of Ric-8A Results in a Gα Protein Deficit and Severe Humoral Immunodeficiency. *J.I.* 195, 2090–2102. doi:10.4049/jimmunol.1500523

Cancer Genome Atlas, N. (2015). Comprehensive Genomic Characterization of Head and Neck Squamous Cell Carcinomas. *Nature* 517, 576–582. doi:10.1038/nature14129

Carloni, V., Mazzocca, A., Mello, T., Galli, A., and Capaccioli, S. (2013). Cell Fusion Promotes Chemoresistance in Metastatic colon Carcinoma. *Oncogene* 32, 2649–2660. doi:10.1038/onc.2012.268

Castaldi, A., Chesini, G. P., Taylor, A. E., Sussman, M. A., Brown, J. H., and Purcell, N. H. (2016). Sphingosine 1-phosphate Elicits RhoA-dependent Proliferation and MRTF-A Mediated Gene Induction in CPCs. *Cell Signal.* 28, 871–879. doi:10.1016/j.cellsig.2016.04.006

Castellone, M. D., Laukkanen, M. O., Teramoto, H., Bellelli, R., Alì, G., Fontanini, G., et al. (2015). Cross Talk between the Bombesin Neuropeptide Receptor and Sonic Hedgehog Pathways in Small Cell Lung Carcinoma. *Oncogene* 34, 1679–1687. doi:10.1038/onc.2014.104

Castillo-Kauil, A., García-Jiménez, I., Cervantes-Villagrana, R. D., Adame-García, S. R., Beltrán-Navarro, Y. M., Gutkind, J. S., et al. (2020). Gαs Directly Drives PDZ-RhoGEF Signaling to Cdc42. *J. Biol. Chem.* 295, 16920–16928. doi:10.1074/jbc.ac120.015204

Cerami, E., Gao, J., Dogrusoz, U., Gross, B. E., Sumer, S. O., Aksoy, B. A., et al. (2012). The cBio Cancer Genomics Portal: An Open Platform for Exploring Multidimensional Cancer Genomics Data: Figure 1. *Cancer Discov.* 2, 401–404. doi:10.1158/2159-8290.cd-12-0095

Chan, A. M., Fleming, T. P., McGovern, E. S., Chedid, M., Miki, T., and Aaronson, S. A. (1993). Expression cDNA Cloning of a Transforming Gene Encoding the Wild-type G Alpha 12 Gene Product. *Mol. Cell. Biol.* 13, 762–768. doi:10.1128/mcb.13.2.762

Chandrabalan, A., and Ramachandran, R. (2021). Molecular Mechanisms Regulating Proteinase-Activated Receptors (PARs). *FEBS J.* 288, 2697–2726. doi:10.1111/febs.15829

Cheng, N., Zhang, Y., Delaney, M. K., Wang, C., Bai, Y., Skidgel, R. A., et al. (2021). Targeting Gα13-Integrin Interaction Ameliorates Systemic Inflammation. *Nat. Commun.* 12, 3185. doi:10.1038/s41467-021-23409-0

Chow, C. R., Ebine, K., Knab, L. M., Bentrem, D. J., Kumar, K., and Munshi, H. G. (2016). Cancer Cell Invasion in Three-Dimensional Collagen Is Regulated Differentially by Gα13 Protein and Discoidin Domain Receptor 1-Par3 Protein Signaling. *J. Biol. Chem.* 291, 1605–1618. doi:10.1074/jbc.m115.669606

Corbisier, J., Galès, C., Huszagh, A., Parmentier, M., and Springael, J.-Y. (2015). Biased Signaling at Chemokine Receptors. *J. Biol. Chem.* 290, 9542–9554. doi:10.1074/jbc.m114.596098

Dermott, J. M., Reddy, M. R., Onesime, D., Reddy, E. P., and Dhanasekaran, N. (1999). Oncogenic Mutant of Gα12 Stimulates Cell Proliferation through Cycloxygenase-2 Signaling Pathway. *Oncogene* 18, 7185–7189. doi:10.1038/sj.onc.1203345

Dong, C. (2021). Cytokine Regulation and Function in T Cells. *Annu. Rev. Immunol.* 39, 51–76. doi:10.1146/annurev-immunol-061020-053702

Dusaban, S. S., Chun, J., Rosen, H., Purcell, N. H., and Brown, J. H. (2017). Sphingosine 1-phosphate Receptor 3 and RhoA Signaling Mediate Inflammatory Gene Expression in Astrocytes. *J. Neuroinflammation* 14, 111. doi:10.1186/s12974-017-0882-x

Dusaban, S. S., Purcell, N. H., Rockenstein, E., Masliah, E., Cho, M. K., Smrcka, A. V., et al. (2013). Phospholipase Cε Links G Protein-Coupled Receptor Activation to Inflammatory Astrocytic Responses. *Proc. Natl. Acad. Sci. USA* 110, 3609–3614. doi:10.1073/pnas.1217355110

El-Haibi, C. P., Sharma, P., Singh, R., Gupta, P., Taub, D. D., Singh, S., et al. (2013). Differential G Protein Subunit Expression by Prostate Cancer Cells and Their Interaction with CXCR5. *Mol. Cancer* 12, 64. doi:10.1186/1476-4598-12-64

Feng, X., Liu, P., Zhou, X., Li, M.-T., Li, F.-L., Wang, Z., et al. (2016). Thromboxane A2 Activates YAP/TAZ Protein to Induce Vascular Smooth Muscle Cell Proliferation and Migration. *J. Biol. Chem.* 291, 18947–18958. doi:10.1074/jbc.m116.739722

Festa, B. P., Chen, Z., Berquez, M., Debaix, H., Tokonami, N., Prange, J. A., et al. (2018). Impaired Autophagy Bridges Lysosomal Storage Disease and Epithelial Dysfunction in the Kidney. *Nat. Commun.* 9, 161. doi:10.1038/s41467-017-02536-7

Flaumenhaft, R., and De Ceunynck, K. (2017). Targeting PAR1: Now what? *Trends Pharmacol. Sci.* 38, 701–716. doi:10.1016/j.tips.2017.05.001

Flori, M., Schmid, C. A., Sumrall, E. T., Tzankov, A., Law, C. W., Robinson, M. D., et al. (2016). The Hematopoietic Oncoprotein FOXP1 Promotes Tumor Cell Survival in Diffuse Large B-Cell Lymphoma by Repressing S1PR2 Signaling. *Blood* 127, 1438–1448. doi:10.1182/blood-2015-08-662635

Forrester, S. J., Booz, G. W., Sigmund, C. D., Coffman, T. M., Kawai, T., Rizzo, V., et al. (2018). Angiotensin II Signal Transduction: An Update on Mechanisms of Physiology and Pathophysiology. *Physiol. Rev.* 98, 1627–1738. doi:10.1152/physrev.00038.2017

Fujii, T., Onohara, N., Maruyama, Y., Tanabe, S., Kobayashi, H., Fukutomi, M., et al. (2005). Gα12/13-mediated Production of Reactive Oxygen Species Is Critical for Angiotensin Receptor-Induced NFAT Activation in Cardiac Fibroblasts. *J. Biol. Chem.* 280, 23041–23047. doi:10.1074/jbc.m409397200

Gadepalli, R., Kotla, S., Heckle, M. R., Verma, S. K., Singh, N. K., and Rao, G. N. (2013). Novel Role for P21-Activated Kinase 2 in Thrombin-Induced Monocyte Migration. *J. Biol. Chem.* 288, 30815–30831. doi:10.1074/jbc.m113.463414

Gan, X., Wang, C., Patel, M., Kreutz, B., Zhou, M., Kozasa, T., et al. (2013). Different Raf Protein Kinases Mediate Different Signaling Pathways to Stimulate E3 Ligase RFFL Gene Expression in Cell Migration Regulation. *J. Biol. Chem.* 288, 33978–33984. doi:10.1074/jbc.m113.477406

Gan, X., Wang, J., Wang, C., Sommer, E., Kozasa, T., Srinivasula, S., et al. (2012). PRR5L Degradation Promotes mTORC2-Mediated PKC-δ Phosphorylation and Cell Migration Downstream of Gα12. *Nat. Cell Biol* 14, 686–696. doi:10.1038/ncb2507

Gao, J., Aksoy, B. A., Dogrusoz, U., Dresdner, G., Gross, B., Sumer, S. O., et al. (2013). Integrative Analysis of Complex Cancer Genomics and Clinical Profiles Using the cBioPortal. *Sci. Signal.* 6, pl1. doi:10.1126/scisignal.2004088

Gavard, J., and Gutkind, J. S. (2008). Protein Kinase C-Related Kinase and ROCK Are Required for Thrombin-Induced Endothelial Cell Permeability Downstream from Gα12/13 and Gα11/q. *J. Biol. Chem.* 283, 29888–29896. doi:10.1074/jbc.m803880200

Girard, M., Dagenais Bellefeuille, S., Eiselt, É., Brouillette, R., Placet, M., Arguin, G., et al. (2020). The P2Y 6 Receptor Signals through Gα Q/Ca 2+/PKCα and Gα 13/ROCK Pathways to Drive the Formation of Membrane Protrusions and Dictate Cell Migration. *J. Cell Physiol* 235, 9676–9690. doi:10.1002/jcp.29779

Goldsmith, Z. G., and Dhanasekaran, D. N. (2007). G Protein Regulation of MAPK Networks. *Oncogene* 26, 3122–3142. doi:10.1038/sj.onc.1210407

Gong, H., Gao, X., Feng, S., Siddiqui, M. R., Garcia, A., Bonini, M. G., et al. (2014). Evidence of a Common Mechanism of Disassembly of Adherens Junctions through Gα13 Targeting of VE-Cadherin. *J. Exp. Med.* 211, 579–591. doi:10.1084/jem.20131190

Gong, H., Shen, B., Flevaris, P., Chow, C., Lam, S. C.-T., Voyno-Yasenetskaya, T. A., et al. (2010). G Protein Subunit Gα 13 Binds to Integrin α IIb β 3 and Mediates Integrin "Outside-In" Signaling. *Science* 327, 340–343. doi:10.1126/science.1174779

Goupil, E., Tassy, D., Bourguet, C., Quiniou, C., Wisehart, V., Pétrin, D., et al. (2010). A Novel Biased Allosteric Compound Inhibitor of Parturition Selectively Impedes the Prostaglandin F2α-Mediated Rho/ROCK Signaling Pathway. *J. Biol. Chem.* 285, 25624–25636. doi:10.1074/jbc.m110.115196

Green, J. A., Suzuki, K., Cho, B., Willison, L. D., Palmer, D., Allen, C. D. C., et al. (2011). The Sphingosine 1-phosphate Receptor S1P2 Maintains the Homeostasis of Germinal center B Cells and Promotes Niche Confinement. *Nat. Immunol.* 12, 672–680. doi:10.1038/ni.2047

Grzelinski, M., Pinkenburg, O., Büch, T., Gold, M., Stohr, S., Kalwa, H., et al. (2010). Critical Role of Gα12 and Gα13 for Human Small Cell Lung Cancer Cell

Proliferation *In Vitro* and Tumor Growth *In Vivo*. *Clin. Cancer Res.* 16, 1402–1415. doi:10.1158/1078-0432.ccr-09-1873

Haak, A. J., Ducharme, M. T., Diaz Espinosa, A. M., and Tschumperlin, D. J. (2020). Targeting GPCR Signaling for Idiopathic Pulmonary Fibrosis Therapies. *Trends Pharmacol. Sci.* 41, 172–182. doi:10.1016/j.tips.2019.12.008

Hashimoto, S., Mikami, S., Sugino, H., Yoshikawa, A., Hashimoto, A., Onodera, Y., et al. (2016). Lysophosphatidic Acid Activates Arf6 to Promote the Mesenchymal Malignancy of Renal Cancer. *Nat. Commun.* 7, 10656. doi:10.1038/ncomms10656

Hauser, A. S., Attwood, M. M., Rask-Andersen, M., Schiöth, H. B., and Gloriam, D. E. (2017). Trends in GPCR Drug Discovery: New Agents, Targets and Indications. *Nat. Rev. Drug Discov.* 16, 829–842. doi:10.1038/nrd.2017.178

He, Z., Yang, Y., Wen, Z., Chen, C., Xu, X., Zhu, Y., et al. (2017). CYP2J2 Metabolites, Epoxyeicosatrienoic Acids, Attenuate Ang II-Induced Cardiac Fibrotic Response by Targeting Gα12/13. *J. Lipid Res.* 58, 1338–1353. doi:10.1194/jlr.m074229

Healy, J. A., Nugent, A., Rempel, R. E., Moffitt, A. B., Davis, N. S., Jiang, X., et al. (2016). GNA13 Loss in Germinal center B Cells Leads to Impaired Apoptosis and Promotes Lymphoma *In Vivo*. *Blood* 127, 2723–2731. doi:10.1182/blood-2015-07-659938

Hedegaard, M. A., and Holst, B. (2020). The Complex Signaling Pathways of the Ghrelin Receptor. *Endocrinology* 161, 161. doi:10.1210/endocr/bqaa020

Hendrickx, G., Boudin, E., Verbeek, M., Fransen, E., Mortier, G., and Van Hul, W. (2020). WNT16 Requires Gα Subunits as Intracellular Partners for Both its Canonical and Non-canonical WNT Signalling Activity in Osteoblasts. *Calcif Tissue Int.* 106, 294–302. doi:10.1007/s00223-019-00633-x

Herroeder, S., Reichardt, P., Sassmann, A., Zimmermann, B., Jaeneke, D., Hoeckner, J., et al. (2009). Guanine Nucleotide-Binding Proteins of the G12 Family Shape Immune Functions by Controlling CD4+ T Cell Adhesiveness and Motility. *Immunity* 30, 708–720. doi:10.1016/j.immuni.2009.02.010

Hilger, D., Masureel, M., and Kobilka, B. K. (2018). Structure and Dynamics of GPCR Signaling Complexes. *Nat. Struct. Mol. Biol.* 25, 4–12. doi:10.1038/s41594-017-0011-7

Hot, B., Valnohova, J., Arthofer, E., Simon, K., Shin, J., Uhlén, M., et al. (2017). FZD10-Gα13 Signalling axis Points to a Role of FZD10 in CNS Angiogenesis. *Cell Signal.* 32, 93–103. doi:10.1016/j.cellsig.2017.01.023

Hou, L., Zhang, Z., Yang, L., Chang, N., Zhao, X., Zhou, X., et al. (2021). NLRP3 Inflammasome Priming and Activation in Cholestatic Liver Injury via the Sphingosine 1-phosphate/S1P Receptor 2/Gα(12/13)/MAPK Signaling Pathway. *J. Mol. Med.* 99, 273–288. doi:10.1007/s00109-020-02032-4

Hu, J., Oda, S. K., Shotts, K., Donovan, E. E., Strauch, P., Pujanauski, L. M., et al. (2014). Lysophosphatidic Acid Receptor 5 Inhibits B Cell Antigen Receptor Signaling and Antibody Response. *J.I.* 193, 85–95. doi:10.4049/jimmunol.1300429

Huang, W., Morales, J. L., Gazivoda, V. P., Lai, J., Qi, Q., and August, A. (2013). The Zinc-Binding Region of IL-2 Inducible T Cell Kinase (Itk) Is Required for Interaction with Gα13 and Activation of Serum Response Factor. *Int. J. Biochem. Cell Biol.* 45, 1074–1082. doi:10.1016/j.biocel.2013.02.011

Ismail, O. Z., Zhang, X., Wei, J., Haig, A., Denker, B. M., Suri, R. S., et al. (2015). Kidney Injury Molecule-1 Protects against Gα12 Activation and Tissue Damage in Renal Ischemia-Reperfusion Injury. *Am. J. Pathol.* 185, 1207–1215. doi:10.1016/j.ajpath.2015.02.003

Janda, C. Y., Dang, L. T., You, C., Chang, J., de Lau, W., Zhong, Z. A., et al. (2017). Surrogate Wnt Agonists that Phenocopy Canonical Wnt and β-catenin Signalling. *Nature* 545, 234–237. doi:10.1038/nature22306

Jiang, L. I., Collins, J., Davis, R., Fraser, I. D., and Sternweis, P. C. (2008). Regulation of cAMP Responses by the G12/13 Pathway Converges on Adenylyl Cyclase VII. *J. Biol. Chem.* 283, 23429–23439. doi:10.1074/jbc.m803281200

Joshi, S., Wels, C., Beham-Schmid, C., Fukunaga-Kalabis, M., Holmen, S. L., Otte, M., et al. (2015). Gα13 Mediates Human Cytomegalovirus-Encoded Chemokine Receptor US28-Induced Cell Death in Melanoma. *Int. J. Cancer* 137, 1503–1508. doi:10.1002/ijc.29506

Justus, C. R., Sanderlin, E. J., Dong, L., Sun, T., Chi, J.-T., Lertpiriyapong, K., et al. (2017). Contextual Tumor Suppressor Function of T Cell Death-Associated Gene 8 (TDAG8) in Hematological Malignancies. *J. Transl Med.* 15, 204. doi:10.1186/s12967-017-1305-6

Kalliora, C., Kyriazis, I. D., Oka, S. I., Lieu, M. J., Yue, Y., Area-Gomez, E., et al. (2019). Dual Peroxisome-Proliferator-Activated-Receptor-Alpha/gamma Activation Inhibits SIRT1-PGC1alpha axis and Causes Cardiac Dysfunction. *JCI Insight* 5, e129556. doi:10.1172/jci.insight.129556

Kalwa, H., Storch, U., Demleitner, J., Fiedler, S., Mayer, T., Kannler, M., et al. (2015). Phospholipase C Epsilon (PLCε) Induced TRPC6 Activation: A Common but Redundant Mechanism in Primary Podocytes. *J. Cell. Physiol.* 230, 1389–1399. doi:10.1002/jcp.24883

Khan, S. M., Sung, J. Y., and Hébert, T. E. (2016). Gβγ Subunits-Different Spaces, Different Faces. *Pharmacol. Res.* 111, 434–441. doi:10.1016/j.phrs.2016.06.026

Ki, S. H., Choi, M. J., Lee, C. H., and Kim, S. G. (2007). Gα12 Specifically Regulates COX-2 Induction by Sphingosine 1-Phosphate. *J. Biol. Chem.* 282, 1938–1947. doi:10.1074/jbc.m606080200

Kihara, Y., Maceyka, M., Spiegel, S., and Chun, J. (2014). Lysophospholipid Receptor Nomenclature Review: IUPHAR Review 8. *Br. J. Pharmacol.* 171, 3575–3594. doi:10.1111/bph.12678

Kim, E.-S., Jeong, J.-B., Kim, S., Lee, K.-M., Ko, E., Noh, D.-Y., et al. (2010). The G12 Family Proteins Upregulate Matrix Metalloproteinase-2 via P53 Leading to Human Breast Cell Invasion. *Breast Cancer Res. Treat.* 124, 49–61. doi:10.1007/s10549-009-0697-2

Kim, K., Lee, J., and Ghil, S. (2018). The Regulators of G Protein Signaling RGS 16 and RGS 18 Inhibit Protease-activated Receptor 2/Gi/o Signaling through Distinct Interactions with Gα in Live Cells. *FEBS Lett.* 592, 3126–3138. doi:10.1002/1873-3468.13220

Kim, K. M., Han, C. Y., Kim, J. Y., Cho, S. S., Kim, Y. S., Koo, J. H., et al. (2018). Gα12 Overexpression Induced by miR-16 Dysregulation Contributes to Liver Fibrosis by Promoting Autophagy in Hepatic Stellate Cells. *J. Hepatol.* 68, 493–504. doi:10.1016/j.jhep.2017.10.011

Kim, T. H., Koo, J. H., Heo, M. J., Han, C. Y., Kim, Y. I., Park, S. Y., et al. (2019). Overproduction of Inter-α-trypsin Inhibitor Heavy Chain 1 after Loss of Gα13 in Liver Exacerbates Systemic Insulin Resistance in Mice. *Sci. Transl Med.* 11, eaan4735. doi:10.1126/scitranslmed.aan4735

Kim, T. H., Yang, Y. M., Han, C. Y., Koo, J. H., Oh, H., Kim, S. S., et al. (2018). Gα12 Ablation Exacerbates Liver Steatosis and Obesity by Suppressing USP22/SIRT1-Regulated Mitochondrial Respiration. *J. Clin. Invest.* 128, 5587–5602. doi:10.1172/jci97831

Kim, Y. M., Lim, S.-C., Han, C. Y., Kay, H. Y., Cho, I. J., Ki, S. H., et al. (2011). Gα 12/13 Induction of CYR61 in Association with Arteriosclerotic Intimal Hyperplasia. *Arterioscler Thromb. Vasc. Biol.* 31, 861–869. doi:10.1161/atvbaha.110.218552

Ko, S. H., Choi, G. E., Oh, J. Y., Lee, H. J., Kim, J. S., Chae, C. W., et al. (2017). Succinate Promotes Stem Cell Migration through the GPR91-dependent Regulation of DRP1-Mediated Mitochondrial Fission. *Sci. Rep.* 7, 12582. doi:10.1038/s41598-017-12692-x

Koo, J. H., Kim, T. H., Park, S.-Y., Joo, M. S., Han, C. Y., Choi, C. S., et al. (2017). Gα13 Ablation Reprograms Myofibers to Oxidative Phenotype and Enhances Whole-Body Metabolism. *J. Clin. Invest.* 127, 3845–3860. doi:10.1172/jci92067

Kuen, D. S., Park, M., Ryu, H., Choi, G., Moon, Y. H., Kim, J. O., et al. (2021). Critical Regulation of Follicular Helper T Cell Differentiation and Function by Gα13 Signaling. *Proc. Natl. Acad. Sci. U S A.* 118, 118. doi:10.1073/pnas.2108376118

Kumar, A., Kremer, K. N., Dominguez, D., Tadi, M., and Hedin, K. E. (2011). Gα13 and Rho Mediate Endosomal Trafficking of CXCR4 into Rab11+ Vesicles upon Stromal Cell-Derived Factor-1 Stimulation. *J.I.* 186, 951–958. doi:10.4049/jimmunol.1002019

Kumar, R. N., Shore, S. K., and Dhanasekaran, N. (2006). Neoplastic Transformation by the Gep Oncogene, Gα12, Involves Signaling by STAT3. *Oncogene* 25, 899–906. doi:10.1038/sj.onc.1209132

Lambright, D. G., Sondek, J., Bohm, A., Skiba, N. P., Hamm, H. E., and Sigler, P. B. (1996). The 2.0 Å crystal Structure of a Heterotrimeric G Protein. *Nature* 379, 311–319. doi:10.1038/379311a0

Leach, K., Wen, A., Cook, A. E., Sexton, P. M., Conigrave, A. D., and Christopoulos, A. (2013). Impact of Clinically Relevant Mutations on the Pharmacoregulation and Signaling Bias of the Calcium-Sensing Receptor by Positive and Negative Allosteric Modulators. *Endocrinology* 154, 1105–1116. doi:10.1210/en.2012-1887

Leach, K., Wen, A., Davey, A. E., Sexton, P. M., Conigrave, A. D., and Christopoulos, A. (2012). Identification of Molecular Phenotypes and Biased Signaling Induced by Naturally Occurring Mutations of the Human Calcium-Sensing Receptor. *Endocrinology* 153, 4304–4316. doi:10.1210/en.2012-1449

Lecointre, C., Desrues, L., Joubert, J. E., Perzo, N., Guichet, P.-O., Le Joncour, V., et al. (2015). Signaling Switch of the Urotensin II Vasoactive Peptide GPCR: Prototypic Chemotaxic Mechanism in Glioma. *Oncogene* 34, 5080–5094. doi:10.1038/onc.2014.433

Lee, C.-W., Rivera, R., Gardell, S., Dubin, A. E., and Chun, J. (2006). GPR92 as a New G12/13- and Gq-Coupled Lysophosphatidic Acid Receptor that Increases cAMP, LPA5. *J. Biol. Chem.* 281, 23589–23597. doi:10.1074/jbc.m603670200

Lee, J. H., Kim, D., Oh, Y. S., and Jun, H. S. (2019). Lysophosphatidic Acid Signaling in Diabetic Nephropathy. *Int. J. Mol. Sci.* 20. doi:10.3390/ijms20112850

Lee, S. J., Yang, J. W., Cho, I. J., Kim, W. D., Cho, M. K., Lee, C. H., et al. (2009). The Gep Oncogenes, Gα12 and Gα13, Upregulate the Transforming Growth Factor-β1 Gene. *Oncogene* 28, 1230–1240. doi:10.1038/onc.2008.488

Li, Y., Liu, M., Yang, S., Fuller, A. M., Karin Eisinger-Mathason, T. S., and Yang, S. (2021). RGS12 Is a Novel Tumor Suppressor in Osteosarcoma that Inhibits YAP-TEAD1-Ezrin Signaling. *Oncogene* 40, 2553–2566. doi:10.1038/s41388-020-01599-z

Lim, W. K., Chai, X., Ghosh, S., Ray, D., Wang, M., Rasheed, S. A. K., et al. (2019). Gα-13 Induces CXC Motif Chemokine Ligand 5 Expression in Prostate Cancer Cells by Transactivating NF-κB. *J. Biol. Chem.* 294, 18192–18206. doi:10.1074/jbc.ra119.010018

Litosch, I. (2012). Negative Feedback Regulation of Gq Signaling by Protein Kinase C Is Disrupted by Diacylglycerol Kinase ζ in COS-7 Cells. *Biochem. Biophysical Res. Commun.* 417, 956–960. doi:10.1016/j.bbrc.2011.12.037

Liu, B., Su, Q., Ma, J., Chen, C., Wang, L., Che, F., et al. (2021). Prognostic Value of Eight-Gene Signature in Head and Neck Squamous Carcinoma. *Front. Oncol.* 11, 657002. doi:10.3389/fonc.2021.657002

Liu, S.-C., Jen, Y.-M., Jiang, S. S., Chang, J.-L., Hsiung, C. A., Wang, C.-H., et al. (2009). Gα12-Mediated Pathway Promotes Invasiveness of Nasopharyngeal Carcinoma by Modulating Actin Cytoskeleton Reorganization. *Cancer Res.* 69, 6122–6130. doi:10.1158/0008-5472.can-08-3435

Liu, W., Li, H., Wang, Y., Zhao, X., Guo, Y., Jin, J., et al. (2017). MiR-30b-5p Functions as a Tumor Suppressor in Cell Proliferation, Metastasis and Epithelial-To-Mesenchymal Transition by Targeting G-Protein Subunit α-13 in Renal Cell Carcinoma. *Gene* 626, 275–281. doi:10.1016/j.gene.2017.05.040

Loskutov, Y. V., Griffin, C. L., Marinak, K. M., Bobko, A., Margaryan, N. V., Geldenhuys, W. J., et al. (2018). LPA Signaling Is Regulated through the Primary Cilium: a Novel Target in Glioblastoma. *Oncogene* 37, 1457–1471. doi:10.1038/s41388-017-0049-3

Lymperopoulos, A., Borges, J. I., Carbone, A. M., Cora, N., and Sizova, A. (2021). Cardiovascular Angiotensin II Type 1 Receptor Biased Signaling: Focus on Non-gq-, Non-βarrestin-dependent Signaling. *Pharmacol. Res.* 174, 105943. doi:10.1016/j.phrs.2021.105943

Mackenzie, A. E., Quon, T., Lin, L. C., Hauser, A. S., Jenkins, L., Inoue, A., et al. (2019). Receptor Selectivity between the G Proteins Gα 12 and Gα 13 Is Defined by a Single Leucine-to-isoleucine Variation. *FASEB j.* 33, 5005–5017. doi:10.1096/fj.201801956r

Mariggiò, S., Bavec, A., Natale, E., Zizza, P., Salmona, M., Corda, D., et al. (2006). Gα13 Mediates Activation of the Cytosolic Phospholipase A2α through fine Regulation of ERK Phosphorylation. *Cell Signal.* 18, 2200–2208. doi:10.1016/j.cellsig.2006.05.003

Masià-Balagué, M., Izquierdo, I., Garrido, G., Cordomí, A., Pérez-Benito, L., Miller, N. L. G., et al. (2015). Gastrin-stimulated Gα13 Activation of Rgnef Protein (ArhGEF28) in DLD-1 Colon Carcinoma Cells. *J. Biol. Chem.* 290, 15197–15209. doi:10.1074/jbc.m114.628164

Masuho, I., Skamangas, N. K., Muntean, B. S., and Martemyanov, K. A. (2021). Diversity of the Gβγ Complexes Defines Spatial and Temporal Bias of GPCR Signaling. *Cell Syst.* 12, 324–337. doi:10.1016/j.cels.2021.02.001

Mathew, D., Kremer, K. N., and Torres, R. M. (2019). ARHGEF1 Deficiency Reveals Gα13-Associated GPCRs Are Critical Regulators of Human Lymphocyte Function. *J. Clin. Invest.* 129, 965–968. doi:10.1172/jci125893

Maziarz, M., Federico, A., Zhao, J., Dujmusic, L., Zhao, Z., Monti, S., et al. (2020). Naturally Occurring Hotspot Cancer Mutations in Gα13 Promote Oncogenic Signaling. *J. Biol. Chem.* 295, 16897–16904. doi:10.1074/jbc.ac120.014698

McLaughlin, J. N., Patterson, M. M., and Malik, A. B. (2007). Protease-activated Receptor-3 (PAR3) Regulates PAR1 Signaling by Receptor Dimerization. *Proc. Natl. Acad. Sci.* 104, 5662–5667. doi:10.1073/pnas.0700763104

McNeil Coffield, V., Helms, W. S., Jiang, Q., and Su, L. (2004). Gα13 Mediates a Signal that Is Essential for Proliferation and Survival of Thymocyte Progenitors. *J. Exp. Med.* 200, 1315–1324. doi:10.1084/jem.20040944

Mende, F., Hundahl, C., Plouffe, B., Skov, L. J., Sivertsen, B., Madsen, A. N., et al. (2018). Translating Biased Signaling in the Ghrelin Receptor System into Differential *In Vivo* Functions. *Proc. Natl. Acad. Sci. USA* 115, E10255–E10264. doi:10.1073/pnas.1804003115

Mikelis, C. M., Palmby, T. R., Simaan, M., Li, W., Szabo, R., Lyons, R., et al. (2013). PDZ-RhoGEF and LARG Are Essential for Embryonic Development and Provide a Link between Thrombin and LPA Receptors and Rho Activation. *J. Biol. Chem.* 288, 12232–12243. doi:10.1074/jbc.m112.428599

Montgomery, E. R., Temple, B. R. S., Peters, K. A., Tolbert, C. E., Booker, B. K., Martin, J. W., et al. (2014). Gα12 Structural Determinants of Hsp90 Interaction Are Necessary for Serum Response Element-Mediated Transcriptional Activation. *Mol. Pharmacol.* 85, 586–597. doi:10.1124/mol.113.088443

Moriyama, S., Takahashi, N., Green, J. A., Hori, S., Kubo, M., Cyster, J. G., et al. (2014). Sphingosine-1-phosphate Receptor 2 Is Critical for Follicular Helper T Cell Retention in Germinal Centers. *J. Exp. Med.* 211, 1297–1305. doi:10.1084/jem.20131666

Mu, G., Ding, Q., Li, H., Zhang, L., Zhang, L., He, K., et al. (2018). Gastrin Stimulates Pancreatic Cancer Cell Directional Migration by Activating the Gα12/13-RhoA-ROCK Signaling Pathway. *Exp. Mol. Med.* 50, 1–14. doi:10.1038/s12276-018-0081-6

Müller, F. E., Schade, S. K., Cherkas, V., Stopper, L., Breithausen, B., Minge, D., et al. (2021). Serotonin Receptor 4 Regulates Hippocampal Astrocyte Morphology and Function. *Glia* 69, 872–889. doi:10.1002/glia.23933

Muppidi, J. R., Lu, E., and Cyster, J. G. (2015). The G Protein-Coupled Receptor P2RY8 and Follicular Dendritic Cells Promote Germinal center Confinement of B Cells, whereas S1PR3 Can Contribute to Their Dissemination. *J. Exp. Med.* 212, 2213–2222. doi:10.1084/jem.20151250

Muppidi, J. R., Schmitz, R., Green, J. A., Xiao, W., Larsen, A. B., Braun, S. E., et al. (2014). Loss of Signalling via Gα13 in Germinal centre B-Cell-Derived Lymphoma. *Nature* 516, 254–258. doi:10.1038/nature13765

Nakanishi, N., Ogata, T., Naito, D., Miyagawa, K., Taniguchi, T., Hamaoka, T., et al. (2016). MURC Deficiency in Smooth Muscle Attenuates Pulmonary Hypertension. *Nat. Commun.* 7, 12417. doi:10.1038/ncomms12417

Nakano, S., Inoue, K., Xu, C., Deng, Z., Syrovatkina, V., Vitone, G., et al. (2019). G-protein Gα13 Functions as a Cytoskeletal and Mitochondrial Regulator to Restrain Osteoclast Function. *Sci. Rep.* 9, 4236. doi:10.1038/s41598-019-40974-z

Nishida, M., Onohara, N., Sato, Y., Suda, R., Ogushi, M., Tanabe, S., et al. (2007). Gα12/13-mediated Up-Regulation of TRPC6 Negatively Regulates Endothelin-1-Induced Cardiac Myofibroblast Formation and Collagen Synthesis through Nuclear Factor of Activated T Cells Activation. *J. Biol. Chem.* 282, 23117–23128. doi:10.1074/jbc.m611780200

Noguchi, K., Ishii, S., and Shimizu, T. (2003). Identification of p2y9/GPR23 as a Novel G Protein-Coupled Receptor for Lysophosphatidic Acid, Structurally Distant from the Edg Family. *J. Biol. Chem.* 278, 25600–25606. doi:10.1074/jbc.m302648200

O'Hayre, M., Inoue, A., Kufareva, I., Wang, Z., Mikelis, C. M., Drummond, R. A., et al. (2016). Inactivating Mutations in GNA13 and RHOA in Burkitt's Lymphoma and Diffuse Large B-Cell Lymphoma: a Tumor Suppressor Function for the Gα13/RhoA axis in B Cells. *Oncogene* 35, 3771–3780. doi:10.1038/onc.2015.442

Olivera, A., Rosenfeldt, H. M., Bektas, M., Wang, F., Ishii, I., Chun, J., et al. (2003). Sphingosine Kinase Type 1 Induces G12/13-Mediated Stress Fiber Formation, yet Promotes Growth and Survival Independent of G Protein-Coupled Receptors. *J. Biol. Chem.* 278, 46452–46460. doi:10.1074/jbc.m308749200

Pang, A., Cheng, N., Cui, Y., Bai, Y., Hong, Z., Delaney, M. K., et al. (2020). High-loading Gα13-Binding EXE Peptide Nanoparticles Prevent Thrombosis and Protect Mice from Cardiac Ischemia/reperfusion Injury. *Sci. Transl Med.* 12. doi:10.1126/scitranslmed.aaz7287

Pang, A., Cui, Y., Chen, Y., Cheng, N., Delaney, M. K., Gu, M., et al. (2018). Shear-induced Integrin Signaling in Platelet Phosphatidylserine Exposure, Microvesicle Release, and Coagulation. *Blood* 132, 533–543. doi:10.1182/blood-2017-05-785253

Papasergi-Scott, M. M., Stoveken, H. M., MacConnachie, L., Chan, P. Y., Gabay, M., Wong, D., et al. (2018). Dual Phosphorylation of Ric-8A Enhances its Ability to Mediate G Protein α Subunit Folding and to Stimulate Guanine Nucleotide Exchange. *Sci. Signal.* 11, eaap8113. doi:10.1126/scisignal.aap8113

Park, H. W., Kim, Y. C., Yu, B., Moroishi, T., Mo, J.-S., Plouffe, S. W., et al. (2015). Alternative Wnt Signaling Activates YAP/TAZ. *Cell* 162, 780–794. doi:10.1016/j.cell.2015.07.013

Patel, M., Kawano, T., Suzuki, N., Hamakubo, T., Karginov, A. V., and Kozasa, T. (2014). Gα13/PDZ-RhoGEF/RhoA Signaling Is Essential for Gastrin-Releasing Peptide Receptor-Mediated Colon Cancer Cell Migration. *Mol. Pharmacol.* 86, 252–262. doi:10.1124/mol.114.093914

Pathe-neuschäfer-rube, A., Neuschäfer-rube, F., and Püschel, G. P. (2005). Role of the ERC Motif in the Proximal Part of the Second Intracellular Loop and the C-Terminal Domain of the Human Prostaglandin F2α Receptor (hFP-R) in G-Protein Coupling Control. *Biochem. J.* 388, 317–324. doi:10.1042/bj20041321

Piccinin, E., Villani, G., and Moschetta, A. (2019). Metabolic Aspects in NAFLD, NASH and Hepatocellular Carcinoma: the Role of PGC1 Coactivators. *Nat. Rev. Gastroenterol. Hepatol.* 16, 160–174. doi:10.1038/s41575-018-0089-3

Plastira, I., Bernhart, E., Joshi, L., Koyani, C. N., Strohmaier, H., Reicher, H., et al. (2020). MAPK Signaling Determines Lysophosphatidic Acid (LPA)-induced Inflammation in Microglia. *J. Neuroinflammation* 17, 127. doi:10.1186/s12974-020-01809-1

Profirovic, J., Strekalova, E., Urao, N., Krbanjevic, A., Andreeva, A. V., Varadarajan, S., et al. (2013). A Novel Regulator of Angiogenesis in Endothelial Cells: 5-hydroxytriptamine 4 Receptor. *Angiogenesis* 16, 15–28. doi:10.1007/s10456-012-9296-7

Qu, C., Liu, Y., Kunkalla, K., Singh, R. R., Blonska, M., Lin, X., et al. (2013). Trimeric G Protein-CARMA1 axis Links Smoothened, the Hedgehog Receptor Transducer, to NF-κB Activation in Diffuse Large B-Cell Lymphoma. *Blood* 121, 4718–4728. doi:10.1182/blood-2012-12-470153

Raghavan, S., Singh, N. K., Gali, S., Mani, A. M., and Rao, G. N. (2018). Protein Kinase Cθ via Activating Transcription Factor 2-Mediated CD36 Expression and Foam Cell Formation of Ly6C Hi Cells Contributes to Atherosclerosis. *Circulation* 138, 2395–2412. doi:10.1161/circulationaha.118.034083

Rasheed, S. A. K., Leong, H. S., Lakshmanan, M., Raju, A., Dadlani, D., Chong, F.-T., et al. (2018). GNA13 Expression Promotes Drug Resistance and Tumor-Initiating Phenotypes in Squamous Cell Cancers. *Oncogene* 37, 1340–1353. doi:10.1038/s41388-017-0038-6

Rasheed, S. A. K., Subramanyan, L. V., Lim, W. K., Udayappan, U. K., Wang, M., and Casey, P. J. (2021). The Emerging Roles of Galpha12/13 Proteins on the Hallmarks of Cancer in Solid Tumors. *Oncogene* 41, 147–158. doi:10.1038/s41388-021-02069-w

Rasheed, S. A. K., Teo, C. R., Beillard, E. J., Voorhoeve, P. M., and Casey, P. J. (2013). MicroRNA-182 and MicroRNA-200a Control G-Protein Subunit α-13 (GNA13) Expression and Cell Invasion Synergistically in Prostate Cancer Cells. *J. Biol. Chem.* 288, 7986–7995. doi:10.1074/jbc.m112.437749

Rasheed, S. A. K., Teo, C. R., Beillard, E. J., Voorhoeve, P. M., Zhou, W., Ghosh, S., et al. (2015). MicroRNA-31 Controls G Protein Alpha-13 (GNA13) Expression and Cell Invasion in Breast Cancer Cells. *Mol. Cancer* 14, 67. doi:10.1186/s12943-015-0337-x

Regué, L., Mou, F., and Avruch, J. (2013). G Protein-Coupled Receptors Engage the Mammalian Hippo Pathway through F-Actin. *Bioessays* 35, 430–435. doi:10.1002/bies.201200163

Rieken, S., Sassmann, A., Herroeder, S., Wallenwein, B., Moers, A., Offermanns, S., et al. (2006). G12/G13 Family G Proteins Regulate Marginal Zone B Cell Maturation, Migration, and Polarization. *J. Immunol.* 177, 2985–2993. doi:10.4049/jimmunol.177.5.2985

Rives, M.-L., Rady, B., Swanson, N., Zhao, S., Qi, J., Arnoult, E., et al. (2018). GPR40-Mediated Gα12 Activation by Allosteric Full Agonists Highly Efficacious at Potentiating Glucose-Stimulated Insulin Secretion in Human Islets. *Mol. Pharmacol.* 93, 581–591. doi:10.1124/mol.117.111369

Ruan, Y., Patzak, A., Pfeiffer, N., and Gericke, A. (2021). Muscarinic Acetylcholine Receptors in the Retina-Therapeutic Implications. *Int. J. Mol. Sci.* 22, 4989. doi:10.3390/ijms22094989

Rümenapp, U., Asmus, M., Schablowski, H., Woznicki, M., Han, L., Jakobs, K. H., et al. (2001). The M3 Muscarinic Acetylcholine Receptor Expressed in HEK-293 Cells Signals to Phospholipase D via G12 but Not Gq-type G Proteins. *J. Biol. Chem.* 276, 2474–2479. doi:10.1074/jbc.m004957200

Sabbir, M. G., Calcutt, N. A., and Fernyhough, P. (2018). Muscarinic Acetylcholine Type 1 Receptor Activity Constrains Neurite Outgrowth by Inhibiting Microtubule Polymerization and Mitochondrial Trafficking in Adult Sensory Neurons. *Front. Neurosci.* 12, 402. doi:10.3389/fnins.2018.00402

Scarlett, K. A., White, E.-S. Z., Coke, C. J., Carter, J. R., Bryant, L. K., and Hinton, C. V. (2018). Agonist-induced CXCR4 and CB2 Heterodimerization Inhibits Gα13/RhoA-Mediated Migration. *Mol. Cancer Res.* 16, 728–739. doi:10.1158/1541-7786.mcr-16-0481

Senarath, K., Kankanamge, D., Samaradivakara, S., Ratnayake, K., Tennakoon, M., and Karunarathne, A. (2018). Regulation of G Protein βγ Signaling. *Int. Rev. Cell Mol Biol* 339, 133–191. doi:10.1016/bs.ircmb.2018.02.008

Seyedabadi, M., Ghahremani, M. H., and Albert, P. R. (2019). Biased Signaling of G Protein Coupled Receptors (GPCRs): Molecular Determinants of GPCR/transducer Selectivity and Therapeutic Potential. *Pharmacol. Ther.* 200, 148–178. doi:10.1016/j.pharmthera.2019.05.006

Shen, B., Delaney, M. K., and Du, X. (2012). Inside-out, Outside-In, and Inside-Outside-In: G Protein Signaling in Integrin-Mediated Cell Adhesion, Spreading, and Retraction. *Curr. Opin. Cell Biol.* 24, 600–606. doi:10.1016/j.ceb.2012.08.011

Shen, B., Estevez, B., Xu, Z., Kreutz, B., Karginov, A., Bai, Y., et al. (2015). The Interaction of Gα13 with Integrin β1 Mediates Cell Migration by Dynamic Regulation of RhoA. *MBoC* 26, 3658–3670. doi:10.1091/mbc.e15-05-0274

Shen, B., Zhao, X., O'Brien, K. A., Stojanovic-Terpo, A., Delaney, M. K., Kim, K., et al. (2013). A Directional Switch of Integrin Signalling and a New Anti-thrombotic Strategy. *Nature* 503, 131–135. doi:10.1038/nature12613

Smrcka, A. V., and Fisher, I. (2019). G-protein βγ Subunits as Multi-Functional Scaffolds and Transducers in G-Protein-Coupled Receptor Signaling. *Cell. Mol. Life Sci.* 76, 4447–4459. doi:10.1007/s00018-019-03275-2

Sobel, K., Monnier, L., Menyhart, K., Bolinger, M., Studer, R., Nayler, O., et al. (2015). FTY720 Phosphate Activates Sphingosine-1-Phosphate Receptor 2 and Selectively Couples to Gα12/13/Rho/ROCK to Induce Myofibroblast Contraction. *Mol. Pharmacol.* 87, 916–927. doi:10.1124/mol.114.097261

Song, M. K., Park, C., Lee, Y. D., Kim, H., Kim, M. K., Kwon, J. O., et al. (2018). Gα12 Regulates Osteoclastogenesis by Modulating NFATc1 Expression. *J. Cell Mol Med* 22, 849–860. doi:10.1111/jcmm.13370

Spoerri, P. M., Strohmeyer, N., Sun, Z., Fässler, R., and Müller, D. J. (2020). Protease-activated Receptor Signalling Initiates α5β1-integrin-mediated Adhesion in Non-haematopoietic Cells. *Nat. Mater.* 19, 218–226. doi:10.1038/s41563-019-0580-4

Sriwai, W., Mahavadi, S., Al-Shboul, O., Grider, J. R., and Murthy, K. S. (2013). Distinctive G Protein-dependent Signaling by Protease-Activated Receptor 2 (PAR2) in Smooth Muscle: Feedback Inhibition of RhoA by cAMP-independent PKA. *PLoS One* 8, e66743. doi:10.1371/journal.pone.0066743

Stecky, R. C., Quick, C. R., Fleming, T. L., Mull, M. L., Vinson, V. K., Whitley, M. S., et al. (2020). Divergent C-Terminal Motifs in Gα12 and Gα13 Provide Distinct Mechanisms of Effector Binding and SRF Activation. *Cell Signal.* 72, 109653. doi:10.1016/j.cellsig.2020.109653

Strathmann, M. P., and Simon, M. I. (1991). G Alpha 12 and G Alpha 13 Subunits Define a Fourth Class of G Protein Alpha Subunits. *Proc. Natl. Acad. Sci.* 88, 5582–5586. doi:10.1073/pnas.88.13.5582

Subramanian, A., Capalbo, A., Iyengar, N. R., Rizzo, R., di Campli, A., Di Martino, R., et al. (2019). Auto-regulation of Secretory Flux by Sensing and Responding to the Folded Cargo Protein Load in the Endoplasmic Reticulum. *Cell* 176, 1461–1476. doi:10.1016/j.cell.2019.01.035

Sunahara, R. K., Tesmer, J. J. G., Gilman, A. G., and Sprang, S. R. (1997). Crystal Structure of the Adenylyl Cyclase Activator G S α. *Science* 278, 1943–1947. doi:10.1126/science.278.5345.1943

Svitkina, T. (2018). The Actin Cytoskeleton and Actin-Based Motility. *Cold Spring Harb Perspect. Biol.* 10, a018267. doi:10.1101/cshperspect.a018267

Syrovatkina, V., Alegre, K. O., Dey, R., and Huang, X.-Y. (2016). Regulation, Signaling, and Physiological Functions of G-Proteins. *J. Mol. Biol.* 428, 3850–3868. doi:10.1016/j.jmb.2016.08.002

Syrovatkina, V., and Huang, X. Y. (2019). Signaling Mechanisms and Physiological Functions of G-protein Gα 13 in Blood Vessel Formation, Bone Homeostasis, and Cancer. *Protein Sci.* 28, 305–312. doi:10.1002/pro.3531

Takefuji, M., Wirth, A., Lukasova, M., Takefuji, S., Boettger, T., Braun, T., et al. (2012). G 13 -Mediated Signaling Pathway Is Required for Pressure

Overload-Induced Cardiac Remodeling and Heart Failure. *Circulation* 126, 1972–1982. doi:10.1161/circulationaha.112.109256

Tan, L., Yan, W., McCorvy, J. D., and Cheng, J. (2018). Biased Ligands of G Protein-Coupled Receptors (GPCRs): Structure-Functional Selectivity Relationships (SFSRs) and Therapeutic Potential. *J. Med. Chem.* 61, 9841–9878. doi:10.1021/acs.jmedchem.8b00435

Tan, W., Martin, D., and Gutkind, J. S. (2006). The Gα13-Rho Signaling Axis Is Required for SDF-1-Induced Migration through CXCR4. *J. Biol. Chem.* 281, 39542–39549. doi:10.1074/jbc.m609062200

Tanaka, M., Okudaira, S., Kishi, Y., Ohkawa, R., Iseki, S., Ota, M., et al. (2006). Autotaxin Stabilizes Blood Vessels and Is Required for Embryonic Vasculature by Producing Lysophosphatidic Acid. *J. Biol. Chem.* 281, 25822–25830. doi:10.1074/jbc.m605142200

Teo, C. R., Casey, P. J., and Rasheed, S. A. K. (2016). The GNA13-RhoA Signaling axis Suppresses Expression of Tumor Protective Kallikreins. *Cell Signal.* 28, 1479–1488. doi:10.1016/j.cellsig.2016.07.001

Tesmer, J. J. G., Sunahara, R. K., Gilman, A. G., and Sprang, S. R. (1997). Crystal Structure of the Catalytic Domains of Adenylyl Cyclase in a Complex with G Sα ·GTPγS. *Science* 278, 1907–1916. doi:10.1126/science.278.5345.1907

Tiacci, E., Ladewig, E., Schiavoni, G., Penson, A., Fortini, E., Pettirossi, V., et al. (2018). Pervasive Mutations of JAK-STAT Pathway Genes in Classical Hodgkin Lymphoma. *Blood* 131, 2454–2465. doi:10.1182/blood-2017-11-814913

Toro-Tapia, G., Villaseca, S., Beyer, A., Roycroft, A., Marcellini, S., Mayor, R., et al. (2018). The Ric-8A/Gα13/FAK Signalling cascade Controls Focal Adhesion Formation during Neural Crest Cell Migration in Xenopus. *Development* 145, 145. doi:10.1242/dev.164269

Trivedi, V., Boire, A., Tchernychev, B., Kaneider, N. C., Leger, A. J., O'Callaghan, K., et al. (2009). Platelet Matrix Metalloprotease-1 Mediates Thrombogenesis by Activating PAR1 at a Cryptic Ligand Site. *Cell* 137, 332–343. doi:10.1016/j.cell.2009.02.018

Tsai, H.-J., Huang, C.-L., Chang, Y.-W., Huang, D.-Y., Lin, C.-C., Cooper, J. A., et al. (2014). Disabled-2 Is Required for Efficient Hemostasis and Platelet Activation by Thrombin in Mice. *Arterioscler Thromb. Vasc. Biol.* 34, 2404–2412. doi:10.1161/atvbaha.114.302602

Unsworth, A. J., Kriek, N., Bye, A. P., Naran, K., Sage, T., Flora, G. D., et al. (2017). PPAR γ Agonists Negatively Regulate α II Bβ3 Integrin Outside-in Signaling and Platelet Function through Up-regulation of Protein Kinase A Activity. *J. Thromb. Haemost.* 15, 356–369. doi:10.1111/jth.13578

van den Bos, E., Ambrosy, B., Horsthemke, M., Walbaum, S., Bachg, A. C., Wettschureck, N., et al. (2020). Knockout Mouse Models Reveal the Contributions of G Protein Subunits to Complement C5a Receptor-Mediated Chemotaxis. *J. Biol. Chem.* 295, 7726–7742. doi:10.1074/jbc.ra119.011984

Wang, J., Hua, T., and Liu, Z.-J. (2020). Structural Features of Activated GPCR Signaling Complexes. *Curr. Opin. Struct. Biol.* 63, 82–89. doi:10.1016/j.sbi.2020.04.008

Wang, L., Guo, D., Xing, B., Zhang, J. J., Shu, H.-B., Guo, L., et al. (2011). Resistance to Inhibitors of cholinesterase-8A (Ric-8A) Is Critical for Growth Factor Receptor-Induced Actin Cytoskeletal Reorganization. *J. Biol. Chem.* 286, 31055–31061. doi:10.1074/jbc.m111.253427

Wang, L., Luo, J.-Y., Li, B., Tian, X. Y., Chen, L.-J., Huang, Y., et al. (2016). Integrin-YAP/TAZ-JNK cascade Mediates Atheroprotective Effect of Unidirectional Shear Flow. *Nature* 540, 579–582. doi:10.1038/nature20602

Wang, L., Wang, D., Xing, B., Tan, Y.-c., Huang, J., Liu, B., et al. (2017). G-protein Gα13 Functions with Abl Kinase to Regulate Actin Cytoskeletal Reorganization. *J. Mol. Biol.* 429, 3836–3849. doi:10.1016/j.jmb.2017.10.020

Wang, N., Huang, H., Xiong, Q., Chen, N., Xi, N., Wu, P., et al. (2019). GNAQ Negatively Regulates Antiviral Innate Immune Responses in a Calcineurin-dependent Manner. *J.I.* 203, 1288–1297. doi:10.4049/jimmunol.1900427

Wang, Y., Li, Y., and Shi, G. (2013). The Regulating Function of Heterotrimeric G Proteins in the Immune System. *Arch. Immunol. Ther. Exp.* 61, 309–319. doi:10.1007/s00005-013-0230-5

Wang, Z., Guan, W., Han, Y., Ren, H., Tang, X., Zhang, H., et al. (2015). Stimulation of Dopamine D3 Receptor Attenuates Renal Ischemia-Reperfusion Injury via Increased Linkage with Gα12. *Transplantation* 99, 2274–2284. doi:10.1097/tp.0000000000000762

Ward, Y., Lake, R., Yin, J. J., Heger, C. D., Raffeld, M., Goldsmith, P. K., et al. (2011). LPA Receptor Heterodimerizes with CD97 to Amplify LPA-Initiated RHO-dependent Signaling and Invasion in Prostate Cancer Cells. *Cancer Res.* 71, 7301–7311. doi:10.1158/0008-5472.can-11-2381

White, J. P., Wrann, C. D., Rao, R. R., Nair, S. K., Jedrychowski, M. P., You, J.-S., et al. (2014). G Protein-Coupled Receptor 56 Regulates Mechanical Overload-Induced Muscle Hypertrophy. *Proc. Natl. Acad. Sci.* 111, 15756–15761. doi:10.1073/pnas.1417898111

Won, H. Y., Min, H. J., Lee, W. H., Kim, S. G., and Hwang, E. S. (2010). Gα12 Is Critical for TCR-Induced IL-2 Production and Differentiation of T Helper 2 and T Helper 17 Cells. *Biochem. Biophysical Res. Commun.* 394, 811–816. doi:10.1016/j.bbrc.2010.03.079

Worzfeld, T., Wettschureck, N., and Offermanns, S. (2008). G12/G13-mediated Signalling in Mammalian Physiology and Disease. *Trends Pharmacol. Sci.* 29, 582–589. doi:10.1016/j.tips.2008.08.002

Wu, M., Chen, W., Lu, Y., Zhu, G., Hao, L., and Li, Y.-P. (2017). Gα13 Negatively Controls Osteoclastogenesis through Inhibition of the Akt-GSK3β-NFATc1 Signalling Pathway. *Nat. Commun.* 8, 13700. doi:10.1038/ncomms13700

Wu, V., Yeerna, H., Nohata, N., Chiou, J., Harismendy, O., Raimondi, F., et al. (2019). Illuminating the Onco-GPCRome: Novel G Protein-Coupled Receptor-Driven Oncocrine Networks and Targets for Cancer Immunotherapy. *J. Biol. Chem.* 294, 11062–11086. doi:10.1074/jbc.rev119.005601

Wu, Y., Xu, J. X., El-Jouni, W., Lu, T., Li, S., Wang, Q., et al. (2016). Gα12 Is Required for Renal Cystogenesis Induced by Pkd1 Inactivation. *J. Cell Sci* 129, 3675–3684. doi:10.1242/jcs.190496

Xie, S., Mason, F. M., and Martin, A. C. (2016). Loss of Gα12/13 Exacerbates Apical Area Dependence of Actomyosin Contractility. *MBoC* 27, 3526–3536. doi:10.1091/mbc.e16-05-0305

Xu, N., Bradley, L., Ambdukar, I., and Gutkind, J. S. (1993). A Mutant Alpha Subunit of G12 Potentiates the Eicosanoid Pathway and Is Highly Oncogenic in NIH 3T3 Cells. *Proc. Natl. Acad. Sci.* 90, 6741–6745. doi:10.1073/pnas.90.14.6741

Yagi, H., Tan, W., Dillenburg-Pilla, P., Armando, S., Amornphimoltham, P., Simaan, M., et al. (2011). A Synthetic Biology Approach Reveals a CXCR4-G13-Rho Signaling axis Driving Transendothelial Migration of Metastatic Breast Cancer Cells. *Sci. Signal.* 4, ra60. doi:10.1126/scisignal.2002221

Yagi, H., Asanoma, K., Ohgami, T., Ichinoe, A., Sonoda, K., and Kato, K. (2016). GEP Oncogene Promotes Cell Proliferation through YAP Activation in Ovarian Cancer. *Oncogene* 35, 4471–4480. doi:10.1038/onc.2015.505

Yagi, H., Onoyama, I., Asanoma, K., Hori, E., Yasunaga, M., Kodama, K., et al. (2019). Gα13-mediated LATS1 Down-Regulation Contributes to Epithelial-Mesenchymal Transition in Ovarian Cancer. *FASEB J.* 33, 13683–13694. doi:10.1096/fj.201901278r

Yanagida, K., Igarashi, H., Yasuda, D., Kobayashi, D., Ohto-Nakanishi, T., Akahoshi, N., et al. (2018). The Gα12/13-Coupled Receptor LPA4 Limits Proper Adipose Tissue Expansion and Remodeling in Diet-Induced Obesity. *JCI Insight* 3, e97293. doi:10.1172/jci.insight.97293

Yanagida, K., Masago, K., Nakanishi, H., Kihara, Y., Hamano, F., Tajima, Y., et al. (2009). Identification and Characterization of a Novel Lysophosphatidic Acid Receptor, p2y5/LPA6. *J. Biol. Chem.* 284, 17731–17741. doi:10.1074/jbc.m808506200

Yanamadala, V., Negoro, H., Gunaratnam, L., Kong, T., and Denker, B. M. (2007). Gα12 Stimulates Apoptosis in Epithelial Cells through JNK1-Mediated Bcl-2 Degradation and Up-Regulation of IκBα. *J. Biol. Chem.* 282, 24352–24363. doi:10.1074/jbc.m702804200

Yang, Y. M., Kuen, D.-S., Chung, Y., Kurose, H., and Kim, S. G. (2020). Gα12/13 Signaling in Metabolic Diseases. *Exp. Mol. Med.* 52, 896–910. doi:10.1038/s12276-020-0454-5

Yang, Y. M., Lee, W. H., Lee, C. G., An, J., Kim, E.-S., Kim, S. H., et al. (2015). Gα12 Gep Oncogene Deregulation of P53-Responsive microRNAs Promotes Epithelial-Mesenchymal Transition of Hepatocellular Carcinoma. *Oncogene* 34, 2910–2921. doi:10.1038/onc.2014.218

Yasuda, D., Kobayashi, D., Akahoshi, N., Ohto-Nakanishi, T., Yoshioka, K., Takuwa, Y., et al. (2019). Lysophosphatidic Acid-Induced YAP/TAZ Activation Promotes Developmental Angiogenesis by Repressing Notch Ligand Dll4. *J. Clin. Invest.* 129, 4332–4349. doi:10.1172/jci121955

Ye, D., and Lin, F. (2013). S1pr2/Gα13 Signaling Controls Myocardial Migration by Regulating Endoderm Convergence. *Development* 140, 789–799. doi:10.1242/dev.085340

Ye, D., Xie, H., Hu, B., and Lin, F. (2015). Endoderm Convergence Controls Subduction of the Myocardial Precursors during Heart-Tube Formation. *Development* 142, 2928–2940. doi:10.1242/dev.113944

Yoo, E. J., Cao, G., Koziol-White, C. J., Ojiaku, C. A., Sunder, K., Jude, J. A., et al. (2017). Gα12facilitates Shortening in Human Airway Smooth Muscle by Modulating Phosphoinositide 3-Kinase-Mediated Activation in a RhoA-dependent Manner. *Br. J. Pharmacol.* 174, 4383–4395. doi:10.1111/bph.14040

Yu, W., Beaudry, S., Negoro, H., Boucher, I., Tran, M., Kong, T., et al. (2012). H2O2 Activates G Protein, 12 to Disrupt the Junctional Complex and Enhance Ischemia Reperfusion Injury. *Proc. Natl. Acad. Sci.* 109, 6680–6685. doi:10.1073/pnas.1116800109

Yu, X., Zhang, Y., and Chen, H. (2016). LPA Receptor 1 Mediates LPA-Induced Ovarian Cancer Metastasis: an *In Vitro* and *In Vivo* Study. *BMC Cancer* 16, 846. doi:10.1186/s12885-016-2865-1

Yuan, B., Cui, J., Wang, W., and Deng, K. (2016). Gα12/13 Signaling Promotes Cervical Cancer Invasion through the RhoA/ROCK-JNK Signaling axis. *Biochem. Biophysical Res. Commun.* 473, 1240–1246. doi:10.1016/j.bbrc.2016.04.048

Yung, B. S., Brand, C. S., Xiang, S. Y., Gray, C. B. B., Means, C. K., Rosen, H., et al. (2017). Selective Coupling of the S1P 3 Receptor Subtype to S1P-Mediated RhoA Activation and Cardioprotection. *J. Mol. Cell Cardiol.* 103, 1–10. doi:10.1016/j.yjmcc.2016.12.008

Zhang, L., Dong, Y., Wang, Y., Hu, W., Dong, S., and Chen, Y. (2020). Sphingosine-1-phosphate (S1P) Receptors: Promising Drug Targets for Treating Bone-related Diseases. *J. Cell Mol Med* 24, 4389–4401. doi:10.1111/jcmm.15155

Zhang, Y., Zhang, J., Yan, R., Tian, J., Zhang, Y., Zhang, J., et al. (2017). Receptor-interacting Protein Kinase 3 Promotes Platelet Activation and Thrombosis. *Proc. Natl. Acad. Sci. USA* 114, 2964–2969. doi:10.1073/pnas.1610963114

Zuo, C., Li, X., Huang, J., Chen, D., Ji, K., Yang, Y., et al. (2018). Osteoglycin Attenuates Cardiac Fibrosis by Suppressing Cardiac Myofibroblast Proliferation and Migration through Antagonizing Lysophosphatidic Acid 3/matrix Metalloproteinase 2/epidermal Growth Factor Receptor Signalling. *Cardiovasc. Res.* 114, 703–712. doi:10.1093/cvr/cvy035

Conflict of Interest: The authors declare that the research was conducted in the absence of any commercial or financial relationships that could be construed as a potential conflict of interest.

Publisher's Note: All claims expressed in this article are solely those of the authors and do not necessarily represent those of their affiliated organizations, or those of the publisher, the editors and the reviewers. Any product that may be evaluated in this article, or claim that may be made by its manufacturer, is not guaranteed or endorsed by the publisher.

Copyright © 2022 Guo, Tai, Wang, Sun, Zhang, Wei, Xiang and Wang. This is an open-access article distributed under the terms of the Creative Commons Attribution License (CC BY). The use, distribution or reproduction in other forums is permitted, provided the original author(s) and the copyright owner(s) are credited and that the original publication in this journal is cited, in accordance with accepted academic practice. No use, distribution or reproduction is permitted which does not comply with these terms.

GLOSSARY

5-HT4R 5-hydroxytryptamine type 4 receptor
AKT protein kinase B
Ang II angiotensin II
AP-1 activator protein 1
AT1R Ang II type 1 receptor
CXCL12 C-X-C motif chemokine 12
CXCR4 C-X-C chemokine receptor 4
DLBCL diffuse large B-cell lymphoma
ERK extracellular regulated protein kinases
FAK focal adhesion kinase
FZD Frizzled
GEF guanine nucleotide exchange factors
GPCRs G protein-coupled receptors
GRP gastrin-releasing peptide
GPR56 g protein-coupled receptor 56
HNSCC head and neck squamous cell carcinoma
I/R ischemia/reperfusion
JNK c-Jun N-terminal kinase
LATS1/2 large tumor suppressor 1/2
LPA lysophosphatidic acid
LPAR LPA receptor
MAPK mitogen-activated protein kinase
MRTF myocardin-related transcription factor
NFAT activated T cell nuclear factor
NFATc1 nuclear factor of activated T-cell c1
NF-κB nuclear factor-kappa B
PARs protease-activated receptors
PI3K phosphatidylinositol 3-kinase
PKC protein kinase C
PLC phospholipase C
PPARγ peroxisome proliferator-activated receptor-γ
RGS regulators of G protein signaling
RhoGEF Rho guanine nucleotide exchange factor
RhoA ras homolog family member A
Ric-8A resistance to inhibitors of cholinesterase 8A
ROCK Rho-associated protein kinase
ROS reactive oxygen species
S1P sphingosine 1-phosphate
SRF serum response factor
Tfh T follicular helper
Th T helper
WNT Wingless/Int-1 lipoglycoprotein
YAP/TAZ yes-associated protein/transcriptional coactivator with PDZ-binding motif

frontiers in Cell and Developmental Biology

ORIGINAL RESEARCH
published: 03 March 2022
doi: 10.3389/fcell.2022.806081

Atorvastatin Induces Mitochondria-Dependent Ferroptosis *via* the Modulation of Nrf2-xCT/GPx4 Axis

Qi Zhang[1], Hang Qu[1], Yinghui Chen[1], Xueyang Luo[1], Chong Chen[1], Bing Xiao[1], Xiaowei Ding[1], Pengjun Zhao[2], Yanan Lu[2], Alex F. Chen[1] and Yu Yu[1]**

[1]Institute for Developmental and Regenerative Cardiovascular Medicine, Xinhua Hospital, School of Medicine, Shanghai Jiao Tong University, Shanghai, China, [2]Department of Pediatric Cardiology, Xinhua Hospital, School of Medicine, Shanghai Jiao Tong University, Shanghai, China

OPEN ACCESS

Edited by:
Xiongwen Chen,
Temple University, United States

Reviewed by:
Qian Xiang,
Peking University First Hospital, China
Jamal Bouitbir,
University of Basel, Switzerland

***Correspondence:**
Yu Yu
yuyu@xinhuamed.com.cn
Alex F. Chen
chenfengyuan@xinhuamed.com.cn

Specialty section:
This article was submitted to Cell Death and Survival, a section of the journal Frontiers in Cell and Developmental Biology

Received: 31 October 2021
Accepted: 03 February 2022
Published: 03 March 2022

Citation:
Zhang Q, Qu H, Chen Y, Luo X, Chen C, Xiao B, Ding X, Zhao P, Lu Y, Chen AF and Yu Y (2022) Atorvastatin Induces Mitochondria-Dependent Ferroptosis via the Modulation of Nrf2-xCT/GPx4 Axis. Front. Cell Dev. Biol. 10:806081. doi: 10.3389/fcell.2022.806081

As one of the cornerstones of clinical cardiovascular disease treatment, statins have an extensive range of applications. However, statins commonly used have side reactions, especially muscle-related symptoms (SAMS), such as muscle weakness, pain, cramps, and severe condition of rhabdomyolysis. This undesirable muscular effect is one of the chief reasons for statin non-adherence and/or discontinuation, contributing to adverse cardiovascular outcomes. Moreover, the underlying mechanism of muscle cell damage is still unclear. Here, we discovered that ferroptosis, a programmed iron-dependent cell death, serves as a mechanism in statin-induced myopathy. Among four candidates including atorvastatin, lovastatin, rosuvastatin, and pravastatin, only atorvastatin could lead to ferroptosis in human cardiomyocytes (HCM) and murine skeletal muscle cells (C2C12), instead of human umbilical vein endothelial cell (HUVEC). Atorvastatin inhibits HCM and C2C12 cell viability in a dose-dependent manner, accompanying with significant augmentation in intracellular iron ions, reactive oxygen species (ROS), and lipid peroxidation. A noteworthy investigation found that those alterations particularly occurred in mitochondria and resulted in mitochondrial dysfunction. Biomarkers of myocardial injury increase significantly during atorvastatin intervention. However, all of the aforementioned enhancement could be restrained by ferroptosis inhibitors. Mechanistically, GSH depletion and the decrease in nuclear factor erythroid 2-related factor 2 (Nrf2), glutathione peroxidase 4 (GPx4), and xCT cystine–glutamate antiporter (the main component is SLC7A11) are involved in atorvastatin-induced muscular cell ferroptosis and damage. The downregulation of GPx4 in mitochondria-mediated ferroptosis signaling may be the core of it. In conclusion, our findings explore an innovative underlying pathophysiological mechanism of atorvastatin-induced myopathy and highlight that targeting ferroptosis serves as a protective strategy for clinical application.

Keywords: ferroptosis, atorvastatin, cardiomyocytes, lipid peroxidation, ROS

INTRODUCTION

Statins, inhibitors of 3-hydroxy-3-methyl-glutaryl-coenzyme A (HMG-CoA) reductase, are the most extensively applied cholesterol-reducing medicine to prevent cardiovascular events (Downs et al., 1998). In addition, statins exhibit pleiotropic cellular effects and have potential role in the treatment of many other conditions, including peripheral arterial disease, idiopathic dilated cardiomyopathy, ventricular arrhythmias, and cancer. Although statins are generally safe, treatment adherence is not optimal in a considerable proportion of patients, resulting in poor cardiovascular outcomes. Among them, the adverse effects of statin-associated muscle symptoms (SAMS) have the greatest health burden (Thompson et al., 2016; Bergt et al., 2017; Ward et al., 2019), including muscular pain, nocturnal muscle cramping, weakness, rare rhabdomyolysis, and amyotrophic lateral sclerosis (ALS)-like muscle wasting conditions (Bai et al., 2021). To date, there is no therapeutic approach for eliminating the adverse effects of statins, and the molecular mechanism underlying the etiology and pathophysiology of the statin-relative adverse effects still remain largely unknown.

Previous studies about SAMS focused on skeletal muscle, and the majority of mechanisms were centered on mitochondrial dysfunction, oxidative stress, immune-mediated necrotizing myopathy, and inhibition of isoprenylation of small G-proteins, owing to impaired mevalonate metabolism upon skeletal muscle damage (Cao et al., 2009; Musset et al., 2016; Thompson et al., 2016; Tiniakou and Christopher-Stine, 2017). But these just account for only a small percentage of it. As for cardiac muscle, a special kind of striated muscle, previous reports demonstrated that the mechanisms of SAMS in cardiac muscle mainly concentrate on mitochondrial dysfunction and apoptosis (Bonifacio et al., 2016; Godoy et al., 2019).

Programmed cell death is a basic physiological process in aging, development, and tissue homeostasis, which is often dysregulated in different pathological conditions. As such, a newly recognized form of programmed cell death, which is termed as ferroptosis (Dixon et al., 2012), has been implicated to play a critical pathogenic role in diverse cardiovascular conditions such as drug side effect or ischemia/reperfusion injury (Tadokoro et al., 2020; Menon et al., 2021). Those reports highlight that targeting ferroptosis may be a cardioprotective strategy (Fang et al., 2019; Tadokoro et al., 2020; Menon et al., 2021). There are two cellular protective systems against ferroptosis: the glutathione-dependent pathway involving GPx4 as well as System Xc−, and the CoQ-dependent pathway involving FSP1 on the plasma membrane (Bersuker et al., 2019; Doll et al., 2019) as well as DHODH in mitochondria (Mao et al., 2021). Whether ferroptosis was involved in the adverse effects of statins and the possible mechanism remains unclear.

In this study, we found that ferroptosis is responsible for atorvastatin-induced muscular injury both in cardiomyocytes and skeletal muscle cells. Mechanistically, atorvastatin induces ferroptosis by suppressing the intracellular anti-oxidative system, Nrf2-xCT/GPx4 pathway, resulting in the lethal lipid peroxidation within muscular cells. Our results for the first time demonstrated that ferroptosis is the pathogenic mechanism of atorvastatin-induced myopathy, providing a novel therapeutic target for improving atorvastatin application strategies.

MATERIALS AND METHODS

Cell Culture and Drug Treatments

HCM, C2C12 and HUVEC were cultured in high-glucose DMEM (Gibco BRL, USA) supplemented with 5% fetal bovine serum (Gibco BRL, USA) without antibiotics in acceptable conditions (5% CO_2, 37°C). Ferrostatin-1 (Fer-1), deferoxamine mesylate (DFO), liproxstatin-1 (Lip-1), RSL3, Z-VAD-FMK and mitoTEMPO (MT) were purchased from Selleck (Selleck, China). Atorvastatin, lovastatin, pravastatin, and rosuvastatin were obtained from MCE (MedChemExpress, China). Fer-1, DFO, Lip-1, RSL3, Z-VAD-FMK and MT were dissolved in dimethylsulfoxide (DMSO) and diluted in a culture medium at ultimate concentrations (0.5 μM with RSL3; 1 μM with Fer-1; 80 μM with DFO; 1 μM with Lip-1; 10 mM with mitoTEMPO; and 2 μM with Z-VAD-FMK). Statins were stocked as 50 mM solutions in DMSO. Final concentrations ranged from 10 to 160 μM.

Cell Viability Assay

In brief, the cultured cells were seeded at the density of 5,000 cells per well in 96-well plates with three replicates. Cells were treated with statins at the dosages of 0, 10, 20, 40, 80 and 160 μM in experimental groups. Meanwhile, the normal culture medium without addition of any statins was set as the control group. Then a Cell Counting Kit-8 (CCK-8) (Sigma, USA) was used to assess cell viability in line with manufacturer's instructions. Cell viability = Absorbance of (experimental group − blank control group)/ absorbance of (control group − blank control group).

Iron Assay

FerroOrange and Mito-FerroGreen probes (DojinDo, Japan) were employed to assess intracellular and mitochondrial iron content, respectively. HCM and C2C12 cells were seeded into 24-well plates and exposed to atorvastatin at the concentrations of 40 uM alone, or other treatments for 24 h. After that, the cells were stained with FerroOrange (1 μM) or Mito-FerroGreen (5 μM) probes along with Hoechst 33,342 (5 μg/ml). After 30 min of lucifuge incubation, the cells were then evaluated by a Leica SP8 confocal fluorescence microscope (Leica Microsystems, Germany).

Detection of Cellular ROS Levels

Intracellular and mitochondrial ROS levels were detected using fluorescent measurement assay by the uptake of 1 μM DCFH-DA (Beyotime, China) and 5 μM MitoSOX Red (Thermo Scientific, USA), respectively. Images were obtained by a Leica SP8 confocal laser scanning microscope (Leica Microsystems, Germany). Fluorescence intensity was measured by ImageJ (National Institutes of Health, USA). The

mean fluorescent intensity of each group was standardized to that of the control group.

Lipid Peroxidation Levels

Lipid peroxidation was measured using C11-BODIPY581/591(Invitrogen™, USA) and MitoPeDPP (Dojindo, Japan) kits. After incubation with C11-BODIPY581/591 and MitoPeDPP solution, lipid peroxidation in the mitochondrial inner membrane was fluorometrically measured at 470 nm using a fluorescence microscope (Leica Microsystems, Germany). The investigation of MDA consistency was strictly conducted in accordance with the manufacturer's instructions (Beyotime, China). For the MDA assay, thiobarbituric acid (TBA) was supplied to supernatants of cell homogenate and softly oscillated for the formation of TBA-MDA mixture. Then the mixture was detected spectrophotometrically at 535 nm, and the BCA protein determination kit (Beyotime, China) was employed for total protein quantification.

Mitochondrial Membrane Potential Levels

Mitochondrial membrane potential (MMP) was estimated by TMRM (Thermo Fisher Scientific, USA) staining. HCM and C2C12 cells were stained with TMRM at an ultimate concentration of 200 nmol/L. Images were acquired by a fluorescence microscope (Leica Microsystems, Germany).

MitoTracker Red CMXRos Staining

To locate the mitochondria, cultured cells were stained with 200 nM MitoTracker Red CMXRos (Thermo Fisher Scientific, USA) for 15 min at room temperature in the dark. Subsequently, cells were washed with PBS and then randomly captured by using a confocal microscope (Leica Microsystems, Germany).

Transmission Electron Microscopy

Cells were fixed with 2.5% glutaraldehyde in 0.1 mol/L of Sorenson's buffer (0.1 mol/L H2PO4 and 0.1 mol/L HPO4 [pH 7.2]) at 4°C overnight, washed three times with PBS, and then treated with 1% OsO4 in 0.1 mol/L of Sorenson's buffer for 2 h at room temperature. After dehydration using an ethanol series and acetone (100%), cells were embedded in acetone and embed-812. Thin sections were cut using an ultramicrotome (Leica Microsystems, Germany), and the sections were subjected to double staining with uranyl acetate and lead citrate and then observed using a transmission electron microscope (Hitachi HT7800, Japan).

Quantitative Real-Time PCR

Total RNA from C2C12 cells was extracted by using the EZ-press RNA purification kit (EZBioscience, USA), according to manufacturer's instruction. Then RNA was reverse-transcribed to cDNA by using a reverse transcription kit (Takara, China). Quantitative PCR was performed by using SYBR Green master mix (Takara, China) on a real-time PCR system (Biorad, USA). The results were normalized to β-actin as an internal control. All data were expressed in terms of fold-change relative to the control samples.

Enzyme-Linked Immunosorbent Assay

The level of CoQ10 and CKMB in HCM was measured by ELISA. After different treatment conditions, the supernatants of HCM were collected for ELISA using CoQ10 and CKMB Enzyme Immunoassay (EIA) kits (Clond-Clone, China), respectively.

GSH/GSSG and GSH-Px Detection

The commercialized GSH/GSSG assay kit and the GSH-Px assay kit were used to measure the intracellular levels of GSH, GSSG, and GSH-Px, respectively (Beyotime, China), in accordance with the instructions of the manufacturer.

Western Blot

Cells were lysed with a cold radio-immunoprecipitation assay (RIPA) (Beyotime, China) lysis buffer plus protease and a phosphatase inhibitor. The protein concentrations were detected by a bicinchoninic acid kit (BCA) (Beyotime, China). Protein sample were separated *via* 12% SDS-PAGE and moved to positively charged nylon (PVDF) membranes (Immobilon-P, Millipore, Switzerland). After blocking with bovine serum albumin (BSA), the membranes were detected using anti-Nrf2 (1:5,000, Abcam), anti-GPX4 (1:1,000, Abcam), anti-SLC7A11 (1:1,000, Abcam), anti-DHODH (1:1,000, Abcam) and anti-β-actin (1:10,000, Abclone). Horseradish peroxidase-conjugated secondary antibodies were diluted 1:10,000 and incubated for 1 h, and chemiluminescence solution and an electrochemiluminescence (ECL) kit (Millipore, USA) were used to detect protein band.

Statistical Analysis

Data were exhibited as mean ± standard deviation (SD). Statistical analysis was performed using unpaired Student's t-tests, one-way or two-way ANOVA, followed by Dunnett's method for multiple comparisons, and Prism 8.0 software (GraphPad Software, United States) was used to perform all the statistical testing and the creation of graphs. Statistical significance was considered at $p < 0.05$. All the experiments were repeated at least three times.

RESULTS

Ferroptosis Contributes to Atorvastatin-Induced Cell Damage in HCM and C2C12 Cells

Above all, we detected the cell viability of statins in different cell lines. As shown in **Figures 1A,E** and **Supplementary Figure S1A**, atorvastatin and lovastatin reduced cell viability with increasing concentrations of statins in HCM, C2C12 and HUVEC, while rosuvastatin and pravastatin did not (**Figures 1A,E** and **Supplementary Figure S1A**). In order to explore whether restriction of ferroptosis could prevent the cell damage induced by atorvastatin and lovastatin, the cells were preprocessed with DFO, Fer-1 or Lip-1 for 2 h and cocultured with atorvastatin or lovastatin for another 24 h. Interestingly, only cell death caused by atorvastatin can be restrained by the treatment with ferroptosis inhibitor, such as DFO (**Figures 1B,F**), Fer-1 (**Figures 1C,G**) and Lip-1 (**Figures 1D,H**), while cell death caused by lovastatin cannot be rescued by

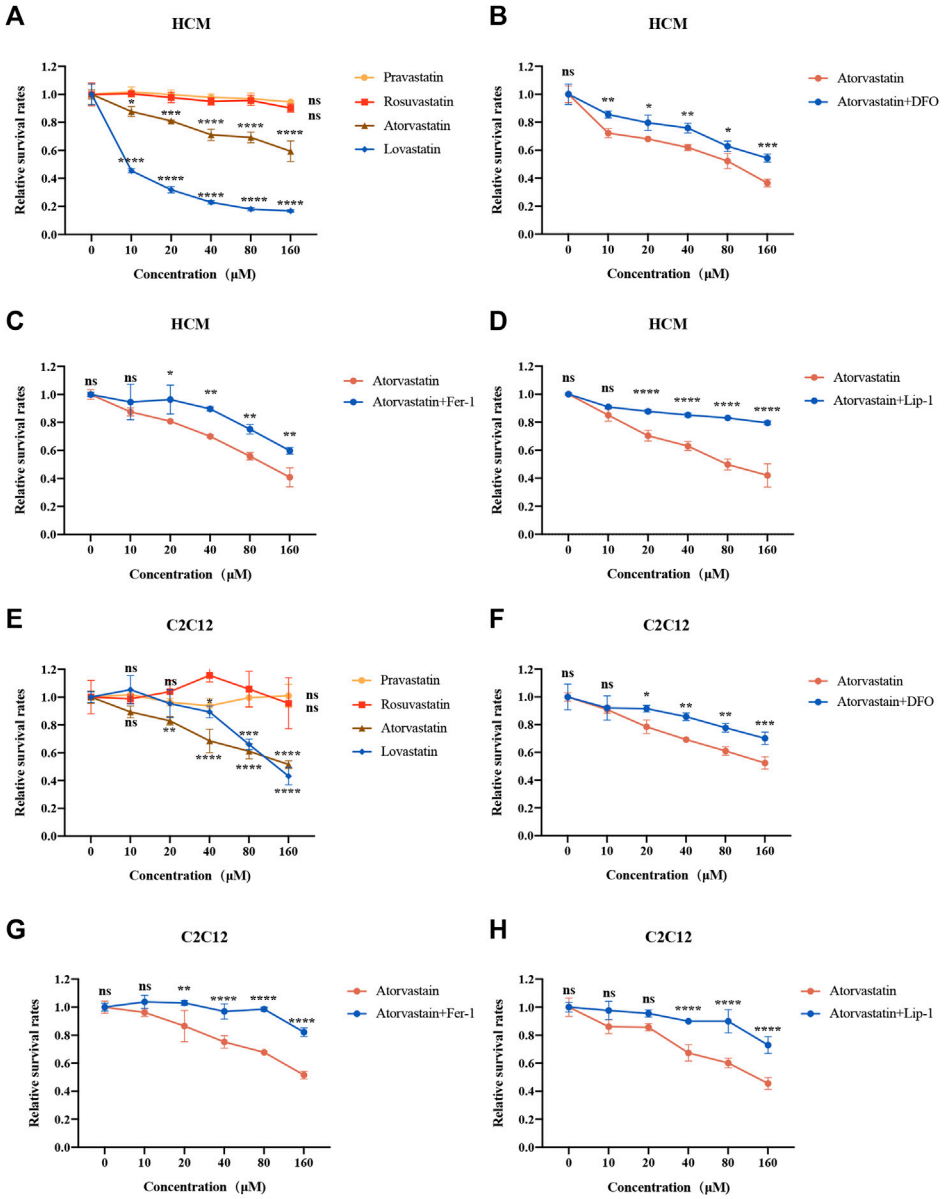

FIGURE 1 | Cell viability of two kinds of muscular cell lines in response to statins for 24 h. **(A)** HCM intervened with increasing concentrations of statins were analyzed by CCK8. **(B–D)** HCM were pretreated with 100 μM DFO, 1 μM Fer-1 or 1 μM Lip-1 for 2 h, followed by the addition of increasing concentration (0–160 μM) of atorvastatin for 24 h and analyzed by CCK-8. **(E)** C2C12 cells intervened with increasing concentrations of statins for 24 h were analyzed by Cell Counting Kit-8 (CCK-8). **(F–H)** C2C12 were pretreated with 100 μM DFO, 1 μM Fer-1 or 1 μM Lip-1 for 2 h, followed by the addition of increasing concentration of atorvastatin for 24 h and analyzed by CCK-8. Data are shown as mean ± SD. ns, no significant; $^{*}p < 0.05$, $^{**}p < 0.01$, $^{***}p < 0.001$, $^{****}p < 0.0001$ vs. the control group. $n = 3$.

Fer-1 in HCM and C2C12 (**Supplementary Figures S2A,B**). As in HUVEC cell lines, only atorvastatin and lovastatin could cause cell death (**Supplementary Figure S1A**), but the cell death induced by atorvastatin or lovastatin could not be rescued by ferroptosis inhibitors (**Supplementary Figures S1B,C**). Results suggested that ferroptosis is related to atorvastatin-induced cell injury, which was restrained within muscular cell lines. Based on the cell viability data, the concentration of 40 μM statins was selected for the deeper research. As anterior studies present that atorvastatin induces apoptosis, we also intervened HCM and C2C12 cells with caspase inhibitor Z-VAD-FMK along with atorvastatin. But our findings were inconsistent with those reported previously as the cell death damaged by atorvastatin could not be rescued by apoptosis inhibitor Z-VAD-FMK (**Supplementary Figures S3A,B**).

Atorvastatin Exposure Leads to Iron Overload in HCM and C2C12 Cells

Intracellular iron overload is a characteristic of cellular ferroptosis; therefore, we detected the level of intracellular iron

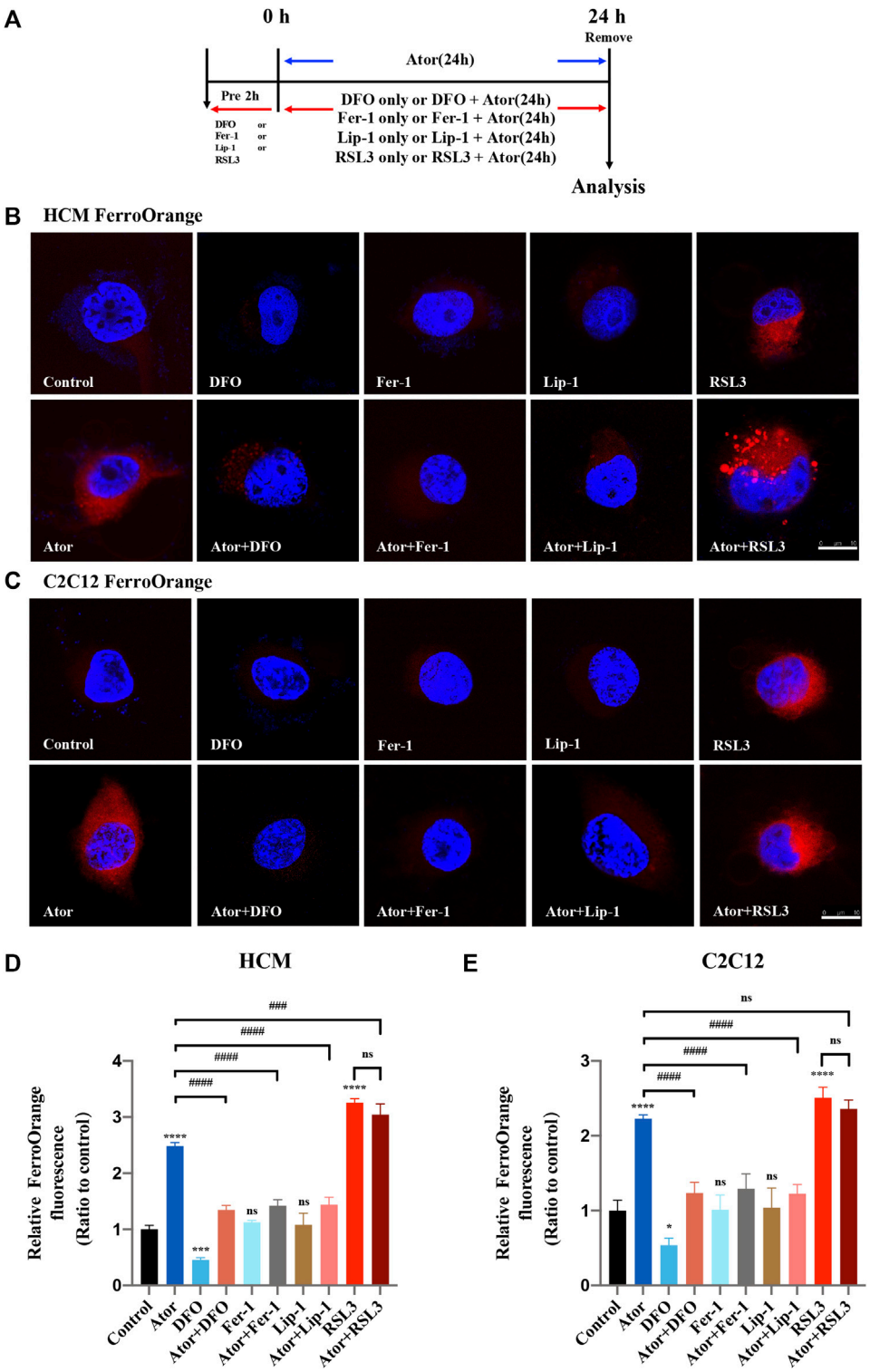

FIGURE 2 | Iron accumulation in atorvastatin-supplemented HCM and C2C12 cells. **(A)** Experimental workflow. The muscular cells were pretreated with 100 μM DFO, 1 μM Fer-1, 1 μM Lip-1 or 0.5 μM RSL3 for 2 h and then intervened with or without 40 μM atorvastatin for another 24 h, or treated with 40 μM atorvastatin alone for 24 h. **(B)** Representative images of HCM treated by atorvastatin alone or with ferroptosis inhibitors DFO, Fer-1 and Lip-1 stained with FerroOrange, an indicator of intracellular Fe^{2+}. **(C)** Representative images of C2C12 stained with FerroOrange. **(D)** Quantification of relative fluorescence intensity of FerroOrange in HCM. **(E)** Quantification of relative fluorescence intensity of FerroOrange in C2C12. Fluorescence intensity was quantified by ImageJ software. The data are shown as mean ± SD. ns, no significant; $^{*}p < 0.05$, $^{***}p < 0.001$, $^{****}p < 0.0001$ vs. the control group; $^{\#\#\#}p < 0.001$, $^{\#\#\#\#}p < 0.0001$ vs. the atorvastatin group. $n = 3$. Scale bar: 10 μm.

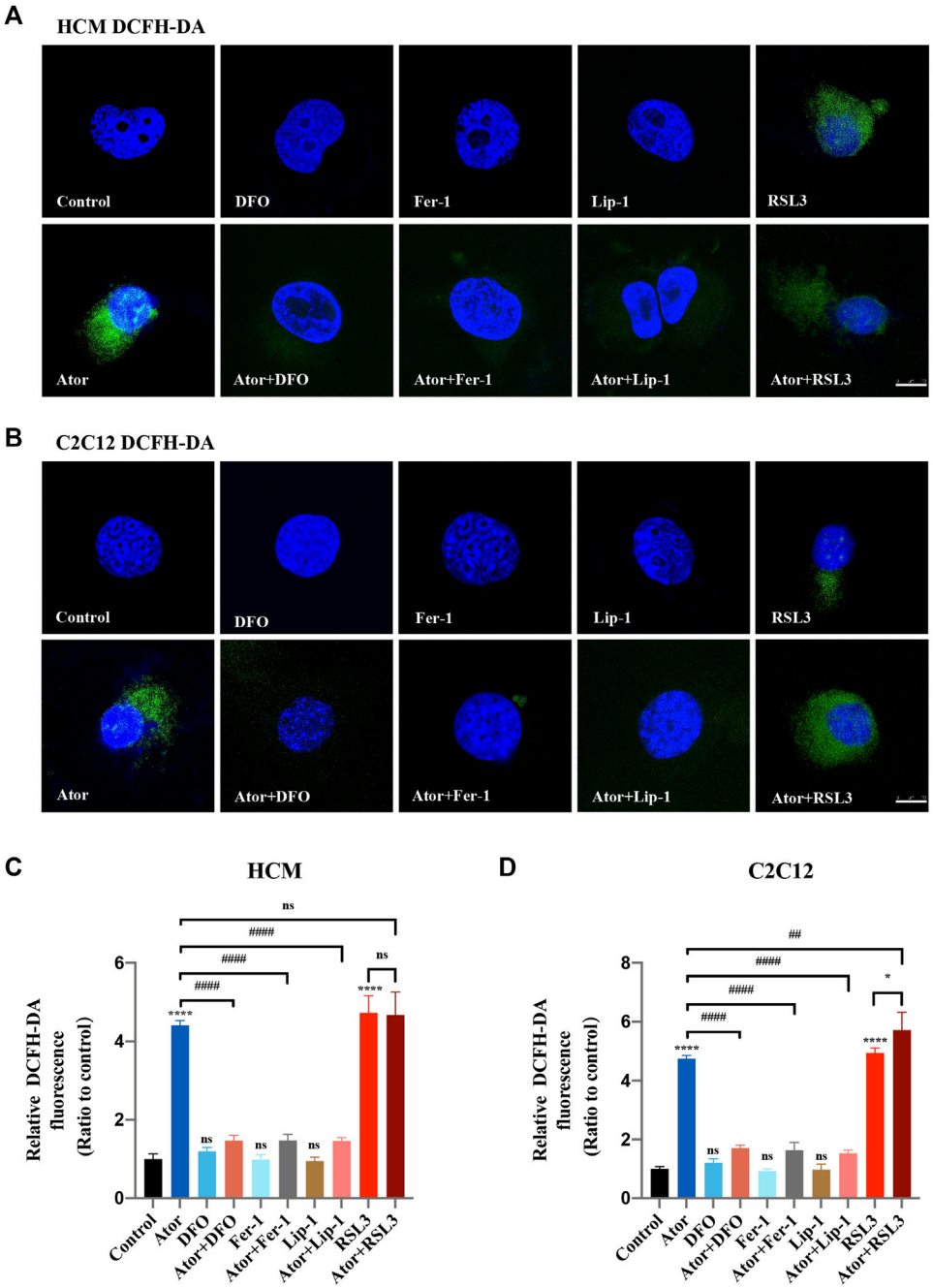

FIGURE 3 | Reactive oxygen species (ROS) generation in atorvastatin-supplemented HCM and C2C12 cells. **(A)** Representative images of HCM treated by atorvastatin alone or with ferroptosis inhibitors DFO, Fer-1 and Lip-1 stained with DCFH-DA, an indicator of intracellular ROS. **(B)** Representative images of C2C12 stained with DCFH-DA. **(C)** Quantification of relative fluorescence intensity of DCFH-DA in HCM. **(D)** Quantification of relative fluorescence intensity of DCFH-DA in C2C12. The fluorescence intensity was quantified by ImageJ software. The data are shown as mean ± SD. ns, no significant; $^{*}p < 0.05$, $^{****}p < 0.0001$ *vs*. the control group; $^{\#\#}p < 0.01$, $^{\#\#\#\#}p < 0.0001$ vs. the atorvastatin group. $n = 3$. Scale bar: 10 μm.

using FerroOrange probes. The muscular cells were pretreated with RSL3, DFO, Fer-1 or Lip-1 and then intervened with or without 40 μM atorvastatin for another 24 h, or treated with 40 μM atorvastatin alone for 24 h (**Figure 2A**). Similar to the ferroptosis inducer RSL3 (Sui et al., 2018), atorvastatin could raise excessive iron content in HCM (approximately 2.5 times than that of the control group; $p < 0.0001$) and C2C12 cells (approximately twofold compared with that of the control group; $p < 0.0001$), as indicated by higher FerroOrange signals than those in the control groups. Interestingly, these iron

accumulations can be remarkably alleviated by ferroptosis inhibitors, such as DFO (about 50%; $p < 0.0001$), Fer-1 (about 48%; $p < 0.0001$) and Lip-1 (about 48%; $p < 0.0001$) in HCM (**Figures 2B,D**), and the rescue effects reappeared as well in C2C12 using DFO (about 50%; $p < 0.0001$), Fer-1 (about 40%; $p < 0.0001$) and Lip-1 (about 50%; $p < 0.0001$) (**Figures 2C,E**). However, pretreated and cocultured with RSL3 groups compared with the atorvastatin alone group have no statistical difference in both HCM and C2C12 cells. These results indicated that overload iron was related to the atorvastatin-induced injury in HCM and C2C12 cells, and the inhibition of ferroptosis could ameliorate it.

Atorvastatin Causes Redox Imbalance in HCM and C2C12 Cells

Since overloading the iron-mediated Fenton reaction followed by the ROS accumulation during ferroptosis process (Dixon et al., 2012), we then used the DCFH-DA reagent to measure the production of total ROS (Kalyanaraman et al., 2012). The staining analysis demonstrated that the ROS level was significantly increased after atorvastatin treatment in HCM (approximately fourfold compared with that of the control group; $p < 0.0001$) (**Figures 3A,C**) and C2C12 (approximately quintuple compared with that of the control group; $p < 0.0001$) (**Figures 3B,D**) cells, which restrained by ferroptosis inhibitors (about 60%; $p < 0.0001$). When atorvastatin cocultured with RSL3, they appear to act synergistically in C2C12, but it was not enough for the synergy in HCM (**Figure 3**).

Ferroptosis Inhibitors Lightened Atorvastatin-Induced Lipid Peroxidation Accumulation in HCM and C2C12 Cells

The expression of PTGS2/COX-2 and 4-HNE, which work as biomarkers for ferroptosis (Hu et al., 2020; Li et al., 2020), increased (approximately 1.5 times than those of the control group; $p < 0.001$) in response to atorvastatin treatment. Furthermore, ferroptosis inhibitors Fer-1 could partly lessen the atorvastatin-induced PTGS2/COX2 (about 20%; $p < 0.05$) or 4HNE expression (about 20%; $p < 0.01$) (**Figures 4A–C**). In addition, there was an increase in MDA, the most general byproduct of lipid peroxidation (Ghosh et al., 2019), from whole cell lysates in atorvastatin-treated HCM and C2C12, and DFO or Fer-1 significantly decreased the level that increased by atorvastatin (**Figure 4D**). We also observed an increase in the BODIPY581/591-C11 signal (Drummen et al., 2002) in atorvastatin-treated cells, manifesting that atorvastatin could cause lipid peroxidation in HCM (about twofold of the control group; $p < 0.0001$) and C2C12 (more than threefold of the control group; $p < 0.0001$) cells. Meanwhile, DFO, Fer-1 and Lip-1 could significantly decrease the lipid peroxidation compared to atorvastatin alone both in HCM (**Figures 4E,F**) and C2C12 (**Figures 4G,H**) represented by the BODIPY581/591-C11 signal. Moreover, treatment with DFO, Fer-1 or Lip-1 alone was unable to produce an increase or decrease in the BODIPY581/591 C11 signal and MDA content, and pretreatment and coculturing with RSL3 compared with the atorvastatin alone group have no statistical difference in both HCM and C2C12 cells. Altogether, lipid peroxidation levels increased after atorvastatin treatment, and lethal lipid peroxidation might serve as a critical medium of atorvastatin correlative muscular injury. However, the MDA content was not increased in other types of statins like lovastatin, pravastatin, and rosuvastatin, which further confirmed the conclusion that only atorvastatin leads to ferroptosis. In addition, the MDA content of other types of statins did not have a significant change when Fer-1 was added (**Supplementary Figure S4**).

Atorvastatin-Induced Ferroptosis is Triggered in Mitochondria

Mitochondrial dysfunction is a crucial factor in myopathies. To analyze the role of mitochondria in atorvastatin-induced ferroptosis, mitochondrial content of Fe^{2+}, ROS and lipid peroxidation were detected. Confocal microscopy results showed that the signal of Mito-FerroGreen (MFG), a mitochondria-specific Fe^{2+} fluorescence indicator, increased threefold compared with the group of atorvastatin alone in HCM (**Figures 5A,C**) ($p < 0.0001$), and it even reached more than fivefold in C2C12 (**Figures 5B,D**) ($p < 0.0001$). DFO, Fer-1 and Lip-1 lessen the trend in HCM and C2C12, respectively. Aforementioned results indicated that atorvastatin will cause free iron accumulation in mitochondria, which could be rescued by ferroptosis inhibitors. When we detected ROS in mitochondria, the condition was similar to the determination of free ferrous iron. Atorvastatin could induce ROS assembling massively in mitochondria, which was partially reduced by ferroptosis inhibitors of DFO, Fer-1 and Lip-1 in HCM (**Figures 6A,C**) and C2C12 (**Figures 6B,D**). To further investigate the role of mitochondria, we used MitoPeDPP to examine the mitochondrial lipid peroxidation. The level of mitochondrial lipid peroxidation labeled with MitoPeDPP was also significantly increased by atorvastatin (more than twofold compared with the control group; $p < 0.0001$), and the increase was rescued by ferroptosis inhibitors in HCM (**Figures 7A,C**). This alteration of mitochondrial lipid peroxidation was reproduced in C2C12 (**Figures 7B,D**). However, pretreatment and coculturing with RSL3 compared with the atorvastatin alone group had no statistical difference in both HCM and C2C12 cells, which may be because of the threshold of the reaction toward oxidative stress. The ferroptosis indicator changed significantly on mitochondria, which was not so different with what occurred intracellularly, suggesting that mitochondria may play a critical role in atorvastatin-induced ferroptosis.

Atorvastatin-Induced Morphological Change of Mitochondria and Breakdown of MMP in HCM and C2C12 Cells

To assess the morphologic features, we used a transmission electron microscope to observe the change of the ultra-microstructure. Shrunk mitochondria with increased membrane density were observed in atorvastatin-treated cells

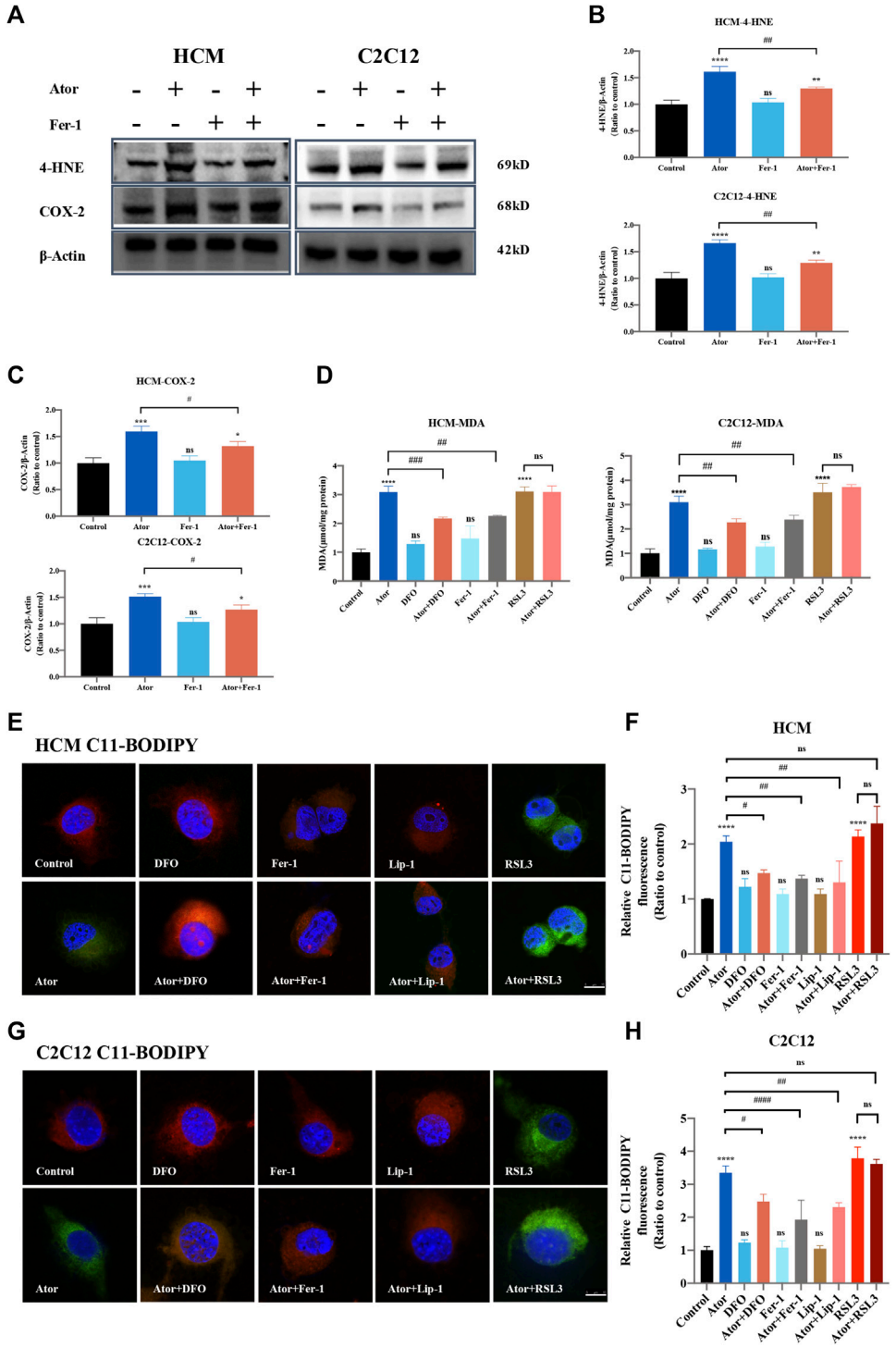

FIGURE 4 | Inhibition of ferroptosis lightened atorvastatin-induced lipid peroxidation accumulation in HCM and C2C12 cells. **(A)** Western blot detection of 4-HNE and COX-2 expression in cells treated with Fer-1 and 40 μM atorvastatin or alone for 24 h. **(B,C)** Quantification of shown blot of HCM and C2C12 in **(A)**. **(D)** MDA content in HCM and C2C12 in response to atorvastatin along or with ferroptosis inhibitors DFO, Fer-1 and RSL3 for 24 h detected by the TBA test. The MDA level was expressed in μmol/mg protein. **(E)** C11BODIPY581/591 was used as the signal of lipid peroxidation to detect the effect of atorvastatin alone or with ferroptosis inhibitors DFO, Fer-1 and Lip-1 in HCM. Red images are representative of non-oxidized lipid, while the green represent oxidized lipid images of muscular cells labeled with C11-BODIPY581/591. **(F)** Relative fluorescence intensity (Green) of intracellular lipid peroxidation in HCM. Quantification of **(E)**. **(G,H)** Lipid peroxidation and the relative fluorescence intensity (green) of intracellular lipid peroxidation in C2C12. Fluorescence intensity was quantified by ImageJ software. The data are shown as mean ± SD. ns, no significant; $^{*}p < 0.05$, $^{**}p < 0.01$, $^{***}p < 0.001$, $^{****}p < 0.0001$ vs. the control group; $^{\#}p < 0.05$, $^{\#\#}p < 0.01$, $^{\#\#\#}p < 0.001$, $^{\#\#\#\#}p < 0.0001$ vs. the atorvastatin group. $n = 3$. Scale bar: 10 μm.

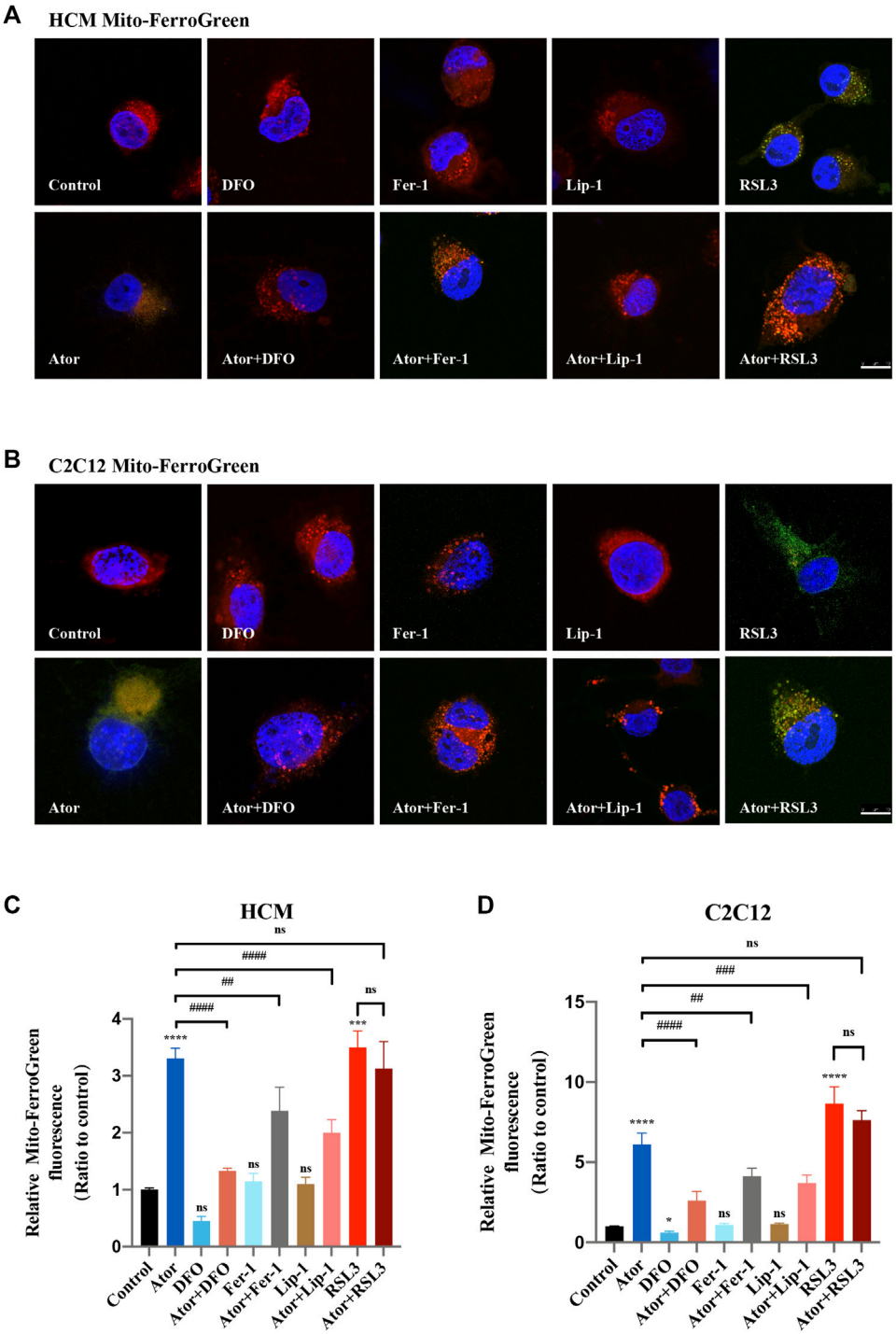

FIGURE 5 | Mitochondrial iron accumulation of atorvastatin exposure in HCM and C2C12 cells. Mitochondrial Fe^{2+} analyzed by Mito-FerroGreen. Treated cell were cocultured with the probe Mito-FerroGreen for 30 min. Red images represent mitochondrial localization using MitoTracker Red CMXRos staining. **(A)** Representative images of HCM treated atorvastatin alone or with ferroptosis inhibitors DFO, Fer-1 and Lip-1 stained with Mito-FerroGreen, an indicator of mitochondrial Fe^{2+}. **(B)** Representative images of C2C12 stained with Mito-FerroGreen. **(C,D)** Quantification of relative fluorescence intensity of Mito-FerroGreen in HCM and C2C12 cells. Fluorescence intensity was quantified by ImageJ software. The data are shown as mean ± SD. ns, no significant; $^{***}p < 0.001$, $^{****}p < 0.0001$ vs. the control group; $^{\#\#}p < 0.01$, $^{\#\#\#\#}p < 0.0001$ vs. the atorvastatin group. $n = 3$. Scale bar: 10 μm.

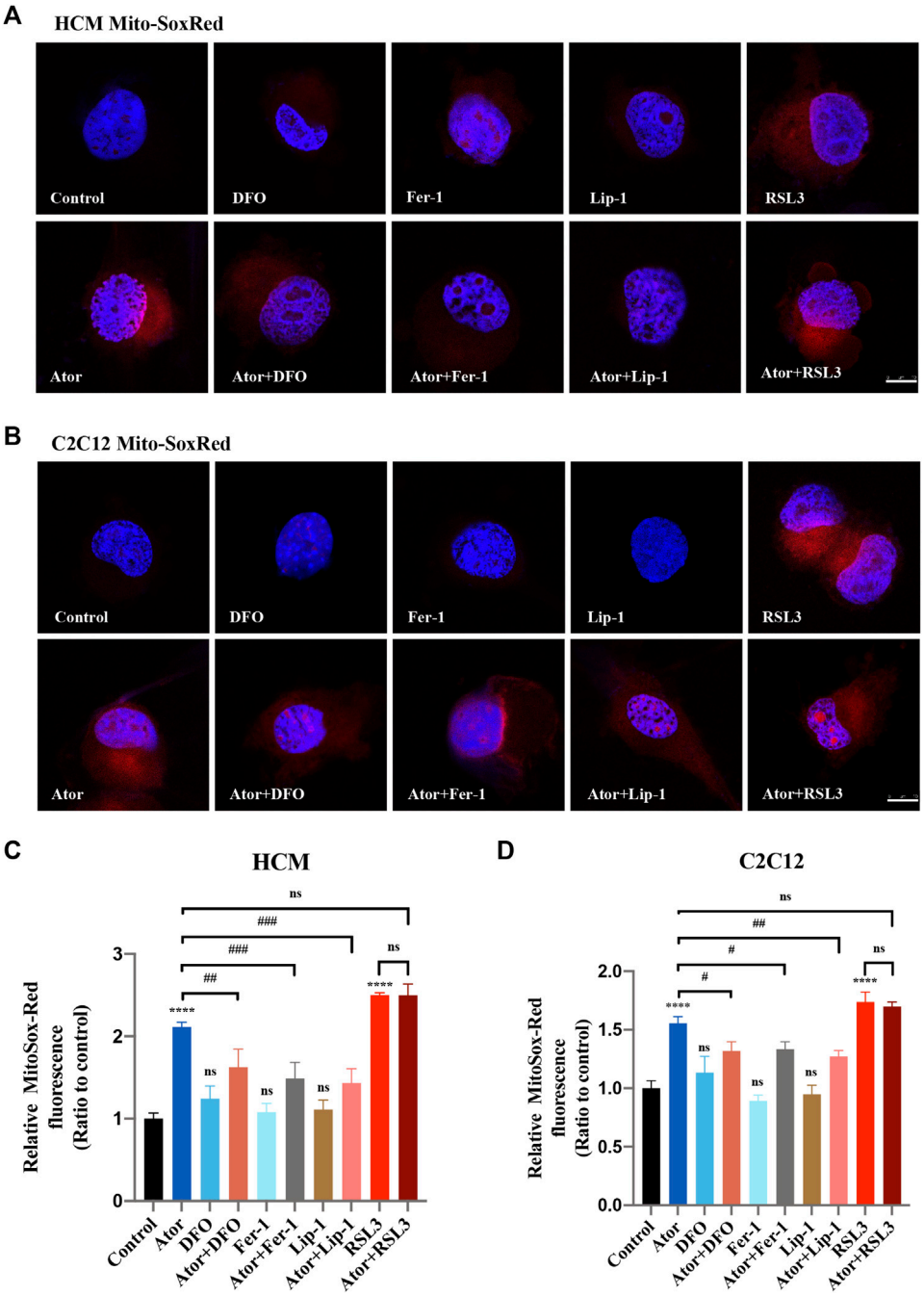

FIGURE 6 | Mitochondrial ROS accumulation of atorvastatin exposure in HCM and C2C12 cells. **(A)** Representative images of HCM treated with atorvastatin alone or with ferroptosis inhibitors DFO, Fer-1 and Lip-1 stained with MitoSox-Red, an indicator of mitochondrial ROS. **(B)** Representative images of C2C12 stained with MitoSox-Red. **(C, D)** Quantification of relative fluorescence intensity of MitoSox-Red in HCM and C2C12 cells. Fluorescence intensity was quantified by ImageJ software. The data are shown as mean ± SD. ns, no significant; $^{****}p < 0.0001$ vs. the control group; $^{\#}p < 0.05$, $^{\#\#}p < 0.01$, $^{\#\#\#}p < 0.001$ vs. the atorvastatin group. $n = 3$. Scale bar: 10 μm.

(**Figures 8A,B**). Fer-1 treatment remarkably ameliorated atorvastatin-induced mitochondrial abnormality, which is consistent with ROS and lipid peroxidation changes in mitochondria of muscular cells. These data provide convincing evidence of the occurrence of atorvastatin-induced ferroptosis in mitochondria of muscular cells. To further verify the effects on mitochondria, we checked the effects of MMP (represents mitochondrial function) by TMRM staining in atorvastatin-supplemented HCM and C2C12 cells. From **Figure 8**, TMRM fluorescence decreased significantly after atorvastatin treatment,

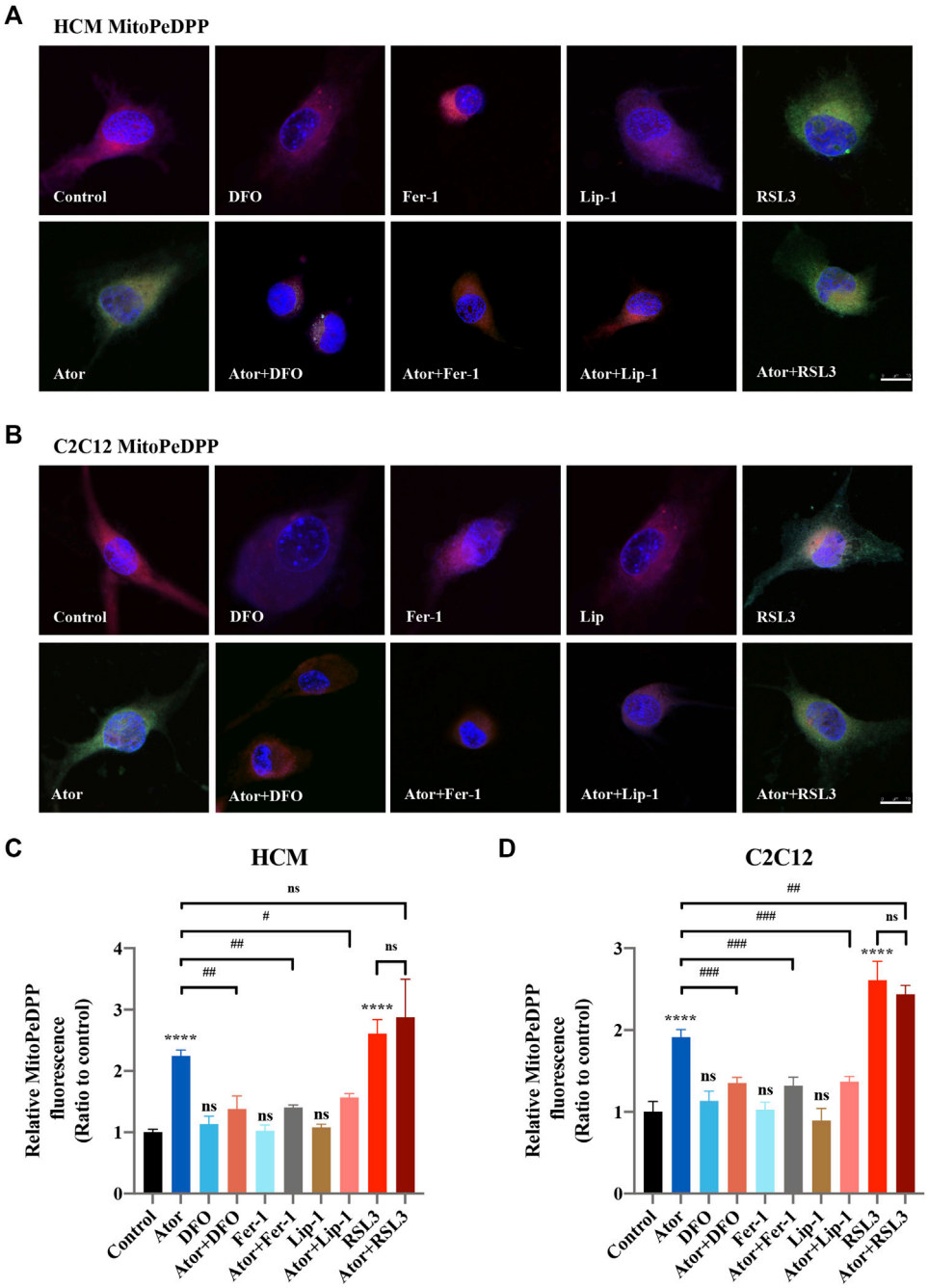

FIGURE 7 | Mitochondrial lipid peroxidation of atorvastatin exposure in HCM and C2C12 cells. Using MitoDeDPP staining detected mitochondrial lipid peroxidation. Red images represent mitochondrial localization using MitoTracker Red CMXRos staining, while the green is representative of mitochondrial lipid peroxidation labeled with MitoDeDPP. **(A)** Representative images of HCM treated atorvastatin alone or with ferroptosis inhibitors DFO, Fer-1 and Lip-1 stained with MitoDeDPP. **(B)** Representative images of C2C12 stained with MitoDeDPP. **(C,D)** Quantification of relative fluorescence intensity of MitoDeDPP in HCM and C2C12 cells. Fluorescence intensity was quantified by ImageJ software. The data are shown as mean ± SD. ns, no significant; $^{****}p < 0.0001$ vs. the control group; $^{\#}p < 0.05$, $^{\#\#}p < 0.01$, $^{\#\#\#}p < 0.001$ vs. the atorvastatin group. $n = 3$. Scale bar: 10 μm.

manifesting that atorvastatin caused a breakdown of membrane potential. The inhibition of ferroptosis by Fer-1 and DFO could recover the abnormal mitochondrial membrane potential caused by atorvastatin. Moreover, mitochondria-targeted antioxidant MitoTEMPO (MT) treatment not only shielded the cells from mitochondrial damage after exposure of atorvastatin as a recovery of TMRM fluorescence intensity appeared in HCM (**Figures 8C,D**) and in C2C12 (**Figures 8E,F**) but also significantly

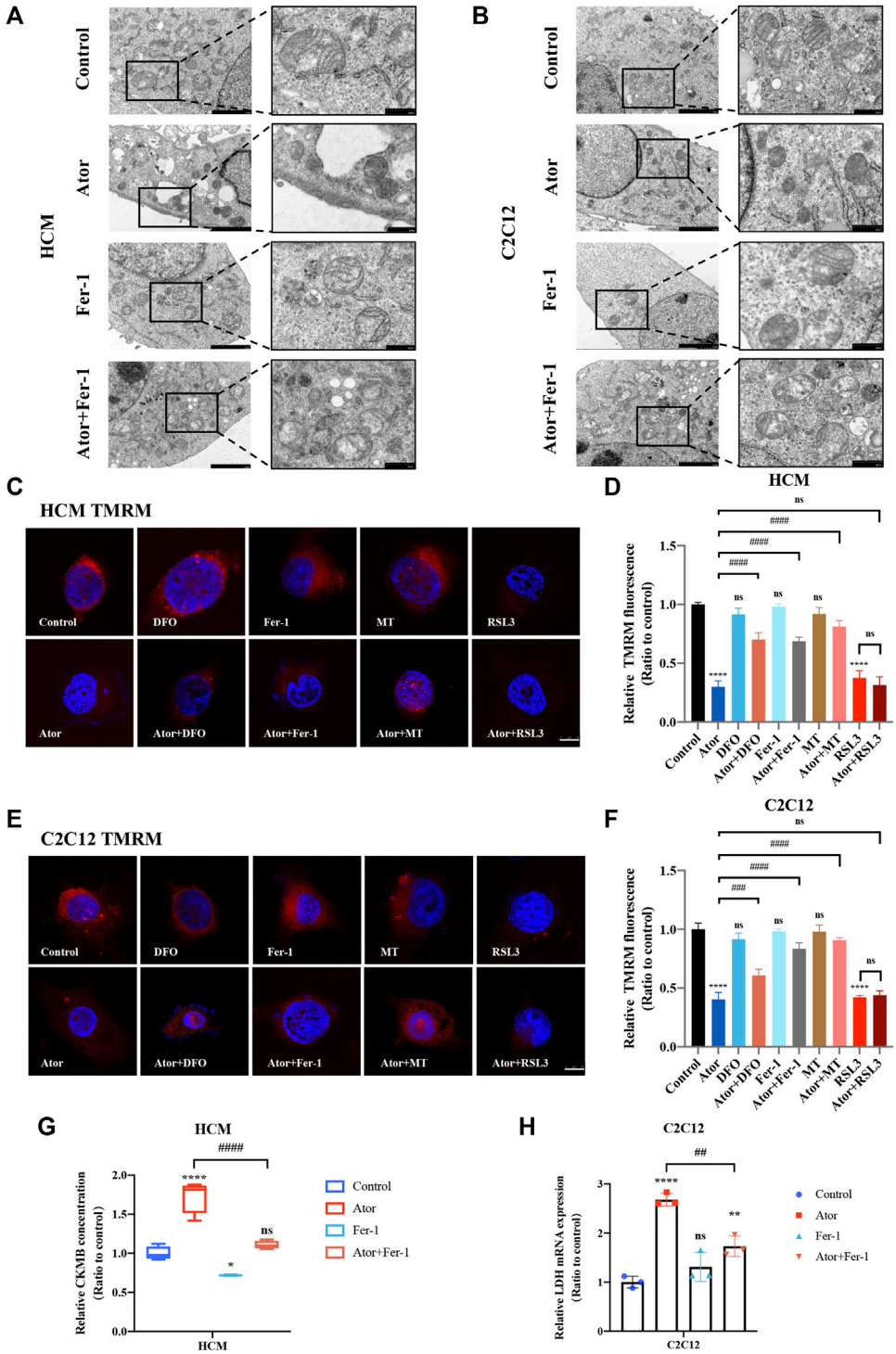

FIGURE 8 | Morphological changes of mitochondria and breakdown of MMP in atorvastatin treated HCM and C2C12 cells. **(A,B)** Transmission electron microscopy images of mitochondria ultrastructure in both HCM and C2C12 cells. Scale bar in left lower inset: 2 μM, right lower inset: 500 nm. **(C)** Representative images of HCM treated atorvastatin alone or with ferroptosis inhibitors DFO, Fer-1 and MT stained with TMRM, an indicator of mitochondrial membrane potential. **(D)** Relative fluorescence intensity of TMRM in HCM. Quantification of **(C)**. **(E,F)** Representative images and relative fluorescence intensity of TMRM in C2C12. **(G)** Relative levels of CKMB in HCM treated by atorvastatin alone or with Fer-1 examined by ELISA. **(H)** Relative mRNA expression of LDH in C2C12 treated by atorvastatin alone or with Fer-1. The fluorescence intensity was quantified by ImageJ software. The data are shown as mean ± SD. ns, no significant; $^{*}p < 0.05$, $^{**}p < 0.01$, $^{****}p < 0.0001$ vs. the control group; $^{\#}p < 0.05$, $^{\#\#}p < 0.01$, $^{\#\#\#}p < 0.001$, $^{\#\#\#\#}p < 0.0001$ vs. the atorvastatin group. $n = 3$. Scale bar: 10 μm.

prevented atorvastatin-induced myocyte death (**Supplementary Figures S5A,B**). Also, pretreatment and coculturing with RSL3 compared with the atorvastatin alone group have no statistical difference toward TMRM in both HCM and C2C12 cells. In general, atorvastatin-induced mitochondria-dependent ferroptosis accompanied with mitochondrial dysfunction is one of the basic matters within muscular cell damage.

Inhibition of Ferroptosis-Lightened Atorvastatin-Induced Myocardial Damage and Muscular Injury in HCM and C2C12 Cells

Creatine kinase-MB (CKMB) works as a representative of myocardial injury biomarker in several cardiovascular conditions like sepsis and acute myocardial infarction (AMI) (Saenger and Jaffe, 2008; Ndrepepa and Kastrati, 2018). To evaluate the myocyte injury potential of atorvastatin, cell free supernatant levels of CKMB were detected by enzyme-linked immunosorbent assay (ELISA). The results indicated that CKMB increased in the atorvastatin group ($p < 0.0001$), which could be restrained by fer-1 to some extents in HCM ($p < 0.0001$). As for skeleton muscle, lactate dehydrogenase (LDH) was selected on behalf of the musculoskeletal injury marker (Milias et al., 2005; Bazzucchi et al., 2019). Elevated LDH after atorvastatin exposure in C2C12 cells (more than two times of the control group; $p < 0.0001$) was also partially ameliorated by fer-1(about 38%; $p < 0.01$) (**Figures 8G,H**). In summary, the inhibition of ferroptosis-alleviated atorvastatin-induced myocardial damage and muscular injury in HCM and C2C12 cells, and ferroptosis was at least partly involved in atorvastatin-caused cell injury.

Nrf2-xCT/GPX4 Pathway Involved in Ferroptosis Induced by Atorvastatin

In order to investigate the mechanism underlying atorvastatin-induced ferroptosis, the GSH/GSSG ratio was tested. As expected, the GSH/GSSG ratio was decreased significantly both in HCM and C2C12 (**Figure 9A**). In addition, glutathione peroxidase (**Figure 9B**) and the expression of GPx4 were downregulated by atorvastatin treatment compared with the control group in HCM (**Figures 9C,D**) and C2C12 (**Figures 9E,F**). As well as the expression of SLC7A11 and Nrf2 was decreased by atorvastatin. Fer-1 could elevate the expression of SLC7A11 and GPx4 compared with that of the atorvastatin alone group, but it did not influence the levels of Nrf2 (**Figures 9C–F**). Aforementioned results imply that the Nrf2-xCT/GPx4 signaling pathway might be involved in atorvastatin-induced ferroptosis. When we isolated mitochondria from cytoplasm, GPx4 was decreased much more significantly in mitochondria (about 60%; $p < 0.001$) than other parts of organelles that exist in cytoplasm (about 20–30%; $p < 0.05$). In mitochondria, the expression of GPx4 was slightly but significantly rescued by ferroptosis inhibitor Fer-1 as well when compared with the single atorvastatin-treated group (**Figures 9G–J**). The results suggested that mitochondria GPx4 may be a key point in pathogenesis of ferroptosis caused by atorvastatin.

To investigate whether the CoQ-dependent system is also involved in atorvastatin-induced ferroptosis, we investigated the CoQ10 levels within atorvastatin exposure in HCM. Our results did not support this hypothesis since there was no statistical difference among groups of CoQ10 and dihydroorotate dehydrogenase (DHODH) (**Supplementary Figures S5A–C**).

DISCUSSION

Despite extensive application of statins, the pathogenesis of statin-induced myopathy remains largely unknown. We observed that atorvastatin administration caused oxidative stress and cell damage, which is the same as the results of hepatic tissue damage (Pal et al., 2015). In the present study, atorvastatin exposure decreased the muscular cell viability in a dose-dependent manner, which could be rescued by ferroptosis inhibitors significantly. At the same time, indicators of ferroptosis such as iron overload, ROS accumulation, and lipid peroxidation occurred in atorvastatin-treatment muscular cells, especially in mitochondria. Although some speculations conjectured that statins will provoke ferroptosis (Chen and Galluzzi, 2018; Chen et al., 2021), but there is only one study that reported that simvastatin caused cancer cell ferroptosis by suppressing the expression of HMGCR (Yao et al., 2021). We first identified that ferroptosis participates in atorvastatin-induced myopathy, providing a potential strategy to prevent atorvastatin-induced heart damage and muscle symptoms by inhibiting ferroptosis.

As it is known that the muscular injury of statins is dose dependent. The dosage selected for research is important, but the dosage of the drug taken by the human body is difficult to convert into the concentration *in vitro*, which involves the rate of absorption and metabolism (Needham and Mastaglia, 2014). Moreover, it is worth mentioning that drug interaction and potent inhibitors of cytochrome P450 (CYP) 3A4 inhibitors (atorvastatin is metabolized by CYP3A4) can significantly increase statin concentrations (Hirota et al., 2020), and clinical research on atorvastatin tends to apply high dose (Pedersen et al., 2005) since high-dose atorvastatin is superior in preventing peripheral arterial disease (Stoekenbroek et al., 2015). Therefore, the relatively high concentrations of statins are also necessary. Among the cell studies, the concentration range of statins is from nanomolar concentrations to micromolar concentrations (Obata and Nakashima, 2016; Cai and Gao, 2021). The concentrations of statins applied *in vitro* were 10 μM (Oh et al., 2020), 20 μM (Qian et al., 2019), 30 μM (Cai and Gao, 2021), 50 μM [atorvastatin was applied to study statin-induced muscle damage in C2C12 and primary murine myoblasts (Hoppstädter et al., 2020)], 60 μM [simvastatin was used to measure the effect of statins on C2C12 myotubes (Moschetti et al., 2021)], 100 μM [atorvastatin was used to investigate the protective effects against doxorubicin-induced cardiotoxicity in H9C2 (Obata and Nakashima, 2016; Li et al., 2019)], and 333.3 μM [which was used to test the efficacy and toxicity of a new hyaluronan-derived nanoparticle delivery system for

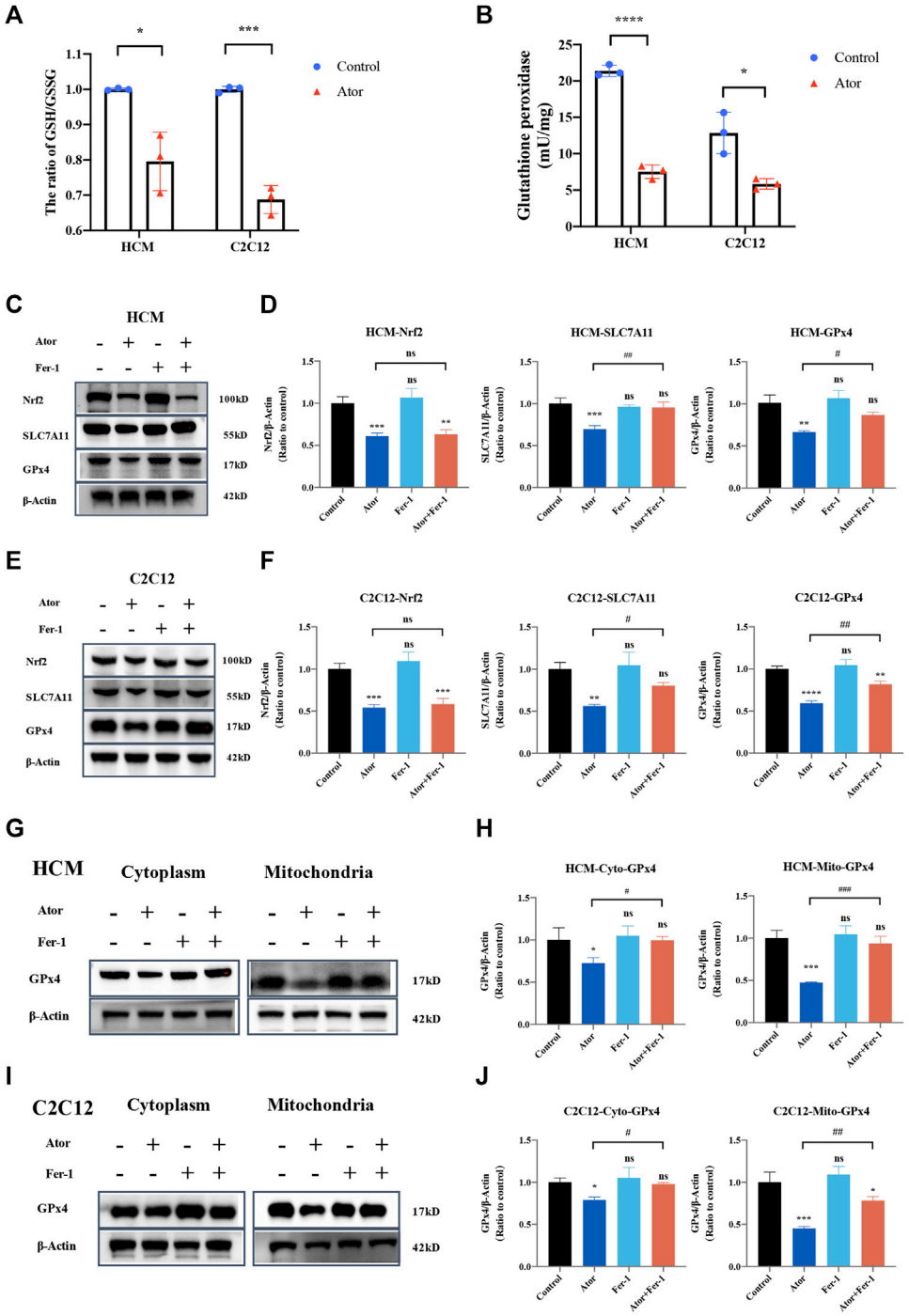

FIGURE 9 | Dysregulation of Nrf2-GPx4/xCT pathway was related to ferroptosis induced by atorvastatin. **(A)** Ratio of GSH/GSSG in lysates from the cultured myocytes. **(B)** Glutathione peroxidase activity in lysates from the cultured myocytes. **(C, D)** Expression of proteins of Nrf2, SLC7A11, and GPx4 in cultured HCM treated by atorvastatin alone or with Fer-1 detected by Western blot. **(E,F)** Expression of proteins of Nrf2, SLC7A11, and GPx4 in cultured C2C12 detected by Western blot. **(G,H)** Expression of GPx4 protein in cultured HCM atorvastatin-treated alone or with Fer-1 in cytoplasm (without mitochondria) or mitochondria detected by Western blot. **(I,J)** Expression of GPx4 protein in cultured C2C12 atorvastatin-treated alone or with Fer-1 in cytoplasm (without mitochondria) or mitochondria in C2C12 detected by Western blot. The fluorescence intensity was quantified by ImageJ software. The data are shown as mean ± SD. ns, no significant; $^{*}p < 0.05$, $^{**}p < 0.01$, $^{***}p < 0.001$, $^{****}p < 0.0001$ vs. the control group; $^{\#}p < 0.05$, $^{\#\#}p < 0.01$, $^{\#\#\#}p < 0.001$ vs. the atorvastatin group. $n = 3$. Scale bar: 10 μm.

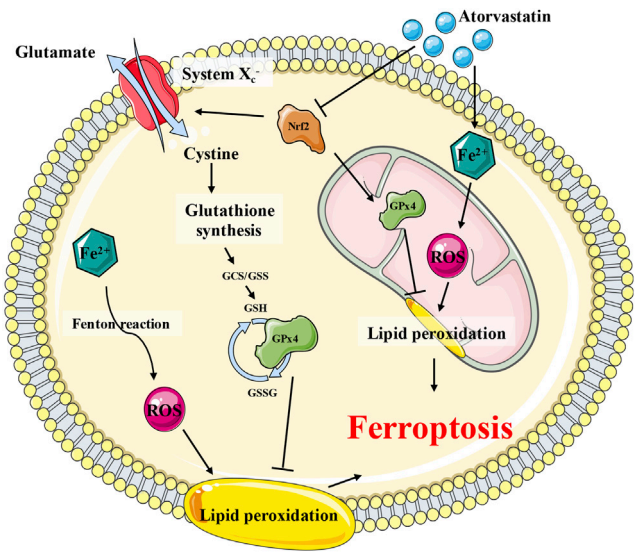

FIGURE 10 | Proposed scheme for the underlying mechanisms of atorvastatin-induced muscular cell ferroptosis. Atorvastatin suppressed the Nrf2, which would, in turn, inhibit the expression of System xc– (SLC7A11) and GPx4 (especially the mitochondrial GPx4), leading to a severe damage to the antioxidant system of ferroptosis. Consistently restraining of System xc– (SLC7A11) brought on GSH depletion, which would exaggerate to the dysfunction of GPx4 as well. The GPx4 enzyme catalyzes the transformation of GSH to GSSG and at the meantime decreases the toxic peroxide to non-toxic hydroxy compounds to protect the structure and function of the cell membrane against peroxides.

simvastatin in tissue-engineered skeletal muscle (Jones et al., 2019)]. The concentration in our study is within the range, and the selected concentration of 40 μM is beneath the IC50 in both HCM and C2C12.

Moreover, we found that only atorvastatin induces ferroptosis, while lovastatin, pravastatin, or rosuvastatin did not. Actually, statins did not always act equally, and the bioequivalence of statins should not be confirmed. The common clinical goal of statins is to reduce LDL-C, but statins have various effects on many other biochemical pathways, and those effects may be commonsensical expected to differ from statins to statins (Trapani et al., 2011; Bergt et al., 2017). For example, for patients who have hypercholesterolemia, only pravastatin but not atorvastatin, could reduce the atherogenic lipoprotein-associated phospholipase A2 (Ky et al., 2008), and lovastatin, but not pravastatin, causes higher mortality of cardiomyopathic hamsters (März et al., 2000). A better comprehension of various molecular pathways is essential and will have suggestions in the decision-making process among specific patient populations.

Overwhelming accumulation of Fe^{2+}, ROS and lipid peroxidation occurs in atorvastatin treatment cells in our study. As is known, ROS plays a major role in atorvastatin induced oxidative stress (Qi et al., 2013; Bouitbir et al., 2012). It contributes to the mitochondrial damage, oxidative injury of the cellular membranes, DNA damage, and so forth (Eruslanov and Kusmartsev, 2010; Bras et al., 2005; Pelicano et al., 2004). In this study, we further identified that ROS was triggered by atorvastatin-induced free iron-overload through a Fenton reaction in muscular cells. The accumulation of ROS subsequently assaulted the bio-membrane system, leading to a lipid peroxidation finally.

Furthermore, mitochondrial dysfunction, in particular impaired function of the electron transport chain, is frequently associated with in statin-associated skeletal muscle damage (Larsen et al., 2013; Bouitbir et al., 2016). We not only confirmed that atorvastatin impairs the mitochondrial function but further found that ferroptosis is involved in the mitochondrial dysfunction since it is effective to protect the mitochondrial function by ferroptosis inhibitor. And our mitochondria ultrastructure results provided convincing evidence that ferroptosis participates in the process of mitochondrial dysfunction induced by atorvastatin.

GPx4 is the most critical ferroptosis defense gene that encodes cytosolic, mitochondrial, and nucleolar isoforms (Yang et al., 2014; Ingold et al., 2018), whose functions include scavenging free radicals and detoxifying various xenobiotics and, consequently, converting itself to its oxidized form, glutathione disulfide (GSSG). In the present study, following atorvastatin intoxication, the expression and function of GPx4 in the mitochondria and intracellular organelles were greatly impaired, indicating that GPx4 may play a critical role in the atorvastatin-induced ferroptosis. This result is consistent with previous study where GPx4 was downregulated as well in atorvastatin-induced liver injury (Kromer and Moosmann, 2009). Another key regulator of the GSH-dependent antioxidation system was System xc–(xCT), an amino acid antiporter that acts as an important reservoir for the supplement of GSH (Jiang et al., 2015; Wang et al., 2017; Ingold et al., 2018; Daher et al., 2019; Koppula et al., 2021). The key component of xCT, SLC7A11, was downregulated by atorvastatin. Nrf2 is the key transcription factor to maintain oxidative homeostasis and is activated under conditions of high oxidative stress, promoting target gene transcription such as GPx4, HO-1, and SLC7A11 (Shin et al., 2018; Dodson et al., 2019). In our results, Nrf2 also was downregulated by atorvastatin, implying that Nrf2 is inhibited by atorvastatin and then suppressed the GPx4 as well as SLC7A11 expression in the process of ferroptosis. Proposed scheme for the underlying mechanisms of atorvastatin-induced muscular cell ferroptosis was diaplayed in **Figure 10**.

Another ferroptosis-defense system is the CoQ-dependent pathway involving FSP1 and mitochondrial DHODH. In our study, CoQ10 levels of atorvastatin exposure in HCM did not have a statistical difference among groups. Therefore, the ubiquinone content may not be the explanation for the observed ferroptosis in atorvastatin treatment. In support of this assumption, it appears that in most patients treated with statins, the skeletal muscle CoQ10 content remains high enough to maintain the ETC function (Banach et al., 2015). In addition, DHODH, the key component of CoQ-dependent system which operates in parallel to mitochondrial GPx4 to inhibit ferroptosis, did not have a statistical difference among groups, either. Therefore, the CoQ-dependent metabolic pathway

was not the mechanism to explain atorvastatin-induced ferroptosis, and more experiment should be conducted to confirm this deduction in the future.

Taken together, our data point toward ferroptosis as an essential molecular mechanism leading to statin-induced muscle damage, providing valuable new insights into homeostatic mechanisms required for the tolerance of the widely prescribed atorvastatin.

DATA AVAILABILITY STATEMENT

The original contributions presented in the study are included in the article/**Supplementary Material**, further inquiries can be directed to the corresponding authors.

AUTHOR CONTRIBUTIONS

YY and AC conceived and designed the experiments. QZ, HQ, YC, XL, CC and BX performed the experiments. QZ, HQ, YC, XL, CC, XD, YL and YY interpreted data obtained from the experiments. QZ, YC and YY wrote the manuscript and prepared figures. PZ and YL critically advised and commented for the project. YY and AC revised the manuscript. All authors contribute to this article and approved the submitted version.

FUNDING

This study is supported by the grants from the National Natural Science Foundation of China (81974021, 82170304, 81930012, 81730013, 81974012, 82170232 and 82070386) and the Natural Science Foundation of Shanghai (20ZR1435500).

ACKNOWLEDGMENTS

We would like to thank Jianhui Wang for his excellent experimental techniques and other members of the AC laboratory for helpful discussion and technical support.

SUPPLEMENTARY MATERIAL

The Supplementary Material for this article can be found online at: https://www.frontiersin.org/articles/10.3389/fcell.2022.806081/full#supplementary-material

REFERENCES

Bai, L., Wang, Y., Huo, J., Li, S., Wen, Y., Liu, Q., et al. (2021). Simvastatin Accelerated Motoneurons Death in SOD1G93A Mice through Inhibiting Rab7-Mediated Maturation of Late Autophagic Vacuoles. *Cell Death Dis* 12 (4), 392. doi:10.1038/s41419-021-03669-w

Banach, M., Serban, C., Sahebkar, A., Ursoniu, S., Rysz, J., Muntner, P., et al. (2015). Effects of Coenzyme Q10 on Statin-Induced Myopathy. *Mayo Clinic Proc.* 90 (1), 24–34. doi:10.1016/j.mayocp.2014.08.021

Bazzucchi, I., Patrizio, F., Ceci, R., Duranti, G., Sgrò, P., Sabatini, S., et al. (2019). The Effects of Quercetin Supplementation on Eccentric Exercise-Induced Muscle Damage. *Nutrients* 11 (1), 205. doi:10.3390/nu11010205

Bergt, S., Grub, A., Wagner, S., Engelke, H., Nöldge-Schomburg, G., Vollmar, B., et al. (2017). Pravastatin but Not Simvastatin Improves Survival and Neurofunctional Outcome after Cardiac Arrest and Cardiopulmonary Resuscitation. *JACC: Basic Translational Sci.* 2 (2), 149–159. doi:10.1016/j.jacbts.2017.01.009

Bersuker, K., Hendricks, J. M., Li, Z., Magtanong, L., Ford, B., Tang, P. H., et al. (2019). The CoQ Oxidoreductase FSP1 Acts Parallel to GPX4 to Inhibit Ferroptosis. *Nature* 575 (7784), 688–692. doi:10.1038/s41586-019-1705-2

Bonifacio, A., Mullen, P. J., Mityko, I. S., Navegantes, L. C., Bouitbir, J., and Krähenbühl, S. (2016). Simvastatin Induces Mitochondrial Dysfunction and Increased Atrogin-1 Expression in H9c2 Cardiomyocytes and Mice *In Vivo*. *Arch. Toxicol.* 90 (1), 203–215. doi:10.1007/s00204-014-1378-4

Bouitbir, J., Charles, A. L., Echaniz-Laguna, A., Kindo, M., Daussin, F., and Auwerx, J. (2012). Opposite Effects of Statins on Mitochondria of Cardiac and Skeletal Muscles: A "mitohormesis" Mechanism Involving Reactive Oxygen Species and PGC-1. *Eur. Heart J.* 33 (11), 1397–1407. doi:10.1093/eurheartj/ehr224

Bouitbir, J., Singh, F., Charles, A.-L., Schlagowski, A.-I., Bonifacio, A., Echaniz-Laguna, A., et al. (2016). Statins Trigger Mitochondrial Reactive Oxygen Species-Induced Apoptosis in Glycolytic Skeletal Muscle. *Antioxid. Redox Signaling* 24 (2), 84–98. doi:10.1089/ars.2014.6190

Bras, M., Queenan, B., and Susin, S. A. (2005). Programmed Cell Death *via* Mitochondria: Different Modes of Dying. *Biochemistry (Mosc)* 70 (2), 231–239. doi:10.1007/s10541-005-0105-4

Cai, S., and Gao, Z. (2021). Atorvastatin Inhibits Proliferation and Promotes Apoptosis of colon Cancer Cells via COX-2/pge2/β-Catenin Pathway. *J. Buon* 26 (4), 1219–1225.

Cao, P., Hanai, J.-i., Tanksale, P., Imamura, S., Sukhatme, V. P., and Lecker, S. H. (2009). Statin-induced Muscle Damage and Atrogin-1 Induction Is the Result of a Geranylgeranylation Defect. *FASEB j.* 23 (9), 2844–2854. doi:10.1096/fj.08-128843

Chen, J. J., and Galluzzi, L. (2018). Fighting Resilient Cancers with Iron. *Trends Cel Biol.* 28 (2), 77–78. doi:10.1016/j.tcb.2017.11.007

Chen, X., Kang, R., Kroemer, G., and Tang, D. (2021). Broadening Horizons: the Role of Ferroptosis in Cancer. *Nat. Rev. Clin. Oncol.* 18 (5), 280–296. doi:10.1038/s41571-020-00462-0

Daher, B., Parks, S. K., Durivault, J., Cormerais, Y., Baidarjad, H., Tambutte, E., et al. (2019). Genetic Ablation of the Cystine Transporter xCT in PDAC Cells Inhibits mTORC1, Growth, Survival, and Tumor Formation via Nutrient and Oxidative Stresses. *Cancer Res.* 79 (15), 3877–3890. doi:10.1158/0008-5472.Can-18-3855

Dixon, S. J., Lemberg, K. M., Lamprecht, M. R., Skouta, R., Zaitsev, E. M., Gleason, C. E., et al. (2012). Ferroptosis: an Iron-dependent Form of Nonapoptotic Cell Death. *Cell* 149 (5), 1060–1072. doi:10.1016/j.cell.2012.03.042

Dodson, M., Castro-Portuguez, R., and Zhang, D. D. (2019). NRF2 Plays a Critical Role in Mitigating Lipid Peroxidation and Ferroptosis. *Redox Biol.* 23, 101107. doi:10.1016/j.redox.2019.101107

Doll, S., Freitas, F. P., Shah, R., Aldrovandi, M., da Silva, M. C., Ingold, I., et al. (2019). FSP1 Is a Glutathione-independent Ferroptosis Suppressor. *Nature* 575 (7784), 693–698. doi:10.1038/s41586-019-1707-0

Downs, J. R., Clearfield, M., Weis, S., Whitney, E., Shapiro, D. R., Beere, P. A., et al. (1998). Primary Prevention of Acute Coronary Events with Lovastatin in Men and Women with Average Cholesterol Levels. *Jama* 279 (20), 1615–1622. doi:10.1001/jama.279.20.1615

Drummen, G. P. C., van Liebergen, L. C. M., Op den Kamp, J. A. F., and Post, J. A. (2002). C11-BODIPY581/591, an Oxidation-Sensitive Fluorescent Lipid Peroxidation Probe: (Micro)spectroscopic Characterization and Validation

of Methodology. *Free Radic. Biol. Med.* 33 (4), 473–490. doi:10.1016/s0891-5849(02)00848-1

Eruslanov, E., and Kusmartsev, S. (2010). Identification of ROS Using Oxidized DCFDA and Flow-Cytometry. *Methods Mol. Biol.* 594, 57–72. doi:10.1007/978-1-60761-411-1_4

Fang, X., Wang, H., Han, D., Xie, E., Yang, X., Wei, J., et al. (2019). Ferroptosis as a Target for protection against Cardiomyopathy. *Proc. Natl. Acad. Sci. USA* 116 (7), 2672–2680. doi:10.1073/pnas.1821022116

Ghosh, S., Serafini, R., Love, C. C., Teague, S. R., Hernández-Avilés, C., LaCaze, K. A., et al. (2019). Effects of media and Promoters on Different Lipid Peroxidation Assays in Stallion Sperm. *Anim. Reprod. Sci.* 211, 106199. doi:10.1016/j.anireprosci.2019.106199

Godoy, J. C., Niesman, I. R., Busija, A. R., Kassan, A., Schilling, J. M., Schwarz, A., et al. (2019). Atorvastatin, but Not Pravastatin, Inhibits Cardiac Akt/mTOR Signaling and Disturbs Mitochondrial Ultrastructure in Cardiac Myocytes. *FASEB j.* 33 (1), 1209–1225. doi:10.1096/fj.201800876R

Hirota, T., Fujita, Y., and Ieiri, I. (2020). An Updated Review of Pharmacokinetic Drug Interactions and Pharmacogenetics of Statins. *Expert Opin. Drug Metab. Toxicol.* 16 (9), 809–822. doi:10.1080/17425255.2020.1801634

Hoppstädter, J., Valbuena Perez, J. V., Linnenberger, R., Dahlem, C., Legroux, T. M., Hecksteden, A., et al. (2020). The Glucocorticoid-induced Leucine Zipper Mediates Statin-induced Muscle Damage. *FASEB j.* 34 (3), 4684–4701. doi:10.1096/fj.201902557RRR

Hu, Z., Zhang, H., Yi, B., Yang, S., Liu, J., Hu, J., et al. (2020). VDR Activation Attenuate Cisplatin Induced AKI by Inhibiting Ferroptosis. *Cel Death Dis* 11 (1), 73. doi:10.1038/s41419-020-2256-z

Ingold, I., Berndt, C., Schmitt, S., Doll, S., Poschmann, G., Buday, K., et al. (2018). Selenium Utilization by GPX4 Is Required to Prevent Hydroperoxide-Induced Ferroptosis. *Cell* 172 (3), 409–422. e421. doi:10.1016/j.cell.2017.11.048

Jiang, L., Kon, N., Li, T., Wang, S.-J., Su, T., Hibshoosh, H., et al. (2015). Ferroptosis as a P53-Mediated Activity during Tumour Suppression. *Nature* 520 (7545), 57–62. doi:10.1038/nature14344

Jones, J. M., Player, D. J., Samanta, S., Rangasami, V. K., Hilborn, J., Lewis, M. P., et al. (2019). Hyaluronan Derived Nanoparticle for Simvastatin Delivery: Evaluation of Simvastatin Induced Myotoxicity in Tissue Engineered Skeletal Muscle. *Biomater. Sci.* 8 (1), 302–312. doi:10.1039/c9bm00986h

Kalyanaraman, B., Darley-Usmar, V., Davies, K. J. A., Dennery, P. A., Forman, H. J., Grisham, M. B., et al. (2012). Measuring Reactive Oxygen and Nitrogen Species with Fluorescent Probes: Challenges and Limitations. *Free Radic. Biol. Med.* 52 (1), 1–6. doi:10.1016/j.freeradbiomed.2011.09.030

Koppula, P., Zhuang, L., and Gan, B. (2021). Cystine Transporter SLC7A11/xCT in Cancer: Ferroptosis, Nutrient Dependency, and Cancer Therapy. *Protein Cell* 12 (8), 599–620. doi:10.1007/s13238-020-00789-5

Kromer, A., and Moosmann, B. (2009). Statin-induced Liver Injury Involves Cross-Talk between Cholesterol and Selenoprotein Biosynthetic Pathways. *Mol. Pharmacol.* 75 (6), 1421–1429. doi:10.1124/mol.108.053678

Ky, B., Burke, A., Tsimikas, S., Wolfe, M. L., Tadesse, M. G., Szapary, P. O., et al. (2008). The Influence of Pravastatin and Atorvastatin on Markers of Oxidative Stress in Hypercholesterolemic Humans. *J. Am. Coll. Cardiol.* 51 (17), 1653–1662. doi:10.1016/j.jacc.2008.01.026

Larsen, S., Stride, N., Hey-Mogensen, M., Hansen, C. N., Bang, L. E., Bundgaard, H., et al. (2013). Simvastatin Effects on Skeletal Muscle. *J. Am. Coll. Cardiol.* 61 (1), 44–53. doi:10.1016/j.jacc.2012.09.036

Li, N., Wang, W., Zhou, H., Wu, Q., Duan, M., Liu, C., et al. (2020). Ferritinophagy-mediated Ferroptosis Is Involved in Sepsis-Induced Cardiac Injury. *Free Radic. Biol. Med.* 160, 303–318. doi:10.1016/j.freeradbiomed.2020.08.009

Li, N., Wen, C., Huang, P., Tao, Y., Jin, F., and Liu, X. (2019). Atorvastatin Reduces Alcohol-Induced Endoplasmic Reticulum Stress in AC16 Cardiomyocytes. *Scand. Cardiovasc. J.* 53 (1), 42–47. doi:10.1080/14017431.2018.1516891

Mao, C., Liu, X., Zhang, Y., Lei, G., Yan, Y., Lee, H., et al. (2021). DHODH-mediated Ferroptosis Defence Is a Targetable Vulnerability in Cancer. *Nature* 593 (7860), 586–590. doi:10.1038/s41586-021-03539-7

März, W., Siekmeier, R., Müller, H.-M., Wieland, H., Gross, W., and Olbrich, H.-G. (2000). Effects of Lovastatin and Pravastatin on the Survival of Hamsters with Inherited Cardiomyopathy. *J. Cardiovasc. Pharmacol. Ther.* 5 (4), 275–279. doi:10.1054/jcpt.2000.16695

Menon, A. V., Liu, J., Tsai, H. P., Zeng, L., Yang, S., Asnani, A., et al. (2021). Excess Heme Upregulates Heme Oxygenase 1 and Promotes Cardiac Ferroptosis in Mice with Sickle Cell Disease. *Blood* 1, 1. doi:10.1182/blood.2020008455

Milias, G. A., Nomikos, T., Fragopoulou, E., Athanasopoulos, S., and Antonopoulou, S. (2005). Effects of Eccentric Exercise-Induced Muscle Injury on Blood Levels of Platelet Activating Factor (PAF) and Other Inflammatory Markers. *Eur. J. Appl. Physiol.* 95 (5-6), 504–513. doi:10.1007/s00421-005-0031-6

Moschetti, A., Dagda, R. K., and Ryan, R. O. (2021). Coenzyme Q Nanodisks Counteract the Effect of Statins on C2C12 Myotubes. *Nanomedicine: Nanotechnology, Biol. Med.* 37, 102439. doi:10.1016/j.nano.2021.102439

Musset, L., Allenbach, Y., Benveniste, O., Boyer, O., Bossuyt, X., Bentow, C., et al. (2016). Anti-HMGCR Antibodies as a Biomarker for Immune-Mediated Necrotizing Myopathies: A History of Statins and Experience from a Large International Multi-center Study. *Autoimmun. Rev.* 15 (10), 983–993. doi:10.1016/j.autrev.2016.07.023

Ndrepepa, G., and Kastrati, A. (2018). Creatine Kinase Myocardial Band - a Biomarker to Assess Prognostically Relevant Periprocedural Myocardial Infarction. *Int. J. Cardiol.* 270, 118–119. doi:10.1016/j.ijcard.2018.07.077

Needham, M., and Mastaglia, F. L. (2014). Statin Myotoxicity: a Review of Genetic Susceptibility Factors. *Neuromuscul. Disord.* 24 (1), 4–15. doi:10.1016/j.nmd.2013.09.011

Obata, T., and Nakashima, M. (2016). Fluvastatin, an HMG-CoA Reductase Inhibitor, Facilitate Adenosine Production in the Rat Hearts via Activation of Ecto-5′-Nucleotidase. *Microvasc. Res.* 107, 1–5. doi:10.1016/j.mvr.2016.04.006

Oh, J., Lee, B. S., Lim, G., Lim, H., Lee, C. J., Park, S., et al. (2020). Atorvastatin Protects Cardiomyocyte from Doxorubicin Toxicity by Modulating Survivin Expression through FOXO1 Inhibition. *J. Mol. Cell Cardiol.* 138, 244–255. doi:10.1016/j.yjmcc.2019.12.007

Pal, S., Ghosh, M., Ghosh, S., Bhattacharyya, S., and Sil, P. C. (2015). Atorvastatin Induced Hepatic Oxidative Stress and Apoptotic Damage *via* MAPKs, Mitochondria, Calpain and Caspase12 Dependent Pathways. *Food Chem. Toxicol.* 83, 36–47. doi:10.1016/j.fct.2015.05.016

Pedersen, T. R., Faergeman, O., Kastelein, J. J., Olsson, A. G., Tikkanen, M. J., Holme, I., et al. (2005). High-Dose Atorvastatin vs Usual-Dose Simvastatin for Secondary Prevention After Myocardial InfarctionThe IDEAL Study: A Randomized Controlled Trial. *Jama* 294 (19), 2437–2445. doi:10.1001/jama.294.19.2437

Pelicano, H., Carney, D., and Huang, P. (2004). ROS Stress in Cancer Cells and Therapeutic Implications. *Drug Resist Updat* 7 (2), 97–110. doi:10.1016/j.drup.2004.01.004

Qian, L., Zhu, K., Lin, Y., An, L., Huang, F., Yao, Y., et al. (2019). Insulin Secretion Impairment Induced by Rosuvastatin Partly Though Autophagy in INS-1E Cells. *Cell Biol Int* 44, 127–136. doi:10.1002/cbin.11208

Qi, X. F., Zheng, L., Lee, K. J., Kim, D. H., Kim, C. S., Cai, D. Q., et al. (2013). HMG-CoA Reductase Inhibitors Induce Apoptosis of Lymphoma Cells by Promoting ROS Generation and Regulating Akt, Erk and p38 Signals *via* Suppression of Mevalonate Pathway. *Cell Death Dis.* 4 (2), e518. doi:10.1038/cddis.2013.44

Saenger, A. K., and Jaffe, A. S. (2008). Requiem for a Heavyweight. *Circulation* 118 (21), 2200–2206. doi:10.1161/circulationaha.108.773218

Shin, D., Kim, E. H., Lee, J., and Roh, J.-L. (2018). Nrf2 Inhibition Reverses Resistance to GPX4 Inhibitor-Induced Ferroptosis in Head and Neck Cancer. *Free Radic. Biol. Med.* 129, 454–462. doi:10.1016/j.freeradbiomed.2018.10.426

Stoekenbroek, R. M., Boekholdt, S. M., Fayyad, R., Laskey, R., Tikkanen, M. J., Pedersen, T. R., et al. (2015). High-dose Atorvastatin Is superior to Moderate-Dose Simvastatin in Preventing Peripheral Arterial Disease. *Heart* 101 (5), 356–362. doi:10.1136/heartjnl-2014-306906

Sui, X., Zhang, R., Liu, S., Duan, T., Zhai, L., Zhang, M., et al. (2018). RSL3 Drives Ferroptosis through GPX4 Inactivation and ROS Production in Colorectal Cancer. *Front. Pharmacol.* 9, 1371. doi:10.3389/fphar.2018.01371

Tadokoro, T., Ikeda, M., Ide, T., Deguchi, H., Ikeda, S., Okabe, K., et al. (2020). Mitochondria-dependent Ferroptosis Plays a Pivotal Role in Doxorubicin Cardiotoxicity. *JCI Insight* 5 (9), e132747. doi:10.1172/jci.insight.132747

Thompson, P. D., Panza, G., Zaleski, A., and Taylor, B. (2016). Statin-Associated Side Effects. *J. Am. Coll. Cardiol.* 67 (20), 2395–2410. doi:10.1016/j.jacc.2016.02.071

Tiniakou, E., and Christopher-Stine, L. (2017). Immune-mediated Necrotizing Myopathy Associated with Statins: History and Recent Developments. *Curr. Opin. Rheumatol.* 29 (6), 604–611. doi:10.1097/bor.0000000000000438

Trapani, L., Melli, L., Segatto, M., Trezza, V., Campolongo, P., Jozwiak, A., et al. (2011). Effects of Myosin Heavy Chain (MHC) Plasticity Induced by HMGCoA-reductase Inhibition on Skeletal Muscle Functions. *FASEB j.* 25 (11), 4037–4047. doi:10.1096/fj.11-184218

Wang, H., An, P., Xie, E., Wu, Q., Fang, X., Gao, H., et al. (2017). Characterization of Ferroptosis in Murine Models of Hemochromatosis. *Hepatology* 66 (2), 449–465. doi:10.1002/hep.29117

Ward, N. C., Watts, G. F., and Eckel, R. H. (2019). Statin Toxicity. *Circ. Res.* 124 (2), 328–350. doi:10.1161/circresaha.118.312782

Yang, W. S., SriRamaratnam, R., Welsch, M. E., Shimada, K., Skouta, R., Viswanathan, V. S., et al. (2014). Regulation of Ferroptotic Cancer Cell Death by GPX4. *Cell* 156 (1-2), 317–331. doi:10.1016/j.cell.2013.12.010

Yao, X., Xie, R., Cao, Y., Tang, J., Men, Y., Peng, H., et al. (2021). Simvastatin Induced Ferroptosis for Triple-Negative Breast Cancer Therapy. *J. Nanobiotechnol* 19 (1), 311. doi:10.1186/s12951-021-01058-1

Conflict of Interest: The authors declare that the research was conducted in the absence of any commercial or financial relationships that could be construed as a potential conflict of interest.

Publisher's Note: All claims expressed in this article are solely those of the authors and do not necessarily represent those of their affiliated organizations, or those of the publisher, the editors, and the reviewers. Any product that may be evaluated in this article, or claim that may be made by its manufacturer, is not guaranteed or endorsed by the publisher.

Copyright © 2022 Zhang, Qu, Chen, Luo, Chen, Xiao, Ding, Zhao, Lu, Chen and Yu. This is an open-access article distributed under the terms of the Creative Commons Attribution License (CC BY). The use, distribution or reproduction in other forums is permitted, provided the original author(s) and the copyright owner(s) are credited and that the original publication in this journal is cited, in accordance with accepted academic practice. No use, distribution or reproduction is permitted which does not comply with these terms.

frontiers | Frontiers in Cell and Developmental Biology

REVIEW
published: 04 May 2022
doi: 10.3389/fcell.2022.826904

Necroptosis and Viral Myocarditis: Tumor Necrosis Factor α as a Novel Biomarker for the Diagnosis of Viral Myocarditis

*Jin Zhou[1], Jing Xu[1], Peng Li[1], Shan Sun[1], Yimiti Kadier[2], Shiying Zhou[2] and Aijuan Cheng[1]**

[1]Tianjin Chest Hospital, Tianjin, China, [2]Hotan District People's Hospital, Tianjin, China

Programmed cell death (PCD), including necroptosis, has emerged as a significant pathway in cardiovascular diseases. The infection of viral myocarditis (VMC) could cause cardiomyocytes degeneration, necrosis, and immune-inflammatory myocardial response. In this review, we summarized and evaluated the available evidence on the pathogenesis, molecule mechanism, diagnosis, and potential treatment strategies of viral myocarditis, with a special focus on the novel mechanism of necroptosis for cardiomyocytes death. Studies have shown that tumor necrosis factor-alpha (TNF-α) is an important cytokine involved in the activation of necroptosis; an elevated level of TNF-α is continually reported in patients suffering from VMC, implicating its involvement in the pathogenesis of VMC. It is of great interest to explore the clinical implication of TNF-α. We subsequently conducted a meta-analysis on the efficacy of serum TNF-α expression level and its diagnostic accuracy on acute viral myocarditis detection. Taken together, the review demonstrates a compelling role of necroptosis involved in the pathogenesis of VMC. Further, applying TNF-α as a serological marker for the diagnosis of VMC may be a useful strategy.

Keywords: necroptosis, viral myocarditis, molecule mechanism, tumor necrosis factor α, diagnosis

OPEN ACCESS

Edited by:
Zhi Qi,
Nankai University, China

Reviewed by:
Jichang Wang,
Sun Yat-sen University, China
Balaji Banoth,
St. Jude Children's Research Hospital, United States

Correspondence:
Aijuan Cheng
ytcaj@sina.com

Specialty section:
This article was submitted to Cell Death and Survival, a section of the journal Frontiers in Cell and Developmental Biology

Received: *01 December 2021*
Accepted: *31 January 2022*
Published: *04 May 2022*

Citation:
Zhou J, Xu J, Li P, Sun S, Kadier Y, Zhou S and Cheng A (2022) Necroptosis and Viral Myocarditis: Tumor Necrosis Factor α as a Novel Biomarker for the Diagnosis of Viral Myocarditis. Front. Cell Dev. Biol. 10:826904. doi: 10.3389/fcell.2022.826904

1 INTRODUCTION

Functional activities of all multi-cellular organisms, maintenance of a homeostatic balance between new cells and those damaged or unrequired cells, or to speak simply, regulating the number of cells, demand a constant effort of cell death (Galluzzi et al., 2009). Cell death is a common and important feature in the growth and development of tissues and organs. Normally, cells are removed in a controlled (programmed) manner, involving a series of biochemical and molecular events, leading to a turnover of damaged or unrequired cells that are supposed to be removed from the body (D'Arcy, 2019). Perhaps the most widely recognized forms of cell death have been described in terms of two types: apoptosis, known as programmed cell death, or necrosis, known as uncontrolled cell death (Kroemer et al., 2009). Necrosis is classically characterized as via an unprogrammed or accidental form that is caused by physical or chemical injury resulting in the rupture of the cell and cellular content leakage into the extracellular space, which ultimately causes the release of damage-associated molecular patterns (DAMPs) (Vandenabeele et al., 2010a). Instead, apoptosis, from a Greek term denoting leaves falling from a tree, is the most well-studied form of programmed cell death and has been characterized as a process controlled by multi-genes and somehow is referred to as programmed cell death (PCD) at the very beginning. Though it was previously thought that necrosis is passive and

unprogrammed, research has now uncovered the caspase-independent processes that resemble necrosis. A new form of programmed cell necrosis, termed necroptosis, and alongside pyroptosis, ferroptosis, and cellular senescence, which is clearly distinct from apoptosis, has now been identified as one of the components of programmed cell death.

2 OVERVIEW OF NECROPTOSIS

Understanding the molecular mechanism of any form of PCD and its roles in disease pathogenesis and development is the key point of current research, which may contribute to effective biomarkers for diagnosis, new therapeutic targets, treatment strategies, and management options.

The word necroptosis is renamed to distinguish from necrosis that can be seen as accidental (unprogrammed) cell death that occurs in response to overwhelming chemical or physical insult, extreme physical temperature, pressure, chemical stress, or osmotic shock (Degterev et al., 2005). Necroptosis is the process of cellular self-destruction that is activated when apoptosis is otherwise prevented. However, the term "necroptosis" had not been generally adopted in the early period that "necrosis" or "necrotic cell death" was also used in the literature (Vandenabeele et al., 2010b). Morphologically, the programmed necrotic cells present a similar character of "necrosis" by cytoplasmic and organelle swelling, disruption of osmotic balance due to the extensive intracellular vacuolation, rupture of the plasma membrane, and cell death. Also, this release of cellular "adjuvants" from the necrotic cells promotes inflammation (Kono and Rock, 2008).

In 1997, Vercammen et al. found that triggering of the TNF receptors leads to necrosis of L929 cells while the Fas antigen results in apoptotic cell death, implicating that cell necrosis may also be regulated by a programmed form, and either necroptosis or apoptosis can occur in the same cell type within the pathways sharing the same cellular components (Vercammen et al., 1997). In addition, it is found that the pan-caspase inhibitor of zVAD-fmk (zVAD), a general inhibitor to block apoptosis, can induce necroptosis in L929 cells and the cell death is dependent on autocrine production of tumor necrosis factor-α (TNF-α) by Wu et al. (Wu et al., 2011). TNF-α has now been demonstrated to trigger programmed necrosis in several cell types (Holler et al., 2000; Lin et al., 2004; He et al., 2009). It was not very clear yet until 2009 that the only molecular component of programmed necrosis was identified as the protein serine/threonine kinase Receptor Interacting Protein 1 (RIP1) (Kono and Rock, 2008; Galluzzi et al., 2009). The role of kinases RIP1/RIP3 was identified in TNF-induced necroptosis in subsequent research (He et al., 2009; Vandenabeele et al., 2010b; Cho et al., 2011). Other cellular receptors that trigger the activation of necroptosis are death receptors of Fas/FasL and Toll-like receptors (TLR4 and TLR3) and cytosolic nucleic acid sensors such as RIG-I and STING, which can induce TNF-α and type I interferon (IFN-I) production promoting necroptosis in an autocrine feedback loop (Chen et al., 2018; Bertheloot et al., 2021).

Broadly speaking, necroptosis is confirmed as a new form of programmed cell death, distinct from necrosis that necrosis is not an uncontrollable passive process at all, but there is a possibility for a controllable form of cell death involving in PCD. Apoptosis was long thought to be the only regulated cell death pathway and the subject of intensive research for decades. On the contrary, its counterpart, necroptosis, has been investigated until recently that it can also be induced by TNF-α following its activation on tumor necrosis factor receptor 1 (TNFR1) (**Table 1**) (Pennica et al., 1984; Gon et al., 1996; Wang et al., 2008). Whereas activation of caspases represents the primary route of apoptosis, necroptosis represents an alternative form of PCD that is caspase-independent (Vandenabeele et al., 2010a). Apoptosis participates in limited individual or small clusters of cells when caspase-independent PCD contributes to the vital process of an immune response, osteogenesis, ovulation, and cellular turnover (Festjens et al., 2006; Sosna et al., 2014). Furthermore, the involvement of necroptosis has been widely implicated in the pathology of various diseases across the body including neurologic, renal, pulmonary, and gastrointestinal systems like pancreatitis (He et al., 2009; Zhang et al., 2009) and cancer; inflammatory diseases such as psoriasis, ulcerative colitis, and Crohn's disease; autoimmune diseases; TIDM; as well as cardiovascular diseases like coronary atherosclerosis, heart failure, myocardial ischemia/reperfusion injury, and myocarditis (Karunakaran et al., 2016; Meng et al., 2016; Moe and Marín-García, 2016; Zhang et al., 2016; Zhou et al., 2018; Sun et al., 2019). Its role has also been identified in the investigation of cell damage by pathogens like vaccinia virus, Shigella and Salmonella, HIV. The programmed processes are important as they have been implicated in the pathology of many diseases (Liu et al., 2015; Yang et al., 2018). The concept of cell death and programmed cell death has dramatically changed over the years.

3 EPIDEMIOLOGY AND PATHOGENESIS OF VIRAL MYOCARDITIS

The understanding of specific viruses affected myocarditis is still unfolding and its pathogenesis remains further investigation. Myocarditis is one of the clinically important cardiovascular diseases induced predominantly by viruses and also by other infectious agents including bacteria, protozoa, and fungi. The disorder is associated with poor prognosis when complicated by left ventricular dysfunction, heart failure, or arrhythmia (Ammirati et al., 2018). Because its specific mechanism has not been fully understood, the absolute incidence and prevalence are hardly recorded and the problem of misdiagnosis is always common. A retrospective study of 1.35 million deaths with certified causes reported myocarditis as the underlying cause of death in 639 cases (Kytö et al., 2007). Among patients visiting the emergency department between 1990 and 2013, the incidence of myocarditis was estimated to be 10–22 out of 100,000 individuals (Collaborators GBODS, 2015).

There are five common viruses associated with viral effect myocarditis that can be categorized as follows: the primary viruses are adenoviruses and enteroviruses such as coxsackie B

TABLE 1 | Difference between necrosis, apoptosis, and necroptosis

	Necrosis	Apoptosis	Necroptosis
Cell death type	Non-programmed cell death	Programmed cell death	
Induced by	Physical/environmental factors outside the cell	Activation of instructions within cell DNA	Outside trauma or deprivation
Activated through	Passive and uncontrollable	Intrinsic pathway: oligomerization of the B-cell lymphoma-2 (BCL-2) family proteins BAK and BAX Extrinsic pathway: engagement of membrane receptors such as TNFR1, or Toll Like Receptors (TLRs)	Following the activation of the tumor necrosis receptor (TNFR1) by TNF-α; other receptors such as death receptors (i.e., Fas/FasL), Toll-like receptors (TLR4 and TLR3), and cytosolic nucleic acid sensors such as RIG-I and STING, which induce type I interferon (IFN-I)
Caspase-dependent manner	Uncontrolled and passive process	Caspase-dependent	Caspase-independent
Occurred Site	Occurred in large fields of cells	Limited to individual or small clusters of cells	Occurred in vital process
Morphological Features	Loss of membrane integrity; cytoplasmic vacuole formation; ruptured mitochondria and lysosomal organelles; release of cytosolic content into extracellular regions	Maintainance of membrane integrity; apoptosis body was phagocytosed by macrophages or adjacent cells	Loss of membrane integrity; myocardial swelling; unclear and strong acidophil staining; pyknosis, karyorrhexis; karyolysis; inflammatory cell infiltration
Inflammatory response	Yes	No	Yes
Gene regulation	No	Yes	Yes
Protective role	—	Preventing cancer and regulating cell growth	DAMPs caused by necroptosis will alert surrounding cells of danger and promote inflammation
Promote disease progression	—	Excessive cell apoptosis can lead to serious diseases such as Parkinson's disease and Alzheimer's disease	Excessive cell necroptosis may contribute to inflammatory diseases such as psoriasis, ulcerative colitis, and Crohn's disease

or echoviruses; viscerotropic viruses, for example, parvovirus B19 have lifelong persistence (Dominguez et al., 2016; Van Linthout et al., 2018), though its exact mechanism may need to be investigated in that these viscerotropic viruses do not play a significant role to the etiology of adult myocarditis (Koepsell et al., 2012); human herpesvirus 6 (HHV6), Epstein–Barr virus and human cytomegalovirus of the lymphotropic viruses; viruses that can indirectly trigger myocarditis by the activation of the immune system, such as human immunodeficiency virus (HIV), influenza A virus, and influenza B virus; and family coronaviruses including the MERS-CoV, SARS-CoV, and SARS-CoV-2 that is recently found to also lead to myocarditis (Topol, 2020; Çınar et al., 2020). The incidence of viral myocarditis in any viral infection is estimated at 3%–6% (Narovlyanskaya and Winokur, 2020). The clinical importance of virus persistence has been demonstrated by Why et al. with higher in-hospital mortality at long-term follow-up (Why et al., 1994).

Research indicates that infection on the myocardium by enteroviruses occurs in three phases (Pollack et al., 2015). In Phase 1, the virus enters into myocytes and activates innate immune response within 7 days: the Coxsackie B viruses exhibit tropism for cardiomyocytes via the coxsackievirus and adenovirus receptor (CAR); the persistent viral replication leads to the dissolution of cardiomyocytes and to necrosis; immune responses can be subsequently activated. High levels of cytokines, such as tumor necrosis factor (TNF), interleukins, and interferons, are produced during this phase. Phase 2 may last for weeks (1–4 weeks), and during this phase, cytokine and chemokine are released; T cell-mediated clearance of virus-infected cells contribute to myocardial injury, necrosis, and production of interleukins and interferons. Commonly, there are two outcomes as viral titers decrease in phase 3. Some individuals experience complete resolution of myocardial injury and normalization of LV systolic function. However, in other patients, ineffective viral clearance and viral persistence throughout the entirety of the stage contribute to dilated cardiomyopathy, featured as chronic inflammation, cardiomyocytes degeneration, hypertrophy, interstitial fibrosis and global remodeling (Pollack et al., 2015).

4 NECROPTOSIS AND VIRAL MYOCARDITIS

4.1 Link Between TNF-α and Viral Myocarditis

Cardiomyocyte is a kind of terminal differentiation cell with limited regenerating ability, and damage factors can induce cardiomyocyte death leading to cardiomyopathy and heart failure. Overwhelming cardiac inflammation and the loss of myocardium is an important pathogenic mechanism in the progress of myocarditis yet the induction of this mechanism is unclear (Kang and Izumo, 2003; Chen et al., 2014; Kühl and Schultheiss, 2014). It was recently found

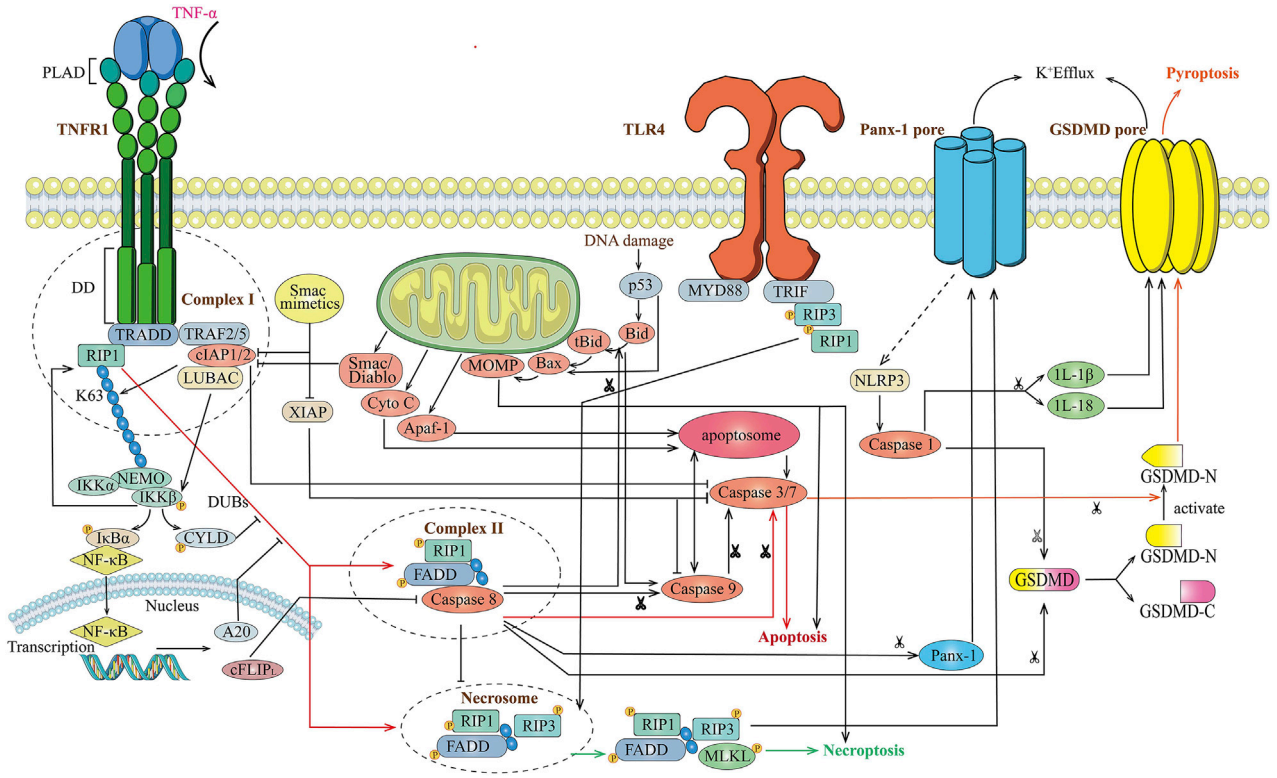

FIGURE 1 | Overview of TNF-induced different cell death signaling mode. Stimulation of cells with TNF leads to recruitment of TRADD and RIP1 to TNFR1, and forms complex I with TRAF2/5, cIAP1/2. The ubiquitination of RIP1 results in IKK-mediated activation of NF-κB and de-ubiquitination of RIP1 results in formation of complex II with FADD and caspase-8, then activates caspase-3 and caspase-7 leading to apoptosis. Meanwhile activated caspase-8 cleaves Gasdermin to form the N-terminal domain (GSDM-N) and C-terminal domain (GSDM-C), which convert apoptosis to pyroptosis. A20 and CYLD block the de-ubiquitination of RIP1 block formation of Complex II and apoptosis. Upon inhibition of caspase-8, RIPK1 activates RIPK3 leading to the formation of the necrosome, which ultimately leads to necroptosis.

that TNF-induced PCD is considered deeply involved in the pathology and development of VMC that necroptosis may be a novel mechanism for cardiomyocyte death in the virus-induced acute myocarditis (Zhou et al., 2018).

Established models and clinical data have demonstrated a causal role for TNF-α in virus-induced myocarditis. (Wang et al., 2016; Zhou et al., 2018; Chen and Deng, 2019). In 2004, the TNF-α mRNA and TNF-α protein had been firstly reported to be significantly more present in viral myocarditis patients than in nonviral myocarditis, accompanying the histologic change of prominent myocardial necrosis compared to TNF-α-negative cases (Calabrese et al., 2004), suggesting that TNF-α mRNA and protein are overexpressed with viral myocarditis of any etiology. The cardiac TNF-α abundance during viral infection was observed (Glück et al., 2000; Wada et al., 2001; Gagliardi et al., 2004); TNF-α gene expression was seen in 80% of the viral positive myocarditis cases; immunohistochemistry for TNFR1/2 was overexpressed in the TNF-α-positive cases while the controls were always negative. Subsequent EMBs showed similar results that the same expression of the pathway was seen in the EMS (Calabrese et al., 2004). Immunostaining reported the marked positivity in the cytoplasm of myocytes. Histologically, the intensity of the inflammatory infiltrate was only significantly noted in the TNF-α-positive case, while there was no difference in terms of extension of fibrosis between all cases. In addition, clinical works demonstrated an association between depressed myocardial function and the elevated TNF-α mRNA and protein levels (Habib et al., 1996; Torre-Amione et al., 1996), suggesting that TNF-α plays an important role in the viral myocarditis pathology of the infiltration of inflammatory cells and activities of inflammatory mediators (Navarro and Mora, 2006). The exact mechanism of how TNF-α contributes to VMC is not well known, and previously it is suspected to be linked to immunity. Clinical studies demonstrated that the TNF-α serum in the VMC group was significantly higher than the controls (Wen et al., 2010; Wang et al., 2016; Chen and Deng, 2019). The possible mechanism currently demonstrated that a cytokine storm after the hyperactivation of the immune system in response to virus infection may cause multiple organ failure through inflammatory cell death; and depending upon the stimulus encounters, different forms of cell death are induced. (Malireddi et al., 2019; Christgen et al., 2020; Malireddi et al., 2020; Samir et al., 2020).

4.2 Distinct TNF Complexes Determine Different Cell Death Signaling Mode

The TNF-induced signaling has multiple outcomes: the mode of gene induction, survival, apoptosis, and necroptosis suggesting

the existence of different molecule mechanisms of signaling complexes or pathways (Amin et al., 2018) (**Figure 1**). Firstly, TNFR1 exists in aggregated receptors recruited by the pre-ligand binding assembly domain (PLAD). The formation of complex I was induced by ligand binding owing to a conformational change in TNFR1 that recruits TNF receptor-associated death domain (TRADD), receptor-interacting protein kinase 1 (RIPK1), a cellular inhibitor of apoptosis (cIAPs), TRAF2 (TNFR-associated factor 2)/5, and (linear ubiquitin chain assembly complex) LUBAC protein. The activation of the NF-κB pathway and K63-linked polyubiquitination of RIP1 ultimately constitute the gene induction and survival mode after TNF stimuli. NF-κB translocates to the nucleus and induces transcription, up-regulating A20 and CYLD. RIP1 is targeted by these deubiquitinases for K63 deubiquitination, which balances the strength and activation of NF-κB signaling through negative-feedback mechanisms (Cho et al., 2009; He et al., 2009; Song et al., 2013). A20 and CYLD removes the K63-ubiquitinaiton of RIP1 promoting the transition of membrane-associated complex I (the gene induction or survival mode) to a secondary cytosolic complex II (the apoptosis and necroptosis mode). Two types of complex II related to a formation of necrosome that can ultimately lead to TNF-induced necroptosis are elucidated: TRADD-dependent or RIP1-dependent. After receptor internalization, an RIP-dependent complex of the secondary cytosolic death-initiating signaling complexes (DISC) is formed in the presence of Smac mimetics, which counteract IAPs and lead to apoptosis through the participation of the RIP1 kinase-dependent activation of caspase-8. RIPK1 is essential for Smac mimetic-stimulated TNF-α-induced apoptosis and is also an important molecular switch for the TNF-induced cell death from apoptosis to necrosis (programmed) as RIP3 did (Wang et al., 2008; Zhang et al., 2009). cIAP ablation prevents RIP1 ubiquitination and proteasomal degradation and favors the formation of the complex II without TRADD but a RIP1-FADD scaffold to activate caspase-8 blocking the necroptosis mode. Therefore, the reduced caspase activity can prevent the apoptotic mode and favor the necrotic mode for TNF stimulation because of the presence of caspase inhibitors, or the adaptor molecule FADD, or the absence of caspase-8. When the Smac mimetic was not cotreated in the TNF signaling, TRADD-dependent complex II is formed that RIP1 and RIP3 are recruited, along with Fas-associated death domain protein (FADD) and caspase-8. Proteolytic inactivation of RIP1 and RIP3 will be prevented in the presence of caspase inhibitors, and that sensitizes some cell lines to TNF-induced necrosis. Otherwise, the apoptotic mode was induced with cleavage of RIP1 and RIP3. The formation of these necrosome shares a common characteristic of the absence of caspase-8 highlighting that caspase recruitment may affect the cell death response. The mixed lineage kinase domain-like protein (MLKL) has been identified as necessary for TNF-α-induced necroptosis, which is an interacting partner of RIP3 that jointly compose the necrosome. (Sun et al., 2012). The involvement of RIP1/RIP3 and the MLKL recruitment and phosphorylation finally lead to the induction of programmed necrosis (Das et al., 2016).

The role of TNF-α in cell death continues to be investigated yet the majority of researches focus on its specific role in inducing cell death. In the murine model, virus infection associates an overall increase in the relative levels of cytokines as to the increased innate immune cell lineages of macrophages and neutrophils with a reduction in the percentage of B cells and T cells. (Karki et al., 2021). The combination of TNF-α and IFN-γ can induce high levels of cell death in BMDMs, but limited levels of cell death are found in other cytokine combinations. Accompanying an increased production of TNF-α peak evidenced in patients with virus infection, the synergism of TNF-α and IFN-γ releasing during the disease course induces PANoptosis and perpetuates a cytokine storm to cause tissue (multi-organ) damage and inflammation. (Karki et al., 2021). Cells can experience extensive crosstalk, leading to PANoptosis (pyroptosis, apoptosis, and necroptosis). Furthermore, there is crosstalk between these pathways. Pyroptosis is a caspase-independent cell death with a concomitant inflammatory response and, thus, has been defined as inflammatory cell death pathways with necroptosis. Caspase-3 is a key protein involved in cell apoptosis mode and can also be induced by TNF-α (or chemotherapy drugs) triggering cell pyroptosis; instead, in several cancer cells, caspase-3 cleaves GSDME to generate GSDME-N and GSDME-C activating the N-terminal fragment and causing plasma membrane lysis. (Hu et al., 2020). When high levels of GSDME were expressed, GSDME cleaved by pro-apoptotic caspases convert apoptosis to pyroptosis. Otherwise, apoptosis was induced. Activated caspase-1 and its recruitment cleavages GSDMD into a 30 KD fragment for oligomerization, and the GSDMD N-terminal domain exhibits pro-pyroptotic activity. (Wang et al., 2020). Cells lacking GSDME showed reduced cell death in response to TNFα-induced inflammatory cell death. (Karki et al., 2021). Collectively, GSDMD-mediated loss of membrane integrity results in pyroptosis implicating the main role executing pyroptosis. (Bertheloot et al., 2021). It is generally known that GSDMD-mediated pyroptosis allows a release of the caspase-1 activated cytokines IL-1β and IL-18. (Frank and Vince, 2019). Whether those inflammasome-activated cytokines contribute to necroptosis-induced inflammation remains investigated. Extrinsic apoptosis, a caspase-dependent process, was induced by activating the cysteine protease caspase-8 to form an apoptosome. The essential feature is the release of cytochrome *c* from mitochondria, regulated by the BCL-2 family, initiator caspases (caspase-8, -9, and -10), and effector caspases (caspase-3, -6, and -7). (Bertheloot et al., 2021). In necroptosis, the molecular mechanism of necroptosis is not entirely clear, further underscoring the differences between the animal model and human necroptosis mechanisms. At the leveling of signaling, there are close interplays between apoptosis and necroptosis. A study has suggested that $cFLIP_L$ (FLIP) blocks caspase-8-dependent apoptosis, and at the same time, the resulting caspase-8-FLIP heterodimers block RIPK3-dependent signaling requiring for necroptosis in the analysis of FADD, RIPK3 and FLIP, RIPK3 double-knockout mice. (Dillon et al., 2012). High intracellular ATP levels enable a cell to undergo apoptosis, and low ATP level favors necroptosis on the contrary (Eguchi et al.,

1997); p53 promotes MOMP to trigger apoptosis and has been recently reported to be required for necroptosis activation (Vaseva et al., 2012); the BCL-2 family of proteins has well-established roles in apoptosis, while their involvement in necroptosis is still under investigation. Current studies have suggested the requirements of the homotypic interactions of RHIMs and the kinase activity of RIPK3 for cell death execution. (Samir et al., 2020).

5 META-ANALYSIS ON THE DIAGNOSTIC VALUE OF TNF-A BASED ON 65 STUDIES

Accordingly, TNF-α plays a prominent role in damaging multi-organs by inducing inflammatory cell death and perpetuating cytokine storm. TNF-α is largely responsible for the timing of iNOS induction by inducing a rapid response. (Karki et al., 2021). Elevated serum TNF-α and mRNA expression in patients with viral myocarditis were consistently observed compared to healthy control implicating the involvement in the pathogenesis of viral myocarditis (Wang et al., 2016; Chen and Deng, 2020). Therefore, we investigated the serum levels of TNF-α, used as serological markers, to identify its VMC values in diagnosis and disease monitoring.

5.1 Methods of Meta-Analyses

5.1.1 Search Strategy

Relevant studies were identified through cross-checking of references and by electronic search of databases including PudMed, Embases, Cochrane Library, Scopus, ScienceDirect, and Chinese National Knowledge Infrastructure (CNKI). The following terms were used in the search strategy: ("necroptosis" OR "programmed necrosis" OR "necrotic cell death"), "viral myocarditis," and "Tumor Necrosis Factor alpha" as well as their abbreviations and synonyms and all possible combination. The detailed search strategy is shown in the supplementary material.

5.1.2 Inclusion and Exclusion Criteria

The studies were included in this analysis if they met the same condition and inclusion criteria as follows: 1) investigation of the TNF-α level and its diagnostic potential for viral myocarditis; and 2) studies provided sufficient data including exact data of the serum TNF-α measurement, sensitivity, and specificity. The exclusion criteria were as follows: 1) studies contributed no data to our analysis; and 2) studies were not in the form of original articles.

5.1.3 Data Extraction and Statistical Analysis

Data were extracted from all eligible studies: the first author's name, year of publication, number of participants, patient characteristics, age, the expression level of TNF-α, diagnostic accuracy data for VMC detection, the optimal cut-off values, etc. Meta-analysis was carried out by STATA 15.0 software. Continuous data of serum TNF-α expression levels in different periods were summarized using STD mean difference (SMDs) and 95%CIs as their effect sizes and a 95%CI excluding the point of no effect indicates statistical significance. The pooled sensitivity, specificity, and area under the curve (AUC) of the area under the summary receiver operating characteristic (SROC) were estimated to show the diagnostic accuracy of serum TNF-α. Heterogeneity across studies was assessed using the I2 statistic, and an I2 > 50% with a p-value < 0.05 was considered as having significant heterogeneity.

5.2 Results

5.2.1 Resutls of Literature Search

We conducted a meta-analysis according to the guidelines set forth by the 2020 PRISM statement and discussed the diagnostic efficiency of serum TNF-α in viral myocarditis. A flow diagram of the study selection is displayed in **Supplementary Figure S1**. In brief, 702 potentially relevant articles were obtained from electronic databases and then 611 of them were excluded after matching the inclusion/exclusion criteria. Finally, 65 studies met the inclusion criteria and were included in the meta-analysis. Quality assessment was conducted according to the QUADAS-2 tool. In detail, all studies demonstrated a moderate risk of bias among the included studies.

5.2.2 Resutls of Meta-Analyses

During our meta-analysis on the existing literature of the clinical researches, serum TNF-α was significantly increased for the myocarditis group with an SMD of 3.54 (95% CI, 2.99–4.08; p < 0.05; **Table 2**) compared to controls in its acute stage. A significant decrease of TNF-α in the recovery period was assessed (SMD −3.23, 95% CI −3.89, −2.56; p < 0.05; **Table 2**) when compared to the acute period. All differences between groups were significant. Significant heterogeneity was observed (I2 >50%, p < 0.05) and a random-effect model was used. Subgroup analysis and sensitivity analysis were also conducted for the assessment of heterogeneity. To account for the potential source of between-study heterogeneity, subgroup analyses were further conducted based on age (children and adults), while no impact of age difference on heterogeneity was found. Both children and adults showed significantly elevated TNF-α levels in the acute stage and decreased TNF-α levels in the recovery stage. When compared to the control group, the VMC group in the recovery stage was still having a significantly higher TNF-α level (SMD 1.41, 95% CI 1.02, 1.81; p < 0.05; **Table 2**) indicating a possible role for TNF-α during the prognosis period.

The application of serum TNF-α for identifying acute viral myocarditis patients presented a pooled sensitivity of 79% (95% CI 0.67–0.88) and specificity of 86% (95% CI 0.74–0.93). The pooled positive likelihood ratio (PLR) was 5.7 (95% CI, 3.0–10.6) and the pooled negative likelihood ratio (NLR) was 0.24 (95% CI, 0.15–0.39). Using a random-effects model, the DOR was 24 (95% CI, 11–53). There was no threshold effect, as indicated by Spearman correlation analysis (−0.44; p = 0.19). We used Deek's funnel plot to evaluate the publication bias of included studies and the shape of the funnel plot showed no between-study heterogeneity (p = 0.19), and no publication bias was found (p = 0.30). The AUC was 0.90 (95% CI 0.87–0.92) implicating that the use of serum TNF-α can provide reliable performance for the diagnosis of VMC (**Supplementary Figures 7, 8s**).

TABLE 2 | Pooled analysis of TNF-α level in comparison to a different stage and subgroup analysis based on age

Comparison	No. of studies	SMD	95% CI	p	I2 (%)	p for heterogeneity
VMC patients vs. control	65	3.6	3.04, 4.15	<0.001	89	0.05
Adult	26	3.40	2.38, 4.41			
Children	39	3.72	3.10, 4.33			
VMC patients in acute vs. recovery stage	32	–3.23	–3.89, -2.56	<0.001	68.6	<0.01
Adult	11	–3.53	–4.71, -2.36			
Children	21	–3.10	–3.94, -2.26			
VMC patients in recovery stage vs. control	32	1.26	0.90, 1.63	<0.001	70.1	0.06
Adult	11	4.48	0.69, 2.28			
Children	21	1.15	0.77, 1.53			

SMD, STD mean difference.
The meta-analyses were calculated from random effect model analysis.

5.3 TNF-α as a Potential Biomarker in VMC

The meta-analysis further confirmed that TNF-α was significantly higher in patients with viral myocarditis and gradually decreased as the disease progressed. Serum TNF-α could be a useful marker for identifying VMC in acute and recovery periods. The virus infection in myocarditis is characterized as a substantial production of TNF-α. Under the strong stimulation of TNF-α, complex II was formed and ultimately caused cardiomyocyte degeneration, necrosis, apoptosis, myocardial interstitial hyperplasia, and an immune-inflammatory response depending on whether caspase-8 is inhibited (Corsten et al., 2012). Overexpression of TNF-α can also confer cytoprotection reducing ischemia-reperfusion (I/R) injury through TRAF2-mediated activation of NF-κB (Burchfield et al., 2010).

6 NECROPTOSIS, CARDIOMYOCYTE DEATH AND VMC PROGRESS

During the evaluation of CVB3-infected myocarditis, serum concentrations of creatine kinase, CK-MB, and cardiac troponin I (cTnI) were significantly increased in the CVB3-infected mice than the noninfected group and the model group with Nec-1, suggesting severe damage to cardiomyocytes in the VMC mice models. Histopathologic features also showed distinct changes between groups. In the CVB3 infected mice, necrosis of most cardiomyocytes was observed, as well as myocardial swelling, unclear and strong acidophil staining, pyknosis, karyorrhexis, karyolysis, cell outline disappearance, and inflammatory cell infiltration. Myofilament and myotome were normal under an electronic electroscope of the control group; the cardiac muscle fibers were well-arranged. In the CVB3 group, mitochondrial swelling and severity vacancy-like denaturation with visible infiltrating mononuclear cells and leukomonocyte revealed that necroptosis is involved in viral myocarditis. Necroptosis has been certified to determine a crucial effort on the pathophysiological change of various diseases. Among patients suffering acute critical illnesses such as MI, septic shock, or acute viral myocarditis, the activation of caspase is inhibited due to the inadequacy of adenosine triphosphate (ATP) a cell can produce. Once the activation of caspases (in this case, caspase-8) was prevented, the necrotic signaling is initiated. Necrostatin-1, a necroptosis pathway inhibitor, can dramatically reduce inflammatory infiltration in cardiomyocytes and promote mice survival via blocking the inhibition of RIP1 kinase (He et al., 2009; Zhou et al., 2018). The study of Wu et al. has also implied that necroptosis is related to experimental autoimmune myocarditis (EAM) (Wu et al., 2021).

The current research progress is the application of the human-induced pluripotent stem cells (hiPSCs) in establishing an *in vitro* model of CVB3-induced myocarditis, investigating the molecular mechanisms of viral myocarditis via iCell® Cardiomyocytes (Kraft et al., 2021). It is said to be newly suitable for cardiomyocytes than other cardiac-like cells since cardiomyocytes represent the target cells of enteroviruses in the human heart, and those cardiac-like and non-cardiac cell lines (HeLa cells, HL-1 cells and H9c2 cells, etc.) that have been used frequently to investigate the mechanism can only distantly represent human cardiomyocytes (Claycomb et al., 1998). Not only the change of histopathology indicating the initiation of necroptosis was a key role in the pathology of VMC; the experiment implicates that the inhibition of RIPK1 and RIPK3 resulted in a reduction of viral replication by around half (Kraft et al., 2021), suggesting that the activity of RIPK1/3 may also be crucial for CVB3 replication. However, how RIPK3 functions on CVB3 replication in the cardiomyocytes remains unknown, and the time element should be specially considered about the "paradox" until the exact mechanism is accurately defined.

7 INSIGHT FROM THE RELATION BETWEEN NECROPTOSIS AND VMC

Necroptosis is not equivalent to the concept of necrosis but illustrates a new concept that cell death can be regulated through a series of signal transductions instead of dying passively, therefore suggesting a new therapeutic option, and blocking the necroptosis pathway may serve as a cardiovascular protective role in acute viral myocarditis. Direct evidence has implicated that necroptosis is the significant contributor to myocardial injury in VMC using Nec-1 to block the

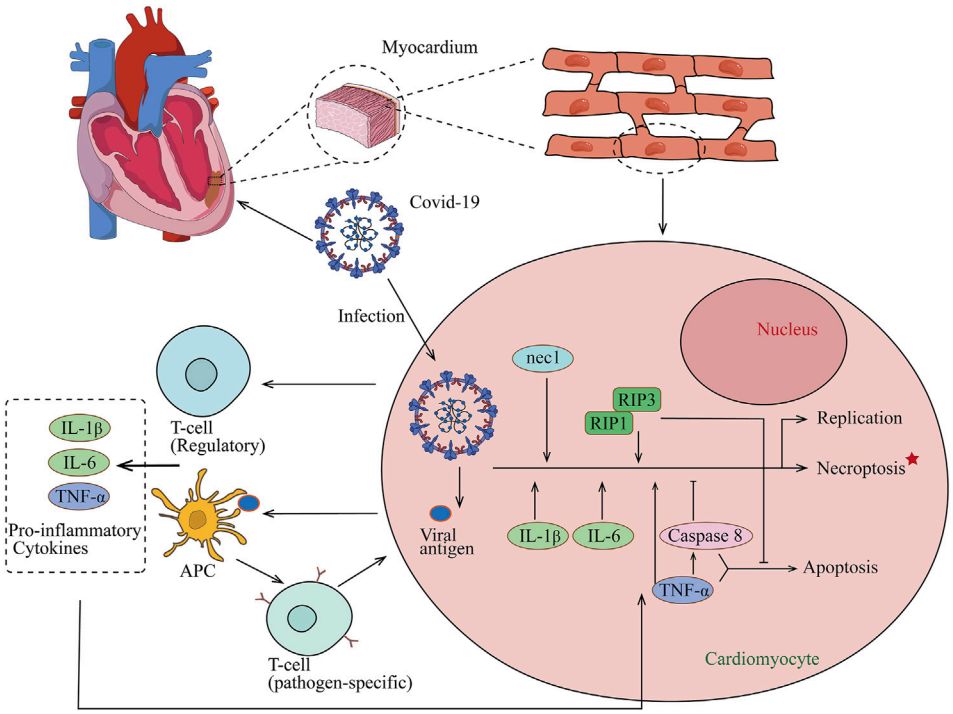

FIGURE 2 | Proposed model for COVID-19 association with myocarditis. After COVID-19 infection, naive T lymphocytes can be primed for viral antigens via antigen-presenting cells, and proinflammatory cytokines of IL-1B, IL-6, and TNF-α which are involved in necroptosis are released into the circulation. The release of cytokines results in a positive feedback loop of immune activation and myocardial damage and also helps the development of COVID-19.

necroptosis signaling pathway and prevents myocardial injury via downregulating RIP1 and RIP3 expression (Zhou et al., 2018). Necrostatin-1, identified as having the ability to attenuate cell necroptosis in various inflammatory diseases, inhibits overexpression and endogenous RIP1 autophosphorylation (Degterev et al., 2008). The CVB3-induced viral myocarditis model showed significantly stronger RIP1 and RIP3 staining in myocardial tissues compared to the controls and demonstrated disseminated distribution. Nec-1 exerts significant downregulation of positivity indicating the protective effect of Nec-1 in VMC. The protective role of Nec-1 has been reported in various diseases (Yang et al., 2018; Liu et al., 2015). Instead of suppressing autophagy, a cell death process involved in many cellular aspects, Nec-1 can be developed as a potential therapeutic target for inflammatory myocarditis. As of now, infection of coronavirus (COVID-19) causes the quick activation of the immune system and continuous inflammatory response (**Figure 2**). Cytokines of IL-1B, IL-6, and TNF-α involved in necroptosis have been proven as key cytokines in the development of COVID-19 (Moore and June 2020). Therefore, using Nec-1 may be a potential strategy to treat COVID-19 (Cao and Mu, 2021). In addition, because RIP3 is an energy metabolism regulator switching TNF-induced apoptosis to necroptosis and the key determinant, the deficiency of RIP3 ameliorated myocardial necroptosis and heart failure by inhibiting cardiac remodeling (Cho et al., 2009; Sun et al., 2012; Zhao et al., 2012; Wu et al., 2013; Humphries et al., 2015; Zhang et al., 2016).

8 FUTURE DIRECTIONS

The updated investigation on programmed cell death provides insight into the pathology mechanism of myocarditis. Necroptosis plays an important role in cardiomyocyte death in acute viral myocarditis. Low sensitivity of viral detection and diagnostic methods hinders the treatment for acute myocarditis and may result in the development of dilated cardiomyopathy in partial patients (Pollack et al., 2015). For the establishment of more appropriate treatment strategies, cytokine TNF-α, inducing necroptosis, presents its significant performance for VMC diagnosis and can be used as a biomarker for subsequent prognosis prediction. Recent researches in the relationship between necroptosis and cardiovascular diseases are still in its beginning stage. While CVB3-induced viral myocarditis is the predominant model for viral myocarditis exploration, other types of viruses associated with inflammation or their relationship with other forms of cell death remains an effort to explore. Currently, researches on necroptosis are insufficient, for example, the roles of death receptor signaling and crosstalk between necrosis, apoptosis, and necroptosis make differentiation difficult to define *in vivo*. Also, the role of necroptosis in diseases across the body including virus induced-cancer is warranted. Optimal window period and markers are poorly defined when marking cell death. Identifying these unknown mechanisms and biomarkers will lead to a novel understanding of necroptosis and new therapeutic treatments for their related diseases. The

application of Nec-1 is worth investigating as it can not only contribute to the comprehension of necroptosis but also contribute to identifying the potential therapeutic targets.

AUTHOR CONTRIBUTIONS

AC contributes to the design of article. JZ contributes to compiling data and writing articles. JX, SS, SZ, YK, and PL contribute to collecting data.

FUNDING

Funded by Tianjin Key Medical Discipline Construction Project.

SUPPLEMENTARY MATERIAL

The Supplementary Material for this article can be found online at: https://www.frontiersin.org/articles/10.3389/fcell.2022.826904/full#supplementary-material

REFERENCES

Amin, P., Florez, M., Najafov, A., Pan, H., Geng, J., Ofengeim, D., et al. (2018). Regulation of a Distinct Activated RIPK1 Intermediate Bridging Complex I and Complex II in TNFα-Mediated Apoptosis. *Proc. Natl. Acad. Sci. USA* 115 (26), E5944–e5953. doi:10.1073/pnas.1806973115

Ammirati, E., Cipriani, M., Moro, C., Raineri, C., Pini, D., Sormani, P., et al. (2018). Clinical Presentation and Outcome in a Contemporary Cohort of Patients with Acute Myocarditis. *Circulation* 138 (11), 1088–1099. doi:10.1161/circulationaha.118.035319

Bertheloot, D., Latz, E., and Franklin, B. S. (2021). Necroptosis, Pyroptosis and Apoptosis: an Intricate Game of Cell Death. *Cell Mol Immunol* 18 (5), 1106–1121. doi:10.1038/s41423-020-00630-3

Burchfield, J. S., Dong, J.-W., Sakata, Y., Gao, F., Tzeng, H.-P., Topkara, V. K., et al. (2010). The Cytoprotective Effects of Tumor Necrosis Factor Are Conveyed through Tumor Necrosis Factor Receptor-Associated Factor 2 in the Heart. *Circ. Heart Fail.* 3 (1), 157–164. doi:10.1161/circheartfailure.109.899732

Calabrese, F., Carturan, E., Chimenti, C., Pieroni, M., Agostini, C., Angelini, A., et al. (2004). Overexpression of Tumor Necrosis Factor (TNF)α and TNFα Receptor I in Human Viral Myocarditis: Clinicopathologic Correlations. *Mod. Pathol.* 17 (9), 1108–1118. doi:10.1038/modpathol.3800158

Cao, L., and Mu, W. (2021). Necrostatin-1 and Necroptosis Inhibition: Pathophysiology and Therapeutic Implications. *Pharmacol. Res.* 163, 105297. doi:10.1016/j.phrs.2020.105297

Chen, D., Tong, J., Yang, L., Wei, L., Stolz, D. B., Yu, J., et al. (2018). PUMA Amplifies Necroptosis Signaling by Activating Cytosolic DNA Sensors. *Proc. Natl. Acad. Sci. USA* 115 (15), 3930–3935. doi:10.1073/pnas.1717190115

Chen, J., and Deng, Y. (2019). Diagnostic Performance of Serum CK-MB, TNF-α and Hs-CRP in Children with Viral Myocarditis. *Open Life Sci.* 14, 38–42. doi:10.1515/biol-2019-0005

Chen, J., and Deng, Y. (2020). Erratum to "Diagnostic Performance of Serum CK-MB, TNF-α and Hs-CRP in Children with Viral Myocarditis". *Open Life Sci.* 15 (1), 597. doi:10.1515/biol-2020-0073

Chen, Z., Yang, L., Liu, Y., Tang, A., Li, X., Zhang, J., et al. (2014). LY294002 and Rapamycin Promote Coxsackievirus-Induced Cytopathic Effect and Apoptosis via Inhibition of PI3K/AKT/mTOR Signaling Pathway. *Mol. Cel Biochem* 385 (1-2), 169–177. doi:10.1007/s11010-013-1825-1

Cho, Y., Challa, S., and Chan, F. K.-M. (2011). A RNA Interference Screen Identifies RIP3 as an Essential Inducer of TNF-Induced Programmed Necrosis. *Adv. Exp. Med. Biol.* 691, 589–593. doi:10.1007/978-1-4419-6612-4_62

Cho, Y., Challa, S., Moquin, D., Genga, R., Ray, T. D., Guildford, M., et al. (2009). Phosphorylation-driven Assembly of the RIP1-RIP3 Complex Regulates Programmed Necrosis and Virus-Induced Inflammation. *Cell* 137 (6), 1112–1123. doi:10.1016/j.cell.2009.05.037

Christgen, S., Zheng, M., Kesavardhana, S., Karki, R., Malireddi, R. K. S., Banoth, B., et al. (2020). Identification of the PANoptosome: A Molecular Platform Triggering Pyroptosis, Apoptosis, and Necroptosis (PANoptosis). *Front. Cel. Infect. Microbiol.* 10, 237. doi:10.3389/fcimb.2020.00237

Çınar, T., Hayıroğlu, M. İ., Çiçek, V., Uzun, M., and Orhan, A. L. (2020). COVID-19 and Acute Myocarditis: Current Literature Review and Diagnostic Challenges. *Rev. Assoc. Med. Bras.* 66, 48–54. doi:10.1590/1806-9282.66.S2.48

Claycomb, W. C., Lanson, N. A., Jr., Stallworth, B. S., Egeland, D. B., Delcarpio, J. B., Bahinski, A., et al. (1998). HL-1 Cells: a Cardiac Muscle Cell Line that Contracts and Retains Phenotypic Characteristics of the Adult Cardiomyocyte. *Proc. Natl. Acad. Sci.* 95 (6), 2979–2984. doi:10.1073/pnas.95.6.2979

Collaborators GBODS (2015). Global, Regional, and National Incidence, Prevalence, and Years Lived with Disability for 301 Acute and Chronic Diseases and Injuries in 188 Countries, 1990-2013: a Systematic Analysis for the Global Burden of Disease Study 2013. *Lancet* 386 (9995), 743–800. doi:10.1016/s0140-6736(15)60692-4

Corsten, M. F., Schroen, B., and Heymans, S. (2012). Inflammation in Viral Myocarditis: Friend or Foe? *Trends Molecular Medicine* 18 (7), 426–437. doi:10.1016/j.molmed.2012.05.005

D'Arcy, M. S. (2019). Cell Death: a Review of the Major Forms of Apoptosis, Necrosis and Autophagy. *Cell Biol Int* 43 (6), 582–592. doi:10.1002/cbin.11137

Das, A., McDonald, D. G., Dixon-Mah, Y. N., Jacqmin, D. J., Samant, V. N., Vandergrift, W. A., et al. (2016). RIP1 and RIP3 Complex Regulates Radiation-Induced Programmed Necrosis in Glioblastoma. *Tumor Biol.* 37 (6), 7525–7534. doi:10.1007/s13277-015-4621-6

Degterev, A., Hitomi, J., Germscheid, M., Ch'en, I. L., Korkina, O., Teng, X., et al. (2008). Identification of RIP1 Kinase as a Specific Cellular Target of Necrostatins. *Nat. Chem. Biol.* 4 (5), 313–321. doi:10.1038/nchembio.83

Degterev, A., Huang, Z., Boyce, M., Li, Y., Jagtap, P., Mizushima, N., et al. (2005). Chemical Inhibitor of Nonapoptotic Cell Death with Therapeutic Potential for Ischemic Brain Injury. *Nat. Chem. Biol.* 1 (2), 112–119. doi:10.1038/nchembio711

Dillon, C. P., Oberst, A., Weinlich, R., Janke, L. J., Kang, T.-B., Ben-Moshe, T., et al. (2012). Survival Function of the FADD-CASPASE-8-cFLIPL Complex. *Cel Rep.* 1 (5), 401–407. doi:10.1016/j.celrep.2012.03.010

Dominguez, F., Kühl, U., Pieske, B., Garcia-Pavia, P., and Tschöpe, C. (2016). Update on Myocarditis and Inflammatory Cardiomyopathy: Reemergence of Endomyocardial Biopsy. *Revista Española de Cardiología (English Edition)* 69 (2), 178–187. doi:10.1016/j.rec.2015.10.015

Eguchi, Y., Shimizu, S., and Tsujimoto, Y. (1997). Intracellular ATP Levels Determine Cell Death Fate by Apoptosis or Necrosis. *Cancer Res.* 57 (10), 1835–1840.

Festjens, N., Vanden Berghe, T., and Vandenabeele, P. (2006). Necrosis, a Well-Orchestrated Form of Cell Demise: Signalling Cascades, Important Mediators and Concomitant Immune Response. *Biochim. Biophys. Acta (Bba) - Bioenerg.* 1757 (9-10), 1371–1387. doi:10.1016/j.bbabio.2006.06.014

Frank, D., and Vince, J. E. (2019). Pyroptosis versus Necroptosis: Similarities, Differences, and Crosstalk. *Cell Death Differ* 26 (1), 99–114. doi:10.1038/s41418-018-0212-6

Gagliardi, M. G., Bevilacqua, M., Bassano, C., Leonardi, B., Boldrini, R., Camassei, F. D., et al. (2004). Long Term Follow up of Children with Myocarditis Treated by Immunosuppression and of Children with Dilated Cardiomyopathy. *Heart* 90 (10), 1167–1171. doi:10.1136/hrt.2003.026641

Galluzzi, L., Kepp, O., and Kroemer, G. (2009). RIP Kinases Initiate Programmed Necrosis. *J. Mol. Cel. Biol.* 1 (1), 8–10. doi:10.1093/jmcb/mjp007

Glück, B., Merkle, I., Dornberger, G., and Stelzner, A. (2000). Expression of Inducible Nitric Oxide Synthase in Experimental Viral Myocarditis. *Herz* 25 (3), 255–260. doi:10.1007/s000590050016

Gon, S., Gatanaga, T., and Sendo, F. (1996). Involvement of Two Types of TNF Receptor in TNF-α Induced Neutrophil Apoptosis. *Microbiol. Immunol.* 40 (6), 463–465. doi:10.1111/j.1348-0421.1996.tb01095.x

Habib, F. M., Springall, D. R., Davies, G. J., Oakley, C. M., Yacoub, M. H., and Polak, J. M. (1996). Tumour Necrosis Factor and Inducible Nitric Oxide Synthase in Dilated Cardiomyopathy. *Lancet* 347, 1151–1155. doi:10.1016/s0140-6736(96)90610-8

He, S., Wang, L., Miao, L., Wang, T., Du, F., Zhao, L., et al. (2009). Receptor Interacting Protein Kinase-3 Determines Cellular Necrotic Response to TNF-α. *Cell* 137 (6), 1100–1111. doi:10.1016/j.cell.2009.05.021

Holler, N., Zaru, R., Micheau, O., Thome, M., Attinger, A., Valitutti, S., et al. (2000). Fas Triggers an Alternative, Caspase-8-independent Cell Death Pathway Using the Kinase RIP as Effector Molecule. *Nat. Immunol.* 1 (6), 489–495. doi:10.1038/82732

Hu, L., Chen, M., Chen, X., Zhao, C., Fang, Z., Wang, H., et al. (2020). Chemotherapy-induced Pyroptosis Is Mediated by BAK/BAX-caspase-3-GSDME Pathway and Inhibited by 2-bromopalmitate. *Cell Death Dis* 11 (4), 281. doi:10.1038/s41419-020-2476-2

Humphries, F., Yang, S., Wang, B., and Moynagh, P. N. (2015). RIP Kinases: Key Decision Makers in Cell Death and Innate Immunity. *Cel Death Differ* 22 (2), 225–236. doi:10.1038/cdd.2014.126

Kang, P. M., and Izumo, S. (2003). Apoptosis in Heart: Basic Mechanisms and Implications in Cardiovascular Diseases. *Trends Mol. Med.* 9 (4), 177–182. doi:10.1016/s1471-4914(03)00025-x

Karki, R., Sharma, B. R., Tuladhar, S., Williams, E. P., Zalduondo, L., Samir, P., et al. (2021). Synergism of TNF-α and IFN-γ Triggers Inflammatory Cell Death, Tissue Damage, and Mortality in SARS-CoV-2 Infection and Cytokine Shock Syndromes. *Cell* 184 (1), 149–168. doi:10.1016/j.cell.2020.11.025

Karunakaran, D., Geoffrion, M., Wei, L., Gan, W., Richards, L., Shangari, P., et al. (2016). Targeting Macrophage Necroptosis for Therapeutic and Diagnostic Interventions in Atherosclerosis. *Sci. Adv.* 2 (7), e1600224. doi:10.1126/sciadv.1600224

Koepsell, S. A., Anderson, D. R., and Radio, S. J. (2012). Parvovirus B19 Is a Bystander in Adult Myocarditis. *Cardiovasc. Pathol.* 21 (6), 476–481. doi:10.1016/j.carpath.2012.02.002

Kono, H., and Rock, K. L. (2008). How Dying Cells Alert the Immune System to Danger. *Nat. Rev. Immunol.* 8 (4), 279–289. doi:10.1038/nri2215

Kraft, L., Sauter, M., Seebohm, G., and Klingel, K. (2021). *In Vitro* Model Systems of Coxsackievirus B3-Induced Myocarditis: Comparison of Commonly Used Cell Lines and Characterization of CVB3-Infected iCell Cardiomyocytes. *Viruses* 13 (9), 1835. doi:10.3390/v13091835

Kroemer, G., Galluzzi, L., Vandenabeele, P., Abrams, J., Alnemri, E. S., Baehrecke, E. H., et al. (2009). Classification of Cell Death: Recommendations of the Nomenclature Committee on Cell Death 2009. *Cel Death Differ* 16 (1), 3–11. doi:10.1038/cdd.2008.150

Kühl, U., and Schultheiss, H. (2014). Viral Myocarditis. *Swiss Med. Wkly* 144, w14010. doi:10.4414/smw.2014.14010

Kytö, V., Saraste, A., Voipio-Pulkki, L.-M., and Saukko, P. (2007). Incidence of Fatal Myocarditis: a Population-Based Study in Finland. *Am. J. Epidemiol.* 165 (5), 570–574. doi:10.1093/aje/kwk076

Lin, Y., Choksi, S., Shen, H.-M., Yang, Q.-F., Hur, G. M., Kim, Y. S., et al. (2004). Tumor Necrosis Factor-Induced Nonapoptotic Cell Death Requires Receptor-Interacting Protein-Mediated Cellular Reactive Oxygen Species Accumulation. *J. Biol. Chem.* 279 (11), 10822–10828. doi:10.1074/jbc.M313141200

Liu, Z. Y., Wu, B., Guo, Y. S., Zhou, Y. H., Fu, Z. G., Xu, B. Q., et al. (2015). Necrostatin-1 Reduces Intestinal Inflammation and Colitis-Associated Tumorigenesis in Mice. *Am. J. Cancer Res.* 5 (10), 3174–3185.

Malireddi, R. K. S., Gurung, P., Kesavardhana, S., Samir, P., Burton, A., Mummareddy, H., et al. (2020). Innate Immune Priming in the Absence of TAK1 Drives RIPK1 Kinase Activity-independent Pyroptosis, Apoptosis, Necroptosis, and Inflammatory Disease. *J. Exp. Med.* 217 (3), 217. doi:10.1084/jem.20191644

Malireddi, R. K. S., Kesavardhana, S., and Kanneganti, T.-D. (2019). ZBP1 and TAK1: Master Regulators of NLRP3 Inflammasome/Pyroptosis, Apoptosis, and Necroptosis (PAN-Optosis). *Front. Cel. Infect. Microbiol.* 9, 406. doi:10.3389/fcimb.2019.00406

Meng, L., Jin, W., Wang, Y., Huang, H., Li, J., and Zhang, C. (2016). RIP3-dependent Necrosis Induced Inflammation Exacerbates Atherosclerosis. *Biochem. biophysical Res. Commun.* 473 (2), 497–502. doi:10.1016/j.bbrc.2016.03.059

Moe, G. W., and Marín-García, J. (2016). Role of Cell Death in the Progression of Heart Failure. *Heart Fail. Rev.* 21 (2), 157–167. doi:10.1007/s10741-016-9532-0

Moore, J. B., and June, C. H. (2020). Cytokine Release Syndrome in Severe COVID-19. *Science* 368 (6490), 473–474. doi:10.1126/science.abb8925

Narovlyanskaya, O., and Winokur, E. J. (2020). Viral Myocarditis. *Dimensions Crit. Care Nurs.* 39 (2), 75–80. doi:10.1097/dcc.0000000000000402

Navarro, J. F., and Mora, C. (2006). Diabetes, Inflammation, Proinflammatory Cytokines, and Diabetic Nephropathy. *Scientific World J.* 6, 908–917. doi:10.1100/tsw.2006.179

Pennica, D., Nedwin, G. E., Hayflick, J. S., Seeburg, P. H., Derynck, R., Palladino, M. A., et al. (1984). Human Tumour Necrosis Factor: Precursor Structure, Expression and Homology to Lymphotoxin. *Nature* 312 (5996), 724–729. doi:10.1038/312724a0

Pollack, A., Kontorovich, A. R., Fuster, V., and Dec, G. W. (2015). Viral Myocarditis-Diagnosis, Treatment Options, and Current Controversies. *Nat. Rev. Cardiol.* 12 (11), 670–680. doi:10.1038/nrcardio.2015.108

Samir, P., Malireddi, R. K. S., and Kanneganti, T.-D. (2020). The PANoptosome: A Deadly Protein Complex Driving Pyroptosis, Apoptosis, and Necroptosis (PANoptosis). *Front. Cel. Infect. Microbiol.* 10, 238. doi:10.3389/fcimb.2020.00238

Song, L., Lin, C., Gong, H., Wang, C., Liu, L., Wu, J., et al. (2013). miR-486 Sustains NF-Kb Activity by Disrupting Multiple NF-Kb-Negative Feedback Loops. *Cell Res* 23 (2), 274–289. doi:10.1038/cr.2012.174

Sosna, J., Voigt, S., Mathieu, S., Lange, A., Thon, L., Davarnia, P., et al. (2014). TNF-induced Necroptosis and PARP-1-Mediated Necrosis Represent Distinct Routes to Programmed Necrotic Cell Death. *Cell. Mol. Life Sci.* 71 (2), 331–348. doi:10.1007/s00018-013-1381-6

Sun, L., Chen, Y., Luo, H., Xu, M., Meng, G., and Zhang, W. (2019). Ca2+/calmodulin-dependent Protein Kinase II Regulation by Inhibitor 1 of Protein Phosphatase 1 Alleviates Necroptosis in High Glucose-Induced Cardiomyocytes Injury. *Biochem. Pharmacol.* 163, 194–205. doi:10.1016/j.bcp.2019.02.022

Sun, L., Wang, H., Wang, Z., He, S., Chen, S., Liao, D., et al. (2012). Mixed Lineage Kinase Domain-like Protein Mediates Necrosis Signaling Downstream of RIP3 Kinase. *Cell* 148 (1-2), 213–227. doi:10.1016/j.cell.2011.11.031

Topol, E. J. (2020). COVID-19 Can Affect the Heart. *Science* 370 (6515), 408–409. doi:10.1126/science.abe2813

Torre-Amione, G., Kapadia, S., Lee, J., Durand, J.-B., Bies, R. D., Young, J. B., et al. (1996). Tumor Necrosis Factor-α and Tumor Necrosis Factor Receptors in the Failing Human Heart. *Circulation* 93 (4), 704–711. doi:10.1161/01.cir.93.4.704

Van Linthout, S., Elsanhoury, A., Klein, O., Sosnowski, M., Miteva, K., Lassner, D., et al. (2018). Telbivudine in Chronic Lymphocytic Myocarditis and Human Parvovirus B19 Transcriptional Activity. *ESC Heart Fail.* 5 (5), 818–829. doi:10.1002/ehf2.12341

Vandenabeele, P., Declercq, W., Van Herreweghe, F., and Vanden Berghe, T. (2010). The Role of the Kinases RIP1 and RIP3 in TNF-Induced Necrosis. *Sci. Signal.* 3 (115), re4. doi:10.1126/scisignal.3115re4

Vandenabeele, P., Galluzzi, L., Vanden Berghe, T., and Kroemer, G. (2010). Molecular Mechanisms of Necroptosis: an Ordered Cellular Explosion. *Nat. Rev. Mol. Cel Biol* 11 (10), 700–714. doi:10.1038/nrm2970

Vaseva, A. V., Marchenko, N. D., Ji, K., Tsirka, S. E., Holzmann, S., and Moll, U. M. (2012). p53 Opens the Mitochondrial Permeability Transition Pore to Trigger Necrosis. *Cell* 149 (7), 1536–1548. doi:10.1016/j.cell.2012.05.014

Vercammen, D., Vandenabeele, P., Beyaert, R., Declercq, W., and Fiers, W. (1997). Tumour Necrosis Factor-Induced Necrosis versus Anti-fas-induced Apoptosis in L929 Cells. *Cytokine* 9 (11), 801–808. doi:10.1006/cyto.1997.0252

Wada, H., Saito, K., Kanda, T., Kobayashi, I., Fujii, H., Fujigaki, S., et al. (2001). Tumor Necrosis Factor-α (TNF-α) Plays a Protective Role in Acute Viral Myocarditis in Mice. *Circulation* 103 (5), 743–749. doi:10.1161/01.CIR.103.5.743

Wang, D., Li, T., Cui, H., and Zhang, Y. (2016). Analysis of the Indicating Value of Cardiac Troponin I, Tumor Necrosis Factor-α, Interleukin-18, Mir-1 and Mir-146b for Viral Myocarditis Among Children. *Cell Physiol Biochem* 40 (6), 1325–1333. doi:10.1159/000453185

Wang, K., Sun, Q., Zhong, X., Zeng, M., Zeng, H., Shi, X., et al. (2020). Structural Mechanism for GSDMD Targeting by Autoprocessed Caspases in Pyroptosis. *Cell* 180 (5), 941–955. doi:10.1016/j.cell.2020.02.002

Wang, L., Du, F., and Wang, X. (2008). TNF-α Induces Two Distinct Caspase-8 Activation Pathways. *Cell* 133 (4), 693–703. doi:10.1016/j.cell.2008.03.036

Wen, H. Y., Jia, W. K., Liu, L., Yang, L., Yang, Y., Sun, X. M., et al. (2010). Clinical Significance of Cellular Immune Function in Patients with Viral Myocarditis. *Xi Bao Yu Fen Zi Mian Yi Xue Za Zhi* 26 (7), 685–686. doi:10.13423/j.cnki.cjcmi.005743

Why, H. J., Meany, B. T., Richardson, P. J., Olsen, E. G., Bowles, N. E., Cunningham, L., et al. (1994). Clinical and Prognostic Significance of Detection of Enteroviral RNA in the Myocardium of Patients with Myocarditis or Dilated Cardiomyopathy. *Circulation* 89 (6), 2582–2589. doi:10.1161/01.cir.89.6.2582

Wu, J., Huang, Z., Ren, J., Zhang, Z., He, P., Li, Y., et al. (2013). Mlkl Knockout Mice Demonstrate the Indispensable Role of Mlkl in Necroptosis. *Cel Res* 23 (8), 994–1006. doi:10.1038/cr.2013.91

Wu, Y.-T., Tan, H.-L., Huang, Q., Sun, X.-J., Zhu, X., and Shen, H.-M. (2011). zVAD-induced Necroptosis in L929 Cells Depends on Autocrine Production of TNFα Mediated by the PKC-MAPKs-AP-1 Pathway. *Cel Death Differ* 18 (1), 26–37. doi:10.1038/cdd.2010.72

Wu, Y., Zheng, Z., Cao, X., Yang, Q., Norton, V., Adini, A., et al. (2021). RIP1/RIP3/MLKL Mediates Myocardial Function through Necroptosis in Experimental Autoimmune Myocarditis. *Front. Cardiovasc. Med.* 8, 696362. doi:10.3389/fcvm.2021.696362

Yang, C., Li, T., Xue, H., Wang, L., Deng, L., Xie, Y., et al. (2018). Inhibition of Necroptosis Rescues SAH-Induced Synaptic Impairments in Hippocampus via CREB-BDNF Pathway. *Front. Neurosci.* 12, 990. doi:10.3389/fnins.2018.00990

Zhang, D.-W., Shao, J., Lin, J., Zhang, N., Lu, B.-J., Lin, S.-C., et al. (2009). RIP3, an Energy Metabolism Regulator that Switches TNF-Induced Cell Death from Apoptosis to Necrosis. *Science* 325 (5938), 332–336. doi:10.1126/science.1172308

Zhang, T., Zhang, Y., Cui, M., Jin, L., Wang, Y., Lv, F., et al. (2016). CaMKII Is a RIP3 Substrate Mediating Ischemia- and Oxidative Stress-Induced Myocardial Necroptosis. *Nat. Med.* 22 (2), 175–182. doi:10.1038/nm.4017

Zhao, J., Jitkaew, S., Cai, Z., Choksi, S., Li, Q., Luo, J., et al. (2012). Mixed Lineage Kinase Domain-like Is a Key Receptor Interacting Protein 3 Downstream Component of TNF-Induced Necrosis. *Proc. Natl. Acad. Sci.* 109 (14), 5322–5327. doi:10.1073/pnas.1200012109

Zhou, F., Jiang, X., Teng, L., Yang, J., Ding, J., and He, C. (2018). Necroptosis May Be a Novel Mechanism for Cardiomyocyte Death in Acute Myocarditis. *Mol. Cel Biochem* 442 (1-2), 11–18. doi:10.1007/s11010-017-3188-5

Conflict of Interest: The authors declare that the research was conducted in the absence of any commercial or financial relationships that could be construed as a potential conflict of interest.

Publisher's Note: All claims expressed in this article are solely those of the authors and do not necessarily represent those of their affiliated organizations, or those of the publisher, the editors, and the reviewers. Any product that may be evaluated in this article, or claim that may be made by its manufacturer, is not guaranteed or endorsed by the publisher.

Copyright © 2022 Zhou, Xu, Li, Sun, Kadier, Zhou and Cheng. This is an open-access article distributed under the terms of the Creative Commons Attribution License (CC BY). The use, distribution or reproduction in other forums is permitted, provided the original author(s) and the copyright owner(s) are credited and that the original publication in this journal is cited, in accordance with accepted academic practice. No use, distribution or reproduction is permitted which does not comply with these terms.

frontiers | Frontiers in Cell and Developmental Biology

ORIGINAL RESEARCH
published: 05 May 2022
doi: 10.3389/fcell.2022.809996

Higenamine Attenuates Doxorubicin-Induced Cardiac Remodeling and Myocyte Apoptosis by Suppressing AMPK Activation

Cuiliu Jin[1†], Yu Chai[1†], Zhimin Hu[1], Wencong Tian[2], Wang Ling[1], Jing Li[2] and Meiping Wu[1]**

[1]*Department of Cardiology, Shanghai Municipal Hospital of Traditional Chinese Medicine, Shanghai University of Traditional Chinese Medicine, Shanghai, China,* [2]*Department of Molecular Pharmacology, School of Medicine, Nankai University, Tianjin, China*

OPEN ACCESS

Edited by:
Rongxue Wu,
The University of Chicago,
United States

Reviewed by:
Jing Wang,
Chinese Academy of Medical Sciences, China
Zhaocai Zhang,
Zhejiang University, China

***Correspondence:**
Jing Li
stellarli@nankai.edu.cn
Meiping Wu
meipingwu@shutcm.edu.cn

†These authors have contributed equally to this work

Specialty section:
This article was submitted to Cell Death and Survival, a section of the journal Frontiers in Cell and Developmental Biology

Received: *05 November 2021*
Accepted: *21 March 2022*
Published: *05 May 2022*

Citation:
Jin C, Chai Y, Hu Z, Tian W, Ling W, Li J and Wu M (2022) Higenamine Attenuates Doxorubicin-Induced Cardiac Remodeling and Myocyte Apoptosis by Suppressing AMPK Activation. Front. Cell Dev. Biol. 10:809996. doi: 10.3389/fcell.2022.809996

Background: As an effective antitumor drug, doxorubicin (DOX) is primarily used to treat solid tumors and hematologic malignancies. However, increasing evidence has emerged indicating its cardiotoxicity, and few solutions have been proposed to counter this side effect. Higenamine (HG) is a natural compound widely found in many Chinese herbs and also serves as a component in many healthcare products. Several studies have demonstrated its cardioprotective effect in different models, but little is known about the underlying influences of HG against myocardial damage from DOX-induced chronic cardiotoxicity.

Methods and Results: C57BL/6 mice and neonatal rat ventricular cardiomyocytes (NRVMs) were used to evaluate the cardioprotective effect of HG against DOX-induced myocardial damage. In mice, DOX (intraperitoneally injected 5 mg/kg every 3 days for 4 weeks) significantly increased cardiomyocyte apoptosis, cardiac atrophy, and cardiac dysfunction, which were significantly attenuated by HG (intragastrically administered with 10 mg/kg every day for 4 weeks). In NRVMs, DOX (3 μM for 24 h) significantly increased cell apoptosis and the level of reactive oxygen species while reducing the level of superoxide dismutase and mitochondrial membrane potential. Remarkably, HG can reverse these pathological changes caused by DOX. Interestingly, the protective effect of HG on DOX-induced cardiotoxicity was independent of the activation of the beta-2 adrenergic receptor (β2-AR), known for mediating the effect of HG on antagonizing ischemia/reperfusion-induced cardiac apoptosis. Furthermore, HG attenuated the abnormal activation of phosphorylated adenosine-activated protein kinase (AMPK). Consistently, AMPK agonists (AICAR) can eliminate these pharmacological actions of HG.

Conclusion: Collectively, our results suggested that HG alleviated DOX-induced chronic myocardial injury by suppressing AMPK activation and ROS production.

Keywords: doxorubicin, higenamine, adenosine-activated protein kinase, cardiac remodeling, myocyte apoptosis

INTRODUCTION

Tumor cardiopathy is a major disease that affects the survival rate and time of tumor patients, where chemotherapy-induced cardiotoxicity accounts for significant complications (Koutsoukis et al., 2018). Doxorubicin (DOX), a cornerstone of chemotherapy, is widely known for its cardiotoxicity, which is difficult to combat in the clinic (Singal and Iliskovic., 1998). DOX-induced cardiomyocyte apoptosis, myocardial atrophy, dilated cardiomyopathy, and myocardial fibrosis contribute to myocardial remodeling, left ventricular dysfunction, and even heart failure (Zhang et al., 2018; Galan-Arriola et al., 2019).

At present, the mechanism of cardiotoxicity induced by DOX is not fully understood. Increasing research has indicated that it might be a multifactorial process including oxidative stress, inflammatory response, mitochondrial damage, disorder of calcium metabolism, induced myocardial cell apoptosis, and autophagy (Mantawy et al., 2014; Wang et al., 2021). Moreover, most drugs which can protect heart remodeling in other types of heart disease fail to do so with DOX-induced cardiotoxicity. The exception to this is dexrazoxane (Yu et al., 2020), the only drug authorized by the FDA to reduce the incidence and severity of cardiomyopathy associated with DOX administration. Furthermore, the administration of dexrazoxane is not 100% effective, so seeking new therapies for the treatment of cardiotoxicity has garnered significant attention. As the primary component of the heart structure, cardiomyocytes are the basis to maintain normal physiological functions of the heart. The fate of cardiomyocytes from DOX treatment has attracted significant attention from the bench to the clinic (Hagag et al., 2020).

Higenamine {HG; 1-[(4-hydroxyphenyl)methyl]-1,2,3,4-tetrahydroisoquinoline-6,7-diol} is the main active ingredient of aconite root, a traditional Chinese herb which was widely used to treat heart failure-like symptoms in Asian countries for thousands of years. Interestingly, HG has been also used as a common component of health products for fat degradation and sports performance in Europe and North America (Lee et al., 2013; Liu and Santillo., 2016). In recent years, a vast number of clinical experimental studies have proven that HG can serve as a cardiotonic, tracheal smooth muscle relaxant, anticoagulant, and anti-inflammatory agent (Tsukiyama et al., 2009; Zhang et al., 2014; Tariq and Aronow, 2015).

Our previous studies have reported that the β2/PI3K/Akt signaling pathway can be activated by HG to inhibit the myocardial injury induced by ischemia-reperfusion (Wu et al., 2016). It has also been found that HG can inhibit myocardial injury and cardiac fibrosis *via* the TGF-β/Smad signaling pathway, which inhibits the activation of cardiac fibroblasts and reduces the deposition of matrix proteins (Zhu et al., 2021). Although these studies have confirmed the therapeutic effect of HG on cardiovascular diseases, it is uncertain whether HG can protect against DOX-induced cardiotoxicity. In the current study, we have examined the effects of HG in chronic DOX-induced heart injury in C57 mice. Using NRVMs, we examined the effects of HG on NRVM apoptosis and the levels of ROS induced by DOX. We also determined the mechanism of HG in this pharmacological function. Here, we have demonstrated that HG remarkably inhibits myocardial apoptosis induced by DOX and restores heart functions. Furthermore, we found that the mechanism of HG in these diseases is different from known pathways, partially through suppressing the abnormal AMPK activation and ROS production, which has not been reported yet.

MATERIALS AND METHODS

Reagents and Drugs

HG was purchased from TAUTO Biochemical Technology Co., Ltd. (Shanghai, China). DOX was procured from MedChemExpress (Shanghai, China). The primary antibodies for cleaved caspase 3, GAPDH, phosphor-AMPKα, and total-AMPKα were purchased from Cell Signaling Technology (Danvers, MA, United States). Cell culture media were purchased from Gibco (Grand Island, NY, United States).

Animal Care

Adult male C57BL/6 mice, 8 weeks of age, were purchased from Shanghai Slac Laboratory Animal Co. Ltd. The mice were routinely kept in the animal room of Shanghai Tongji University. The protocols were approved by the Laboratory Animal Ethics Committee of Shanghai Tongji University (Shanghai, China; Permit No. TJHBLAC-2019-057). All animal procedures were performed in accordance with the Shanghai University of Traditional Chinese Medicine guidelines and the National Natural Science Foundation of China (NSFC).

Doxorubicin Injection Model

To mimic chronic cardiotoxicity of DOX *in vivo*, we exposed the mice to continuous intraperitoneal injection of vehicle saline or DOX. The mice in DOX and DOX + HG groups were intraperitoneally injected with 5 mg/kg DOX every 3 days for 4 weeks. For HG treatment, HG was dissolved in a vehicle consisting of 10% (vol/vol) DMSO in 40% β-cyclodextrin. The mice were then randomized to receive either HG (10 mg/kg) or vehicle (10% DMSO in 40% β-cyclodextrin) treatment administered intragastrically once daily for 4 weeks. The aforementioned procedure is described in **Figure 1**. After 4 weeks, the general condition and survival of the mice were observed.

Neonatal Rat Ventricular Cardiomyocytes Isolation, Culture, and Treatment

NRVMs were isolated from 2- to 3-day-old suckling Sprague Dawley rats following the methods previously published (Golden et al., 2012). In brief, the rat hearts were excised; their ventricles were separated and washed in Hank's balanced salt solution (HBSS) three times and then digested repeatedly with type II collagenase containing HBSS. The cells were collected by 100 × g centrifugation and resuspended in Dulbecco's modified Eagle medium (DMEM), supplemented with 15% fetal bovine serum (FBS), 100 IU/ml penicillin, and 100 g/ml streptomycin.

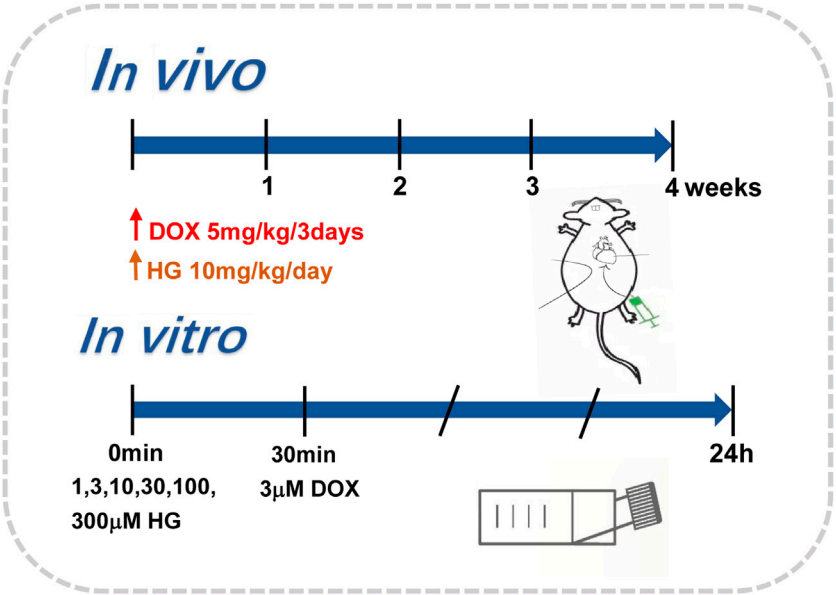

FIGURE 1 | Administration modes *in vivo* and *in vitro*.

Fibroblasts were then removed by differential adherent culture and placed at 37°C for 90 min. The cell suspension was collected and plated directly into six-well plates with 5-BrdU in a density of about 3×10^5 cells/ml. After 24 h, the cells were washed several times with PBS and treated with DMEM containing 10% fetal bovine serum. Cardiomyocytes were treated with DOX (3 μM) for 24 h, with or without different interventions. The aforementioned procedure is described in **Figure 1**.

Echocardiography

Cardiac function was assessed by transthoracic echocardiography and using a Vevo 2100 ultra-high resolution small animal ultrasound imaging system (Fujifilm, Toronto, ON, Canada). Left ventricular systolic and diastolic functions, LV ejection fraction (EF%), and fractional shortening (FS%) were measured.

Assessment of Cell Viability

Cell viability was measured by using the Cell Counting Kit-8 (CCK-8). In brief, after 24 h of treatment, cells were incubated with CCK-8 solution (Beyotime, China). To facilitate the reaction, stained cells were incubated at 37°C for 3 h. At the end of the treatment, the absorbance at 450 nm was measured using a BioTek® Epoch microplate reader (BioTek Instruments, Inc. United States).

Assessment of Reactive Oxygen Species Levels

Intracellular reactive oxygen species levels were assessed by using a DCFH-DA fluorescence probe (Beyotime, China). In brief, after 24-h treatment, cells were incubated with a 10 μM DCFH-DA fluorescence probe for 30 min at 37°C in the dark. The fluorescence intensity was determined by flow cytometry.

Assessment of Superoxide Dismutase Levels

Intracellular superoxide dismutase levels were measured by using superoxide dismutase kits (Beyotime, China), following the manufacturer's instructions. The data were measured by using a BioTek® Epoch microplate reader (BioTek Instruments, Inc. United States).

Western Blot Analysis

Western blot analysis was performed as described previously (Knight et al., 2016). In brief, cell and heart samples after various treatments were collected to extract the proteins. The protein concentration was determined by using a BCA protein assay (Thermo Fisher Scientific, Rockford, IL, United States). The protein samples were separated by SDS-PAGE and transferred to PVDF membranes. PBST containing 5% (m/v) BSA (in Tris buffer containing 0.1% Tween 20) was used to block the membrane at room temperature for 2 h. The cells were then incubated with anti-AMPK (1:1000), anti-P-AMPK (THR 172, 1:1000), anti-cleaved caspase 3 (1:1000), and anti-GAPDH (1:1000) primary antibodies at 4°C overnight. Subsequently, the membrane was washed with PBST and exposed to the corresponding secondary antibody (1:6000) at room temperature for 2 h. A Bio-Rad imaging system (Bio-Rad, Hercules, CA, United States) was used to detect fluorescence signals, and Image Lab software (Bio-Rad, Hercules, CA, United States) was used to quantify the signal.

Hematoxylin–Eosin Staining

Hematoxylin–eosin staining was performed as described previously (Cardiff et al., 2014). Mice hearts were collected,

fixed, embedded, and sectioned, in accordance with the standard protocol. In short, the heart sections were dewaxed with xylene and dehydrated with ethanol. The sections were incubated in the hematoxylin staining solution at room temperature for 5–10 min, washed with distilled water for 5 min, re-stained with eosin staining solution for 3 min, and finally washed with distilled water for 5 min. The sections were soaked in 75, 85, 95, and 100% ethanol for 2 min, and then heart sections were cleaned in xylene and sealed with neutral resin.

Wheat Germ Agglutinin Staining

Wheat germ agglutinin (WGA) staining was performed as described previously (Wang et al., 2019). In brief, heart sections were dewaxed with xylene and dehydrated with ethanol. The heart tissues were preheated in a pressure cooker containing 0.01 M citrate solution, incubated with glycine at room temperature for 20 min, and washed with PBS for 5 min. WGA staining solution was prepared at a dilution of 1:50. The staining solution was dropped on the glass slide and incubated at room temperature for 1 h in the dark. The slides were then washed three times with PBS, taking 5 min per wash. DAPI sealing solution was then added to seal the heart sections. Images were collected by using a fluorescence microscope. Image-Pro software (Media Cybernetics) was used to quantify the mean cardiomyocyte cross-sectional area (CSA).

Terminal Deoxynucleotidyl Transferase–Mediated dUTP Nick-End Labeling Staining

TUNEL staining was performed in accordance with the instructions of the TUNEL kit (Roche, Switzerland). In brief, the tissue sections were dewaxed and rehydrated following standard protocols. The tissue sections were incubated for 30 min at 37°C with proteinase K working solution (20 μg/ml in 10 mM Tris–HCl, pH 7.4–8). The blocking solution (5% goat serum in PBS) was then added and incubated for 1 h at room temperature. The TUNEL reagent was added to the samples and incubated at 37°C for 1 h in the dark. After washing with distilled water three times (5 min each), DAPI dye solution was added and incubated at room temperature for 10 min. After washing with distilled water twice, images were taken under a fluorescence microscope. The images were obtained from three random regions of each mouse heart section. The apoptotic index was expressed as the percentage of TUNEL-positive nuclei to DAPI-stained nuclei.

Measurement of Mitochondrial Membrane Potential

The mitochondrial membrane potential (MMP) was evaluated by staining with a cationic dye, 5,5,6,6-tetrachloro-1,1,3,3-tetraethylbenzimidazolylcarbocyanine iodide (JC-1, Beyotine, China), in accordance with the manufacturer's instructions. In brief, neonatal rat cardiomyocytes were inoculated into six-well plates; the culture medium was aspirated, and the cells were washed with PBS. Afterward, 1 ml of the culture medium and 1 ml of the JC-1 staining solution were added and the mixture was incubated at 37°C for 20 min. After incubation, the cells were washed twice with 1X buffer and the culture medium was added. The images were normalized by fluorescence imaging using a Leica inverted fluorescence microscope.

Immunohistochemistry

For immunohistochemistry, the heart paraffin sections were heated using the pressure cooker for antigen retrieval and 8% goat serum was used to block non-specific binding sites incubated with anti-P-AMPK (ab23875, Abcam) and anti-T-AMPK antibody (ab131512, Abcam), followed by incubation with goat anti-rabbit EnVisionTM+/horseradish peroxidase (HRP) reagent, and stained using a DAB detection kit (GeneTech, Shanghai, China). Negative control was obtained by replacing primary antibody with PBS. Immunohistochemistry paraffin sections were visualized by light microscopy.

STATISTICAL ANALYSIS

All data are presented as mean ± SEM. Statistical analysis was performed using Prism 8.0 one-way ANOVA, followed by Bonferroni's post hoc test for comparisons of multiple groups. p-values < 0.05 were considered statistically significant.

RESULTS

Higenamine Attenuates DOX-Induced Cardiac Injury *In Vivo*

To explore the function of Higenamine in cardiac injury induced by DOX *in vivo*, C57BL/6 mice were intraperitoneally injected with 5 mg/kg of DOX every 3 days for 4 weeks to mimic the chronic myocardial injury induced by DOX. For HG intervention, mice were randomized to receive either HG (10 mg/kg) or vehicle [10% (vol/vol) DMSO in 40% β-cyclodextrin] treatment administered intragastrically once daily starting from the first day of DOX injection. As shown in **Figure 2A**, after 4 weeks, there was no statistical difference in the survival rate among each group. DOX-induced heart atrophy was assessed by global morphology. Daily HG application reversed this pathological deterioration (**Figure 2B**). H&E staining was used to evaluate cardiac remodeling, and WGA staining was performed to illustrate the cross-sectional area of each cardiomyocyte. Using H&E staining, we found a similar tendency of morphological changes in the global shape (**Figure 2C**). Consistently, WGA staining indicated that HG can reverse the DOX-induced cross-sectional area (CSA) reduction of cardiomyocytes (**Figures 2D,E**), suggesting that HG attenuates DOX-induced cardiac remodeling *in vivo*.

Higenamine Improves Doxorubicin-Induced Cardiac Dysfunction *In Vivo*

To evaluate the effects of HG on the cardiac dysfunction induced by DOX, we monitored cardiac function by echocardiography (**Figure 3A** and **Table 1**). As depicted in **Figures 3B,C**, compared with the normal saline group, the

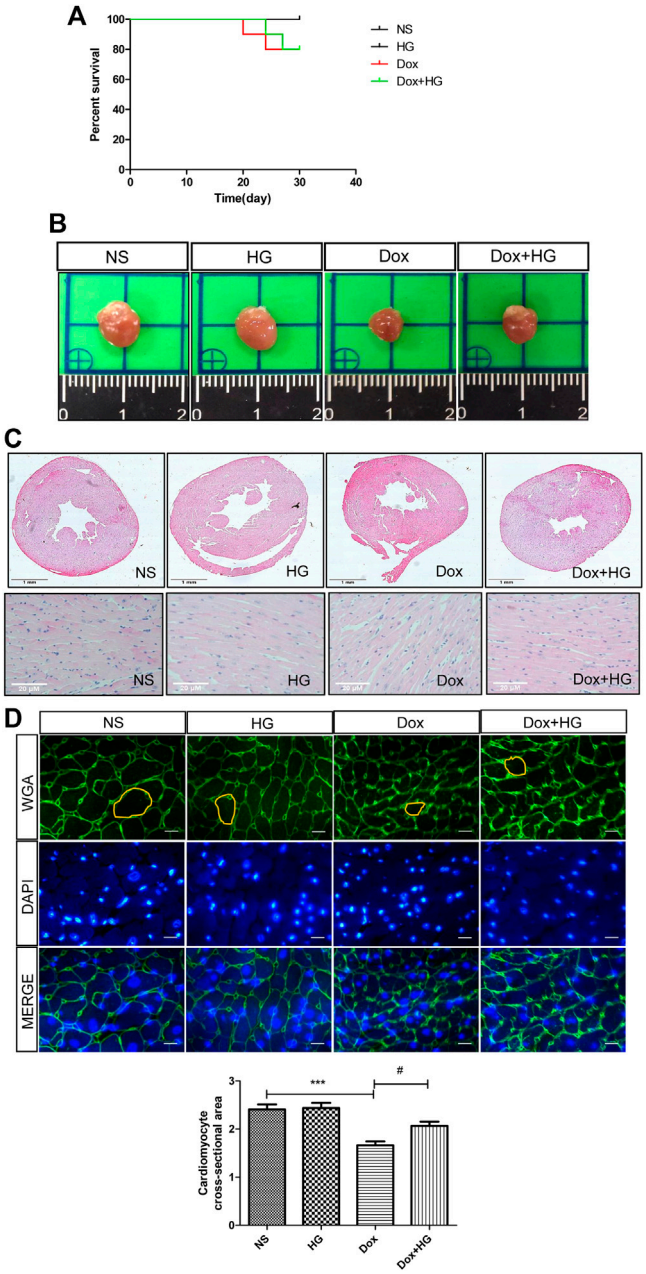

FIGURE 2 | HG attenuated DOX-induced cardiac injury *in vivo*. **(A)** Survival curve of mice. **(B)** Representative heart images of each group. Mice were injected with normal saline (NS) or DOX (5 mg/kg/3 days) and systemically administrated with HG (10 mg/kg/day) during DOX injection for 4 weeks. **(C)** Schematic diagram of HE staining of the heart cross-sectional area for each group. **(D)** Schematic diagram of representative heart tissue WGA staining for each group of mice. **(E)** Quantification of the cross-sectional area of single cardiac muscle cells after WGA staining. All values are presented as mean ± SEM; statistical analysis was performed using Prism 8.0 one-way ANOVA. * $p < 0.05$ DOX vs NS; # $p < 0.05$ DOX + HG vs DOX. Animal numbers: NS, n = 8; HG, n = 7; DOX, n = 10; Dox + HG, n = 10.

cardiac function in the DOX model group decreased, reflected by the ejection fraction (EF) and shortening fraction (FS) ($p < 0.05$). With HG application, EF and FS were significantly rescued ($p < 0.05$). Consistently, DOX induced heart atrophy as reflected by the stroke volume (SV), and this deterioration is markedly attenuated in mice receiving treatment with HG ($p < 0.05$) (**Figure 3D**). Using the ELISA kit to detect BNP levels in serum, the results showed that DOX can also promote BNP content in serum, and HG can reduce BNP content (**Supplementary Figure S3A**). All these results suggest that HG has a protective effect on cardiac remodeling and heart failure induced by DOX.

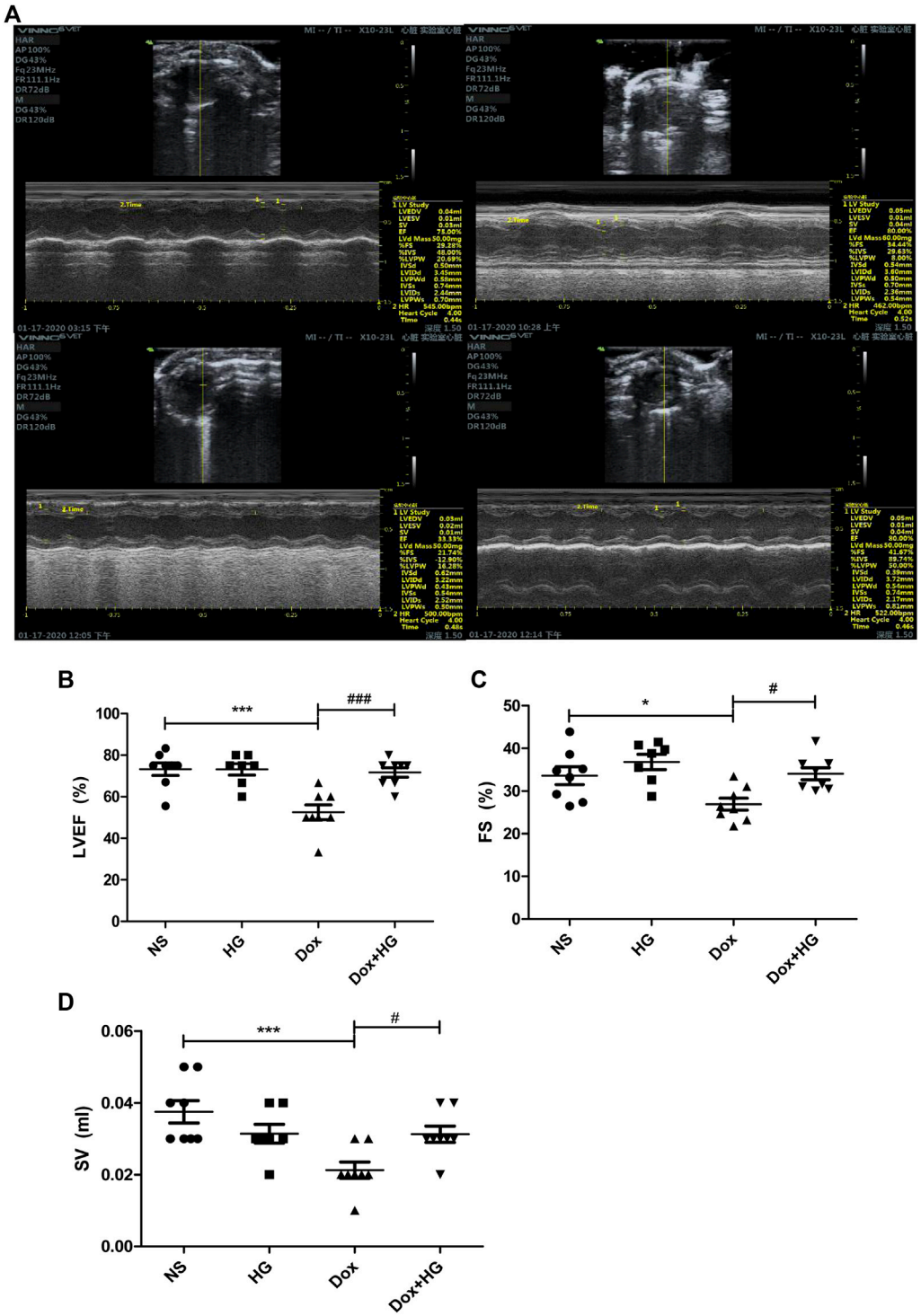

FIGURE 3 | HG improved DOX-induced cardiac dysfunction *in vivo*. **(A)** Representative M-mode echocardiographic images of mice in each group at 4 weeks. **(B–D)** Summary of **(B)** ejection fraction (EF), **(C)** shortening fraction (FS), and **(D)** stroke volume (SV) data in each group. All values are presented as mean ± SEM; statistical analysis was performed using Prism 8.0 one-way ANOVA. * $p < 0.05$ DOX vs NS; # $p < 0.05$ DOX + HG vs DOX. Animal numbers: NS, n = 8; HG, n = 7; DOX, n = 10; DOX + HG, n = 10.

TABLE 1 | Echocardiographic indexes in each group of mice.

Parameter	NS	HG	Dox	Dox + HG
EF (%)	73.195 ± 8.028	73.096 ± 6.751	52.5 ± 9.393*	71.668 ± 6.123#
FS (%)	33.606 ± 5.522	36.829 ± 4.379	26.875 ± 3.683*	34.073 ± 3.753#
LVEDV (ml)	0.053 ± 0.016	0.043 ± 0.007	0.04 ± 0.007	0.044 ± 0.009
LVESV (ml)	0.015 ± 0.010	0.011 ± 0.003	0.019 ± 0.003	0.013 ± 0.004
SV (ml)	0.038 ± 0.008	0.031 ± 0.006	0.021 ± 0.006*	0.031 ± 0.006#
IVSd (mm)	0.509 ± 0.101	0.461 ± 0.029	0.544 ± 0.074	0.509 ± 0.066
IVSs (mm)	0.7 ± 0.053	0.683 ± 0.085	0.635 ± 0.072	0.649 ± 0.107
LVIDs (mm)	2.495 ± 0.393	2.22 ± 0.171	2.519 ± 0.154	2.311 ± 0.219
LVIDd (mm)	3.744 ± 0.354	3.516 ± 0.160	3.445 ± 0.142	3.506 ± 0.259
LVPWs (mm)	0.709 ± 0.077	0.797 ± 0.098	0.639 ± 0.109	0.679 ± 0.070
LVPWd (mm)	0.586 ± 0.068	0.603 ± 0.070	0.543 ± 0.079	0.509 ± 0.054
HR(beats/min)	539.00 ± 37.964	510.714 ± 65.226	500.75 ± 31.52	482.625 ± 35.6

*p < 0.05 vs NS; #p < 0.05 vs Dox.
Values are expressed as mean ± SEM.
EF, ejection fraction; FS, fractional shortening; LVEDV, left ventricular end-diastolic volume; LVESV, left ventricular end-systolic volume; SV, stroke volume; IVSd, diastolic interventricular septal thickness; IVSs, systolic interventricular septal thickness; LVIDs, left ventricular internal diameter in systole; LVIDd, Left ventricular internal diameter in diastole; LVPWs, left ventricular posterior wall thickness at systole; LVPWd, left ventricular posterior wall thickness at diastole; HR, heart rate.
All values are presented as mean ± SEM; statistical analysis was performed using Prism 8.0 one-way ANOVA.

Higenamine Inhibited Doxorubicin-Induced Cardiomyocyte Apoptosis *In Vivo*

Cardiomyocyte apoptosis is a pivotal pathological process of DOX-induced myocardial injury. To evaluate the effect of HG on DOX-induced cardiomyocyte apoptosis, TUNEL staining and Western blots were performed on mice hearts. As expected, TUNEL staining showed that mice with DOX had a significantly increased number of apoptotic cardiomyocytes compared to the normal saline group, and HG could inhibit DOX-induced cardiomyocyte apoptosis (**Figures 4A,B**). Similarly, Western blot results showed that compared to the saline control mice, the expression level of cleaved caspase 3 in mice with DOX was largely increased ($p < 0.05$). After application with HG, the protein level of cleaved caspase 3 was significantly decreased ($p < 0.05$) (**Figures 4C,D**). Combined with the TUNEL staining, these results confirmed that HG could attenuate DOX-induced cardiac apoptosis in mice. Doxorubicin has been proved to lead to adverse ventricular remodeling of the heart in the chronic progressive approach, mainly involved in cardiac fibrosis. In order to detect the degree of myocardial fibrosis after DOX stimulation, we performed PSR staining and Masson staining. The results showed that myocardial fibrosis did not increase after injecting DOX for 4 weeks, and HG treatment did not remarkably reduce myocardial fibrosis and the perivascular collagen volume area (**Supplementary Figures S1A–D**).

Higenamine Protected Doxorubicin-Induced Neonatal Rat Ventricular Myocyte Apoptosis *In Vitro*

Various concentrations of DOX were used to stimulate NRVMs for 24 h *in vitro*. As shown in **Figure 5A**, 1–3 μM DOX was enough to cause death of half of the NRVMs ($p < 0.05$). As the concentration of DOX increased, the proportion of NVRMs that died also increased. In order to further explore whether HG can inhibit DOX-induced cytotoxicity in NRVMs *in vitro*, we first tested cytotoxicity of HG. After incubation with various concentrations of HG for 24 h, the activity of NRVMs did not significantly decrease when the concentration of HG was less than 1 mM, indicating that HG itself has no obvious cytotoxic effect on NRVMs (**Figure 5B**). Based on the results depicted in **Figure 5A**, we used 3 μM DOX-induced NRVM death as the cell model and added varying concentrations of HG 30 min prior to DOX. The results showed that when the concentration of HG was under 30 μM, it could not effectively inhibit DOX-induced NRVM death ($p > 0.05$). However, when the concentration of HG reached 100 μM, it could significantly inhibit DOX-induced cytotoxicity ($p < 0.05$) (**Figure 5C**). Next, we evaluated whether the effect of HG was rooted in its inhibition of apoptosis. As anticipated, DOX observably increased the expression of cleaved caspase 3, by Western blot ($p < 0.05$) (**Figures 5D, E**). At concentrations less than 30 μM, HG had no effect on cell apoptosis ($p > 0.05$). Conversely, the expression of the cleaved caspase 3 protein obviously decreased as the concentration of HG increased above 30 μM (**Figure 5D**). To further test whether HG protects DOX-induced myocardial cell activity in a time-dependent manner, we added HG 30 min in advance and then DOX to stimulate cardiomyocytes for 48 h and found that HG could still protect the activity of DOX-induced cardiomyocytes (**Supplementary Figure S2A**). Thus, for the subsequent *in vitro* studies, the cells were treated with 3 μM DOX for 24 h with a concentration of 100 μM HG.

Higenamine Alleviates Doxorubicin-Induced Neonatal Rat Ventricular Myocyte Oxidative Stress Injury *In Vitro*

Oxidative stress injury is a central pathogenesis of DOX-induced myocardial apoptosis. Oxidative stress injury is primarily due to the imbalance between oxidative and antioxidant systems. Here, oxidative stress comprises an increase in reactive oxygen species and a decrease in antioxidant enzymes. We evaluated mean fluorescence intensity (MFI) to reflect the level of intracellular ROS. As shown

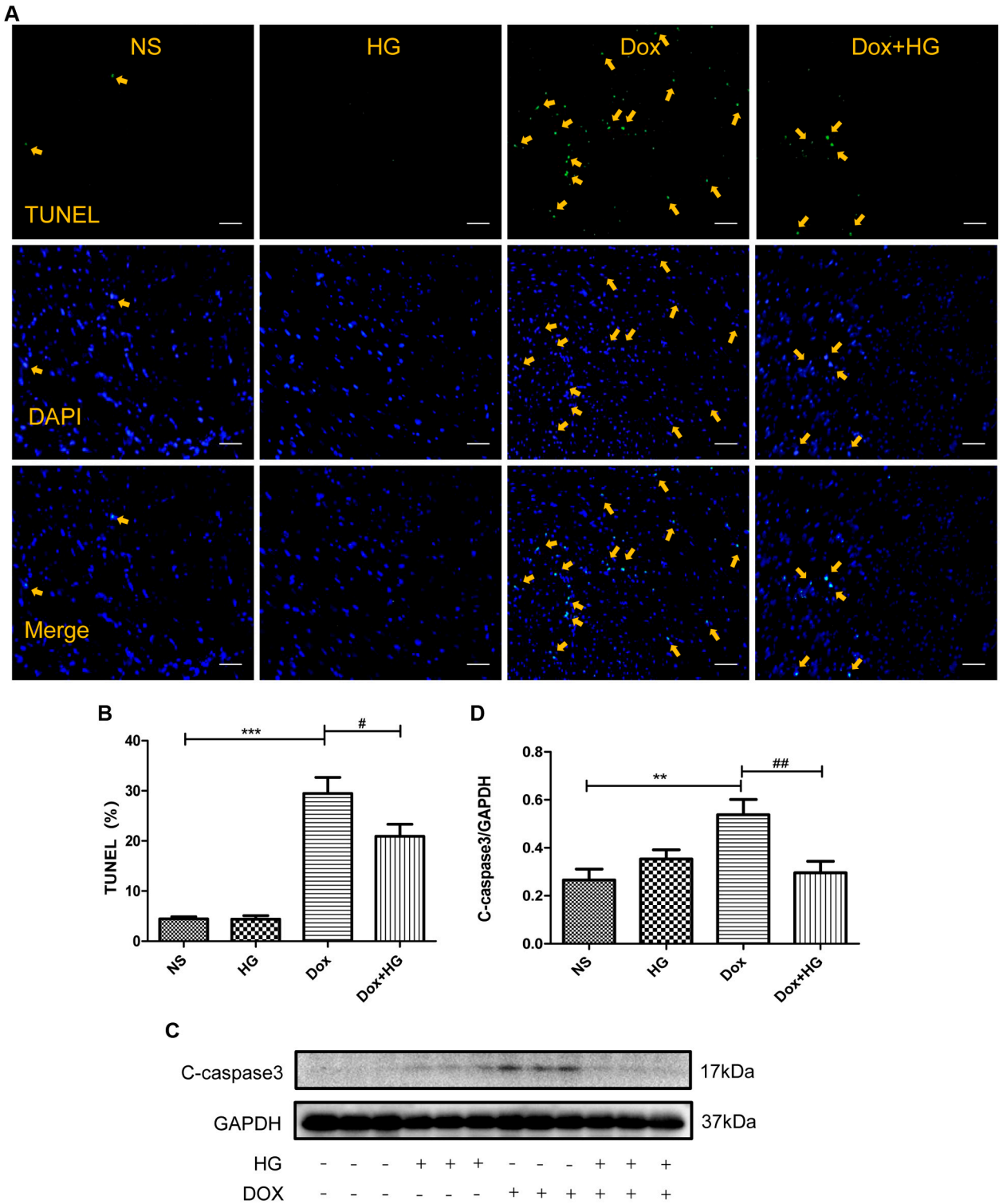

FIGURE 4 | HG inhibited DOX-induced cardiomyocyte apoptosis *in vivo*. **(A)** Representative TUNEL staining image of a myocardial section. Nuclei of apoptosis cells are marked with orange arrows. **(B)** Quantitative data of nuclei of apoptosis cells in mice evaluated by TUNEL staining. **(C)** Western blot analysis of GAPDH, cleaved caspase 3 in cardiac tissues expressed in mice. **(D)** Quantitative data of cleaved caspase 3 expressed in mice. All values are presented as mean ± SEM; statistical analysis was performed using Prism 8.0 one-way ANOVA. * $p < 0.05$ DOX vs NS; # $p < 0.05$ DOX + HG vs DOX. Animal numbers: NS, n = 8; HG, n = 7; DOX, n = 10; DOX + HG, n = 10.

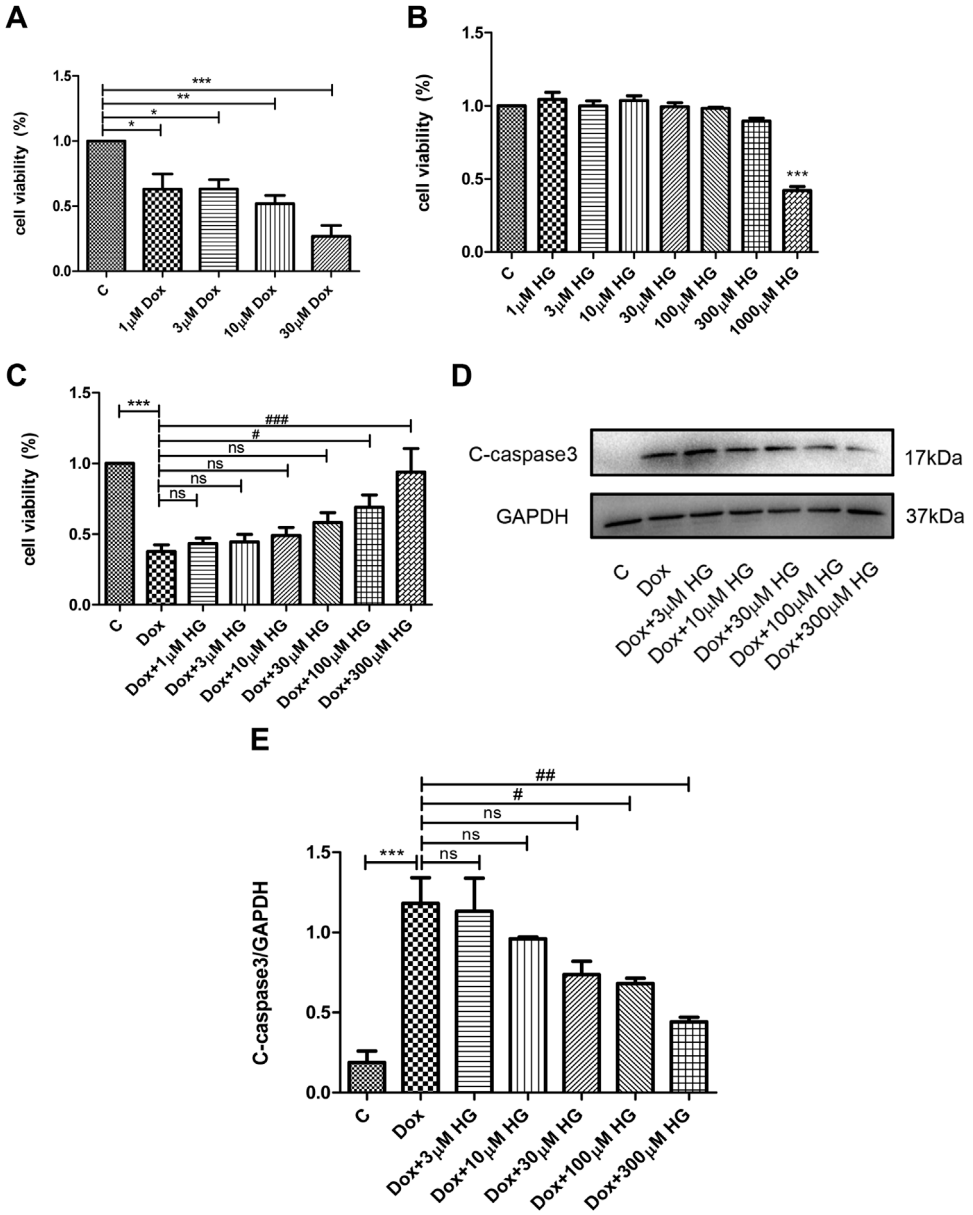

FIGURE 5 | HG inhibited DOX-induced NRVM apoptosis *in vitro*. **(A)** NRVMs were treated with DOX (1, 3, 10, and 30 μM) for 24 h after detection by the CCK8 reagent. **(B)** NRVMs were treated with HG (1, 3, 10, 30, 100, 300, and 1000 μM) for 24 h after detection by the CCK8 reagent. **(C)** NRVMs were pretreated with HG (1, 3, 10, 30, and 100 μM) for 30 min after treatment with DOX for 24 h. Cell activity was detected by using the CCK8 reagent. **(D)** Protein level of cleaved caspase 3 was detected by Western blot. **(E)** Quantitative data of cleaved caspase 3 expressed in NRVMs. The aforementioned experiments were repeated more than three times. All values are presented as mean ± SEM; statistical analysis was performed using Prism 8.0 one-way ANOVA. * $p < 0.05$ DOX vs Control C and HG vs Control C; # $p < 0.05$ DOX + HG vs DOX; ns, $p > 0.05$ DOX + HG vs DOX.

in **Figure 6A**, DOX increased ROS production in NRVMs, while HG pretreatment can alleviate DOX-induced ROS production. In addition, we evaluated the level of superoxide dismutase (SOD) in NRVMs, as shown in **Figure 6B**. Here, HG could reverse the DOX-induced decrease in the expression of SOD.

The mitochondrial membrane is the premise of ATP production and necessary for maintaining mitochondrial function. The stability of mitochondrial membrane potential is conducive for maintaining normal physiological functions of cells. During oxidative stress, free radicals are not sufficiently eliminated from the cell, leading to the decline of mitochondrial membrane potential and the damage of mitochondrial function. JC-1 was used to detect the changes of mitochondrial membrane potential in NRVMs by fluorescence microscopy and analyzed by Image-Pro Plus. As shown in **Figures 6C,D**, DOX exposure changed

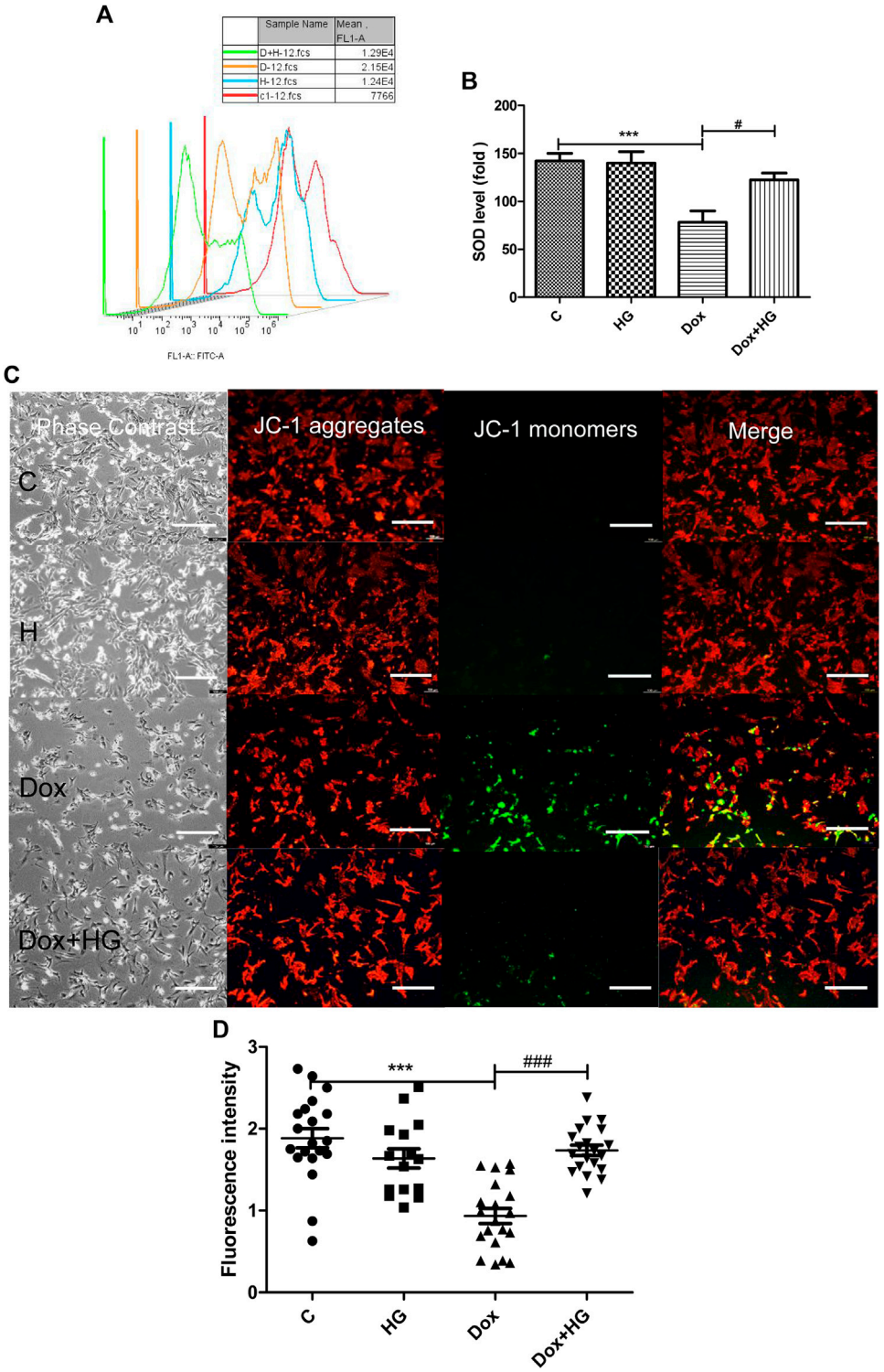

FIGURE 6 | HG alleviated DOX-induced NRVM oxidative stress injury *in vitro*. **(A)** Content of ROS activity in NRVMs. **(B)** Content of SOD activity in NRVMs. **(C)** Mitochondrial membrane potential in cardiomyocytes were detected by using the JC-1 probe. The images were recorded using a microscope (Laika) at ×40 magnification. **(D)** Quantitative data of the JC-1 red-to-green fluorescence intensity ratio. The aforementioned experiments were repeated more than three times. All values are presented as mean ± SEM; statistical analysis was performed using Prism 8.0 one-way ANOVA. * $p < 0.05$ DOX vs Control C; # $p < 0.05$ DOX + HG vs DOX.

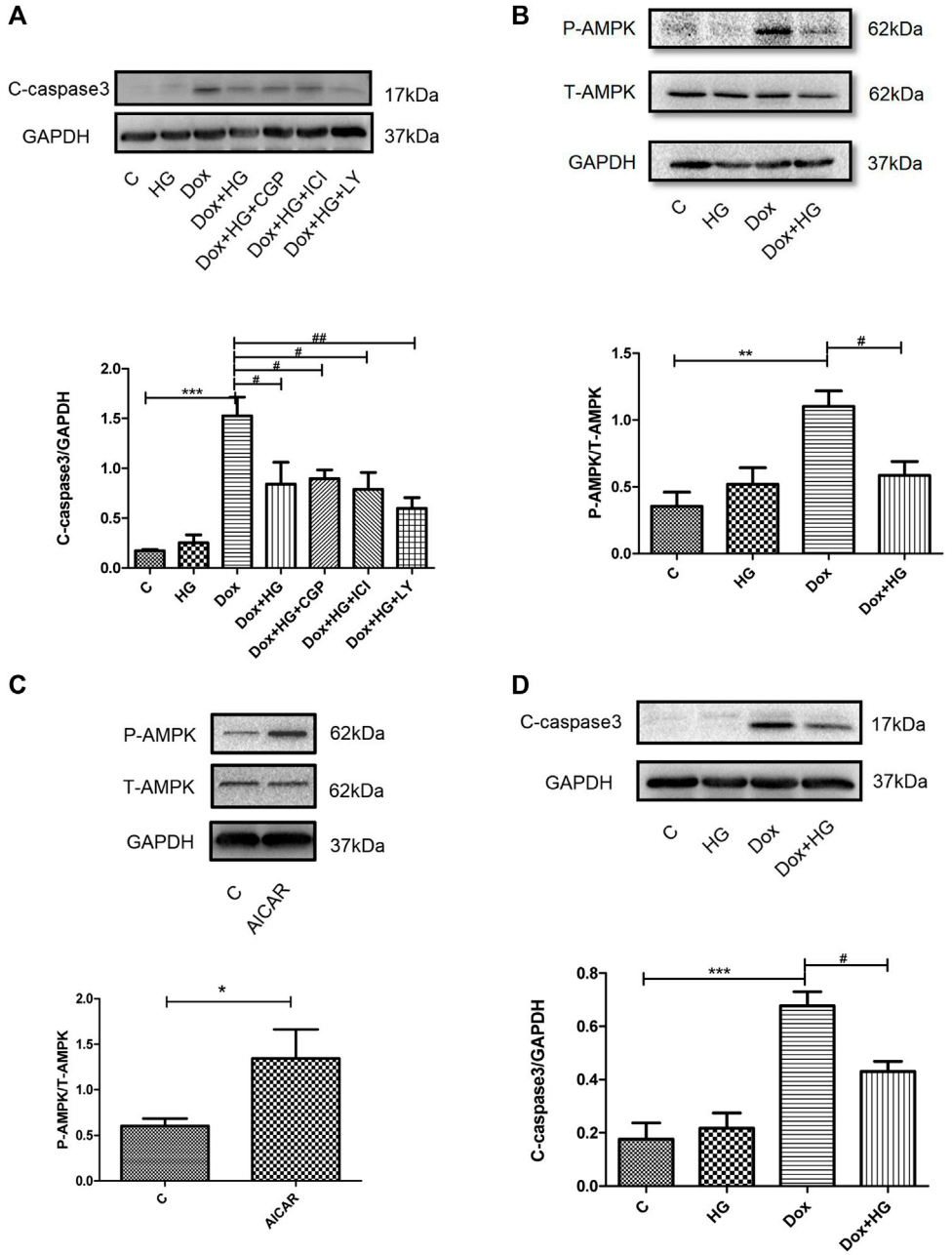

FIGURE 7A | HG blocked the AMPK signal pathway in neonatal ventricular myocytes and in mice. **(A)** Effect of HG was not eliminated in the presence of CGP20712a (1 μM), ICI118551 (0.5 μM), and LY294002 (1 μM). **(B)** Western blot representative images and analysis of the expression of phosphorylated and total AMPK in neonatal ventricular cardiomyocytes. **(C)** Western blot representative images confirmed the efficacy of the agonist AICAR. **(D)** In the absence of agonist AICAR, HG could inhibit DOX-induced cardiomyocyte apoptosis. **(E)** AICAR blocked the inhibitory effect of HG on DOX-induced cardiomyocyte apoptosis. **(F)** Immunohistochemical staining of the phosphorylated and total AMPK in each group of 4 weeks and the phosphorylated AMPK-positive cell for quantitative analysis in mice hearts; scale bar: 100 μM. The aforementioned experiments were repeated more than three times. All values are presented as mean ± SEM; statistical analysis was performed using Prism 8.0 one-way ANOVA. * $p < 0.05$ DOX vs control C, AICAR vs control C, DOX vs NS; # $p < 0.05$ DOX + HG vs DOX; ns, $p > 0.05$ DOX + HG + AICAR vs DOX + AICAR. Animal numbers: NS, n = 8; HG, n = 7; DOX, n = 10; DOX + HG, n = 10.

JC-1 from a polymer to monomer, resulting in a decrease of red fluorescence and increase in green fluorescence, which suggested the loss of mitochondrial membrane potential in NRVMs after DOX treatment. Notably, pretreatment with HG can significantly improve the ratio of red to green fluorescence, indicating that HG can improve DOX-induced mitochondrial dysfunction.

Topoisomerase IIβ (Top 2β) is a protein that helps DNA in fixing topological difficulties and protects cells from being destroyed. DOX interacts with DNA and topoisomerase, forming the Top2–DOX–DNA

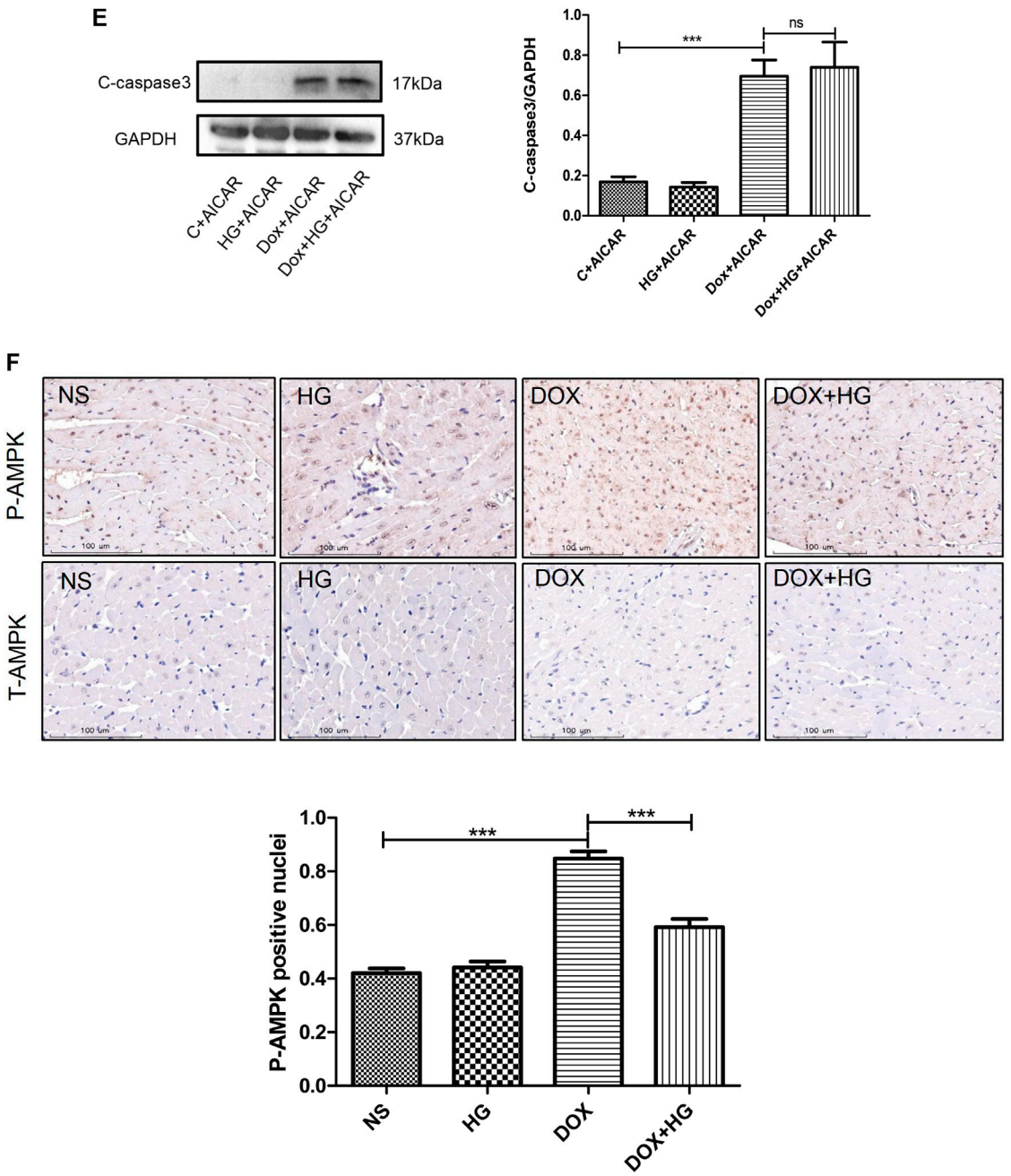

FIGURE 7B | (Continued).

complex, which increases double strand breakage, leading to cytotoxic effects (Tewey et al., 1984). As previously defined, Top 2β is an essential driver of DOX-induced cytotoxicity and DNA damage in cardiomyocytes (Zunino and Capranico, 1990). To explore whether HG is related to DOX-induced DNA damage by interfering with Top 2β, we detected Top 2β mRNA levels by qRT-PCR. We also observed that DOX administration reduced the Top 2β mRNA levels, but the levels of Top 2β were not reversed by HG intervention (**Supplementary Figure 2B**).

Higenamine Blocked the AMPK Signal Pathway in Neonatal Rat Ventricular Myocytes and Mice

Previous studies have shown a similar structure of HG and catecholamine, which activates both β1- and β2-adrenergic receptors (AR). Our former studies reported that HG can reduce myocardial apoptosis induced by ischemia/reperfusion through activation of the β2/PI3K/Akt signaling pathway (Wu et al., 2016). We attempted to determine whether the inhibitory

effect of HG on DOX-induced myocardial apoptosis is through the same pathway as that in ischemia/reperfusion-induced apoptosis. Here, we used specific β1-AR (CGP20712a), β2-AR (ICI118551), and PI3K inhibitors (LY294002). Interestingly, pretreatment with these three inhibitors did not change the protective effect of HG on DOX-induced NRVM apoptosis (**Figure 7A**), suggesting that the effect of HG on DOX-induced NRVM apoptosis is independent of the signaling pathway in ischemia/reperfusion disease.

To explore the molecular mechanism of HG in DOX-induced NRVM apoptosis, we examined the AMPK signaling pathway, a typical pathway that participates in DOX-induced NRVM damage. Our results showed that the phosphorylation of AMPK was significantly increased in DOX-treated NRVMs, while HG significantly inhibited the phosphorylation of AMPK (**Figure 7B**). To further verify whether the AMPK signaling pathway contributed to the cardioprotective effect of HG, we used the AMPK-specific agonist, AICAR. As shown in **Figure 7C**, AICAR can increase the phosphorylation of AMPK, indicating the effectiveness of the agonist. In the absence of AMPK agonist AICAR, HG could inhibit DOX-induced NRVM apoptosis (**Figure 7D**). In the case of presence of AICAR, we found that the inhibitory effect of HG on DOX-induced NRVM apoptosis cold be blocked by AICAR (**Figure 7E**). Furthermore, the result of immunohistochemical staining showed that DOX treatment led to an increase in the level of phosphorylated AMPK-positive cells, and HG inhibited the number of phosphorylated AMPK-positive cells (**Figure 7F**). These results suggested that HG can inhibit DOX-induced NRVM apoptosis, and the protective effect of HG on the heart at least partially depends on the AMPK signaling pathway.

DISCUSSION

The cardiotoxic side effects of DOX, a typical anthracycline antitumor drug that has been prescribed for several decades around the world, have restricted the outcome for patients. At present, a few people have been successful in solving this problem. Dexrazoxane is the only drug that has been approved by the Food and Drug Administration (FDA) as a cardiac protective agent against DOX-induced cardiotoxicity (Kane et al., 2008). However, its use has been controversial due to its carcinogenic potential (Reichardt et al., 2018). Therefore, it is urgent to find new drugs to protect against DOX-induced cardiotoxicity. In Oriental Asia, aconite roots, a traditional Chinese medicine, has been commonly used to treat similar symptoms for thousands of years (Zhang et al., 2017). Higenamine (HG) is the main effective compound extracted from this Chinese herb. Recently, it has also been used as a common component in health products for fat degradation and sports performance in Europe and North America. Previous studies have shown that HG has positive inotropic and chronotropic effects on cardiomyocytes as well as antioxidant, antiapoptotic, and vasodilator effects (Zhang et al., 2014; Tariq and Aronow., 2015).

The aim of this study was to investigate the effect of HG on DOX-induced chronic cardiotoxicity. During our study, other groups reported the protective effect of 6-gingerol combined with HG on DOX-induced chronic heart injury (Chen et al., 2013; Wen et al., 2019; Wen et al., 2020). Herein, we provide further evidence that HG can prevent DOX-induced oxidative stress injury and improve cardiomyocyte apoptosis in neonatal rat cardiomyocytes *in vitro*. A DOX model was used to mimic clinical cardiotoxicity induced by chemotherapy drugs *in vivo*. We found that HG reduced DOX-induced myocardial atrophy and cardiomyocyte apoptosis and improved cardiac dysfunction and cardiac remodeling in mice. In general, our chronic cardiotoxicity mouse model and DOX cytotoxicity model demonstrated that HG could reduce DOX-induced cardiotoxicity.

The pathogenesis of DOX-induced cardiotoxicity has been a controversial and complex topic. Oxidative stress injury is one of the common causes of cell dysfunction and a vital factor in the pathogenesis of many diseases. Several studies have shown that DOX can accumulate in mitochondria, destroying the electron chain, increasing the content of ROS, and causing the imbalance of antioxidant and oxidative systems. This induces myocardial oxidative stress damage, further leading to myocardial cell apoptosis and ultimately causing cardiac dysfunction and even heart failure. In our study it also demonstrated that DOX can induce the increase of ROS, and the decrease of SOD content and mitochondrial membrane potential, all of which is consistent with previous research results. HG intervention can improve mitochondrial dysfunction, restore the mitochondrial membrane potential, promote the expression of superoxide dismutase, and reduce the production of ROS, indicating that HG can reduce DOX-induced oxidative stress injury.

Excessive production of reactive oxygen species can activate mitochondrial anion channels, further open mPTP channels, and reduce the mitochondrial membrane potential, all of which facilitate apoptosis triggered by the mitochondrial-dependent pathway (Sinha et al., 2013). In our *in vivo* study, TUNEL staining and Western blots showed that DOX could induce the increase of TUNEL-positive nuclei and the abundance of apoptosis protein cleaved caspase 3, indicating that DOX could induce cardiomyocyte apoptosis. Simultaneously, after HG intervention, the number of TUNEL-positive nuclei and the abundance of the apoptosis protein decreased significantly. These results indicated that HG could reduce cardiomyocyte apoptosis. In addition, we found that EF, FS, and SV were significantly improved after HG intervention, indicating that HG could improve DOX-induced cardiac dysfunction in mice.

Topoisomerase IIβ (Top 2β) is considered to be an important driver of the DOX-induced cardiotoxicity. Studies have found that DOX binds to Top 2β when entering the body, and a Top2–DOX–DNA complex is formed, which promotes ROS production, impairs mitochondrial function, and induces cardiomyocyte apoptosis (Tewey et al., 1984). In addition, dexrazoxane, the only drug that has been shown to prevent and treat DOX-induced cardiotoxicity, was reported to antagonize DOX-induced DNA damage by interfering with Top 2β (Lyu et al., 2007). Unfortunately, in our study, HG did not affect DOX-induced Top 2β expression.

The most well-known molecular target of HG is β-AR (Tsukiyama et al., 2009). Previous studies, including our own laboratory findings, have shown that HG is a β2-AR agonist in bronchorelaxation, and HG, through the activation of the β2/PI3K/Akt signaling pathway, inhibits cardiomyocyte apoptosis and protects myocardia from ischemia-reperfusion injury. Moreover, researchers have found that the heart-strengthening effect of HG is achieved through the β-adrenergic receptor pathway. In this study, we utilized the β1-AR agonist CGP20712a, β2-AR agonist ICI118551, and PI3K agonist LY294002 to investigate the mechanism of DOX-induced apoptosis inhibition by HG. Our studies found that HG could still protect against the DOX-induced apoptosis of cardiomyocytes. Notably, our results showed that HG inhibited DOX-induced cardiomyocyte apoptosis independent of the β-AR signaling pathway, suggesting that HG may have a new pharmacological target for anti-cardiomyocyte apoptosis induced by DOX.

Adenosine-activated protein kinase (AMPK) plays a key role in the regulation of biological energy metabolism. Previous studies have found that AMPK is a major regulator of lipid metabolism and glucose metabolism and is a hot topic in the study of diabetes and other metabolic diseases (Madhavi et al., 2019). In recent years, studies have revealed that the AMPK signaling pathway is also closely related to cardiovascular disease (Howell et al., 2011). Several studies support that the AMPK signaling pathway plays an important role in DOX-induced cardiac dysfunction (Feng et al., 2018). On the one hand, it is believed that activation of the AMPK signaling pathway can promote DOX-induced cardiomyocyte apoptosis (Liu et al., 2018). On the other hand, a few studies suggest that inhibition of the AMPK signaling pathway can play an antiapoptotic role in cardiomyocytes (Lv et al., 2012), which differs from the mainstream opinion of the AMPK signaling pathway. During our *in vitro* and *in vivo* study, DOX can significantly induce the phosphorylation of AMPK, while HG pretreatment can inhibit the phosphorylation of AMPK and protect cardiomyocytes from DOX-induced apoptosis. When AMPK agonist AICAR was added, the effect of HG disappeared. Therefore, the protective effect of HG may be achieved by inhibiting the AMPK signaling pathway. In the future, it is of great significance to study whether HG is related to the AMPK signaling pathway and the interaction between HG and AMPK signaling pathways.

CONCLUSION

In this study, we found a new role of HG in tumor cardiopathy by inhibiting DOX-induced cardiomyocyte apoptosis. In addition, we demonstrated that this protective effect worked partially through the suppression of the AMPK signaling pathway. In the future, it is of great significance to study whether HG is related to the AMPK signaling pathway and the interaction between HG and AMPK signaling pathways.

DATA AVAILABILITY STATEMENT

The original contributions presented in the study are included in the article/**Supplementary Material**, further inquiries can be directed to the corresponding authors.

ETHICS STATEMENT

The animal study was reviewed and approved by National Natural Science Foundation of China. Written informed consent was obtained from the owners for the participation of their animals in this study.

AUTHOR CONTRIBUTIONS

All authors listed have made a substantial, direct, and intellectual contribution to the work and approved it for publication.

FUNDING

This research was supported by grants from the National Natural Science Foundation of China, No. 81973826 (to MP-W) and National Natural Science Foundation of China No. 81904167 (to WL).

SUPPLEMENTARY MATERIAL

The Supplementary Material for this article can be found online at: https://www.frontiersin.org/articles/10.3389/fcell.2022.809996/full#supplementary-material

REFERENCES

Cardiff, R. D., Miller, C. H., and Munn, R. J. (2014). Manual Hematoxylin and Eosin Staining of Mouse Tissue Sections. *Cold Spring Harb. Protoc.* 2014 (6), pdb.prot073411–658. doi:10.1101/pdb.prot073411

Chen, Y.-L., Zhuang, X.-D., Xu, Z.-W., Lu, L.-H., Guo, H.-L., Wu, W.-K., et al. (2013). Higenamine Combined with [6]-Gingerol Suppresses Doxorubicin-Triggered Oxidative Stress and Apoptosis in Cardiomyocytes via Upregulation of PI3K/Akt Pathway. *Evidence-Based Complement. Altern. Med.* 2013, 1–14. doi:10.1155/2013/970490

Feng, Y., Zhang, Y., and Xiao, H. (2018). AMPK and Cardiac Remodelling. *Sci. China Life Sci.* 61 (1), 14–23. doi:10.1007/s11427-017-9197-5

Galán-Arriola, C., Lobo, M., Vílchez-Tschischke, J. P., López, G. J., de Molina-Iracheta, A., Pérez-Martínez, C., et al. (2019). Serial Magnetic Resonance Imaging to Identify Early Stages of Anthracycline-Induced Cardiotoxicity. *J. Am. Coll. Cardiol.* 73 (7), 779–791. doi:10.1016/j.jacc.2018.11.046

Golden, H. B., Gollapudi, D., Gerilechaogetu, F., Li, J., Cristales, R. J., Peng, X., et al. (2012). Isolation of Cardiac Myocytes and Fibroblasts from Neonatal Rat Pups. *Methods Mol. Biol.* 843, 205–214. doi:10.1007/978-1-61779-523-7_20

Hagag, A. A., Badraia, I. M., El-Shehaby, W. A., and Mabrouk, M. M. (2020). Protective Role of Black Seed Oil in Doxorubicin-Induced Cardiac Toxicity in Children with Acute Lymphoblastic Leukemia. *J. Oncol. Pharm. Pract.* 26 (6), 1397–1406. doi:10.1177/1078155219897294

Howell, N. J., Ashrafian, H., Drury, N. E., Ranasinghe, A. M., Contractor, H., Isackson, H., et al. (2011). Glucose-Insulin-Potassium Reduces the

Incidence of Low Cardiac Output Episodes After Aortic Valve Replacement for Aortic Stenosis in Patients with Left Ventricular Hypertrophy. *Circulation* 123 (2), 170–177. doi:10.1161/CIRCULATIONAHA.110.945170

Kane, R. C., McGuinn, W. D., Dagher, R., Justice, R., and Pazdur, R. (2008). Dexrazoxane (Totect): FDA Review and Approval for the Treatment of Accidental Extravasation Following Intravenous Anthracycline Chemotherapy. *Oncologist* 13 (4), 445–450. doi:10.1634/theoncologist.2007-0247

Knight, W. E., Chen, S., Zhang, Y., Oikawa, M., Wu, M., Zhou, Q., et al. (2016). PDE1C Deficiency Antagonizes Pathological Cardiac Remodeling and Dysfunction. *Proc. Natl. Acad. Sci. U.S.A.* 113 (45), E7116–E7125. doi:10.1073/pnas.1607728113

Koutsoukis, A., Ntalianis, A., Repasos, E., Kastritis, E., Dimopoulos, M.-A., and Paraskevaidis, I. (2018). Cardio-Oncology: A Focus on Cardiotoxicity. *Eur. Cardiol.* 13 (1), 64–69. doi:10.15420/ecr.2017:17:2

Lee, S.-R., Schriefer, J. M., Gunnels, T. A., Harvey, I. C., and Bloomer, R. J. (2013). Acute Oral Intake of a Higenamine-Based Dietary Supplement Increases Circulating Free Fatty Acids and Energy Expenditure in Human Subjects. *Lipids Health Dis.* 12, 148. doi:10.1186/1476-511X-12-148

Liu, D., Ma, Z., Di, S., Yang, Y., Yang, J., Xu, L., et al. (2018). AMPK/PGC1α Activation by Melatonin Attenuates Acute Doxorubicin Cardiotoxicity via Alleviating Mitochondrial Oxidative Damage and Apoptosis. *Free Radic. Biol. Med.* 129, 59–72. doi:10.1016/j.freeradbiomed.2018.08.032

Liu, Y., and Santillo, M. F. (2016). Cytochrome P450 2D6 and 3A4 Enzyme Inhibition by Amine Stimulants in Dietary Supplements. *Drug Test. Anal.* 8 (3-4), 307–310. doi:10.1002/dta.1863

Lv, X., Yu, X., Wang, Y., Wang, F., Li, H., Wang, Y., et al. (2012). Berberine Inhibits Doxorubicin-Triggered Cardiomyocyte Apoptosis via Attenuating Mitochondrial Dysfunction and Increasing Bcl-2 Expression. *PLoS One* 7 (10), e47351. doi:10.1371/journal.pone.0047351

Lyu, Y. L., Kerrigan, J. E., Lin, C.-P., Azarova, A. M., Tsai, Y.-C., Ban, Y., et al. (2007). Topoisomerase IIβ-Mediated DNA Double-Strand Breaks: Implications in Doxorubicin Cardiotoxicity and Prevention by Dexrazoxane. *Cancer Res.* 67 (18), 8839–8846. doi:10.1158/0008-5472.CAN-07-1649

Madhavi, Y. V., Gaikwad, N., Yerra, V. G., Kalvala, A. K., Nanduri, S., and Kumar, A. (2019). Targeting AMPK in Diabetes and Diabetic Complications: Energy Homeostasis, Autophagy and Mitochondrial Health. *Cmc* 26 (27), 5207–5229. doi:10.2174/0929867325666180406120051

Mantawy, E. M., El-Bakly, W. M., Esmat, A., Badr, A. M., and El-Demerdash, E. (2014). Chrysin Alleviates Acute Doxorubicin Cardiotoxicity in Rats via Suppression of Oxidative Stress, Inflammation and Apoptosis. *Eur. J. Pharmacol.* 728, 107–118. doi:10.1016/j.ejphar.2014.01.065

Reichardt, P., Tabone, M.-D., Mora, J., Morland, B., and Jones, R. L. (2018). Risk-Benefit of Dexrazoxane for Preventing Anthracycline-Related Cardiotoxicity: Re-Evaluating the European Labeling. *Future Oncol.* 14 (25), 2663–2676. doi:10.2217/fon-2018-0210

Singal, P. K., and Iliskovic, N. (1998). Doxorubicin-Induced Cardiomyopathy. *N. Engl. J. Med.* 339 (13), 900–905. doi:10.1056/NEJM199809243391307

Sinha, K., Das, J., Pal, P. B., and Sil, P. C. (2013). Oxidative Stress: The Mitochondria-Dependent and Mitochondria-Independent Pathways of Apoptosis. *Arch. Toxicol.* 87 (7), 1157–1180. doi:10.1007/s00204-013-1034-4

Tariq, S., and Aronow, W. (2015). Use of Inotropic Agents in Treatment of Systolic Heart Failure. *Ijms* 16 (12), 29060–29068. doi:10.3390/ijms161226147

Tewey, K. M., Rowe, T. C., Yang, L., Halligan, B. D., and Liu, L. F. (1984). Adriamycin-Induced DNA Damage Mediated by Mammalian DNA Topoisomerase II. *Science* 226 (4673), 466–468. doi:10.1126/science.6093249

Tsukiyama, M., Ueki, T., Yasuda, Y., Kikuchi, H., Akaishi, T., Okumura, H., et al. (2009). β2-Adrenoceptor-Mediated Tracheal Relaxation Induced by Higenamine from Nandina Domestica Thunberg. *Planta Med.* 75 (13), 1393–1399. doi:10.1055/s-0029-1185743

Wang, L., Yuan, D., Zheng, J., Wu, X., Wang, J., Liu, X., et al. (2019). Chikusetsu Saponin IVa Attenuates Isoprenaline-Induced Myocardial Fibrosis in Mice Through Activation Autophagy Mediated by AMPK/mTOR/ULK1 Signaling. *Phytomedicine* 58, 152764. doi:10.1016/j.phymed.2018.11.024

Wang, Y., Lu, X., Wang, X., Qiu, Q., Zhu, P., and Ma, L. (2021). Atg7-Based Autophagy Activation Reverses Doxorubicin-Induced Cardiotoxicity. *Circ. Res.* 129 (8), e166–e182. doi:10.1161/CIRCRESAHA.121.319104

Wen, J., Wang, J., Li, P., Wang, R., Wang, J., Zhou, X., et al. (2019). Protective Effects of Higenamine Combined with [6]-Gingerol Against Doxorubicin-Induced Mitochondrial Dysfunction and Toxicity in H9c2 Cells and Potential Mechanisms. *Biomed. Pharmacother.* 115, 108881. doi:10.1016/j.biopha.2019.108881

Wen, J., Zhang, L., Wang, J., Wang, J., Wang, L., Wang, R., et al. (2020). Therapeutic Effects of Higenamine Combined with [6]-gingerol on Chronic Heart Failure Induced by Doxorubicin via Ameliorating Mitochondrial Function. *J. Cel. Mol. Med.* 24 (7), 4036–4050. doi:10.1111/jcmm.15041

Wu, M.-p., Zhang, Y.-s., Zhou, Q.-m., Xiong, J., Dong, Y.-r., and Yan, C. (2016). Higenamine Protects Ischemia/Reperfusion Induced Cardiac Injury and Myocyte Apoptosis Through Activation of β2-AR/PI3K/AKT Signaling Pathway. *Pharmacol. Res.* 104, 115–123. doi:10.1016/j.phrs.2015.12.032

Yu, X., Ruan, Y., Huang, X., Dou, L., Lan, M., Cui, J., et al. (2020). Dexrazoxane Ameliorates Doxorubicin-Induced Cardiotoxicity by Inhibiting Both Apoptosis and Necroptosis in Cardiomyocytes. *Biochem. Biophysical Res. Commun.* 523 (1), 140–146. doi:10.1016/j.bbrc.2019.12.027

Zhang, K. W., Finkelman, B. S., Gulati, G., Narayan, H. K., Upshaw, J., Narayan, V., et al. (2018). Abnormalities in 3-Dimensional Left Ventricular Mechanics with Anthracycline Chemotherapy Are Associated with Systolic and Diastolic Dysfunction. *JACC: Cardiovasc. Imaging* 11 (8), 1059–1068. doi:10.1016/j.jcmg.2018.01.015

Zhang, N., Lian, Z., Peng, X., Li, Z., and Zhu, H. (2017). Applications of Higenamine in Pharmacology and Medicine. *J. Ethnopharmacology* 196, 242–252. doi:10.1016/j.jep.2016.12.033

Zhang, Z., Li, M., Wang, Y., Wu, J., and Li, J. (2014). Higenamine Promotes M2 Macrophage Activation and Reduces Hmgb1 Production Through HO-1 Induction in a Murine Model of Spinal Cord Injury. *Int. Immunopharmacology* 23 (2), 681–687. doi:10.1016/j.intimp.2014.10.022

Zhu, J.-X., Ling, W., Xue, C., Zhou, Z., Zhang, Y.-S., Yan, C., et al. (2021). Higenamine Attenuates Cardiac Fibroblast Abstract and Fibrosis via Inhibition of TGF-β1/Smad Signaling. *Eur. J. Pharmacol.* 900, 174013. doi:10.1016/j.ejphar.2021.174013

Zunino, F., and Capranico, G. (1990). DNA Topoisomerase II as the Primary Target of Anti-Tumor Anthracyclines. *Anticancer Drug Des.* 5 (4), 307–317.

Conflict of Interest: The authors declare that the research was conducted in the absence of any commercial or financial relationships that could be construed as a potential conflict of interest.

Publisher's Note: All claims expressed in this article are solely those of the authors and do not necessarily represent those of their affiliated organizations, or those of the publisher, the editors, and the reviewers. Any product that may be evaluated in this article, or claim that may be made by its manufacturer, is not guaranteed or endorsed by the publisher.

Copyright © 2022 Jin, Chai, Hu, Tian, Ling, Li and Wu. This is an open-access article distributed under the terms of the Creative Commons Attribution License (CC BY). The use, distribution or reproduction in other forums is permitted, provided the original author(s) and the copyright owner(s) are credited and that the original publication in this journal is cited, in accordance with accepted academic practice. No use, distribution or reproduction is permitted which does not comply with these terms.

Advantages of publishing in Frontiers

OPEN ACCESS
Articles are free to read for greatest visibility and readership

FAST PUBLICATION
Around 90 days from submission to decision

HIGH QUALITY PEER-REVIEW
Rigorous, collaborative, and constructive peer-review

TRANSPARENT PEER-REVIEW
Editors and reviewers acknowledged by name on published articles

Frontiers
Avenue du Tribunal-Fédéral 34
1005 Lausanne | Switzerland

Visit us: www.frontiersin.org
Contact us: frontiersin.org/about/contact

REPRODUCIBILITY OF RESEARCH
Support open data and methods to enhance research reproducibility

DIGITAL PUBLISHING
Articles designed for optimal readership across devices

FOLLOW US
@frontiersin

IMPACT METRICS
Advanced article metrics track visibility across digital media

EXTENSIVE PROMOTION
Marketing and promotion of impactful research

LOOP RESEARCH NETWORK
Our network increases your article's readership